PROCEEDINGS

5th international conference on nondestructive testing

Montreal, Canada, 1967

DISCLAIMER

This report was prepared as an account of work sponsored by an agency of the United States Government. Neither the United States Government nor any agency Thereof, nor any of their employees, makes any warranty, express or implied, or assumes any legal liability or responsibility for the accuracy, completeness, or usefulness of any information, apparatus, product, or process disclosed, or represents that its use would not infringe privately owned rights. Reference herein to any specific commercial product, process, or service by trade name, trademark, manufacturer, or otherwise does not necessarily constitute or imply its endorsement, recommendation, or favoring by the United States Government or any agency thereof. The views and opinions of authors expressed herein do not necessarily state or reflect those of the United States Government or any agency thereof.

DISCLAIMER

Portions of this document may be illegible in electronic image products. Images are produced from the best available original document.

MASTER

PROCEEDINGS OF THE
FIFTH INTERNATIONAL CONFERENCE
ON
NONDESTRUCTIVE TESTING

© Crown Copyrights reserved

Available by mail from the Queen's Printer, Ottawa,
and at the following Canadian Government bookshops:

HALIFAX
1735 Barrington Street

MONTREAL
Æterna-Vie Building, 1182 St. Catherine Street West

OTTAWA
Daly Building, Corner Mackenzie and Rideau

TORONTO
221 Yonge Street

WINNIPEG
Mall Center Building, 499 Portage Avenue

VANCOUVER
657 Granville Street

or through your bookseller

Price: $30.00 Catalogue No. M37-1267

Price subject to change without notice

The Queen's Printer
Ottawa, Canada
1969

18

Permission granted in 2008 from the Crown Copyright to DOE/OSTI to offer an Internet copy of this document, with the following disclaimer: "The Government of Canada makes no representation and expressly disclaims any liability relative to the accuracy or completeness of the work".

Designed and prepared by

D. A. SHENSTONE

Public Relations and Information Services
Department of Energy, Mines and Resources
Ottawa

MASTER

PROCEEDINGS OF THE
FIFTH INTERNATIONAL CONFERENCE
ON
NONDESTRUCTIVE TESTING

© Crown Copyrights reserved

Available by mail from the Queen's Printer, Ottawa,
and at the following Canadian Government bookshops:

HALIFAX
1735 Barrington Street

MONTREAL
Æterna-Vie Building, 1182 St. Catherine Street West

OTTAWA
Daly Building, Corner Mackenzie and Rideau

TORONTO
221 Yonge Street

WINNIPEG
Mall Center Building, 499 Portage Avenue

VANCOUVER
657 Granville Street

or through your bookseller

Price: $30.00 Catalogue No. M37-1267

Price subject to change without notice

The Queen's Printer
Ottawa, Canada
1969

18

Permission granted in 2008 from the Crown Copyright to DOE/OSTI to offer an Internet copy of this document, with the following disclaimer: "The Government of Canada makes no representation and expressly disclaims any liability relative to the accuracy or completeness of the work".

Designed and prepared by

D. A. SHENSTONE

Public Relations and Information Services
Department of Energy, Mines and Resources
Ottawa

23 Conf-670505--

5

PROCEEDINGS OF THE FIFTH INTERNATIONAL CONFERENCE ON NONDESTRUCTIVE TESTING

[Held at Montreal, Canada, May 21—26, 1967].

6

20 507p.
21 $30.00

31 Conference on Nondestructive Testing, Montreal, 1967.

INTERNATIONAL
CONFERENCE ON
NDT
CANADA, 1967

Sponsored by the Canadian Council for Nondestructive Technology, Inc.

Release for Announcement in
Nuclear Science Abstracts

INTERNATIONAL COMMITTEE FOR NONDESTRUCTIVE TESTING

Officers, 1963-67

President
W. E. Havercroft,
CANADA

Vice President
R. D. Barer,
CANADA

Secretary
E. T. Watterud,
CANADA

Delegates

Dr. Ekkehart Krainer,
AUSTRIA

Prof. Dr. Georges-A. Homès
BELGIUM

ing. Lubomir Cizek, CSC.,
CZECHOSLOVAKIA

Prof. Giorgia Moravia,
ITALY

Prof. Dr. Hiroshi Kihara,
JAPAN

A. de Sterke,
NETHERLANDS

Prof. Dr. Ignacy Malecki,
POLAND

Prof. Dr. Manuel de Miro,
SPAIN

Dr. J. Salokangas,
FINLAND

Prof. Dr. Paul G. Bastien,
FRANCE

Dr. R. Seifert,
GERMANY

Dr. L. Mullins,
ENGLAND

H. Swedenborg,
SWEDEN

R. Hornung,
SWITZERLAND

P. Scribante,
SOUTH AFRICA

Dr. Gerold H. Tenney,
U.S.A.

Prof. Dr. P. K. Oshchepkov,
U.S.S.R.

Jon Christian Walter
NORWAY

SOME ACTIVITIES AT THE CONFERENCE

The head table at the conference banquet

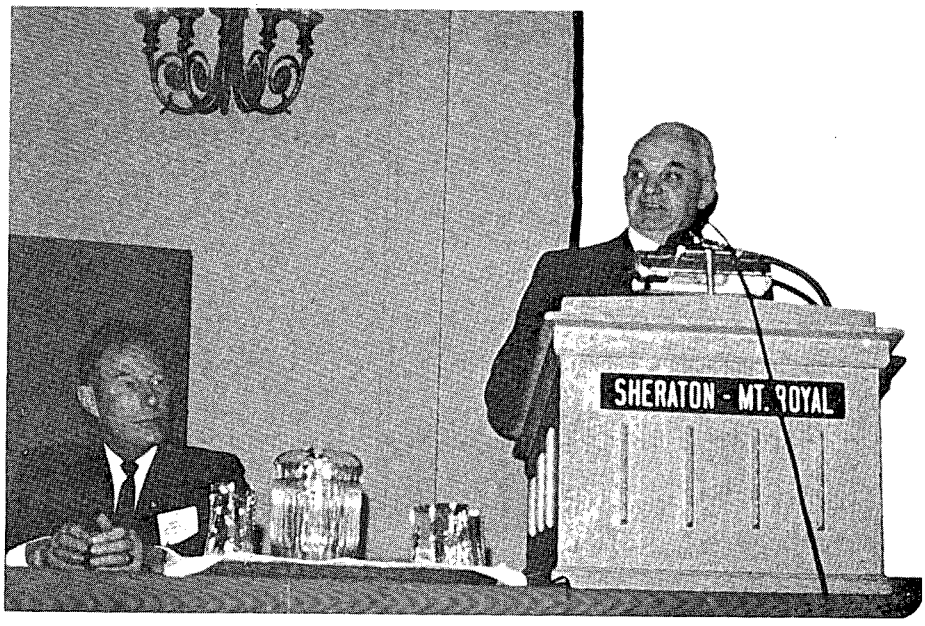

Dr. John Convey, Director, Mines Branch, opens the conference

Some international delegates gather after the day's session

CONTENTS

INTRODUCTION ix

SESSION 1—EVALUATION OF MATERIAL QUALITY

Advances in the Application of Nondestructive Testing to Cast Iron, *A. G. Fuller, U.K.* 2
The Evaluation of Small Surface Laps in Aluminium Alloy Die Forgings, *J. G. Harris, U.K.* 8
Dynamic Tests for Nondestructive Analysis of Lumber Quality, *W. L. Galligan* and *R. F. Pellerin, U.S.A.* 15
Nondestructive Testing of the Elasticity and Strength of Wood, *N. D. Popescu, Romania* 20
Controlling the Electric Field of Low-frequency Dielectric Nondestructive Testing Devices, *J. R. Zurbrick, U.S.A.* 27

SESSION 2—ULTRASONICS—IDENTIFICATION AND MEASUREMENTS

The Relationship between Ultrasonic Inspection Results, Slag Inclusions, and Fatigue Strength, *S. Malmqvist, Sweden* 34
Ultrasonic and Metallurgical Evaluation of Flaws in Large Rotor Forgings, *R. W. Renner, H. A. Greenberg* and *W. G. Clark, Jr., U.S.A.* 37
The Ultrasonic Inspection of Steel Sheets with Lamb Waves, *E. Isono* and *T. Ueno, Japan* 43
Underwater Wall-Thickness Measurements and Weld Testing by Ultrasonics, *H. Jünke, Germany* 50
Wall Thickness and Wall-thickness Tolerance Measurement, *W. Grabendörfer* and *A. Droege, Germany* 54
Ultrasonic Defect-size Determination with Double-probe and Single-probe Techniques, *E. Mundry* and *H. Wüstenberg, Germany* 58

SESSION 3—THERMAL METHODS

Infrared Nondestructive Testing—Past, Present and Future, *R. Vanzetti, U.S.A.* 64
Dynamic Infrared Detection of Fatigue Cracks, *E. J. Kubiak, B. A. Johnson* and *R. C. Taylor, U.S.A.* 69
An Analytical Approach to Infrared Nondestructive Testing, *A. W. Schultz, U.S.A.* 74
Thermal Nondestructive Testing with Cholesteric Liquid Crystals, *W. E. Woodmansee* and *H. L. Southworth, U.S.A.* 81

SESSION 4—TESTING OF WELDS

The Activities of the International Institute of Welding in the Domain of Nondestructive Testing, *A. de Sterke, Netherlands,* and *G. A. Homès, Belgium* 88
Ultrasonic Inspection of Weldments Using the Delta Technique, *B. T. Cross* and *G. J. Posakony, U.S.A.* 96
Practical Quality Evaluation of Welds by Ultrasonics, *T. Fuji* and *M. Sato, Japan* 100
Analysis of the Strengths of Aluminum Repair Welds, *S. Leonard, J. K. S. Lee* and *J. S. Chasty, U.S.A.* 104
Inspection and Tracking of Welds Using the New Magnetic Reaction Analyzer, *G. H. Smith* and *R. C. McMaster, U.S.A.* 108
Scientific Principles of Introscopy, *P. K. Oshchepkov, U.S.S.R.* 114

SESSION 5—VISUAL AIDS IN NONDESTRUCTIVE TESTING

Television Systems for Nondestructive Testing, *H. Berger, U.S.A.* 118
Optical Methods for Studying Ultrasonic Propagation in Transparent Media, *H. L. Whaley, K. V. Cook, R. W. McClung,* and *L. S. Snyders, U.S.A.* 125
A Thermoluminescent Image-detection Method for Neutron Radiography, *J. Kastner, H. Berger* and *I. R. Kraska, U.S.A.* 132
Ciné-fluoroscopic Studies in the Production of Castings, *R. Halmshaw, J. D. Lavender* and *R. L. Durant, U.K.* 134

SESSION 6—MEASUREMENTS OF STRESS AND ELASTIC PROPERTIES

Ultrasonic Methods in the Study of Mechanical Characteristics of Iron and Carbon Steels, *W. J. Bratina, J. T. McGrath, R. I. Moore, Canada; O. M. M. Mitchell,* and *R. E. Love, U.S.A.* 140
Elasticimétrie et inélasticimétrie automatiques entre −200° et +250°C, *M. Sepaser, P. Azou* and *P. Bastien, France* 145
Humidity Insensitive Strain-indicating Coatings with Increased Sensitivity (Aerosol Stresscoat), *J. S. Borucki, U.S.A.* 151
Measurement of Surface-residual Stress by Nondestructive Methods, *W. J. McGonagle* and *S. S. Yun, U.S.A.* 159
Ultrasonic Determination of High-order Elastic Constants in Elastically Deformed Metal Rods, *H. D. Tietz, Germany* 164
Application of the Laser-beam Technique in Mechanical Testing of High-temperature Materials, *D. R. Axelrad, Canada* 169

SESSION 7—MAGNETIC AND EDDY-CURRENT METHODS

Experiences and Results in the Application of Magnetography in Industry, *P. Muller, Germany* 174
Sur la détectabilité des défauts macroscopiques des matériaux conducteurs par des essais électriques, *N. Andreescu, E. Lăbuscă* and *S. Vasiliu, Romania* 188
The Mill Inspection of Steel Pipe at 2150°F, *M. M. Godshall, R. A. Nance* and *J. W. Allen, U.S.A.* 192
Computer Design of Eddy-current Tests, *C. V. Dodds* and *W. E. Deeds, U.S.A.* 199
Eddy-current Inspection of Rod During Hot Rolling, *A. Arnelo* and *A. Von Heijne, Sweden* 203
In-line Utilization of New Eddy-current Test Systems for the Crack Inspection of Semi-finished and Mass Produced Parts, *F. Förster, Germany* 209

SESSION 8—SURFACE METHODS AND NEUTRON RADIOGRAPHY

Removal Techniques in Penetrant Inspection Processes, their Development and Effect on Sensitivity, *R. E. Birley, N. H. Hyam* and *J. Tebbenham, U.S.A.* 222
Mechanisms Contributing to Fluorescence and Visibility of Penetrants, *B. Graham, U.S.A.* 225
Nondestructive Replica Methods for Surface Examination, *D. Scott* and *A. I. Smith, U.K.* 233
Improved Resolution Neutron Radiography, *B. L. Blanks, D. A. Garrett* and *R. A. Morris, U.S.A.* 242
Application of Neutron Radiography Using a Pool Reactor, *W. A. Carbiener, U.S.A.* 247
The Present Aspects of Neutron Radiography in Toshiba, *T. Inouye, S. Kawasaki, N. Wakabayashi,* and *K. Ogawa, Japan* 250

SESSION 9—STANDARDIZATION—GENERAL

Development of Radiographic Standards for Castings, *S. Goldspiel, U.S.A.* 256
The Development of Reference Radiographs for Steel Welds—Mil-Std-779, *R. M. Gustafson* and *E. L. Criscuolo, U.S.A.* 269
Nondestructive Testing Standardization in Great Britain, *C. C. Bates* and *C. Campkin, U.K.* 274
Correlation of Conductivity to Mechanical Properties of Age-Hardenable Aluminum Alloys Using Eddy-current Methods, *D. D. Seltzer, U.S.A.* 283
Contrôles non destructifs de gaines d'éléments combustibles prototypes de réacteurs à neutrons Rapides, *J. P. Dufayet, A. Samoel* and *B. Spriet, France* 291

SESSION 10—ULTRASONICS AT ELEVATED TEMPERATURES

Ultrasonic Testing of Solids at Elevated Temperatures, *L. C. Lynnworth* and *E. H. Carnevale, U.S.A.* 300
The Ultrasonic Testing of Hot Steel Products, *S. Sekino* and *Y. Sasaki, Japan* 307
A Continuous Ultrasonic Test Installation for Steel Strip with Automatic Recording of Data, *L. Brand, Germany* 310
Ultrasonic Evaluation of the Tensile Strength of Brittle Materials, *Z. Pawlowski, Poland* 314
Project Apollo—Automated Ultrasonic Bond-quality Inspection, *C. C. Kammerer, U.S.A.* 322

SESSION 11—APPLICATIONS

Nondestructive Detection of Contents, Radiation Leakage and Sources in Containers Packed for Transportation, *J. Domanus, Poland* 328
Progress in Nondestructive Testing in Aero Engine Manufacture, *I. L. F. Glover, U.S.A.* 335
Application of the Ultrasonic Testing Technique to the Quality Evaluation of Cast Iron Rolls, *S. Sasaki* and *K. Ono, Japan* 341
Composite Nondestructive Testing of Steel Castings: the Radiographic-Ultrasonic Method, *R. Rackwal, Poland* 344
Ultrasonic Nondestructive Inspection of Round Tubes and Bars by the Rotating Probe Method, *C. E. Hohl, U.S.A.* 347
Automated Quality Control of Electrical Steel in a Production Line, *J. A. Vdovin* and *A. J. Kadochnikov, U.S.S.R.* 352

SESSION 12—X-RAY TECHNIQUES

Radiography of Parts with Wide Variations in Thickness, *J. H. d'Adler-Racz, U.S.A.* and *M. Sevrin, Belgium* 358
Errors Due to the X-Ray Technique in Stress Measurement, *M. Iwamoto* and *H. Kikuchi, Japan* 361
L'Influence de la sensibilité spectrale des émulsions et de la composition spectrale des rayonnements ionisants dans la qualité des images radiographiques, *P. A. Ruault, France* 365
Relations Between Radiographic Image Quality and Film Density, *W. Bock, E. Mundry* and *D. Schnitger, Germany* 372
Layer-radiography with a Betatron, *Y. Ishii* and *A. Kanno, Japan* 378
Radiography Within the Energy Range 100 kV to 15 MeV with Orwocolor Films, *H. U. Richter* and *D. Linke, Germany* 383

CONFERENCE INTRODUCTORY

SESSION 13—RADIOGRAPHY

A Method for the Classification of Industrial X-Ray Film, *D. Polansky* and *E. L. Criscuolo, U.S.A.* 390
Evaluation of the Strength of Castings Based on Radiography, *Z. Godlewski, Poland* 393
Automation in Radiology, *R. Halmshaw, U.K.* 398
The Radiographic Evaluation of a Welded Structure Designed with Fatigue Strength, *H. Kihara* and *Y. Ishii, Japan* 403
Flaw Detection in Finned, Thin-walled Tubes, *V. V. Gorsky, V. T. Pronyakin, E. M. Lovyakin* and *V. M. Zakharov, U.S.S.R.* 410

SESSION 14—ULTRASONIC STANDARDIZATION

A Proven Method of Selection and Standardization of Ultrasonic Probes, *L. Niklas* and *H. Stoll, Germany* 414
Ultrasonic Evaluation of Mechanical Inhomogeneities of Materials, *L. Malecki, Poland* 419
Focused Ultrasonic Beams, *J. T. McElroy, U.S.A.* 422
Some Examples of Ultrasonic Testing in Swedish Industry, *J. Tiljander, G. Folkestad* and *S. Ingevald, Sweden* 428
Theory and Application of Ultrasonic Multiple Echoes in Specimens with Semi-permeable Interfaces, *E. Mundry, Germany* 435
Evaluation of Small Discontinuities in Non-metals with Microwaves, *D. W. Prine, U.S.A.* 441

SESSION A—TRAINING AND QUALIFICATION

Personnel Qualifications for NDT in the U.S.A., *H. Hovland, U.S.A.* 446
Training and Certification of NDT Personnel in the U.K., *B. R. Byrne* and *L. Mullins, U.K.* 448
Education and Qualification of NDT Personnel in Japan, *Y. Tada, Japan* 453
Certification of Radiographic Personnel in Canada, *W. E. Havercroft, Canada* 456

SESSION B—CORRELATION OF WELD DEFECTS

How Dangerous are Weld Defects? *R. Weck, U.K.* 460
The Detection and Identification of Weld Defects, *A. de Sterke, Netherlands* 467
Standards for the Acceptance of Weld Defects, *R. B. McCauley, U.S.A.* 472

REPORT SESSION 478

INTRODUCTION

The Fifth International Conference on Nondestructive Testing was held in the Mount Royal Hotel, Montreal, Canada, May 21 to 26, 1967 for the purpose of promoting international collaboration in all matters relating to the development and use of nondestructive test methods. Canada's invitation to host the Conference was approved by the Standing Committee for International Cooperation in the Field of Nondestructive Testing, now the International Committee for Nondestructive Testing, at the fourth meeting of the committee held in London, England, September 10, 1963.

The conference was sponsored by the Canadian Council for Nondestructive Technology Inc., who solicited aid from many organizations, and individuals. An Organizing Committee was formed and given the responsibility of preparing and conducting the conference within the terms of reference established by the International Committee for Nondestructive Testing.

Members of the International Committee and the recognized nondestructive testing societies in the member countries publicized the conference and promoted interest among members. Several countries established committees for the purpose of reviewing and screening technical papers prior to their submission for presentation at the Conference.

The languages of the conference were English and French and facilities for simultaneous translation were provided at all sessions. In addition to the technical sessions there were two principal sessions where invited papers were presented and discussed.

The conference was attended by 736 delegates from 23 countries. From more than 150 papers submitted 82 were selected for presentation by authors from 14 different countries. All session meetings and social activities were held in the Mount Royal Hotel, in which most of the conference delegates were housed.

Activities related to the Conference included a program for the ladies in which more than 80 participated, local plant visits, a post conference tour of southern Ontario, a banquet and other social events.

The International Committee for Nondestructive Testing held two meetings at which requests for committee membership were approved and a revised form of the committee's Terms of Reference were adopted. The Committee accepted an invitation from Germany to host the Sixth International Conference on Nondestructive Testing in May 1970.

The Canadian Welding Society and the Canadian Council of the American Society for Metals held regional meetings in Montreal in conjunction with the Fifth International Conference on Nondestructive Testing.

The Canadian Welding Society held its Sixth National Conference in the Laurentian Hotel. Technical papers presented at the three-day conference featured the special applications of welding, fabrication and design used in turbo trains, hydrofoil vessels, turbines, bridge and building construction, locomotives etc. The papers dealt with many of the new welding processes.

The Canadian Council of the American Society for Metals sponsored a Regional Conference on Metal Processing, a two-day conference held in the hotel Chateau Champlain. The technical papers presented were concerned with solidification and coasting, drawing and forming, metal cutting, heat treating and finishing.

The Canadian Welding Society and the American Society for Metals sponsored an International Exposition for Metals, Testing, Welding and Fabricating at the Show Mart Building. This exposition, which included one of the largest displays of nondestructive testing equipment ever shown, was attended by more than 6,000 visitors.

Several thousand visitors from around the world, interested in the production, fabrication and testing of metals gathered in Montreal as a result of the Exposition and the combination of Society Conferences.

The success of the Fifth International Conference on Nondestructive Testing was due in large measure to the interest displayed by the societies, government agencies, industry and organizations and individuals who participated.

To all of them is due a sincere vote of thanks.

International Exposition for Metals, Testing, Welding and Fabricating

An International Exposition sponsored by the Canadian Welding Society and the American Society for Metals was held in the Show Mart, Montreal, May 22-25. More than 100 companies and their affiliates from Canada, United States, Europe and Asia presented exhibits, covering operations on the production, selection and use of metals, equipment and methods for nondestructive testing, physical testing, welding, brazing and all types of metal fabrication machines.

The display of NDT equipment and scientific equipment was provided by the following companies:

Automation Industries Inc., Sperry Products Division
Balteau Electric Corporation
Bausch & Lomb Inc.
L. E. Baxter Limited
Branson Instruments, Inc.
The Budd Company, Instruments Division
Canadian Eastman-Kodak
Carveth Metallurgical Ltd.
W. E. Carveth Ltd.
Central Scientific Company
Electro-Physical Instruments Ltd.
Geoscience Instruments Ltd.
Instrom Canada Ltd.
Isotopin–Laboratorium
Karl Deutsch Germany
Krautkramer Ultrasonics Inc.
Drs. J & H Krautkramer
M.T.S. Systems Corporation
Magnaflux Corporation
Magnetic Analysis Corporation
Mohr and Federhalf A.G.
Philips Electronic Instruments & C. H. F. Muller
Photo Import Agencies—Gevaert Films
Picker X-Ray Corporation—Holger Andreason
Polaroid Corporation of Canada Ltd.
Rich. Seifert and Company
Spectra Research Ltd.
Wilhelm Tiede
Toshiba, Tokyo Shibaura Electric Company Limited
Technical Marketing Services
Vickers Instruments
Welsh Scientific Co.

Some 80 other exhibitors displayed metals, welding and shop fabrication equipment.

Supporting Companies

H. G. Acres & Co. Ltd.
Algoma Steel Corporation Ltd.
Anaconda American Brass Ltd.
Associated Inspection Services
Atomic Energy of Canada

Babcock Wilcox & Goldie-McCullogh
L. E. Baxter Limited
B & W Heat Treating Ltd.
Branson Instruments Ltd.
Bristol Aerospace Limited
Budd Instruments Ltd.

Canadair Ltd.
Canadian Council A.S.M.
Canadian General Electric Co. Ltd.
Canadian Iron Foundries Ltd.
Canadian Kodak Company Ltd.
Canada Machinery Corporation
Canadian National Railways
Canadian Oxygen (1963) Ltd.
Canadian Pacific Railway
Canadian Steel Foundries

Catalytic Construction of Canada Ltd.
Canadian Welding Bureau
Canadian Welding Society
Canadian Westinghouse Company Ltd.

De Havilland Aircraft of Canada Ltd.
Dominion Bridge Company Ltd.
Dominion Foundries and Steel Ltd.
Dominion Steel & Coal Corporation
J. & H Krautkramer

Electro Physical Instruments Ltd.

Fahralloy Canada Ltd.
Ferrania Photo Sales Ltd.
Ferranti Packard Ltd.
Frankel Structural Steel Ltd.

Horton Steel Works Ltd.
Phillip A. Hunt Co. (Canada) Ltd.

Imperial Oil Ltd.
Independent Inspection Service
Industrial Nondestructive Testing Ltd.

Lake Ontario Steel Company

National Steel Car Corporation
North American Inspection Services
Northern Electric Co. Ltd.

Ontario Chapter Society for N.D.T.
Orenda Ltd.

Philips Electronic Industries Ltd.
Picker X-Ray Engineering Ltd.
Procor Limited

Renfrew Aircraft & Engineering Co. Ltd.
Rich-Seifert (J. Roch)

Steel Company of Canada

Toronto Iron Works Ltd.

Union Carbide Canada Ltd.
United Aircraft of Canada Ltd.
United Electrical X-Ray Company Ltd.

Visu-Ray Limited

Warnock-Hersey Company Ltd.
Williams and Wilson
Wilhelm Tiede

X-Ray and Radium Ltd.

The Government of the United States of America
—The Naval Air Systems Command
—The Office of Naval Research

Many companies, both Canadian and foreign, provided assistance to the conference. Their contributions were essential to the organization of a conference of this scope, and were wholeheartedly appreciated by all registrants.

The Organizing Committee of the 5th ICNDT wishes to sincerely thank the following organizations for their distinct and invaluable contribution to the organization of this conference;

The Society for Nondestructive Testing Inc.
The Standing Committee for International Co-operation within the Field of Nondestructive Testing
The Department of Industry, Government of Canada
The Department of Trade and Commerce, Government of Canada
The Department of Energy, Mines and Resources, Government of Canada
The Montreal Convention Bureau.

Social Activities

The official delegates from the participating countries and members of the International Committee for Nondestructive Testing were welcomed at a reception held on Sunday, May 21, at "The Expo '67 Club" on the Expo site.

The official banquet on Thursday, May 25, was the highlight of the many receptions held during the Conference. More than 500 guests of the Canadian Council for Nondestructive Technology, the Canadian Welding Society, the American Society for Metals and of the International Exposition for Metals, Testing, Welding and Fabricating, were in attendance. Professor J. Gordon Parr, Dean of Engineering, University of Windsor, Windsor, Ontario, as an excellent Master of Ceremonies, maintained the spirit of international friendship expressed by the delegates and guests. Dancing and entertainment followed the banquet.

Ladies' Program

More than 80 ladies who had accompanied delegates to the meetings of the three participating Societies took part in a program of visits and social activities arranged by the Conference Ladies Reception Committee. A hospitality room provided a meeting place to obtain information and to get acquainted. Visitors enjoyed a bus tour of greater Montreal, attended a fashion show, visited the Planetarium and a large modern shopping centre. Luncheons were arranged and time provided for a day at Expo '67.

Post-Conference Tour
May 28-June 3, 1967

The post conference tour was attended by 23 delegates from the United Kingdom, the U.S.S.R. and the U.S.A. The tour began in Montreal on Sunday, May 28, and terminated in Toronto on June 3. The delegates visited industrial plants, government laboratories and a university and were entertained at several social gatherings. The itinerary was as follows:

Monday, May 29, Ottawa
The National Research Council Radiological and Mechanical Laboratories and the Parliament Buildings of Canada. A City tour.

Tuesday, May 30, Kingston
The Aluminium Research Laboratories and the Aluminum Company of Canada. A tour of Fort Henry.

Wednesday, May 31
Travel to Toronto with a visit to Edwards Botanical Gardens.

Thursday, June 1, Toronto
Sheridan Park Research Complex with visits to the British American Oil Company Research Centre and laboratories of the Atomic Energy of Canada. The Steel Company of Canada new Research Laboratory.

Friday, June 2, Hamilton
Dominion Foundries and Steel Ltd. The Engineering Buildings and Nuclear Reactor of McMaster University.

Saturday, June 3, Niagara Falls
The delegates were given the opportunity of seeing the scenic beauty of Niagara Falls and the nearby points of interest.

Plant Visits

An organized tour was arranged to Air Canada Ltd., Airline Maintenance Base, Dorval, Que. In the modern nondestructive testing laboratory the latest equipment and test methods used in the aircraft industry were seen by the delegates.

Individual plant visits to other organizations were arranged at the request of the delegates.

OPENING SESSION

Welcoming addresses were given by W. E. Havercroft, General Chairman; V. G. Behal, General Co-Chairman and by L. Hanigan, City Councillor on behalf of His Worship the Mayor of Montreal.

The keynote address was delivered by Dr. John Convey, Director, Mines Branch, Department of Energy, Mines and Resources, Ottawa.

Welcoming Addresses

W. E. Havercroft, General Chairman

On behalf of the Organizing Committee of the Canadian Council for Nondestructive Technology it is my privilege to welcome you to the Fifth International Conference on Nondestructive Testing.

It is very gratifying to know that so many distinguished visitors from Canada and from many parts of the world are gathering here this week to share information in the rapidly expanding field of nondestructive testing.

Previous successful conferences held in Brussels, Belgium; Chicago, U.S.A.; Tokyo, Japan; and London, England, taught us to have confidence in each other and in our profession. It is this confidence, which I hope will be fostered this week, that has made possible this Fifth International Conference on Nondestructive Testing.

You will have the opportunity to share information and record the progress of nondestructive testing as it is presented by authors of 82 technical papers from 13 different countries.

You will also have the opportunity to renew old friendships and to create new international friendships among the many people you will meet.

We hope our visitors from abroad will get to know their Canadian hosts and will help Canada celebrate her 100th birthday.

Some of you will have an opportunity to see other parts of Canada, to visit EXPO'67. We hope you retain fond memories of Canada and of the Fifth International Conference on Nondestructive Testing.

With the hope that the international cooperation and friendship established at the previous conferences will be maintained and continued at future conferences I have the honour to officially open the Fifth International Conference on Nondestructive Testing.

V. G. Behal, General Co-Chairman

As Chairman of the Organizing Committee of the Fifth International Conference on Nondestructive Testing, it is my pleasure and great privilege, to welcome you to participate in the conference and acquaint you with some of the other activities we have arranged for, or co-sponsored, for your added enjoyment and benefit.

Firstly, about 82 technical papers will be presented here, at the Mount Royal Hotel, the headquarters of the Conference, by representatives of 13 nations to visitors from 24 countries. Our pre-registration and current registration figures indicate that a total attendance at this conference will exceed 700 visitors.

The First Eastern Canadian Regional Conference of the American Society for Metals, organized by representatives of eight of the fourteen Canadian Chapters, with headquarters at the Chateau Champlain, will present 14 papers on Modern Metal Processing, during their two-day conference, held May 24th and 25th.

The Sixth National Convention of the Canadian Welding Society will be held on May 23rd, 24th and 25th, with 36 papers being given at the Convention Headquarters, the Laurentian Hotel.

The Canadian Welding Society, together with the American Society for Metals, headquarters at Metals Park, have organized and will operate an International Exposition for Metals, Testing, Welding and Fabricating, sponsored by all the participating societies, and this show, held at the Show Mart, covers 75,000 square feet of space, containing what is believed to be the largest exhibition of nondestructive testing equipment ever assembled under one roof, with the balance representing metals and materials industries. The Exposition will be open daily throughout the week of our conference, until Thursday night, while our conference continues throughout Friday.

The Organizing Committee of the Conference has planned a comprehensive ladies program and ladies of the other participating societies are welcome to join this group, as provisions have been made, based upon pre-registration, to accommodate all who wish to participate.

Conversely, registrants to the NDT Conference are cordially invited to attend any of the ASM or CWS lectures they might be interested in, and we urge all delegates to visit the Metals Exposition; all these activities are free to conference registrants.

The ASM group expect an attendance of 300, while the CWS will have as many as 500 registrants.

There have been four successful conferences held prior to this one, but when again will you be able to gather for such an occasion in a country celebrating the centennial of its Confederation, in a large, cosmopolitan centre such as Montreal, a city combining the new-world efficiency with an old-world charm, and during Expo '67, or its equivalent?

You may note that we shall have simultaneous sessions, served by bilingual translation, further adding to the truly international flavour of our gatherings.

The simultaneous sessions were necessary to provide and cover all of the material thought to be required for a group of this calibre, gathered here from around the globe.

As stated before, we were fortunate in being able to arrange our conference during Expo '67, the first Class I International Exposition ever held on this continent, and while this has created some problems, for which under the circumstances we feel that you will forgive us, it was well worth it, as we are certain that you will find this event unforgettable, and the highlight of this week's nontechnical activities.

Anyone wishing to join in the post-conference tour or any of the several tours arranged for plants in Montreal, is asked to please contact the registration desk.

On Sunday, May 28, the now reinstated post-conference tour departs from Montreal for Ottawa, and the following week will be spent travelling by bus through Kingston, Upper Canada Village, Toronto, Sheridan Park, Hamilton, to Niagara Falls, with visits to research establishments, industrial concerns, and also points of interest for scenic beauty along the way. The tour will spend Saturday, June 2, at Niagara Falls, and participants will be returning to Montreal that night.

Receptions along the way have also been provided for and we do hope that each one of you will enjoy his visit to Canada, and during your stay you will meet some of the people, too numerous to introduce, but whose great efforts over an extended period have made our plans a reality, and who I wish to thank publicly for their magnificent support.

I hope you will find your visit here both enjoyable and profitable and that we shall have the opportunity to meet with each one of you personally, throughout the week, to either renew old acquaintances or make new ones, to help develop the spirit of international co-operation and understanding, so badly needed in the world today.

Keynote Address

Dr. John Convey, Director, Mines Branch

The response shown by this gathering to an international conference on nondestructive testing is indicative of the rapid progress and expansion that is occurring in this area of technology.

The rate of increased knowledge and of the scientific achievements of today demands a more rapid exchange of information between nations and individuals than ever before. The advanced communications of today by means of satellites etc. merely paves the way for a personal contact between individuals and for distinguished scientists, engineers, educators etc. to gather together at international conferences such as this. The exchange of scientific information on an international level is essential to maintain progress in any scientific field and to provide an attitude of trust between nations.

Although we are blessed with an abundance of minerals and elements which can be extracted from our environment and made to serve us in many ways, our supply of raw materials is not inexhaustible. We already feel the shortage of these materials in numerous ways and must seriously begin to consider the wastage of time and materials.

Nondestructive testing, although a relatively new part of our technology, is playing an important role in this endeavour. With it we have a means of assuring the serviceability of a single part whose failure can lead to the loss of a structure that wastes expensive and critical materials and thousands of man hours of labour. Or we can use it to assure the reliability of thousands of commonplace articles of everyday life in which we must soon expect built-in quality and a reasonable life, rather than built-in obsolescence.

Much waste could be avoided if more thought were given at the time of design of a component as to how its quality can be determined. Many times inspection costs could be appreciably reduced if this had been done. Perhaps the day will come when the quality-control expert will be a part of the design team.

Material savings are quite evident where quality control is maintained at each step of the fabricating process. More and more quality control through nondestructive testing is being integrated into assembly operations as an integral part of the production cycle and more and more use is made of the automatic feed back of computerized data to prevent the occurrence of anomalies during the process.

Management's responsibility to operate at a profit demands proper quality control. Quality control, and in particular some nondestructive testing personnel, are making decisions whose value in dollars to an organization may be equal or higher than decisions made by top management. It is management's responsibility to encourage these people to keep abreast of new developments in their field. One manner of doing this is by participation in meetings such as this.

The extensive research and development occurring in the field of nondestructive testing will be exemplified this week. We are more demanding of the properties of many of our materials than we were in the past, and of course we have much to learn of the properties of newer materials. In space technology and nuclear activities, for example, we are demanding nondestructive tests capable of finding discontinuities, fluctuations etc. that were relatively unimportant a short time ago. We now concern ourselves with a misplaced atom and its effect upon the properties and serviceability of the part. We expect materials to withstand higher stresses under greater extremes of temperature and in extremely difficult environments.

At the other end of the scale we must be more and more concerned with the safety of the individual and of entire populations in an area. In daily life we are becoming encircled with more and greater hazards such as the transportation or storage of gases and chemicals which could wipe out an entire town or city.

The importance of nondestructive testing in this area should not be ignored.

During this week you will learn of the development of many new and fascinating nondestructive testing methods. For example, you will learn of recent developments in the electronic imaging of X-rays which provide instantaneous information on the structure of materials. As mentioned earlier, you will find this method, in common with so many other test methods, has applications in the automatic in-line process control of materials.

In the field of ultrasonics we now have television ultrasonic imaging systems to provide information comparable to the fluoroscopic and radiographic test methods.

The use of heat as the probing medium for nondestructive tests is also expanding. Thermal sensitive phosphors and paints are being used as indicating coatings to show unbonded areas on such things as honeycomb panels. Thermal and infrared nondestructive test techniques appear to have a great future in aerospace applications. It has been suggested that structures or machines subject to heating during service may have built-in sensing and alarm systems which will indicate overloading, deterioration of the part or even the initiation of discontinuities.

There has been definite progress in recent years, especially in Europe, in the development and application of electromagnetic methods of nondestructive testing. There have been several advances in the production of eddy-current and magnetic analysis test systems adaptable to in-service plant inspection.

The use of neutron radiography and microwaves, newcomers to the family of nondestructive tests has already shown promise as a probing medium for use in areas where present test methods are inadequate.

The ultimate value of all these commonplace and exotic test methods depends upon the integrity of the equipment used and the skill and knowledge of the operators. The increased use of computerized systems, with automatic read-out of information is dependent upon the equipment and its operator. With the development of miniaturized NDT equipment it is most important that the training and education of nondestructive testing personnel be not neglected. It is to be hoped that the information absorbed during this week by the highly qualified people attending this conference will be passed on for the benefit of those who cannot obtain it at first hand.

CANADIAN COUNCIL FOR NONDESTRUCTIVE TECHNOLOGY INC.

HAVERCROFT, W. E., President, Dept. of Energy, Mines and Resources, Ottawa.

BEHAL, V. G., Vice-President, Dominion Foundries and Steel Ltd., Hamilton, Ont.

DALY, M. O., Secretary, Hawker Siddeley Canada Ltd., Canadian Steel Foundries Div., Montreal, Que.

GILL, E. A., Treasurer, Canadian General Electric Co. Ltd., Toronto, Ont.

BAXTER, L. E., Director, L. E. Baxter Ltd., Montreal, Que.

VEZINA, G. E., Director, Canadian National Railways, Montreal, Que.

MICHAUD, R., Director, Electro Physical Instruments Ltd., Montreal 29, Que.

BARER, R. D., Director, Pacific Naval Laboratories, Esquimalt, B.C.

VAN DEN ANDEL, J., Director, Canadian Westinghouse Ltd., Hamilton, Ont.

BOWE, E., Director, Warnock-Hersey Co. Ltd., Montreal, Que.

Conference Executive

HAVERCROFT, W. E., General Chairman, Dept. of Energy, Mines and Resources, Ottawa.

BEHAL, V. G., General Co-Chairman, Chairman Organizing Committee, Dominion Foundries and Steel Ltd., Hamilton, Ont.

BAXTER, L. E., Co-Chairman Organizing Committee, Chairman Arrangements, L. E. Baxter Ltd., Montreal, Que.

GILL, E. A., Chairman Finance, Canadian General Electric Co. Ltd., Toronto, Ont.

MICHAUD, R., Secretary Organizing Committee, Electro Physical Instruments Ltd., Montreal 29, Que.

DALY, M. O., Chairman Publicity, Hawker Siddeley Canada Ltd., Canadian Steel Foundries Div., Montreal, Que.

BENSON, J. E., Chairman Technical Papers, Canadian General Electric Co. Ltd., Peterborough, Ont.

VEZINA, G. E., Co-Chairman Arrangements, Canadian National Railways, Montreal, Que.

HERRING, R. D., Co-Chairman Arrangements, Williams & Wilson Ltd., Montreal, Que.

TARDIF, H. P., Co-Chairman Technical Papers, Canadian Armament Research and Development Establishment, Quebec, Que.

BIRD, J. A., Co-Chairman Finance, The Steel Co. of Canada Ltd., Hamilton, Ont.

PALMER, J. D., Co-Chairman Publicity, Ontario Research Foundation, Toronto, Ont.

Ladies' Committee

MICHAUD, MRS. R., Chairman.

DALY, MRS. M., Co-Chairman.

CAIE, MRS. J. W., Secretary.

MEMBERS OF INTERNATIONAL COMMITTEE FOR NONDESTRUCTIVE TESTING

Australia. Mr. G. J. Timbs, Hon. Secretary, Non-Destructive Testing Association of Australia, N.S.W. Branch, Science House, 157 Gloucester St., Sydney, Australia.

Austria. Dr. E. Krainer, Eisenhutte Osterreich, Leoben, Montau Hochschule, Austria.

Belgium. Prof. Dr. G. A. Homès, 118 rue Gabrielle Brussels 18, Belgium.

Burma. Mr. H. H. Law Yone, Research Officer, Union of Burma Applied Research Institute, Pagoda-Kanbe Roads, Rangoon, Burma.

Canada. Mr. W. E. Havercroft, Dept. of Energy, Mines and Resources, 568 Booth St., Ottawa, Canada.

Czechoslovakia. Ing. L. Cizek CSC., Czechoslovak Scientific and Technical Society, Praha 1, Siroka 5, Czechoslovakia.

Denmark. Mr. H. Vinter, 345 Park Allé, Copenhagen, Glostrup, Denmark.

Finland. Dr. J. Salokangas, The State Institute for Technical Research, Lonnrotinkatu 37, Helsinki, Finland.

France. Prof. Dr. P. G. Bastien, 15 rue Pasquier Paris 8°, France.

Germany. Dr. R. H. Seifert, Boganstrasse 41, 207 Ahrensburg, Germany.

Great Britain. Dr. L. Mullins, Research Laboratories Kodak Ltd., Harrow, Middlesex, England.

Italy. Dr. F. Baldi, Centro Sperimentale, Metallurgica S.P.A., Rome, Italy.

Japan. Prof. Dr. H. Kihara, 483 Numabukuro, Nakano-ku, Tokyo, Japan.

Netherlands. Mr. A. de Sterke, Chief Research Engineer, Röntgen Technische Dienst N.V., Delftweg 144, Rotterdam 8, Netherlands.

Norway. Mr. J. C. Walter, Director, Rontgenkontrollen, Forsknings-veien 1, Oslo, Norway.

Poland. Prof. Dr. I. Malecki, Nowowiejska 22 m. 12, Warsaw, Poland.

Spain. Prof. Dr. M. de Miro, Instituto de la Soldadura, Director, Departamento Asistencia Technica Y Ensenanza, Serrano 144-A Madrid, Spain.

Sweden. Mr. H. Swedenborg, Tekniska Rontgencentralen AB, Huvud-kontoret 1, Stockholm 50, Sweden.

Switzerland. Mr. R. Hornung, c/o Gebr. Sulzer AG., Abt. 15133, Winterthur, Switzerland.

South Africa. Mr. P. Scribante, South African Bureau of Standards, Private Bag 191, Pretoria, South Africa.

United States of America. Dr. G. H. Tenney, Society for Non-destructive Testing Inc., 704 Forty-Seventh St., Los Alamos, New Mexico, 87511, U.S.A.

Union of Soviet Socialist Republics. Prof. Dr. P. K. Oshchepkov, States Committee of Devices and Automatisation, Ogarev St. 5, Moscow, K-9, U.S.S.R.

INTERNATIONAL COMMITTEE FOR NONDESTRUCTIVE TESTING

(formerly The Standing Committee for International Co-operation within the Field of Nondestructive Testing)

Minutes of the
FIFTH MEETING
of the International Committee, held on Sunday, 21st May, 1967
at 2:00 p.m. at the Mount Royal Hotel, Montreal, Canada.

The following were present:

Mr. W. E. Havercroft (Chairman)	Canada
Mr. R. D. Barer (Vice-Chairman)	Canada
Mr. E. T. Watterud (Secretary)	Canada
Prof. Dr. G. Homès	Belgium
Dr. R. H. Seifert	Germany
Mr. C. C. Bates	Great Britain
Mr. W. C. Heselwood	Great Britain
Dr. F. Baldi	Italy
Prof. Dr. H. Kihara	Japan
Mr. A. de Sterke	Netherlands
Prof. Dr. I. Malecki	Poland
Dr. Z. Pawlowski	Poland
Mr. P. Scribante	South Africa
Mr. H. Swedenborg	Sweden
Mr. R. B. Socky	U.S.A.
Dr. G. H. Tenney	U.S.A.

1. *Apologies for Absence*

The Chairman reported that apologies for absence from the meeting had been received from Dr. E. Krainer (Austria), who had nominated Dr. Seifert to represent him; H. Vinter (Denmark), Dr. J. Salokongas (Finland), Dr. M. de Miro (Spain) and R. Hornung (Switzerland). Prof. Moravia had been prevented by illness from attending and had asked that Dr. Baldi act in his place. The Committee endorsed a suggestion by Dr. Tenney that a note of regret at Prof. Moravia's absence and wishes for his recovery be signed by all members in attendance, and forwarded to him.

The meeting expressed sincere regret at the announcement by the Chairman of the recent death of Mr. Pemberton of Great Britain. Mr. Pemberton was President of the Fourth Conference in London.

2. *Minutes of Previous Meeting*

The Minutes of the two meetings of the Committee held on 10 September and 13 September in London, were adopted.

3. *Terms of Reference*

The Chairman reported that a Working Group composed of himself, Dr. Tenney, Dr. Seifert, Prof. Malecki and Dr. Mullins had developed Draft No. 4 of the Terms of Reference for the Committee, based on Draft No. 3 that was adopted at the London Conference. Copies of Draft No. 4 had been submitted to the Committee for comment in July 1966, with the result that official approval had been expressed by seven member countries and no indication of disapproval had been received.

At the suggestion of Dr. Tenney the draft was given a general review. This resulted in agreement on a change in the title of Clause 3 from "Object" to "Objectives" and a corresponding change in Clause 3.1. Dr. Tenney suggested standardization of the spelling of the term "nondestructive". After some discussion the Committee agreed, on a motion by Dr. Tenney, seconded by Prof. Malecki, to accept the one-word spelling of the term. This decision would be reflected in appropriate changes throughout the draft.

Mr. Bates recommended that, since the draft had been provided to all members some months earlier, giving them ample time for consideration, its adoption should be resolved at this meeting. This was agreed and, on a motion by Mr. Bates, seconded by Mr. de Sterke, Draft No. 4 was adopted, subject to the editorial changes recorded above.

Dr. Tenney expressed the congratulations of the Committee to the Chairman for his leadership in pushing development of the Terms of Reference through to successful completion.

4. *Venue for Sixth Conference*

The Chairman read a letter from Dr. Seifert confirming the offer made at the London Conference that Germany would be pleased to host the Sixth Conference in 1970. Dr. Seifert supported his written invitation with a verbal statement pointing out that 1970 is an appropriate year in that it will be the 75th Anniversary of Roentgen's discovery of X-rays. He indicated that the Conference would be planned for May, probably in Berlin.

Dr. Seifert's invitation was greeted with favour and enthusiasm. Prof. Malecki noted the possibility of difficulties, from a political point of view, in arranging for entry of delegates from some countries into West Berlin.

Dr. Seifert stated that this possibility had been recognized, but expressed the hope that the choice of Berlin would pose no problem politically, since the city had much to commend it as the site for a nondestructive testing conference. It was agreed that the final choice of the site in Germany must be left to the discretion of Dr. Seifert and his colleagues according to the circumstances encountered at the time. The Committee agreed unanimously on a motion by Mr. Barer, seconded by Dr. Tenney, that the next conference be held in Germany in 1970.

5. *Invitation for Seventh Conference*

The Chairman recalled that tentative invitations had been advanced by both Poland and France for future conferences. Prof. Malecki confirmed Poland's willingness to host a conference in 1973, but suggested that the matter be discussed at the meeting on Thursday when, it was hoped, Prof. Azou of France would be present.

6. *Membership Changes*

The Chairman noted two changes in membership of the Committee since the London meetings. Mr. P. Scribante had replaced Mr. A. Middlecote as the representative of South Africa, and Mr. J. C. Walter was the new member from Norway, replacing Mr. A. Markestad.

The Chairman reported also that interest has been expressed in committee membership by Argentine, Australia, Czechoslovakia and Hungary. A tentative request in writing from Australia would be raised for consideration on Thursday.

Dr. Tenney reported that Yugoslavia also has indicated an interest in joining the Committee. He thought that a formal request could be expected from that country shortly.

The meeting agreed with Dr. Seifert and Dr. Tenney that additions to the Committee membership should be encouraged, and promised a favourable reception to all membership requests that fulfil the conditions outlined in the Terms of Reference.

7. *Information Dissemination*

The Chairman invited general discussion on proposals advanced at various times in the past for particular activities that might be pursued by the Committee. Included amongst these were such items as the establishment of specific work projects, development of a multilingual glossary of Ndt terms, and exchange of information amongst member countries. He noted that the circulation of yearly progress reports from member countries, as recommended at the London meetings, had not been effectively carried forward.

Mr. Bates reported on the formation of the Research Centre, set up in the United Kingdom, which would include an information and documentation service on nondestructive testing, and proposed that this might be used by members of the International Committee as a facility for exchange of information.

Dr. Seifert thought that member countries should participate more actively in the exchange and circulation of reports on nondestructive testing. He promised to call for such reports from members on a regular basis during the period leading to the next conference.

Dr. Tenney agreed that dissemination of the rapidly growing body of knowledge in nondestructive testing is most desirable. He recommended the distribution to all member countries of the journals of national societies as one means of furthering circulation of information.

Prof. Malecki referred to the program being pursued by UNESCO on the problem of information dissemination. He recommended that the International Committee keep in touch with this activity.

Prof. Homès pointed out the problem created by the tremendous amount of data and information that is being developed. He stressed the importance of being selective in the quality and kind of information distributed.

Mr. de Sterke stated that the International Institute of Welding has undertaken to establish liaison with the organizers of future conferences on nondestructive testing, and noted that this would have the effect of bringing all pertinent IIW documentation to the attention of Committee members.

In closing the discussion on the topic of information distribution, the Chairman expressed the hope that the opinions and ideas advanced would prove useful to Dr. Seifert and his colleagues in their plans and preparations for the Sixth Conference.

8. *New Business*

The Chairman invited discussion on a proposal that had been submitted to each of the members by Mr. L. E. Baxter concerning his establishment of an information distribution and international secretariat service. The Chairman noted that this proposal was an independent and personal effort on the part of Mr. Baxter, who felt that this service would prove beneficial to member countries in providing for the dissemination of information from a central agency.

Prof. Homès, Mr. Bates, Mr. de Sterke and Prof. Malecki, in turn, stated general opposition to the principle and philosophy of Mr. Baxter's proposal. The Committee concurred with these views and, though expressing appreciation of Mr. Baxter's proposal, agreed that formation of an international secretariat was not desirable at this time. The Chairman undertook to notify Mr. Baxter of the Committee's reaction.

The meeting adjourned at 4:30 p.m., to reconvene on Thursday, 25 May.

INTERNATIONAL COMMITTEE FOR NONDESTRUCTIVE TESTING

Minutes of the
SIXTH MEETING
of the International Committee held on Thursday, 25th May, 1967
at 2:00 p.m. at the Mount Royal Hotel, Montreal, Canada

The following were present:

Mr. W. E. Havercroft (Chairman)	Canada
Mr. R. D. Barer (Vice-Chairman)	Canada
Mr. E. T. Watterud (Secretary)	Canada
Prof. Dr. G. Homès	Belgium
Dr. M. Baimler	Czechoslovakia
Ing. L. Cizek	Czechoslovakia
Prof. P. Y. Azou	France
Dr. R. H. Seifert	Germany
Mr. C. C. Bates	Great Britain
Mr. W. C. Heselwood	Great Britain
Dr. F. Baldi	Italy
Prof. Dr. H. Kihara	Japan
Mr. A. de Sterke	Netherlands
Prof. Dr. I. Malecki	Poland
Dr. Z. Pawlowski	Poland
Mr. P. Scribante	South Africa
Mr. H. Swedenborg	Sweden
Dr. Y. Badlevski	U.S.S.R.
Prof. Dr. P. K. Oshchepkov	U.S.S.R.
Mr. R. B. Socky	U.S.A.
Dr. G. H. Tenney	U.S.A.

1. *Minutes of Previous Meeting*

It was agreed that the Committee name shown as the heading for the Minutes of the meeting held on 21 May should be changed to reflect the form accepted in the Terms of Reference.

Mr. Bates asked that the second paragraph of Item 7 be altered to read as follows:

> "Mr. Bates reported on the formation of the Research Centre, set up in the United Kingdom, which would include an information and documentation service on nondestructive testing, and proposed that this might be used by members of the International Committee as a facility for exchange of information."

The meeting agreed on a motion by Mr. Barer, seconded by Mr. Bates, that the minutes, amended as indicated above, be adopted. The corrected version would be distributed to the members by mail.

2. *Business Arising out of the Minutes*

Prof. Azou reported, in connection with Item 5 of the minutes, that he had discussed the question of venue for the Seventh Conference with Prof. Malecki, and expressed his support of the proposal that Poland host the conference.

3. *Committee Membership*

The Chairman tabled a letter from Czechoslovakia requesting membership on the International Committee. Statements of support for this request were made by Prof. Oshchepkov, Dr. Tenney, Prof. Malecki and Dr. Seifert, and these were enthusiastically endorsed by the other members. The result of this was a motion by Prof. Oshchepkov, seconded by Dr. Tenney and carried unanimously to welcome Czechoslovakia as a full member of the Committee. At this point the two Czechoslovakian delegates, Ing. L. Cizek and Dr. M. Baimler joined the meeting, with Dr. Cizek expressing appreciation on behalf of Czechoslovakia for acceptance of their membership application.

The Chairman reported that a considerable interest has been expressed on the part of Australia in obtaining membership on the Committee although no official request has yet been made. Dr. Tenney suggested that the Australian membership interest be followed up by a letter from the Chairman with the suggestion that their official request for membership be submitted to Dr. Seifert who will be the next Chairman and who would handle the membership application by a postal ballot.

(Note: Subsequent to the meeting it was learned that an official Australian request for membership had arrived. It has been decided therefore that Mr. Havercroft would submit the application to postal ballot, with completed ballots to be returned to Dr. Seifert.)

4. *Comments on Fifth International Conference*

In inviting frank comments and opinions of the members on any and all aspects of the Fifth International Conference, the Chairman reported that the post conference tour, originally cancelled on account of the marginal interest displayed prior to the conference, had now been rescheduled in view of somewhat increased interest discovered since the conference had opened. He made the observation that the unexpectedly large number of delegates had resulted in the shortage of some conference items such as portfolios and certain items of literature, and had posed as well certain registration problems and inconvenience for some delegates.

Prof. Homès noted that at least one of the sessions had encountered some difficulty in that questions to the session panelists, written in French, had gone unanswered, presumably because of translation difficulties. He suggested that at least one bilingual or multilingual person should be included among the administrators of each session to avoid this kind of difficulty in future conferences. He stressed also the importance of maintaining a close liaison arrangement between session chairmen, slide projector operators and the audience.

Dr. Tenney emphasized the desirability of having preprints of all papers made available to delegates prior to the conference. He

suggested also, for future conferences, that the Terms of Reference of the International Committee should be provided to all delegates upon their registration.

Mr. Bates strongly supported Dr. Tenney's suggestion for paper preprints. He noted that some delegates had failed to obtain a copy of the conference program in advance of the conference, prior to their departure from home. He observed also that the holding of simultaneous sessions proved inconvenient in some instances, when delegates found themselves faced with the problems of having separate papers of equal interest to them being presented at the same time.

Prof. Oshchepkov expressed the wish that technical sessions could be translated into more than one language.

Mr. de Sterke, in commenting on the suggestion concerning preprints, stated that success was achieved at a technical conference held in Warsaw in the technique of providing rather full summaries of technical papers in place of complete preprints. He expressed appreciation of the arrangements for the Fifth Conference that permitted a majority of delegates to be housed in the same hotel as the venue of the conference itself. He recommended this arrangement for future conferences wherever possible.

Prof. Malecki expressed his recognition of difficulties faced by a conference committee in selecting technical papers from the variety offered from the different countries concerned. He recommended the technique of having the National Committees in each of the countries provide assistance and recommendations on the choice of papers from their countries. He urged also that care be taken in the arrangement of session time-tables to avoid the simultaneous presentation of sessions on similar topics, thereby echoing the earlier comment of Mr. Bates. Prof. Malecki thought also that a better balance should be sought in the selection of papers of a scientific or research nature versus those of applied technology. He supported the point made earlier by Mr. de Sterke that summaries of technical papers in advance of a conference could serve almost as well as full preprints with less practical difficulty in execution.

Mr. Heselwood asked whether delegates will have access to early press coverage of the conference or to copies of the technical papers, for purposes of reporting to their individual firms.

Mr. Scribante stressed the desirability of having the technical paper presentations remain closely on schedule. Dr. Seifert commented also on the problem of keeping technical sessions to their time schedules. He thought that the use of such techniques as warning lights to speakers might be helpful in maintaining time schedules.

Dr. Seifert expressed his appreciation of the criticisms and suggestions offered by the members, since he realized that these were intended largely for the benefit of the next conference. He made particular comment on the problem of selecting the most qualified technical papers from those offered for a conference, stating that it would be the plan of the German Committee to accept only those papers that have been recommended by the National Committees of the countries concerned. The Chairman warned, through the experience of the Canadian group, that a problem of time could be encountered in arranging for acceptance of papers by National Committees prior to their final acceptance by the conference committee.

In reply to a question by Dr. Tenney, the Chairman stated that 20 copies of preprints of their papers are being provided to all authors on a complimentary basis. Additional copies will be provided as required, at a nominal charge.

5. *New Business*

Mr. Bates tabled a two-part proposal by the British delegation, as follows:

1. That the committee agree that the appropriate time has arrived for establishment of an International Committee to co-ordinate the preparation of International Recommendations on Nondestructive Testing.
2. That it be further agreed by all delegates that they will request their official National standards organizations to recommend to the International Organization for Standardization (ISO) that ISO does establish and support a Technical Committee to deal with Nondestructive Testing.

The Committee joined Dr. Pawlowski in strong support for an approach to ISO concerning establishment of a Technical Committee on Nondestructive Testing.

Dr. Pawlowski expressed the hope that a significant percentage of research and scientific type papers can be attracted to future conferences. He thought also that it would be desirable to arrange between-conference meetings of groups of nondestructive testing people who have a common interest in various aspects of the subject. This technique would prove valuable in the exchange of information between conferences.

Prof. Homès supported Dr. Pawlowski's suggestion concerning between-conference meetings of representatives having common nondestructive testing interests.

Mr. Barer recommended that the term "Testing" in "Nondestructive Testing" be considered for replacement by a more appropriate term. He expressed the feeling that the term "testing" has a somewhat inferior connotation to some people. He thought that the term "technology" might be a better choice, and would have the added advantage of maintaining the well known and well established initials NDT. It was agreed, that no particular action could be taken at this time on Mr. Barer's proposal, but Mr. Barer asked that the subject be introduced for formal discussion at the next International Committee meeting.

The meeting adjourned at 4:15 p.m.

TERMS OF REFERENCE

(Adopted in Montreal, Canada, May 21, 1967)

1. *Definition*

1.1 Nondestructive testing is a procedure which covers the inspection and/or testing of any material, component or assembly by means which do not affect its ultimate serviceability.

1.2 In the present state of the knowledge the following techniques of nondestructive testing are included.

a) radiography and fluoroscopy by X-ray, gamma-rays and neutrons.
b) X-ray diffraction, X-ray crystal analysis.
c) electron diffraction.
d) X-ray spectroscopy.
e) ultrasonic methods.
f) eddy-current methods.
g) electrical and thermal conductivity tests.
h) the use of surface penetrants.
i) the use of magnetic tests.

This list is not intended to be exclusive but indicative of the nature of tests involved.

2. *Name*

The organization shall be known as the International Committee for Nondestructive Testing. The abbreviated term "International Committee" used below will be taken to refer to this organization.

3. *Objectives*

3.1 The objectives of the International Committee shall be to promote international collaboration in all matters relating to the development and use of all methods of nondestructive testing.

3.2 To this end, the International Committee shall, in association with National Organizations in nondestructive testing:

3.2.1. Encourage the organization of international conferences on the methods and uses of nondestructive testing at intervals of three to four years.

3.2.2. Assist in the formulation of international standards on nondestructive testing in collaboration with the International Organization for Standardization (ISO) and National Standards Bodies.

3.2.3. Encourage the formation of national bodies so that accredited national representatives to this committee can be appointed.

3.3 The International Committee shall not engage in commercial or trade activities, and shall not concern itself with wage rates, prices or markets.

4. *Membership*

4.1 The International Committee shall be made up of one representative of each country, nominated by *an appropriate* national body in that country, which has registered its intention to collaborate and co-operate in the work of the International Committee.

4.2 Each country may nominate a second representative to the International Committee. He shall not be entitled to vote except in the absence of the first representative.

4.3 Although a country's nominee may be attached to a commercial organization, it shall be understood that he represents his country's interests in the development of the uses and methods of nondestructive testing and must not concern himself within the International Committee with those aspects debarred by paragraph 3.3 above.

4.4 Countries that wish to join the work of the International Committee shall make written application to the President currently in office, and their application shall be voted on by the International Committee at the next international conference, or by postal ballot. A majority vote in keeping with 10.3 in favour of their application will be necessary to ensure their representation on the International Committee.

4.5 It is desirable in the interests of continuity to maintain the same representative on the International Committee. However, countries may change their representative provided the President currently in office is advised by the National Organization concerned prior to the next meeting of the International Committee.

5. *Officers*

5.1 The officers of the International Committee shall be a President, Vice-President and Secretary.

5.2 All officers of the International Committee shall be appointed by the country that will host and organize the next International Conference, in accordance with the following:

5.2.1 The President and Secretary shall be from, and located in, the host country.

5.2.2. The Vice-President need not be from the host country.

6. *Steering Committee*

6.1 A Steering Committee shall be formed by the host country and shall consist of the Officers defined in Section 5, and preferably one or two other members.

6.1.1. The other member or members may be from the host country or from National Organizations from other countries represented on the International Committee.

6.1.2. It is suggested that a member of a former Conference Organizing Committee be a member of the Steering Committee in order to benefit from past experiences and to help maintain continuity between conferences.

6.2 The functions of the Steering Committee shall be:

6.2.1 To organize the forthcoming Conference.

6.2.2 To make recommendations to the International Committee as appropriate.

7. *Duties*

7.1 *President*—The President, during his term of office, and with the aid of the Steering Committee, shall organize and conduct the forthcoming international conference in accordance with direction put forward by the National Organization, or other such body responsible for the Conference. He shall administer all actions of the International Committee and act as Chairman or appoint an alternate for all meetings of the International Committee.

7.2 *Vice-President*—The duties of the Vice-President shall be designated by the President.

7.3 *Secretary*—In co-operation with the President, the Secretary shall be responsible for terminating as expeditiously as possible, all activities of the Conference, including the publication of the transactions.

8. *Term of Office*

8.1 The term of all officers shall start immediately following the completion of one conference, and shall terminate upon the completion of the next.

8.2 It is desirable that officers be named prior to the beginning of their term of office.

9. *Venue and Frequency of International Conferences*

9.1 At each conference, the International Committee shall decide on the country which will act as host for the next conference, and will also discuss venues of subsequent conferences and encourage tentative invitations from member countries.

9.2 The normal interval between International Conferences under the aegis of the International Committee shall be three *to* four years.

9.3 The time of the year and venue for each conference will be settled by the National Organization of the country acting as host.

10. *Procedure*

10.1 The International Committee shall meet at least once during each International Conference; and preferably at the beginning and the end of the conference.

10.2 Between meetings, decisions where necessary, will be sought by postal ballot, in accordance with item 10.3.

10.3 A majority vote corresponding to at least two-thirds of the countries represented on the International Committee will be necessary on all matters put to a vote. In a postal vote, those countries which do not reply by the stipulated date will be considered to be in favour of the motion.

10.4 At meetings of the International Committee, all voting shall be by show of hands of those present.

11. *Finance*

11.1 The expenses incurred in relation to an International Conference shall be borne by the host country.

11.2 Such expenses as apply to an International Conference may be recovered from the registration fee charged for delegates attending the conference.

11.3 The International Committee will not be expected to give any financial aid to countries organizing International Conferences.

12. *Official Languages*

The official language of each conference will be English. French, however, may also be used and contributions spoken in French may by request be translated into English. Contributions in English will not be translated into French. The language of the host country may be used if simultaneous translation into English is provided. Where a speaker wishes to use any other language, he must make available an English text at the time, or provide an interpreter.

13. *Changes of Terms of Reference*

13.1 Any proposed changes to these Terms of Reference must be communicated to each member of the International Committee at least *nine months* before the next meeting.

13.2 Such proposed changes, provided they are seconded, shall be voted upon by the International Committee at its next meeting.

14. *Relations with the International Organization for Standardization*

Although the terms of reference allow for discussion of matters requiring standardization, it must be understood that all requests for standardization must be dealt with by the National Standards Organization of the countries represented on the International Committee, and all communications with the International Organization for Standardization shall be through the National Standards Organization, *where they exist.*

15. *Publications*

15.1 The publication of any official statement arising from the International Conference, or from the International Committee, can be authorized only by the International Committee.

15.2 In general, the publication of such statements will be undertaken by each country represented on the International Committee.

LIST OF AUTHORS

d'ADLER-RACZ, J. H., Balteau Electric Corp., Belgium.
AXELRAD, D. R., Micromechanics of Solids Lab., McGill University, Canada.
ALLEN, J. W., Instruments Division, Budd Co., Phoenixville, U.S.A.
ANDREESCU, N., Institute for Atomic Physics, Romania.
ARNELO, A., Essem M Metotest, Sweden.
AZOU, P., École centrale des arts et manufactures, France.
BASTIEN, P., École centrale des arts et manufactures, France.
BATES, C. C., Corrosion & Welding Engineering Ltd., U.K.
BERGER, H., Argonne National Laboratory, U.S.A.
BIRLEY, R. E., Rolls Royce Ltd., U.K.
BLANKS, B. L., Nondestructive Testing Group, Los Alamos Scientific Laboratory, U.S.A.
BOCK, W., Bundesanstalt für Materialprüfung, Berlin-Dahlem, Germany.
BORUCKI, J. S., Magnaflux Corporation, U.S.A.
BRAND, L., Theodor Wupperman, Leverkusen, Germany.
BRATINA, W. J., Ontario Research Foundation, Canada.
CAMPKIN, C., Central Electricity Generating Board, S. Western Region, U.K.
CARBIENER, W. A., Battelle Memorial Institute, U.S.A.
CARNEVALE, E. H., Panametrics Inc., U.S.A.
CHASTY, J. T., Lockheed Missiles & Space Co., U.S.A.
CLARK, W. C. jr., Westinghouse Research Lab., U.S.A.
COOK, K. V., Metals & Ceramics Division, Oak Ridge National Laboratory, U.S.A.
CRISCUOLO, E. L., U.S. Naval Ordnance Laboratory, U.S.A.
CROSS, B. T., Automation Industries Inc., U.S.A.
DEEDS, W. E., Metals & Ceramics Division, Oak Ridge National Laboratory, U.S.A.
DODD, C. V. III, Metals & Ceramics Division, Oak Ridge National Laboratory, U.S.A.
DOMANUS, J., Electrotechnical Institute, Poland.
DROEGE, A., J. & H. Krautkramer, Germany.
DUFAYET, J. P., Cen Cadarache, France.
DURANT, R. L., Royal Armament Research & Development Establishment, U.K.
FOLKESTAD, G., Stal-Laval Turbine Co., Sweden.
FÖRSTER, F. DR., Institut Dr. Förster, Reutlingen, Germany.
FUJI, T., Japan Steel & Tube Corp., Japan.
FULLER, A. G., British Cast Iron Research Association, U.K.
GALLIGAN, W. L., Wood Technology Section, College of Engineering Research Div., Washington State University, U.S.A.
GARRETT, D. A., Nondestructive Testing Group, Los Alamos Scientific Laboratory, U.S.A.
GLOVER, I. L. F., Bristol Siddeley Engines Ltd., U.K.
GODLEWSKI, Z., Electrotechnical Institute, Warsaw, Poland.
GODSHALL, M. M., Instruments Division, The Budd Co., Phoenixville, U.S.A.
GOLDSPIEL, S., U.S. Naval Applied Science, U.S.A.
GORSKY, V. V., State Committee on Utilization of Atomic Energy, U.S.S.R.
GRABENDÖRFER, W., J. & H. Krautkramer, Germany.
GRAHAM, B., Magnaflux Corporation, U.S.A.
GREENBERG, H. D., Westinghouse Research Laboratory, U.S.A.
GUSTAFSON, R. M., U.S. Naval Ordnance Laboratory, U.S.A.
HALMSHAW, R., Royal Armament Research & Development Establishment, U.K.
HARRIS, J. G., James Booth Aluminium Ltd., U.K.
HAVERCROFT, W. E., Dept. of Energy, Mines & Resources, Canada.
HESELWOOD, W. C., The United Steel Companies Ltd., U.K.
HOHL, C. E., Krautkramer Ultrasonics Inc., U.S.A.
HOMÈS G. A., Universities of Brussels and Mons, Belgium.
HOVLAND, H., Automation Industries Inc., U.S.A.
HUSAREK, V., Société Française d'électro-physique, France.
HYAM, N. H., Brent Chemical Products Ltd., U.K.
INGEVALD, S., The Swedish Steam Users Assoc., Sweden.
INOUE, T., Tokyo Shibaura Electric Co. Ltd., Japan.
ISHII, Y., Tokyo Institute of Technology, Japan.
ISONO, E., Fuji Iron & Steel Co. Ltd., Japan.
IWAMOTO, M., Railway Technical Research Institute, Japan.
JOHNSON, B. A., General American Transportation Corp., U.S.A.
JÜNKE, H., Kammer der Technik, Magdeburg, Germany.
KADOCHINIKOV, A. L., Academy of Sciences of U.S.S.R., U.S.S.R.
KAMMERER, C. C., North American Aviation Inc., U.S.A.
KANNO, A., Tokyo Institute of Technology, Japan.
KASTNER, J., Argonne National Laboratory, U.S.A.
KAWASKI, S., Tokyo Shibaura Electric Co., Japan.
KIHARA, H., University of Tokyo, Japan.
KIKUCHI, H., Railway Technical Research Institute, Japan.
KRASKA, I. R., Argonne National Laboratory, U.S.A.
KUBIAK, E. J., General American Transp., U.S.A.
LABUSCA, E., Institute for Atomic Physics, Romania.
LAVENDER, J. D., Royal Armament Research & Development Establishment, U.K.
LEE, J. K. S., Lockheed Missiles & Space Co., U.S.A.
LEONARD, S., Lockheed Missiles & Space Co., U.S.A.
LOUVAKIN, E. M., State Committee on Utilization of Atomic Energy, U.S.S.R.
LOVE, R. E., Corning Glass Works, U.S.A.
LYNNWORTH, L. C., Panametrics Inc., U.S.A.
MALECKI, I., Academy of Sciences, Poland.
MALMQVIST, S., Saab Aktiebolag, Sweden.
MITCHELL, O. M. M., Bell Telephone Laboratories, U.S.A.
MOORE, R. I., Ontario Research Foundation, Canada.
MORRIS, R. A., Nondestructive Testing Group, Los Alamos Scientific Laboratory, U.S.A.
MULLER, P., Institut Dr. Förster, Reutlingen, Germany.
MUNDRY, E., Bundesanstalt für Materialprüfung, Berlin-Dahlem, Germany.
McCAULEY, Prof., R. B., Ohio State University, U.S.A.
McCLUNG, R. W., Metals & Ceramics Division, Oak Ridge National Laboratory, U.S.A.
McELROY, J. T., Automation Industries Inc., U.S.A.
McGONNAGLE, W. J., Associated Midwest Universities, U.S.A.
McGRATH, J. T., Ontario Research Foundation, Canada.
McMASTER, Dr. R. C., Ohio State University, U.S.A.
NANCE, R. A., Instruments Division, The Budd Co., Phoenixville, U.S.A.
NIKLAS, L., J. & H. Krautkramer, Germany.
OGAWA, K., Tokyo Shibaura Electric Co. Ltd., Japan.
ONO, K., Hitachi Research Laboratory, Hitachi Ltd., Japan.
PAWLOWSKI, Z., Institute for Basic Technical Problems of the Polish Academy of Sciences, Poland.
PELLERIN, R. F., Wood Technology Division, College of Engineering Research Div., Washington State University, U.S.A.
POLANSKY, D., U.S. Naval Ordnance Laboratory, U.S.A.
POPESCU, N. D., The Mining Institute of Petrosani, Romania.
POSAKONY, G. J., Research Division, Automation Industries Inc., U.S.A.
PRINE, D. W., Magnaflux Corporation, U.S.A.
PRONVAKIN, V. T., State Committee on Utilization of Atomic Energy, U.S.S.R.
RACHWAL, R., Electrotechnical Institute, Warsaw, Poland.
RENNER, R. W., Westinghouse Research Laboratories, U.S.A.
RICHTER, H.-U., VEB. Schwermaschinebau Karl Liebnecht, Magdeburg, Germany.
RUAULT, P. A., Gaz de France, France.
SAMOËL, A., Cen Cadarache, France.
SASAKI, S., Hitachi Research Laboratory, Hitachi, Japan.
SASAKI, Y., Yawata Iron & Steel Co., Japan.
SATO, M., Japan Steel & Tube Corp., Japan.
SCHNITGER, D., Bundesanstalt für Materialprüfung, Berlin-Dahlem, Germany.
SCHULTZ, A. W., Space Systems Division, Avco Corporation, U.S.A.
SCOTT, D., National Engineering Laboratory, U.K.
SEKINO, S., Yawata Iron & Steel Co., Japan.
SELTZER, D. D., Martin Marietta Corporation, U.S.A.
SEPASER, M., Centre national de la recherche scientifique, France.
SEVRIN, M., Usines Balteau, Belgium.
SMITH, A. I., National Engineering Laboratory, U.K.
SMITH, G. H., F. W. Bell Inc., U.S.A.
SNYDERS, L. S., Metals & Ceramics Division, Oak Ridge National Laboratory, U.S.A.
SOUTHWORTH, H. L., The Boeing Co., U.S.A.

SPRIET, B., Cen Cadarache, France.
de STERKE, A., Röntgen Technische Dienst. NV, Netherlands.
STOLL, H., J. & H. Krautkramer, Germany.
TADA, Y., Kyowa Electronic Instruments Co., Japan.
TAYLOR, R. C., General American Transportation Corporation, U.S.A.
TEBBENHAM, J., Brent Chemical Products Ltd., U.K.
TENNEY, C., Nondestructive Testing Group, Ohio State University, U.S.A.
TIETZ, H. D., Kammer der Technik, Magdeburg, Germany.
TILJANDER, J., Test Central Laboratories, ASEA, Sweden.
UENO, T., Fuji Iron & Steel Co. Ltd., Japan.
VANZETTI, R., Raytheon Co., U.S.A.
VASILIU, S., Institute for Atomic Physics, Romania.
VDOVIN, J. A., Academy of Sciences of U.S.S.R., U.S.S.R.
VON HEIJNE, A., Essem M Metotest, Sweden.
WAKABAYSHI, N., Tokyo Shibaura Electric Co. Ltd., Japan.
WHALEY, M. L., Oak Ridge National Laboratory, U.S.A.
WECK, R., British Welding Research Assoc., U.K.
WOODMANSEE, W. E., The Boeing Co., U.S.A.
WUSTENBERG, H., Bundensanstalt für Materialprüfung, Germany.
YUN, S. S., IIT Research Institute, U.S.A.
ZAKHAROV, V. M., State Committee on Utilization of Atomic Energy, U.S.S.R.
ZURBRICK, J. R., Space Systems Division, AVCO Corporation, U.S.A.

LIST OF DELEGATES

A

Allen, John W.
The Budd Company
Phoenixville, USA

Allinson, John D.
Canadian Westinghouse Co. Ltd.
Port Hope, Canada

Aman, John
DuPont de Nemours & Co.
Hollywood, USA

Anastasia, A.
Radio Corp. of America
Princeton, USA

Anderson, M. B.
Atomic Energy of Canada Ltd.
Ottawa, Canada

Anderson, W.
Wabush Mines Co. Ltd.
Sept Iles, Canada

Andreasen, A. C. H.
Andrex Company
Copenhagen, Denmark

Arneson, T.
Sarnia Inspection Co. Ltd.
Scarborough, Canada

Arsenault, Jacques
Quebec North Shore and Labrador Rly.
Sept Iles, Canada

Astakhov, Nirolav
Moscow Research Inst. of Introscopy, USSR

Astley, Fred B.
DuPont de Nemours & Co.
Wilmington, USA

Astier, Paul
C. E. R. C. A., Paris, France

Atkinson, G. E.
Anaconda American Brass Ltd.
New Toronto, Canada

Aube, Bert
Combustion Engineering-Superheater Ltd.
Sherbrooke, Canada

Azou, Pierre
Ecole Centrale, Paris, France

B

Bacon, John P.
The Budd Company
Phoenixville, USA

Badlevski, Dr. Y. N.
Moscow Research Inst. of Introscopy, USSR

Bagnell, M. J.
M. E. L. Equipment Co. Ltd.
Crawley, Eng.

Bagnato, Roy C.
Photo Importing Agencies
Toronto, Canada

Baimler, Dr. Miroslav
Peaceful Use of Atomic Energy,
Prague, Czechoslovakia

Baker, James M.
Boeing Co.
Seattle, USA

Balcome, G. H.
Aluminum Co. of Canada Ltd.
Montreal, Canada

Baldi, Dr. Francesco
Centro Sperimentale Metalurgico
Rome, Italy

Barer, R. D.
Pacific Naval Laboratory
Victoria, Canada

Barnard, Lt. James W.
U.S.A.F.
Winnetka, USA

Baron, Ed.
DuPont de Nemours Co.
Chicago, USA

Barton, Dr. John P.
S.A.R. Centre d'études nucléaires
Grenoble, France

Barton, L. G.
Canadian Armed Forces
Trenton, Canada

Basile, George R.
Reactive Metals Inc.
Niles, USA

Bates, Colin C.
Corrosion & Welding Eng. Ltd.
Redhill, Eng.

Battema, John
Phillips Electrical Institute
Mt. Vernon, USA

Baxendale, F. W.
Canadian Arsenals Ltd.
St. Paul L'Ermite, Canada

Baxter, L. E.
L. E. Baxter Limited
Montreal, Canada

Beale, R.
DeHavilland Aircraft Co.
Downsview, Canada

Beares, William S.
Buffalo X-Ray Co.
Buffalo, USA

Becker, George L.
Lockheed Aircraft Service Co.
Jamaica, USA

Behal, V. G.
Dominion Foundries & Steel Ltd.
Hamilton, Canada

Bell, E. C.
Air Canada
Dorval, Canada

Bencze, S. M.
Dominion Engineering Co.
Lachine, Canada

Bennett, G. H.
Northern Electric Co. Ltd.
Montreal, Canada

Benson, J. E.
Canadian General Electric Co.
Peterborough, Canada

Berger, Harold
Argonne National Laboratory
Argonne, USA

Bergeron, Armand E.
Nondestructive Test Br., Code 131M2, U.S. Navy
San Francisco, USA

Bernisson, Charles M.
Eastman Kodak Company
Rochester, USA

Bilan, V.
Canadair Ltd.
Montreal, Canada

Billings, Robert
X-Ray & Radium Ltd.
Toronto, Canada

Bills, Duane L.
World Tool & Engr. Co.
Minneapolis, USA

Bird, J. A.
Steel Co. of Canada Ltd.
Hamilton, Canada

Birley, R. E.
Rolls-Royce Ltd., Derby, Eng.

Bishop, K.
Chase Brass & Copper Co.
Waterbury, USA

Black, A. D.
Watson & Sons
Wembley, Eng.

Black, W. A.
Republic Steel Corp.
Cleveland, USA

Blackham, L. A.
Rank Organization
Brentford, Eng.

Blair, A. S.
Stewarts & Lloyds Ltd.
Bellshill, Scotland

Blakeman, Denis
Public School Board
Edmonton, Canada

Blythe, Dr. W.
San Jose State College
San Jose, USA

Bly, James H.
Applied Radiation Corp.
Walnut Creek, USA

Bobbin, John E.
Branson Instr. Co.
Stamford, USA

Boekamp, K. M.
General Dynamics Convair
San Diego, USA

Bogart, H. G.
Magnaflux Corporation
New York, USA

Bolinger, Maurice
Wm. Powell Company
Cincinnati, USA
Bologna, Nino
Magnaflux Corporation
Chicago, USA
Bond, A. R.
British European Airways
Hounslow, Eng.
Bonnett, G. M.
Newport News S. & D. D. Co.
Newport News, USA
Borchelt, W. C.
Procter & Gamble Co.
Ivorydale, USA
Borkowski, Don
James Electronics Inc.
Chicago, USA
Borucki, J.
Magnaflux Corporation
Chicago, USA
Bosko, John
Canoga Park, USA
Bott, William H.
Dept. Energy, Mines and Resources
Ottawa, Canada
Boyd, C. E.
G. D./Convair, San Diego, USA
Bradley, James W.
General Motors Institute
Flint, USA
Bramhall, F. M.
Racey MacCallum & Bluteau
Montreal, Canada
Brand, Lutz
Theodor Wuppermann GmbH
Leverkusen, Germany
Bratina, Dr. W. J.
Ontario Research Foundation
Toronto, Canada
Brodie, N. W.
B.C. Hydro & Power Authority
Vancouver, Canada
Brunke, T. A.
Aluminum Co. of Canada Ltd.
Kingston, Canada
Buckles, John H.
Arrowhead Products Co.
Los Alamitos, USA
Buckrop, Roy L.
Rock Island Arsenal
Rock Island, USA
Bussche, van der
Inenieurbuero Mueller
Mannheim, Germany
Bywater, Fred
Ontario Hydro
Toronto, Canada

C

Cahill, A. D.
Algoma Steel Corporation
Sault Ste. Marie, Canada
Calaluca, Alex M.
U.S. Army Tank Automotive Cd.
Madison Heights, USA
Cale, Norman H.
Anaconda American Brass Co.
Waterbury, USA
Callihan, R. E.
Automation-Forster Co.
Boulder, USA
Campbell, G.
Automation Products
Danbury, USA
Campkin, C.
Central Electricity Generating Bd.
Clifton, Eng.
Candlish, J. R.
Ontario Hydro
Pickering, Canada
Carbiener, Wayne A.
Battelle Memorial Inst.
Columbus, USA
Carlsen
Andrex Company
Copenhagen, Denmark
Carroll, K. C., Idaho Nuclear Corpn., USA
Carson, R. D.
Automation Industries Inc.
Danbury, USA
Carter, S. W.
Avco Corporation
Sherborn, USA
Cauthen, E. C.
General Dynamics Corporation
Fort Worth, USA
Chamberland, M.
Trenton, Canada
Chapman, Pat
North American Inspection Ser.
Oakville, Canada
Chebookjian, Shant L.
Polaroid Corporation
Cambridge, USA
Chevy
Le Parc
Isere, France
Cipywnyk, H.
Steel Co. of Canada Ltd.
Hamilton, Canada
Cizek, Ing. Lubomir
Nat. Research Institute for Materials,
Prague, Czechoslovakia
Clark, B. H., Jr.
Union Carbide Corporation
Charleston, USA
Coenen, Albert
Agfa-Gevaert Inc.
Teterboro, USA
Coembs, John
Standard Oil of California
Richmond, USA
Coenraads, C.
Technical Operations Inc.
Burlington, USA
Colivas, C.
Vulcan Inspection & Drafting Ltd.
Mount Royal, Canada
Constantin, Ionescu
Ministry of Education
Bucharest, Romania
Convey, Dr. John
Dept. Energy, Mines and Resources
Ottawa, Canada
Cook, Jeffrey F.
McDonnell Company
St. Louis, USA
Cornillon, Jacques
SUD Aviation
Point Pleasant, USA
Corney, George M.
Eastman Kodak Company
Rochester, USA
Corsi, Dr. Ferruccio
Philips (Milan)
Milan, Italy
Cosgrove, Don G.
General Dynamics
Fort Worth, USA
Cosh, L. A.
Dupont of Canada Ltd.
Montreal, Canada
Cowan, Peter
North American Inspection Serv.
Oakville, Canada
Cox, Patrick W.
Procter & Gamble Co.
Cincinnati, USA
Crenshaw, James R.
ARO Inc.
Tennessee, USA
Cressman, R. N.
Bethlehem Steel Corp.
Bethlehem, USA
Criscuolo, E. L.
U.S. Naval Ord. Laboratory
Maryland, USA
Crisp, D. M.
Canadian Kodak Limited
Toronto, Canada
Cross, B. T.
Automation Industries
Boulder, USA
Cross, Newbold O.
Esso Research & Eng.
Florham Park, USA
Culham, H. D.
Orenda Limited
Toronto Airport, Canada
Cunningham, J.
2362 Zela Street
Victoria, Canada

D

D'Adler-Raez, Jos. H.
Balteau
Liege, Belgium
Daly, Maurice
Canadian Steel Foundries Ltd.
Montreal, Canada
Dann, M. V. H.
Wisconsin Centrifugal Inc.
Waukesha, USA
Darcy, G. A., Jr.
U.S. Army Mat. Res. Agency
Watertown, USA
De Carlo, Victor A.
Union Carbide Nuclear Co.
Idaho Falls, USA
Dedieu, Jacques
Vallourec
Aulnoye Nord, France
Denton, C. J.
Battelle-Northwest Co.
Richland, USA
DePue, Dr. Leland A.
Naval Research Laboratory
Washington, USA
Desandre-Navarre, C.
Commissariat à l'énergie atomique
St. Paul lez Durance
(B. du R.), France
Desbordes, J. C.
Commissariat à l'énergie atomique
Paris, France

Destribats, M. Thérèse
Commissariat à l'énergie atomique
Paris, France
Deutsch, Dr. V.
Wuppertal, Germany
Devictor, M.
Commissariat à l'énergie atomique
Paris, France
Devine, C. M.
Imperial Oil Enterprises Ltd.
Edmonton, Canada
Devine, G. M.
Krautkramer Ultrasonics Inc.
Stratford, USA
Dick, Paul
General Electric Co.
Philadelphia, USA
Dodd, Caius V.
Oak Ridge National Labs.
Oak Ridge, USA
Dodge, D. D.
Ford Motor Co.
Detroit, USA
Dollansky, K. W.
Combustion Engineering-Superheater Ltd.
Sherbrooke, Canada
Douglas, W.
Orenda Ltd.
Toronto Airport, Canada
Dowell, K.
Agfa-Gevaert Inc.
Teterboro, USA
Dowling, J. V.
Automation Industries Inc.
Danbury, USA
Downes, G. W.
Vitosonics Ltd.
Hertford, Eng.
Drieseberg, W.
Ultrasonic Testing Serv.
Burlington, Canada
Driscoll, D. E.
U.S. Army Mat. Res. Agency
Watertown, USA
Drummond, Walter N.
United Aircraft of Canada Ltd.
Longueuil, Canada
Dubitski, Dr. Leo
Moscow Research Inst. of Introscopy
USSR
Dudzinski, Joseph J.
U.S. Army Tank-Autom. Command
St. Clair Shores, USA
Dukes, W. A.
Explosives Research & Dev.
Essex, Eng.
DuMond, T. C.
American Society for Metals
Metals Park, USA
Dutra, John A.
San Francisco Bay Naval Shipyard
Vallejo, USA

E

Edwards, F. H.
Bragg Laboratory
Sheffield, Eng.
Edwards, R.
EMI-Cossor Electronics Ltd.
Dartmouth, Canada
Egorov, K.
Moscow Research Inst. of Introscopy
USSR
Eisenstein, N.
Barnes Engineering Co.
Stamford, USA
Elliott, Dana
Los Alamos Scientific Laboratory
Los Alamos, USA
Emery, Edwin R.
Westinghouse Company
Blairsville, USA
Ensminger, Dale
Battelle Memorial Inst.
Columbus, USA
Epstein, A. J.
Mobil Chemical Company
Matuchen, USA
Erickson, Neil R.
Dow Chemical Company
Midland, USA
Exton, C. H.
Magnaflux Limited
London, Eng.

F

Fairchild, J. F.
Air Canada
Montreal Airport
Montreal, Canada
Fang, Dr. H. Y.
Lehigh University,
Bethlehem, USA
Fehr, Dr. Robert O.
Branson Instruments Inc.
Stamford, USA
Ficare, Dr. Ing. Paolo
Aeroporto Di Fiumicino
Italy
Field, G.
Automation Industries Inc.
Danbury, USA
Fielder, A. W.
British Overseas Airways Corp.
London, Eng.
Figuaroa, Carlos
Industrial Nucleonics Corp.
Columbus, USA
Fink, L.
Navy Department
Washington, USA
Fiola,
Aluminum Co. of Canada Ltd.
Arvida, Canada
Fisher, Harold L. D.
A.E.C.L.
Pinawa, Canada
Fletcher, S. G.
Latrobe Steel Company
Latrobe, USA
Flis, E. T.
Canadian Kodak Sales Ltd.
Toronto, Canada
Flora, John N.
Battelle Memorial Inst.
Columbus, USA
Fogler, Henry H.
Eastman Kodak Co.
Rochester, USA
Folkestad, Gosta
Stal-Laval Turbin AB
Finspong, Sweden
Forest, Y. L.
Canadian Kodak Sales Ltd.
Toronto, Canada
Förster, Dr. F.
Institut Dr. Förster
West Germany
Foster, R. Paul
Winchester, USA
Foxall, Robert H.
McKay Machine Co.
Youngstown, USA
Frederick, C. L.
Nortec
Richland, USA
Fritsch, Werner
Mannesmann Tube Co. Ltd.
Sault Ste. Marie, Canada
Froot, H. A.
IBM Corporation
Hopewell Junction, USA
Fry, E. M.
Bell Telephone Lab. Inc.
Whippany, USA
Fuji, Takashi
Japan Steel & Tube Co.
Tokohama-shi, Japan
Fuller, A. C.
British Cast Iron Research Assoc.
Birmingham, Eng.
Fuller, Richard
Eastman Kodak Co.
Rochester, USA
Fulton, C. W.
Aluminum Co. of Canada Ltd.
Montreal, Canada

G

Gabacorti, Giovani
Alitalia Airlines
Montreal Airport,
Montreal, Canada
Gallagher, Donald V.
San Francisco Bay Naval Shipyard
Vallejo, USA
Galligan, Wm. L.
Irvington Machine Wks. Inc.
Portland, USA
Gamiche, David L.
U.S. Army Tank Automotive Cd.
Warren, USA
Gans, Martin
Internat. Nondestructive Testing Ltd.
Las Vegas, USA
Garcia, Leonard
Uresco Inc.
Montebello, USA
Gauthier, G. P.
Warnock-Hersey Co. Ltd.
Lasalle, Canada
Gentile, Dr. Ralph G.
The Babcock & Wilcox Research Center
Alliance, USA
Gerard, Jacques S. L.
Métallurgie et mécanique nucléaires
Dessel, Belgium
Giasson, Albert
Quebec North Shore and Labrador Rly.
Sept. Iles, Canada
Gibbs, F. Eugene
Kaiser Aluminum & Chemical Corp.
Spokane, USA
Gibson, Walter J.
Babcock & Wilcox Co. Inc.
Alliance, USA
Gill, E. A.
Canadian General Electric Company
Toronto, Canada

Gleekman, Dr. Lewis W.
Wyandotte Chemical Corp.
Wyandotte, USA

Glover, I. L. F.
Bristol Siddeley Engines Ltd.
Bristol, Eng.

Gooderham, R. M.
Canadian Welding Bureau
Toronto, Canada

Golani, Dave
United Aircraft Canada Ltd.
Longueuil, Canada

Goldspiel, S.
U.S. Naval Appl. Scientific Lab.
Brooklyn, USA

Golia, Matthew J.
Ohio State University
Columbus, USA

Gordon, Morton
Metal & Pipeline Endurance Ltd.
London, Eng.

Gorinine, Igor
Union "Svetlana"
Leningrad, USSR

Gorski, V.
Moscow Research Inst. of Introscopy
USSR

Gottfeld, F. H.
F. H. Gottfeld GmbH
Germany

Grady, Edward C.
New York State D.P.W.
Albany, USA

Graham, Bruce
Magnaflux Corporation
Chicago, USA

Granitsas, George A.
American Optical Co.
Southbridge, USA

Gray, Allen G.
American Society for Metals
Metals Parks, USA

Green, D. T.
Picker Industrial Products
Cleveland, USA

Greene, Arnold
Testing Laboratories Inc.
East Natick, USA

Greenberg, German
Pittsburgh, USA

Grimm, Donald E.
Las Vegas, USA

Grosvenor, R. J.
Steel Co. of Canada Ltd.
Hamilton, Canada

Gusse, Donald
General Dynamics
Pomona, USA

Gustafson, Roy M.
Navy Dept.
Washington, USA

H

Hake, Guest
Atomic Energy of Canada,
Chalk River, Canada

Haller, L. B.
Magnaflux Corporation
Chicago, USA

Halmshaw, Ronald
Ministry of Defence
Kent, Eng.

Halsey, G. H.
McCreary Tire & Rubber Co.
Indiana, USA

Hansen, H. Harold
Hansen Engineering & Machine Co.
Lynn, USA

Harding, N. G.
Ardrox Limited,
Niagara on the Lake, Canada

Harmon, W. C.
Republic Steel Corp.
Cleveland, USA

Harris, J. G.
James Booth Aluminum Ltd.
Birmingham, Eng.

Hart, Earle C.
Aerospace Corporation
El Segundo, USA

Hastings, C. H.
AVCO Corpn.
Weston, USA

Havercroft, W. E.
Dept. Energy, Mines & Resources,
Ottawa, Canada

Hay, Robert H.
Aluminium Laboratories Ltd.
Kingston, Canada

Hayashi, Hiroshi
Japan Industrial Testing Co.
Kanagawaken, Japan

Heisman, A.
Radio Corp. of America
Princeton, USA

von Heijne, Axel
Essem Metotest AB
Skultuna, Sweden

Hemingway, A. V.
STD. Services Ltd.
Staffordshire, Eng.

Hennekens, Robert C.
IBM Corp.
White Plains, USA

Henry, Edwin B. Jr.
U.S. Steel Corporation
Pittsburgh, USA

Herman, R. S.
Olin Mathieson,
New Haven, USA

Herring, R. D.
Williams & Wilson Ltd.
Montreal, Canada

Heselwood, W. C.
The United Steel Co. Ltd.
Rotherham, Eng.

Hetherington, M. J.
Stewarts & Lloyds Ltd.
Northants, Eng.

Hill, Colin
Esso Ltd.
Port Coquitlam, Canada

Hills, A. B. Farley,
British Aircraft Corporation
Lancashire, Eng.

Hitt, W. C.
Automation Industries Inc.
Danbury, USA

Hoeller, Dr. P.
Huttenwerk Oberhausen AG
West Germany

Hogervorst, G. F.
Toronto Iron Works Ltd.
Toronto, Canada

Hohl, Cary
Krautkramer Ultrasonics Inc.
Stratford, USA

Hoitsma, B.
Cooper Alloy Corp.
Hillside, USA

Holden, William O.
The Seybold Co.
Cincinnati, USA

Holeer, Dr. Paul
Huttenwerk Oberhausen AG
West Germany

Holliday, Robert L.
R. L. Holliday Co.
Pittsburgh, USA

Homès, Prof. Dr. G. A.
Universities of Brussels & Mons
Brussels, Belgium

Hooker, P. R.
Automation Industries Inc.
Danbury, USA

Horne, Harold W.
Imperial Oil Enterprises Ltd.
Dartmouth, Canada

Hovey, C. M.
Bristol Aerospace Ltd.
Winnipeg, Canada

Hovland, H.
Automation Industries Inc.
Danbury, USA

Huffstatler, R. O.
Westinghouse Atomic Co.
West Mifflin, USA

Huggins, B. E.
UK Atomic Energy Authority
Aldermaston, England

Hughes, E. T.
Westinghouse
West Mifflin, USA

Hunter, D. O.
Battelle-Northwest Co.
Richland, USA

Husarek, V.
Société Française d'électrophysique
Sartrouville, France

Hutchinson, Lew
Lake Ontario Steel Co.
Whitby, Canada

Huth, Dr. John
Naval Ship Systems Command
Washington, USA

I

Ishibashi, Yasuo
Nihon University
Narashino City, Japan

Imai, Takashi
Tokyo Shibaura Electric Co. Ltd.
Kawasaki, Japan

Imai, Yasuho
1st Research Inst. of Japan Def. Agcy.
Tokyo, Japan

Ingevald, Sture
Swedish Steam Users' Assoc.
Stockholm, Sweden

Inoue, Tamon
Tokyo Shibaura Electric Co.
Cambridge, USA

Irsak, J. E.
Switzer Brothers
Cleveland, USA

Irwin, John Schwenk
Walnut, USA

Ishii, Yugoro
Tokyo Inst. Technology
Tokyo, Japan
Ishiri, Yugoro
Tokyo, Japan
Isono, Eiji
Fuji Iron & Steel Co.
Kanagawa, Japan
Iwamoto, Mitsugu
Railway Technical Research Inst.
Tokyo, Japan

J

Jackson, V. C.
Union Carbide Corporation
Oak Ridge, USA
Jacobsen, K. M.
Brent Chemical Products Ltd.
Middlesex, Eng.
Jaeger, Gerhard
Deutsche Lufthansa
Frankfurt, Germany
Jahn, George H.
Mannesmann Tube Co. Ltd.
Sault Ste. Marie, Canada
Janis, Carl G.
IBM Corporation, Vestal, USA
Jarrett, Fred W.
CBL Industries Inc.
Cleveland, USA
Javor, Dr. Tibor
Research Inst. for Civil Eng.
Bratislava, Czechoslovakia
Jean, Harlan D.
Allison Div. G.M.C.
Indianapolis, USA
Jenkins, T. Clifford
Lockheed Georgia Co.
Marietta, USA
Jehu, L.
Dominion Bridge Co. Ltd.
Montreal, Canada
Johnson, E. D.
Canadian Welding Bureau
Toronto, Canada
Johnson, Philip D.
A.S.N.T. Inc.
Evanston, USA
Jones, K. H.
Canadian Kodak Sales Ltd.
Toronto, Canada
Jones, R. D.
Canadian Steel Wheel Ltd.
Montreal, Canada
Judd, T. W.
Republic Steel Corporation
Cleveland, USA
Jorgensen, Axel V.
F. L. Smith & Co.
New York, USA
Junkins, W. Alva
Industrial Heat Treating Co.
Indianapolis, USA
Jurenka, J.
Dominion Bridge Co. Ltd.
Montreal, Canada
Justice, Bryant E.
General Dynamics Co.
New York, USA

K

Kadota, Kazuto
Mitsubishi Heavy Ind. Ltd.
Kobe Shipyard,
Kobe, Japan
Kallas, D. H.
U.S. Naval Applied Science Lab.
Brooklyn, USA
Kammerer, C. C.
Long Beach, USA
Karlsson, Bengt
Royal Swedish Air Force
Malmslatt, Sweden
Kasel, Richard S.
Van Water's & Roger's Inc.
Los Angeles, USA
Kastner, Jacob
Argonne National Laboratories
Argonne, USA
Keady, Timothy V.
Eastman Kodak Co.
Rochester, USA
Kean, Harold S.
QAD-Philadelphia Naval Shipyard
Philadelphia, USA
Kearney, M. A.
Automation Industries Inc.
Danbury, USA
Keene, Samuel J. Jr.
Nasa-Goddard
Greenbelt, USA
Kenney, D.
Picker X-Ray Co.
Boston, USA
Kihara, Hiroshi
University of Tokyo
Tokyo, Japan
Kirchner, E.
Phillips Elec. Inst.
Mt. Vernon, USA
Kistler, James F.
Hewlett-Packard Co.
Waltham, USA
Klinker, Lt. Col.
U.S. Army, Arlington, USA
Knapp, Randy
Combustion Engineering-Superheater Ltd., Sherbrooke, Canada
Knell, M.
Kodak Limited
London, Eng.
Kojima, Kobei
Osaka University
Osaka, Japan
Korowac, E. Gene
Picker X-Ray Eng. Ltd.
Calgary, Canada
Krafka, Edward G.
Toronto, Canada
Kraimer, Dr. Phil Ekkehard
Bohler & Co. AG
Austria
Krapf, G.
DuPont of Canada Ltd.
Montreal, Canada
Kraus, Heinz
Canadair Ltd.
Montreal, Canada
Krause, W.
Teletype Corporation
Skokie, USA
Krautkramer, H.
Krautkramer Ultrasonics Inc.
Stratford, USA
Kriesz, H. W.
Holger Andreasen
Copenhagen S., Denmark
Kristjanson, Carl H.
Shell Canada Ltd.
Montreal East, Canada
Krock, Dr. R. H.
P. R. Malloy & Company
Burlington, USA
Kubiak, E. J.
General American Transp.
Niles, USA
Kuntz, P.
Agfa-Gevaert Inc.
Teterboro, USA

L

Lakovicz, William
Anaconda American Brass Co.
Detroit, USA
Lamarche, R. M.
Department of National Defence
Ottawa, Canada
Larson, Robert W.
Larpen Supply Company
Milwaukee, USA
Latichenko, Vitold
Institut Mehuniki Polimezov
USSR
Lavender, J. D.
B.S.C.R.A., Yorkshire, Eng.
Law, R.
Canadian Vickers Shipyards Ltd.
Montreal, Canada
Laycraft, N. E.
Dept. of Public Works,
Ottawa, Canada
Leipner, M. N.
Picker X-Ray Corp.
New Haven, USA
Lemonde, Claude
Dept. of National Defence
Montreal, Canada
Leonard, Sheldon
Lockheed Missiles/Space Co.
Organization 48-10
Sunnyvale, USA
Leopold, Dr. S.
Gevaert Agfa Nu.
Antwerp, Belgium
Levy, Lionel
Aerospace Corp.
San Bernardino, USA
Lewis, W. H.
Lockheed-Georgia Co.
Marietta, USA
Liebowitz, Harold
Department of the Navy
Washington, USA
Lindfeldt, Olof
Scandinavian Airline Services
Stockholm, Sweden
Lindsay, James
Scottish Aviation Ltd.
Ayrshire, Scotland
Litting, B. G.
International Combustion Ltd.
Derby, Eng.
Littlewood, Dr. R.
Steel Co. of Canada Ltd.
Hamilton, Canada
Lobbon, Richard A.
Picker X-Ray Corp.
Philadelphia, USA
Lomerson, Edwin O. Jr.
Pratt & Whitney Aircraft Co.
East Hartford, USA

Lopos, Jose Augusto
Aeroporto Congonhas
S. Paulo, Brazil

Louks, D. C.
Atlas Steel Co.
Welland, Canada

Low, Ian A. B.
Lambton College
Sarnia, Canada

Luini, Louis A.
General Dynamics Corp.
Groton, USA

Lynnworth, Lawrence C.
Panametrics Inc.
Waltham, USA

Lucas, Werner
Krautkramer,
Berlin, Germany

M

MacKessy, R. J.
F. W. Bell Inc.
Columbus, USA

MacMillan, Keith C.
Lawrence Radiation Lab.
Livermore, USA

Malecki, Dr. Ignacy
Polish Academy of Science
Warsaw, Poland

Malik, M. P.
Deutsche Lufthansa
Hamburg, Germany

Malmqvist, Sven
Saab Aktiebolog
Linkoping, Sweden

Malter, Don
McDonnell-Douglas Co.
St. Louis, USA

Mansfield, V.
The Rauland Corp.
Chicago, USA

Marble, J. D.
General Electric Co.
Cincinnati, USA

Marcus, E. Mason
General Dynamics/Electric Boat Co.
Groton, USA

Marechal, M.
Balteau Electric Company
Stamford, USA

Markert, Dieter
Seifert X-Ray Corp.
King of Prussia, USA

Marshall, Duncan A.
Internat. Radiographic & Insp. Serv.
Edmonton, Canada

Martin, Don
Idaho Nuclear Corporation
Idaho Falls, USA

Martin, R. A.
Canadian Pacific Airlines
Vancouver, Canada

Martin, James
Deuterium of Canada Ltd.
Glace Bay, Canada

Martin, James H.
Fairbanks Morse (Canada) Ltd.
Kingston, Canada

Mather, K.
Waterways Experiment Station,
Jackson, USA

Mathers, Mrs. K.
Waterways Experiment Station
Jackson, USA

Mathews, E. S.
Switzer Bros. Inc.
Cleveland, USA

Mathews, G. W.
Philips Electronics Ltd.
Toronto, Canada

Matting, Prof. Dr. Ing. H. A.
Betatron-Gruppe
Hannover, Germany

May, H. E.
General Electric Co.
Evendale, USA

May, Harley E.
General Electric Co.
Cincinnati, USA

Mayer, Bruce C.
General Electric Co.
Pleasanton, USA

Mayer, R. J.
McDonnell Aircraft Corp.
St. Louis, USA

Mayo, W. H.
U.S. Steel Corp.
Pittsburgh, USA

De Meester, Dr. Paul
University Leuven
Leuven, Belgium

Melmon, Ernest L.
Sicucar Ind. X-Ray
San Francisco, USA

Menetrier, J.
Appareils Gamma Siar
Paris, France

Mercer, W. R.
Electro Physical Instr. Ltd.
Brampton, Canada

Merchant, Harry G.
Imperial Oil Enterprises Ltd.
Brights Grove, Canada

Michaud, R.
Dorval, Canada

Migel, H.
Magnaflux Corporation
Chicago, USA

Miller, Edward C.
Oak Ridge National Laboratory
Oak Ridge, USA

Miller, T. R.
BIX Limited
Buzzard, England

Minuto, C.
Procol
Milan, Italy

Mitchell, C. A.
X-Ray Prod. Co.
Norristown, USA

Mitchell, K. M.
Canadian Kodak Co.
Toronto, Canada

Monahan, J.
Phillips Elec. Inst.
Mt. Vernon, USA

Morgan, Charles T.
Charles T. Morgan Co. Inc.
Hawthorne, USA

Mori, Makoto
Tokyo Denki-Seiki Electronics Ltd.
Tokyo, Japan

Morris, Roger A.
Los Alamos Scientific Lab.
Los Alamos, New Mexico, USA

Moss, M.
Racey, MacCallum & Bluteau Ltée.
Montreal, Canada

Mueller, R. A.
McDonnell Aircraft Corp.
St. Louis, USA

Muller, Dr. Paul
Wurttemberg, Germany

Muller, Dipl. Ing. W.
Ludwigshafen
Rheingonheim, Germany

Muenow, Richard
James Electronics Co.
Chicago, USA

Mundry, Ing. Eberhard
Bundesanstalt fur Materialprufung (BAM)
Germany

Munoz, Joseph
Paris, France

Murray, J. J.
U.S. Army Research Office,
Durham, USA

McCarthy, A.
Crane Limited
Hamilton, Canada

McCauley, Roy B.
Ohio State University
Columbus, USA

McClung, Robert
Oak Ridge National Laboratory
Oak Ridge, USA

McCuaig, R. R.
Polymer Corp. Ltd.
Sarnia, Canada

McEachern, A. D.
Atomic Energy of Canada Ltd.
Chalk River, Canada

McElroy, J. T.
Automation Industries
Boulder, USA

McFarlane, T. W.
Magnaflux Corporation
Chicago, USA

McGlynn, J.
Canadian Bechtel Ltd.
Montreal, Canada

McGonnagle, Dr. Warren J.
Elmhurst, USA

McGoughey, William C.
c/o Wm. C. McGoughey Co.
New Fairfield, USA

McKinnon, Jack
Warnock-Hersey International Ltd.
St. John's, Canada

McLellan, D. J.
Wolverine Tube
London, Canada

McMaster, Dr. Robert C.
The Ohio State University
Columbus, USA

N

Nakamura, Harumasa
National Research Inst. for Metals
Tokyo, Japan

Nance, Roy A.
Budd Company Automation Ind.
Phoenixville, USA

Neiley, R. Y.
Automation Industries Inc.
Danbury, USA

Nelles, J. S.
Atomic Energy of Canada Ltd.
Chalk River, Canada

Nemet, A.
British National Committee for NDT
Surrey, England

Nesbitt, Charles D.
Photo Products Dept.
Wilmington, USA

Niklas, Dr. J.
J. & H. Krautkramer A. G. A. E.
Cologne, Germany

Nisbet, Ronald T.
Engineering Test Services Inc.
Torrance, USA

Nostrand, C.
Phillips Elect. Inst.
Mt. Vernon, USA

Nute, P. R.
Automation Industries Inc.
Danbury, USA

O

O'Connor, D. T.
Magnaflux Corporation
Chicago, USA

O'Donnell, Harry
Electric Boat Div.,
General Dynamics
Groton, USA

Offner, Walter W.
X-Ray Engineering Int.
San Francisco, USA

O'Halloran, Daniel E.
Northrop Norair
Hawthorne, USA

Ohlson, Herbert B.
Kaiser Aluminum & Chem. Corp.
Spokane, USA

Oliver, Robert B.
Union Carbide Corp.
Kokomo, USA

Olsson, Dexter A.
Bethlehem Steel Corp.
Bethlehem, USA

Opeldus, Andreas
C. H. F. Muller, GmbH
Hamburg, Gr.

Orr, Dr. L. W.
Tecumseh Products Laboratory
Ann Arbor, USA

Oshchepkov, Prof. P. K.
Moscow Research Inst. of Introscopy
USSR

Ostrofsky, Bernard
American Oil Company
Whiting, USA

P

Paddan, H. F.
Grumman Aircraft Eng. Corp.
Bethpage, USA

Pade, Earl R.
Alcoa
New Kensington, USA

Page, O.
Samuel Fox & Co. Ltd.
Sheffield, Eng.

Palfy, Pavol
Slovnaft Refinery-CSSR
London W., Eng.

Palijenko, Basil
Ontario Hydro
Toronto, Canada

Palmer, J. D.
Ontario Research Foundation
Toronto, Canada

Park, I. M.
Steel Co. of Canada
Hamilton, Canada

Parks, C. J., Jr.
G. C. Optronics Inc.
Ann Arbor, USA

Parker, F. C.
Stamford, USA

Parker, Phil
Parker Research Co.
Dunedin, USA

Parkinson, E. P.
Canadair Limited
Montreal, Canada

Parkinson, John Keith
Montreal Locomotive Works Ltd.
Montreal, Canada

Parsons, Austin
Zenith Radio Corporation
Chicago, USA

Passeri, Alfonso J.
Pratt & Whitney Aircraft Co.
East Hartford, USA

Patience, J.
Canadian Vickers Shipyards Ltd.
Montreal, Canada

Patriquin, D. B.
Warnock-Hersey Internat. Ltd.
Dartmouth, Canada

Patterson, F.
DeHavilland Aircraft Co.
Downsview, Canada

Paul-Hus, C.
Canadian Vickers Shipyards Ltd.
Montreal, Canada

Pawlowski, Z.
Polish Academy of Sci.
Warsaw, Poland

Peare, H. J. S.
Rolls-Royce of Canada Ltd.
Montreal, Canada

Pellerin, Roy F.
Washington State University
Pullman, USA

Pender, T. L.
Wisconsin Centrifugal Inc.
Waukesha, USA

Pennell, Franklin H.
DeLaval Turbine Co.
Trenton, USA

Perks, R.
Agfa-Gevaert Inc.
Teterboro, USA

Perrone, Nicholas
Office of Naval Research
Washington, USA

Persson, Hilding
National Swedish Road Board
Stockholm, Sweden

Pester, Peter
Kodak A. G. Stuttgart
West Germany

Phillips, G. S.
Aluminum Co. of Canada Ltd.
Toronto, Canada

Pickles, L.
Catalytic Con. of Canada
Sarnia, Canada

Plachta, Edwin S.
Carborundum Co.
Niagara Falls, USA

Placke, E. A.
AMF Tuboscope Inc.
Houston, USA

Plekhanov, A.
Moscow Research Inst. of Introscopy
USSR

Pludek, V. R.
Canadian Vickers Shipyards Ltd.
Montreal, Canada

Pluhar, A. J.
Dominion Bridge Co. Ltd.
Winnipeg, Canada

Plummer, Fred L.
American Welding Society
New York City, USA

Polansky, Daniel
U.S. Naval Ordnance Lab.
Silver Spring, USA

Posakony, G. J.
Automation Industries
Boulder, USA

Poulard, S. J.
Commissariat à l'énergie atomique
Paris, France

Preston, Don
Rolls-Royce of Canada Ltd.
Montreal, Canada

Prime, David W.
Magnaflux Corporation
Chicago, USA

Pritchett, Leslie D.
Boeing Company
Renton, USA

Promisel, N. E.
National Research Council
Washington, USA

Prusak, John J.
IBM Components Div.
Hopewell Jct., USA

Pychyl, Walter A.
Stelco-Page Hersey Wks.
Welland, Canada

R

Rafat, Abolghasem
National Iranian Oil Co.
Tehran, Iran

Rao, T. Shama
Fairey Aviation Ltd.
Dartmouth, Canada

Reeves, L.
L. E. Baxter Ltd.
Toronto, Canada

Reinsmith, Gerald
U.S. Army Weapons
Rock Island, USA

Renner, R. W.
Westinghouse Research Labs.
Pittsburgh, USA

Reynolds, Robert E.
Eastman Kodak Co.
Whittier, USA

Richards, A. E.
Williams & Wilson Ltd.
Toronto, Canada

Richard, Jacques
Ville de Montreal
Montreal, Canada

Rigbey, James V.
Ford Motor Co. of Canada Ltd.
Windsor, Canada

Robards, Chester F.
Bardel Inc.
Cleveland, USA

Roberts, P. R.
Dominion Bridge Co. Ltd.
Montreal, Canada

Robinson, Gary C.
Reading & Bates Offshore
Houston, USA

Robinson, R. D.
Canadian Kodak Company
Toronto, Canada

Roch, J. F.
Electro Physical Inst. Inc.
Montreal, Canada

Rochon, Dr. C. A.
NAA Space & Info. Control Systems Div.
Downey, USA

Roffman, Eugene
Philadelphia, USA

Rolfe, J. E.
Magnaflux Corporation
Chicago, USA

Rossie, James
ITT Cannon
Los Angeles, USA

Rothrouff, Regis G.
Westinghouse Electric Corp.
Cheswick, USA

Ruault, Pierre
Gaz de France
Paris, France

S

Saito, Sadaichi
The Sanpo Inc.
Tokyo, Japan

Sakar, Rosella Peter
McConnell Air Force Base
Wichita, USA

Samson, J. B.
Dominion Bridge Co. Ltd.
Montreal, Canada

Samuels, L. E.
Defence Standards Laboratories
Melbourne, Australia

Samusch, Manfred
Rich. Seifert & Co.
Hamburg, Germany

Samusch, Mrs. Manfred
Rich. Seifert & Co.
Hamburg, Germany

Sasaki, Soji
Hitachi Ltd.
Hitachi, Japan

Sato, Thom-o
Inst. of Technology
Magoya, Japan

Sattler, Frank J.
T. R. W. Inc.
Cleveland, USA

Sauerwein, Dr. Kurt J.
Isotopen-Laboratorium
Dusseldorf, Germany

Sawamura, Shogo
Tokushu Tokyo Co. Ltd.
Tokyo, Japan

Schaper, Eng. H.
Inst. fur Werkstoffkunde
der Technischen Hochschule
Hannover, Germany

Schiebel, R. O.
Magnaflux Corporation
Chicago, USA

Schickert, Lothar
Deutsche Lufthansa
Hamburg, Germany

Schmidt, Dr. A.
Ont. Dept. of Health
Toronto, Canada

Schneeman, Justin G.
X-Ray Products Corp.
Pico Rivera, USA

Schock, H. E.
Radio Corp. of America
Camden, USA

Schoff, Harold A.
Anaconda American Brass Co.
Waterbury, USA

Schremp
Canadian Kodak Sales Ltd.
Toronto, Canada

Schultz, Arnold W.
Avco Corporation, Lowell, USA

Schumacher, Dr. Rudi
C. H. F. Muller GmbH
Hamburg, Germany

Schwartz, Gerard
United Aircraft of Canada Ltd.
Longueuil, Canada

Schwartz, Kurt J.
Univ. Tech. Test Laboratory
Collingdale, USA

Schwartz, Richard J.
Quebec Iron & Titanium Corporation
Tracy, Canada

Schwartzbart, H.
11T Research Institute
Chicago, USA

Scribante, P.
Bureau of Standards
Pretoria, S. Africa

Searles, C. E.
Lockheed Cal. Company
Burbank, USA

Sebistianowich, C. A.
Supreme Precision Casting (1963) Ltd.
Ville St. Laurent, Canada

Seeboth, Henry
Larpen Industries
Milwaukee, USA

Seeytyd, Leopold
Gevaert Agfa NU
Antwerp, Belgium

Seibyl, W.
Picker X-Ray Co.
Cleveland, USA

Seifert, Dr. Richard
Rich. Seifert & Co.
Hamburg, Germany

Seidl, John E.
Martin-Marietta Co.
Orlando, USA

Sekino, Shozo
Yawata Iron & Steel Co. Ltd.
Kukuoka, Japan

Selner, R. H.
Joliet, USA

Seltzer, David D.
Martin-Marietta Co.
Orlando, USA

Serjeznov, Dr. A. L.
St. Polsunov ab,
Novosibirsk, USSR

Seybold, Robert W.
The Seybold Co.
Cincinnati, USA

Shafer, James D.
Detec Inc.
Cleveland, USA

Shahdadi, Mohammad
National Iranian Oil Co.
New York, USA

Shanks, Osborne
Warnock-Hersey Co. Ltd.
Toronto, Canada

Sharpe, Roy Samuel
U.K. Atomic Energy Auth.
Berkshire, Eng.

Shaw, Carl B.
Automation Industries Inc.
Boulder, USA

Shimomura, T.
Ataka New York Inc.
New York, USA

Shiraiwa, Toshio
Sumitomo Metal Industries
Hyogo, Japan

Simon, L. E.
Pacific Missile Range
Point Mugu, USA

Simpson, T.
Williams & Wilson Ltd.
Toronto, Canada

Sinclair, Neil A.
General Dynamics Elect. Corp.
Groton, USA

Siry, Andre
Imperial Oil Enterprises
Montreal, Canada

Skeie, Kermit
Uresco Inc.
Downey, USA

Smetana, Robert
Detec Inc.
Cleveland, USA

Smith, G. H.
F. W. Bell Inc.
Columbus, USA

Smith, Dr. Kenneth
Torrance, USA

Smith, Lee
X-Ray Engineering Internat.
San Francisco, USA

Smyth, D.
Mannesmann Tube Co.
Sault Ste. Marie, Canada

Socky, R. B.
General Electric Company
Philadelphia, USA

Southey, R. M.
Shawinigan Chemicals Ltd.
Shawinigan, Canada

Spring, D. N.
Canadian Kodak Company
Toronto, Canada

St. Pierre, Paul A.
Baie Comeau, Canada

Starkey, B. J.
EMI-Cossor Electronics Ltd.
Dartmouth, Canada
Stein, David
Picatinny Arsenal
Dover, USA
Stemple, Godfrey A.
Baltimore Gas & Electric Co.
Baltimore, USA
Sterke, A. de
Rontgen Technische Dienst NV
Rotterdam, Holland
Stevens, C. R.
Williams & Wilson Ltd.
Montreal, Canada
Stevens, Harold B.
Shawinigan Chemical Ltd.
Shawinigan, Canada
Stevens-Guille, P. D.
Atomic Energy of Canada Ltd.
Chalk River, Canada
Stewart, R. E.
DuPont Company
Clifton, USA
Stillman, Jerry
Hughes Company
Canoga Park, USA
Storing, D.
Agfa-Gevaert Inc.
Teterboro, USA
Stotts, R. B.
Wolverine Tube
Dartmouth, Canada
Strader, L. B.
Rocketdyne
Canoga Park, USA
Strother, R. G.
Magnaflux Corporation
Chicago, USA
Stubbeman, A. W.
Almar-York Co. Inc.
Fort Worth, USA
Struminski, Prof. F.
Moscow Research Inst. of Introscopy, USSR
Suckow, R. G.
Symington Wayne Company
Depew, USA
Sulmont, Alain
Vallourec, Paris, France
Swedenborg, Hakan
Tekniska Rontgencentralen AB
Stockholm, Sweden
Sweeney, Robert J.
Irving Refining Ltd.
Saint John, Canada
Switucha, N. M.
Dept. of Industry,
Ottawa, Canada

T

Tada, Yoshiaki
Kyowa Electronic Inst. Co.
Tokyo, Japan
Tait, John
North American Inspection Serv.
Oakville, Canada
Tait, William H.
Dominion Foundries and Steel Ltd.
Hamilton, Canada
Takata, Saburo
Orenda Ltd.
Malton, Canada
Tardif, Dr. H. P.
C.A.R.D.E.
London, Eng.
Taylor, C. W.
Dosco Steel Ltd.
Sydney, Canada
Taylor, Edward H.
Canadian Pacific Rly.
Montreal, Canada
Tehon, S. W.
Tecumseh Products Co.
Ann Arbor, USA
Tenney, Gerold H.
University of California
Los Alamos, USA
Teres, J.
MAA, Air Force Materials Lab.
Wright Patterson Air Force Base
Ohio, USA
Thams, R. W.
Picker X-Ray Corp.
Cleveland, USA
Thomas, H. P.
X-PER-X Ltd.
Montreal, Canada
Thomas, W. E.
Magnaflux Corporation
Chicago, USA
Thome, Paul
Commissariat Energie Atomique
Yvette, France
Tillou, Jos. H.
Allis-Chalmers Atomic Energy Div.
Bethesda, USA
Titleman, Morton S.
Dominion Bridge Co.
Lachine, Canada
Tomlinson, Daniel W.
Eastman Kodak Co.
Rochester, USA
Trapp, W. J.
MAMD Air Force Materials Lab.
Wright Patterson Air Force Base
Ohio, USA
Treca, Maurice
Sud Aviation
Laboratoire Central
Courbevoie, France
Triller, J. M.
United Electric X-Ray Co.
Toronto, Canada
Trueman, G. F. R.
Rolls-Royce of Canada Ltd.
Montreal, Canada
Turner, R. P.
Magnaflux Corporation
Chicago, USA
Turner, Ralph E.
Eastman Kodak Company
Rochester, USA
Turnbull, K. L.
United Electric X-Ray Co. Ltd.
Toronto, Canada
Tuskey, John
Lake Ontario Steel Co.
Whitby, Canada
Tweedie, R. P.
Dominion Bridge Company
Montreal, Canada

V

Valade, (Ing.) J. P.
X-PER-X Ltd.
Montreal, Canada
Van Valkenburg, H. R.
Automation Industries Inc.
Danbury, USA
Van den Andel, J.
Canadian Westinghouse Co.
Hamilton, Canada
Vanderputten, Willem
Magnaflux Corporation
Chicago, USA
Vanier, Guy
Royal Canadian Air Force
Ottawa, Canada
Van Kirk, Keith
Magnaflux Corporation
Chicago, USA
Vareika, William E.
Gillette Safety Razor Co.
South Boston, USA
Vaupel, Prof. O.
Ihnestrasse, Germany
Vaupel, Mrs. Maria C.
Ihnestrasse, Germany
Vdovin, I.
Inst. of Metrology
Sverdlovsk, USSR
Veprek, Louis F.
Adv. Dev. Grumman Aircraft Co.
Bethpage, USA
Vezina, George E.
Canadian National Rlys. Co.
Montreal, Canada
Vicki, Frank J.
Pratt & Whitney Aircraft Co.
East Hartford, USA
Vriend, Jan
Canadian Arsenals Ltd.
Montreal, Canada
Vurpillot, Bernard
Laboratoires Ville Marie Inc.
Laval, Canada

W

Walker, Alfred
National Research Council
Ottawa, Canada
Walker, H. D.
Eastern Air Lines Inc.
Miami, USA
Walther, Karl G.
Krautkramer,
Cologne, Germany
Waltz, Marion D.
Youngstown Sheet & Tube Co.
Youngstown, USA
Wang, Shih-Ping
The Rauland Corp.
Niles, USA
Washburn, J. C.
Phillips Elect. Inst.
Mt. Vernon, USA
Watanabe, F. M.
Aluminum Co. of Canada Ltd.
Alma, Canada
Watterud, E. T.
Dept. Defence Production
Ottawa, Canada
Webborn, T. J. Haydn
The Unit Inspection Co. Ltd.
Swansea, S. Wales
Webster, R. R.
Jones & Laughlin Steel Corp.
Pittsburgh, USA

Weeber, Helmut
Max-Planck-institut
Dusseldorf, Germany
Weinbaum, Hillel
A. M. F. Tuboscope Inc.
Houston, USA
Weisner, L. W., Jr.
E. I. DuPont de Nemours & Co.
Aiken, USA
Wells, Dennis C.
Wells-Krautkramer Ltd.
Hertfordshire, Eng.
Wenk, Sam
Varian Co.
Palo Alto, USA
Wesanko, Morris W.
Canadian General Elect. Company
Peterboro, Canada
Whaley, Hubert L., Jr.
Union Carbide Co.
Oak Ridge, USA
White, LeRoy A.
American Oil Co.
Whiting, USA
Wildsmith, A.
Orenda Ltd.
Toronto Airport, Canada
Wilkins, R. W.
IBM Corporation
Oswego, USA
Wilkinson, P.
Orenda Ltd.
Toronto Airport, Canada
Willcox, D.
Rolls Royce of Canada Ltd.,
Montreal, Canada
Williams, E.
Babcock Wilcox & Goldie McCulloch
Galt, Canada
Williams, F. S.
M-7, Naval Air Engineering
Philadelphia, USA
Williamson, Alan
Via-U-Ray Ltd.
Waterloo, Canada
Wilson, Donald W.
Canadian Vickers Ltd.
Montreal, Canada
Wilson, Cdr. W. B.
RCN
Victoria, Canada
Winterton, Dr. K.
Dept. Energy, Mines and Resources
Ottawa, Canada
Wiskel, S. J.
Research Council of Alberta
Edmonton, Canada
Wloszek, Joseph
Cleveland, USA
Woodmansee, Wayne E.
Boeing Company
Seattle, USA
Wren, Howard D.
Armco Steel Corp.
Middletown, USA
Wunder, Dr. Charles J.
Milwaukee School of Eng.
Milwaukee, USA
Wyckoff, H. S.
Automation Industries Inc.
Danbury, USA
Wynsewski, Roy E.
Gen. Aniline & Film Corpn.
New York, USA

Y

Yamaguchi, Tomio
Mitsubishi Heavy Industries Ltd.
Kobe, Japan
Yamamoto, Miaki
Tokyo/Keikiseizosho
Otaku, Japan
Yeh, William C.
Calumet & Hecla Inc.
Calumet, USA
Yonsmitsu, I. D.
Canadian General Electric Co.
Peterborough, Canada
Yurick, Andrew N.
Mobil Oil Corporation
Paulsboro, USA

Z

Zakraysek, Louis
General Electric Co.
Syracuse, USA
Zettler, R. M.
Quebec North Shore and Labrador Rly.
Sept Iles, Canada
Zillman, Joachim
Materialprufung
Berlin, Germany
Zurbrick, John
Avco Space Systems Div.
Lowell, USA

Technical Session 1/ Evaluation of Material Quality

Advances in the Application of Nondestructive Testing to Cast Iron

A. G. FULLER, U.K.

ABSTRACT: The properties of cast irons used for most engineering purposes depend upon the form and amount of graphite in the casting and its matrix structure. For the routine inspection of the many thousands of castings used, reliable, easy to operate, nondestructive testing procedures are required. The British Cast Iron Research Association has been instrumental in developing resonant frequency methods of testing and demonstrating the application of established eddy-current procedures for these purposes. The application of these procedures and the development of suitable testing conditions are described and examples of typical foundry applications are illustrated.

Introduction

The function of engineering design is to devise and select methods of producing assemblies or components in such a way that while these components or assemblies will perform satisfactorily in service their production costs are minimized. This involves consideration of the selection of materials having suitable properties, the efficient use of this material and methods of forming this material to its required final shape. While the materials for producing some components are obvious, there are many cases in which more than one alternative method is feasible.

A casting has many advantages over fabrications, particularly where components are to be produced in appreciable quantities. These advantages stem from the general freedom in design available for castings, with a resultant efficient use of material and a reduction in the number of parts required to complete the assembly. Iron castings in particular may be economically produced by the use of simple melting processes to produce castings having a wide range of mechanical properties in combination with generally good machinability, while special properties such as heat, corrosion and abrasion resistance may be obtained by alloying. The extent of usage in engineering is reflected by the fact that in 1965 when the United Kingdom production of iron castings was about 4,000,000 tons, just over 24 per cent (1,000,000 tons) of the castings were used by the automobile industry alone.(1)

The cast irons most widely used for engineering purposes are of three types: grey (flake), nodular or malleable. During solidification of the flake and nodular graphite irons the eutectic is precipitated in the form of discreet grains containing austenite and graphite. These grains are referred to as eutectic cells. In grey irons the graphite is present as a network of interconnected flakes within each eutectic cell, whereas in nodular iron during the production of which the molten metal is treated with magnesium, the graphite is present as a spherulitic nodule at the centre of each eutectic cell. For a given matrix structure the tensile strength of both grey and nodular cast irons depends upon the form and amount of graphite. High-carbon, high-silicon irons containing large quantities of coarse graphite flakes have the lowest tensile strength, irons of lower carbon and silicon content contain less graphite which is, in itself, present as finer flakes, have higher tensile strengths, while changing the form of the graphite from flake to nodular results in a large increase in strength. Malleable cast irons are produced by the heat treatment of low-carbon, low-silicon irons which, when originally cast contain no graphite which has formed during solidification; instead, the carbon in solution is precipitated as iron carbide. Heat treatment breaks down the iron carbide to produce nodules of aggregated graphite.

The matrix structure of grey and nodular irons or the heat-treated white (malleable) irons may vary. Usually, in the as-cast condition flake and nodular graphite engineering irons have a substantially pearlitic matrix, while some malleable irons are heat-treated to give this structure. Pearlitic irons which have hardnesses ranging between 170 and 330 Brinell, depending on the fineness of the structure, have reasonable machinability combined with good wear resistance and strength, the machinability decreasing with increasing amount of pearlite and with increasing fineness of the structure (increasing hardness). Generally by the heat treatment of cast irons having other types of matrix structure, a ferritic matrix may be obtained. Irons with this type of matrix are softer (hardness between 100 and 150 Brinell) than the pearlitic irons, have a lower tensile strength for a given form and amount of graphite, but have improved ductility and machinability. Sorbitic, acicular or martensitic structures may also be obtained by heat treatment or by appropriate alloying, producing iron having hardnesses between 280 and 420 Brinell; provided that in these irons free carbides are not present, machining operations can be carried out without undue difficulty. The presence of free carbides, however, with hardnesses up to 800 DPN and above, even in small amounts, markedly reduce machinability and decrease tool life. This is particularly so if the carbides are present in a massive form.

Typical properties (2) of a number of cast irons used for engineering purposes, which show the influence of the form and amount of graphite and the matrix structure upon properties, are illustrated in Table 1.

In order to satisfy customers that castings do, in fact, have the required properties, foundries require nondestructive tests that will:

1. Assess the form and amount of graphite
2. Assess the matrix structure

With these tests available, the facility exists for the inspection, if required, of every casting, giving to the designer and user of iron castings confidence in the selection of the material for even the most arduous engineering applications.

Table 1

Type of Iron	Matrix	Mechanical Properties			
		Tensile Strength Tons/in²	Kg/mm²	Elongation per cent	Hardness BHN
High-carbon, coarse flake graphite	Pearlitic	11–13	17–21	<1	180–240
Lower carbon, fine flake graphite	Pearlitic	15–19	24–30	<1	190–250
Low-carbon, fine flake graphite	Acicular	23–28	36–44	<1	290–350
Nodular graphite	Pearlitic	40–48	63–76	3–4	240–290
Nodular graphite	Ferritic	24–32	38–50	8–25	130–170
Malleable	Pearlitic	28–38	44–60	4–10	150–240
Malleable	Ferritic	18–22	28–35	6–14	110–149

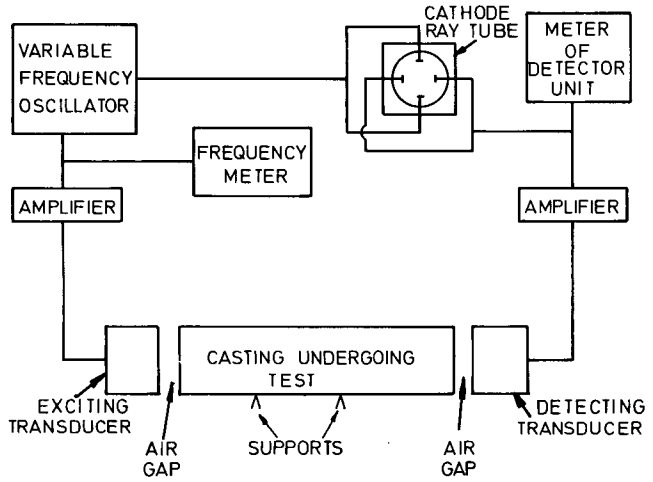

Figure 1. Block diagram of apparatus used for sonic testing.

Developments in the Testing of Cast Iron at BCIRA

Resonant Frequency Measurements

The principal features of the apparatus developed for resonant frequency measurements are shown in Figure 1. The output from the variable-frequency oscillator is fed to a transducer which converts the electrical energy from the oscillator to mechanical vibrations in a component under test. The component is supported near to the transducer on a rigid test bench. The frequency of the oscillator is adjusted and as it approaches resonant frequency the component will begin vibrating and may be heard to ring if the resonant frequency is within the audible range. When the frequency of the oscillator coincides with the resonant frequency, the amplitude of mechanical vibrations and noise emitted will be at maximum. Contact between a component to be tested must be reduced to a minimum to avoid the mass of the transducer affecting the resonant frequency. For metallic components electro-magnetic transducers may be used and an air gap left between the components and the transducers, thus overcoming problems of surface preparation. The amplitude of vibration in components being tested is measured using a detecting transducer, again separated from the casting by an air gap, this transducer being connected to a meter to indicate the amplitude of vibration and to a cathode ray tube to indicate the condition of resonance by the formation of Lissajous figures.

For most materials, including cast irons, the resonant frequency is well defined, making the test simple to operate. However, for any one material there are variations in the sharpness of its definition as the material and properties vary. This sharpness is a measure of the damping capacity of the material and may be used to demonstrate differences in the material structure and properties. Damping-capacity measurements are, however, very sensitive to extraneous noise and vibration and since in cast iron they provide no more information than can be obtained by resonant-frequency measurements, the use of damping capacity as a foundry control test has not been developed.

Castings of complex shape will resonate at a number of fundamental frequencies and their corresponding under- and overtones. These frequencies result from a combination of longitudinal flexural and torsional stresses in the vibrating casting. One fundamental frequency (as identified by the appearance of a single loop on the cathode ray screen) will be found at which the amplitude of vibration is much greater than at any of the other frequencies. This predominant fundamental resonant frequency is usually well separated from other resonant frequencies and is thus especially suited for use in assessing the graphite structure of the iron casting.

For flake and nodular graphite cast irons the relationship between graphite form and resonant frequency is illustrated in Figure 2. The casting having the best nodular graphite structure (top left) had the highest resonant frequency, while the casting having a flake graphite structure (bottom right) had the lowest resonant frequency. As the spheroidal form of the graphite degenerated towards a flake form the resonant frequency progressively decreased. The subtle difference in structure between those at the top left and top right is easily recognizable by sonic testing, since the resonant frequency of a casting may easily be measured with an accuracy of 1 part in 10,000. This application represents an important use of sonic testing in the foundry, namely the assessment of the perfection of the nodular graphite structure obtained in magnesium-treated irons, and this type of test may be carried out irrespective of the matrix structure of the cast iron, since no prediction of tensile strength, which the matrix also affects, is involved. When, however, the matrix structure remains consistent, that is, the castings are produced from similar charges and melted under similar conditions, sonic testing may be used as a method of predicting tensile strength, irrespective of whether the graphite is in a flake or nodular form. In order to do this a calibration curve must be constructed relating the resonant frequency of each type of casting with its tensile strength. This is done by measuring the resonant frequency of a large number of castings of this type, determining the range of variation in the predominant fundamental resonant frequency expected, selecting castings having resonant frequencies within the range and carrying out destructive tests in the critical regions of interest to the designer. When the calibration curve has been completed a minimum resonant frequency may be determined, below which the casting should not be accepted, as is illustrated by the curve for pearlitic nodular iron crankshafts shown in Figure 3. The

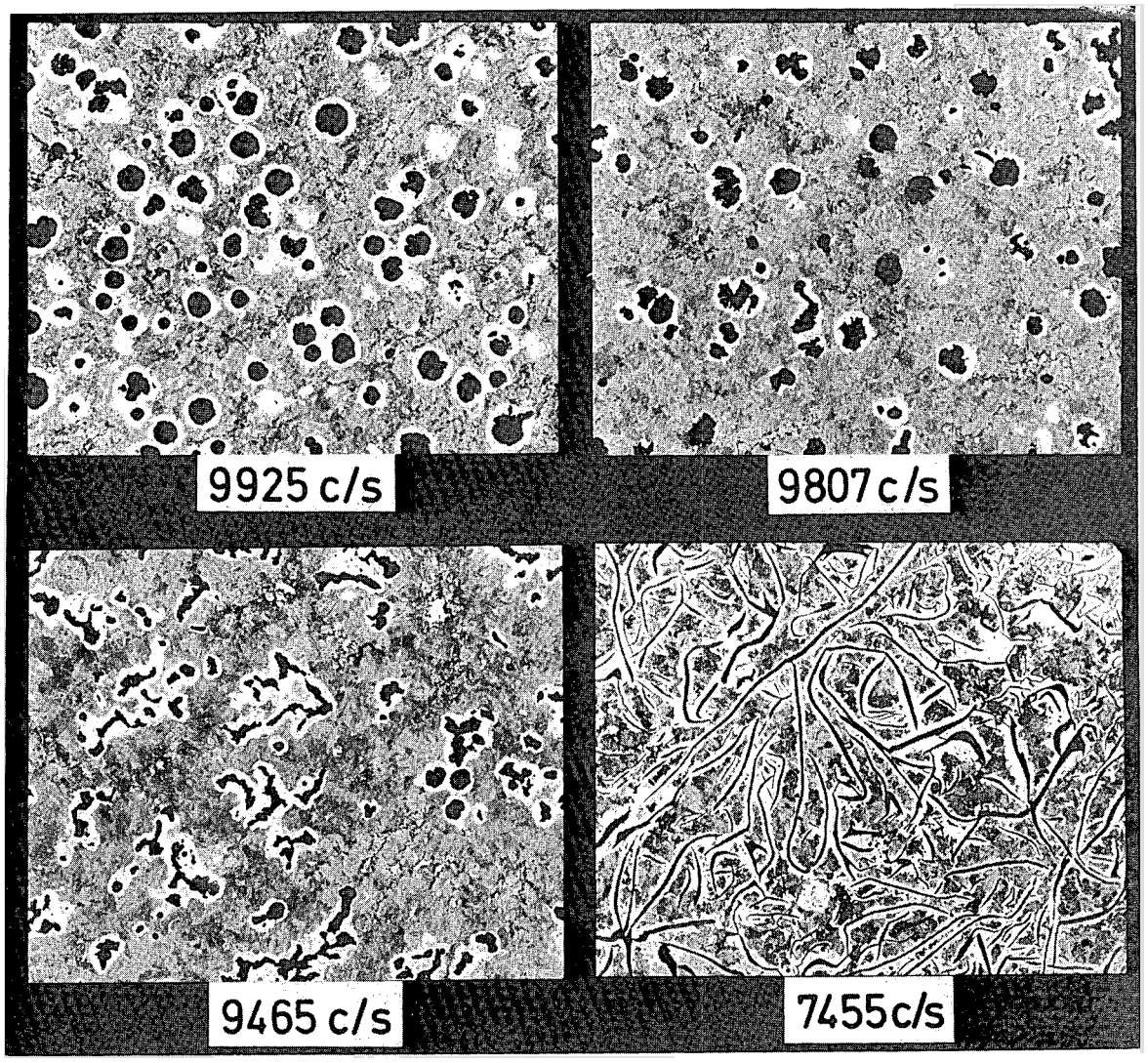

Figure 2. Variations in resonant frequency with changes in graphite form. Ref. PI/33/1/65. x 100. Etched 4 per cent Picral.

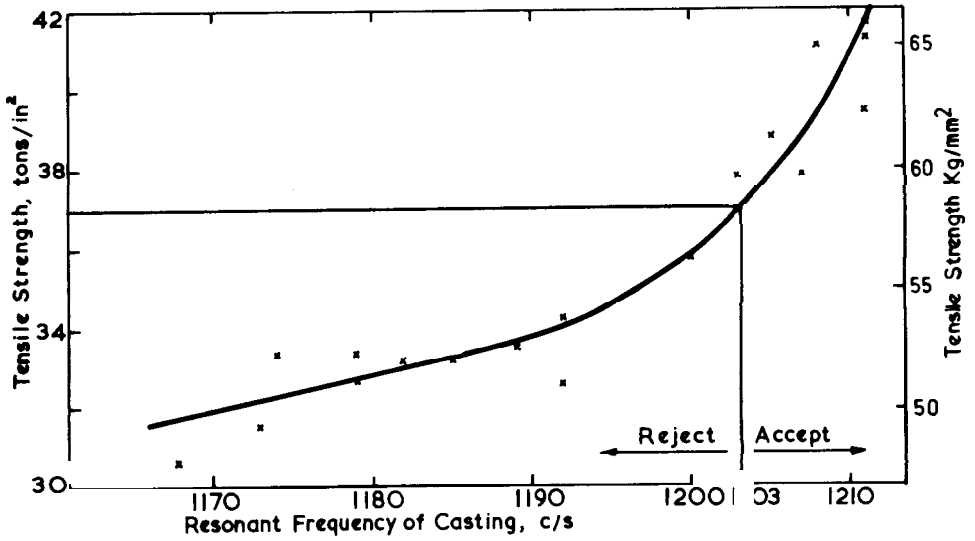

Figure 3. Relationship between resonant frequency and tensile strength for pearlitic nodular iron crankshafts.

accuracy with which the tensile strength may be predicted is ± 5 per cent of the tensile strength determined by conventional destructive methods. However, because of the need to construct calibration curves relating resonant frequency with tensile strength, sonic testing is applicable only when large numbers of castings of the same type have to be inspected. Where only a small number of castings are to be inspected, the cost of constructing calibration curves is not usually justified and in these circumstances ultrasonic-velocity measurements are most convenient, since a calibration curve relating velocity with tensile strength may be established using separately cast test bars, the final tests, of course, being carried out on the castings themselves. Often castings are subject to minor design changes to take account of modification in service conditions. Provided that these changes are small, it is usually unnecessary to construct a completely new calibration curve. An acceptable alternative is to produce at the same time a number of castings of both the old and new design and to reposition the calibration curve by an amount equal to the difference in resonant frequency between castings of the two designs.

The advantages of sonic testing over ultrasonic testing lie almost exclusively in its ease of operation. The separation of the castings from the transducers by an air gap, the size of which is not important, eliminates coupling problems. The apparatus itself is easy to use and well within the capability of an unskilled worker, who is required only to tune the oscillator until the casting resonates and then decide whether the frequency of resonance as recorded on a digital frequency meter exceeds the minimum specified. Furthermore, most castings are tested with their major axes between the transducers, so that the effect of variations in casting size is small, particularly in relation to the changes in resonant frequency which occur as a result of changes in graphite structure, while additionally the apparatus is flexible, being suitable for the inspection of castings ranging in size from 1 or 2 in. (25-50 mm) up to 20 ft (6,000 mm) and in type from circular discs such as clutch plates, to 6-cylinder diesel engine blocks.

Existing Nondestructive Testing Methods

It has long been known that changes in the form and amount of graphite in a cast iron will cause changes in the velocity of the propagation of ultrasonic energy through the casting, or in the attenuation of the ultrasonic energy in its passage through the casting. Both of these techniques have, in fact, been described in published papers (3,4) as nondestructive tests applicable in foundries for the assessment of casting quality, in which the tensile strength may be estimated to within ±5 per cent of the tensile strength determined by conventional destructive tests.

For the routine checking of a large number of castings the ultrasonic techniques do have disadvantages. For ease of operation, both velocity and attenuation methods depend upon the fact that two parallel surfaces on the casting can be found, one from which the ultrasonic energy can be transmitted and the other from which a well-defined reflection may be obtained. This limitation may make the application of these methods of testing difficult in the case of castings of complex design, where the need for testing may, in fact, be greatest. The use of couplants, either water or oil, will cause either rusting or staining of the casting surface. While in some cases this may not be important, unsightly stains or smears will, for other applications, render the casting unacceptable or require additional operations before painting or other surface treatment. Also to ensure good coupling some preparation of the casting surface may occasionally be necessary. If velocity measurements are used, the measured time for the travel of ultrasonic energy through the casting may have to be corrected for variations in casting dimension if these variations are large compared with the thickness of the section being tested. This may be particularly important in the testing of thin-section castings. If attenuation measurements are made by the simplest technique of measuring the height of the trace on the cathode ray screen representing the reflected energy, reproducibility in testing cannot be guaranteed unless the performance of all the probes and instruments used can be standardized, and will also vary significantly depending upon the efficiency of coupling between the probe and the casting. Jarvis (4) recognized the deficiency of attenuation measurements in this respect and developed a special testing system using concentrically arranged transmitting and receiving crystals in a probe coupled to a specially cast test bar through an oil column. A test on a separately cast bar is useful as an internal foundry control test, but is not a substitute for tests carried out on castings themselves. Finally, in order to obtain good results, ultrasonic testing requires the services of skilled operators, but the recruitment of suitable people for this purpose is not particularly easy, since technically trained personnel are reluctant to accept a job involving the routine testing of many thousands of components per week.

Ultrasonic testing does, however, have the advantage that due to the directional properties of the ultrasonic waves, testing may be carried out in a critical location specified by the designer and will, of course, as well as assessing the physical properties, indicate whether or not a defect is present within its location.

Hardness measurements have been and still are widely used for the assessment of matrix structure. There are, however, a number of disadvantages, perhaps the most important being the need to prepare a flat, ground surface on the casting before testing can be carried out. This is a time consuming operation which may also, in certain circumstances, render the casting unacceptable for further use. In this sense at least, hardness measurements do not constitute a completely nondestructive test. Furthermore, hardness testing itself is, even with the use of automatic hardness testing machines, a comparatively slow operation.

For the assessment of the form and amount of the graphite and the matrix structure, there was a clear need for the development of nondestructive testing which fulfilled the following conditions:

1. No surface preparation of castings is necessary and hence completely nondestructive
2. Insensitive to small changes in the dimensions of the castings
3. Rapid in operation
4. May be used on a routine basis by unskilled labour
5. Gives results of an acceptable standard of accuracy which are reproducible.

The British Cast Iron Research Association has developed tests suitable for both purposes, the form and amount of the graphite being assessed by resonant frequency measurements (sonic testing) and the matrix structure being assessed by eddy-current methods. The applications of these techniques are described below.

While for simplicity of operation, sonic testing is most useful for the prediction of the tensile strength of castings having similar matrix structures, where, in the as-cast condition the matrix structure contains varying proportions of ferrite and pearlite, it is still possible to assess directly the form and amount of the graphite present, but if it is also required to predict tensile strength, an additional measurement sensitive to changes in matrix structure must be made and a combination of resonant frequency and the secondary measurement used in

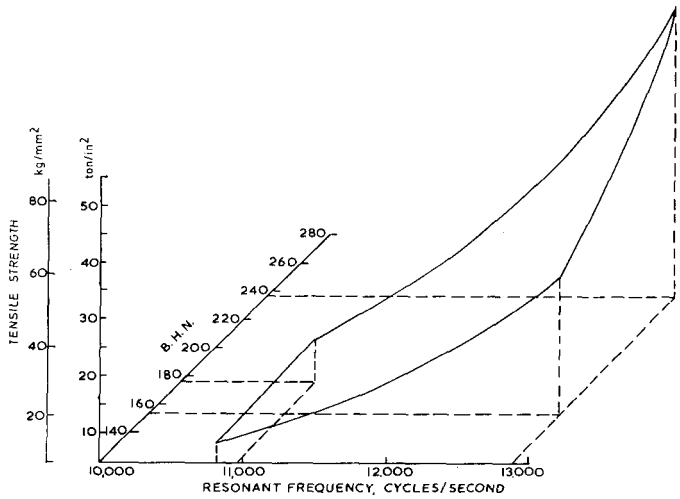

Figure 4. Variation of tensile strength with Brinell hardness and graphite (form in terms of resonant frequency).

predicting tensile strength. In practice, hardness measurements fulfil the purposes of the secondary measurement and three-dimensional calibration curves may then be constructed (Figure 4), which may be reduced to a nomogram form for routine control purposes.

For internal foundry control purposes a useful extension of sonic testing procedures is the development of a simple test bar(5) which may be removed from the mould 15 minutes after casting and sonically tested after removal of the gating system used to fill the casting. The bar may then be tested without any further preparation, e.g. shotblasting or grinding, so that within 20 minutes an estimate of the quality of the metal used to produce the castings will have been obtained. This is not sufficiently rapid to prevent the pouring of unsatisfactory metal, but at least action can quickly be taken both to restore control of the melting process and to segregate castings of unsatisfactory quality so that no further additional money is spent in preparing them for sale.

Eddy-Current Testing

While the work carried out by the BCIRA on sonic testing represents the development of a completely new method of testing for determining the properties of cast irons, in the following section the work of BCIRA in the field of eddy-current testing has involved the evaluation of well established procedures using commercially available equipment to provide knowledge of the conditions under which eddy-current-testing procedures may be used for the evaluation of the matrix structure. This work has formed the background to the successful application of eddy-current-testing procedures for this purpose in many foundries in the United Kingdom.

While a substantial proportion of the flake and nodular graphite irons are required to be pearlitic, a considerable proportion of malleable irons are required to be substantially ferritic. Malleable iron castings are usually comparatively small components used in considerable numbers in automobile manufacture, where high-speed machining is of great importance. In substantially pearlitic malleable irons the maintenance of the optimum ferrite-pearlite ratio is desirable in order to obtain the correct properties and machining characteristics, whereas in ferritic malleable iron, the presence of pearlite, particularly as a rim on the outside of the castings, while not seriously impairing the mechanical properties of the whole casting, will cause considerable machining difficulties. The BCIRA therefore undertook to investigate the use of eddy-current-testing procedures primarily as a technique to differentiate between ferrite and pearlite or to measure the ferrite-pearlite ratio.

With any graphite type, variation in remnant magnetism between ferritic and pearlitic structures is small and in no way consistent. The electrical resistivity of ferritic structures is always less than that of pearlitic structures but only by a small margin. The coercive force of ferritic structures is, however, always about one-third of that of pearlitic structures, while the maximum permeability of ferritic structures is about three times higher than that of pearlitic structures. Thus measurements of coercive force or maximum permeability were considered to be the most suitable for the development of an eddy-current-testing procedure.

Variations in coercive force show as a change in phase of the cyclic signal on the cathode ray tube display of eddy-current-testing apparatus and changes in permeability which cause changes in induction show as variations in amplitude. Instrumentally it is much more convenient to measure changes in amplitude than changes in phase, so that sorting is most conveniently done by measurement of amplitude and by implication of permeability. However, because permeability changes with field strength and since the permeability of ferrite is higher than that of pearlite by a factor of three at low field stengths but only by a small amount at high field strengths (6) ideally, conditions of testing require a measurement of permeability at low field strengths.

Using a Magnatest QP3/203 instrument operating with a magnetizing field frequency of 10 cycles/sec, BCIRA have demonstrated the sensitivity of the instrument in separating structures over the range from fully ferritic to martensitic, produced by heat treating a series of castings of similar analysis. To obtain all these results on one span of the cathode ray tube, gain levels were set very low; under normal use higher gain levels would have been set to obtain greater speed over the hardness range being investigated. The results shown in Figure 5 revealed a continuous variation of test indication from those obtained with a soft ferritic structure to those of an unannealed white iron. This would be expected from considerations of the metallurgy of the matrix since the change from ferritic to an unannealed white iron structure is a reflection of the amount of cementite (iron carbide) in the matrix, either as free carbide or combined with ferrite in pearlite. The curve from the white iron to the martensitic structure is not necessarily continuous because of the basic change of structure and insufficient results are available to be sure on this point which, for practical purposes, is at present of no great importance.

Changes in the chemical composition of the iron will affect the relationship between hardness and the eddy-current indication. However, the effects of changes in carbon and manganese content could be ignored for practical purposes, but changes in silicon content could alter the readings considerably. This was not unexpected since it is well known that the presence of silicon in ferro-magnetic materials has a considerable effect upon their magnetic properties. These effects were, however, observed at low magnetic field strengths. At high magnetic field strengths changes in carbon content could be expected to affect the eddy-current indication as a result of the effect of graphite on the saturation induction and manganese would be expected to have an effect similar to silicon.

Variations in casting dimensions will also influence the eddy-current indication, this effect being most pronounced in the case of small castings lying wholly within the coil system. Variations in the size of the casting affect the distance between the casting and the coil and hence the magnetic coupling between the two, while variations in the length of the casting in the axial plane of the coil alter the air-path length of the magnetic

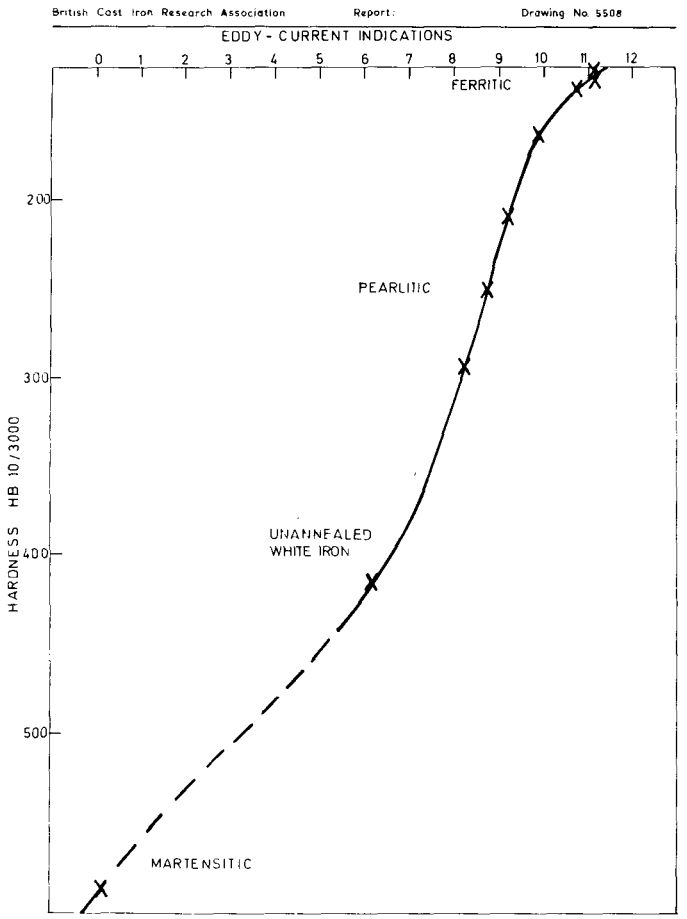

Figure 5. Eddy-current-test indications with varying matrix structure.

field and hence the magnetic induction obtained in the casting. These effects may be minimized by making the axial length of the coil small compared to the axial length of the casting, the diameter of the coil $1\frac{1}{2}$ to 2 times the diameter of the casting, when the casting may be considered as a disc in the plane of the coil, by arranging the testing system so that the parts of the casting least likely to be dimensionally inaccurate are in the magnetic field, and by jigging the castings so that they always occupy the same position relative to the magnetic field. When using hand probes placed against the casting for the inspection of large castings as opposed to the coil system described, the distance between the hand probe and the casting and the location of the hand probe must be kept constant.

Alternating magnetic fields do not penetrate deeply into ferro-magnetic materials since the outer layers screen the inner layers and prevent the magnetic field from building up. The depth of penetration is not a discreet value since the magnetic field does not have an absolute value at one internal layer and a zero value slightly farther on. However, the fact that the magnetic field is not uniform over a cross-section of the test-piece shows that eddy-current testing gives a greater indication of the magnetic properties of the outer layers of the test-piece than of the inner. Experimental measurements, however, suggest that at a testing frequency of 10 c/s material at a greater depth than 0.3 in. has little effect on eddy-current indication, while at frequency of 50 c/s the corresponding depth is of the order of 0.1 in. Eddy-current testing is, therefore, essentially a test on the surface properties of castings; since, however, machining usually only involves the removal of metal from the surface of castings this feature is not a serious disadvantage.

Tests on commercial castings heat treated to various hardness levels have shown that eddy-current testing is a good indication of the hardness of the castings, the accuracy being obtained at a field strength of 12 oersteds, being ± 10 points Brinell in the range of hardness 180 to 300 BHN (Figure 6). In practice, foundries using eddy-current-testing apparatus for the assessment of matrix structure usually find that its advantage lies in its speed of operation and absence of casting preparation necessary compared with conventional hardness testing. The speed that can be achieved, of course, depends on the mechanical handling of castings and then in order to use the full potential of the technique automatic sorting gates are incorporated, these gates being triggered by electronic sensing systems working from the cathode ray tube display. Such systems are in use in malleable iron foundries in the United Kingdom.

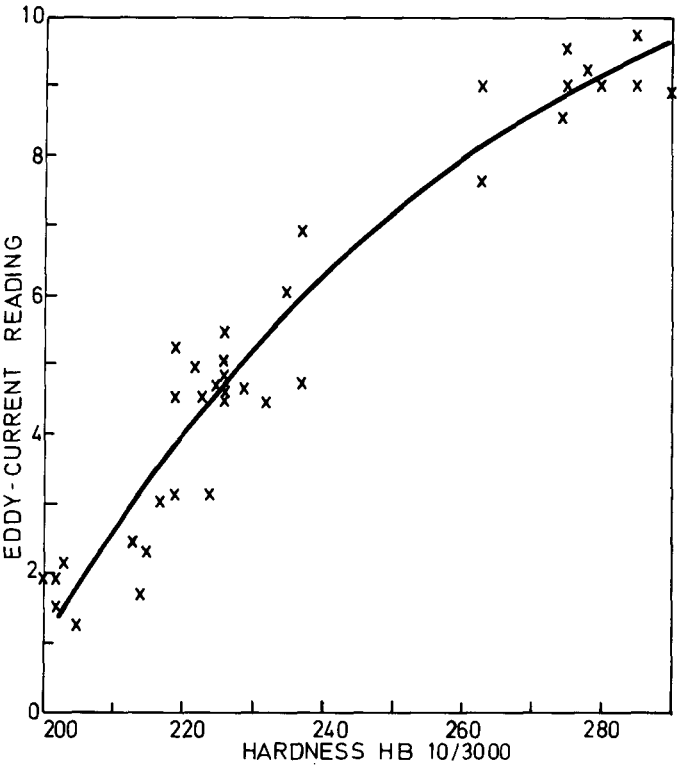

Figure 6. Eddy-current reading vs. hardness.

Because high testing rates are one of the main attractions of eddy-current testing and because a calibration curve must be produced for each type of casting to be inspected, eddy-current-testing systems are most suitable when many components of the same design have to be tested. To produce a calibration curve, readings are taken on a number of castings and destructive tests done on samples covering the range of reading obtained. Such castings can then not be used for further setting of the range since the removal of the surface for Brinell reading necessarily changes the shape of the casting and if this occurs in an area in which eddy currents circulate the reading will be altered.

Summary

This paper describes developments by the British Cast Iron Research Association applicable particularly to the testing of large numbers of iron castings of similar design. Sonic testing used to assess graphite form and amount, is an easily operated nondestructive test which, by the construction of calibration curves may be used to predict, under specified conditions, the tensile strength of castings to within ± 5 per cent of their tensile

strength determined by conventional destructive methods. Eddy-current testing may be used as a replacement for hardness testing as a control procedure in the foundry industry for assessing the matrix structure of castings and is particularly useful when a mechanical handling system is used to take advantage of the high potential testing speed of the eddy-current apparatus, and when an accuracy of ± 10 points Brinell is acceptable.

These techniques are two of a number available to the inspection department of foundries to ensure that their products conform to the customer's specification. The quality of iron castings supplied to the customer is by no means dependent solely upon nondestructive tests carried out on finished castings. Throughout each stage of the production process, other control tests are applied to the sand used for producing moulds and to the metal as it is melted and before it is cast. In the commonly accepted connotation of the words 'nondestructive testing', these tests are often overlooked since they do not apply to the finished product. However, in combination with the developments described in this paper, founders are able to operate a complete quality-control system for all grades of cast iron. This is reflected by the increasing use of castings as replacements for fabrications and forgings, e.g. the use of nodular iron automobile crankshafts.

Acknowledgment

The author wishes to thank the Director and Council of the British Cast Iron Research Association for permission to publish this paper.

References

(1) *Foundry Trade Journal,* 1966, v. 120, March 3rd, pp 294.
(2) Angus, H. T. Physical and engineering properties of cast iron, 1960, B.C.I.R.A. Alvechurch, Birmingham, pp 44-53.
(3) Ziegler, R. and Gerstner, R. Giesserie, 1958, v. 45, April 10th pp 185-193.
(4) Jarvis, J. A. F. Proc. 4th Internat. Conf. on Nondestructive Testing, 1964, Butterworths London, pp 173-175.
(5) Lovett, R. R. and Carter, N. *British Foundryman,* 1965, v. 58, March, pp 77-82.
(6) Hillman, M. H. BCIRA *J. Res. and Devel.* 1954, v. 5, April pp 188-248.

The Evaluation of Small Surface Laps in Aluminium Alloy Die Forgings

J. G. HARRIS, U.K.

ABSTRACT: Surface laps, or folds, form during forging due to local metal-flow conditions. In certain circumstances, components can be used containing laps, if they can be evaluated. To determine the effectiveness of evaluation by red dye penetrant, forgings of one type which exhibited small laps, were examined by an eddy-current crack-depth instrument and ultrasonic surface waves, followed by cut-up testing.

Consideration of the results from ten laps showed the limitations of the methods. The red dye penetrant test showed up open deep laps but not open shallow ones with constricted laps running from them. The eddy-current crack-depth meter indicated laps with a minimum, maximum depth of about 0.02 in. (0.5 mm). Surface-wave ultrasonic testing revealed the lap length along the surface and in the forging, and a simulative standard test block was developed.

By using the results from the surface-wave ultrasonic and eddy-current testing in terms of the cut-up test results, it is possible, with limitations, to evaluate a lap.

Introduction

Die forgings are usually made into highly stressed components which use the forged structure to maximum advantage. Light alloy forgings are of particular value in the aero space field of application. During the manufacture of the actual component, the forged surface is often machined away and with it go small surface laps. Sometimes the forged surface is used but a blemish-free surface is required, so careful cleaning and polishing procedures are employed to prepare the surface. This is then followed by careful inspection to ensure that the surface is satisfactory. In the case under consideration, advantage is taken of the forged shape to obtain an efficient design without the high cost of elaborate machining in a part of the component which is highly stressed but which will tolerate small forging laps. Single forged components can contain areas of all three categories and, even when blemishes are to be removed by localized polishing, it is often an advantage to be able to evaluate the laps before deciding upon the mode and degree of dressing. This can save the necessity of repeated polishing and inspection to determine if the lap has been removed. In practice the performance of forged components is proved first by static and dynamic tests simulating service conditions and then by subsequent service with the periodic inspection.

The forging laps, which are surface folds, are due to several causes. Damage originating at a previous stage of manufacture—perhaps from a forging tool—is forged over and causes a fold. This type of lap can be random from random damage, but the process may regularly cause surface damage in a certain region. The blank which is die forged may, itself, have been previously forged or it may be a piece of cast, rolled or extruded material. The forging is carried out hot and the metal flow in the die is likely to be influenced by the local surface conditions which, in turn, are influenced by blank shape, position in the die, die roughness and lubricant conditions. This means that in practice, sometimes the metal finds it easier to flow locally in from the surface rather than to flow along the die surface, and this usually occurs in certain areas in the forging, depending upon shape.

Procedures are adopted to minimize the lap formation, but with many forgings it is impossible to avoid them completely and where the final forged shape is to be used on the component, they may have to be removed or, at least controlled. Before their removal, the laps have to be detected and then it is often impractical to remove them mechanically from the final die forging, as the component would become too small in size. Control is exercised by not completely die forging, inspecting for laps, polishing them out and then finally die forging. As this operation does not move much metal, the severity of any laps formed on this last stage is limited and if any occur, they are more likely to be removable with light polishing. As forged, the surface is obscured by surface

oxidation and burnt-on lubricant and this is removed by pickling with a 10% sulphuric acid and 1% sodium fluoride solution. At this stage, some evidence of laps can be seen visually as lines and roughness but there is little guide to the severity. There are various nondestructive methods available to help in their detection and possibly in their evaluation. There is little evidence available on what, in practice these methods will detect, so an investigation was carried out evaluating defects followed by cut-up tests.

Investigation

The nondestructive methods available for detection of defects and for assessment were penetrant tests, ultrasonic surface wave examination, and the use of an eddy-current instrument which indicates crack depth. The forgings selected for examination were about 20 in. (50 cm) in diameter and contained a series of deep radial recesses as shown in Figure 1A. The laps form towards the base of the slope where the surface metal tends to flow into the forgings rather than along the surface. The visible effect after pickling, is shown in Figure 1B.

Three pickled Duralumin forgings were selected from a batch, a commercial red dye water-washable penetrant to DTD.929 was applied to the surface by hand and left for twenty minutes. This was then removed by spray rinsing with water and dried with compressed air. A light film of developer was applied to the surface and left to stand for up to twenty-four hours. Some of the laps in the recesses or pockets were revealed by red dye seepage and the length of the seepage was noted.

Next, a commercial eddy-current instrument was used to evaluate the laps in the pockets. This instrument operates at a frequency of around 0.5 MHz with a small hand-held test probe. Lift-off effects on a curved surface can be phased out and the instrument indicates on a meter the depth of a crack. The meter calibration was known by comparison with, and from experience of, the depth of normal to the surface fatigue cracks. The instrument remained in balance on curved surfaces but near the pocket sides, the light alloy sides influenced the probe, causing an unbalance and deflection of the meter and this prevented complete lap evaluation. The pockets were examined for maximum defect indication in terms of the maximum meter signal, and for indication of length of defect along the surface.

The pockets were then examined by ultrasonic surface waves using commercial equipment with a miniature probe ⅞ in. (22 mm) × 0.6 in. (15 mm) at a frequency of 4 MHz. The equipment used was one which had an amplifier with a reasonably linear response. Oil was used as a couplant but care was taken to avoid oil in front of the probe which would have absorbed and reflected some of the ultra sound. The instrument was standardized on a defective sample kept for the purpose. The probe directed towards the rim was moved across the pockets and angled for maximum defect signal. The defect length along the surface was assessed by measuring the distance between the position of the probe centre line at positions just either side of the defect which did not produce a defect signal.

Lastly, ten defects were selected and sectioned. Micro sections were examined and drawings made of the defects revealed. The micro sections were machined away on a lathe and the

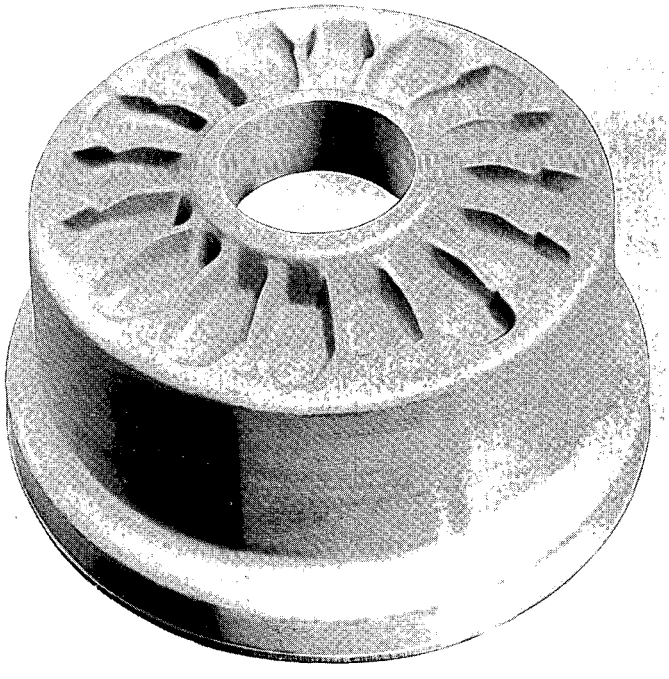

Figure 1A. General view of forging, showing recesses.

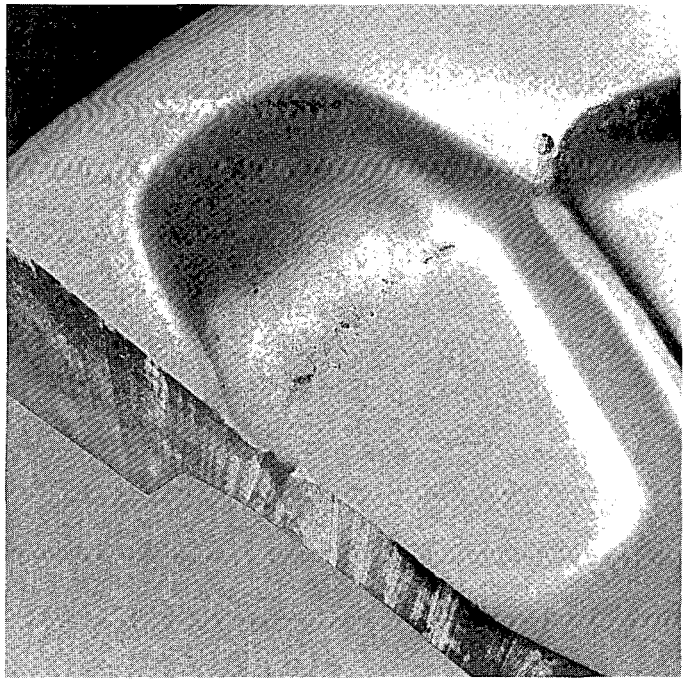

Figure 1B. Appearance of the lap in the surface of the recess after pickling.

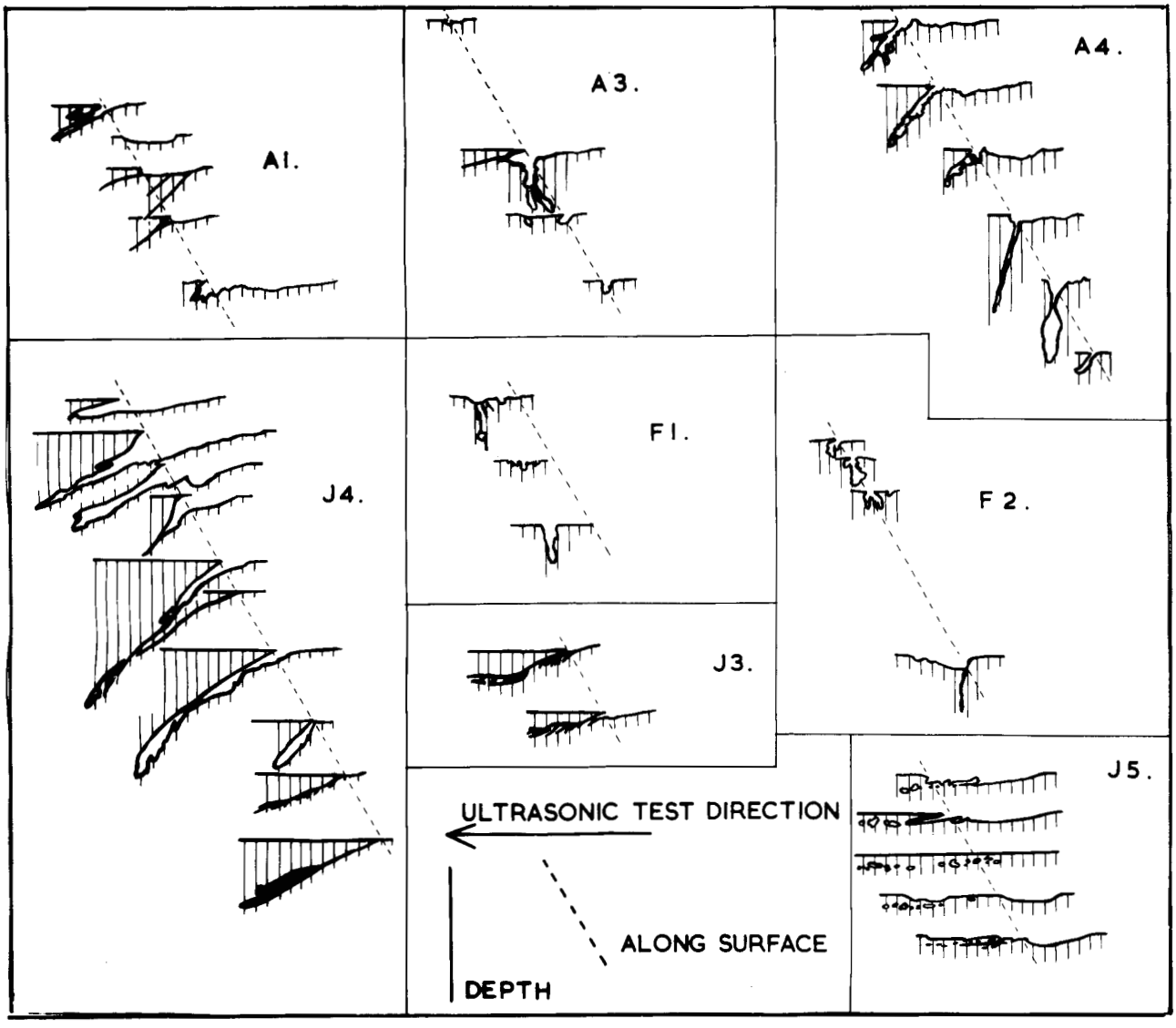

Figure 2. Isometric view of laps. Magnification X 16.

sections polished, etched, examined and drawn every 1/16 in. (1.6 mm). The results were combined and drawn on isometric graph paper and are shown in Figure 2. It will be seen that the laps revealed were most irregular in shape, angle and dimensions. The laps generally sloped away from the surface in the direction of the ultrasonic test. The lap in the first one sectioned was not discovered as it was not wide and a satisfactory preparatory technique had not been developed, and in another it was not clear whether the lap had been found or whether the evidence had been confused with a damage mark but again, it was one of little width.

The results of all the tests are summarized in Table 1 which lists the maximum indications and sizes.

Consideration of Results

Penetrant Tests

Red dye penetrant tests clearly showed two of the defects as lines. These were the defects that were open about 0.004 in. (0.1 mm) and were at least 0.02 in. (0.5 mm) deep. Three others showed seepage spots but two of these had open parts of some depth while the third was a tight lap except near the surface, where it was about 0.002 in. (0.05 mm) wide and 0.004 in. (0.1 mm) deep. Three of the defects which did not reveal seepage, tended to be open and shallow with tight or constricted laps running from them. Lap (A4) 0.036 in. (0.91 mm) deep and 7/16 in. (11 mm) along the surface was not detected by this means and thus shows the limitations of the process as an aid in indicating which pockets need polishing before final die forging, or as a means of evaluation of the finally forged surface.

The penetrant testing was a standard process carried out under works conditions and is probably capable of improvement. There is a need to study the performance of various penetrants using different test conditions on the shop floor to obtain optimum performance.

Table 1

Forging and No.	Penetrant	Eddy Current		Ultrasonic		Size from Sections			
		Max. Signal	Surface Length	Max. Signal	Surface Length	Max. Depth	Max. Internal Length	Surface Length	Angle
A1	3 small spots	2		4	1″ (25 mm)	0.021″ (0.53 mm)	0.028″ (0.71 mm)	0.5″ (13 mm)	30/45°
A2	nil	nil		3.8	¼″ (6 mm)	Damage and a small lap.		0.003″ (0.08 mm)	
A3	¼″ line (6 mm)	2		5	⅞″ (22 mm)	0.024″ (0.61 mm)	0.029″ (0.74 mm)	0.31″ (8 mm)	15/90°
A4	nil	10	½″ (13 mm)	7	⅝″ (16 mm)	0.036″ (0.91 mm)	0.036″ (0.91 mm)	0.44″ (11 mm)	50–(80°)
F1	nil	2		4	¾″ (19 mm)	0.021″ (0.53 mm)	0.021″ (0.53 mm)	0.31″ (8 mm)	90°
F1X	nil	nil		3	¼″ (6 mm)	not found			
F2	3 spots	2		3	1¼″ (32 mm)	0.021″ (0.53 mm)	0.021″ (0.53 mm)	1″ (25 mm)	85°
J3	3 small spots	nil		4.5	½″ (13 mm)	0.013″ (0.33 mm)	0.038″ (0.96 mm)	0.19″ (5 mm)	20°
J4	1½″ line (38 mm)	5		8	2″ (50 mm)	0.048″ (1.22 mm)	0.071″ (1.8 mm)	1.5″ (38 mm)	25°
J5	nil	nil		4.2	½″ (13 mm)	0.004″ (0.10 mm)	0.024″ (0.61 mm)	0.12″ (3 mm)	15°

Eddy-Current Test

The eddy-current inspection was carried out at a frequency of about 0.5 MHz. The probe was circular and had a spread with a reduction to about half signal strength of about ± 0.04 in. (1 mm). Maximum signal was obtained when the lap was along a probe diameter. The probe presumably produces a flux normal to the surface in the material under test and the eddy-current flow is disturbed by the lap surfaces. The lap has greater influence on the probe and hence the instrument reading, the deeper it penetrates and, for a given length, the more normal to the surface it lies. The more acute the lap is to the surface, the less disturbance there is, presumably, to the eddy-current flow. The largest value of the lap length multiplied by the sine of its angle at the surface, obtained from the cut-up tests, is plotted against maximum meter reading in Figure 3. As the instrument was working at maximum sensitivity the figure indicates that it cannot detect laps below about 0.018 in. (0.46 mm) deep even when they are normal to the surface. The slope of the response line was similar to that expected from normal-to-the-surface fatigue cracks. The maximum lap length multiplied by the sine of the angle to the surface is not necessarily the same as the maximum depth, as the lap can change angle in the metal and the longer the lap in the metal, the more likely this is to occur.

To confirm the effect of lap length on the instrument response, simulative test blocks were prepared. Slots 0.014 in. (0.35 mm) wide were sawn into blocks of aluminium alloy. The blocks were heated and then squeezed so that the slots were closed. The blocks were then machined down so that the defects were of the required depth. The surface was finally prepared by

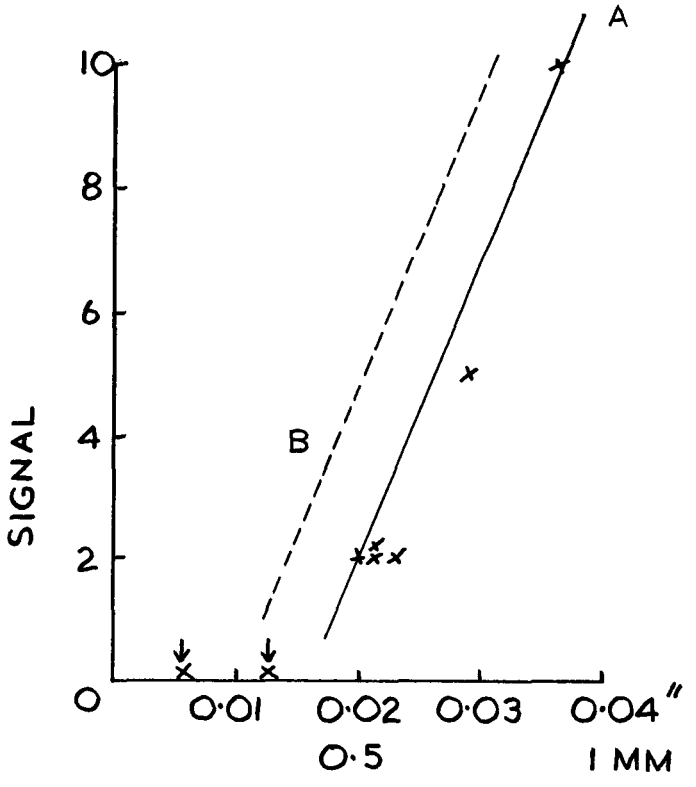

Figure 3. Eddy-current test results. Line A—relates lap length in the component multiplied by sine of the angle to the surface at the surface, with meter reading. Line B—relates length of normal to the surface "defects" in test blocks, with meter reading.

hand grinding, with graded silicon-carbide and then the blocks were solution-treated by heating at their solution-treatment temperature and quenching in cold water. This procedure seemed to yield a consistent response. The compressional surface residual stresses induced by quenching no doubt tended to keep the "defect" closed.

The results from the blocks with normal-to-the-surface "defects" confirmed that the instrument meter reading increased largely linearly with defect depth and that it increased from zero to a maximum of 10 with an increase in depth of about 0.020 in. (0.5 mm). Although the same sort of response was obtained from the simulative test blocks as the actual laps described, the actual meter readings were greater from the former as also were meter readings from fatigue cracks. This means that the laps were longer than originally estimated, rather like discontinuities detected by longitudinal ultrasonic waves which are usually larger than estimated by comparison with flat bottomed holes drilled in test blocks. The eddy-current-instrument meter reading increased for a given size of "defect" with increase in conductivity of the material and as this varies with alloy and heat-treatment condition, it is important to bear this in mind when making comparisons. There was an effect of surface shape, which was small with a concave surface of 6 in. (15.5 cm) diam and with a convex surface of 4 in. (10 cm) diam but with more concave surfaces there is more surrounding metal and the lap has less influence on the probe. With a concave surface of 1 in. (25 mm) diam which is similar to the forging under consideration, the signal was reduced by 30%. Tests with test blocks spaced apart with feeler gauges indicated that the meter reading decreased with increase in gap width. The signal had fallen to half with a gap of about 0.04 in. (1 mm) so a gap of a few 0.001 in. (0.025 mm) had only a small effect. An attempt was made to demonstrate the effect angle of "defects" using simulative test blocks of the type described but this was unsuccessful using this equipment. With another similar eddy-current instrument indicating conductivity operating at a lower frequency and with a larger diameter probe, the signal, expressed as a charge in conductivity due to the presence of a discontinuity, was found to vary with "defect" length multiplied by the sine of the angle to the surface.

Simulative test blocks are of use in checking instrument performance and in setting the controls to obtain a consistent response.

Due to the lack of sensitivity in the tests, the instrument did not perform well on estimating the length of the laps along the surface. The narrow ones measuring less than 0.2 in. (0.51 mm) along the surface were not detected at all and only in the case of the lap which gave a full-scale signal, did it provide good agreement with the determined size. The probe was influenced by the side walls of the pockets, which caused an unbalance and a meter deflection. This effect could probably be reduced by using a probe with improved screening.

Ultrasonic Tests

Ultrasonic examination at 4 MHz revealed a defect in all ten pieces. A variety of signal heights were obtained and the lengths of the laps along the surface were estimated. The surface waves were able to detect the laps even when they occurred near the pocket wall. The ultrasonic test overestimated the lap length along the surface compared with the length found in the cut-up tests, which, due to the difficulty of determining the end of the defect, probably underestimated the true length. The difference was generally 0.3 in. (0.76 mm).

Ultrasonic surface-wave inspection is sensitive to surface defects and is of considerable help in their detection but it was not known to what extent the quantitative information obtained would be useful. Work with standard blocks consisting of plates with machined grooves across their surfaces did not look promising. With the grooves normal to, and sloping away in the direction of, the ultrasonic wave, the defect signal height increased with the depth of the groove until it was half a wave length deep, then it decreased to an amount depending upon the groove angle, as shown in Figure 4A. The peak was reduced and broadened by roughening the groove surface and there was a tendency for the signal to increase slightly again with increases in groove depth. The effect was explained by the ultra sound being reflected at the groove barrier when it was a proportion of the wave length; the larger the barrier, the more was reflected and the bigger the signal. As the groove became longer, some of the ultra sound travelled along it and the signal height was primarily controlled by the angle of the sharp corner. The larger the angle to the surface, the larger the signal as more was reflected and less travelled along the groove (Figure 4B).

The results from test blocks indicated that at a test frequency of 4 MHz, a sloping defect 0.01 in. (0.25 mm) long in the component would be indicated by a larger signal than from one 0.02 in. (0.5 mm) long in the component and that for defects longer than 0.02 in. (0.5 mm), the signal height would be largely dependent upon angle and not on its length. This was not borne out in practice and the maximum ultrasonic signal was found to vary substantially with the maximum lap length in the component, and to be largely independent of angle, as shown in Figure 5. It was concluded that there was not a sharp corner to produce a signal and that the signal was being produced by the roughness of the lap; the longer the lap was, the greater the roughness and the greater the signal. The effect can be demonstrated by machining 0.001 in. (0.025 mm) deep, 45° grooves adjacent to one another on a plate surface. The signal height increases with the number of grooves.

This work suggested the construction of a simulative test block. Test blocks used for surface-wave work often contain slots and in use, the edges become damaged, coated with oil and dirty and this affects the signal. It was decided to coat the test block containing the 0.001 in. (0.025 mm) grooves with epoxy resin. This was done and at first the layer of resin absorbed much of the ultra sound, so it was polished down to reduce its thickness until a signal of the required height was obtained from the grooves. In practice one groove is sufficient. The resin protects it and prevents contamination by oil and dirt.

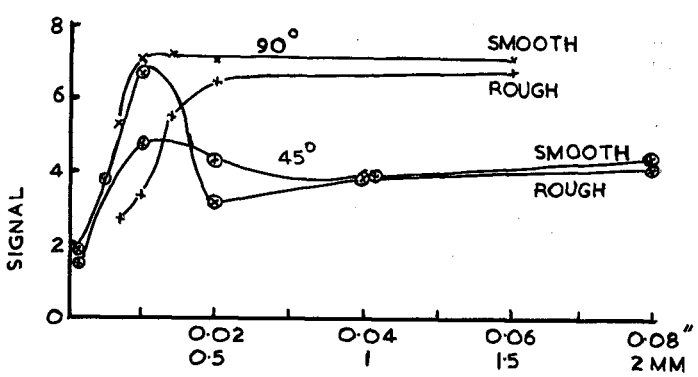

Figure 4A. Ultrasonic surface-wave test at 4 MHz relating ultrasonic signal height with the length of the groove machined into the test blocks. This length is the length of the groove face from the surface.

Ultrasonic surface-wave testing indicates the lap length in the component substantially independent of the angle. If a sharp corner does occur, a signal from this will contribute to that from the lap and its length will be overestimated. This errs on the side of safety. The signal was not influenced by the length of the lap along the surface, owing to the narrowness of the beam. The laps would be expected to be longer along the surface compared with the maximum length found in the component, and sectioning revealed ratios of between 5:1 and 48:1; most of them being in the range 11:1 to 22:1. The longest lap in the component was found to be 0.071 in. (1.8 mm). The smallest length of lap in the component that can be detected depends upon the instrument sensitivity setting, but if this is too high minor surface imperfections are detected. Laps 0.01 in. (0.25 mm) long or less in the component and $\frac{1}{4}$ in. (6 mm) along the surface can be detected if required.

General Consideration

In deciding whether the component which contains laps is acceptable, it is necessary to know the lap length, angle in the component, depth and its surface length. The long lap normal to the surface is likely to be more dangerous than one at an acute angle to the surface. Using the experimentally determined results an evaluation is possible. The ultrasonic test assesses the length of the lap on the surface and the length in the component, and this is followed by the eddy-current test. Thus, if a lap is long on the ultrasonic test and yet reacts as a shallow one on the eddy-current test, then the long lap is at an acute angle to the surface. The sizes can be estimated using the experimentally determined information in Figures 3 and 5. Table 2 compares the estimated values with the measured values.

The ultrasonic estimate of length from the graph was within about ± 10% of that measured with the exception of lap A4, which was considerably overestimated. The eddy-current estimates from the graph of length multiplied by the sine of the angle to the surfaces was within ± 3% of that measured. Owing to these inaccuracies the angle was not estimated well, particularly at large angles to the surface when a small variation of length multiplied by the sine of the angle is equivalent to a disproportionate variation in angle. The results at less than 40° appeared better but the result for lap A3 is misleading because the lap consisted of two parts, one at a large angle and the other at a small angle. It would appear, however, that when the eddy-current indication is small compared with the ultrasonic indication then the lap is at a small angle to the surface. The maximum lap length multiplied by the sine of the angle to the surface at the surface agreed well with the maximum depth except when the lap was long, when it had more opportunity to change direction in the forging.

Having evaluated the laps, it is possible to run tests simulating the use of the component to show that this region of the component has a longer life than more critically stressed parts. It is also possible to check this region during the actual life of the component.

For more general application of these methods of evaluation there is a need for a more sensitive eddy-current crack-depth meter with perhaps a more finely focused probe with better screening and it is necessary to determine the limitations of the methods by studying more forging laps, both the random type and others of the same type in similar and in different geometric circumstances.

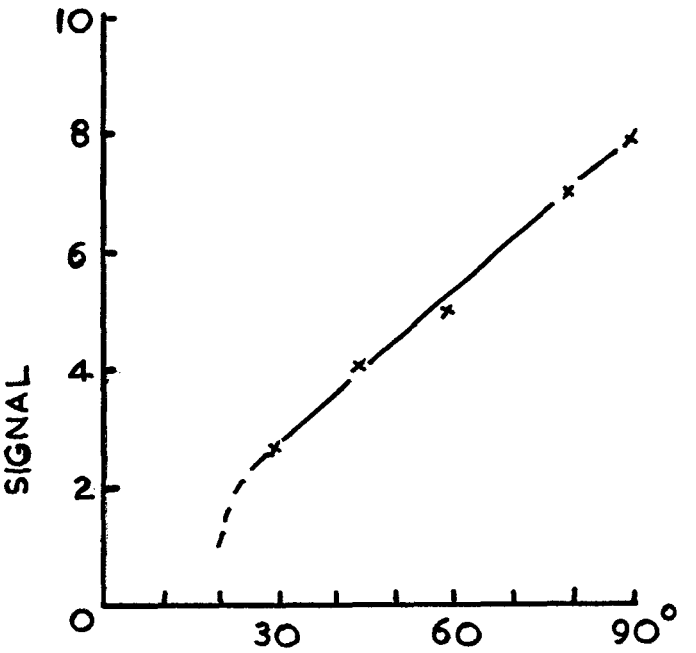

Figure 4B. Ultrasonic surface-wave test relating ultrasonic signal height with the angle of 0.04" (1 mm)-deep grooves cut in test blocks.

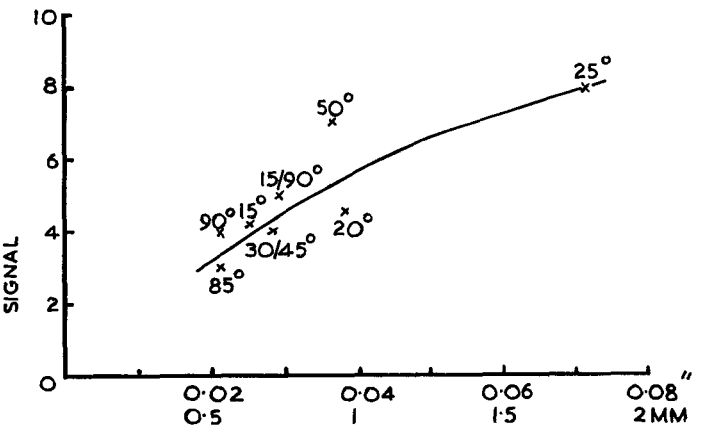

Figure 5. Ultrasonic surface-wave test relating ultrasonic signal height with the length of the laps at various angles in the forgings.

Conclusion

Despite the limitations, nondestructive means can provide information on small forging laps, particularly those that occur regularly in the same area due to local conditions, and have the same sort of characteristics. After pickling the forging, the laps show surface markings and roughness and with some knowledge of the size and direction, it is possible, with certain components, to use them without incurring the considerable expense of completely removing them by localized polishing.

Examination by red dye penetrant as normally carried out under production conditions, has considerable limitations. "Deep" open laps were the only ones well indicated while constricted ones with rounded openings were not indicated. The deepest one not shown was of 0.036 in. (0.91 mm) maximum depth and $\frac{7}{16}$ in. (11 mm) long, along the surface.

The eddy-current methods produced a meter reading that was proportional to the length of the lap in the forging, multiplied by the sine of the angle of the lap to the surface at the

Table 2

Forging and No.	Maximum measured		Measured	Estimated from Figures 3 and 5		
	Length in forging L_1	$L_1 \times$ sine angle to surface A_1	Angle A_1	Length in forging L_2	$L_2 \times$ sine angle to surface A_2	Angle A_2
A1	0.028″ (0.71 mm)	0.020″ (0.51 mm)	45°	0.025″ (0.64 mm)	0.020″ (0.51 mm)	53°
A2	—	—	—	0.021″ (0.53 mm)	<0.018″ (<0.46 mm)	<59°
A3	0.029″ (0.74 mm)	0.023″ (0.58 mm)	90°	0.033″ (0.84 mm)	0.020″ (0.51 mm)	36°
A4	0.036″ (0.91 mm)	0.036″ (0.91 mm)	77°	0.056″ (1.4 mm)	0.037″ (0.94 mm)	42°
F1	0.021″ (0.53 mm)	0.021″ (0.53 mm)	90°	0.025″ (0.64 mm)	0.020″ (0.51 mm)	53°
F1X	—	—	—	0.018″ (0.46 mm)	<0.018″ (<0.46mm)	<90°
F2	0.021″ (0.53 mm)	0.021″ (0.53 mm)	85°	0.019″ (0.48 mm)	0.020″ (0.51 mm)	90°
J3	0.038″ (0.96 mm)	0.013″ (0.33 mm)	20°	0.030″ (0.76 mm)	<0.018″ (<0.46 mm)	<36°
J4	0.071″ (1.8 mm)	0.029″ (0.74 mm)	25°	0.071″ (1.8 mm)	0.026″ (0.66 mm)	21°
J5	0.024″ (0.61 mm)	0.006″ (0.15 mm)	15°	0.028″ (0.71 mm)	<0.018″ (<0.46 mm)	<40°

surface. The minimum lap that it would detect normal to the surface was about 0.018 in. (0.46 mm) long. Maximum lap length multiplied by the sine of the lap angle agreed well with the maximum lap depth except when the lap was long and altered its angle in the forging. The instrument was insufficiently sensitive to indicate lap surface lengths successfully.

Ultrasonic surface-wave inspection was the most sensitive method. It provided an indication of the length of the lap in the component and by moving the probe, an indication of the length along the surface. Laps 0.01 in. (0.25 mm) long and less in the component, and ¼ in. (6 mm) along the surface were detectable. The principal can be used to construct a simulative test block consisting of a machined notch covered with an epoxy resin, which is more resistant to the effects of dirt and damage than the usual slotted blocks.

The present equipment combined provides much information about laps in a particular circumstance. By reference to experimentally determined results, the 4-MHz ultrasonic surface wave indicates defect length along the surface and in the component, and the eddy-current test indicates the lap length multiplied by the sine of the angle to the surface at the surface. By considering the geometry of the two results, it is possible to estimate whether the lap is at an acute angle to the surface or 45° and greater. With zero signal on the eddy-current test, a maximum angle can be estimated. If the lap is "long" it may alter its angle in the forgings and become deeper than the length and angle would at first suggest.

The results indicate that some success has been achieved in evaluating laps and that for more general application there is a need for the development of the techniques. A more sensitive eddy-current crack-depth instrument with a more finely focused probe is required and more laps of similar and different forms in various geometric circumstances require evaluation followed by cut-up examination.

Acknowledgments

The author wishes to acknowledge the help provided by his colleagues, particularly by K. Tipping, and to thank the management of James Booth Aluminium Ltd., for permission to submit this paper. Acknowledgment is also made to E. W. Peppitt of the Dunlop Rim & Wheel Co., for his assistance with the eddy-current tests.

Dynamic Tests for Nondestructive Analysis of Lumber Quality

WILLIAM L. GALLIGAN and ROY F. PELLERIN, U.S.A.

ABSTRACT: Structural lumber has been used as a versatile engineering material for many years. Building practice in the last fifty years in the United States has required that lumber be segregated into quality classes; however, this segregation has been relatively inaccurate. Nevertheless, until recently this grading system, based on visual inspection of the lumber and on clear wood strength, has been considered adequate. As engineering practice in building has improved and the competition of other materials has increased, the inefficiencies of the visual grading system have become more evident and the need for accurate grading of lumber for modulus of elasticity and modulus of rupture has become more apparent.

Nondestructive testing machines capable of measuring the modulus of elasticity of lumber came into use in 1962. These machines also assign each piece of lumber an allowable fibre stress based on a correlation between modulus of elasticity and modulus of rupture. Several of these machines are in use.

Two new, dynamic methods of machine grading lumber are under development at Washington State University. One method, using transverse vibrations, measures both frequency of vibration and rate of vibration decay in order to more accurately predict modulus of rupture. The second method yields the modulus of elasticity of lumber through measurement of the rate of propagation of longitudinal stress waves which are induced by impact. Features of each of these new methods suggest commercial applications.

Application of both transverse vibration and wave-propagation methods for measurement of lumber properties have illustrated the improvement in grading efficiency that is possible with piece-by-piece nondestructive analysis.

Introduction

List of Symbols

A_1	Amplitude of first cycle
A_n	Amplitude of n^{th} cycle
c	Velocity of propagation, ft/sec (cm/sec)
E	Modulus of elasticity, pounds per square inch (psi), (kiloponds per square centimetre, kp/cm^2)
E_d	Modulus of elasticity, determined by dynamic means, psi (kp/cm^2)
E_v	Modulus of elasticity determined by transverse vibration, psi (kp/cm^2)
E_I	Modulus of elasticity determined by impact-induced stress wave propagation, psi (kp/cm^2)
f	Allowable design fibre stress, psi (kp/cm^2)
f_n	Natural frequency, hertz
g	Acceleration due to gravity, 386 inches per second per second (980 cm per second per second)
I	Moment of inertia, inches^4 (centimetres^4)
I	E_I modified by instrumentation used for measurement of rate of wave propagation, psi (kp/cm^2)
k	Constant dependent upon mode of support for a beam vibrating at its fundamental frequency (e.s., k=1.57 for beams supported at the ends)
kilopond	Weight of a kilogram mass
L	Length, inches (centimetres)
$\log_e$	Natural logarithm
n	Number of cycles
R	Modulus of rupture, psi (kp/cm^2)
W	Weight, pounds (grams)
δ	Logarithmic decrement
ρ	Density, pounds per cubic foot (grams per cubic centimetre)

In engineering design and construction the world over, lumber plays a major role. Using 1962 figures from the United States as an example, the wood industry contributed $25 billion to the gross national product. (14) In volume of product, lumber production alone in that same year was estimated at 37.3 billion board feet in the United States. Of this tremendous total about 27 billion board feet were used for residential and industrial construction. In this role as a structural material, lumber competed with many other products, most commonly concrete, steel, plywood and composition materials.

As a construction material, lumber is placed in different categories depending upon size and intended use. The category of interest in this paper is structural lumber, a product defined as lumber which is 2 in. or more thick and 4 in. or more wide. This lumber is intended for use where allowable working stresses must be known. In the lumber industry today there are two distinctly different bases for assigning these working stress values. The traditional method, visual grading, is truly nondestructive, but is not sufficiently accurate to provide a product that can reach its potential as an engineering material. It is the basic purpose of this paper both to illustrate the need for new, accurate nondestructive methods of assigning lumber properties and to discuss two dynamic methods that are under active development at Washington State University.

Lumber Grading Problems

The grading of lumber in a nondestructive way for classification as an efficient engineering material poses many problems to the engineer and scientist. These problems involve the basic fact that wood is a heterogeneous and anisotropic natural product as a result of the manner of tree growth. (16) The anisotropy results from an orientation of wood-cell formation which produces an orthorhombic structure. The longitudinal properties of the wood are those corresponding to the longitudinal direction of tree growth while the tangential and radial properties of wood refer to the circular pattern of cell formation with respect to the vertical axis of the tree. The elasticity and strength values of the wood are highest in the longitudinal direction and, while there are differences between tangential and radial values, both are much lower than longitudinal properties.

The heterogeneity of lumber is commonly characterized by a wide range of sizes and types of flaws such as knots. Often these flaws may influence design or become stress risers in strength applications. Just as common as visible flaws, however, but often misunderstood, is the fact that clear wood (free of visible flaws) contributes to lumber heterogeneity also because of widely variable mechanical properties. Wood material is also hygroscopic and the moisture content of the wood influences the mechanical properties.

Another variable which must be considered is species. The many biological differences between species influence the mechanical properties and, while the average strength and the average modulus of elasticity of one species may be higher than that of another, the wide variability of individual specimens causes wide overlapping of properties.

One might ask why, with these problems, lumber is a popular construction material. This is because the ratios of strength and stiffness to weight are very advantageous. Also wood is available in many parts of the world, it is economical, and it is quite easy to fabricate into attractive and effective products. As an engineering material, lumber is being challenged more every day as other materials compete with ever-increasing effectiveness. This is partially because of the adaptability of the other materials to quality-control programs. These quality-control programs, in turn, yield better estimates of cost of production, more efficient distribution and more assurance of reasonable factors of safety in design. In attempting to meet this challenge, the lumber industry is faced with grading a material that is highly variable. The characteristics of wood mentioned briefly above are the basic problems with which nondestructive testing must cope if lumber is to remain effective as an engineering material.

Visual Grading

During the early years of lumber stress-grading development, efficiency in the cutting, grading and distribution of lumber was not as critical as it is today. Grading rules were highly conservative. These rules, based on limited sampling and on visual inspection, have been subject to review periodically ever since, in step with increasing competition and changes in mill practice, yet basic visual grading concepts remain largely intact. (5)

Visual grading is a method in which the average strength value of clear wood of each species is used as a basis for the strength of the actual lumber which, of course, is anything but clear in many cases. To arrive at design stress values, the clear-wood values first are adjusted downward by factors which recognize the variability of clear wood, the effects of long-term loading in actual use, and a "safety" or accidental overload factor. The adjusted clear-wood strength values then are multiplied by a further reduction factor, termed the strength ratio, which estimates the effect that a certain size of knot or other defect will have on strength. This procedure is outlined in ASTM Standard D 245-64T. (1) Visual grading may be classed as a nondestructive test because the strength-ratio values have been used to develop criteria upon which a visual grader in the lumber mill applies judgment in order to classify each piece of lumber as it passes down the production line.

Several problems are inherent in the visual grading technique. Some of these are technical problems based on the fundamentals of the method; several of them are practical problems present in the mill. Basically, visual grading is a method that tends to assure safety at the expense of efficient grading by undervaluing all pieces of a species through the use of a "variability factor" not based on the actual sample being visually tested. The strength properties of clear wood have a wide degree of variation and this must be taken into consideration in the method since no test of the clear-wood properties is made on the production line. Modulus of elasticity values, for example, can vary by a factor greater than two, and strength values have approximately the same variation. Further, the application of a strength ratio to the clear-wood strength value assumes that the visual grader can assess at a glance which of the competing flaws in the lumber is controlling and that this decision is sufficient to assign proper grade to that particular piece of lumber. The variability and inaccuracy resulting from these procedures must be compensated for by the methods used in arriving at working stress values.

A new visual grading practice has been developed which will be covered by ASTM Standard D-2555T. (1) Unfortunately, when viewed strictly from the point of view of nondestructive testing, this method does not remedy any of the weaknesses in the existing practice, but was adopted for other reasons. It allows the grouping of species of different over-all quality for estimation of mechanical properties. This new method is based on an extensive survey of density samples taken in the forests of the United States and uses a correlation between density and strength in clear wood to assign the allowable stresses. There is a wide variation in density within the tree, both vertically and transversely and one must be cognizant of the statistical problems that are present when assigning a strength value based on a density sample taken from a tree which must represent not only that tree but all the trees in its immediate area.

This discussion of visual grading methods has been meant to be critical purely from the technical point of view of nondestructive testing, that is, from the position that an adequate nondestructive test must be accurate with regard to *each piece*. In practice, these two visual grading methods were not designed specifically to do this. For example, the modulus of elasticity

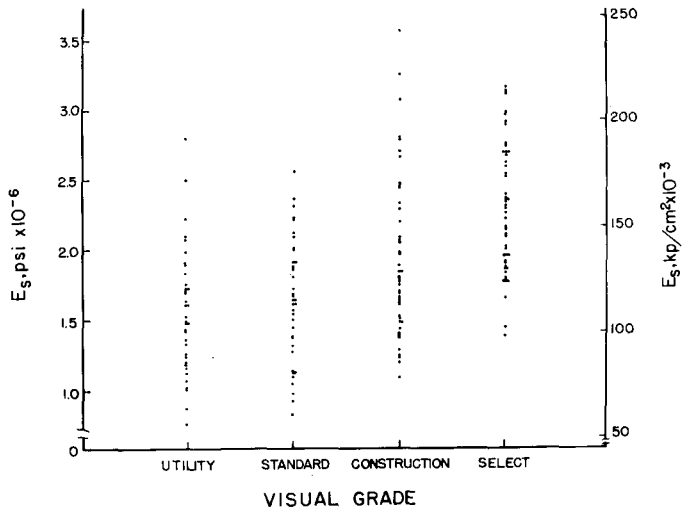

Figure 1. Variation of static modulus of elasticity (E_s) measured on edge among four visual grades of nominal 2 x 6-in. Douglas fir lumber.

allowed for all lumber of a given species has been the supposed average value for the species. This is an inaccurate base for design use since there are many values much higher and much lower than the average. Figure 1 illustrates this problem. The moduli of elasticity (E) for 172 pieces of Douglas fir nominal 2 × 6 in. lumber were measured by static bending. The resulting E_s values are plotted for the four visual grades represented among the lumber specimens. According to the visual grade rules all of these specimens would be used in design at a value of 1.92 x 10^6 psi (135 x 10^3kp/cm^2). (15) Recent modifications to these grading rules have applied a sliding E-value scale so that the lower grades of lumber are restricted to lower moduli of elasticity for design. As is shown in Figure 1, however, this cannot be very effective because the visual method of classifying lumber by grade is inaccurate for modulus of elasticity.

The great inaccuracies of visual grading with regard to single-piece properties are compensated for by a conservative system of assigning design stress values. Of course, statistically, many pieces are capable of use at higher design values, but cannot be so used because they cannot be identified by this visual grading system. (5) For illustration, a typical sample of a population from one visual grade with an allowable design fibre stress in bending of 1750 psi (123 kp/cm^2) had actual rupture values of from 3675 psi (258 kp/cm^2) to 13,808 psi (966 kp/cm^2). When these rupture values were adjusted downward for long-term loading and for accidental overload, corresponding allowable design values ranged from 6575 psi (460 kp/cm^2) to approximately 1750 psi (123 kp/cm^2).

One effect of visual grading is to prevent the industry from marketing lumber at its design potential. To accomplish this latter goal, nondestructive testing must be employed in its true sense, for efficiency and quality control of each piece.

Nondestructive Testing in the Lumber Industry

Traditionally, the only nondestructive testing of lumber other than visual grading has been measurement of moisture content through the use of electrical resistance and capacitance methods. With these exceptions, nondestructive testing did not make its influence felt on the lumber industry until the advent of the machine graders, termed rapid-bending machines, in 1962. These machines measure the modulus of elasticity of individual lumber specimens that are passed through them endwise. (5) (3) They accomplish this by measuring the bending deflection resulting from a known load or by measuring the load required to accomplish a given amount of deflection. Special

features of some machines include sensitivity to low-point elasticity; that is, the ability to detect sections of the lumber which may have modulus of elasticity much lower than the average of the piece.

Working stresses are determined from the machine *E*-values by a very useful regression between *E* and modulus of rupture (*R*). (5) In some cases visual grading restrictions are placed on the machine results to achieve even greater accuracy. (13). The *E-vs-R* relationship is the result of years of research, and study continues in an effort to improve further the working correlation.

Four basic types of rapid-bending machines have been developed. These are the "CLT-1" developed by Potlatch Forests, Inc., Lewiston, Idaho; the "Stress-O-Matic" lumber grader developed originally by the Western Pine Association in Portland, Oregon; a machine developed at the Forest Products Laboratory, Princes Risborough, England; and a machine that sorts lumber in three structural grades and was developed in Australia by the Forestry Commission of New South Wales. Experiences with the Australian machine are typical. Species that have low average elasticity and strength have yielded a very useful percentage of material with safe working stresses well over that allowed by visual methods (3).

Research is active in other areas of nondestructive testing for lumber, for example, optical systems for identifying splits, knots, and stain in lumber. In some of these applications, however, the objective is to determine flaws that will cause rejection of the material for a particular end use. An example is detection of areas that may be severe stress risers and thus precipitate failures. Need still exists, however, for improved methods that can examine anisotropic, heterogeneous lumber to estimate its basic working design values, since discrimination of flaws and defects alone will not permit optimizing lumber use as an engineering material. Two new NDT systems now being studied at Washington State University show promise for prediction of lumber quality. These are characterized as dynamic systems operating under very low stress conditions. One system uses transverse vibrations while the other employs longitudinal wave propagation. High accuracy is expected from these systems. Fixed and portable commercial units are possible since both systems are largely electronic in nature.

Transverse Vibration

A transverse vibration method for nondestructive testing of structural lumber was developed at Washington State University by Pellerin. The special virtue of this method is that it enables the assignment of fibre strength and modulus of elasticity values independently for each piece of lumber. This procedure should lead to a more accurate determination of strength than is now possible.

The vibration approach is based on transverse oscillations that permit measurement of two fundamental properties of materials, namely energy storage and energy dissipation. These fundamental properties were hypothesized by Jayne (8,9) to be related to the same mechanisms that control the mechanical properties, i.e., modulus of elasticity and modulus of rupture, respectively.

The outward manifestation of energy storage of material is its natural frequency in vibration and, through well established equations relating natural frequency to modulus of elasticity, a direct calculation of this modulus can be made. For a beam, the relationship is expressed for transverse vibration as follows:

$$E_v = \frac{f_n^2 \; WL^3}{k^2 \; I_g} \qquad (1)$$

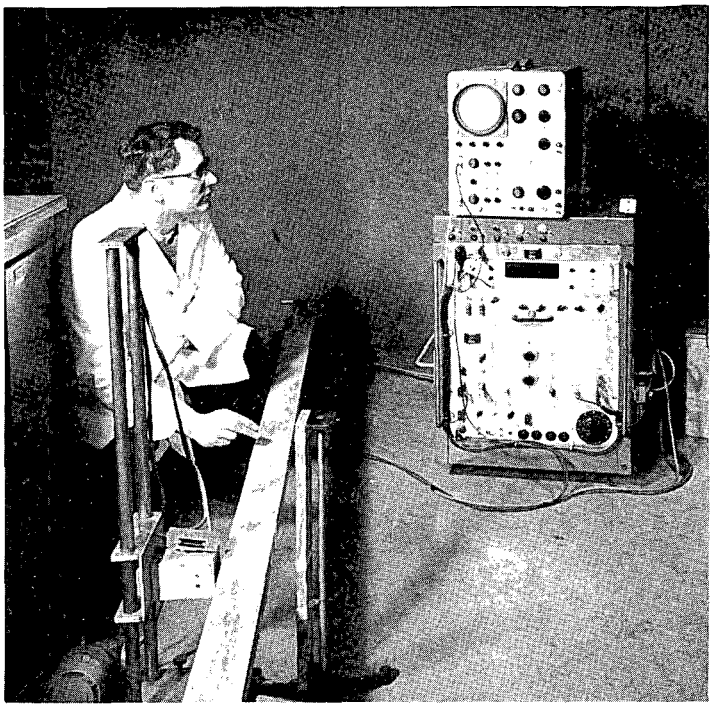

Figure 2. Transverse vibration testing of structural lumber. The console in the background measures the frequency and the log decrement of free vibrations. The vibration amplitude is detected by the photocell unit in the foreground and is observed in the oscilloscope.

In contrast, the mathematical relationship involving energy dissipation and modulus of rupture has not been well established. However, Jayne's hypothesis of causal relationship (8) indicated the possibility of developing a system by which energy dissipation might be made to predict modulus of rupture. Thus, the problem was first to develop a means of measuring energy dissipation and, second, to develop correlative information sufficient to prove the existence of a useful relationship between energy dissipation and strength.

The method developed for this purpose involved the use of free transverse vibration. (11) In this case, energy dissipation is measured as the rate of decay, or logarithmic decrement (δ), of the amplitude of the vibration of the vibrating body and is expressed in the form:

$$\delta = \frac{1}{n} \log_e \frac{A_1}{A_n} \qquad (2)$$

where A_1 and A_n are the amplitudes of two oscillations n cycles apart.

The relationships between the vibrational parameters, E_v and δ, described above and the mechanical properties of lumber have been investigated by several researchers, (7,8,9,10) all of whom agree on the relationship of frequency to modulus of elasticity, but have conflicting conclusions concerning the usefulness of logarithmic decrement in predicting modulus of rupture.

Application of both frequency and logarithmic decrement analysis to full-size lumber at Washington State University revealed correlation coefficients of 0.98 and higher between the dynamic modulus of elasticity, E_v, and the static modulus, E_s. (11) More significant, however, were correlation coefficients as high as 0.92 which were revealed between a combination of vibration parameters (E_v/δ) and the modulus of rupture. This success was attributed to newly developed electronic equipment and procedures which refined the measurement of logarithmic decrement and natural frequency of lumber subjected to free

transverse vibrations. A photograph of the present laboratory equipment is shown in Figure 2.

The frequency of the vibrating lumber is determined by measuring the period of oscillation. The logarithmic decrement is measured by counting the number of oscillations which occur between two predetermined amplitudes, A_1 and A_n. The gates of the counter are set electronically to trigger at amplitudes such that the natural logarithm of the ratio A_1 to A_n is equal to unity. Hence, the number of oscillations that occur between these amplitudes is the reciprocal of logarithmic decrement.

Following development of equipment and demonstration of technical feasibility, the transverse-vibration method was applied in studies pointed toward commercial applications. Another dynamic test method, stress-wave propagation, has been studied at Washington State University with a similar pattern of development, although it has not been under study for as long. Following a discussion of stress-wave propagation research, results of both methods are compared to visual grading.

Stress-Wave Propagation

Like transverse vibration, the stress-wave propagation method is a dynamic analysis, but it differs in that the direction of the excitation is longitudinal and the frequency of excitation is about 1000 times higher than for transverse vibration. Despite these basic differences, both methods yield very similar values of modulus of elasticity for construction lumber.

The propagation of longitudinal stress waves in solids is influenced in a complex manner by both the mechanical and physical properties of the medium. To describe the propagation for practical use, the complex expressions commonly are simplified to elementary, one-dimensional wave propagation theory as applied to an isotropic, homogeneous material. If a specimen has lateral dimensions which are small compared with the wavelength of the propagating wave, this simplified theory yields the following equation relating the velocity of propagation, c, with the modulus of elasticity and density (ρ) for a prismatic bar:

$$c = \sqrt{E/\rho} \qquad (3)$$

At Washington State University, research on stress-wave propagation in wood has involved wavelengths much larger than the lateral dimensions of the specimen. This wavelength-dimension relationship was obtained by simple impact on the end of wood specimens that were in the form of small, clear prismatic rods. When wave-velocity measurements were made on the prismatic rods, Equation (3) yielded E-values which agreed closely to the corresponding static moduli. (2) Modulus of elasticity values determined from the impact-induced wave propagation were labeled E_1.

Following this initial work with prismatic rods, the study of wave propagation was extended to wood specimens of commercial interest in the form of structural lumber. (4) This was a great challenge to the stress-wave propagation method because of the number of knots, splits, and grain deviations commonly present. However, initial laboratory studies determined that the dynamic E of construction lumber calculated from Equation (3) agreed well with the static E obtained from simple bending. More study of wave propagation with structural lumber was encouraged and particular emphasis was placed on development for nondestructive lumber grading.

Early efforts to measure modulus of elasticity of lumber employed a simple pendulum to provide a reproducible impact-induced stress wave, a trigger circuit and a delayed-sweep oscilloscope to make the measurement of rate of stress-wave propagation. (4) With the time delay adjustment of the oscilloscope, the elapsed time between impact and the arrival of the energy wave at the other end of the specimen was measured in microseconds. Knowing the dimensions and weight of the lumber, the value of E_1 was calculated from Equation (3). A correlation coefficient of 0.956 between the static modulus (E_s) and the dynamic modulus (E_1) illustrated the reliability of the stress-wave method. The least-squares relationship was $E_1 = 0.956\ E_s + 0.101 \times 10^6$ psi. When these same lumber specimens were tested by transverse vibrations, the least-squares line obtained was $E_v = 0.969\ E_s + 0.074 \times 10^6$ psi. The close agreement between the two slope values (0.956 and 0.969) illustrates the excellent correspondence between elastic moduli determined at far different excitation rates.

Since the initial research, the measurement system has been under continuous revision to achieve greater commercial feasibility. These changes have included sophistication in the trigger system and use of an electronic counter for readout. Figure 3 is an over-all view of the equipment. The device in the foreground imparts a reproducible impact to the lumber; the electronic counter is shown in the background.

Modifications to the instrumentation often have introduced artificial factors in the time measurements, which, in turn, produce E-values calculated from Equation (3) which may not be in one-to-one relationship with the static E-values. (4) When this occurred, the calculated parameter was labeled I to distinguish it from the true dynamic value, E_1. These I-values, of course, are adjustable to the modulus of elasticity by a regression.

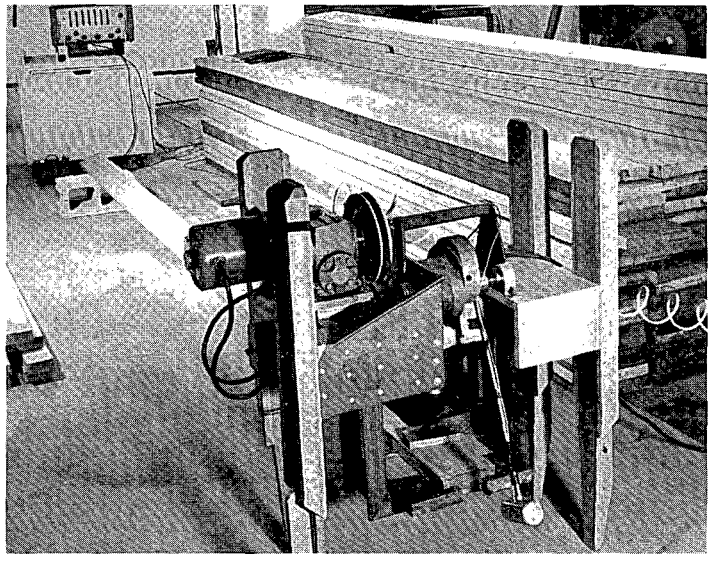

Figure 3. Apparatus for measurement of rate of stress-wave propagation in structural lumber. The device in the foreground imparts a reproducible impact to the lumber. A transducer sensitive to strain is positioned at the far end of the lumber to transmit a signal to the electronic counter.

Dynamic Test Results

As indicated previously, both transverse vibration and longitudinal wave propagation have a demonstrated capability for measuring the modulus of elasticity. Figure 4 depicts the E_s, E_v and I values of the Douglas fir specimens shown in Figure 1. Although the dynamic tests predict the wide range of E_s values, visual grade methods in force in mid-1966 would allow only a design E of 1.92×10^6 psi (125×10^3 kp/cm^2) at 15% moisture content for all of these pieces.(15) In Figure 4, E_s is a static measurement on edge; E_v was determined with vibration in the flat plane of the nominal 2 × 4-in. lumber. Note that the wave-propagation data is labeled I since changes in instrumentation yielded an artificially high value of E_1 from Equation (3).

To demonstrate further the effect of piece-by-piece nondestructive testing, a sample of 50 clear, western hemlock,

nominal 2 × 4 in. lumber specimens, 16 ft (488 cm) in length were chosen from a sample population of 250 to be tested by both dynamic methods. The basis of choice of the sample was the 25 predicted to have the highest strength by E_v/δ and the 25 predicted to be the lowest strength by E_v/δ. By current visual grading methods, these pieces would be classified as select structural and allowed an E of 1.68×10^6 psi (118×10^3 kp/cm^2) at 15% moisture content. (15) Figure 5 illustrates the actual E-values, both static and dynamic, that were found in these 50 specimens. Both the E_s and E_v measurements were made on edge. It is clear that not only is a wide variability present in clear lumber, but that to utilize the E potential, modern NDT is required.

The select structural grade in hemlock is permitted one design fibre-stress value, 1750 psi (123 kp/cm^2) at 15% moisture content by visual rules. (15) The specimens of Figure 5 were broken on edge in a testing machine and the modulus of rupture values (R) were compared with the strength predicting parameter E_v/δ. Figure 6 shows the R-values graphed against E_d/δ where E_v was used for the dynamic $E(E_d)$. Because this sample population was not truly normal in the statistical sense, no regression lines were calculated. The data was analyzed, however, on the basis of machine grades using the E_d/δ concept. The machine was assumed to grade the lumber in E_d/δ groups of 40×10^6 psi (282×10^4 kp/cm^2). This segregation is shown by the vertical lines. In two groupings where sufficient specimens were present, the allowable fibre-stress values were calculated by recognized methods which take into account variability,, duration of load, and accidental overload.(6) The allowable fibre-stress values, 2030 psi (143 kp/cm^2) and 3400 psi (239 kp/cm^2) are depicted by the horizontal dashed lines in the respective E_d/δ groups. Both fibre-stress levels are appreciably higher than permitted by the visual grade as shown by the dashed line at 1750 psi (123 kp/cm^2). These differences are typical of results obtained when comparing presently operating machine graders with the visual system. It must be noted that the data collected in Figure 6 were not part of a large study and thus should not be used to arrive at actual design values. The purpose of this data was to portray the differences in the existing practices of the industry and the improvement in efficiency to be gained by NDT. For more detail on these methods many references are available. (6, 12)

Nondestructive testing is a must for the wood industry if it is to remain abreast technologically. The advent of the machine graders and presence of new dynamic methods is only the beginning. These methods at present are far from optimized and the NDT industry can contribute to their improvement. High efficiency will probably result from a marriage of the best features of the visual system and the piece-by-piece thoroughness of the automated nondestructive test.

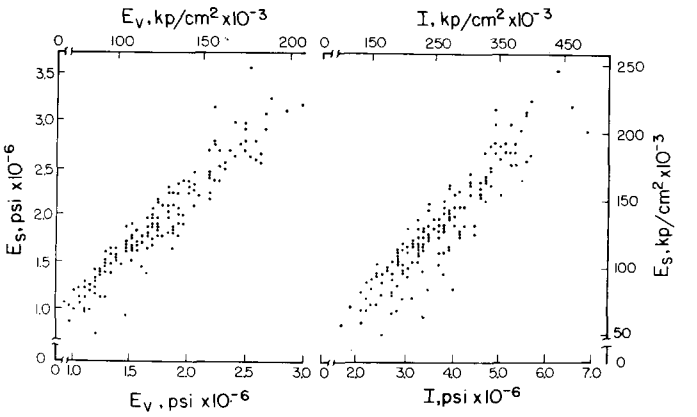

Figure 4. Static modulus of elasticity (E_s) of the specimens of Figure 1 graphed against the transverse vibration modulus of elasticity, E_v, and the impact-induced wave propagation modulus I.

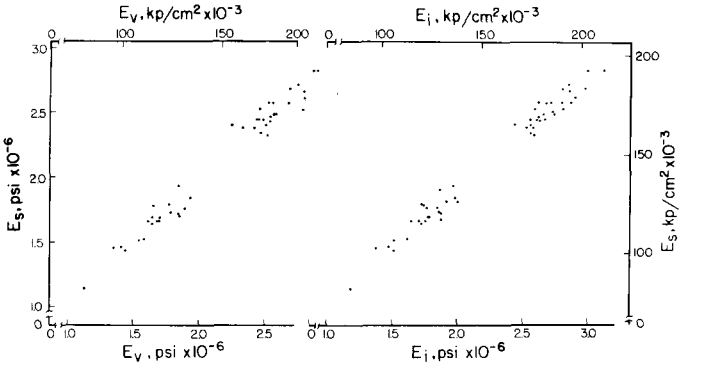

Figure 5. Comparison of the static moduli of elasticity of two groups of 25 specimens of nominal 2 x 4-in., clear hemlock with the moduli determined by dynamic methods. The E_V plot is shown on the left; the plot on the right compares E_I with E_S.

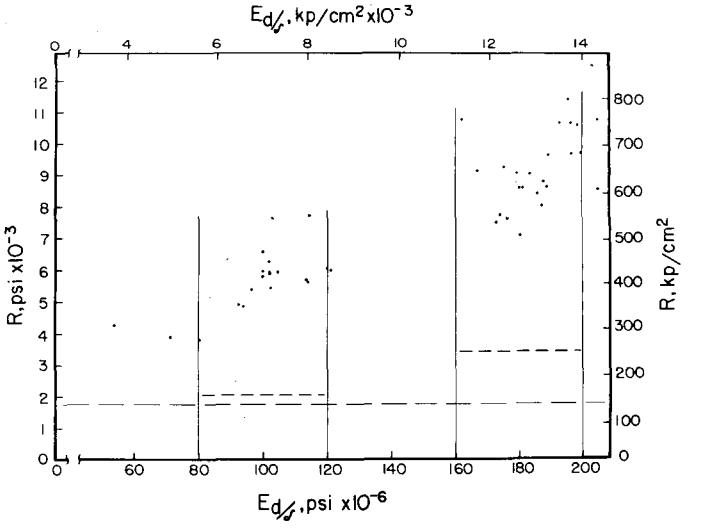

Figure 6. An illustration of the visual grading and machine grading for estimate of allowable fibre stress. The long dashed line is the allowable design fibre stress by visual grade for these two samples of clear hemlock lumber. The two short dashed lines typify the allowable stress levels as they would be calculated from nondestructive machine grading. The dynamic elasticity used in E_d/δ for this plot was determined by transverse vibrations.

References

(1) *ASTM Standards 1966,* Part 16.

(2) Bertholf, L. D. Use of elementary stress wave theory for prediction of dynamic strain in wood, *Washington State Inst. Technol.* Bull. 291, Washington State Univ., 1965.

(3) Booth, H. E. The machine grading of timber, *The Australian Timber J.,* v. 30(8), Sept. 1964, 81-89.

(4) Galligan, W. L., and Courteau, R. W. Measurement of the elasticity of lumber with longitudinal stress waves and the piezoelectric effect of wood, *Second Symp. NDT of Wood,* Pullman, Washington Tech. Extension Serv., College of Eng., Washington State Univ., 1965.

(5) Galligan, William L. and Pellerin, Roy F. Nondestructive testing of structural lumber, *Materials Evaluation,* XXII, No. 4, 1964, 169.
(6) Hilbrand, H. C. and Miller, D. G. Machine grading-theory and practice, *Forest Prod. J.,* v. XVI, no. 11, 1966, 28.
(7) James, W. L. Vibration, static strength and elastic properties of clear Douglas fir at various levels of moisture content, *Forest Prod. J.,* v. XIV, no. 9, 1964, 409.
(8) Jayne, B. A. The vibrational properties of wood as indices of quality, *Forest Prod. J.,* v. IX, no. 11, 1959, 413.
(9) ————Development of vibrational nondestructive test for construction lumber, Washington State Univ. Res. Rept., No. 61/15-108, 1961. (Unpublished.)
(10) Miller, D. G. Nondestructive testing of crossarms for strength, *Canada Dept. Forestry,* Pub. 1021, 1963.
(11) Pellerin, R. F. A vibrational approach to nondestructive testing of structural lumber, *Forest Prod. J.,* v. XV, no. 1, 1965, 93.
(12) *Proc. Second Symp.-NDT of Wood,* William L. Galligan, Editor. Washington State Univ., Tech. Extension Serv., College of Eng., Pullman, Washington.
(13) "Standard Grading and Dressing Rules No. 15," Revised Sept. 1, 1964. Supplement XIV for Mechanically Stress Rated Lumber. West Coast Lumber Inspection Bureau, Portland, Oregon.
(14) "Timber Trends in the United States," Forest Service, U.S. Department of Agriculture, Forest Resource Report No. 17, February, 1965.
(15) "Western Wood Products 1965 Standard Grading Rules," Western Wood Products Association, Portland, Oregon, January, 1965.
(16) Youngs, Robert L. Nondestructive testing of wood—Status, needs, and possibilities, *Materials Evaluation,* v. XXIII, no. 8, 1965, 372.

Nondestructive Testing of the Elasticity and Strength of Wood

N. D. POPESCU, ROMANIA

ABSTRACT: The method of testing described is based on the principle of coupled oscillations. Bending and torsional oscillations are generated in the test piece with the aid of two pendulums of identical weight. The period of the beats produced by the super-position of the pendulum oscillation against the test-piece oscillation is used to determine the mechanical characteristics.

A theoretical relationship is established between the elastic characteristics of a test piece and the beat. Using this relationship the elastic characteristics of five types of wood species are determined and these are compared with the results obtained by an ultrasonic method.

Relationships between the speed of the respective elastic longitudinal waves, the beat period, and the mechanical strength of the wood are then derived experimentally.

As wood is an anisotropic material, an anisotropic coefficient is used instead of the transverse contraction coefficient. The anisotropic coefficient can be determined using the test method described in this paper.

Introduction

Symbols and Notations Used

E = longitudinal elasticity module of the test-piece
G = transverse elasticity module of the test-piece
M = mass of a pendulum
M_1 = mass of the horizontal lever
$2a$ = distance between the axes of pendulum supports
m = mass of the tested test-piece
I = axial inertia moment of the test-piece
I_p = polar inertia moment of the test-piece
I_{M1} = inertia moment of the horizontal lever
l_o = length of the mathematical pendulum, synchronous with the physical one
I_{mo} = moment of inertia of the test-piece on the unity length in relation with its geometrical axis
L = theoretical length of the test-piece
T = period proper to pendulums
ζ_e = period of beats (in the case of bending oscillations)
ζ_g = period of beats (in the case of torsion oscillations)
ρ = wood density
δ = wood specific weight
g = acceleration of the free fall
V'_L = propagation speed of the longitudinal elastic waves through the bars
μ = transverse contraction coefficient
α = coefficient of anisotropy
R_c = resistance to compression
R_t = resistance to tension

Study of the elastic characteristics of wood by the classical method is difficult as the test-piece used to determine the longitudinal elastic modulus E is destroyed during the test and therefore cannot be used to determine the transverse elastic modulus G. A second test-piece must then be used to determine the latter and this may not have the same properties, as the elastic and strength characteristics of wood vary not only from one species to another, and from one tree to another, but even in the same tree we obtained different results from different places.

It is therefore impossible to establish any relationship between the two elastic moduli using the classical methods.

The method described in this paper, called the "coupled oscillation" method, enables us to determine on the same test-piece all the elastic and strength characteristics of wood, as the tests are done without destroying the material.

In principle the method relies on the generation of bending and torsional oscillations in the test-piece by using two coupled pendulums of identical weight. The pendulums are coupled to the sample and generate a beat frequency in it due to the interference between the oscillations of the pendulums and the natural oscillations of the sample.

The beat frequency depends on the oscillation frequency of the pendulums and the natural oscillations of the test-piece. The latter is determined by the elastic characteristics of the test-piece material. Consequently a direct relationship between the elastic characteristics of a material and the beat frequency can be determined. This is shown by the oscillations of the pendulums and can be easily measured.

To perform the tests, the test-piece of cylindrical or square cross-section, is placed in a vertical position with the bottom embedded in a base, and the top fixed to a horizontal lever, at the end of which are hung the identical pendulums on knife-edge wedges. The knife-edges are placed so that the pendulum axes can oscillate either in the same plane or in different planes. In the first case, the movement of the pendulums generates bending oscillations, while in the second the oscillations generated are torsional.

If a pendulum is deflected from its equilibrium position and then released, it will begin to oscillate and due to the elasticity of test-piece, the pendulum at the opposite end of the horizontal lever will also oscillate.

As the amplitude of the oscillation of the first pendulum begins to decrease, the oscillation amplitude of the second pendulum increases, reaching a maximum when the first pendulum has stopped. After this, the first pendulum begins to oscillate again while the oscillation amplitude of the second decreases until the pendulum stops. The time between two successive stoppings of a pendulum represents the beat period. The problem to be solved lies in establishing the relationship between the elastic constants of the material and the beat period.

Determination of Relationship Between Elastic Constant and Period of Beat

The equipment as used for determining the longitudinal elastic modulus E is shown schematically in Figure 1. This can be considered as a system with three degrees of liberty, the generalized coordinates being:

x—The displacement of the top of the test-piece;

θ—The position of the first pendulum;

φ—The position of the second pendulum.

We adopt the hypothesis that the horizontal bar B-C has a linear translation (motion) and we neglect the work of the force which represents the weight of this bar.

In the case of a bar of length L, mass m, inertia moment I, and elastic modulus E, embedded at one end and free at the other, considering only fundamental oscillations and neglecting the influence of harmonics, we can write for small oscillations that the potential energy W and the oscillation pulsation ω the following equations:

$$W = \frac{\pi^4}{64} \cdot \frac{EI}{L^3} x^2 \tag{1}$$

$$\omega^2 = \frac{\pi^4}{64\left(\frac{3}{4} - \frac{2}{\pi}\right)} \cdot \frac{EI}{mL^3} \tag{2}$$

From a dynamic point of view we can consider the bar as an undamped linear oscillator with the elastic constant c and equivalent mass q:

$$W = \frac{1}{2} c\, x^2 \tag{3}$$

$$\omega^2 = \frac{c}{q} \tag{4}$$

We can then derive the following values for c and q:

$$c = \frac{\pi^4}{32} \cdot \frac{EI}{L^3} \tag{5}$$

$$q = \frac{3\pi - 8}{2\pi} m = 0.226\, m \tag{6}$$

Using the Lagrange equations, the system of differential equations is obtained which describes a movement of the system. After linearizing this becomes

$$\left.\begin{aligned} n\ddot{x} + l_0\ddot{\theta} + l_0\ddot{\varphi} + kx = 0 \\ \ddot{x} + l_0\ddot{\theta} + g\theta = 0 \\ \ddot{x} + l_0\ddot{\varphi} + g\varphi = 0 \end{aligned}\right\} \tag{7}$$

where:

$$n = \frac{q + M_1 + 2M}{M} \text{ and } k = \frac{c}{M}$$

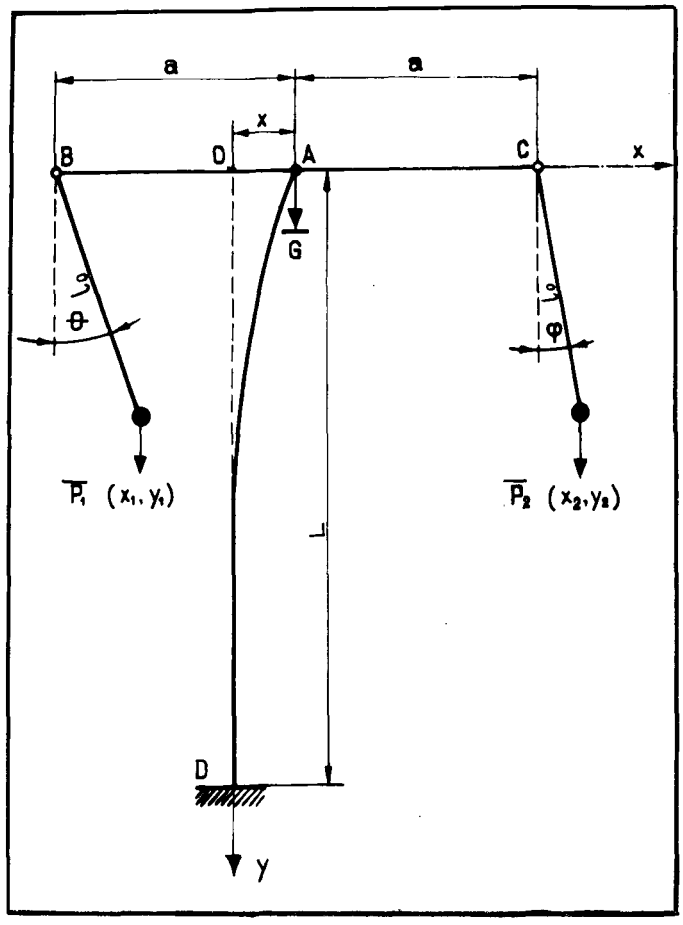

Figure 1

The particular solutions of this system have the form:

$$\left.\begin{aligned} x &= A \sin(\omega t + \psi) \\ \theta &= B \sin(\omega t + \psi) \\ \varphi &= C \sin(\omega t + \psi) \end{aligned}\right\} \tag{8}$$

Using these relations, the system of equation (7) becomes:

$$\left.\begin{aligned} A(n\omega^2 - k) + B l_0\omega^2 + C l_0\omega^2 = 0 \\ A\omega^2 + B(l_0\omega^2 - g) = 0 \\ A\omega^2 + C(l_0\omega^2 - g) = 0 \end{aligned}\right\} \tag{9}$$

This system of equations in A,B,C, is compatible with unbanal solutions, if the determinant of the coefficients of unknown quantities is null:

$$\begin{vmatrix} (n\omega^2 - k) & l_0\omega^2 & l_0\omega^2 \\ \omega^2 & (l_0\omega^2 - g) & 0 \\ \omega^2 & 0 & (l_0\omega^2 - g) \end{vmatrix} = 0 \tag{10}$$

Solving this equation, the following expressions for pulsations are obtained:

$$\left.\begin{aligned} \omega_I^2 &= \omega_0^2 \\ \omega_{II,III} &= \frac{\omega_0^2 + \omega_1^2 \pm \sqrt{(\omega_0^2 \pm \omega_1^2)^2 - 4\delta\,\omega_0^2\omega_1^2}}{2\delta} \end{aligned}\right\} \tag{11}$$

where:

$$\left.\begin{aligned} \omega_0^2 &= \frac{g}{l_0} \text{ (the square of pulsations proper to the pendulums)} \\ \omega_1 &= \frac{k}{n} = \frac{c}{q + M_1 + 2M} \\ \delta &= 1 - \frac{2}{n} = \frac{q + M_1}{q + M_1 + 2M} \end{aligned}\right\} \tag{12}$$

By the superposition of the pulsation oscillations ω_I over the pulsation oscillations ω_{II} or ω_{III} the phenomenon of beats is obtained, the pulsation of the beats being:

$$\omega_b = \omega_0 - \sqrt{\frac{\omega_0^2 + \omega_1^2 + \sqrt{(\omega_0^2 + \omega_1^2)^2 - 4\delta^2\omega_0^2\omega_1^2}}{2\delta}} \qquad (13)$$

Taking into account the relations (5), (6), (12) and the expressions:

$$\omega_0 = \frac{2\pi}{T} \; ; \; \omega_b = \frac{2\pi}{\zeta_e} \; ; \qquad (14)$$

from equation (13) we obtain:

$$E = A + B\,\zeta_e \qquad (15)$$

where:

$$A = \frac{128\,L^3\,(0.226\,m + M_1)}{\pi^2\,T^2\,I} \qquad (16a)$$

$$B = \frac{128\,L^3\,M}{\pi^2\,T^3\,I} \qquad (16b)$$

It can be seen, therefore, that the longitudinal elastic modulus E can be determined without any difficulty if the period of beats ζ_e is known when A and B are constants of the test-piece and equipment. For the case when the equipment is used for determining the transverse elastic modulus G, the axes of the two pendulums must oscillate in parallel planes, as is shown in Figure 2A, and Figure 2B. This installation can also be considered as a system of three degrees of liberty, its generalized coordinates being

φ–for the rotation of the lever B-C,
δ–for the position of the first pendulum,
θ–for the position of the second one.

Taking into account the fact that the bar A-D can be replaced from a dynamic viewpoint with an equivalent undamped linear oscillator, of elastic constant k and equivalent inertia moment having the expressions:

$$\left.\begin{aligned} K &= \frac{G\,I_p}{L}, \\ \eta &= (I_{M_1} + \frac{I_{mo}}{3}L), \end{aligned}\right\} \qquad (17)$$

and proceeding as in the previous case, we obtain:

$$G = C + D\,\zeta_g, \qquad (18)$$

where:

$$\left.\begin{aligned} C &= \frac{4\pi^2 L}{I_p\,T^2}\,(I_{M_1} + \frac{I_{mo}}{3}L), \\ D &= \frac{4\pi^2\,L\,Ma^2}{I_p\,T^3}. \end{aligned}\right\} \qquad (19)$$

Hence in the case of the transversal elastic modulus G, the problem is also reduced to measuring the beat frequency on an experimental basis, the coefficients C and D being the constant values of the test piece and the equipment.

Design of the Experimental Equipment

The actual experimental equipment designed to meet the theoretical requirements already described is so designed that it can be used not only for determining the longitudinal elastic modulus E but also for determining the transversal elastic modulus G by changing only the plane of oscillation of the pendulum axes and ensuring—in the case of determining elastic constant G—that displacement of the top of the test-piece should not take place.

Figure 3 shows the equipment with the test-piece mounted for the determination of the elastic modulus E.

The base of the equipment, an iron plate 11 in. × 9.8 in. × 1.4 in. In the centre of the space is a device for rigidly fixing the bottom of the test-piece.

The top of the test-piece is fixed by means of a similar device, on a horizontal lever, at the end of which are mounted two pairs of hard steel holders which constitute the supports for the pendulums.

Two of these supports are placed on each side of the test-piece—perpendicularly on the axis of the horizontal lever—at a distance 3.35 in. from the axis of the test-piece.

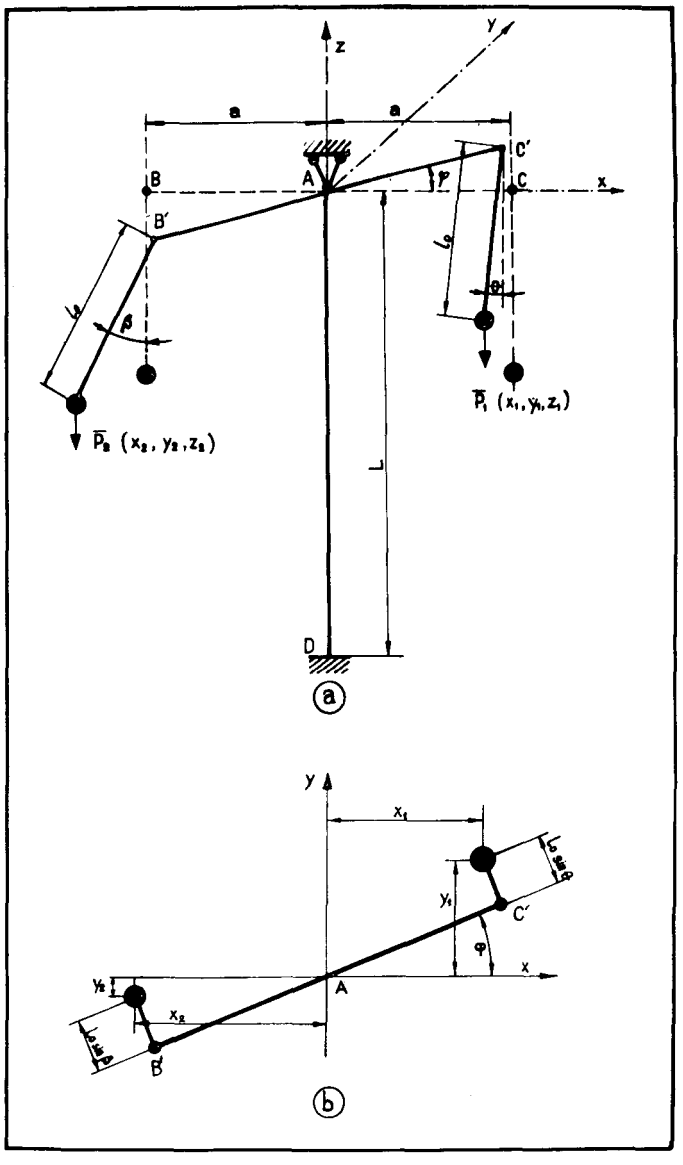

Figure 2

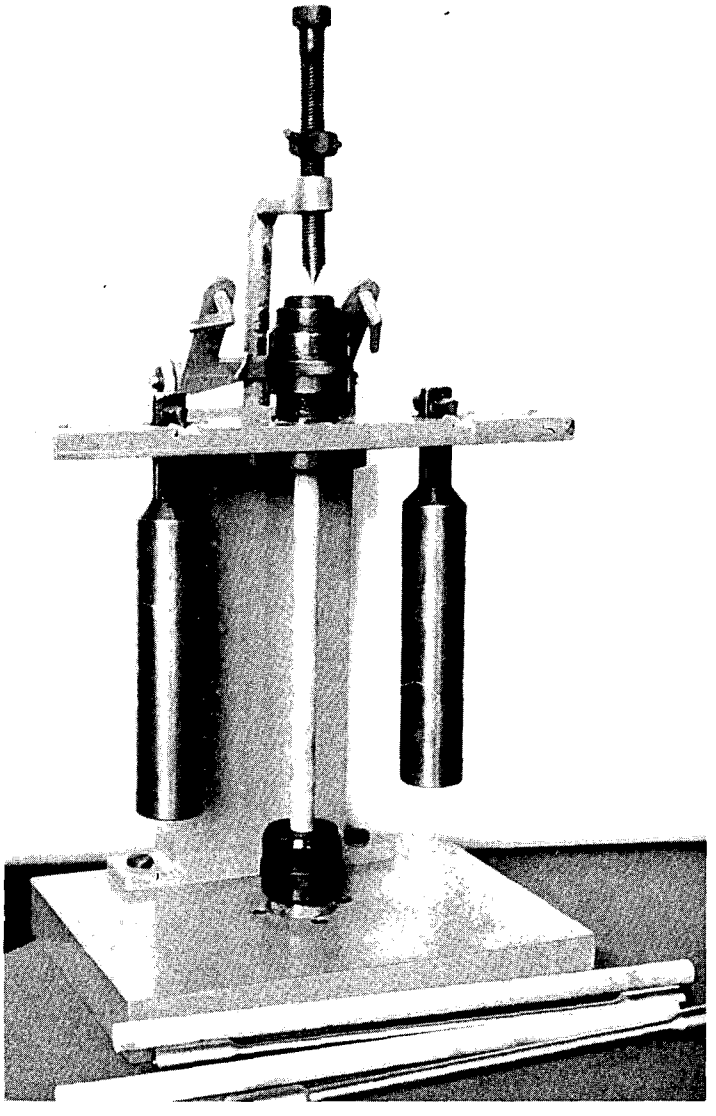

Figure 3

The two pendulums are supported by hard steel knife-edges on these supports, one on each side of the test-piece.

Thus the pendulums can oscillate only in the plane containing the axis of the horizontal lever and the axis of the test-piece, whereas the top of the test-piece can be displaced.

For the determination of the transverse modulus of elasticity G the two pendulums are placed on the other pair of supports which are also mounted on a horizontal lever, symmetrical to the test-piece at a distance of 5.35 in. from it.

As these supports are on the axis of the horizontal lever, the axes of the pendulums can oscillate only in normal and parallel planes between them on the plane determined by the axis of the test-piece and the axis of the horizontal lever, so that the oscillation makes the horizontal lever rotate and thus twists the test-piece.

A special device which allows the top of the test-piece to rotate only around its own axis prevents any displacement of the top of the test-piece. The two pendulums are cylindrical and are made of iron.

In this way the apparatus is made ready to test for the transverse elasticity modulus G.

The two pendulums are cylindrically shaped and are made of iron, like the other details of the apparatus.

As the test-pieces are of small dimension, their mass can be neglected, and thus in equations (16) and (19) we can take $m=I_{m_0}=0$, obtaining for coefficients A,B,C and D the following expressions:

$$\left.\begin{aligned} A &= \frac{128\,M_1}{0.0491\,\pi^2\,T^2}\cdot\frac{L^3}{d^4}\,;\quad B=\frac{128\,M}{0.0491\,\pi^2\,T^3}\cdot\frac{L^3}{d^4}\,;\\ C &= \frac{4\pi^2\,I_{M_1}}{0.0982\,T^2}\cdot\frac{L}{d^4}\,;\quad D=\frac{4\pi^2\,M\,a^2}{0.0982\,T^3}\cdot\frac{L}{d^4}\,; \end{aligned}\right\} \tag{20}$$

where d is the diameter of the test-piece.

The characteristics of the apparatus are:

$$\left.\begin{aligned} M &= 0.0105\ \text{lb/in}^{-1}.s^2,\\ M_1 &= 0.0112\ \text{lb/in}^{-1}.s^2,\\ T &= 0.750\ \text{s.},\\ a &= 5.35\ \text{in.},\\ I_{M_1} &= 0.1553\ \text{lb. in. } s^2., \end{aligned}\right\} \tag{21}$$

and for the coefficients A,B,C and D the following values result:

$$\left.\begin{aligned} A &= 5.25\frac{L^3}{d^4}\,;\quad B=6.58\frac{L^3}{d^4}\,;\\ C &= 111\,\frac{L}{d^4}\,;\quad D=284\,\frac{L}{d^4}\,. \end{aligned}\right\} \tag{22}$$

For verifying the proper operation of the apparatus, the elastic constants of a steel bar, with the length $L=8.47$ in. and a diameter $d=0.28$ in. were determined.

In this case the equations which permit the calculus of elasticity moduli can be written under the form:

$$\left.\begin{aligned} E &= 519.057 + 650.451\,\zeta_e,\\ G &= 152.972 + 391.389\,\zeta_g. \end{aligned}\right\} \tag{23}$$

Measuring the period of beats for the two types of tests, the following values were obtained:

$$\left.\begin{aligned} \zeta_e &= 44\ s,\\ \zeta_g &= 28\ s. \end{aligned}\right\} \tag{24}$$

By replacing these values in equation (23) E and G were obtained.

$$\left.\begin{aligned} E &= 29.138.900\ \text{lb/in}^2\\ G &= 11.111.864\ \text{lb/in}^2. \end{aligned}\right\} \tag{25}$$

For these values of E and G a transverse contraction coefficient resulted, $\mu=0.31$.

These data, corresponding with those determined by classical methods for this kind of steel, show that the apparatus operates with good accuracy.

Experimental Results Obtained on Wood

Samples and Materials Used

Five species of wood were tested, namely fir, beech, oak, elm, and acacia. As we were also interested in the determination of the mechanical properties at various positions in the tree-trunk, samples were taken from various positions as shown in Figure 4. The sample size used was 0.79 × 0.79 × 14.77 in. with the axis of the sample parallel to the wood fibres.

The test-pieces were free from flaws and were found to have a humidity of 15%. Tests were carried out at 20°C. In order to check the results the samples were tested not only by the method described but also by the well-known ultrasonic method.

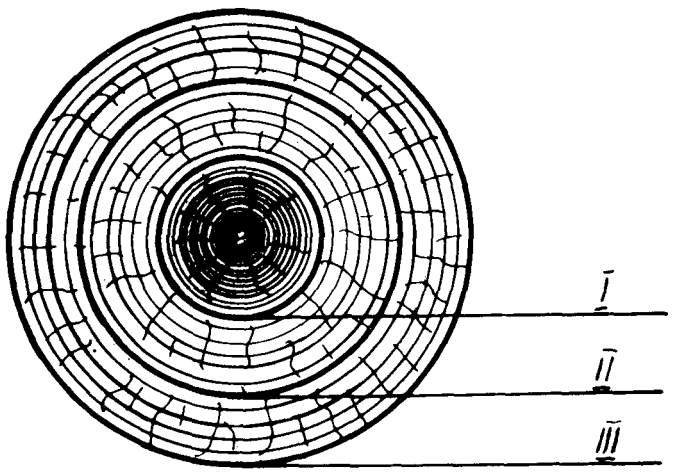

Figure 4

The speed of propagation of longitudinal elastic waves V'_L in the direction parallel to the fibres was first determined. The samples were then cut into two parts, a test-piece of 0.79 × 0.79 × 2.37 in. and another of 0.79 × 0.79 × 12.4 in. The shorter test-pieces were tested in compression to determine the resistance to compression *Rc*, and the longer test-pieces were turned on a lathe to a diameter of 0.59 in. in their central portion and were then tested by the method described, and then broken in the tensile machine.

Determination of Mechanical Characteristics by Ultrasonics

Measurement of the velocity of longitudinal elastic waves in the test-pieces was done by means of the Ultrasoniscope LIN-2 (1). The transmitter and receiver were placed at each end of the test-piece so that the elastic waves travelled parallel to the fibres. The measured speeds are given in column 4, of Table 1.

In the same table we also give the specific weights δ (column 3), the compression strength *Rc* (column 6), and the tensile strength *Rt* (column 9), as well as the mechanical characteristics calculated from the propagation velocity of elastic longitudinal waves.

At a frequency of 100 kHz the wave-length of the ultrasonic wave is greater than 1.5*d* where *d* is the thickness of the test-piece. Hence the propagation of waves through the test-piece is described by the relation

$$V'_L = \sqrt{\frac{E}{\rho}} \quad . \tag{26}$$

Under an explicit form this relation becomes:

$$E = \rho\, V'^2_L = \frac{\gamma}{g}\, V'^2_L \, . \tag{27}$$

Using this expression, the elastic moduli will calculate it as shown in column 5, Table 1.

When these values are plotted graphically, as shown in Figure 5A, the pairs of values

$$R_c = a\,\gamma\, V'_L - b, \tag{28}$$

The points may be plotted as a straight line, the equation for which is ‡28, where *a* is in inches and *b* in lb/sq in. are coefficients determined experimentally. Equation 28 can be verified from a dimensional point of view when *Rc* is in lb/sq in. if we take gamma in lb/sq in. cubed and V'_L is in inches.

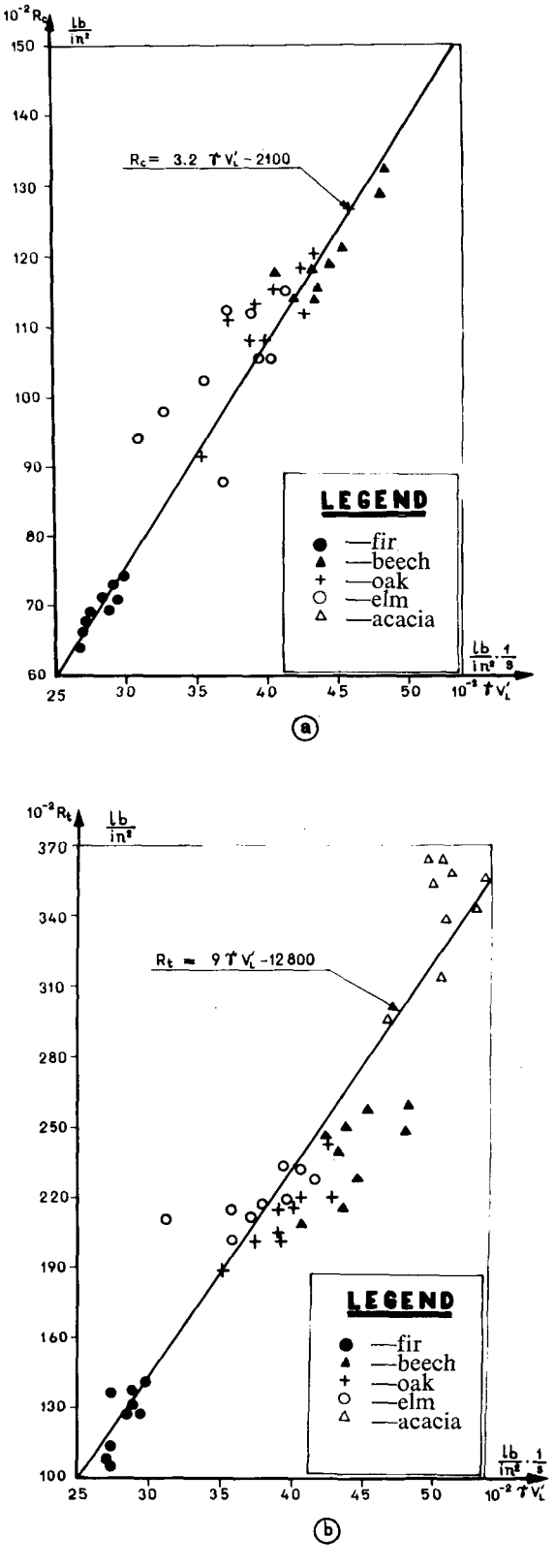

Figure 5

The values of the coefficients *a* and *b* for all wood specimens being *a* = 3.2s, *b* = 2100 lb/sq in.

Table 1

Test Zone	No.	l_0^2 lb/in³	$l_0^{-2}V_L'$ in/s	E lb/in²	R_c lb/in² Det.	Cal.	Diff. %	R_t lb/in² Det.	Cal.	Diff. %
1	2	3	4	5	6	7	8	9	10	11
				Fir Wood						
	1	1,50	1.831	1.298.860	6.900	6.687	−3,10	13.500	11.914	−11,70
	2	1,52	1.910	1.437.540	7.330	7.212	−1,61	13.640	13.390	− 1,83
I	3	1,51	1.905	1.416.960	6.970	7.116	+2,10	13.080	13.120	− 0,31
	Mediate			1.384.453	7.066	7.005	−0,86	13.406	12.808	− 4,46
	4	1,53	1.950	1.504.440	7.460	7.452	−0,01	13.920	14.065	+ 1,04
	5	1,51	1.884	1.380.240	7.110	6.988	−1,72	12.800	12.760	− 0,31
II	6	1,52	1.929	1.456.210	7.040	7.276	+3,37	12.800	13.570	+ 6,02
	Mediate			1.446.963	7.203	7.245	+0,58	13.173	13.465	+ 2,22
	7	1,50	1.790	1.240.470	6.400	6.492	+1,44	11.800	11.365	− 4,02
	8	1,50	1.810	1.267.900	6.620	6.588	−0,48	12.090	11.635	− 3,77
III	9	1,50	1.818	1.275.680	6.750	6.604	−2,17	11.650	11.680	+ 0,26
	Mediate			1.261.350	6.590	6.561	−0,44	11.846	11.560	− 2,22
				Beech Wood						
	10	2,80	1.551	1.740.000	11.380	11.820	+3,87	21.500	26.350	+22,50
	11	2,78	1.568	1.761.430	11.510	11.852	+2,97	25.080	26.440	+ 5,44
I	12	2,82	1.528	1.704.080	11.800	11.724	−0,65	23.900	26.080	+ 9,15
	Mediate			1.735.170	11.563	11.798	+2,03	23.493	26.290	+16,15
	13	2,72	1.634	1.873.680	11.940	12.108	+1,40	22.760	27.160	+19,35
	14	2,71	1.770	2.193.590	12.930	13.260	+2,55	24.790	30.400	+22,70
II	15	2,73	1.762	2.193.100	13.220	13.324	+0,79	25.920	30.580	+18,00
	Mediate			2.086.790	12.696	12.897	+1,58	24.490	29.380	+19,95
	16	2,60	1.551	1.616.000	11.800	10.828	−8,15	21.630	23.560	+ 8,95
	17	2,62	1.725	2.011.400	12.090	12.364	+2,27	25.640	27.880	+ 8,75
III	18	2,61	1.613	1.755.560	11.650	11.372	−2,38	24.620	27.790	+12,90
	Mediate			1.794.320	11.849	11.521	−2,77	23.963	26.410	+10,20
				Oak Wood						
	19	2,72	1.302	1.189.440	9.120	9.228	+1,18	18.880	19.060	+ 0,96
	20	2,76	1.417	1.430.800	11.300	10.444	−7,60	21.640	22.480	+ 3,87
I	21	2,74	1.363	1.316.480	11.090	9.868	−11,0	20.100	20.860	+ 3,77
	Mediate			1.312.240	10.503	9.847	−6,25	20.207	20.800	+ 2,96
	22	2,92	1.456	1.593.760	11.800	11.500	−2,54	24.200	25.450	+ 5,15
	23	2,92	1.464	1.609.790	11.150	11.564	+3,71	21.920	25.630	+16,90
II	24	2,90	1.495	1.670.910	12.010	11.788	−1,85	25.080	26.260	+ 4,70
	Mediate			1.624.820	11.650	11.617	−0,28	23.733	25.780	+ 8,72
	25	2,76	1.449	1.492.000	10.650	10.700	+0,47	21.500	23.200	+ 7,93
	26	2,74	1.425	1.431.310	10.800	10.380	−3,88	21.390	22.300	+ 4,26
III	27	2,78	1.460	1.526.560	11.510	10.892	−5,36	21.980	23.740	+ 8,04
	Mediate			1.483.290	10.986	10.657	−3,00	21.623	23.080	+ 6,75
				Elm Wood						
	28	2,49	1.488	1.417.100	8.830	9.740	+10,30	20.100	20.500	+ 1,98
	29	2,53	1.464	1.398.670	9.400	9.772	+ 3,54	21.080	20.590	− 2,32
I	30	2,54	1.488	1.447.740	9.680	9.996	+ 3,27	21.620	21.220	− 1,85
	Mediate			1.421.170	9.303	9.836	+ 5,74	20.933	20.770	− 0,78
	31	2,53	1.594	1.660.440	10.520	10.828	+2,92	23.160	23.560	+ 1,73
	32	2,53	1.542	1.522.200	11.080	10.380	−6,32	23.380	22.300	− 4,63
II	33	2,56	1.615	1.722.240	11.510	11.148	−3,14	22.800	24.460	+ 7,30
	Mediate			1.634.960	11.036	10.785	−2,25	23.113	23.440	+ 1,41
	34	2,59	1.377	1.267.360	10.240	9.324	− 8,95	21.400	19.330	− 9,66
	35	2,60	1.425	1.361.570	11.090	9.772	−11,90	21.070	20.590	− 2,21
III	36	2,61	1.512	1.540.500	10.520	10.540	+0,19	21.950	23.450	+ 6,84
	Mediate			1.389.810	10.616	9.878	−6,95	21.473	21.123	− 1,63
				Acacia Wood						
	37	3,18	1.464	1.756.820	13.500	12.812	−5,10	29.600	29.140	− 1,55
	38	3,31	1.633	2.252.340	14.950	15.020	+0,47	35.450	35.350	− 0,40
I	39	3,24	1.551	2.012.000	13.800	13.996	+1,42	30.600	32.470	+ 6,12
	Mediate			2.007.200	14.083	13.943	−1,00	31.883	32.320	+ 1,37
	40	3,02	1.631	2.071.320	13.940	13.644	−2,15	36.500	31.480	−13,75
	41	3,00	1.672	2.168.630	13.660	13.964	+2,20	36.200	32.380	−10,55
II	42	3,01	1.691	2.224.330	14.220	14.188	−0,22	35.600	33.010	− 7,30
	Mediate			2.154.760	13.940	13.932	−0,06	36.100	32.290	−10,80
	43	3,13	1.511	1.848.600	13.220	13.068	−1,15	35.200	29.860	−15,15
	44	3,16	1.652	2.234.210	14.220	14.636	+2,92	34.300	34.270	− 0,09
III	45	3,14	1.611	2.104.960	13.660	14.092	+2,43	33.900	32.740	− 3,43
	Mediate			2.062.590	13.700	13.932	+1,70	34.466	32.290	− 6,30

Table 2

Test Zone	No.	Period of beats ζe	ζg	Elastic Characteristic lb/in² E	G	α
1	2	3	4	5	6	7
			Fir Wood			
	1	40	7,0	1.345.760	146.525	
	2	43	7,3	1.444.718	152.472	
I	3	41	7,3	1.378.746	152.472	
	Mediate			1.389.741	150.489	14.4
	4	45	7,0	1.510.690	146.525	
	5	40	7,1	1.345.760	148.507	
II	6	43	7,0	1.444.718	146.525	
	Mediate			1.433.722	147.186	15.4
	7	36	6,5	1.213.816	136.612	
	8	37	6,0	1.246.802	126.700	
III	9	39	6,6	1.312.774	138.595	
	Mediate			1.257.797	133.969	14.7
			Beech Wood			
	10	51	13,5	1.708.606	275.387	
	11	52	14,0	1.741.592	285.300	
I	12	49	12,7	1.642.634	259.527	
	Mediate			1.697.610	273.404	8.4
	13	56	13,0	1.873.536	265.475	
	14	65	10,5	2.144.090	215.912	
II	15	59	11,6	1.972.494	237.720	
	Mediate			1.996.706	239.702	12.6
	16	47	13,0	1.576.662	265.475	
	17	65	10,5	2.144.090	215.912	
III	18	51	12,5	1.708.606	255.562	
	Mediate			1.809.786	245.649	10.7
			Oak Wood			
	19	35	14,0	1.180.830	285.300	
	20	42	13,5	1.411.732	275.387	
I	21	39	13,5	1.312.774	275.387	
	Mediate			1.310.778	278.691	5.3
	22	45	12,0	1.510.690	245.650	
	23	46	12,5	1.543.676	255.562	
II	24	48	12,5	1.609.648	255.562	
	Mediate			1.554.671	252.258	8.3
	25	44	12,0	1.477.704	245.650	
	26	42	11,5	1.411.732	235.737	
III	27	45	12,5	1.510.690	255.562	
	Mediate			1.466.708	245.647	7.9
			Elm Wood			
	28	44	11,5	1.477.704	235.737	
	29	42	10,5	1.411.732	215.912	
I	30	43	12,0	1.444.718	245.650	
	Mediate			1.444.718	232.433	8.4
	31	49	12,0	1.642.634	245.650	
	32	44	10,0	1.477.704	206.000	
II	33	48	11,0	1.609.648	225.825	
	Mediate			1.576.662	225.825	9.9
	34	37	11,0	1.246.802	225.825	
	35	39	11,5	1.312.774	235.737	
III	36	41	10,5	1.378.746	215.912	
	Mediate			1.312.774	225.824	7.6
			Acacia Wood			
	37	50	20,0	1.675.620	404.250	
	38	67	18,0	2.236.382	384.600	
I	39	58	17,0	1.939.508	344.775	
	Mediate			1.950.503	377.875	6.3
	40	59	21,0	1.972.494	424.075	
	41	63	15,0	2.104.438	305.125	
II	42	66	19,0	2.203.396	384.425	
	Mediate			2.093.442	371.208	7.2
	43	55	17,0	1.840.550	344.775	
	44	65	19,0	2.144.090	384.425	
III	45	58	18,0	1.939.508	384.600	
	Mediate			1.974.716	371.266	6.6

Equation ♯28 can then be written as:

$$R_c = 3.2\ \gamma\ V'_L - 2100 \tag{29}$$

Column 7, Table 1, shows the resistance to compression calculated using this formula, which is then compared in column 8 with a resistance compression obtained experimentally.

The relative error is found to be less than ± 10% (except in two places where the error is 11% and 11.9% respectively). This shows that equation 29 represents satisfactorily the relationship between the compression strength of wood and the speed of elastic longitudinal waves travelling parallel to the wood fibres.

A similar relation can also be obtained between the tensile strength R_t and the speed V'_L:

$$R_t = c\ \gamma\ V'_L - d \tag{30}$$

where c (in s) and d (in lb/sq in.) are coefficients determined experimentally.

From the graph shown in Figure 5b we obtain: $c = 9s$, $d = 12.800$ lb/sq in.

$$R_t = 9\ \gamma\ V'_L - 12.800 \tag{31}$$

Table 1, column 10 shows the tensile strength calculated from the equation ♯31, which can be compared with the experimentally determined tensile strength shown in column 11.

The relative error is less than ± 16% (with the exception of the samples taken from the second zone of beech wood, where the relative error reached the value of ± 22.7%).

We note that a better correlation could be obtained if an equation similar to that shown in expression ♯30 were calculated for each species of wood separately.

Testing Wood by Coupled Oscillations

Tests were performed with the apparatus described in reference 2, patent ♯43349 (2), on cylindrical test-pieces with a diameter of $d = 0.59$ in. and a calculus length $L = 8.47$ in.

The following values result for the coefficients A,B,C and D given by equation (22):

$$\left.\begin{aligned} A = 26320\left(\text{in}\ \frac{\text{lb}}{\text{in}^2}\right);\ B = 32986\left(\text{in}\ \frac{\text{lb}}{\text{in}^2}\cdot\frac{1}{s}\right) \\ C = 7750\ \left(\text{in}\ \frac{\text{lb}}{\text{in}^2}\right);\ D = 19825\left(\text{in}\ \frac{\text{lb}}{\text{in}^2}\cdot\frac{1}{s}\right) \end{aligned}\right\} \tag{32}$$

With these values, equations (15) and (18) become:

$$\left.\begin{aligned} E &= 26320 + 32986\ \zeta_e \\ G &= 7750\ + 19825\ \zeta_g \end{aligned}\right\} \tag{33}$$

The periods of beats ζ_e and ζ_g were measured for each test-piece, after which the values of the elastic characteristics E and G were calculated with equation (33).

The results of the tests are given in Table 2, which comprises both the periods ζ_e and ζ_g (columns 3 and 4) and the values of the elasticity moduli E and G (columns 5 and 6) calculated with equation (33).

The modulus of elasticity E, determined by the coupled oscillation method, has been compared with those established by ultrasonics, in Figure 6, where in the ordinate the modulus of elasticity E calculated by ultrasonics was taken, and in the abscissa the values of the modulus of elasticity E, determined by the oscillation method.

Thus a series of points have been obtained, the coordinates of which are simply the values of the elasticity modulus E, determined for test-pieces taken from the same zone (the values written in the illustration represent the arithmetic mean of the elasticity modulus E, determined for three test-pieces taken from the same zone of the tree trunk of a species), established by the two methods.

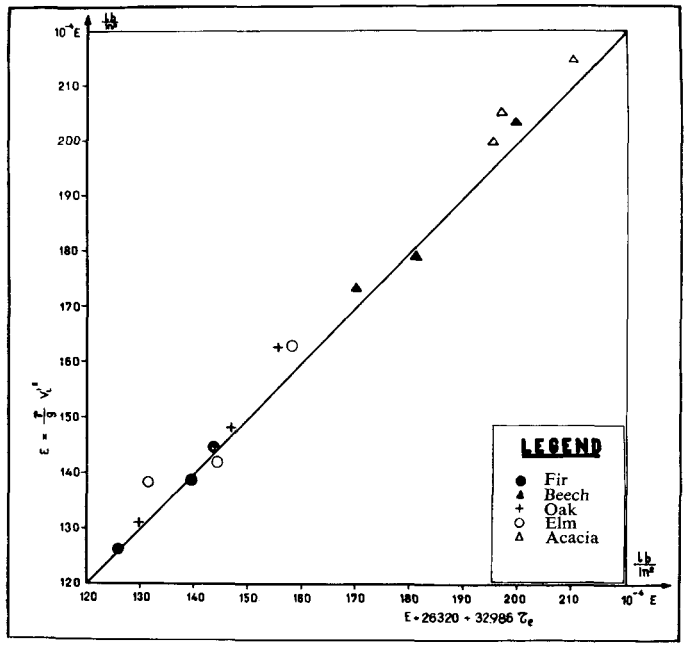

Figure 6

We see that the results obtained by the two methods are almost identical, the coupled oscillation method having the advantage in making possible the determination, on the same test-piece, the transverse elasticity modulus G also, using a very simple installation.

Interpretation of Results of the Coupled Oscillation Method

Analyzing the results from testing the five wood species we find that the average values of the elasticity modulus vary within relatively broad limits:

—fir:	E =	1.257.979 – 1.433.722	lb/in²
	G =	133.969 – 150.489	lb/in²
—beech:	E =	1.697.610 – 1.972.494	lb/in²
	G =	239.702 – 273.404	lb/in²
—oak:	E =	1.301.778 – 1.554.671	lb/in²
	G =	245.647 – 278.691	lb/in²
—elm:	E =	1.312.774 – 1.576.662	lb/in²
	G =	225.824 = 232.433	lb/in²
—acacia:	E =	1.950.503 – 2.093.442	lb/in²
	G =	371.266 – 377.875	lb/in²

We notice that the longitudinal elasticity modulus E, in all species, is maximal for wood of the second zone and minimal in the first zone (except for fir, for which the minimal was obtained in the third zone).

The transverse elasticity modulus G, in all species is maximal in the first zone, and minimal in zone three (except for beech, for which the minimal was obtained in the second zone).

Wood being an anisotropic material, it is not possible to determine the transverse contraction coefficient μ on the basis of the well-known relation:

$$\mu = \frac{E}{2\,G} - 1, \tag{34}$$

as for isotropic materials.

The application of this equation in the case of wood gives values for μ much above the maximum limit which is 0.5.

Nevertheless, a coefficient can be obtained to characterize the degree of anisotropy for wood in comparison with another material that is considered isotropic.

Taking α, the coefficient of anisotropy and comparing it with glass (which has a transverse contraction coefficient of $\mu' = 0.25$) we can define this coefficient by the relation:

$$\alpha = \frac{\frac{E}{2G} - 1}{\mu_s} = \frac{\frac{E}{2G} - 1}{0.25} = \frac{E - 2G}{0.5\,G} \tag{35}$$

Substituting in this expression the values of E and G, determined for glass, we obtain $\alpha_s = 1$ (a case in which the material is isotropic).

The values of the coefficients of anisotropy α, for each zone and wood species are given in column 7, Table 2.

We note, that for all species the coefficient of anisotropy is maximal in the second zone and minimal in the first (with the exception of elm for which the minimal is in the third zone).

If in equations (29) and (31) respectively we replace V'_L with the value given in equation (26) we obtain:

$$R_c = 3.2\sqrt{\gamma g E} - 2100 \tag{36}$$

$$R_t = 9\sqrt{\gamma g E} - 12.800 \tag{37}$$

Substituting E in these relations from equation (33), we have:

$$R_c = 3.2\sqrt{\gamma_0(26320 + 32986)\,\zeta_e} - 2.100 \tag{38}$$

$$R_t = 9\sqrt{\gamma_0(26320 + 32986)\,\zeta_e} - 12.800 \tag{39}$$

Thus two simple relations were obtained which enable us to determine the resistance compression and the resistance to stretching, on the basis of the period ζ_e, obtained by testing wood test-pieces by the coupled oscillation method.

As the elasticity moduli E, determined by ultrasonics are approximately equal, it follows that equations (38) and (39) enable us to determine the strength characteristics of wood with the same degree of precision, as do equations (29) and (31).

Conclusions

The tests carried out on five species of wood have led to the following conclusions:

1. The ultrasonic method, and the coupled oscillation method enable us to determine with the same precision the elasticity modulus E, as well as the resistances to compression and stretching.

2. The coupled oscillation method, using a more simple and cheaper installation enables us to determine both the transverse elasticity modulus G and the coefficient of anisotropy α. Thus for testing wood, this method prevails from all points of view.

3. The great advantage of the coupled oscillation method lies in the rapidity of carrying out the tests, without using any source of energy, as well as in the fact that the test is done without destruction of the material and it is possible to determine on the same test-piece all the elastic and strength characteristics of the materials and to study the influence in time of the different factors which act on these materials.

The disadvantage of the method, when compared to ultrasonics lies in the fact that the tests can be carried out only on test-pieces.

4. The study done has shown that for all wood species the elastic and strength characteristics vary from one test-piece to another, depending on the zone of the tree-trunk cross-section out of which it was taken.

5. Of all the wood species studied, elm has the best elastic and strength characteristics and a minimum coefficient of anistropy, for all the three zones of the tree-trunk.

References

(1) Popescu, N. D. Method and apparatus for determining the propagation speed of ultrasonic impulses through materials. Patent, Rumanian Socialist Republic, ‡4032/1963.

(2) ————Device for determining the elastic constants of materials, without destruction. Patent, Rumanian Socialist Republic, ‡43349/1965.

Controlling the Electric Field of Low-Frequency Dielectric Nondestructive Testing Devices

JOHN R. ZURBRICK, U.S.A.

ABSTRACT: Materials research and development programs at Avco provided the need and the opportunity to investigate the feasibility of nondestructively evaluating variability in numerous nonmetallic materials through low-frequency electric-field response. These efforts led to the development of controlled-field capacitance probes which provide high sensitivity, stability, precision and accuracy. Materials evaluation studies showed that when the projected electric field is adequately controlled and defined, particularly with reference to the electric complex plane, the quantitative response values contain as much, and in some cases even more, information on materials condition and properties as traditional dielectric tests.

The theoretical and practical properties of electric fields projected from the various capacitance test devices developed at Avco are discussed, including concepts of electric-field projection pattern, field direction, effective depth of field, and stray field projection and interception. The basic principles of probe design and construction used to control the projected field are discussed and examples shown.

Highly definitive correlations between electric-field response and such materials properties as modulus of elasticity, degree of cure, density, and moisture content for unfilled and glass-fabric-reinforced polymeric resin systems are presented. The growing future potential of low-frequency electric-field measurement as an important nondestructive test method is emphasized.

Introduction

A Need for Nondestructive Testing

An increasing quantity of nonmetallic materials is providing design advantages in critical aerospace applications. Evaluation of the performance reliability of these materials in service requires nondestructive testing. For reasons of inherent anisotropy and profoundly different electrical properties, among others, extrapolation of nondestructive testing techniques from metals experience has been largely frustrated.

Research and development programs at Avco Space Systems Division have dealt with this problem for the case of fibre-reinforced composites designed for structural, primary load-bearing applications. (1, 2)

Experience has shown that all composites, particularly those produced under laboratory or batch-production conditions, vary significantly in composition and properties, both within a part and between like parts, even in the absence of gross defects. While we recognize the seriousness of gross defects, it is the inherent variability which determines the true reliability of a material under specific design criteria.

The approach taken was that of carefully studying the detailed physical and mechanical properties typifying reinforced plastics, and the specific properties of each fibre or matrix included in the composite. This, combined with the knowledge and understanding of energy forms applicable to nondestructive testing, provided the basis for a fresh analysis of the problem.

Emphasis was placed then on developing nondestructive test techniques that would provide quantitative indications directly linked to the kind, degree and location of relevant variability occurring in fabricated composites. Variability in reinforced plastics has been traced to local changes in resin content, porosity content, degree of cure, and moisture content, to name the most prevalent.

Using the Electric Field

One energy form, the low-frequency electric field, offered one of the greatest potentials for evaluating reliability of reinforced plastics. Traditional dielectric testing, based on the theory of parallel capacitor plates, is being widely used for determining the electrical properties of electrically insulating materials. Many of these are a filled or reinforced plastic.

A review of nondestructive testing literature early in our work pointed up the almost complete lack of applied low-frequency (1 kHz to 100 kHz) electric-field measurements. Some limited practical applications had been accomplished, mostly in the areas of thickness measurement, pinhole detection and the determination of moisture content. (3) The most logical step was to adapt the electric field in general to the special purposes of nondestructive testing.

The first goal was to develop a suitable projected electric field, a field that could intercept a known volume of the material in question and provide a characteristic response. By projecting the field, a one-side probing technique could be developed for the all-too-frequent situation where physical access is limited to just one side, as in completed assemblies. This approach offered quick, on-the-spot information, a factor of prime economic importance in practical nondestructive testing evaluations.

By comparison, in most traditional dielectric tests, a machined specimen or limited section of material must be placed in the electric field between parallel capacitor plates with adequate shielding surrounding the test arrangement. Hence, the development needs and constraints were clear. Most important, development was certainly required.

A search of existing dielectric test methods and apparatus provided a starting point for the development effort. The discussions of ASTM test method D 150 covered the traditional methods. (4) A particularly remarkable contribution was that of J. J. Knudsen and co-workers at the Delsen Corporation almost 10 years ago. (5) Their pioneering development of a proprietary instrument the D-K Analyzer, for dielectric measurements using a coplanar capacitance probe, appeared at first to provide a ready system for nondestructive dielectric testing. Our own experience with this instrument, however, revealed its practical shortcomings, which explained to us the noteworthy absence of this instrument and technique in nondestructive testing literature.

The greatest difficulty lay in the interpretation of capacitance-probe response. Particular difficulty was encountered when more than one variable in the material was changing at the same time. This was further complicated by "probe effects" which had no apparent relationship to materials variation. The only alternative was to begin at the beginning and build up a firm understanding of capacitance-probe theoretical and practical characteristics along with a knowledge of empirical design factors.

In our development program over the past 4 years, we studied the theoretical electron-distribution character of the coplanar capacitor, (6) and learned how physically to control the electric field. We built prototype probes for moisture determinations and materials variability evaluations to test out practical designs as well as solve in-house testing problems. These studies proved that a properly controlled, well defined projected electric field can yield even more quantitative information on material condition and properties than traditional dielectric test methods.

Corollary to its feasibility, electric-field response measurements must be intelligently applied to a given nondestructive testing problem. This requires the test engineer and operator to be completely familiar with the working characteristics of the capacitance probe. In hope of stimulating wider interest, this paper provides an initial familiarization for those concerned with nondestructive testing. It describes the parameters controlled in a projected electric field, the characteristics common to coplanar capacitance-probe devices, the effect of materials variables on indicated response, and preliminary correlations between electric-field response and materials properties.

Controlling the Projected Field

Definition

In the broadest sense, a dielectric probe is any device that behaves as a capacitor while producing an electric field capable of interacting with a given volume of material. For nondestructive test purposes, the probe must be so designed that specimens of specific geometry are not required but rather that point-by-point or scanning measurements of the component in the whole may be accomplished.

General Probe Characteristics

An understanding of the apparently universal characteristics exhibited by projected electric-field capacitance probes goes a long way toward intelligently applying them to nondestructive testing. The special characteristics of the parallel-plate capacitor and its mathematical model are familiar to many. Should the parallel capacitor be opened in the manner of a hinge until both plates lie in the same plane, the field once "captured" becomes projected outward. The field is then free to extend omnidirectionally and without limit; the familiar analytical relationships become useless. Distribution of this field, in terms of strength and vector direction, is partly a function of the capacitor plate shapes and proximity to each other, requiring an entirely new analytical model.

This simple picture of two capacitor plates side-by-side in space is the basic configuration of a coplanar dielectric probe having an "uncontrolled" electric field. Such a configuration is obviously quite useless as the field is sensitive to all objects in the surrounding environment, and to all other electric fields existing in that environment.

To be used as a quantitative measuring instrument the capacitance probe must demonstrate sound instrument qualities:

—stability over a long time-period
—measurement precision
—high sensitivity (where needed)

In addition, it must provide an appropriate and determinable depth of penetration so that the volume of material interrogated is known. These considerations provide firm guidelines for probe development investigations.

Capacitance Element Design

Two steps are required in controlling the projected electric field. First the field is attenuated or "grounded out" in all directions except the desired direction.(7) Objects in the surrounding environment, including the probe handle and operator's hands, no longer can influence probe response. Second, the gradient energy of the field is concentrated close to the face of the probe, diminishing with distance from the probe face. It lies within a given geometrical area of resolution, so that sensitivity is high and volume of material interrogated is established. Objects that are in front of the probe but beyond its depth of field exert negligible effect on probe response. Detailed distribution of the field energy over the probe-face active area, and point-in-space electric field vector, are also important design factors.

The effective depth of penetration (depth of field) characteristic of the probe-face design may be established with some "standard" material such as polymethylmethacrylate (PMMA) sheet. Depth of field is defined as that thickness of material beyond which no further addition of the same material will influence indicated electric-field response. Although indicating instrument sensitivity may influence the exact depth of penetration value, the cut-off of response with thickness for the probes investigated has been remarkably constant and sharp over a wide range of sensitivities. The dielectric character of the material under test does influence depth of penetration, generally being an inverse function of dielectric constant.

Although the design of a probe-face element, in terms of electrode size, proximity, and shape, controls the basic direction and pattern of the projected electric field, the test-material geometry exerts a definite influence on field pattern and therefore on probe design. For this reason, a design must be matched to the particular nondestructive testing situation.

Probe Construction

The general construction of the coplanar probe shown in Figure 1 was developed as a result of experience gained in testing aerospace vehicle components and materials. Probes of this type have been convenient to use and are relatively easy to make. Total weight and weight distribution, handle size, cable terminal location and position, cable flexibility and length, and assembly techniques are all factors of the design. The printed-circuit probe element has been found to provide the greatest design flexibility necessary for proper control of the projected electric field. This manufacturing technique has greatly aided the rapid transition of experimental face designs into finished dielectric probes while providing inherent stability to them.

Indicating Instrumentation

As defined, the probe device is basically a capacitor and therefore any capacitance-responsive instrumentation system conceivable through the wizardry of electronics may be used to indicate electric-field response characteristics. The emphasis in this paper is concentrated on the probe, since the indicating instrumentation may be selected to meet specific test condition needs. While the material under test will dictate probe design, the various needs for a given level of sensitivity, range of measured values, test frequency, and operator skill will influence the indicating equipment selected.

A general-purpose system assembled in our laboratory for voltage response measurements is shown in Figure 2A. It was used first to study the frequency and voltage characteristics of various probe designs, and to measure variables in reinforced plastic panels. The Ballantine Direct Capacitance Meter, Figure 2B, contains the essentials of the laboratory system in a single package. The meter is calibrated in capacitance values which are sufficiently accurate for low-loss materials. The probe attached to the meter was specifically designed for determination of moisture content in sheet materials 0.10 in. (0.25 cm) to 0.50 in. (1.27 cm) thick.

Where the complex impedance function of electric-field response contains the desired materials-variability information, a true capacitance bridge circuit is used. Simultaneous changes in dielectric constant and dissipation factor from point to point in the material cause corresponding changes in electric-field response phase shift and attenuation. These are sensed by the bridge circuitry as reactive impedances and resistive impedances, and displayed, at balance, as relative capacitance and relative dissipation factors. These values relate to the specific probe and connecting cables used. Thus, a complex impedance plane diagram may be developed from these values for a given probe, and used to interpret material-variability indications observed.

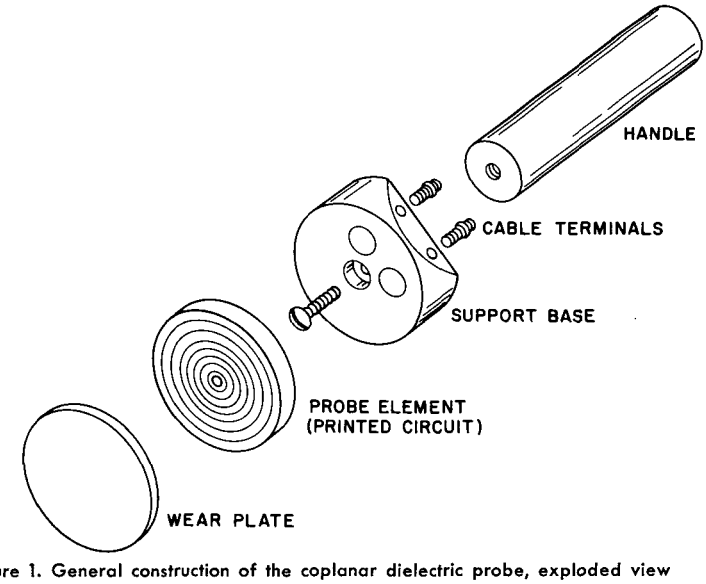

Figure 1. General construction of the coplanar dielectric probe, exploded view

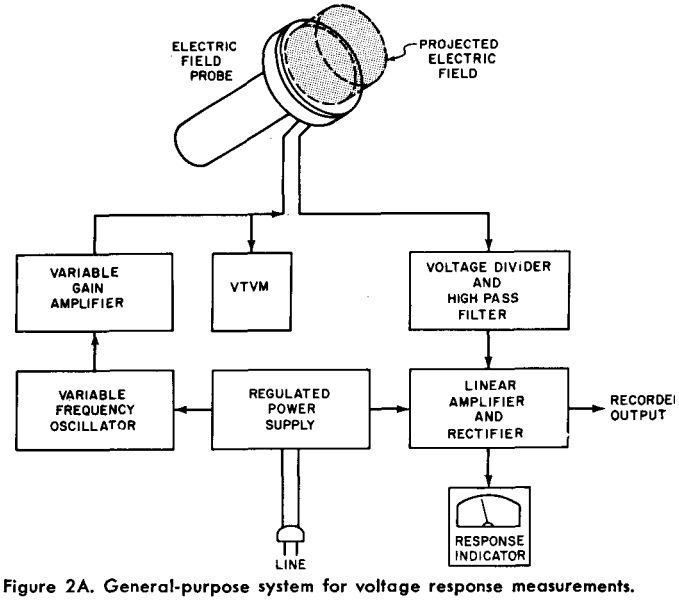

Figure 2A. General-purpose system for voltage response measurements.

Gating circuits, blinking lights, horns and buzzers, strip-chart recorders, capacitive controlled oscillators, multiple-frequency techniques, and automatic bridges, to name a few, are all useful to nondestructive dielectric testing.

Figure 2B. AVCO/SSD-designed probe attached to a commercial direct capacitance meter.

Effects of Materials Variables

Basic Studies

Once generalized capacitance-probe character and design were understood, interest was focused on the response of the projected electric field to compositional and geometrical parameters in various nonmetallic materials. The studies first involved thermoplastic sheet materials in order to limit and control the influencing variables. From this work, a more distinct understanding of empirical field-response relationships was gained.

Complex Dielectric Property Influence

As may be seen from the graphs in Figure 3, material changes that influence either dielectric constant or dissipation factor consistently influence capacitance-probe electric field response. For plastic materials, such changes may correspond to changes in average molecular weight, molecular weight distribution, extent of cure, mixture ratios, moisture absorption, and so on.

The relationships in Figure 3 were obtained with an Avco/SSD-designed probe having a 2-in. (5.1-cm) dia. and an effective depth of field of 1.5 in. (3.8 cm) (referenced on PMMA). The blocks of material evaluated were 4 in. (10.2 cm) square by 3 in. (7.6 cm) thick. Measurements were taken simultaneously at 10 kHz with 3 volts RMS input to the probe. The indicating instrumentation was a General Radio Capacitance Bridge Assembly, Type 1620-A.

Thickness and Volume Effects

Almost every nondestructive testing energy form is influenced by the geometry of the test material, and nondestructive dielectric testing is no exception. Figure 4A exhibits the primary influence of thickness, while Figure 4B exhibits the secondary influence of material area presented to the probe. Although they may be lumped together as a "volume factor", confusion is avoided by separating them as shown. The same 2-in. (5.1-cm) dia. by 1.5-in. (3.8-cm) depth-of-field probe was used in this case but at 1 kHz and 50 volts RMS input. The Ballantine Direct Capacitance Meter, Model 520, provided response indications.

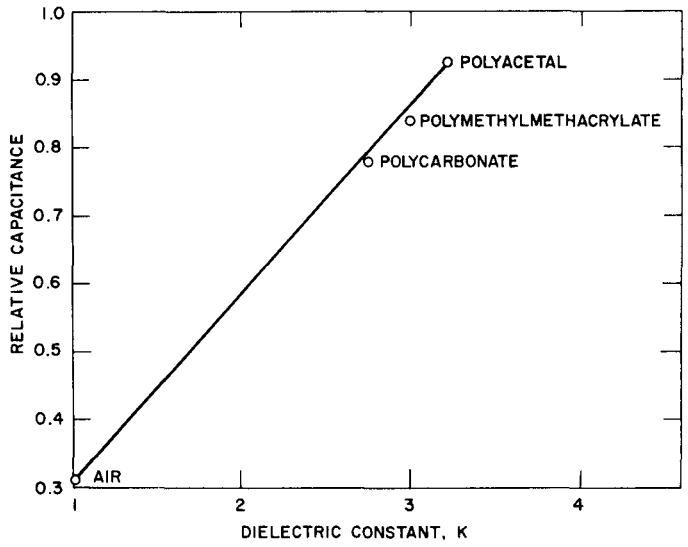

Figure 3A. Relative capacitance response to dielectric constant in thermoplastic materials.

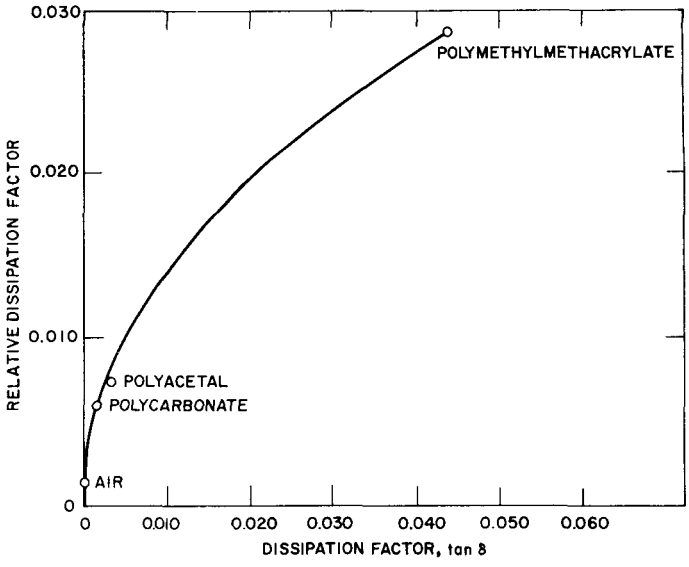

Figure 3B. Relative dissipation factor response to dissipation factor in thermoplastic materials.

Note in Figure 4A the characteristic response curves with thickness typical of coplanar probes. The probe studied here is useful for materials-variability determinations independent of thickness variation at thicknesses greater than 1.5 in. (3.8 cm). It is useful for thickness measurements independent of materials variation at thicknesses less than 0.2 in. (0.51 cm). Between 0.2 in. (0.51 cm) and 1.5 in. (3.8 cm), the field response contains both variables and at best is difficult to interpret.

In Figure 4B, the influence of increased area presented to the probe was one of increased energy loss, which accounted for the decreased capacitance values. For thicknesses greater than 1.5 in. (3.8 cm), the influence became constant when area presented was equal to or greater than approximately ten times the probe-face area of resolution.

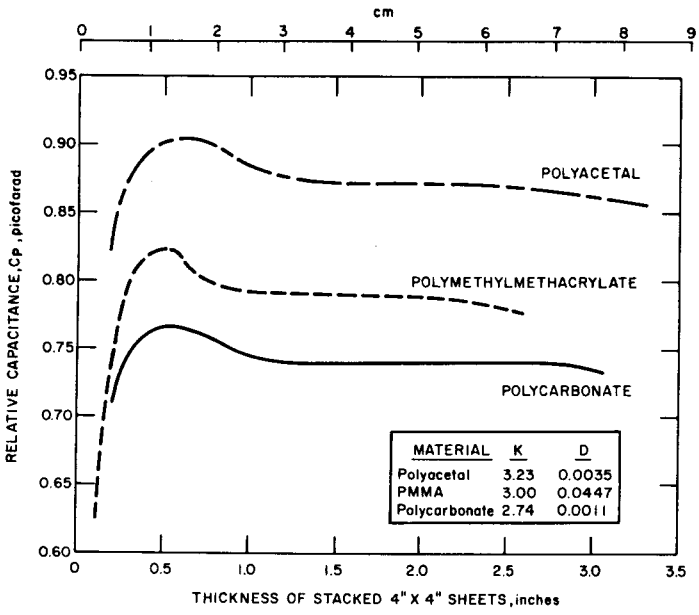

Figure 4A. Thickness effect on electric field response with the 2-in. (5.1 cm) diam. by 1.15-in. (3.8 cm) depth of field probe for three thermoplastic materials.

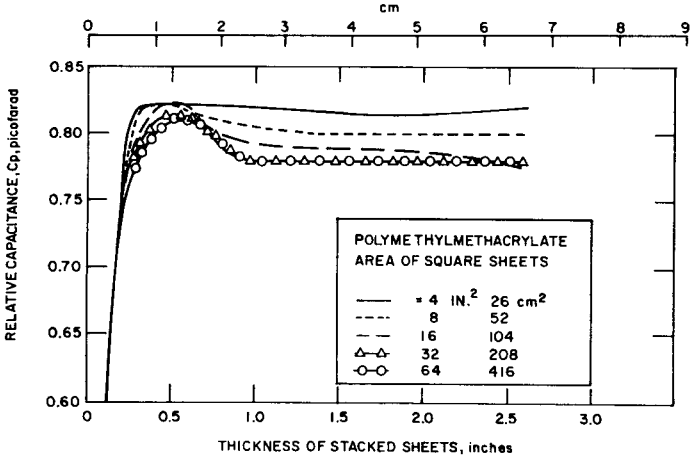

Figure 4B. Parametric effect of area presented to the dielectric probe.

Preliminary Correlations

Studies on Representative Reinforced Plastics

Dielectric probe measurements in unfilled cast resins and glass fabric laminates produced from them, in the continuing U.S. Air Force-sponsored nondestructive testing program, provided a valuable opportunity to refine techniques and sharpen the interpretation of response indications. Preliminary correlations between materials properties and electric-field response values obtained in these studies have established the practical feasibility of nondestructive dielectric testing.

Degree of Cure

Figure 5 shows two relationships developed for a cast epoxy system. Series B represents an 80% to 90% extent of reaction (degree of cure) range, and Series C a 95% to 98% range. Although cure conditions were similar, the physical and electrical properties of the two series were distinctly different, as may be seen in these correlations.

Figure 5A is particularly significant in that the probe used had a $\frac{1}{4}$-in. (0.64-cm) × $\frac{1}{4}$-in. (0.64-cm) area of resolution and an 0.030-in. (0.76-mm) depth of field, while the tensile specimens were nominally $\frac{3}{4}$ in. (1.9 cm) thick.

The relative capacitance data in Figure 5B were obtained with a probe having a 1-in. (2.54-cm) × 1-in. (2.54-cm) area of resolution and an 0.060-in. (1.52-mm) depth of field. Density increase in Series B came as the normal result of advancing cure. The corresponding decrease in relative capacitance values is in harmony with dielectric theory and test experience.

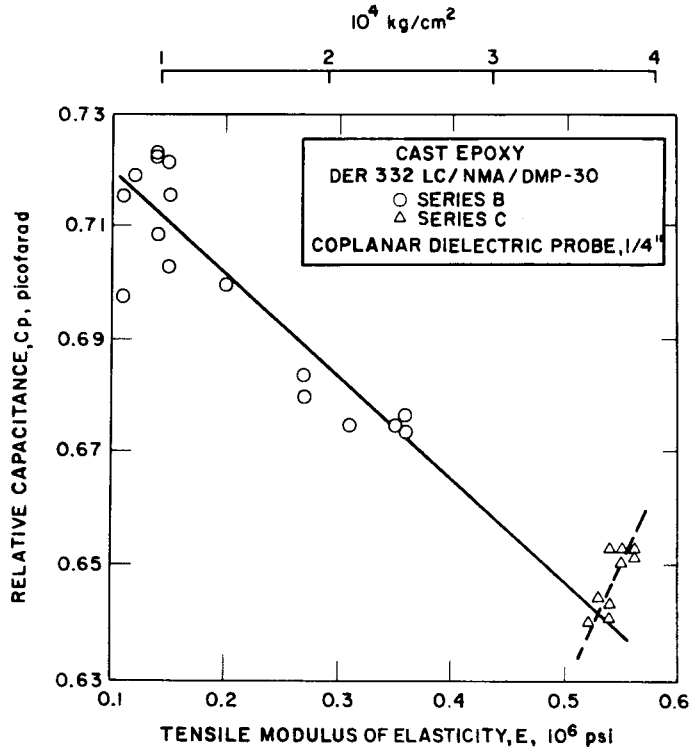

Figure 5A. Electric field response vs. tensile modulus relationship for range of resin degree of cure.

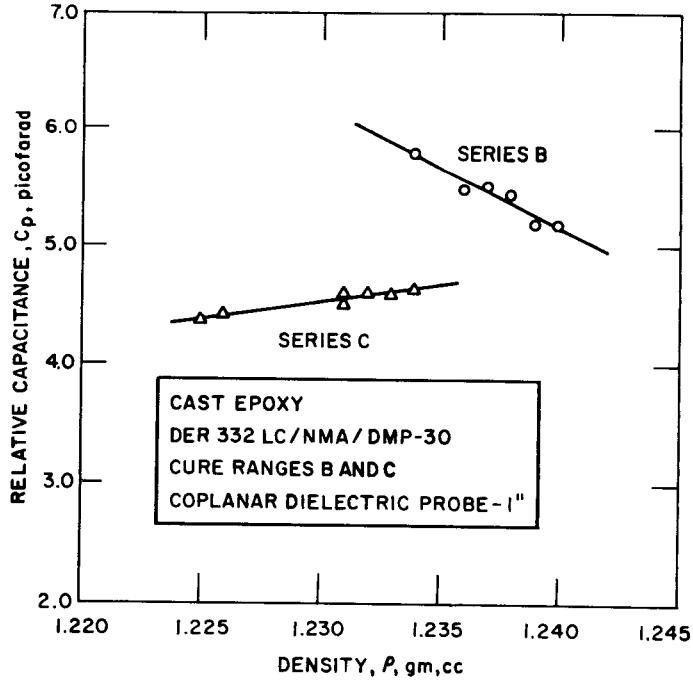

Figure 5B. Electric-field response vs. resin density for two degree of cure ranges.

However, Series C behaved quite oppositely. Further investigation disclosed that volatiles had been lost during post-cure operations, resulting in a small amount of distributed microporosity throughout the castings. In fact, as post-cure temperatures were increased, more volatiles were lost, resulting in lower densities with slight advances in resin cure.

Returning to Figure 5A, the distributed microporosity influence on tensile modulus is quite evident as indicated by the dashed line. However, this correlation does show the predominant and consistent influence of degree of cure on both tensile modulus and electric-field response.

Glass Fabric Laminate Variability

The correlations in Figure 6 extend the dielectric probe technique into much more complex systems. These glass-fabric laminates were viewed as a highly anisotropic, three-component system consisting of glass, resin, and distributed porosity. The compositional and geometrical occurrence of each is essentially random within fairly broad limits, i.e., 25% to 40% by weight resin content and 0.5% to 10% by volume porosity content.

Laminates represented in Figure 6A were prepared from the same epoxy resin system studied in Figure 5. In this correlation, the electric field responded linearly to glass content and porosity content as they influenced density in machined specimens.

In Figure 6B, density was determined on as-fabricated 9-in. (23-cm) × 16-in. (41-cm) polybenzimidazole resin laminates at 32 points using a nondestructive gamma radiation gauging technique. These values were correlated with relative capacitance values obtained at the same test locations on each laminate. The two laminates, N-1 and N-2, prepared under very similar fabrication conditions, exhibited one set of dielectric properties as shown in the correlation. The third laminate (N-4) had been prepared under somewhat different fabrication conditions. The dramatic effect of fabrication conditions on electrical character is vividly reflected in the resulting correlation.

Note that correlations involving materials variability have involved electric-field response changes measured in tenths, hundredths, and even thousandths of a picofarad. These are quite sensitive measurements. By comparison, moisture content determinations involve electric-field response changes at the picofarad level (2 picofarads for each per cent of moisture), as shown in Figure 7. Dielectric probe determination of moisture content has been relatively easy as a result of the high dielectric constant (81) exhibited by water vapor at room temperature.

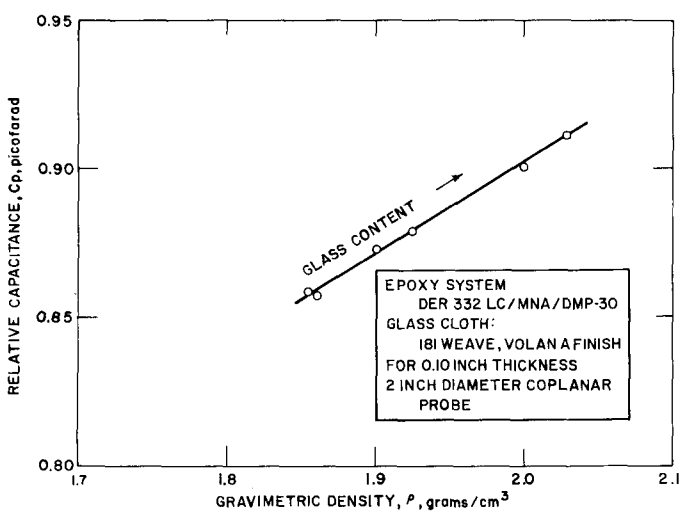

Figure 6A. Electric-field response vs. density for glass fabric reinforced epoxy laminate system.

Because of this, even small moisture content changes in a material must be avoided when it is being dielectrically evaluated for variability.

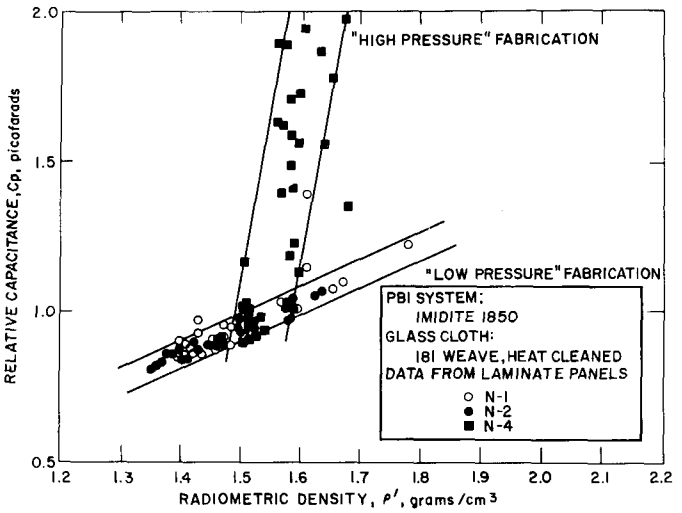

Figure 6B. Electric-field response vs. density for glass fabric reinforced polybenzimidazole laminate system.

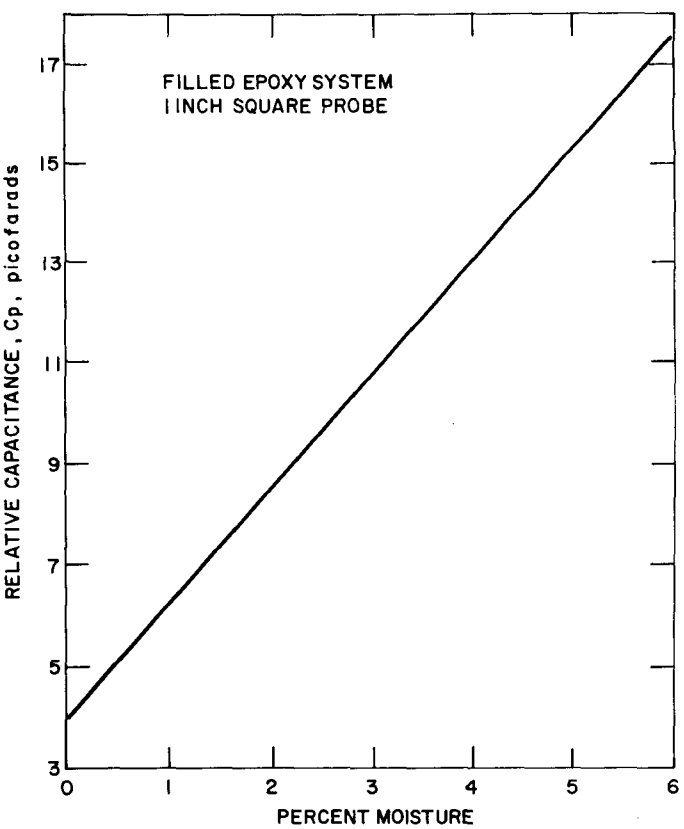

Figure 7. Typical calibration curve for dielectric probe determination of moisture content.

Summary

The increasing use of reinforced plastics, mixed composites, wood, ceramics and other nonmetallics in critical military and civilian applications has provided the need for nondestructive dielectric testing as a tool to assure reliability. A basic understanding of projected electric-field response character has been developed and test studies have proven the utility of the capacitance-probe for nondestructive test evaluation of materials variability. The lesson we learned was that each nondestructive

test situation will require a properly controlled projected field as provided by a dielectric probe of specific design, with indicating instrumentation selected to meet the readout conditions dictated by the over-all nondestructive testing problem itself.

The low-frequency electric-field form of energy generally has received relatively little attention in the search for methods and techniques applicable to solving nondestructive testing problems. As more is learned of its capabilities for evaluating nonmetallic materials, the electric-field method will grow to full stature among those familiar methods being widely applied today.

References

(1) Zurbrick, J. R. and Chiklis, C. K. Development of nondestructive methods for the evaluation of organic non-metallic materials, Tech. Rept. AFML-TR-65-267 (October, 1965), 188 pages.

(2) Zurbrick, J. R. Development of nondestructive methods for the quantitative evaluation of glass-reinforced plastics, Tech. Rept. AFML-TR-66-269, (June, 1966), 101 pages.

(3) McMaster, R. C., editor, Nondestructive Testing Handbook, The Ronald Press Co., New York (1963), vol. I, pp. 5.21-22.

(4) A-C Loss Characteristics and Dielectric Constant (Permittivity) of Solid Electrical Insulating Materials, (D150), 1966 Book of ASTM Standards, Part 29.

(5) Oleesky, S. S. and Mohr, J. G. Handbook of Reinforced Plastics of the SPI, Inc., Reinhold Publishing Corporation, New York (1964), pp. 568-574.

(6) Lynnworth, L. C. Inspection of material uniformity and thickness using dielectric measurements, *Proc. Fourth Internat. Conf. on Nondestructive Testing*, London (September, 1963), pp. 283-290.

(7) Operating Instructions, Type 1620-A Capacitance Measuring Assembly, (October, 1963), General Radio Company, West Concord, Mass., p. 19.

The Relationship between Ultrasonic Inspection Results, Slag Inclusions, and Fatigue Strength

SVEN MALMQVIST, SWEDEN

ABSTRACT: A small steel pressure vessel, fatigue stressed in service, was inspected by ultrasonics for inclusions that were thought to impair its fatigue strength. Therefore the relation between fatigue strength and ultrasonic indications caused by inclusions had to be established. This was done for bar material from which the vessels were fabricated—a chromium-molybdenum steel equivalent to SAE 4130 heat-treated to 100 kp/mm² (140 kpsi) ultimate tensile strength—as well as for the vessels themselves.

The bar material was inspected by ultrasonics to select test samples with a high inclusion rate. From the test samples, fatigue-test pieces were prepared perpendicular to the rolling direction. The test pieces were also inspected by ultrasonics and the indications recorded.

In addition, fatigue tests were performed with pressure vessels made from the same type of bar material. They were inspected by ultrasonics using the same technique as for the fatigue-test pieces.

When comparing the results of the fatigue tests with those of the ultrasonic inspection it was evident that, for both the bar material and the pressure vessels, the best relationship existed between the fatigue strength and the *sum* of the ultrasonic flaw echoes.

Introduction

A hydraulic cylinder barrel, fatigue stressed in service, was manufactured from steel bar material, containing some abnormally heavy slag inclusions. Fatigue cracks originated from these inclusions causing leakage of the hydraulic oil through the barrel wall. Therefore it was necessary to inspect the barrels by ultrasonics in order to differentiate barrels with heavy slag inclusions from acceptable ones.

It was also of interest to investigate the relationship between the fatigue properties and ultrasonic inspection results for the barrels, and for the bar material from which the barrels were fabricated.

Investigation of the Bar Material

The material concerned was a chromium-molybdenum steel equivalent to SAE 4130 and heat-treated to a strength level of 100 kp/mm²(140 kpsi).

The fatigue-test pieces were prepared from bars in the transverse direction, which was of special interest because the pressure vessels were also stressed in this direction.

To get adequate test-pieces, bar material in stock was inspected by ultrasonics for inclusions. Bars with heavy inclusions were then used for the preparation of test-pieces.

Test samples from the bars were .16 × 1.38 × 1.97 in. (4 × 35 × 50 mm) in size and sheet material of the same composition was welded to both ends of these samples to get test-pieces of sufficient length. After heat treatment to the required strength level, machining and grinding, the test-pieces had the shape suitable for the Amsler high-frequency pulsator used for the fatigue testing.

All test-pieces were inspected by ultrasonics to observe possible defects that might influence the fatigue strength. This inspection was performed with a normal pulse-echo apparatus with miniature probes for surface waves and for transverse waves with 70° incidence in steel. The conditions for the ultrasonic inspection were held as constant as possible by using reference blocks with artificial defects for calibration. The echo traces on the oscilloscope screen were recorded on 35-mm film with a Robot camera.

Fatigue testing was performed in an Amsler high-frequency pulsator with a frequency of 90 c/s. The stress pulsated between 0 and a maximum.

The results were compared with the ultrasonic indications (flaw echoes); high echoes evidently were associated with a short fatigue life, but the results were very scattered.

This being so, the correlation between the number of cycles to failure and the sum of the flaw echoes from various locations of the test-piece was investigated. This sum was obtained by measuring the heights of the echoes on the film recordings of the oscilloscope screen trace. In this way the scatter was considerably reduced (Figure 1).

From fatigue testing at other maximum stress levels than that represented by Figure 1 (40 kp/mm²) (57 kpsi) it was observed that the scatter increased as the maximum stress limit was reduced.

Investigation of Cylinder Barrels

The cylinder barrels were fabricated from bar material with a diameter of 4.7 in. (120 mm). The material was the same chromium-molybdenum steel—equivalent to SAE 4130—as mentioned above and the barrels were heat-treated to the same strength level as the fatigue-test pieces, 100 kp/mm² (140 kpsi). The cross-section of the tested part of the barrel is shown in Figure 2; its total length was 9 in. (230 mm).

For the ultrasonic inspection of the barrels the same equipment as for the fatigue-test pieces was used. The probes were placed on one of the flat parts of the surface, where very good coupling was achieved. Both flat surface areas were used for scanning and in this way each half of the barrel could be scanned separately. A specially designed curved probe was used for scanning the inner surface. In this case the degree of coupling could be estimated from the indication from the wave travelling around the barrel and entering the probe from the back side (Figure 2). The inner surface was scanned on three equally spaced sources.

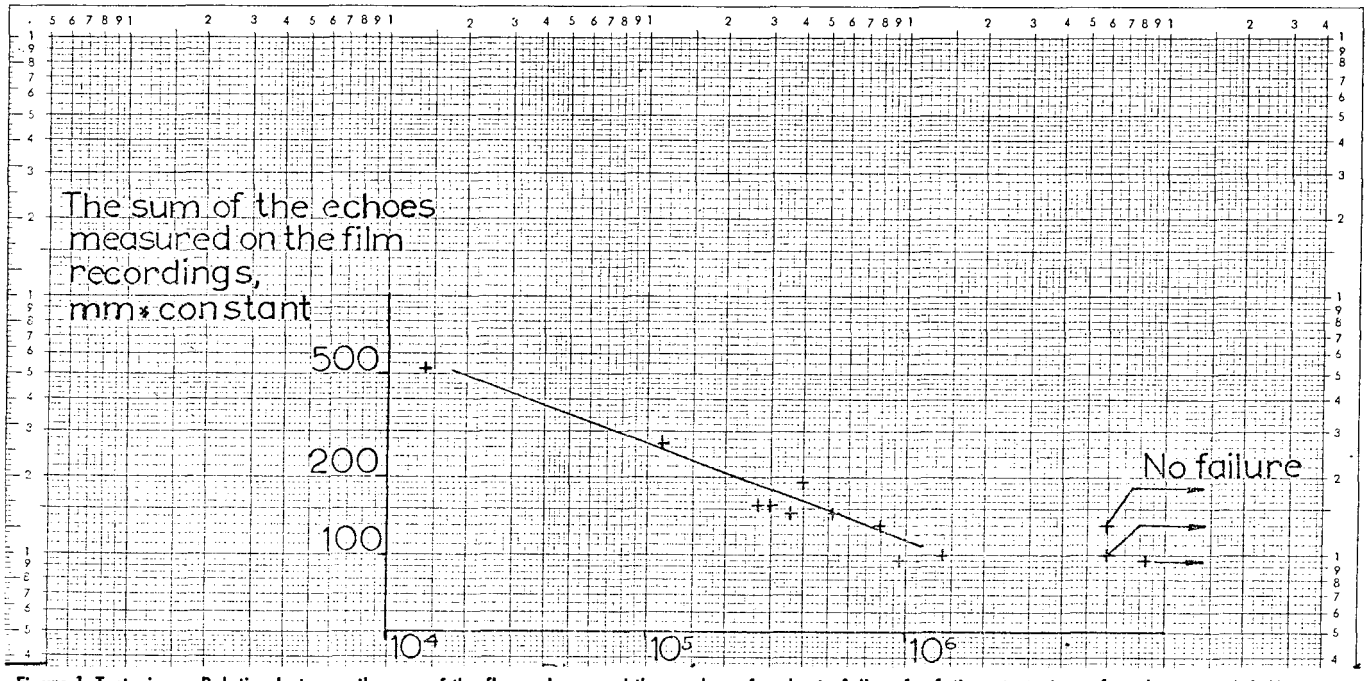

Figure 1. Test-pieces. Relation between the sum of the flaw echoes and the number of cycles to failure for fatigue test-pieces from bar material. Max. stress 40 kp/mm².

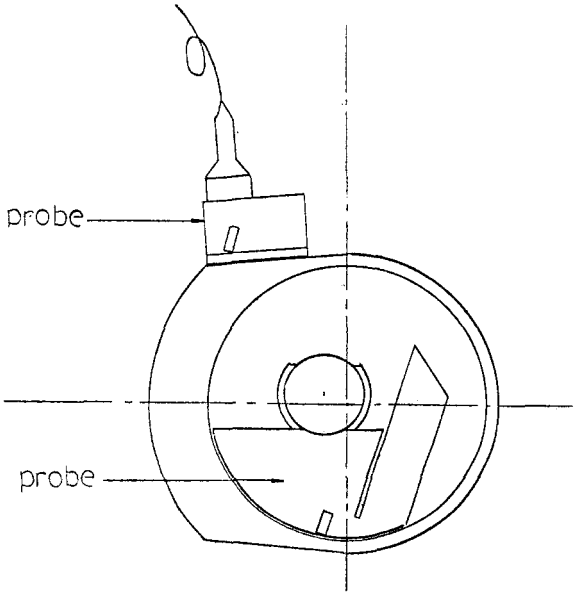

Figure 2. Cross-section of the cylinder barrel; inner dia 2.37 in. (60 mm) and wall thickness .12 in. (3 mm).

The flaw echoes were compared with those caused by artificial defects in a reference plate and in a reference barrel of the actual thickness. The artificial defects consisted of holes with square sections of .04 × .04 in., .08 × .08 in., .12 × .12 in. (1 × 1 mm, 2 × 2 mm, 3 × 3 mm) and so on, designated defects no. 1, 2, 3 etc.

The penetration of the sound beneath the surface was controlled on a barrel with a wedge-shaped slot in the wall. At one end the slot fully penetrated the wall and then its depth decreased linearly to zero along the barrel. Thus it was shown that the whole wall thickness could be covered by scanning from both the outer and the inner surface with surface-wave probes. As an additional precaution a probe for transverse waves with 70° incidence in steel was used.

The number and magnitude of the flaw echoes were recorded. In the first place smaller indications than those corresponding to echoes from the reference defect no. 1 were not taken into account.

Fatigue testing was performed with some of the cylinder barrels. A plug with a tube for hydraulic oil was inserted into the open end of the barrel and a hydraulic pump exerted pressure in the barrel alternating between zero and a maximum value. The number of cycles until leakage occurred was recorded.

Results

The results were compared with the ultrasonic indications (flaw echoes). As for the fatigue-test pieces high echoes were associated with a short fatigue life, but the results were very scattered.

In this case, too, the correlation between the number of cycles to failure and the sum of the flaw echoes from various locations of the test barrel was investigated (Figure 3). In this

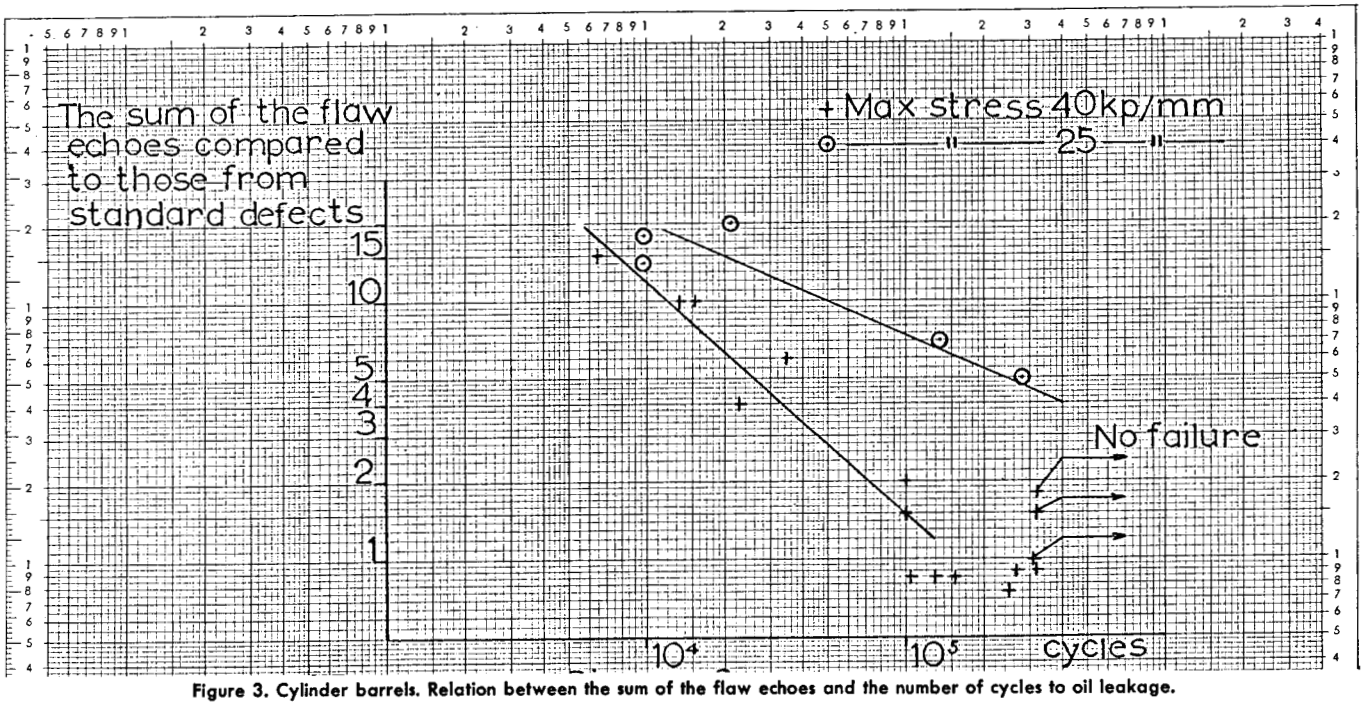

Figure 3. Cylinder barrels. Relation between the sum of the flaw echoes and the number of cycles to oil leakage.

way, the scatter was reduced. However, the scatter increased as the maximum pressure was reduced.

After fatigue testing the cylinder barrels were broken up along the fatigue cracks and examined. In all barrels having given flaw echoes the fatigue cracks had started from slag inclusions, which could be observed in crack surfaces.

In some cases locations having given flaw echoes were sectioned. These sections were prepared for micro-examination and determination of the size of the slag inclusions. Echoes equivalent to the standard defect no. 1 were observed to be due to slag inclusions with a maximum cross-section of 50-150 μm (2-6 mils) and echoes corresponding to standard defect no. 4 to inclusions with 400-600 μm (16-24 mils) maximum cross-section.

Summary

For both test-pieces and barrels, a fairly good correlation was found to exist between fatigue life and the sum of the flaw echoes. This could be expected because both are functions of the inclusion rate of the steel. However, several factors influence both these sets of data, resulting in the scatter observed.

First, the fairly small number of test-pieces and barrels must be considered.

Fatigue life varies with size, shape and position of inclusions. For example, an inclusion oriented perpendicularly to the direction of the principal stress has a higher notch effect than when in a parallel position. The notch effect also is higher for an inclusion close to the surface than if it is situated at a greater depth.

The size, shape and orientation of an inclusion can make it more or less ideal as a reflector for ultrasound and its position is also important because the sensitivity of the surface-wave probe decreases with the depth under the surface. Attention must also be paid to the varying coupling conditions involved.

Taking the random distribution of size, shape and position of the inclusions into considerations, it is not surprising that their influence is better expressed by the *sum* of the flaw echoes than by the individual echoes.

Discussion

Q. DAVID STEIN, Picatinny Arsenal, Dover, USA:
Was there any correlation between location where oil leakage first occurred and location of flaws? Unless this correlation exists, one would question the value of the studies described.

A. Yes, in all barrels having given flaw echoes, the fatigue cracks—and as a consequence the oil leakages—started from slag inclusions, which could be observed in the crack surfaces. My paper gives this information under the heading "Results".

Ultrasonic and Metallurgical Evaluation of Flaws in Large Rotor Forgings

R. W. RENNER
HERMAN A. GREENBERG
W. G. CLARK, Jr., U.S.A.

ABSTRACT: Flaw size in large alloy steel rotor forgings is currently evaluated by either a back reflection or a reference block ultrasonic testing technique, as specified in ASTM A418. This paper describes the development and application of the reference block technique for the inspection of rotor forgings. Included is a discussion of the many variables in the test which, if uncontrolled, could seriously affect ultrasonic reflection amplitude and lead to erroneous estimates of flaw size. A relatively simple inspection technique is presented by means of which inspectors can report flaw size directly in terms of equivalent reflecting area. Nine case histories are presented showing the correlations between ultrasonic data and metallographic appearance of flaws found in large turbine generator rotor forgings.

Introduction

Ultrasonic evaluation of small flaws (less than 1 sq in. in area) in parts having flat surfaces is frequently based on a comparison with flat-bottom holes in reference blocks made from the same material. By performing the comparison at identical test depths the effects of attenuation in the material and radiation decay of the sound beam are compensated for automatically. The inspection of turbine-generator rotor forgings presents the additional problem of testing from curved surfaces of several different diameters.

Two distinct procedures have evolved for the ultrasonic inspection of rotor forgings and are described in ASTM Specification A418; namely, the per cent of back reflection technique and the reference block technique. The per cent of back reflection technique relies on reporting the amplitudes of flaw reflections which exceed a specified percentage of the back reflection from either the bore of the rotor or, if unbored, the opposite side. This procedure automatically provides compensation for attenuation differences from rotor to rotor, couplant losses and surface finish variations. In order to provide meaningful results, compensation must be provided for forging geometry and flaw orientation, depth, and area by utilizing correction factors based on experimental measurements on rotor forgings. Attenuation within a specific rotor is considered negligible at the 1-MHz frequency used for testing. A detailed description of the per cent of back reflection testing technique was presented at the 15th Annual Convention of the Society for Nondestructive Testing in Philadelphia, Pa. on October 20, 1956 by Serabian.(1)

The Reference Block Technique

The reference block technique relies on reporting the amplitudes of flaw reflections which exceed a specified percentage of a distance-amplitude reference line which is based on experimental measurements on rotor forgings. This procedure automatically compensates for flaw depth and forging geometry, while permitting direct measurement of flaw area. Flaw orientation is compensated for by correction factors based on additional experimental measurements on rotor forgings. Compensation for attenuation differences from rotor to rotor is not considered necessary since attenuation measurements made on rotors during the past three years show that attenuation differences between rotor forgings of the same composition are quite small. The test procedure also provides compensation for surface finish which must be 250μ in. or better, in accordance with specification requirements. Compensation is not provided for couplant since this potential variable is held constant by a test specification requirement.

This paper presents refinements in the reference block technique as developed and applied by Westinghouse over the past two decades and includes case histories that illustrate the correlation obtained between ultrasonic data and the metallographic appearance of flaws.

Variables Considered

To obtain meaningful comparisons between ultrasonic flaw reflections in a rotor forging with those from flat-bottom holes in reference blocks, attention must be paid to the many variables that can affect the measured amplitudes of signals both in the blocks and in the rotor forging. The effects of these variables and the compensation provided for each are discussed.

Flaw Depth: The amplitude of the ultrasonic response from a given size flaw or flat-bottom hole will vary as the test distance from the transducer increases, as shown in Figure 1. The solid curve is based on theoretical calculations (2) for a 2¼-MHz frequency, 1⅛-in.-dia transducer and a Ni-Mo-V rotor steel, ASTM Specification A469 Class 4; included are data points obtained experimentally from $\frac{1}{16}$-in.-dia flat-bottom holes at different depths in rotor steel blocks of two sizes, 2 in. and 7 in. square. The curves shown in Figure 2 are based on experimental measurements on a 38-in.-dia. rotor and a 17½-in.-dia rotor. The data points are from ¼-in.-dia flat-bottom holes in both cases. Figure 3 illustrates a combination of all of the curves from Figures 1 and 2 taken to a common base at the peak points and reveals that the relative shapes of the curves for the two different diameters and the flat surfaces are reasonably comparable. Consequently, it was concluded that a composite curve could be developed from the Figure 3 data that would be reasonably

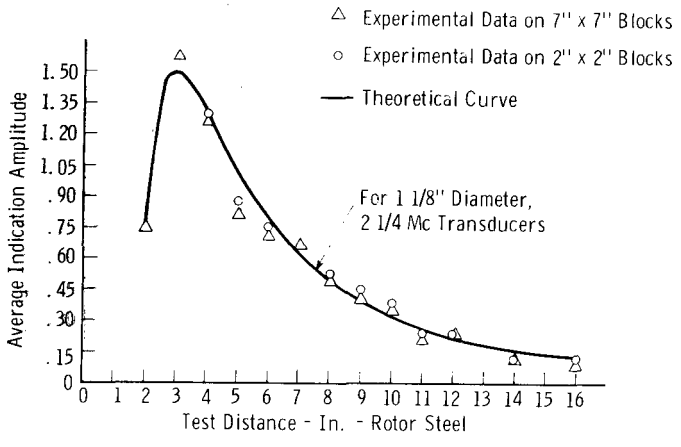

Figure 1. Theoretical and experimental distance-amplitude response from 1.16-in.-dia flat-bottom holes in flat test blocks.

applicable for rotors of all diameters for the specific test frequency of 2¼-MHz and the transducer size of 1⅛-in.-dia. This composite curve is shown in Figure 4. The curve was extended beyond 16 in. by extrapolation since a logarithmic plot of the curve in this far field region is a straight line.

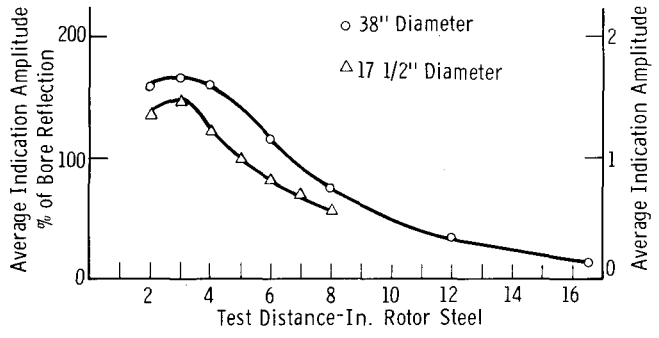

Figure 2. Experimental distance amplitude response from ¼-in.-dia flat-bottom holes in 17½-in. and 38-in.-dia rotors. Average of 2¼-MHz, 1½-in.-dia quartz transducers.

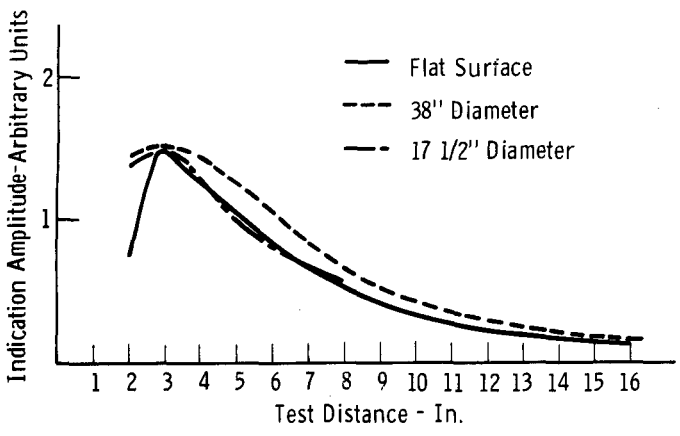

Figure 3. Combination of Figures 1 and 2 to a common amplitude at a 3-in. test distance.

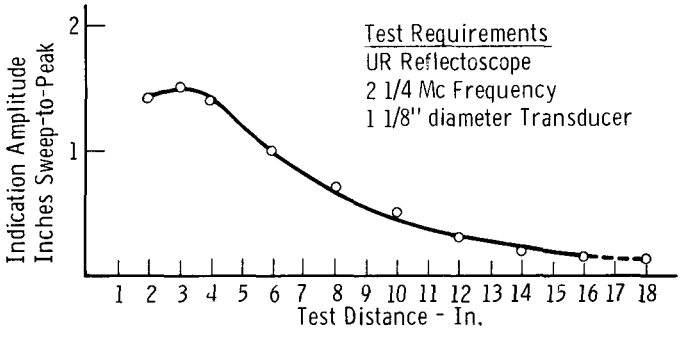

Figure 4. Composite curve of Figures 1 and 2 for all rotor diameters.

Flaw Area: In accordance with ultrasonic theory, the amplitude of ultrasonic reflection is proportional to the reflecting flaw area for flaws considerably smaller than the transducer. By establishing the distance-amplitude curve for a flat-bottom reflector of specified diameter, the equivalent diameter of a small flaw can be estimated by comparison of its amplitude against the curve. This was first accomplished by making the reference curve amplitude represent the reflecting area of a $\frac{1}{16}$-in.-dia flat-bottom hole of 0.003 sq in. area but was subsequently modified, for ease in measurement, so that the curve now represents a reflecting area of 0.010 sq in.

Flaw Orientation: The relationship between flaw reflection amplitude and that from flat-bottom holes comes closest to being valid when the flaw is in a plane normal to the sound beam. As the angle of the flaw shifts from this plane, the amplitude of ultrasonic response decreases rapidly; consequently, to obtain proper evaluation of flaw size, compensation must be provided for the effects of flaw orientation. To obtain the desired compensation, the effects of misorientation of a flat reflector on the amplitude of ultrasonic response were determined experimentally(2) for a 2¼-MHz frequency and a 1⅛-in.-dia transducer. These data are shown in Figure 5 as a curve of correction multiplier versus misorientation angle.

In order to use the correction multiplier from Figure 5, the displacement angle of the flaw from the position normal to the sound beam must be determined. In large forgings this can be accomplished by utilizing the variation in beam spread at different frequencies as described by Serabian(1) in 1956. This procedure involves pinpointing both the surface location directly over the flaw and the flaw depth at a 5-MHz frequency since this frequency will provide minimum beam divergence and maximum loss of back reflection when over the flaw. The surface location is then noted where maximum reflection from the flaw is obtained when using a highly divergent 1-MHz test-frequency for which the assumption is made that some portion of the sound beam strikes the flaw at normal incidence. Knowing the flaw depth and the displacement between the two transducer positions, the flaw orientation can be determined geometrically.

Forging Diameter: To validate the use of a fixed amplitude reference curve when testing rotors of different diameter, it was necessary to provide a correction for the effect of curvature. This was accomplished by both theoretical calculation and experimental measurement(2) for a 2¼-MHz frequency, a 1⅛-in.-dia transducer, and an SAE #20 oil couplant. From these data, correction multipliers for the effects of each curvature change were determined as shown in Figure 6.

Test Blocks: When evaluation of flaw size by the reference block technique was first devised, the reference line for reporting flaw reflection amplitudes was established by utilizing two rotor steel blocks which contained $\frac{1}{16}$-in.-dia flat-bottom holes of 0.003 sq in. area, at test depths of 3 and 11 in. At that time, a straight-line correction was provided for test depths from 3 in. to 11 in. by connecting the points of maximum reflection amplitude from the 3-in. and 11-in.-distant test holes with a line drawn on the transparent shield over the cathode ray tube of the test instrument. Correction for distances under 3 in. and over 11 in. was limited to extending the amplitudes at these specific points as straight horizontal lines from 3 in. to 0 in. and from 11 in. to greater depth. Amplitudes of flaws were then reported as a percentage of the 0.003-sq-in. reference line and correction multipliers were applied to this value to compensate for the effects of curvature and flaw orientation. To avoid the necessity of carrying heavy steel test blocks, aluminum test blocks were made that provided distance-amplitude responses that were equivalent to the steel blocks.(3)

The previously described procedure was revised in a number of respects to arrive at the technique now employed. The first revision was to abandon the B_3-B_{11} reference line and to substitute in its stead the actual distance-amplitude correction curve developed by Ying for a 2¼-MHz frequency and a 1⅛-in.-dia transducer from theoretical considerations and later confirmed by experimental data, see Figures 1 to 4. This change provided greater accuracy when estimating flaw size beyond an

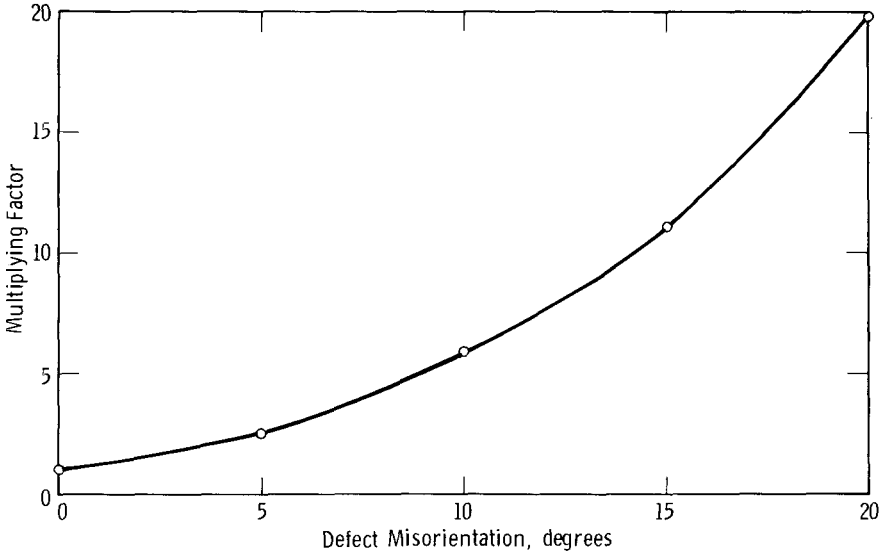

Figure. 5. Correction multiplier for defect misorientation from normal to the ultrasonic beam when making use of $2\frac{1}{4}$-MHz, $1\frac{1}{8}$-in.-dia quartz transducers.

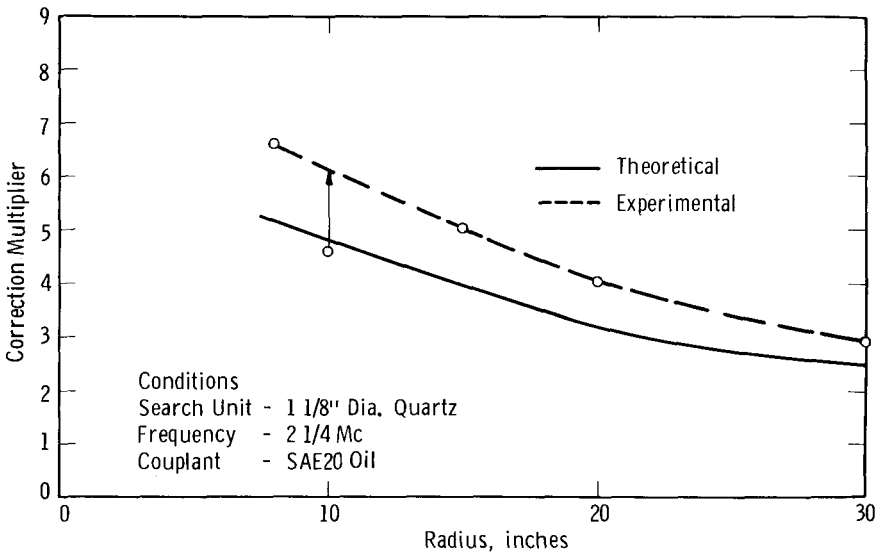

Figure 6. Correction multiplier for compensating for the effect of forging curvature on ultrasonic reflection amplitude.

11-in. test depth in the critical bore region of rotor forgings. Since it was no longer necessary to have two test blocks, the procedure was changed to permit the substitution of a commercially available reference block. The reference block used for this purpose was ASTM E127-64, Type 3-0600; it is readily available from ALCOA with a guaranteed accuracy of ± 10%. A test distance of 6 in. was chosen in order to provide a measurement well beyond the Fresnel zone of the specified $2\frac{1}{4}$-MHz, $1\frac{1}{8}$-in.-dia transducer, yet short enough so that the test block could be readily transported and handled.

A second revision that was made was to adjust the relationship between the experimental distance-amplitude data and the reference block amplitudes so that the fixed amplitude reference curve drawn on the test screen represented a reflecting area of 0.010 sq in. rather than 0.003 sq in. This was done so that field inspectors could more quickly estimate flaw size from ultrasonic reflection amplitude by simply multiplying the flaw reflection amplitude, measured as a per cent of the reference line, by 0.010 sq in. to obtain an estimate of flaw area. This value, of course, requires subsequent correction if the flaw is found to be misoriented from a position normal to the sound beam.

In order to assure that the distance-amplitude curve for the 0.010-sq in. reflecting area was high enough to be easily readable for discontinuities near the bore, the amplitude of this curve at a 12-in. test depth was arbitrarily adjusted to be 0.30 in. on the test instrument screen; this adjustment was made possible by increasing the prescribed tuning level for the ASTM E127-64T, Type 3-0600 reference block. Thus, we now have developed the distance-amplitude curve for a 0.010-sq in. reflecting area with an amplitude of 0.30 in. at a 12-in. test distance for a 38-in.-dia rotor. This curve is, of course, only valid for a $2\frac{1}{4}$-MHz test frequency, $1\frac{1}{8}$-in.-dia transducer, and a Type UR Reflectoscope tuned to a prescribed level on a Type 3-0600 aluminum reference block.

It was considered desirable to apply the correction for curvature directly to the instrument tuning level so that all testing would be performed at the same defect-sensitivity regardless of forging diameter. In order to do this the established amplitude value on the Type 3-0600 aluminum block for a 38-in.-dia rotor was utilized as a basing point for setting the instrument sensitivity and this value was varied in accordance with the experimental correction-multiplier vs. curvature data provided by A. Ying for larger and smaller rotor diameters. Amplitude settings for rotor curvatures from 12 in. to 80 in. may be found in Table 1.

Table 1

Amplitude Settings on ASTM Reference Block #3-0600 for Rotor Curvatures from 12 to 80 in.

dia, in.	Indication Amplitude, in. (s/p)
12 - 15	6.6
15 - 20	6.0
20 - 25	5.3
25 - 30	4.7
30 - 35	4.2
35 - 40	3.9
40 - 45	3.6
45 - 50	3.3
50 - 55	3.1
55 - 60	2.9
60 - 65	2.7
65 - 70	2.5
70 - 75	2.4
75 - 80	2.2

Attenuation: The effects of attenuation on ultrasonic reflection amplitude in a specific forging are generally considered to be small in comparison to the radiation decay of the sound intensity with distance. Actually, by making use of a distance-amplitude curve based on experimental measurements in rotor steel, compensation is automatically provided for even the small amount of attenuation that is present in the material. Experimental measurements by W. Knorr and H. G. Ricken(4) indicated that attenuation differences in alloy steels are slight at the $2\frac{1}{4}$-MHz frequency that is utilized for flaw evaluation. The variation in attenuation from rotor to rotor has therefore been assumed to be negligible and accumulated attenuation measurements on production rotors during the past three years have verified this assumption.

Surface Roughness: Experimental and theoretical determinations(2) of the effect of surface roughness on the amplitude of ultrasonic reflection reveal roughness to be a variable of con-

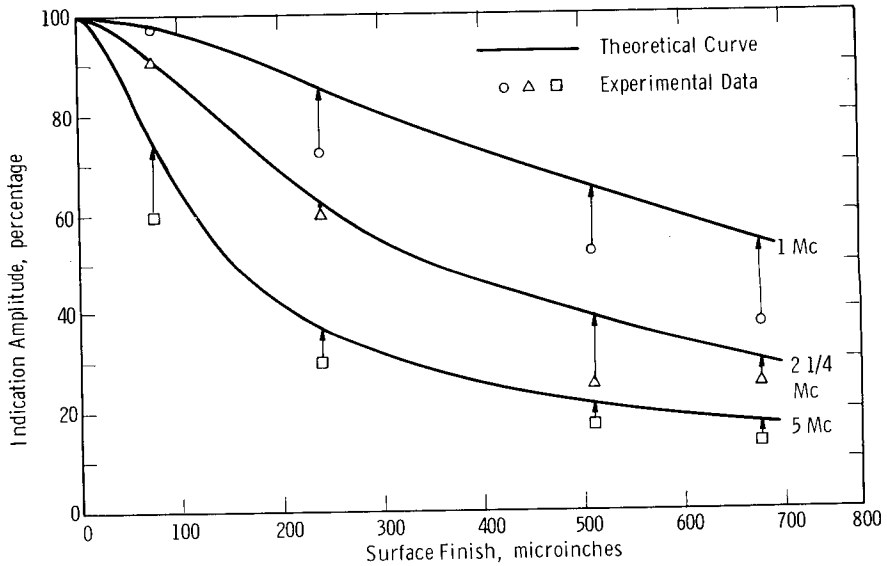

Figure 7. Effect of surface roughness on ultrasonic reflection amplitude.

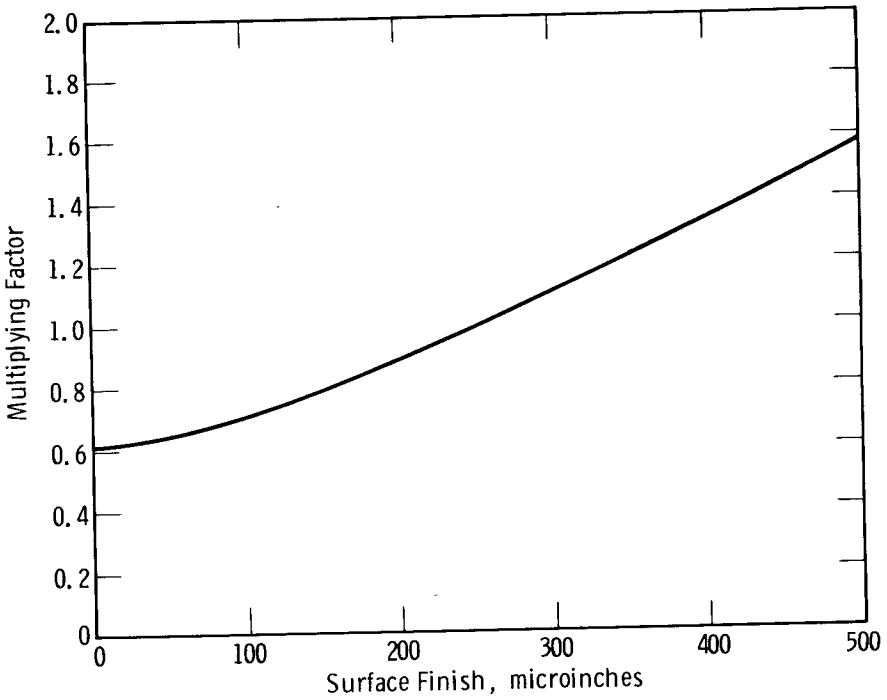

Figure 8. Correction multiplier for surface roughness when making use of $2\frac{1}{4}$-MHz, $1\frac{1}{8}$-in.-dia quartz transducers.

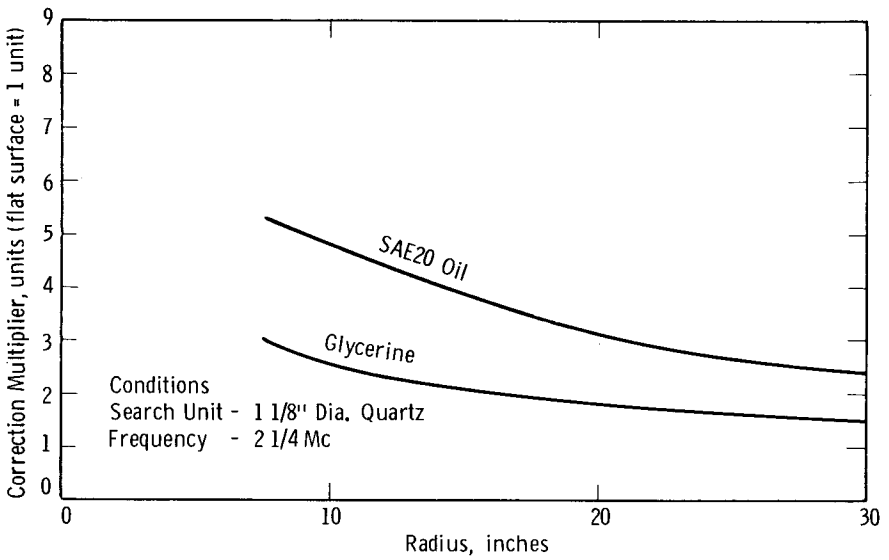

Figure 9. Theoretical effect of SAE20 oil and glycerine on correction multiplier used for compensating for the effect of curvature on ultrasonic reflection amplitude.

siderable significance. These data are shown in Figure 7 for a $2\frac{1}{4}$-MHz frequency, $1\frac{1}{8}$-in. dia search unit and SAE #20 oil couplant. To provide correction for different surface roughness conditions, the experimental data for the $2\frac{1}{4}$-MHz test were replotted, as shown in Figure 8, to present appropriate correction factors for various surface roughnesses with unity being a 250-microinch finish; 250 microinch is the minimum acceptable finish in accordance with our specification requirements. This value was selected because it can be readily provided by conventional mill machining practices. Surface roughness can be measured by use of commercially available instruments.

Waviness, which is caused by machine or work-load deflection vibrations during machining, will similarly affect the amplitude of ultrasonic response. Consequently, the effect of this variable is eliminated by a specification requirement that the waviness shall not exceed 0.001 in. as measured by a dial indicator mounted in a tool-post holder.

Couplant: On a curved surface the type of couplant used for ultrasonic inspection can have a considerable effect on the amplitude of ultrasonic response. Figure 9 shows the results of a theoretical comparison of required multiplying factors for curvature correction when making use of SAE #20 oil and glycerine. These results indicate variations as great as 2:1 even though both couplants provide equivalent ultrasonic responses on flat surfaces; for this reason, the use of SAE #20 oil as a couplant has been made a test specification requirement.

Instrumentation: There are many ultrasonic test instruments available commercially and each has different electrical characteristics so that ultrasonic evaluations performed with one instrument cannot be readily repeated with an instrument made by a different manufacturer. Some have tuned pulsers while others are untuned; some have broad-band receivers while others are narrow-band; and some have a video presentation while others have a radio-frequency (RF) presentation. In addition, there are differences in characteristics such as deflection linearity, pulse-repetition rate, and dynamic range. Because of these differences, it is necessary to eliminate instrumentation as a variable by specifying a specific instrument for evaluating flaw size by the reference block technique. The specified instrument must be of the same type that was used to obtain the previously detailed experimental data, i.e., RF, narrow-band, tuned pulser.

In addition to the instrumentation, the transducer and frequency used for flaw evaluation must also be controlled by specification. For this purpose, a $2\frac{1}{4}$-MHz, $1\frac{1}{8}$-in.-dia quartz transducer is specified since this is the type of unit used to obtain the experimental data on which compensation and correction are based. Any variation in frequency, transducer diameter, or transducer material from that specified will invalidate the experimentally established distance-amplitude reference line. Quartz was selected as the transducer material since it will provide the best reproducibility of the various transducer materials which are available; a $2\frac{1}{4}$-MHz frequency was selected in order to permit detection of flaws as small as $\frac{1}{16}$-in. dia near the centre of rotors; and a $1\frac{1}{8}$-in.-dia search unit was selected to permit the greatest amount of inspection coverage per scan.

Application of the Technique

The reference block technique, as presently applied, requires the use of a Sperry Type UR Reflectoscope, a $2\frac{1}{4}$-MHz test frequency, a $1\frac{1}{8}$-in. dia quartz search unit, an SAE #20 oil couplant, and a maximum surface roughness of 250 microinch on the rotor being tested. If any of these conditions are changed, the subsequently described test procedure for evaluating flaw size may no longer be completely valid since all the experimental compensation factors were obtained specifically for these conditions.

After satisfying the above requirements, evaluation of flaw size in rotors is accomplished by the following simple procedure:

1. Draw a distance-amplitude curve on the transparent shield over the test instrument cathode ray tube similar to the curve shown in Figure 4.
2. Adjust the Reflectoscope sensitivity to obtain a reflection amplitude from the ASTM 3-0600 reference block in accordance with the values given in Table 1.
3. Perform the ultrasonic test and measure the amplitudes of flaw reflection as a percentage of the distance-amplitude curve. Multiply these values by 0.010 sq in. to obtain initial estimations of each flaw area.
4. Determine the orientation angle of the flaw from a position normal to the sound beam and apply the correction indicated in Figure 5 to the value obtained in step 3.
5. Measure the surface roughness at the transducer location and apply the correction indicated in Figure 8 to the value obtained in step 4 to obtain a final estimate of the approximate equivalent reflecting area of the flaw.

Example of Flaw-Size Evaluation

Conditions:

A 40-in.-dia rotor with a 250-microinch surface finish is tested in accordance with Section III requirements and procedures. A 0.25-in. s/p flaw reflection is observed at a 16-in. test distance and is found to be from a flaw oriented at an angle of 5° from a plane normal to the sound beam.

Evaluation Procedures:

1. From Figure 4, a 0.25-in. s/p indication at a 16-in. test distance is found to be 170% of the .15-in. s/p reference line amplitude.
2. From Figure 5, a correction factor of $2\frac{1}{2}$ is required for a 5° defect angularity.
3. From Figure 8, a correction factor of 1 is required for a 250-microinch surface.
4. Multiplying the indication amplitude (170%) by the orientation correction factor ($2\frac{1}{2}$), by the surface roughness correction factor (1), and then by the standard reference area (0.010 sq in.) results in an estimated flaw reflecting area of 0.042 sq in. This is equivalent to a $\frac{15}{64}$-in.-dia flat-bottom hole so the defect can be considered as being at least $\frac{15}{64}$-in. in diameter, and probably larger due to factors discussed in the next section of this paper.

Limitations of the Evaluation Procedure

If the evaluation is conducted in the prescribed manner, there is only one limiting factor for which provision has not been included. That is the effect of certain physical characteristics of the flaw. These include: the shape of the flaw, whether smooth or rough and rounded or flat; the nature of the flaw, whether a void or an inclusion and the number of flaws in a confined area, whether single or concentrated. As a result, estimates of flaw size based on comparison with ideal reflectors (flat-bottom holes) are usually too low.

Evaluation of Flaw Severity

The actual evaluation of flaw severity is not based solely on the amplitude of ultrasonic reflection; many other factors must be taken into consideration such as the type of indications (stationary or travelling, sharp or bulbous, single or clustered), the surface area over which the flaw is detected, and the effect the flaw has on the back reflection amplitude. Evaluation of these factors provides a reasonable estimate of the orientation, extent and nature of a specific flaw, particularly when combined with previous experiences with flaw evaluations and a thorough understanding of the processes involved in the fabrication of the part being inspected. However, with the current state of the art, it is still not possible to report the exact size and precise nature of discontinuities detected ultrasonically in large rotor forgings. When an ultrasonic indication present in a rotor forging is considered to be caused by a discontinuity of sufficient size to increase the stress beyond allowable design criteria, the discontinuity is considered detrimental regardless of its nature and, if possible, removed by trepanning or overboring. If the flaw or defective condition cannot be completely removed by one of these methods, the forging is rejected.

Every rotor forging purchased by Westinghouse is evaluated individually and a decision as to the acceptance or rejection of each reportable discontinuity is reached at a meeting of the responsible metallurgical and mechanical engineers and quality control personnel. Fortunately, the advent of vacuum degassing and other metallurgical innovations have greatly reduced the number of questionable ultrasonic indications found in large forgings. Table 2 shows the results of the ultrasonic inspection of 260 generator rotor forgings supplied to and inspected by the Large Rotating Apparatus Department (LRAD) at East Pittsburgh from 1960 through 1966. It should be noted that approximately 87% of the rotor forgings inspected had no ultrasonic indications and of the 35 forgings with indications, only six were bad enough to be rejected. Several additional rotor forgings, however, were known to have been rejected by suppliers prior to examination by Westinghouse personnel.

Table 2

Cumulative Results of Ultrasonic Inspection of Generator Rotor Forgings* from 1960 through September, 1966

Specified Minimum Yield Strength (psi)	Rotors with Reportable Ultrasonic Indications	Rotors Without Reportable Ultrasonic Indications	Rotors Overbored	Rotors Accepted	Rotors Rejected
55,000	6	46	2	49	3
65,000	1	29	2	30	0
75,000	7	47	1	54	0
85,000	11	61	8	72	0
95,000	10	42	4	49	3
Total	35	225	16	254	6

*Inspection performed by Westinghouse inspectors. These figures do not include forgings rejected by mill inspectors and not submitted to Westinghouse.

Case Histories

Nine typical case histories involving the correlation of ultrasonic data with destructive evaluation of rotor forgings were examined in relation to this paper, but space does not permit their publication.*

Summary

This paper has presented the considerations involved in the development of the reference block technique for ultrasonic testing of large rotor forgings presently in use at Westinghouse. Correlation of ultrasonic data with destructive evaluation has proven the effectiveness of this technique for revealing the presence, location, and approximate size of small discontinuities in large rotor forgings. The data provided as the result of this inspection technique have been used to make engineering decisions regarding the acceptability of each rotor forging for its intended application. The value of this tool and its application has been proven by the excellent service performance of Westinghouse large rotating apparatus.

* The author may be in a position to supply them to those interested.

References

(1) Serabian, S. Influence of geometry upon an ultrasonic defect-size determination in large rotor forgings, presented at 15th Ann. Conv., Soc. for Nondestructive Testing, Philadelphia, Pa., Oct. 20, 1956.

(2) Ying, Andrew S. C. and Baudry, R. A. A theoretical approach to the evaluation of ultrasonically detected flaws in rotor forgings, presented at Winter Ann. Meeting, Am. Soc. Mech. Engrs., New York, N.Y., Nov. 25-30, 1962.

(3) Greenberg, H. and Hughes, E. T. Ultrasonic testing of generator rotors, Western Metals Congr., ASM, 1957.

(4) Knorr, W. and Ricken, H. G. Investigations on the measurement of sound attenuation and ultrasonic determination of defect size in steel forgings (translated from *Archiv Eisenhuttenwesen,* v. 33, 1962, #5, 317-325).

The Ultrasonic Inspection of Steel Sheets with Lamb Waves

E. ISONO AND T. UENO, JAPAN

ABSTRACT: We have studied the attenuation and reflection of Lamb waves in the frequency range of 1 MHz to 5 MHz.

1. The attenuation follows the relationship for the equation proposed by Lehfeldt and Höller.

2. Effects of curvature and pickling of steel sheets on the attenuation are negligible, but grain size larger than a certain size influences the attenuation.

3. Appreciable damping was observed at some temperatures corresponding to the Snoek peak.

4. The reflection of Lamb waves at artificial and natural defects shows constant reflection ratio.

5. The frequency spectra of Lamb waves influence the attenuation and other behaviour of them.

Introduction

Increased demands for high-quality steel sheets have brought about much progress in nondestructive inspection by ultrasonics, especially by using the pulse-reflection method with Lamb waves. But there have been few reports on analytical studies of ultrasonic inspection by Lamb waves compared with those of longitudinal waves.

In this paper are presented some fundamental studies on the nondestructive testing of steel sheets using Lamb waves.

The thicknesses of steel sheets used were from 0.8 mm to 3.1 mm, and a variable-angle probe with plexiglas was used throughout this experiment.

The attenuation and reflection of Lamb waves under various conditions were analyzed.

Attenuation of Lamb waves

Attenuation Equation of Lamb Waves and the Measurement of Attenuation

In order to treat quantitatively the inspection result by Lamb waves, we confirmed the attenuation equation. There are two equations for the attenuation of Lamb waves proposed by Lehfeld (1) and Höller(2) (equation 1), and Niklas(3) (equation 1′):

$$P = Poe^{-\alpha r}\, 1/\sqrt{r} \qquad (1)$$

$$P = Poe^{-\alpha r}\, 1/r \qquad (1')$$

where α is the attenuation constant in neper of the Lamb waves used, P is the amplitude of the Lamb waves at a round-trip distance (r) from the probe to the end of a sheet and Po is the amplitude at $r = 1$ and $\alpha = 0$.

In order to examine the equations, we used a ratio of P/P_{50} for convenience of measurement, where P_{50} is the amplitude of an echo whose height is 50% on the oscilloscope. Then the logarithm of P/P_{50} is given as follows:

$$20 \log P/P_{50} + 10 \log r = 20 \log Po/P_{50} - \alpha r \qquad (2)$$

similarly we obtained equation (2′) from equation (1′)

$$20 \log P/P_{50} + 20 \log r = 20 \log Po/P_{50} - \alpha r \qquad (2')$$

Using a 2.3-mm-thick uniform grain size stainless steel sheet, with a flat surface and no attenuation, we measured the amplitude of an end echo 20 log P/P_{50} at 20-cm intervals of r at 1 MHz and 2.25 MHz, plotted in the two ways mentioned above, and found the attenuation of Lamb waves closely follows the equation given by Lehfeldt and Höller.

From equation (2), we can get the attenuation constant α from the slope of plots 20 log P/P_{50} + 10 log r versus r. In this way, we can measure the attenuation α in steel sheets for each mode of Lamb waves within the error of ± 1.5 dB/m, using a commercial ultrasonic flaw detector and a variable-angle probe with plexiglas wedge whose beam index is constant at any available incident angle. When using a variable-angle probe whose beam index changes at various incident angles, we could not get a reliable attenuation α value. In this probe, a change in thickness of the oil layer as a medium of contact influences the echo height of the Lamb waves and care should be taken to keep the oil layer constant in order to get reliable attenuation of the Lamb waves.

Effect of Curvature, Scale and Grain Size of Steel Sheets on Lamb-Wave Attenuation

To make practical the application of ultrasonic Lamb waves to steel sheets, we measured the effects of curvature, scale and grain size on the attenuation, using the same procedure and units mentioned above.

Table 1

Increase of Attenuation Constant after Pickling and Curvature Making Against "as-rolled" State (dB/m)

Sample (mm)	Mode	As-rolled state	After pickling	After making curvature Radius (m)		
				0.5	1.0	1.5
1.9	S_1	7.0	0	3.0	1.5	−0.5
	S_2	14.0	−2.0	0	3.0	1.0
	S_0	12.5	0.5	−2.0	0.5	1.0
	A_1	20.0	1.0	3.0	1.0	−0.5
2.3	S_1	12.5	−0.5	4.0	0.5	0.5
	S_2	9.0	2.0	−1.0	−0.5	2.0
	A_1	20.0	0	0	−1.5	−0.5
3.1	S_1	25.5	0	−0.5	−0.5	−1.5
	S_2	20.0	0	−2.0	−1.5	−0.5
	S_3	12.5	−1.0	−1.0	0.5	1.0
	A_1	21.5	0	0.5	−1.0	0

We made up several samples 40 cm wide x 100 cm long from hot-rolled 1.9, 2.3 and 3.1-mm-thick sheets. The rolling direction of each sample was perpendicular to its longitudinal direction, to which Lamb waves were transmitted. First we measured the attenuation constant of the sample for each mode of Lamb waves at 2.25 MHz, then one part of them was pickled to remove scale and the rest were bent to a curvature of 0.5-, 1.0- and 1.5-m radius to their rolling direction. Again we measured the attenuation constant of pickled and bent samples.

The attenuation constants of the samples with and without scale and those of the samples with various curvatures are shown in Table 1. From these results we can see that the effect of mill scale and curvature (0.5- to 1.5-m radius) on the attenuation constant is almost negligible.

In order to test the effect of grain size on the attenuation constant, we measured mild steel samples with various thicknesses and grain sizes. The grain size was controlled by annealing as shown in Table 2. Table 3 shows the increase of the attenuation constant after the annealing. From these results it is apparent that the attenuation constant increases with the grain size and the propagation becomes very difficult for larger grain sizes such as ASTM No. —1 or —2.

Table 2

ASTM Ferrite Grain Size Number of Samples

Sample		Annealing Temperature (°C)			
Thickness (mm)	As rolled	900	1000	1100	1200
1.2	5~10	4	3~4	3~4	−2
1.9	6~9	4	3~4	−1	−2~−3
2.3	5~10	4~5	3~4	0~−1	0~−2
3.1	4~6	4~5	3~4	3	−1~−2

Table 3

Increase of Attenuation Constant after Annealing. (dB/m)

Sample (mm)	Frequency (MHz)	Mode	As-rolled state	Annealing temperature (°C)			
				900	1000	1100	1200
1.2	2.25	A_1	8.0	7.0	7.0	8.0	x
		S_0	16.0	20.5	22.0	x	x
	1	S_0	1.0	2.0	1.0	4.5	5.5
1.9	2.25	A_1	20.0	14.0	11.0	x	x
		S_0	12.0	13.5	14.5	x	x
		A_0	7.0	12.0	10.0	19.5	x
	1	S_0	6.0	1.0	1.5	4.0	x
2.3	2.25	S_1	11.5	3.0	2.5	3.5	x
		A_1	19.0	7.0	8.5	8.5	x
	1	S_0	11.0	2.0	3.0	2.5	x
3.1	2.25	S_1	24.0	10.0	8.5	11.0	x
		S_0	20.0	10.0	8.0	12.5	x
		A_1	21.0	5.0	5.5	5.0	x
	1	S_0	11.5	0	0.5	1.0	x

Effect of Temperature of Steel Sheets on the Attenuation of Lamb Waves

For the on-line inspection of steel sheets, it is necessary to know the effect of temperature on the attenuation. For this reason, we measured the attenuation of mild steel (rimmed and killed), 18-8 and 13 Cr stainless steel sheets at higher temperature. The samples tested were heated in the electric furnace from room temperature to about 500°C. The temperature of samples was measured with three welded thermocouples inside the furnace. The temperature difference between the three points

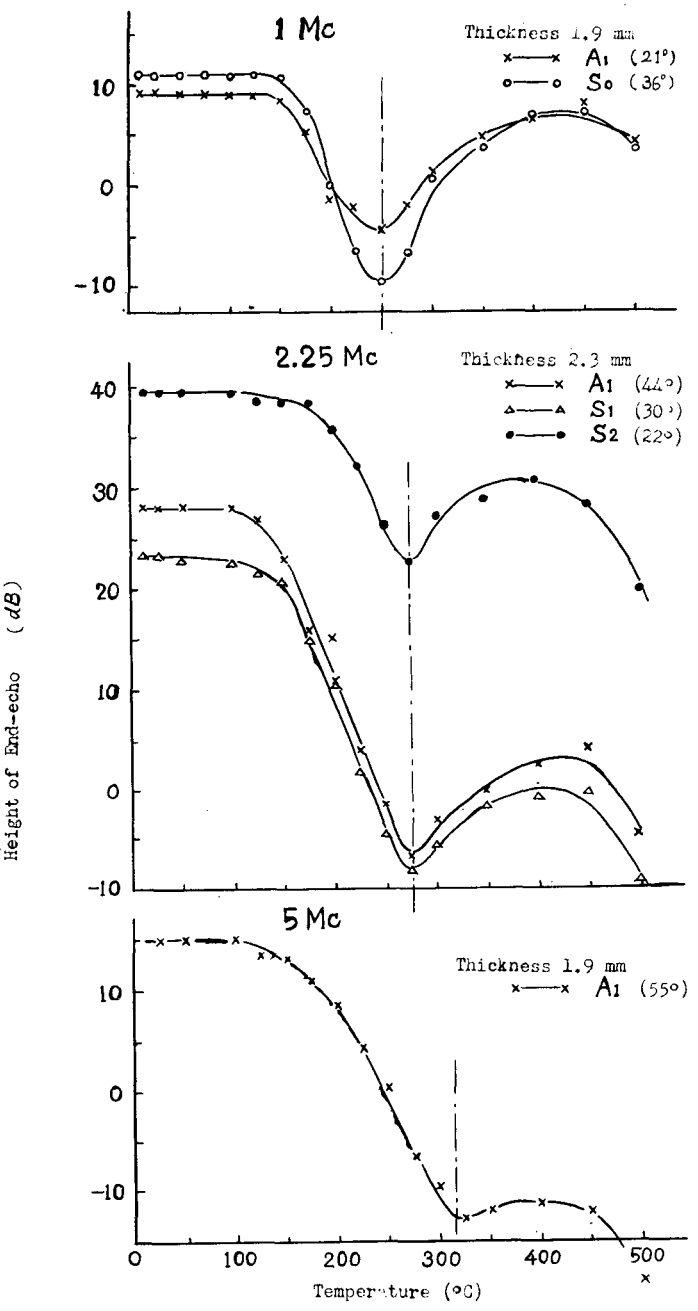

Figure 1. Effect of temperatures and frequencies on Lamb-wave attenuation of rimmed steel sheets.

was within the range of ± 8°C. The variable-angle probe was then placed on the outside end of the sample and the end echo height of every mode of Lamb waves available was measured against the temperature of the sample. The maximum temperature at the point of contact of the probe was 95°C, and the contact was only momentary so that the measurement might not be influenced by heat.

Figure 1 shows the effect of temperature upon attenuation at 1, 2.25 and 5 MHz for rimmed steel samples. Similar data were developed in the same way for samples of high-strength, low-alloy steel, 18-8 and 13 Cr stainless steel.

The end echo in the sample of rimmed steel shows a large decrease (20-45dB) when the temperature is between 250°C to 310°C, while the killed steel shows a small damping. Conversely, stainless steels and high-tensile steel show different tendencies and do not show any peak of attenuation.

From these experimental results and the knowledge of internal friction measurement (4), we may infer that the large attenuation of ultrasonic Lamb waves in the mild steel sample is due to Snoek damping caused by carbon or nitrogen dissolved in α-iron.

The above results were confirmed by measuring the Snoek peak of the same sample by internal friction (1.5 c/sec).

In this area, some consideration should be given to the inspection of low-carbon steel sheets at temperatures above 200°C.

Analysis of a Defect Echo in the Inspection by Lamb Waves

In order to analyze a defect echo, it was necessary to get the relationship of a defect echo amplitude of Lamb waves to their transmitting distance. We obtained equation (3) of a defect echo, assuming the proportion of reflection of the Lamb waves to be R:

$$P_F = RPoe^{\alpha r}\, 1/\sqrt{r} \quad (\alpha: neper) \qquad (3)$$

where P_F is the amplitude of a defect echo and R is the reflection ratio of the Lamb waves at the defect.

As previously, equation (4) was derived from equation (3)

$$20 \log P_F/P_{S0} + 10 \log r = 20 \log R + 20 \log Po/P_{S0} - \alpha r \ (\beta: dB) \qquad (4)$$

If the defect is uniform and perpendicular to the propagating direction of the Lamb waves and always covers the entire beam width of the waves, R is expected to be independent of the propagating distance and constant. Conversely, if the defect is point-like, R is expected to be dependent on the distance and variable.

Comparing equation (2) with (4), we know that, in the case of a constant R, if we plot $20 \log P/P_{S0} + 10 \log r$ versus r and $20 \log P_F/P_{S0} + 10 \log r$ versus r, both curves will be linear, the absolute value of the slope is an attenuation constant and the difference of ordinates between two curves at the same distance r is equal to $20 \log R$. In the case of a variable R both curves might be linear, but the difference of ordinates ($20 \log R$) will change depending on r as illustrated in Figure 2.

Effect of the End Form of Steel Sheets on the Reflection of Ultrasonic Lamb Waves

In equation (1) or (3), we assume that the Lamb waves are completely reflected at the end of the sheets. However, it is possible that the type of reflection may depend on the form of the sheets. Therefore before studying the reflection of Lamb waves at a defect it is necessary to check the effect of the end form.

We used 2.3-mm-thick cold-rolled steel sheet with fairly uniform grain size as a sample. The end forms were sheared, roundly finished (radius equal to thickness) and machined perpendicular to the rolling faces. As a measure of the effect of the reflection at an end, we employed $20 \log Po/P_{S0}$ which is equal to the ordinate at $r=0$ of a linear line derived by plotting $20 \log P/P_{S0} + 10 \log r$ versus r like Figure 2.

The reflection of symmetrical modes is 0-2 dB higher at the roundly finished end than at the perpendicularly finished end and the reflection of asymmetrical modes is 1-2.5 dB higher at the perpendicularly finished end than at the roundly finished end. The difference in the reflection between the as-sheared end and the machined end is within ± 2.5 dB.

Reflection of Lamb Waves at Artificial Defects

We measured the reflection of Lamb waves at 1 and 2.25 MHz at artificial defects machined in the same 2.3-mm-thick sheet

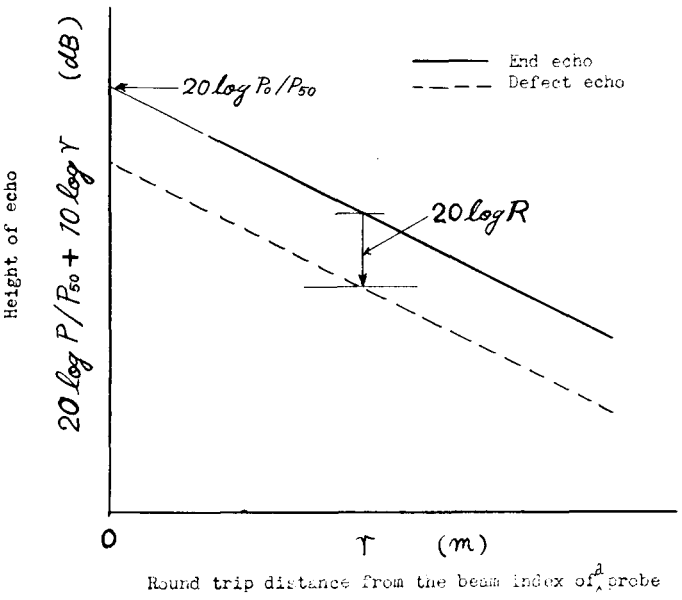

Figure 2. Relationship of attenuation constant and reflection ratio.

used in the previous experiment. As mentioned, the form of the ends does not seriously influence the reflection of the waves, so we used the perpendicularly finished end.

For the artificial defects, we used machined grooves and holes. For the groove-type defect, four different widths (1, 2, 5 and 10 mm) and four different depths (0.3, 0.5, 1.0 and 1.5 mm) were used. For hole-type defects, drilled holes of four different diameters (1, 2, 5 and 8 mm) were used.

First we measured the end-echo amplitude in the sample without any artificial defects, then machined the defects, measured the amplitude of the defect echo and end echo which passed through the defect, and plotted these data as in Figure 2. Measurement was made at 20-cm interval of r and the sensitivity of the detector was kept constant by the standard test-piece. (5)

As explained before, the reflection ratio R of such a groove is expected to be constant, in other words the slopes of the two plotted lines as illustrated in Figure 2 are the same, and equal to the attenuation constant of the testing mode. In Table 4 the absolute values (dB/m) of both slopes are shown for 1 and 2.25 MHz. They were almost the same within the experimental error for the given testing mode. In some S_0 cases at 1 MHz an echo was not reflected at the groove and therefore is not listed in Table 4. In Figure 3 the reflection ratio $20 \log R$ versus the groove width is shown for each mode at 1 and 2.25 MHz for different depths. It should be noted that, for the groove width over 2-5 mm, the $20 \log R$ has a tendency toward becoming constant for each groove depth and that there seems to be no simple relationship between the groove depth and the R value. Both slopes of the end echoes of the sample with and without a groove are nearly equal.

The experimental results on drilled holes are shown in Figure 4. At 2.25 MHz there is little difference between the slope of the defect-echo amplitude versus r and that of an end-echo amplitude versus r of the sample without a hole. In other words the reflection ratio R of the drilled hole is dependent on r. At 1 MHz we could not get a clear defect echo when the S_0 was used and the ratio R was found to be independent of r. when the A_1 mode was used. In Table 5 the 20-log-R-value at r=0.4 m and 1.4 m for 2.25 MHz is shown. The slopes of the end echo versus r with and without the drilled hole are different at 2.25 MHz and equal at 1 MHz.

Table 4
Gradient of End Echo Before Machining and that of Groove Echo (dB/m)

Groove		2.25 MHz						1 MHz			
		A_1		S_1		S_2		S_0		A_1	
Depth (mm)	Width (mm)	End	Groove	End	Groove	End	Groove	End	Groove	End	Groove
0.3	1	20.5	19.5	8.5	10.0	8.2	7.5	11.5	—	1.5	3.1
	2		20.2		9.0		7.0		—		2.7
	5		18.5		9.0		4.7		—		2.7
	10		17.0		9.0		8.5		—		0.9
0.5	1	20.0	19.5	8.5	8.2	8.5	8.5	11.5	—	1.5	1.6
	2		20.7		8.2		6.7		—		1.6
	5		19.5		8.2		6.3		—		1.6
	10		21.0		8.2		6.3		—		1.6
1.0	1	19.5	19.0	8.5	8.2	8.2	8.5	11.5	—	2.5	3.0
	2		19.0		8.2		8.5		13.5		3.1
	5		19.0		8.5		8.5		9.2		2.5
	10		19.0		9.0		8.5		8.7		2.6
1.5	1	20.7	21.0	8.5	8.5	8.2	8.5	11.0	14.0	2.8	3.2
	2		21.0		8.5		8.5		14.0		3.0
	5		21.0		8.7		8.5		13.2		4.2
	10		21.0		8.5		8.5		14.0		2.5

Table 5
Reflection Ratio of Drilled Hole at 2.25 MHz (dB)

Mode	$\frac{r}{(m)}$	Dia of hole (mm)			
		1	2	4	8
A_1	0.4	−28.9	−26.9	−23.4	−21.7
	1.4	−30.4	−28.9	−26.2	−24.7
S_1	0.4	−29.7	−28.4	−25.9	−22.2
	1.4	−31.7	−31.2	−27.9	−24.7
S_2	0.4	−29.2	−27.2	−24.0	−21.5
	1.4	−33.2	−30.9	−27.9	−25.7

Reflection of Lamb Waves at Natural Defects

After studying the reflection of the Lamb waves with artificial defects, we tried to observe the reflection with natural lamination defects.

First we measured the reflection ratio of similar laminations in 2.1-mm-thick, hot-rolled sheet by Lamb waves at 2.25 and 1 MHz.

From equation 4, the reflection ratio can be expressed as follows:

$$20 \log R = 20 \log P_F/P_{50} - 20 \log Po/P_{50} + 10 \log r + \alpha r \quad (5)$$

Although the sample was laminated, the plotted curve 20 log P/P_{50} + 10 log r versus r was linear. We could get 20 log Po/P_{50} and α from this linear line. After measuring the defect-echo amplitude 20 log P_F/P_{50} at the lamination, we calculated the reflection ratio 20 log R from equation (5). The 20 log R values at 2.25 MHz, S_2 and 1 MHz, S_0 modes for several samples are shown in Table 6.

It is interesting to note that although the lamination width confirmed by the magnetic particle method ranged from 8 mm to 50 mm the reflection ratio is almost constant for each mode. This coincides with the previous experimental results derived with the groove-type defect. S_1 and A_1 modes at 2.25 MHz do not show any clear echo at the lamination.

We also measured the reflection ratio of the same kind of lamination in 0.8-mm-thick cold-rolled mild steel. Figure 5 is an example of this experiment by the S_0 mode at 2.25 MHz. In this case the lamination is rather smaller than the above sample and the reflection ratio is between −20 to −30 dB.

In our experience, there is no definite relationship between the reflection ratio at the lamination and its size. It will be necessary for quality control on the production line to grasp the relationship by checking natural defects and the height of echo

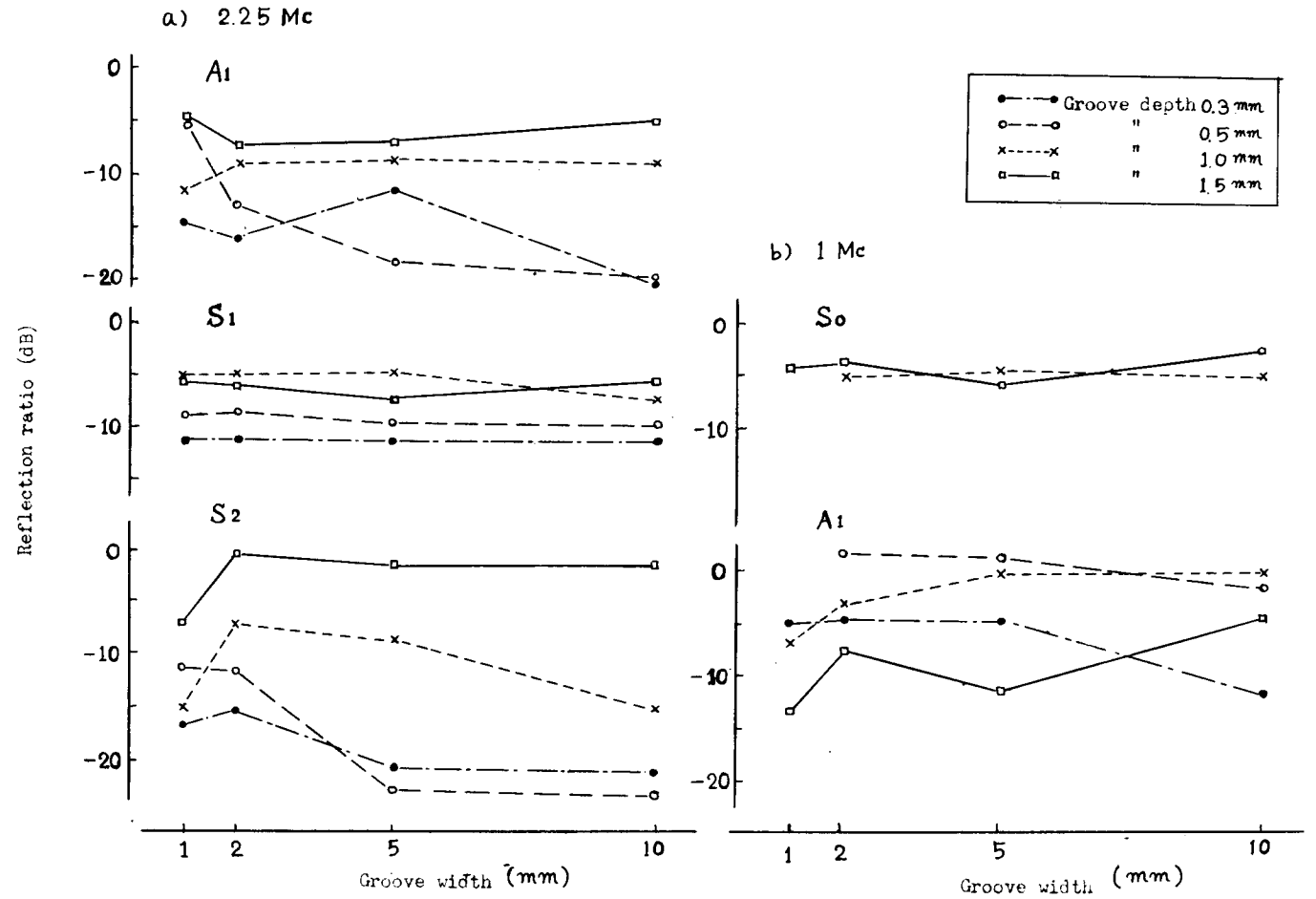

Figure 3. Effect of groove size on reflection ratio.

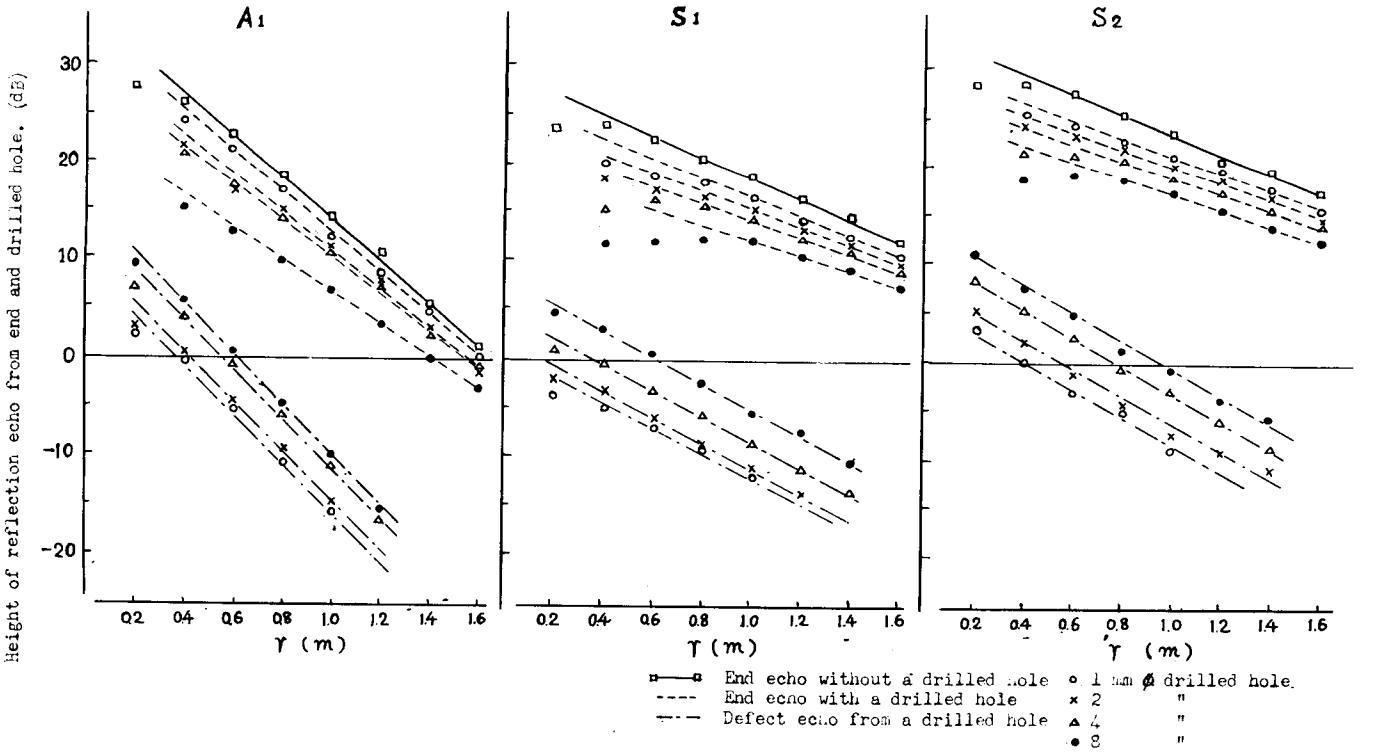

Figure 4. Relationship of end echo height and reflection echo from a drilled hole (2.25 MHz, 2.3-mm sheet).

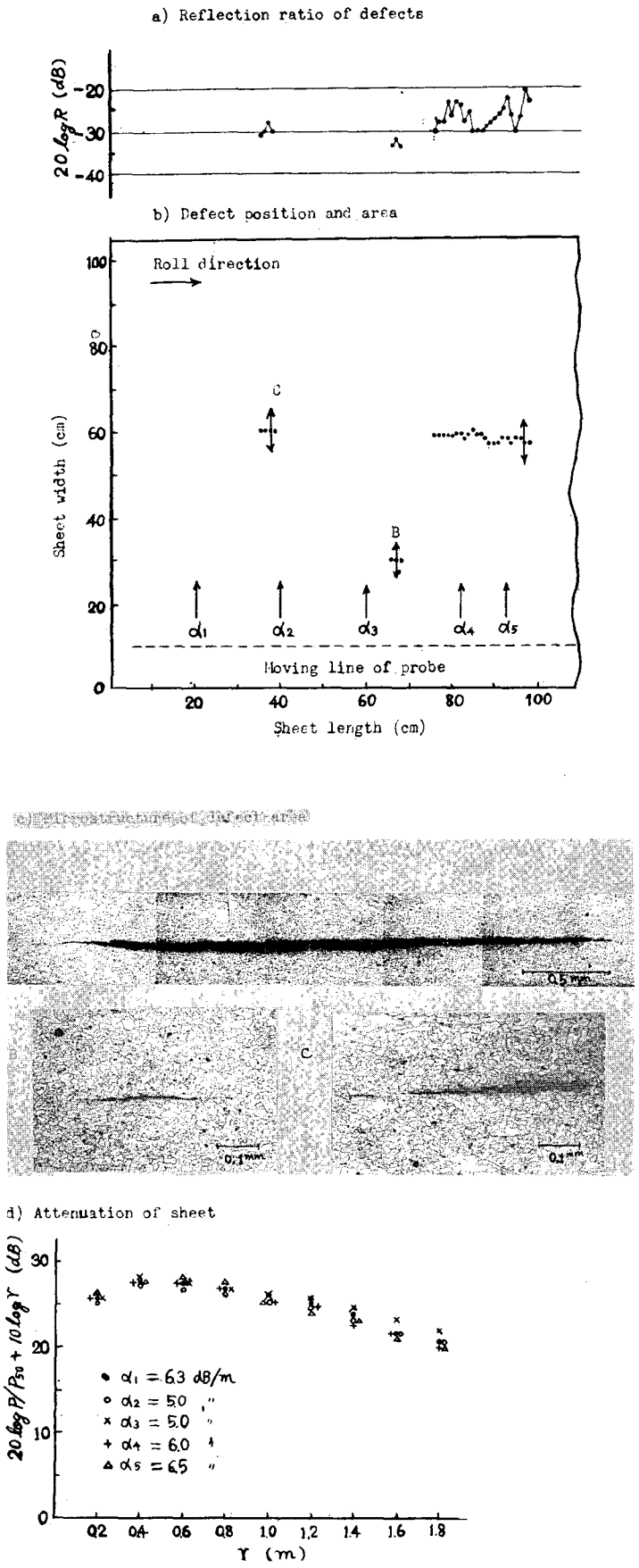

Figure 5. **Example of data sheet of inspected sample (0.8-mm sheet, 2.25 MHz, S_0 mode).**

Table 6
Examples of Reflection Ratio of Lamination
(2.1-mm-thick steel)

	Item	Sample No. 2	7	13	14	15
2.25 MHz, S_2	$20 \log \frac{p_F}{p_{50}}$	8.0	6.5	10.0	12.5	11.0
	αr ($r=0.4$)	2.5	5.0	4.5	6.0	5.0
	$10 \log r$	−4.0	−4.0	−4.0	−4.0	−4.0
	$-20 \log \frac{p_0}{p_{50}}$	−39.0	−42.5	−43.5	−46.0	−40.0
	Total (20 log R)	−32.5	−35.0	−33.0	−31.5	−38.0
1 MHz, S_0	$20 \log \frac{p_F}{p_{50}}$		−6.0	−3.0	−4.5	−7.0
	r (m)		0.7	0.4	0.4	0.4
	α (dB/m)		11.5	5.5	11.0	15.5
	αr		8.0	2.5	4.4	6.2
	$10 \log r$		−1.5	−4.0	−4.0	−4.0
	$-20 \log \frac{p_0}{p_{50}}$		−28.5	−26.0	−25.0	−23.5
	Total (20 log R)		−28.0	−30.0	−29.1	−28.3

Table 7
Attenuation Constants and Reflection Ratio Measured by Different Ultrasonic Flaw Detectors

Flaw Detector	Mode A_1 (dB/m)	A_1 20log$R$ (dB)	S_1 (dB/m)	S_1 20log$R$ (dB)	S_2 (dB/m)	S_2 20log$R$ (dB)
A'1*	22.5	−11.0	11.5	−7.8	12.0	−18.5
A 1	19.5	−12.3	8.5	−8.5	8.5	−17.0
B 1**	19.5	−11.0	9.0	−6.3	8.5	−10.8
B 2	25.8	− 9.3	8.0	−6.7	10.0	−12.5
B 3	19.0	−10.8	12.0	−6.5	8.3	−20.8

*A1, A'1 means the different type of detectors made by maker A.
**B1, B2, B3 means the same type of detectors made by maker B.

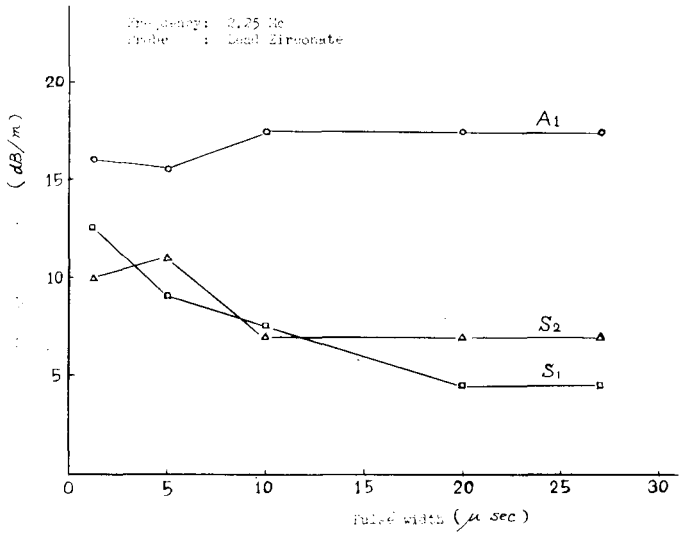

Figure 6. Relationship of pulse width and attenuation constant with rectangular pulse modulated wave. (Arenberg's Pulsed Oscillator and Wide Band Amplifier.)

reflected at it. Furthermore every available mode at a certain frequency is not necessarily useful for nondestructive inspection and care should be taken to use effective modes.

Effect of Frequency Spectrum on the Attenuation and Reflection Ratio of Lamb Waves

Only one type of ultrasonic flaw detector was used in the experiments described above and it was possible that another detector might get different results. In order to check this, we measured the attenuation constant and reflection ratio of Lamb waves with several types of flaw detectors, using the same method as that used in the previous experiment. The measurement of the reflection ratio was made at a groove 0.5 mm deep and 5 mm wide in a 2.3-mm-thick steel sheet. As shown in Table 7, different detectors showed different reflection ratios. First, we thought the narrow band width (0.5 MHz) of the amplifier in a detector might have influenced the results. Therefore, we made the same measurement again with broader band width (2.2 MHz) of the B1 detector by changing the circuit. But the same results were obtained. Different detectors may generate pulses with a different frequency spectrum and the different spectrum may cause different behaviour of Lamb waves. Using a rectangular, pulse-modulated wave transmitter, a wide-band amplifier and a synchroscope we tried to confirm this. We measured the attenuation constant of Lamb waves at 2.25 MHz with the same 2.3-mm-thick sheet, changing the pulse width from 1.25μ sec to 27μ sec. The results are shown in Figure 6. Attenuation constants of S_1 and S_2 modes increase almost to the value measured by the B1 detector when the pulse width decreases while the attenuation of the A1 mode stays constant and is almost equal to the value measured by the B1 detector.

From these results we may conclude that the shape or frequency spectrum of the pulse influences the measurement of Lamb waves.

When group velocity is not a constant, the pulse suffers considerable dispersion if the frequency spectrum is appreciable and the pulse length has to be considerably longer to obtain useful results.(6) Usually the pulse widths of detectors are not constant and the frequency spectra are different among detectors. Therefore comparison of quantitative measurements of Lamb waves among detectors seems to be difficult although each detector can make the measurements.

The authors would like to acknowledge the invaluable help and advice given by Professor Dr. M. Onoe of Tokyo University.

References

(1) Lehfeldt, W. Ultraschall-Prüfung von Blechen mittels Plattenwellen. Materialprüf. 4 (9) 1962, . 331-337.

(2) Höller, P., and Lechky, E. Prüfung von 3 bis 20 mm dicken Stahlblechen mit Ultraschall-Plattenwellen. Arch. Eisenhütt. 33 (10) 1962, P. 699-710.

(3) Niklas, L. Plattenwellen Materialprüf. 4 (1) 1962, P. 12-20.

(4) Delatte, J. Influence du cobalt sur le coefficient de diffusion du l'azote dans la ferrite, Metaux. Corr. Ind. 36, 1961, P. 161-168.

(5) "NDI Standard Test Piece Type Pl for Ultrasonic Testing by Lamb Waves" specified by the Japanese Society for NDT.

(6) Mason, W. P. Physical Acoustics and the Properties of Solids, p. 100 D. Van Nostrand, 1958.

Discussion

Q. R. N. CRESSMAN, Bethlehem Steel Corp., Bethlehem, U.S.A.— Two critical aspects of Lamb-wave inspection for production applications are:

1. The need for closely controlling the test angle, and 2. maintaining uniform coupling at test speeds of several thousand fpm. Have you developed any methods for overcoming these difficulties? Have you found that any particular Lamb-wave mode is most sensitive to laminar-type defects?

A. As you point out, the strict control of test-angle is essential in Lamb-wave inspection. The control is done as indicated below, and we have been carrying out Lamb-wave inspection in the production process in our Hirohata works. At first we tried to use the wheel-type *variable* angle probe made by Sperry Products Co., but the ultrasonic echo on a CRT fluctuated so much that it proved impractical. We solved the problem by using a solid frame to which a wheel-type *fixed* angle probe was fixed, with a manual angle-changing mechanism. Regarding your second query, we have been trying to carry out inspection of steel sheets at high speed, but so far the maximum inspection speed is 120m/min and rust-preventing oil is used as a coupling medium. At 2.25 MHz, S_2 mode is found to be very sensitive to some laminations in 2-mm-thick steel sheets, and other modes are found to be quite useless. At the same frequency, S_0 is found to be effective in the inspection of 0.8-to-1.0-mm-thick sheets. General rules for the selection of suitable modes for steel sheet inspection have not yet been established.

Underwater Wall-Thickness Measurements and Weld Testing by Ultrasonics

HARTMUT JÜNKE, GERMANY

ABSTRACT: *The application of underwater ultrasonic testing by using a submerged pulse system is dealt with. Laboratory tests on wall-thickness measurements, weld testing and crack detection are described with respect to application under water, for which waterproof housing for a battery-powered pulse system was developed. Tests were carried out to a depth of 32.8 ft. (10 m). They showed that pressure and water do not influence sound transmission of the recording equipment, and that accurate testing is possible under water. Special conditions that occur when testing under water are noted and the practical application of measuring wall thicknesses of sheet piling is described.*

Introduction

Ultrasonic material testing has found acceptance in nearly all branches of industry and technology, and is expanding its field of application more and more. Most tests of course are carried out at plants and building sites on land. Structures in water or underwater are normally tested for manufacturing defects out of water, but if such structures are in operation, checking for loading defects is an extremely difficult and complex task. Underwater welds, for example, cannot be tested by conventional means, so that we must turn to ultrasonic testing as a method offering the best conditions for underwater testing. In 1959 the Akademiet for de Tekniske Videnskaber Svejsecentralen Kopenhagen undertook tests to measure the wall thickness of sheet pilings by underwater ultrasonics (1). In 1963-65 similar methods were used to measure the thickness of steel sheet pilings in East Germany (2). In all tests reported the diver put the probe on the prepared spot, but the equipment remained out of water. Using prearranged signals by cord or by telephone the diver and the equipment operator communicated with each other. This kind of testing is applicable when a static reading is required, where the probe is not moved, as in the case of doing wall thickness measurements. The ultrasonic test, however, is a dynamic one and is not confined to measurement. The test-piece must be evaluated by coordinating the movement of the probe and the movement of the screen image, and the inspector must watch the probe movement and the screen simultaneously. Accordingly it is necessary to submerge the equipment. As far as power supply difficulties are concerned, battery powered ultrasonic equipment has been developed.

Underwater ultrasonic inspection has special significance in measuring wall thickness, weld tests, and in detecting cracks in ships' hulls. Dock fees, which amount to about $2,000 may be reduced (3) as the tests may be carried out during normal hours when the ship is at anchor in a harbour, or even in the roads.

Laboratory Investigations

Only battery powered equipment can be used for underwater testing so the investigations were carried out with this kind of set-up. Pulse system equipment USK 4 made by Krautkramer, Köln, was used.

Wall Thickness Measurements

Since it is better to read the wall thickness directly from the screen without recalculation, a waterproof 6-MHz, dual-crystal probe was used, with waterproofed cable connections.

In the case of sheet pilings water may get behind the plate. Therefore, the influence on the screen image due to water at the back side of the plate had to be cleared up. Further, the effect on the screen image of a gap of water between the probe and the plate required examination; because of the corroded surfaces there will nearly always be a gap. However, investigation showed that water at the back side of a plate will not influence the result of the wall thickness measurement.

A probe radiates sound in itself when submerged; as it approaches the object under test an echo arises from the surface of the sample at the normal incidence of sound. Depending on the distance between the probe and the test surface, an echo arises a certain distance from the transmission point (initial pulse indication). It coincides with the initial pulse when the probe touches the sample.

Dual-crystal probes are built to indicate reflecting targets lying close below the surface, and very near to the probe—about 0.04-in. (1-mm) steel in this case. Thus spurious echoes had to be expected if the water gap between probe and test surface became more than 0.01 in. (0.25 mm) (i.e. about 0.04-in. (1-mm) steel). Figures 1a to 1h show how different gaps influence the recording of the measured wall thickness of 0.915-in. (5-mm) steel. At first one can see that up to a gap thickness of 0.04 in. (1.0 mm) in Figure 1 a clear separation of zero echo and measured echo takes place. With a gap of 0.08 in. (2.0 mm) a positive reading is impossible; with a gap of 0.12 in. (3.0 mm) the measuring echo is covered totally by the echo from the surface. Further, with increasing distance the zero echo shifts to greater distances, while the distance between the zero echo and the measuring echo remains constant. Working with a constant gap this shifting may be taken into account and the equipment adjusted, so that a precise measurement within the limits of the pulse system is possible. Measurements of small thicknesses showed that a gap thickness of 0.02 in. (0.5 mm) should not be exceeded.

The minimum thickness to be measured is 0.12 in. (3.0 mm) of steel for the chosen pulse system with an accuracy of 0.02 in. (± 0.5 mm) on rough surfaces. The upper limit is 1.2 in. (30 mm) of steel. Above this the multiple-echo method has to be used.

To keep a gap of 0.02 in. (0.5 mm) a probe holder was built. A guide tube simultaneously serves normal sound incidence.

Weld Testing and Crack Detection

Testing of welds and ship hulls to find fatigue cracks requires an oblique angle of incidence. At first we tried to use the probe holder developed for wall thickness measurements, adjusting a normal probe to a certain angle, determined according to Snell's law. A 4-MHz immersion probe was used. However the probe radiated sound through the housing into the holder and the surrounding water, producing a number of spurious echoes. Therefore, a refracting prism was made (Figure 3) by which, depending on the wedge angle, shear waves were radiated into the plate at the desired refractive angle. The investigations were carried out to test a welded joint 0.39 in. (10 mm) thick.

Firstly, however we had to determine in the laboratory whether water on the testing side or the back side, or simultaneously on both sides, impaired sound transmission in the plate and with it the reading. A waterproof box was welded on to the back side of the sample, shutting off one side. Thus

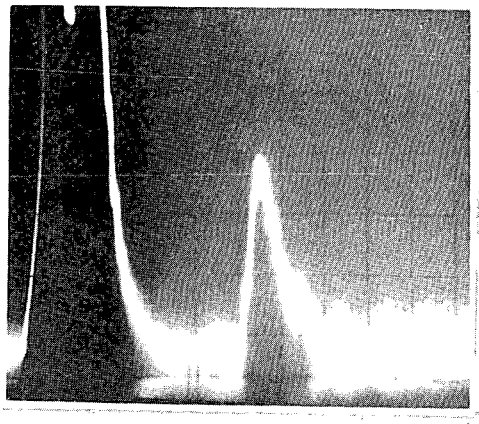

Fig. 1a
d= 0 mm

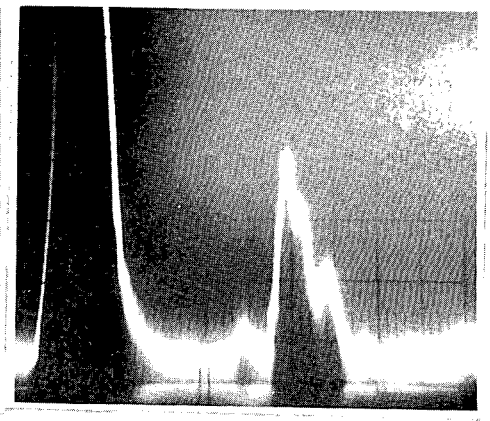

Fig. 1b
d= 0,35 mm (0,014 in)

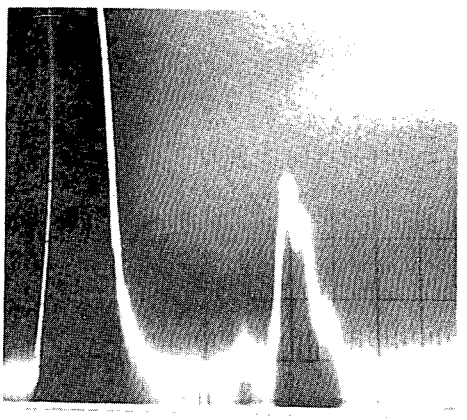

Fig. 1c
d= 0,5 mm (0,02 in)

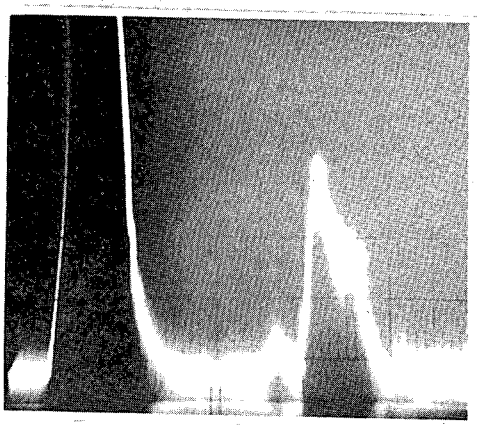

Fig. 1d
d= 0,85 mm (0,034 in)

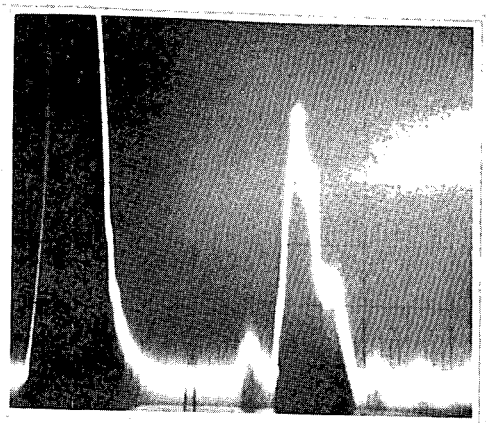

Fig. 1e
d= 1,0 mm (0,04 in)

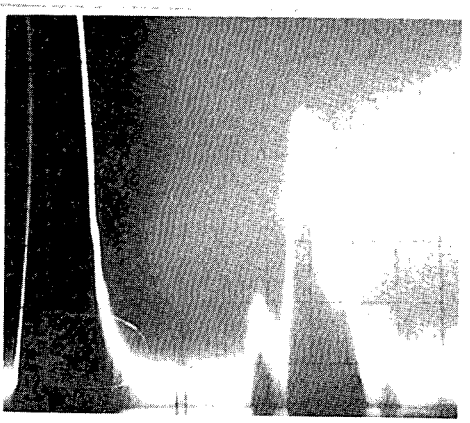

Fig. 1f
d= 1,5 mm (0,06 in)

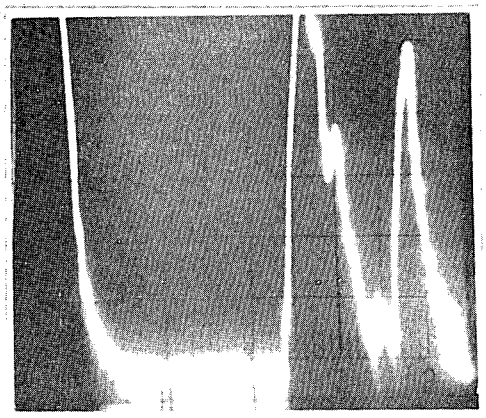

Figure 1. Screen images of the wall-thickness measurement of a thickness of 1.195 in. (5 mm) having different gaps of water, d.

we were able to make underwater tests of one part of the weld exposed to air only, and by flooding the box make similar tests on the same weld exposed to water.

The tests showed that in no case did the water impair the reading.

Application of this method to the checking of fatigue cracks in ships' hulls was also tested. The tests were applied to double-plated hulls. Under operating conditions cracks occurred in the outer plating, beginning on the inner side. Because of the double plating the only possible test was by ultrasonics carried out from the water side. The tests showed that the formation of cracks is detectable by underwater checking. This means that ships need not go into dock for checking.

These results had to be checked in greater depths of water, because the laboratory tests had been performed without water pressure, and the pulse system itself was out of water, too. Thus, it was necessary to develop a waterproof housing.

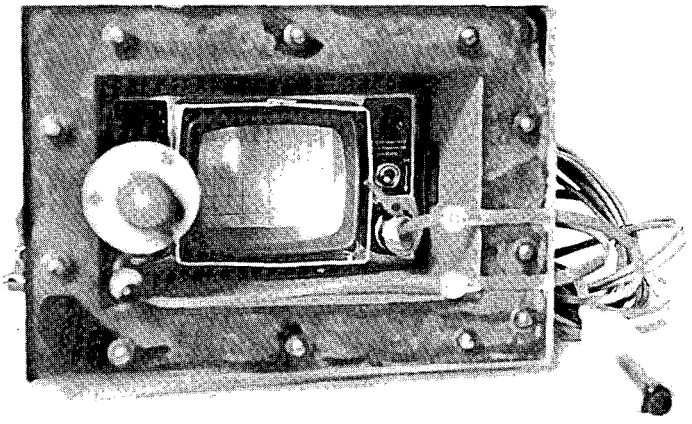

Figure 2. View of the housing for wall-thickness measurements (photo by author).

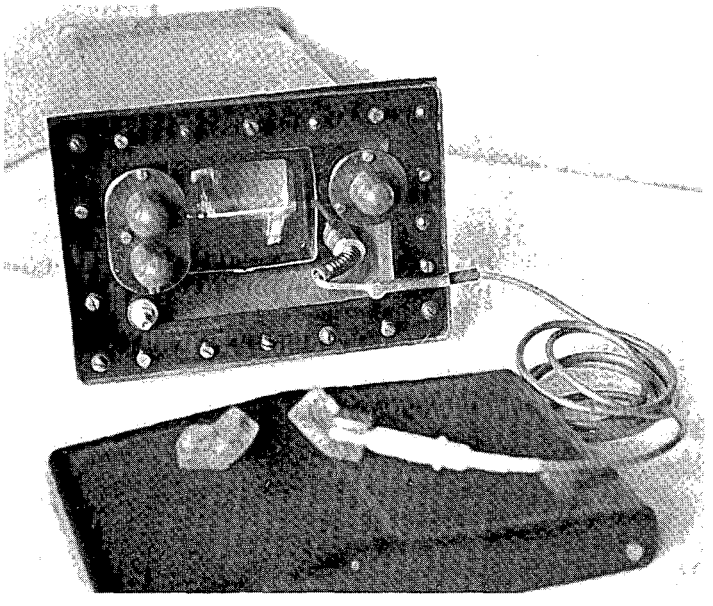

Figure 3. View of the housing for testing welds and for crack detection, with prisms and prepared weld (photo by author).

Equipment Set-Up

There were four requirements for construction of the housing.

1. It had to be waterproof and resistant to compression.
2. A satisfactory view of the screen had to be maintained, even under unfavourable water conditions.
3. The pulse system had to be operated from outside.
4. A simple method for changing batteries had to be incorporated.

In relation to the pulse system these requirements led to the following construction: A housing of 0.08-in. (2-mm) steel sheet was produced to fit the pulse system. The bottom (back wall of the pulse system) consisted of 0.39-in. (10-mm) steel plate welded to the housing. Inside the bottom there was a cover, waterproofed by a rubber-ring gasket, mounted by four screws. A battery change could be made quickly by opening the cover without taking the pulse system out of the housing.

The front side of the housing was equipped with a plexiglass pane, 0.58 in. (15 mm) thick. In this pane were the openings for the control knobs and the probe cables. The pane was bolted to the housing and waterproofed by a rubber gasket. By removing the pane the pulse system could be taken out of the housing.

To adjust the pulse system the openings in the pane were waterproofed by rubber sleeves into which extension control knobs were fitted. Thus the pulse system could be handled from outside. In deeper water, the sleeves would be compressed and the pulse system could not be operated without corresponding counterpressure. Therefore, the housing was provided with a valve, by means of which a high-pressure corresponding to the water depth could be produced. By this means a leak could be detected at once by the formation of air bubbles when the equipment was immersed, but before water could enter the housing. The probe cables were led out between the pane and the rubber gasket, the pane being drilled parallel with the surface, so that the cables, lying within a rubber gasket would be pressed into the rubber gasket of the pane. This kind of sealing proved useful up to 1.5 (21.3 lb/in.^{2}) overpressure, corresponding to a water depth of 49.2 ft (15 m). Preliminary tests showed that the calibration of the pulse system did not vary by switching on or off. The pulse system was tested by switching on and off approximately one hundred times, measuring a reference thickness after every switch-on.

Accordingly, when measuring wall thicknesses, it was only necessary to handle the switch-on knob, which simultaneously controlled the gain. Only one outside lead was provided. Figure 2 shows the construction of the housing for wall thickness measurements. Cable connections out of the housing were covered by a rubber tube and sealed by varnish.

To carry out weld and crack testing the pulse system had to be adjusted to the probe used and to the material under test. Therefore, it was necessary to handle every control knob, and all knobs had to be led out. Figure 3 shows the construction of the housing for weld tests, and also the construction of the angle probes and the prepared weld.

To prevent condensation in the housing due to humidity when the equipment was submerged, a bag filled with silicagel was placed in the housing, which prevented the pane from becoming covered with moisture.

The development of an underwater housing of this type was influenced by technical and time considerations. Of course, it is possible to place the pulse system in a cast housing that is resistant to compression without producing a counterpressure. The version developed, however, fulfilled all requirements, because such underwater tests are rarely, if ever, carried out in greater depths than 42.2 ft (15 m). Further developments provide for an improvement in operating the equipment and the connection of a compressed air cylinder to the housing, to vary, at will, the internal pressure below water surface.

Tests Below Water Surface

Safety precautions required special diver training for light divers when engaged in underwater tests, because the submerged diver was subjected to great physical loads and had to acclimatize himself to near-weightlessness in the altering rhythms of movement. The latter was the greatest difficulty in underwater testing. Slight movements, such as guiding or contact-pressuring of the probe would move the inspector out of position. When testing *in situ* it was advantageous to support the inspector by ladders. The inspector could fasten himself to the subject under test by use of a magnet.

At first, the tests were carried out in an enclosed basin down to a depth of 16.4 ft (5 m), at which depth the photos were taken. In open water, photography was impossible, as no underwater camera was available.

Figures 4 and 5 show tests for checking welds. The divers wore lead belts to get support below water surface. The equipment was trimmed by a lead weight in such a manner that it would stay upright. When testing in a greater depth of water the equipment may be slung, and the inspector is not bothered by weight, as the equipment almost floats in the water.

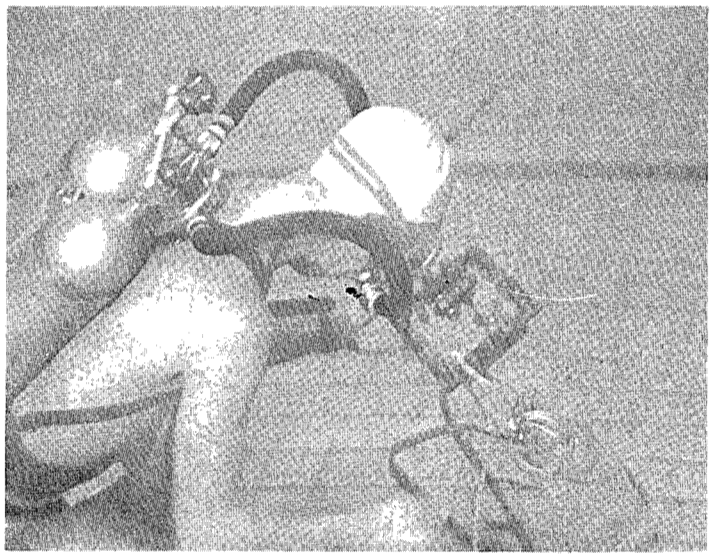

Figure 4. Test checking in 16.4 ft (5m) of water (photo by author).

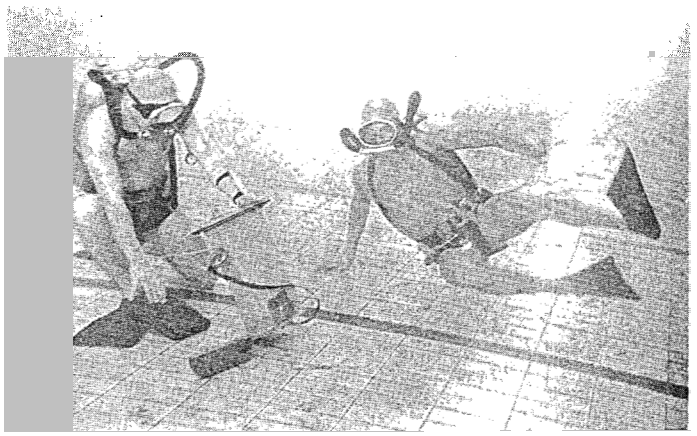

Figure 5. Test checking in 16.4 ft (5m) of water (photo by author).

Tests to a depth of 32.8 ft (10 m) showed that water pressure did not influence sound propagation and recording, nor did the presence of water at both sides of the plate change the reading. The same behaviour can be expected at greater depths, i.e. at greater pressures. The depth limit of 32.8 ft (10 m) was chosen so as not to complicate the tests by adhering to certain surfacing and half-compression times and also to minimize danger to the diver as far as possible.

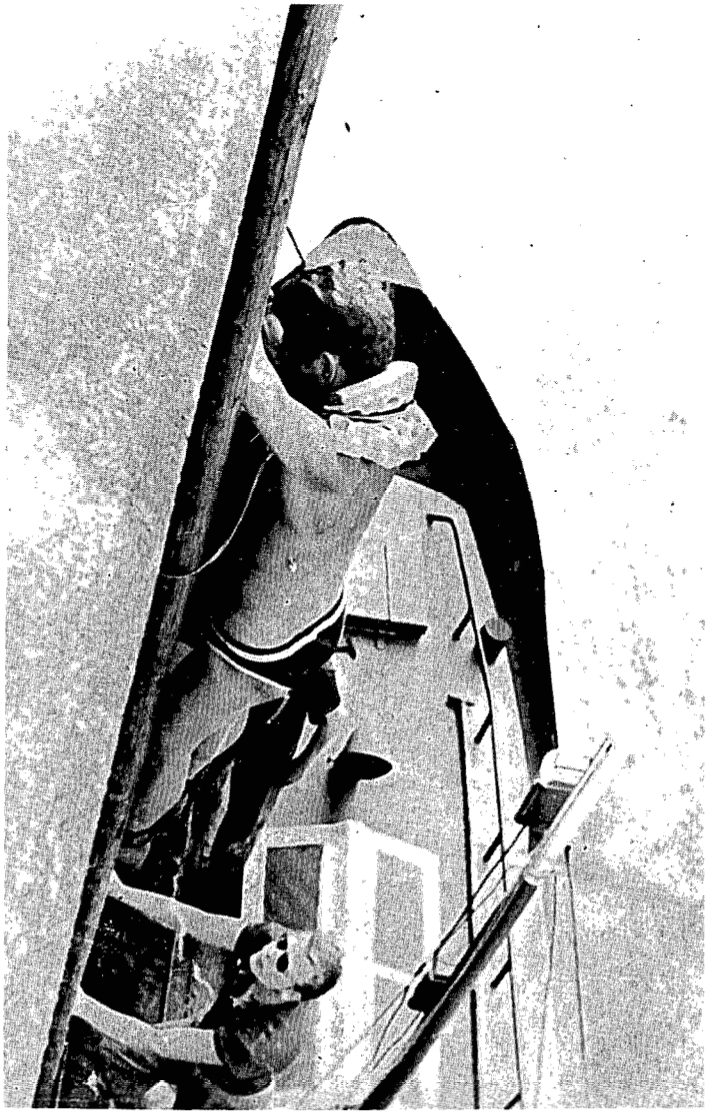

Figure 6. Wall thickness measurements of sheet piling in a harbour (photo by author).

The properties of the system were not changed by pressure, the reading remaining constant for more than three hours.

If a subject under test ranged some metres in depth it was advantageous to begin the test at the deepest point. Within the housing, pressure was produced corresponding to that depth. The water pressure acting against the internal pressure of the rubber sleeves permitted movement, and adjusting the equipment was possible without difficulty. Surface air was blown down corresponding to the depth, to establish a balanced position.

Because of working and safety conditions it was necessary to employ two inspectors. They communicated by writing with a pencil on a white resin plate, fastened to one arm, and also used the plate to make notations on the tests.

Figure 5 shows that in spite of lead weights movement was very difficult under water. The inspector had to put the test-piece on one of his flippers, anchoring himself against the pressure resulting from contact of the probe on the test-piece.

Because the screen was luminous a reading could easily be made under water. The oscilloscope had enough luminosity to permit recognition of the screen dial, although strong turbidity in open water tended to obscure it and make a reading complicated.

Such situations occurred when doing wall-thickness measurements of sheet pilings in a harbour. Therefore, the distance between the screen and the pane of the housing was so placed that the diver could watch the screen without difficulty by touching his goggles to the pane. Thus, even in mud a reading was possible.

A test was made on sheet piling built some ten years ago (Figure 6). The results showed that the existing wall thickness was good for about twenty years at least. Thus it was established that the pilings were strong enough to support a crane without renewing the wall. If it had not been posisble to make the measurements, the pilings would have been renewed simply as a safety precaution; the tests resulted in considerable savings.

Summary

This paper has dealt with the significance of underwater ultrasonic testing. The problems were tested in a laboratory and battery powered pulse system, type USK 4 made by Krautkramer, Köln was used. Wall-thickness measurements were carried out by use of a 6-MHz-double-crystal-probe. Tests showed that the distance between the probe and the test surface may be a maximum of 0.02 in. (0.5 mm) for a satisfactory reading. Accuracy of measurement amounts to 0.02 in (±0.5 mm). Plate thickness is measurable from 0.12 in. (3 mm) upwards. Testing of welds and detecting of cracks in plates of ships' hulls is also possible. Water at both sides of a plate does not influence sound propagation or equipment indication.

The construction of a waterproof housing for the pulse system has been described. Tests were carried out down to a depth of 32.8 ft (10 m) using a submerged pulse system for the first time. The tests proved satisfactory operation of the equipment and showed that no difference appeared in the indication. They also showed that practical measurement of the thickness of sheet piling is possible.

The results show that it is possible to carry out successful underwater ultrasonic tests, thereby opening up a new field of application in ultrasonic testing. Proper application of such testing could significantly increase the safety of underwater or in-water metal structures and substantially reduce costs of inspection.

References

1. N. N. Wanddickenmessungen an Stahlspundwanden unter Wasser. Das Echo, Nr. 9 Dec. 1961 p. 117/118. Dr. J.u.H. Krautkramer, Gesell.f.Elektrophysik, Koln.
2. Liesche, M., Rauschert, M. Forschungsauftrag "Stahlkorrosion". Poseidon, Zeitschr.f. Tauchsport, Tauchertechnik Heft 10 (1965) p. 18/22.
3. Evans, D. J. Ultrasonic inspection in the oil refining and related industries. Nondestructive Test. 15 (1957) Nr. 3, p. 156/160.
4. Winters, W. R. Nondestructive testing protects nation's marine industry. Mat. Eval. Vol. XXII Aug. 1964 Nr. 8, p. 361/362.

Wall Thickness and Wall Thickness Tolerance Measurement

W. GRABENDÖRFER and A. DROEGE, GERMANY

ABSTRACT: Measuring the exact wall thickness of products of which only one side is accessible is a substantial and important part of nondestructive testing. This paper describes the measuring problems and the requirements found in practice. It presents a summary of the available measuring methods and their latest developments, as well as some examples of application. The accuracies, and limitations in meeting the stated requirements are described.

Introduction

Generally the practical requirements are subdivided as follows:

a) Checking of wall thicknesses during or immediately after manufacture.

b) Inspecting wall thicknesses of material in operation, i.e. routine plant checks of critical parts, for example, in the chemical industry and in power plants.

Objects of the first group have smooth, non-corroded surfaces. The wall surfaces of the second group, however, will be found in most cases too severely corroded by aggressive media and high temperatures. It is in these corroded areas that the remaining minimum wall thickness has to be measured.

On new products (i.e. tubes, plates, vessels) a continuous measuring system, that is mechanized as much as possible, is required. The critical structural parts in industrial plants, however, must be scanned by hand in most cases.

Reading of the measured values must be easy, preferably by means of large scales or digital presentation, so that unskilled labour can make routine checks. Evaluating results from continuous measuring systems must also be simple, that is, presenting wall thickness values on a recorder, automatic sorting of specimens whose wall thickness is above or below certain limits or visual indication of the minimum thickness value.

The well known classical procedures for measuring wall thicknesses and their characteristics are the following:

The Multiple-Echo Method

The method of measuring wall thickness by a series of multiple echoes on a calibrated pulse-echo instrument is well known, and has been used for a long time. This method, however, is limited to scanning the specimen under test point by point, and is also limited to smooth surfaces. Besides, the operator must carefully read the screen at each measuring point. If the operator reads the values for the three-to-fivefold wall thickness (i.e. he evaluates 3 to 5 multiple echoes) he can obtain a measuring accuracy of 1 to 2 per cent. Depending on the probe frequency this measurement can be accomplished down to a wall thickness of about $\frac{1}{8}$ in. (3 mm). When a sequence consists of at least 4 to 5 multiple echoes measurements can be facilitated (down to 4 mm) by an ancillary electrical device supplementing the pulse-echo unit. When using this "wall thickness meter", the echo sequence excites a tunable oscillating circuit. As soon as the operator has found the resonant point by turning the tuning condenser, the wall thickness value can be read directly from a scale.

In cases where the walls are thicker, the multiple echoes on the screen are widely separated, making it possible to record wall thickness values. For this purpose, the echo sequence is

generated via a water column, i.e. by immersion technique. For recording purposes only, the distance between the echo from the water/steel boundary surface and the first back echo is needed; a transit-time monitor produces a voltage proportional to the echo distance. If such a system is used to scan spirally (i.e. tubes), the wall thickness along this spiral line can be recorded continuously. At probe frequencies, between 4 and 6 MHz, the echo widths are widened by rough surfaces, and thus limit the application of this recording method to wall thicknesses in excess of about $\frac{1}{4}$ to $\frac{1}{3}$ in. (6 to 8 mm).

The Resonance Method

The ultrasonic resonance method is quite a different procedure: The frequency of the transmitted continuous ultrasonic wave is varied continuously between certain limits. The wall being measured resonates when it is equal to an integral number of half wavelengths of the sound beam used. The wall thickness can be determined from the frequency of the resonant points. The measuring device "Vidigage" makes the resonant points visible on the screen, and the wall thickness is read from special scales. Another device applying the same principle shows the resonant points by lighting annularly arranged glow lamps. Values are read from a circular scale, shiftable around the centre. The resonant points are indicated acoustically by another device. The above resonance devices enable point to point measuring, if good coupling is provided.

Some years ago the resonance method was improved, thus enabling wall thickness measurements by interconnecting a water column. Since proper coupling is guaranteed by the immersion technique the resonance method can be applied for continuous measuring, at least for plates and precision tubes with smooth surfaces. An ancillary device also helps to receive a signal that is proportional to the wall thickness and to record it.

Compared to the pulse-echo method, the resonance method can measure wall thicknesses down to approximately 0.5 mm (20 thou).

SE-Probe Method

All these methods are limited to smooth wall surfaces. The pulse-echo method indicates corroded areas by disappearance of the multiple echo sequence. Corroded pits are not indicated in a correspondingly clear manner by the resonance method. Since, however, the measurement of remaining minimum wall thickness is the main task of the plant check there is great interest in an easy and dependable method. For several years the SE-probe has been successfully used for this purpose. This probe consists of a transmitter and a receiver giving only a small indication of the material surface. The first clear indication following comes from the back-wall. This back echo is used to read the exact wall thickness from the screen of a pulse-echo instrument (the scale dimensions on the screen are spread to obtain sufficient accuracy). Normally the full screen width matches a material thickness of 0.4 in. (10 mm). It is significant that in most cases a readable back echo can be achieved even if a corrosion pit is present on the inner wall surface. In cases where the "outside" surface (accessible for measurements) is heavily corroded, measurements are only possible in a place where sufficient coupling is achieved in spite of the rough surface. Since the echo indicates clearly and directly the remaining wall thickness, the location of the minimum residual wall thickness can be found by shifting the probe and watching the movements of the echo on the screen. To obtain good accuracy (approx. ± 0.1 mm resp. ± 4 thou) it is important to check the calibration of the unit by means of a step test block at certain intervals (Figures 1, 2).

It is obvious that continuously operating wall thickness measuring devices can be made, using this simple procedure. Using this method, it is possible to measure down to 0.04 to

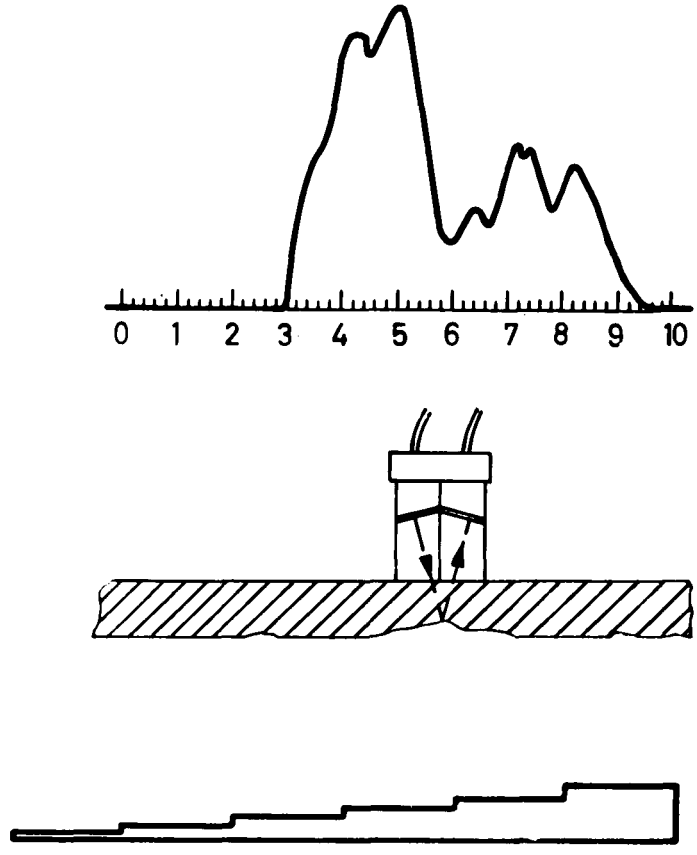

Figure 1. Wall thickness measuring with SE-probe (b) and 10-mm scale expansion.

Figure 2. Wall thickness measuring at corroded tubes with SE-probe.

.06 in. (1 to 1.5 mm) (contrary to the multiple-echo method with a normal probe). Since the "overcoupling echo" from the coupling gap between probe and surface can be lower than the back echo by 14 db, an automatic wall thickness tolerance measuring system can be easily constructed by means of additional signal monitors. There will be difficulties, however, arising from mechanizing the scanning. Because of the ratio of sound velocities of water to steel = approx. 1:4, a change of the water gap by only 0.1 mm is equivalent to 0.4 mm change in steel thickness. Even if the probe is mounted with accurate mechanical devices, with the surfaces normally found in practice, it is not possible to keep the coupling gap within 0.1 mm. This, however, is necessary to avoid an error of more than 0.4 mm wall thickness.

The SKE-Probe

To correct this, the development of the SE-probe was continued. A third crystal was inserted to obtain a reference echo from the surface. The distance between this crystal and the contact surface of the probe is shorter, so that the reference echo resulting from it appears before the small overcoupling indication of the normal SE-probe crystals. Besides, the amplitude of this reference echo can be adjusted independently from the other echoes. As soon as the distance between probe and specimen surface changes, both echoes—the reference echo and the back echo (the latter corresponding to the wall thickness), shift exactly in parallel. Thus this surface echo can be a reference echo for wall thickness measuring if the evaluating monitor gate is "attached" to this echo. Figure 3 shows the construction and the echo of the described SKE-probe. For continuous measurement, the transmitter and receiver are designed as water chambers as indicated in Figure 3. When the probe is lifted from the surface the reference echo (1) and the back echo (3) shift to the right by the same distance, of course the undesired overcoupling echo (2) shifts also. The distance between echoes (1) and (3), which corresponds to the sum of the probe constant and the wall thickness to be determined, is read. Lifting the probe up to 0.80 in. (2 mm) does not influence the oscillogram and the result. When exceeding 0.80 in. (2 mm) the overcoupling echo becomes very large, thus preventing an automatic evaluation of the oscillogram by a monitor. At this point certain factors influencing the accuracy of the SE method should be considered. Each echo on the screen shows "knots" on the rising (and falling) flank resulting from the rectified high-frequency oscillations of the pulse. Since the rising flank of the echo is used when reading the screen, the reading can differ by the distance between two knots when applying different echo heights for measurements. In the worst case—if the echo being read is not high enough—the reading can be shifted to the high side by 2 or 3 knots. Since the distance between two knots corresponds exactly to one wavelength, the resultant error can be easily stated: i.e. 0.02 in. (0.5 mm) for 6 MHz measuring frequency when shifting the flank by one knot. (Half the wavelength results from the time difference being divided into its way back and forth when applying the reflection method.) Therefore, during measurements the operator must be careful always to read at the same echo height (as it was being done during calibration procedure) and always before the same knot within the indication.

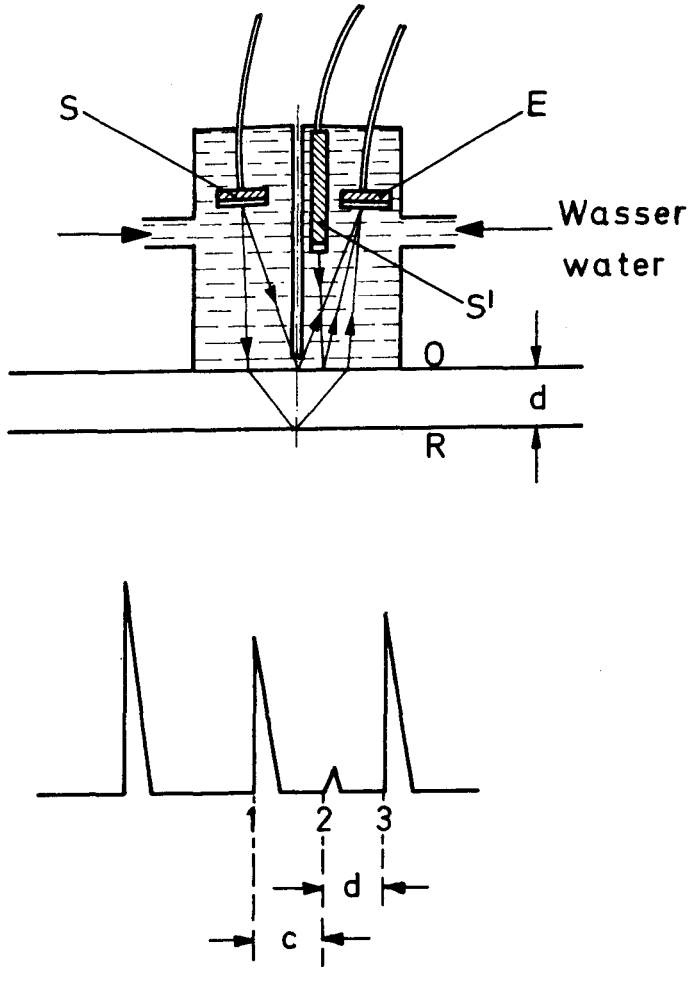

Figure 3. Scheme and oscillogram of SKE-probe. 1 (S'-O-E) = reference echo. 2 (S-O-E) = overcoupling echo. 3 (S-R-E) = back echo. 1-3 = echo distance to be evaluated by monitor for thickness measurement. c = probe constant.

The continuous wall thickness measurement of tubes can be used as an example of the possibilities of automatic thickness control. A simple system operates as follows: A signal monitor gate whose width is adjusted to the tolerance wall thickness will be attached to the reference echo of the SKE-probe. As soon as the tube wall thickness falls below this tolerance (during spiral scanning) the monitor triggers. The signal may be used directly for marking the point below tolerance or for controlling a sorting device via a storage element. Of course, a second monitor channel can be added showing wall thicknesses above a maximum tolerance value.

On the other hand, the wall thicknesses can be analogously registered by a recorder via a transit-time monitor whose gate is also attached to the reference echo of the SKE-probe. This method, however, is somewhat elaborate owing to the great quantity of recording paper to be evaluated. In most cases this is not desirable for wall thickness inspection during production.

In all cases, it is important to know the minimum wall thickness which was found when checking the whole tube. An ancillary unit was developed to store smaller value as found, or the result is erased by the operator. Simultaneously the digital reading of wall thickness is presented by luminous numerals, and the minimum reading can also be printed after a tube has passed through.

A variation of the above system, where the tube (longitudinal direction) is subdivided into sections, e.g. 200 mm long, has been in use for some time. The section where the thickness falls below tolerance is marked, and can be cut off consequently, or a printed tape for each tube shows in proper sequence the minimum thickness for each section. Since during measuring procedure in most cases (i.e. tube testing) defects must be detected at the same time, other, rather complex evaluation devices are required for the combined data evaluation.

High-Temperature Measurements

All measuring methods must be critically reviewed on their performance at higher temperatures, i.e. temperatures of approx. 200 to 600°C (400 to 1100°F). (Objects with temperatures close to 600°C are very seldom encountered, according to our experience). There are two problems when measuring these "hot" specimens:

1) Coupling medium. Even at high temperatures it must not evaporate, develop blisters, or melt, thus preventing probe coupling.
2) Protection of crystals, cement layers and probe connections from the heat. The crystals and their cementing (sensitive to heat) on the damping body must not contact the hot specimen. Therefore, heat-resistant adaptors (not too sound-absorbing) must be used.

The measuring method first mentioned—evaluating a multiple-echo sequence on the calibrated screen—can be easily adapted to hot material by using a normal probe with plastic adaptor (the latter normally made of "Lekutherm") and silicone vacuum grease, bitumen or other special greases for coupling. Owing to the relatively high absorption of ultrasonic waves in the plastic adaptor only one or two multiple echoes appear, the first one being followed by the echoes of the wall thickness to be read. Reading the screen must be done quickly, since the adaptor heats up during prolonged contact of the hot surface, thus changing the sound velocity within the adaptor and causing a drift of the echo. The absorption increases continuously, so that the echoes to be evaluated disappear with more or less rapidity. For this reason the oscillograms must be photographed as soon as they appear, for calculation of the thickness later. This means a procedure which is time-consuming and not very elegant for practical operation. Additional time is required between the photographing of the screen and the conclusions to be drawn from the screen photographs. However, this was the only dependable measuring method for a long time.

To solve the above problem, another method was developed: The echo sequence from the wall to be measured was generated by a "water pistol", thus applying the principle that a powerful water jet of approximately $1\frac{3}{16}$ in. (30 mm) dia destroys the steam film on the hot surface of the test object. This achieves good coupling of the sound beam being transmitted via the water jet. The critical requirement, however, is that this jet must hit the surface exactly vertical to obtain an echo sequence. By this method measurements could be made up to temperatures of approx. 600°C (1100°F). It may be of interest that hot ingots (temperatures higher than 1100°C (1800°F) were successfully tested for inner defects by means of the water pistol. As far as the coupling and the measuring technique is concerned, it is possible therefore, to measure wall thicknesses at these high temperatures. However, tension cracks could develop in tubes when they are hit by the cold water jet. Of course, both the above methods are applicable for non-corroded walls only. It was of great interest to find out at how high a temperature the SE-probe method could be used. Consequently SE-probes were built with highly heat-resistant material, so that the SE method could be used for pointwise wall thickness measuring (applying silicone vacuum grease for coupling on hot surfaces for temperatures up to 500-600°C (900-1100°F)). Between readings the probe must be cooled in a cold-water bath. Here too, heating of the probe influences the screen indications. If the temperature increases the oscillogram shifts in regard to the non-visible zero point, because the sound velocity in the plastic delay blocks changes. Besides, due to the increased temperature the absorption within the blocks increases so that the amplitude of the echo to be read quickly decreases. The screen must be read quickly, immediately after the echo appears. An automatic camera will make this easy and foolproof. As soon as the probe makes contact, the echo is photographed by releasing the camera shutter (highly sensitive film) via a monitor triggered by the echo. This relieves the operator from the difficult task of catching the echo at the right moment in each reading.

SE-probes made of highly heat-resistant material, of course, can be arranged in SKE grouping (auxiliary crystal for generating a reference echo). This will be advantageous when measuring at high temperatures, because the reference echo is shifting on the screen in nearly the same manner as the back echo. Therefore, a tolerance-measuring signal monitor or a

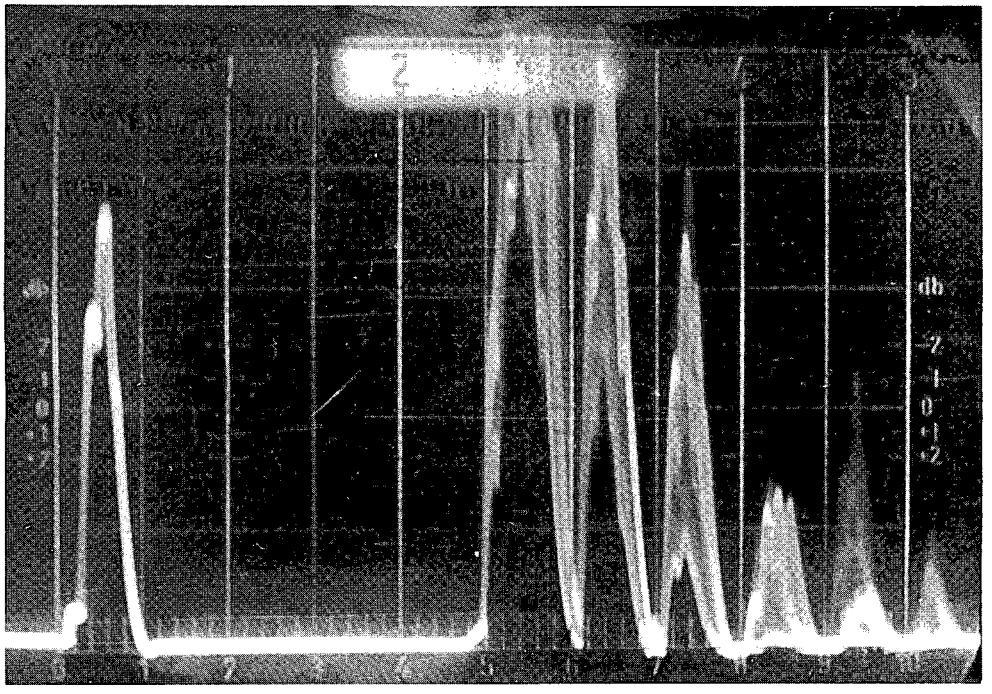

Figure 4. Measuring with SE-probe at high temperatures (oscillogram).

transit-time monitor with auxiliary indicator can be used for read-out, if the monitor gate is attached to the reference echo. Measuring will no longer be possible if the amplitudes of reference and back echo become too small owing to increasing absorption within the probe. The echo shift is of only trifling influence on the readings (Figure 4). The remaining wall thickness of corroded tubes can be determined as temperatures between 500 and 600°C (900-1100°F) as described above. One must be satisfied, however, with a measuring accuracy of ± 0.5 mm (± 20 thou) which, according to experience, is sufficient for practice. While the wall thickness of hot corroded tubes is already being done extensively by heat-resistant SE-probes, the more elegant method using SKE-probes is still undergoing tests.

Presently there are only a few automatic measuring systems. Most of the wall-thickness inspection is made in conjunction with flaw detection. During recent years only, industry has been interested in systematic wall thickness inspection of new tubes. For thin wall a continuous wall thickness inspection of the critical cans for nuclear elements for reactors, and other precision tubes, became possible by extending the resonance method to the immersion technique. Testing installations for longitudinal and transverse defects always have a recording and measuring device working in conjunction with the immersion/resonance method. (Figure 5)

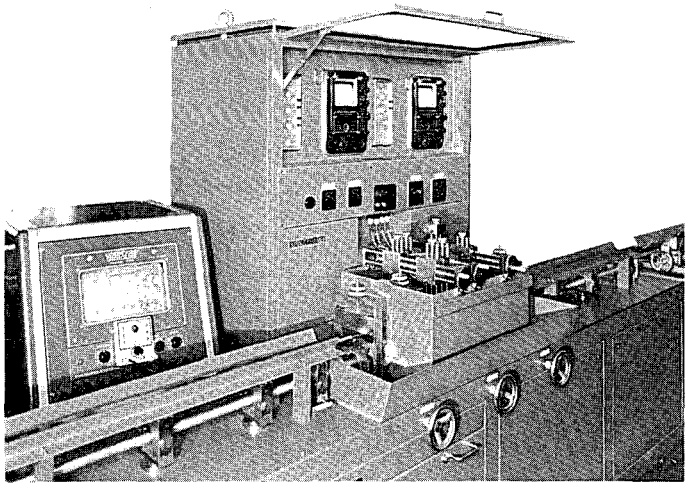

Figure 5. Test equipment for precision tubes, wall thickness measuring with immersed resonance method.

An installation for testing tubes in oil fields has been operating for several years using wall-thickness tolerance measuring equipment with normal SE-probes. The smooth tube surface insures very good probe guidance so that the required accuracy of ± 0.2 mm (± 8 thou) can be kept. Besides registering defect indications this installation also records wall thicknesses outside of pre-selected minimum and maximum values.

At present, tube testing installations are being developed for continuously checking the wall thickness of the tubes using the SKE method. Evaluation devices can be connected to these systems to process the results from flaw inspection and wall thickness measurement according to different programs. The program for a certain installation can be selected according to the practical requirements; for example, marking the tubes at the defective thin points and sorting them into different quality groups.

Experiments for supplementing the defect inspection of the different tube testing installations by wall-thickness measuring devices suitable for continuous operation are still in the initial stage. Within two or three years the results of performance of these measuring installations can be expected.

Summary

The nondestructive wall-thickness measurement can be subdivided as follows:

Checking the wall thickness during production and measuring the wall thickness during plant inspection. The differences of both problems and their requirements are discussed.

There are different measuring methods:
Evaluation of multiple echoes (pulse-echo method), the resonance method, measuring according to SE method and further development (SE-probe with auxiliary crystal).

In addition, the performance of the above methods is investigated. It is shown that particularly the SKE-probe, as developed from the SE-probe, is best suited for automatic measuring installations. The way to make the best use of this probe in tube testing installations and to evaluate the measuring data, mostly together with the defect data is described. Furthermore the possibilities of measuring the wall thickness of hot specimens is discussed. In this case highly heat-resistant material is adapted to both normal probes and SE probes. Both methods based on the pulse transit-time measurements can be applied for temperatures up to a maximum 600° C (1100° F). When using a "water pistol", higher temperatures can be measured. For determining the remaining wall thickness of corroded inner wall surfaces (cold or hot specimens) only the SE-probe method can be applied.

Ultrasonic Defect-size Determination with Double-probe and Single-probe Techniques

E. MUNDRY AND H. WÜSTENBERG, GERMANY

Introduction

List of Symbols

b =	Distance emitter-receiver
b_N =	Distance emitter-receiver, related to the near field length of the emitter
$C;c$ =	Proportional coefficient
d =	Diameter of the emitter or the receiver
$D = d/\lambda$ =	Diameter of the emitter over the wavelength λ
f =	Diameter of the flaw
$F = f/\lambda$ =	Diameter of the flaw over the wavelength λ
G =	Relative size of flaw $= f/d = \frac{S_F}{S_0}$
$H_{Fi}h_F$ =	Level of flaw echo amplitude
H_∞ =	Level of echo amplitude for infinite size of flaw
i =	$\sqrt{-1}$
k =	Wave number $= \frac{2\pi}{\lambda}$
$\overline{P_F}$ =	Average sound pressure on the flaw surface

$\overline{P_R}$ = Average sound pressure on the receiver surface

$\overline{P_R}^*$ = Average sound pressure at the receiver, calculated with respect to the distribution of sound pressure on the flaw surface

P_0 = Sound pressure on the emitter surface

$r(x)$ = Distance between the surface elements dS_0 and dS_F as a function of x

S_F = Flaw surface

S_R = Receiver surface

S_0 = Emitter surface

dS_F = Surface element of the flaw

dS_0 = Surface element of the emitter

x = Distance between emitter and flaw

$X = \frac{x}{\lambda}$ = Distance emitter-flaw, related to the wavelength λ

$X_N = \frac{4X}{D^2}$ = Distance emitter-flaw, related to the near field length of the emitter.

In evaluating ultrasonic echo indications by the method of flaw-size determination two ranges of flaw size must be distinguished: when a flaw is larger than the cross-section of the ultrasonic beam, it can be scanned by moving the probe. Where the largest dimension of the flaw is smaller than the beam diameter, the amplitude of the echo indication is a measure for the flaw size because of the characteristic relation between the acoustic pressure and the probe-flaw distance. This relation was used by Krautkramer (1) to develop his diagram for flaw-size determination.

Krautkramer's diagram is applicable only for a single-probe technique, in which the ultrasonic probe works as emitter and receiver, so that the distances emitter-flaw and flaw-receiver are always equal to one another. In some cases, however, a double-probe technique, using two angle-probes, must be applied, since the reflecting surfaces of the flaws are mainly oriented perpendicular to the scanning surface of the specimen, e.g. when testing butt welded joints in thick plates (2,3) or flash-butt weldings of large cross-sections (Figure 1). Thereby the whole cross-section is scanned by moving the probes countercurrently. Using such a test method, the distances emitter-flaw and flaw-receiver are different from each other. Therefore Krautkramer's diagram cannot be applied for flaw-size determination in a double-probe technique. Since the total pulse path emitter-flaw-receiver is of equal length for all flaw positions—this may be considered to be a characteristic of this technique—Lack (2) and de Sterke (3) have assumed that the amplitude of a flaw echo does not depend on the flaw position in the cross-section. Accordingly such a flaw-size determination would prove to be much easier than when using a single-probe technique.

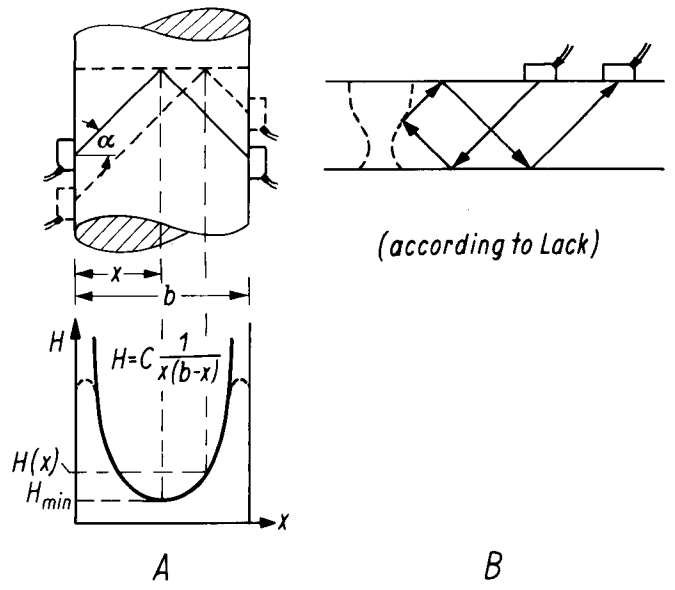

Figure 1. Double-angle probe technique and qualitywise dependence on echo amplitude.

This assumption, however, is wrong. Therefore this paper deals with the theoretical calculation of the dependence of the echo amplitude on the position and the size of a flaw for the general case of different distances emitter-flaw and flaw-receiver, which includes the single-probe technique as a special case. The theoretical results are confirmed by experiments.

Calculation of Echo Amplitude

A simple calculation shows that the echo amplitude H in an arrangement like Figure 1a must depend on the flaw position x in a specific way: If the near-field length of emitter, flaw and receiver are negligibly small compared to the pulse path sections $x/\cos\alpha$ and $(b\text{-}x)/\cos\alpha$, the well known decrease of sound pressure in the far field leads to a simple formula for the echo amplitude H being proportional to the sound pressure:

$$H = \frac{C}{x\,(b-x)} \qquad (1)$$

This function is plotted in Figure 1a (full curve). Of course, near-field influences must not be neglected in practice. Due to their remarkable dependency on the special ratio between total pulse path and near-field length for any test problem they can be indicated only qualitywise in the diagram (dotted lines). Therefore a diagram for the flaw-size determination with a double-probe technique, which is as universally useful for this technique as is Krautkramer's diagram for the single-probe technique, cannot be found. Since the experimental determination of such diagrams for every practical case would not be practical, we shall attempt to calculate them theoretically.

Analogous Model and Presumptions

According to Huyghens' principle, reflecting surfaces can be replaced by hole-type diaphragms of equal geometric shape, because both, excited in the same way, will produce ultrasonic fields of equal kind. Hence the theoretical considerations are based upon the following imaginary model: A piston source and a receiver of equal kind are at a given distance in diametral position directed towards each other, and a hole-type diaphragm, moving along the axis between emitter and receiver, represents the flaw (Figure 2 top).

The following conditions are assumed:

1) Emitter and receiver are circular piston sources of the same diameter.
2) The flaws are also of circular shape.
3) One ultrasonic pulse consists of so many single oscillations that it can be replaced by a continuous harmonic wave.
4) Only longitudinal waves are taken into account, i.e. the medium is assumed to be a fluid.
5) The echo amplitude is proportional to the arithmetic average of the sound pressure at the receiver.
6) The ultrasonic extinction will be neglected.
7) The exact calculation of the echo amplitude leads to a sextuple integral, which cannot be solved analytically and hardly determined numerically. That's why preliminarily the additional assumption must be made, that the flaw behaves like a piston source oscillating with that average of amplitude which is produced by the emitter at the position of the flaw.

Reduction of the Problem to the Calculation of the Average Sound Pressure at the Flaw

According to Rayleigh the sound pressure at one point of the flaw surface is

$$P_F(x) = c\,P_0 \int_{S_0} \frac{e^{-ik\,r(x)}}{r(x)}\,dS_0 \tag{2}$$

Its average is

$$\overline{P_F}(x) = c\,P_0 \frac{1}{S_F} \int_{S_F} \int_{S_0} \frac{e^{-ik\,r(x)}}{r(x)}\,dS_0 dS_F \tag{3}$$

The average sound pressure $\overline{P_R}$ at the receiver, whose average value is proportional to the wanted echo amplitude, is obtained analogously to Equation 3, assuming condition No. 7:

$$\overline{P_R} = \overline{P_F}(x)\,\frac{1}{S_R}\,c \int_{S_R} \int_{S_F} \frac{e^{-ik\,r(b-x)}}{r(b-x)}\,dS_F dS_R \tag{4}$$

In this equation the order of integrating can be interchanged, because the variables of integration are independent. Moreover, it is according to condition No. 1, $S_0 = S_R$. Using Equation 3, we get

$$\int_{S_R} \int_{S_F} \frac{e^{-ik\,r(b-x)}}{r(b-x)}\,dS_F dS_R = \int_{S_F} \int_{S_0} \frac{e^{-ik\,r(b-x)}}{r(b-x)}\,dS_0 dS_F \tag{5}$$

$$= S_F \frac{\overline{P_F}(b-x)}{c\,P_0}.$$

Putting this result into Equation 4, and then dividing Equation 4 by P_0, the ratio of sound pressures is obtained, as follows:

$$\frac{\overline{P_R}}{P_0} = \frac{\overline{P_F}(x)}{P_0}\,\frac{\overline{P_F}(b-x)}{P_0}\,G^2 \text{ with } G^2 = \frac{S_F}{S_0} \tag{6}$$

The level of the wanted flaw-echo amplitude h_F in decibels is then

$$h_F = 20\log\frac{\overline{P_R}}{P_0} = 20\log\frac{\overline{P_F}(x)}{P_0} + 20\log\frac{\overline{P_F}(b-x)}{P_0} + 20\log G^2 \tag{7}$$

At its right side this equation contains the average sound pressures $\overline{P_F}(x)$ and $\overline{P_F}$ (b-x) at the flaw surface at the distances x and (b-x) to the emitter as an unknown value. Thereby the calculation of the echo amplitude h_F for all positions is reduced to the calculation P_F (x) within the range $0 < x < b$.

Average Sound Pressure at the Flaw Surface

The calculation* of the ratio of sound pressures $\overline{P_F}$ (X)/P_0, leads to

$$\frac{\overline{P_F}(x)}{P_0} = e^{-i2\pi x} - \frac{4}{\pi} \int_0^{\pi/2} \sin^2\varphi\; e^{-2\pi i\sqrt{x^2 + F^2\cos^2\varphi}}\,d\varphi$$

$$- \frac{D+F}{2F} \int_0^{\pi/2} \sin\varphi\; e^{-i2\pi\sqrt{x^2 + \frac{1}{4}(D+F)^2\cos^2\varphi}}\,d\varphi$$

$$+ \frac{D-F}{2F} \int_0^{\pi/2} \sin\varphi\; e^{-i2\pi\sqrt{x^2 + \frac{1}{4}(D-F)^2\cos^2\varphi}}\,d\varphi$$

$$+ \int_0^{\pi/2} \sin\varphi\; e^{-i2\pi\sqrt{X^2 + F^2\cos^2\varphi}}\,d\varphi \tag{8}$$

After splitting up the four integrals of this equation into their real and imaginary parts, they can be determined precisely by means of a computer, using Simpson's method. With regard to the zero points of the integrants, the intervals for numerical integration were selected so that the possible error is $\leqslant 1\%$.

Due to the experiments described later the average sound pressure was calculated for the relative flaw sizes $G = 0.1$; 0.2; 0.3; . . . ; 1.0 and within the range $0 \leqslant X \leqslant 600$ with the value $D = 14.3$. For the values $D = 10$ and $D = 31.8$—i.e. $k\,d/2 = 100$ according to (4)—the special case $G = 1.0$ was calculated additionally. In order to determine the diffraction losses this special case was calculated in another way by Seki, Granato and Truell (4). Our results agree exactly with those reported in (4). The case $G = 1.0$ is equivalent to that of a hole-type diaphragm of infinite size between emitter and receiver, if the flaw of the size $G = 1.0$ is replaced by the receiver.

Distribution of Sound Pressure at the Flaw Surface

The echo amplitudes can be calculated from Equation 6 without any admissible large error, save when the distribution of the sound pressure at the flaw surface is negligible. Therefore Equation 6 is applicable only for small flaws with $G \ll 1$, or for larger flaws inside the far field. In all other cases condition No. 7 must be set aside, and the distribution of sound pressure at the flaw surface must be considered. This is done by dividing the flaw surface into concentric ring zones and one internal range of circular shape with $G = 0.2$, and by calculating* the average sound pressures on these ring zones. Instead of Equation 6 the result for the average sound pressure at the receiver is now

$$\frac{\overline{P_R}}{P_0} = G^2 \frac{\overline{P_F}(x)}{P_0}\,\frac{\overline{P_F}(b-x)}{P_0}\Bigg|_{G=0.2} +$$

$$+ \sum_{n=1}^{m} \frac{[G^2_{n+1}\overline{P_F}_{n+1}(x) - G^2_n\,\overline{P_F}(x)]\,[G^2_{n+1}\overline{P_F}_{n+1}(b-x) - G^2_n\overline{P_F}_n(b-x)]}{P^2_0\,(G^2_{n+1} - G^2_n)} \tag{9}$$

with $m = m(G_{max})$. By using the logarithms of this equation the level of the wanted echo amplitudes is obtained analogously to Equation 7.

Diagrams for Flaw-size Determination and Verification by Experiments

According to Krautkramer (1) the abscissa axis of all diagrams were divided into units of the near-field length $d^2/4\lambda$ of the emitter, although the admissibility of such a normalization cannot be read from Equation 8 and was verified numerically only for the special case $G = 1.0$.

The agreement between the results calculated from Equation 6 and those calculated from Equation 9 within the range $X_N > 2.5$ is so good, that for this range the relatively simple

* Detailed calculation is available from the authors.

* Detailed calculation is available from authors.

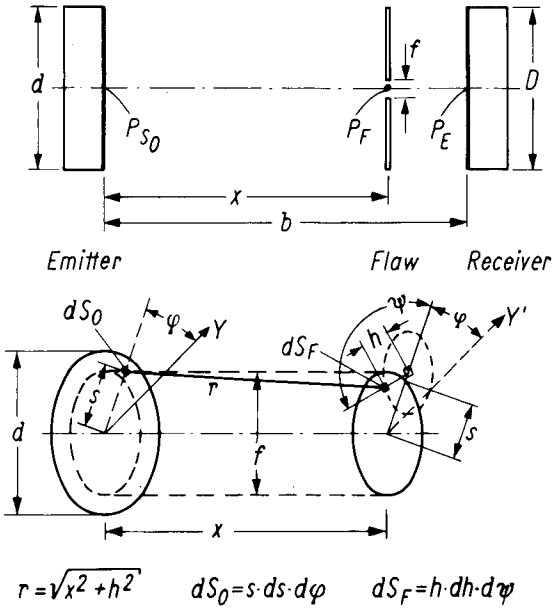

Figure 2. Analogous model for flaw-size determination.

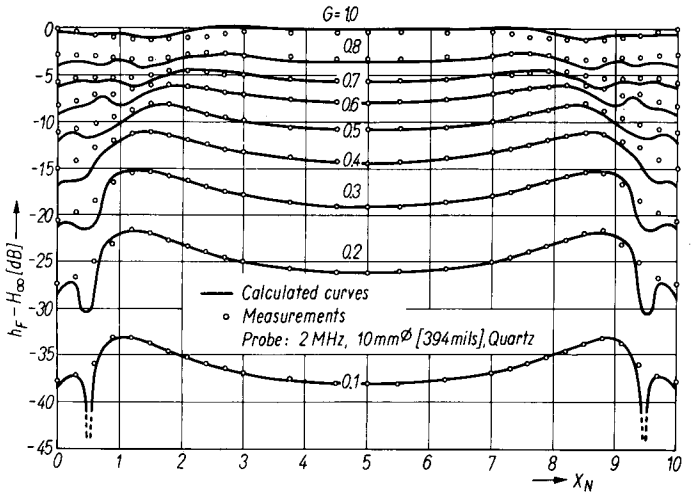

Figure 3. Calculated and measured echo amplitudes for different flaw positions X_N and (flaw) sizes G (double-probe technique).

Equation 6 and Equation 7 respectively, can be used. For the range $X_N \leq 2.5$ the echo amplitudes were calculated from Equation 9 and converted into decibels.

In order to check the theoretical results, experiments were carried out using two normal probes of equal kind, and hole-type diaphragm of different diameters in an immersion technique, so that the experimental arrangement was a complete analogy to the imaginary model according to Figure 2. Additional experiments were carried out on a test-piece with flat-bottom holes using two angle probes in an arrangement like Figure 1a.

Diagrams for a Double-probe Technique

Figure 3 shows the calculated levels of echo amplitudes h_F[dB]—$H\infty$[dB] for the relative flaw sizes $G = 0.1; 0.2; 0.3; \ldots; 1.0$ and for a total pulse path $b_N = 10$ near-field lengths as a function of the flaw position X_N. The reference value $H\infty$ corresponds with a hole-type diaphragm of infinite diameter. In theory $H\infty$ was calculated from Equation 8 with the values $G = 1.0$ and $X_N = 4X/D^2 = 10$; experimentally it was measured when the diaphragm was omitted. Due to the constant length of the total pulse path the ultrasonic extinction has no influence on such a diagram. The diagram contains the theoretical results as a full curve and is compared to the measured values.

The trend of the curves corresponds completely with the expectations derived from the simple considerations cited under Calculation of Echo Amplitude. The deviations of the theoretical results from the experimental ones inside the near-field range for flaw sizes $G > 0.5$ are probably caused by the kind of approximation in the derivation of Equation 8*. Some tests made with better methods of approximation are not yet finished. The striking minimum for $G = 0.1$ and $X_N = 0.5$ is not clear in the experiments, since the interference length of the pulses is too small for small values of X_N.

The different shapes of the curves in Figure 4 confirm the remarkable dependency of near-field influences on the ratio between total pulse path and near-field length. For small values of b_N the shape of the curves is converted completely. Thus the prediction 2 is verified; i.e. it is impossible to develop one diagram of general validity for all cases.

The results of the additional experiments with flat-bottom holes agree nearly as well with the theory as the results of the experiments with the hole-type diaphragms. The near-field length of angle probes was taken from (8). It is clear that the real flaw size follows approximately from the measured value by multiplication with the factor $1/\sin\alpha$ (Figure 1a).

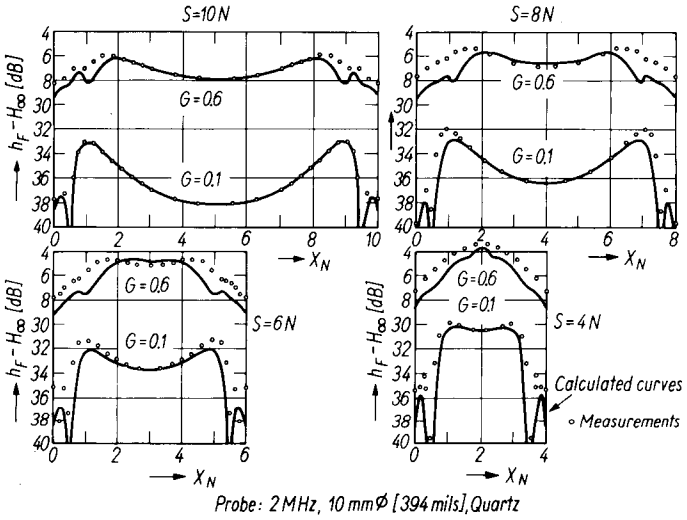

Figure 4. Diagrams like Figure 3 for different total pulse paths b_N.

Diagram for the Single-probe Technique

As already mentioned, the theory must include Krautkramer's diagram as a special case for equal distances emitter-flaw and flaw-receiver. In Figure 5 such a calculated diagram is shown, which also contains the values measured by Krautkramer (1). The differences between theory and experiments are analogous to those in Figure 3 and can be explained in the same manner.

Conclusions

Up to now it is not certain whether the results of these considerations are applicable to the sound field of transverse waves of angle probes. Due to the results of the additional experiments with flat-bottom holes it appears possible, but further experiments must be made. Moreover, the results of practical

* Detail available from authors.

applications may be incorrect, when the shape of real flaws deviates too much from the circular or when their reflection factor is considerably smaller than 1.0. This is possible, for example for flaws in flash-butt weldings, and therefore further investigations should be made.

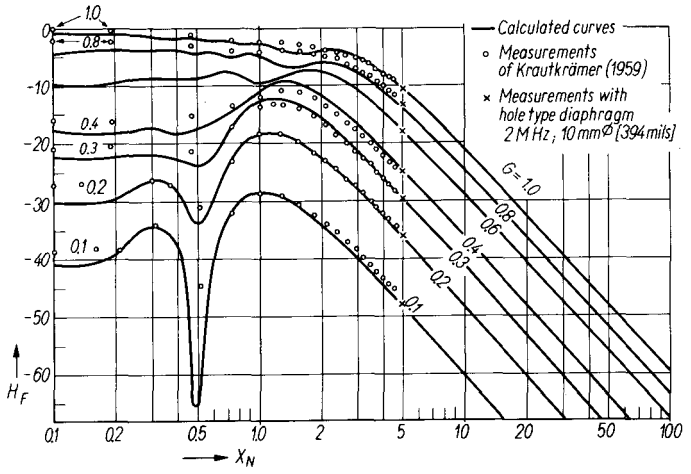

Figure 5. Calculated and measured echo amplitudes for different flaw positions X_N and (flaw) sizes F (single-probe technique).

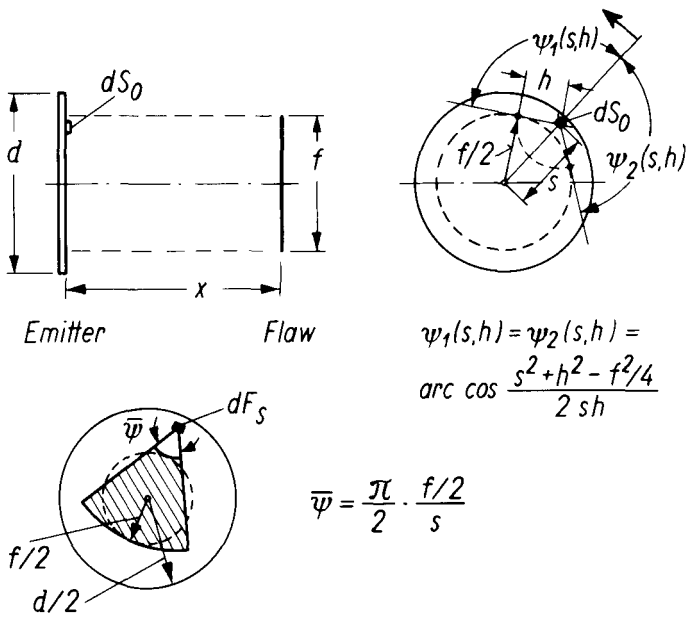

Figure 6. Definitions and coordinates for the calculation of average sound pressure at the flaw.

Summary

The diagram for the flaw-size determination developed by Krautkramer is useless for a double-probe technique—e.g. for tests of weldings of large cross-sections—since the emitter-flaw distance in general is not equal to the flaw-receiver distance. According to such a technique a more general diagram for defect-size determination was developed.

The theoretical considerations are based upon an analogous model containing a piston source and a receiver of equal kind at a given distance and a hole-type diaphragm as a flaw, which moves between emitter and receiver. The relation between echo amplitude, defect size and position was calculated approximately.

This general theory comprises two well known special cases:

1) The middle position of the diaphragm between the emitter and the receiver represents exactly the conditions for Krautkramer's diagram for the single-probe technique.
2) If the diameter of the hole in the diaphragm approaches infinity, the theory results in the diffraction losses calculated by Seki, Granato and Truell.

Experiments in a water basin and the theoretical results agree well. Additional experiments using two angle probes and flat-bottom holes as flaws have shown the practicability of the theory.

References

(1) Krautkramer, J. Fehlergrössenermittlung mit Ultraschall; Archiv für Eisenhüttenwesen 30 (1959), 11, p. 693/703

(2) Lack, B. J. Ultrasonic examination of welds in thick plate using a double probe inline technique; *Brit. Weld. J.* (1962), Feb., p. 54/60

(3) de Sterke, A. Ultrasonic examination of welded joints in steel plate of thicknesses up to 300 mm; IIW/IIS Doc. V-318-66/OE

(4) Seki, H., Granato, A., Truell, R. Diffraction effects in the ultrasonic field of a piston source and their importance in the accurate measurement of attenuation; *J. Acoust. Soc. Am.*, 28 (1956), 2, p. 230/38

(5) Kimura, K. Approximate calculations of flaw echo height in ultrasonic pulse echo method; Transactions of National Research Institute for Metals, 4 (1962); 2, p. 104/10

(6) Tjaden, K. Absorption longitudinaler Ultraschallwellen in Aluminium bei hohen Temperaturen; *Acustica*, 11 (1961)

(7) Williams, A. O. Piston Source at high frequencies; *J. Acoust. Soc. Am.*, 23 (1959), 1, p. 1

(8) Krautkramer, J. Nahfeldlänge und Fehlergrössenbestimmung bei Winkelprüfköpfen; Proceedings on the III National Conference on Non-Destructive Testing (Warsaw) 3.-6.X. 1966, p. 79/85

Technical Session 3/ Thermal Methods

Infrared Nondestructive Testing–Past, Present and Future

RICARDO VANZETTI, U.S.A.

ABSTRACT: The physical principles upon which infrared techniques for NDT are resting, and the two basic application approaches are discussed: heat injection from without, and heat generation from within. A short description of the performance capabilities of the infrared test equipment today available is added, with special mention of the Fast Scan Microscope for the evaluation of microelectronics.

Key applications of infrared NDT are described, with emphasis placed on the ability to detect characteristics and conditions that are difficult or impossible to detect by conventional means. Welding control and quality assessment of microwelds by means of infrared detectors "looking" at the weld area through optical fibres is presented as the latest breakthrough in a field where only visual inspection has been so far available, short of destructive testing.

The automated infrared troubleshooting and maintenance console is described, with emphasis on its capability to recognize typical infrared "signatures" of good and of defective electronic units. Fault part isolation and detection of deteriorating trends in time to prevent catastrophic failures takes place in 100 seconds and is documented in printed information. A cost comparison of this approach versus the conventional techniques is presented.

Finally, the concept of infrared-to-visible conversion is presented, with the foreseeable development of visual checkout capability for quick, at-a-glance test and troubleshooting in the field with the use of just one piece of test equipment—the human eye.

Introduction

For almost a century, it has been known that all physical matter radiates infrared energy as a function of the temperature of the emitting surface and of its emissivity factor, but only during the current decade is a significant effort being carried out to take advantage of this phenomenon for nondestructive test and evaluation of materials and of electronics.

The evaluation of materials is usually based on the observation of the thermal pattern created when a known heat gradient is applied between two predetermined points of the target. This is called "energization from without." The presence of any discontinuity, or anisotropy or other irregularity along the heat-flow path, will be reflected in a variation of the surface temperature distribution. In turn, this condition will alter the radiation pattern as detected by the infrared test equipment.

The evaluation of electronics, instead, is based on the measurement of the heat developed "from within", due to electrical power dissipation. The extreme sensitivity of the infrared detectors today available allows the measurement of thermal gradients as small as 0.005°C, which is beyond even the most exacting requirements. In practice, the capability of reading a Δ of 0.05 degrees C is quite adequate for the evaluation of electronic components operating at low power level.

Infrared Equipment for NDT

"Radiometer" is the general name for any instrument capable of detecting and measuring infrared radiation. According to the operational characteristics, radiometers are divided in two groups: point detectors and scanners. In turn, the scanners can be line scanners or area scanners. For most applications, the area scanners are the preferred type of equipment.

The sensing element of the radiometer is the detector. According to whether its operation is based on a thermally induced phenomenon, or on a photon-generated condition, the detectors are broadly grouped as thermistor bolometers, and quantum detectors. In turn, the quantum detectors are divided in photoconductive, photovoltaic and photoelectromagnetic cells. The speed of response of the quantum detectors is about three orders of magnitude faster than that of the thermistors, since the photon-carrier transformation takes place directly, without the need to wait for a temperature increase of the detector.

When the temperature of the elements under evaluation is close to 300°K (the so-called conventional "ambient" temperature), the spectral peak of the infrared radiation emitted lies in the 9-micron region. While this is no problem for the thermistor bolometers, whose spectral response is essentially flat, quantum detectors must be cooled to cryogenic temperature in order to operate at this wavelength. According to the spectral coverage that is desired, different quantum detectors can be used, each of them requiring cooling at some "optimum" temperature for most NDT applications. The most sensitive detector is the copper-doped germanium cell, which must be cooled at 4°K for best operation.

Cooling can be achieved by thermoelectric means (down to 200°K), or by cryogenic generators (down to 20°K), or by liquefied gases (down to 4°K with liquid helium). Progress is continuing at a fast pace in this field, so that the use of cooled detectors is becoming less difficult as time goes by.

Finally, according to the optical system used, the radiometers can be of "telescope" or of "microscope" type. Instruments of the first group are used for evaluation of large targets, such as cases of rockets, tracts of high-voltage power lines, etc. When working at closer range, these same instruments can be used for thermal analysis of conventional size electronics. Infrared scanning radiometers are presently made by Barnes Engineering, Philco-Sierra Division, Automation Industries, Conotron Industries, Huggins Labs., Infrared Industries, Servo Corp. of America and Raytheon Company.

Infrared microscopes are rapidly gaining acceptance for the evaluation of microelectronics. The fast trend towards more and more complex circuitry integrated onto a single semiconductor chip makes the infrared microscope an unrivalled tool for assessing the working condition of any active element of the circuitry. And the number of active elements per chip is rapidly

growing: large arrays of logic units are packing many hundreds and even several thousands of discrete elements onto a single crystal of very small dimensions.

The fast response of the quantum detector makes it possible to measure and record the transient conditions that are sequentially developing during warmup, from the instant when electric energy is applied, until final thermal equilibrium is reached. The Fast Scan Infrared Microscope (Figure 1), developed for NASA by Raytheon Company, scans a 1-mm^2 chip with a 50-line raster in one second, thus allowing detection of details during warmup, before lateral heat transfer might wipe them out.

Other infrared microscopes, of the point-detector type, are made by Philco-Sierra Division, and by Barnes Engineering. Scanning sub-stages can be used with these instruments to scan the whole area of the semiconductor chip.

Major NDT Applications

Materials bonding, especially the area of adhesive bonded structures, has been for several years a field of application for infrared techniques. At present a program is in progress at Lockheed-California for the evaluation with infrared techniques of jet motor blades, fuselage sections, radomes, primary control surfaces, and other structures formed by bonding together various laminated metallic elements. The infrared scanner used for this program has a thermal resolution of 0.2°C, a spatial resolution of 0.2 × 0.2 in. for a closely located target 10 in. × 10 in. in size, and the capability of scanning much larger areas.

Infrared scanning of a large target is shown in Figure 2. A Polaris A3 rocket motor is being inspected for proper curing and adhesion of the propellant to the containing structure, composed of an intermediate layer of material called "liner" and the outside fiberglass envelope. Infrared scanning takes place when the rocket motor cools down after heat-soaking at a higher-than-ambient temperature. Any void or discontinuity of the bond between core and liner, and between liner and envelope, shows up as a cool area in the infrared scan. In order to cover the whole surface of the rocket, the infrared scanner is mounted on a carriage that slides up or down a custom-designed metal tower while the rocket can rotate around its vertical axis. The equipment was built by Lockheed Missiles & Space Division for the U.S. Naval Weapons Station at Concord, California.

Figure 1. Fast-scan infrared microscope.

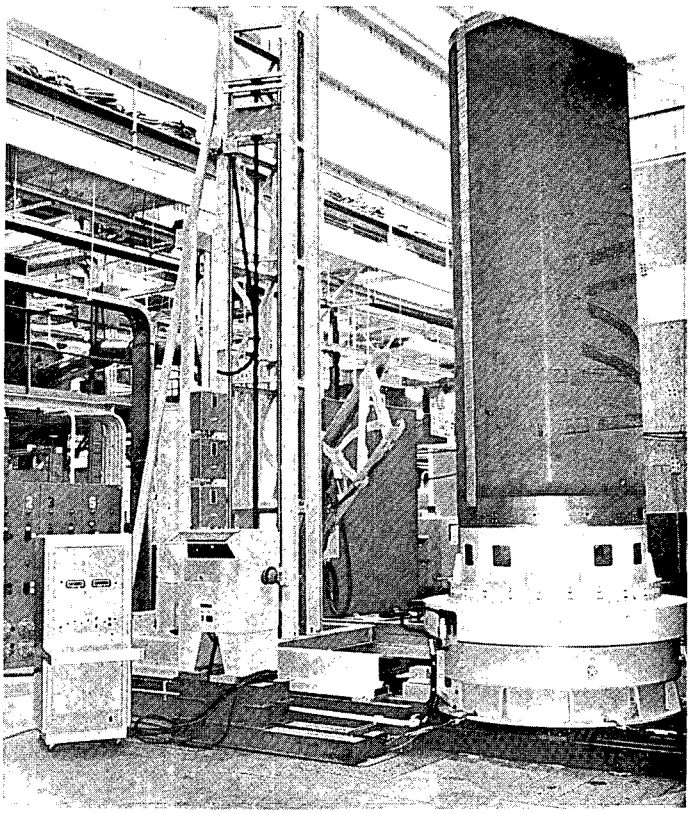

Figure 2. Testing Polaris A3 motors. (Photo Lockheed Missile & Space Co., Sunnyvale, Calif.)

Another project using infrared scanning for bond evaluation is now in process at Boeing-Vertol in Philadelphia, Pa. An especially designed scanner built by Philco-Sierra is used to check the bond cementing the glass-laminated "skin" of helicopter blades to the aluminum honeycomb structure used as the "core" material.

So much for large objects. At the other end of the dimensional spectrum, a program that appears as a real breakthrough is in progress at Raytheon. Since the advent of microelectronics, the use of microwelding has been rapidly increasing, to the point that at present complex systems contain microwelds by the hundreds of thousands. Short of destructive testing, quality control of these welds has been relying solely on visual inspection. A feasibility program completed last year has proved that the welding process can be monitored and controlled by an infrared system while the weld is being made.

The infrared control setup is shown in Figure 3. The detector "looks" at the metal puddle generated by the welding current, through a bundle of optical fibres whose far end is located between the two electrodes of a parallel gap welder. The amplitude of the infrared signal displayed in the oscilloscope trace is proportional to the temperature of the metal at the point where the weld is made.

Figure 4a shows the scope trace of a poor weld, as evidenced by the hidden cavity revealed by the photomicrograph. Figure 4b shows the scope trace of a good weld, as confirmed by its photomicrograph. The bonding appears complete, with even and uniform fusion at the interface between the two elements of the weld.

The great advantage of this system is the convenience of using the detector output as the controlling element of a feedback loop. In this way, just the right amount of current is

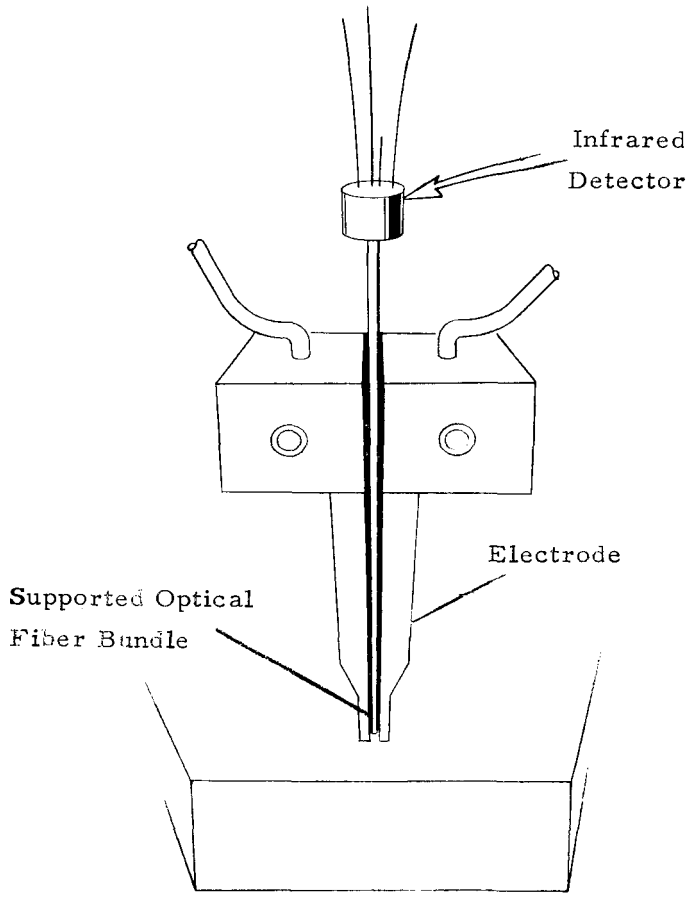

Figure 3. Parallel-gap welder with infrared control system. (Arnold Crowley, Raytheon Co., Waltham, Mass.)

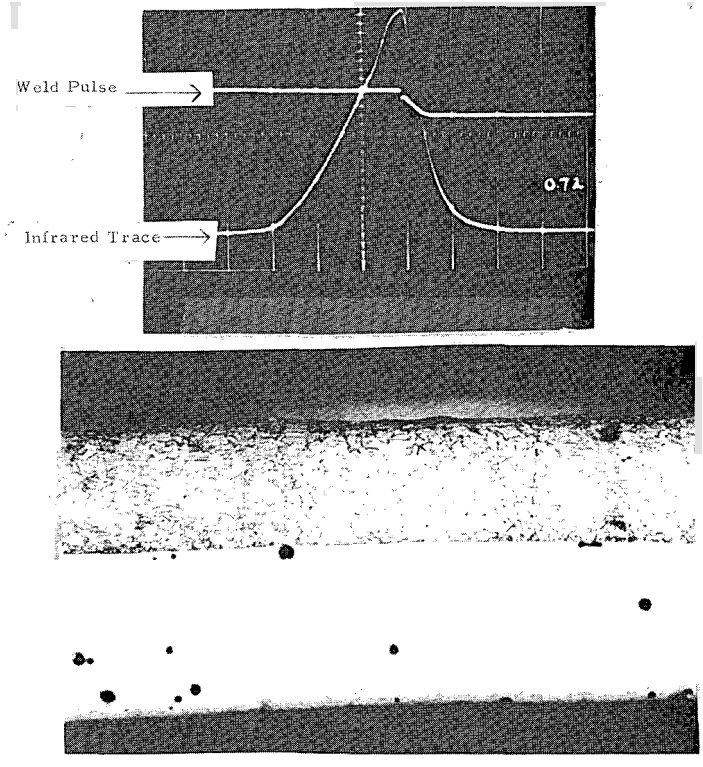

Figure 4a. IR response and micrograph of inadequate microweld. (Arnold Crowley, Raytheon Co., Waltham, Mass.)

supplied to form the weld, which is kept at the optimum temperature, during a pre-determined length of time, for optimum weld quality. Variations in the dimensions of the welded elements, or in their electrical resistivity are automatically compensated for, so that it becomes impossible to generate a poor weld. And in the event of equipment malfunction, the oscilloscope trace will immediately show a nonconforming response requiring prompt correction. Polaroid photo-recording of the oscilloscope trace thus becomes the quality certificate of each weld.

Electronics evaluation of conventional size component boards is being carried out by the Quality Assurance groups of several companies. When this operation is performed on newly designed assemblies, it is as a phase of engineering design evaluation, or as a reliability study for life expectancy prediction. In this function it can substantially contribute to raise the quality of the unit, by allowing correction of unsound electrical or mechanical conditions that otherwise would have remained undetected.

When infrared scanning of electronic assemblies takes place during the manufacturing phase, it is always on a comparison basis. In other words, the infrared pattern of the unit under evaluation is compared against the "standard" pattern of the approved sample. A match (within the pre-determined tolerances) indicates a good unit, while any deviation indicates a discrepancy to be corrected. The type of correction needed is indicated by the physical location of the deviations, so that fault isolation becomes easy, fast and foolproof.

The basic requirement for the success of such an operation is the perfect repeatability of the infrared scanning process. Rigid, consistent, invariable spatial relationship between detector and target is the essential prerequisite for an infrared system designed to test production units.

With these requirements in mind, Raytheon built the Compare System shown in Figure 5. The rotating table where the electronic production units are mounted for pre-heating and subsequent scanning has 16 positions where boards of similar or different type can be mounted in any sequence. The

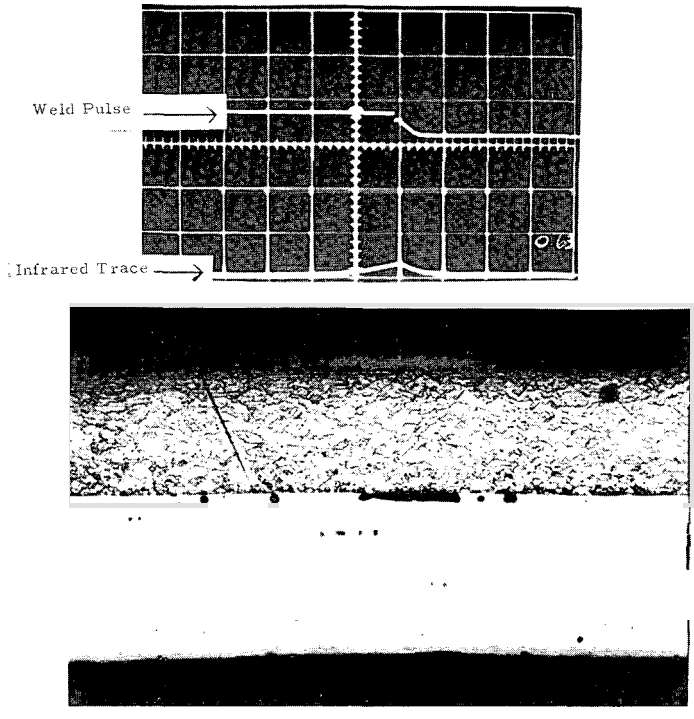

Figure 4b. IR response and micrograph of good microweld. (Arnold Crowley, Raytheon Co., Waltham, Mass.)

units can contain conventional discrete components or integrated circuits of any type and size. As the table rotates, every board is brought and held in the target plane for the 50 seconds during which the scanning takes place.

During the scanning, electronic "windows" open up in a programmed sequence, to allow reading the temperature of as many as 250 components per every board. This information, called "infrared profile", is held in a magnetic core memory and compared against the profiles stored in a punched-tape memory. These profiles are: the "standard" profile of a good unit, and the "failure" profiles of as many defective units as required. The comparison operation takes 50 seconds, at the end of which time the system indicates in the digital display the number of the failure exhibiting the closest resemblance to the unit under investigation, and the number of points (if any) of discrepancy. At the command of the operator, the system prints out the list of the points showing a discrepancy along with the magnitude of every discrepancy. Fault-part isolation can be carried out on the basis of this information by analysts having adequate knowledge of the circuitry.

At an operating speed of one unit every 100 seconds, the Compare System can troubleshoot up to 36 units per hour. Lowering this figure to a very conservative 15 units, the System still performs the work of 15 conventional troubleshooters, if we assume 1 hour as the average time required for a manually performed troubleshooting operation of a complex board.

An added bonus is the elimination of wasted material and rework, since the Compare's diagnosis is generally precise and eliminates the removal of good components (which unfortunately happens all too often in conventional troubleshooting).

Finally, the capital investment in an instrument of the calibre of the Compare System is more than repaid by the savings obtained in eliminating 15 troubleshooting stations, with all the related conventional test equipment, such as signal generators, power supplies, oscilloscope, meters, etc.

Maintenance of electronic equipment can be carried out on a rational basis with the help of the Compare System. For this purpose, the original profile of each board of the equipment is recorded on the punched tape at the time when the equipment leaves the factory. In the field, at pre-determined time intervals, the maintenance personnel loads the boards onto the rotating table, and lets the Compare System check the actual infrared profile of every board against its original one. A perfect match indicates no drift whatsoever, therefore no need for replacement. A less-than-perfect match indicates a deteriorating trend to be watched. In this case, the printout information gives the magnitude of the variation for every component that is affected and from this information, the maintenance technician can decide if and when a replacement is needed. And when the replacement takes place, the infrared profile of the new board is recorded in the memory in place of the profile of the replaced board. In this way, catastrophic failures can be avoided, and replacements are made only when really needed. Quite a difference from the still in-use system of blind replacements based on statistical calculations and without even the certitude that the new unit is better than the discarded one!

In the microelectronics field, the Fast Scan Infrared Microscope performs its work in a similar way, except for the fact that it operates at very high efficiency, to compensate for the extremely low level of the energy radiated by the targets. Figure 6 shows how the oscilloscope traces depicting the warmup along a single scan line of an integrated circuit are altered in amplitude and shape when the semiconductor chip is poorly bonded to the substrate. The oscilloscope traces were photographed respectively at 1, 6, 16, and 46 seconds after electrical energization of the unit, and are thus plotting the speed at which the warmup takes place. We can see that the good unit shows a rather slow warmup so that at the end of 46 seconds the temperature has reached approximately 70°C. The bad unit at the end of the same time has reached approximately 95°C. In the lower part of Figure 6 are the radiographs of the circuit, showing the quality of the chip-to-header bond. No voids are seen under the good unit, while a large void is detectable under the "poorly cemented" chip.

Future Developments

The recent development of glasses having good transmissivity in the spectral region around 9 microns will permit bringing out onto an open surface the infrared radiation emitted by elements hidden behind non-transparent bodies, or inside opaque envelopes or potting compounds. These glasses belong to the Arsenic-Selenium-Tellurium family, and can be drawn in fibres

Figure 5
The Compare System.

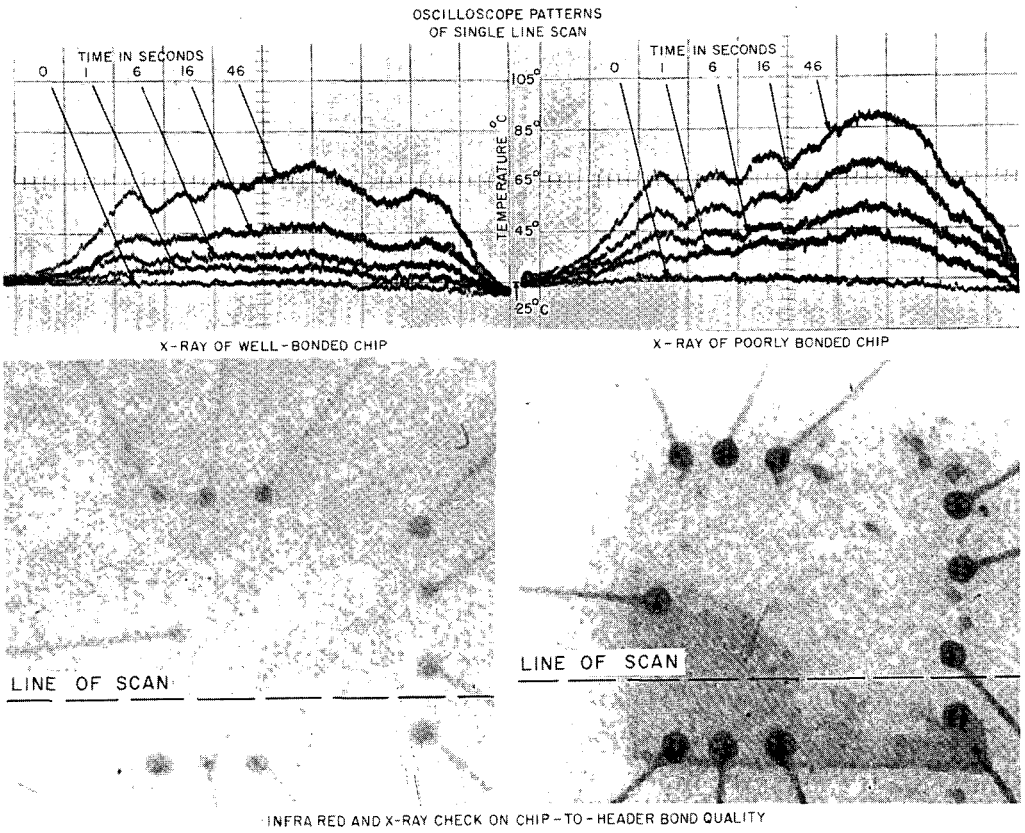

Figure 6
Quality of semiconductor chip bonding seen by infrared microscope.

measuring a few thousandths in diameter. An infrared detector scanning the terminations of fibres whose other end is facing a surface emitting infrared radiation in the spectral range between 2 and 13 microns, will, in effect, "see" this surface and be able to measure its temperature.

Frequency conversion, from infrared to visible, will be next, probably with the use of luminescent phosphors similar to the type produced by the U. S. Radium Corp. These phosphors require ultraviolet excitation to produce luminescence, which is "quenched" by an increase in temperature. The thermal image therefore appears as a negative, with respect to the temperature distribution.

The availability of frequency converters, coupled with infrared transmitting fibres and possibly with light transmitting fibres at the output of the converter, will make it possible to do away with infrared test equipment. Since the infrared radiation has been converted into visible light, the human eye can be used as the only piece of test equipment necessary to effect instant evaluation and troubleshooting of electronics. To eliminate the difficulties of making quantitative measurements at a glance, the fibre terminations can be arranged in a pattern of sequential decrease (or increase) in intensity. Any variation in the thermal regime of an element will alter the brightness of the corresponding fibre termination, and the eye will notice at once that the brightness sequence has been altered. Visual checkout and troubleshooting will be fast, easy and will not require the use of equipment of any kind.

Conclusion

The number of applications of infrared techniques for NDT is rapidly increasing, thanks to the availability of infrared test equipment especially designed for this purpose. Besides the steady progress in the materials evaluation work, a great expansion in the field of electronics is shaping up, to cover the various areas of design evaluation, process control, production test and troubleshooting, and maintenance.

Perhaps the fastest progress will take place in microelectronics NDT, where the absence of competition by conventional methods makes the adoption of a new approach an imperative need.

Infrared NDT, whatever be the field where it is applied, could be the final step to 100% automation. The fact that the infrared equipment's output is an electric signal that lends itself to appropriate processing and display makes it possible to incorporate infrared test equipment into an automated manufacturing facility.

Beyond this point, which is already within today's capability, we can foresee interesting applications of infrared-to-visible conversions for checkout and field maintenance of electronics by visual means only. Still much research and development needs to be done to reach this point, but the fundamental physical principles upon which these developments are predicated are well understood, and leave no doubt that their implementation into working equipment will bring about the expected successful results.

Discussion

Q. A. D. MCEACHERN, Atomic Energy of Canada Ltd., Chalk River, Canada:

Have you applied these techniques to integrated circuits?

A. Yes. NASA's Fast Scan Infrared Microscope has been used for this purpose. It is capable of scanning a 1 mm² semiconductor chip in 1 second, with a 100-line raster, and the infrared profile so generated can yield information that is not obtainable by conventional test means. The technique is useful for design evaluation and for quality control purposes.

Q. N. O. CROSS, Esso Research & Engineering, Florham Park, USA:

Are IR to visible light converters presently commercially available? If so, in what portions of the IR spectrum are they capable of use?

A. Yes. For the 5 to 10 micron region of the infrared spectrum, conversion to visible light can be achieved in two ways: a) using limine scent phosphors of the type currently produced by U.S. Radium Corporation—for instance, their "RADELIN ♯1807"; b) using liquid crystals, which are currently produced by Westinghouse and by Boeing.

Q. D. D. DODGE, Ford Motor Co., Detroit, USA:

Have any circuits been devised to automatically correct for emissivity variations in metals?

A. Yes. Automatic emissivity correction can be achieved by the system shown in Figure A. The concept is sound, but I have never had an opportunity to use it. Application of this principle is illustrated in Figure A; radiation from the test surface is composed of emitted radiation due to its temperature and reflected radiation from a reference heater. When the total radiation from the test surface matches that from the reference heater, the heater temperature is proportional to the test surface temperature. Since the sum of emissivity and reflectivity is always unity, any change in test surface emissivity will cause a corresponding change in the amount of heater radiation reflected from the surface. Thus, at a specific temperature the total test surface intensity (emitted plus reflected energy) remains constant regardless of its emissivity. This principle has been used in a radiation pyrometer by British Scientific Instrument Research Association Chislehurst, Kent, England.

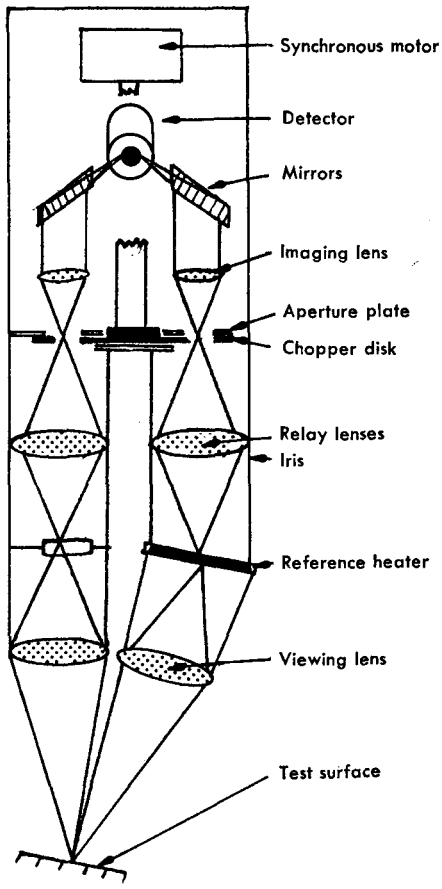

Figure A. Reflection compensates for emissivity

Dynamic Infrared Detection of Fatigue Cracks

E. J. KUBIAK, B. A. JOHNSON, and R. C. TAYLOR, U.S.A.

ABSTRACT: A noncontacting, nondestructive inspection system is described, that can rapidly locate, in real time, the position and extent of fatigue cracks in aircraft and missile structures. The automated infrared system was developed for the USAF for use in their Sonic Test Facility at Wright-Patterson AFB. This facility is capable of subjecting large aircraft or missile structures to the intense sound fields experienced in actual flight or launch.

In addition to presenting the basic concepts of the method, this paper 1) describes briefly the design of the system that was developed for the USAF, 2) discusses test results, and 3) presents conclusions and indicates future applications of the technique.

Introduction

At the Fourth International Conference on Nondestructive Testing held in 1963, a paper entitled "Dynamic Infrared Inspection Techniques" was presented by M. B. Levine and B. A. Johnson. The paper presented the basics of several techniques and discussed potential areas of applications. Since then, an automated infrared inspection system for detecting surface or near-surface fatigue cracks has been developed for the USAF for use in their Sonic Test Facility at Wright-Patterson Air Force Base, Dayton, Ohio. This facility is capable of subjecting large aircraft or missile structures to the intense sound fields experienced in actual flight or launch.

One of the primary instrumentation requirements of the facility is a noncontacting, nondestructive inspection system capable of rapidly locating, in real time, the position and extent of flaws or cracks which develop in the experimental structure during the course of the test. An investigation of standard nondestructive testing inspection techniques, such as X-ray, photographic, eddy current, and ultrasonics, revealed that none of these were directly suitable for automated inspection during the test, although recently conceived high-speed X-ray and eddy-current techniques could be used to advantage by stopping the tests periodically and inspecting during the nontest intervals. This is, of course, a time consuming procedure, particularly if the purpose of the tests is to study crack propagation.

General American Transportation Corporation had earlier successfully applied infrared techniques to the detection of voids and flaws buried in rubber and plastic structures. While metals, due to their higher thermal conductivity, present a much more difficult problem (as the rate of heat flow is faster and the thermal gradients that develop are smaller), analytical studies indicated that infrared techniques should be applicable to the thin metallic skin type of construction normally used in aircraft and missiles. However, these studies also indicated that infrared techniques would be limited to detecting in metals only flaws very close to the surface, such as fatigue cracks.

Basic Concepts

The basic concept of infrared inspection is predicated on the fact that flaws and defects within a body change the thermal characteristics of the body. If heat-flow exists in the body and various other conditions are proper, this thermal characteristic change will manifest itself as a surface temperature difference or gradient. In other words, the body will exhibit a different thermal radiation signature if it contains flaws than it would if it contained no flaws. A high-speed scanning infrared detection system can then sense these gradients or signatures and convert them into electrical signals that can be recorded and interpreted.

The important point to remember, however, is that heat-flow must be present for infrared methods to detect flaws in materials and structures. This heat-flow can be achieved either by action within the flaw or by injecting heat from an external source. These heat-flow generation methods are known respectively as passive and active systems. For fatigue-crack detection, a passive system would rely on the heat generated by either an incipient crack or by the friction between the sides of a complete crack. Analytical studies showed that the amount of heat generated by an incipient or complete crack in metallic aircraft or missile structures was not sufficient in most cases to create a significantly different thermal signature. Therefore, the heat injection method, or active system, was investigated for this application.

Many different methods can be conceived for injecting energy into a structure so as to cause flaws to generate a measurable surface-temperature gradient on the structure. The method that works best depends on the particular application, that is, on the size of the structure, the material of which the structure is fabricated, the type of flaw to be detected, and the location of the flaw in the structure. For example, if the structure is of cylindrical shape and the flaw is buried somewhere in the wall of the cylinder, the simple procedure of heating the cylinder interior with hot water or steam and monitoring the thermal signature of the cylinder exterior may allow the flaws to be located and their size defined. However, such simple methods are not applicable to all cylindrical structures. The size, location, and thermal conductivity of the flaw, the thickness and thermal conductivity of the wall material are all parameters that can determine whether or not a flaw would cause a measurable surface-temperature gradient to be generated. Another feature of the heat injection system that has to be considered is whether energy should be injected continuously or in pulses. Again the selection of the best heat injection method and mode of operation depends upon the particular application. Analytical studies aid the selection, but often the best arrangement is found only by experimental testing. Additional techniques that have been used or considered for heat injection sources are: 1) hot-air jets, 2) plasma jets, 3) direct flames, 4) inductive heating coils, 5) contacting tape heating coils, 6) infrared and arc lamps, and 7) lasers.

For the detection of fatigue cracks in the skin of aircraft and missile structures from a distance, the best detection method was found to be a system which injected heat into a small area or spot on the skin surface by means of a radiant heat source and then measured the resulting temperature rise of the surface at or near that spot with a radiometer. To facilitate the rapid inspection of an aircraft structure, the source and radiometer spots are optically scanned in synchronism over a 10×10-degree field. Figure 1a shows a plan view of a specimen with a fatigue crack being scanned by this technique and Figure 1b shows the resultant temperature versus position profile obtained for one scan.

By scanning at constant velocity, each point on the surface receives the same amount of energy over the same period of time. Therefore, the rise in surface temperature due to the injected energy will be the same unless something happens to disrupt the thermal characteristics of the surface. A fatigue crack open to the surface or near the surface will cause just such a perturbation of the thermal characteristics. As the heat-source spot approaches the fatigue crack, heat-flow away from the spot area will not be omnidirectional—the crack represents a restriction to heat-flow. Therefore, the surface temperature will rise rapidly as the heat injection spot approaches the crack. This is shown graphically in Figure 1b. With the source and radiometer spots concentric as shown in Figure 1a, the surface temperature should theoretically drop back down to the level

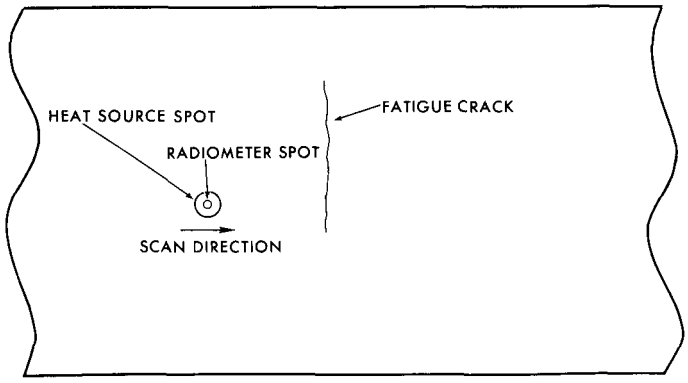

a. Plan View of Specimen Being Scanned

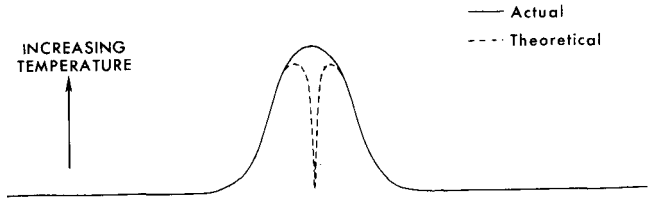

Figure 1. Moving heat-spot geometry and resultant temperature profile.

for "sound" material when the heat spot is centred over the crack, because now heat-flow is once again omnidirectional. And when the heat spot is just to the right of the fatigue crack, the surface temperature rises again because heat cannot flow back through the crack. This is shown graphically in Figure 1b by the dotted lines.

In practice, this effect is seldom observed—the actual measured temperature is more like the solid line. The primary reason for this is the resolution of the heat source and radiometer spots; they are of finite size and therefore some averaging is achieved. Also high scanning rates have a tendency to "smear" the temperature profile.

It should be pointed out that different effects can sometimes be achieved if the radiometer spot is located either ahead or behind the heat-source spot. The best location depends upon scanning speed and the properties of the material being inspected. By performing multiple scans an area of the specimen surface can be inspected. By employing a facsimile recorder of the type often used for ultrasonic scanning, a C-scan record of surface temperature changes versus x-y coordinates can be obtained which will graphically display the extent and location of fatigue cracks.

We have labeled this technique of inspecting an area with moving source and radiometer spots as dynamic infrared detection. Following is a brief description of the system. Typical test results are shown, several conclusions are stated, and future applications of the technique are discussed.

Description of USAF Fatigue-crack Detection System

Figure 2 illustrates the significant features of the infrared system for detecting fatigue cracks. In its simplest form the system can be considered to consist of: 1) a heat source, 2) an infrared radiometer, and 3) an optical scanning system. The heat source consists of a compact xenon arc lamp and both reflective and refractive optics. The focusing of the energy on the specimen being inspected is accomplished with pyrex lenses which serve the additional purpose of filtering out energy with wavelengths above 3 microns (30,000 Å). The reason for this filtering is discussed later. The size of the source spot is approximately $\frac{3}{8}$-in. (0.95 cm) dia. The system as designed for the USAF operates at a maximum distance of 6 ft (approx. 183 cm) from the specimen to the optical axis of the system.

The infrared radiometer consists of an 8-in. (20.32 cm) dia Cassegrainian optical system, a long-wavelength pass-interference filter, and a mercury doped germanium (Ge:Hg) detector cooled with liquid helium. The radiometer spot is approximately .060 in. (.152 cm) dia. The long-wavelength pass-interference filter has a sharp cut-on at 5 microns (50,000 Å) to insure that the infrared detector "sees" only radiation emitted by the specimen and that it does not "see" energy from the source reflected off the specimen surface. The use of pyrex refractive optics in the source further insures this condition by absorbing most of the arc lamp's radiation above 3 microns (30,000 Å). The electrical signal from the Ge:Hg detector, after electronic processing, is used to modulate the intensity of the facsimile recorder print-out.

Two different signal processing techniques, one employing a carrier system and the other employing a d-c system, can be used. In the carrier system, radiation is optically chopped at 600 cps just before it reaches the Ge:Hg detector. The lower frequency (generated by scanning action) components representing temperature changes are superimposed on the 600-cps carrier. After synchronous demodulation, differentiation, and amplification, the signal is fed to the facsimile recorder. In the d-c system, the radiation is unchopped and the lower frequency components representing temperature changes are differentiated and amplified directly. Each system has its advantages and disadvantages, of course. A carrier system is capable of determining absolute temperature but it also has limited dynamic range or bandwidth. At a carrier frequency of 600 cps, the system bandwidth is approximately 60 cps. The d-c system, while it yields no absolute temperature information, is capable of considerably greater bandwidth although it is not as responsive to extremely low-frequency components as is the carrier system. This limitation is brought about by the low-frequency response of the preamplifier. For detecting fatigue cracks in metallic aircraft skins, the d-c system was demonstrated to be superior. For this application, absolute temperature is not significant—rate of change of temperature is the important factor. In addition, the extremely low frequency components are not of interest either because they do not in general represent fatigue cracks—they are usually due to larger surface area defects such as general surface condition or emissivity changes. Regarding the latter, the system responds to emissivity changes so that an abrupt emissivity change could be interpreted as a fatigue crack unless precautions are taken. Two general techniques can be applied, constant emissivity coatings, or an emissivity compensation system. The compensation system determines the actual emissivity (by reflection techniques) at each point that a temperature measurement is made and it automatically adjusts the detector output for emissivity changes. Although this technique is more universally applicable, it does add considerable complexity. For this application, constant emissivity coatings were selected and they performed well. It should also be recognized that the use of a constant emissivity coating improves the efficiency of the entire system because it increases both the absorptivity and emissivity of the surface from something like 0.1 to about 0.9.

The scanning system consists of an oscillatory motion and a translatory motion. The oscillatory motion generates the constant velocity and retrace scans. The translatory motion generates the movement in a direction perpendicular to the velocity and retrace scans, so that multiple-like scans result. In our system, the oscillatory motion is accomplished by oscillating the two front surface scan mirrors at constant velocity and with a high-speed retrace. The translating motion is achieved by moving the entire optical system (source, radiometer, and oscillatory scanning system) along its optical axis.

Figure 3 is a photograph of the system. The mobile cart on the right contains (from right to left) the radiometer, the scanning system, and the heat source. The mobile cart on the

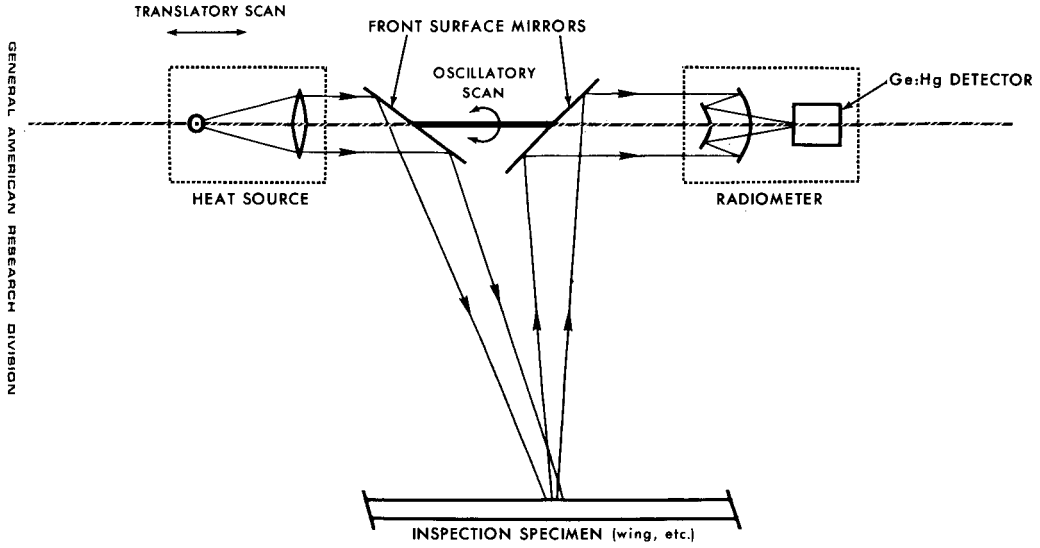

Figure 2
Block diagram of dynamic infrared system.

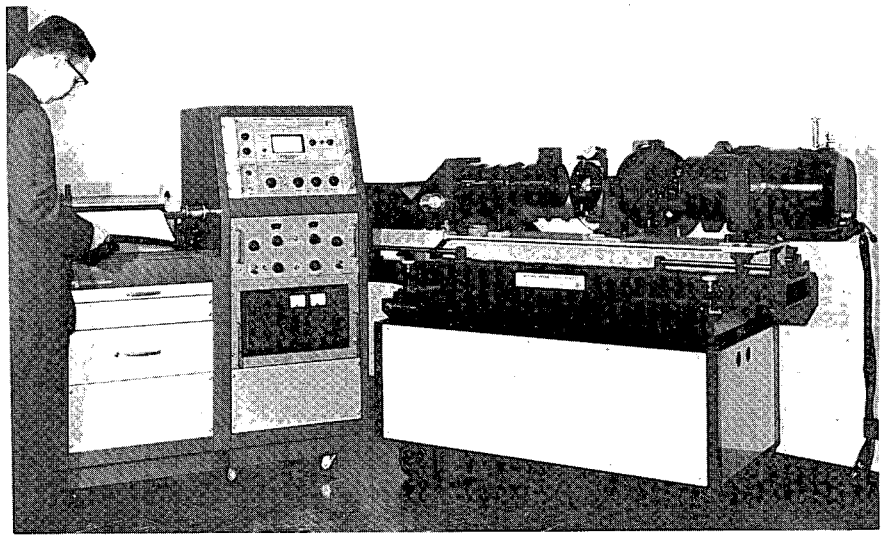

Figure 3
Photograph of actual system.

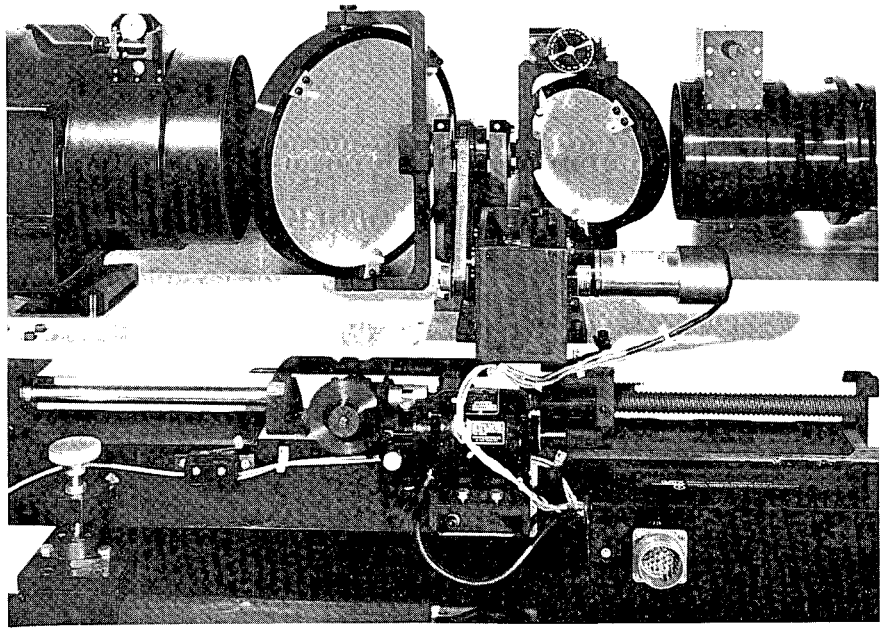

Figure 4
Photograph of oscillatory scanning system.

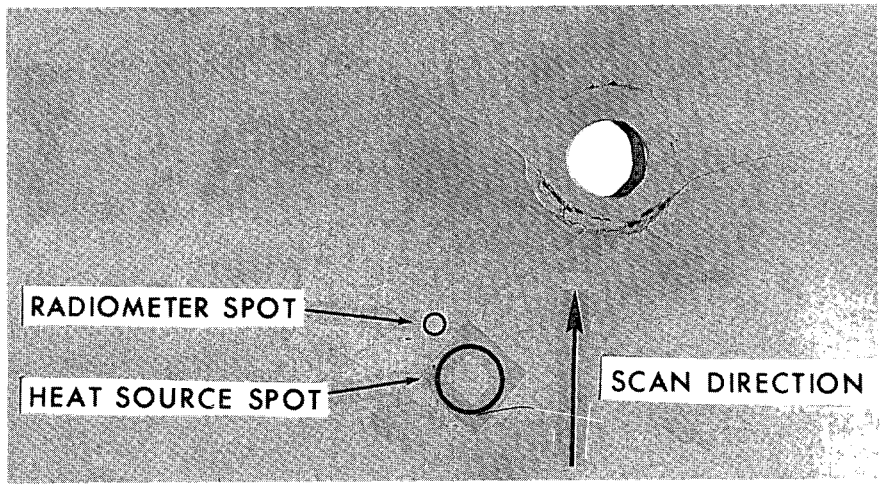

Figure 5
Photograph of fatigue cracks around hole.

left contains the necessary electronics and facsimile recorder. Figure 4 is a back view of the oscillatory scanning system showing the two scanning mirrors and the oscillatory mechanism. The mirror yoke is driven through a precision-programmed cam by a high-speed, high-resolution stepping motor operating at a maximum speed of 1500 steps/sec. An identical stepping motor is used to drive the helix of the facsimile recorder. A common pulse generator and amplifier assures that the two stepping motors stay in step. In this way the oscillatory scan motion and recorder helix drive are synchronized. The time required to inspect a given area of a specimen depends on how close, physically, the multiple line scans are made. This usually depends on the size of cracks that are to be detected. At a working distance of 6 ft (183 cm), a 12 × 12-in. (30.48-cm) square area will be inspected in a maximum of 3 minutes. This is the time required for 50-per-cent overlap of the radiometer spots for successive scans at maximum scanning speed.

Test Results

Figure 5 is a photograph of a .090-in. (.229-cm)-thick aluminum panel with fatigue cracks emanating from a ⅜-in. (0.95-cm)-dia hole. The location of the source and radiometer spots and the direction of scan are also shown. Figure 6 is a photograph of the facsimile recorder output for this specimen.

There are several interesting points to note in Figure 6. Probably the most intriguing is that one of the cracks showed up lighter than "sound" material and the other showed up darker. This effect is due to two factors: 1) the relative position of the radiometer spot with respect to the source spot, and 2) the direction of scan relative to the inclination of the crack. Referring back to Figure 5, it can be seen that for the positive-sloped (running from the third quadrant up to the first) crack, the radiometer spot crossed the crack ahead of the source spot. In so doing, the infrared detector "sees" a temperature change from that corresponding to "sound" material (because the source spot isn't close enough to the crack to cause a temperature rise) to a lower temperature (because the material on the other side of the crack has not as yet received any heat). Because our radiometer electronics performed a differentiation of the detector signal, this change was detected as a negative-going change and thereby printed lighter than the "sound" areas did. For the negative-sloped (running from the second quadrant down to the fourth quadrant) crack, the radiometer and source spots cross the crack at approximately the same time. Under this condition, the infrared detector "sees" a temperature rise, the electronics interpret it as a positive-going change, and the result is an indication darker than that for "sound" material.

It was interesting to note that even if the direction of scan was parallel to crack inclination, an indication of the start and end of a crack was obtained. This is very encouraging because theory would indicate that this orientation would result in only a slightly different absolute temperature pattern than that for a "sound" material. The start and end of the crack are detected by this system only because differentiation of the signal is used.

The dark area following the hole (the white area) is due to the electronics being saturated by a large positive-going signal at the top edge of the hole. This same effect is observed at the ends of a specimen. Changes in the electronics would minimize this effect.

Conclusions and Future Applications

Several conclusions can be drawn from the work to date. Dynamic infrared inspection is capable of detecting and locating

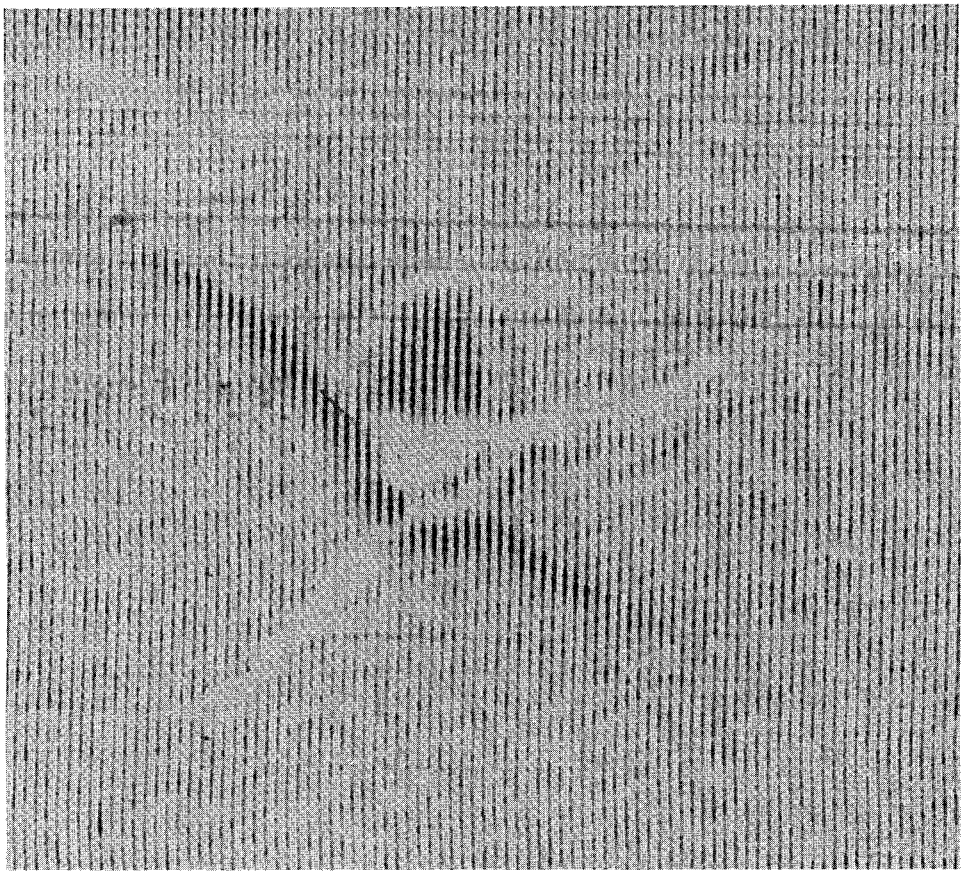

Figure 6
Photograph of C-scan record from facsimile recorder.

fatigue cracks in the metallic skin of aircraft and missile structures. However, in its present state of development the technique is limited to surface or near-surface defects such as fatigue cracks. In lower conductivity materials, of course, the method will respond to defects farther below the surface. In addition, the resolution of the system is not as yet maximized. The system as developed for the USAF will detect surface cracks that can also be found optically with a little magnification or by dye penetrants. Subsurface cracks that can be found with this system can also be detected with eddy currents. Of course, none of these other methods are consistent with requirements of the Sonic Test Facility for which this equipment was developed. This comparison with other techniques does illustrate the present capability of the technique.

This present capability, however, is far from the ultimate that can be reached with the technique. With the rapid advances being made in gas lasers, the use of a CW laser in place of the arc lamp is an improvement worth investigating. Because of the laser's inherent high degree of collimation and higher energy density, the resolution of the present system can be increased. An added advantage of the laser that must not be overlooked is its capability to inject heat from greater distances. Imagine the potential of a technique that could inspect a structure for defects from a distance of 30 ft (914.4 cm) or more!

The technique, of course, has applications other than the detection of surface or near-surface fatigue cracks in thin metals. In low-conductivity materials, such as rubber, plastics, wood, and bonded fibrous materials, its advantages are particularly attractive for detecting debonds or buried voids or flaws. However, with the rate at which power levels of gas lasers are being increased, it is also easy to visualize the technique becoming useful in more massive metal structures in the near future. Its inherent advantages of being noncontacting, and capable of permanent and instant record output are often (as was the case with detecting fatigue cracks in a sonic environment) just what the engineer or researcher requires in a NDT method.

Bibliography

(1) Levine, M. B., and Johnson, B. A., Dynamic infrared inspection techniques, 4th Internat. Conf. on NDT, London, England, September, 1963.

(2) Schmitz, G., and Levine, M. Investigation of fatigue failure detection systems using infrared techniques, RTD-TDR-63, 4293, Oct. 1964, USAF Contract AF 33(657)-8828.

(3) Sachs, H. L. A thermal infrared inspection procedure for detection and location of flaws in solid propellant rocket cases, Proc. Fourth Annual Symposium on NDT of Aircraft and Missile Components.

(4) Green, D. R. Infrared instrument for NDT heat transfer testing, Proc. Fourth Annual Symposium on NDT of Aircraft and Missile Components.

(5) Maley, D. R. Applied research to establish infrared detection methods for NDT analysis of metallic and ceramic structures, Contract AF 33(616)-7725.

Discussion

Q. ALFONSO J. PASSERI, Pratt & Whitney Aircraft Co., East Hartford, USA:

What is the limit of resolution for detecting cracks (smallest size crack) in low conductivity metals, such as those used in turbine blades and vanes.

A. The smallest size crack which can be resolved with this system has a length of approximately $\frac{1}{4}$ in. (6.35 mm) and a depth of $\frac{1}{16}$ in. (1.585 mm)—the width of the crack can be infinitely small as long as there is an actual separation of the material. It should be pointed out, however, that in order to be able to detect any surface defect with this system it is necessary for heat to flow primarily along the surface and not into the material. Therefore the system is limited to detecting surface defects in fairly thin materials. This is particularly true in high thermal conductivity materials such as metals.

An Analytical Approach to Infrared Nondestructive Testing

ARNOLD W. SCHULTZ, U.S.A.

ABSTRACT: A theoretical analysis of the infrared radiometric scan method is presented in a generalized parametric form that can be applied to a wide range of problems concerned with void detection. Principles of the method and the several facets involved in surface image formation of voids and their radiometric detection are detailed in a manner that provides a practical foundation for designing test techniques and establishing inspection procedures. Working graphs for determining test parameters for a range of void characteristics are given, and their use is illustrated. Limited preliminary experimental evidence is presented to substantiate, in part, the validity of the analysis.

The thermal diffusivity and thermal conductivity of a material must be known if the theory is to yield specific quantitative results. Two convenient and rapid transient radiation methods are discussed. One is an extension of a well-known, through-transmission method for measuring diffusivity absolutely. The other is now undergoing development at the Avco Corporation, Space Systems Division, and is a novel comparative method for determining diffusivity and conductivity when only one surface of a material is accessible. A desirable characteristic of both methods is that knowledge of heat flux input is unnecessary.

Introduction

During the past year, Avco SSD has been involved in nondestructive evaluation of materials used in space vehicle heatshield applications by employing, among several methods, infrared scanning. This method has been successfully used in a variety of problem areas (1-4). In the course of reviewing for background information the many papers dealing with infrared scanning, it became apparent that many investigators preferred a trial-and-error approach for establishing the several experimental parameters necessary to radiometrically observe voids within a material. Only a few papers hinted at approaching a scanning problem analytically. Since Avco problems include a multitude of material types, which can contain voids at all depths, it was decided that an analysis of the general problem of thermally detecting voids in materials by scanning would (1) probably facilitate determining experimental parameters, (2) make possible the optimization of experimental results, and (3) provide a basis for proposing inspection specifications. This paper, then, is essentially both a summary of this analysis and a report on some of the experiments performed.

The infrared radiometric scan method consists of introducing focused heat continuously over the surface of a material and, simultaneously, monitoring radiometrically the resultant

temperature rise in the scan path after a suitable time delay. During this delay, heat is conducted away from the surface into the material at a rate that depends upon the influence that the material properties have on heat flow. Variations in surface temperature arise from variability in these properties, which include such discontinuities as voids, cracks, and inclusions. For voids, the time delay at which a maximum surface temperature disturbance occurs is critically dependent upon (a) characteristics of the material itself and (b) void size, shape, and location. Proper design of a test technique for detection must consider (1) the separation between the heat source and the radiometer field-of-view at the surface; (2) the scan velocity of the source-detector system, with respect to the material surface; (3) the heat-source characteristics; and (4) the response, sensitivity, and resolution of the radiometer. By "proper design" is meant an optimized situation for detection: i.e. compatibility between the criterion of minimum heat input to the material (consistent with nondestructive testing) and sufficient image contrast at the material surface to permit reproducible detection of the void. This image contrast is a time-varying quantity and in this method is regarded to be of most concern.

The physics of the scan method is treated here as a sequence of separate problems. As the principles of the method are well known they are discussed as briefly as possible, consistent with complete analysis. The objective is to show that a source of heat moving over a surface creates a system of isotherms that are centred about the source and move at the same velocity as the source; thus a radiometer focused at a point that follows the source by a fixed distance continuously observes one of the isotherms and, hence, a constant temperature, even for real cases where heat losses from the surface exist and where the material is of finite thickness.

Image formation theory is then presented in sufficient detail to provide a basis for designing void-detection techniques and for extending these techniques to other problem areas requiring the use of the infrared scan method. The theory treats heat-source types in terms of mathematical approximations and develops the concept of surface-image contrast of a characteristic void shape in a general parametric form suitable for broad application. This is followed by a discussion of the effect of heat-pulse shape on image contrast with illustrations of two types of heat pulses typically generated by real sources. Source design is then viewed in terms of desirable pulse-shape characteristics and source size, and examples of the use of the theory for the two pulse types are given.

Image detection is treated next from the viewpoint of interacting image characteristics with characteristics of the radiometer. Detection is assumed possible when this interaction satisfies established criteria for observability. Limited experimental results are then offered as preliminary evidence for validating the analysis in part.

Involved throughout the theory are the parameters' thermal diffusivity and thermal conductivity. These parameters must be known for a material, should quantitative results be desired. Their rapid infrared experimental determinations are available from the author. Such determinations, made either by an extension of a well-known absolute through-transmission method or by a novel one-surface comparative method, are now undergoing development at Avco.

Principles of the Scan Method

Should a source of heat be regarded as a point of constant intensity moving at a constant velocity over a plane surface of homogeneous material at uniform temperature, the spatial distribution of the higher temperature created on the surface takes the form of a system of concentric, oval-shaped isotherms. These isotherms move at the velocity of the source and diminish exponentially in magnitude, such that the gradient is steeper in front of the source than to the rear of the source. The temperature of one of these isotherms is described by Equation 1 for an adiabatic situation where all heat losses from the surface are neglected (5).

$$T_I = T_A + \frac{q_0}{2\pi kL} e^{-\frac{vx}{2\alpha}} K_0\left[\frac{v}{2\alpha}\sqrt{x^2 + y^2}\right], \qquad (1)$$

where

T_I = Temperature of isotherm on surface
T_A = Temperature of surface prior to heating
q_0 = Point source heat strength at surface
k = Thermal conductivity of material
L = Thickness of material
v = Velocity of heat source
α = Thermal diffusivity of material
x = Surface coordinate moving in the direction of the straight-line scan, in which the heat source is fixed, such that $x = x_0 - vt$ where x_0 is the coordinate fixed on the material, and vt is the separation between the moving and stationary systems
K_0 = Modified Bessel function of the second kind, zero order
y = Surface coordinate perpendicular to the scan direction

Examination of equation 1 shows that at a fixed position on the surface T_I is a function of time since x is a function of time; whereas for a fixed separation between the moving source and radiometer, which observes T_I, x is constant, and T_I depends only on q_0. Consequently, continuous evaluation over a surface results in the radiometer sensing a constant temperature, or radiation intensity.

For real cases, radiation and convection heat losses from the surface to the environment and conduction of heat from the surface into the material, cause distortion in the shape of the moving system of isotherms. This can be seen by incorporating these losses into Equation 1, which results in the following equation for the conditions of material homogeneity and semi-infinite thickness (6):

$$T_I = T_A + \frac{q_0}{2\pi kr} e^{-\frac{vx}{2\alpha}} e^{-r\left[\left(\frac{v}{2\alpha}\right)^2 + \frac{h}{k}\right]^{1/2}} \qquad (2)$$

where

r = $(x^2 + y^2 + z^2)^{1/2}$
z = Depth coordinate perpendicular to the scan direction
h = Coefficient of surface heat transfer (including radiation and convection)

Even though distortion exists, the temperature sensed by the radiometer at the surface ($z = 0$) remains constant and is obviously less than that sensed at the same radiometer-to-heat source separation for the no-loss case described by Equation 1.

If the material appears finite in thickness and is homogeneous, then the temperature sensed by the radiometer will be greater or less than that for the condition of semi-infiniteness, depending on the degree of impedance to heat flow that exists at the finite boundary. Finiteness arises when the heat source-to-radiometer spacing is greater, in terms of time, than the transit time required for heat to diffuse to a depth at which impedance to the heat flow changes. If, for example, the diffusivity at the boundary is greater than that of the material itself, the resulting surface temperature will be less than that for the case of semi-infiniteness. The heat source-to-radiometer spacing is then an important quantity, since void detection depends critically upon the transit time of the heat to and from the void. This spacing, S, can be described by the relation

$$S = vt_s , \qquad (3)$$

where t_s is the time delay between heating and temperature detection of a point in the scan path on the material surface. The radiometer senses a constant temperature for a particular S- or t_s-value that is related to a particular depth in a material.

Since a void creates a time-dependent temperature disturbance at the material surface, there exists an optimum spacing that corresponds to a maximum localized disturbance. This disturbance will appear either positive or negative relative to the undisturbed temperature, depending on the mechanism for heat transfer at the void. This mechanism is regarded either as predominantly one of radiation or one of conduction. To determine which mechanism exists, the void is assigned a conductivity equivalent that permits, ideally, the same quantity of heat to flow through the void by conduction as would flow by radiative transfer. Comparison of this equivalent conductivity with the conductivity of the material itself determines, to a first approximation, whether the void acts as a heat source or as a heat sink. Should the void be assumed to have a cylindrical shape, its axis being parallel to the flow of heat and its walls being adiabatic and exhibiting grey body characteristics, then its equivalent conductivity can be expressed as (7, 8)

$$k_e = 4\sigma \epsilon F l T^3 \tag{4}$$

where

σ = Stefan-Botzmann constant
ϵ = Total emissivity of void walls
F = View factor (=0.5 if void diameter and length are equal)
L = Void length
T = Average absolute temperature of void

When k_E is less than the conductivity of the material, the predominant mechanism can be regarded as one of conduction; the void then acts as a heat source, and the surface temperature disturbance will appear positive, the image of the void appearing as a hot spot at the surface. One interesting aspect of Equation 4 suggests that a material can be heated to a temperature where the T for a void results in a value for k_E equal to the conductivity of the material itself. In this situation the void is not discernible, since it creates no surface temperature disturbance. Additional heat would cause the void image to appear as a cold spot.

Image Formation

The formation of an image on a material surface is time-dependent, and, as indicated previously, many variables influence its temperature contrast. It is the optimization of this contrast with regard to image detection that is of principal interest here. As a starting point, use has been made of image theory studies performed at Avco that have considered stationary heat sources, particular ranges of void sizes, and somewhat general boundary conditions (9). The results of these studies have been adapted for application to the scan method.

Heat Sources

Heat sources are regarded here to be radiative only and to consist of two types, (1) those that produce a uniform intensity at the surface of a material and (2) those that produce a nonuniform, but symmetric, intensity at the surface. Both types of distributions can be produced by, for example, a point source of heat. Such a source when located a considerable distance beyond a surface will produce a nearly uniform distribution over a small area at the surface which can be defined by an aperture. The same source located near the surface will produce a spatially symmetric-shaped, cosine-squared intensity distribution. Reflecting or transmitting optical devices can be used to obtain a variety of intensity distributions.

Image Contrast of Voids

Rather than attempting to obtain the temperature distribution about the void, the approach taken for obtaining the image contrast of a void at the surface was to first determine the disturbed surface temperature caused by the presence of the void and to then determine the disturbed temperature deviation from the undisturbed. In this development it is assumed that (1) the material is homogeneous, exhibits constant thermal properties, and is finite in thickness; (2) the void is cylindrically shaped, with its axis perpendicular to the surface; and (3) the heated surface area is disc-shaped, is large compared to the circular area of the void, and is located directly above the void. This last condition is necessary to permit the use of a "point-source solution." This solution assumes that the undisturbed heat flux at a depth in the material corresponding to the upper tip of the void can be considered as concentrated at the centre of the tip. The point-source strength at the tip is then assumed to equal the heat that is reflected by the tip. The accuracy of this approximation is well within 10 per cent if the void is small, a criterion that will be defined.

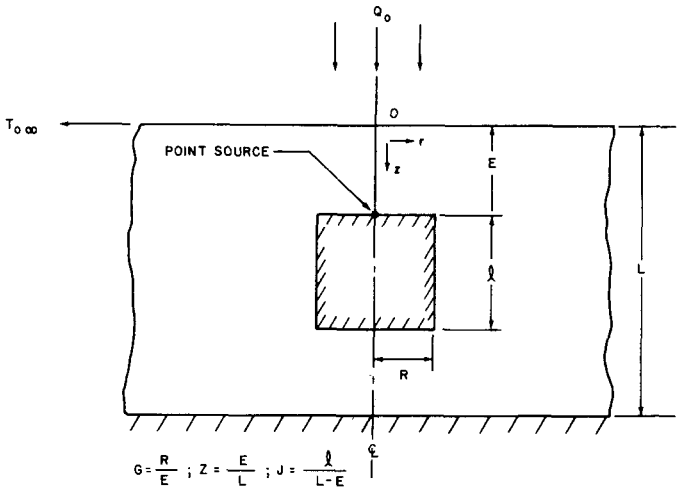

Figure 1. Geometry for void problem

To provide a basis for broad application, the size and location of the void in the material are described by three dimensionless parameters, G, Z, and J, the geometry for which is illustrated in Figure 1. These parameters are defined as:

$$G \equiv \frac{R}{E} \; ; \; Z \equiv \frac{E}{L} \; ; \; J \equiv \frac{l}{L-E} , \tag{5}$$

where the length of the void is l, its radius is R, and its depth below the surface of a material (that is L units thick) is E. The limits of G are 0 to infinity, where the former value indicates the absence of a void. The top of the void is located by Z, which may vary from 0 to 1, where the former value indicates a semi-infinite material. J may vary from 0 to 1, with the former value being a slit-void, and the latter value a full-depth void. A void is considered to be small, and results of this analysis are then valid when the condition $G \leq 0.5$ exists. It is to be noted that a void with a $G = 0.5$ and $Z = 0.5$ is physically quite large.

In terms of surface temperature disturbance and these geometrical parameters, the image contrast of a void can then be described by the following dimensionless relationship:

$$\psi = \frac{T_0 - T_{0\infty}}{GQ_0R/k} , \tag{6}$$

where ψ is this dimensionless temperature disturbance; $T_{0\infty}$ is the undisturbed, constant-scan surface temperature when no void is present; T_0 is the disturbed surface temperature directly above the void; Q_0 is the surface heat flux; and k is the material thermal conductivity. The quantities Q_0 and k are usually known in an experiment, and G and R are the variable parameters, so that it is then necessary to develop relationships for T_0 and $T_{0\infty}$.

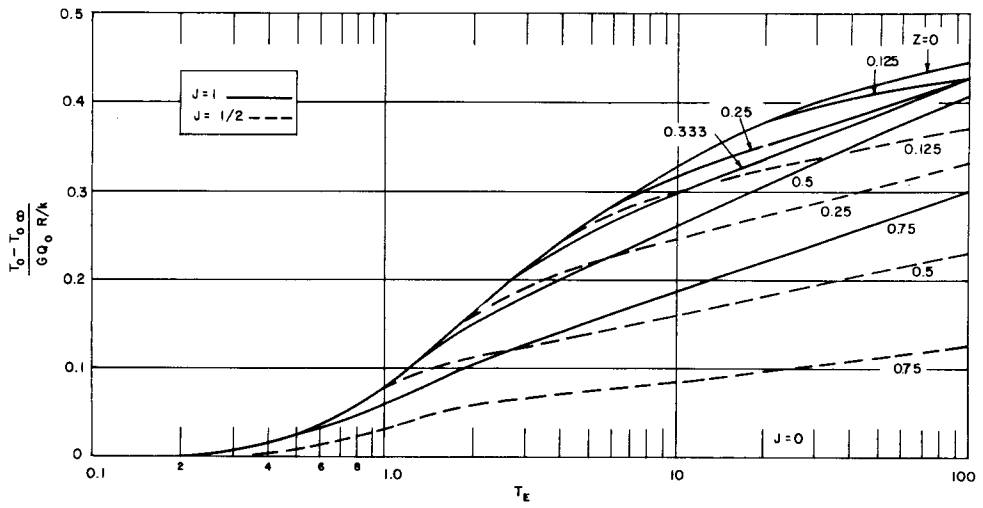

Figure 2
Surface temperature disturbances for small voids ($G \leq 0.5$)

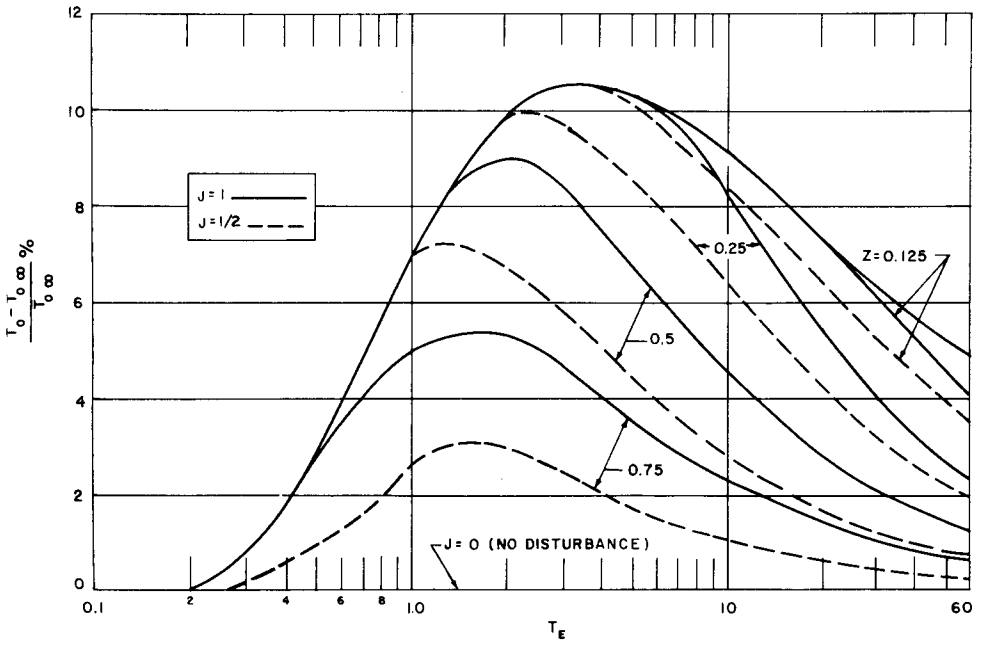

Figure 3
Percent change in surface temperature for small voids ($G \leq 0.5$)

For a homogeneous finite slab heated on one surface with a constant and uniform flux, $T_{0\infty}$ is given closely by

$$T_{0\infty} = T_A + \frac{2Q_0R}{\sqrt{\pi}\,kG}(T_E)^{1/2}, \qquad (7)$$

for the condition $\alpha t \leq L^2/3$, or $T_E \equiv \alpha t/E^2 \leq 1/3Z^2$ (References 9 and 10).

The quantity T_A is the temperature of the surface prior to heating, and the quantity T_E is a dimensionless characteristic time, where t is the time during which heating occurs. This condition is equivalent to stating that the material appears semi-infinite during heating. As an example, if the top of a void is located at a depth equal to one-half the material thickness, then $Z = 0.5$, and Equation 7 is valid as long as $T_E \leq 1.3$. The disturbed temperature T_0 has been obtained for small voids by the point-source solution. This involves a complex mathematical development* and results in an expression that consists of summing series of complimentary error functions that are mainly dependent on T_E and Z.

Parametric graphs of ψ as a function of T_E for $G \leq 0.5$ and for several values of J and Z are shown in Figure 2; these indicate the disturbance to be expected from various void sizes during heating. It is seen that a small void length (J-value) produces a small disturbance, and for the case of no void ($J = 0$) there is no disturbance. Also, as void depth Z increases, the disturbance decreases. Further, it is noted that, for particular T_E- and J-values, the disturbance varies little as a function of Z for $Z \lesssim 0.5$, especially for early times, and that ψ will equal 0 when $Z = 1$ (no void).

A quantity that can be more useful than ψ is the per cent change in surface temperature caused by a void, graphs for which quantity are shown in Figure 3 as a function of T_E for several void parameters. This figure illustrates vividly the time-dependent nature of surface image contrast. An interesting facet of each function is the exhibition of one maximum, which occurs at approximately $T_E = 2$. Heating of the surface for periods greater or less than this value results in a diminished contrast. As an example of the use of Figure 3: Should $G = 0.5$, $Z = 0.5$, and $J = 1$ for a void, then at $T_E = 2$ the disturbance shall correspond to a change in surface temperature equal to 9 per cent. At a surface temperature ($T_{0\infty}$) equal to 100° F a contrast of 9° F can then be expected.

The image of a void at the surface is not sharply defined, but rather exhibits a spatial temperature or intensity distribution that is time-dependent. Temperature disturbances as a function of radial position for several void characteristics and T_E-values are shown in Figure 4.

*Available from the author.

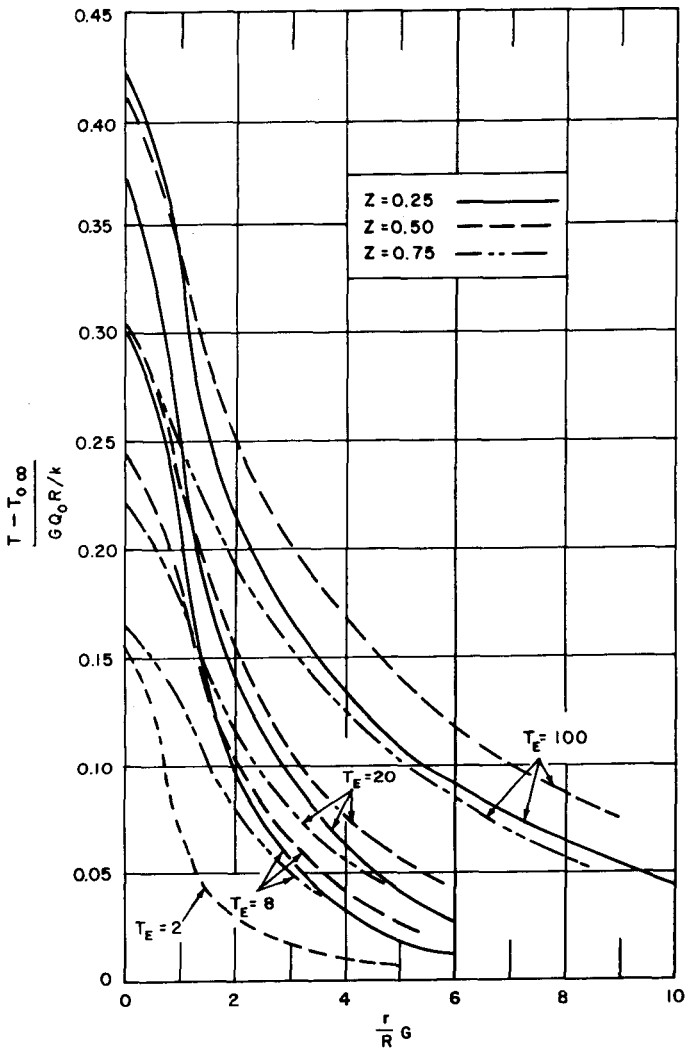

Figure 4. Surface temperature disturbances for small voids for J = 1 as a function of radial position.

Heat Pulse Shape

It is important to remember that these results for temperature disturbance are applicable only for stationary and constant heat fluxes that are introduced at the surface of a material and directly over a void which can be treated mathematically by a point-source solution. By using principles of convolution and superposition, it is possible to adapt these results to the case of a time-varying heat pulse for application in the scan method. To a close approximation, convolution permits a varying heat flux to be represented by the superposition of a few uniform fluxes. Consequently, a stationary disc-shaped heat source can be replaced by a moving source of the same shape that emits a time-varying flux that is approximated by the superposition of several uniform-in-time-and-space fluxes.

Knowledge of pulse shape is essential, then, for determining the mathematical approach to be used for obtaining image contrast. A consideration basic to determining pulse shape is the requirement of the appropriate dimension of the heat source relative to that for the void, consistent with the use of the point-source solution. This determination has been performed by experiment, and the conclusion is that the heat source should have a diameter approximately five times the desired inspection depth for small voids (1). Diameters larger or smaller than this diminish surface temperature contrast. Consequently, if the disc-source diameter (D) must equal $5E$ for optimum image contrast, then, since $G = R/E \leq 0.5$ for small voids, the diameter must be equal to or greater than 10 void radii ($D \geq 10R = 10\,GE$). It is noted that, although the diameter selected for the area to be heated is a function of inspection depth, this diameter probably does not have as critical an effect on contrast as do other parameters; thus a range of depths are probably observable using a single source size in practice.

In illustration of the theory, two common heat source pulses will be discussed, pulse shape being described either by the temporal distribution of intensity or by pulse amplitude as a function of pulse length. Should a disc source be uniform in intensity, then the pulse shape viewed at a point on the surface directly above the void, as the source moves over this point, shall appear to be essentially a square wave. Should the spatial intensity distribution over the disc be non-uniform, but symmetric (cosine-square), the pulse shape shall exhibit symmetry.

Pulse length observed at a point on a surface, for the centre of a disc source passing over the point, is given simply by

$$\tau D = \frac{D}{v}\,, \tag{8}$$

where v is the velocity of the moving source. Should, for example, the disc source be replaced by a rectangular source, the pulse length would still be described by (8), except that D would be replaced by the length of the rectangle in the scan direction.

The pulse amplitude of the square-wave produced by the uniform disc source is

$$A_u = Q_0\,, \tag{9}$$

where Q_0 is the heat flux at the surface after correction for the surface emissivity. The amplitude for the cosine-squared intensity distribution is

$$A_v = \frac{\epsilon Q_P}{4\pi H^2}\cos^2\theta\,, \tag{10}$$

where ϵ is the emissivity of the surface; Q_P is the strength of the point heat source; and H is the perpendicular distance from the source to the surface. The angle between H and the ray from the source to the surface is θ, which is subjected to the boundary condition $0 \leq \theta \leq \arctan D/2H$, where $D/2$ defines the radius of the disc-shaped area on the surface that undergoes heating.

Use of Theory

The theory is useful for calculating image contrast and scan technique parameters, which include velocity and spacing of the heat source-radiometer system, source size, heat flux, and surface temperature for uniform and time-varying heat pulses.

As an example of the use of the theory for a uniform flux: It is desired to determine whether a void having a radius $G = 0.5$ and a length $J = 1$ exists at a depth $Z = 0.5$ in a material of diffusivity α. A uniform flux is available over a disc-shaped area of diameter D. From Figure 3, a maximum change of 9 per cent occurs at $T_E = 2$. Since $T_E = \alpha\, t/E^2$, the time for optimum observation then occurs at $t = 2E^2/\alpha$. But: $D = 10GE = 5E$, so that $t = 2D^2/25\ \alpha$, which is the pulse length of the square wave. Recalling that the heat source to radiometer spacing S equals vt_s and that $\tau_D = D/v$, we find then that $S = Dt/\tau_D$. Normally, the condition $t > \tau_D$ or $S > D$, must be met so that the radiometer shall not view the surface during heating and, consequently, shall not record infrared radiation either emanating from the source or reflected by the surface. Thus, optimum observation of the surface shall follow immediately after heating, any delay shall result in diminished contrast. This is an important consequence of the theory for a square pulse. Other investigators have normally used high-flux, short-time pulse techniques. Theory implies, however, that optimum

contrast is achieved by slowly injecting a comparatively small flux into the surface, an obvious advantage of which is the over-all reduction in final surface temperature.

From Figure 2, the surface temperature disturbance is seen to equal 0.15 at $T_E = 2$. The minimum required flux, Q_0, can thus be determined, first by using the disturbance value to solve for Q_0, then by eliminating T_o–$T_{o\infty}$, using the value of per cent difference, and finally by solving (Equation 7) for $T_{o\infty}$. It may be important to determine this minimum Q_0, since properties of the material may undergo change should surface temperature be excessive.

Use of convolution is necessary to determine the surface temperature disturbance and the velocity and spacing of the heat source-radiometer system for the time-varying flux case. Illustrated in Figure 5 is a cosine-squared flux in terms of the relative pulse

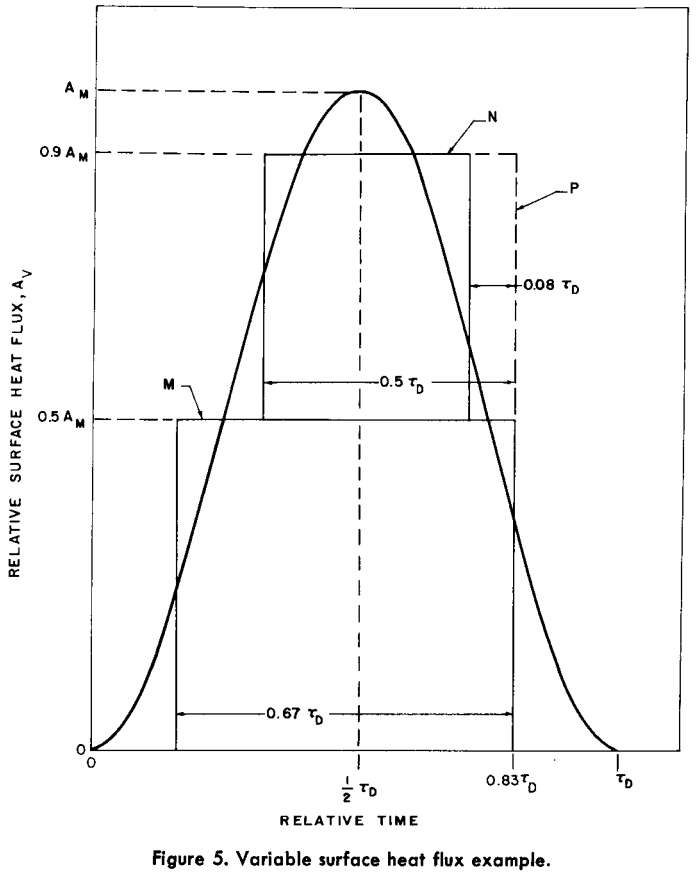

Figure 5. Variable surface heat flux example.

time τ_D and the maximum amplitude A_M. A sample disturbance calculation, for the same parameters as above, is included in the figure, the variable flux being represented at 0.83 τ_D by three uniform fluxes, labeled M, N, and P, with magnitudes of 0.5 A_M, 0.4 A_M, and –0.4 A_M and with pulse times of 0.67 τ_D, 0.5 τ_D and 0.08 τ_D respectively. The step-by-step calculation consists of first determining a T_E-value for each flux using the relation $T_{EN} = \alpha\, t_N/E^2 = 0.08\, \alpha\, \tau_D/E^2$ as an example of the N component. Then, from Figure 2, dimensionless temperature disturbances ψ for each of the three T_E-values are obtained for $Z = 0.5$ and $J = 1$. Each ψ is then multiplied by its corresponding flux value, as, for example, $\psi_P\ Q^0 = -0.4\ \psi_P\ A_M$. The resulting three weighted fluxes are added giving the product of A_M and the sum $0.5\ \psi_M + 0.4\ \psi_N - 0.4\ \psi_P$. Multiplication by the appropriate GR/k-value then yields the temperature disturbance $T_0 - T_{0\infty}$. By this procedure, the disturbance at other times can be quickly calculated. The per cent change in temperature is obtained by using (Equation 7) to divide each ψ by the corresponding $G(T_{0\infty} - T_A)k/Q_0$ R-value and then summing the individual per cent changes.

The maximum temperature disturbance and per cent change in temperature occur during heating, so that the radiometer shall observe infrared radiation reflected from the surface (unless appropriate filtering is used) and superposed upon the radiation emanating from the heated surface. This is a disadvantage that does not exist for the square-pulse case. Of course, the surface can be observed after heating, but image contrast shall have diminished.

Image Detection

Knowledge of the spatial intensity distribution of the image and of the resolution, sensitivity, and response of the radiometer, together, provide all of the information needed to determine whether an image is detectable. The output signal $V(T)$ from a radiometer can be conveniently related to the input signal $W(T)$ by means of a generalized transfer function, which accounts for the effects on detection of surface emissivity, sensitivity, collector optics, spatial resolution, and spectral response. This transfer function g is defined as

$$\frac{V(T)}{W(T)} \equiv g = C_E C_T C_0 R(d) S_R \eta \quad , \tag{11}$$

where $W = \epsilon\lambda\sigma A_S T_{0\infty}^4$ is the background radiation incident to the radiometer from the surface area A_S, covered by radiometer field-of-view, and $\epsilon\lambda$ is the spectral emissivity corresponding to the spectrum sensed by the radiometer. C_E accounts for the effect of change in emissivity $\Delta\epsilon_\lambda$ of the image relative to background, and is equal to $1 + \beta(\Delta\epsilon_\lambda/\epsilon_\lambda)$, where $\beta = A_I/A_S$, and A_I is the image area covered by the radiometer field-of-view. C_T accounts for the effect of temperature change and equals $1 + 4\beta[(T_0 - T_{0\infty})/T_{0\infty}]$, where T_0 is assumed constant over A_I. C_o accounts for the effect of the radiometer collector optics and equals $[4(1+\mu)^2 f\#^2]^{-1}$ where μ is the magnification of the optical system, which equals $(A_D/A_S)^{1/2}$, and A_D is the area of the detector. $f\#^2$ is the f-number, or optical speed of the system, and equals f/2nd, where f is the system focal length and d is the diameter of the optical collector or field stop. $R(d)$ accounts for optical resolution and equals $J_1(d_0/d)/(d_0/d)$, where J_1 is the Bessel function of zero order, and d_0 is the diameter of the blur circle due to spherical aberration and collector size. S_R is the responsivity of the radiometer, usually given in units of volts per watt.

η accounts for the spectral response, or wavelength limitation, and equals

$$\int_{\lambda c}^{\lambda_c} E_\lambda(T) d\lambda / \sigma\, T_{0\infty}^4 \quad ,$$

where E_λ is the photon density characteristic of the material surface at $T_{0\infty}$, and λ_c is the wavelength cutoff of the detector. From C_E, it is seen desirable to have a surface that exhibits a high ϵ_λ, to increase radiometer output voltage, and, ideally, to have a $\Delta\epsilon_\lambda$ equal to zero to reduce signal noise.

Noise diminishes the useful signal from the radiometer. This effect can be stated as

$$V_D = V_N(\Sigma^2 - 1)^{1/2} \quad , \tag{12}$$

where V_D is the detectable output signal voltage from the radiometer, V_D is noise voltage, and $\Sigma \equiv V(T)/V_N$, where $V(T)$ is the output signal voltage. A criterion for image detectability occurs when $\Sigma > 1$. V_N can be related to temperature through a radiometer figure of merit termed Noise Equivalent Temperature (NET), the mathematical definition of which is available from the author. This quantity indicates the minimum target temperature that can be observed by the radiometer to obtain a $\Sigma = 1$. Small values of NET indicate high radiometer sensitivity and performance.

Field-of-view Image Interaction

As the field-of-view of the radiometer A_S intercepts the area of the image A_I, an increase in signal voltage is produced that is proportional to the total radiance emitted by the areal segment of A_I that is viewed. The results of this interaction shall be discussed qualitatively, first in terms of voltage shapes for four idealized signals and then for a real situation.

Ideally, it is assumed that the image is sharply defined and emits a uniform and constant radiation intensity. In all cases, as A_S moves at a constant velocity over A_I, the total length of response equals either the sum of the lengths l_s and l_I or the diameters of A_S and A_I in the direction of scan. For the case where $l_I \ll l_s$, the pulse shape, or response, is nearly square and exhibits slightly canted skirts having a base length equal to l_I in terms of scan time. $A_S l_s I$ increases so that $l_I < l_s$, both the signal amplitude and the response length increase, and the canted skirts occupy more of the total response length. When $l_I = l_s$, the amplitude increases further, and the response shape is triangular and of length equal to twice l_s. For $l_I > l_s$, the signal amplitude and skirts do not change further, but the response length increases, the amplitude being established by A_S. Consequently, should amplitude signify the existence of a void image, optimum response would occur when $A_S = A_I$; further reduction in A_S would diminish amplitude. Moreover, should A_I lie in a background of larger objects (e.g., emissivity changes), the optimum A_S would be that just equaling A_I, since the response to the larger objects would have been reduced, and signal contrast would be enhanced.

For image observation, it is important to compare pulse length in terms of time with the response time of the entire detection system. Should the time for A_I to pass by A_S be less than two system time constants, the image would be considered unobservable. Practical considerations require the pulse length to exceed two, and preferably ten, time constants; where one constant is the time necessary for the system to produce 67 per cent of its maximum amplitude response to a step-function signal.

The spatial resolution capability of the radiometer is another important quantity for observing images. High resolution is required to detect small images. One measure of this quantity uses the distance between the intercepts of a canted skirt, such distance taken at 10 per cent below and 10 per cent above the maximum and minimum signal levels, respectively(12).

In reality, a void image is not sharply defined, but exhibits a radiant intensity distribution that is a function of radial position, void depth, and time, as shown in Figure 4. Since the temperature decreases with distance from the image centre, the apparent size of the image shall depend upon the minimum temperature that can be discerned by the radiometer, which temperature is its NET. As the time T_E increases, the temperature disturbance increases, and the image appears larger and more blurred. The effect of this blurring on radiometer response can be estimated by determining the change in NET caused by the change in differential radiance $\partial N_T / \partial T$ as temperature increases.

Experimentation

A complete experimental evaluation of the analysis has as yet to be performed. Some evidence, however, of its validity can be demonstrated in the scan results shown in Figure 6. A slab of a low-k material, which contains 4 large holes ($G \gg 0.5$) drilled into its rear surface ($J = 1$), was scanned over its front surface. A constant set of test parameters was used but with three different heat source-to-radiometer—field-of-view separations. The temperature rise of the surface was a few degrees above ambient.

It is immediately obvious from the figure that (1) the voids have created "hot" surface images, and (2) that the surface temperature disturbance $T_0 - T_{0\infty}$ decreases as the dimensionless radius of the voids decreases. As the source-to-field-of-view separation increases, the following effects are observed: (1) the undisturbed surface temperature $T_{0\infty}$ decreases; (2) the disturbance caused by void A decreases at a faster rate than that due to the other voids; and (3) the widths of void images A and B have increased and are beginning to merge. In general, then, all of these observations are in accord with projections from the analysis. Although these voids are considered large, it can be inferred from the trend of the G- and Z-values that a small void ($G \leq 0.5$) with a Z of approximately 0.3 and greater can probably be discerned. An obvious conclusion that can be drawn from the figure is that the separation distance is a more critical parameter for the A and B voids that are nearer to the surface.

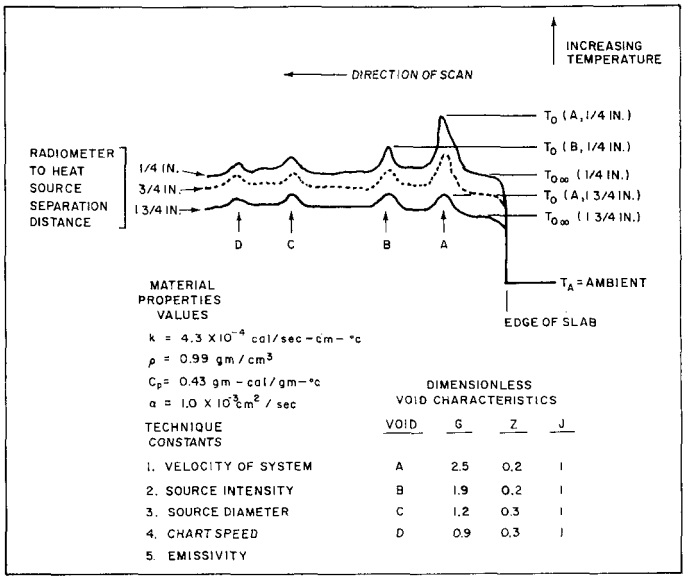

Figure 6. A superposition of actual radiometer scan recordings obtained for three different heat source to radiometer field-of-view separations moving at a constant velocity relative to a slab containing four voids that have various characteristics.

Discussion

The preceding analysis is somewhat general in scope in that the results are applicable to a range of small voids located in homogeneous materials. Clearly, much experimentation is required to evaluate the validity of the analysis, but once validated it should provide a foundation upon which test techniques can be designed, and inspection procedures specified. Extension of many of these results to other varied problems employing infrared scanning should not be difficult.

Application of the transient through-transmission diffusivity method to low thermal conductivity materials yields accurate absolute values, as well as values that are a function of thickness and are needed in the analysis. The fact that additional evidence supporting the validity of the "finite pulse-time effect" has been demonstrated is regarded as noteworthy. The one-surface, comparative method used for determining either the thermal conductivity or the diffusivity of solids presents a potentially highly useful tool for the nondestructive evaluation of materials. The intrinsic ability of this tool to permit rapid determinations in localized regions in various geometrical shapes is both unique and desirable.

References

(1) Maley, D. R., and Posakony, G. J. A thermal scanning technique for nondestructive testing. Proc. Fourth Annual Symposium on NDT of Aircraft and Missile Components, San Antonio, Texas (February 26-28, 1963), pp. 11-35.

(2) Gericke, O. R., and Vogel, P. E. J. Infrared bond defect detection system. *Materials Evaluation* (February, 1964).

(3) Sacks, H. L. A thermal infrared inspection procedure for detection and location of flaws in solid propellant rocket cases. Proc. Fourth Annual Symposium on NDT of Aircraft and Missile Components, San Antonio, Texas (February 26-28, 1963), pp. 99-114.

(4) Maley, D. R., Apple, W. R., and Posakony, G. J. Inspection of reinforced plastics by thermal nondestructive techniques. Proc. Symposium on Testing Techniques for Filament Reinforced Plastics, Wright-Patterson AFB, Ohio, AFML-TR-66-274 (September, 1966), pp. 578-604.

(5) Jakob, M., *Heat Transfer,* Vol. I (New York: Wiley, 1959), p. 359.

(6) *Ibid,* pp. 346, 352.

(7) *Ibid,* p. 87.

(8) Bird, R. B., Stewart, W. E., and Lightfoot, E. N. *Transport Phenomena* (New York: Wiley, 1963), p. 442.

(9) Beck, J. V., and Hurwicz, H. Study of thermal discontinuities and associated temperature disturbances in a solid subject to a surface heat flux, Part II. Avco TR-9-59-14 (April 28, 1959).

(10) Carslaw, H. S., and Jaeger, J. C. *Conduction of Heat in Solids* (London: Oxford, 1959), p. 75.

(11) Marks, B. G., Revesz, G., and Walker, M. The thermal plotter and its uses in microcircuit analysis and testing. Proc. Third Annual Meeting of the Infrared Techniques for Electronics Committee, Huntsville, Alabama (February 19-21, 1964), published by Soc. for Nondestructive Testing, Inc.

(12) Berger, W. M. Application of isothermal mapping as a reliability tool. Internal Report, Sierra Electronic Division, Philco, p. 4.

Thermal Nondestructive Testing with Cholesteric Liquid Crystals

W. E. WOODMANSEE and H. L. SOUTHWORTH, U.S.A.

ABSTRACT: The properties of a family of liquid crystals which scatter light over small temperature intervals near room temperature are described. Simplified methods of applying cholesteric films to test surfaces for thermal mapping are discussed. A technique for obtaining permanent flaw patterns with liquid crystals is given. The application of liquid crystalline materials to evaluation of aerospace cooling panels, thermal visualization of Lüder lines in aluminum alloys, and flaw detection in adhesively bonded titanium components is described. A comparison is drawn between the applicability of cholesteric liquid crystals and thermally quenched phosphors for nondestructive testing problems.

Introduction

The unique response of cholesteric liquid crystals to temperature changes arises through subtle modifications of their anisotropic structure. The effects of the altered molecular arrangement are most easily seen as shifts in the colors scattered by thin liquid crystalline films illuminated with white light. To explain the light scattering and other optical properties of cholesteric materials, Oseen (1) proposed a structure consisting of a series of parallel planes each of which contains molecules with their long axes aligned. A thin ($\leq$100 microns) cholesteric film is thus thought to be composed of a series of molecular planes parallel to the supporting surface with adjacent planes rotated by a small angle so that the locus of vectors along the principal molecular axis in successive planes through the film thickness describes a helix. Fergason (2) has discussed the mechanism by which circularly polarized light may be scattered by this structure and estimated that an angular displacement of 7 minutes in the orientation of successive planes is sufficient to shift the principal wavelength of light scattering over the entire visible spectrum. The delicate balance of this helical structure may be altered by the presence of trace amounts of various chemicals (3), electric fields (4,5) and thermally. The distinctive changes in the scattered colors produced by small temperature changes have been used in a number of thermal nondestructive testing problems (6). This paper discusses simplified techniques for performing thermal mapping with liquid crystals, and testing applications are described in which these materials have been successfully employed.

Properties of Liquid Crystalline Mixtures

Several factors should be considered in choosing liquid crystals for thermal mapping. The following criteria have been used to evaluate our materials: (1) Distinctive color changes should be seen over a small temperature increment: (2) the colors should be observed at a given temperature both by heating or cooling: (3) the color changes should occur rapidly in response to temperature changes: (4) the cholesteric materials should remain liquid when stored at room temperature: (5) the color-temperature behavior should be stable with time.

The graph in Figure 1 gives the color-temperature response of a cholesteric system we have studied extensively. The solid line in each set of curves represents the temperature at which red scattering commences for a given composition. The dashed line indicates the temperature at which scattering occurs in the blue spectral region. An example of light scattering by one of these mixtures over the red to blue portion of the visible spectrum may be seen in the lower right hand portion of Figure 1. The liquid crystals were applied to a copper bar heated at one end to maintain a stable temperature gradient along its length. Thermocouple measurements were made of the principal scattered colors to give the temperature seen in the graph. More detailed measurements of spectral response

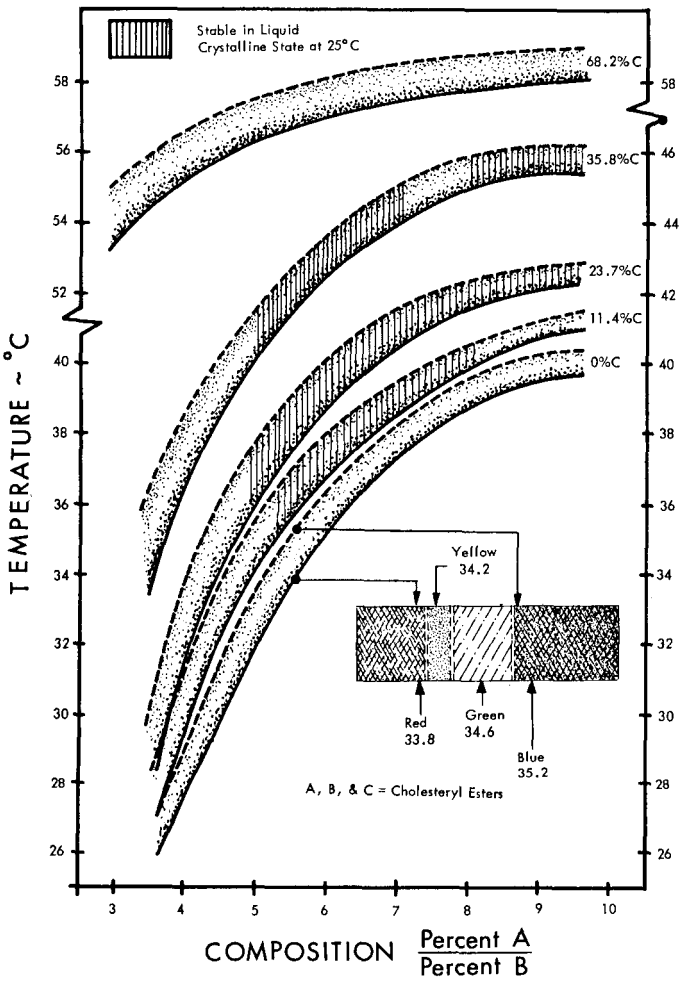

Figure 1. Temperature response of cholesteric liquid crystals.

have also been made with a Beckman spectrophotometer, but for rapid evaluation of the properties of a series of mixtures, the temperature gradient method has been used most frequently. This family of cholesteric mixtures provides considerable latitude in obtaining color response over a small temperature increment at any temperature between room temperature and 60°C.

All of the mixtures shown in the graph exhibit completely reversible color-temperature behavior. The speed with which the color changes may be induced was observed by thermally pulsing a one-mil polymeric film painted with liquid crystals which change from red to blue scattering from 25°C to 26°C.

A flash bulb positioned behind the film was used to heat the film while movies were taken of the response of the liquid crystals. With light scattering initially in the red spectral region, at 64 frames/sec. the film appeared violet within one frame, or about 15 milliseconds after flashing the bulb.

Although many of the mixtures shown in Figure 1 will solidify within a few days at room temperature, this can be prevented by dissolving the cholesteric materials in solvents such as chloroform, hexane, or benzene. It is however, often desirable to use liquid crystals free from solvent and application of the pure liquid crystals is simplified if they remain fluid when stored at room temperature. Samples of mixtures corresponding to the cross-hatched areas on the color-temperature plots have not crystallized during 12 months storage at approximately 25°C. Many nondestructive testing applications of liquid crystals are based on the detection of thermal gradients, and the absolute surface temperature is not significant. For precise sensing of specific temperatures with liquid crystals, however, it is important to insure they are not contaminated by oils, solvents, or vapors, which can greatly change their temperature response characteristics. Changes induced by contamination can be effectively reduced, however, by careful storage of the liquid crystals. For example, the color-temperature response of materials stored in a vacuum (~1 mm Hg) for one year was within 1°C of their initial behavior.

Thermal Mapping with Liquid Crystals

In thermal mapping, colors are seen with liquid crystal films owing to temperature-dependent light scattering in discrete spectral bands approximately 50 millimicrons wide. The non-scattered incident white light is transmitted by the film, and if the surface supporting the film is reflective, the color isotherms due to scattering are indistinct. In our initial work with liquid crystals we used a number of different black paints between the liquid crystals and reflective test surfaces to absorb transmitted light and thus enhance the scattered colors. These intensified the colors but the application, drying time, and subsequent removal of the paint frequently took much longer than the thermal tests.

To reduce the time needed for thermal mapping with liquid crystals, two novel techniques have been developed. To obviate the underlying black paint when testing large areas, we have added black filler materials directly to the liquid crystals. By adding finely divided carbon black, black tempera paint, or 325-mesh metallic or nonmetallic particles to the cholesteric mixtures, reflections from metal test-objects are greatly reduced. As the colors appear microscopically to be developed from small 'domains' in the cholesteric film, the light-absorptive material can be dispersed between the scattering regions without greatly attenuating the brilliance of the colors seen from the film. A comparison between the colors seen with clear and filled liquid crystals may be seen in Figure 2. The honeycomb panel on the left has clear liquid crystals applied over a black Krylon paint while the panel on the right was painted with the same liquid crystal mixture with the addition of carbon black. Generally we use from 10 to 30 weight per cent filler depending upon the reflectivity of the surface to be examined. Brushing may be used to apply either the clear or filled liquid crystals without solvent or by adding 10-20 volume per cent benzene, hexane, or chloroform; the mixture may be readily sprayed with an air brush or self-contained spray can using a Freon propellant. To remove the chemicals following testing, a rubber scraper may be used to collect the bulk of the liquid crystals which can then be reused. Final cleaning is accomplished by a solvent wipe.

For small, fixed test areas a flexible vacuum frame was devised to hold a thin polymeric film coated with filled liquid crystals against the test surface. Frames were fashioned from lengths of rubber vacuum tubing adhesively joined at the ends to form a continuous ring. A series of holes drilled in the inner wall of the tubing and a metal tube sealed in the outer wall permit evacuation of the volume between the tubing, polymer film, and test surface. Replacement of the film bearing the liquid crystals was simplified by sealing it to the vacuum tubing with double-backed adhesive tape. If the film is initially stretched across the frame, gradual application of a vacuum initially pulls the centre of the film against the surface and, as the vacuum is increased, the entire film is pressed tightly against the part to be examined. With careful evacuation, very little air is trapped under the film and in most applications the added thermal barrier of the film has not significantly decreased the

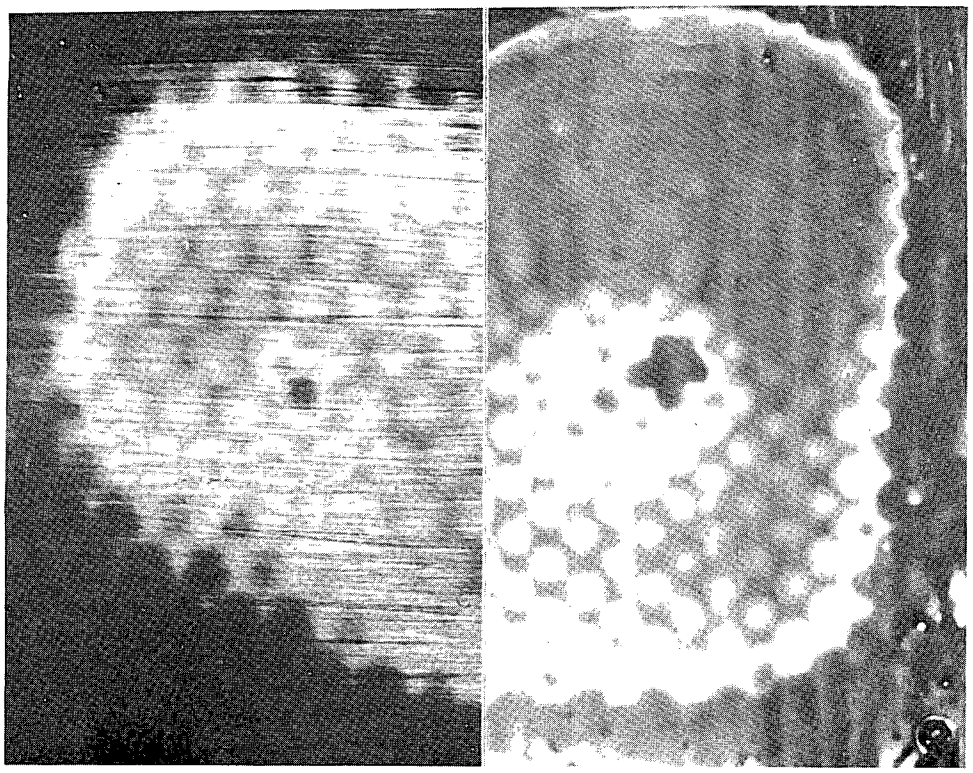

Figure 2
Clear and carbon-filled cholesteric liquid crystals used in thermal mapping on honeycomb structures. Left: Clear liquid crystals applied to flat black surface (.010 in Ti face sheet-phenolic core). Right: Liquid crystals containing 20 weight per cent carbon black (.010 in. Ti face sheet-Ti core).

sensitivity of the thermal test. The flexible ring allows some latitude in working with irregularly shaped parts and contoured surfaces may also be tested in this manner. Thin teflon films, and for lower temperatures, saran films have been reused thirty times without replacement resulting in a significant reduction in chemical costs and testing time.

Recording liquid crystal temperature patterns photographically is relatively straightforward. A technique which is helpful in reducing glare from the crystals is the use of polarizing filters over both the camera lens and the flash or flood lamps used for illumination. If photographs are not required, the locations of discrete anomalies revealed by the thermal patterns in a part may be retained by tracing the outline of the suspect area with a cotton swab to remove the crystals. When filled liquid crystals are used, this leaves a clear indication of the size and shape of the flaw.

Another method of retaining certain flaw indications utilizes a transition observed with liquid crystals at temperatures above the light-scattering range. If a cholesteric film is slowly heated beyond the violet scattering temperature, it will appear clear until it reaches the temperature at which the anisotropic properties of the liquid crystals are destroyed by thermal energy, and the film behaves as an isotropic liquid. Near this transition point—about 60°C with our most commonly used materials—the film has a faint grey or light blue appearance. This has been associated with Rayleigh scattering by the homeotropic state of cholesteric substances. If a test object exhibiting a 'hot spot' is carefully heated until the anomalous area reaches the homeotropic state, as evidenced by the appearance of Rayleigh scattering, the abrupt change in viscosity (7) of the liquid crystals at this temperature will produce a distinctive textural difference in the film over the questionable area. An example of an after-image obtained in this manner may be seen in Figure 3. The light square in the centre of the photo corresponds to a bonding anomaly in a honeycomb sandwich composite consisting of a 0.012″ Ti skin bonded to phenolic core with a polyimide adhesive. This flaw, produced by a lack of adhesive, was quickly detected by cycling the panel through the light-scattering temperatures of the cholesteric film. To 'fix' the flaw indication, the panel surface was uniformly heated until the liquid crystals over the flaw reached the homeotropic state. At this point heat injection was stopped. The reduction in viscosity of the film in this state gives the film a smoother,

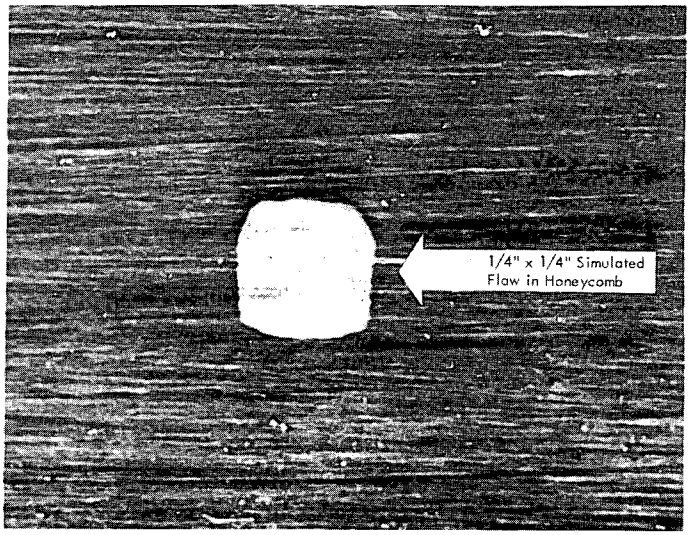

Figure 3. Stable flaw indication in cholesteric liquid crystals obtained by heating to the cholesteric-isotropic transition temperature.

more uniform appearance which persists upon cooling below the light-scattering temperatures. In addition, if the surface is slowly reheated to the scattering temperatures, the colors seen over the flaw area appear much more intense, as in Figure 3, than adjacent portions of the film which did not reach the homeotropic state. The altered textural and scattering properties

of liquid crystals treated in this way appear to be stable, and clear flaw patterns have been preserved for 24 hours after testing.

Coolant Panel Evaluation with Liquid Crystals

A thermal mapping problem for which liquid crystals have demonstrated utility is the detection of restricted coolant channels in aerospace components. By controlling the temperature of fluid circulating through cooling panels it has been possible to quickly reveal blockages by the color patterns developed on the surface. The panel sketched in Figure 4 had aluminum face sheets diffusion-bonded to a core containing a series of parallel $\frac{1}{4}$-in.-wide ribs separated by lightening cavities. On the top and bottom of each rib, coolant slots 0.030 in. wide and 0.080 in. deep were machined along the centre line. Fluid reaches the coolant channels from a header system $\frac{3}{16}$ in. wide and 0.090 in. deep around the periphery of the panel. Two pins were inserted in coolant slots of the sample panel to simulate channel blockage. One of these blocked only the channel on one side of a rib, while the other pin extended completely through a second rib and blocked the channels on both the top and bottom of the rib.

To determine if the blockages could be detected with liquid crystals, the input to the header was connected to a laboratory water tap and hot water and cold water alternately circulated through the panel. Liquid crystals which scattered light at approximately 30°C were applied over a water-base black paint on one surface of the panel. The single-channel blockage was on the unpainted side of the panel to establish whether flow restrictions in both top and bottom cooling channels were detectable by inspection from one side. A photo of the thermal indication seen with the panel is shown in Figure 4. The large elliptical pattern on the left side of the panel was due to the blockage in both upper and lower channels and the smaller ellipse at the right was caused by the channel blockage on the opposite side of the panel. The panel was initially cooled by circulating cold water through it and the photo shows the results obtained during a heating cycle. Owing to the flow restrictions in the artificially blocked channels, the panel surface over the blockages briefly remained one or more degrees Centigrade cooler than portions of the panel with normal flow rates. The blockages were readily detected with liquid crystals. This type of test is well suited to the use of a vacuum frame to hold a film supporting liquid crystals in intimate contact with the coolant panel surface.

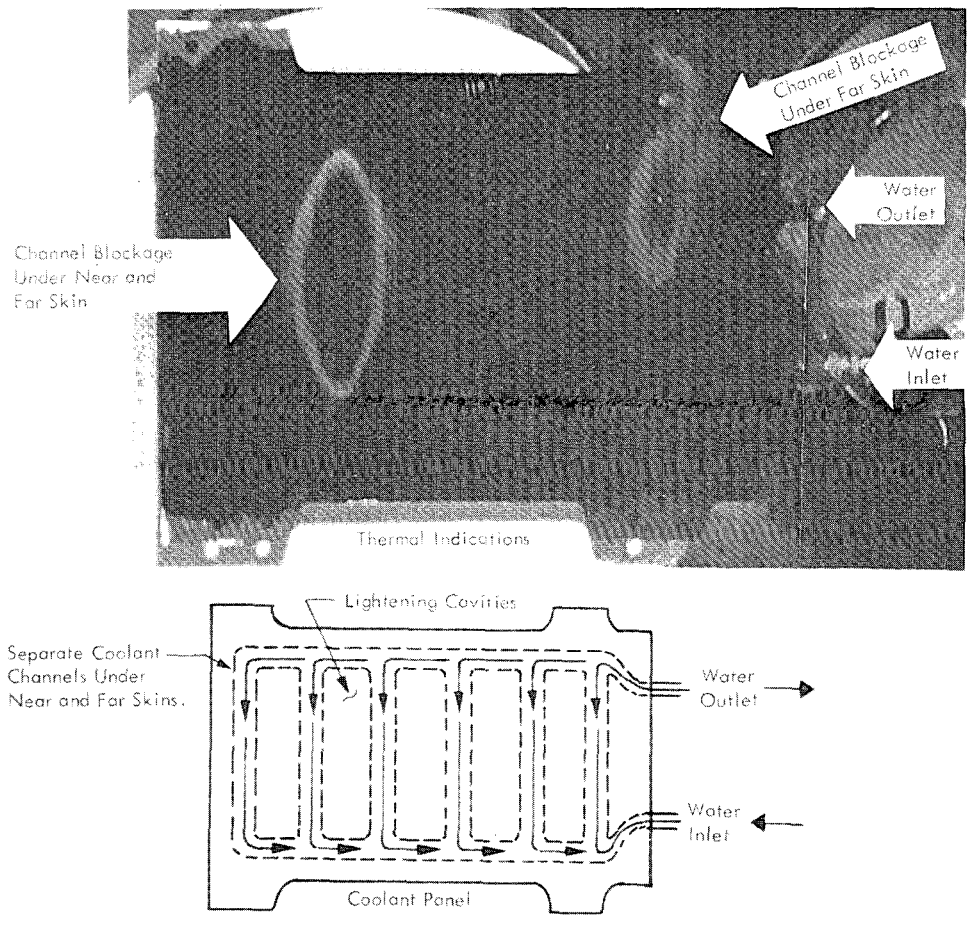

Figure 4
Liquid crystal thermal test of coolant panel.

A similar test was successfully conducted on a copper cooling baffle. The baffle contained sixty-six 0.085-in.-dia cooling holes parallel to the side of the baffle at a depth of 0.115 in. The hole separation was nominally 0.200 in. As before, the wall of the baffle was coated with liquid crystals while hot and cold water was injected alternately into the baffle. By rapidly pulsing the water temperature it was possible to obtain a relatively stable temperature pattern which revealed twelve artificially blocked holes in the baffle.

Flaw Detection in Adhesively Bonded Titanium Composites

The thermal properties of titanium composite structures being evaluated for aerospace structures are, in many instances, well suited to nondestructive testing with liquid crystals, to reveal voids generated by entrapment of volatile products from adhesives, lack of adhesive, crushed core, faulty adhesive splices, and nonuniform filleting. Any of these bonding anomalies could

adversely affect bond strength and liquid crystals have been effective in detecting these conditions in a number of sandwich panels consisting of titanium face sheets bonded to titanium core or phenolic core and in titanium metal-to-metal bonds. The advantage of this method of thermal testing, where applicable, is the speed with which relatively large surface areas can be examined in detail. Among the disadvantages are the necessity for careful control of the rate and uniformity of heat injection in the test surface, and careful interpretation of the thermal indications associated with bonding irregularities. The thickness of metal between the surface painted with liquid crystals and the bond line being examined is one of the most important factors determining the sensitivity of these tests. As the skin thickness increases, more lateral heat flow occurs which reduces the flaw-related surface-temperature gradients. These gradients are produced by the effects of bonding anomalies on heat flow through the skin thickness and flaws will be less sharply defined with thicker skins.

In order to establish the effect of skin thickness upon the sensitivity of liquid crystal thermal tests, a series of test panels was fabricated with simulated flaws prepared by removing the adhesive in areas of $\frac{1}{4}$ in. × $\frac{1}{4}$ in., $\frac{1}{2}$ in. × $\frac{1}{2}$ in., and 1 in. × 1 in. Titanium face sheets varying in thickness by 0.010 in. increments from 0.010 in. to 0.080 in. were bonded with a polyimide adhesive to titanium core for the first set of samples, and to phenolic core for the second set. Each panel was painted with cholesteric materials containing 20 weight per cent carbon black. The red to blue transition of the mixture in these tests was 35.0 to 36.0°C. The panel face sheet over the simulated flaws was alternately heated and cooled to cycle the surface through the temperature 'window' in which light scattering occurs. Two 1000-watt photoflood lamps heated the test surface which was then convectively cooled with an air jet. The results of these tests are summarized in Tables 1 and 2. In most cases the flaw indications were easily seen, however, with the thicker skins it is doubtful that the flaws denoted by a question mark would have been found if their presence were not known. These results are meaningful only for voids comparable in shape to the simulated flaw and do not imply that long narrow flaws could be seen as readily as a square flaw of the same area. Table 3 contains the results of similar tests on a series of titanium metal-to-metal bonded panels with different skin thicknesses. When these panels were bonded, the adhesive evidently flowed into the void areas provided by removing portions of the adhesive. The temperature pattern seen on these panels revealed a number of small bond irregularities due to volatile products generated while the adhesive was being cured. The approximate areas of the smallest voids associated with the thermal indications seen with the different skin thicknesses are given in Table 3. The flaws seen with heat injection and cooling from the near side only are listed together with the flaws seen with near-side heating and far-side cooling. These estimates are only meaningful in evaluating the ability of liquid crystals to locate, in titanium composites, voids comparable to the flaws simulated for these tests.

Fatigue, Flow, and Fracture of Metals

The sensitivity and rapid response of liquid crystals to small temperature variations signalled their potential usefulness in studies of fatigue, flow, and fracture phenomena. It was felt that thermal conversion of mechanical energy during deformation could be detected and visualized with the aid of liquid crystals in a manner leading to increased understanding of flow and fracture processes. A few of the phenomena of current interest are: non-homogenous plastic flow; size and configuration of plastic enclaves at crack tips; location of

Table 1

Artificial Flaws Detected by Liquid Crystals in Ti Skin/Ti Honeycomb Sandwich Panels

Face Sheet Thickness (in.)	Programmed Flaw Areas		
	$\frac{1}{4}$ in. × $\frac{1}{4}$ in.	$\frac{1}{2}$ in. × $\frac{1}{2}$ in.	1 in. × 1 in.
.010	X	X	X
.020	X	X	X
.030	X	X	X
.040	?	X	X
.050	0	X	X
.060	0	X	X
.080	0	0	?

X—Detected
?—Questionable
0—Not Detected

Table 2

Artificial Flaws Detected by Liquid Crystals in Ti Skin/HRP Honeycomb Sandwich Panels

Face Sheet Thickness (in.)	Programmed Flaw Areas		
	$\frac{1}{4}$ in. × $\frac{1}{4}$ in.	$\frac{1}{2}$ in. × $\frac{1}{2}$ in.	1 in. × 1 in.
.010	X	X	X
.020	X	X	X
.030	X	X	X
.040	X	X	X
.050	0	X	X
.060	0	?	X
.070	0	?	X
.080	0	0	?

X—Detected
?—Questionable
0—Not Detected

Table 3

Void Areas Detected by Liquid Crystals in Ti/Ti Bonded Panels

Face Sheet Thickness (in.)	Smallest Flaw Detectable	
	Front Heating and Cooling	Front Heating Far Side Cooling
.010	.014	.009
.020	.011	.014
.030	.009	.009
.040	.009	.009
.050	.059	.059
.060	.234	.059
.070	.240	.240
.080	.860	.590
.090	.540	.540
.100	.540	.540

initial slip and slip saturation during fatigue; and fatigue crack initiation and growth characteristics. Local generations of heat can be expected with each of these. Contemporary studies conducted with miniaturized strain-measuring devices and temperature-sensing instrumentation are seriously limited by the necessity of predicting, before testing, the location of expected anomalies (8). Otherwise, the placement of strain gauges and thermocouples or selection of lines of scanning with infrared detectors introduces a large element of chance.

The utility of liquid crystals in such studies has been examined and established by a limited amount of testing of fatigue and static tensile specimens. Small thermal gradients created by strain concentrations were readily revealed within gross areas of both types of test specimens. The tip of a growing fatigue crack was vividly delineated by a zone of indicated temperature rise having a size compatible with the expected plastic enclave. In testing of sheet metal tensile specimens, the inception of plastic instability and its location was readily discernible by a local increase in temperature before necking of the specimen became visible.

During these tests a short series of highly transitory, flickering color changes of unknown origin were frequently observed prior to rupture. Assuming that these thermal transients were associated with unstable plastic flow, an aluminum alloy (5456 in the H321 condition) was selected which exhibits very prominent strain irregularities above its yield point. These cause a characteristic serrated load-strain curve as indicated schematically in Figure 5. Local thermal disturbances were revealed by liquid crystals on tensile specimens of this alloy which corresponded to the irregularities of the load-strain recording.

Coincident with the above tests, a production problem developed involving "Lüder bands" or "stretcher-strains" appearing during stretch-forming large panels of 2024-T3. This aluminum alloy and temper is not commonly known to be prone to such forming difficulties. Materials which exhibit a pronounced yield point, such as mild steels, or a serrated load-strain curve, as in some aluminum alloys, tend to develop these defects. Whether they develop, commonly depends on the prior thermal-mechanical history.

Lüder bands result from unstable plastic flow and appear abruptly as local bands of thinning. A laboratory investigation of the stretch-forming problem was initially hindered by inability to detect or control the responsible strain irregularities in uniaxial tensile specimens. Application of liquid crystals greatly facilitated the investigation by permitting visual observation of the formation, location and orientation of the Lüder bands and led to being able to produce them at will. They could be initiated after a critical amount of plastic elongation followed by a rest period at constant load. Resumption of straining resulted in their appearance, and single bands could then by cyclically induced by sudden increase in rates of strain from zero to 0.1 min.$^{-1}$. Single bands could also be induced under steady load by a sharp blow of a lead hammer on the lower crosshead.

Liquid Crystals—Thermally Quenched Phosphors

Limited comparative tests have been performed with our liquid crystals and commercially available (U. S. Radium Corporation #1807) thermally quenched phosphors. The intensity of visible light emitted by these phosphors, with suitable ultraviolet illumination, changes by as much as 25 per cent per degree Centigrade (9). Their useful temperature range is room temperature to 80°C. Due to the nature of the temperature-response mechanisms in these two types of indicators, it is to be expected that there will be differences in their ability to give visual temperature information. The liquid crystals are, in some instances, more easily used as they may be viewed with white indoor lighting or in bright sunlight. Testing with the phosphors, of course, must be conducted in darkened areas with ultraviolet exciting radiation. As noted earlier, our liquid crystals provide thermal indications over a narrow temperature increment. The phosphors, on the other hand, exhibit changes in intensity of light emission over a much broader range of temperature. This feature of the phosphors has been advantageous in examining honeycomb sandwich panels with complex geometry. For example, a honeycomb composite containing a doubler around

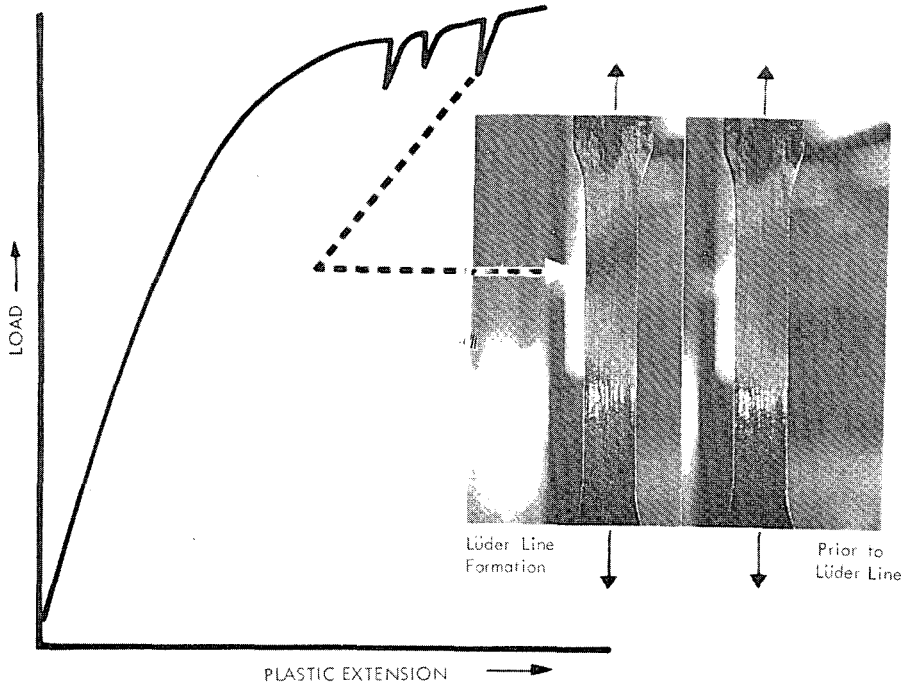

Figure 5
Visualization of Lüder-line formation with liquid crystals on aluminum tensile specimen.

the outer edge will, when heated uniformly from the front, reach higher temperatures over the metal skin bonded directly to the honeycomb than over the skin bonded to the doubler. This is due to the greater heat capacity of the metal-to-metal construction. The phosphors are frequently able to give thermal indications over several areas differing in temperature due to structural difference, and thus allow simultaneous evaluation of the bonds over these areas. With the liquid crystals it is necessary to examine such areas separately as each passes through the temperature 'window' over which light scattering occurs.

When used to visualize the temperature distribution on the back of a human hand, liquid crystals produced a more detailed thermal pattern due to the venous bed than was seen with phosphors. Similarly, liquid crystals gave much more obvious indications of Lüder-line formation in aluminum alloys. Although the thermally quenched phosphors are not susceptible to contamination by oils, greases, solvents, etc., we have observed a permanent degradation of phosphors exposed to sunlight for approximately a week. Generally, if a small thermal gradient may be related to a material property, liquid crystals can probably reveal it more effectively. If sensitivity is desired over a broader range of temperature, thermally quenched phosphors may be more suitable.

Conclusions

Cholesteric liquid crystals may be used to detect small temperature gradients in a number of areas of interest to nondestructive testing. In addition to the examples discussed above, liquid crystals have been successfully used to locate shorts in multilayer electronic circuit boards, to determine the uniformity of conductive coatings on aircraft windshields, in a penetrant detection application, and in several medical skin-temperature visualization studies. In thermal mapping studies in which surface contact is possible, the simplicity and convenience of their application and interpretation make liquid crystals a very useful testing tool. The direct surface temperature indications generally allow one to quickly determine the applicability of thermal testing to a problem and to establish optimum heating and cooling techniques necessary to reveal the desired material property.

Acknowledgments

The assistance of Gary Waterman in developing our liquid crystals and conducting many of these tests is gratefully acknowledged. Wilbur Wilson is to be commended for his patient efforts in the bond-evaluation study.

References

(1) Oseen, C. W. The theory of liquid crystals. Trans. Faraday Soc. *29* 883 (1933).

(2) Fergason, J. L. Cholesteric structure—I, Optical properties. Molecular Crystals *1*, 293 (1936).

(3) Fergason, J. L., Goldberg, N. N. and Nadalin, R. J. Cholesteric structure—II, Chemical significance. Molecular Crystals *1*, 309 (1966).

(4) Harper, W. J. Voltage effects in cholesteric liquid crystals. Molecular Crystals *1*, 325 (1966).

(5) Muller, J. H. Electric field effects in cholesteric liquid crystals. Z. Naturforschg—20a, 849 (1965).

(6) Woodmansee, W. E. Cholesteric liquid crystals and their application to thermal nondestructive testing. Materials Evaluation *24*, 564 (1966).

(7) Porter, R. S. and Johnson, J. F. Order and flow of liquid crystals: The cholesteric mesophase. J. Appl. Phys. *34*, 55 (1963).

(8) Williams, F. R. G., Taylor, C. J. and Mitchell, P. J. Studies of metal fatigue by infrared techniques. Applied Materials Research, April 1966.

(9) Byler, W. H. and Hays, F. R. Fluorescence thermography. Nondestructive Testing May-June 1961.

Discussion

Q. E. J. KUBIAK, General American Transportation, Niles, USA:

Surface finish required for vacuum film method? Sensitivity of technique over complete colour range?

A. The test must be clean to permit use of the vacuum film technique, however, relatively rough surfaces may be examined in this way due to the uniform force exerted by atmospheric pressure which holds the plastic in intimate contact with the test surface. The colour response of cholesteric materials with which we have worked is generally linear in terms of the thermal shift of the wavelength of maximum scattering from the red to the blue visible colours. The wavelength of maximum scattering then decreases much more slowly with increasing temperature. The red to blue shift of the chemicals we have used occurs in response to temperature changes of 1.0 to 1.5°C.

Q. GERHARD JAEGER, Lufthansa German Airlines, Frankfurt, Germany:

Is the method already in use during production and construction of airplanes?

A. Thermal testing has been used to a limited extent on current aircraft to determine, for example, the uniformity of conductive defrost coatings on Boeing 707 windshields. Extensive thermal testing of preliminary design titanium bonded structures for the SST has been performed with cholesteric liquid crystals.

Q. DAVID STEIN, Picatinny Arsenal, Dover, USA:

Can you give me information on the application of cholesterol crystals on leakage detection?

A. James Fergason did some work on identification of gases by their effects upon the color-temperature response of cholesteric compounds and mixtures. This technique could be adapted to leak detection in some instances although the susceptibility of liquid crystals to contamination from sources other than the gas being sensed will probably limit their use in this aplication.

Q. HAROLD BERGER, Argonne National Laboratory, Argonne, USA:

Would you please comment on the quantitative aspects of temperature differences that can be detected with the liquid crystal method?

A. Spectral shifts from the red to blue regions of the visible spectrum have been observed with temperature changes of 0.1°C. The limit to the thermal sensitivity obtainable with cholesteric liquid crystals has not been established.

Q. H. SCHWARTZBART, 11T Research Institute, Chicago, USA:

Are the crystals strain sensitive?

A. The chemicals we have used do not exhibit strain sensitivity. Some colour response to mechanical stress has been described for cholesteryl oleyl carbonate and the carbonate formed with nonylphenol but stress induced colour changes are much less pronounced than those produced chemically or thermally.

Technical Session 4/ Testing of Welds

The Activities of the International Institute of Welding in the Domain of Nondestructive Testing

A. DE STERKE, NETHERLANDS and
G. A. HOMÈS, BELGIUM

Introduction

At the Annual Assembly of the International Institute of Welding in 1964, it was considered desirable to establish liaison with the organizers of future international conferences on nondestructive testing.

For this reason a liaison group was formed in IIW Commission V, dealing with testing, measurement and control of welds.

It was proposed that a list of documents relating to the testing of welds, as published by Commission V of the IIW, should be made available together with a report on the activities of Commission V and its sub-commissions.

In the following, a general outline of the structure, scope and activities of the International Institute of Welding is given, with particular reference to Commission V.

Foundation and Objects

The foundation of the International Institute of Welding in 1948 was the result of striking successes in the application of welding. Confronted with the technical problems raised at each stage in its development, which was rich in discoveries and from which many lessons were to be learned, specialists in the different countries concerned felt the need to exchange information and to meet for discussion; many personal contacts had already shown that there was a marked desire to work together at an international level so as to link and coordinate exertions which, though often resulting in brilliant successes within the different countries, were being made quite independently of each other.

The establishment of an international body met a Dutch-inspired suggestion put forward at the symposium held at Utrecht, 1947. A first meeting, convened by the (British) Institute of Welding, of which J. L. Adam was President, took place the same year in London. A provisional committee was then set up to draft the constitution of the proposed institute and to define its structure.

The committee was able to complete quickly its difficult task, meetings being held successively in Paris on the invitation of the (French) Institut de Soudure and in Bâle on that of the "Société Suisse de l'Acétylène".

In June 1948, at the end of a two-day international meeting convened by the "Institut Belge de la Soudure" and held in Brussels under the auspices of the Belgian Minister of Economic Affairs, the International Institute of Welding was founded at the offices of the "Fonds National de la Recherche Scientifique" by the representatives of the following thirteen countries: Austria, Belgium, Denmark, France, Italy, the Netherlands, Norway, South Africa, Spain, Sweden, Switzerland, the United Kingdom and the United States.

Such was the original nucleus which, through the work of the General Secretariat, so many more members were later to join.

Today 31 countries participate in the work of the IIW. The other countries that have joined since 1948 are: Argentina, Australia, Bulgaria, Canada, China, Czechoslovakia, Finland, Germany, Hungary, Israel, Japan, New Zealand, Poland, Rumania, Turkey, Uruguay, U.S.S.R., Yugoslavia.

The participating organizations in the different countries are listed at the end of this document.

On 11th June 1948, the first Governing Council meeting was held at the offices of the "Institut Belge de la Soudure".

Composed of delegates previously nominated by the member societies, it then appointed the first officers, electing a President, three Vice Presidents, a Treasurer and a Secretary General; it drew up the annual budget and organized the initial series of technical commissions. The commissions were made responsible for dealing with the technology of the various welding and allied processes, standardization, terminology, metallurgical and constructional problems and also with the testing, measurement and control of welds.

In an article of the constitution it is stated that an objective of the Institute shall be, either by itself or in collaboration with other bodies, "to promote the development of welding by all processes".

That such an expansion would lead to a natural, but also fruitful, rivalry between the different welding processes was clearly foreseen by the founders, as were the difficulties which might result from it. For this reason it was stated in another article of the constitution that "the Institute shall not engage in commercial or trade activities and in particular shall not concern itself with prices, wage rates, markets or agencies".

Indeed, the action of the Institute cannot be other than disinterested. In the course of its work difficult problems may arise, in particular when new processes appear, because the Institute's duty is simultaneously to promote progress and to prevent competitive advantages being gained from its support.

For this reason the Institute has laid down its policy clearly and firmly in the constitution and bylaws.

It is also stated that the Institute shall assist in the formulation of international standards for welding in collaboration with the International Standards Organization. It has been able to do this effectively as a result of its close participation in the work of ISO/TC 44. Finally, it is laid down that the I.I.W. shall periodically organize assemblies, with a view to the promotion of team work at an international level.

Technical Structure

The activity of the IIW as a whole depends essentially on the work of its technical commission. Unlike many international organizations whose principal activity takes the form of holding, at regular or irregular intervals, congresses at which papers on certain previously chosen themes are presented, the IIW has tried to obtain its results from the continuous cooperative work of a limited number of members and experts who constitute working technical commissions.

The advantages of this formula, which was deliberately chosen on the foundation of the IIW, seem today to have been proved by experience.

The working sessions of the IIW commissions, subcommissions and working groups enable detailed and practically uninterrupted work to be carried out since, between meetings, the members correspond with each other and, if necessary, with members and chairmen of other commissions.

Under these conditions it is possible not only to compare different opinions and to draw conclusions, but also to prepare programs of work, to allocate this work between the participants, to collect experimental results, to carry out investigations, etc.

At present, the IIW has the following sixteen commissions:

Commission I	—	Gas welding and allied processes.
Commission II	—	Arc welding.
Commission III	—	Resistance welding.
Commission IV	—	Documentation.
Commission V	—	Testing, measurement and control of welds.
Commission VI	—	Terminology.
Commission VII	—	Standardization.
Commission VIII	—	Health and safety.
Commission IX	—	Behaviour of metals subjected to welding.
Commission X	—	Residual stresses, stress relieving and brittle fracture.
Commission XI	—	Pressure vessels, boilers and pipelines.
Commission XII	—	Special arc welding processes.
Commission XIII	—	Fatigue testing.
Commission XIV	—	Welding instruction.
Commission XV	—	Fundamentals of design and fabrication for welding.
Commission XVI	—	Welding of plastics.

Publication of the Work of the IIW

On the foundation of the IIW arrangements were made to ensure that the work which had been accomplished should be made known. These arrangements have resulted, firstly, in the publication and sales, under the auspices of the IIW, of a certain number of documents and secondly, in the publication in the technical press of documents recommended for publication by the IIW.

Since 1949 abstracts of welding literature have been published in an IIW periodical "Bibliographical Bulletin for Welding and Allied Processes".

In "Welding in the World", another bilingual quarterly journal, the International Institute of Welding has published since 1963 the principal documents recommended for publication by its technical commissions, reports by chairmen of commissions and general information on the activities of the IIW.

Influence of the IIW at an International Level and Liaisons with Other International Organizations

The Institute has attempted to ensure that all necessary liaison is maintained with international groups and organizations whose objectives have points in common with its own activities.

In the first place, it may be mentioned that the IIW became a member of the Union of International Engineering Organisations (UATI) on the foundation, in March 1951, of this body, which was established on the initiative of UNESCO with a view to bringing together non-governmental international technical organizations for the discussion of common problems.

Apart from permanent contact with this group of international organizations, the IIW maintains liaison with the International Standards Organisation (ISO), and particularly with its Committee ISO/TC 44 "Welding" and its sub-committees, in connection with standardization problems in welding and testing.

In this connection, the results of the technical work of the IIW, which are of interest from the point of view of international standardization are considered by ISO, which uses them as a basis of discussion with a view to the preparation

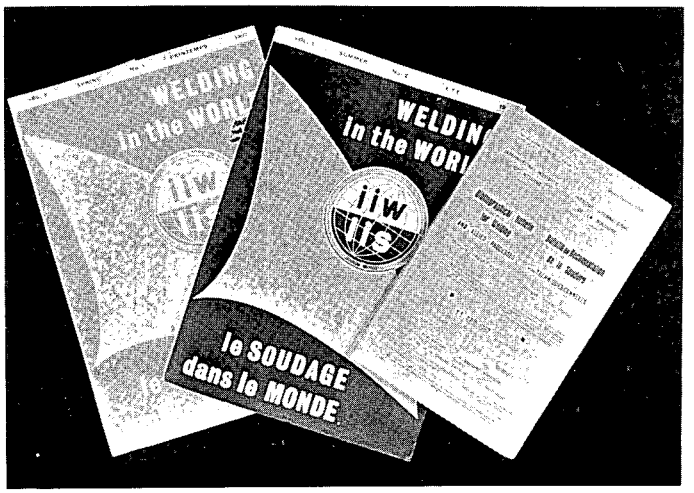

Figure 2. Publications of the IIW.

of international recommendations. In addition, ISO frequently asks the IIW to give it authoritative advice on the technical problems which arise in the discussion of questions studied within its committees. Although the IIW's liaison with ISO is principally with ISO/TC 44, it nevertheless maintains contact with other committees, among which may be particularly mentioned ISO/TC II "Unification of Boiler Codes" and certain of its sub-committees and ISO/TC 17 "Steel".

As regards international specifications, there is also co-operation with the International Electro-Technical Commission.

Commission V: Testing, Measurement and Control of Welds

Chairman: Mr. H. L. Carson (United Kingdom),
Vice-Chairman: Mr. M. Evrard (France),
Membre d'Honneur: Prof. G. A. Homès (Belgium),
Secretary: Mr. J. Th. Eering (Netherlands),
Secretarial Assistant: Miss E. Sauer (Netherlands)

Commission V was established in 1948, to study all methods of weld testing. Its first Chairman was P. Goldschmidt-Clermont (Belgium). He was succeeded in 1950 by Professor G. A. Homès (Belgium), who was in turn succeeded in 1963 by the present Chairman, H. L. Carson (United Kingdom).

The late L. van Ouwerkerk (Netherlands) played a very active part in the early life of the Commission and was its Vice-Chairman from 1954 until his death in 1958.

The 31-member countries of the IIW are each entitled to appoint one delegate and one or more technical experts to serve on the Commission. At present, the number of persons so accredited is 103 and about half this number can usually be relied upon to attend each year on the four days when the Commission meets during the Annual Assembly. To work effectively with such a large number of people and to give adequate attention to the wide range of subjects which come within its terms of reference, the Commission is divided into the following sub-commissions:

Sub-Commission V-A—Radiography;
Sub-Commission V-C—Ultrasonics;
Sub-Commission V-D—Destructive Tests;
Sub-Commission V-E—Methods of Nondestructive Testing other than radiography and ultrasonics;
Sub-Commission V-F—Welding Defects and their Significance.

Each sub-commission holds its own meetings (usually two per year) in the periods between the Annual Assemblies of the full Commission. At each Annual Assembly, the work of the sub-commissions is carefully reviewed and, where appropriate, recommendations are made by Commission V for the publication of reports and/or their transmission to other Commissions of the IIW or to the International Standards Organisation.

Certain other commissions of the IIW also find themselves involved in weld testing matters. Sometimes they find it convenient to refer these matters to Commission V, but on other occasions they find it more convenient to establish a special sub-commission or working group of their own and to invite Commission V to nominate one or more members to assist in the work. An example of such intercommission collaboration is Sub-Commission III-G. This sub-commission was established by Commission III (Resistance Welding) to enquire into the efficacy of nondestructive testing as applied to resistance spot welds. More than half the members of Sub-Commission III-G are also members of Commission V. Other examples are the working groups on nondestructive testing established by Commission XI (Pressure Vessels, Boilers and Pipelines) and Commission XV (Fundamentals of Design and Fabrication for Welding). On both of these working groups Commission V is represented.

General co-ordination of the work of all the commissions of the I.I.W. is achieved through the good offices of the Scientific and Technical Secretary and by the Technical Committee and an annual meeting of chairmen of commissions.

In the sections which follow, an attempt is made to give a résumé of the past and present activities of all the sub-commissions, except Sub-Commission V-D. This Sub-Commission is omitted since it is not concerned with nondestructive testing.

All documents approved for publication by the IIW bear a reference beginning "IIS/IIW". Many of them may be purchased from the national welding institutes which are members of the IIW, but where this is not possible, orders can be placed with *Le Secrétariat Scientifique et Technique de l'IIS*, 32 Boulevard de la Chapelle, Paris, 18e, France. A catalogue of all IIW publications is available from the same address.

Sub-commission V-A: Radiography

Chairman: Mr. M. Evrard (France),
Secretary: Mr. J. Th. Eering (Netherlands).

In 1949 a Working Group, presided over by the late L. van Ouwerkerk (the Netherlands) was created for the purpose of initiating general investigations into the problems involved in the application of radiography to the examination of welds.

Later, three other working groups were created with the object of investigating:

—Image quality indicators (1950);
—The appearance of weld radiographs and the behaviour of the welds in service (1950);
—The possibilities of using radio-isotopes (1951).

These preliminary studies led to the formation of Sub-Commission V-A in 1952, with L. van Ouwerkerk (the Netherlands) as its first Chairman. Following the death of Mr. van Ouwerkerk in 1958, H. Vinter (Denmark) took over the Chairmanship, and on his resignation for business reasons in 1963, the present Chairman, M. Evrard (France) was appointed.

For convenience of administration, Sub-Commission V-A is at present divided into the following sections:

1) Section A—"Study of the fundamental aspects of radiography"
2) Section B—"Study of the technological aspects of radiography".

These sections are both presided over by the Chairman of the Sub-Commission, who can appoint:

—Drafting committees (3 or 4 members at most) to study a particular matter and to draft an appropriate document on it;
—Rapporteurs, to make studies of a limited nature in accordance with clearly defined terms of reference.

Achievements

The achievements of Sub-Commission V-A may be summarised as follows:

1) *Image Quality Indicators (IQI).*
   After a very comprehensive study of the existing IQI's, two types were finally recommended for international use:
   a) The step-with-hole indicator with steps in the geometrical ratio of 1.25 and holes of a diameter equal to the thickness of the steps.
   b) The wire indicator with wire diameters in the geometrical ratio of 1.25.

Both types are described in document IIS/IIW-62-60.

Subsequently, rules were established for the reading of these IQI (Doc. IIS/IIW-185-65). The IQI are now used extensively and their international standardization is in course of study by ISO.

2) *Recommended practices for radiographic examinations* have been established for the following:

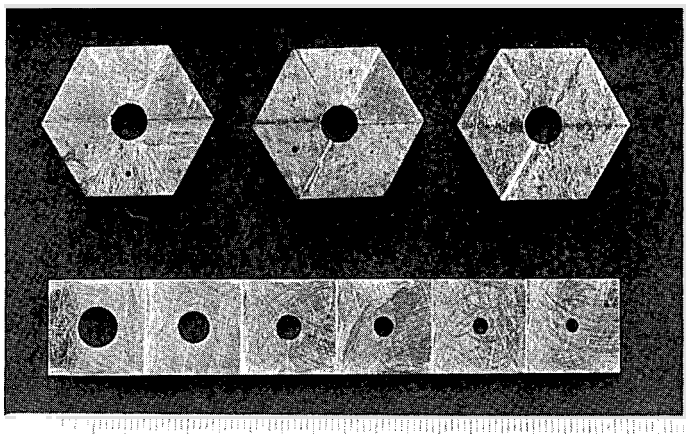

Figure 3. Some of the "step with hole" radiographic image quality indicators.

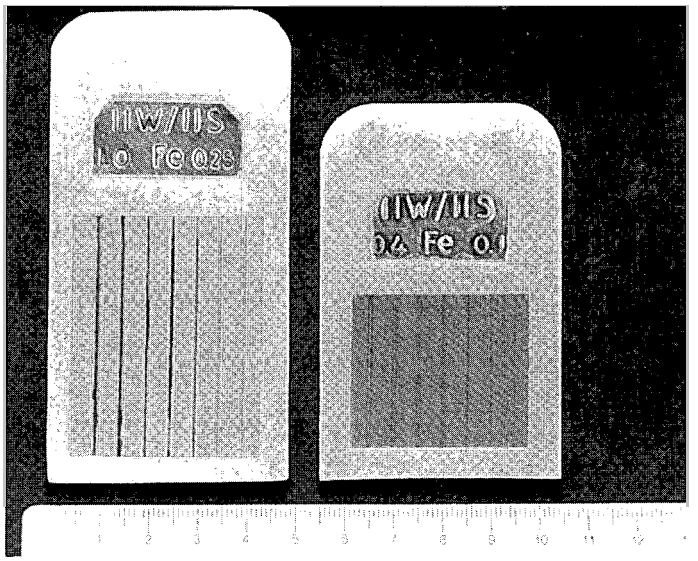

Figure 4. Some of the wire type radiographic image quality indicators.

a) Fusion welded joints for steel plates up to 500 mm (IIS-IIW-6-58).
b) Circumferential fusion welded butt joints in steel pipes up to 50 mm wall thickness (IIS/IIW-36-59).
c) Fusion welded joints in aluminum and its alloys and magnesium and its alloys up to 50 mm (IIS/IIW-35-59).
d) Resistance spot welds in aluminum and its alloys (V-322-66/OF).

3) *Collections of reference radiographs* which are published under the auspices of the I.I.W. by four member countries, comprising:
a) A collection for steel; the first edition which dates from 1952, was supplemented in 1953, 1954 and 1966. It now contains 86 cards with the reference radiographs either in the form of transparencies or copies on paper.
b) A collection for aluminum and light alloys (1962 edition) containing 51 radiographs, some of which refer to resistance spot welds.
c) A booklet of prints of radiographs of welds in steel, primarily intended for educational purposes.

4) *Handbook on radiographic apparatus and techniques.* (Doc. IIS/IIW-46-60), published in three languages, English, French and Swedish.

5 *Study of radiographic films.*
Knowledge of the characteristics of films is essential for good radiography.
The results of the work are contained in "Recommendations for sensitometric tests of radiographic films for use without intensifying screens or with lead screens". (Doc. IIS/IIW-184-65).

6) *Calibration of X-ray equipment.*
This is a rather difficult problem, requiring tests which cannot easily be performed by normal users of the equipment. However, the studies resulted in a recommendation for determining the focal spot size of X-ray tubes. (Doc. IIS/IIW-183-65).

7) *Study on the detectability of fine cracks by radiography.*
A report for information was prepared on this subject (Doc. V-288-65/OE), but has not yet been published.

Work in Progress:

1) *Studies to define the conditions required in practice to obtain optimum image quality.*
In these studies, the two recommended IQI's are being used. It has been shown that it is necessary to investigate the conditions under which the films are read and at the same time to define the possible variations in the recording of image quality for each type of IQI.

2) *Study of radiographic films.*
The investigations in this field are directed towards a classification of films.

3) *Recommended practice for the radiographic examination of fusion butt welds in steel plates with a thickness between 50 and 200 mm.*
In this document, the use of radioactive isotopes, generators of high energy X-rays, such as linear accelerators and betatrons, are being considered.

4) *Collections of reference radiographs.*
This refers in the first instance to the steel collection. There is a certain degree of opposition to the classification of the cards by colours.

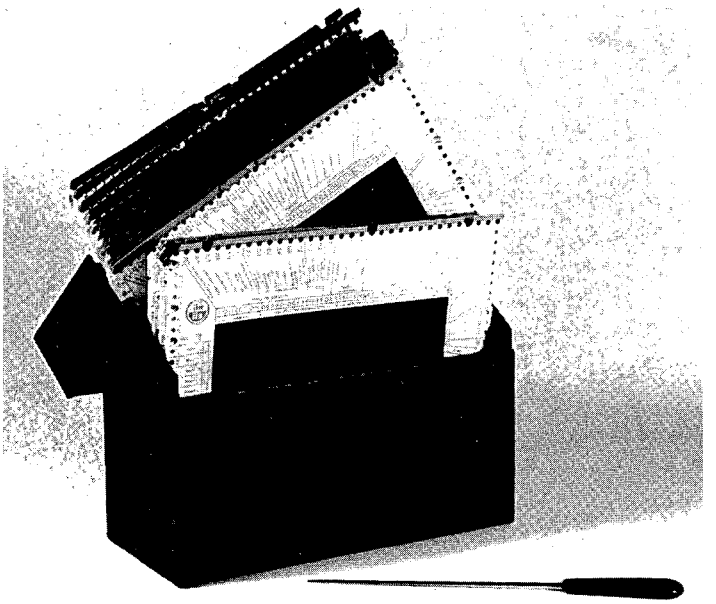

Figure 5. Collection of reference radiographs.

As a result of an enquiry amongst users of the collection, it appears that 47% use the collection for educational purposes, and 42% use it as an acceptance standard.
Under these conditions, the present collections will be retained for a number of years, but a new collection is also envisaged in which each card will bear a macrograph illustrating the defect revealed by the radiograph.

5) *Study of the possibility of using radiographic examination for brazed joints, friction welds or electron beam welds joining identical or dissimilar metals.*
6) *Study of the possibility of using radiography for the examination of those welded connections to pressure vessels illustrated in I.I.W. document XI-125-65.*
(This study is being undertaken at the request of Commission XI.)
7) *Study of the application of automatic procedures in radiographic examination.*

Sub-commission V-C: Ultrasonics

Chairman: Prof. P. Bastien (France),
Secretary: Mr. M. Evrard (France).

In 1949, the International Institute of Welding formed a Working Group under the Chairmanship of Professor G. A. Homès (Belgium), which was charged with enquiring into the use of ultrasonics in the examination of welds. Following on this preliminary work, Sub-Commission V-C was established in 1952, with Professor Homès as Chairman. In 1953, Mr. A. de Sterke (Netherlands) succeeded him as Chairman, and in 1954 he was in turn succeeded by the present Chairman, Professor P. Bastien (France).

Since its formation, Sub-Commission V-C has made extensive use of working groups of limited periods of existence. Each has been entrusted with the study of a clearly defined problem and has been able to have recourse where necessary to laboratories for the conduct of experimental work in accordance with a carefully pre-arranged program, and to pass on documents specimens from one laboratory to another.

For the solution of simpler problems, the Sub-Commission appoints rapporteurs who are asked to carry out particular investigations and place the results of these before the Sub-Commission for general discussion.

At the present time, two working groups are in being with responsibility for the following:

a) Terminology,
b) Study of calibration blocks and the determination of probe characteristics.

Rapporteurs have responsibility for the following:

c) Attenuation of ultrasonic waves in metals, particularly, steel plates;
d) Establishment of a unified procedure for the checking of ultrasonic flaw detection equipment;
e) Study of a means for assessing the dimensions of weld flaws revealed by ultrasonic testing;
f) Presentation and recording of the results of an ultrasonic examination;
g) Study of the limitations inherent in the use of ultrasonics for weld examinations;
h) Study of the possibilities of using ultrasonics for the examination of welded nozzles in the pressure vessels indicated in Doc. XI-125-65. This study is being made at the request of Commission XI (pressure vessels, boilers and pipelines).

The normal conclusion of a rapporteur's work is either the production of a document or the formation of a working group to further advance the study of the subject.

Achievements

These are as follows:

1) *Calibration block:*
Important work has been done in this field. Test-pieces and blocks were exchanged between the different countries interested in this question. The result was a calibration block recommended by the IIW (IIS/IIW-23-59) and adopted in varying degrees, by a number of countries. This block has been standardized in Germany and France and is included in a British Standard on calibration blocks. It is now being studied by ISO.

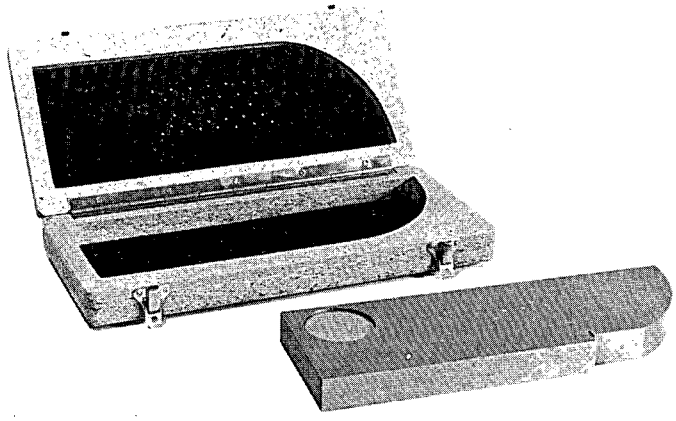

Figure 6. Dutch version of IIW. calibration block.

2) *Response curves for ultrasonic waves for typical weld defects (IIS/IIW 127-64).*
Groups of laboratories made experiments on test-pieces containing defects, which were circulated between these laboratories. One of the results was the establishment of a method for distinguishing planar defects (cracks, cold cracks, hot cracks . . .) from volumetric defects (cavities, blow holes . . .), according to the appearance of the echoes and their variation when the probe was moved.
3) *Recommended practice for the examination of welds by ultrasonics (IIS/IIW-205-66).*
4) *List of terms used in ultrasonic testing (first edition, comprising the list of terms in three languages (1959)).*
5) *List of terms used in ultrasonic testing (second edition, comprising definitions of terms in two languages and the list in eleven languages (now being printed)).*
6) *Unified procedure for the checking of ultrasonic equipment.*
(Approved for publication but not yet published.)

Work in Progress

1) Study of calibration blocks, by a Working Group, in order to determine the influence of the form of the block and to specify means for defining the characteristics of the ultrasonic beam (beam index, angle of incidence, distribution of energy in the beam).
2) *List of terms.*
Preparation of supplementary lists in other languages.
3) *Attenuation of ultrasonic waves in plates.*
4) *Training of ultrasonic testing operatives.*
For the time being, this study is restricted to the gathering of information.
5) *Study of means for determining the sizes of defects found by ultrasonics.*
This is a very difficult problem, but it is of fundamental importance.

6) *Study of the limitations of ultrasonics in weld inspection.*
7) *Study of the application of ultrasonics for the detection of defects in brazed joints, friction welds and electron beam welds, as well as lack of fusion in welds, made by the CO_2 process.*

Summarizing it can be said that, although the program of Sub-Commission V-C is very comprehensive, the subjects under investigation and the mutual discussions are sufficiently clearly defined to lead to results which will make it possible to improve and develop the techniques of ultrasonic examination.

Sub-Commission V-E: Methods of Nondestructive Testing Other than Radiography and Ultrasonics

Chairman: Mr. A. de Sterke (Netherlands)
Secretary: Mr. S. A. Lund (Denmark).

In 1955, Sub-Commission V-E was established to undertake work in field other than radiography and ultrasonics, under chairmanship of Mr. A. de Sterke.

The working procedure normal in the other sub-commissions was also adopted for Sub-Commission V-E. In particular the system of rapporteurs to deal with specific items.

The duty of this sub-commission was in the first place to study methods of surface inspection, such as magnetic particle testing and testing with penetrant liquids.

As a consequence of the diversity of view on the use of the magnetic particle method as a means for the detection of subsurface defects, it was decided to restrict initial consideration to the application of the magnetic test, to weld defects in or near the surface.

A document was prepared and approved for publication. (Doc. IIS/IIW-94-62, ex Doc. V-186-61) "Considerations on the influence of various factors in magnetic particle inspection of surface defects in welds".

A study of the use of penetrant liquids resulted in the preparation of Doc. V-236-63/OE "Recommended practice for the application of penetrant testing", which was subsequently published as Doc. IIS/IIW-182-65.

A further study in the domain of penetrant testing was concerned with the development of an artificial demountable crack specimen. A great number of designs, some taken from published literature and others originating from the discussions in the sub-commission, were tried and modified to incorporate improvements.

The latest design is under investigation with a view to checking on the reproducibility of the results it gives.

Work has also been undertaken on the detection of subsurface defects by the magnetic particle method, but at the moment, no final agreement has been reached on an international scale on the scope of the method in this application. The study on this latter subject has stimulated interest in the development of the magnetographic methods which unlike the particle method uses magnetic tape as the detecting and recording medium.

Factors such as surface condition, magnetic characteristics of the material, the way in which magnetic fields are applied, etc. are being studied together with the shape, size and other particulars of magnetic powders.

Present evidence suggest that surface condition is the dominating factor in the detectability of sub-surface flaws.

Another investigation being undertaken by the sub-commission is concerned with the application of eddy-current techniques for the detection of weld defects and the determination of flaw size.

After completion of the present program, other items to be studied will include the testing of brazed joints and welds made with special techniques (electron beam etc.); the automatic examination of welds by magnetic, eddy-current and penetrant methods.

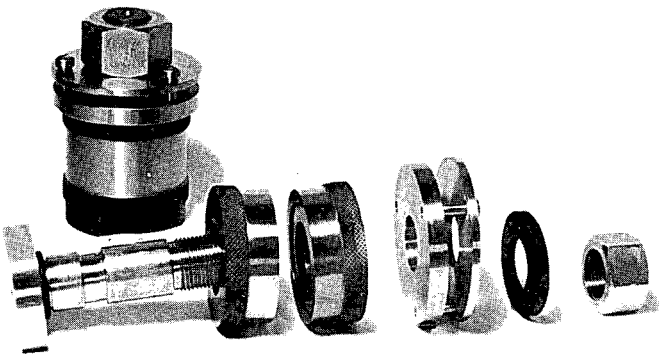

Figure 7. Test-piece for the evaluation of penetrants and developers.

Sub-commission V-F: Welding Defects and Their Significance

Chairman: Mr. J. G. Young (U.K.)
Vice-Chairman: Mr. J. J. Chène (Switzerland)

In 1963 Mr. J. G. Young was appointed rapporteur on this subject and in 1964 a working group was created to draft terms and definitions for weld defects. At the 1966 Annual Assembly this activity was given Sub-Commission status under the Chairmanship of Mr. Young with Monsieur J. J. Chène as Vice-Chairman. The terms of reference of Sub-Commission V-F are to draw up terminology and explanations for weld defects; to assess research studies on the influence of defects in service behaviour; to classify defects at different levels and to devise acceptance criteria.

At the time of preparation of this document the detailed work program is not available.

Work of Other I.I.W. Commissions in the Domain of Nondestructive Testing

SUB-COMMISSION III-G: NONDESTRUCTIVE TESTING OF RESISTANCE SPOT WELDS.

Chairman: Dr. H. G. Taylor (U.K.)
Secretary: Mr. H. L. Carson (U.K.)

Sub-Commission III-G was formed by Commission III (Resistance Welding) at the Annual Assembly in 1959. It has as its object the investigation of the scope of nondestructive testing methods for the assessment of the mechanical strength of resistance spot welds.

One of the first acts of the Sub-Commission was to initiate a program of co-operative research into means for testing spot welds in mild steel and aluminium alloys containing heavy metals such as copper. This work is still in progress and already it has shown that no single method of nondestructive testing is likely to be self sufficient.

The first interim report on the investigations was issued in 1962 (Doc. III. G-12-62/OE) and this was later revised and re-issued as Doc. III. G-12A-63/OE. It recommended that a combination of special X-ray and ultrasonic techniques should be used for the examination of spot welds in steel, and that a very sensitive X-ray technique should be employed to reveal the heavy-element migration ring in the case of aluminium alloys containing heavy elements. In this latter case, it is believed that the presence of the heavy-element migration ring is a clear indication that a weld nugget has been formed and that, therefore, the weld has satisfactory

adhesion and thus mechanical strength. However, more tests require to be made before these recommendations can be regarded as final.

A report on the work done in Italy in association with Sub-Commission III-G was published by GALLINARO in "Revista Italiana Della Saldatura", XIV, 6, pp. 305-317, Novembre-Decembre, 1962.

This was later translated into English and issued to Sub-Commission III-G as Doc. III-G-17-63, and to Commission III as Doc. III-222-64. Its English title is: "Radiographic Inspection of Spit Welds in Primary Aircraft Structures".

The Sub-Commission is also following with interest work being undertaken by independent bodies throughout the world, particularly work in Germany where ultrasonic transducers are contained in the welding electrodes and thus permit a rapid check to be made of spot-weld quality simultaneously with production.

The possibility of applying eddy-current and special magnetic methods to assess the mechanical strength of spot welds is under consideration, and certain preliminary tests are at present being made.

COMMISSION IV "DOCUMENTATION"

One of the jobs of Commission IV is to prepare contributions for the publication "Bibliographical Bulletin for Welding and Allied Processes".

This quarterly bulletin in two languages, French and English, publishes about 2,500 abstracts of articles relating to welding and allied processes.

Documents relating to nondestructive testing are included, in particular under the headings "Properties of welds and testing methods" and "Study and testing of welded constructions".

Commission IV also organizes exhibitions of publications which are almost always held on the occasion of the Annual Assemblies of the IIW.

Research reports and periodicals devoted to welding and allied processes are exhibited and these frequently include items relating to nondestructive testing.

COMMISSION VI "TERMINOLOGY"

Since its creation, Commission VI has occupied itself with the establishment in the form of a "Multilingual collection of terms for welding and allied processes", a list of technical terms, used in welding and allied techniques.

The parts already published, contain:

1) general terms—welding procedure—characteristics and inspection of welds.
2) Gas welding.
3) Arc welding.
4) Resistance welding.
5) Heat treatment.

As indicated by the title, the first part contains terms relating to testing of welds. It comprises lists of terms in 12 languages:

German, English, Danish, Spanish, Finnish, French, Italian, Dutch, Norwegian, Serbo-Croat, Slovene, Swedish and a supplement for the following languages:

Polish, Russian, Slovak, Czech, and Turkish.

At the present time the Commission is preparing a revision of the volume.

COMMISSION VII "STANDARDIZATION"

This Commission studies problems concerned with the standardization of welding and allied processes. Its activity is oriented towards the transmission to the International Organization for Standardization (ISO) and to the "Commission Electrotechnique Internationale" (CEI) of documents drafted by the IIW. In turn it refers to the interested technical commissions of the IIW, the results of the work done in the ISO and CEI in the field of the activities of the IIW.

In this respect the very close liaisons existing between the IIW and ISO Committee TC 44 "Welds" and its different sub-commissions in particular Sub-Committee 5 "Testing and Control of Welds" which studies the documents drafted by the IIW (Commission V), should be noted.

Moreover, Commission VII is continuously occupied with reviewing standards existing in different member countries of the IIW, including of course those relating to nondestructive testing of welds.

The first review, made about 5 years ago, resulted in a publication concerning 21 countries; a new review is in progress and will probably interest a greater number of countries.

COMMISSION XI "PRESSURE VESSELS, BOILERS AND PIPELINES"

This commission is charged with the study of welding in the specific field of pressure vessels, boilers and pipelines. Also the examination of welds in such structures is given full attention.

As a result of close cooperation between Commission XI and Commission V, a Working Group "Non-destructive Testing" was constituted by Commission XI under the Chairmanship of Prof. G. A. Herpol (Belgium) with the task of drawing up recommendations for the radiographic inspection of welds in boilers and pressure vessels.

This work was divided into two parts. The first part led to a proposal regarding the qualitative principles on which the choice of the amount of radiography might be based. Not a specification or a code but suggestions regarding the "Radiography of welds of boilers and pressure vessels". This document was published as Doc. IIS/IIW-85-61.

The suggestions in the document were based on the acceptance of the idea that the conditions of sound design and good material selection have been fulfilled. With regard to the latter, it should be observed that only mild- or low-alloy steels of standard quality were considered.

On the basis of a number of criteria, pressure vessels are divided into three classes, determining the extent to which radiography should be applied.

In the second part of the work, quantitative limits of the above mentioned criteria are proposed.

The document prepared by the Working Group bears the number XI-159E-66 and is entitled: "Radiography of welds of boilers and pressure vessels Part II: Limit values of the criteria".

It is based on a reasonable evaluation of the risks associated with the vessel as a consequence of:

a) the gravity of the accident that can result from a failure, from the point of view of both the human risk and the economic risk.
b) the assumption of the existence of a defect in the vessel itself, which can initiate a failure.

As fundamental criteria for the amount of radiography, pressure and the production of pressure and volume are taken.

A number of corrective criteria are given, derived from such influences as service temperature, manufacturing temperature, nature of the contents, residual stresses, material thickness, nature of the load and the properties of the material.

COMMISION XIV "WELDING INSTRUCTION"

Charged with the study of the problems concerning all aspects of welding instruction, Commission XIV made the necessary efforts to explore the work of other technical commissions of the IIW and to acquaint teaching staffs with this work.

In this light, the work of Commission V is taken into consideration by Commission XIV, in particular with respect to nondestructive testing either for the training of personnel working in the field of testing welded constructions, or with respect to the use of these tests for the qualification of welders.

COMMISSION XVI "WELDING OF PLASTICS"

This Commission studies all problems concerned with the welding of plastics; the scientific aspects, technical aspects, industrial applications, documentation and education.

A good deal of work is also devoted to the nondestructive testing of welds in high polymers.

Both the aspects of radiographic and ultrasonic examination are investigated. Here, particular problems not known in the testing of metals come to the fore, especially the low absorption coefficient for radiation which introduces particular problems, for instance with regard to the image quality indicators used.

For the ultrasonic inspection of welds, special measures must be taken to compensate for the relative high acoustic absorption of the material and also in other respects, for instance the refractive index when angle probes are used, differ from those found in the testing of welds in metals.

For the radiographic inspection, collections of reference radiographs are in preparation.

The collection will consist of 30 radiographs, showing different discontinuities occurring in welds in plastics.

List of Member Societies of the I.I.W.

Country	
ARGENTINA	Instituto Argentino de Soldadura P.O. Box 643, BUENOS-AIRES
AUSTRALIA	Australian Welding Institute, 323 Daking House, Rawson Place, SYDNEY, New South Wales.
AUSTRIA	Oesterreichische Gesellschaft für Schweisstechnik, Objekt 221, Arsenal, VIENNE III. Schweisstechnische Zentralanstalt Schumanngasse 31 VIENNE XVIII.
BELGIUM	Institut Belge de la Soudure, 21, Rue des Drapiers, BRUXELLES 5.
BULGARIA	Section "Soudure" NTS—Union Scientifique-Technique de Bulgarie, Rue Radovski 108 SOFIA.
CANADA	Secretary Canadian Council of the IIW 7, Pleasant Boulevard TORONTO (Ontario). Canadian Welding Society P.O. Box 9, Station I, TORONTO 6 (Ontario). Canadian Welding Bureau 1393 Yonge Street TORONTO (Ontario) Mines Branch, Dept. of Energy, Mines and Resources, 568 Booth Street, OTTAWA (Ontario).
CHINA	Institute of Welding The Chinese Mechanical Engineering Society Shan Li Ho, PEKING.
CZECHOSLOVAKIA	Výskumný Ustav Sváracsky 135 Ul. Februárového Vitazstva BRATISLAVA.
DENMARK	Dansk Svejseteknisk Landsforening c/o Mr. Erik Kongshavn, 345 Park Allé COPENHAGEN, GLOSTRUP. Svejsecentralen 345 Park Allé COPENHAGEN, GLOSTRUP.
FINLAND	Suomen Hitsausteknillinen Yhdistys r.y. Finlands Svetstekniska Förening r.f. Vuorimiehenkatu 14 A 6 HELSINKI.
FRANCE	32, Boulevard de la Chapelle PARIS (18e) Institut de Soudure Société des Ingénieurs Soudeurs 32, Boulevard de la Chapelle PARIS (18e).
GERMANY	Deütscher Verband für Schweisstechnik e.V. Schadowstrasse 42 DÜSSELDORF (22a).
HUNGARY	Gépipari Tudomanyos Egyesület Section of Welding Szabadsag tér 17 BUDAPEST 5.
ISRAEL	Israel Institute of Metals, Institut des Métaux d'Israël Technion—Israël Institute of Technology P.O.B. 4910 HAIFA.
ITALY	Instituto Italiano della Saldatura Viale Sauli 3-5 GENOVA.
JAPAN	Japan Welding Society 1-11 Kanda Sakuma-cho Chiyoda-ku TOKYO.
NETHERLANDS	Stichting Nederlands Instituut voor Lastechniek, Zeestraat 62, DEN HAAG.
NEW ZEALAND	New Zealand Institute of Welding P.O. Box 1270 WELLINGTON.
NORWAY	Norsk Sveiseteknisk Forening Kr. Augusts gt. 5 II OSLO.
POLAND	Instytut Spawalnictwa Ul. H. Wiatreka 16/18 GLIWICE.
RUMANIA	Centre Technique de Recherches de Timisoara Bul. Mihai Viteazul 24 TIMISOARA.
SOUTH AFRICA	South African Institute of Welding 107-112 Pharmacy House 80, Jorissen Street—P.O. Box 10836 JOHANNESBURG.
SPAIN	Departamento de la Soldadura Centro Nacional de Investigaciones Metalurgicas Ciudad Universitaria MADRID 3.
SWEDEN	The Swedish Pressure Vessel Commission (Tryckkärlskommissionen) P.O. Box 791 STOCKHOLM 1. Svetstekniska Foreningen I.V.A. Box 5073 STOCKHOLM 5. Tryckkarlskommissionen I.V.A. Box 5073 STOCKHOLM 5.

SWITZERLAND	Association Suisse pour la Technique du Soudage St. Albanvorstadt 95 4000 BALE 6.
TURKEY	Istanbul Teknik Universitesi Makina Fakültesi—Makina Malzemesi ve Imâl Usulleri Enstitüsü Gümüssuyu 87 ISTANBUL.
UNITED KINGDOM	Institute of Welding 54, Princes Gate—Exhibition Road LONDON, S.W. 7.
URUGUAY	Instituto Uruguayo de la Soldadura Chana no. 2274 bis MONTEVIDEO.
U.S.A.	American Council of the I.I.W. 345 East 47th Street NEW YORK 17, N.Y.
U.S.S.R.	The U.S.S.R. National Welding Committee Comité National de Soudure de l'U.R.S.S. Prospekt Lenina 490 MOSCOU B-134. The U.S.S.R. Scientific Research Institute of Electric Welding Machinery Institut Russe de Recherche Scientifique du Matériel de Soudage Électrique VNNIESO Ulitsa Acad. Pavlova 8 LENINGRAD P-22. Mechanical Engineering Society Société des Constructions Mécaniques NTO Mashprom B. Cherkasskii Per 7 MOSCOU K-12.
YUGOSLAVIA	Savez Drustava Za Tehniku Zavarivanja Sfij. Erjavceva 15/I LJUBLJANA. Association des Sociétés de Soudure de Yougoslavie Kej 13 Novembri b.b. SKOPJE.

Ultrasonic Inspection of Weldments Using the Delta Technique

B. T. CROSS and G. J. POSAKONY, U.S.A.

ABSTRACT: The delta technique is an ultrasonic weld inspection method for rapidly accepting good welds. This new method employs several ultrasonic search units positioned in a configuration characteristic of the method. Its primary advantage is its ability to detect randomly oriented weld defects with nearly equal reliability.

The delta technique has been tested with contact, manual water bubbler ultrasonic wheels, manual immersion, and automatic C-scan immersion ultrasonic systems. These tests performed under field and laboratory conditions have detected a variety of defect conditions including lack of fusion, porosity, metallic and non-metallic inclusion, and cracks. Correlation studies made between weld radiographs and ultrasonic delta, C-scan recordings show excellent correlation.

This paper discusses the principles and potential application for the delta technique in the inspection of welded structures.

Introduction

While ultrasonic weld inspection techniques are widely used in Europe, they have gained only limited acceptance in the United States. The reasons for the limited acceptance are, in part, the result of inherent limitations of the standard ultrasonic techniques to detect and identify randomly oriented defect conditions in a weld.

While performing research on weld inspection, the Research Division of Automation Industries, Inc., developed a unique technique for weld evaluation. This new approach, called the "delta technique" employs two or more ultrasonic search units positioned in a manner characteristic of this method. The primary feature of this technique is its ability to detect randomly oriented flaw conditions in weldments with nearly equal reliability. A second significant feature is the relative insensitivity to the weld bead condition.

A variety of welds and weld conditions have been studied in numerous positions and at different frequencies. The defect information collected during these tests was displayed on facsimile recordings similar to conventional ultrasonic C-scans. In all the work that has been performed, any defect detected with radiographic techniques was also detected with the delta technique, and it was established that the condition of the weld bead and the orientation of the flaw had only minor influence on the capability of the system.

While the accomplishments of the delta technique are encouraging, there are certain limitations. One is the inability to clearly define defects, such as group porosity. Since delta scans provide a facsimile recording of weld, test results can be compared with radiographs. Excellent correlation was obtained for crack type defects, but closely spaced bits of porosity appeared as single large indications. Although this inability to define group porosity exists, the technique successfully detects group porosity, laminar defects, and vertical defects in one operation.

The delta technique was developed as a supplement to standard ultrasonic weld evaluation methods, a supplement that provides a means for rapidly accepting good welds.

The Delta Operation

While the analysis of the ultrasonic energy entering and leaving a weld zone is complicated, the concept of delta weld inspection is relatively simple. The outline drawing of Figure 1 shows the general principle. The sound energy is introduced into the material under investigation at an angle that produces shear-wave energy in the material. In welds, the energy is usually introduced in the parent metal next to the weld. The sound propagates in the material until it strikes an interface, which is defined as anything having an acoustic impedance different than the parent material and resulting in an interruption in the propagation pattern of the sound beam. An interface may be an inclusion, a crack, lack of weld penetration, lack of fusion, etc. At the interface, a variety of things may occur. The conditions that have been identified are listed as follows:

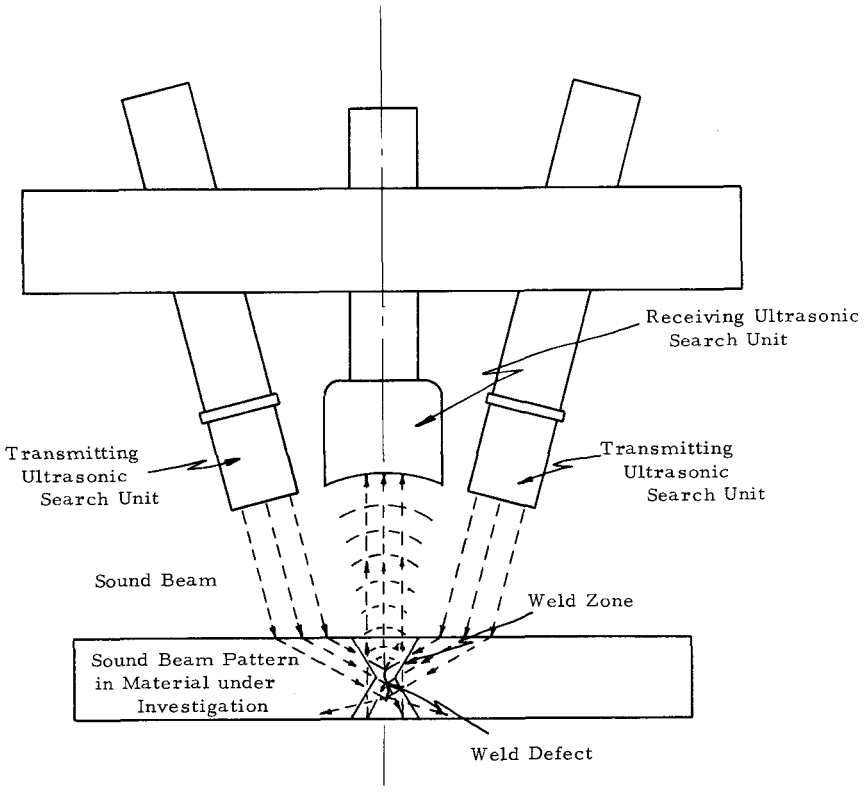

Figure 1
Sketch of delta configuration.

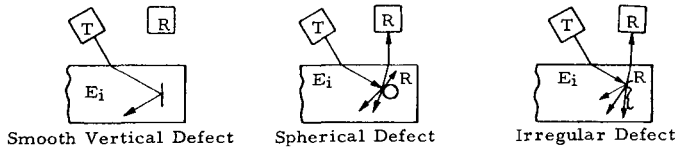

Figure 2A. Reflected Energy

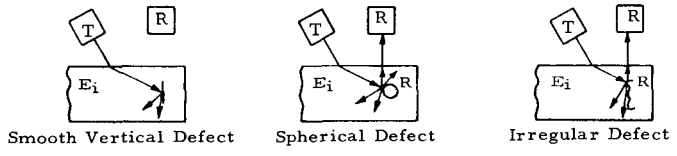

Figure 2B. Mode Converted Energy (Direct)

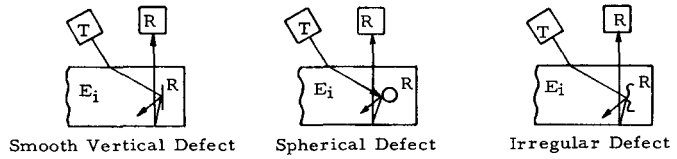

Figure 2C. Mode Converted Energy (Indirect)

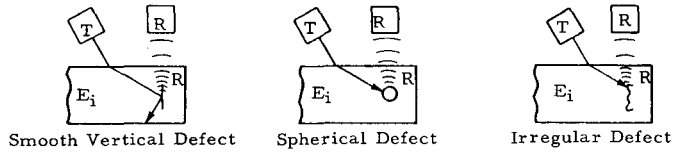

Figure 2D. Reradiated Energy

Figure 2. Redirected sound energy.

A. The sound energy may simply be reflected from the interface. This type of energy remains as shear energy as long as it is in the material.

B. The energy may be mode-converted from shear to longitudinal. This does not imply that the shear energy has been absorbed. The shear energy and the longitudinal energy occur simultaneously in the material and merely propagate in a manner that is characteristic to that particular form of energy. Both the longitudinal energy and the shear energy propagate from the defect as a direct reflection, but the angles of propagation and the speed of travel are different.

C. The energy may be reradiated. This phenomenon is not thoroughly established or understood. Experiments have established the apparent existence, but the manner in which it occurs is not clear. In concept, the defect acts as a new source for sound energy generation.

The various methods for redirecting the sound energy incident on the flaw or defect are pictured in Figure 2. The various path lengths have been verified by determining the time required for the energy to propagate along a particular path length.

Figure 2A shows the path for direct reflected energy from three different types of defects. The incident energy, E_i, is shear and the energy, R, is likewise shear. Figure 2B shows the path length for mode-converted energy that is redirected from the different defects. The incident energy, E_i, is shear, but the energy, R, is longitudinal. This has been established by measuring travel time. Figure 2C shows a mode-converted energy path that can provide additional information about the defect. The importance of Figure 2C is to show that there is more than one way in which energy can get back to the receiving search unit. Figure 2D shows the concept for reradiated energy. This energy appears to travel at the speed of

a longitudinal wave, but it radiates in many directions. The source for the energy shown in Figure 2D is not currently established.

The schlieren photograph shown in Figure 3 describes the various modes of energy redirected at a metal-to-air interface. The defect is a machined slot having a vertical wall normal to the top and bottom of the part. A seal is used to guarantee a metal-to-air interface. A rubber wedge is used to block the reflected incident beam, thus preventing this energy from obscuring the defect information. Defect information is visible at both the top and bottom surfaces; however, energy patterns at the bottom surface give a better picture of energy redirection at the interface. The near-vertical beams are caused by mode conversion as shown in Figures 2B and 2C. Part of the transmitted beam misses the interface and is visible leaving the bottom surface at the incident angle (Figure 3A). The shear energy reflected at the interface is evident at the bottom surface. The vertical energy beam leaving the part surface is believed to be the reradiated beam. The schlieren photograph inserted in Figure 3A shows the normal or uninterrupted sound beam pattern.

Any energy that is redirected from the defect can provide information about the defect. The energy collected at the receiving search unit contains information about the defect regardless of which path it followed to the receiver. The receiving search unit is usually focused to increase the angle of capture of the redirected energy. In thinner materials, the various path lengths are sufficiently short that they give the

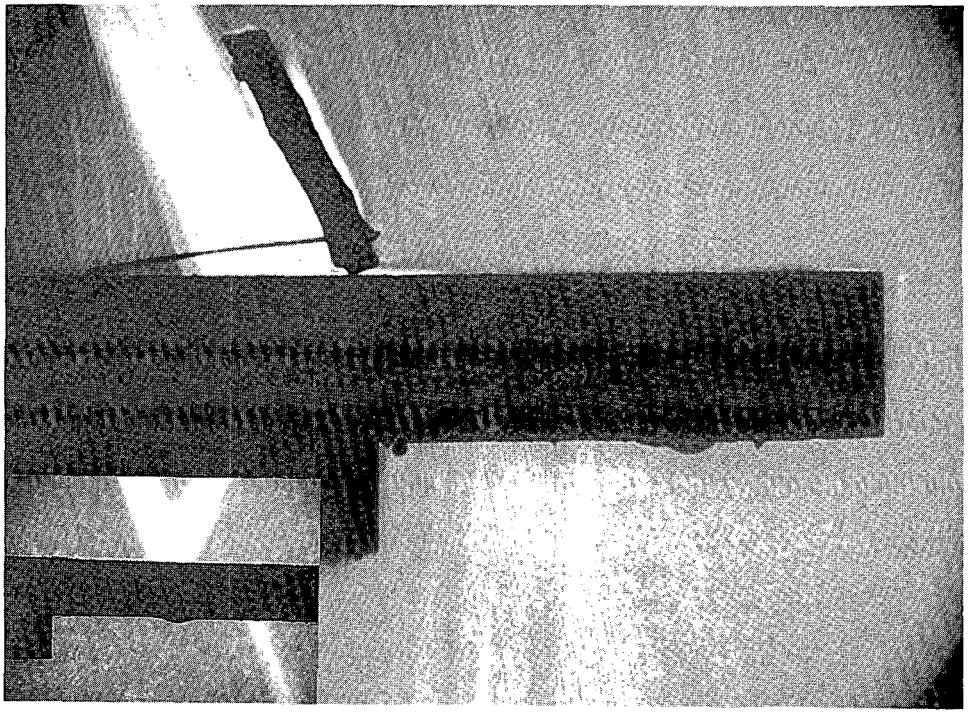

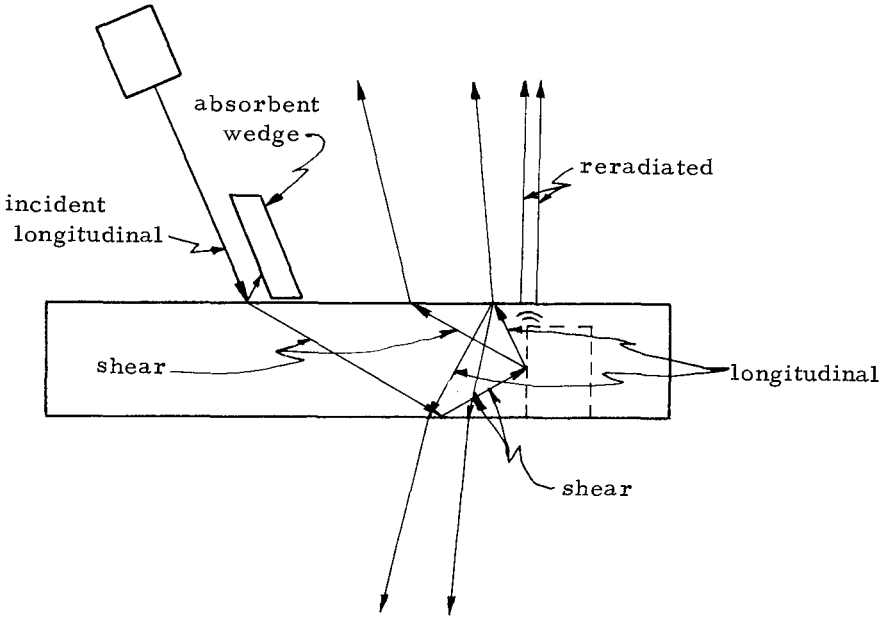

Figure 3
Schlieren image of various modes of redirected energy.

appearance of occurring at nearly the same time. In the thicker materials, the various paths and modes can be separated and identified.

Separation of the various modes or redirected energy is not necessary in locating defects. The main purpose of this phase of weld inspection is to assure the detection of all defects. The probability of detecting all defects is enhanced by using all modes of energy. In a good weld, no energy is received because the normal propagation path of the transmitted energy is not interrupted (insert in Figure 3A).

Defect evaluation with the delta technique is accomplished by selecting any one of the various modes of redirected energy, preferably the reradiated mode, and carefully examining the defect and the surrounding weld area. The characteristic pattern of propagation for the reradiated energy mode is spherical, and apparently originates at the defect boundaries. This spherical propagation of energy allows reception of defect information with a normal receiver placed directly over the defect. Defect information may be displayed on a facsimile recorder in the same manner as conventional C-scans. The receiver position being directly over the defect when flaw information is received makes the facsimile recording a true plan view of the defect location.

The physical position of search units in the delta configuration must allow the incident sound energy to strike the defect while the receiver is directly over the defect. In thin welds, this requirement is easily satisfied; however, as weld thickness increases, the size of the transmitter search unit must increase accordingly. To prevent the size of the transmitter search unit from becoming prohibitive, a shuttle configuration may be employed (see Figure 4). The shuttle delta configuration moves the transmitted sound beam back and forth, scanning the entire weld thickness; this allows inspection of thick welds with moderate search units.

Another factor to consider in the delta operation is the quantity of ultrasonic energy available for defect detection in thicker welds. Because of energy partition at the defect interface, the energy levels of the redirected modes are less than normally used in weld inspection. The addition of a second transmitter search unit and the use of selected search-unit types have increased the available energy levels to reliable states. Proper positioning of the second transmitter search unit effectively doubles the quantity of energy present. The search units are selected to give the maximum loop gain.

Test Results

Typical results of weld inspection with the delta technique are shown in Figures 5 and 6. The welds in Figures 5A and B are $\frac{3}{4}$-in. steel butt welds. The weld in Figure 6A is a $\frac{1}{2}$-in. aluminum butt weld; Figure 6B is a 1-in. aluminum butt weld. Comparison of the delta scans with the radiographs shows the correlation of weld defect data that can be obtained with the delta technique. The test results shown in Figures 5 and 6 were made at average inspection speeds of 10 ft/hr (3 m/hr). This rate of weld inspection is not the maximum speed of inspection allowable using the delta technique, although it is typical of the inspection speed used to obtain well defined defect images comparable to those shown.

The delta technique has been used successfully to inspect welds and other parts in both hand-held devices and automated systems. The size of these various delta configurations has ranged from devices 6 in. × 10 in. × 14 in. (15.3 cm × 25.4 cm × 35.6 cm) for inspecting welds 4 in. (10 cm) thick to a device $\frac{3}{8}$ in. dia × $\frac{3}{4}$ in. (9.5 mm dia × 1.9 cm long) for inspecting small fillet welds.

Conclusions

Further use of the delta technique appears to be unlimited. This inspection method could be used in the following ways:

A. A crawling device to circle the hull of a submarine for automated girth-weld inspection;
B. A hand-held device for on-the-spot inspection of weld repairs;

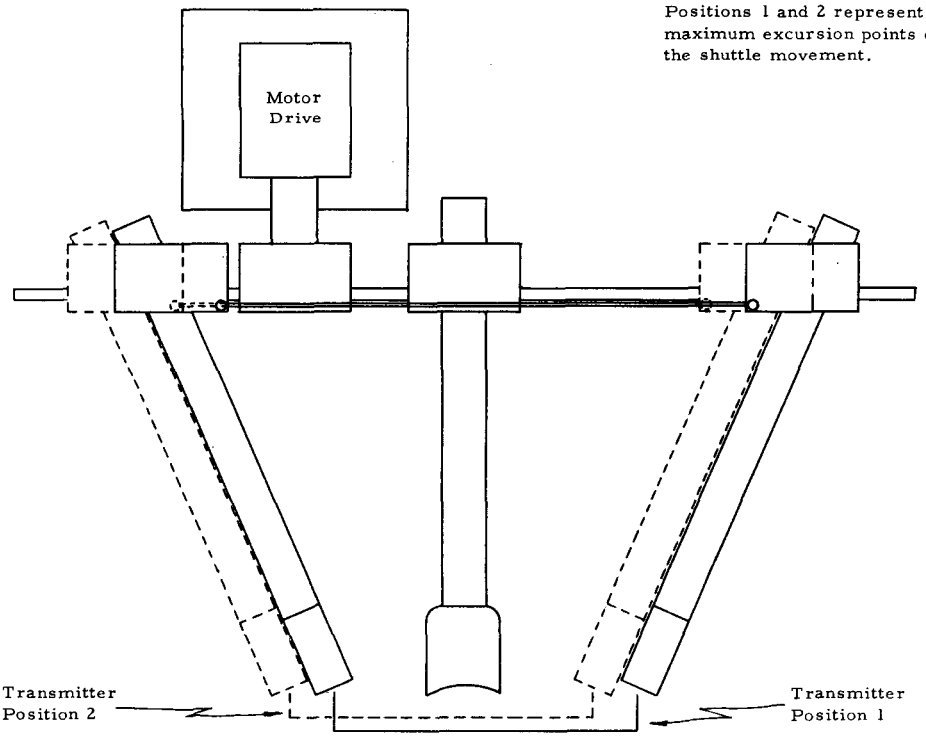

Figure 4
Dual-transmitter shuttle delta system

Facsimile Recording using Delta Technique

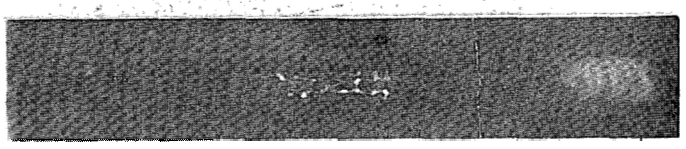

Photograph of Radiograph
(A)

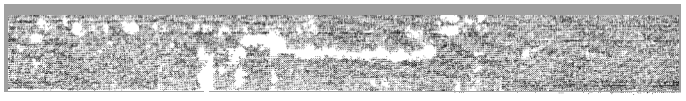

Facsimile Recording using Delta Technique

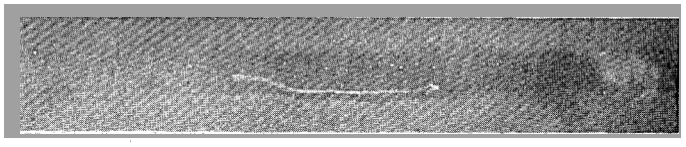

Photograph of Radiograph
(B)

Figure 5. Comparison between delta scan and radiograph.

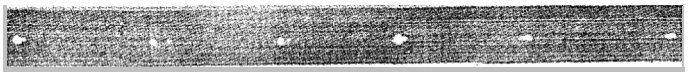

Facsimile Recording using Delta Technique

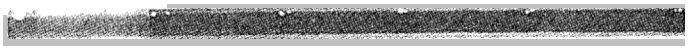

Photograph of Radiograph
(A)

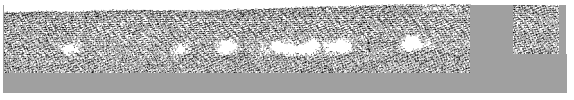

Facsimile Recording using Delta Technique

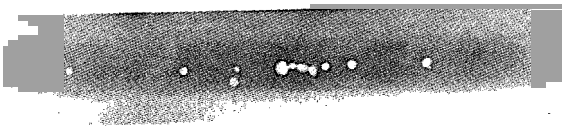

Photograph of Radiograph
(B)

Figure 6. Comparison between delta scan and radiograph.

C. A device mounted in an ultrasonic wheel for inspection of parts that prohibit an excessive use of couplant overflow, or

D. A split-collar device for inspecting welded tubing or pipeline welds.

Although future application appears unlimited, the delta technique in its present state is a research tool. This technique must remain a research tool until its operation has been further evaluated and is better understood.

Acknowledgment

The research work with the delta technique has been sponsored in part by the following organizations: The U.S. Air Force, Materials Laboratory, Wright Patterson Air Force base; U.S. Navy, Naval Air System Command, Washington, D.C.; National Aeronautics and Space Administration, Marshall Space Flight Center, Huntsville, Alabama; and Automation Industries, Inc.

Practical Quality Evaluation of Welds by Ultrasonics

T. FUJI and M. SATO, JAPAN

ABSTRACT: A study was made of the ultrasonic inspection method applied to weldments in ship's hulls under construction and to underground pipelines.

(1) Sensitivity of the ultrasonic instrument and the transducer used were calibrated against a standard test block established tentatively by the Japanese Society for Nondestructive Inspection in 1966.

(2) In order to employ the ultrasonic method for weldments in ship's hulls under construction, quality evaluation standards for the method were established by trial.

Ultrasonic indications were classified in 6 grades similar to those established by the Japanese Industrial Standards for radiography, by taking into consideration both the echo-signal amplitude and the extent of lateral movement possible while still receiving a continuous echo signal.

(3) Segment-type steel pipes used in shield tunnelling operations cannot be radiographically inspected, because only the inside of the casing is accessible. Acceptance standards for the ultrasonic inspection of welds of segment-type steel casings were established by trial using tests similar to (2) above.

(4) An automatic scanning system involving movement of the probe and the use of standard reflection pieces was developed. The standard reflection pieces were found very useful for monitoring scanning conditions similar to the image-quality indicator in radiography.

Introduction

The ultrasonic method applied specifically to weld inspection does not provide as accurate a record as does the radiographic method. Therefore, in Japan, critical weld assemblies are almost all radiographically inspected rather than ultrasonically inspected to determine the internal quality of weldments.

Recently, however, the ultrasonic method is gradually coming into use to detect internal defects of weld assemblies, as this method has certain advantages over the radiographic method.

In order to employ the ultrasonic method for weld assemblies, many unsolved problems were studied, among which were:

(1) Suitable test equipment; (2) Calibration for sensitivity; (3) Method of quality evaluation for weld; (4) Automatic scanning system by moving probe; (5) Standard reflection piece for monitoring automatic scanning.

Standard Test Block for Calibrating Sensitivity

Before initiating weld inspection, the level of sensitivity of the ultrasonic equipment and transducer should be calibrated.

For this purpose, we used the standard test block, known as NDI—STB—A2T, which was established tentatively by the Japanese Society for Nondestructive Inspection in 1966.

The standard test block (NDI—STB—A2T) for calibrating sensitivity is made up as follows:

(1) Material: Rolled steel for welded structure with 50 Kg/mm² tensile strength.
(2) Normalizing: 925°C 15 minutes, air cooling
(3) Stress relief: 625°C 50 minutes, furnace cooling
(4) Grain size: McQuaid—Ehn No. 7—8

The block is 15 mm thick, 150 mm wide and 300 mm long as shown in Figure 1, and is finished by surface grinding to an accuracy of ± 0.1 mm.

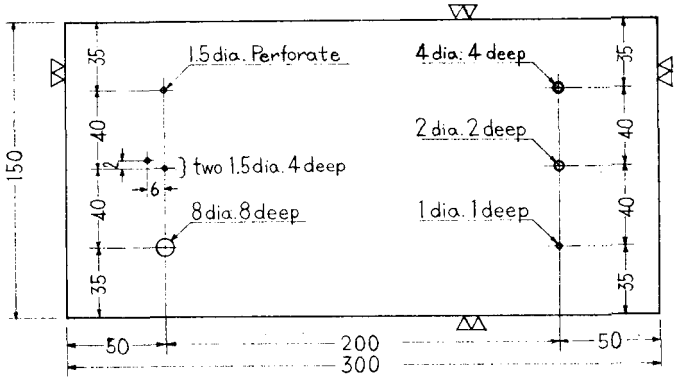

Figure 1.

The block has four different sized flat-bottomed drill holes and one perforated drill hole for calibrating sensitivity, and two flat-bottomed drilled holes for measuring resolution.

For calibrating sensitivity, the probe is placed on the same surface as the drill holes, and is then moved so as to find the maximum echo-signal amplitude at 1 skip distance. The level of sensitivity is calibrated by the maximum echo-signal amplitude from the specific drill hole. For example, the maximum echo-signal amplitude from the 2-mm-deep hole at the first reflection is set at 50% of full scale on the cathode ray tube by adjusting the grain control.

To alter the grade of inspection of the weldment, the levels of sensitivity are alternated by varying the hole size and setting the amplitude.

For measuring resolution of the flaw detector and probe system, the probe is placed on the same surface as the drill holes, and is then moved so as to obtain the equivalent echo-signal amplitudes from two adjacent drill holes (1.5 mm dia, 4 mm deep) at 1 skip distance.

The resolution is measured by the clarity of separation of the two echo-signal amplitudes from the two adjacent drill holes.

Application to a Weld of a Ship's Hull under Construction

Critical weld parts of a ship's hull have been radiographically inspected and evaluated, and classified in 6 grades according to JIS* (Japan Industrial Standard) in Japan.

To apply the ultrasonic method to the weldment in a ship's hull, we established the quality evaluation standards for the ultrasonic method by trial.

As radiographs are classified in 6 grades according to JIS, ultrasonic indications were also classified in 6 grades by taking into consideration both the echo-signal amplitude and the extent of lateral movement possible while still receiving a continuous echo signal, as shown in Table 1.

Table 1

Echo signal amplitude (%) / Extent of lateral movement (mm)	5	6 10	11 15	16 20	21 30	30
5 Max.	A	A	B	C	D	E
6—10	A	B	C	D	E	F
11—20	B	C	D	E	F	F
21—30	C	D	E	F	F	F
31—40	D	E	F	F	F	F
41 Min.	E	F	F	F	F	F

As the classified JIS grades for radiography are too stringent, especially in regard to porosity, the quality-evaluation standards for ultrasonics impose very severe grades on echo-signal amplitude.

During construction, in our shipyard, both ends of the submerged, machine-arc-welded butt joint of a ship's hull are inspected ultrasonically instead of radiographically.

The flaw detection is carried out as follows:

Thickness of material: About 20—35 mm
Test equipment: Krautkramer, USK—5 M
Probes: Frequency, 2 and/or 4 MHz
Angle, 70°
Scanning: Manual, ½-1 skip distance
Sensitivity: The maximum echo-signal amplitude from the 2-mm-dia, 2-mm-deep hole of the test block at 1 skip distance is set at 50% of full scale on the cathode ray tube.

Before using ultrasonic inspection, we had used both ultrasonic and radiographic inspection for the machine-welded parts of a ship's hull, owing to the reliable checks that could be made with ultrasonic inspection.

Correlation between ultrasonic and radiographic results in the classified grades on the whole corresponded well in the above tests, save in some cases, as follows:

The ultrasonic method could not detect fine porosity when the sensitivity was at a low level, but the radiographic method could not detect a large enough defect to be recorded by the ultrasonic echo signal.

* See Appendix.

In conclusion, the quality evaluation standards for both the echo-signal amplitude and the extent of lateral movement possible while still receiving a continuous echo signal corresponded well with the classified radiographic grades, and gave good evaluation of the internal quality of the weld.

Underground Casing Welds

Until recently, underground casings have been constructed in the open, on the ground. However, urban traffic conditions now make this impractical, and they are now constructed from separate pieces, or segments.

We have constructed many segment-type steel casings for high-pressure town water in a number of large cities in Japan. Details of segment-type steel casings are as follows:

Diameter:	About 1500-3500 mm
Length of unit pipe:	750-2000 mm
Thickness:	About 10 mm
Materials:	High-yield-point steel
Division:	4-6 per circumference
Joint preparations:	**Single-Vee with backing ring**
Welding:	Manual or semi-automatic

The segment-type casings used for shield tunnelling cannot be radiographically inspected, because only one side of the casing is accessible. Therefore ultrasonic inspection is the only nondestructive testing method that can be used to determine the internal quality of the weld part of the casing.

The practice of flaw detection is as follows:

Test equipment:	Krautkramer, USK–5 M
Probes:	Frequency 4 MHz Angle 70° Normal probe when detecting for penetration to backing ring
Scanning:	Manual, ½-1 skip distance
Sensitivity:	The maximum echo-signal amplitude from the 4-mm-dia, 4-mm-deep hole of the NDI–STB–A2T test block at 1 skip distance is set at 50% of full scale on the cathode ray tube.

The acceptance standards for ultrasonic inspection of a weld for segment-type steel casings were established by trial on the same basis as used for a weld in a ship's hull, as shown in Table 2.

Table 2

Echo signal amplitude (%) Extent of lateral movement (mm)	12 Max.	12–25	25 Min.
0–20	A	A	B
21–50	A	B	C
51–80	B	C	C
81–100	C		

A (small defect)..... Good
B (medium defect)..... Fair
C (large defect)..... Poor

To check the correlation between ultrasonic results of welded test plates and their mechanical properties, about 100 welded test plates 10 mm thick containing various sized internal defects, were mechanically tested after being classified according to the above acceptance standards.

The results of the tensile strength test gave mean values of grade B and grade C as about 95% and 90% respectively of the mean value of grade A.

Results of the fatigue strength test, showing the difference of strength according to the above grades were observed qualitatively. However, fatigue strength is affected by the position of the defect. Test plates with surface or sub-surface defects showed lower fatigue strength than those with internal defects of the same size.

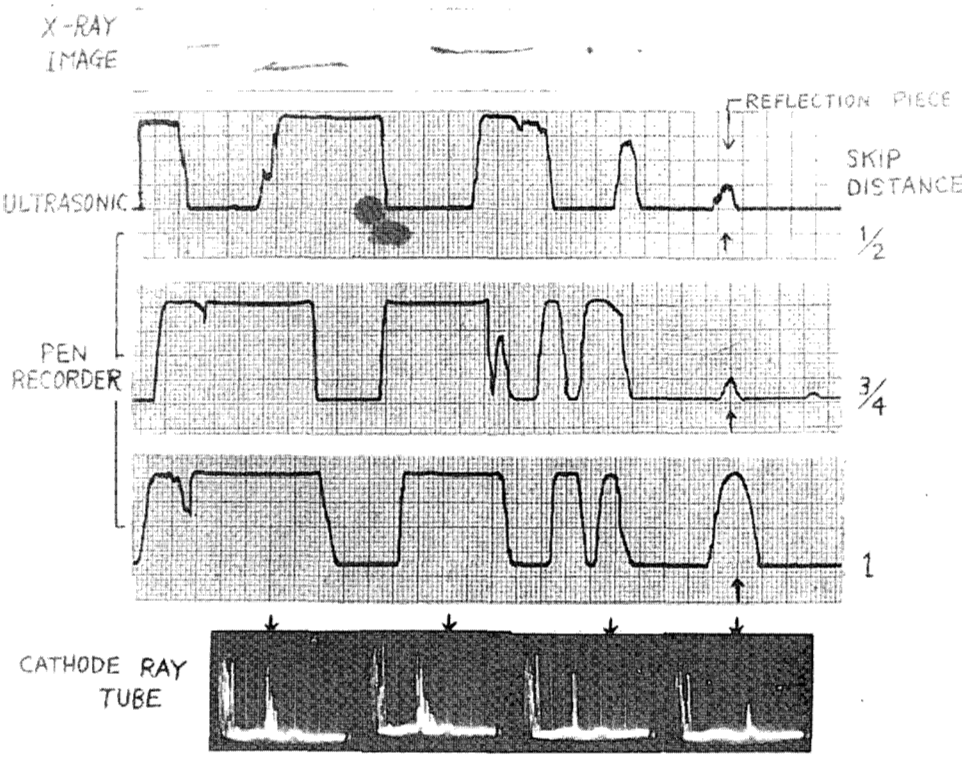

Figure 2.

For segment-type steel pipes fatigue strength is not a major requirement, but the welds themselves receive repeated stresses and require fatigue strength. Therefore, the acceptance standards for the entire welded structure demanded consideration of fatigue strength, based not only on the echo-signal amplitude and the extent of lateral movement, but the position of defects as well.

Automatic Scanning System by Moving Probe

As is well known, the weak point in ultrasonic testing lies in the recording of results, especially by manual scanning, and an automatic scanning and recording system for weld inspection has been developed for moving objects, as for example welded pipes in the factory.

However, when the objects cannot be moved, such as a large object or fixed one, the probe system must be moved in order to achieve automatic scanning.

Our automatic scanning and recording system by moving probe is as follows:

Drive:	Alternating current motor
Transmission:	Gear and chain
Moving direction:	Parallel to welded seam
Moving length:	600 mm
Probe:	Angle 70°, 2 MHz
Probe-to-weld distance:	Adjustable, but usually probe is fixed in three positions ($\frac{1}{2}$, $\frac{3}{4}$, and 1 skip distance)
Test equipment:	Krautkramer, USIP—10 W
Monitor:	2 channels gate No. 1 for weld part gate No. 2 for reflection piece

One example of records for welded test plate is shown in Figure 2. The records consist of 3 charts received from different probe-to-weld distances.

By comparing the 3 charts, we can recognize internal defects, including shape, size, position and kind of defect. If necessary, more critical examination may be done by manual scanning with a high-frequency, small-sized probe.

We can recognize internal defects from the recording chart, but we do not know the scanning conditions, such as sensitivity level, probe contacting condition, etc. In order to monitor the scanning conditions, we use the standard reflection pieces.

The standard reflection piece is made of synthetic resin and is similar to the wedge of an angle probe. When this piece is placed on the parent material near the welded seam as shown in Figure 3, the echo signal from its surface appears on the cathode ray tube beside, and to the right of, the echo signal from the defect.

To pick up the echo signal from this piece and reject the needless echo signal, we use a 2-channel monitor. No. 1 gate of the monitor is used for the weld part and No. 2 gate for the standard reflection piece.

Standard reflection pieces are very useful for monitoring the scanning conditions, such as sensitivity level, probe contacting condition etc., with a function similar to the image-quality indicator in radiography.

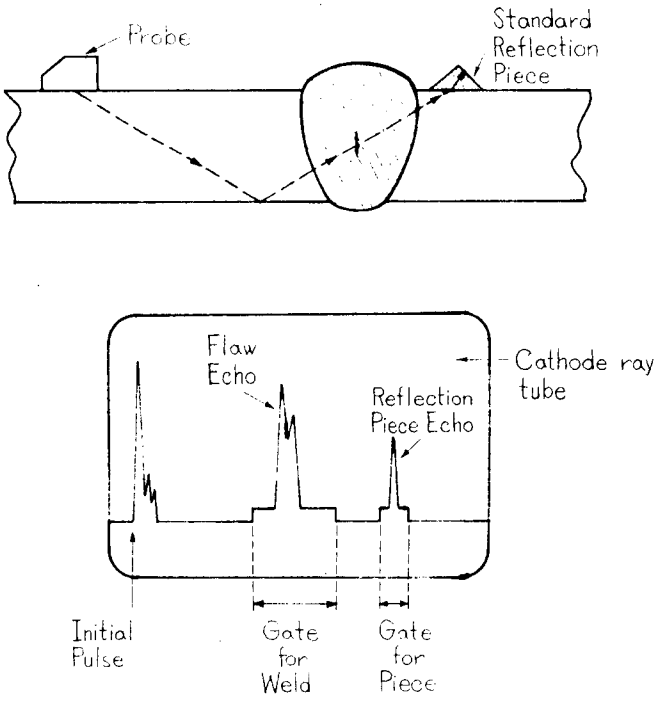

Figure 3.

Appendix

Japanese Industrial Standard
(JIS Z 2341-1955)
Radioactive Ray Penetration Test
for Metals
(EXTRACTION)

"4. *Grading Classification of Test Results*

"4.1. The evaluation of radiographic test results shall be made by photographic-negative taken direct.

"4.1.1 The weld zone shall be classified into 6 grades according to the standard shown in Table 3."

Table 3

Maximum thickness of test specimen (mm)	5.0 Max	5.1–10.0	10.1–20.0	20.1–50.0	50.1 Min
Grade 1	0	0	1 Max	1 Max	1 Max
Grade 2	2 Max	3 Max	4 Max	5 Max	6 Max
Grade 3	4 Max	6 Max	8 Max	10 Max	12 Max
Grade 4	8 Max	12 Max	15 Max	18 Max	20 Max
Grade 5	12 Max	18 Max	25 Max	30 Max	40 Max
Grade 6	Having a greater number of defects than Grade 5				

Remarks: The numerals in the Table indicate the number of defects found in the area of 10 x 50 mm in the region of highly concentrated defects. The sizes of defects are assumed to be less than 2 mm in length but those exceeding 2 mm shall be multiplied by the coefficients given. A defect exceeding 12 mm and containing a crack shall be considered of Grade 6.

Size of defects mm	2.0 Max	2.1–4.0	4.1–6.0	6.1–8.0	8.1–10.0	10.1–12.0
Cœfficients	1	4	6	10	15	20

Analysis of the Strengths of Aluminum Repair Welds

SHELDON LEONARD, JAMES K. S. LEE and JOHN S. CHASTY, U.S.A.

ABSTRACT: A program was conducted to (1) determine the effects of multiple repair welding on the tensile strengths of 6061-T6 fusion welds, and (2) develop a nondestructive test method to monitor the changes in strength due to these repairs. The program was limited to the analysis of fusion welded 0.090-in. 6061-T4 material; the weldments were subjected to uniaxial tensile loading after artificially age-hardening to the T6 condition.

Successive repair welding produced significant strength reductions as determined by the uniaxial tensile test data. These reductions ranged from 6,600 psi (16 per cent of control average) for one repair cycle to 15,600 psi for three repair cycles. In contrast, welded samples containing extreme amounts of porosity rejectable to MIL-R-45774-STD II, failed at higher average strength values than weldments subjected to single and multiple repair cycles.

The effects of multiple repairs were expressed in terms of electrical conductivity measured in the heat-affected zones of the parent metal. These data were statistically analyzed and compared with the mechanical test results. The conductivity measurement method devised during the course of this investigation readily indicated weld area strength by changes of the conductivity in the heat-affected zone of the metal. Ultimate weld strength relative to heat effects can be predicted with a confidence level of 95 per cent based on prior test data.

Introduction

Radiography is the nondestructive test most widely used for the inspection of thin-gauge aluminum fusion welding. Cracks, inclusions, porosity, and similar type defects are readily detected by this method. Anomalies are recorded pictorially in essentially true size in two dimensions. Considering the amount of information provided, interpretation is relatively easy. Although the ultrasonic method has been shown to be effective for the inspection of certain weld alloys, thicknesses, and joint designs, radiography is still superior.

This superiority, however, has had a negative effect. Reliance on radiography by most of those concerned with weld quality has retarded the development and use of other weld-inspection methods. Weld-quality specifications are usually based on radiographic standards, which limit the use and acceptance of results of other nondestructive tests. The limitations of radiography to provide a complete quality evaluation are not widely known nor understood. These limitations are emphasized in the case of the nondestructive inspection of aluminum repair welds.

This report describes a program conducted by Lockheed Missiles and Space Company (LMSC) to perfect a nondestructive test which would provide quantitative information of repair weld strength. These data are vital in situations involving multiple repair welds of heat-treatable aluminum alloys.

Background

Two factors motivated the study to analyze the strengths of repair welds nondestructively. One was the misuse of radiographic information in rendering dispositions of repaired welds. The other factor was the little attention shown to metallurgical changes occurring in the parent metal adjacent to repairs in relation to the importance placed on the presence and magnitude of porosity in such welds.

The misuse of X-ray inspection came as the result of placing too much importance on it. This was revealed in several ways. First, the weld specification would usually indicate radiography as the only nondestructive test. Second, the X-ray standard contained thorough descriptions of grades of porosity, including formulae for calculating porosity area per unit length of weld and minimum distances permitted between porosity. All this information implied a direct relationship between porosity in a weld and the performance (strength) of the weld. This implication was made regardless of alloy, welding technique, or type of service imposed on the weld. This implied relationship, not verified for the alloy in question, could, and occasionally did, lead to a weld being repaired many times until it passed X-ray inspection. In the meantime, the metallurgical changes arising from these repairs were not evaluated. Fortunately, experienced shop liaison engineers prevailed on the matter of porosity, resulting in a broader range of acceptance.

The following brief discourse provides a basis for understanding why the present study was necessary.

Conditions affecting the quality and performance of welds fall into two categories. The first category covers defects that are visible or would be visible if the interior of the weld were accessible. Cracks, inclusions, porosity, undercut, and mismatch are examples of visible types of flaws. These are defined and referred to as first-order defects. The other category contains those anomalies that are not visible without high magnification or that manifest themselves in ways not revealed by light energy. These are second-order defects; examples are adverse stress concentrations, severe redistribution of alloying constituents, intergranular and other insidious forms of corrosion, gross variations in chemistry, and micro conditions of first-order defects such as microcracks and microporosity.

It follows that nondestructive tests of welds, or any other material objects, also divide into two groups. The first are those methods that provide visual evidence of first-order defects and, hence, are qualitative. The most widely employed methods, namely radiography, dye penetrant, magnetic particle, and ultrasonic flaw detection make up most of this first group.

The second group of nondestructive tests reveals the presence of second-order defects by measuring some characteristic of the object. Quantitative nondestructive test data are available for correlation to the object's performance. Electrical conductivity and ultrasonic attenuation are examples of these types of tests.

Applying the foregoing information to the situation of evaluating the quality of repaired aluminum fusion welds, it was evident that radiography alone was not adequate. Consequently, in late 1964, a preliminary investigation was performed to determine the effects of multiple repairs on 0.090-in.-thick 6061-T4 aluminum welds.

Two effects, namely ultimate strength and electrical conductivity, were monitored in the repaired areas. The objectives were: (a) to establish the amount of strength reduction caused by the heating from multiple repairs cycles and (b) to devise a quick and accurate nondestructive test to indicate the magnitude of this strength reduction.

Owing to the small number of test coupons (18, exclusive of controls), firm conclusions could not be drawn. This did not prevent the indication of several interesting relationships. For instance, each successive repair cycle reduced the ultimate and yield strengths of the weld specimens. The repairs to the weld nugget areas resulted in a greater strength reduction per repair cycle than did repairs to the weld fusion zone. Changes in electrical conductivity of the weld areas were inversely related to the ultimate and yield strengths, e.g., as the physical strengths of the weld areas were reduced due to multiple repairs, the electrical conductivity values increased. The information obtained from this brief investigation justified repeating the study on a larger, more detailed scale.

Procedure

General

To evaluate the effect of the weld heat damage due to repair welds, it was necessary to fabricate a series of welded test plates on which the various repair cycles could be made. These welded test plates were then machined into test coupons suitable for both eddy-current conductivity evaluation and mechanical testing. Shop personnel, equipment, and fabrication methods were used when possible since it was felt that such a procedure would more closely represent actual hardware fabrication and, therefore, be more meaningful to future shop applications. All laboratory functions were performed by LMSC's Manufacturing Research personnel in the welding, metallurgical, and nondestructive testing laboratories. These functions included electrical conductivity measurements using the eddy-current method, repair welding, age hardening, and mechanical testing.

Detail

A 48 × 144-in. sheet of 0.090-in. bare 6061-T4 material was sheared into 36 equal 4 × 48-in. pieces. After degreasing and edge preparation, the pieces were assembled and welded to make eighteen 8 × 48-in. test plates. The test plates were then radiographed to confirm the over-all weld quality and were eddy-current tested to establish the as-welded electrical conductivity of the heat-affected zone. Next, the control and test coupon locations were established and identified by steel stencil. Each plate contained eight test coupons and six control coupons. Although the final coupon width for both coupon types was $1\frac{1}{4}$ in., the test coupons at this stage were 4 in. wide in order to provide a heat-sink distance between repaired areas (see Figure 1).

The test-coupon repair areas were prepared for repair welding by rotary filing a $\frac{1}{8} \times \frac{1}{2} \times 0.060$-in. groove in either the weld-nugget area or the fusion zone, depending upon which repair type was designated. After repair welding, the beads were removed. The plates were again radiographed to confirm the repair-weld quality and were eddy-current tested to measure the heat-affected zone conductivity. The above procedure was then repeated on those coupons designated as second or third repair cycles. All repairs and conductivity measurements were made on the "top" side of the test plate weld, not on the "drop-through" side. Finally, the plates were sheared into coupon blanks and the blanks were machined into coupons. A final radiographic check and a conductivity measurement of each coupon were made and recorded. The entire group of coupons were age hardened and mechanically tested for ultimate tensile strength (UTS). The conductivity and UTS data were then statistically analyzed.

The test plates were welded per Lockheed Aircraft Corporation Specification No. 1422, using the tungsten-inert gas process. The welding technique was: 275 amps., 26 VAC, 10-in./min head travel, 7/32-in. tungsten electrode, "L" wire feed, and 4043 weld wire. The direction of weld head travel was 90° to the rolling mill direction. All test-plate welds chosen for this investigation were acceptable to MIL-R-45774-STD I. Three in. of plate weld from each end were discarded because of possible weld start-or-stop problems.

Both the control and the test coupons were $\frac{3}{4}$ in. in width at the reduced section dimension and conformed to Federal Test Method Standard No. 151A, paragraph 4.1.3. The test coupons consisted of two main groups or categories: (a) those repaired in the weld-nugget area and (b) those repaired in the fusion zone. Each main group was further divided into three categories of one, two, and three repair cycles. There were 16 coupons in each of the six categories. Each test coupon category, in turn, was represented by 14 control coupons. The control coupons were tested in the unrepaired condition and, therefore, represented the over-all weld quality of the test plate from which the various test coupons were taken. Each coupon was identified as to plate source, location in the plate, repair type (weld nugget or fusion zone), and number of

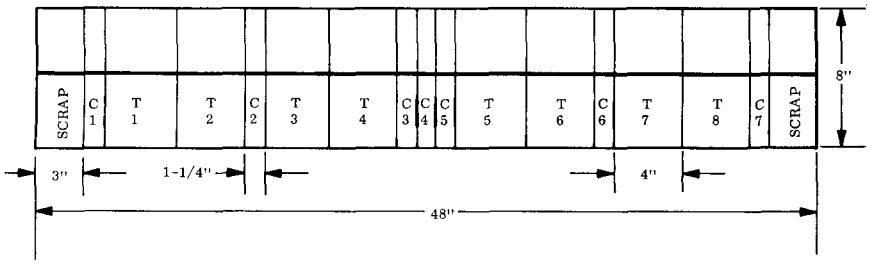

C = CONTROL COUPON BLANK
T = TEST COUPON BLANK

Figure 1
Typical test plate layout.

repair cycles. The repair welding was manually performed with the tungsten inert-gas process using 4043 weld wire.

Eddy-Current Conductivity Test Method

The electrical conductivity measurements were made with an E.D. 500 and an F.M. 103. Both are Magna-test instruments sold by the Magnaflux Corporation of Chicago, Ill. Each was used individually or in combination. All three procedures yielded essentially the same results. The nondestructive test data reported here were obtained by using the E.D. 500 unit with a Flex E. C. number 1 probe. This probe is a special, small diameter ($\frac{1}{8}$-in.) element which has a very small area of influence on a specimen. Because of its high degree of sensitivity and resolution, the probe can be placed adjacent to the weld and can readily distinguish conductivity changes that occur in the heat-affected zones of aluminum fusion welds.

The coupon conductivity was measured in the following manner. The instrument probe was placed on an area of the parent metal not affected by the weld heat, the probe was then moved slowly towards the weld, and the conductivity rise caused by the heat-affected zone was noted. The heat-zone conductivity peak, as well as the parent metal values, were recorded (see Figure 2).

The relative conductivity differences derived from the E.D. 500 unit were converted to absolute unit differences through the use of the F.M. 103 instrument. Throughout this phase of the program, the E.D. 500 measurements were carefully and frequently checked with the F.M. 103 unit. This somewhat involved procedure was necessary because the F.M. 103 probe was large in diameter ($\frac{3}{8}$ in.) and hence averaged the specimen's conductivity, making it unsuited to read small heat-zone changes. The Flex E.C. number 1 probe did not function in the F.M. instrument, therefore the above procedure evolved. All conductivity measurements were related back to the three standards furnished with the F.M. 103 instrument and were expressed as a percentage of the International Annealed Copper Standard (IACS).

Statistical Analysis

A portion of the data, randomly selected, was analyzed, while the rest of the data was used as a check on the analysis. A linear relationship was assumed between the tensile strength and the difference in IACS as measured. The correlation coefficient was calculated to check the linearity assumption. An analysis was then performed to determine the minimum strength for a given difference in IACS with a confidence level of 95 per cent. An analysis of variance was also performed to estimate if there was any significant variation between the control and the test coupon.

The experiment consisted of 12 groups of control and 12 groups of test coupons. From each set of control and test coupons, four data points were randomly selected and analyzed. Thus, 48 data points of the 177 recorded were analyzed. The nomenclature "Y" was the unit tensile strength in hundred pounds, and "X" was the difference between the maximum heat-zone conductivity and the stock. Conductivity was measured in IACS.*

Discussion of Results

The results of both the mechanical tests and electrical conductivity measurements were in agreement with the study discussed under Background. Each successive repair cycle reduced the UTS of the weld area and increased the conductivity of the heat-affected zone. These results are shown by category and repair location in the bar charts of category averages in Figures 3 and 4. The above category-average data are also shown in Figure 5 as a curve of UTS versus heat-affected zone conductivity.

Statistical Results

The curve in Figure 6 indicates the minimum UTS (with a 95 per cent confidence level) for a given heat-zone conductivity difference. The derivation of this curve and the statistical analysis employed are discussed in the Appendix.

Strength Reduction

From the Figure 3 bar chart, it is apparent that no great strength loss difference exists between a weld-nugget repair and a fusion-zone repair. The significant factor is that an average strength loss of 11,200 psi resulted when any given weld area was subjected to three successive repairs. This average strength loss represents 28 per cent of the average as-welded control coupon strength. The greatest individual strength loss resulting from three repair cycles was 15,600 psi, or 40 per cent. It was not an objective of this program to establish biaxial or polyaxial stress loading on repaired aluminum-alloy weldments.

Figure 3 also indicates that an average loss of 16 per cent can be expected when only a $\frac{1}{2}$-in. length of weld or fusion zone is removed and rewelded. In general shop practice, the length of a weld repair is usually much longer than the $\frac{1}{2}$-in. maintained in this investigation. Also, the width of a repair usually exceeds the $\frac{1}{8}$-in. specified in this investigation. Repairing a longer and wider grind-out will, in turn, induce more heat into the parent metal and will result in a greater heat-zone strength loss.

* Statistical data available from the authors.

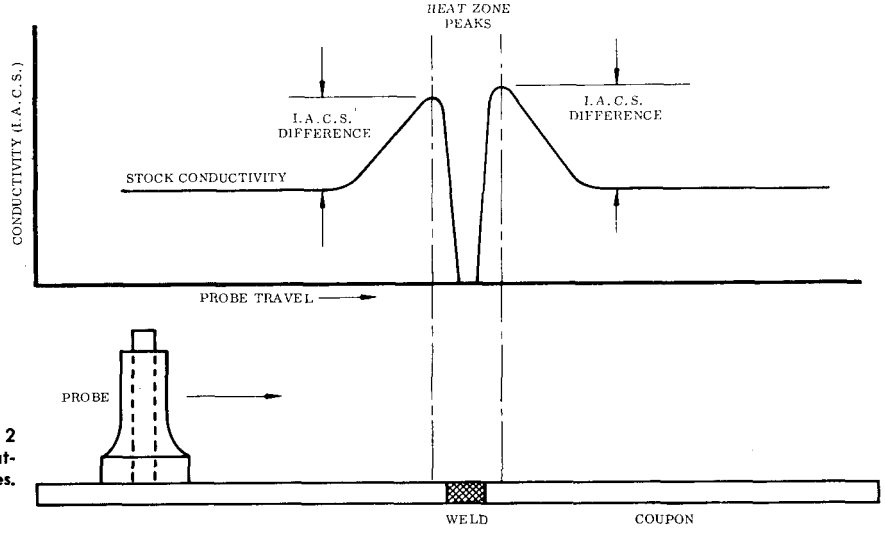

Figure 2
Maximum conductivity at heat-affected zones.

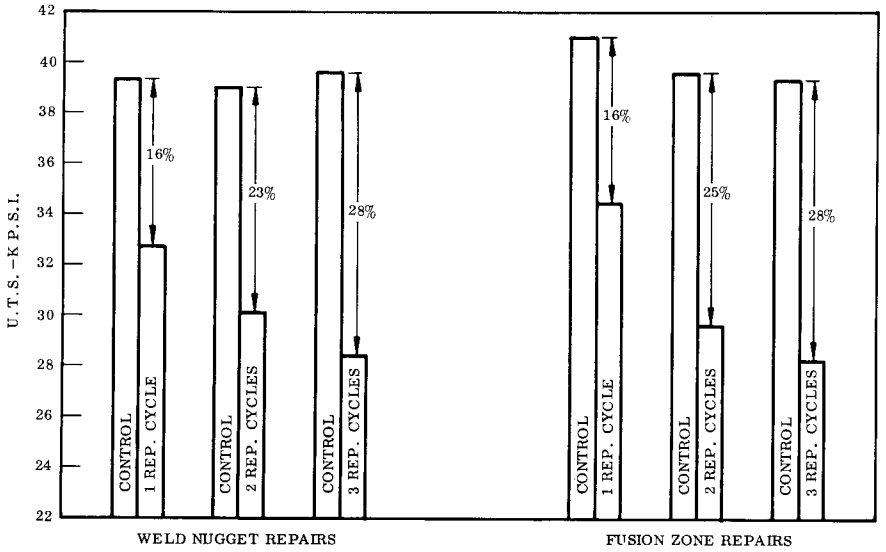

Figure 3
Percentage reduction of ultimate tensile strength (category averages).

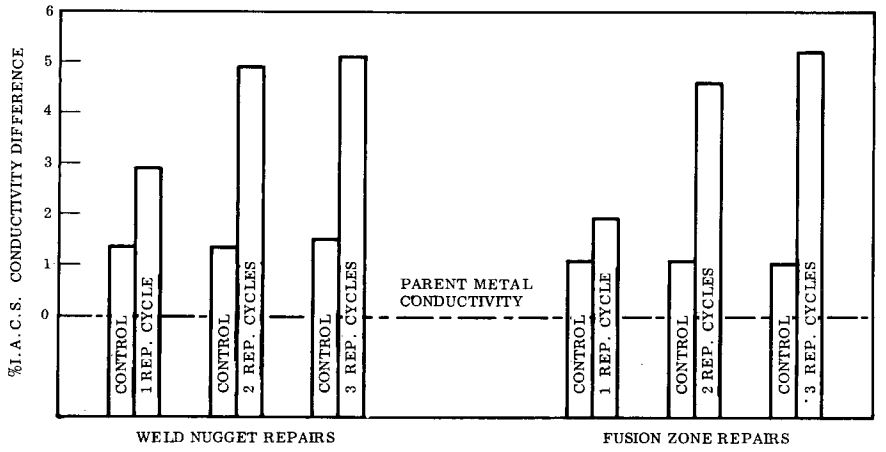

Figure 4
Conductivity increase (category averages).

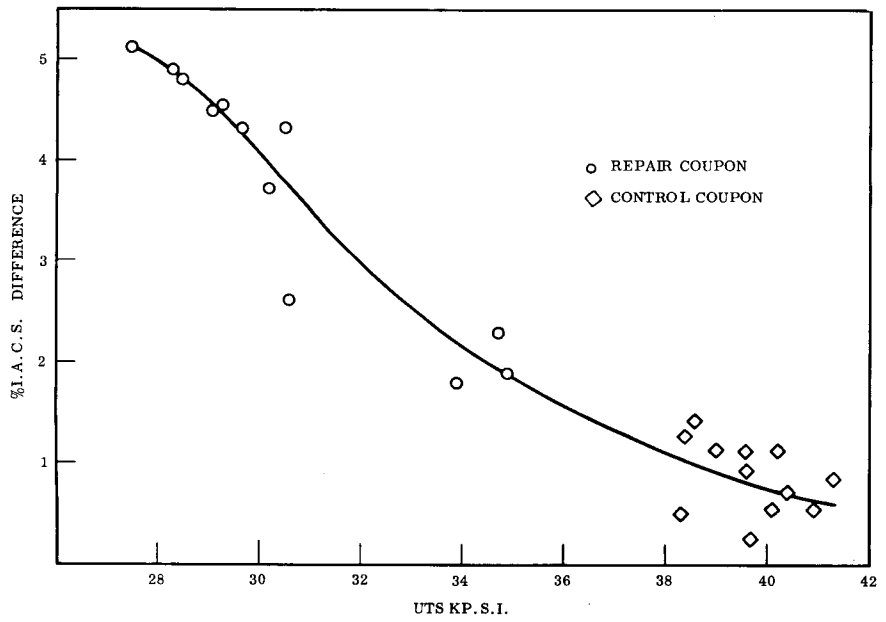

Figure 5
Ultimate tensile strength vs. conductivity (category averages).

A repair-weld strength analysis,* conducted by C. Gott of the Martin-Denver Co. on 2024-T6 aluminum alloy welds, showed similar strength losses for one, two, and three successive repair cycles. The Martin-Denver study did not employ eddy-current strength analysis methods.

Conductivity Measurements

The data in Figure 4 clearly indicate that increasing the number of repair cycles will raise the conductivity of the heat-

* Martin-Denver Co., *Effects of Multiple Repairs on 2024-T6 Aluminum Alloy Weld Joints,* Laboratory Report 62-11-3, Denver, Colorado, 13 Nov. 1963.

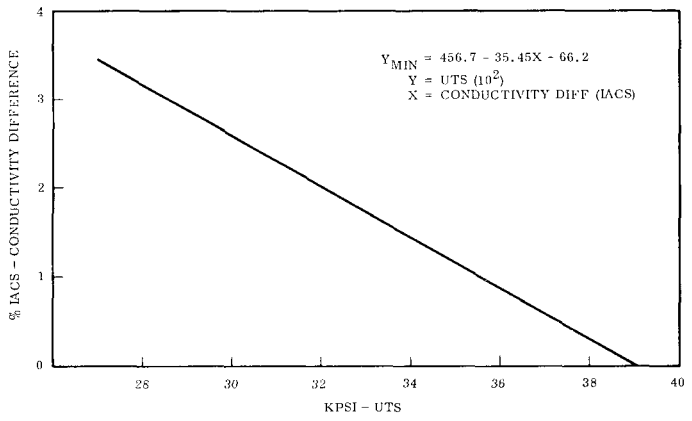

Figure 6. Minimum ultimate tensile strength (95 per cent confidence level) vs. conductivity difference.

affected zone and, in addition, weaken the parent metal in this area. The weld heat distribution of the test plates before repair welding was uniform, as evidenced by nearly identical conductivity measurements taken along each weld edge, and by an even distribution of control coupon fracture locations on either edge of the weld. In contrast to the as-welded control coupons, the manually repaired test coupons displayed a varying edge-to-edge heat distribution and conductivity pattern, particularly those coupons repaired in the fusion zone. Of all the repaired coupons, both weld nugget and fusion zone, 96 per cent failed in the heat-affected zone having the greater conductivity. This again points up the heat damage caused by repair welding.

The curve in Figure 5 reveals the relationship between the weld area heat-zone conductivity average and the average UTS. Of particular interest is the isolation of the control-coupon averages from any of the repaired-coupon averages. This phenomenon could be used as a quick post-weld evaluation to determine the uniformity of the welt-heat distribution and the subsequent size of localized heat-damaged areas. Of greater importance, an eddy-current conductivity check of a repaired area would be a nondestructive strength analysis of the repair heat-affected zone.

Other Results

In addition to the coupons used in this investigation, several other test specimens containing excessive as-welded porosity and drilled holes were subjected to physical testing and radiographic inspection. The as-welded porosity (and, of course, the drilled holes) were far in excess of the minimum acceptable voids in MIL-R-45774-STD II. A comparison of these data to those from coupons of repeatedly repaired welds and radiographically clear, indicated the absence of any relationship between radiographic quality and mechanical strength.

Conclusions

Multiple weld-repair cycles to a given area in a 0.090-in.-thick 6061-T4 aluminum alloy fusion weld reduces the average UTS of the weld joint due to heat damage in the adjacent parent metal. Of significance is the great amount of this strength reduction, i.e., from 16 to 28 per cent of the control average, depending upon the number of repair cycles.

The average electrical conductivity of the heat-affected parent metal increases with each successive repair cycle. These average increases ranged from 2.4 per cent IACS for one repair to 5.3 per cent IACS for three repair cycles.

The UTS of a 6061-T6 aluminum alloy fusion weld joint can be predicted with a confidence level of 95 per cent, if the electrical conductivity of the heat-affected T4 parent metal is known.

The eddy-current strength analysis described herein can be applied before a second or third repair cycle is attempted. A nondestructive strength analysis at this stage could influence a decision as to whether to continue the repair and further weaken the heat zone parent metal, or accept the weld area in its present condition. Obviously, the type and magnitude of the radiographically revealed defect would be a factor in this decision.

Eddy-current strength analysis is recommended as a supplement to, rather than a replacement for, present test and inspection methods.

Inspection and Tracking of Welds Using the New Magnetic Reaction Analyzer

GEORGE H. SMITH and
ROBERT C. McMASTER, U.S.A.

ABSTRACT: A new eddy-current instrument, the Magnetic Reaction Analyzer has demonstrated strong potential as both a sensitive nondestructive test and a guidance control for welded products and automatic welding operations. The magnetic reaction analyzer differs from the conventional coil instruments in that a Hall element is used to sense the magnetic reaction fields. Use of a Hall element as an eddy-current detector in the pickup probe facilitates high resolution and reduced sensitivity to lift-off variations which are always detrimental to an eddy-current system in an industrial environment. The magnetic reaction analyzer in its differential form is useful to perform sensitive nondestructive inspection of welded parts on process lines, in weld mills, or at distribution points whether the test parts are moving at high or low speeds or are fixed statically in jigs. This differential analyzer produces an unusually pronounced magnetic reaction at the edge of conductive materials and at many welds. This reaction is used to form a control signal to track precisely the position of welds and weld preparations so that inspection heads can be accurately referenced to the weld and welding torches, and electrodes can be critically positioned relative to the preparation in automatic welding operations.

Introduction

One of the most interesting application areas of the new magnetic reaction analyzer is its employment in the inspection and tracking of welds and weld preparations. The analyzer systems use Hall elements as detectors, and as a consequence they exhibit a combination of characteristics unlike any conventional eddy-current system. These characteristics are used to definite advantage in the formulation of test and control systems for welded products. A description of the absolute and differential analyzers and their operating principles as they relate to evaluation and location of welds and weld preparations are presented in this paper.

The Hall Element as an Eddy-current Detector

The Hall effect has opened new doors to eddy-current testing. This phenomenon, discovered in 1879 by E. H. Hall, makes it possible to have an eddy-current probe that responds directly to the magnetic vector amplitudes and is insensitive to the frequency of test. Thus, the Hall element introduces the eddy-current probe that is not sensor-limited, as all coil pickups (detectors) must be, by virtue of this inherent sensitivity-dependence on frequency.

A diagrammed representation of a Hall element is shown in Figure 1a. Typically, they are thin (2-10 mils) and rectangular in shape; a common size is 30 × 60 mils. The Hall voltage, measured across the width, is proportional to the product of control current through the element and the magnetic vector component perpendicular to its surface. Therefore, by maintaining the control current constant, a linear response to the normal magnetic vector field is provided across the Hall voltage terminals. The sensitive area of a Hall element is generally circular with a diameter equal to the element width. Good resolution is attainable with this point sensitivity even at very low frequencies.

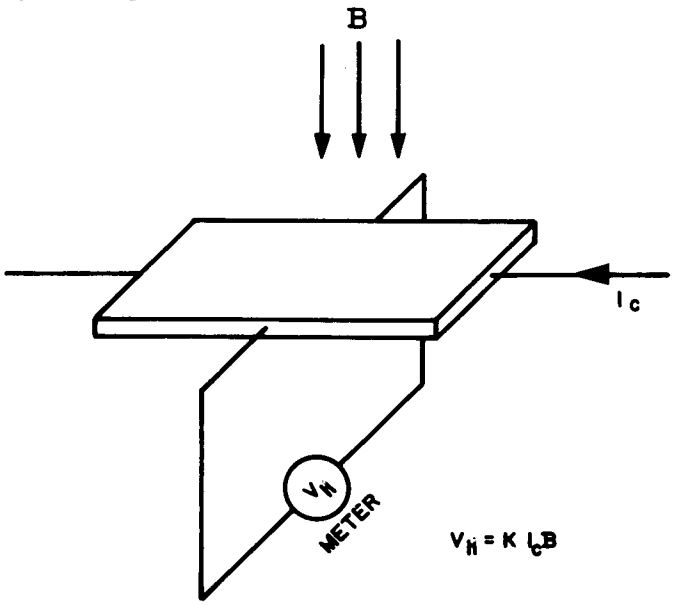

Figure 1a Hall element operation.

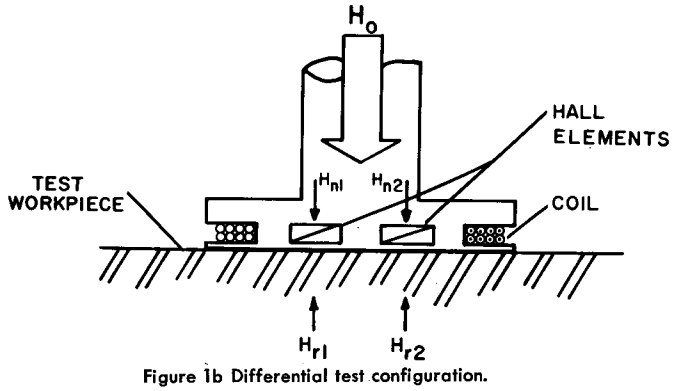

Figure 1b Differential test configuration.

When the Hall element is used as a detector in an eddy-current probe, excitation is provided by a coil that surrounds or is positioned near the Hall element (or elements, when multiple detectors are used). Sensitivity is essentially constant for a given Hall detector for all frequencies of excitation, a feature unattainable with coil pickups. Nearly 100 per cent coupling efficiency of the magnetic vector fields is common because the Hall element can easily be positioned near the test surface. Size, shape and location of the excitation coil are variables that produce significant effects on the probe sensitivity and in a predictable fashion. As the coil diameter (or cross-sectional area for noncircular coils) is increased, two effects are readily apparent.

First, the depth of eddy-current penetration increases. Since penetration depth also increases as the excitation frequency is lowered, two variables of the eddy-current test can be used to improve penetration into the product under test; or where it may be desirable to use a relatively high-test frequency, the depth of penetration can be adjusted by varying the excitation-coil diameter. This can all be done without loss of resolution or sensitivity since the Hall element is the detector.

A second effect that is apparent when the excitation-coil diameter is increased, is a reduction in the effects of lift-off (spacing between probe and test surface). Often normal production-line vibrations introduce lift-off signal variations to an eddy-current inspection system that are considerably larger than those produced by the defect signals which are of real interest. Unless these lift-off signals can be reduced in such a system, the product inspection is a useless operation. The magnetic reaction analyzer probe can be simply designed to give a desired lift-off sensitivity on flat surface and many contoured surface inspections without a sacrifice in sensitivity or resolution, both of which are essentially constant for a given Hall element. Therefore, analyzer probes with large excitation coils provide excellent eddy-current penetration and effectively normalize sensitivity to lift-off, such that variations of ¼ in. can be tolerated for some production tests.

Description of the Magnetic Reaction Analyzers

The Hall element is used for detection in all magnetic reaction analyzer systems. This has produced a new concept in eddy-current testing that features an absolute analyzer with internal standardization, and a differential analyzer useful for both sensitive inspection of a product and accurate control of the production process.

Absolute Magnetic Reaction Analyzer

Direct readout of all of the components of the magnetic vector plane are produced by the absolute magnetic reaction analyzer. The magnetic vector plane might well be considered one of the most direct and most easily understood of the complex plane representations. The means by which these vector quantities are produced and displayed has been covered in several previous papers (1-3). Further treatment of this subject can be found in the new edition of the Nondestructive Testing Handbook (4). A brief description and the performance characteristics of the absolute analyzer that are pertinent to the subject matter of this paper is summarized here.

The absolute analyzer, though not used in industrial application, serves the function of establishing the initial feasibility, optimum test frequency and often the final test-probe design. The instrument provides constant current, variable frequency excitation to the test probe over a frequency range of 20 Hz to 100,000 Hz. A typical absolute probe is composed of a coil that encircles a Hall detector where the magnetic axis of each is aligned, so that nearly 100 per cent coupling efficiency is commonly achieved.

An increase in the magnetic reaction vector H_r is experienced for either an increase in test frequency, electrical conductivity, or thickness for their materials. This would be expected since all of these parameters increase the eddy-current density within a test material. Therefore, when inspection is performed at a fixed test frequency, any material discontinuities

that alter the conductivity or thickness (geometry) of the product under test will be reflected in the magnetic reaction of the eddy-current test.

In practice, a test frequency is chosen to penetrate the material to the desired inspection depth. Coil diameter can be increased for even greater penetration depth. Then fabricated or natural discontinuities can be evaluated in absolute magnetic reaction units (a scale referenced to the fixed excitation amplitude of the probe coil). It is generally possible to determine the smallest discontinuity (of a defined type) that is detectable in the light of normal variations of conductivity and geometry within the test material. When these normal property variations are prohibitive, which is commonly true, a differential probe can be used to minimize these inconsequential variables.

Differential Magnetic Reaction Analyzer

The concept of the magnetic reaction analyzer has been carried further so that high-sensitivity differential testing can be effectively performed in an industrial environment. All characteristics of the absolute analyzer are utilized and even apparently insignificant absolute analyzer variations often can serve as a basis for a practical production test.

A differential magnetic reaction analyzer is depicted in Figure 2a. This instrument provides an excitation field for two Hall detectors that may be located within a single probe. The outputs of the detectors are connected differentially, so that the indicated output of the analyzer represents the difference between the two detector outputs. A high-attenuation filter plug-in module facilitates noise-free operation in electrically noisy environments. The system block diagram in Figure 2b shows that the indicated vector output is the difference of the net magnetic vectors at two discrete test locations.

Differential testing with the differential analyzer is generally performed with a test probe in which two Hall detectors are encircled by a single excitation coil. A configuration of this type is diagrammed in Figure 1b. Local property variations within a product such as defects, voids and metallurgical nonhomogeneities can often be detected with this type of configuration to the exclusion of long-term variables such as gradual changes in wall or material thickness, physical properties or heat-treat condition. This is because long-term variables do not change abruptly, and hence affect two closely spaced Hall detectors in like manner. This same probe configuration is used to formulate precise guidance systems for process control applications.

Defects, voids and metallurgical nonhomogeneities within a material that, at least in part, lie in planes parallel to the axis of the test probe can often be detected with standard differential analyzer system when a local change in conductivity or

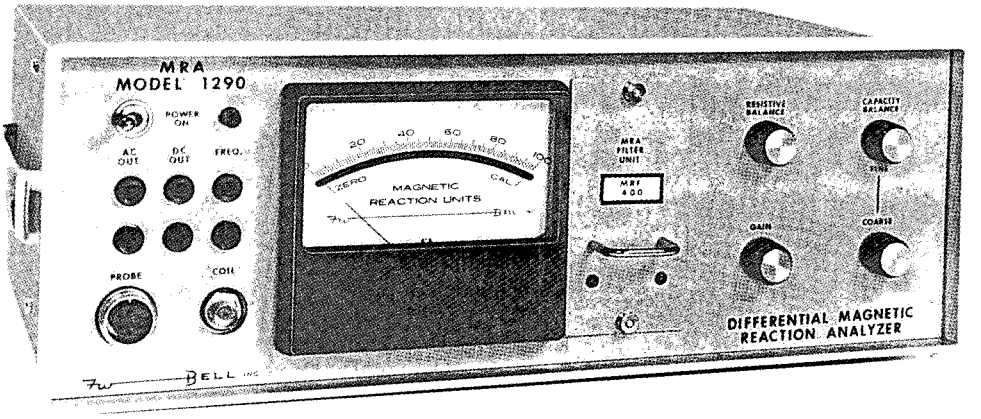

Figure 2a
Differential magnetic reaction analyzer (F. W. Bell, Inc.).

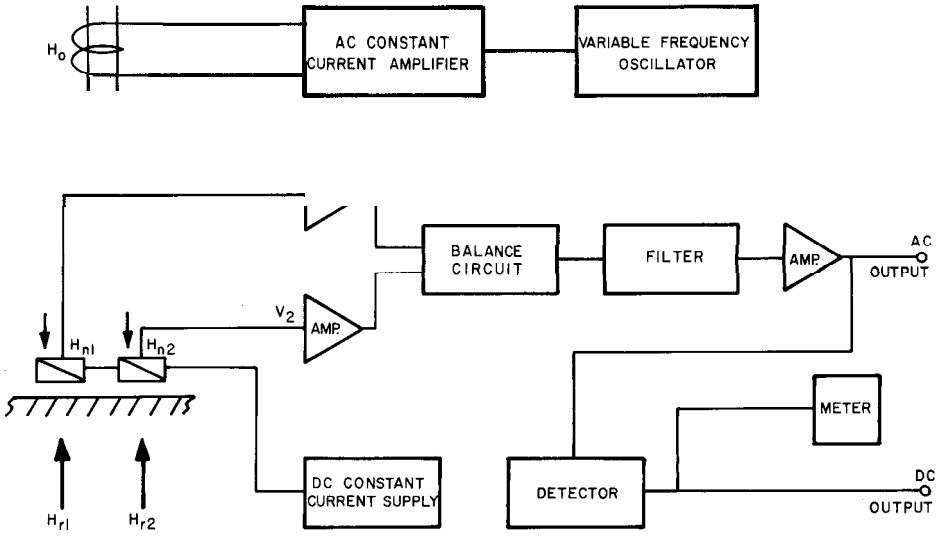

Figure 2b
Block diagram of differential analyzer (F. W. Bell, Inc.).

BLOCK DIAGRAM MRA 1290

geometry is produced by the discontinuity. Laminar defects that lie totally in planes parallel to the surface of the test part are not detectable with probe techniques since the flow of eddy currents is also in planes parallel to the surface except when diverted by edges of, or transverse discontinuities within, the test part.

Eddy-current inspection with probe systems has, in general, been highly unsuccessful because of the false output signals resulting from mechanical noise and vibration. Because lift-off response of the magnetic reaction analyzer probes is totally predictable and controlled, this noise problem can usually be resolved even in demanding production environments. Even further lift-off compensation is afforded by the differential probe configuration since both Hall elements sense identical lift-off changes and their outputs are connected in electrical opposition (differentially).

Inspection of Welds

Weld inspection is most efficiently performed when only the weld zone is included in the inspection. When an additional area is covered by the test, excessive power units are sometimes necessary and resolution required to detect small defects is generally sacrificed. In particular when the weld is longitudinal, a line inspection is all that need be performed with the analyzer by scanning the probe along the weld zone. On weld mills, inspection can even be performed with a near-stationary probe as the weld passes under it. Where curved welds or weld skew must be followed, tracking of the weld position is many times feasible using an analyzer system to provide positioning correction.

Depending on the required level of sensitivity, an inspection path from 0.030 in. to $\frac{1}{2}$ in. can be provided with a standard differential probe that has two Hall elements in it $\frac{1}{4}$ in. apart, each being an $\frac{1}{8}$ off-centre. Typically very high sensitivity can be achieved with a scan path width of about $\frac{1}{8}$ in. This is accomplished by twisting the test probe within a fixture so that the effective spacing between the Hall elements, with respect to the direction of scan along a weld, is $\frac{1}{16}$ in. If each element is considered to have an effective range of $\frac{1}{16}$ in., then together they will scan two adjacent $\frac{1}{16}$-in. paths—a total scan-path width of $\frac{1}{8}$ in.

The depth to which inspection can be performed may be adjusted, using the variable of test frequency and, when necessary, the excitation coil diameter. However, it is sometimes advantageous to select the coil diameter and/or shape to minimize the pesky effects of lift-off. On large parts large-area excitation coils facilitate deep penetration (to 1 in. in brass and around $\frac{3}{4}$ in. in most aluminum alloys) and can tolerate unusually large lift-off variations (to $\frac{1}{4}$ in. on steel). By selecting the appropriate test frequency either surface or subsurface discontinuities can be emphasized for a given material, since the depth of penetration varies inversely with the root of the test frequency. If only surface discontinuities or leakers are of interest, a high-test frequency would be a logical choice.

Inspection of welded tubing is commonly accomplished with encircling eddy-current coils, even though nearly all objectionable defects are located in the weld zone. Much higher sensitivity and, consequently, far more critical inspection of the weld in welded tubing can be performed with a differential analyzer probe referenced to the weld seam. This is logically so, since encircling coils must view the total body of the tube, and property variations throughout the body of the tubing produce signal variations that only serve to mask the information of interest from the weld zone. Because the resolution of the weld area is so greatly improved, sensitivity to lack of fusion, root defects, and other inside-diameter weld imperfections is often possible.

Figure 3 depicts differential analyzer output signals for scans made along a longitudinal weld seam for two pieces of stainless steel tubing. Both welds appeared good on the $3\frac{1}{2}$-in.-dia tube outside-diameter surfaces, but further examination showed that weld penetration was not complete at the root of the weld on the inside-diameter surface of one.

Tracking of Welds and Weld Preparations

An interesting characteristic of the basic analyzer probe design is its unusually pronounced reaction to the edge of a conductive

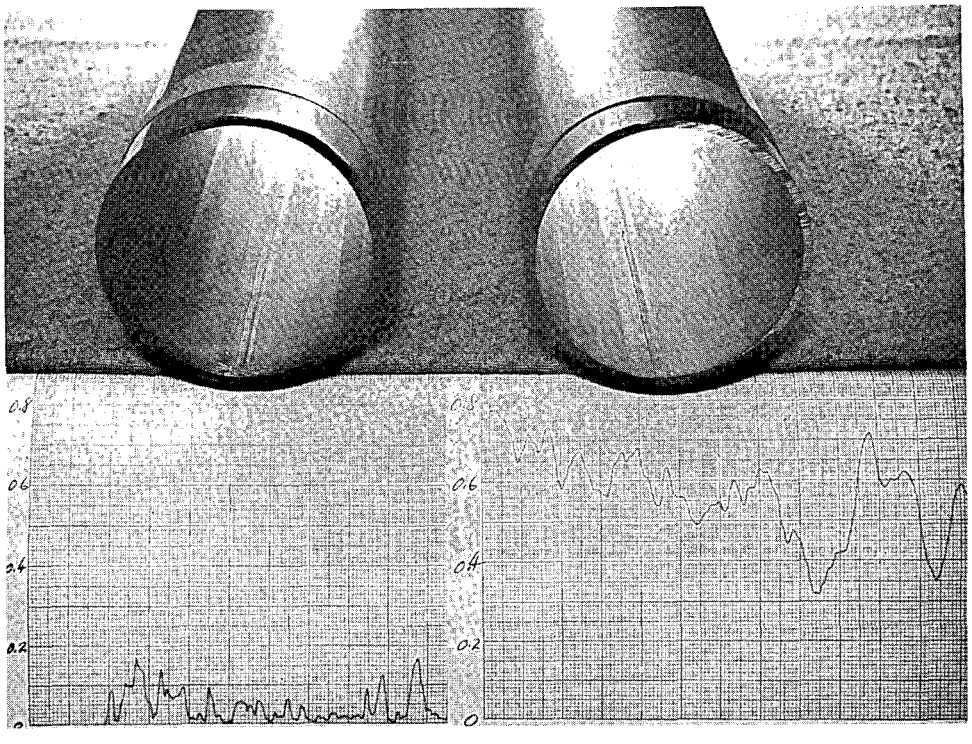

Figure 3
Differential analyzer output signals for weld seam scans of two stainless steel tubes, 3-½ OD.

material. When the probe of the magnetic reaction analyzer is remote from edges of the test material, consistent readings are obtained over conducting materials of uniform properties and thickness. Negligible effects upon signals are observed as the probe is moved towards the edge of the specimen, so long as the magnetizing coil of the probe remains wholly over the test material. However, when the Hall detector is just within the edge of the material, it is subject to the strong demagnetizing effect of the distorted eddy-current path. If the Hall detector is just outside the edge of the conducting test material, this magnetizing effect is reversed. This distortion and reversal is shown in Figures 4(a)-(d).

This remarkable effect is the result of the point sensitivity of a Hall detector being located in a relatively large excitation field area. Just outside the material edge the magnetic reaction (H_r) of the eddy currents is reversed from its normal direction and aids the exciting field (H_0) of the excitation coil. Numerous applications in process control, weld tracking and guidance of automatic welding electrodes are now feasible using this magnetic-reaction analyzer concept.

At an edge of a material or at a through-crack location, the circular eddy-current paths are totally diverted along the edges (Figure 4d) and significant differences in H_r, the magnetic reaction field, are noted. If a longitudinal variation in conductivity, permeability, or geometry (such as many welds represent) exists along a material, only a certain percentage of the eddy currents are diverted along the line of property discontinuity or weld. Often this variation is sufficient to produce enough change in the magnetic reaction so that a weld is easily detected and useful as a control signal for guidance systems.

If an absolute probe (single Hall detector probe) is scanned across a weld zone, an increase in the magnetic reaction vector, H_r, is normally experienced at the weld. The exact location of the weld can be easily defined in this manner. However, when positioned to the side of the weld it is impossible to discriminate one side of the weld from the other by merely observing the reaction signal, since both provide identical information.

If instead, a differential probe is positioned over the weld such that the two Hall detectors straddle the weld, not only the amount of offset, but also the direction of offset from the weld is indicated. Figure 5 depicts the three possible probe positions over a weld and the corresponding differential analyzer ac output signals. As the probe senses any wander of the weld from the balance (centred) position, the control signal created commands a servo-controlled system to immediately eliminate the positioning error. Such positioning correction is useful for guidance of inspection transducers on, or a given distance away from, a weld, or for precise referencing of welding electrodes or arcs along the weld preparation.

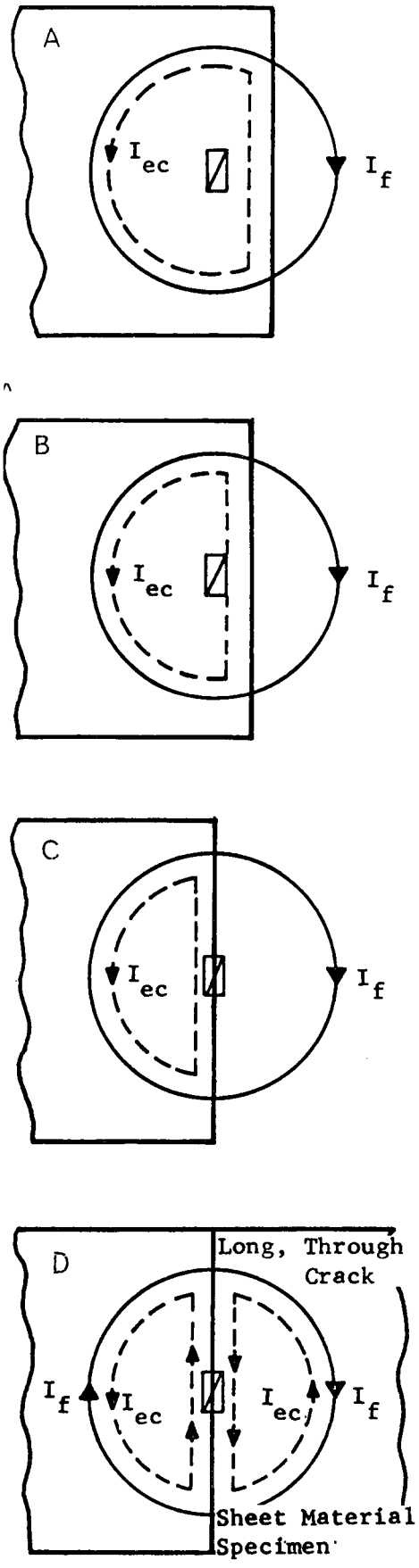

Figure 4
A. Path of eddy current when probe magnetizing coil extends partially over edge of sheet material. Demagnetizing field of eddy currents is increased as flow path approaches Hall device (shown as black square in centre of magnetizing coil). B. Path of eddy current when Hall device at probe centre approaches edge of sheet material. (very high demagnetizing field acts upon Hall detector). C. Path of eddy current when Hall device at probe centre is located outside edge of sheet material. In this case, the magnetic field of eddy current is reversed, and aids the magnetizing coil, resulting in field strengths greater than probe coil magnetization at the Hall detector. D. Eddy-current distribution when probe is located over a long, through crack in thin sheet material. (Note that eddy currents flow in opposite directions along each side of the through crack, producing an intense reversed magnetic reaction field due to the clockwise effective current flow which aids the field of the magnetizing coil current, I_f).

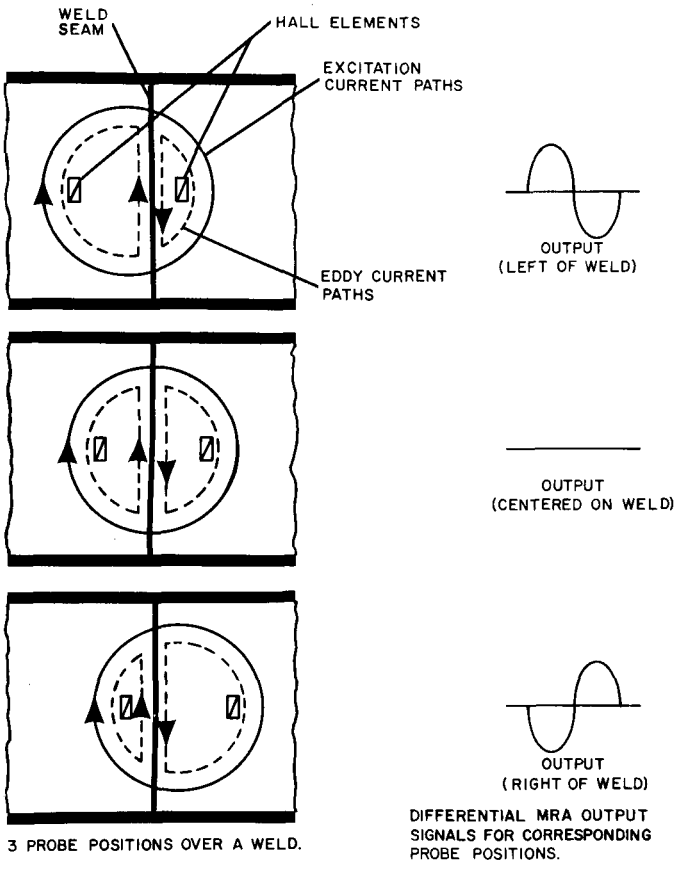

Figure 5 Differential MRA output signals produced for various probe positions over a weld.

Accuracy of such a tracking signal is limited by the backlash in the mechanical gearing and can conceivably be held to a fraction of a mil for applications that require such precision. Normal variations in material properties can also serve to limit the accuracy, but often metallurgical and geometrical nonhomogeneities can be normalized in the preparatory stages of a production process.

Many applications may not require this degree of accuracy, so that other means of control may be entirely suitable. One such possibility is the use of reversing dc motor control. In this case, the ac output of the differential analyzer is used to feed a standard synchronous detector and electronic gate combination which can directly furnish signals for multi-speed dc motor correction.

Tracking and Inspection Systems

The differential form of the magnetic reaction analyzer is useful as both a critical inspection and accurate guidance control system. When sensitive inspection of a weld must be performed at production rates of speed, both functions can often be accomplished with identical electronic systems. The advantages in terms of maintenance, personnel training, and general simplicity of using identical systems are evident.

Of paramount importance in the successful operation of systems of this type is a well engineered mechanical referencing unit. It is many times necessary in this area of mechanical fixturing to attempt a best-effort type of design and hope that in the final testing it will prove to be adequate. This nonscientific approach can only be eliminated when it is possible to produce sound, reliable, lift-off curves in terms of absolute, not relative, units that are readily reproducible without referring to fabricated standards that often prove to be dissimilar.

Conditions common to production, such as vibrational noise, are represented in early test stages of system development with the magnetic reaction analyzer, and studies are made of these conditions that result in tabularized and plotted relationships. These data are all in terms of magnetic reaction units, an absolute unit scale that is established within the absolute analyzer unit. This internal standardization that produces an identical calibration on every absolute analyzer makes data meaningful and reproducible in remote locations without any reference to test standards or blocks of material that can change with time and environmental conditions.

When the fundamentally important relationships have been determined for a given application, the test or control system mechanical unit can be designed from this information on a knowledgeable basis. Tolerances for various motions and mating parts can be dictated so that the unit will be adequate but not unnecessarily overdesigned, an expensive element in any type of system.

An example of a dual-function test and control system and mechanical referencing unit is shown in Figure 6. This is a production unit to track and inspect the weld on small-diameter tubing. This is typical of the magnetic reaction analyzer systems that are finding broad areas of application in industrial welding processes because of their linear sensitivity at all frequencies, sensitive point resolution, and minimized lift-off sensitivity.

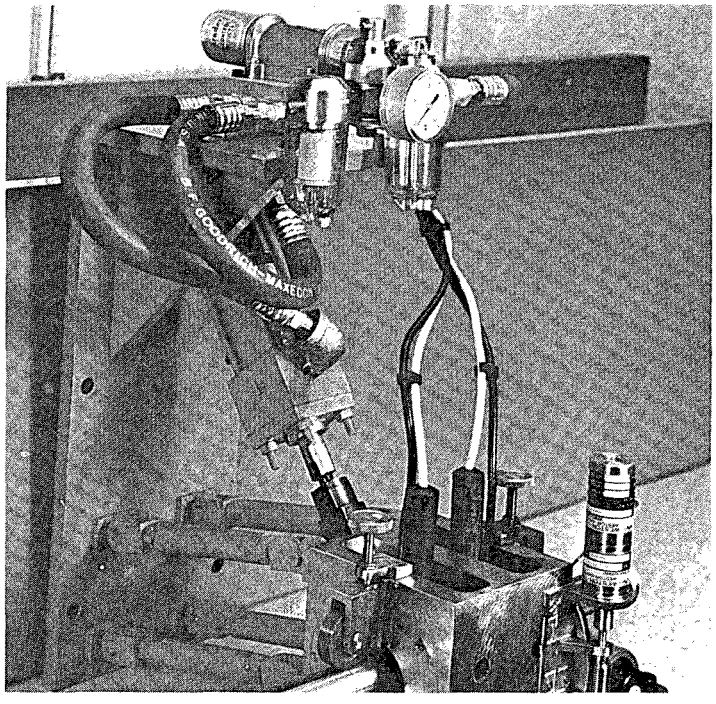

Figure 6 Mechanical referencing unit used for tracking and inspection of welds on small diameter tubing.

References

(1) McMaster, Robert C. The magnetic reaction analyzer—A new eddy-current nondestructive test. Presented at *Am. Soc. for Metals Congr.,* November, 1965.

(2) McMaster, Robert C. and Smith, George A. The magnetic reaction analyzer—A new tool for maintenance inspection and control. Presented at *Am. Soc. Mech. Engrs.,* Plant Engineering and Maintenance Conference, April, 1966.

(3) ——Principles of the magnetic reaction analyzer (A new probe-coil type eddy-current test). Presented at *Soc. Nondestructive Testing,* November, 1966.

(4) McMaster, Robert C., Editor;—Complex plane representations of eddy-current test condition; The magnetic vector plane. Nondestructive Testing Handbook, 1967.

Scientific Principles of Introscopy

P. K. OSHCHEPKOV, USSR

Introscopy, a new trend in science and technology, has of late emerged and developed in the Soviet Union as a natural requirement of modern technical progress.

In the most general sense introscopy means direct vision inside opaque bodies and media. Its main aim is to develop methods and apparatus which ensure the study of the inner properties and qualities of materials, parts of machines and processes, which are impenetrable to usual light, without destroying them.

There are very few transparent bodies and media in nature because the visible part of the spectrum of electromagnetic waves constitutes only a very small part of the multiformity of the known types of radiation. Such bodies and media can literally be counted on the fingers. They are water, air, vacuum, quartz, rock salt, fluorite and several more natural formations. There are also very few artificial transparent materials. Of these only glass and a few plastics may be mentioned. Opaque bodies constitute the overwhelming majority in nature.

However, if the type and spectral composition of the radiation is chosen correctly, it is possible, on the basis of transforming these invisible radiations into optical visible images, to make the whole world, as it were, transparent. In this connection it is not out of place to mention here that for a flux of neutrino-type elementary particles even the terrestrial globe is transparent.

The achievements of physics (beginning with the discoveries of Becquerel and Roentgen), especially those of modern technical electronics, have made it possible to consider introscopy one of the practically soluble problems of our time.

The needs of production, research, medicine, etc., urgently require the development of high-speed methods of obtaining, treating and establishing the fullest possible—i.e., multiple-unit —information directly from the inner spheres of the investigated or controlled bodies and media. By making extensive use of the most diverse types and spectra of penetrating radiations, introscopy as a method of producing and obtaining multi-unit information, is one of the real methods of solving such problems.

The physical basis of introscopy is the interaction of the penetrating radiations with the substance in which they are propagated. This interaction may express itself in a change and in variation of the absorption coefficient of radiations in the manner of their propagation inside the radiated body, as well as in a change of the characteristics correspondingly connected with reflection, diffusion, dispersion, polarization, diffraction, nuclear reactions, magnetic resonance and other phenomena.

In the most general sense the capacity of introscopy to inform is determined by the physical nature of the penetrating radiation and the mechanism of its interaction with the substance of the radiated or controlled body, namely, the intensity, spectrum and geometry of distribution of the flux of penetrating radiations; the material, structure and geometry of the object being studied; the speed with which the multi-unit information is obtained and treated; the method of registering the images in the invisible fluxes of penetrating radiations; the share of the effectively absorbed energy in the receiving element; the type and parameters of the transformer and amplifier of the images; the method of discriminating the images of introscopic information; and the type of logical and computing machines used.

Many types of optically formed or spatially distributed fluxes of penetrating radiations, from gamma-quanta of high energies to radio waves of millimetre and submillimetre bands, and from high-frequency resilient oscillations to corpuscular radiations, may be used as agents capable of carrying multi-unit information about the internal structure, composition and properties of opaque bodies and media. Fluxes of neutrons and other particles with a still higher penetrating ability may also be used for the same purposes.

Nowadays many new scientific and technical problems are solved on the basis of already known technical elements and of finding new interrelationships between them. This also applies to the problem of introscopy. It is confirmed by the example of using the near infrared radiation for purposes of introscopy. The "MIK-I"-type infrared microintroscopes, first built in the Soviet Union, have made it possible to effect direct vision in single crystals of silicon, gallium arsenide and a number of other semiconductor materials.

However, the problem hinges on finding fundamentally new technical ways, owing to the special demands made of such apparatus.

What are the most essential and most important methods of technical solution?

The specific character of simultaneous reception and transformation of multi-unit information through optically formed or volumetrically distributed fluxes of radiant energy consists in the fact that many types of radiations cannot be directly transformed into a distributed electron flux by the known methods of transformation, for example, through the external photoeffect. The reason is that in some cases (e.g. long-wave infrared radiation, submillimetre and millimetre radio waves) the energy of separate quanta is fundamentally insufficient to overcome the work of photo-electron yield, while in other cases (e.g. gamma-quanta and high energy accelerated particles) the energy of the quanta or particles is too great to produce such an effect, and leads to their negligibly low absorption in the surface layer of the emitter.

The solution to this problem was found through elaboration of an entirely new principle of receiving and transforming optically formed or spatially distributed fluxes of radiant energy. This principle rests on the fact that the received radiation is in this case used, not for direct influence on the photoelectric cathode, as is done in all the usual electron-optic transformers, but for the creation of a so-called electric potential relief (electric image) outside the electron-vacuum apparatus. The electric potential relief is then used for controlling the secondary electron or photo-electron emission inside the electron-vacuum apparatus. To transfer the external electric potential relief into the electron-vacuum system, it was necessary to develop new materials which combine vacuum strength and properties of anisotropic electric conductivity, i.e., electric conductivity only in one direction (Figure 1).

Technically the new principle of transforming distributed fluxes of penetrating radiations was embodied in "Unikon-55"-type universal transformers. The principle of action of such apparatus can be explained as follows (Figure 2): the electric relief created in the receiving element and reflecting the received image in the flux of invisible radiations directly, and with the

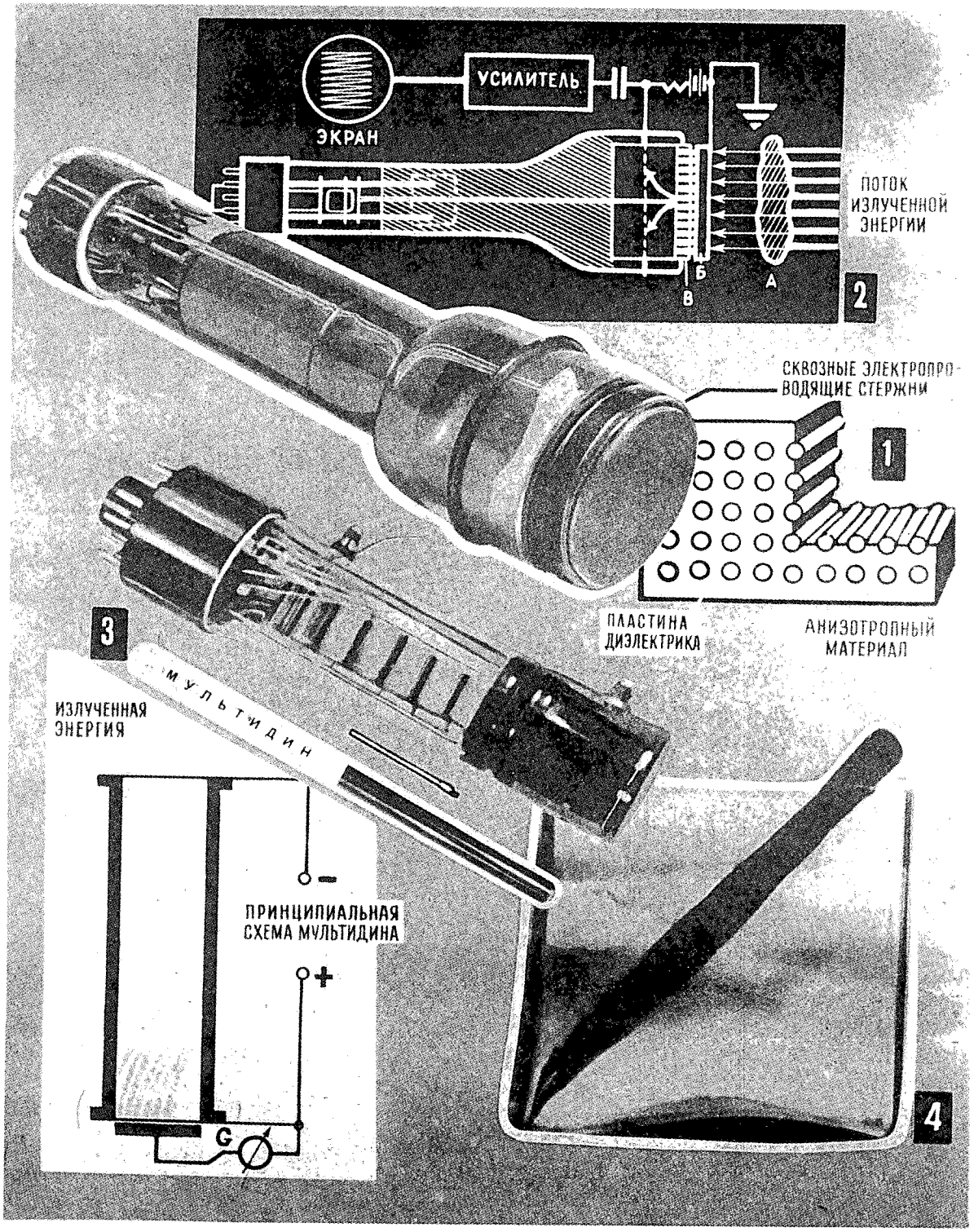

Figure 1. Material possessing electric conductivity only in the direction of the axis of the apparatus. Figure 2. Fundamental scheme of "Unikon": A-body being studied; B-receiving element. Figure 3. A multidyne. Above it are a match and a normal multistage photoelectronic multiplier shown for comparison. Figure 4. Introscope screen showing pincers immersed in a cuvette containing an opaque liquid.

same spatial distribution in the plane of reception, is transmitted within the electron-vacuum apparatus. This transfer is effected because the anisotropic material of the inlet of the apparatus has electric conductivity only in the direction of the axis of the apparatus. In all other directions this material acts as an insulator. Such material may number from 1,000 to 10,000 and more conducting elements per one square centimetre.

The anisotropic material of the inlet of such a transformer is covered on the inside, i.e., on the side of the vacuum, with a thin film that possesses secondary-electron emission, and secondary electrons will therefore be emitted from this film when the electron beam passes over its surface. The value of the secondary-emission current will follow exactly the value of the electric potential at the point of interaction of the electron beam

with the surface of the emitter, and the current from the collector will carry television information corresponding to the received image in the penetrating beams.

The principle of reception and transformation of penetrating radiations through the external electric potential relief is universal and in its further development it will ensure a considerable expansion of the different types of radiation used for purposes of introscopy.

In the apparatus in which the principles and methods of introscopy are used the receiving and transforming elements are in one complex with the radiating devices. This extends the possibilities of introscopy because insufficient intensification of the received multi-unit information may in this case be compensated for by the power of the radiation source. However, we must take into consideration the fact that in its further development introscopy will undoubtedly come across such materials and processes that their control is possible only at weak and ultra-weak radiation fluxes. This is dictated by the requirements of biological protection, when using any penetrating radiations, as well as by the necessity of obtaining information on very small physical changes in the media in question.

These requirements bring forward the problem of developing methods of simultaneous reception and amplification of the weak radiation fluxes and isolating signals which lie below the background level. Theoretical and experimental studies have shown many basic principles of radio engineering, and electronics may successfully be transferred to the sphere of light, magnetic, semi-conductor and even mechanical phenomena. Here, too, there are extensive prospects for using, in photoelectronics, principles analogous to those of radio engineering and also for finding such properties in them as differ qualitatively from those of radio engineering.

In the reception of single-channel information it was possible to show that the elaborated principle of photoelectronic supergeneration (analogous to the superregenerator) displays not only considerable amplification (about 10^5-10^6)—high sensitivity to a weak signal—but also makes it possible to receive a weak signal against a background which exceeds the received signal 100-fold and more. This is particularly important in studying images of objects with a weak contrast. The phenomenon thus discovered has a high degree of non-linearity.

The subsequent development of this principle relative to simultaneous reception of multi-unit information has led to the creation of a system of multichannel electronic amplification.

The many years working out systems of multichannel secondary electron amplification have resulted in putting into practice the principle of uninterrupted secondary-electron amplification which we named, for the sake of brevity, multidyne.

The distinguishing feature of multidyne is the absence of separating electrodes (unlike all types of photomultipliers) and the possibility of making the smallest desirable amplifiers (down to the size of a micron). The coefficient of multidyne amplification is in principle unlimited. Only the thermal stability of the material itself is the limit.

The principle on which the multidyne works can be seen in Figure 3. Only one tension is fed to the tube, made of high-resistance, but nevertheless conducting, material. An increasing distributed potential is placed along the tube and, consequently, an increasing electrical field inside the tube. Under the action of this field the electron emitted from any point of the inner surface of the tube will move along a parabola. And, if the calibre of the tube, i.e., the ratio of the length of the channel to its diameter, is large enough (about 50-60), the electron will soon meet with the opposite wall of the tube at a point whose potential will in this case necessarily be higher than the potential at the point of its emission. Thus the electron, picking up this difference in potentials, will cause a secondary emission at the point of incidence. This will be followed by a chain electron multiplication which will very soon lead to amplification of the primary signal a thousand—, a millionfold, and even more.

A single-channel multidyne, but not the smallest, compared with the usual photoelectron multistage multiplier, is shown in Figure 3. This multidyne is the size of a match, but multidynes can be made scores and even hundreds of times smaller.

This principle has now been theoretically and experimentally confirmed. An engineering realization of various systems of multidynes and further development of their theory will make a serious contribution to technical electronics and radio engineering; this principle of amplification is now being developed in many countries.

No development of high-speed methods of controlling and investigating materials and processes, especially when studying very important objects, is thinkable unless the results of radiation can be recorded at the same speed. The "Unikon"-type universal electronic transformers make it possible simultaneously to solve this problem also, since the use of materials with anisotropic electric conductivity permit of transferring the distribution of the electric charges inside the vacuum system without any distortion to any dielectric material outside the vacuum system. The methods of developing such electric charges on dielectric materials are already well enough known.

Such electronic videographic recording of the results of observations in the form of images, graphs, figures and codes will also be very useful for computing engineering. In such devices the rate of printing may be brought up to 20,000 signs a second.

The multi-unit introscope information obtained in fluxes of penetrating radiations is conditioned by the interaction between the quanta or particles of radiations of various energy and the substance being studied. In evaluating the information obtained an important role must be played by methods of analysis, particularly spectral methods of its investigation. Elaboration of systems of coloured and stereoscopic introscopy may be one of the possible results of such investigations. But for the nearest practical problems the spectral analysis of information makes it possible to separate the irregular anomalies from the regular ones in the process of studying the substance. With the existing highly sensitive primary elements this becomes very important.

Such are the basic scientific and technical problems of introscopy formulated in their most general fundamental significance. It should be noted that these fundamental propositions give rise to an enormous number of scientific and practical problems.

Stemming from the aforementioned problems is the necessity of working out specialized analogs and computers for discerning the introscopic images obtained and studying the information capacity of penetrating radiations during interaction with substance.

The importance of introscopy is hard to over-estimate. It has vast fields of application. It is necessary to many branches of the national economy, practice, scientific experiment and medicine. In engineering, for example, it is necessary in studying the quality of metals and, especially, new materials developed on the basis of minor materials and polymers, plastics, ceramics and pyroceramics, for improving the methods of defectoscopy, determining the sizes of types and orientations of defects, the

degree of reliability in the work of aggregates, in studying fatigue stress, internal stresses, etc. In metallurgy the application introscopy is necessary for studying and controlling the kinetics of high-temperature processes on the metal-slag borderline; for automatically controlling the quality of hot and cold metal in the process of rolling on blooming and slab mills; in tube- and sheet-rolling production. In the chemical industry the methods of introscopy are needed for active control of a number of technological processes.

Introscopy will play an important role in building for it may be used in studying the strength of building materials and structures. Introscopy will also find application in geology and hydraulic engineering.

Introscopy has found one of its first applications in studying the quality of semi-conductor materials and the optic efficiency and homogeneity of single crystals impenetrable to visible light. But this is only the beginning. In the field of semi-conductor materials, and in the field of quantum radio electronics much is still to be done to extend the application of introscopy to make it possible not only to observe structural and chemical anomalies, but also to study electrical processes at the border of transition with different conductivity, to observe the real distribution of currents inside semi-conductors, and to study the topology of thermal fields, etc.

Infrared microintroscopes have made it possible to see directly into single crystals of semi-conductor materials. In scientific experiments introscopy is needed for studying the relief of magnetic, electromagnetic and ultra-high-frequency fields, in radio astronomy—for studying the spatial structure of radio signals—and in biochemical and encephalographic research—for studying pathological changes in the living organism.

To improve the work of ports and airfields under unfavourable meteorological conditions, it is also necessary to have means of seeing through opaque or barely transparent obstacles. Under these conditions introscopy can solve the problem of seeing through fog, rain, clouds, etc.

There is no need to list further the fields of application of introscopy. It is sufficient to suggest that its application will be wider than that of microscopy and telescopy, since introscopy rests not on a narrow region of visible light, but on the enormous range of electromagnetic radiations, as well as other types of radiation, including corpuscular fluxes and resilient oscillations.

In summing up we may merely state that the emergence of introscopy was in a measure predetermined by the development of such now powerful branches of technology as computing engineering. It is generally known that the achievements already made in this field have widened the prospects for developing the most diverse systems of automatic control and regulation. It has now become possible to use computing engineering in many branches of science and technology, from metallurgy and machine building to scientific experimentation and from agrotechnics to medicine and biology. Automation, systems of control or, in a more general sense, cybernetic devices offer unlimited opportunities for application and are of paramount importance to the national economy because, in the long run, a consistent rise in labour productivity, which society needs so much, depends on their development. But effective utilization of this large store of devices may be ensured only if the means of obtaining objective primary information are ensured. Insufficient attention has as yet been devoted to problems of developing techniques of obtaining such information, and a clearly marked gap between the requirements and the possibilities has formed as a result. As an example, mention may be made of the fact that a number of the most highly developed countries now already have several thousand electronic computers, whereas for control of industrial processes, i.e., for control with feedback, and improvement of the processes, the number of machines in use is only in the hundreds. The control of technological processes, the determination of the degree of dependability and quality of materials, parts of machines and structures, and especially the technical diagnosis of particularly expensive objects require new and high-speed methods of obtaining primary information.

All the now existing pick-ups, electrical, mechanical, thermal, ultrasonic and other values make it possible to obtain information mainly of a local or composite character. The ammeter, for example, makes it possible to measure the strength of electric current in the chain of a semi-conductor apparatus, but furnishes no information on the distribution of current inside this apparatus. The nominal value of a certain ohmic resistance does not as yet mean that its physical properties are homogeneous in cross-section or surface, that it does not have zones of dangerous concentration of possible overload, etc. The temperature of the exhaust gas of a jet engine has a complex spatial distribution. The same may be said about the distribution of internal forces of stress. The temperature of the human body also shows a complex picture of its distribution along the surface, as well within the internal organs.

These conditions very naturally gave rise to the necessity for multi-unit information characterized by the spatial distribution of these and other similar physical properties inside the studied or controlled body. Many problems of modern technology can no longer be solved without such information. This is particularly important in the problem of technical diagnosis which determines the degree of dependability of various devices, schemes and structures.

Modern technical progress presents a number of other requirements which determine such a problem.

Most things and materials used in modern technology are, as is well known, impenetrable to visible light. That is why the problem of penetrating inside opaque bodies and media must be solved by the new trend in science and technology—introscopy—which, as has already been stated, in the most general sense means seeing inside. In a broader sense this implies a complex of means which makes it possible to obtain multi-unit information in the form of an electric potential relief capable of being subsequently treated quantitatively or logically by means of electronic computers. Direct visual perception of information on cathode-luminescence or other screens is, as it were, a specialty of introscopy.

Practically speaking, in the final analysis our eye also works to elaborate electrical impulses. The neurons of the cerebral cortex actually treat not the image on the retina of our eye, but the sum of electrical signals reaching them along optic nerves. This suggests a rather important analogy with bionics for the subsequent development of introscopy.

All the means of modern electronic computing engineering with its systems of control and automation may be regarded as a complex of means for treating information and issuing command signals, whereas introscopy is the obtaining of primary information for such treatment. The development of techniques of penetrating inside opaque bodies and media with the aid of all available types of radiations and fields, is destined to play an increasingly important role.

Technical Session 5/Visual Aids in NDT

Television Systems for Nondestructive Testing

HAROLD BERGER, U.S.A.

ABSTRACT: The methods of operation of a number of unusual television techniques are discussed, as are the capabilities of each system in regard to sensitivity, resolution, contrast, and speed of response. Emphasis is placed on those television techniques which respond to X-radiation, infrared, ultrasound, and neutrons; ultraviolet and light sensitive television systems also receive some attention. In addition to the discussions of each system, the general areas of application of television systems for nondestructive testing are outlined. Included is a discussion of the advantages and limitations of television techniques as applied to the nondestructive testing area. Several methods for recording and using test data from such television systems are given. An extensive bibliography is included.

Introduction

The dictionary definition of television refers to this term as the transmission and reproduction of a scene by a device which converts light into an electrical signal and then back into light. This definition is unduly restrictive, in that one can use television techniques to display images formed by radiations other than light. Many such radiations involve other portions of the electromagnetic spectrum, such as infrared, ultraviolet, or X-radiation. Radiations outside the electromagnetic spectrum, such as ultrasound or neutrons have also been used with television techniques. All of these radiations can be very useful for nondestructive testing applications. It is primarily these unusual television systems and their potential for nondestructive testing with which this report is concerned.

Many of the systems make use of television camera tubes which are directly sensitive to the radiation of interest. Others employ some detection device which converts the radiation of interest into a radiation, such as light, which can be more easily handled by conventional techniques. The characteristics of the detection devices are discussed, with particular attention being devoted to the sensitivity, resolution, and contrast capabilities of the detection device, and of the complete television system. Data recording techniques for nondestructive testing television systems are also discussed since many application situations require that inspection records be retained for later examination.

Electromagnetic Spectrum Television Systems

Of course, the largest percentage of television systems in use are those devoted to the detection of light. Many light-sensitive television systems are used for the observation, inspection, or control of inaccessible processes, and may, therefore, properly be designated as nondestructive testing television systems. Since these light-sensitive systems are outside the primary interests of this report, we shall give a few references to such studies (1-7) and then consider other television techniques.

By far the majority of these other television systems now in use are those used in medical and industrial X-ray imaging systems. Such systems respond to a wide range of X-ray energies and are available in many forms. These include those in which the camera tube itself responds to X-radiation (8-11), and other systems in which the X-radiation is converted to light by means of fluorescent screens (12-15), or image intensifier tubes (16-20). These latter systems make use of light-sensitive television equipment to provide a television presentation of the converted X-ray image. Such equipment has been used to present X-ray images in the high-Mev X-ray energy range (14, 15, 18-21) and, in the other extreme, has been used to view X-ray diffraction patterns (22) and medical X-ray images (12, 16, 17) in the Kev energy range.

It is difficult to generalize as to the performance capabilities of these systems, since so many different types are available. Generally, however, those television techniques which employ phosphor screens to detect the X-ray beam, as in the image intensifier and fluorescent screen systems, provide resolution capabilities in the 0.25 to 0.50-mm range. An order of magnitude improvement in resolution can be obtained if one uses a small X-ray vidicon camera technique (11). The resolution improvement in this case comes at the expense of useful image area, and the X-ray intensity required for viewing. This latter property, of more interest for medical rather than industrial applications, varies from a value of about 30 R/min at the face of the X-ray vidicon tube for a routinely useful image presentation, to values about 1/1000 of that for medical X-ray examinations with X-ray image intensifier systems.

The image area covered in an X-ray television system presentation is of some importance. For industrial inspection applications a traversing mechanism for moving a large object through the inspection area can, in some cases, reduce the importance of this property. Nevertheless, for examinations of very heavy objects, or in cases in which it is desirable to view at once an object area large enough so that the viewer can easily orient himself (this is of some importance in medical applications, for example), the area factor can be important. Sizes vary from the scanned area of a small X-ray vidicon camera tube (11) (about 1.2 × 0.95 cm) to the 30-cm-dia fluorescent screen sizes used in commercially available fluorescent screen-image orthicon television systems (23). Image intensifier tube systems typically provide useful X-ray detection diameters betwen 12.5 and 22 cm although tubes having detection diameters as large as 27.5 cm have been built (24). X-ray

vidicon tubes having useful detection diameters as large as 30 cm have also been used in some medical X-ray investigations (25).

The contrast capabilities of the various systems are given in a recent review (23) by Vincent et al. Thickness changes as small as 1.5 per cent can be detected under optimum conditions with most of the X-ray television systems; for most practical conditions, penetrameter sensitivities in the range of 2 to 4 per cent can be achieved.

The other two portions of the electromagnetic spectrum of interest from a television point of view are those on either side of the visible spectrum, namely ultraviolet and infrared. The ultraviolet region has not received much attention from a nondestructive testing point of view, so it will receive little attention here. Camera tubes directly sensitive to ultraviolet radiation have been made and used, however, primarily for biological work in the field of ultraviolet microscopy (26).

In the infrared region, there has been a wide range of activity in the development of image intensifier and other imaging devices. Only a few of these latter devices readily lend themselves to television techniques since they include phosphor (27) or other coating techniques (28-30), mechanical scan techniques with point detectors (31), and oil film imaging techniques (32). Image intensifier tubes and other camera tube techniques utilizing photoemissive layers (33) do lend themselves very well to television techniques. However, these devices are limited to the near infrared region (to about 1.2 μ) and are useful for testing applications for materials only at fairly high temperatures (one would need a temperature almost that required for incandescence, or about 450°C). Photoconductive television camera tubes (34) for response in that spectral range are also available and have similar limitations.

Vidicon television camera tubes directly sensitive to infrared wavelengths in the 2 μ and higher region have also been described (35-37). A camera tube having response to a wavelength of 2.3 μ has been evaluated for use in nondestructive testing applications (37). This tube, easily used with glass optics and with standard closed circuit television equipment, was shown to be useful for observing hot objects having a temperature at least 170°C. At object temperatures of 350°C or higher, a surface temperature difference as small as 3°C was detectable. The speed of response of the tube was comparable to other vidicon systems (11) in that it displayed an image of a 12-mesh screen moving as fast as 45 cm/min without appreciable blur.

The type of image presented is illustrated in Figure 1, which is a reproduction of three frames of a kinescope motion picture recording. The image shows a cooling, metal jacketed reactor fuel pin; sodium is contained inside the jacket to provide heat transfer between the fuel and the jacket. As the fuel pin cools after having been heated to about 500-600°C by a radiant heater, the portion of the fuel pin containing sodium cools more slowly since a greater mass is involved. Therefore, this technique reveals the sodium level; it is shown on the figure by the obvious difference in surface temperature (white represents a higher temperature) and is indicated by the pointing finger.

Ultrasonic Television System

Ultrasonic techniques lend themselves to television methods, a fact which was recognized long ago (38). In fact, a great deal of effort has been expended in past years to devise methods for imaging ultrasonic patterns by one method or another, at least partially because it was realized that an image presentation of the ultrasonic information eases some of the interpretation problems. Much of this effort is described in several review articles (39-41).

Television system studies in the ultrasonic field have been devoted almost exclusively to the development of television camera tubes directly sensitive to ultrasonic radiation. One such system, shown in Figure 2, illustrates the basic method used. In all cases, the charge pattern developed by a piezoelectric detector is read by an electron scanning beam, thereby providing the video signal. There are a number of differences in the various proposed systems, such as the use of an electron multiplier in the ultrasonic camera tube (42), the use of the piezoelectric target inside the camera tube rather than the double use of the target as the vacuum window of the tube (43) (a technique which can yield larger inspection areas), the use of low-velocity electron scanning beams as opposed to high-velocity scans (44), and the use of pulsed ultrasound rather than the continuous-wave technique now mostly used (43, 45).

Each of these systems provides excellent sensitivity to ultrasound. One report (44) indicates that camera tubes can show response to ultrasonic intensities as low as 10^{-11} watts/cm^2. Generally, the tubes respond to ultrasonic intensities in the order of 10^{-7} to 10^{-9} watts/cm^2; in actual inspection use the ultrasonic intensities used are appreciably higher.

The resolution capabilities of these systems depend upon the ultrasonic frequency used and on the geometry of the image arrangement. For a through-transmission system with a relatively thin object, as shown in Figure 2, one can resolve discontinuities as small as 1 mm, at a frequency of 2 MHz. The resolution would improve with increasing frequency. Resolution capabilities in the order of 1.7×10^{-3} mm at frequencies of 15MHz have been reported (46), and interest has been expressed in system frequencies as high as 100 MHz for ultrasonic microscopy techniques (46).

In some respects, the resolution capability of an ultrasonic television system is associated with the diameter of the inspection area. Those systems employing high frequencies must make

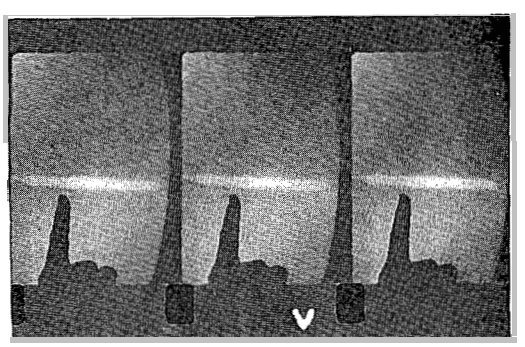

Figure 1
Three frames of an infrared television system kinescope motion picture recording showing a thermal image of a sodium-filled, metal jacketed reactor fuel pin. The finger points to the white-grey image dividing line which is the sodium level inside the metal jacket.

use of very thin piezoelectric receiving transducers, since the resolution of such systems is limited by the larger value of the ultrasonic wavelength, or the thickness of the receiver. Therefore, for high-resolution, high-frequency operation, a thin receiving transducer in a camera tube must be supported inside a vacuum window (43), or, if used as the vacuum window, it must be bolstered by some support such as a metal grid (46), or must be small in diameter if it is to have the necessary strength for use. For systems employing the transducer as the vacuum window of the tube, transducer diameters of 10 cm, 5 cm, and 2.5 cm are typical for 1 MHz 2 MHz and 5 MHz operation, respectively (47).

The sensitivity of ultrasonic television methods for the detection of defects is generally very good, particularly with the direct through-transmission system for the inspection of relatively thin objects (47). Presentations with a continuous wave system would appear as shown in Figure 3. The inspected object in this case was a flat reactor fuel element; it was placed close to the camera tube, angled to eliminate standing wave patterns (48), and translated vertically past the camera tube to provide a complete inspection. The defect noted in Figure 3 was a jacket-core unbonded area which impeded the transmission of the 2 MHz ultrasound. In terms of defect detection, one of the major advantages of the ultrasonic television method over conventional ultrasonic techniques, concerns detection of small discontinuities. For example, in a recent comparison of the transmission of thermal and ultrasonic energy through bonded samples (49), areas of small, suspect, unbonded regions could be found much more easily by the television technique.

Speed of inspection is another potential advantage, in that inspection samples, such as the flat fuel plate indicated above, can be translated through the inspection area as fast as the inspector can follow the motion on the kinescope presentation. In the case of the fuel element, linear object movement (47) as fast as 120 cm/min could be used; the inspection area was about 4.4 cm in diameter.

As one might anticipate, the continuous-wave ultrasonic systems can present standing-wave problems. These can be eliminated or lessened by angling a flat inspection object (48), or by using a thin ultrasonic attenuator between object and camera tube (50). Pulsed systems should eliminate many of these problems, a fact which explains, at least partially, the present development efforts in such systems. Pulsed systems now in use employ a much slower television frame rate (in the order of seconds), as compared to the conventional rates offered by continuous-wave systems. Therefore, at the present stages of development, one can choose a continuous-wave system at conventional television frame rates (1/30 sec, for U.S.A.), a system which can follow rapid object movement but which may have some problem with standing waves, or a slower frame rate, pulsed system. The commercial availability of the former system, coupled with the advantages offered by the fast information rate (a defect indication is much more readily detectable if the observer can watch it move across the kinescope than if the image is stationary), account for the more widespread use of the continuous-wave systems at the present time. As pulsed systems improve (45), particularly if one can gain the improved sensitivity offered by storage systems (46), this situation may change.

Thermal Neutron Television Techniques

Thermal neutrons are a more recent addition to the radiations which can be used with television techniques. The development which has made this possible is the neutron image intensifier (51, 52), a vacuum device which converts a thermal

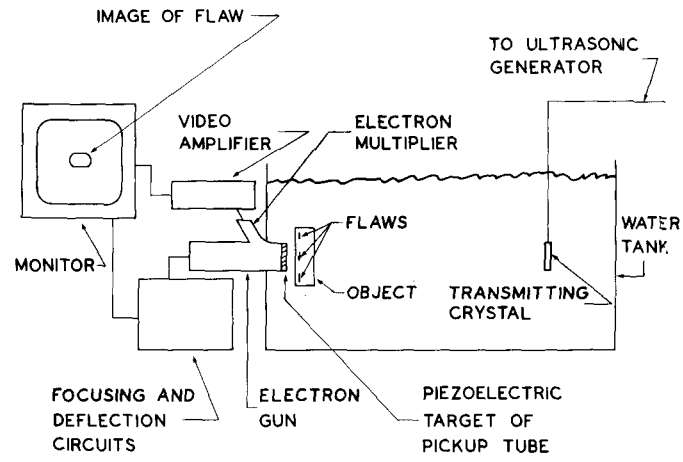

Figure 2a. Diagram of an ultrasonic television system, arranged for through-transmission inspection. The camera tube extends into the water tank from the left.

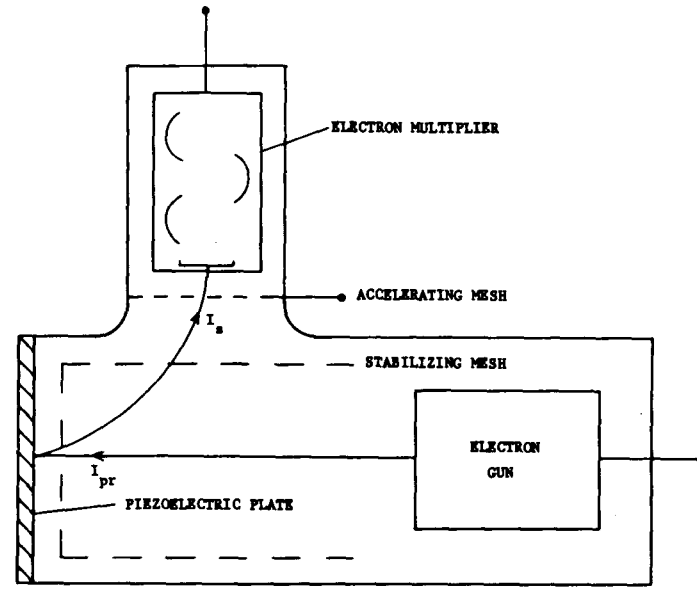

Figure 2b. Schematic diagram of the ultrasonic camera tube.

neutron image into a bright, small visible image. The operation of the intensifier tube involves the conversion of the neutron image into a light image by means of a neutron scintillator. An adjacent photoemissive layer yields an electron image which is then voltage-accelerated towards a small light-emitting, phosphor screen at the output end of the tube. A diagram of such a tube is shown in Figure 4.

The neutron scintillator, as shown in Figure 4, is a mixture of ^{6}LiF and a phosphor powder, in a resin binder. Although the phosphor used in the first tubes and indicated in Figure 4 was ZnCdS(Ag), ZnS(Ag) phosphor used in later tubes has yielded improved results (53) in terms of light yield and in terms of relative neutron-to-gamma response ratio. The basic operation of the tube remains the same for either phosphor; the absorption of neutrons by the ^{6}Li results in prompt alpha particle emission which stimulates the phosphor and yields light.

The gain of the intensifier tube, as in the case of similar tubes used to detect X-radiation, results from the acceleration of the photoelectrons liberated from the photoemissive surface

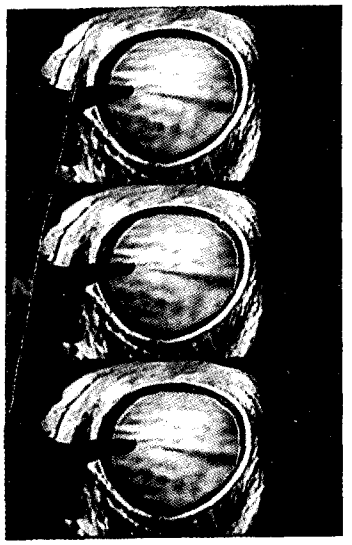

Figure 3
Three frames of a continuous-wave ultrasound television system kinescope motion picture recording, showing a long, narrow jacket-core separation in a stainless steel jacketed, flat reactor fuel element. The finger points to the long, dark defect area within white, ultrasound transmission image. The 5 cm diameter camera tube was overscanned during this presentation with 2 MHz ultrasound; the piezoelectric target image is only in the central round white area.

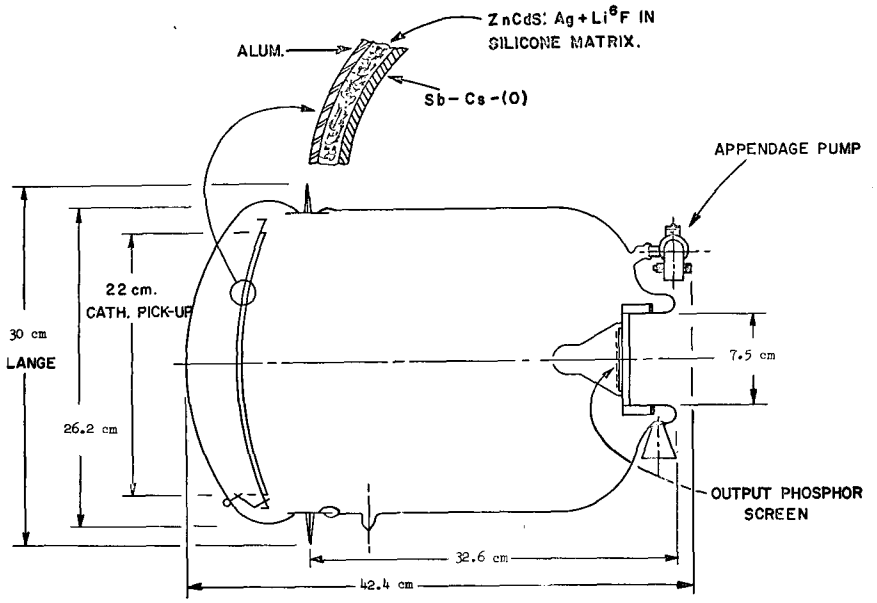

Figure 4
A diagram of a neutron image intensifier tube.

adjacent to the scintillator, and from the minification of that electron image at the time it stimulates the output phosphor. The light yield is linear (52) with neutron intensity, at least in the neutron intensity range from 10^3 to 10^7 neutrons/cm^2-sec; for this higher neutron intensity, an output phosphor brightness as high as 50-ft-Lamberts has been achieved. The light yield from these tubes is such that one can readily detect the light image with a closed circuit vidicon television system for thermal neutron intensities of 10^5 neutrons/cm^2-sec or higher. Image orthicon television systems, which are more sensitive (54) by factors of at least 100 times can be used to improve the response by that factor. Direct observation of the signal at the output phosphor screen of the tube by dark-adapted observers has been accomplished for thermal neutron intensities as low as 100 neutrons/cm^2-sec. Of course, with these lower intensities, one would need some storage device in the imaging system, electronic or photographic, in order to accumulate signal information long enough to obtain radiographically useful images (55, 56).

The resolution capability of the neutron image intensifier tube, and the associated television system is limited by the thickness of the neutron scintillator target in the tube and/or by the neutron imaging geometry for standard line television systems (55). High-contrast images as small as 0.35 mm have been observed through the television system(53).

The contrast sensitivity which can be observed through the television system follows the pattern observed in other penetrating radiation fluoroscopic systems (23), in that best contrast values can be realized in a fairly narrow range of sample thickness. This is shown in Figure 5, in which contrast values for steel, lead, and natural uranium are plotted as a function of inspection sample thickness. These data are for a thermal neutron intensity of 2×10^7 neutrons/cm^2-sec and for visual detection of the thickness change on the television monitor (525 line, 1/30-sec frame time, interlaced system). For very small sample thicknesses the observed contrast is reduced because a fairly large percentage thickness change is necessary to present a given transmitted radiation intensity change. For the larger sample thicknesses, the limitations involve deviation in the number of quanta or neutrons used to present the image, and the results of increased scatter in the thicker inspection samples. This portion of the contrast curve might

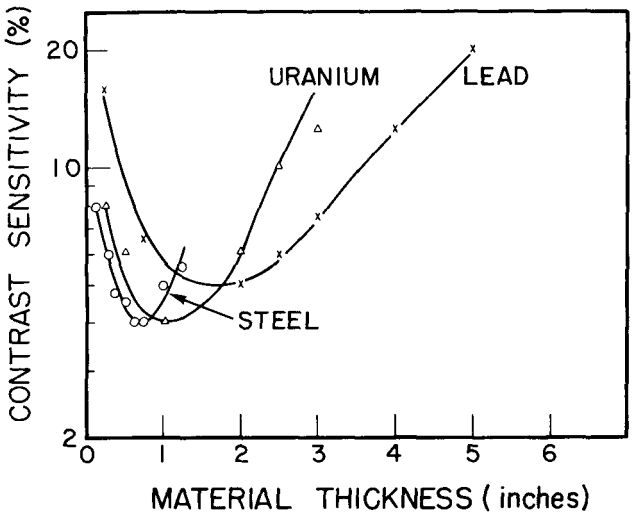

Figure 5. Thickness changes detectable by direct observation of the neutron television system monitor, for steel, lead, and natural uranium. Optimum contrast sensitivities are observed for a narrow thickness range centred about a 1-1/2 half-value layer sample thickness. The thermal neutron intensity was 2 x 10^7 neutrons/cm^2-sec.

be improved by using longer accumulation times (longer than the 0.2 sec normally used for visual observation), and for grids to reduce the influence of the scattered neutrons.

The motion capability of the system is generally good at high neutron intensities. For a thermal neutron intensity of 2×10^7 neutrons/cm^2-sec, a vidicon television system used with the neutron image intensifier has presented good images(55) of relatively high-contrast objects moving as fast as 5 m/min. The limitation on speed in this case is the vidicon rather than the image intensifier. An image orthicon televison system used with the intensifier tube under similar conditions has presented useful television images of high contrast objects moving 2 to 3 times faster than the object motion followed by the vidicon system.

One additional property of this television system is its relative response to neutron and gamma radiation; this is because of the application of neutron imaging techniques for radioactive inspection material, and because of the potential use of such a system with smaller, possibly portable neutron sources (57). Many such neutron sources would have an appreciable gamma radiation background (58).

Intensifier tubes containing ZnS(Ag) in the neutron scintillator target of the tube have been shown to yield an equal output phosphor brightness for either a ^{60}Co gamma radiation intensity of 600 R/hr, or 10^6 thermal neutrons/cm^2-sec. Therefore, if one has available a high-neutron intensity, one can neutron-image through relatively high values of gamma radiation intensity. With a thermal neutron intensity of 2×10^7 neutrons/cm^2-sec, useful neutron images for some applications (53, 59) can be obtained even with gamma intensities as high as 10,000 R/hr.

Although the neutron image intensifier has been developed to a useful state and enables one to assemble a simple neutron television system, other techniques appear to be potentially useful for neutron television techniques. A neutron scintillator, for example, could be used as the neutron-to-light converter, the image then being picked up by a sensitive television system. Argonne work with such a system with the very sensitive neutron scintillator (60) developed at MIT, and now commercially available through Nuclear Enterprises, Ltd. (type NE421), revealed that an image orthicon television system would present useful television images for neutron intensities about 5×10^6 neutrons/cm^2-sec. Of course, one could improve the performance of such a system by using a light image intensifier to amplify the light signal presented to the television camera. Commercially available light image intensifiers can provide gain factors (61) in the range of 10^5; a gain of this magnitude would provide such a system with a neutron sensitivity comparable to that of the neutron image intensifier.

Discussions and Conclusions

Certainly the foregoing material proves that a wide variety of radiations useful for nondestructive testing applications can be used with television techniques. Among the many areas of application are the observation of dimensional changes, as with visible or X-ray systems, the observation of internal structure or details in opaque objects with X-ray, neutron, or ultrasound systems, and the location or identification of bonding variations with systems employing infrared or ultrasonic radiation. Many of the references cited in the discussion of each system describe applications in greater detail. As a general statement, the nondestructive test technique involved in a television method can be used for the same types of applications as are normally associated with the technique. Although in many cases, the dynamic nature of the television method adds application areas which cannot normally be considered with standard techniques.

Among the advantages offered by television techniques is the fact that the information is presented as an image, thereby easing some of the test interpretation problems presented by other inspection techniques. This advantage is perhaps of most importance in the case of ultrasonic techniques because competing imaging methods are not widely used for ultrasonic nondestructive testing. Even in cases in which imaging methods are routinely used for nondestructive testing, the television method provides the significant advantage of an essentially immediate image presentation. In addition, television can be used to provide continuous surveillance of inspection objects as they are heated, stressed, or used in service. The fact that the inspector can easily orient the inspection object in the radiation beam (62) in order to present an optimum inspection result can also be very helpful.

In some cases, similar advantages to those given above can be obtained with other than television systems, as in the case of X-ray fluoroscopy, for example. However, if we add the facts that television systems allow the operator to control the brightness and contrast of his image presentation, that remote and/or multiple viewing of the inspection image is readily obtainable, and that a variety of information recording and processing techniques readily adapt themselves to the electronic television systems, then the over all advantages of television techniques become more apparent.

Limitations of television techniques include the facts that quantitative measurements on the inspection sample often present problems and that, in low signal situations, much of the dynamic nature of the television technique may be lost because of the need to accumulate signal information for long enough periods to obtain useful images. As far as the first limitation is concerned, recent work at General Electric (63) has shown the feasibility of an electronic gating method to measure the temperature of a small portion of an infrared television scene to a reasonable degree of accuracy. Similar techniques appear possible with other television methods, thereby providing a means for obtaining numerical data. As far as the low signal-image presentation rate problem is concerned, it may be regarded as an advantage that storage techniques are readily available

for accumulating signal over an extended period of time. Some storage can be accomplished directly in the camera tube (25, 54, 64); electronic storage tubes (65) and the associated electronics (66) offer versatile techniques for extended storage capability.

In the matter of information recording (47), the techniques available include photography of the television monitor presentation, either still or motion picture (examples of motion picture records are given in Figures 1 and 3) and magnetic-tape recording. Each of these provides a permanent record of the inspection. The magnetic-tape method permits the inspector to review the test information immediately, if desired. Polaroid film still photography would provide similar advantages.

Another recording technique which appears potentially useful is a paper, electrostatic printing method, such as the Videograph system developed by the A. B. Dick Co. A resolution capability of less than 1 mm, and the capability for displaying at least seven shades of grey make this system attractive for many recording applications (67). It appears to be particularly adaptable to slow-scan television systems and/or to modified single-line scan systems in which the paper speed matches that of the object movement through the inspection area. A system of this type is now being considered for use with the ultrasonic television system as applied to the inspection of flat reactor fuel elements. A 1:1 recording of the ultrasonic transmission pattern through the inspection sample should result.

We should also consider those cases in which one need not look at the inspection image at all, but would automatically obtain interpretation information by means of physical masking techniques (21), or by computer methods (68). Such techniques are particularly attractive in cases involving large numbers of inspections. Computer techniques lend themselves very well to television inspection methods, in that one could easily compare an electronic signal inspection result to a stored signal containing acceptable-limit information, in order to determine acceptance or rejection. Such techniques appear to have an important future in nondestructive testing.

References

(1) Barratt, P., and Waters, I. M. Application of closed-circuit television in the nuclear industry, *J. Brit. Inst. Radio Engrs.*, 20, 225, 1960.

(2) Sardyko, V. I. Application of television in science and industry in the USSR, *J. Brit. Inst. Radio Engrs.*, 20, 449, 1960.

(3) Carroll, E. C. Closed circuit television for industrial applications, *Iron and Steel Eng.*, 37, No. 7, 78, July, 1960.

(4) Mayne, L. B. Some applications of closed circuit television in industry, *Machinery* (London), 101, 463, Aug. 29, 1962.

(5) Syke, G., and Burns, C. Closed-circuit television for the inspection of fast-moving surfaces, *J. Inst. Elec. Engrs.*, 9, 296, 1963.

(6) Blythe, R. E. Industrial television in the generating industry, *Indust. Electron.*, 1, 707, 1963.

(7) Oudin, J. Nuclear television, *Nuclear Eng.*, 11, 609, 1966.

(8) Cope, A. D., and Rose, A. X-ray noise observations using a photoconductive pickup tube, *J. Appl. Phys.*, 25, 240, 1954.

(9) Heinje, L., Schlagen, P., and Bruining, H. An Experimental photoconductive camera tube for television, *Philips Tech. Rev.*, 16, 23, July, 1954.

(10) Jacobs, J. E., and Berger, H. Large-area photoconductive X-ray pickup-tube performance, *Electrical Eng.*, 75, 158, 1956.

(11) Mitchell, J. P., and Rhoten, M. L. Closed-circuit television system for X-ray inspection, *J. Soc. Motion Picture and Television Engrs.*, 71, 444, 1962.

(12) Morgan, R. H., and Sturm, R. E. The Johns Hopkins fluoroscopic screen intensifier, *Radiology*, 57, 556, 1951.

(13) Polansky, D., and Criscuolo, E. L. Characteristics of a closed-link television X-ray system, *Nondestructive Testing*, 14, No. 3, 18, 1956.

(14) Pruitt, J. S. Use of crystal to display high energy X-ray images, *Nondestructive Testing*, 17, No. 6, 359, 1959.

(15) Elsip, P., and Lewis, R. J. Television and industrial fluoroscopy, *Brit. J. Nondestructive Testing*, 6, 10, March, 1964.

(16) Coltman, J. W. Fluoroscopic image brightening by electronic means, *Radiology*, 51, 359, 1948.

(17) Teves, M. C., and Tol, T. Electronic intensification of fluoroscopic images, *Philips Tech. Rev.*, 14, 33, Aug., 1952.

(18) Lueckerath, W., Fink, K., and Flossmann, R. A nondestructive method to detect pipes and cavities in hot steel blooms during the rolling-process by means of betatron, X-ray-image-intensifier and television set-up, *Nondestructive Testing*, 18, 27, 1960.

(19) Green, D. T., and Niklas, W. F. An image intensifier tube with high gain for 1 Mev photons, *Materials Evaluation*, 22, 465, 1964.

(20) Nishibori, K., Makino, S., Hashimoto, K., and Kobayashi, M. Nondestructive testing of thick steel plate by means of a betatron, X-ray image intensifier and television system, *Proc. Fourth Internat. Conf. on NDT*, Butterworths, London, 1964, pp. 88-91.

(21) Berger, H., and Pace, A. L. Field performance of a television X-ray system, *Nondestructive Testing*, 15, 26, 1957.

(22) Goetze, G. W., and Taylor, A. Direct viewing and rapid photographic recording of X-ray diffraction patterns, *Rev. Sci. Instr.*, 33, 353, 1962.

(23) Vincent, B. J., Pollitt, C. G., and Halmshaw, R. Image-intensifier systems, *Physics Indust. Radiol.*, edited by R. Halmshaw, Heywood, London, 1966, pp. 407-438.

(24) Hardenberg, J. J. C. An apparatus for cinefluorography with an 11-inch X-ray image intensifier, *Philips Tech. Rev.*, 20, 331, 1959.

(25) Chejfec, G., Danemann, H. A., Milewski, J., Texter, E. C., and Barborka, C. J. Fluorocinematographic and manometric studies of esophageal motility in patients with achalasia, *IRE Trans. on Med. Electron.*, 7, 225, 1960.

(26) Zworykin, V. K., Ramberg, E. G., and Flory, L. E. "Television in Science and Industry", John Wiley, New York, 1958.

(27) Urbach, F., Nail, N. R., and Pearlman, D. The observation of temperature distributions and of thermal radiation by means of non-linear phosphors, *J. Appl. Phys.*, 39, 1011, 1949.

(28) McGonnagle, W. J. "Nondestructive Testing", McGraw-Hill, New York, 1961, pp. 70-91.

(29) Fergason, J. L. Liquid crystals, *Sci. Am.*, 211, 77, Aug., 1964.

(30) Woodmansee, W. E. Cholesteric liquid crystals and their application to thermal nondestructive testing, *Materials Evaluation*, (to be published).

(31) Barnes, R. B. Thermography of the human body, *Science*, 140, 870, 1963.

(32) McDaniel, G. W., and Robinson, D. Z. Thermal imaging by means of the evaporograph, *Applied Optics*, 1, 311, 1962.

(33) Kruse, P. W., McGlauchlin, L. D., and McQuistan, R. B. "Elements of Infrared Technology", John Wiley, New York, 1962, pp. 281-288.

(34) Taylor, S., An infra-red sensitive television camera tube, in "Advances in Electronics and Electron Physics", edited by J. D. McGee and W. C. Wilcock, Vol. 12, Academic Press, New York, 1960, pp. 263-275.

(35) Redington, R. W., and Van Heerden, P. J. Doped silicon and germanium photoconductors as targets for infrared television camera tubes, *J. Optical Soc. Am.*, 49, 997, 1959.

(36) Heimann, W., and Kunze, C. Development of an infra-red vidicon-type pick-up tube with a lead sulphide target, in "Advances in Electronics and Electron Physics", edited by J. D. Mc-

Gee, W. C. Wilcock, and L. Mandel, Vol. 16, Academic Press, Inc., New York, 1962, 217-255.
(37) Berger, H., and Kraska, I. R. Characteristics of an infrared vidicon television system, *Materials Evaluation*, 24, 197, 1966.
(38) Sokoloff, S. "Means For Indicating Flaws in Materials", U.S. Patent 2,164,125, June 27, 1939.
(39) Spengler, G. Problem of acoustical-optical image conversion, *Nachrichtentechnik*, 3, 399, 1953.
(40) Rozenberg, L. D. Survey of methods used for the visualization of ultrasonic fields, *Soviet Physics—Acoustics*, 1, 105, 1955.
(41) Berger, H., and Dickens, R. E. A review of ultrasonic imaging methods, with a selected, annotated bibliography, *Argonne Nat. Lab. Rept.*, ANL-6680, 1963.
(42) Jacobs, J. E., Berger, H., and Collis, W. J. An investigation of the limitations to the maximum attainable sensitivity in acoustical image converters, *IEEE Trans. on Ultrasonic Eng.*, 10, 83, 1963.
(43) Lawrie, W. E., and Feith, K. E. Electronic imaging of ultrasonic fields, *J. Acoustical Soc. Am.*, 34, 719, 1962 (abstract).
(44) Smyth, C. N., Poynton, F. Y., and Sayers, J. F. The ultrasound camera, *Proc. IEE*, 110, 16, 1963.
(45) Sayers, J. F. The future of ultrasonic cameras in industrial inspection, *Ultrasonics*, 4, 92, April, 1966.
(46) Jacobs, J. E. The ultrasound camera, *Sci. J.*, 1, 60, April, 1965.
(47) Berger, H. A television system for ultrasonic imaging, *Argonne Nat. Lab. Rept.*, ANL-7042, 1966.
(48) Berger, H., and di Novi, R. A. Angular positioning of thin metallic samples for optimum continuous-wave ultrasonic imaging, *J. Acoustical Soc. Am.*, 36, 2053, 1964.
(49) di Novi, R. A. Correlation of the heat transfer properties and ultrasonic transmission properties of bonds, *Argonne Nat. Lab. Rept.*, ANL-7074, 1966, p. 18.
(50) Muenow, R. A. A preliminary study of resistance welds by improved ultrasonic image conversion techniques, *Materials Evaluation*, 23, 449, 1965.
(51) Kallmann, H., and Kuhn, E. "Neutron Image Converter", U.S. Patent 2,270,373, Jan. 20, 1942.
(52) Berger, H., Niklas, W. F., and Schmidt, A. An operational neutron image intensifier, *J. Appl. Phys.*, 36, 2093, 1965.
(53) Dolon, P., Berger, H. and Niklas, W. F. An improved neutron image intensifier tube, *13th Nuclear Science Symp.*, Oct. 19-21, 1966, Boston, Mass., to be published in Proceedings.
(54) Mesner, M. H. Television's toughest challenge, *Electronics*, 38, No. 10, 80, May 17, 1965.
(55) Berger, H. Characteristics of a thermal neutron television imaging system, *Materials Evaluation*, 24, 475, 1966.
(56) Berger, H. "Neutron Image Intensifier", Supplement to Encyclopaedic *Dictionary of Physics, edited by J. Thevlis*, Pergamon Press, London, to be published.
(57) Warman, E. A. Neutron radiography in field use, *Materials Evaluation*, 23, 543, 1965.
(58) Berger, H. "Neutron Radiography", Elsevier Publishing Co., Amsterdam/London/New York, 1965.
(59) Berger, H., and Beck, W. N. Neutron television system inspection of radioactive fuel capsules, *Am. Nuclear Soc.*, Winter Meeting, Oct. 31-Nov. 3, 1966, Pittsburgh, Pa., to be published in Transactions.
(60) Wang, S. P., Shull, C. G., and Phillips, W. C. Photography of neutron diffraction patterns, *Rev. Sci. Instr.*, 33, 126, 1962.
(61) Ruggles, P. C., and Slark, N. A. Improvements in light amplifier operation, *IEEE Trans. Nuclear Sci.*, 11, No. 3, 100, 1964.
(62) McMaster, R. C., Rhoten, M. L., and Mitchell, J. P. The X-ray vidicon television image system, *Materials Evaluation*, to be published.
(63) Cedar-Brown, R. I., and Harris, J. E. Infrared measurements in real time, presented at 24th Nat. Conv., Society for NDT, October, 1965. See also General Electric Co., Defence Electronics Division, Electronics Laboratory, Ithaca, New York, Report Volume I, "Design Studies of a Real-Time Infrared Measurements System", Final Report, Contract NASA 8-11715, Jan. 15, 1965.
(64) Zworykin, V. K., and Morton, G. A. "Television", John Wiley, New York, 1954.
(65) Knoll, M., and Kazan, B. "Storage Tubes and Their Basic Principles", J. Wiley, London, 1952.
(66) Greatorex, C. A., Image storage techniques applied to diagnostic radiology, in "Advances in Electronics and Electron Physics", Vol. 16, edited by J. D. McGee, W. L. Wilcock and L. Mandel, Academic Press, New York, 1962, pp. 593-600.
(67) Dahl, H., A. B. Dick Co., Chicago, Illinois, private communication, 1965. Some data on the system were also obtained from J. P. Mitchell, Ohio State University, Columbus, Ohio, 1965.
(68) Leonard, S., and Eppler, W. G. Radiographic film reading and analyzing by electronic methods, *Materials Evaluation*, 22, 428, 1964.

Discussion

Q. DR. J. P. BARTON, S.A.R., Centre d'Etudes Nucleaires, Grenoble, France:

First, I would like to comment on the neutron image intensifier described in this paper. First I wish to congratulate those concerned with the development of this instrument; an idea which is already proving of interest in Japan, the U.K., and France, as well as in the USA. One important point, in my view, needs further elaboration. In previous publications on this neutron image intensifier it has been suggested that a main advantage of the technique is that it will make possible neutron radiography with low output neutron sources such as small generators and radioactive sources. In the account just given it was stated that the instrument enables images to be seen with very low intensity neutron beams, mentioning figures as low as 10^2 or 10^3 neutrons/cm^2-sec. I think this might be misleading. The point is open to discussion, but in my view the quality of a neutron radiograph obtainable from a low intensity (small source) neutron beam is limited by the statistical fluctuations of the few neutrons forming the image. Amplifying the signal from each individual neutron by means of the intensifier and television system cannot overcome this. The simple procedure of using a scintillator screen next to a fast film can provide an image with an integrated neutron exposure of as little as 10^5 n/cm^2. This is, in a way, already too efficient; the quality is already severely limited by statistics; and in order to get good radiographs less efficient methods (e.g. slower films) must be used requiring integrated doses of 10^7 or 10^8 n/cm^2. I think it will be useful to point out therefore, that if ordinary immobile neutron radiographs of even moderate quality are required the image intensifier system cannot provide any advantage even for small source, low beam intensity techniques. The advantages are certainly immediate presentation of the image, or presentation after short integration times, and also inspection of objects in motion. I have already discussed this point with Mr. Berger and perhaps it would be useful if he would comment here on whether he would accept or reject these views.

Second, for the neutron image intensifier system contrast sensitivity is, of course, a most important characteristic and some figures have been mentioned. The important stage in the instrument is the neutron converter screen which consists in this case of a Li^{6}F-ZnS scintillator. On this subject I can now answer a question which I myself asked at the last conference in this series in LONDON, and which is relevant here. In a paper on neutron radiography it was suggested that a scintillator screens of this type could provide only much inferior contrast sensitivity as compared with foil-film conversion methods. (10 per cent contrast sensitivity for lead and uranium when using the scintillator screen, and 2 per cent when using direct foil techniques). That scintillation techniques were basically inferior

to foil techniques was questioned becaused no physical reasons could be seen to explain the difference. We have therefore performed some tests to compare the contrast provided by Li^6F-ZnS scintillator screens and metal foil (gadolinium) screens used in direct exposure methods. The tests were for thin sections of cadmium and plastic, so that it is truly the neutron contrast which is being measured and not a gamma ray effect. Results indicate that the scintillator provides at least as good a contrast as the foil converter. The previous large difference noted between the scintillator and foil methods for uranium and lead may therefore have been a special effect under the experimental circumstances due to:

1) use of different films for scintillator and film; 2) different statistical fluctuations due to neutron doses required; and 3) the gamma ray effect which will enhance the contrast for heavy metal test blocks such as uranium and lead.

A. I have to agree with Dr. Barton's first comment to the effect that, whatever detector is used, one must accumulate sufficient information to present an image with the desired detail and contrast. In the specific case of the small neutron source, where one may have a thermal neutron beam intensity for radiography in the order of 10^3 neutrons/cm^2-sec., a neutron radiograph taken with a scintillator-film detector will require an exposure time of a few hundred seconds. On such a radiograph one will be able to resolve high contrast detail in the order of 0.1 mm. With the neutron image intensifier detector, viewed directly in a thermal neutron intensity of 10^4n/cm^2-sec., observable resolution degrades to about one cm. Although one can make gross observations at lower intensities, obviously the image quality becomes very poor. I believe that each detector has some advantages and that the choice of detector may actually be dictated by the application requirements. Certainly, I have to agree, that in cases where film results of reasonable quality are desired, the scintillator approach with film supplies an inexpensive, efficient detection system. The neutron image intensifier offers no advantage in that situation. The brightness gain of the intensifier makes it easier to detect the signal but one must still accumulate sufficient information to obtain a statistically meaningful image. The image intensifier does offer an advantage if there is a requirement for observing object movement, or for making rapid, gross detail observations.

Regarding Dr. Bartons second comment, I am pleased to learn that further work has been done on this question of the contrast one can observe with a scintillator-film detector. The three reasons that have been mentioned undoubtedly were contributing factors to the poorer contrast we observed with scintillator methods.

Optical Methods for Studying Ultrasonic Propagation in Transparent Media

H. L. WHALEY, K. V. COOK,
R. W. McCLUNG and L. S. SNYDERS, U.S.A.

ABSTRACT: The schlieren and photoelastic methods for viewing continuous and pulsed ultrasonic waves propagating in transparent media were investigated. Limitations, possible applications, and results of the investigation of each system are discussed. Emphasis is placed on equipment improvements for the development of optimum systems for nondestructive testing applications.

Introduction

Techniques involving ultrasound are widely used in the field of nondestructive testing. However, much of the basic theory concerning the behaviour of ultrasonic is based on light-wave or optic theories and experimental observations. In general, the correlation of light-wave and ultrasonic phenomena is good; therefore, efforts to visualize ultrasonic propagation in transparent media have not been pursued with a great amount of effort.

Since there are optical methods, such as those based on the schlieren principle and the photoelastic effect, for observing ultrasonic propagation, we felt that much could be learned by observing basic ultrasonic phenomena such as reflection, refraction, and the effects of surface waves and Lamb waves. Observation of ultrasonic transducer-beam symmetry, collimation and focussing, and modes of propagation for actual applications, such as tubing inspection, could be of practical benefit and should lead to much improved techniques. The possibility of using a visual technique in flaw detection is also intriguing.

For these reasons we have developed systems for making visual observations of ultrasound by the schlieren and photoelastic methods. These methods have been used by many others in the past for a number of applications including aerodynamics (1) and ultrasonics (2–4). Very few of the publications in this field, however, discuss the experimental setups in detail, and this lack of detailed description imposes a hardship on those who wish to utilize the techniques. Our studies of the necessary equipment covered different combinations of light sources, collimating lenses, ultrasonic generators, and other accessories, and we have developed advanced systems which are optimized for the desired results.

Equipment

The 78.7-in. (2-m) optical bench with the schlieren equipment is shown in Figure 1. This bench was used for both the schlieren and photoelastic methods of viewing ultrasound. The following schlieren components are mounted on the bench, from left to right:

1. An argon-jet spark light source which can supply a pulse of light with duration of 0.2 μsec from an electric discharge of 3 joules and which also contains an incandescent pilot light for convenience in alignment.
2. An achromatic lens for collimating the light from the source.
3. A water-filled tank into which ultrasound is introduced.
4. A second lens for refocussing the parallel light rays.
5. A vertically adjustable slit which blocks the refocussed parallel light rays and passes diverted rays.

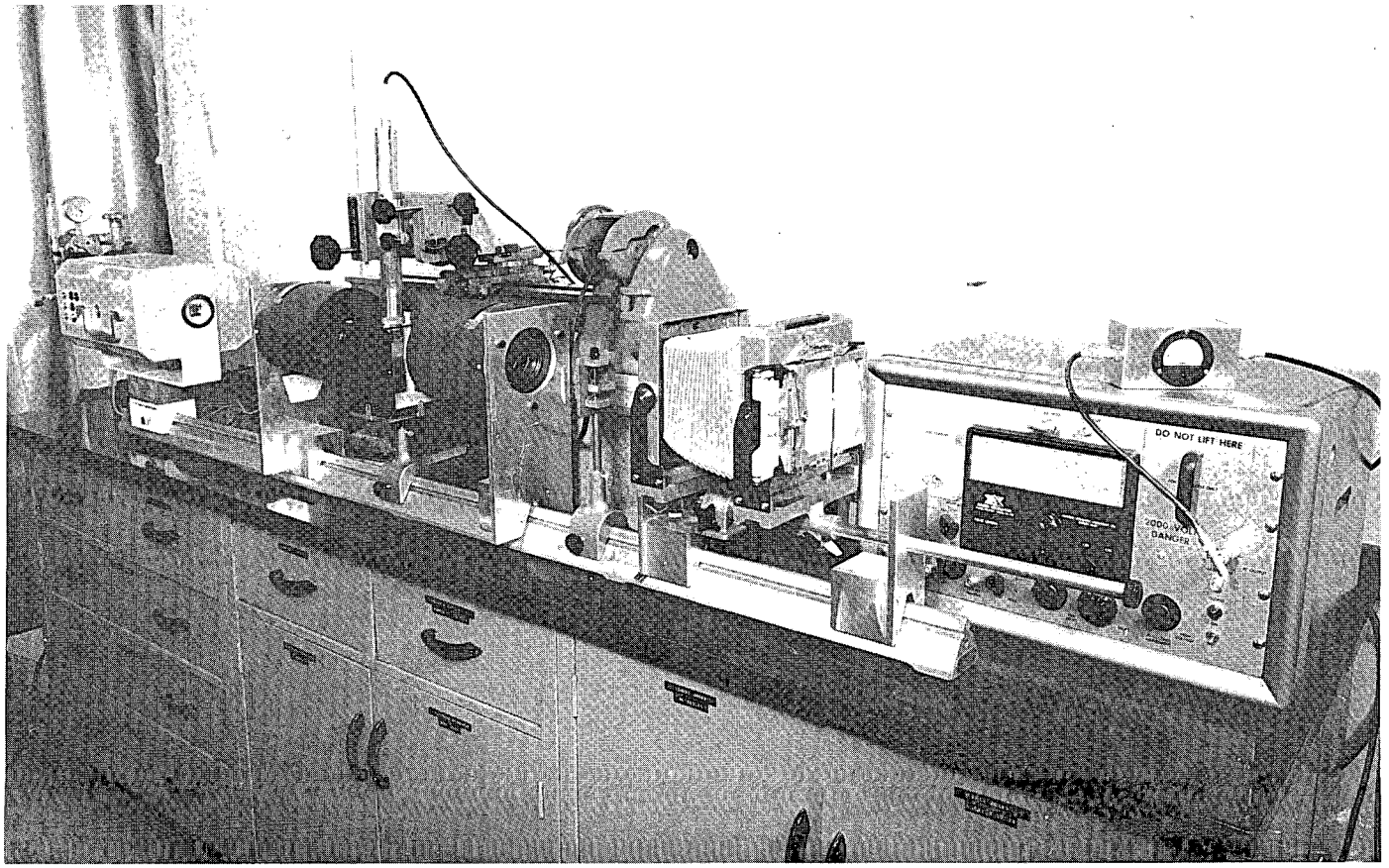

Figure 1. Optical bench with schlieren equipment

6. A Calumet view camera which has a ground glass screen for viewing the images produced by ultrasonic propagation in the water-filled tank, and a 4- × 5-in. (10.16- × 12.70-cm) Polaroid attachment for photographing the images.

The Arenberg generator, shown on the right in Figure 1, supplies the ultrasonic transducer with an electrical driving signal having a frequency adjustable from 350 kc to 25 Mc in either a continuous wave or pulsed mode of operation. A delay line and pulse generator are also used to trigger the jet spark light source in proper sequence with the generated pulse of ultrasound.

All the above equipment, except the water-filled tank and the movable slit, is used in the photoelastic method as well as the schlieren method. In addition, polarizing plates are required for the photoelastic method. Additional information on equipment used is given in the Appendix.

Schlieren Method

The schlieren optical system for viewing ultrasound derives its name from its original use in Germany for the detection of inhomogeneous regions in glass which occur often in the form of streaks or "schliere" (5).

General Principles of the Technique

A number of theories have been advanced to explain how an ultrasonic beam or pulse is made visible by the schlieren optical system. Willard (6) has discussed the manner in which Raman and Nath treat the optical diffraction by ultrasound as a result of the phase modulation of the wave front by the sound beam.

Debye and Sears (7) rejected the phase-grating explanation of the effect and developed a theory "based on the assumption of a volume scattering, in which every volume of the liquid contributes to the total scattering in accordance with Maxwell's equations." Neither of these theories appears to be adequate to account for all of the effects observed. Recently Mayer (8), Breazeale and Hiedemann (9), and many others have demonstrated through the direction of their work that interest in the theoretical aspects of this problem still exists.

For our purposes we shall assume that ultrasonic propagation diverts or diffracts parallel light rays, thereby allowing its visualization by the schlieren optical system as illustrated in Figure 2. Light from a bright source is focussed on slit S_1. A lens I_1, at a distance from S_1 equal to its focal length, f, collimates the light from the source. If there is no optical disturbance of the light between L_1 and L_2, the second lens, L_2, will refocus it in the plane of S_2, a vertically adjustable slit. The dark field at the screen or photographic plate at the far right of Figure 2 is produced by setting S_2 to block out essentially all the undisturbed light with one of its edges. If there is some optical disturbance between L_1 and L_2, some light rays will be altered from their parallel alignment so that light will miss S_2 and appear at the plane of the screen. For example, if the disturbance is a speck of dust, an image of the speck will appear in the image plane of the second lens as illustrated in Figure 2. The screen is so placed that a disturbance midway between L_1 and L_2 would be in sharp focus at the screen by making the distances p and q in Figure 2 conform to the well-known formula of geometrical optics,

$$\frac{1}{f} = \frac{1}{p} + \frac{1}{q} \quad . \tag{1}$$

Such an optical system will render a sound beam in water visible in the manner described below.

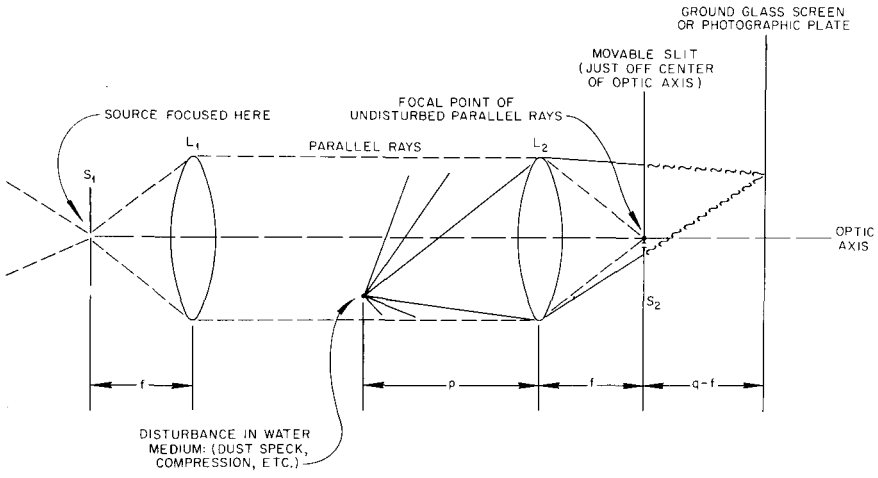

Figure 2
Schlieren optical system.

A glass-walled tank is filled with water and placed midway between L_1 and L_2. An ultrasonic crystal is submerged in the water and activated by an oscillator, sending ultrasonic energy through the water perpendicular to the direction of travel of the parallel light rays. The ultrasonic waves traversing the water are pressure waves traveling at the speed of sound in water. A single complete vibration of the transducer produces a region of increased density followed by a region of decreased density of the water as compared to the density of undisturbed water. These areas of density change disturb the rays of parallel light by refraction, and images of these regions appear on the screen. If the screen is placed so that the object and image size are the same, the image on the screen in stop-motion consists of sets of narrow horizontal bright and dark lines. The width of a bright line-dark line pair is equal to the wavelength of the sound in the water.

Development of the Optical System

The direction taken in the experimental program was first to establish a sensitive optical schlieren system without using ultrasound, and then determine optimum components and manner of operation for both pulsed and continuous wave (cw) modes of ultrasonic propagation. For convenience, before actual introduction of ultrasonics, the schlieren image for comparing these components was provided by introducing thermal gradients into the water in the tank.

Most schlieren systems described in the literature incorporate a pinhole as the light source and a circular opaque obstacle to block out the undeviated light. However, we found that a pair of slits proved to be a far superior arrangement with better image contrast and ease of adjustment. The apparent reason for this is that the deviation of the light beams from their original path by stress waves is always extremely slight, so only very small solid angles of deviated light are available and these can be admitted readily by a narrow slit. Any other scattering mechanism, such as particles in the water or on the glass walls of the water tank that scatter the parallel beams through a large solid angle, will not show up as brightly with the slits, resulting in better contrast in the image. The best results were obtained with a pair of slits made by electrodischarge machining. The slits were machined in 0.007-in. (0.018-cm) thick metal sheets and were 0.01 in. (0.025 cm) wide × 0.5 in. (1.27 cm) long. With the installation of the best slits and the accurate alignment of the achromats, the optical system was sufficiently sensitive that convection currents in air rising from a human hand could be seen when a high-intensity mercury arc light source was used.

After the sensitivity of the optical system had been maximized, an ultrasonic transducer, driven by a power oscillator, provided the disturbance of the collimated light necessary to produce a schlieren image. There are several ways to improve the schlieren image of the ultrasound. The windows of the water tank should be as nearly strain-free as possible and kept free of fingerprints, dust, and air bubbles during use. In this connection, we initially used a fused quartz glass tank but later found that a plexiglass tank made from $\frac{1}{4}$-in. (0.635-cm) sheet was adequate. Further improvement can be achieved if the precision achromatic lenses are cleaned only when necessary and then with extreme care. The importance of such factors is greater for systems with poor sensitivity.

We found that our use of collimating slits, as previously discussed, provided an improved tolerance for scattering centres such as dust. In addition, although the use of distilled water in the tank is recommended in some references, tap water was found to work equally well.

One extremely important consideration in the quality of the resultant schlieren image is the perpendicularity of the direction of the collimated light and ultrasound beam. For an ideal diffraction grating, the thickness of the grating is assumed to be zero and to have no effect on the diffraction even if the incidence of the light on the grating is not normal. If the light is not incident normally, the diffraction grating formula simply changes from

$$d \sin \theta = n\lambda, \tag{2}$$

where d is the grating spacing, n is the order number, λ is the wavelength of the light, and θ is the diffraction angle, to

$$d(\sin \theta + \sin i) = n\lambda, \tag{3}$$

where i is the angle by which the direction of the light incident on the grating differs from the normal. However, the ultrasound beam always has considerable thickness, and if it is inclined with the parallel light rays so that a light ray crosses both compressions and rarefactions, its net deflection may be cancelled, and the schlieren image will not occur. In our experimental setup, the transducer was mounted in the end of a search tube normally used for immersed ultrasonic testing. The tube was clamped in a manipulator (for angular adjustment), which was in turn mounted on a 6-in. (15.24-cm) lathe bed. This arrangement allowed for convenient alignment of the sound beam approximately normal to the direction of the light. The alignment was completed by further adjustment of the manipulator while viewing the schlieren image on the ground glass screen. For many transducers, the beam image was visible

when it deviated from normal by as much as 10°. The extent of tolerable deviation was affected by both beam diameter and ultrasonic frequency.

Refinements for Viewing Continuous Wave Ultrasound

Continuous ultrasonic waves (produced by applying a continuous sine wave to the ultrasonic transducer) were observed using the Arenberg oscillator in the cw mode of operation. A number of light sources were tried in an effort to develop the most sensitive cw system. A 10-w zirconium arc lamp, a 150-w projector lamp of a common variety, a 100-w mercury arc lamp, and the pilot light in the jet spark light source were compared. Use of the mercury arc source always resulted in a more sensitive system; however, because of the convenience of using the pilot lamp in the jet spark light source, it was generally used. The continuous wave system is sensitive enough that a dim image of the ultrasonic beam was observed using a common flashlight as the light source.

The intensity of the schlieren images is obviously related to the intensity of the ultrasonic energy which in turn depends on the voltage applied to the transducer. For the best images, the highest operating voltages are desirable, but extreme care must be taken because higher voltages shorten the transducer life. For continuous-wave operation, the possibility of transducer damage exists because heat is a byproduct of the transducer operation. In some cases this could be observed in the schlieren image as a thermal gradient adjacent to the transducer. To prevent the overloading of a transducer, a current meter was used in the output circuit. If the transducer became warm during operation, the meter reading was noted, and the current was kept less than that value in subsequent operations. With the Arenberg oscillator, the range of frequencies over which a good schlieren image of the ultrasound occurs for a given transducer is usually large. For example, a crystal with a resonant frequency of 5 MHz gave a good image at 2.25 MHz, and a 10-MHz transducer was photographed working at 3 MHz. However, for the best image, the crystal should be operated near its resonant frequency.

Refinements for Viewing Pulsed Ultrasound

Use of the schlieren system with pulsed ultrasound allows the tracing of ultrasound through transparent media and the isolation of reflections, refractions, and other phenomena from the transmitted pulse. This is accomplished by synchronizing a pulsed light source with a pulsed oscillator using an adjustable delay of the signal triggering the light flash.

Since a rather bright light source is needed for good schlieren work, finding an appropriate pulsed light source was not easy. We wanted a source with sufficient energy per flash and a high enough repetition rate that continuous adjustment of the delay time would make the pulse appear to travel in an unbroken path. The first light source used was a General Radio Strobotac which we happened to have on hand. Figure 3 is a block diagram of the pulsed system used with the Strobotac. A triggering signal taken from the pulsed oscillator was fed through an appropriate delay circuit to activate the Strobotac whose light pulse has a duration of approximately 1 μsec. The stroboscopic effect caused the pulse to appear to stand still at a variable distance from the transducer, dependent upon the amount of delay. Although the intensity of the image was not as great as we desired, visualization of pulses was possible with this system. We were able to resolve individual cycles within a pulse as high as 2.25 MHz using this light source. The ability to operate at high repetition rates allows the Strobotac to be used with commercial ultrasonic equipment having repetition rates as high as 600 cycles/sec.

An argon-jet spark was considered and selected as one of the better available pulsed light sources. The instrument incorporates large capacitors in which an electrical charge is stored before being discharged in a brilliant spark. A laminar jet of argon gas flows steadily between the two electrodes to channel the spark when it occurs so that it will follow exactly the same path each time. This permits accurate focussing of the spark on a slit. A pilot lamp whose position is optically equivalent to that of the spark is used for convenient focussing of the spark on a slit. The pulse of light from the spark is extremely brilliant and of short duration, three joules of energy being dissipated in only 0.2×10^{-6} sec. The repetition rate is low (on the order of once a second at maximum), but it can be used for visual as well as photographic work. Owing to this low repetition rate, triggering was accomplished through the use of an auxiliary pulser designed and fabricated at ORNL. The output pulse was fed to both the Arenberg oscillator and through the delay and amplifier circuitry to the light source. Figure 4 is a block diagram of the pulsed system with the jet spark light source. Individual cycles were resolved, within pulses, at frequencies up to 4 MHz with this system before the compressions became so close together that resolution was lost owing to pulse movement.

Results and Applications

With the cw system for viewing ultrasound, beam images have been obtained using a variety of quartz and ceramic transducers

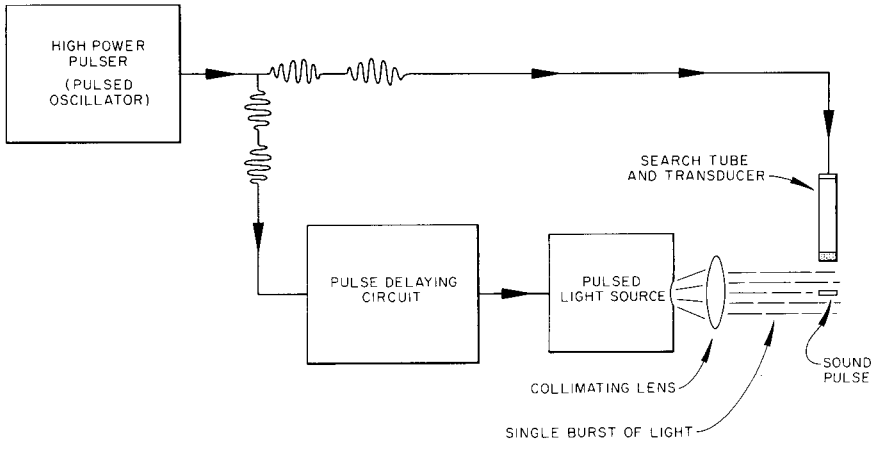

Figure 3
Block diagram of the pulsed system used with the Strobotac.

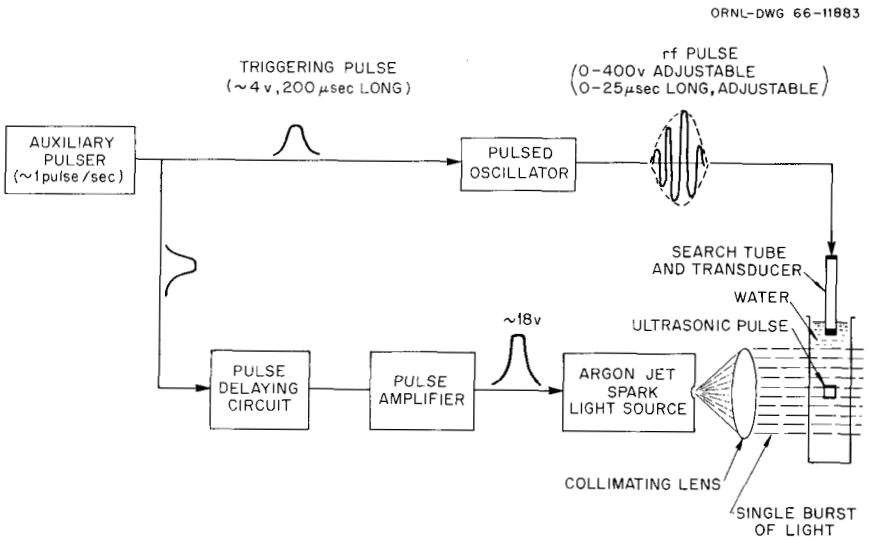

Figure 4
Block diagram of the pulsed system used with the argon-jet spark light source.

for a range of frequencies from 2.25 MHz through 25 MHz. The cw method has been used to make cursory examinations of a few of our transducers; the active area of one transducer, for example, was observed to be substantially reduced due to a blistered epoxy coating on its face. The cw method has also been applied to viewing beam collimation, the location of focal points of focussed transducers, and the reflection of beams from flat and curved reflectors. Figure 5 shows a continuous 5-MHz beam reflected from a piece of aluminum with a curved reflecting surface. Note how the reflected beam is focussed.

The pulsed method of viewing ultrasound with our system is more sensitive than the cw method, although both are useful. The Arenberg oscillator delivers greater voltages to the transducer in the pulsed mode of operation. The higher voltages

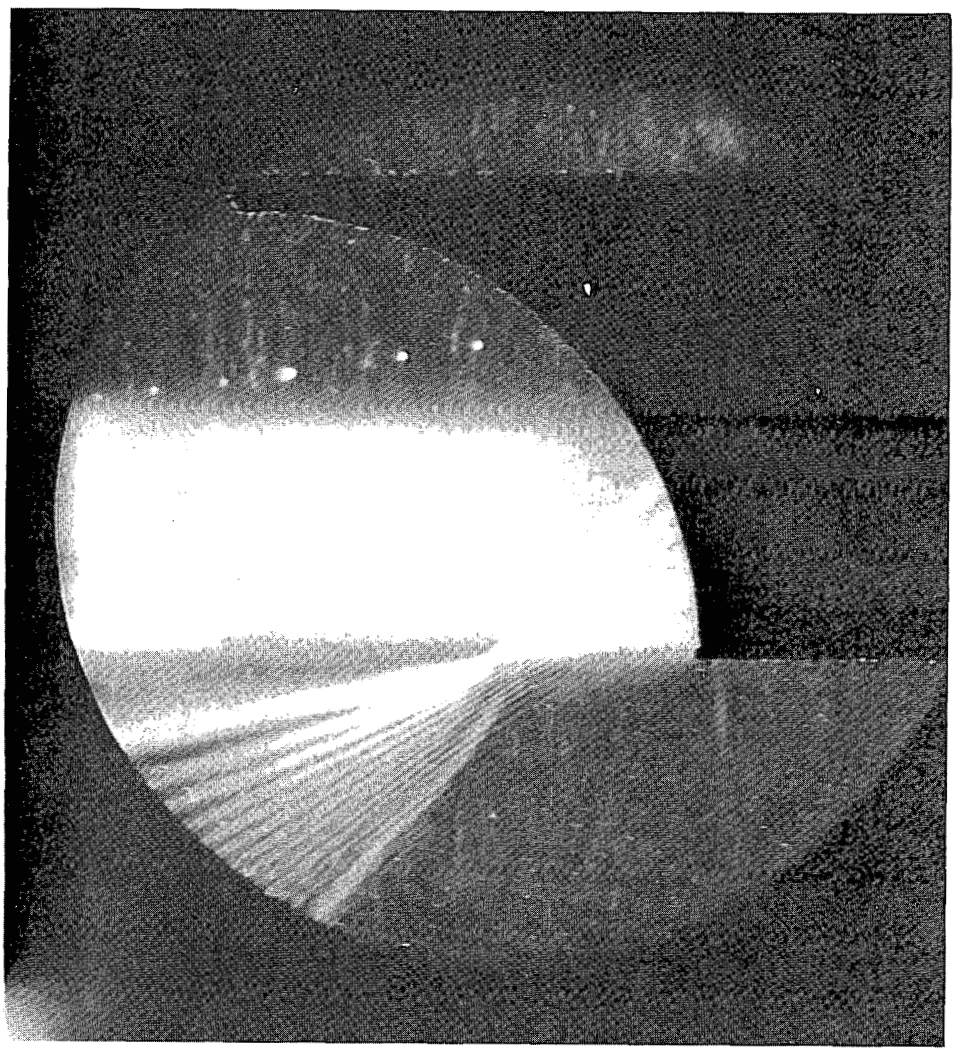

Figure 5
Continuous 5-MHz beam reflected from a piece of aluminum with a curved surface.

applied to the transducer increase the amplitude of its vibrations and, thus, of the local density changes in the water. These more pronounced density changes increase the contrast of the schlieren image by making the density gradient between compressions steeper. The fact that sharper images of pulses can be obtained than for the corresponding cw beam allows ultrasonic pulses to be observed in some situations where the use of cw ultrasound alone would not suffice. One case in which this proved possible is shown in Figure 6. We wanted to photograph the ultrasound in a plexiglass block, but only negative results were obtained with the cw system. The attempt with the pulsed system was, however, successful. Outside the block, interference patterns can be seen from the interaction between compressions that have been reflected, and others starting later in time. With the pulsed system, we were able to view images over a frequency range from 0.8 to 25 MHz. The progress of the pulses could be followed in detail both by eye and by making a series of photographs. Reflections and scattering at interfaces were observed by proper adjustment of the delay time. In one instance, the pulsed system was used to get an estimate of ultrasonic velocity for a low-velocity rubber material. This estimate was made by observing the time in microseconds required to delay a pulse through a known thickness of the material.

For the work with ultrasound in solids, ordinary glass and transparent epoxy blocks were employed as well as the Plexiglass already mentioned. Results obtained with the epoxy were much poorer than for the plexiglass at all frequencies. The glass had small attenuation but such large acoustic impedance that most of the incident sound was reflected from its surface. Contact crystals gave about the same results as the immersed type. The plexiglass was by far the best material that we found for both the cw and pulsed schlieren work with transparent solids. In the plexiglass the ultrasonic indication is very bright near the surface where it enters; however, owing to its high attenuation, we have been able to observe penetration to only about 2.0 in. (5.08 cm). Observations have also been made of ultrasonic behaviour around drilled holes in plexiglass. Further work is needed on observations of internal reflection, refraction, mode conversion, and reflection from drilled holes, notches or other discontinuities. Selected materials will need low acoustic impedance and attenuation.

Photoelastic Method

We have also used another method to view ultrasonic propagation in transparent solids. This method is based on the photoelastic effect and uses monochromatic light and a polariscope to observe the stress patterns introduced by the ultrasonic propagation (10).

General Principles

The photoelastic method (11) as adapted for viewing ultrasound employs a polariscope, which in its simplest form is an optical polarizer, an analyzer, and a light source. Our polariscope was assembled by altering the schlieren system already available (Figure 1). The water tank and second slit were removed and a polarizer, a quarter-wave plate, an unstressed transparent epoxy solid, another quarter-wave plate, and an analyzer in that order were set up on the optical bench between the collimating and refocussing lenses. For this approach, pulsed ultrasound was introduced by a transducer attached directly to the epoxy solid. The jet-spark light source was triggered as before with the auxiliary pulser.

If polarized light is passed through an unstressed transparent plate, through an analyzer whose plane of polarization is normal to that of the polarizer, and then projected on a ground glass screen, a darkened light field will be observed. Some solid materials have the optical property of being able to split an

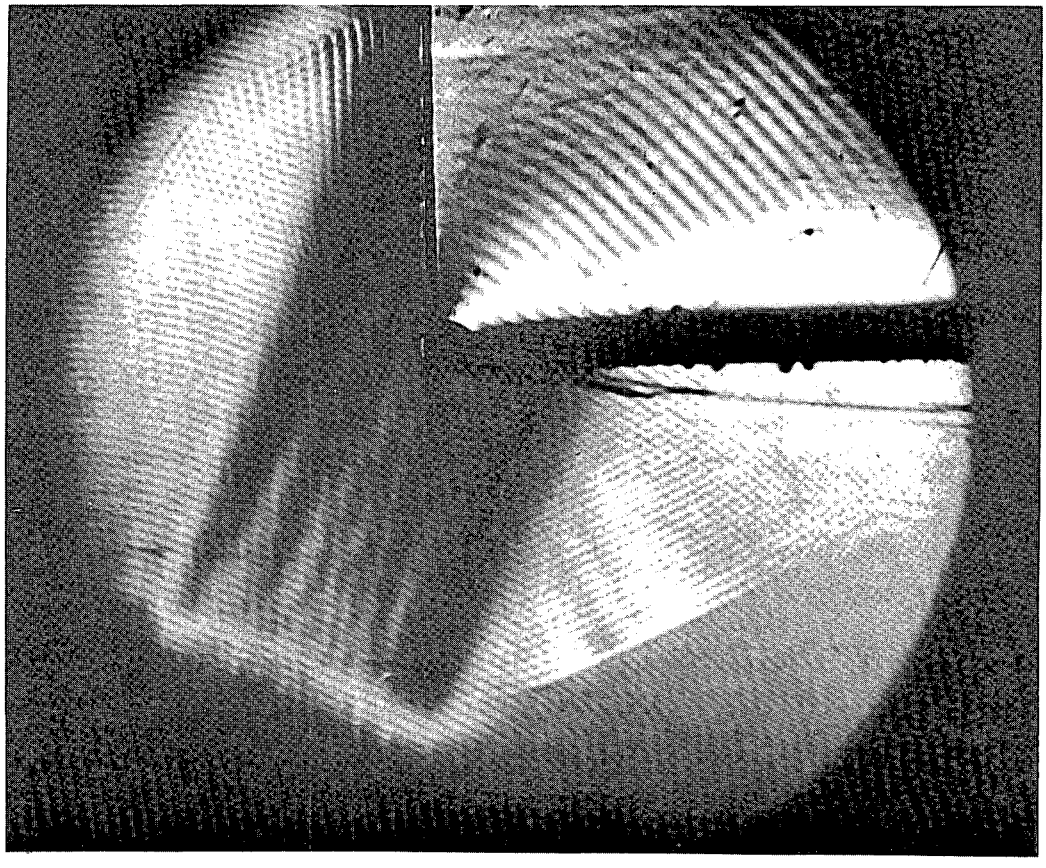

Figure 6
Incident pulse (2.25 MHz) on the corner of a plexiglass block (shown in upper right-hand corner of figure).

incident light ray into two components which are polarized in planes at right angles to each other (a phenomenon called birefringence). Almost any solid material becomes birefringent when stresses are introduced. At each point of the stressed solid, the planes into which an incident light ray is split are coincident with the planes of maximum and minimum stress. The polariscope arrangement causes an interference pattern to occur which is characteristic of the stress-caused birefringence. These are bright areas on the darkened field at the ground glass screen. If the stresses introduced are travelling ultrasonic pulses, they can be viewed and photographed with the aid of the polariscope.

Results and Applications

We have used the photoelastic method to observe ultrasound in transparent solids and to measure quantitatively the intensity of the ultrasound in the material. By successive measurements as the sound propagated, attenuation could be determined. A $\frac{1}{4}$-in. (0.635-cm) plate of transparent epoxy was molded with attention to producing a model free of permanent stresses. Ultrasonic pulses in a frequency range of 0.5 to 1.0 MHz were introduced into the solid, and the photoelastic image of the resulting stress was photographed. Measurements on the fringe orders allowed evaluation of the principal stress magnitudes as a function of ultrasonic penetration. Strain-gauge measurements compared favourably with results of photoelastic method. The frequency range was restricted on the pulse-intensity measurements since our Arenberg oscillator became unstable below 0.5 MHz, and the amount of movement of the pulse during the duration of the light flash became too large compared to the ultrasonic wavelength above 1.0 MHz. The upper frequency limit for the photoelastic method should be comparable to that for the schlieren technique where resolution of individual cycles is not a necessity. This has not, however, been determined for our setup.

Of course, the photoelastic method is suitable for continuous-wave as well as pulsed observation; although, again, frequency limits for the equipment in our setup have not been determined. Preliminary indications are that the schlieren method affords greater sensitivity for visual observation, while the photoelastic method may be better adapted to quantitative determinations. Since birefringence does not occur for liquids, the photoelastic method cannot be used to view interface effects at liquid-solid interfaces for submerged solids, a use for which the schlieren technique works very well.

Epoxy was the only solid to which the photoelastic technique was applied. Although it was chosen for its high photoelastic response, there may be other materials that would allow better photoelastic observation of ultrasonic phenomena in solids.

Summary and Conclusions

Visual means of observing ultrasonic phenomena show promise of being valuable tools in nondestructive testing. After studying many different combinations of equipment, we have developed a highly sensitive optical system with which we can observe both cw and pulsed ultrasound in transparent solids and liquids by a schlieren technique and in transparent solids by a photoelastic technique. The schlieren technique seems especially promising for visual study of ultrasonic phenomena at water-solid interfaces and inside some transparent solids while the photoelastic method is useful for quantitative study of stress-strain mechanics in transparent solids. There are good reasons for believing that the schlieren method can be applied to flaw detection although work on this problem is still in the early stages.

References

(1) Holder, D. W. and North, R. J. "Schlieren Methods", Notes on Applied Science No. 31, National Physical Laboratory, Her Majesty's Stationery Office, London, 1963, p. 56.

(2) Aldridge, E. E. A numerical study of the mode of working of the ultrasonic micrometer used in thickness measurements of stainless steel tubing, UKAEA, Harwell, England, April 1966, AERE M-1742.

(3) Fitch, C. E. Mater. Evaluation XXII(3), 124, 1964.

(4) Ensminger, D. Ultrasonic testing of thin plates, presented at the 1964 Spring National Convention of the Society for Nondestructive Testing, Los Angeles, Calif., March 1964.

(5) Holder, D. W. and North, R. J. as 1 above, p. 1.

(6) Willard, G. W. *J. Acoust. Soc. Am.*, 21 101, 1949.

(7) Debye, P. and Sears, F. W. *Proc. Natl. Acad. Sci. U.S.*, 18, 410, 1932.

(8) Mayer, W. G. *Ultrasonic News*, Spring 1961.

(9) Breazeale, M. A. and Hiedemann, E. A., *Naturwissenschaften*, 45, 157, 1958.

(10) Snyders, L. S. The photoelastic observation of ultrasonic waves in a transparent plate, Oak Ridge Nat. Lab., ORNL-TM-1671 (in press).

(11) Heywood, R. B. "Designing by Photoelasticity", Chapman and Halls, London, 1952.

Appendix

Equipment

Optical bench	78.7 in. (2 m) The Ealing Corporation Cambridge, Massachusetts
Pulsed oscillator	Model PG-650-C with Modification No. 2 Arenberg Ultrasonic Laboratory, Inc. Jamaica Plain 30, Massachusetts
Four-volt pulser	Built at ORNL
Pulse amplifier	Built at ORNL
Delay line	Model 102 E.S.C. Electronics Corporation Palisades Park, N.J.
Pulsed light source	Model 7 Argon Jet Light Source Lunartron Electronics Luton, England
View camera	Calumet Manufacturing Company Chicago, Illinois
Achromatic lenses	Kodak Aero-Ektars, f/2.5, 7-in. focal length Free Style Sales Company Los Angeles, California
Zirconium arc lamp	10 watts George W. Gates Company, Inc. Franklin Square, L.I., New York
Mercury arc lamp	100 watts General Electric Company
Strobotac	Model 1531-A General Radio Company Concord, Massachusetts

A Thermoluminescent Image-Detection Method for Neutron Radiography

JACOB KASTNER, HAROLD BERGER and I. R. KRASKA, U.S.A.

ABSTRACT: A thermoluminescent method for displaying thermal-neutron images is described. A sheet of ^{6}LiF, exposed to the imaging neutrons for periods as long as is necessary to capture the image, can be made to reproduce the image by means of the light emission produced by heating at any time after the exposure. The excellent storage capability of this detection method makes it attractive for use with relatively low-intensity neutron radiographic beams. Images can be obtained for total thermal neutron exposures of about 10^9 n/cm^2. A high-contrast resolution capability of about 0.125 mm and a contrast sensitivity of about 10 per cent have been demonstrated.

A number of photographic methods for detecting thermal-neutron images have been described (1-3) and applied to neutron radiographic inspections (4,5). The methods can be divided into two main categories: the direct-exposure method, in which film is used in the neutron imaging beam either by itself or in conjunction with some type of converter screen, and the transfer method, in which the neutron image is detected by a screen of some potentially radioactive material, an autoradiograph of the screen later providing a film image. One feature that these methods lack is the ability to integrate neutron image information in the presence of interfering gamma radiation for long periods of time, as would probably be required in most thermal-neutron imaging situations involving nonreactor neutron sources. The thermoluminescent image detection method described offers some advantage in this respect. A preliminary report describing the technique has been made (6). Now, however, information concerning resolution and contrast capabilities can be given. Also, the speed of technique has been substantially improved since the initial report.

When a thermoluminescent phosphor is exposed to ionizing radiation, many of the freed electrons become trapped at lattice imperfections in the crystalline solid. They remain trapped when stored at or below the temperature at which the exposure was made. If the temperature is raised, the probability of escape is increased, and the electrons are released, subsequently recombining with opposite-charge carriers with the emission of light, the intensity of which is proportional to the ionizing exposure. In an intensity-versus-time plot, the peaks of emittted light intensity become narrower at faster heating rates, although the areas under the peaks remain constant.

The Harshaw Chemical Company, Cleveland, in cooperation with Cameron of the University of Wisconsin (7) has developed activated ^{6}LiF crystals specifically for neutron dosimetry. The material is identified as TLD-600 (95.6% ^{6}Li) and is extremely sensitive to thermal neutrons. The material is available in powder, or single-crystal form.

For imaging purposes, a thin (for good resolution) sheet of ^{6}LiF, either single or multicrystalline, extending over a reasonable area, is all that need be exposed to the neutron imaging beam. Once the neutron exposure is complete, the light can be released either by heating the LiF to a temperature of 210°C or by irradiating the LiF with ultrasound (8). The resultant light image can be observed visually or detected on film. The use of film, preferred in most cases, can be accomplished simply by placing film in contact with the LiF during the heating or ultrasonic process.

Practically speaking, the placing of film directly on a heated thermoluminescent detector does introduce some problems. Therefore, it is desirable to separate the film from the heated thermoluminescent detector. The initial studies were made simply by photographing (6) the thermoluminescent detector during its period of light release, the entire heating and photographic process being carried out in a darkroom. The separation of film and detector in this manner, however, does result in a significant loss of available light, and the number of neutrons needed to prepare a picture is relatively large. With this camera technique, a total exposure of about 10^{11} thermal n/cm^2 was needed to prepare a useful neutron photograph on 3000 speed Polaroid film (Type 47), with a natural lithium-fluoride pressed powder detector (6). Point A on Figure 2 represents a thermal exposure of 10^9n/cm^2.

This speed figure can be substantially improved upon. For example, the use of a single LiF crystal eliminates some light loss due to scattering. This has improved the speed of the process by a factor of about 1.5 times. Better light collection by the use of a fibre optic assembly can result in a significant speed improvement. Preliminary tests of this type, made with inexpensive fibre optics,* indicate that a speed improvement of about 20 times over the camera technique can be achieved. Although these preliminary tests have yielded a speed result, the image area available was too small to prepare useful neutron images. A typical fibre optic result is shown in Figure 1. In addition to providing a speed comparison, these preliminary results have shown that a fibre optic length of only a few cm will be satisfactory for film use; this is long enough to eliminate problems due to film heating.

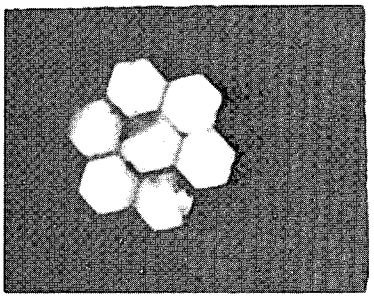

Figure 1
A positive print of a thermoluminescent neutron radiograph made with the film resting on a light guide during the period of light release from the thermoluminescent LiF.

An additional speed improvement can be obtained if the LiFR is Li-6 enriched. The speed factor improvement due to enrichment can be estimated by noting the speed improvement which can be achieved with LiF-ZnS(Ag) type neutron scintillators (4) if one uses natural lithium, and then Li-6-enriched material. Argonne (National Laboratory) results with such scintillators indicate that one can achieve a speed improvement of about 3 times. If one combines all these speed improvement factors (1.5 × 20 × 3), the result is about a factor of 100. Therefore, one would anticipate that a useful neutron radiograph with thermoluminescent techniques could be obtained with a total thermal neutron exposure of about 10^9 n/cm^2. This has been experimentally confirmed.

* A hexagonal fibre optic bundle (fibres are 0.0125 mm, or 0.0005 in. dia), approximately 3 mm across the flats, was used to piece together a rod about 1 cm in dia and 2 cm long. The image conduit used was type 40,643, American Science Center, Inc., Chicago, Ill. 60646.

The advantages of this method are predicated on its ability to integrate thermal-neutron image information for long periods of time without saturating, even in the presence of interfering gamma radiation. The transfer-exposure photographic technique (1-4) can be used to eliminate essentially the influence of gamma radiation on the neutron image, but the length of time one can accumulate information is limited because the activity of the recording screen will eventually become saturated. One does not have this saturation problem if the direct-exposure photographic method is used, but the thermoluminescent type of detector offers a superior neutron-to-gamma response ratio. It has been shown (4,9) that metal converter screens and X-ray film used as direct-exposure thermal-neutron detectors yield about equal film response for an exposure of 10^5 thermal n/cm² or 1 mR of ^{60}Co gamma radiation. For ZnS neutron scintillators instead of metal converter screens, this relationship can be improved so that a thermal-neutron exposure of only about 10^4 n/cm² is required to equal the film response of 1 mR of ^{60}Co gamma radiation. Thermoluminescent detectors employing the low Z^6 LiF have an even better relative neutron-gamma response; work in this laboratory indicates that one needs only about 5000 n/cm² (thermal) to produce the same amount of light as that produced by a gamma-ray exposure of 1 mR. Even if the two methods were comparable in their relative neutron-gamma response ratio, the reciprocity-law failure response of the scintillator technique, particularly at low light levels, is a disadvantage (10). (A reciprocity-law failure response refers to the fact that the response of film to light shows a maximum response for a certain range of light intensities. Above or below that range a greater exposure—light intensity × time—is required to produce the same film darkening.) At lower thermal neutron intensities, such as one might anticipate from a small accelerator or radioactive source arranged to yield a thermal neutron beam, the response of the scintillator direct-exposure detectors would be impaired because of the lower film response to the low light levels from the scintillator. The thermoluminescent detector, however, could be exposed to the neutron beam long enough to accumulate the energy needed for a large light release after the exposure. Reciprocity-law failure responses, therefore, could not influence this detector.

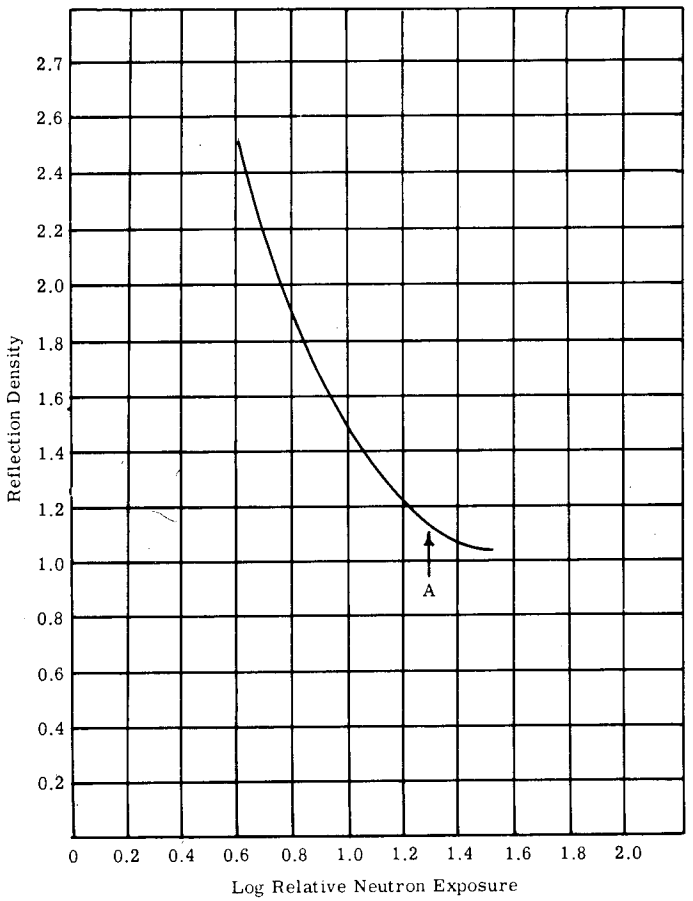

Figure 2. Polaroid film reflection density obtained on photographing thermoluminescent light releases from a variety of thermal-neutron exposures of a ^{6}LiF detector, as described in the text. The film used was Polaroid Type 47, 3000 speed. Point A represents a thermal-neutron exposure of 10^9n/cm². The curve shown is an average of several trials. Individual data points fell within a reflection density range of 0.1 from this average curve.

At the present stage of development, the thermoluminescent neutron imaging technique can provide a high-contrast resolution capability of about 0.125 mm (0.005 in.). Such a result is shown in Figure 3. The neutron image of a cadmium test object containing several through holes 0.020 in. (0.5 mm) dia is shown. The hole spacings in this cadmium object continually decrease. A hole separation at least as small as 0.125 mm can be observed.

Figure 3a
A positive print of a portion of a thermoluminescent neutron radiograph of a cadmium test piece containing a number of through holes 0.020 in. (0.5 mm) in dia. Hole separations, left to right are approximately 0.030 in. (0.75 mm), 0.020 in. (0.5 mm), 0.010 in. (0.25 mm), and 0.005 in. (0.125 mm). Closer hole spacings do not appear to be resolved.

Figure 3b
A print of a thermoluminescent neutron radiograph showing an image of a different cadmium test object. Hole sizes in the cadmium are, top to bottom 0.040 in. (1 mm), 0.75 mm, 0.5 mm, and 0.35 mm. The image was obtained by photographing the light release from a pressed and sintered powder LiF sample. The sample was cracked at the time of this picture.

Figure 4 shows that the technique is capable of displaying grey scale. Tests with uranium indicate that a thickness change of about 10 per cent can be neutron-imaged with 0.5-in.-thick material.

The thermoluminescent detector, even in its present stage of development, offers a number of advantages. These include

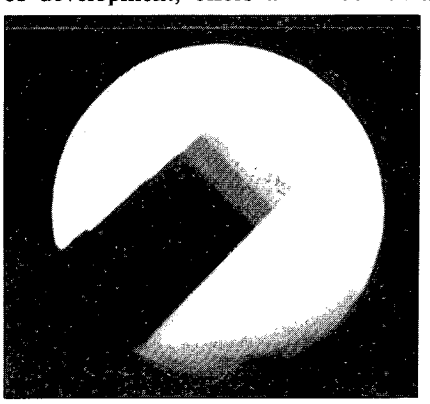

Figure 4
A thermoluminescent radiograph showing grey scale; the object was a cardboard stepped wedge.

the ability to accumulate thermal-neutron image information for extended periods without saturation* or reciprocity-failure response problems, and equal or better relative neutron-gamma responses than other available direct detection methods. These advantages are particularly important in cases involving relatively low neutron intensity beams and interfering gamma radiation. This is most likely to be the case when small accelerator or radioactive neutron sources are used for neutron radiography, or when the neutron radiographic technique is being used for the radiographic inspection of a thick, neutron attenuating material. The thermoluminescent technique may provide a very useful neutron image detector in these situations.

* It is true that thermoluminescent LiF will eventually saturate because, in principle, the traps can all be filled. In practice, this generally requires megarad orders of total dose.

References

(1) Kallmann, H. Neutron radiography, *Research* (London), 1, 254, 1948.

(2) Thewlis, J. Neutron radiography, *Brit. J. Appl. Phys.*, 7, 345, 1954.

(3) Berger, H. Comparison of several methods for the photographic detection of thermal neutron images, *J. Appl. Phys.*, 33, 48, 1962.

(4) ——— Neutron Radiography, Elsevier Publishing Co., Amsterdam, 1965.

(5) Proc. Technical Session Neutron Radiography; 24th National Convention, Society for Nondestructive Testing, published by the Society for Nondestructive Testing, Evanston, Illinois, 1965.

(6) Kastner, J., Berger, H. and Kraska, I. R. LiF thermoluminescence for neutron image storage, *Nuclear Applications*, 2, 252, June, 1966.

(7) Cameron, J., Zimmerman, D., Kenney, G., Bush, R., Bland, R. and Grant, R. Thermoluminescent radiation dosimetry utilizing LiF, *Health Phys.*, 10, 25, 1964.

(8) Frank, M. and Herforth, L. Zur thermolumineszendosimetrie mit CaF_2 "Mn", *Kernenergie*, 6, 435, 1961.

(9) Watts, H. V. Neutron radiography—Why and how (Ref. 5).

(10) Berger, H. Photographic detectors for neutron diffraction, *Rev. Sci. Instr.*, 33, 844, 1962.

Ciné-Fluoroscopic Studies in the Production of Castings

R. HALMSHAW, J. D. LAVENDER and R. L. DURANT, U.K.

ABSTRACT: A television/fluoroscopic X-ray image intensifier system has been used to study the pouring and solidification of castings in steel and other materials.

The apparatus produces a fluoroscopic image on a high-definition television monitor screen, from a 12-in.-dia primary fluorescent screen, and the display image is filmed with a suitably synchronized 16-mm ciné camera.

The apparatus has been used to study the flow of molten steel through various gating systems.

The formation of internal defects in the steel during solidification has also been studied, in particular the formation of gas cavities. A particular advantage of this technique is that the time during the casting process at which defects form is easily determined; gas bubbles can be seen to form and under certain conditions can also be seen to disappear again, presumably as the gas is absorbed by the metal.

Further applications of this ciné-fluoroscopic technique to the production of castings in nonmetallic materials are described. Again, the formation of various casting defects can be clearly shown. Possible future developments to extend the range of the equipment for this type of work are discussed.

Introduction

The direct viewing of an X-ray image on a screen, i.e. fluoroscopy, has had only a limited application in industry, largely because many of the specimens which require to be examined are of such a thickness that only a very low-brightness image is possible. However, electronic image intensifier systems now available produce bright enough images for viewing in an ordinary room.

For the work to be described a Marconi X-ray television-fluoroscopy apparatus was used. In this the image on the fluorescent screen is transferred directly on to a $4\frac{1}{2}$-in. image orthicon camera tube, by means of a Schmidt mirror optical system (Figure 1). The use of television circuitry enables very large gains in amplification, i.e. image brightness, to be obtained;

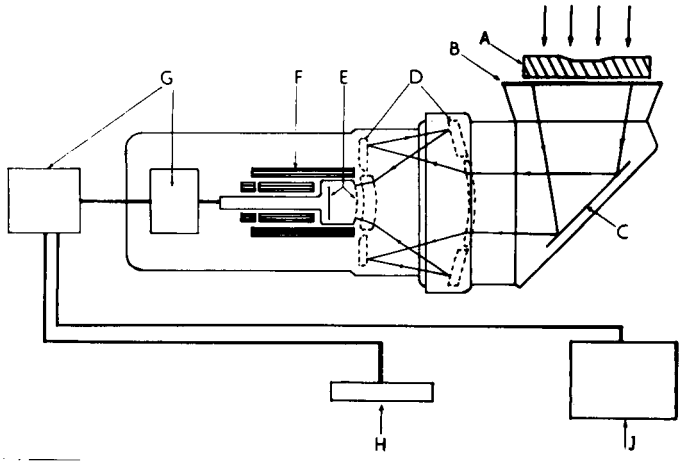

Figure 1 Diagram of Marconi image intensifier.

A—specimen
B—fluorescent screen
C—plane mirror
D—Schmidt optical system
E—pick up screens in image orthicon
F—orthicon focussing coils
G—amplifiers
H—control box
J—display monitor

Crown Copyright reserved. Reproduced by permission of the Controller of H.M. Stationery Office.

image contrast control is available, and electronic image-size magnification is possible. With the present equipment the final image can be either natural-size or magnified × 1.6.

Thus, many of the limitations of conventional fluoroscopy are overcome, and one can make use of an unique advantage of fluoroscopy—the ability to see an X-ray image of a moving specimen.

The equipment has been used to study the flow and solidification processes when liquid steel and other casting materials are poured into a mould.

So far as is known these preliminary experiments represent the first application of fluoroscopic techniques to the casting of ferrous metals.

Experimental Arrangements

The broad principle of the image intensifier equipment has already been described; the final image is produced on a 14-in. television monitor tube. This can be a long or short persistence tube—the latter being more suitable when filming a moving image, and the former for direct viewing.

The television image is a 1000-line triple-interlace scan, to provide image definition to match that attainable on the fluoroscopic screen, and this triple-interlace causes special problems in synchronization when recording with a ciné camera. The triple interlace is locked to the 50 c/s mains, each of the three scans taking 1/50th of a second. Thus a complete triple scan takes 3/50th sec (0.06 sec) and there are $16\frac{2}{3}$ complete scans per second. In a ciné camera with a 180° shutter, running at 16 frames/sec, the shutter is open and shut alternately for periods of 1/32 second (0.03 sec) so that even assuming correct phasing, each frame of the film cannot record the full information over the 1000-line scan; to do this the framing speed would have to be no faster than $8\frac{1}{3}$ frames/sec. If the camera covers only part of the screen image, i.e. less than the full 1000 lines, the framing speed on each frame can be increased to record full information.

If the framing speed is not matched to the television scan speed, and also adjusted to the correct phase relationship, an unexposed strip occurs on each frame of the ciné film, which on projection has the appearance of a moving band across the image.

As an alternative to 16-mm ciné-film recording, a Sony videotape recorder has also been used. This does not eliminate the usefulness of the film record, but enables an instant playback of the recorded event to be made, without the inevitable delays of film processing. It also permits editing before filming, and enables a continuous recording of up to two hours to be made.

The largest transportable X-ray set which could be used adjacent to the steel melting facilities was a 300-kV, 15mA machine, and all the experiments described have been done with this equipment.

During the steel pouring operation an operator was relatively close to the X-ray beam and adequate radiation protection had to be provided. Protection of the image intensifier equipment from the heat of the mould, from accidental splashes or overspill of molten steel was also obviously essential.

The first experiments used a horizontal X-ray beam, and the X-ray tube and image intensifier were each surrounded by Dexion-framed, lead-ply boxes (Figure 2). A focus-to-film distance of about 30 in. was used. The box holding the image intensifier had a 12-in. dia opening opposite the fluorescent screen; the screen was covered with $\frac{1}{8}$-in. Dural and $\frac{1}{4}$-in. asbestos board and this proved entirely adequate in preventing

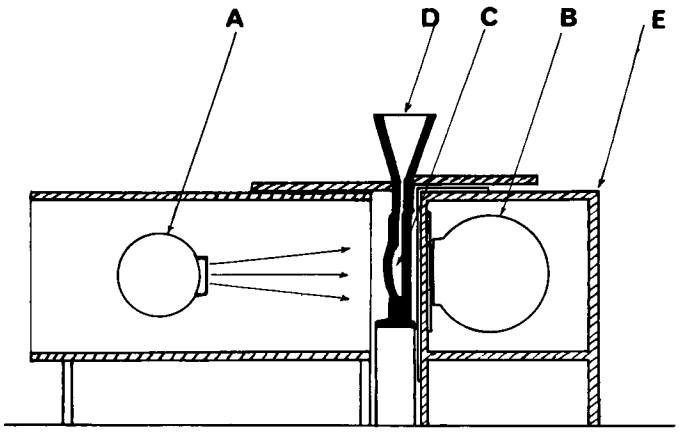

Figure 2 Sketch of set-up for a vertical mould and a horizontal X-ray beam.

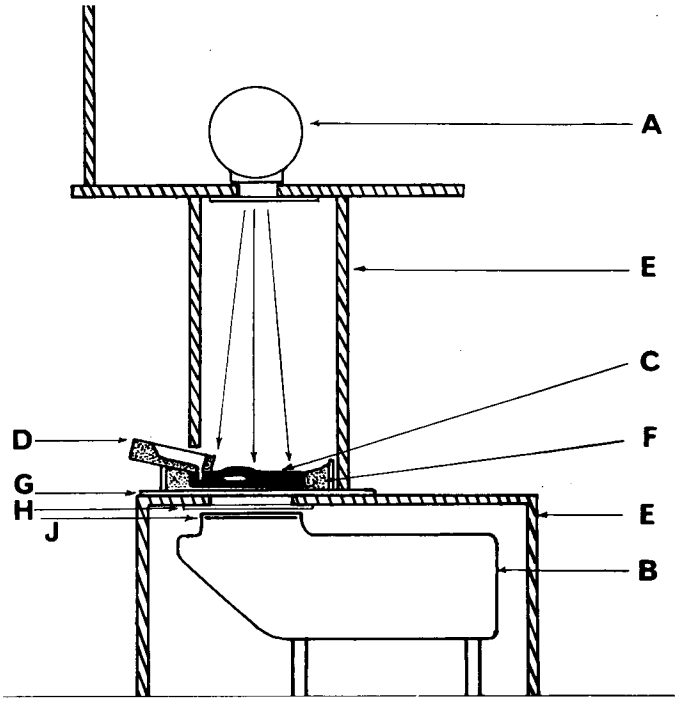

Figure 2A Sketch of set-up for a horizontal mould and a vertical X-ray beam.

A—X-ray tube
B—image amplifier
C—mould
D—pouring cup
E—lead-ply box
F—sand box round mould
G—steel sheet
H—asbestos sheet
J—fluorescent screen

heat from reaching the fluorescent screen from the hot mould. The mould, gate assembly and pouring cup were assembled in the space between the two boxes so that the nearest face of the mould was 1 in.-$1\frac{1}{2}$ in. from the fluorescent screen.

From this experience a similar protective unit, utilizing a vertical X-ray beam and horizontal moulds was built. (Figure 2A.) The protection for the fluorescent screen was a $\frac{1}{8}$-in. sheet of steel with asbestos sheet below, and a second asbestos sheet protected the X-ray tube window. In general the moulds were supported in sand boxes with sand surrounds to contain overspill of molten metal. The arrangements used to protect the fluorescent screen from heat were adequate for the sizes of casting and moulds used, but there was evidence that better heat protection would be necessary with larger castings. With this vertical arrangement, also, a bursting mould or extensive overspill in pouring could conceivably cause considerable damage to the fluorescent screen and the optical system of the image intensifier.

Sensitivity

In radiography, sensitivity is usually measured with some standard form of image quality indicator (I.Q.I.), and the following tables show values of sensitivity which have been obtained with this equipment under static conditions, with 300-kV X-rays (as used for these experiments) and for three higher X-ray energies.

I.Q.I. Sensitivities (per cent)

Thickness of steel (in.)	300 kV X-rays		400 kV X-rays	1 MV X-rays	5 MV X-rays	
	hole-type I.Q.I.*	wire-type I.Q.I.	wire-type I.Q.I.	wire-type I.Q.I.	wire-type I.Q.I.	hole-type I.Q.I.*
¼	9.5	3.9				
½	6.2	3.2	2.8	4.8	4.0	
¾	4.8	2.4	—	—	—	
1	6.3	3.1	1.6	3.1	—	
1½	7.0	4.2	1.6	2.6	2.1	
2	—	—	1.6	2.0	—	—
2½	—	—	1.9	1.9	1.2	—
3½	—	—	—	4.0	0.9	—
4½	—	—	—	6.5	0.9	2.5
6½	—	—	—		0.9	2.5
8½	—	—			1.1	2.3
10½	—	—			2.4	2.5

* The hole-type I.Q.I. has drilled holes of depth equal to diameter and the sensitivity is given as a percentage of the specimen thickness.

Castings in sand moulds. I.Q.I. Sensitivities in terms of metal thickness, using 300 kV X-rays

Thickness Penetrated	Hole type I.Q.I Sensitivity (%)
¼″ steel + ¾″ sand	20
½″ steel + ¾″ sand	12
1″ steel + ¾″ sand	10
1¼″ steel + ¾″ sand	10

These sensitivity values were obtained with flat plate specimens. It was found that if there was X-radiation reaching the fluorescent screen round the sides of the specimen, then the sensitivity deteriorated very markedly. Adequate edge-masking was found to be absolutely essential, and specimens such as thin bars were the most difficult on which to get good defect sensitivity.

For the later experiments, when the formation of defects was being studied, masks were cut from ¼-in. steel, with apertures slightly smaller than the projected area and shape of the castings, and the mould was positioned accurately over these before pouring.

Attention to the pattern of casting, from the point of view of ability to provide radiographic masking is probably the most important single factor in the technique. For experiments to show only metal flow, masking was not necessary.

From the point of view of sensitivity, also, it is desirable to use a size of casting that will comfortably fill the fluorescent screen image. A small casting, with a lot of unused image-area on the screen is likely to result in an image of unnecessarily poor sensitivity.

Results

The equipment was used first to study a variety of casting and gating problems in steel. In some of these experiments the molten metal was deliberately "gassed" and abnormal casting conditions were used in order to produce casting defects.

Some of the experiments performed were:—

(1) The study of the influence of design and dimensions of a simple gating system.

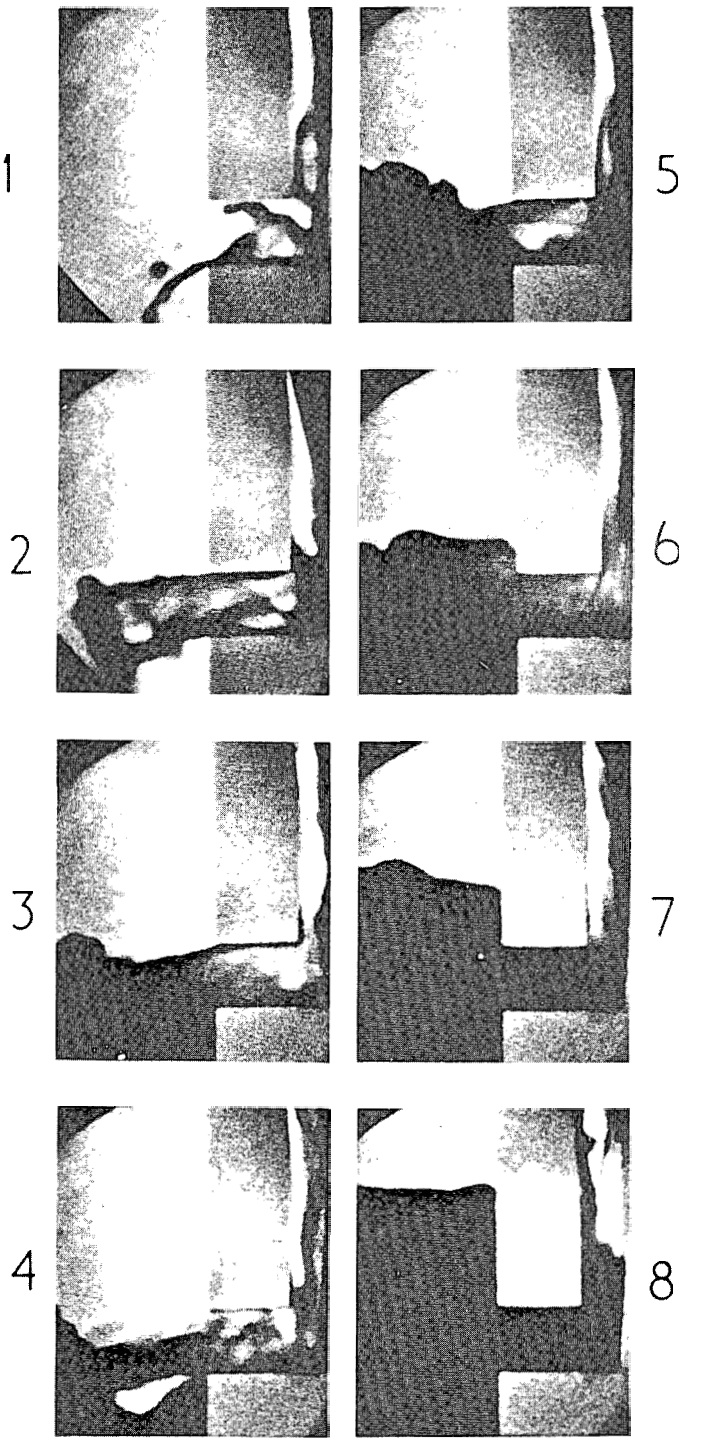

Figures 3, 3A Prints at 0.24-sec intervals, from ciné film, showing metal flowing through two gating systems.

Two tests moulds were produced using the CO_2 sodium silicate process; the only variation was in the ingate, one was 1 × 1½-in. section, Figure 3, and the second ¾ × ¾-in. section, Figure 3A, both sprues being 12 in. high, untapered and of 1-in. dia.

Thus these represented an unpressurized and a pressurized system. The steel was a nominal 0.3 per cent carbon steel poured at 1620°C, and the moulds were held in a vertical position during pouring.

Considering first the unpressurized system, Figure 3, the flow of metal out of the runner bush with the absence of any choking effect at the gate was insufficient to cause the gate or any

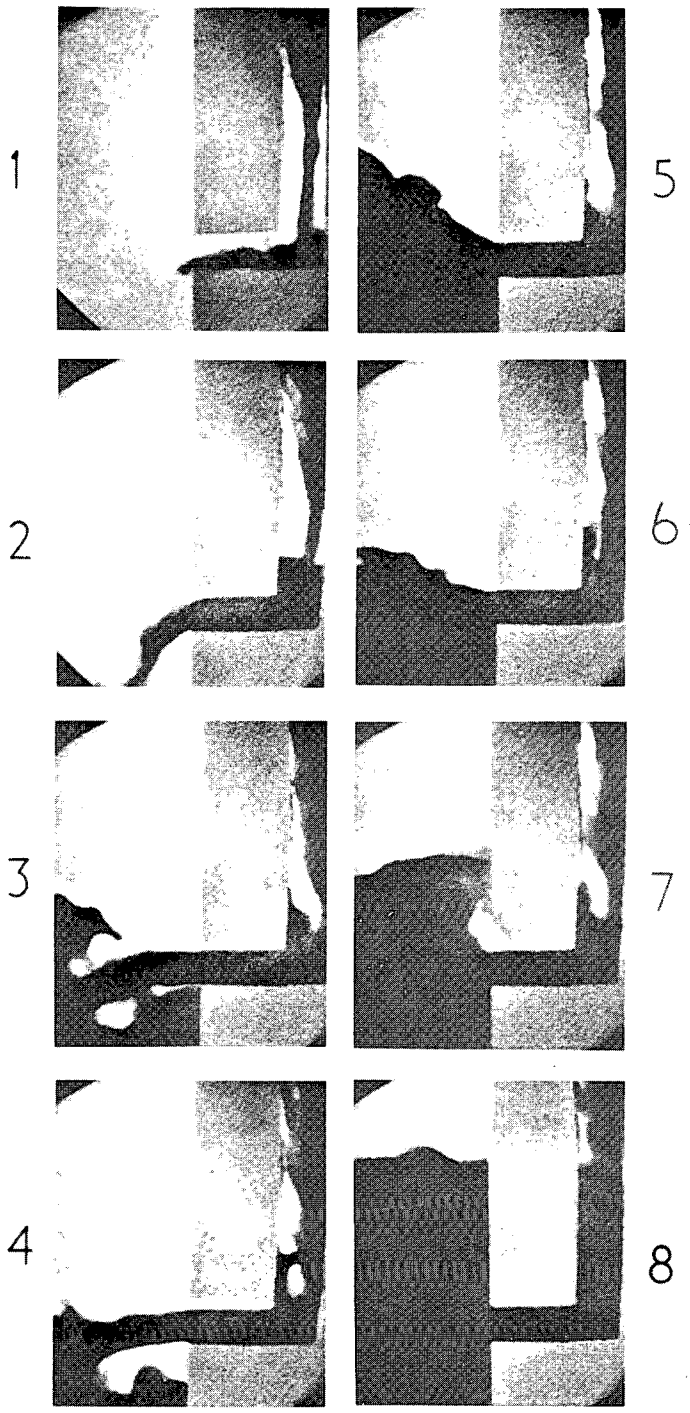

part of the sprue to be filled. The fall of metal to the bottom of the sprue, and the 90° change of direction at the gate resulted in much turbulence and air entrapment in the early stages. However, as would be expected, when the height of the metal in the casting exceeded the level of the ingate, the levels of metal in the casting cavity and sprue naturally equalized. Thus further metal was introduced into the casting with little further turbulence or air aspiration.

However, with the pressurized system, Figure 3A, although the ingate became full at an early stage, the metal velocity from the gate was obviously greater, and the metal in the casting cavity was consequently more turbulent; it appeared that air was being introduced into the casting at a later stage than with the unpressurized system.

As these castings were small and there was some difficulty in keeping the runner bush filled with metal, the experiments were repeated with a larger mould which would take longer to fill, and the steel was poured from a much larger bottom-pour ladle. A greater range of ingate sizes was also investigated.

Further investigations will require more carefully controlled experiments and consideration being given to the following factors: (a) the steel composition, (b) the pouring temperature, (c) the pouring rate, (d) the volume of steel which is to be poured. It is recognized that there are also other variables affecting gating studies, which will have to be considered during the investigation.

(2) The gating of commercial moulds for casting small Alcomax and Almico magnets of various shapes.

Results have been obtained on two specific patterns:

(a) A small circular magnet approximately 1 in. dia × 1 in. thick;

(b) A bar magnet $\frac{3}{8}$ in. wide × $\frac{1}{4}$ in. thick × 4 in. long approximately.

The shell mould for the circular magnet was designed to produce eight magnets, four on each side of the central horizontal runner; it was cast in a horizontal position.

A study of the series of photographs, Figure 4, shows that the central runner filled completely before any steel entered the ingate of any individual magnet. There was a temporary

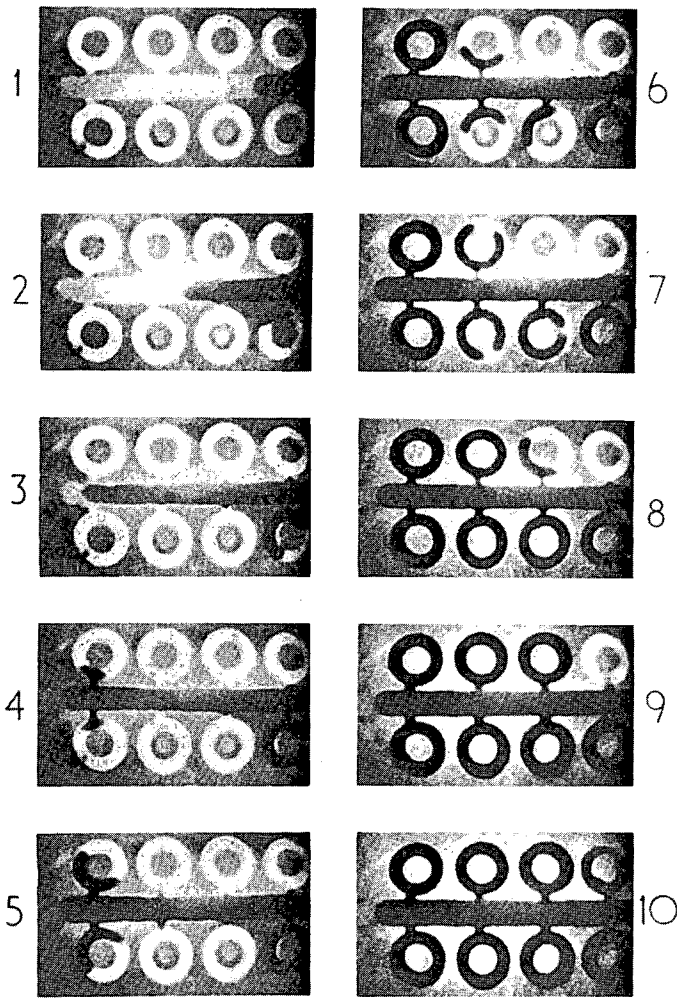

Figure 4 The running of small Alcomax magnets, in a horizontal mould. The prints are at 0.24-sec intervals.

stoppage at each separate ingate before the metal stream impinged on the central core of the magnet. This temporary stoppage and resultant impingement on the core could produce oxide formation and core wash owing to the effect of liquid pressure. A second important factor which requires further study is the random filling of the magnet cavities.

In the mould for the bar magnet fourteen magnets were produced in each shell mould, seven on each side of the central runner; this mould also was cast in a horizontal position.

As occurred in the circular magnet, the central runner filled completely before liquid metal began to fill the individual bar magnets; again these magnets filled in a random manner. It was noted, in addition, that the liquid steel ran along one side of the bar of the magnet and then round the other side before it was completely filled (Figure 5).

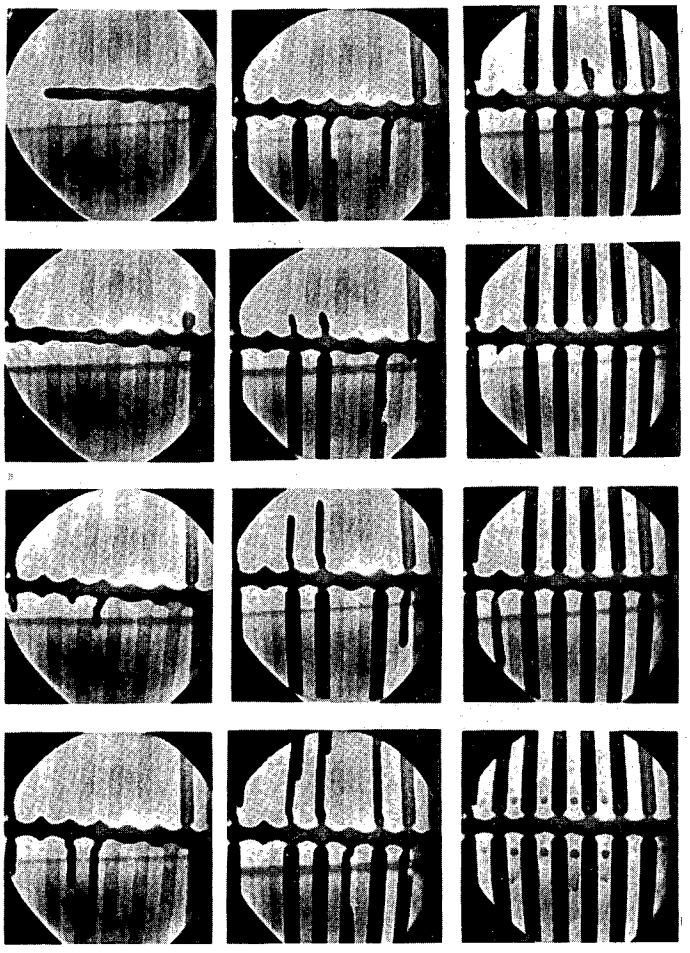

Figure 5 Small bar magnets in a horizontal mould. The prints are at .24-sec intervals.

(3) The filling and formation of flaws in a thin plate, cast vertically in a greensand mould.

This plate, 8 in. × 6 in. × 1½ in. was cast in a variety of steels—rimming steel, silicon-killed steel, aluminium-killed steel, aluminium-killed steel with various hydrogen contents produced by "steaming"—to study the filling of the mould and the development of internal defects. The formation of a cold shut, of gas-holes and of gross gas cavitation was observed. Some of the steels appeared to flow very inadequately.

Gas-hole Formation

Castings were made in shell moulds with variations in the hexamine-content of the resin, to study the effect on the formation of gas holes in the casting.

In one experiment, a 0.3-per cent carbon steel silicon deoxidized, at a temperature of 1600°C, was cast into a shell mould of a horizontal plate 6 in. × 6 in. × ⅜ in. by way of an ingate, ⅜ × ½ in. wide. The shell mould mix contained 96 per cent silica sand and 4 per cent resin as a physical bond. In order to set the resin during the production of a shell, approximately 12 per cent of the resin weight of hexamine was added. This hexamine addition can lead to the formation of gas holes in the casting by the evolution of nitrogen and to ensure the formation of gas cavities in these particular castings, the hexamine content was increased to 20 per cent of the resin weight.

After cooling, one of the castings was examined visually and was found to have an excellent clean surface. It was then sectioned, the sectioning being carried out with due regard to particular features which had been observed on the ciné-radiographs.

The ciné-radiographs (Figure 6) show:—

(i) After the formation of a sound clean solid skin, gas holes begin to form after 3-5 seconds. They did not form, however, in the region adjacent to the ingate due to liquid metal conditions in this zone; (ii) They enlarge quickly and unite, at about 7-10 seconds; (iii) A large central cavity forms at a position immediately adjacent to the ingate, at 15 seconds; (iv) Liquid steel returning from the ingate begins to fill the cavities which had originally formed, at 27 seconds; (v) Owing to internal gas pressure inside the solid steel skin, or due to lack of liquid steel fluidity, complete filling of the central cavity does not occur; (vi) Gas holes form in the secondary liquid feed metal adjacent to the ingate, at about 32 secs.

The liquid supplied under (iv) above may differ in composition from the liquid steel which initially entered the mould and a metallurgical investigation was made to determine whether this was the case.

Two main points of interest arise out of this investigation.

(i) The formation of the gas cavities and the centre-line defect which occurred during solidification were interconnected. The central cavity was centre-line shrinkage and its formation was unquestionably influenced by the pressure exerted by nitrogen evolution during solidification of the molten steel.

(ii) Gas cavities formed inside a solid steel skin during the early (3-5 seconds) stages in the solidification process. Liquid steel from the ingate filled certain parts of the centre-line shrinkage area and some of the gas cavities, giving rise to dark etching segregate zones.

Cast Explosive

Liquid RDX/TNT has been poured into a mould to simulate a G.W. warhead, of a shape likely to develop hot-tearing. It was demonstrated that the tears form a very long time after pouring, 20-30 minutes, but that the rate of formation of each tear is comparatively rapid. Not enough experiments have been made however for this to be taken as a generally valid conclusion.

The Formation of Hot Tears in Steel

A mould was designed so as to produce a wide hot tear with the plane of the tear approximately in line with the X-ray beam. The formation of the tear was clearly visible and the tear propagated very slowly over a period of several minutes.

Discussion of the Results

This image-intensifier equipment is basically medical equipment and is not specifically designed for the study of steel casting production. Several developments or modifications would be worthwhile.

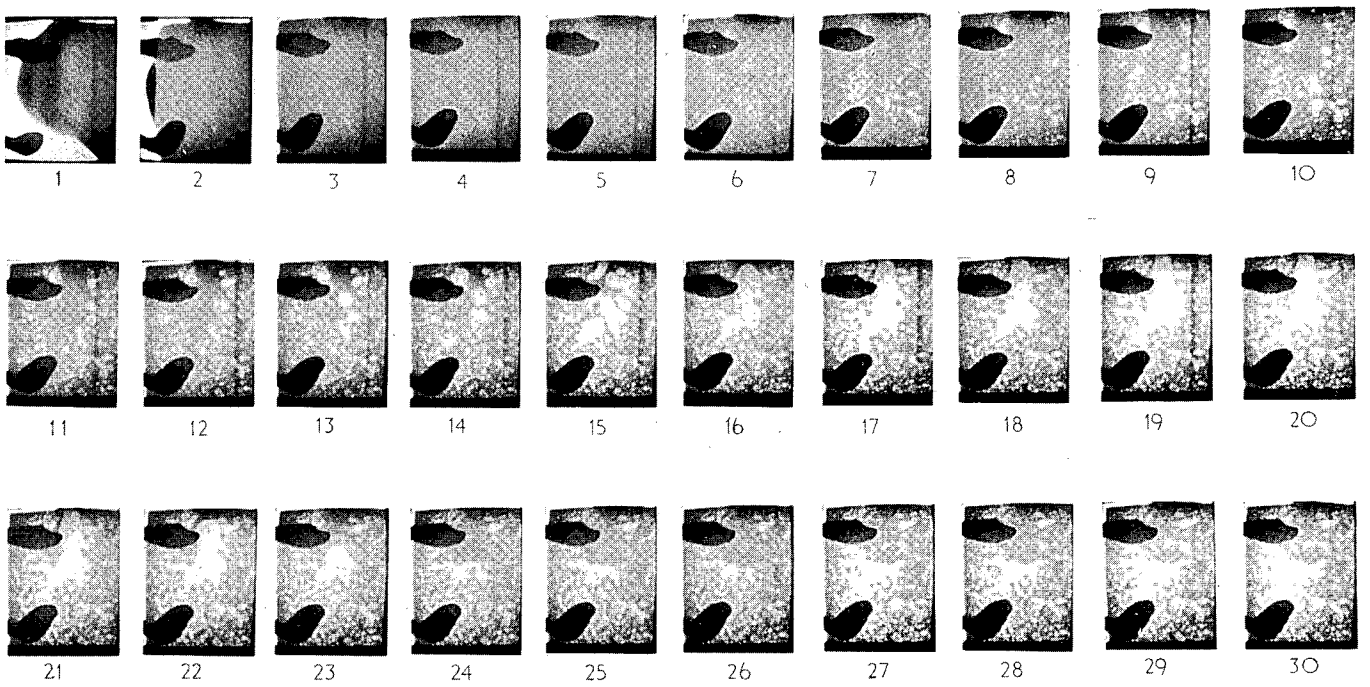

Figure 6 Silicon-deoxidized steel being cast in a shell mould. The prints are at 0.64-sec intervals.

X-ray Equipment

With the 300-kV X-ray set there is a fairly severe limitation on the penetrable thickness of steel when the thickness of the mould and the protective sheets are taken into account. The practical casting thickness is probably not greater than about $1\frac{1}{4}$-in. if good defect sensitivity is required. Higher energy X-rays would extend this thickness, 1-MV X-rays to about $2\frac{1}{2}$-in. steel and 2-MV X-rays possibly to 4-in. steel, although radiation protection problems would become more severe. Still higher energy X-rays such as are produced by the betatron and linac might be worth considering, and the steel thickness could then certainly be increased to about 8-in., but it should be remembered that the maximum area of casting which can be covered at any one position is a 12-in.-dia circle, and with this limitation penetration of very large thicknesses may not be very useful.

The use of high-energy X-rays will preclude hand-pouring of the molten steel, because of radiation hazards.

As the casting thickness is increased, so the heat-protection problem will become more serious. One solution would be to stand the casting and mould some distance away from the fluorescent screen. In order to minimize image blurring in these conditions, a fine-focus X-ray set would be desirable and in the 1-MeV or 2-MeV energy region, a Van de Graaff set would be the most suitable.

Image Intensifier

To extend the usefulness of the Marconi 12-in. image intensifier for this particular application it would be worthwhile:—

(i) to have a range of electronic image magnification, from $\times 1$ to about $\times 4$, so that the image of a small casting can be enlarged to fill the screen;

(ii) to be able to film at faster framing speeds, to slow down rapid motion; this can already be done to at least 60 fps, with a special continuous-feed ciné camera, but this has not been used for these experiments;

(iii) to extend the area of casting or mould which can be covered at one view by using a larger fluorescent screen. A flexible optical system would be the ideal solution, so that the screen area covered could be varied from, say, 4 in. $\times$ 4 in. to 24 in. $\times$ 24 in.

(iv) to have a primary fluorescent screen capable of absorbing and utilizing a greater proportion of the incident X-ray energy. This is especially important if high-energy X-rays are to be used.

Foundry aspects

An automatic, remote-controlled pouring system, both from the point of view of radiation safety and standardization of pouring technique, is essential for future experiments.

More consideration of the most suitable mould shape, method of support, and the use of pre-assembled moulds, masks, pouring boxes, etc., on a base plate ready to be slid into position as a complete unit, will certainly produce better results when setting-up time between pours is limited.

Conclusions

It has been demonstrated that a television/fluoroscopy image intensifier equipment can be used to study the pouring and solidification of small steel castings, and larger castings in lower density materials. The development of internal defects during solidification of the castings has been shown, and the flow of molten steel into small moulds through various gating systems has been studied.

The image intensifier has been used in conjunction with a 300-kV X-ray set and a synchronized ciné camera for this work and possible future developments on the equipment to extend its usefulness to this application are discussed.

Since the ciné recording speed is 25 frames/sec, it is also possible to produce single frames from the film record which show detail and specific conditions occurring at any given instant in the mould, on a known time-scale.

Technical Session 6/ Measurement of Stress & Elastic Properties

Ultrasonic Methods in the Study of Mechanical Characteristics of Iron and Carbon Steels

W. J. BRATINA, J. T. McGRATH, and R. I. MOORE, CANADA,
O. M. MRACEK MITCHELL, AND R. E. LOVE, U.S.A.

ABSTRACT: Measurement of the ultrasonic wave attenuation in the MHz frequency range associated with the vibration of free dislocation segments, i.e. dislocation damping, was explored as a potential nondestructive technique for the study of mechanical characteristics of metals over a wide temperature range (−150° to +150°C). Studies of strain aging and the ductile-brittle transition were made in iron and carbon steels. The amount of dislocation damping observed upon application of an external stress was used as a measure of the depinning of dislocations from interstitial atoms. This quantity was observed to decrease with aging time in the strain-aging study and as the temperature was lowered in the investigation of the ductile-brittle transition. A unit for automatically recording the amplitude of two echoes was used in conjunction with a variable-frequency pulse-modulated rf source, a linear or logarithmic amplifier and a dual-pen chart recorder. Cryostats suitable for ultrasonic attenuation studies of mechanical characteristics down to liquid nitrogen temperature are described. A magnetic field (up to 1 kOe) was applied by means of a solenoid and strain was applied by an Instron machine.

Introduction

Applications of ultrasonic techniques fall into two broad categories characterized by low and high ultrasonic intensity. An important application of the low-power ultrasonics is in the field of nondestructive testing, and either a travelling-wave pulse-echo technique or a resonance technique has been used. The principal applications of ultrasonic nondestructive testing are: 1) evaluation of the structural integrity of a material; 2) determination of the dimensions; and 3) determination of physical properties, particularly mechanical and magnetic characteristics. While the first two applications are widely used, there has been only a limited amount of work done in exploring the potentialities of the ultrasonic technique in the study of mechanical properties of materials. This paper discusses some of the physical properties that can be obtained from ultrasonic measurements.

The ultrasonic attenuation α in a material is in general the sum of several components:

$$\alpha = \alpha_D + \alpha_M + \alpha_S + \alpha_X$$

where α_D is the dislocation damping which is a measure of the energy absorbed by vibrating dislocations (1), α_M is the magnetomechanical damping (2, 3), α_S is the loss due to scattering of the wave (4), and α_X represents all other losses including bond losses. The first two components depend strongly on the mechanical and the magnetic state of the material, while the magnitude of scattering component depends on grain size and slip-band structure. The usefulness of the absolute attenuation as a measure of mechanical properties is therefore limited. Some typical values of absolute attenuation measured at 5 MHz on demagnetized ferrous specimens were as follows (in dB/cm): for Fe—0.08% C alloy in a quenched condition, $\alpha = 0.30$ to 0.45; for Armco iron annealed at 700°C for 2 hours, $\alpha \sim 0.30$; for 0.20% carbon steel with the same annealing treatment, $\alpha \sim 0.18$; and for a high carbon steel ($\sim$ 1.0% C) in the spheroidized condition, $\alpha \sim 0.14$.

The magnitudes of some of the components can be estimated by measuring the change in attenuation $\Delta\alpha$ as a function of parameters such as elastic strain or stress, strain rate, magnetic field strength, temperature, time and the number of stress cycles. A promising approach to a study of mechanical properties appears to be in terms of dislocation characteristics. The dislocation damping component of attenuation is sensitive to the dislocation structure since it is a measure of the energy absorbed by vibrating dislocations. In order to separate the dislocation damping from the other attenuation components ($\alpha_M, \alpha_S, \alpha_X$) the change in attenuation $\Delta\alpha$ can be measured versus elastic strain as a function of several parameters: strain rate, time and temperature.

Previous work on mechanical characteristics of fcc and bcc metals using ultrasonic techniques has been reviewed recently (5-8). In particular, the application of measurements of attenuation changes to studies of metal fatigue concerned primarily with the internal changes associated with cyclic stressing and not with surface crack detection (9, 10) have been discussed (8, 11, 12). Ultrasonic studies have been only recently extended to liquid nitrogen temperature (13). The experimental technique at temperatures above 150°C is still unsatisfactory, although the approach used by Lord (14) is promising. This paper discusses the application of an ultrasonic technique to the study of two metallurgical and mechanical phenomena, strain

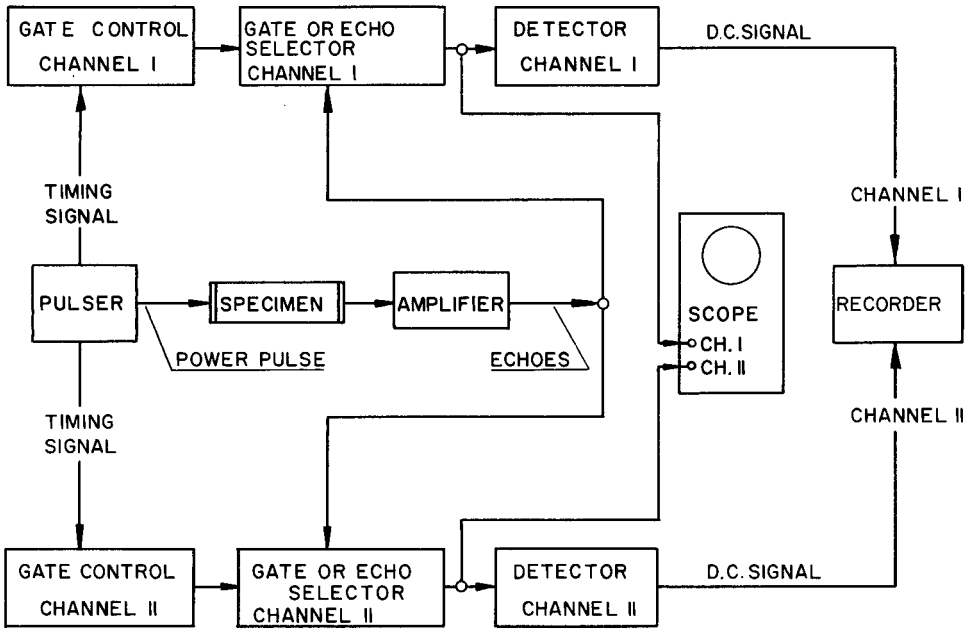

Figure 1
Block diagram of two-channel echo-selection and detection unit.

aging and ductile-brittle transition. The specialized equipment used in these studies, a unit for automatically recording the amplitude of two echoes and cryostat assemblies, is described.

Ultrasonic Instrumentation

The attenuation of longitudinal ultrasonic waves propagating along the specimen axis was measured in most cases by the transmission (double-ended) pulse-echo technique. X-cut quartz transducers (Valpey Corporation) were largely used and the coupling medium was either a hydraulic fluid Plexol (Rohm and Haas Company) or Dow Corning 200 Fluid, 1000 cS viscosity. Measurements of ultrasonic attenuation as a function of various parameters are facilitated by automatic continuous recording of the attenuation on a chart. Electronic equipment of great sensitivity, accuracy and versatility was designed. Figure 1 shows a simplified block diagram of the echo selection and detection unit which can be used to select two echoes and record their amplitudes simultaneously. A full description of the electronics will be reported elsewhere (15). Recently a modified and completely transistorized version was built at the Ontario Research Foundation and is undergoing testing. A pulser, either Arenberg Ultrasonic Laboratory PG-650-C or Ultrasonic Attenuation Comparator described by Chick et al. (16), was used as a variable-frequency pulse-modulated rf source. Either a Leeds and Northrup Speedomax H Azar Recorder or Moseley Dual Pen Strip Chart Recorder was used. The changes in the amplitude of a single echo can be used to monitor the changes in attenuation provided the over-all acoustic level remains constant. If, however, the impedance of the bond changes with temperature as it usually does in the temperature range of interest, the attenuation must be determined from the difference in amplitudes of at least two echoes. In this case the use of a logarithmic i.f. amplifier (LEL Model IML-1-30-08-50) enabled widely separated echoes to be monitored simultaneously. An echo near the start of the echo train and

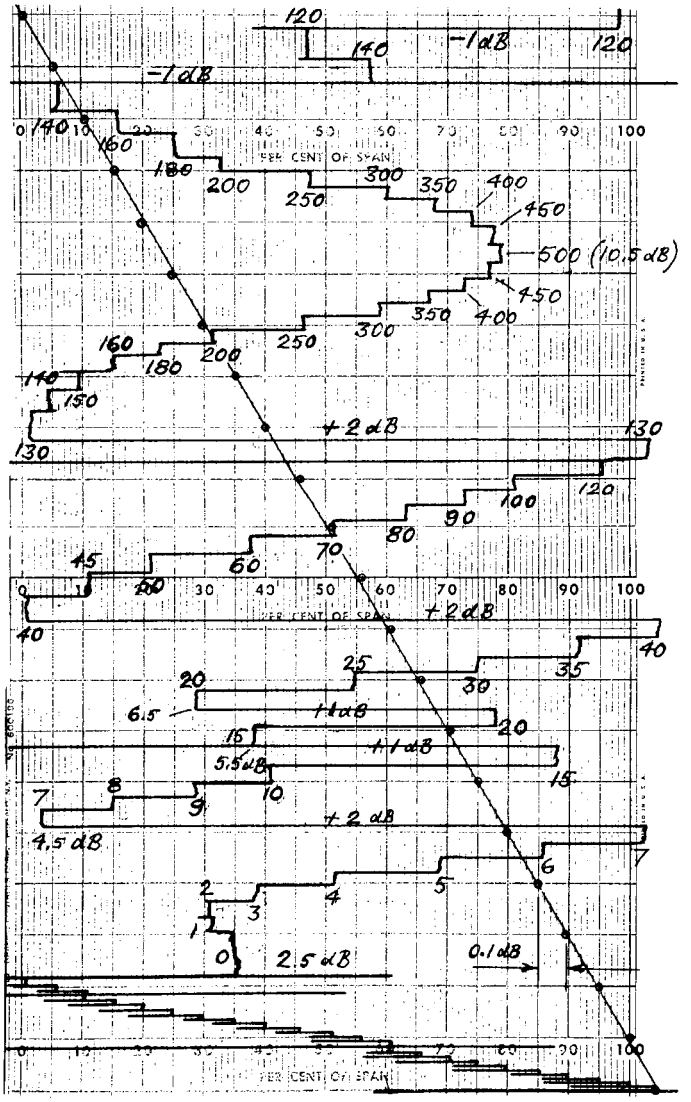

Figure 2. Typical recorder trace of one selected echo (6th echo). Full-scale sensitivity is 100 mV. The calibration trace (at the bottom) and calibration curve (diagonal line) in steps of 0.1 dB are shown. The change in echo amplitude is caused by the application of a progressively increasing magnetic field (0 to 500 Oe). Material is 0.20% C steel, annealed (700°C, 2 hr) and demagnetized.

one at a long delay time are both amplified without saturating the output stage.

Figure 2 shows a typical recording of one echo in a 0.20%C steel specimen in the annealed (700°C, 2 hr) and demagnetized condition. Very good linearity and great sensitivity with little background noise is noted. The attenuation changes observed were caused by an axially applied magnetic field. The data are replotted in Figure 3 and show magnetomechanical damping as a function of the magnetic field strength H. The results can be compared with those on a similar material reported earlier (3). The small maximum in attenuation, curve a, is associated with the internal stress present in annealed two-phase material (17). The attenuation maximum in curves bb and cc is caused by remanent magnetism.

Cryostats

The cryostat shown in Figure 4a was designed for measurement of ultrasonic attenuation during tensile stressing. A prototype of the present cryostat was reported earlier (13). The cryostat consisted of two stainless steel containers insulated by Styrofoam and separated by a Styrofoam gasket through which various connections to the specimen were introduced. The desired temperature was obtained by filling the containers with a specific quantity of liquid nitrogen. Temperatures down to liquid nitrogen temperatures were obtained. Temperature gradients were reduced to ±1°C by surrounding the specimen with a split cylinder of copper. The gradients were ±2°C if a magnetic field of 500 to 1000 Oe (0.4 to 0.8A) was applied in order to

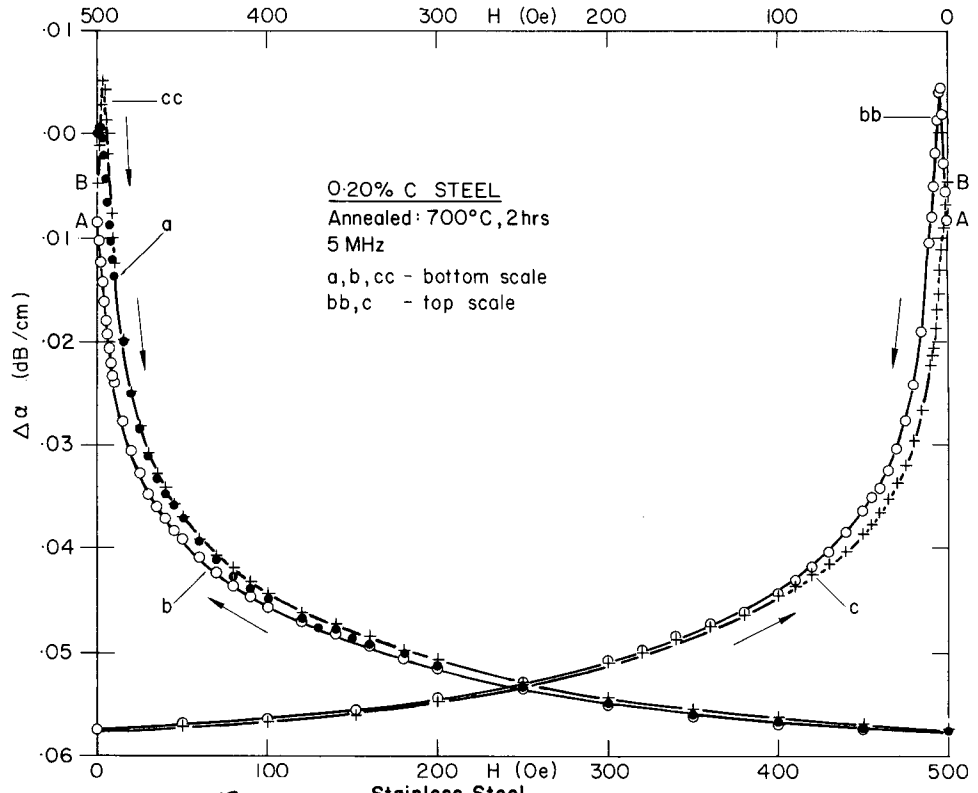

Figure 3
The data from Figure 2 are replotted, curve a (full circles, bottom scale). Included is also a complete Δα—H hysteresis curve: curve b (open circles, bottom scale) is continued through the point A into curve bb (open circles, top scale), and curve c (crosses, bottom scale) is continued through the point B into curve cc (crosses, top scale).

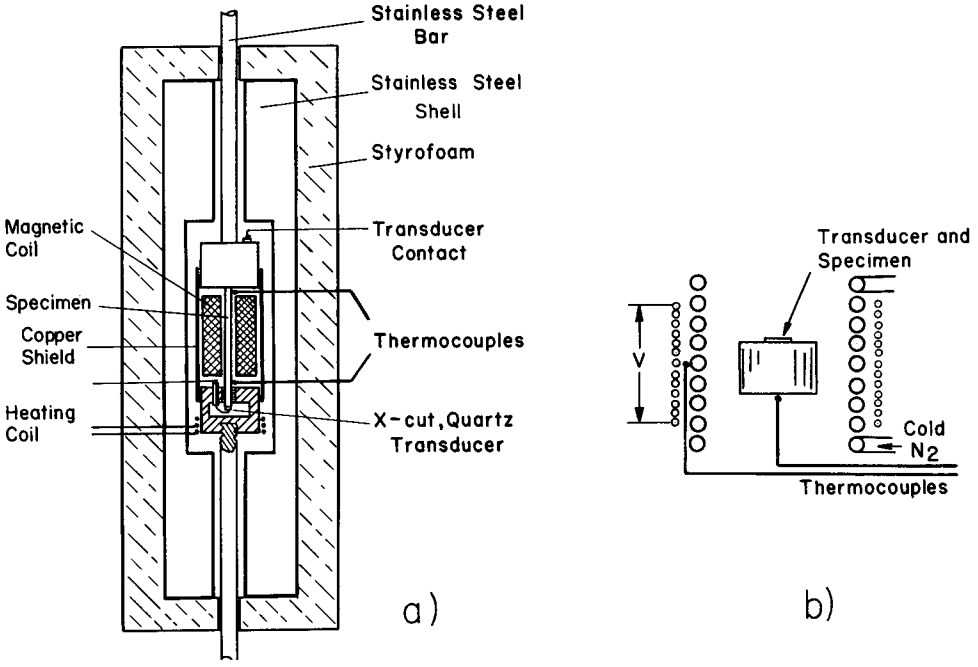

Figure 4
Two types of cryostat assembly

suppress the magnetomechanical component of attenuation α_M because of the unavoidable heat dissipation in the solenoid. In the liquid helium temperature range superconducting magnets may prove to be useful.

Another cryostat arrangement (18) which has been used for short specimens, about 10 mm long, in the temperature range from $-150°$ to $+150°$C is shown schematically in Figure 4b. The specimen was heated above room temperature by a resistance heater surrounding the specimen and cooled below room temperature by a stream of cold nitrogen gas obtained as boil-off from a storage can of liquid nitrogen in which another resistance heater was immersed. Each heater in turn was controlled by a temperature controller equipped with linear programming (Mohawk Scientific Corporation), which automatically changed the temperature of the specimen. Styrofoam insulation (not shown) surrounded the specimen and coils.

Experimental Results

The basis for the application of dislocation damping α_D to the study of mechanical characteristics was essentially dislocation-dislocation and point-defect-dislocation interactions. The work described here is limited to bcc metals, mainly iron and carbon steels in which the important point defects are interstitial nitrogen, carbon and oxygen. The interstitial-dislocation interactions are particularly strong and mainly responsible for the well known mechanical characteristics such as yielding, serrated stress-strain curve, strain aging, ductile-brittle transition, and the knee in the S-N curve. The use of dislocation damping measurements to yield information on strain aging and ductile-brittle transition is discussed.

Strain Aging

The changes in mechanical properties occurring in the bcc transition metals following plastic deformation are associated to a large extent with strain aging (19, 20). The process is interpreted in terms of pinning of the dislocations generated during deformation by interstitial atoms. The progress of strain aging is accompanied by a gradual decrease in the concentration of interstitial atoms in solid solution and by a return of the yield point. The latter phenomenon is the basis for the conventional technique applied in the study of strain aging.

The technique used in the present work, a study of dislocation damping α_D, is unique in the respect that it represents a direct measure of dislocation pinning by interstitial atoms (21). In a deformed material there is initially ($t = 0$) a large number of free dislocations and dislocation damping is a maximum. At a temperature low enough to suppress the diffusion of interstitials sufficiently ($T \sim$ liquid nitrogen temperature) this condition will remain unchanged for prolonged periods of time. At room temperature however, pinning of dislocations by interstitial atoms occurs readily and dislocation damping decreases with time, obeying, in general, the Granato-Hikata-Lücke equations (22). The decay of dislocation damping with time at 25°C after prior deformation, is virtually completed for Fe — 0.08% C alloy in the quenched condition at $t < 1$ sec; for annealed Armco iron at $t \sim 30$ min, for annealed 0.20% carbon steel at $t \sim 24$ hr, and for a high-carbon steel ($\sim$ 1.0% C) in spheroidized condition at $t > 72$ hr. However, because the dislocation damping depends on the fourth power of the dislocation loop length, it is a sensitive indicator of only the initial stages of pinning. For example, pinning of each dislocation segment by one interstitial atom results in a reduction of the dislocation damping to $\frac{1}{16}$ of its initial value. At this stage, the pinning is far from complete even though most of the change in attenuation has taken place. Dislocation damping at MHz frequencies is essentially amplitude independent, i.e., the ultrasonic strain amplitude ($\sim 10^{-7}$) is too small to induce a breakaway of dislocations from interstitials. However larger strains can cause a breakaway of the dislocations from the pinning centres and cause an increase of the attenuation. The return of the yield point is associated with breakaway strains many orders of magnitude larger than the ultrasonic strain ($\sim 10^{-3}$).

To study the progress of strain aging, therefore, it is necessary to apply an external strain to the specimen. A previously deformed high-carbon steel specimen ($\sim$ 1.0% C) was chosen for convenience, since it is characterized by very slow strain aging at room temperature. An elastic strain of 6.6×10^{-4} applied at a strain rate $\dot{\epsilon} = 0.85\times10^{-4}$ sec^{-1} resulted in a rise in attenuation which was essentially dislocation damping associated with dislocations pulled away from the interstitial pinning centres by the applied strain. The increase in attenuation is subject to a decay with time for a given strain. One-hour decays at a strain of 6.6×10^{-4} are shown in Figure 5 at 25°C after various aging times (0 to 1280 min) at a selected aging temperature of 175°C. The gradual permanent immobilization of dislocation loops in a strain aging sense with aging time is noted and corresponding dislocation damping is shown as a dashed curve versus log aging time. Similar series of curves were obtained at other aging temperatures. This method, employing dislocation damping is not only the most direct way of determining the degree of immobilization of dislocation loops and therefore the degree of strain aging, but can provide a measure of pinning strength over a wide range of strains up to the yield strain. This

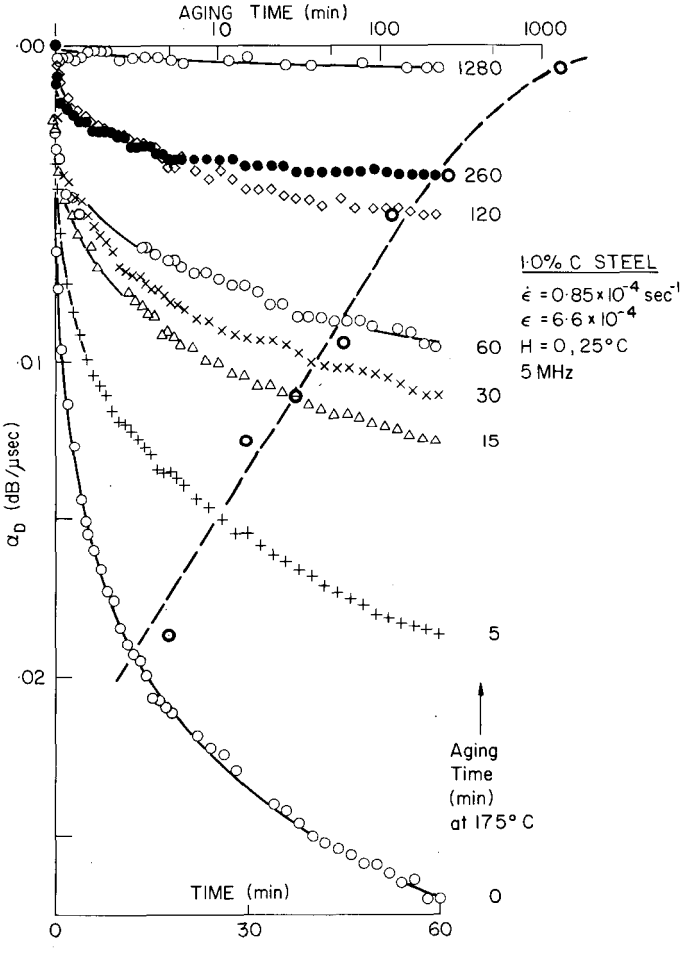

Figure 5. Decay of dislocation damping with time at 25°C in a 1.0% C steel at a strain of 6.6 × 10^{-4}. Decay curves obtained after various aging times at 175°C are shown. The 1-hr values are replotted versus log aging time (dashed curve).

ultrasonic technique therefore appears to be capable of measuring the quantities essential in the strain aging process and it may well be developed into a nondestructive method.

Ductile-Brittle Transition

The mechanical properties of most transition bcc metals are strongly dependent on temperature, as manifested by the ductile-brittle transition. The embrittlement is a function of material (composition, structure, grain size, thermal and mechanical history) and the test conditions (temperature, strain rate). In current practice, the transition temperature range is determined by impact testing, i.e., a fracture load is applied at a very high strain rate ($\dot{\varepsilon} = 10^2 - 10^3$ sec^{-1}) to a notched specimen. The test is so severe that it satisfies most practical conditions.

In the present experiment (Figure 6) the dislocation component of ultrasonic attenuation was measured in a 1.0% carbon steel as a function of external elastic strain (up to 6.6×10^{-4}) at a series of temperatures in the range 25° to −124°C. The strain rate was rather low ($\dot{\varepsilon} = 0.85 \times 10^{-4}$ sec^{-1}) compared with the strain rates employed in impact testing; thus embrittlement is expected to occur at temperatures much below the impact testing transition. The change in attenuation with strain, shown in Figure 6, is essentially the dislocation damping, although a correction for a small magnetomechanical component should be made. A field of 500 Oe nominal, applied by an axial solenoid, was not large enough to suppress the magnetomechanical damping completely because of imperfect flux closure. A larger field was not desirable because of excessive heat dissipation in the cryostat chamber. The magnitude of magnetomechanical damping correction can be estimated from the results at −124°C. The initial decrease in attenuation versus strain is caused by magnetomechanical damping and the subsequent rise by dislocation damping.

The main feature of Figure 6 is a gradual decrease in dislocation damping with temperature for a given strain. Strain-amplitude-independent damping is, according to the Granato-Lücke theory, proportional to the product: $A \cdot B \cdot L^4$ where Λ is the dislocation density, B is the dislocation damping constant, and L is the average loop length of vibrating dislocations. Application of an elastic strain, as in Figure 6, does not change the dislocation density because dislocation generation cannot occur at these strains. In a series of other experiments in the same temperature range it was established that there is practically no change in B. This leaves the average loop length as the only variable. These experiments therefore provide direct proof that the breakaway of dislocations from interstitials becomes increasingly more difficult as the temperature is decreased. If, however, the elastic strain is increased beyond the value in Figure 6 an additional breakaway is possible and further lowering of the temperature would be necessary to suppress it. Large plastic flow and ductility of a material is associated with a high number of free dislocations while a lack of free dislocations will promote embrittlement. It appears from the results in Figure 6 that as the temperature is decreased, it becomes more difficult to obtain free dislocations which would participate in plastic flow and therefore the ability of the material to deform in a ductile manner is reduced because of lack of dislocations.

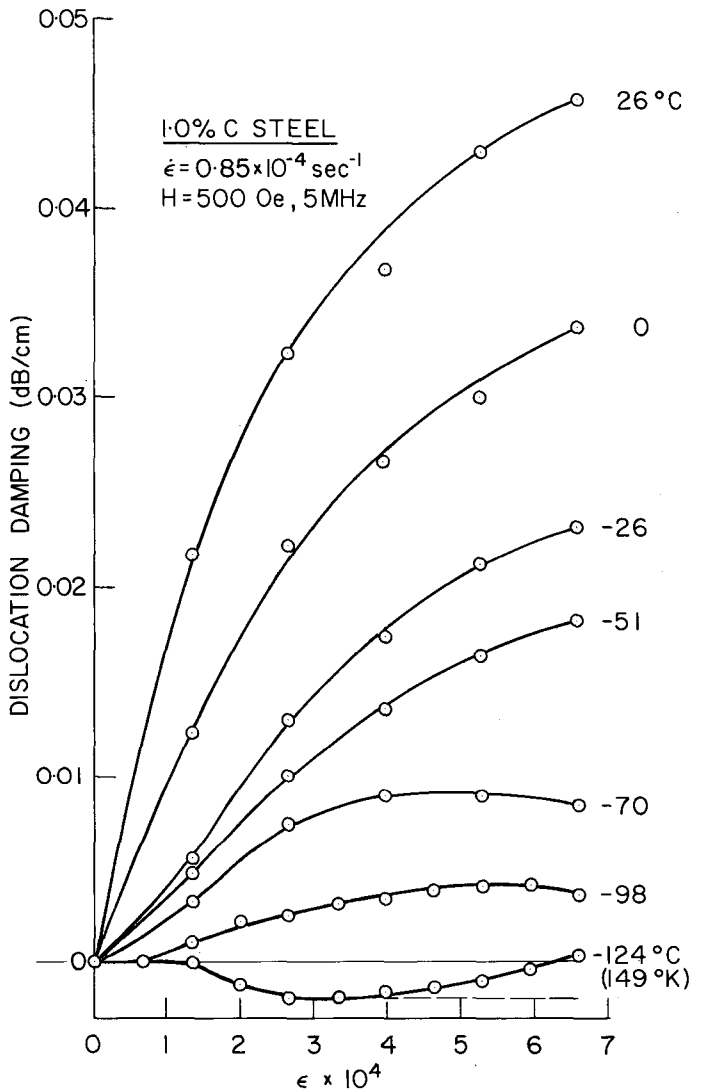

Figure 6. Dislocation damping at various temperatures in a 1.0% C steel strained elastically to a maximum strain of 6.6 × 10^{-4} at a strain rate of 0.85 × 10^{-4} sec^{-1}.

Comments

Basic studies of material properties with ultrasonic techniques indicate that these techniques might be applied to complex problems in nondestructive testing. In particular, with further basic work, nondestructive testing instrumentation and techniques might be developed for: 1) following the course of fatigue in metals and the possibility of predicting fatigue behaviour within some limits; 2) measuring internal stress; 3) indicating the extent of strain aging and the associated changes in mechanical properties; and 4) following ductile-brittle transition phenomena and developing a criterion for embrittlement behaviour.

Acknowledgments

The major part of this work was supported by the Province of Ontario through the Department of Economics and Development.

References

1. Granato, A. V. and Lücke, K. The vibrating string model of dislocation damping. Physical Acoustics (W. P. Mason, Ed.), Academic Press Inc., New York, 1966, Vol. 4A, 225–276.
2. Bratina, W. J., Martius, U. M. and Mills, D. Magnetic contribution to the ultrasonic attenuation in annealed and deformed steel (SAE1020). *J. Appl. Phys.*, 1960, **31**, 241S.
3. Martius, U. M. and Bratina, W. J. Frequency dependence of ultrasonic wave attenuation in Armco iron and low-carbon steel. *J. Appl. Phys.*, 1961, **32**, 280S.

4. Papadakis, E. P. Rayleigh and stochastic scattering of ultrasonic waves in steel. *J. Appl. Phys.*, 1963, **34**, 265.
———— From micrograph to grain-size distribution with ultrasonic applications. *J. Appl. Phys.*, 1964, **35**, 1586.
5. Hikata, A. Effect of plastic deformation on ultrasonic attenuation in metals. *Bull. Govt. Mech. Lab.*, Japan, 1960, **39**, 1.
6. Hirone, T. Quality inspection of materials by ultrasonic method in Japan. *Proc. 3rd Intern. Conf. Nondestructive Testing,* Pan-Pacific Press, Tokyo, 1961, 317.
7. Truell, R., Elbaum, C. and Hikata, A. Ultrasonic methods in the study of plastic deformation. Physical Acoustics (W. P. Mason, Ed.), Academic Press Inc., New York, 1966, Vol. 3A, 199–221.
8. Bratina, W. J. Internal friction and basic fatigue mechanisms in bcc metals, mainly iron and carbon steels. Physical Acoustics (W. P. Mason, Ed.) Academic Press Inc., New York, 1966, Vol. 3A, 223–291.
9. Rasmussen, J. G. Prediction of fatigue failure using ultrasonic surface waves. *Nondestructive Testing,* 1962, **20**, 103.
10. Klima, S. J., Lesco, D. J. and Freche, J. C. Application of ultrasonics to detection of fatigue cracks. *Experimental Mechanics,* 1966, **6**, 154.
11. Truell, R., Chick, B., Anderson, G., Elbaum, C. and Findley, W. Ultrasonic methods for the study of stress cycling effects in metals. WADD TR 60-920, 1961.
12. Chick, B., Hikata, A., Anderson, G., Findley, W., Elbaum, C. and Truell, R. Ultrasonic methods in the study of fatigue and deformation in single crystals. ASD-TDR-62-186, Part II, 1963.
13. Love, R. E., Bratina, W. J. and McGrath, J. T. Ultrasonic methods in the study of plastic deformation of body centered cubic metals. *Proc. 5th Intern. Conf. Acoustics,* Liège, 1965, paper D42.
14. Lord, A. E. High-temperature operation of vacuum-evaporated, thin-film acoustic wave transducers. *J. Appl. Phys.*, 1966, **37**, 4593.
15. Moore, R. I., Mitchell, O. M. M. and Bratina, W. J. Automatic recording of ultrasonic attenuation. (To be published.)
16. Chick, B., Anderson, G. and Truell, R. Ultrasonic attenuation unit and its use in measuring attenuation in alkali halides. *J. Acoust. Soc. Am.*, 1960, **32**, 186.
17. Mills, D. and Bratina, W. J. Residual stress studies in ferromagnetic materials by ultrasonics. *Proc. Symp. Physics and Nondestructive Testing,* Southwest Res. Inst., San Antonio, Texas, 1963, 356.
18. Mitchell, O. M. M. Dislocation relaxations in single-crystal and polycrystalline niobium and tantalum at megahertz frequencies. *J. Acoust. Soc. Am.*, 1967, **41**, 1058.
19. Baird, J. D. Strain aging of steel. *Iron and Steel,* 1963, May, 186; July, 368; August, 400; September, 450.
20. Imgram, A. G. Strain aging of refractory metals. DMIC Rept. 134, 1960.
21. Mitchell, O.M.M. and Bratina, W. J. Strain aging studies by dislocation damping. *J. Metals,* 1964, **16**, 83.
22. Granato, A. V., Hikata, A. and Lücke, K. Recovery of damping and modulus changes following plastic deformation. *Acta Met.* 1958, **6**, 470.

Élasticimétrie et inélasticimétrie automatiques entre −200 et +250°C

MAURICE SEPASER, PIERRE AZOU et PAUL BASTIEN, FRANCE

Les problèmes relatifs au comportement soit élastique soit inélastique des matériaux ont toujours été à l'ordre du jour d'un grand nombre de laboratoires compte tenu du double intérêt pratique et théorique qui se rattache aux grandeurs physiques correspondantes. La littérature scientifique fait d'ailleurs état de nombreuses publications dont l'article de McSkimin (1) donne une bonne vue d'ensemble.

Cependant dès que l'on veut choisir une technique de mesures, on doit s'orienter soit vers les méthodes statiques ou quasi-statiques, soit vers celles utilisant vibrations ou ondes. Notre but n'est pas ici de dégager les avantages et inconvénients mutuels. Toutefois, l'inconvénient majeur des méthodes statiques réside dans la durée de l'expérimentation nécessaire pour obtenir un résultat complet au point de vue élastique et inélastique. A titre d'exemple, la détermination simultanée du module d'Young, du coefficient de Poisson et de la constante de temps de relaxation dans un essai de traction simple, pour une température donnée, nécessite un appareillage compliqué et extrêmement sensible si l'on ne veut pas par une charge trop importante du matériau, altérer l'élasticité de celui-ci.

Afin d'éviter ces difficultés, l'utilisation d'ondes sous forme d'impulsions ou d'ondes permanentes a été faite depuis longtemps. Florisson, Cabarat, Förster, pour ne citer que les plus connus, ont pu, avec une mise en oscillation tant capacitive qu'inductive ou par percussion et dans un domaine souvent restreint de température, mesurer pratiquement un seul coefficient d'élasticité et l'amortissement intérieur de l'éprouvette utilisée. Cependant de nombreux problèmes expérimentaux se posaient, notamment au point de vue du réglage des dispositifs de mise en oscillation du matériau. Ces difficultés s'aggravaient pour des mesures à une température autre que l'ambiante.

Le but de notre recherche, objet de cette communication, était de mettre au point, dans un domaine aussi étendu que possible de températures, un appareillage permettant, avec le minimum de réglages en cours d'essai, d'obtenir l'ensemble des coefficients d'élasticité et l'amortissement intérieur. Dans la suite de cet exposé, nous envisagerons successivement: le principe de la méthode, la réalisation pratique et des exemples pris dans l'ensemble de nos résultats expérimentaux.

Principe de la méthode

Nous avons choisi de déclencher, dans une éprouvette cylindrique dont la longueur est grande par rapport à son diamètre, un ensemble complexe d'ondes faisant intervenir simultanément les

trois modes de vibrations libres: longitudinales (dans le sens de l'axe du cylindre) transversales et de torsion.

Coefficients d'élasticité

La connaissance de deux des vitesses de phase de propagation de ces divers types d'ondes permet d'obtenir l'ensemble des coefficients d'élasticité suivant les relations indiquées ci-après. Cependant il ne faut pas oublier que les expressions obtenues pour ces diverses vitesses dépendent considérablement des conditions aux limites et qu'en particulier la vitesse de phases des ondes longitudinales peut s'exprimer de trois manières:

$$V_e = \sqrt{\frac{E}{\rho}}$$

barre de faible diamètre

$$V_e = \sqrt{\frac{E}{\rho} \frac{1-\nu}{(1+\nu)(1-2\nu)}}$$

matériau de grande section avec sollicitation locale

$$V_e = \sqrt{\frac{E}{\rho} \frac{1}{1-\nu^2}}$$

plaque de faible épaisseur

E étant le module d'Young, ν le coefficient de Poisson et ρ la masse volumique.

La considération des vitesses de phase des ondes longitudinales V_e et de torsion $V\tau$ permet d'atteindre les coefficients d'élasticité E et ν pour une éprouvette de faible diamètre par rapport à la longueur lorsque s'établit dans celle-ci une propagation stationnaire conservatrice ou dissipative. Si l'on désigne par F_e la fréquence du mode fondamental en propagation longitudinale et F_t la même caractéristique pour la torsion, on peut écrire:

$$E = 4\rho L^2 F_e^2 \quad (1)$$

$$G = \mu = 4\rho L^2 F_t^2 \quad (2)$$

G module de cisaillement, μ premier coefficient de Lame et L longueur de l'éprouvette.

À partir de E et G (ou μ on obtient les autres coefficients élastiques: λ second coefficient de Lame, χ coefficient de compressibilité et ν coefficient de Poisson.

$$\nu = \frac{E}{2\mu} - 1 = \frac{1}{2}\left(\frac{F_e}{F_t}\right)^2 - 1 \quad (3)$$

$$\lambda = \mu \frac{2\nu}{1-2\nu}$$

soit

$$\lambda = 4\rho L^2 F_t^2 \frac{(F_e/F_t)^2 - 2}{3 - (F_e/F_t)^2} \quad (4)$$

et

$$\chi = 3 \cdot \frac{1-2\nu}{E}$$

soit

$$\chi = \frac{3}{4\rho L^2 F_L^2}\left[3 - \left(\frac{F_L}{F_T}\right)^2\right] \quad (5)$$

De l'examen des diverses relations il apparaît immédiatement que seule l'expression de ν est indépendante de ρ et de L. Il en résulte que, si l'on envisage les trois mesures de F_e, ν, F_t, le coefficient de Poisson sera le seul coefficient accessible directement. Pour évaluer les deux autres coefficients il sera indispensable de réaliser simultanément ou parallèlement une détermination de masse volumique et de longueur aux différentes températures étudiées. Dans une première approximation, comme le groupement ρL^2 fait intervenir ces deux paramètres simultanément, on s'aperçoit que

$$\rho L^2 = (1 - \alpha\theta)\rho_o L_o^2$$

α étant le coefficient de température dans la dilatation linéaire. Une simple dilatométrie doit donc permettre de dégager l'influence du facteur ρL^2.

Pour le seul coefficient accessible directement, ν, la précision théorique se déduit de la relation (3) et du mode de mesure. Nous mesurons et enregistrons directement la valeur

$$R = \frac{F_L}{F_T} ,$$

d'où

$$\nu = \frac{1}{2}R^2 - 1 \text{ et } d\nu = RdR$$

R est mesuré à $0{,}5 \cdot 10^{-4}$ près et vaut toujours 1,6 à 1,7 d'où $d\nu \# 10^{-4}$. Une modification sur l'un des appareils de mesure nous permet de mesurer un nombre $R' = k R$ $(k < 1)$ et de l'enregistrer face à une échelle qui permet la lecture directe du coefficient de Poisson ν. Cette échelle, linéaire, coïncide avec la graduation du papier millimétré et conserve en pratique la précision théorique.

Coefficient d'inélasticité

Par suite de l'amortissement intérieur, dont nous n'analyserons pas ici les origines, toute vibration libre présente une décroissance en fonction du temps. Celle-ci apparaît comme étant de forme exponentielle si l'amortissement est du type fluide. L'amplitude A_i de la vibration, quel que soit son mode $(i = e, \tau, t)$, peut donc s'exprimer par la relation

$$A_i = A_{io} \exp\left(-\frac{t}{\tau_i}\right), \tau_i$$

étant la constante de temps de la décroissance. On caractérise souvent l'amortissement intérieur δ_i par le décrément logarithmique des oscillations libres amorties. Par définition

$$\delta_i = \frac{1}{n} \text{Log}_e \frac{A_{io}}{A_{in}}$$

A_{io} et A_{in} étant deux valeurs maximales séparées par n pseudo-périodes. Il est commode de prendre n tel que $nT_i = \tau_i$ (T_i pseudo-période) il vient alors:

$$A_{in} = A_{io} \exp(-1)$$

d'où

$$\delta_i = \frac{1}{n} \text{Log}_e \left[\frac{A_{io}}{A_{io}\exp(-1)}\right] = \frac{1}{n}$$

Le décrément logarithmique des oscillations libres est alors égal à l'inverse du nombre d'oscillations comprises entre deux amplitudes telles que la seconde est égale à la première divisée par e.

Cependant il est possible que ce nombre soit ou trop grand ou trop faible. On peut, dans de telles conditions, travailler avec un temps de mesure différent. Par exemple on fixe le rapport

$$\frac{A_{io}}{A_{in}} = \exp(+K),$$

le décrément logarithmique devient dans ce cas

$$\delta_l = \frac{K}{n}.$$

Cette dernière formule est d'un emploi plus aisé que la première. Elle montre de plus que l'on peut, à un coefficient multiplicatif près, considérer que le décrément logarithmique δ_l est inversement proportionnel au nombre d'oscillations libres comprises entre deux amplitudes de rapport imposé.

Théoriquement il est possible de définir trois amortissements intérieurs correspondant aux trois modes de vibration. Cependant la réalisation pratique de la mesure n'est pas toujours simple car ils peuvent être d'ordre de grandeur différent. Nous espérons, toutefois, réaliser simultanément ces trois mesures car elles permettraient de vérifier si l'amortissement intérieur est à une même fréquence indépendante ou non du mode de sollicitation: compression, cisaillement ou torsion.

Réalisation pratique

Pression résiduelle et température

Afin de limiter au maximum les pertes par échange avec l'environnement, la mesure se fera sous pression résiduelle faible de l'ordre de 10^{-3} à 10^{-4} Torr. Ceci a de plus l'avantage de protéger l'échantillon contre une pollution due à ce même environnement. Cependant, la réalisation de ces basses pressions nécessite la mise en action de pompes mécaniques qui peuvent transmettre des vibrations parasites au support de l'éprouvette. Pour pallier à cet inconvénient, nous avons employé une technique d'adsorption locale par azéolithes refroidis à la température de l'air liquide. Cette méthode présente de plus l'avantage d'éviter la sortie, hors de l'enceinte de mesure, de canalisations. La conductivité thermique est ainsi diminuée et l'homogénéisation des températures accrue.

Le domaine de température, compris entre −200 et +250°C est réalisé par une enceinte générale (figure 1) étanche au vide comprenant à l'intérieur deux compartiments: l'un en partie basse pour les azéolithes et l'autre en partie haute pour un four entièrement métallique, de forme cylindrique et dont la section est légèrement supérieure à celle de l'éprouvette de mesure. L'ensemble est maintenu à −200°C par immersion dans un vase Dewar, et l'éprouvette peut, grâce au four intérieur, subir un cycle imposé de température (figures 2 et 3).

Type d'éprouvette

L'éprouvette constituée par un cylindre de 20 cm de long et de 8 à 10 mm de diamètre est maintenue en son milieu par trois vis de fixation comme dans l'élasticimètre Cabarat. On y réalisera donc un nœud de vibrations au point de vue des amplitudes tant en vibrations longitudinales que de torsion. Les extrémités de l'éprouvette doivent être bien parallèles afin de ne pas introduire de dispersion dans les fréquences des vibrations libres.

Vibration et détection

La mise en vibration a été, avec la détection, l'un des problèmes les plus délicats. En effet, pour obtenir une automaticité maximale, il était nécessaire de concevoir un dispositif sans réglage

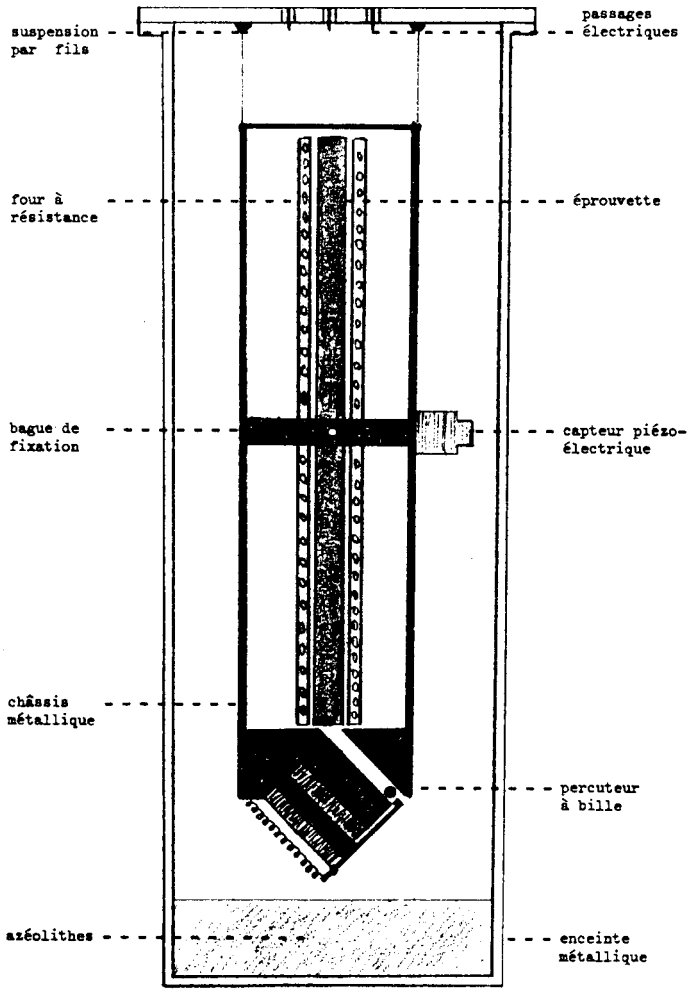

Figure 1. Enceinte de mesure.

après la mise en place dans l'enceinte de mesure. La solution adoptée consiste en un mécanisme à ressort, déclenché par une commande électrique, qui envoie une unique bille d'acier (diamètre 4 mm) percuter, toutes les cinq secondes, l'extrémité inférieure de l'échantillon. Ce mécanisme est réglé pour que les contraintes imposées restent dans le domaine élastique et que l'inclinaison de la percussion détermine l'apparition des trois modes de vibration. Après chaque choc, la bille est automatiquement récupérée par le mécanisme en vue de son utilisation ultérieure.

La détection est assurée sans introduire d'amortissement supplémentaire par l'intermédiaire du support médian. En effet, si la section médiane est un nœud de vibration au point de vue amplitude, elle se comporte comme un ventre de vibration au point de vue contrainte. Celle-ci déclenche par effet latéral une déformation qui réagit sur les trois vis de fixation lesquelles transmettent à un capteur piézoélectrique l'information désirée. Il a été fait choix d'un titanate de baryum dont la limite supérieure d'utilisation est +250°C. On trouve là, la limitation supérieure de notre appareillage dans son état actuel. L'emploi d'un capteur différent pourrait permettre un emploi à une température plus élevée. On peut également concevoir un renvoi par matériau rigide et non conducteur thermiquement dans une zone plus froide. Dans une telle optique, la limite d'utilisation deviendrait celle du four intérieur. Pour les longueurs d'éprouvettes employées, il n'existe pas de problèmes en relation avec le temps de réponse du capteur.

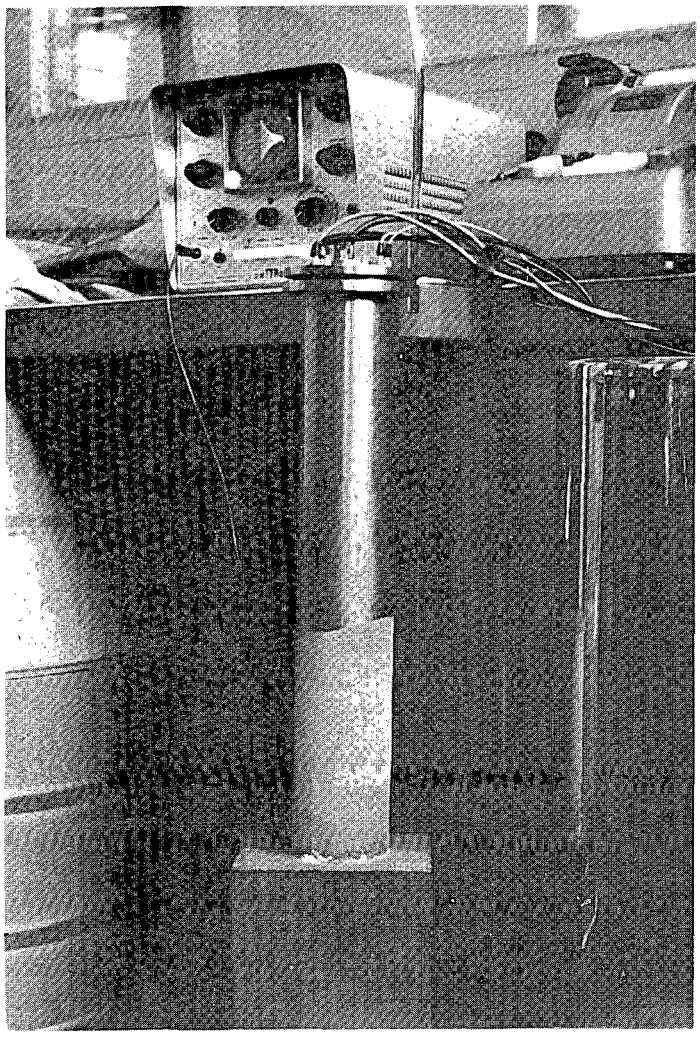

Figure 2. Enceinte de mesure.

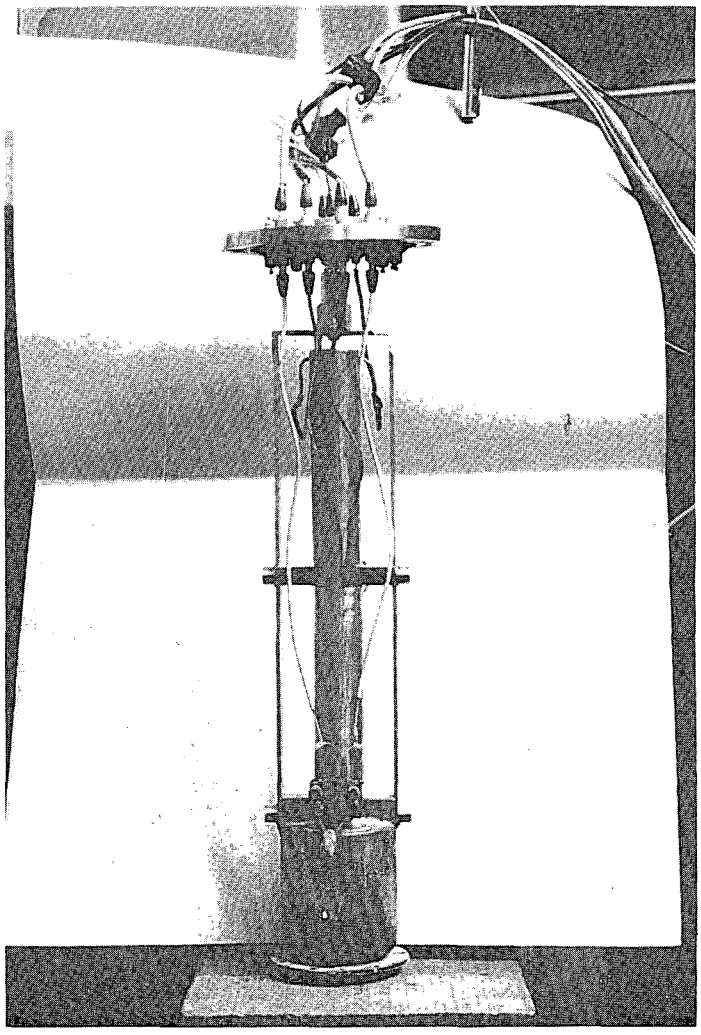

Figure 3. Disposition intérieure.

Inscription et enregistrement

L'information électrique délivrée par le capteur piézoélectrique est dirigée alternativement sur deux amplificateurs sélectifs calés l'un sur la fréquence F_e et l'autre sur celle F_t. À la sortie de ceux-ci, la fréquence est mesurée par un fréquencemètre électronique qui simultanément agit sur une imprimante par l'intermédiaire d'un transcripteur, et sur un enregistreur potentiométrique grâce à un convertisseur analogique. L'enregistrement est du type X-Y: avec en abscisses X la température grâce à la force électromotrice d'un thermocouple disposé au contact de la section médiane et avec en ordonnées Y la fréquence, soit F_t, soit F_e, suivant la commande d'un programmateur assurant le déroulement normal des opérations avec la séquence des mesures suivantes: «Fréquence longitudinale—Fréquence de torsion—2 fois l'amortissement intérieur en longitudinal».

L'enregistrement de l'amortissement intérieur est réalisé par le fréquencemètre numérique fonctionnant en compteur commandé par deux déclencheurs à niveaux réglés une fois pour toutes et imposant donc à notre mesure la valeur du coefficient K mentionnée sous la rubrique «Coefficient d'inélasticité».

Signalons l'avantage possible du convertisseur analogique assurant la transformation de la valeur numérique en différence de potentiel d'enregistrement. En effet il est possible de sélectionner trois chiffres successifs dans le nombre affiché par le compteur. Il apparaît tout de suite avantageux pour une fréquence qui varie peu d'utiliser les chiffres de droite (3 sur 5 dans notre cas) et pour un amortissement intérieur qui varie relativement plus au point de vue dispersion d'utiliser les chiffres de gauche. Nous avons, en première approximation, employé cette méthode ce qui permet, même sur les courbes enregistrées, d'avoir une très bonne précision sur la mesure. Nous y atteignons pratiquement la même précision (1 Hz sur 10 KHz) que pour le compteur numérique.

Nous pourrions dans l'état actuel de notre appareil mesurer l'amortissement intérieur en torsion. Cependant, le signal dû à l'onde longitudinale a une amplitude très supérieure à celle de la torsion. La fréquence F_t est souvent difficile à obtenir pure pendant une durée suffisante. Aussi avons-nous transformé l'amplificateur sélectif de F_t en oscillateur synchronisé par la seule fréquence des ondes de torsion. Cette méthode est extrêmement intéressante pour les matériaux présentant un amortissement intérieur élevé qui entraîne une décroissance trop rapide des oscillations, laquelle ne permet plus une mesure satisfaisante de la fréquence. Dans la version future, pour les températures élevées, nous utiliserons cette méthode en élasticimétrie.

Enfin nous projetons d'améliorer notre appareillage en lui adjoignant un dispositif électronique qui, donnant directement le rapport F_e/F_t, permettra de représenter la variation du coefficient de Poisson sans calculs auxiliaires.

La figure 4 est une vue d'ensemble de l'installation.

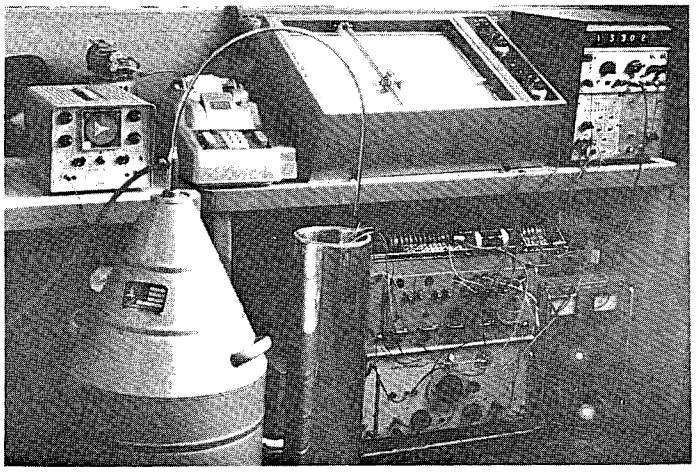

Figure 4. Vue d'ensemble du montage.

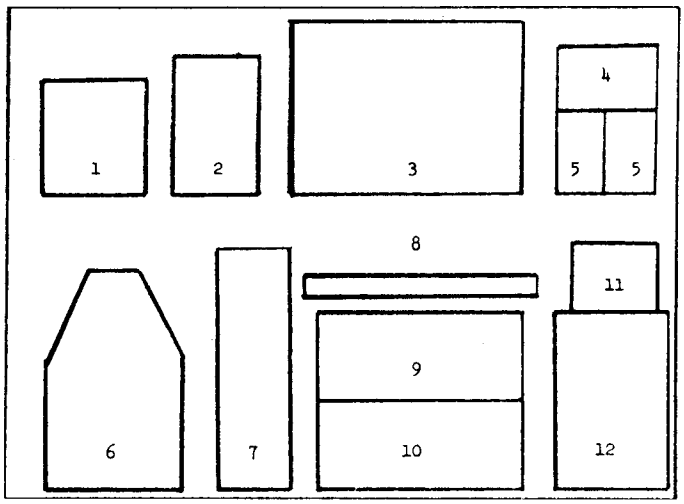

1. Oscillographe.
2. Imprimante.
3. Enregistreur.
4. Chronomètre.
5. Transcripteurs.
6. Air liquide.
7. Vase Dewar.
8. Combinateur.
9. Amplificateurs et bascules.
10. Amplificateur sélectif.
11. Auto-transformateur.
12. Alimentation de tension.

Résultats expérimentaux

Performances de l'appareil

La fréquence de répétition des mesures est de 5 secondes. Pour un essai, dans lequel la température évolue entre −200 et + 250°C, avec une vitesse quasi constante de montée en température égale à 1°5/mn, la durée totale de l'opération est de 5 heures environ. L'enregistreur effectue environ 3.600 pointés dont deux courbes de fréquences de 900 pointés chacune et une courbe d'amortissement intérieur de 1.800 pointés. L'intervalle de température entre deux pointés est de 0,125°C environ, soit un pointé de F_e tous les 0°5 (de même pour F_t). L'examen des courbes obtenues montre que la dispersion sur les mesures de fréquences est extrêmement faible. Par contre il n'en est pas de même en général, pour la mesure des amortissements intérieurs. À ce sujet dans nos prochaines expérimentations nous songeons à modifier la séquence des mesures en adoptant la suivante:

—Fréquence en longitudinal—Fréquence en torsion

—Rapport des deux fréquences avec 5 chiffres significatifs

—Amortissement intérieur en longitudinal répété dix fois et sommé sur le compteur numérique en obtenant ainsi une moyenne sur dix essais de l'amortissement intérieur.

La fréquence de chaque mesure au lieu d'être, en températures de 0°5, deviendrait 1°75. Compte tenu de la très faible dispersion sur les fréquences cet intervalle n'est nullement excessif.

Actuellement, la valeur du coefficient de Poisson est calculée manuellement tous les 10°C, intervalle qui est apparu satisfaisant. Un léger inconvénient de l'appareil actuel réside dans le fait que les deux fréquences sont mesurées à 0°125 d'écart. Il en résulte que la précision sur la mesure de ν est moins bonne que celle prévue théoriquement. Nous estimons que l'erreur absolue est actuellement en pratique égale à ± 1 demi-unité sur le troisième chiffre significatif.

Résultats expérimentaux

À titre d'exemple nous avons groupé quelques courbes enregistrées et reproduites par dessin car les pointés sont trop fins pour être photographiés. Estimant qu'une énumération de la totalité des résultats n'avait pas un intérêt fondamental, nous avons voulu faire apparaître les caractéristiques essentielles de nos résultats:

Reproductibilité des résultats. Les courbes obtenues sur un même échantillon de zirconium, ou de cuivre (figures 6 et 9) mettent en évidence la très bonne reproductibilité des résultats dans le domaine des fréquences et donc du coefficient de Poisson.

En ce qui concerne l'amortissement intérieur, il ne faut pas espérer obtenir une dispersion aussi faible que sur les fréquences car le nombre de causes d'erreurs expérimentales est nettement plus élevé dans ce cas. Les variations notables de cette caractéristique sont cependant très nettement mises en évidence avec une bonne reproductibilité comme la variation de δ lors du passage au point de Curie d'un monel ainsi qu'il apparaît à la figure 7.

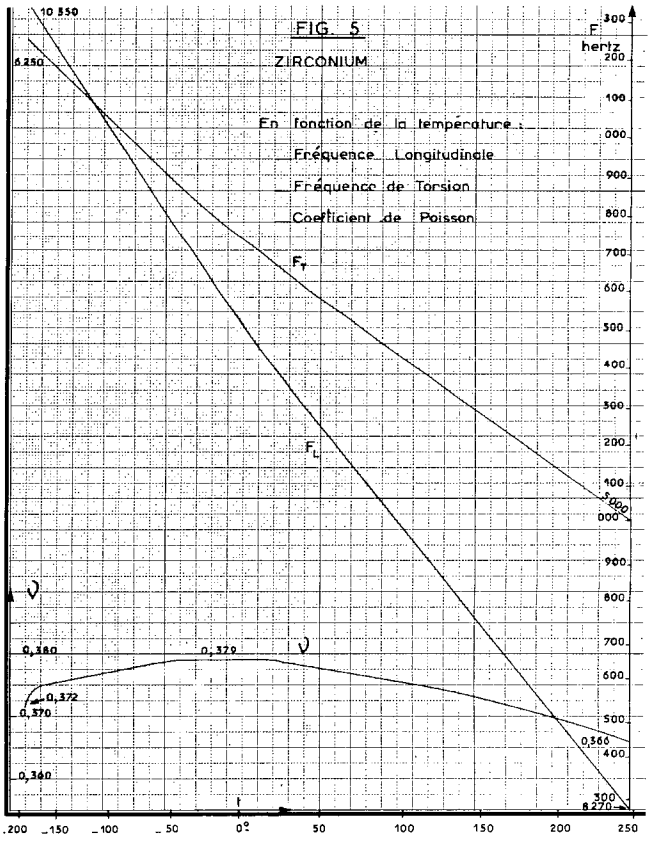

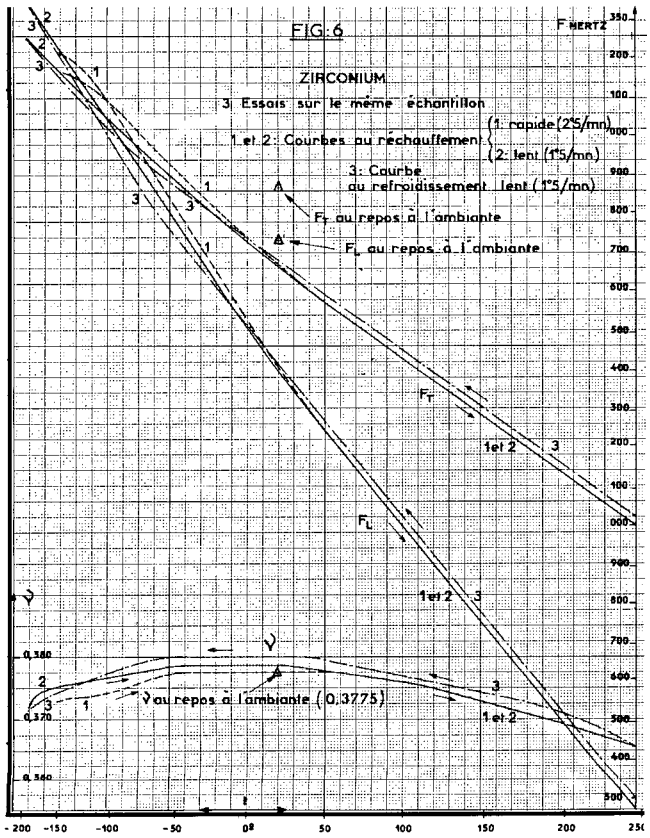
FIG. 6
ZIRCONIUM
3 Essais sur le même échantillon
1 et 2 : Courbes au réchauffement (1: rapide (2°5/mn), 2: lent (1°5/mn))
3 : Courbe au refroidissement lent (1°5/mn)
F_T au repos à l'ambiante
F_L au repos à l'ambiante
F_T
F_L
1 et 2
3
ν
ν au repos à l'ambiante (0,3775)
F HERTZ
t°

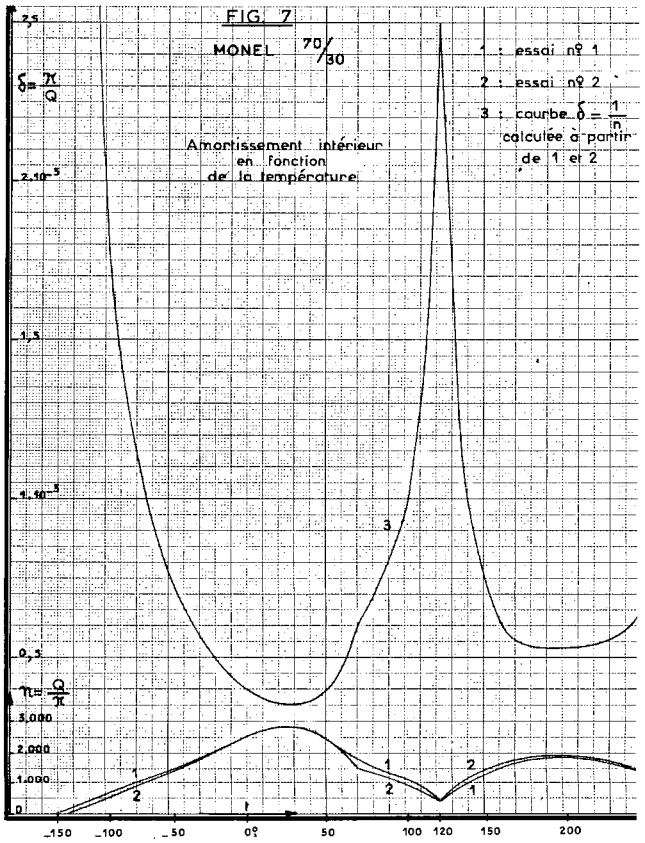
FIG. 7
MONEL 70/30
1 : essai n° 1
2 : essai n° 2
3 : courbe $\delta = \frac{1}{n}$ calculée à partir de 1 et 2
Amortissement intérieur en fonction de la température
$\delta = \frac{\pi}{Q}$
$\eta = \frac{Q}{\pi}$
t°

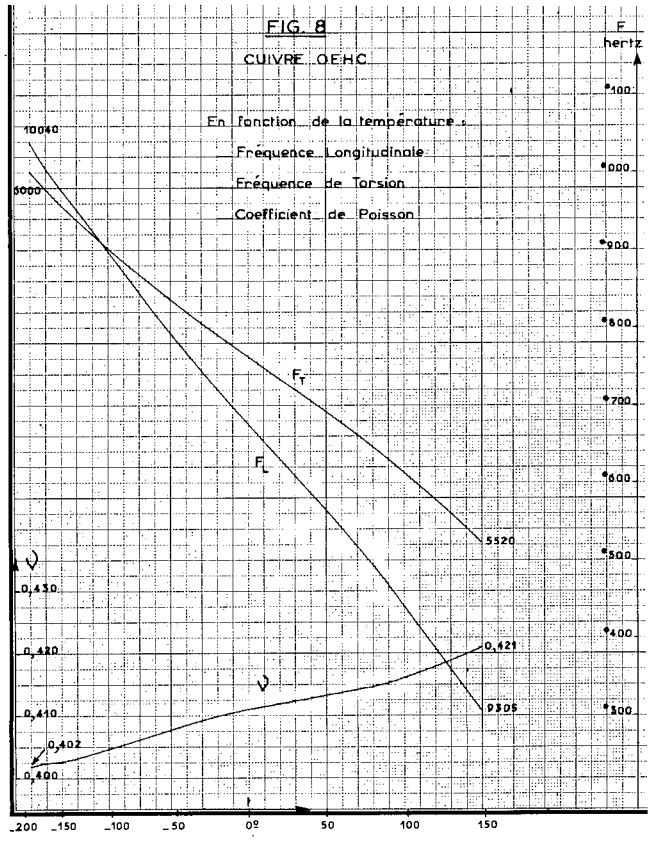
FIG. 8
CUIVRE OFHC
En fonction de la température :
Fréquence Longitudinale
Fréquence de Torsion
Coefficient de Poisson
F_T
F_L
5520
9305
ν
0,421
0,402
F hertz
t°

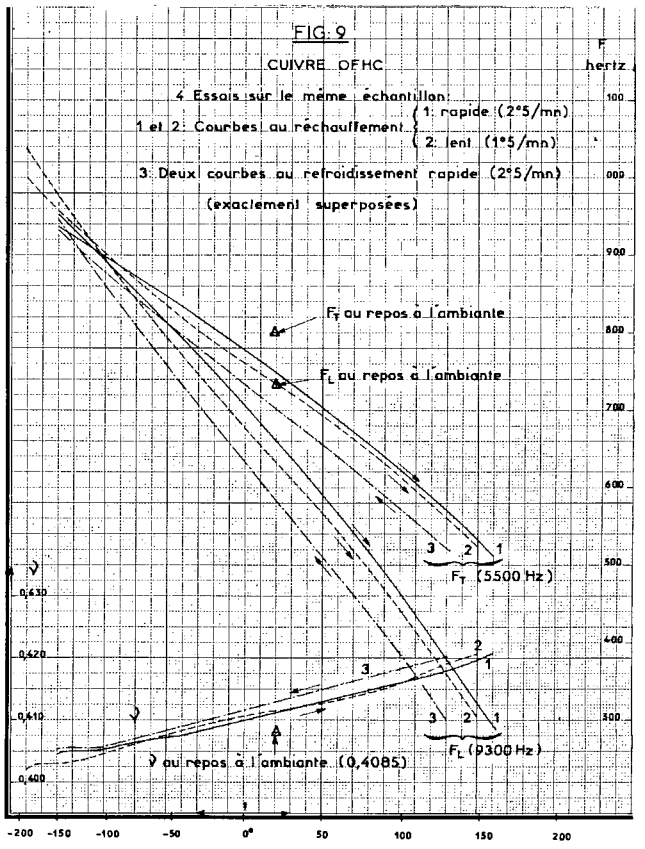
FIG. 9
CUIVRE OFHC
4 Essais sur le même échantillon:
1 et 2: Courbes au réchauffement (1: rapide (2°5/mn), 2: lent (1°5/mn))
3: Deux courbes au refroidissement rapide (2°5/mn) (exactement superposées)
F_T au repos à l'ambiante
F_L au repos à l'ambiante
F_T (5500 Hz)
F_L (9300 Hz)
ν au repos à l'ambiante (0,4085)
F hertz
t°

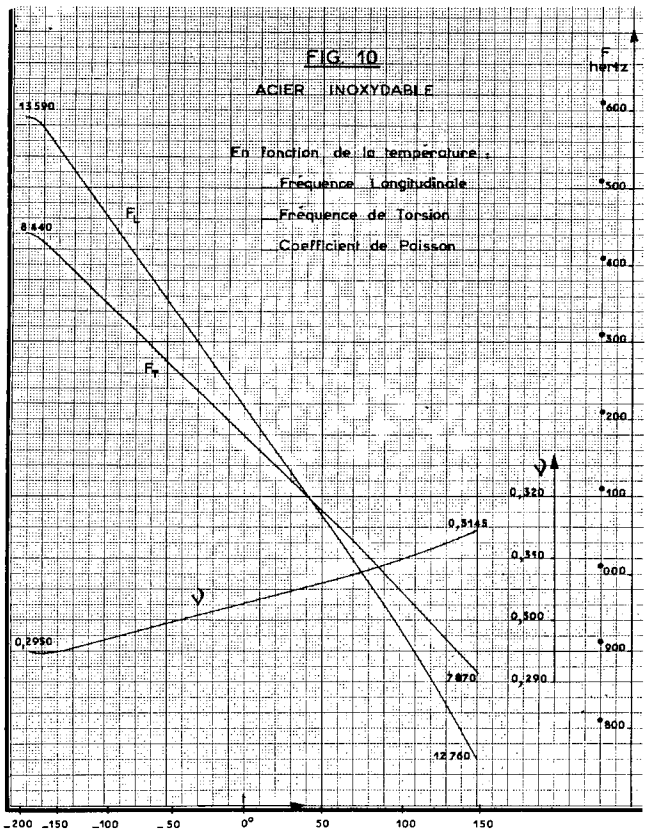

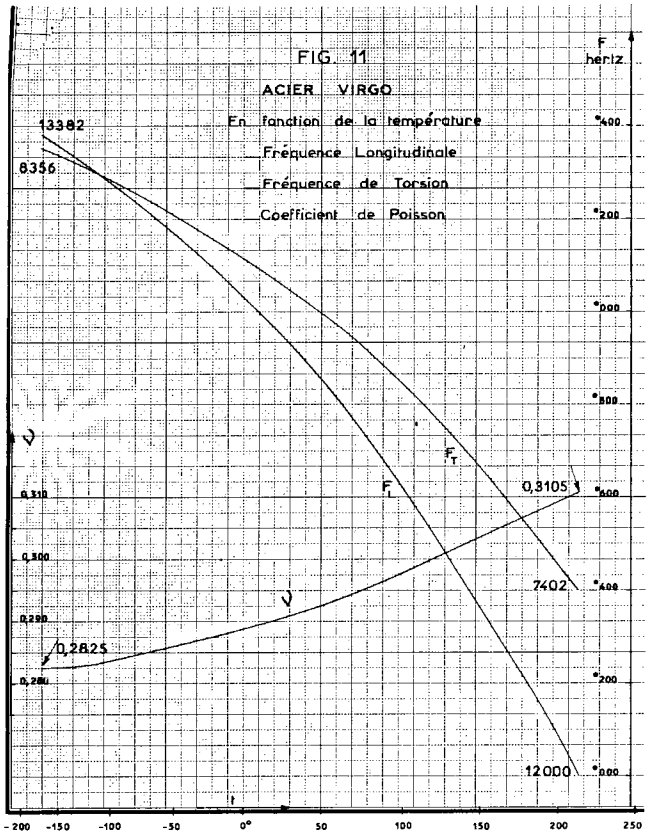

Cinétique des transformations. Bien que travaillant à des vitesses de montée en température très faibles de l'ordre de 1°5/mn il nous est apparu que les modules d'élasticité étaient très influencés par la cinétique. D'une manière générale on ne trouve pas les mêmes valeurs pour une température stabilisée depuis un certain temps et pour une structure en évolution même à la vitesse indiquée (figures 6 et 9).

Influence de la température. Le coefficient de Poisson ne subit pas une variation monotone en fonction de la température quelle que soit la nature du matériau. C'est ainsi que pour les aciers inoxydables (figures 10 et 11) et pour le cuivre (figure 8) le coefficient de Poisson augmente continûment avec la température. Par contre pour le zirconium (figure 5), ce paramètre passe par un maximum étalé autour de 0°C. Il est à remarquer que nos valeurs sont toutes légèrement supérieures à celles publiées dans la littérature pour des matériaux identiques.

Conclusions

L'ensemble expérimental mis en application semble être particulièrement adapté aux mesures d'élasticité et d'inélasticité par voie automatique sur éprouvettes présentant une certaine dimension. Son avantage certain réside dans l'obtention numérique et graphique des valeurs permettant le calcul des coefficients désirés. La stabilité du réglage et une totale automaticité lui permettent d'assurer un bon rendement sous simple surveillance. Nous pensons pouvoir extrapoler cet appareillage, limité actuellement à + 250°C, afin d'atteindre, du moins en élasticimétrie, des températures plus élevées.

Référence

1. McSkimin, H. J.: Physical Acoustics, Vol. 1. Ed. New York Academic 1964, p. 272–334.

Humidity Insensitive Strain-Indicating Coatings with Increased Sensitivity (Aerosol STRESSCOAT)

JAMES S. BORUCKI, U.S.A.

ABSTRACT: A series of strain-indicating coatings have been developed for aerosol and bulk use which are designed to operate over a temperature range comparable to the standard brittle lacquer coatings now in use. They act independently of humidity, making coating selection and testing significantly easier. Inherent properties of these coatings allow for testing at strain sensitivities as low as 150 microinches per inch of strain. Individual coatings are designed to operate at a nominal strain sensitivity threshold of 500 microinches per inch of strain. Several of the chemical and physical properties of this new series of coatings as well as their performance characteristics are discussed and compared to the existing STRESSCOAT lacquers.

Introduction

The same strain-indicating coatings have been used successfully in experimental stress analysis for many years. Stress analysts and design engineers have been able to successfully determine the distribution, direction, location and magnitude of inherent tensile strains through the use of STRESSCOAT* lacquers. They have used these coatings both quantitatively and qualitatively (more generally as a qualitative tool to show where and in what direction to place strain gauges). On the usual complicated engineering structures such coatings will point directly to the areas of highest strain, show the direction of the principle tension and, if properly controlled, will yield quantitative values of sufficient accuracy for practical design purposes.

The chemistry of the STRESSCOAT lacquers, their application technique and their over-all physical characteristics have remained the same over many years. They are sensitive to both temperature and humidity; there is a definite effect of humidity on coating strain-sensitivity and the minimum coating strain-sensitivity obtainable is about 400 microinches per inch. The solvent carrier (carbon disulfide) is well known to users of brittle coatings; it is very flammable and requires careful handling. The odour is quite definite and distinctive.

Recently a new series of strain-indicating coatings have been developed which represent great improvement over the existing industrial standard. The new series of brittle lacquers function the same as the standard brittle lacquers now in use. The crack patterns which occur during loading form at right angles to the principal tension stress. They differ, however, from the old in that they act completely independently of humidity which makes coating selection and testing significantly easier. In addition inherent chemical properties of these coatings allow for testing at strain-sensitivity levels as low as 150 microinches per inch without thermal crazing. This is a significant advantage since it permits testing at low load levels and with a high degree of coating sensitivity. Furthermore, the chemical composition of this new series makes it possible to package them in aerosol spray cans, the convenience of which is now established.

This development involved a great deal of study and experimentation in solvent, resin and plasticizer chemistry. The project goals were to produce a series of coatings with improved functional, chemical, and physical characteristics. From a functional standpoint we have been able to eliminate humidity as a test variable. In addition we have been able to increase the sensitivity of the coatings so that strain sensitivities as low as 100 microinches per inch are obtainable without evidence of thermal crazing (Figure 1).

Coating Chemistry

The solvent system for the new series of lacquers is carbon disulfide, the same solvent as used for years in STRESSCOAT. Over the years several attempts have been made to find a suitable replacement solvent. Many single solvent systems or azeotropic blends of solvents are available that have similar physical properties (boiling point, vapour pressure, evaporation rate, flash point, solubility characteristics, refractive index, surface tension and molecular weight) but none were found to produce the same functional characteristics in the coating as carbon disulfide. Tables 1 and 2 list a few of the solvents and solvent blends evaluated.

Ideally, we would like to replace carbon disulfide with a nonflammable solvent of low toxicity and with the same functional characteristics in the coating as CS_2.

* Trade Mark Registered in the U.S.A. by Magnaflux Corporation.

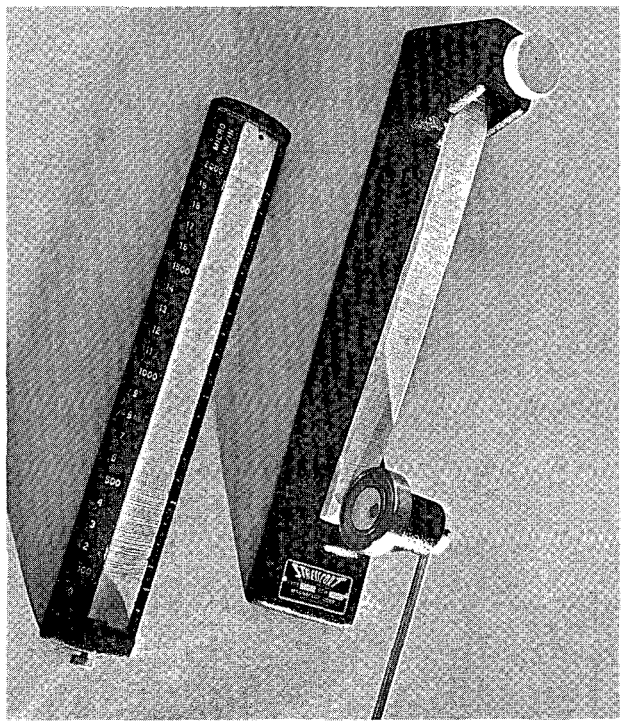

Figure 1. STRESSCOAT lacquers with increased coating sensitivity.

One of the basic difficulties in finding a suitable solvent replacement lies in the solvent retention characteristics of the resin base. Any number of solvents or solvent systems, flammable or nonflammable will serve as a carrier solvent for a brittle lacquer. The coating will dry out and crack patterns will be formed. The formed crack patterns, however, are inconsistent and unreliable; their strain threshold values vary greatly depending on the degree of solvent retention in the coating. The more highly volatile solvents rupture through the resin coating leaving craters which impair crack formation. Few solvents will diffuse through the deposited resin coating as completely, uniformly and as predictably as carbon disulfide. In addition very few solvents or solvent systems have been found which produce the unique bubble structure and bubble density in the dried resin film thought necessary to good crack-pattern formation.

With further research we hope eventually to find a replacement solvent for carbon disulfide.

Most of the synthetic and natural resins commercially available today were evaluated before selecting those which provided the best functional characteristics. Our study included the consideration of the following parameters: 1) chemical type (generic classification), 2) melting point consistency, 3) solvent release characteristics, 4) chemical purity, 5) chemical stability, 6) toxicity ratings, 7) solubility characteristics and 8) temperature sensitivity response.

Since the brittleness of the strain-indicating coating can be controlled to a large extent by the plasticizer system used it is extremely important that the proper chemical combination be found. Each coating in the brittle lacquer series is formulated to meet specific strain-sensitivity requirements over a specific temperature range. This means that the resin is plasticized to a specific brittleness by the selected plasticizer.

There are many plasticizers commercially available today which are suitable for use in brittle coatings. It is important, however, that they are: 1) nonvolatile, 2) chemically stable, 3) nontoxic, 4) soluble in resin-solvent system, 5) impart

Table 1

Solvents Evaluated for STRESSCOAT Lacquer

	Solvent	b.p. at 760 mm Hg.
1	Vinyl 2-Chlorethyl Ether	39 °C
2	Trimethyl Borate	68 °C
3	Trichlorotrifluorethane	47.5°C
4	Methyl Acetate	56.3°C
5	Ethyl Formite	54.2°C
6	Dimethyl Formel	42.3°C
7	Vinyl Propyl Ether	65.1°C
8	Pentane	36.1°C
9	Ethyl Acrylate	44.9°C
10	Dimethyl Ketone (Acetone)	56.1°C
11	1-Chloropropane (Propyl Chloride)	46.6°C
12	Cis 1,2 Dichloroethylene	60.1°C
13	1 Bromobutane (n Butyl Bromide)	101.3°C
14	1-Chlorobutane (n Butyl Chloride)	78.5°C
15	2-Bromobutene (Butyl Bromide, secondary)	91.2°C
16	2-Bromo-2-methyl propane (butyl Bromide tertiary)	73.3°C
17	2-Chlorobutane (Butyl Chloride, Sec.)	68.0°C
18	2-Chloro-2-methyl propane	51.0°C
19	Benzene	79.6°C
20	Carbon Disulfide	46.5°C
21	Tetrachloroethylene	47.6°C
22	Methylene Chloride	40.7°C
23	2, Chloropropane	36.0°C
24	2, 2 Dimethylbutane	49.7°C
25	2, 3 Dimethylbutane	58.0°C
26	2-Methyl-2-Butane	38.5°C
27	Cyclopentane	49.3°C
28	1, 3 Pentadiene	42.1°C
29	Methylpropyl Ether	39.1°C
30	Diethylamine	55.5°C
31	1, 2 Epoxy 2-methyl propane	55.5°C
32	Tert-butyl chloride	51.0°C
33	Propylamine	48.5°C
34	Trimethyldiborane	45.5°C
35	2-Chloropropane	36.5°C
36	Chloropropane	44.6°C
37	2-Propenal	52.5°C
38	Dimethylsulfide	36.0°C
39	Ethanethiol	35.5°C
40	1-Chloropropane	37.0°C
41	1, 1-Dichloroethane	57.4°C
42	1, 1, 2-Trichloro-1, 2, 2-Trifluoroethane	47.6°C
43	Dichloromethylsilane	41.9°C
44	Trans 1, 2 Dichloroethylene	48.9°C
45	Bromo Chloromethane	68.0°C
46	Cis & Tram 1, 2 Dichloroethylene	50 to 58°C
47	1, 2 Dichloroethane	83°C
48	2 Bromopropane	59.6°C
49	1, 4 Dochloropentane	58 to 60°C
50	1-Chloropropane	37°C
51	3-Chloropropane	44.6°C
52	Bis (2-(2-methoxyethoxy) ethyl) Ether	68.0°C
53	Petroleum Ether	50 to 60°C
54	1, 1, 2 Trichloroethylene	86°C
55	Chloroform	61°C

craze resistance to coating, 6) impart good flow-out characteristics to the coating and 7) compatible with selected resins and solvents.

The plasticizer system has a profound affect on the viscoelastic nature of the applied resin coating. The plasticizer affects greatly both the drying and thermal craze characteristics of the resin coatings. These properties are discussed later.

Table 2

Cosolvent Systems Evaluated

	Solvents	Ratio
1	Chlorobromomethane/Methylene chloride	1:3
2	Cis 1, 2 dichloroethylene/Methylene chloride	2:1
3	Trans 1, 2 dichloroethylene/Methylene chloride	1:1
4	Cis & Trans 1, 2 dichloroethylene/Methylene chloride	1:1
5	Methylene Bromid/Methylene chloride	1:3
6	Methylene Iodide/Methylene chloride	1:3
7	Carbon Disulfide/Methylene chloride	1:2
8	Freon TF/Methylene chloride	1:3
9	Petroleum Ether/Methylene chloride	1:3
10	Petroleum Ether/Chlorobismomethane	1:5
11	Chloroform/Methylene chloride	1:3
12	Chloroform/Chlorobromomethane	1:3
13	1, 2 Dichloroethane/Methylene chloride	1:3
14	Benzene/Methylene chloride	1:9
15	1-Bromisbutane/Methylene chloride	1:5
16	2-chloropropane/Methylene chloride	1:5
17	1-Bromo-3-chloropropane/Methylene chloride	1:4
18	Acetone/chlorobromomethane	1:3
19	Acetone/Methylene chloride	1:1
20	Acetone/Benzene	3:1
21	Benzene/Chlorobromomethane	1:4
22	1, 1, 2-Trichloroethylene/Acetone	2:1
23	Chloroform/2-chloropropane	1:1
24	Chloroform/Tetrachloroethylene	1:2
25	1-Bromobutane/Acetone	1:1

Coating Performance Characteristics

Throughout our development many brittle coating formulations were made up and evaluated. Many adjustments were required in order to obtain the proper ratio of plasticizer-to-resin to solvent. The coating characteristics and their performance properties were thoroughly evaluated and compared to the established performance standards of normal STRESSCOAT.

Preliminary tests consisted of calibrating each coating and evaluating the quality of the coating and the crack pattern produced. Those coatings which produced an acceptable coating and crack pattern were tested further, but in greater detail. The standard STRESSCOAT calibration procedure was used to calibrate the coatings under test, i.e., calibration bars were sprayed, dried at a pre-selected temperature for 18 hours and then tested. A load was applied to the coated calibration strips with a standard cantilever device which produced crack patterns in the coatings. The last crack indicated the strain threshold value for that coating.

The following performance characteristics for this new series of strain-indicating coatings were studied; 1) solvent-release properties, 2) resistance to crazing, 3) sensitivity requirements of coating (minimum strain threshold value), 4) effect of bubble structure on coating performance, 5) effect of coating thickness on coating performance, 6) effect of relative humidity on coating performance, 7) compression load response (strain threshold vs hold time—strain threshold vs release time), 8) effect of application technique on coating performance.

Solvent Release Properties

In determining the solvent-release properties of each particular coating the following procedure was employed. Calibration strips were coated, one-half were dried at room temperature and one-half at approximately 100°F. The coatings were dried for 18 hours and then tested at the same temperature at which they were dried, but those dried at 100°F were also tested at room temperature. It is most desirable to have the strain-sensitivity value when dried at 100°F and tested at room

temperature to be close to the strain sensitivity when dried and tested at room temperature. This would indicate that most of the solvent carrier was being released under room temperature drying conditions and not remaining as a residual solvent to act as a plasticizer and soften the coating, thus affecting coating sensitivity.

Resistance to Crazing

Brittle coatings are inherently susceptible to crazing; both to drying craze and to thermal craze. Both have a marked adverse effect on the appearance and performance of the coating. Thermal craze occurs from a spontaneous failure of the coating, due to temperature change. It is the result of the difference in thermal contractions between the substrate and coating. On the other hand, drying craze may occur on rather thick coatings of normal strain sensitivities; it is usually caused by uneven drying of the coating. In thick coatings the outer surface dries first and some shrinkage occurs before the coating beneath the top layer has dried. The coating progressively shrinks as drying continues until it fails in the form of a crack. Through the proper selection of plasticizers, however, we were able to develop a coating series which affords a great deal of resistance to both thermal and drying craze.

Sensitivity Requirement of Coating

The new series of coatings has been designed to yield strain sensitivities of less than 200 microinches per inch (0.0002 in./in. strain). The thermal craze point is approximately 125 to 150 microinches per inch. Temperature change obviously affects coating sensitivity. An increase in temperature will soften the coating, thus making it less sensitive; a decrease in temperature makes the coating more brittle. The temperature-sensitivity response of these new coatings is in the order of 35 microinches per inch per degree of temperature change. This temperature-strain sensitivity response is illustrated quite graphically in Figure 11.

Since these coatings are inherently more sensitive than the standard STRESSCOAT lacquer, the nominal strain-threshold value has been shifted down to 500 microinches per inch—i.e., each coating in the series has been calibrated to yield a strain-sensitivity threshold value of 500 microinches per inch when dried and tested at the designated temperature.

Coating Performance

Effect of Bubble Structure

Normal STRESSCOAT lacquers as well as the new series produce a coating with a fine, dense bubble structure. This is attributed mostly to the manner in which carbon disulfide escapes or diffuses through the coating during evaporation. It is believed that this type of bubble structure aids in the orientation and production of a detailed crack pattern with a predictable end point (strain threshold-last crack). A comparison can be made to a crack in a piece of glass. If holes are drilled at both ends of the crack it will not progress any further; otherwise it will progress unpredictably. With the various solvents evaluated we were unable to produce a coating with an equivalent bubble structure. Several of the experimental coatings were completely void of air bubbles; for the most part these coatings produced definite crack patterns, but they were inconsistent and unpredictable in that there were wide variations in sensitivity.

Effect of Coating Thickness

The effect of coating thickness on strain sensitivity was measured by calibrating the brittle coatings at various thicknesses (0.002 in. to 0.010 in.). Test results on the coatings evaluated indicated that within a thickness range of 0.002 in. to 0.008 in. there is little change in sensitivity. These results for the most part parallel normal STRESSCOAT. From a coating thickness of approximately 0.004 in. to 0.008 in. there is little change in strain sensitivity for both coatings. Figure 2 illustrates this relationship graphically.

Effect of Humidity

The effect of humidity on the standard STRESSCOAT lacquers has been known for many years; it is one of the determining factors in selecting a coating for use. An increase in humidity will increase the coating strain-sensitivity response, while a decrease in humidity will decrease it, thus making the coating more brittle. In some instances the influence of humidity on a coating can be an asset, but in most instances it is a hindrance. In either case it is one more test variable which must be considered. In the new series of lacquers, however, we have been successful in eliminating humidity as a test variable; these coatings act completely independently of humidity.

The effect of humidity on the resin coatings evaluated was measured by calibrating at a constant temperature and by varying the humidity conditions. Changes in sensitivity could then be attributed directly to the effect of humidity on the coatings. Figure 3 compares the effect of humidity on standard STRESSCOAT lacquer (ST-1204) and compares its response to a typical coating in the new series. Note that the standard lacquer changes 600 microinches per inch from 22 to 100% R.H. whereas the humidity-insensitive coating changes only 50 microinches per inch.

Compression Loads

This new series of lacquers responds to compression loads about the same as the established series of lacquers. Figure 4 illustrates coating compression strain-sensitivity response to release time (with compression hold time constant). Figure 5 illustrates

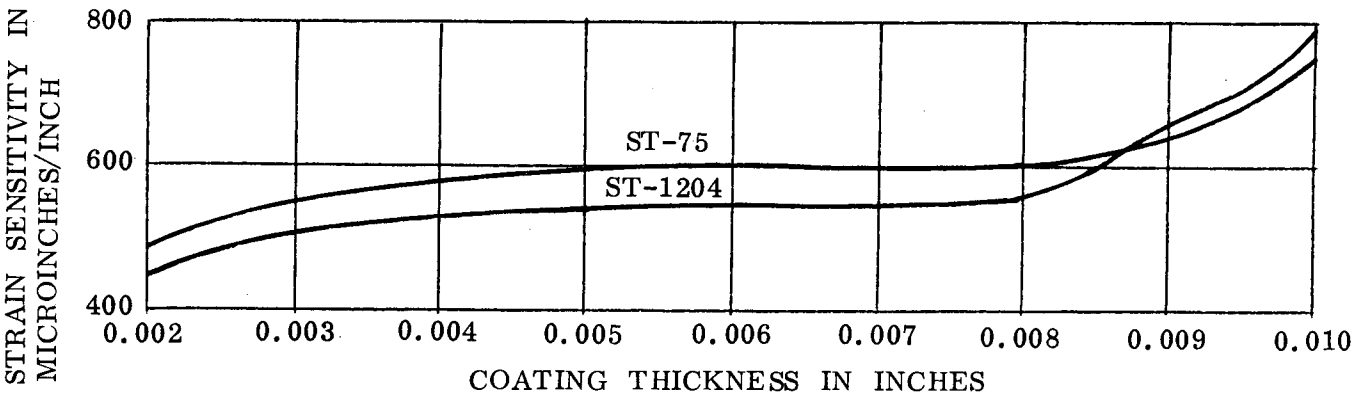

Figure 2. Coating thickness vs. strain sensitivity.

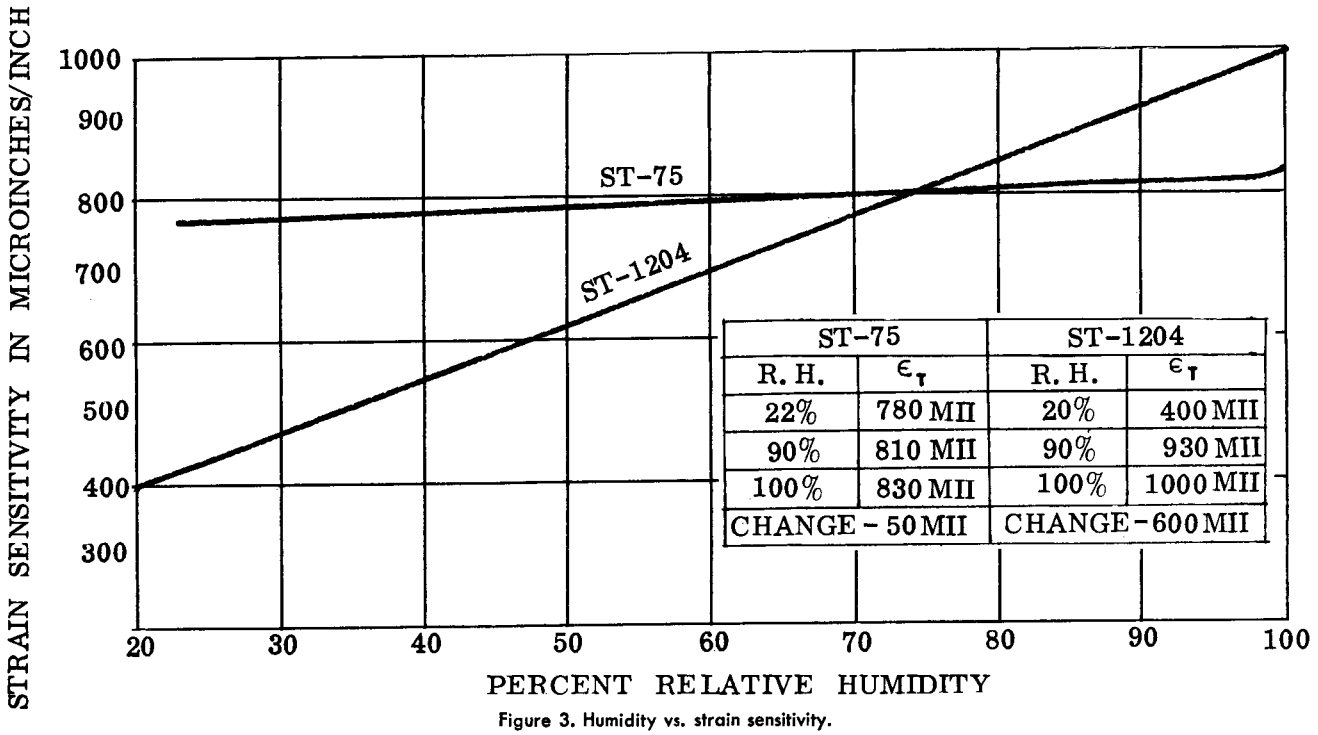

Figure 3. Humidity vs. strain sensitivity.

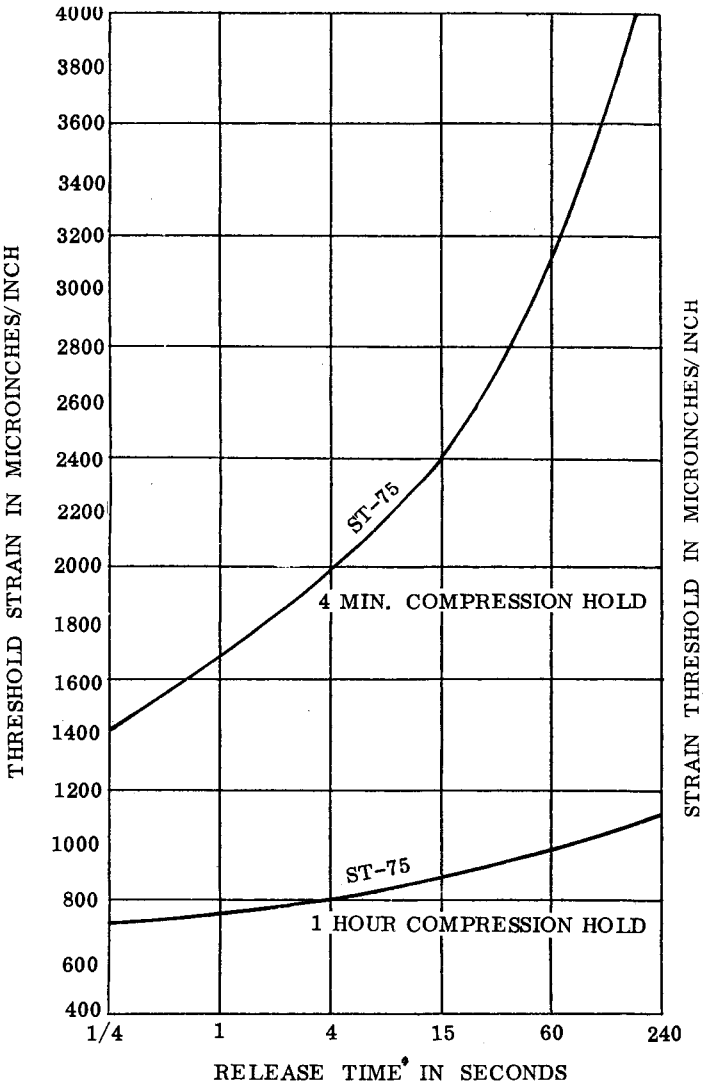

Figure 4. Compression threshold vs. release time.

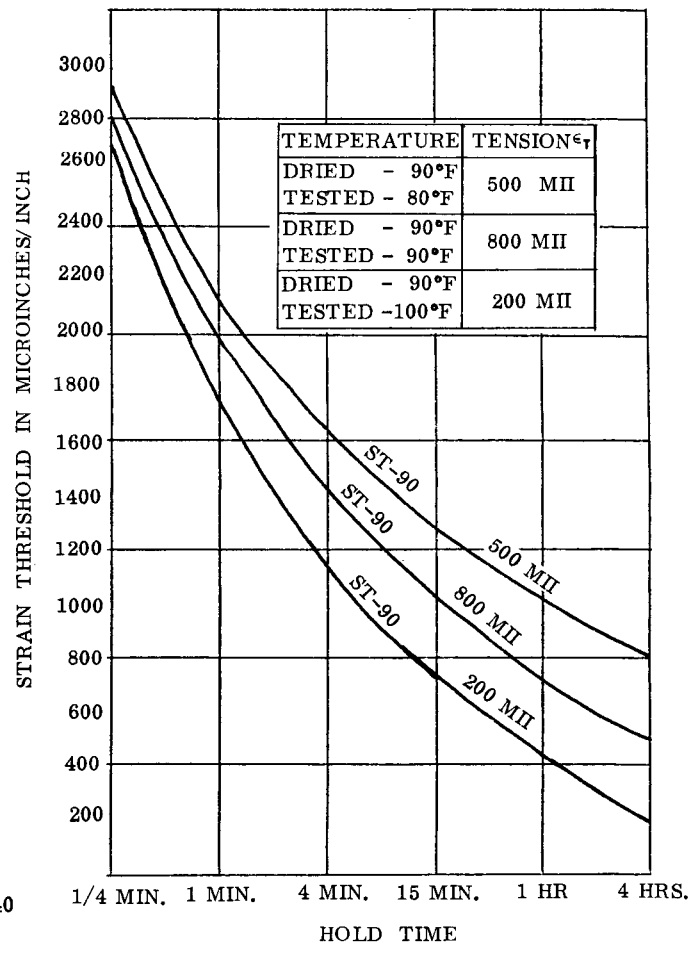

Figure 5. Compression threshold vs. hold time.

compression strain-sensitivity response to hold time (with release time held constant). Figures 6 and 7 illustrate the response of the standard STRESSCOAT lacquers under the same test conditions. Both coatings react about the same in compression.

Creep Properties

STRESSCOAT is normally considered to be a very brittle material. However, under the influence of time and load, the coatings tend to creep and relieve the stress within the coating which was induced by the original load placed on the base structure. For this reason creep-correction values for this series of coatings have been established. Figure 8 illustrates the effect of time and load on this series of coatings. Figure 9 is included to compare the creep properties of the standard series with the new.

Effect of Application Technique on Coating Performance

Application technique can certainly affect the performance of the coating. Too wet a spray will cause the coating to run, build up in certain areas and in general dry unevenly. Coating thickness variations beyond the limits described will affect strain sensitivity of the coating. Too dry a spray, on the other hand, will produce a very dry, dusty coating. In such a coating crack-pattern formation is generally very uneven and difficult to see.

With the proper application technique, however, uniform coatings of the proper film thickness (average 0.006 in.) can be applied rather consistently.

There are many variables in the spray technique which can influence the over-all coating quality. The spray gun or aerosol itself can be the cause of improper application if they are found to be defective. In the case of spray gun application the air supply to the spray gun can cause problems if it is contaminated with oil or moisture. The air pressure on the spray gun must be accurately controlled; too high an air pressure will cause "dusting". If the air pressure is too low the coating will run, and dry unevenly. In practice an average air pressure of 8 to 12 psig is used. There are many other factors that influence the quality of the applied coating; 1) distance of spray from the part, 2) direction of the spray, 3) number of passes

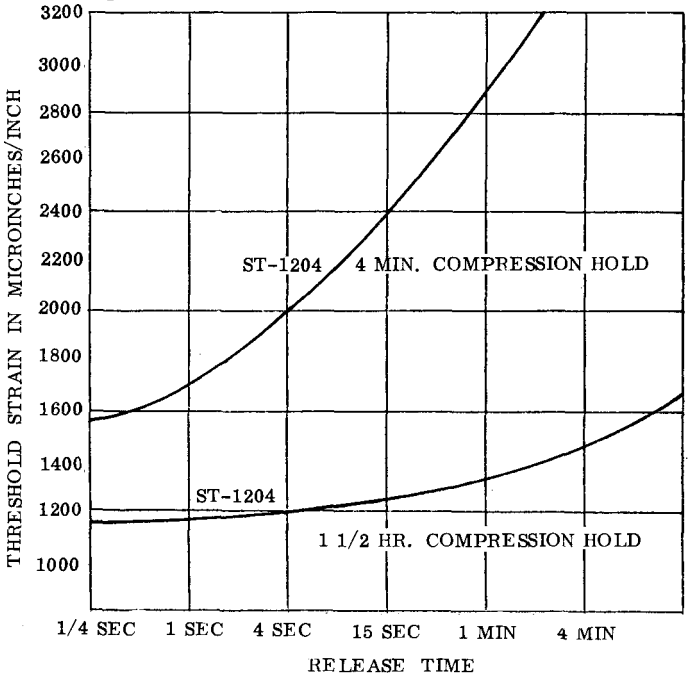

Figure 6. Compression threshold vs. release time. Standard STRESSCOAT series, 800 tension threshold.

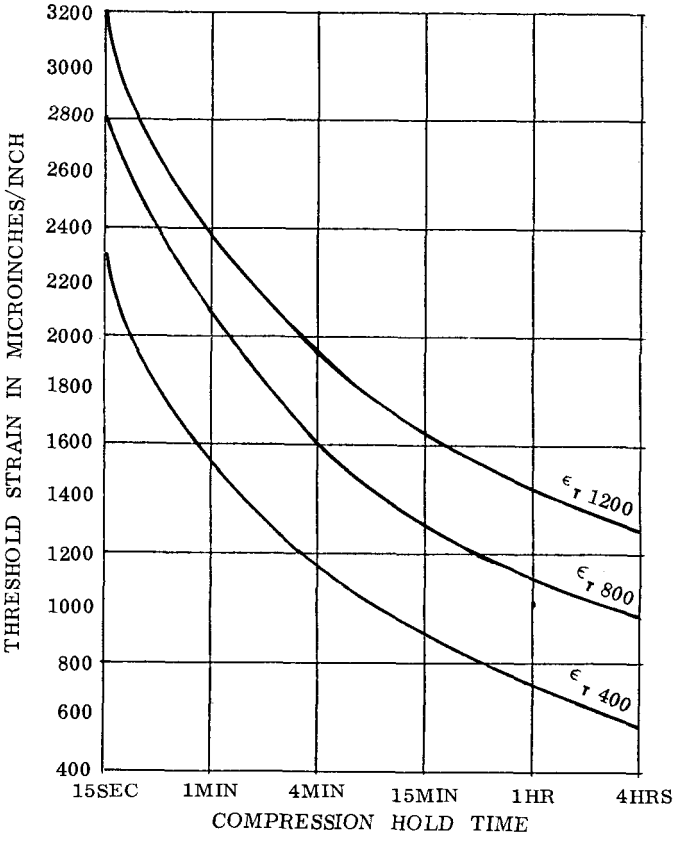

Figure 7. Compression threshold vs. hold time.

required to build up the coating, 4) time lapse between passes and 5) speed with which the spray passes are made. Consistent and reliable results, however, are usually obtained if the operating instructions are followed.

Analysis of Selection Charts

Both series of coatings are operative over a wide temperature range (0 to 130°F) for both indoor and outdoor use. Coating identification and selection, however, differ greatly as illustrated in Figures 10 and 11. Table 3 identifies the coatings in this new series. The coating number actually represents the test temperature for which the coating was designed. Coatings should be dried at test temperature or slightly higher and coatings designed for use below 70°F should be dried at 70° and then brought down to the test temperature in the same manner as existing STRESSCOAT lacquers.

The coatings are calibrated to yield a nominal strain threshold sensitivity of 500 microinches per inch when dried and tested at the designated temperature. Temperature change affects coating sensitivity. An increase in temperature will soften the coating, thus making it less sensitive; a decrease in temperature makes the coating more brittle thus making it more sensitive. The temperature-sensitivity response is in the order of 35 microinches per inch per degree temperature change. With these new coatings strain sensitivities of less than 200 microinches per inch are obtainable without crazing. The craze point is approximately 150 microinches per inch. Above 800 microinches per inch the crack patterns tend to close upon release of the load; it is therefore suggested that STATIFLUX powder be employed to detect these patterns above this strain level. With the standard STRESSCOAT lacquer the coatings are calibrated to yield a nominal strain threshold sensitivity

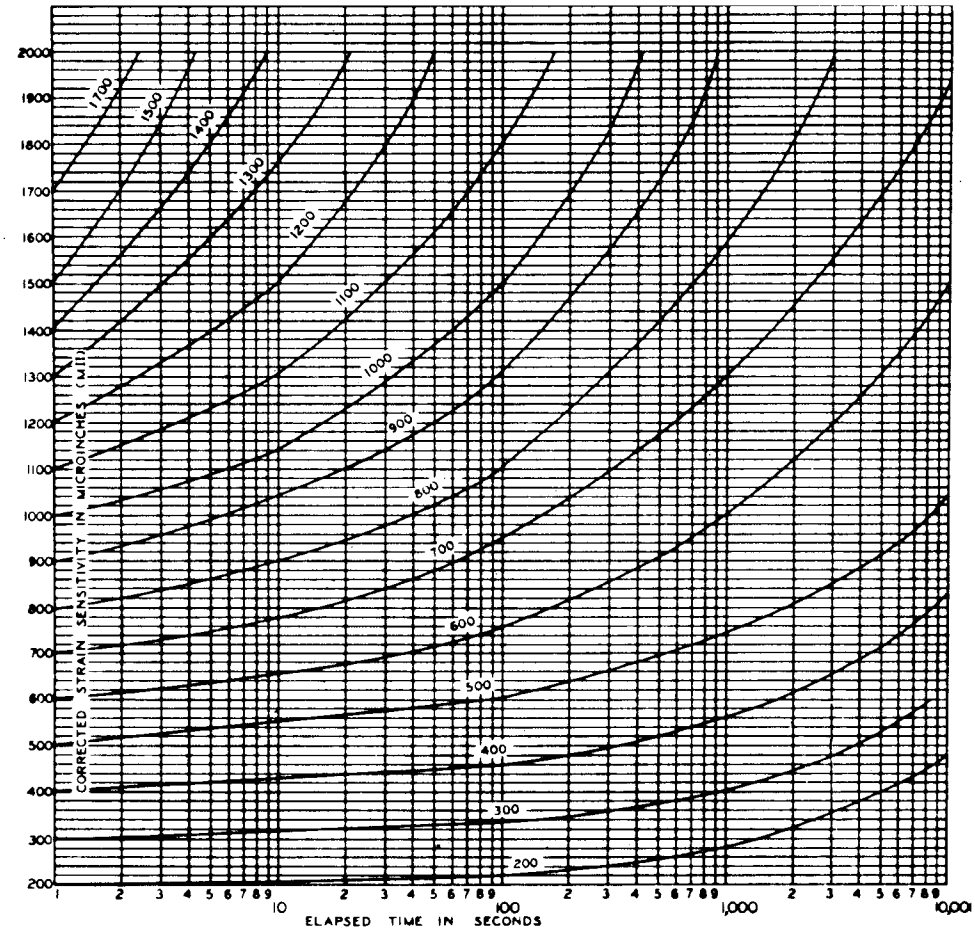

Figure 8
Aerosol STRESSCOAT creep correction chart.

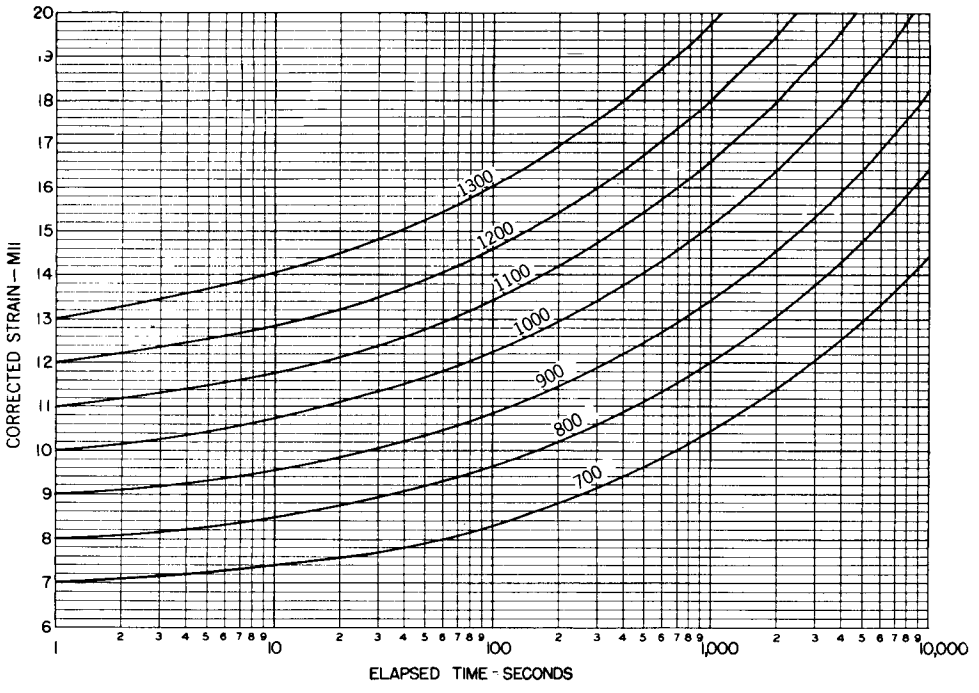

Figure 9
Comparison of creep properties of the standard series with the new series.

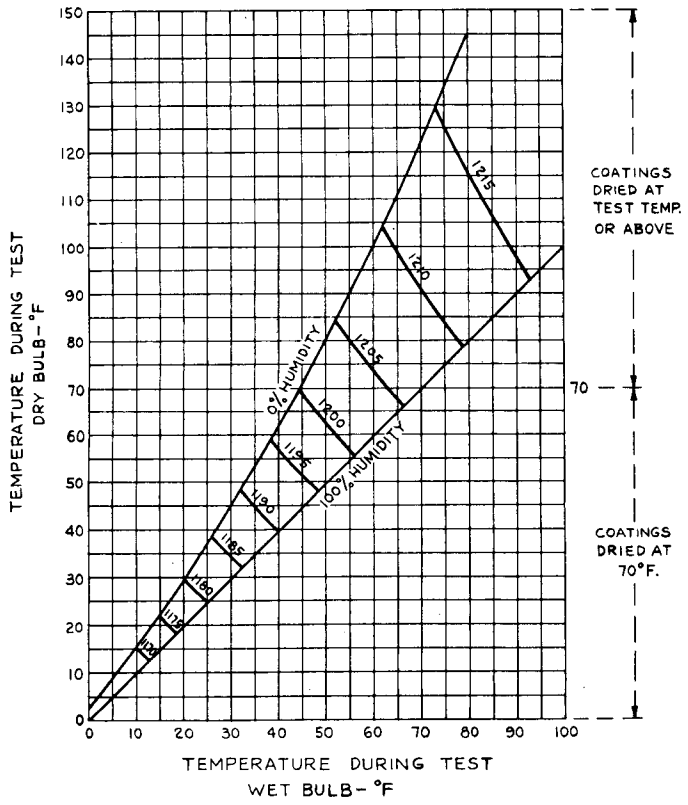

Figure 10. STRESSCOAT coating selection chart.

value of 700 microinches per inch. The craze point is approximately 400 microinches per inch and the patterns tend to close above 1000 microinches per inch.

Application of Aerosol STRESSCOAT Materials

The best procedure to follow to obtain optimum results using the spray-can lacquer is as follows. Clean the test specimen thoroughly with aerosol cleaner; it is nonflammable and evaporates quickly. Parts should be tested for cleanliness before proceeding. The aluminum undercoat is then applied. It provides a uniform background on all types of parts regardless of their surface finish, whether dull or polished. Spray at a distance of 6 to 12 in. (shake can at intervals), moving across the part rapidly and evenly, applying a very thin film, just enough to provide an even, uniform coating. The undercoat dries quickly and within 15 minutes the STRESSCOAT lacquers can be applied by spraying at an average distance of about 4 to 8 in. from test structure. Spray by moving across the part *very rapidly* and with even passes. The coating should be built up slowly with several passes as described above to an average coating thickness of about 0.006 in.

The coating should be dried at the temperature indicated in the selection chart. Coating the part in the afternoon and testing the next morning is a typical drying procedure. Overnight drying is recommended for all coatings.

Table 3

Coatings	Drying Temp.	Test Temp.	Nominal Strain Sensitivity (in microinches/inch)
ST–10	70° F.	10° F.	500
ST–20	70° F.	20° F.	500
ST–30	70° F.	30° F.	500
ST–40	70° F.	40° F.	500
ST–50	70° F.	50° F.	500
ST–60	70° F.	60° F.	500
ST–70	70° F.	65° F.	500
ST–75	75° F.	60° F.	500
ST–80	80° F.	75° F.	500
ST–85	85° F.	80° F.	500
ST–90	90° F.	85° F.	500
ST–95	95° F.	90° F.	500
ST–100	100° F.	100° F.	500

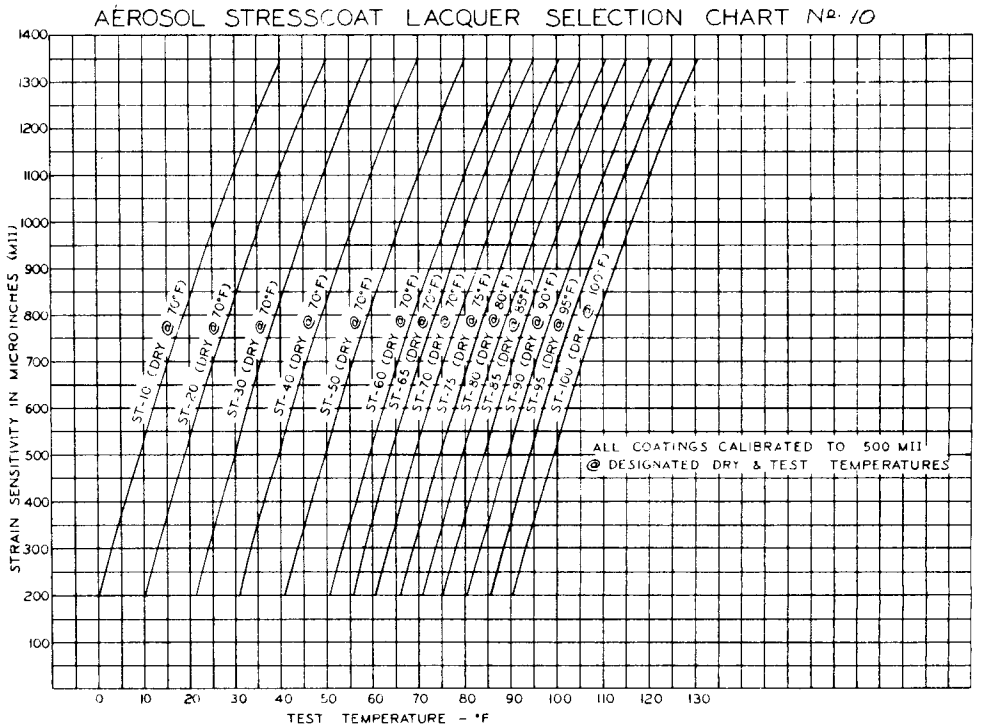

Figure 11
Aerosol STRESSCOAT lacquer selection chart.

Summary

The new series of coatings described represent an improvement in the use and application of the coatings used in the brittle lacquer test method employed in experimental stress analysis. We believe they will provide the stress analyst and design engineer with a more sensitive coating, unresponsive to humidity and more convenient to use.

Measurement of Surface-Residual Stress by Nondestructive Methods

WARREN J. McGONAGLE
and S. S. YUN, U.S.A.

Introduction

Residual stresses are those stresses that exist in a material when all the external forces are removed. These stresses can be macroscopic, microscopic, or have the dimensions of the crystal lattice. These internal stresses can arise in a number of ways, as from nonuniform cooling or quenching, from mismatch of parts which are constrained mechanically prior to welding or joining, and from mechanical working such as rolling, drawing, machining, or grinding. The deleterious effects of residual stresses are warpage during machining or grinding, lack of dimensional stability with time, and reduced resistance to premature failure by fatigue or stress corrosion. The residual stresses are superimposed on the load stresses, and if the combined stresses exceed a certain critical value they may cause failure of a component.

Various methods have been used to study residual stress. These methods include: (a) electrical and mechanical strain gauges developed especially for studying stresses in weldments (1–4), (b) photoelastic coatings (5), (c) acoustoelastic effect (6), (c) photoelastic effect (7,8), magnetic (9), and X-ray (10, 12).

This paper is concerned with the discussion of X-ray and ultrasonic methods for the study of surface residual stresses induced in a machined or ground specimen of simple geometry. Although it is not possible to obtain a complete pattern or distribution of the surface residual stresses existing throughout a specimen before and after machining, the average magnitude of the surface residual stresses on a machined or ground specimen can be estimated by measuring the change in lattice spacing by X-ray and by measuring the velocity of propagation of surface ultrasonic waves (13,14).

Surface Residual Stresses Induced in Machined Material

Literature is available on the effects of machining operations in producing stresses in structural parts. Much of this literature is controversial and the results are often inconclusive.

Investigation has shown that the total residual stresses on the surface of a machined part are the combined effects of the machining or grinding operation and the accompanying heat involved in the process of removing the material. The combined effects of the mechanical operations and accompanying phenomena are to produce surface layer stresses that might be beneficial (compressive) or harmful (tensile) to the service life of a part. Once the existence of the stress is known, the problem becomes one of making measurements to find the magnitude of the stress, depth of stressed layer, and nature of the stress, whether tensile or compressive.

Although there are many factors that determine the final configuration of surface residual stresses in a machined piece, some general features of the residual stresses have been observed by various investigators and reported in the literature. No discussion is presented in this paper on the effect of the specific tools, shapes, sharpness of the cutting edges, and modes of cutting in relation to the induced total residual stresses, but a series of figures in references 15-18 serve to illustrate the residual stress patterns in various materials for different cutting parameters employed. As Figures. 1 and 2 indicate, the maximum residual stresses (either compressive or tensile) are induced at the surface of the material; then the sign of the residual stress along the depth of the material changes to balance the stresses introduced at the very near surface. As will be seen later, this general characteristic of residual stress due to machining can be utilized in interpreting the experimental results obtained for a given material.

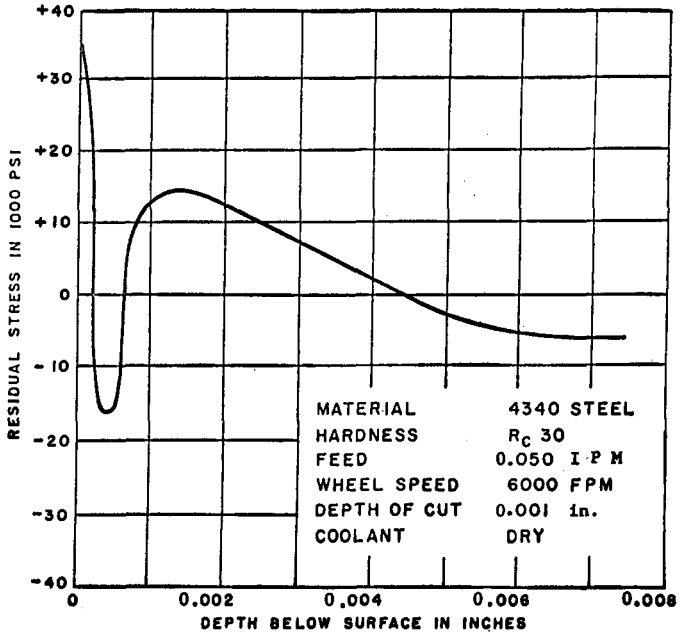

Figure 1. Residual stress resulting from grinding operations on a workpiece.

This work was supported by U.S. Air Force.

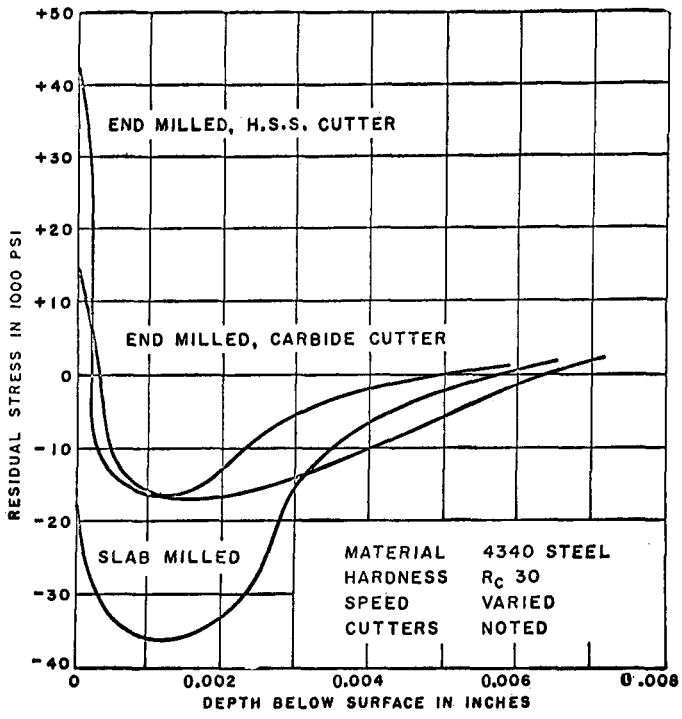

Figure 2. Comparison of residual stress resulting from parameter change in milling operation.

Nondestructive Residual-Stress Measuring Methods

X-Ray Method (10,12,19-25)

One of the most extensively used nondestructive methods for residual stress determination is X-ray diffraction. The X-ray method is based on measuring the change in the crystal lattice spacing caused by the residual or applied stresses in the specimen. Elastic strains caused by stress in metals that have crystalline structures can be determined by measuring the lattice parameters by X-ray diffraction since the lattice parameter of a metal in the unstressed state is known or can be determined nondestructively without machining or drilling. X-ray diffraction techniques are applicable only to crystalline materials having randomly oriented small grains.

When a monochromatic X-ray wave is reflected from the atomic planes, the diffraction of X-rays satisfies the Bragg equation:

$$n\lambda = 2d \sin \theta \quad \text{.....(1)}$$

where λ = the wavelength of incident beam
θ = the angle between incident or reflected beams and surface of reflecting lattice planes
d = the lattice spacing
n = the order of reflection ($n = 1, 2, 3, \ldots$)

Equation 1 shows that if the wavelength of the X-ray is known, the interplanar spacing, d, can be determined by measuring the angle θ. The residual stresses are then deduced from the lattice strains by using mathematical relations deduced from the theory of elasticity. The precision in measuring the interplanar spacings depends on the precision in measuring θ. To evaluate the effective errors, the Bragg equation is differentiated with respect to θ;

$$\frac{\Delta d}{d} = \cot \theta \cdot \Delta \theta \quad \text{.....(2)}$$

This equation shows that the larger the angle θ, the better the precision that can be obtained. Since it is difficult to measure θ to better than 0.005°, diffraction angles of 60° and preferably over 70° are used to select X-ray radiation wavelengths for the particular material to be investigated. In most cases the optimum conditions cannot be employed because of adverse X-ray scattering by the specimen. When this condition occurs, other diffraction planes must be chosen at the expense of the precision of analysis.

Two general techniques are used in the recording of diffraction patterns: (a) photographic and (b) X-ray diffractometer. In both techniques the preceding analysis assumes isotropic material. In general, this assumption is not valid for the individual grains of the specimen even when it is valid for the specimen as a whole. This consideration, together with the fact that a diffracted beam comes from only those grains having a certain orientation in the specimen, has given rise to much uncertainty concerning the correct values to use for macroscopic or average values of Young's modulus and Poisson's ratio (22, 26, 27).

An approximate average sensitivity of macroscopic strain measurement is given in Table 1. It should be noted that these values are all determined from the average values of lattice residual strain in the specimen. The composition of the specimen also affects the test results (28).

Table 1

Summary of Residual Stress Measuring Methods

	X-Ray Diffraction		
	Film Technique	Diffractometer	Ultrasonic Method
Quality of Measurement			
Approx. strain sensitivity, μ in/in	400	300	3 ksi[a]
Approx. reproducibility	±5–10 ksi	±5–10 ksi	±5–10 ksi
Determine stress components	Yes	Yes	Possible
Applicable to uneven stress field	Yes	Yes	Possible
Surface or interior strains	Surface	Surface	Interior stress
Effects from Variations in Materials	Affected	Affected	Affected
Field Application			
Field (F) or laboratory (L)	L, F	L	L, F
Remote indicating	No	No	Yes
Cost and Time			
Complexity of equipment[b]	4	4	4
Time required[c]	3	3	1
Required operator skill[d]	4	4	4

[a] Sensitivity in stress is given: ksi = 10^3 psi.
[b] 1 to 4: Less expensive → expensive.
[c] 1 to 4: Short → long.
[d] 1 to 4: Less experienced → highly experienced.

The average sensitivity in X-ray residual stress measurement is approximately 5,000 psi (25, 29), and the reproducibility is also within this sensitivity at a point in a given specimen. The measurements at the different points in the specimen yield greater uncertainty in reproducibility. However, it has been found that the difference in the residual stress value obtained by X-ray methods and that of destructively measured specimens is generally greater than 5,000 psi.

Ultrasonic Method

The velocity and attenuation of ultrasonic waves are influenced by the physical and mechanical properties of the medium (13, 14, 30, 31). If residual stresses exist in metals, for example, these properties change; therefore, it is possible to detect the changes in velocity or attenuation and relate them to the residual stresses in the specimen.

The velocity of an elastic wave, v, propagating through a homogeneous elastic medium is given by

$$v = \frac{\sqrt{E}}{\rho} \tag{3}$$

where E is the elastic modulus and ρ is the density. A change in E or ρ would affect the velocity. The density and elastic modulus of metal change, in general, as a compressive or tensile stress is applied. These changes are a second-order effect on the velocity of ultrasonic waves; therefore, the fractional change in velocity is very small—approximately 0.0005% per 10^4 psi—in most metals.

The techniques developed in recent years for accurately measuring velocity are capable of detecting the velocity difference by one part in 10^6. In some single crystals and polycrystalline metals, this change corresponds with a stress of less than 10^3 psi (32). The fact that the velocity changes in commercial metals caused by the other factors (such as inhomogeneity, preferred orientation and grain structure) are approximately the same order of magnitude as the changes caused by the residual stresses complicates the stress analysis in many applications (33).

Assuming that these effects are eliminated by the relative measurement of ultrasonic velocity in stress-free and stressed specimens, the expected sensitivity of stress measurement is of the order of 10^4 psi.

Attenuation measurements of ultrasonic waves in metals, as a function of applied stress, yield a relationship which can be used in determining the state of residual stress in a specimen (34). However, the difficulties in experimental techniques and interpretation of data in terms of the residual stresses in the specimen make this technique less desirable than the velocity technique.

The accuracy and dependability of the attenuation techniques are not well established as yet, and the measurement of residual stress by ultrasonic absorption is more or less qualitative at present.

Only limited applications of ultrasonic techniques have been reported in residual stress analysis (34). Most of the ultrasonic techniques are in the development stage, and are used primarily in laboratory applications.

Velocity Measurements

Determinations of the transit time and the path length of an ultrasonic pulse propagated through a specimen can be used to determine changes in the wave velocity. Variations of the measured time as a function of applied stress may be used to determine the amount of change in velocity due to an applied load. There are many sources of error in this technique. For example, the bonding of the transducer to the specimen is very critical. Variations in temperature can make an apparent change in transit time.

In addition to the stress, other factors can alter the velocity, such as a preferred grain orientation of differing amounts of metallurgical or mechanical treatment and varying concentrations of alloying elements.

The fact that the change in velocity is small indicates the limitations of the conventional pulse-echo technique. A number of precision experimental arrangements for absolute velocity measurement have been described by Forgoes and McSkimin (35,36). These systems are capable of determining the transit time to a few parts in 10^5 or better, and had been able to determine third-order elastic constants in single crystals. The "sing-around" technique, as it has been called, is very convenient for measuring small differences in the transit time of ultrasonic pulses. A selected pulse or received signal from the specimen is used to re-trigger the transmitter, so that the pulse of energy thereafter repeats itself at a frequency determined by the effective ultrasonic time. Changes in transit time are determined by a change in repetition frequency measured on an electronic counter. The circuitry is stable, and accurate measurements can be obtained.

Of prime importance in the application of Rayleigh waves for measuring surface residual stress is their effective generation and detection in the medium of interest; this requires adaptation to complex geometries, roughness of the surfaces, different surface shapes, and other characteristics of the surface.

The three general techniques of generating surface waves are:

(1) Use of mode conversion of compressional waves incident upon the surface at a critical angle (37).
(2) Use of a comb structure to provide spatially periodic coupling of a compression wave to the surface (38).
(3) Use of specially dimensioned Y-cut quartz crystal in contact with the surface (37).

In the present work, surface waves were generated by a variable angle transducer system. The angle of incidence of longitudinal waves to a specimen was adjusted such that the following relation was satisfied:

$$\frac{V_L}{V_R} = \sin \theta_{cr} \tag{4}$$

where

V_L = velocity of longitudinal wave in a wedge.
V_R = Rayleigh wave velocity generated in specimen.
θ_{cr} = critical angle for the Rayleigh wave.

Using the sing-around technique one can determine the absolute velocity of the surface waves in the specimen or merely the change of the velocity with respect to the unstressed or standard test specimen. Figure 3 is a schematic diagram of the electronic instrumentation.

In the sing-around technique a pulse from a pulsed oscillator drives the transducer. A surface wave is propagated through the specimen for a given distance and the signal detected by a second transducer. The received signal re-triggers the pulsed oscillator for the next pulse. The repetition frequency is the reciprocal of the electronic delay time and the acoustic travel time. For a given distance between the transducers, the surface-wave velocity can be calculated. As improvement on this technique is to superimpose the received and transmitted signal by introducing an external trigger pulse generator and vary the repetition frequency, the received and original signal are superimposed to obtain the travel time. Using this modified sing-around technique the surface-wave velocity can be measured accurately to 1 part in 10^5.

Experimental Results

Typical test results obtained for 4340 steel (at 150 and 220 ksi strength levels) are given in Figure 4. The results show that the fractional change in velocity of the surface wave is approximately proportional to the strain produced by the applied stress. The slopes of the stress curve vs. velocity change, at different frequencies, are the same within experimental error. Therefore, a calibration curve at one frequency can be used for other frequencies of the surface waves in the case of uniaxially stressed specimens.

Using these calibration curves, the stress values determined ultrasonically were superimposed on destructively determined

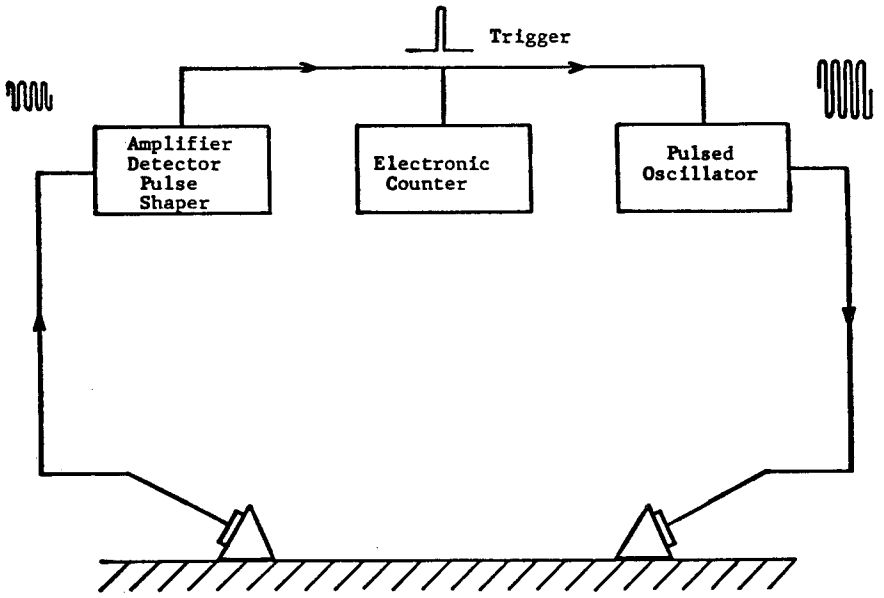

Figure 3
Basic apparatus for measuring Rayleigh-wave velocity by the sing-around method.

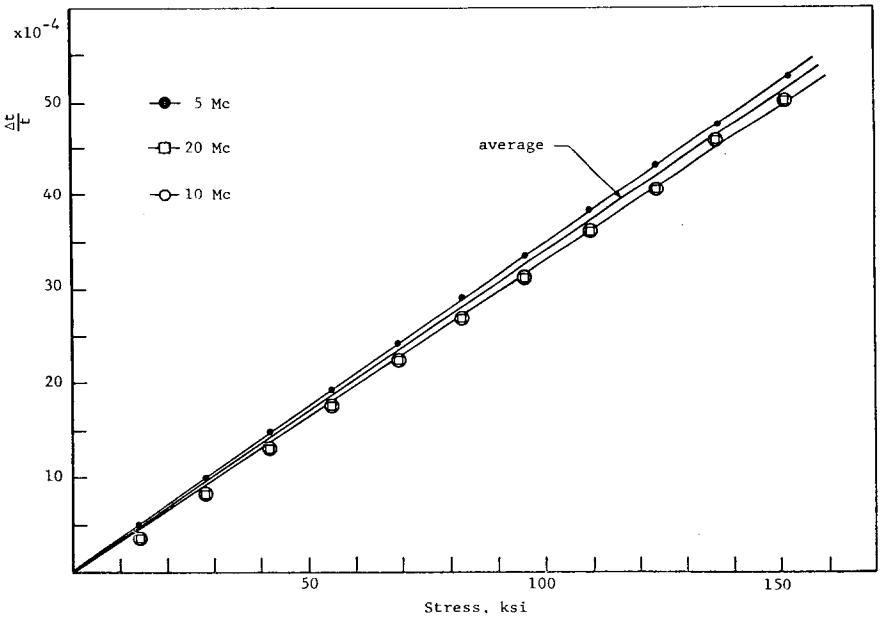

Figure 4
Ultrasonic calibration curve for 4340 steel at 220 ksi strength level.

stress-depth curves for several materials. Although correlation of the ultrasonic measurements at three different frequencies was not consistent, the maximum values of residual stress agreed reasonably well within the experimental error.

In order to determine the degree of correlation between the actual stress distribution in the specimens tested and the ultrasonic data, the variations of the ultrasonic data with the X-ray data were compared as the stressed layers were removed from the surface of the specimen by electropolishing.

Even though the stress-dependent calibration curve shows little scatter in the measurements, the correlation between ultrasonic measurements and destructively determined stress-depth curve can be poor. There are two major reasons for poor correlation: The first is the variation in residual stress along the length of ground specimens, as indicated by destructive tests. The residual stress, determined destructively, shows an integrated value for the entire length of the specimen, while the ultrasonic measurement shows an integrated value over a length of 1 or 2 in. (the distance between the transducers), and the X-ray measurement gives the stress at a point. The poor correlation between ultrasonic measurements and destructively determined stress-depth curves is also associated with the deficiency in reproducibility of destructively determined stress-depth curves.

To give a much more significant indication of the capability of the ultrasonic method, a comparison of ultrasonic with X-ray residual stress determination has been made. Specimens of 4340 steel at 150 ksi and 220 ksi strength level were ground. Residual stresses were determined by X-ray method and ultrasonic technique at three different frequencies: 5, 10, and 15 MHz. In the as-ground condition, X-ray residual stress determinations were made at positions $\frac{1}{2}$ in. either side of the centre, and ultrasonic determinations were made at three different frequencies with the transducer set 1 to $1\frac{1}{2}$ in. apart over the centre section of the specimen. After the X-ray and ultrasonic measurements were made, a layer of material was removed from the surface of the specimen. Then, X-ray and ultrasonic measurements were made. Another layer of material

was removed from the surface of the specimen, followed by X-ray and ultrasonic measurements. This process of layer removal by means of electropolishing and measuring was repeated several times to obtain residual stress data as a function of depth.

These results are given graphically in Figures 5 and 6. The data show that the residual stresses determined at a given frequency decreased as the stressed layers were removed from the surface of the specimens. The rate at which the residual stress decreased as a function of depth was approximately the same for both 15- and 10-MHz surface waves. This is only approximately true for 5-MHz waves. For the 5-MHz waves, after a given amount of material has been removed, the values of residual stress remain relatively constant. This variation can be explained by the fact that the wavelength of the 5-MHz surface wave is approximately 20 $\times$ 10^{-3} in. Thus, as the stressed layers are removed, the interior part of the specimen has more effect on the measurements than does the immediate surface where only small residual stress remains. The residual stress values determined at higher frequencies are greater than those determined at lower frequencies. The values of maximum stress determined by the ultrasonic method were lower for all four specimens than were the maximum values obtained by the X-ray method. This was expected, since the X-ray method interrogates stress at the smaller amount of the specimen than does the ultrasonic method.

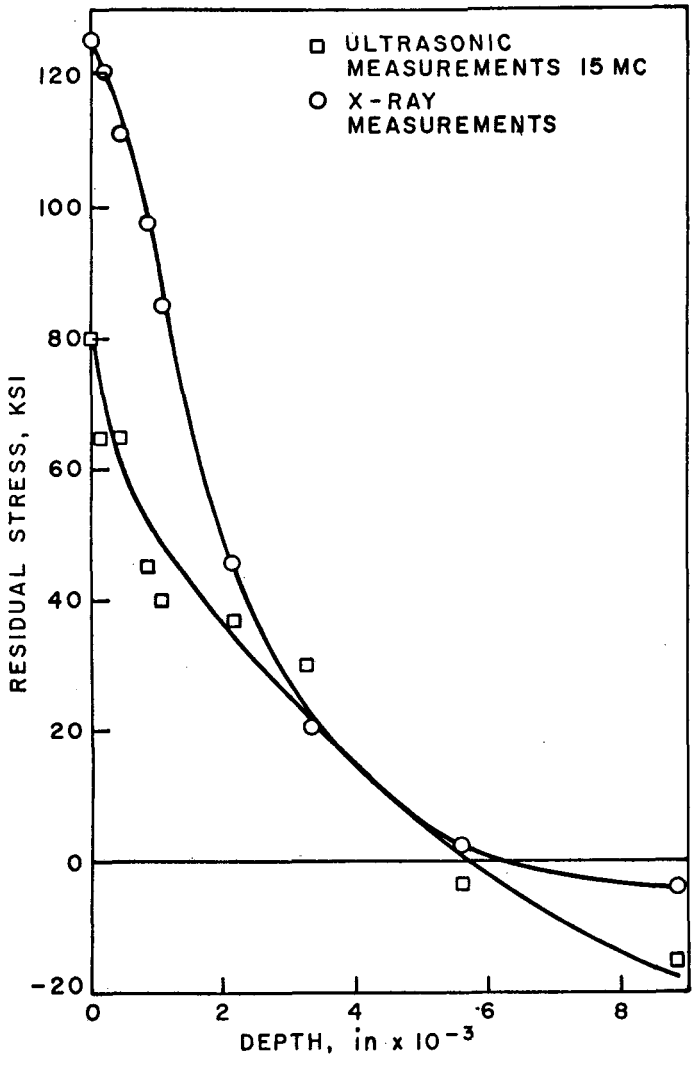

Figure 5. Ultrasonic and X-ray measurements of residual stress for 4340 steel specimen—as functions of amount of material removed.

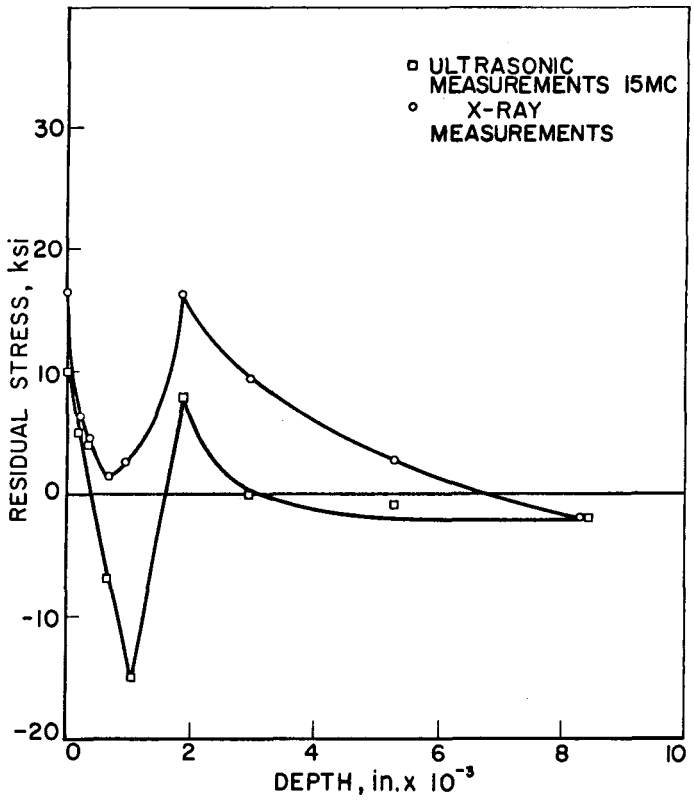

Figure 6. Ultrasonic and X-ray measurements of residual stress for 4340 steel specimen—as functions of amount of material removed.

The 15-Mc ultrasonic data correlates fairly well with X-ray data. This suggests that if the X-ray value is used as the reference, the residual stress at various depths can be plotted from the values determined by the ultrasonic method. This is contingent on the establishment of correction factors for each different surface wave frequency.

Summary

Although the layer-removal correlation between ultrasonic and X-ray measurement does not represent the actual stress distribution of the specimens tested prior to the removal of each layer, the X-ray value does represent the stress values at the surface after removal of each layer. Therefore, any degree of correlation between the values obtained ultrasonically and from X-ray diffraction at each surface shows the feasibility of ultrasonic determination of surface residual stresses at different layers. Further work is required in order to determine the correlation factor which can be used for different materials at different frequencies.

References

1. Masubuchi, K. Nondestructive measurement of residual stresses in metals and metal structures, RSIC 410, Redstone Scientific Information Center, U.S. Army Missile Command, Redstone Arsenal, Alabama, April, 1965.
2. Gunnert, R. Measuring of residual stresses and strains, Document No. X-286-62-OE, Commission X of the Internat. Inst. Welding, 1962.
3. Treuting, R. G., Wishart, H. B., Lynch, J. J., and Richards, D. G. Residual Stress Measurements, *Am. Soc. Metals,* 1952.
4. Hetényi, M., editor, *Handbook of Experimental Stress Analysis,* New York, John Wiley and Sons, Inc., 1950.
5. Zandman, F. Photoelastic-coating technique for determining stress distribution in welded structures, *The Welding J.,* 39, 5, Research Suppl., 191s, 1960.

6. Benson, R. W., and Realson, V. T. Acoustoelasticity, *Prod. Eng.*, 30, 29, 56, July, 1959.
7. Crites, N. A., Graver, H., Hunter, A. R. Experimental stress analysis by photoelastic techniques, *Prod. Eng.*, 33, 18, 57, September, 1962.
8. Holister, G. S. The photo-elastic method applied to material research, *Appl. Res.*, 1, 3, 149, October, 1962.
9. Mills, D., and Bråtina, W. J. Residual stress studies in ferromagnetic materials in ultrasonics, *Proc. Symp. Physics and NDT*, 1963.
10. Vaughan, D. A., and Crites, N. A. Measurement of stress by X-ray diffraction, *Prod. Eng.*, 34, September, 1963.
11. Hyler, W. S., and Jackson, L. R. Precautions to be used in the measurement and interpretation of residual stresses by X-ray technique, in Residual Stresses in Metals and Metal Construction, New York, Reinhold Publishing Co., 1954.
12. Barrett, C. S. X-Ray Analysis, Chapter 18 in reference 4 above.
13. Firestone, F. A., and Frederick, J. R. Refinements in supersonic reflectoscopy—polarized sound, *J. Acoust. Soc. Am.*, 18, 200, 1946.
14. Frederick, J. R. Use of ultrasonic surface waves in the determination of residual stress in metals, *J. Acoust. Soc. Am.*, 32, 1499, 1960.
15. Field and Zlatin, AMC Contract 33 (038) 9948, Curtiss-Wright Corp., Volume 2, 164.
16. Frisch, J., and Thomsen, E. G. Residual grinding stresses in mild steel, *Trans. ASME*, 73, 337, 1951.
17. Henriksen, E. K., Cook, H. R., and Starnes, J. C. Determination of residual stresses in aircraft materials, Convair Report MRT, 57-101 (1956).
18. Osgood, W. R. Residual Stresses in Metals and Metal Construction, Reinhold Publishing Corp., New York (1954).
19. Norton, J. H., and Rosenthal, D. Stress measurement by X-ray diffraction, *Proc. Soc. Exptl. Stress Anal.*, 1, 2, 73-76, 1944.
20. Norton, J. T., and Rosenthal, D. Recent contributions to the X-ray method in the field of stress analysis, *Proc. Soc. Exptl. Stress Anal.*, 5, 1, 71-77, 1947.
21. Norton, J. H., and Rosenthal, D. Applications of the X-ray diffraction method of stress measurement to problems involving residual stresses in metals, *Proc. Soc. Exptl. Stress Anal.*, 1, 2, 77-81, 1944.
22. Isenberger, H. R. Bibliography on X-ray Stress Analysis, St. John X-ray Laboratory, Califon, New Jersey (1949).
23. Koistinen, D. P., and Marburges, R. E. A simplified procedure for calculating peak position in X-ray residual stress measurements on hardened steel, *Trans. ASM*, 51, 537, 1959.
24. Vaughan, D. A., and Crites, N. A. Measurement of stress by X-ray diffraction, *Prod. Eng.*, 34, 20, Sept. 30, 1963.
25. Macherauch, E., Basis and problems of X-ray determining of elastic stress, *Materialprüfung*, 5, 14, 1963.
26. Bollenrath, F., Hauk, V., and Osswald, E. Roentgenographische Spannungsmessungen bei Uberschreiten der Fliessgrenze an Zugstaben aus unlegiertem Stahl, *Z. Ver. Deut. Ing.*, 83, 129, 1939.
27. Condon, E. V., and Odishaw, H. (eds.), Handbook of Physics, Part 8, The Solid State, McGraw-Hill Book Company, Inc., New York, 1958.
28. Maucherauch, E. A. new aspect in X-ray residual stress analysis, *Proc. Symp. Physics and NDT*, 1966.
29. Martin, D. E., Evaluation of methods for measurement of residual stress, TR-147, *Soc. Auto. Engrs.*, New York (1960).
30. Bratina, W. J., and Mills, D. Investigation of residual stress in ferromagnetics using ultrasonics, *Nondestructive Testing*, 18, (1), 110, 1960.
31. Rollins, F. (Midwest Research Institute), Ultrasonic methods for nondestructive measurement of residual stress, WADD Tech. Rept. 61-42, Part 1 (May, 1961).
32. McSkimin, H. J. Variations of the ultrasonic pulse-superposition method for increasing the sensitivity of delay time measurement, *J. Acoust. Soc. Am.*, 37, 864, 1965.
33. Hikata, A., Truell, R., Granato, A., Chick, B., and Lücke, K., Sensitivity of ultrasonic attenuation and velocity changes to plastic deformation and recovery in aluminum, *J. Appl. Phys.*, 27, 4, 396, 1956.
34. Kihara, H., and Masubuchi, K. Residual stresses and distortions in weldments, *Sampo Co.*, Tokyo, in Japanese, 1957.
35. Forgoes, R. L. Improvements in the sing-around technique for ultrasonic velocity measurements. *J. Acoust. Soc. Am.*, 32, 1697, 1960.
36. Reference 32 above.
37. McGonnagle, W. J. Nondestructive Testing, Gordon & Breach, New York (1966).
38. Viktorov, I. A. Investigation of methods for exciting Rayleigh waves, *Soviet Phys-Acoustics*, 7, 236, 1962.

Ultrasonic Determination of High-Order Elastic Constants in Elastically Deformed Metal Rods

D. TIETZ, GERMANY

ABSTRACT: The determination of traditional elastic (second-order) constants by ultrasonics is well known as applied to monocrystalline and polycrystalline materials. However, for the solution of many problems in the physics of metals and the theory of elasticity it is necessary to make use of elasticity of a higher order, i.e. the theory of nonlinear elasticity. Third-order elastic constants can also be determined with ultrasonics. The equations developed by Hughes and Kelly, and Toupin and Bernstein for polycrystalline material serve as bases for such determinations. The measurement of the velocity of longitudinal and transverse waves (the plane of vibration parallel and perpendicular to the direction of load) by linear elastic loading of tensile stress and pressure are determined by moduli of the third order. Three third-order moduli have been determined in aluminum. Two third-order moduli have been determined in steel and Armco iron. The different equations have been compared and discussed. The moduli can be used in experimental stress analysis with ultrasonics (acoustoelasticity).

Introduction

The determination of elastic moduli in crystalline media from the measurement of ultrasonic velocity is an important and useful use of ultrasonics in the physics of metals. Hooke's law describes the linear connection between stress and strain and is valid for many practical cases. However the present-day development of the physics of solids requires a nonlinear connection between stress and strain.

The theory of nonlinear elasticity is usefully applied (1), for example, in the description of the change of volume or density of elastic material with internal stresses or dislocations,

and in the description of strain and stress about lines of dislocation (2). The attenuation of hypersonic waves ($> 10^9$ cycles/sec) can be explained by the aid of the nonlinear theory of elasticity. Within this range of frequency can be obtained phonon-phonon interaction (3, 4). The nonlinear theory of elasticity has an essential importance for the description of the finite deformation of monocrystalline and polycrystalline materials (5, 6) and for the description of the change of elastic constants with hydrostatic pressure (7). In this connection it is apropos to discuss the propagation of ultrasonics in elastic deformed media (8).

The Nonlinear Theory of Elasticity

The function of strain energy can be described as a polynom expression (9):

$$\phi = \phi_v + yc_{ij}\eta_{ij} + \tfrac{1}{2}\, c_{ij}{}^{kl}\eta_{ij}\eta_{kl} + c_{ijklmn}\eta_{ij}\eta_{kl}\eta_{mn} + \qquad (1)$$

with $i, j, k, l, m, n = 1, 2, 3$

η_{ij} signifies the Lagrange components of strain, c the elastic moduli with the strain energy ϕ. ϕ is the energy at the beginning. It is null, when ϕ is null before the deformation begins. $Yc_{ij}\eta_{ij}$ represents potential energy. This can be ignored because the reference point of the energy is unimportant, under the assumption that the linear elastic behaviour is ordinarily stopped after the third term. We obtain, then, the above elastic second-order constants, c_{ijkl}. However, c_{ijklmn} represent third-order elastic constants, and are important in the non-linear theory of elasticity. The moduli constitute a sixth-order tensor with 720 components. Only 56 components are independent from one another in the triclinic system (10, 11). Birch (12) employs the expression of tensor c_{pqr} for third-order moduli with which p,q,r traverse values of 1 to 6, corresponding to the condition $p \leqq q \leqq r$. The shortened expression for the Lagrange components of the strain is analogous.

Only three elastic third-order moduli still exist for isotropic media, namely

$$\left.\begin{aligned} c_{123} &= \mathrm{l} \\ c_{144} &= \mathrm{m} \\ c_{456} &= \mathrm{n} \end{aligned}\right\} \qquad (2)$$

These are the so-called Murnaghan constants (13).

Equations for the Determination of Third-order Constants.

The determination of third-order elastic moduli for crystals and isotropic media is relatively difficult, for example, by using the Poynting effect. Measurement of the velocity of ultrasonics allows third-order elastic moduli to be determined not only with polycrystalline material but also with monocrystalline material under uniaxial tension or pressure, and hydrostatic pressure. In this way Bateman, Mason and McSkimin (14) have determined all six elastic moduli for the cubic monocrystal of germanium, while Hughes and Kelly (13) have calibrated the three moduli for polycrystalline iron.

Hughes and Kelly (13) and in a similar way Toupin and Bernstein (8) have derived the relations for the change of velocity of ultrasonics under small uniaxial pressure by primary isotropic media.

Toupin and Bernstein (8) indicate the following equations for a wave propagation perpendicular to the direction of load with utilization of the relations

$$E = \frac{\mu(3\lambda + 2\mu)}{\lambda + \mu} \qquad (3)$$

and

$$\nu = \frac{\lambda}{2(\lambda + \mu)} \qquad (4)$$

longitudinal wave

$$\frac{d v_L}{d\sigma} = \frac{1}{2E v_{L_o} \delta_0} \left[-\nu(4\lambda + 8\mu + 3\nu_1 + 10\nu_2 + 8\nu_3) + (1 + \nu)(\nu_1 + \nu_2) \right] \qquad (5)$$

transverse wave, direction of vibration in direction of load

$$\frac{dv_{11}}{d\sigma} = \frac{1}{2E v_{T_o} \delta_0} \left[-\nu(4\mu + 3\nu_2 + 4\nu_3) + (1 + \nu)(2\mu + \nu_2 + 2\nu_3) \right] \qquad (6)$$

transverse wave, direction of vibration perpendicular to the direction of load

$$\frac{d v_1}{d\sigma} = \frac{1}{2E v_{T_0} \delta_0} \left[-\nu(4\mu + 3\nu_2 + 4\nu_3) + (1 + \nu)\nu_2 \right] \qquad (7)$$

Accordingly v_{Lo} is the velocity of the longitudinal wave and v_{To} the velocity of the transverse wave in an unstressed medium; δ_0 is the density before loading. The expressions ν_1, ν_2, ν_3 represent third-order moduli.

Measurements and Results

The velocities of ultrasonics have been measured under uniaxial tension for the alloy AlCuMg. Tension and compression were applied to steel C45 and Armco iron. The direction of vibration of the transverse wave was in the direction of the load ($\nu\perp$) and perpendicular to the direction of the load ($\nu\|$). The direction of propagation was perpendicular to the direction of load in all cases. All these values were measured with increasing and decreasing load in order to detect hysteresis, but no differences were found. An interferometer was used for the measurements. Extensive observations of the errors of this method showed that the error of measurement was 0.1 °/∞, when the probe-to-specimen contact was constant; the number of equalized echoes from the specimen were the same in the series of measurements, and the readings on the spindle of the interferometer were precise. Further, the water temperature was determined to an accuracy of 0.1°C. The temperature was measured before the equalization started and when it was finished, and the measurement of the relative change of velocity was much improved in comparison with the previous examinations for different probe-to-specimen contacts (15). The rods used were 30 mm wide and 20 mm thick; the pressure rods were thicker. Consequently, the dimensions were not influenced by the method of measurement (16). The transverse contraction was determined and taken into consideration in determining the velocity.

An aluminum device was developed for the probe with a straight extension of the cable to achieve an approximate constant probe-to-specimen contact in the range of elastic tension or pressure deformation (Figure 1). The ultrasonic velocity was therefore not influenced. The pressure of the probe-to-specimen contact was applied with two steel springs. The probes rested in a U-shaped clamp that formed part of the device, thereby avoiding tilts at the probe-to-specimen contact. The angular measure of the device was established to determine the position of the vibration plane for transverse-wave probes as related to the pressure or tension direction. All planes parallel to the specimens were ground. The contact between the transverse-wave probes and the specimens did not have a special

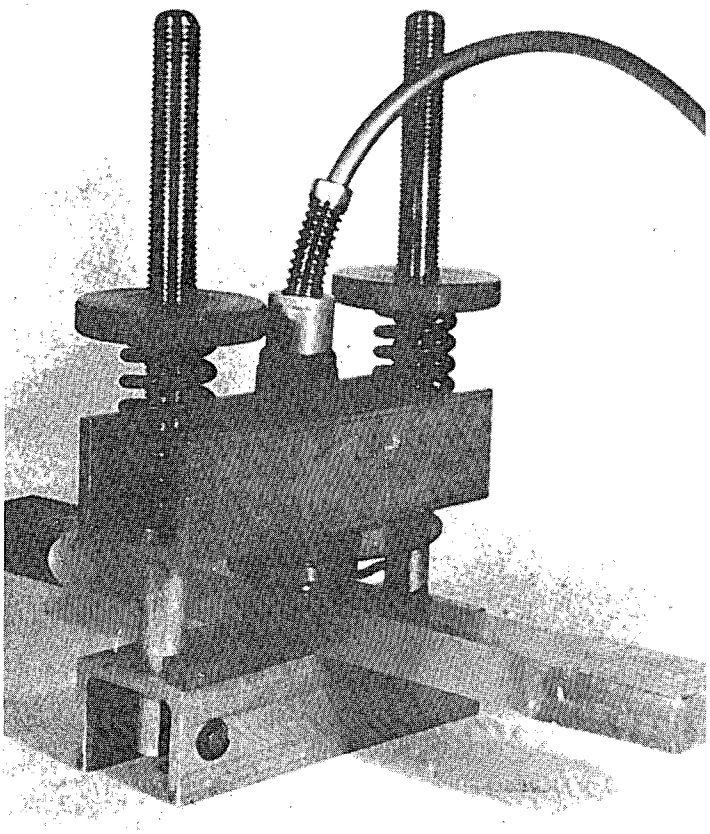

Figure 1. Aluminum probe device with a straight cable connection to maintain constant probe-to-specimen contact.

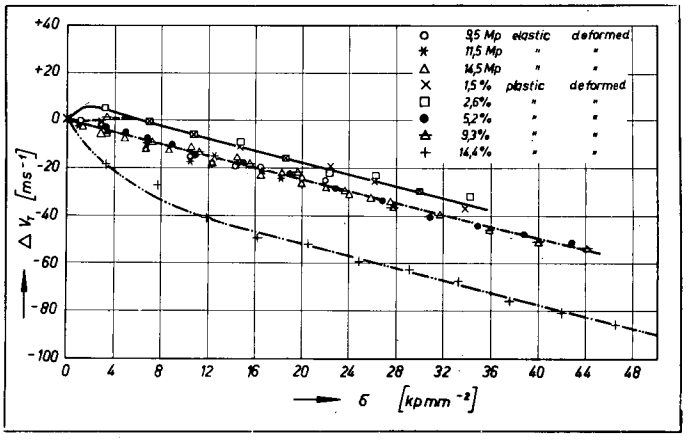

Figure 2. Velocity change of transverse wave. Plane of vibration in the tension direction, 4 MHz, material AlCuMg, different stretch degrees.

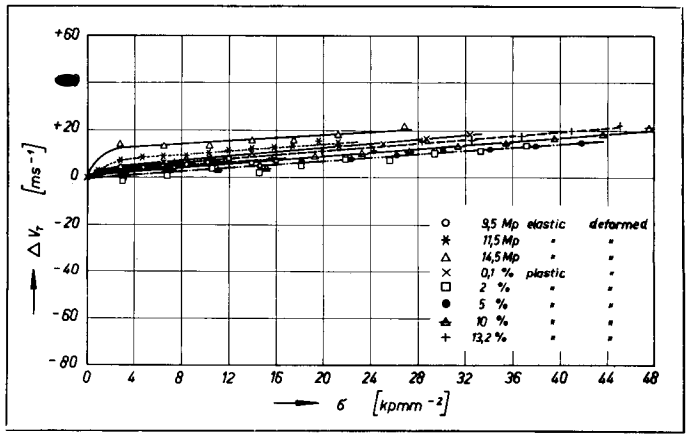

Figure 3. Velocity change of transverse wave. Plane of vibration perpendicular to the tension direction, 4 MHz, material AlCuMg, different stretch degrees.

coupling medium, with which the specimens could be degreased. The influence of frequency was not located for any media in this range, i.e. from 2 to 6 MHz. A frequency of 4 MHz was selected, and a good high-frequency disintegration in the multiple echoes resulted.

Primary examination of the alloy AlCuMg specimens was made. Applying the same stress, higher dilation than with steel was found, owing to the low Young's modulus. X-ray examinations showed that stronger texture and internal pressure stresses of 11 kp mm^{-2} exist on the surface of the material. Different stretch degrees were applied to detect the influence of plastic deformation and of internal stresses. The Δv-values are related to the value of the beginning of every line of load. Figure 2 is a graphic illustration of the velocity change of the transverse wave whose plane of vibration lies in the direction of tension. Changes in ultrasonic velocity were determined in the elastic load range of 9.5, 11.5 and 14 Mp. All values showed a linear behaviour and a decrease in the transverse-wave velocity. The straight lines are superposed. A change in the stresses ($\Delta\sigma$) of 10 kp mm^{-2} shows a change in the transverse-wave velocity ($\Delta v\|$) of —13.0 kp mm^{-2}. The stretching was then applied up to 1.5, 2.5, 5.2, 9.2 and 14.4%. All graphs showed a linear decrease in the transverse velocity with an increase in the tensile stress.

The transverse-wave velocity was then determined at the point where the vibration plane lies perpendicular to the direction of load. Different degrees of stretch were chosen again for a parameter of graphs (Figure 3). Three graphs were developed up to 9.5, 11.5 and 14.5 Mp without plastic deformation. After loading stresses above 3 kp mm^{-2}, the graphs showed a linear shape. All three graphs lie parallel to each other. With an increase of the stress by 10 kp mm^{-2} the velocity increases by 4.2 ms^{-1}. This value is nearly the same as that found for a specimen with 4.3 ms^{-1}.

The gradual plastic dilations of 0.1, 2, 5, 10 and 13.2% show for the following elastic dilations a linear course of graphs with partial small variations for low load. The change of longitudinal velocity for small tensile stress is determined analogously. A variation of 10 kp mm^{-2} yields a change of longitudinal wave velocity of 9.6 ms^{-1} (Figure 4).

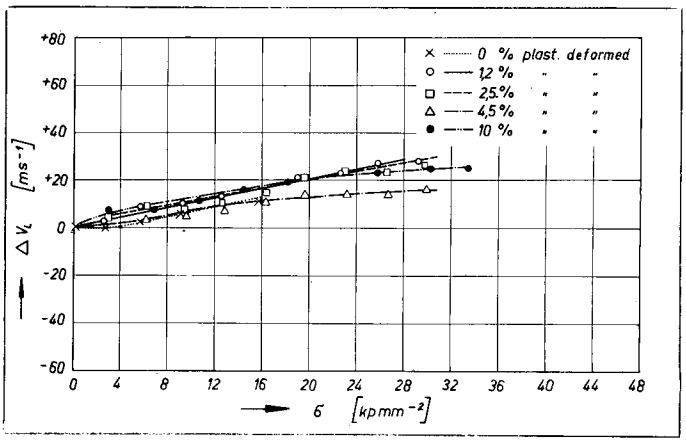

Figure 4. Velocity change of longitudinal wave, 4 MHz, material AlCuMg, different stretch degrees.

In the same way the transverse velocity change for different load steps for Armco iron was determined. This material does not show distinct internal stresses on the surface. Stresses smaller than 1 kp mm^{-2} in the axis direction were obtained with X-rays and are in the error range of this method; the texture is fine. The Armco iron specimens were examined in the unstretched state and with plastic dilation of 2.5 and 11%. The graphs again indicate linear processes that lie parallel to each other. The changes are small. The decrease amounts to 1.4 ms^{-1} for an increase of the 10 kp mm^{-2} in tensile stress. The direction of the vibration plane lies in the direction of tension. When the vibration plane lies perpendicular to the tensile direction, the increase of 1.4 ms^{-1} is obtained for an increase of load. The last value is not precisely relative to the small change in velocity.

Later, pressures were applied to the Armco iron specimens. The change of the transverse-wave velocity amounted to 2.0 ms^{-1} for a pressure increase of 10 kp mm^{-2}. The change of velocity was a linear increase, and this value conformed with the value of 1.8 ms^{-1} found for the increase in tensile stress. When the vibration plane of the transverse wave lay perpendicular to the pressure direction, the exact change of velocity was not obtained. The measurement of the longitudinal velocity did not give precise results of the velocity change.

Examinations were then made to steel C 45. The material was tempered (normalized and stress-relief annealing) before the test as were the Armco specimens. X-ray determination of internal stress only showed values on the surface smaller than 0.5 kp mm^{-2}, which are in the range of errors of the X-ray method. The texture is fine.

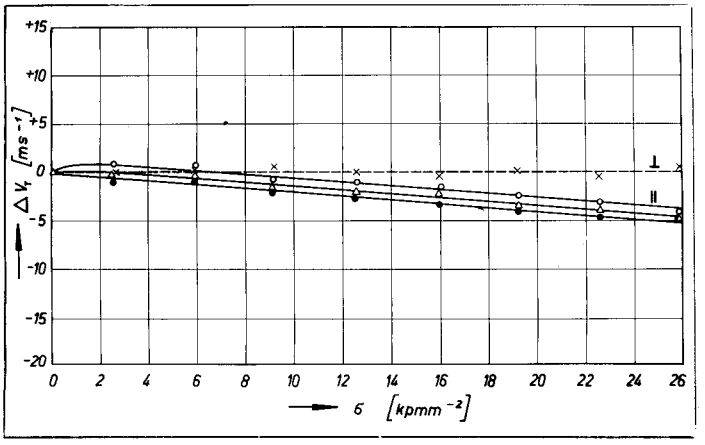

Figure 5. Velocity change of transverse wave. Plane of vibration parallel with and perpendicular to the direction of load, 4 mc, material C45, tensile stress.

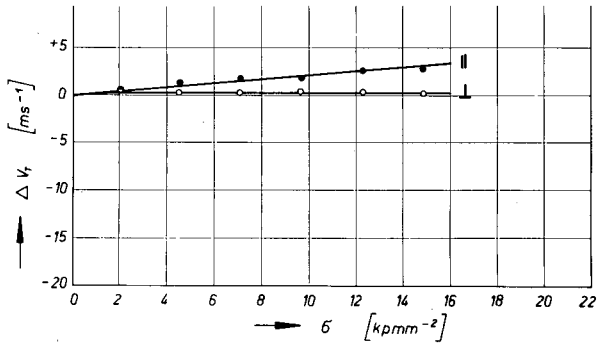

Figure 6. Velocity change of transverse wave. Plane of vibration parallel with and perpendicular to the direction of load, 4mc, material C 45, pressure stress.

A variation in tensile stress of 10 kp mm^{-2} effects a variation in transverse-wave velocity of 2 ms^{-1}. In this case the vibration plane lay in the direction of the load. When the vibration plane was perpendicular to the direction of tension, the change was not measured (Figure 5). Results of pressure on C 45 were analogous with those on Armco iron. The transverse-wave velocity was increased by 2.1 ms^{-1} for an increased pressure stress of 10 kp mm^{-2} (Figure 6). The vibration plane was parallel to the pressure direction. When the vibration plane was perpendicular to the direction of load, the change was not measured again. A plastic stretched rod, a stretched and then normalized and stress-relief annealed rod, and a hardened specimen were investigated under an elastic pressure load for determination of other influences. The measurement values are listed in Table 1.

Table 1

material	$\Delta\sigma$ [kpmm^{-2}]	ΔE [%]	Δv_{11} [ms^{-1}]	Δv_1 [ms^{-1}]	Δv_L [ms^{-1}]
AlCuMg	+10	0.135	−13.0	+4.2	+9.6
Armco iron	+10 −10	0.046	−1.8 +2.0	+1.4 ≈0	≈0 ≈0
C 45 normalized	+10 −10	0.047	−2.0 +2.0	≈0 ≈0	≈0 ≈0
C 45 stretched	−10	0.047	+2.1	≈0	≈0
C 45 stretched, normalized and stress-relief annealed	−10	0.047	+2.0	−0.6	≈0
C 45 hardened	−10	0.047	+2.7	≈0	≈0

Assembly of velocity change in dependence of stress change

Δv_{11}: change of transverse-wave velocity vibration plane in direction of load

Δv_1: change of transverse-wave velocity vibration plane perpendicular to the direction of load

Δv_L: change of longitudinal-wave velocity

Discussion of Measurement Values

All the measurement values are listed in Table 1.

The results of measurements of transverse-wave velocity are proportional to the modification of stress for the measured range and for the investigated material. An inversion of the load inverts the sign of the values only. This pointed up the value of the transverse-wave velocity, especially when the vibration plane lay parallel to the direction of load. The velocity of the transverse wave with the vibration plane perpendicular to the load direction was affected by the load also. The change in longitudinal-wave velocity was observed with the stress load only with the alloy AlCuMg. Other materials had irregular variations only. It is interesting to note that conclusions arrived at by Mager (17) and Bergman and Shabender (18) measured under the same conditions with steel and aluminum have a different quantitative change and trend of change.

The Murnaghan (5,6) constants can be determined by using the equations of Hughes and Kelly (13). The changes in longitudinal-wave velocity and in two transverse-wave velocities have been determined for AlCuMg. Now, third-order moduli can be determined by the Murnaghan constants *l*, *m*, *n*. The pressure examination yielded the following values:

$l = 465\,040$ kp mm^{-2}
$m = -64\,640$ kp mm^{-2}
$n = -44\,530$ kp mm^{-2}

The constants can be influenced by the pronounced texture and internal stresses of this material. With the Armco iron material under tensile stress and with the steel C 45 (stretched and tempered) under pressure stress, based upon the equations of Hughes and Kelly, the following values were found:

Armco iron (tension) $m = 61\,120$ kp mm^{-2}
$n = -96\,220$ kp mm^{-2}
C 45 (pressure) $m = -135\,150$ kp mm^{-2}
(stretched and tempered) $n = -77\,770$ kp mm^{-2}

In comparison, the values in the literature for iron are:

	l [kp mm^{-2}]	m [kp mm^{-2}]	n [kp mm^{-2}]
Hughes and Kelly	$-3.55.10^4$	$-10.51.10^4$	$+10.0.10^4$
Seeger and Buck	$-1.6.10^4$	$-6.2.10^4$	$-15.9.10^4$

The values in the literature also differ from one another. Those of Seeger and Buck (1) are determined by the Poynting effect, and the measured values in this paper agree as to the order of magnitude with values of the literature. The velocities of different load steps enter into the equations of Hughes and Kelly. The moduli l, m, n are dependent on the corresponding magnitude and sign of the stresses. The equations are true only for infinitesimal stresses.

It is more straightforward to consider the equations of Toupin and Bernstein. The changes of the velocity Δv are dependent on the changes of stresses $\Delta\sigma$ only. The elastic moduli are determined by the density δ_0 and the transverse-wave velocity v_{T0} in the unstressed medium and by the changes of velocity and stress. The Lamé constants are as follows:

AlCuMg: $\nu_1 = 42\,270$ kp mm^{-2}
$\nu_2 = -82\,210$ kp mm^{-2}
$\nu_3 = -79\,520$ kp mm^{-2}
Armco iron $\nu_2 = -43\,690$ kp mm^{-2}
$\nu_3 = -86\,750$ kp mm^{-2}
C 45 $\nu_2 = -42\,680$ kp mm^{-2}
$\nu_3 = -91\,440$ kp mm^{-2}
C 45 (stretched and tempered) $\nu^2 = -16\,570$ kp mm^{-2}
$\nu_3 = -93\,500$ kp mm^{-2}

The moduli result from the tensile experiment for AlCuMg and Armco iron and from the pressure experiment for C 45. The values for Armco iron are not conclusive. The value for $\Delta v\perp$ with 1.4 ms^{-1} differs from the measurements with steel where the values are very small or not detectable. A comparison with the values in the literature cannot be made, as they are not known. The equations of Toupin and Bernstein describe the measured behaviour better than the equations of Hughes and Kelly. The ratio $\frac{\Delta v}{\Delta\sigma}$ is independent of the sign of Δv_{11}, $\Delta v\perp$ and $\Delta\sigma$. This is in agreement with the measured values. The Lamé constants are also independent of the load direction.

Furthermore the equations of Toupin and Bernstein are independent of the velocity value with the single load step, in contrast with the equations of Hughes and Kelly. The ratio $\frac{\Delta v}{\Delta\sigma}$ can be determined more exactly by the compensating straight line than by the velocity with a definite stress. The relation between $\Delta\sigma$ and Δv is linear according to the equations of Toupin and Bernstein. The measurement values point up the verification of these relations although the equations concern infinitesimal stresses only.

The linear change of the transverse-wave velocity with the change of the stress is appropriate for the experimental analysis of stress due to outside load. It is significant that internal stresses do not change with load change (Table 1). The following expression for a plane state of stress due to linear behaviour of the curves $\Delta v = f(\sigma)$ is analogous to the photoelasticity:

$$v_1 = v_0 + c_1\sigma_1 + c_2\sigma_2$$
$$v_2 = v_0 + c_1\sigma_2 + c_2\sigma_1$$

The difference of principal stresses σ_1 and σ_2 can be determined from the effect of the double refraction in analogy to the photoelasticity (19, 20). The separate determination of the principal stresses σ_1 and σ_2 is possibly from the described method and from the combination of equations (6) and (7) with equation (8).

The constants c_1 and c_2 can be determined from a test specimen of the same material with uniaxial state of stress. Here the following is used for the uniaxial state of stress:

$$\Delta\sigma = \sigma_1,\sigma_2 = 0\,,\ \Delta v_1 = v_0 - v_1 \text{ and } \Delta v_1 = v_2 - v_0\,.$$

The factors c_1 and c_2 contain the third-order constants. The values $v_0 - v_1$ and $v_2 - v_0$ are the changes of transverse-wave velocity, where the vibration plane lies in the direction of σ_1 resp. σ_2, v_0 is the velocity before loading.

References

1. Seeger, A. and Buck, O. Die experimentelle Ermittlung der elastischen Konstanten höherer Ordnung. Z. Naturforschung *15a*, 1960, p. 1056.
2. Seeger, A. and Mann, E. Anwendung der nichtlinearen Elastizitätstheorie auf Fehlstellen in Kristallen. Z. Naturforschung 14a, 1959, p. 154.
3. Truell, R. and Elbaum, Ch. High frequency ultrasonic stress waves in solids, *in* Handbuch der Physik, Akustik Bd. 2, Berlin/Göttingen/Heidelberg, 1962.
4. Mason, W. P. Phonon viscosity and its effect on acoustic wave attenuation and dislocation motion, *J. Acoust. Soc. Am.*, 32, 1960, 4, p. 458.
5. Murnaghan, F. D. Finite deformation of an elastic solid, *Am. J. Math. 59, 1937*, p. 235.
6. Murnaghan, F. D. Finite Deformation of an Elastic Solid, John Wiley & Sons, Inc., New York, 1951.
7. Birch, F. Finite elastic strain of cubic crystals, *Phys. Rev.* 71, 1947, 11, p. 809.
8. Toupin, R. A. and Bernstein, B. Sound waves in deformed perfectly elastic materials, *J. Acoust. Soc. Am.*, 33, 1961, 2, p. 216.
9. Hearmon, R. F. S. Third-order elastic constants, *Acta Cryst.* 6, 1953, p. 331.
10. Bhagavantam, S. and Suryanarayana. *Nature, London,* 160, 1947, p. 750.
11. Hearmon, R. F. S. The elastic constants of anisotropic materials, III. *Phil. Mag.*, Suppl. 5, 1956, p. 323.
12. Birch, F. Finite elastic strain of cubic crystals, *Phys. Rev.*, 71, 1947, 11, p. 809.
13. Hughes, D. S. and Kelly, J. L. Second-order elastic deformation of solids, *Phys. Rev.*, 92, 1953, 5, p. 1145.
14. Bateman, T., Mason, W. P. and McSkimin, H. J. Third-order elastic moduli of germanium, *J. Appl. Phys.*, 32, 1961, 5, p. 928.
15. Freyer, G. and Tietz, H.-D. Beitrag zum Problem der Schallgeschwindigkeitsmessung Werkstoffprüfertagung, 1964.
16. Freyer, G. and Tietz, H.-D. Beitrag zum Problem der Schallgeschwindigkeitsmessung mit Ultraschall Feingerätetechnik 14, 1965, 11 S. 516.
17. Mager, H. Über die Spannungsabhängigkeit der Ultraschallgeschwindigkeit in Metallstäben, Dissertation Philosophische Fakultät der Universität Köln, 1953.
18. Bergman, R. H. and Shabender, R. A. Effect of statically applied stresses on the velocity of propagation of ultrasonic waves, *J. Appl. Phys.* 28, 1958, 12, p. 1736.
19. Benson, R. W. and Realson, V. J. Acoustelasticity, *Prod. Eng.* 20, July 1959, p. 56.
20. Rollins, F. Ultrasonic method for nondestructive measurement of residuals, United States Air Force, WADD Techn. Rep. 61-42, 1961.

Application of the Laser-Beam Technique in Mechanical Testing of High-Temperature Materials

D. R. AXELRAD, CANADA

ABSTRACT: This paper is concerned with the arrangement of a mechanical test apparatus for the testing of high-temperature materials such as BN, Si_3N_4, SiC, WoC, etc. by using a laser beam technique. An intense light beam is generated by means of a solid-state ruby laser (Al_2O_3 with 0.04% Cr_2O_3) which permits a fast local temperature rise of the test-piece of up to 400°C above a steady-state temperature. The latter can be chosen within the range of 0–1600°C. The test equipment consists of a high-temperature furnace and control circuit, the laser device including the power supply and control unit, and electronic strain measuring devices for the measurement of longitudinal and transverse deformation of the specimens due to thermal shock. Some of the test results obtained by using this technique, as well as metallographic investigations of material specimens of "0-grade" tungsten carbide-cobalt compounds, are briefly discussed.

Introduction

In previous publications (1, 2) the arrangement of a mechanical testing apparatus for the performance of constant-stress tests on high-temperature materials in an isothermal temperature field has been discussed.

This paper deals with the arrangement for the testing of such materials when subjected to thermal cycling or shock loads. Tests of this type have become increasingly important for the study of the mechanics of fracture, e.g. the micro-crack formation and propagation through such materials. The technique briefly discussed in this paper involves a high-power pulsed laser beam which is used as a heat source for the production of local heat shocks on the material specimens.

Lasers in general are light amplifiers, which possess enough positive feed-back to produce oscillation by stimulation of radiation at optical frequencies. They consist essentially of three parts, the active medium or generator producing the required amplification by means of stimulated emission, the resonator supplying the necessary feed-back and finally the power source which feeds enough energy to the active medium in order to maintain the amplification by the process of stimulated emission. The equipment discussed subsequently uses a solid-state "ruby" laser of sufficient power to permit a local temperature jump of up to + 400°C from a steady-state reference temperature within the range 0-1600°C.

Arrangement of High-temperature Equipment for Thermal Cycling and Shock Tests

Test Furnace and Temperature Control

The technique discussed in this section has been used so far for the shock testing of high-temperature materials only. The arrangement of the test apparatus is shown schematically in Figure 1 (plan view).

The equipment consists essentially of the high-temperature test apparatus, the laser system and photo-electric optical strain measuring devices. The specially designed furnace for the testing of high-temperature materials is described in detail in reference (1). It is of the resistance type, using graphite rods as the heating element. As may be seen from Figure 1 the furnace contains six channels that are insulated by carbon tubes to permit the mounting of the temperature-control sensing devices, the optical system for the laser beam focussing, the device for the local cooling of specimens, as well as optics and probes required for the strain measurements in both the longitudinal and radial direction of the specimen. The temperature range of this furnace is from 0 to 2000°C and covers, therefore, the region above half melting point of most of the refractory metals. For the protection of specimens against oxidation all tests are carried out in an argon atmosphere (99.8% purity and flow rate of approximately 0.8 cu ft/min). The furnace permits the performance of thermal shock and/or cycling tests of various metals above and below a steady-state pre-set temperature level ranging from 400 to 1600°C. It is also possible to apply an external mechanical load to the specimen by an appropriate load train. This arrangement permits the application of uni-axial as well as bi-axial stresses to the specimen.

For the supply of an instantaneous local heat shock on a particular specimen, the laser beam is used. The energy output of the latter can be adjusted so as to give either a very intense point source on the metal surface, or the energy can be spread over a larger area on the surface of the specimen to allow for

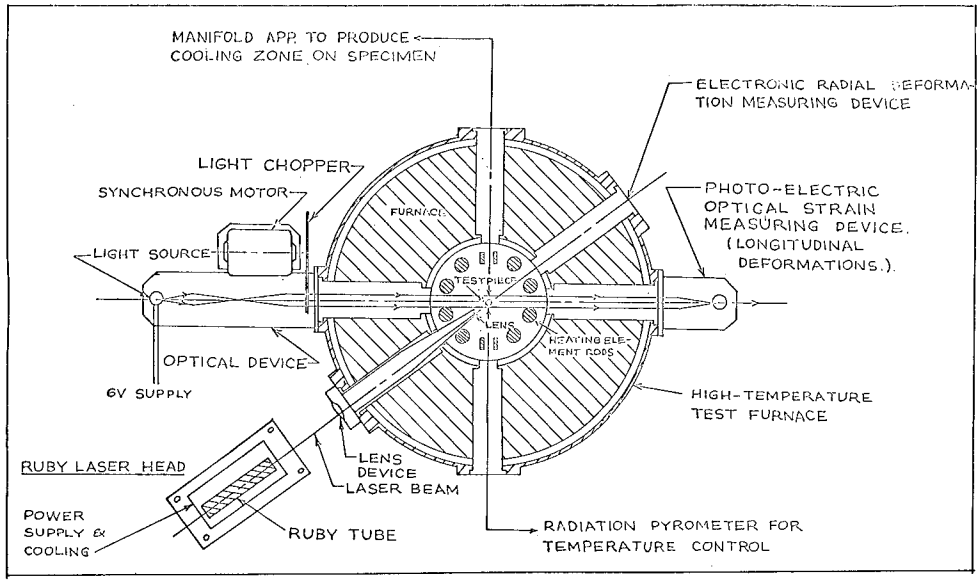

Figure 1
Laser-beam arrangement for materials testing. Plane view.

local heating. An adjustment of this kind depends on the response characteristic of the material to the radiant optical energy and varies with the type of material under investigation.

To ensure proper test conditions for the case of cycling tests for instance, the temperature control has to satisfy the following requirements:

(i) A steady-state temperature field must be maintained at any pre-set level over the range of 400 to 1600°C for any length of time.

(ii) The temperature must be controlled to permit an upwards or downwards jump from the steady-state temperature at a pre-set level.

The present equipment permits a temperature jump of up to ± 400°C in a required time interval. In the case of investigations on high-temperature materials, the pulse duration is often of the order of 10^{-1} seconds or less during shock tests. In order to meet condition (i) above, which is also the requirement for isothermal stress testing, a high-speed radiation pyrometer is used. This pyrometer is focussed through an aperture in the heating element (see Figure 1) on to the centre of the specimen under test and the temperature of the latter is recorded on a strip-chart recorder. The recorder contains retransmitting slide wires; thus, any difference between the position of the slide wire and "master steady point control" (e.g. corresponding to a pre-set temperature level) causes an error signal which is transmitted to a rate controller. The latter in turn controls a silicon rectifier-type power controller, which permits more or less current to pass through the heating element. To prevent the passage of too high currents through the heating elements during the initial starting period of the furnace, a maximum current over-ride is built into the power controller.

In order to meet condition (ii) it is necessary that the heating elements remain at a constant temperature during the thermal cycling. Hence, after each cycle, or a number of cycles, the specimen returns to its initial steady-state temperature. For this purpose a second sensing device is used in the form of a tungsten-tungsten rhenium thermocouple which is mounted close to one of the resistor rods. This thermocouple governs the rate controller by means of a voltage transducer and vertical indicator. Thus, during cycling the heating element remains at a constant temperature. By switching to "off-normal" either a cooling or heating cycle can be produced depending on the position of the high-low selector. Both high and low steady-point controls are adjusted to control the amplitude and the cycle in the same way as for the steady-state condition. This control circuit is indicated in Figure 2.

However, during cycling tests a second controller is employed, which either works into an argon-jet controlled system manifold (for cooling cycles) or into the ruby laser device for heating cycles and/or shocks. By switching from normal to off-normal the duration of the cycles can be adjusted for manual or automatic control. The type of cycle required for a specific test on a specimen is achieved by 4 timers and 4 four-position switches. Finally it should be noted that the power input of the control system is 220 volts, single phase, at maximum 12 KVA. Owing to the special design of the graphite heating element, the voltage, after passing through the power controller, is stepped down to 50 volts.

The Ruby Laser System

The solid-state laser system for this type of testing consists of the laser head, power and control unit. The laser head contains a ruby laser rod (Al_2O_3 .04% Cr_2O_3) one end of which is di-electrically coated. For the excitation of the ruby a flash lamp with a 6½-in. arc gap (water cooled) is used. The laser head is made in the form of an elliptical cavity, which is split

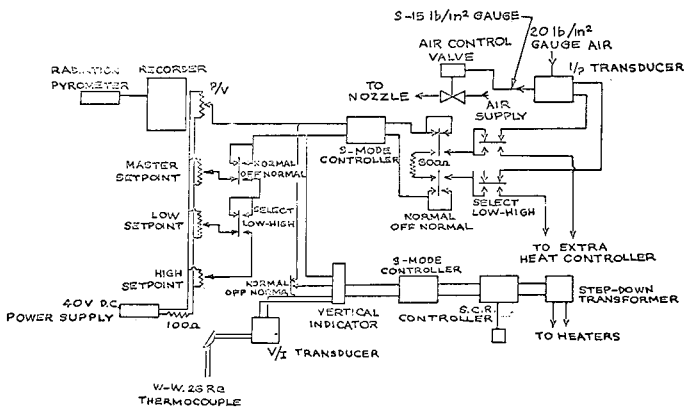

Figure 2. Schematic diagram of temperature-control chart.

and hinged for quick opening of the jacket. Thus the water cooled unit has the flash lamp at one focus and the ruby rod at the other. For ease of operation the laser head is mounted on a base plate to facilitate positioning and proper focussing. Further, there are two manifolds in the base of the laser-head mounting for the distribution and control of the cooling water. The inlet manifold is equipped with flow regulators set to regulate the flash lamp and ruby at 1 gpm and the cavity with ¾ gpm, respectively. Finally the elliptical cavity is purged with dry nitrogen in order to maintain its high reflectance and also to avoid any discomfort, which may be caused due to the generation of ozone when the flash lamp is operated.

The power supply to the laser head is a 208-volt, 3-phase, 60-cps unit in which the maximum stored energy is 18,000 joules at 4 KV. The charging voltage of the power supply unit is 0-4 KV and the power output is 15-30 KV. For the modes of operation either manual firing by panel, a remote firing button, or an automatic firing can be employed. The pulse repetition of this unit is 0.1 to 16 pps. The power unit also contains, as a safety feature, an adjustable lamp-voltage safety circuit, a fail-safe capacitor bank dumping circuit and a circuit breaker. The power supply is arranged with a control unit in which a specially designed current-limiting transformer, charging the capacitor through a silicon rectifier, is employed. Feed-back from the bank voltage is used to maintain a pre-set level with an accuracy of about .2 per cent of the maximum voltage. A pause generator is further employed to provide the necessary delay after each firing of the flash lamp. This gives the flash lamp sufficient time to de-ionize completely and thus prevent any hold-over which could lead to its destruction. When the capacitor bank charges above a pre-set level an adjustable lamp-voltage protection circuit stop is built into the charging and initiates the capacitor dumping circuit. Thus the front-panel control has three positions: normal, normal kilovoltmeter, peak memory circuit for use at high repetitive rates, and a triggering voltage for the flash lamp. In the manual operation of the laser the laser head fires and the power supply does not recharge. The manual firing mechanism is governed either by panel or remote button. For automatic operation the automatic pulse generator permits a 2-pulse/min to 16-pps operation. The laser control circuit mentioned above is included in the diagram of Figure 2.

Energy Output

For the nondestructive testing of high-temperature materials a proper control of the laser energy which is absorbed at the surface of the test-piece is required. Theoretical calculations of laser energies at metal surfaces are discussed in references

(3, 4). For the practical assessment of such energies fairly accurate measurements can be obtained by means of a ballistic "thermo-pile". The latter is a calorimetric device which measures temperature rise due to the absorbed radiation. It consists of two bright nickel-plated silver cones and 10 series-connected iron-constant thermocouples. The thermocouples are arranged so that the hot junctions are attached to the receiver cone. The radiant energy of the laser beam is directed to the input hole of the receiver cone and almost completely absorbed due to multiple reflections (Mendenhall-wedge effect). The temperature rise of the receiver with respect to the reference cone causes an emf, which can be monitored by an externally connected microvoltmeter. The peak emf induced is then linearly related by a proper calibration to the total input energy. The surface of the receiver cone is specially treated to resist any destructive effects due to the high-power pulse encountered in laser work. The main functional characteristics of this instrument are its time-constant (7 secs) the maximum energy input (300 joules) and the maximum power density (10^8 watts/cm). The instrument works with a maximum error in measurement of up to 2.5 millijoules or 5 per cent.

Laser-Metal Interaction

For the purpose of discussing nondestructive testing by means of the laser-beam technique the interaction effects between the latter and the material surfaces should be briefly mentioned. There are mainly three effects which can be stated as follows:

(i) Absorption of the laser energy at the metal surface.
(ii) Effects of this absorption on and near the metal surface.
(iii) Changes to the micro-structure in the affected region of the specimen.

Since the laser beam, in contrast to the conventional light beam, is a monochromatic source with a high degree of directionality, it can be relatively simply focussed on to a target to induce either thermal shock or a continuous heating of the metal surfaces. As mentioned already, apart from the focussing, the adjustment of the energy output of the laser beam is possible by a regulating device described above. The energy absorption can be calculated by means of a phenomenological theory in terms of the amount of material which is vaporized during the short period of the laser-beam action on the metal. For this purpose the thermal properties of the absorbing medium and the laser pulse itself are significant parameters in the formulation. Such calculations based on the conventional thermodynamics are usually employed as a first approximation. By using some simplifying assumptions, the temperature rise as a function of time and depth of penetration into the medium can be obtained from the conventional heat-transfer theory (3, 4). It is also possible to consider the light beam as a "buried line source" for calculating the depth of penetration of specific materials. This approach, in calculating the depth of penetration induced by the pulse of a solid state laser beam for some of the non-ferrous metals, has been used by the writer. In calculations of this type one of the main parameters involved is the difference between the observation time and the time at which the energy is absorbed. An estimate of the time constant involved can thus be made on basis of the work in reference (4). For power densities of the order of 10^7 watt/sq cm, the time constant for metals is approximately 1-2 μ sec. It may be inferred from observations made on various metals and the calculated depth of penetration that almost all the laser energy of the pulse is utilized in vaporizing the material. For instance, the penetration depth produced by a laser beam (pulse intensity 5000 joules/sq cm) in stainless steel has been found to be 0.76 mm. For a pulse characteristic of 10^9 watt/sq cm and 44 n secs duration the calculated penetration depth for the same material was 1.8 μ. It should be noted in this context that in studying penetration depths of various metals the interaction effect also depends on whether a Q-switched laser or an ordinary laser system is employed. In general, investigations revealed that increasing the power of the pulse of a given shape will increase the depth by a factor less than the ratio of the power of the laser beam. This indicates that the energy absorption is actually confined to the surface of the metal.

Apart from the above effect, which is due to the conversion of light to heat at the metal surface, two other effects should be mentioned, i.e. the electric field phenomenon, and the field emission. The former is known as the Schottky effect and the "work function" of the material, i.e. the minimum energy to be supplied for the removal of an electron from the metal surface will be decreased if an external field is present. The field emission effect can be regarded as being due to a narrowing of the potential barrier encountered by the electron at the surface of the metal. Both these effects, however, have been observed for the d.c. electric fields and so far as laser-beam interactions with metal surfaces are concerned there is at present insufficient experimental evidence of these two effects. It can be concluded therefore that the thermal effect is essentially the predominant one.

Some Experimental Results

The structural aspects of the high-temperature materials mentioned earlier, which may be tested with the laser-beam technique, are discussed in numerous publications. Some results obtained from isothermal constant-stress tests on such materials are given in reference (5). For the description of the laser-beam technique a specific material such as tungsten-carbide-cobalt compound is briefly discussed. Two series of this compound material were used for either short-time creep tests or thermal-shock tests. The "0-grade" series of this material consisted of a dispersion of Wc particles (0.5μ) in a cobalt-matrix, where the latter varied between 8 to 25 per cent of the total volume. A micrograph of the original structure before testing is shown in Figure 3. For the purpose of delineating the structure and to make the grain boundaries clearly visible, etching was carried out. Thus specimens were first prepared by etching in base etchant ($HCl/CH_3\ COOH/H_2O_2$) and without repolishing were then electrolytically etched by application of ($NaOH/K_3\ FeCN_6$). Micrographs of cross-sectional areas of the test samples show that the Wc phase consisted of rhombic shaped particles with rather smooth grain boundaries. At a later stage of the

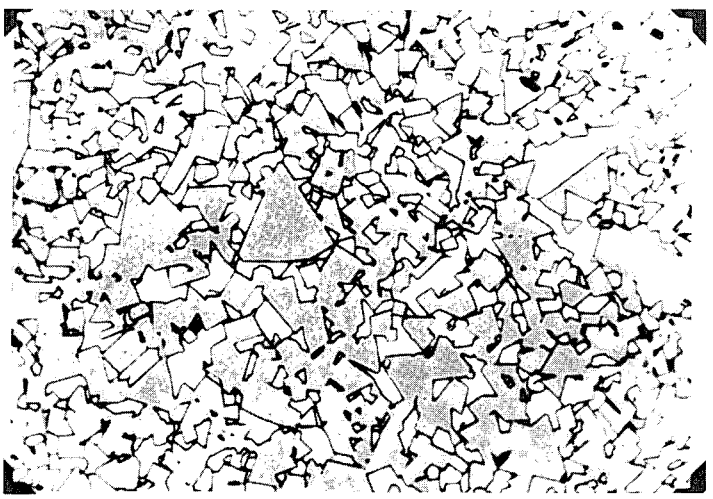

Figure 3. Micrograph of "0-grade series" specimen before testing. Transverse section (Etched X1500). Material: 75% WC, 25% Co, Type "YO".

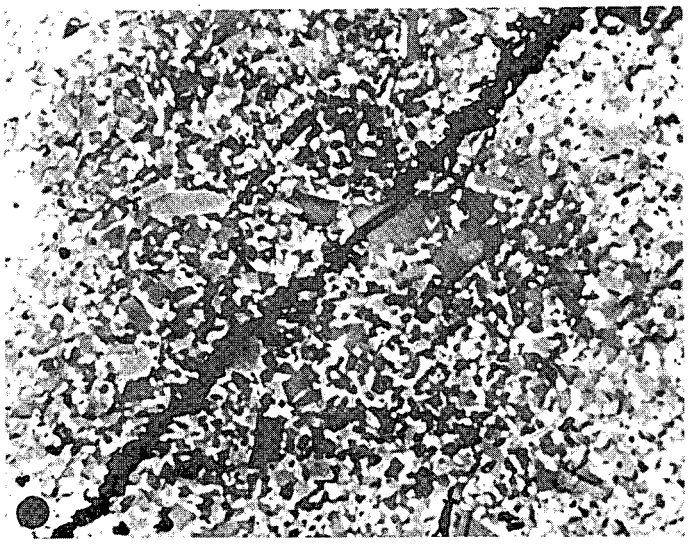

Figure 4. Micrograph of "0-Series" specimen (101) after short-time load test. (Test temp. 1200°C load 3.6 ton/in^2, duration of test 410 min) (Etched, magnification X1500).

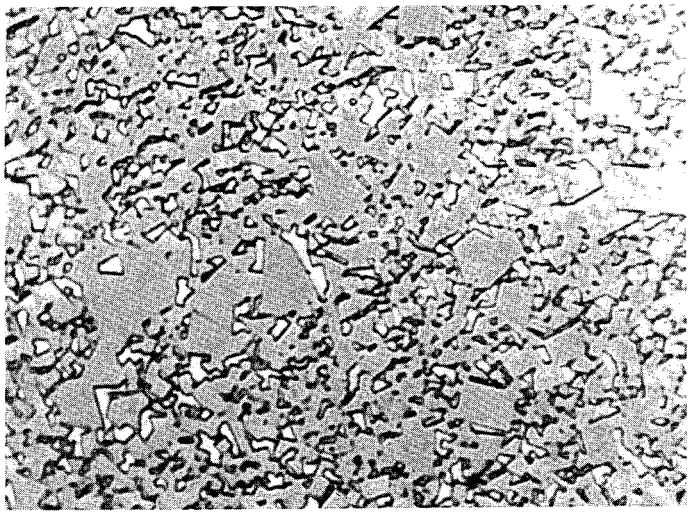

Figure 5. "0-Series" specimen (102) (Type JO–91% WC, 9% Co) before exposure to laser beam (Magnification X1400).

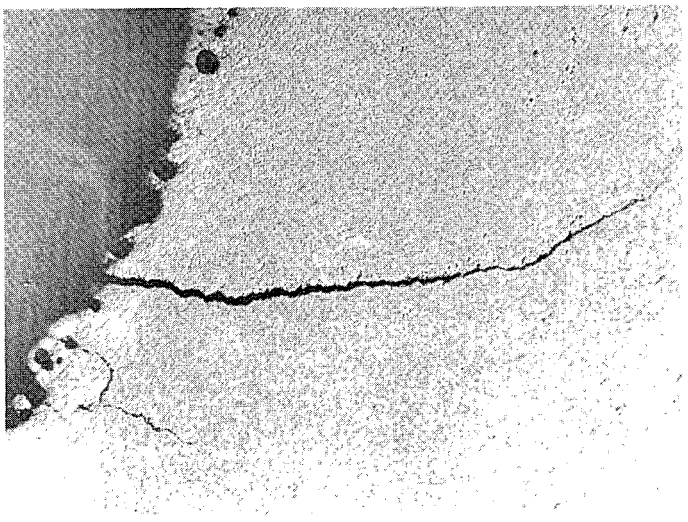

Figure 6. Affected area of specimen (102). Edge of crater formed by laser beam. (Unetched, magnification X180).

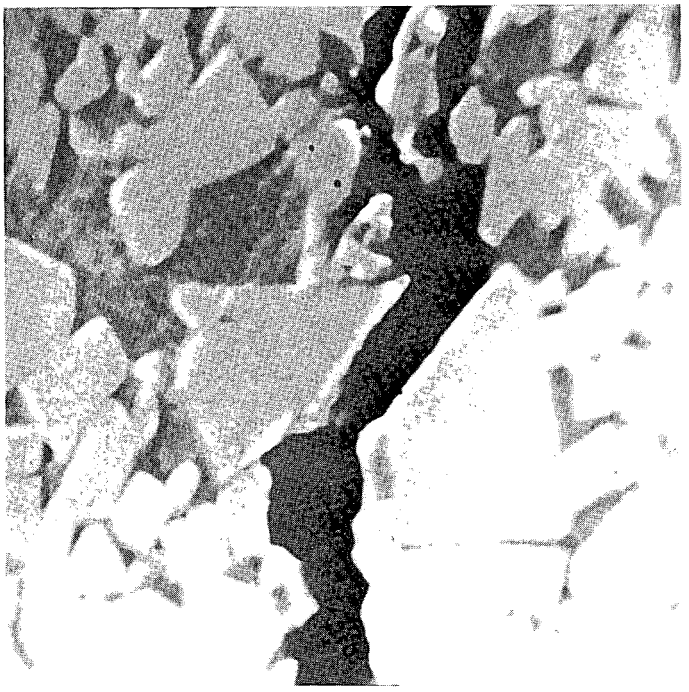

Figure 7. Micrograph of affected area exposed to laser beam showing crack formation. (Scanning electron-microscope, magnification X5180).

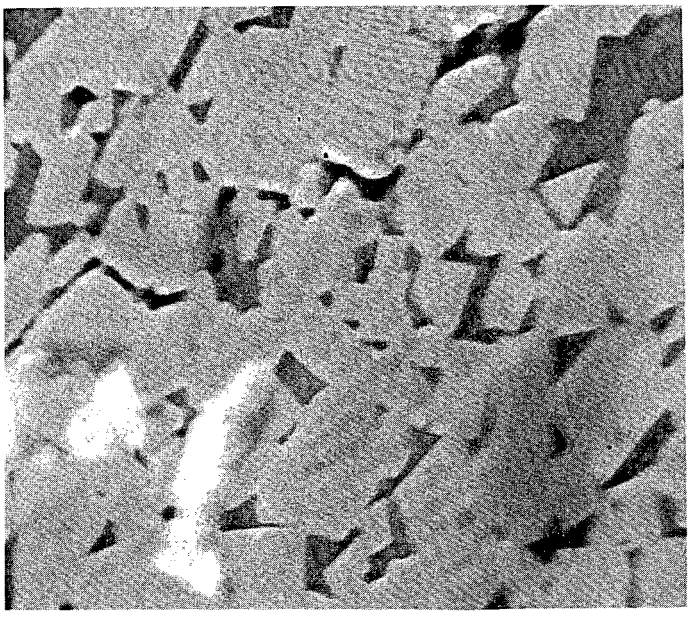

Figure 8. End section of crack shown in Figure 7. (Scanning electron-microscope, Magnification X5900.)

steady-state tests micrographs revealed the formation of subgrains. From micrographs obtained at the final stage of the constant-stress test, a crack formation within larger grains (transgranular), followed by an inter-crystalline spreading of this crack was observed, e.g. a continuous propagation through the cobalt matrix (Figure 4). For the testing of the same compound ("0-type series" specimen) by means of the laser-beam technique, the latter was adjusted to an energy output of approximately 30 joules. This caused strong interaction between the laser beam and the metal specimen. A typical micrograph of such a test piece before exposure to the laser beam is shown in Figure 5. For discussing the interaction effect between the laser beam and the specimen, the effect of several shocks

applied to the specimen causing, finally, a crater-like penetration into the metal surface is of interest. The micrograph obtained is shown in Figure 6. This figure also reveals the initiation of micro-cracks which is presently under study by the author and his co-workers, in a similar way as the investigation carried out by the researchers mentioned in reference (6). Thus in order to illustrate the laser-beam application, this type of observation is shown here, although for the case of ordinary shock tests the laser-beam energy is reduced so as to avoid crater formation. The affected area and in particular the region of the micro-crack formation (Figure 6) was then followed up to a higher magnification. A further study of this region, employing a scanning electron-microscope, revealed a similar material response due to thermal shock, as that obtained from the steady-state testing of the same material. Similar to the latter type of testing, cracks started at the transition zone (affected area by the laser beam) with an inter-crystalline crack developing deeper into the cobalt matrix.

The propagation of the crack was then observed in several subsequent micrographs. However, it was difficult to assess the end of the crack propagation since the microstructure in this region becomes more like that of the unaffected section of the specimen. A typical micrograph of the propagating crack and the end of the crack merging with the structure in the unaffected region of the specimen are shown in Figures 7 and 8, respectively. In conclusion it should be mentioned that further mechanical testing as well as metallographic investigations are intended in order to obtain more accurate information on the laser beam-metal interactions.

References

1. Axelrad, D. R.: *J. Sci. Instr.*, 9, Dec., 1962.
2. ————————.: *Proc. Inst. Mech. Eng.*, 180, part 3A, 1966.
3. Verber, C. M. and Adelman, A. H. *J. Appl. Phys.*, 36, 1522, 1965.
4. Ready, J. F.: *J. Appl. Phys.*, 36, 424, 1965.
5. Axelrad, D. R.: *Trans. Soc. Rheology*, 9, 1219, 1965.
6. Kryemer, V. I., Tunanov, S. I., Kamenski, D. S. and Pavola, Z. I. *Phys. of Metals and Metallography*, 17, 1964.

Technical Session 7/ Magnetic & Eddy-Current Methods

Experiences and Results in the Application of Magnetography in Industry

P. MÜLLER, GERMANY

Introduction

There are many requirements in the technology of modern nondestructive testing. There is not only a demand for highly sensitive methods and apparatus with high resolution, but it is essential that such methods be applicable under in-line conditions; the apparatus must be rigid, reliable, simple to operate and quickly and easily serviced. The method has to be economic, not only in direct costs but also indirect costs, such as unnecessarily high rejection rate. For that reason a basic requirement for a method for detecting defects is that it should be able to discriminate within a fairly reasonable range of error between serious and not serious defects. A modern seam-finding installation should have an adjustable acceptance limit. In addition, the high reliability of an automated system compared with that of human inspectors plus high labour costs makes automatic systems a necessity. This paper deals with new instruments based on the magnetographic principle, which are used for automatic defect detection in ferrous materials and which are capable of meeting all the above requirements.

Principles of Magnetography

Magnetography is an advanced technique of magnetic particle inspection. It is used for seam-finding in ferrous materials and makes use of the magnetic leakage field or stray field generated by a defect when a test part is suitably magnetized. The magnetic leakage field, which in the conventional technique of using magnetic ink, attracts a seam of magnetic particles is, in magnetography, replaced by a magnetic tape. This tape consists of a highly wear-resistant neoprene material in which very small magnetic particles are uniformly distributed. Such a tape is placed on the test part and while the test part is magnetized the magnetic leakage field is copied on to the tape. Later, the tape is scanned by a probe that is sensitive to magnetic fields and thus the leakage field imprinted into the tape is transduced into electric voltage. Magnetography was first developed and described by F. Foerster in 1950 in Europe and in 1951 in the United States*. The practical use of magnetography was jeopardized for many years because there was no tape material available with the necessary high wear-resistance on the one hand and that also possessed sensitive enough magnetic characteristics to obtain comparable or even better results than magnetic ink.

The principles of magnetography are most easily explained by means of a photograph of an early prototype of a magnetographic weld tester. In Figure 1 a welded tube is seen which travels from the right side of the picture to the left. The tube is magnetized by means of two pairs of contact brushes which send a current through the tube longitudinally, thus generating a magnetizing field in a circumferential direction. A wheel, covered with thick sponge rubber rides on the tube; on the sponge rubber is an endless magnetic tape. As the tube travels from the right side of the picture to the left, the wheel rotates without slippage between the tape and the tube. If there is a defect in or near the welded zone of the tube the leakage field due to this defect is imprinted on the tape and as the wheel rotates clockwise, this leakage field is detected by the scanning disc mounted at the left side of the wheel. This disc rotates at a speed of 60 cps. On the disc is a Foerster probe which transduces the magnetic leakage field into an electric signal. The signal is transduced from the rotating disc to the electronic cabinet by means of contactless transformers; as the tube goes on, the wheel with the magnetic tape keeps turning and on its right hand side there is an eraser which demagnetizes the tape so that it is ready for a new print.

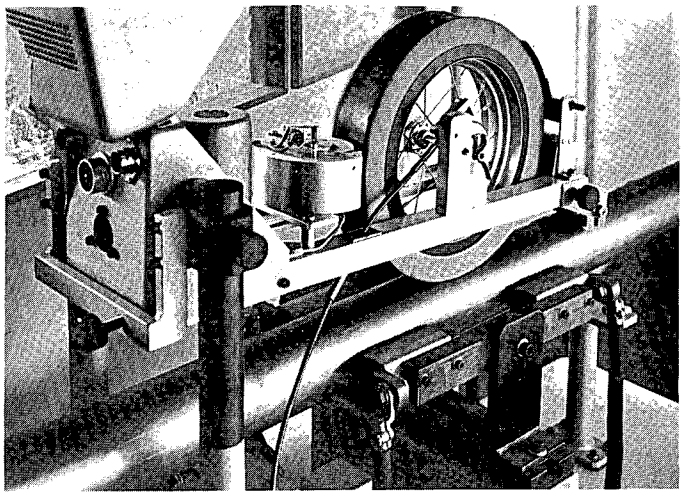

Figure 1. Foerster magnetography weld tester.

* Lecture given by F. Foerster at the Metal Show in Detroit Oct. 1951.

Figure 2 shows the miniaturized Foerster probe used for detecting the leakage field. This is an absolute field probe that can be modified to, for example, a differential probe. There are three main features to the Foerster probe; its very small size—only about .040 in. large; its response voltage. (The electric signal per Oersted is approx. 10,000 times higher than the corresponding signal of a conventional Hall crystal); its extremely wide range of frequency response, which allows very high scanning frequencies. Figure 3 shows that the upper limit frequency of this probe is approximately 2 MHz. This is possible because the probe is driven with very high frequency between 10 and 30 MHz. Hall probes are normally driven no higher than 100 kc, so that the upper limit of their frequency response curve is about 100 times lower than that of a miniaturized Foerster probe.

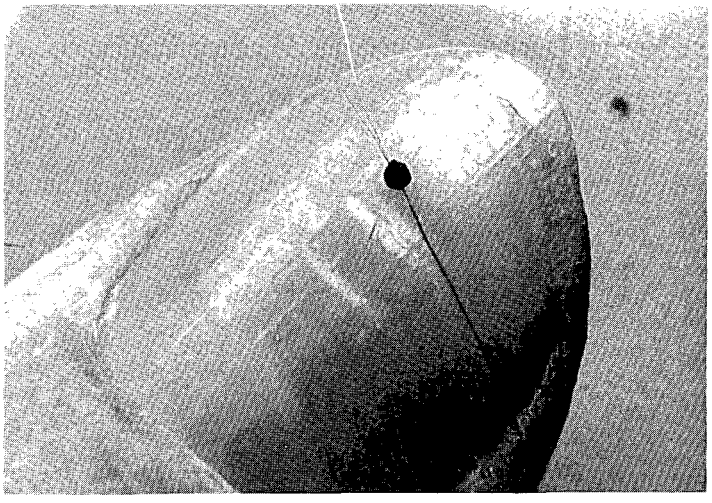

Figure 2. Foerster micro probe.

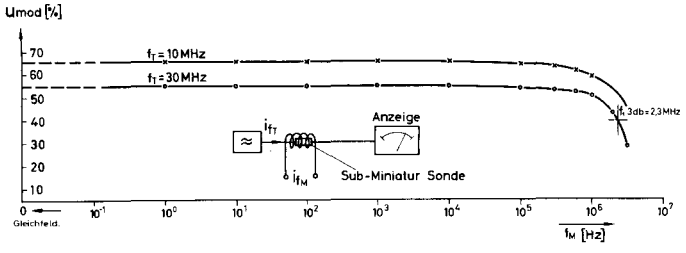

Figure 3. Frequency range of the Foerster mini probe.

As an example of a modern design instrument, Figure 4 shows a magnetography hand unit, with cabinet open; this is called a hand roller as it is used for special purposes, specifically for cross checking the conditioning department under in-line conditions. Such a unit is light weight and portable. Various fixtures and mountings at both bottom ends of the scanner allow its adaptation to test parts of various dimensions.

Theory of Magnetic Test Methods

Finding defects through magnetic methods requires a suitable way of magnetization. For magnetography it is essential that the test parts be magnetized with direct fields only. It is of no importance whether there is a constant direct field or a pulsed direct field but alternating fields cannot be used because they would erase any signal from the tape as the tape moved away from the surface of the test part. The example of a low carbon steel, C15, Figure 5, shows the basic relations between the tangential field strength H_T (the magnetizing field), the induction

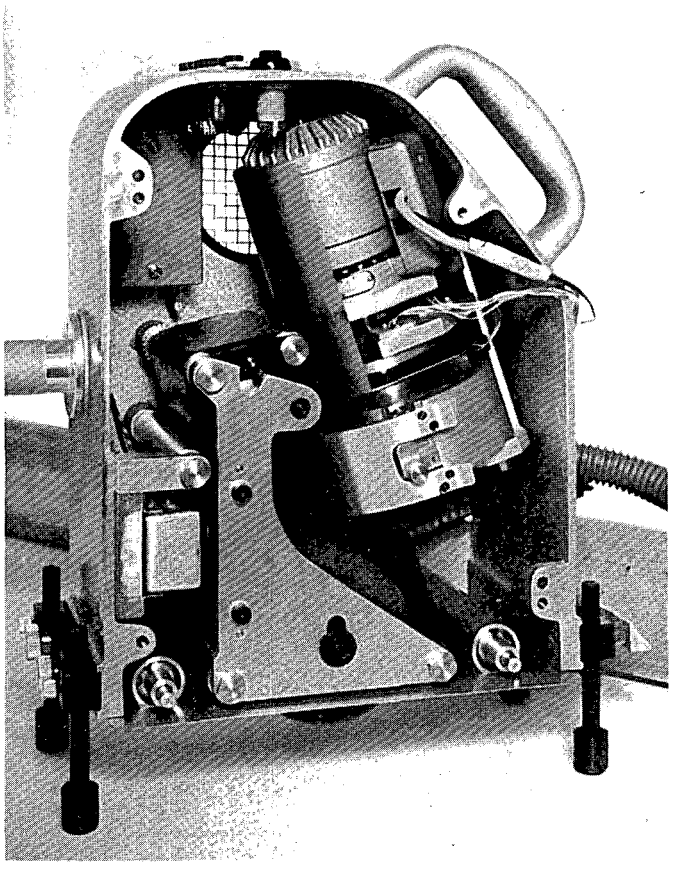

Figure 4. Hand-roller.

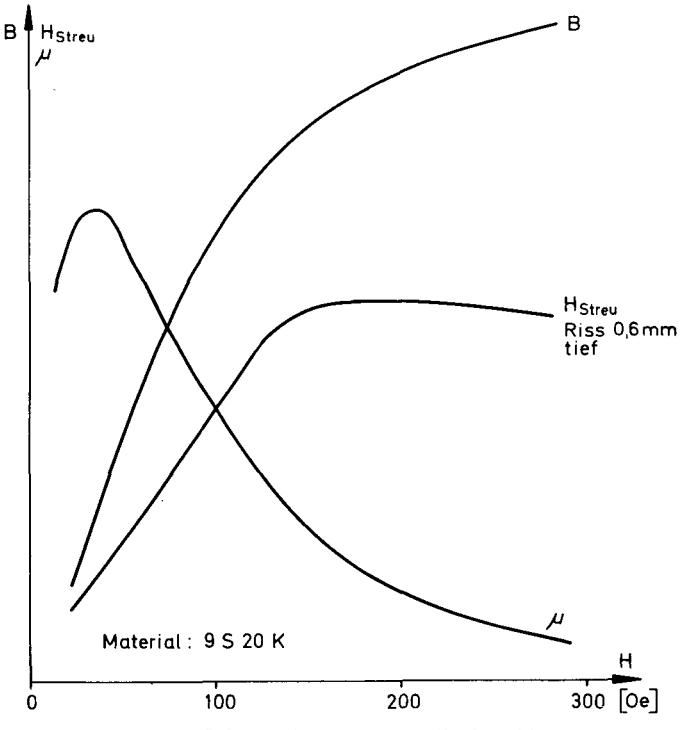

Figure 5. Basic relations between H_T, B and H_{st}.

B, the magnetic stray flux and the differential permeability which is given by the differential quotient of dB/dH. It shows that for small magnetizing fields there is practically no stray flux at all. Only after the magnetizing field is higher than a certain lower

limit does the stray flux penetrate the surface. The permeability μ starts with a fairly small value of initial permeability at the tangential field strength of $H_T=0$ and reaches a peak value which is higher by approximately 1 magnitude than the initial permeability and from that point on it decreases and approaches the H_T axis at the value of $\mu=1$ as H_T becomes infinite. This picture shows that there is no use applying extremely high magnetizing fields in order to obtain a high defect resolution. The reasonable working range of a stray flux method is between the point where the B curve reaches about 70% of its saturation value and the saturation point of the B curve.

The experimental findings as shown in Figure 5 indicate that the stray flux and the permeability decrease for high magnetizing field strengths. Experimental experience also shows that for high magnetizing field strength not only defects like seams, laps, slivers, etc. have a stray field but also surface irregularities produce an increasing stray flux. This led Foerster and Stambke* to make a thorough theoretical investigation on the basic correlation between the permeability of a material and the stray flux of defects of various shapes. Figure 6 shows the results of these calculations. They were made for the idealized conditions of a very thick and wide steel blade in which elliptical holes as indicated in the figure were drilled. These holes have varying ratios of their axes vertical to the magnetic field, and of their axes parallel to the field. The ordinate in Figure 6 is the ratio of the magnetic field H in such a hole over the magnetic induction B in the sound material far from the hole. The abscissa is the ratio of the axis vertical to the magnetic field over the axis parallel to the magnetic field.

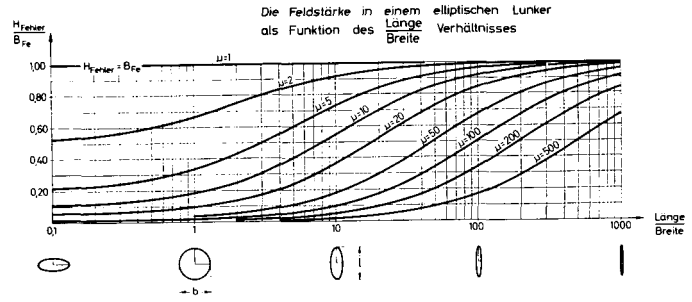

Figure 6. Field strength of the magnetic leakage field as a function of the 1/b ratio.

It is evident that for a material of $\mu=1$, which means a nonferromagnetic material, the magnetic field in such a void is exactly the same as in the material itself irrespective of the shape of the defect, as there is no difference between the magnetic properties of the void and the sound material. But looking at a material with a permeability of 20 we note that in a void (the ratio of the axis vertical to the magnetic field over the axis parallel to the magnetic field $=0.1$) which is parallel to the flux lines there is a magnetic field which is only approximately 5% of the induction in the sound material. As for such a material the void gets a large extension vertical to the flux lines compared with its extension parallel to the flux lines, the magnetic field in the void will increase. For a ratio of the axis of 10 : 1 (permeability of 20) we have a field of 36% and for a ratio of 100 : 1 we have a field of 84% of the flux in the sound material. For a material of high permeabilities between $\mu=50$ and $\mu=500$ there is only a very small magnetic field in such a void for all ratios of its axes smaller than 10 : 1. In contrast to this for a material with a permeability of $\mu=5$ the magnetic field in a void with a ratio of the axis of 10 : 1 is approximately 70% of a void, with an extremely high ratio of the axis of 1000 : 1. It will be shown that the magnetic field in such a void is representative of the stray flux of a surface defect which we obtain when we cut such a blade along its symmetrical plane in two halves, as shown in Figure 7. Keeping this in mind, Figure 6 teaches us that the magnetic stray flux in a very wide defect is approximately the same as the stray flux in very narrow defects if the permeability is very low, for example between $\mu=2$ and $\mu=10$. But the stray flux in such a wide defect is very small compared with the stray flux in a very narrow defect if the permeability of the material is between $\mu=20$ and $\mu=500$.

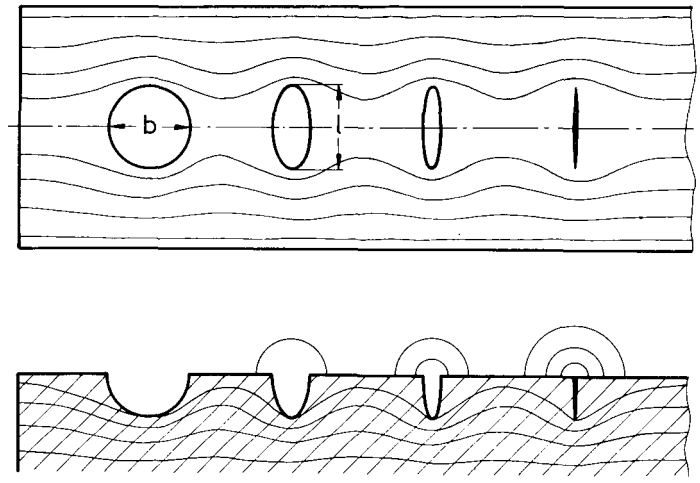

Figure 7. Increase of the magnetic leakage field as a function of the 1/b ratio

Going back to Figure 5 this proves that the background noise due to surface irregularities will increase as we utilize too high a tangential field strength, because in the area of high tangential field strength μ decreases very rapidly. The magnetizing tangential field strength must be such that, if possible, μ should not become smaller than 20. Figure 8 shows why the operation of cutting the blade along its symmetrical plane in two halves is allowed (*see* Figure 7). The stray field in an infinitely deep defect is homogeneous except in the area near the surface of the material. Figure 8 shows that the tangential component of the stray flux of a defect decreases according to hyperbolic function, the variable of which is given by the ratio of the distance a from the surface of material over the width b of the defect. In addition, Figure 8 shows that stray flux at the surface of an infinitely deep defect is still approximately 85% of the stray flux

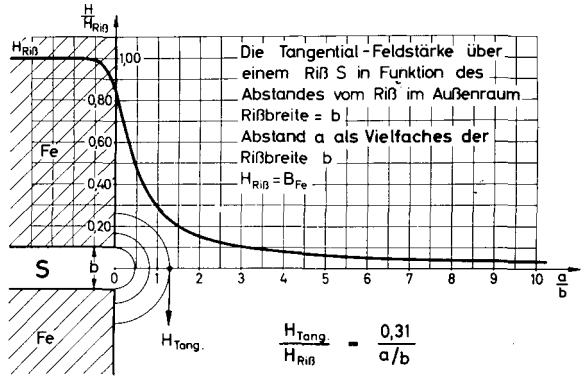

Figure 8. Tangential component of the stray flux.

* These theoretical results will be published in a monograph by F. Foerster "Magnetography—a New Method for Nondestructive Testing" to be published in 1967.

inside the defect. For this reason the conditions in such a defect are not changed too much when we cut a blade in two halves through its symmetrical plane as shown in Figure 7. It should be noted that the conditions described above are the same for any magnetic test method whether using magnetic ink or magnetography.

We have looked at the various conditions of the stray field that occur for surface defects. We should also look at the conditions as we meet them for subsurface defects. For doing so the ASTM has proposed a test ring the dimensions of which are very similar to the dimensions shown in Figure 9. The difference between the ring shown in Figure 9 and the ASTM test ring is that the latter has double the number of bore holes as the ring we use, and propose to use, for further investigations. The holes we use cover the same range of depth beneath the surface. Because the stray flux of the holes deep beneath the surface is so wide it interferes with the stray flux of two neighbouring holes when the dimensions of the original ASTM ring are used. The ring as shown in Figure 9 is magnetized by a central conductor and is very suitable for the investigation of depth penetration in methods for detecting subsurface defects.

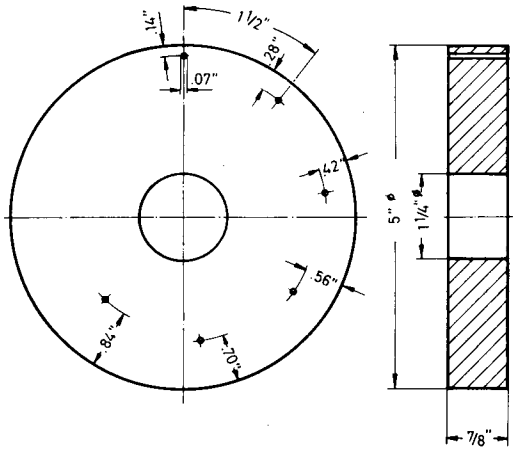

Figure 9. Test ring for the detection of subsurface defects.

Figure 10 shows the absolute leakage field of such a test ring. Looking at the top curve in Figure 10, which was obtained by measuring directly on the surface, we notice that the signal of the hole nearest to the surface is about 7 times higher than that obtained from the hole deepest beneath the surface. But as the spacing between the surface and the probe is increased the ratio between the indications of the hole nearest and farthest to the surface decreases. In addition Figure 10 shows that the signal

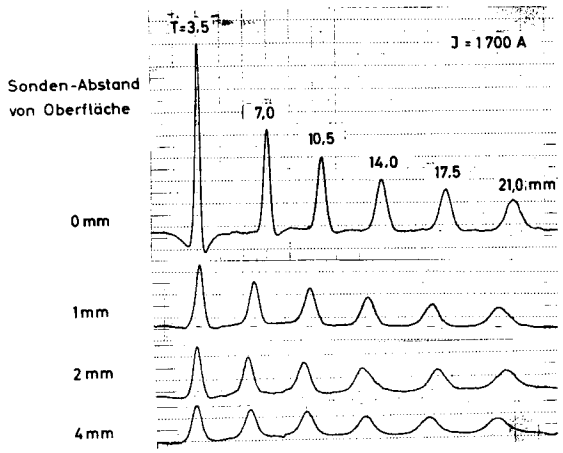

Figure 10. Leakage field of the holes in the ASTM test ring.

due to the hole nearest to the surface is much narrower than that due to the holes farther away from the surface. The width of the signal increases as the depth of the hole beneath the surface increases. The Fourier-analysis of the signals obtained from these various holes shows more high-frequency spectral lines in defects near the surface and more low-freqency spectral lines in the defects far away from the surface. This gives us the opportunity of using electronic filters of suitable characteristics in order to obtain, for example, a comparatively higher gain of signals due to subsurface defects or, if we wish, of signals due to surface defects. By using suitable filters and an advanced technique of probe configurations it is possible to obtain a magnetographic indication of the holes in the test ring (Figure 11) which shows that the penetration of the magnetographic method is nearly twice as deep as that of the conventional powder method. Figures 10 and 11 show one can discriminate between the surface defects and subsurface defects by means of evaluating their frequency spectra. In doing so one complication has to be overcome: in total, a surface defect has a signal of higher intensity as shown in the upper curve of Figure 10. Therefore, the lower band components of such a defect are still fairly high. That means in a band-pass filter which is tuned to the low-frequency band we "see" surface and subsurface defects with similar intensity. In a band-pass filter tuned to the high-frequency band we "see" surface defects only because subsurface defects have practically no high frequencies in the spectrum of their defect signals. By this we can use a suitable logical combination circuitry. A defect which is "seen" in the low and in the high-frequency band must be a surface defect whereas a defect "seen" in the low-frequency band can only be a subsurface defect. Accordingly it is possible to avoid mistaking small surface defect for a comparatively large subsurface defect. In the practical use of magnetography this is

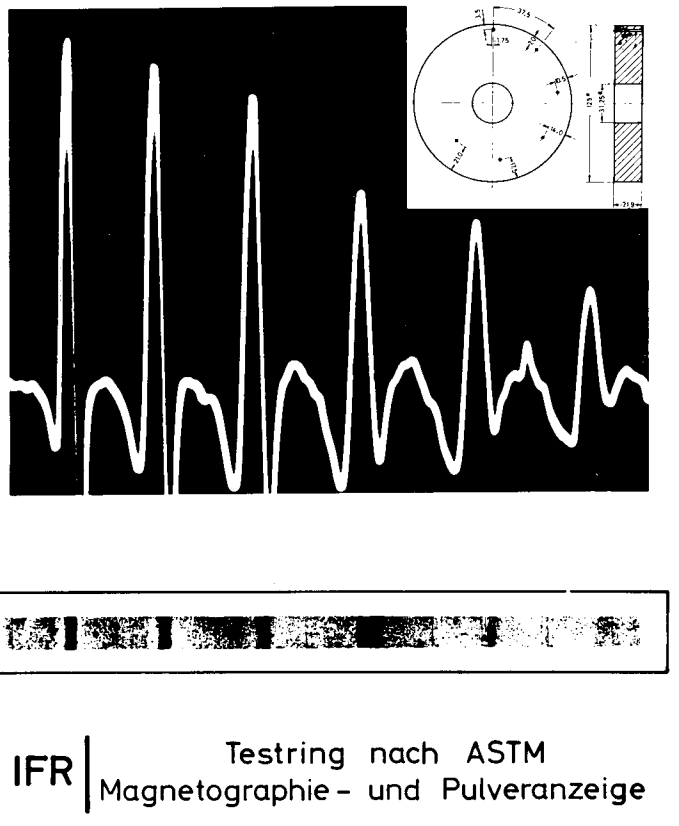

Figure 11. ASTM ring, magnetography and powder indication.

an extremely important feature as it prevents, for instance, the rejection of tubes merely because of relatively harmless small surface defects.

It has been claimed that under laboratory conditions with magnetic particles a very well trained and experienced inspector is able to tell the depth of a defect below the surface from the width of the particle indication. Without arguing about that, it is evident that under in-line conditions at a test speed of, for example 100 ft/min a group of inspectors working round the clock in three shifts will never be able to discriminate reliably between surface and subsurface defects.

The deeper penetration of the magnetographic method compared with the flux method can be explained in brief. The force attracting a magnetic particle is F=H. grad H. F means the force, H means the magnetic field. The magnetic field H near the defect is defined as $H = H_o + H_{st}$ where H_o is the undistorted field and H_{st} is the stray field. A magnetic field H resp. a stray field H_{st} decreases as the distance between the defect and the surface increases and the gradient H does the same. As the gradient of the undistorted field is small compared with the gradient of the leakage field it is $H + H_{st}$. This means that a force acted upon by a particle decreases with a higher power than the leakage field itself decreases. With a Foerster probe we measure directly the leakage field H_{st}. It is shown in Figure 10 that the geometrical extension of the stray field increases as the depth of the defect below the surface increases. The Foerster microprobe has a very suitable size compared with the size of the stray field of a subsurface defect. For reason of its geometrical size the Foerster probe is able to integrate over a substantial portion of the stray field. The stray field of a subsurface defect is wide and therefore integrated by the probe but the narrow stray field of a surface defect will not be integrated to such an extent. With magnetic particles it is not possible to make use of such an integration effect. The size of particles has to be kept very small for the sake of keeping the particles movable at all, because a subsurface defect attracts a particle with a very small force only.

In Figure 12 a practical example is shown. Our magnetographic system is systematically optimized by utilizing a magnetic tape with suitable physical properties, a suitable probe configuration, suitable filters and a suitable field strength. In a relatively thin transformer sheet there was a defect in the lower weld of the sheet. This is shown in the upper part of Figure 12 in which a filter setting was used which was sensitive for surface defects only. When a handroller as shown in Figure 4 was rolled over the upper weld there was an indication as shown in the top chart of Figure 12. When the instrument was rolled along the lower weld there was an indication as shown in the chart second from the top. After utilizing a filter setting suitable for the detection of subsurface defects, nearly the same records were obtained in inspecting the upper weld or the lower weld as shown in the two charts at the bottom of Figure 12.

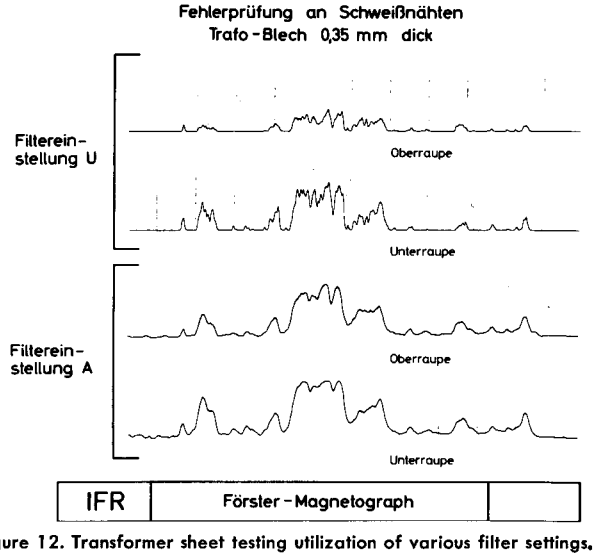

Figure 12. Transformer sheet testing utilization of various filter settings.

The theoretical outline of magnetography shows that this method is applicable for a very large variety of problems, specifically such problems where there is a physical limitation for the utilization of the particle method. In this field a large amount of application work has been done but within this paper it is not possible to give a summary about this work*.

Automatic Weld Testing

In contrast to the particle method, magnetography allows the automation of the test procedure. In the past years priority has been given to the design of automatic test machines for the inspection of semi-finished parts such as pipes and billets.

The Magnetographic Weld Tester

The most interesting application of magnetography in the field of tube inspection is the inspection of longitudinal welds in resistance or high-frequency welded tubes with diameters larger than 2 in. Such an installation is shown in Figure 13. The magnetization of the test parts is maintained by means of a magnetic

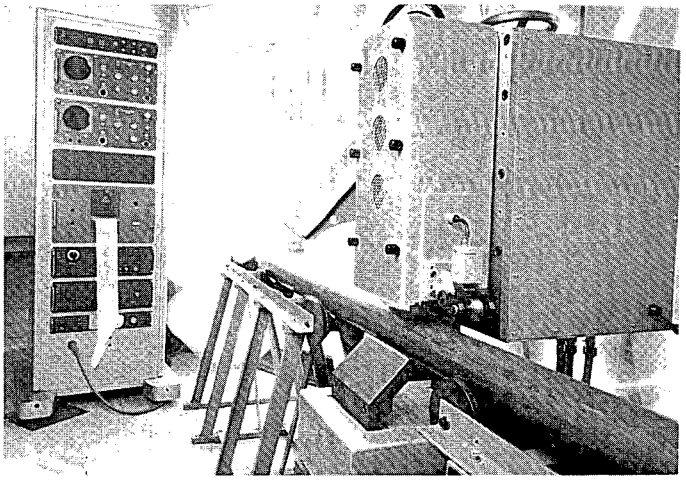

Figure 13. Magnetography tube inspection unit.

yoke which is fed with a D.C. current. The yoke is supported on a floating suspension and is guided by the tube itself. By this means a constant air gap between the yoke and the test-pieces is maintained and it is ensured that the tangential field strength across the weld is constant. In order to avoid any unnecessary friction or even a slight amount of slip between the tape and the tubes the tape is driven by an electro-motor which is synchronized with the speed of the tube. An electric clutch with an electrically adjustable torque makes sure that a slight error in the synchronizing system of the electro-motor does not involve slipping of the tape. In this case the electromagnetic clutch takes over that small amount of slippage. As welded tubes are never entirely clean and as, specifically, tubes made from hot-rolled strip always have some loose scale on the surface the tape might get very dirty and spoiled with parasite magnetic signals after a certain period of operation. For that reason there are rotating brushes to keep the tape clean. In addition, not the front side of the tape is scanned but the back side. By this means the test

*A wide variety of industrial applications of the magnetographic method is covered in the Foerster monograph already mentioned.

system itself is never in direct contact with that side of the tape which touches the tubes.

As mentioned above the evaluation of the results is done in two separate channels with two separate filter settings, one for surface defects and one for subsurface defects and as described above there is a logic combination circuitry which controls the automatic spray guns which give paint marks in different colours for I.D. and O.D. defects. In addition there is a digital data evaluation system in the cabinet. The evaluation is slightly different according to the application for endless tubing or for tubing cut in lengths.

For endless tubing there is a wheel which continuously counts the length of tube and which gives a signal after every 30 or every 300 feet of tube. In a digital counter system the number of defects is counted. Each time after the tube has travelled 30 (or 300) feet there comes the signal from the device measuring the length of the tube. This signal makes the digital counter system print the number of defects which were present in the past 30 feet of tube and also resets the counter printer to zero. Now, for the next 30 feet of tube the number of defects is counted and is printed after the tube has travelled another 30 feet and so on. By this means we have continuous printing of the statistical distribution of defects over a total length of the tube produced in a day or in a shift.

For tubes which are cut in lengths the recording by means of such a digital record is done in a very similar way except that this time the number of defects per tube is counted and printed.

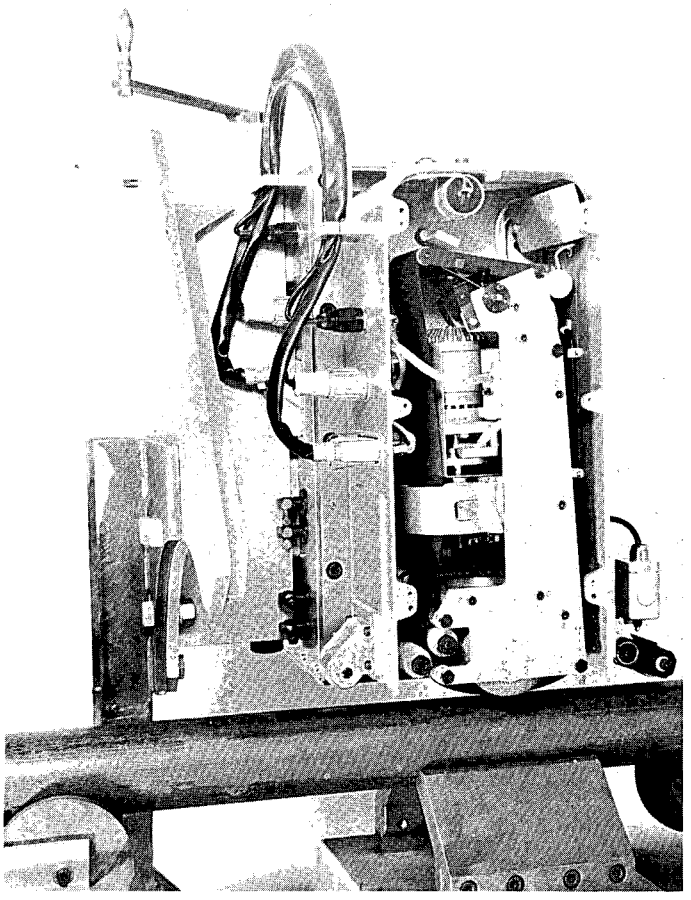

Figure 14. Test head of tube inspection unit.

The unit also contains a device for lifting the test head off when the leading or trailing edge of a tube comes through, thus avoiding any damage to the tape by a sharp flash of the sawn tube ends. There is another problem in inspecting tubes cut in lengths; it is essential that the tube is so positioned that the weld is on top. For this reason an automatic weld finder has been developed which is able to detect the weld. When it is getting near the weld, it produces a signal voltage which will be balanced to zero when the weld finder is exactly over the centre of the weld. Figure 15 shows the features of such a weld finder which is not only able to find the weld but also to feed a control system which maintains the weld in its proper position. It should be noted that, for the magnetograph, the position of the weld is not critical. The wander of the weld can be as much as ± 1 in. or ±20°, whichever value of the two is the smallest.

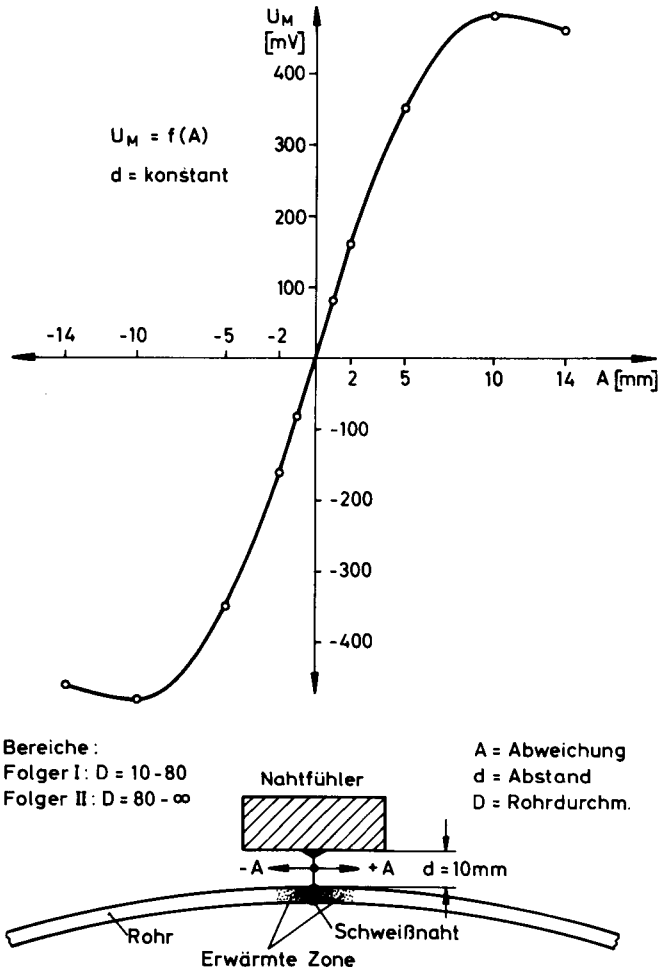

Figure 15. Weld finder.

The maximum test speed of such a system is given by the pitch of the scanner. There is a simple relation

$$p = \frac{v}{n}$$

in which v means the speed of the tube or of the tape, n the number of scans per unit of time and p the pitch. As we have 60 turns/sec of the scanner and in the scanning disc there are four probes we scan 240 lines/sec transverse to the tape resp. the weld. If we read the test speed of the tube in feet/min and the pitch in inches we obtain an equation

$$p = \frac{v}{12{,}000}$$

which means that for a test speed of 120 feet/min the pitch is .1 in. As the probe looks at a width of approx. .06 in. we would entirely cover the surface at a test speed of approx. 70 feet/min. In weld testing it is essential to find pinholes and it has been said pinholes are extremely short so that it was not possible to exceed the test speed of 70 feet/min. This problem has been investigated by thoroughly analyzing such defects that seemed to be pores after the tube had undergone hydraulic tests. Figure 16 shows, left on top, the magnetic-particle indication obtained by two such pores and, right on top, the particle indication as obtained by a good piece of welded tube. When the frequency filter of the magnetograph was adjusted for the finding of surface defects the record chart showed the two pores and showed them to be very short. But when the filter was set for looking at subsurface defects as it was done in the second chart on the left, or even to a larger extent on the chart at the bottom left, it turned out that there were not only pores but that quite a considerable length of the tube was defective and only in two very short spots was the defect open to the surface. On the right side of Figure 16 a chart obtained from a good length of tube for every one of three filter settings is shown. Figure 16 proves three facts: a) the hydraulic test is not reliable enough because if there had not been those two short pores the whole defective length of the tube under inspection would have been classified as good; b) magnetic ink has a fairly poor depth penetration for welded tubes because even a good tube can collect powder in the welded area. The long subsurface defect as shown on the left side in Figure 16 was not detected by magnetic ink; c) normally a pore is not a short defect but in the vicinity of a pore the weld is bad, too.

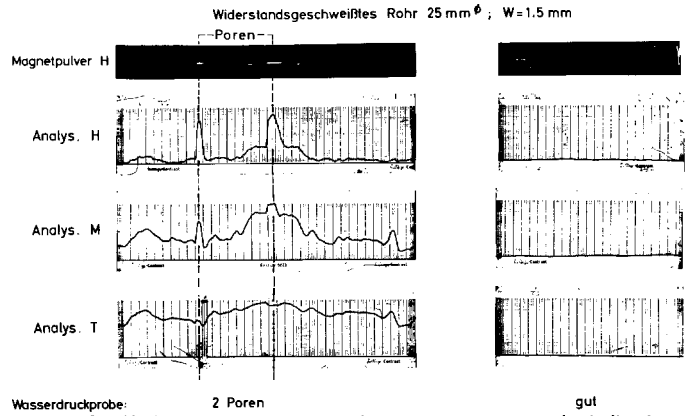

Figure 16. Hydraulic test—powder indication—magnetography indication.

The last statement is of great importance for the maximum test speed which can be obtained. As a pore is—at least underneath the surface—a fairly long defect, the pitch of scanning helix can be made as wide as $\frac{1}{8}$ in. or more without running the risk of missing the pore. That the welded zone in a tube induces a certain background "noise" to the particle indication is also true to some extent for the magnetographic weld inspection. To some extent it is possible to eliminate this background noise by means of filters but under normal conditions the penetration of the magnetographic method in welds is restricted to about $\frac{1}{4}$ in. to $\frac{5}{16}$ in. of wall thickness. It is evident that heavier walls can be inspected, too, but the resolution for I.D. defects will decrease with heavier wall thickness.

Calibration of the Weld Tester by Means of Standard Defects

For weld testing, API standards have been elaborated. According to API a defect of 12.5% of the wall thickness at the inner wall of a tube should be detected and, e.g. the calibration of ultrasonic weld testers should be made with such standards because it is more convenient to machine such artificial defects. The API standards propose among others a v-notch which is open under 45°. It is shown in this paper that the magnetic stray flux depends a lot on the geometrical shape of the defect. For this reason we investigated how a v-notch which is indicated by the magnetograph compared with an artificial defect of the same depth but having vertical flanks and a width of .004 in. The results are shown in Figure 17. The left part of Figure 17 refers to an I.D. defect and the right side to an O.D. defect. A notch gives a reading which is very similar to an artificial defect although the sensitivity to such a notch is slightly reduced. It can still be used for calibration purposes. As the normal working range is between 60 and 80 Oersteds (tangential field strength) the difference in reading is not too serious. For outside defects there is practically no difference in reading at all but this is true under the assumption that the v-notch is filled with wax or similar material so that the tape is not pressed into the bottom of the notch but is a laid plane on the surface of the test-piece. These findings may be a little bit surprising with reference to the findings in Figures 6 and 7 but it is to be noted that a v-notch is much different from an ellipsis. Figure 17 proves that it is possible to calibrate the magnetograph with both a v-notch and a "normal" artificial defect. This may be of special interest because there is a tendency to eliminate the v-notch from the API standards.

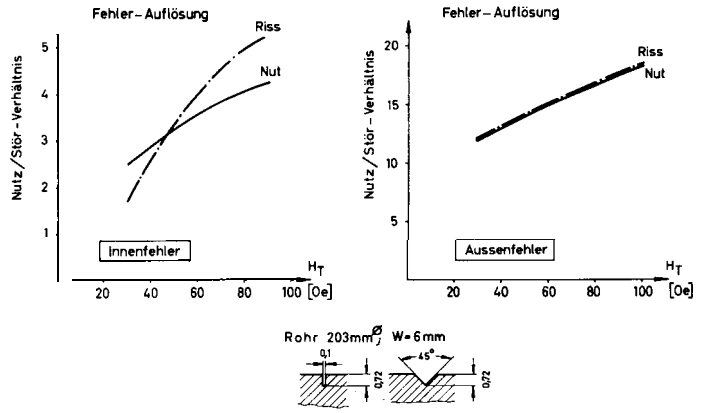

Figure 17. Magnetography tube testing. Indication of a v-notch and artificial defect with vertical flanks.

Practical Results in Weld Testing

The weld tester has been used with good success both for bright and for hot-rolled welded tubes. Initially there was some problem in making the system insensitive to dirt. To solve this problem the first step was to scan the back side of the tape and to brush the tape by means of rotating brushes. In addition dust proof gears and bearings for driving the magnetic belt were used, all electrical contacts were sealed and care was taken that any wear parts could be exchanged easily. In addition the tubes under inspection were slightly cleaned of oil or grease by a steam jet. It does not matter if the tube is humid but it should not be dripping wet. It developed that these conditions can be easily maintained without any substantial cost or other inconvenience. Figures 18 and 19 show two typical results of magnetographic weld inspection. Figure 18 was obtained by inspecting a resistance welded tube in which, during inspection, the welding current was continuously decreased. After this the tube was cut in lengths of 8 feet each. The first tube was without defects. At the end of the second tube there was a slight defect. The third tube was defective at four areas and it was surprising that there was a periodicity of these defects. Although

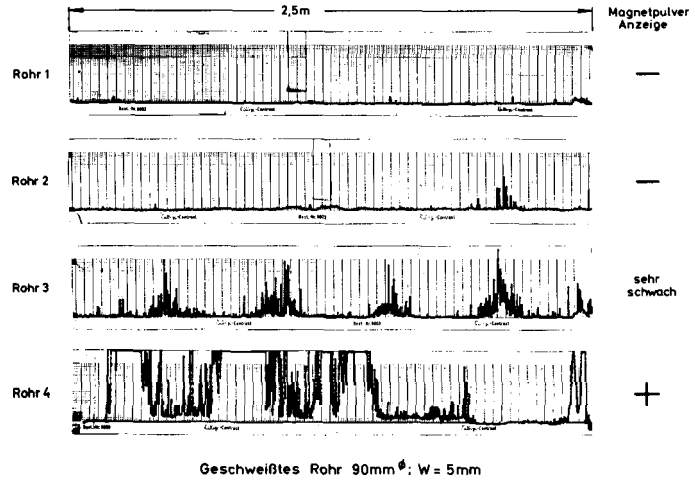

Figure 18. Magnetography inspection of a resistance welded tube; current continuously decreased.

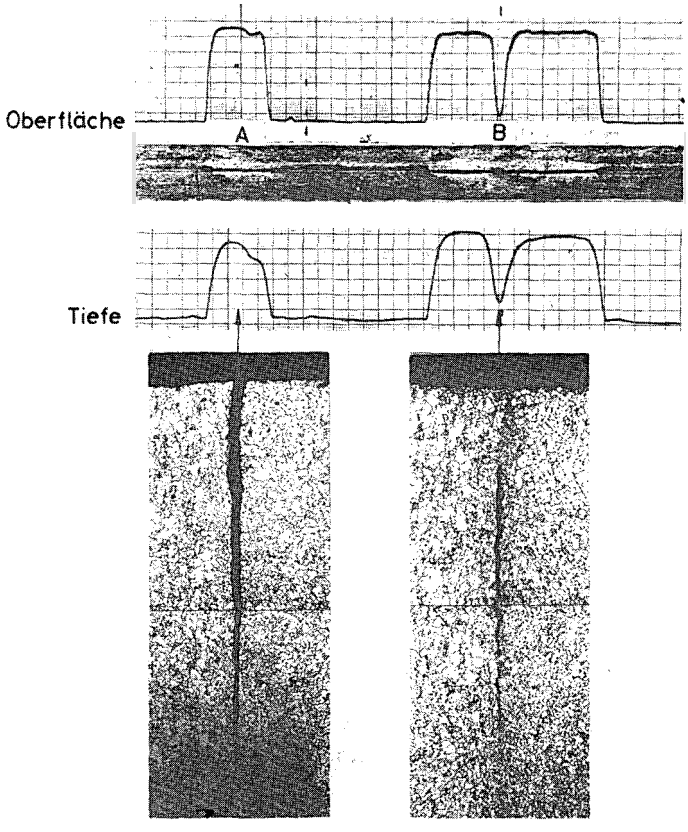

Figure 19. Magnetography and powder dications of surface an subsurface defects.

the chart obtained from tube No. 4 is swamped it can be seen that this periodicity continues on the tube. The reason for this periodicity was an eccentricity of the welding wheel. Owing to the varying pressure of the welding wheel on the tube most defects were in the zone of too low welding pressure. This picture shows that such an evaluation permits not only the finding of defects but the reason they occur. Figure 19 shows an interesting result obtained from a weld that had two defects, one of which was open to the surface and one which, over a certain length, "dove" underneath the surface. In spot B the channel for surface defects shows no signal at all (and no particle indication) but the subsurface channel still showed a decrease of the defect in that spot but clearly showed that the defect was still there. The combination of the upper and lower chart shows that in section B there must be a subsurface defect (as described above this evaluation is done automatically in the logic circuitry).

Record charts as shown in Figures 18 and 19 are normally not made under in-line conditions, only for calibration and evaluation purposes. Under in-line conditions statistical evaluation by a counter printer and automatic paint marking by spray guns have proved to be more practicable. The method has been used for wall thicknesses as heavy as $\frac{1}{2}$ in. but under these circumstances I.D. defects as small as $12\frac{1}{2}\%$ could no longer be found. When the wall thicknes is $\frac{1}{2}$ in. I. D. defects of 20 to 25% can be found. It turned out that the flash at the inner side of the tube is not critical in principle. The resolution for I.D. defects is best when the flash is removed so far that it is not higher than .008 in. In total it could be proved that the magnetographic weld tester has become a reliable practicable and sensitive tool for automatic in-line inspection of welded tubes.

Billet Inspection

Besides weld testing, the automatic billet inspection is an application of the magnetograph which is urgently needed and very interesting, both from a principal and from a technological point of view.

Principal Problems

The principle of a fully automatic billet inspection system is shown in Figure 20. The billet is magnetized by means of

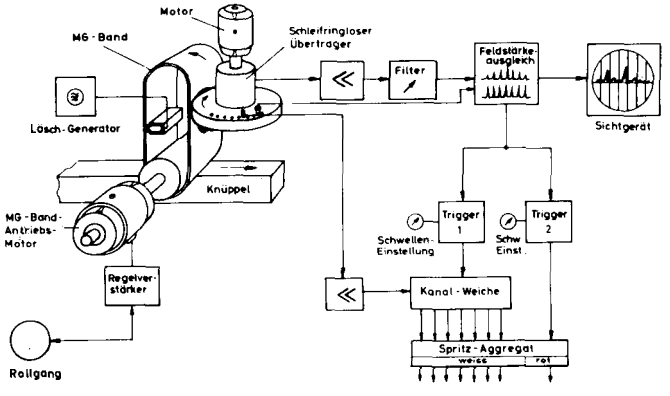

Figure 20. Principle of an automatic billet testing system.

copper-bronze contact brushes placed at the vertical faces of the billet near the test head (the brushes are not shown in the block diagram). The tape is pressed to the billet face by means of a sponge rubber wheel; tape and wheel are so flexible that it assures the tape going round the corners of the billet, thus extending inspection to the corners. As the billet moves from left to right the magnetic tape travels upwards to the rotating disc in which is the magnetic sensing device. As the tape travels on, it comes to the eraser which demagnetizes it; it is then driven by a speed-controlled electro-motor, the speed of which is controlled by the speed of the conveyor table. The electro-motor is coupled to the driving system of the belt by an electromagnetic clutch as already described for the weld tester. The voltage of the magnetic field probe is transduced from the rotating disc to the amplifier by a contactless transformer. After amplification

the signal is filtered and fed to a sensitivity-control system. This system is necessary because the magnetic field strength around a cross-section of the billet is not homogeneous but is higher in the centre part of the billet than near the corners. This sensitivity-control system makes sure that defects near the corners of the billet are indicated with the same sensitivity as defects in the centre part. From the sensitivity-control system a signal goes to an oscilloscope where it is displayed. Parallel to the oscilloscope the signal goes to a trigger system. The threshold of the two triggers can be continuously adjusted. The left trigger system is used to indicate defects that are no longer acceptable but are only so deep that it is still economic to condition them. The right trigger system is operated only if there is a very deep defect, so deep that conditioning of the billet is no longer possible or advisable and the billet has to be rejected. This trigger system operates one spray gun only which paint-marks the billet with red, indicating that the billet is scrap. The trigger system that operates when there are comparatively small defects feeds its signal to a channel gate which divides the width of the billet up into seven channels. If there is a defect that can still be conditioned it is important to know not only that there is a defect in a given cross-section but also to know its exact location to avoid unnecessary time in finding it. As this channel system divides the width of the billet up into equal strips of $\frac{3}{4}$-in. width, the location of any defect is paint-marked with fair accuracy. Conditionable defects are normally painted with white paint.

The sensitivity-control system is an important part of the billet tester and has involved a number of thorough investigations. To understand what such a sensitivity-control system has to do we look at Figure 21, which shows the directions of the magnetic flux lines around a billet cross-section for a billet with a cross-section of 2 in. × 2 in. and one with a cross-section of approx. $2\frac{3}{4}$ in. × $2\frac{3}{4}$ in. The billet shown on the left of Figure 21 is the smaller and it was magnetized with a tangential field strength of 60 Oersteds in the centre part of the face. In comparison the billet in the centre, of the same dimensions, was magnetized with tangential field strength of 120 Oersteds in its centre. The comparison of the behaviour of the flux lines under

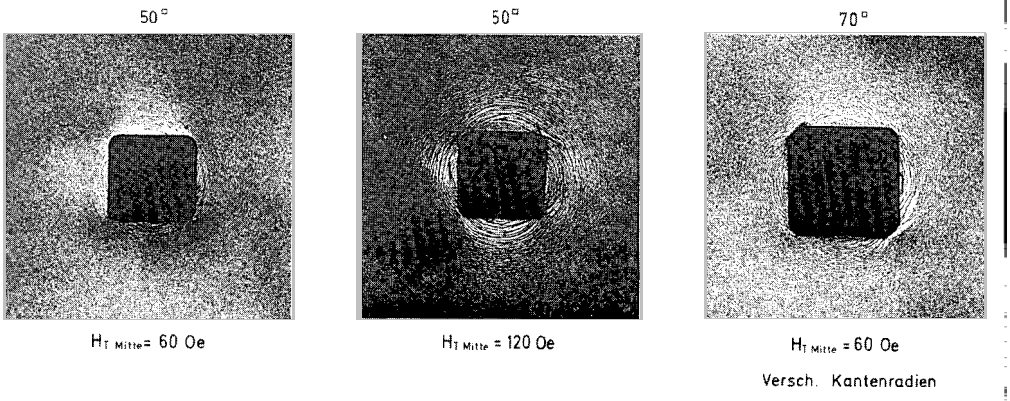

Figure 21
Magnetographic field distribution around a billet.

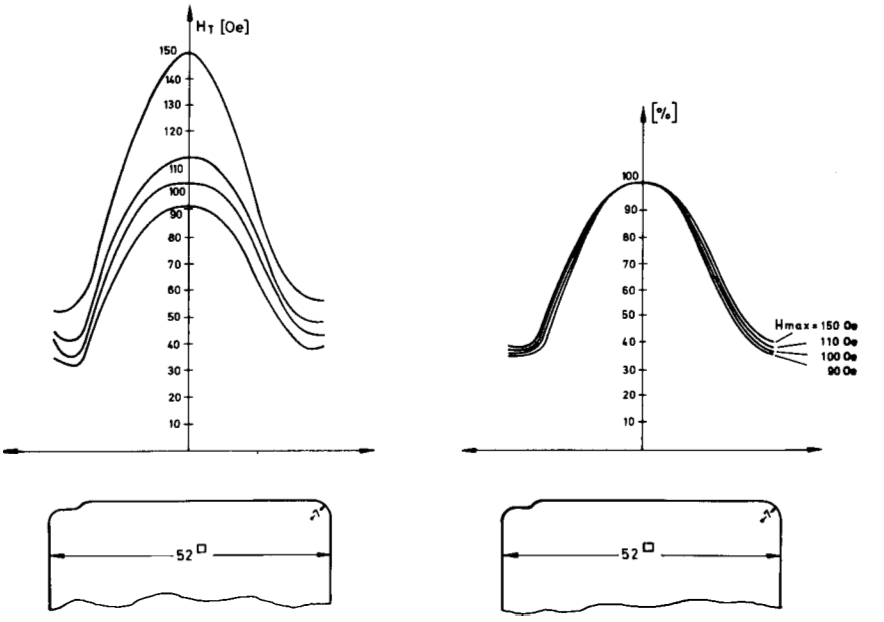

Figure 22
Distribution of the magnetic field across the

IFR	Verteilung der Tangentialfeldstärke H_T über die Knüppelbreite

high or low magnetization shows that under low magnetization the flux lines enter the surface of the billet face nearly rectangularly in the areas near the corners, but on the highly magnetized billet the flux lines follow a path which is much less inclined to the surface. This means that with too low a magnetization there is no substantial tangential field strength near the corners of the billet, and therefore it is not possible to find longitudinal defects near the corners if the billet is under too low a magnetization. It can be clearly seen that under the higher magnetization there is still a component of a flux line parallel to the surface face, which means that every longitudinal crack, no matter whether in the centre part of the face or at the corners, will have a stray flux.

The billet on the right side of Figure 21 was magnetized with the same field strength as that on the left. In general the field lines behave similarly on the two although that on the right is larger. There is a certain similarity law in the behaviour of the magnetic flux lines. Another feature in the right picture is interesting. It shows that irregularities in the shape of the billet also mean an irregularity in the path of the flux lines. For this reason it is to be expected that substantial irregularities in geometrical shape of a billet will slightly affect the distribution of the magnetic field around its cross-section. This feature is of some theoretical interest, but it can be shown that it does not unduly restrict the accuracy and reproducibility of magnetographic testing.

Figure 22 shows some of the results of the investigation of the distribution of the magnetic field across the billet face. On the left part the distribution of the magnetic field across the billet face has been plotted for various magnetizing currents. The currents were selected such that in the centre part of the billet there were magnetic field strengths of 90, 100, 110 and 150 Oersteds. In the right side these curves are plotted in relative values. In the left, the field strengths are plotted in absolute values for all four curves. In the right they are plotted in relative values and the maximum field strength of each curve is defined as 100%. This figure shows that there is a similarity in all these field-strength curves but there is a clear tendency that, for a high magnetization the field strength near the corner is relatively higher than that for the low magnetization. It can also be seen that the surface irregularity on the left corner of

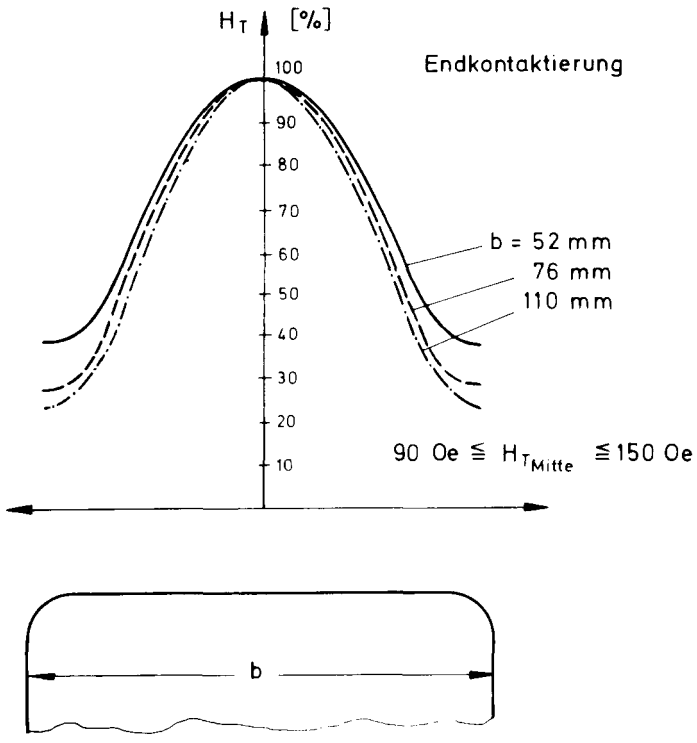

Figure 23. Distribution of the magnetic field across the billet face.

the billet influences the distribution curve of the magnetic-field strength.

It was mentioned that for various dimensions of the billets there was a certain similarity law of the distribution of the magnetic field. This is true for any constant billet size. If we plot one average curve instead of the four curves on the right side of Figure 22 and evaluate such curves for billets of various dimensions, we find results as shown in Figure 23. In a large billet the decrease of the tangential field strength across the billet face is sharper than that for a smaller billet. But the compensation circuits as described in Figure 20 are capable of compensating this decrease for any billet size for which the billet tester is built.

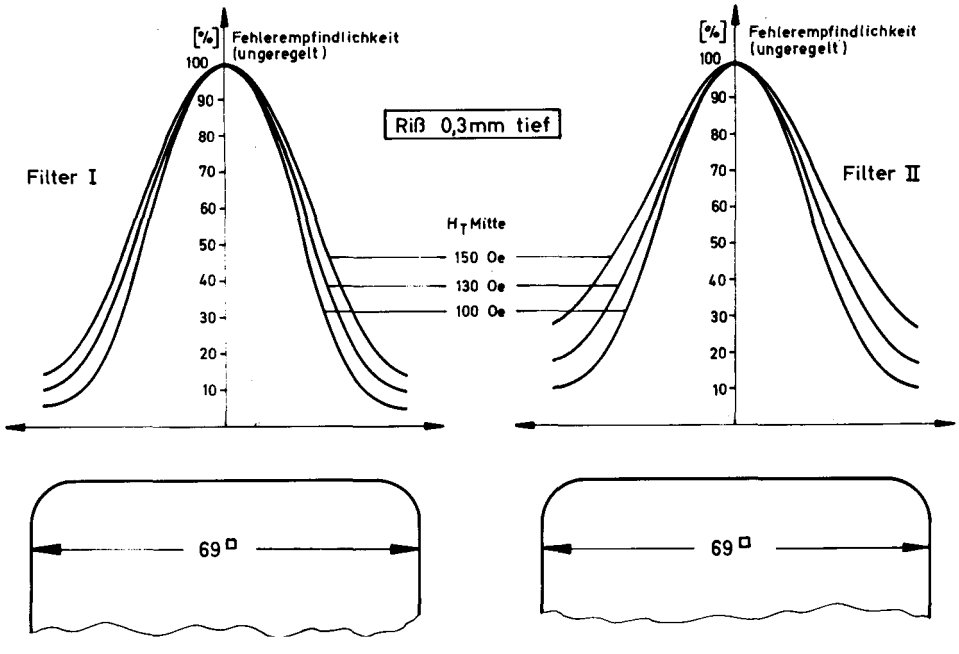

Figure 24
Sensitivity of the magnetographic system.

Figure 24 shows an example of how the sensitivity of the magnetographic system is affected by this distribution of the tangential field strength. The sensitivity of the magnetographic indication decreases stronger than the field itself decreases. Incidentally, the comparison between the left and the right family of curves in Figure 24 shows that by using adequate filters the drop of the sensitivity near the corners of the billets can be considerably reduced. This is because the frequency spectrum of a magnetographic defect signal varies as a function of the magnetizing field strength. By using a suitable filter and a suitable field strength the sensitivity curve of the magnetographic indication can be made very similar to the distribution of the tangential field strength. Figure 24 shows that for larger defects this distribution curve may look different from the curve for small defects because in the centre part of the billet a certain saturation of the signal may occur. Thus the indication is no longer linear. In the range of those defects in the vicinity of the acceptance limit—normally anywhere between .010 in. and .030 in.—the curves are so similar that the sensitivity control system as described in Figure 20 works quite satisfactorily.

Because there is a certain influence of the shape of the crack on the sensitivity, and also because the sensitivity control system cannot work absolutely accurately in the full range of all defect sizes, we obtain a band of error as shown in Figure 25. This practically means that it is possible to set a certain acceptance limit (according to the customer's specifications), i.e. a certain crack depth D. If such an acceptance limit is requested we have to set our trigger signal according to the dashed horizontal line in Figure 25. This makes sure that all defects deeper than D are paint-marked. Under these circumstances it will happen that some defects smaller than D are paint-marked also; by reason of their shape, the magnetographic system is more sensitive to them. It is important that a lot of defects—namely all defects underneath the dashed horizontal lines—are not paint-marked and for this reason need not be conditioned. On an average there is a much larger number of shallow defects than deep ones as shown in Figure 26. The distribution of the length of defects versus their depth varies very strongly according to the quality and the milling conditions of the billets. The evaluation of a large number of defects has shown that the decrease of the length of defects is within the hatched area of Figure 26.

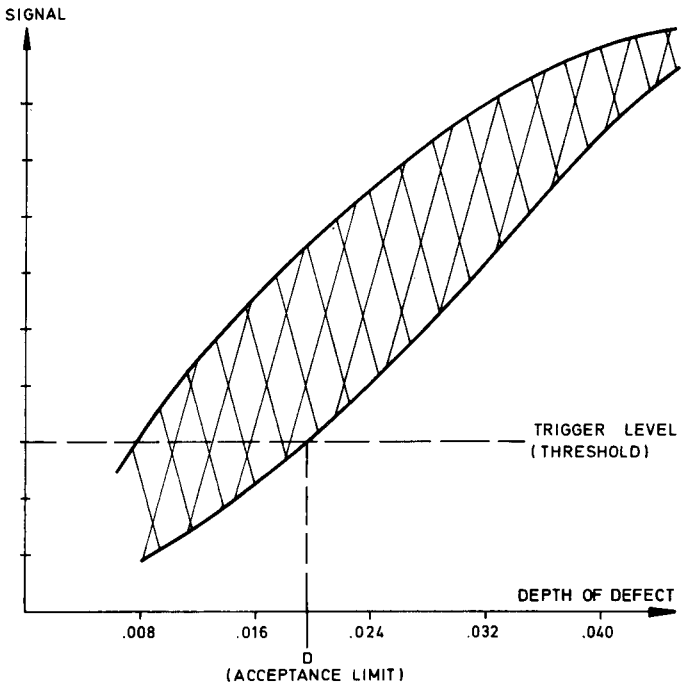

Figure 25. Band of error.

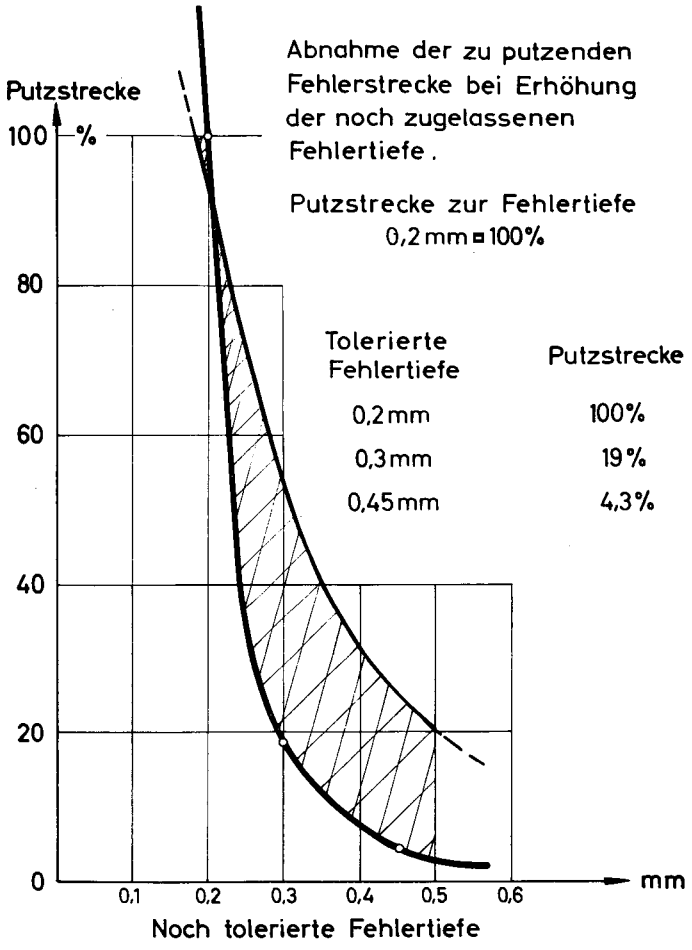

Figure 26.

Features of the Automatic In-Line Billet Tester

Figure 27 shows two of the test heads which inspect the opposite faces of the billet (the protective cabinet is removed). The billet goes on its diamond and the two test heads are placed under 45° to the vertical. The test heads are suspended (floated) so that they can follow the curvatures of the billet in two coordinates. On the lower test head, which examines the underside of the billet, the sponge rubber wheel and the contact system can be clearly seen. It should be noted that the contact brushes for the injection of the magnetizing current are placed very close together to ensure that the uninspected end is no longer than $2\frac{1}{2}$ in. After the billet has gone through the test station as shown it enters another very similar station which looks at the other two faces of the billet. By this means all four sides are inspected in continuous flow. Figure 28 shows a more complete view of one such twin unit which can be used for billets in the size range between 2 in. × 2 in. to $4\frac{1}{2}$ in. × $4\frac{1}{2}$ in. The adjustment to other billet sizes can be made very simply by turning the handle shown in the picture. The picture also shows the arrangement of the spray guns. Figure 29 shows the installation of a twin unit in a line. The unit is placed between two rigid stands which keep the billet in proper position by means of pinch

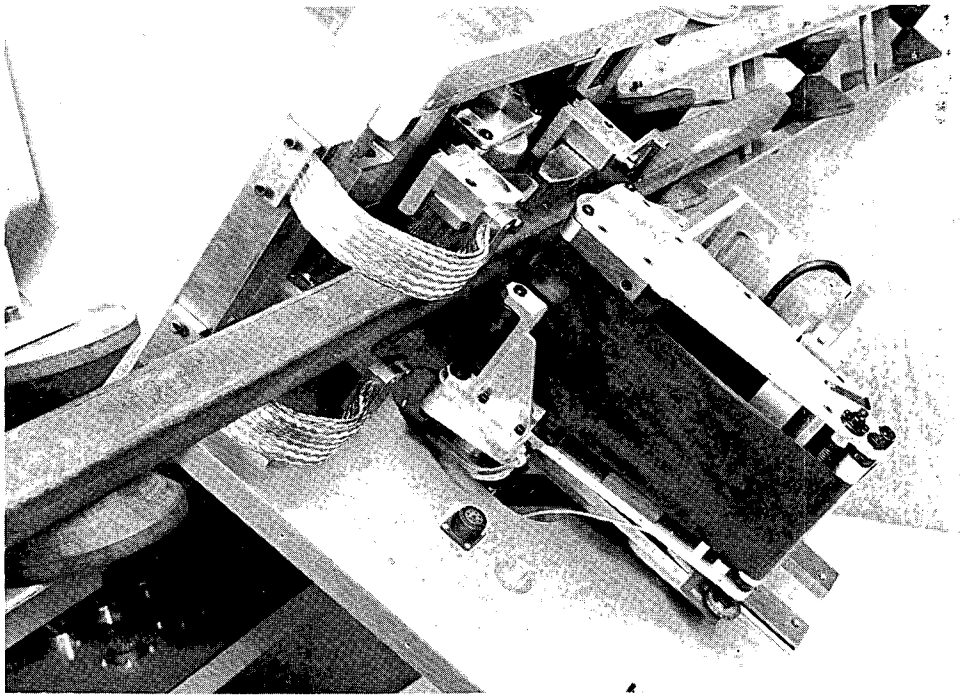

Figure 27.
Magnetography billet inspection test head.

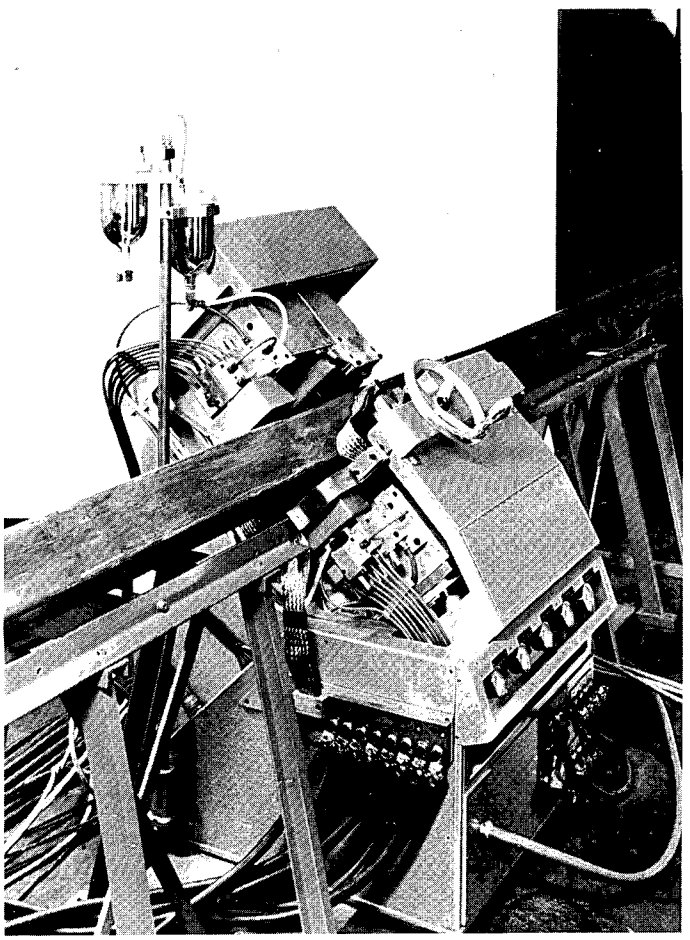

Figure 28. Magnetography billet inspection twin unit.

rollers. The controls for the unit and for the conveyor table and for some fail-safe devices are included into a control desk. Electronically, the unit is built up completely in solid-state design. The billets travel with a velocity of approx. 100-120 feet/min. The space requirements are fairly modest as each one of the two twin units does not require more than 5 to 6 feet floor space (including the pinch roller stands) so that the total longitudinal space required is approx. 10 to 12 feet. Such a unit can be operated by one inspector and the operation itself is so simple that an intelligent operator without any special education can run it. For nearly a year such an apparatus has been used 16 or 24 hours a day. The Figure 30 shows the through-put rate that

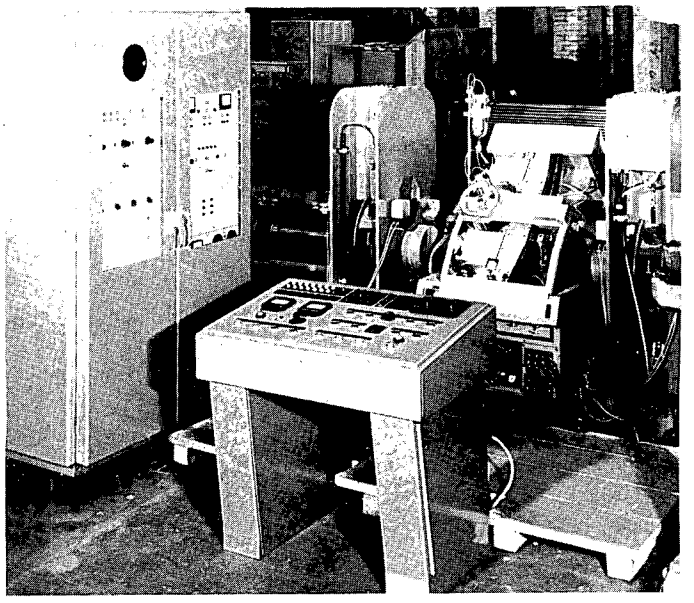

Figure 29. Magnetography billet testing test unit.

can be achieved. The maximum resolution under in-line conditions is .008 in. to .012 in. according to surface conditions. In most cases a better resolution than .012 in. is not practicable because mostly such defects are not serious and therefore would only cause unnecessary expense for conditioning if they were marked. The installation is used for billets with a descaled surface only. Scale on the billet does not substantially jeopardize the measurement itself, but it is not possible to inject enough current through a scaled surface. For that reason the billets which are inspected are shot-blasted. In close cooperation with some producers of the blasting equipment it has been possible to provide a shot-blasting system which is able to clean the billets well enough to maintain a proper current injection on the one side and to keep the costs for shot-blasting so low that the total costs for the magnetographic inspection are more economic than for normal particle testing.

Tabelle 1

Knüppellänge in Meter		1.5 m	3 m	4.5 m	6 m	9 m	12 m
Nutzeffekt η		0.5	0.6	0.65	0.7	0.75	0.8
Knüppelabmessung in mm		To/Monat (2 Schichten)					
50	□	6200	7400	8000	8700	9300	10000
75	□	14000	17000	18000	19500	20600	22000
100	□	25000	30000	32500	34500	36400	40000
120	□	36000	43000	47000	50000	53600	58000
150	□	56000	67000	70000	78000	83500	90000
180	□	80000	97000	106000	113000	120000	128000

Monatlich geprüfte und signierte Tonnenzahl für verschiedene Knüppelabmessungen

Figure 30. Magnetography billet testing throughput rate.

Figures 31 and 32 show practical results as they were obtained under in-line conditions. Figure 31 represents, on the left column, the total number of all defects present in all of 14 billets each of $2\frac{1}{2}$ in. $\times$ $2\frac{1}{2}$ in. in cross-section and 10 feet long. The total number of defects was defined as 100%. These billets were visually inspected and the inspectors were told that it was a very important selection and had to be checked with special care. The bottom part of the right column shows the total number (percentagewise) of all defects detected and removed after visual inspection but before magnetographic inspection. The Figure also shows that by visual inspection only approximately 65% of all defects were detected and conditioned. After conditioning those billets were inspected with the magnetograph and there another 35% of defects were found. Of these 35% about 15% were negligible as their depth was less than .012 in. but 20% were deeper than .012 in. and the maximum depth of the defects still present and not detected by visual inspection was .088 in. All the defects not removed after visual inspection were visible, but the inspectors had not seen (conditioned) them.

These do not result from a one-shot examination. In many demonstrations and investigations in a large number of steel companies it has been verified that under normal conditions of visual inspection approximately 20% of all visible defects are not detected by normal inspection routine. This shows that the reliability factor of an automatic system is much higher than that of a system that depends on the human eye or on the concentration and attention of an inspector.

Figure 32 shows the analogous result of comparison between magnetography and particle inspection. The total circle (360°) represents the total number of defects present in the bunch of steel billets. The section "marked by flux inspector

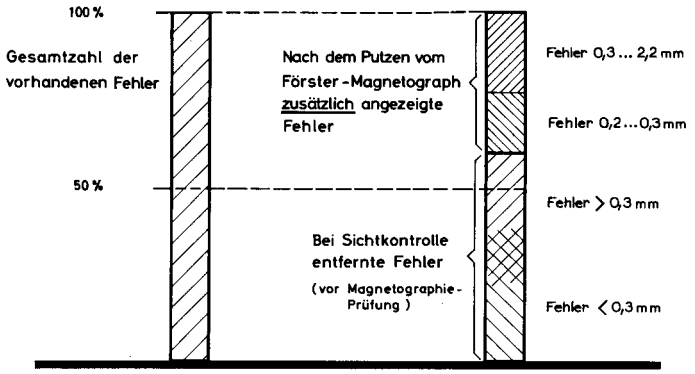

Figure 31. Visual inspection of billets and magnetography testing.

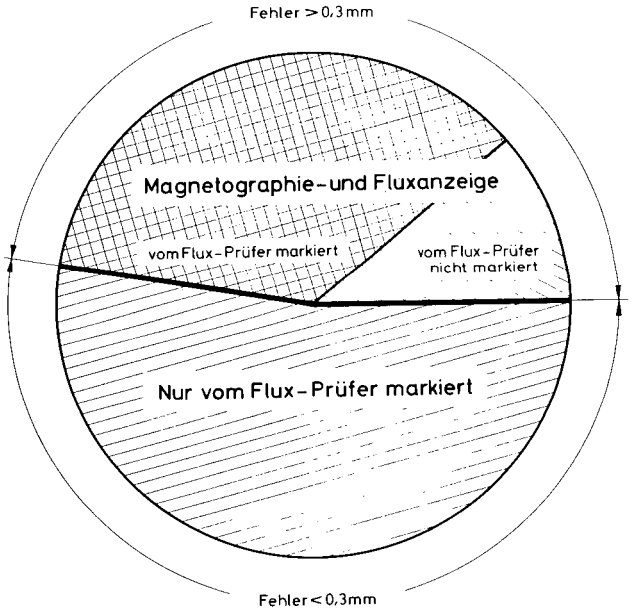

Figure 32. Billet testing by means of flux method and magnetography method.

only" shows the total number of defects marked by the flux inspectors only. The second section in the upper part of the circle "marked by magnetograph and by flux inspector" were paint-marked by the flux inspector and by the magnetograph. The section on the upper right part "not marked by flux inspector but marked by magnetograph" showed magnetograph paint-marks but all the defects represented by that section were not marked by the flux inspectors. It is important to know that all these defects clearly showed a particle indication but the flux inspectors had missed them and thus they were not marked.

The lower section of the diagram "marked by flux inspector only" showed no paint mark by the magnetograph. The depths of all these defects were measured and it could be shown that none was deeper than .012 in. (.012 in. was the acceptance limit to which the instrument was calibrated). All defects that were paint-marked by the magnetograph were deeper than .012 in. This Figure shows clearly that with the particle inspection the twofold number of defects had to be removed compared with magnetographic indication, but of these twofold numbers approximately 50% were of no significance and on the other hand, the number of approximately 20% of really serious

defects—i.e. such defects which were deeper than .012 in.—had not been paint-marked and according to this would not have been removed. Possibly the quantitative correlation as shown in Figure 32 is not always as good as this, specifically with free cutting steels, the error of the magnetographic indication being higher than for the steel qualities investigated in Figure 32. Even in these circumstances, we draw the conclusion from Figures 31 and 32 that flux inspection is influenced by human factors like attention, error, fatigue etc. as is the case with visual inspection. Again, approximately 20% of all defects are not paint-marked, i.e. not removed. Visual inspection and particle inspection both depend on the human factor. In both types of inspection the human factor is the same, which means that approx. 20% of all defects are not marked (not removed).

Practical Results

Over a long test in a conditioning line such a billet tester works reliably and the time needed for maintenance and repair is reasonably low. It is a great advantage that only one inspector per shift is needed and it is not necessary to train and have available a large number of trained and good inspectors day and night.

In comparison with visual inspection it has proved to be a money-saver for conditioning because the throughput rate of a man conditioning the billets is nearly doubled if the defects are clearly paint-marked so that the man no longer needs to look for the crack. A special conditioning table ensuring a very high hourly throughput rate has been developed and is available.

Development Work

Looking to the future, the trend is to the development of a fully automatic conditioning line. Some investigations and practical experiments for such a line are already going on and in the near future it seems to be possible that billets will be inspected at a speed of about 70–90 feet/min and that by means of a magnetic memory or a similar control system, defects found by an automatic magnetographic system will be removed automatically in a continuous flow of billets, on all four sides at almost the same time.

At least one step towards a semi-automatic conditioning device will be done within a few months. A normal commercial grinding machine will be equipped with a magnetographic test head which will control the operations of such a grinding machine. The principle of such a test device is shown in Figure 33. Here the billet is loaded on a wagon and contacted at its ends so that there is no need for taking the tight scale off (only loose scale disturbs the testing procedure). After the billet is moved from the left to the right on the wagon it is inspected on its upper side by the magnetographic test head and the results are stored in a 7-channel memory which again controls the positioning of the grinding machine so that the inspected

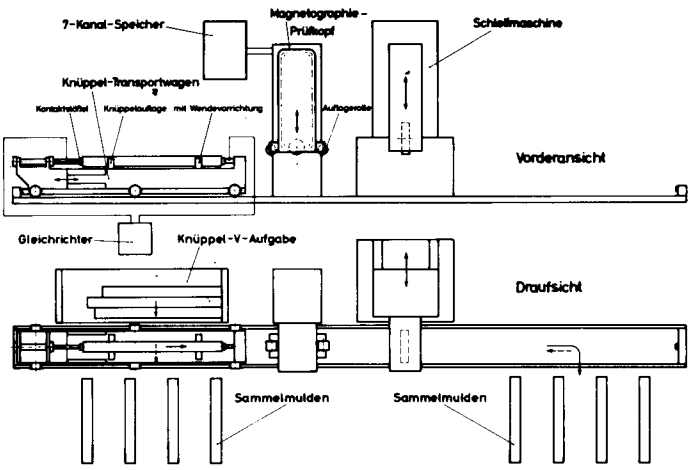

Figure 33. Magnetography billet test device.

billet face is completely conditioned when it arrives at the right side of Figure 33. The operation is repeated for each face of the billet. This method is very promising for high-quality steel and is certainly more reliable and much more economic than grinding all the billet faces.

An example shows that the complete grinding of all four billet faces does not always effect the result desired, i.e. ground billets without any defects. A larger quantity of ground chromium alloy billets was checked up for remaining defects with the magnetographic hand-roller shown in Figure 4. The result was quite surprising. At an average of 1 m each there was still a defect to be found, the depth of which surpassed the tolerance limit.

Investigations and development work on fully automatic conditioning lines are going on. Further results will be reported in due time.

Summary

Magnetographic test systems have proved to be a useful tool for automatic in-line inspection, specifically of welded steel tubes and of steel billets. Inspection is independent of the most serious obstacle to high reliability: the human factor. Under in-line conditions any method depending on the attention and judgment of inspectors finds no more than 80% of all serious defects.

Sur la détectabilité des défauts macroscopiques des matériaux conducteurs par des essais électriques

NICOLAE ANDREESCU, ELENA LĂBUSCĂ et S. VASILIU, ROMANIA

RÉSUMÉ. Ayant constaté le fait que la conductibilité électrique est un paramètre qu'on peut employer pour le contrôle préliminaire de l'homogénéité d'une série de pièces d'un matériel nucléaire, bon conducteur électrique, les auteurs indiquent une méthode simple et précise pour la mesure rapide de la conductibilité électrique. Cette méthode est applicable pour des mesures en série de pièces ayant la même forme et les mêmes dimensions, permettant ainsi une première sélection.

Pour détecter les non-homogénéités locales, les auteurs ont expérimenté un système de mesure original, utilisant un dispositif à quatre contacts, disposés en croix. Deux des contacts opposés servent pour le passage d'un courant électrique dans le matériel et les deux autres, pour la mesure de la différence de potentiel électrique entre deux points, symétriques par rapport à l'axe des contacts de courant. La valeur mesurée de la différence de potentiel indique le degré de non-homogénéité locale. On peut estimer la grandeur de ces zones de non-homogénéité à l'aide de cette différence de potentiel, par le calcul du champ électrique dans le matériel. Sur ces considérations on peut élaborer une méthode efficace d'essai non destructif, qui peut avoir un large domaine d'application. Il est nécessaire aussi de tenir compte des particularités du matériel étudié, tels que l'anisotropie, etc.

Les auteurs présentent les résultats expérimentaux obtenus pour le graphite nucléaire, et les comparent avec ceux obtenus à l'aide des ultra-sons.

Introduction

Les conditions de qualité imposées par l'utilisation courante des différents matériaux dans la technique moderne, impliquent, en général, non seulement que les pièces élaborées à partir d'un matériel aient certaines propriétés spécifiques, mais aussi que ces propriétés soient les mêmes pour toutes les pièces d'une série,—c'est-à-dire qu'il faut que la reproductibilité en série des caractéristiques soit assurée. Il est donc nécessaire que les pièces de série, fabriquées à partir d'un même matériel, soient ressemblantes en ce qui concerne l'ensemble de leurs caractéristiques, mais aussi, chaque pièce doit présenter un degré d'homogénéité suffisamment élevé, au point de vue structure et propriétés. Lorsqu'il s'agit de cette homogénéité des propriétés dans la masse même du matériel,—il est généralement connu que la présence des défauts macroscopiques,—tels que fissures, pores, zones de discontinuité, inclusions, etc,—peut déterminer, dans une mesure moins ou plus large,—des variations locales des propriétés mécaniques, physiques, etc. En fonction des conditions imposées par l'utilisation respective, on peut admettre un certain degré de non-homogénéité, au point de vue microstructure,—à condition que, dans l'ensemble, les variations locales des propriétés déterminées par les défauts microstructuraux ne dépassent pas les valeurs moyennes qui caractérisent le matériel et n'empêchent pas que les pièces respectives fonctionnent en bonnes conditions.

À partir des considérations ci-dessus, il en ressort la nécessité de contrôler, par les méthodes les plus diverses et les plus sensibles, la qualité des matériaux, y compris le contrôle de la reproductibilité en série des caractéristiques et aussi l'homogénéité de chaque pièce séparée.

L'étude présente se réfère aux expériences effectuées sur le graphite nucléaire, qui nous ont permis de mettre au point un système de contrôle non destructif, par des mesures des propriétés électriques. Considérant le cas des matériaux conducteurs, la mesure de la conductibilité électrique peut être utile pour apprécier l'uniformité d'une série complète de pièces et aussi évaluer le degré d'homogénéité de chaque pièce.

Évaluation de l'uniformité des pièces de graphite par le contrôle de la résistivité globale

La mesure de la résistivité globale d'une pièce de graphite nucléaire est relativement facile, étant donné que la plus grande partie des pièces de graphite utilisées pour fin nucléaire ont une forme simple et régulière. Si un lot de pièces est suffisamment homogène, la mesure de la résistivité doit conduire à une série de valeurs très rapprochées, même si les dimensions diffèrent d'une pièce à l'autre.

Ainsi, la mesure relativement rapide de la résistivité globale de chaque pièce fournit des indications précieuses d'après lesquelles on peut apprécier le degré de ressemblance des pièces de la série controlée avec une pièce—étalon, dont les propriétés spécifiques (résistances mécaniques, propriétés thermiques, section d'absorption, etc) ont été déterminées a priori avec beaucoup de précision.

Considérant le cas des pièces de graphite de forme parallélépipèdique, nous avons appliqué, pour ces mesures rapides de la résistivité globale, une méthode qui utilise un dispositif ayant un contact sur chacune des quatre facettes du parallélépipède (figure 1).

Les contacts, ayant la forme de lames minces (couteaux), sont situés dans les deux axes de symétrie de la section de la pièce et exercent une certaine pression sur toute la longueur de leur contact avec la surface latérale. Si on fait passer par le matériel, à l'aide des contacts A et B (figure 1), le courant I, on peut recepti-

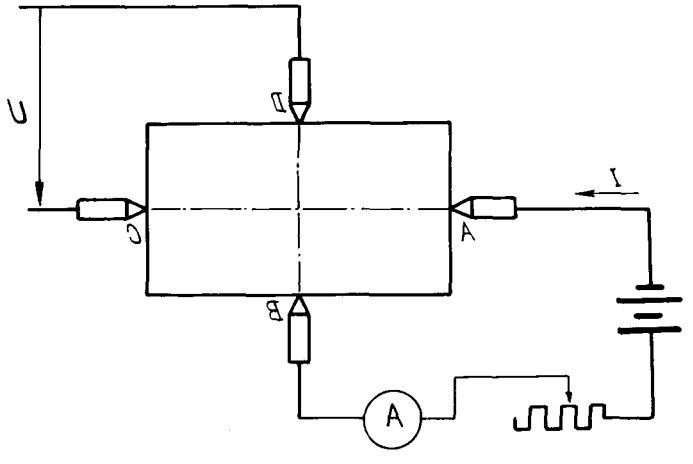

Figure 1. Dispositif pour déterminer la résistivité globale.

ner une tension U entre les contacts C et D. En notant avec g l'épaisseur de la pièce (la hauteur du parallélépipède), on peut écrire (1):

$$\rho = \frac{\pi g U}{I \ln_2} \qquad (1)$$

La validité de l'équation (1) est assurée seulement lorsqu'on fait respecter les conditions de symétrie ci-dessus mentionnées, et

si les contacts lamellaires A, B, C et D assurent un bon contact électrique sur toute l'épaisseur g. Le dispositif est construit pour autocentrer les contacts en fonction des dimensions du parallélépipède de graphite, qui peuvent varier dans certaines limites. Il assure le contact électrique par le pressage des lames sur les surfaces latérales de la pièce mesurée. Il permet donc une manipulation légère et rapide, et peut être utilisé dans le cas des mesures en série. Il faut encore remarquer que, à cause de la technologie de fabrication, (2), les pièces en graphite nucléaire présentent une anisotropie suffisamment grande, en fonction de la direction de pressage utilisée pour la mise en forme des pièces. À cause de cette anisotropie, la résistivité mesurée dans la direction de pressage, ρ_2 est plus petite par rapport à la résistivité ρ_1, mesurée dans le plan perpendiculaire à la direction du pressage.

Si les électrodes A, B, C et D sont placées parallèlement à la direction de pressage, le passage du courant électrique a lieu dans le plan perpendiculaire, dans lequel le matériel est isotrope, (le champ électrique est identique dans n'importe quel plan de ce type) et la relation (1) permet la détermination de ρ_1.

Si les quatres éléctrodes sont placées perpendiculairement par rapport à la direction de pressage, le champ électrique reste un champ plan, mais dans ce plan le matériel est anisotrope, et la valeur qu'on peut calculer à l'aide de l'équation (1) a les dimensions d'une résistivité et représente une fonction $\rho_p(\rho_1, \rho_2)$ laquelle est dépendante de ρ_1 et ρ_2 et peut servir à la sélection des pièces requises pour déterminer le degré d'uniformité.

Le tableau suivant contient quelques données expérimentales concernant des mesures effectuées sur quelques lots de pièces en graphite nucléaire, avec le dispositif et la méthode ci-dessus décrits.

Les valeurs de ρ_1 et ρ_2 contenues dans le tableau ont été déterminées avec une méthode que nous allons décrire tout de suite.

On peut constater que les différences entre les valeurs de ρ_p, pour les pièces appartenant à un même lot, sont inférieures à 5%, les erreurs expérimentales étant approximativement 3%. À l'aide de ces mesures nous avons fait une première sélection des pièces en graphite: a) des pièces pour lesquelles les valeurs de ρ_p ne présentent pas des différences plus grandes que 5% et qui sont considérées comme suffisamment homogènes; b) les autres pièces, pour lesquelles les différences dans les valeurs de ρ_p ont dépassé 5%, et qui sont considérées comme insuffisamment homogènes. Ces valeurs de ρ_p sont indiquées dans le Tableau 1. L'examen ultérieur de ces pièces, par des procédés que nous allons décrire, a montré qu'en effet ces pièces ont des non-homogénéités, dont la présence explique les variations observées dans les valeurs de ρ_p.

Tableau 1

Catégorie	Pièce	g [cm]	ρ_p [Ω cm]	ρ_1 [Ω cm]	ρ_2 [Ω cm]
a	1	2,64	$1{,}15\times10^{-3}$	$1{,}41\times10^{-3}$	$1{,}11\times10^{-3}$
	2	2,74	$1{,}115\times10^{-3}$	$1{,}39\times10^{-3}$	$1{,}11\times10^{-3}$
	3	2,68	$1{,}115\times10^{-3}$	$1{,}33\times10^{-3}$	$1{,}14\times10^{-3}$
	4	2,7	$1{,}12\times10^{-3}$	$1{,}37\times10^{-3}$	$1{,}0\times10^{-3}$
b	1	2,61	$1{,}32\times10^{-3}$	$1{,}55\times10^{-3}$	$1{,}32\times10^{-3}$
	2	2,64	$1{,}30\times10^{-3}$	$1{,}43\times10^{-3}$	$1{,}17\times10^{-3}$
	3	2,91	$1{,}37\times10^{-3}$	$1{,}64\times10^{-3}$	$1{,}22\times10^{-3}$
	4	2,66	$1{,}34\times10^{-3}$	$1{,}45\times10^{-3}$	$1{,}19\times10^{-3}$
c	1	2,7	$1{,}51\times10^{-3}$	$1{,}78\times10^{-3}$	$1{,}4\times10^{-3}$
	2	2,6	$1{,}48\times10^{-3}$	$1{,}74\times10^{-3}$	$1{,}33\times10^{-3}$
	3	2,7	$1{,}465\times10^{-3}$	$1{,}6\times10^{-3}$	$1{,}25\times10^{-3}$
	4	4,97	$1{,}53\times10^{-3}$	$1{,}76\times10^{-3}$	$1{,}38\times10^{-3}$

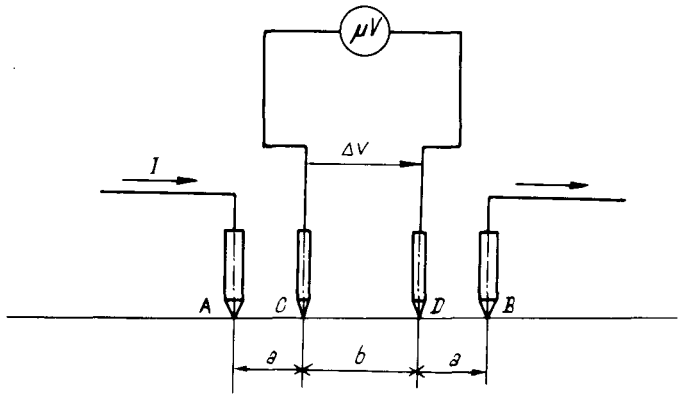

Figure 2. Dispositif qui permet la mesure des résistivités locales.

La mesure des résistivités locales ρ_1 et ρ_2

Dans nos recherches nous sommes partis de l'hypothèse qu'on peut faire l'évaluation du degré d'homogénéité d'une pièce par la détermination de la résistivité en chaque point de la pièce. Étant donné que le graphite est anisotrope, il a été nécessaire de déterminer les fonctions ρ_1 (x, y, z) et ρ_2 (x, y, z), et d'examiner ces deux champs scalaires pour apprécier le degré d'homogénéité de la pièce étudiée.

On peut montrer (3), qu'en utilisant un dispositif simple (fig. 2), qu'on fait promener sur la surface de la pièce, on peut mesurer la résistivité locale. Ce deuxième dispositif que nous avons réalisé, implique aussi quatre électrodes, mais qui sont cette fois placées en ligne droite, —les électrodes A et B étant employées pour l'introduction d'un courant I dans le matériel et les électrodes C et D pour la mesure de la tension.

Le contact des électrodes avec le matériel peut être considéré comme ponctuel. D'après (3), si les dimensions de la pièce sont sensiblement plus grandes que 2 a + b, l'effet périphérique peut être négligé et on peut déduire les relations:

$$\rho_1 = \frac{\Delta V}{I}\,\frac{\pi a\,(a+b)}{b} \tag{2}$$

lorsque la ligne commune des quatre électrodes coïncide avec la direction de pressage, et

$$\sqrt{\rho_1\rho_2} = \frac{\Delta V}{I}\,\frac{\pi a\,(a+b)}{b} \tag{3}$$

lorsque la ligne commune est située dans le plan perpendiculaire à la direction de pressage.

En effectuant deux mesures dans deux directions perpendiculaires, une de ces directions étant obligatoirement perpendiculaire à la direction de pressage, on obtient, pour une valeur donnée du courant, les valeurs ΔV^1 et ΔV^2, à partir desquelles on peut déduire les valeurs de ρ_1 et de ρ_2. Il est évident que ces valeurs représentent la moyenne des valeurs des résistivités locales réelles, moyenne valable pour le matériel qui remplit l'espace autour des contacts du dispositif illustré dans la figure 2.

Les relations (2) et (3) deviennent approximatives lorsque le dispositif à mesurer est placé très près de n'importe quelle limite de la pièce, ou lorsque l'épaisseur de la pièce n'est pas suffisamment grande. Par exemple, pour les valeurs: a = 0,45 cm et b = 1 cm, l'épaisseur de la pièce mesurée doit être > 1,5 cm et le dispositif ne doit pas être placé plus proche qu'un centimètre des bords de

la pièce. Le contrôle de l'homogénéité peut donc être réalisé pour des zones relativement superficielles des pièces excepté pour les zones périphériques. Pour pouvoir produire une perturbation donnée dans les tensions ΔV mesurées, un défaut existant dans la pièce doit être d'autant plus grand tant qu'il est situé plus profondément dans le matériel. Pourtant, en choisissant une épaisseur convenable de la pièce, notamment celle qui dépasse très peu le minimum pour lequel les relations (2) et (3) ne sont plus affectées, et en effectuant les mesures sur les deux facettes opposées de la pièce, on peut déterminer le degré d'homogénéité du matériel.

La méthode peut donc être utilisée pour la vérification de l'homogénéité, mais son importance principale est de permettre la détermination de ρ_1 et de ρ_2.

Détermination des non-homogénéités locales par la méthode des quatre contacts disposés en croix

La sensibilité du système de mesure, utilisant le dispositif illustré dans la figure 2, peut être considérablement agrandie si les deux contacts de tension (C et D) sont placés de façon symétrique par rapport à l'axe des contacts de courant (A et B), tel que nous l'avons representé dans la figure 3.

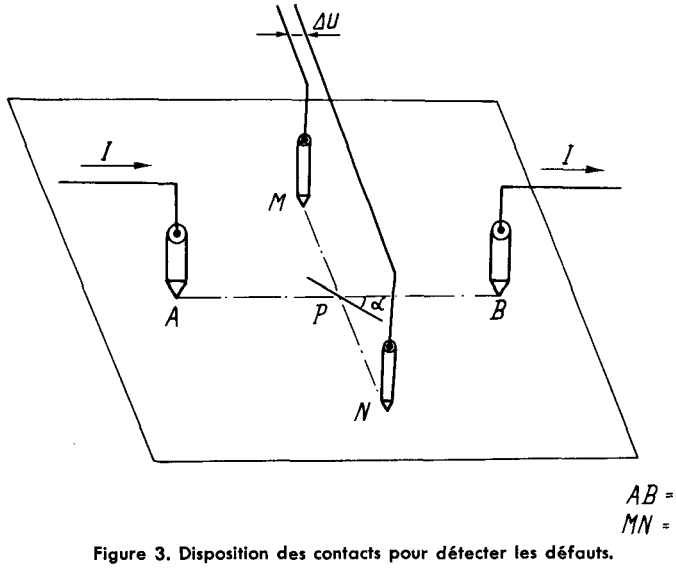

Figure 3. Disposition des contacts pour détecter les défauts.

Considérant ce dernier cas, si les dimensions de la pièce mesurée, dans le plan où l'on place le dispositif, sont beaucoup plus grandes que 1 et c et si le matériel est homogène et isotrope—pour tout courant I, introduit dans le matériel à l'aide du dispositif, —la tension qui apparaît entre les points M et N doit être nulle.

Mais si, dans la zone considérée, il y a une non-homogénéité non symétrique par rapport à l'axe A — B, on peut détecter une tension ΔU qui apparaît entre les points M et N, tension qui est d'autant plus grande que les dimensions de cette non-homogénéité (fissure, pore, zone avec ρ différente) sont plus grandes et qu'elle est située plus proche de la surface de la pièce.

Maintenant, si nous considérons le cas d'une fissure ayant la forme d'un demi-cercle de rayon r, petit par rapport aux dimensions 1 et c, cette fissure étant localisée dans le point P, et orientée perpendiculairement sur le plan de la surface de la pièce et inclinée avec l'angle α par rapport à l'axe AB, — un calcul approximatif (4) fournit pour ΔU l'expression suivante:

$$\Delta U = \frac{8\rho\, I r^3}{\pi l^2 c^2} \sin 2\alpha \qquad (4)$$

Lorsque le matériel est anisotrope, et le dispositif à mesurer est placé dans le plan perpendiculaire à la direction de pressage, alors, dans les mêmes conditions, la valeur de ΔU est donnée par la relation:

$$\Delta U = \frac{8\sqrt{\rho_1\rho_2}\, I r^3}{\pi l^2 c^2} \sin 2\alpha \qquad (5)$$

Si le dispositif est situé dans un plan parallèle à la direction du pressage et l'axe AB incliné avec l'angle φ par rapport à cette direction, alors, même si le matériel est homogène, une tension apparaît qui peut être exprimée, d'après (4), par la relation:

$$\Delta U' = \frac{I\sqrt{\rho_1\rho_2}}{\pi}\left[\frac{1}{\sqrt{\left(\frac{1}{2}\sin\varphi - \frac{c}{2}\cos\varphi\right)^2 + \frac{\rho_2}{\rho_1}\left(\frac{1}{2}\cos\varphi + \frac{c}{2}\sin\varphi\right)^2}} - \frac{1}{\sqrt{\left(\frac{1}{2}\sin\varphi + \frac{c}{2}\cos\varphi\right)^2 + \frac{\rho_2}{\rho_1}\left(\frac{1}{2}\cos\varphi - \frac{c}{2}\sin\varphi\right)^2}}\right] \qquad (6)$$

On peut encore écrire cette relation de la forme suivante:

$$\Delta U' = \frac{1}{\pi}\sqrt{\rho_1\rho_2}\, k_1 \qquad (7)$$

ou

$$k_1 = \frac{1}{\sqrt{\left(\frac{1}{2}\sin\varphi - \frac{c}{2}\cos\varphi\right)^2 + \frac{\rho_2}{\rho_1}\left(\frac{1}{2}\cos\varphi + \frac{c}{2}\sin\varphi\right)^2}} - \frac{1}{\sqrt{\left(\frac{1}{2}\sin\varphi + \frac{c}{2}\cos\varphi\right)^2 + \frac{\rho_2}{\rho_1}\left(\frac{1}{2}\cos\varphi - \frac{c}{2}\sin\varphi\right)^2}} \qquad (8)$$

L'expression K_1 peut se présenter sous la forme d'une famille de courbes, pour des valeurs données de 1 et c, en fonction de l'angle φ, ayant comme paramètre le rapport

$$\frac{\rho_2}{\rho_1}$$

ainsi comme nous l'avons représenté sur la figure 4.

Dans ces conditions, la tension produite entre les points M et N, à cause de la fissure demi-circulaire située en P (4) sera donnée par l'expression:

$$\Delta U'' = \frac{8I\sqrt{\rho_1\rho_2\, r^3}\sin 2\alpha}{\pi l^2 c^2\left[\cos^2(\varphi+\alpha) + \frac{\rho_1}{\rho_2}\sin^2(\varphi+\alpha)\right]} \cdot \frac{1}{\left(\sqrt{\sin^2\psi + \frac{\rho_2}{\rho_1}\cos^2\psi}\right)^3} \qquad (9)$$

Dans le but d'éliminer l'influence de $\Delta U'$ sur le dispositif à mesurer, on peut utiliser un montage de compensation impliquant un galvanomètre spécial, où l'on cherche à placer l'axe AB du dispositif parallèlement ou perpendiculairement à la direction de pressage pour que $\Delta U' = 0$ (voir fig. 4).

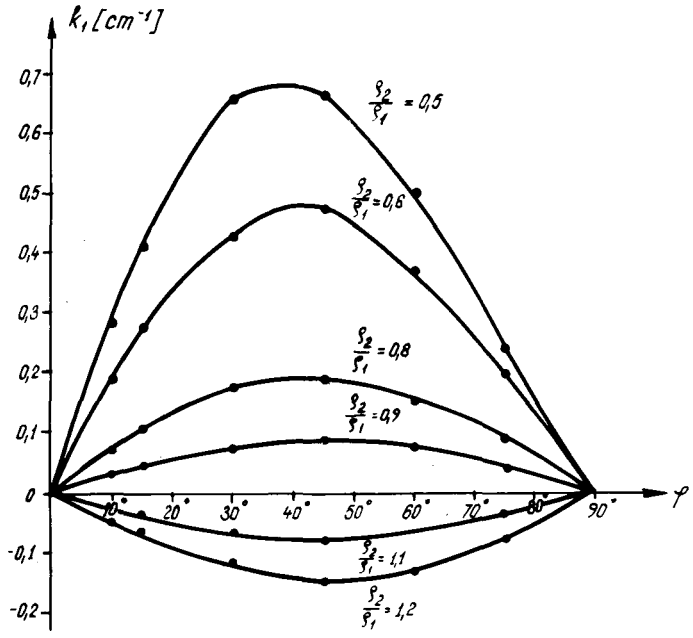

Figure 4. Variation de k_1, en fonction de ϕ, pour différents $\frac{\rho_2}{\rho_1}$.

Comme il est difficile de réaliser cette condition, en pratique, les fissures éventuelles qui pourraient exister dans le matériel et qui sont orientées le long d'une des deux directions ci-dessus mentionnées, pourraient rester non identifiées. On a donc décidé pour nos mesures sur le graphite, d'effectuer les essais dans le plan perpendiculaire à la direction de pressage, pour augmenter la précision de la méthode. Ce cas implique la condition que la plus petite dimension des pièces en graphite soumises au contrôle soit orientée dans le sens du pressage. Il en ressort donc qu'il est nécessaire de tenir compte de cette condition dans le procédé de mise en form des pièces en graphite.

La valeur minimum du rayon de la fissure demi-circulaire superficielle qui peut être détectée sur les pièces en graphite étudiées ressort de la relation (5):

$$r = \sqrt[3]{\frac{\pi l^2 c^2 \Delta U}{8 \sqrt{\rho_1 \rho_2}\, I}} \tag{10}$$

et, considérant les valeurs: $\alpha = 45°$; $\rho_1 = 1{,}78 \times 10^{-3}\ \Omega$ cm $\rho_2 = 44 \times 10^{-3}$ Ωcm; $\Delta U_{min} = 2\mu V$; $l = 0{,}9$ cm; $c = 0{,}5$ cm; $I = 5A$

on trouve finalement:

$$r_{min} \simeq 0{,}27 \text{ mm}$$

L'effet perturbateur des fissures existant dans le matériel sur la symétrie du champ électrique vers l'axe AB du dispositif, décroît d'autant plus que les fissures se trouvent localisées plus profondément dans l'intérieur de la pièce.

Ainsi, une fissure de forme circulaire (considerée ici pour simplifier les calculs), située à la prodondeur a, et dont le plan est incliné avec l'angle α par rapport à l'axe AB, produit,—lorsque le dispositif de mesure est situé dans le plan perpendiculaire à la direction de pressage,—une tension entre les points M et N (4), donnée par l'expression:

$$\Delta U = \frac{r^3\, lc \sqrt{\rho_1 \rho_2}\, I \sin 2\alpha}{8\pi \left(\sqrt{\frac{l^2}{4} + \frac{\rho_2}{\rho_1} a^2} \right)^3 \left(\sqrt{\frac{c^2}{4} + a^2} \right)^3} \tag{11}$$

La valeur minimale du rayon de la fissure détectable est, dans ce cas:

$$r = \sqrt[3]{\frac{\pi l^2 c^2 \Delta U}{8 \sqrt{\rho_1 \rho_2}\, I}}\, k_2 \tag{12}$$

ou:

$$k_2 = \sqrt{\left(1 + 4 \frac{\rho_2}{\rho_1} \frac{a^2}{l^2}\right) \left(1 + 4 \frac{a^2}{c^2}\right)} \tag{13}$$

La figure 5 représente la variation de k_2 en fonction de la profondeur a, pour $l = 0{,}9$ cm, $c = 0{,}5$ cm et

$$\frac{\rho_2}{\rho_1}$$

compris entre 0,6 et 1.

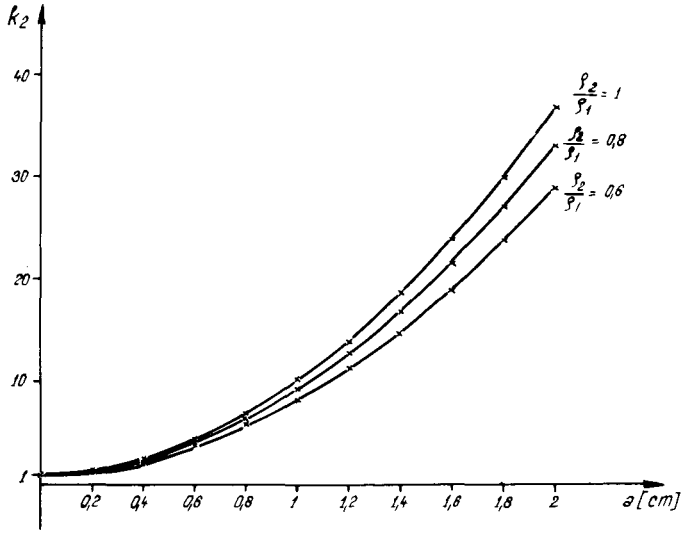

Figure 5. Variation de k_2, en fonction de la profondeur, pour différents $\frac{\rho_2}{\rho_1}$.

On constate que le rayon minimum de la fissure détectable croît relativement vite avec la profondeur, et peut atteindre, —dans les conditions exposées, des valeurs jusqu'à neuf fois plus grandes, pour une profondeur d'approximativement 1 cm. Il en ressort donc que pour avoir une efficacité suffisante, la méthode ne peut être utilisée que sur des pièces dont l'épaisseur est relativement petite. Dans le cas de notre dispositif l'épaisseur doit être au-dessous de 1,5 cm. En tenant compte qu'on fait le contrôle sur les deux surfaces parallèles, il en ressort que la profondeur que nous devons considérer sera réduite à la moitié et par conséquent le rayon minimum de la fissure détectable sera 1,4 mm, pour a = 0,75 cm.

Il faut remarquer aussi, le fait que les dimensions de la fissure minimum détectable dépendent de $(\rho l)^{-\frac{1}{3}}$, tandis que le pouvoir dissipé aux contacts A et B croît avec ρI^2, fait qui démontre que la méthode est d'autant plus précise que le matériel a une resistivité plus grande.

La précision des relations (4) (5) (9) (10) (11) et (12) décroît lorsque les dimensions du défaut augmentent et que sa forme s'éloigne trop de celle d'un cercle. Mais, il est évident que la valeur de la différence de potentiel entre les points M et N, croît au fur

et à mesure que la grandeur du défaut augmente. On peut donc établir une corrélation entre ΔU et le degré d'homogénéité du matériel, en spécifiant qu'il s'agit d'un dispositif à mesurer ayant certaines dimensions, lequel est utilisé pour un courant donné I.

On peut aussi établir pour une certaine utilisation, un seuil déterminé ΔU_0, au-dessous duquel la pièce contrôlée peut être considérée conforme aux conditions techniques. La méthode que nous avons décrite est facile à appliquer et est plus sensible dans le cas du graphite, que la méthode fondée sur l'utilisation des ultra-sons.

Les essais que nous avons faits à l'aide des ondes ultra-sonores ont montré qu'avec le graphite, comme dans la majorité des matériaux poreux, l'absorption d'énergie est très importante (5), et par conséquent on ne peut utiliser que les méthodes de transmission. Ces dernières sont toutefois moins précises que les méthodes de réflexion et impliquent une interprétation plus compliquée des données expérimentales.

Les déterminations que nous avons faites sur le graphite en utilisant la méthode de transmission directe, nous ont permis de détecter les défauts de grandes dimensions ayant des sections qui dépassaient 1–2 cm^2. Les données expérimentales étaient incertaines dans le cas des défauts plus petits. Le dispositif avec les quatre contacts disposés en croix, décrit ci-dessus, ayant $l = 0{,}9$ cm, $c = 0{,}5$ cm pour $I = 1$ A, conduit à l'apparition de tensions de l'ordre des millivolts pour des défauts de l'ordre de 1 cm^2, c'est-à-dire des tensions 10^3 fois plus grandes que celles correspondant aux défauts minimes détectables de l'ordre de 0,1 mm^2.

Conclusions

La valeur de la résistivité globale d'une pièce fabriquée à partir d'un matériel conducteur peut servir pour apprécier l'homogénéité d'une série complète de pièces, élaborées de la même façon.

La mesure de ce paramètre peut être réalisée avec précision et rapidité à l'aide du dispositif décrit ci-dessus (fig. 1), lequel est adaptable à toutes sortes de pièces ayant une forme régulière.

Les non-homogénéités locales macroscopiques peuvent être détectées par la mesure locale de la résistivité, mesure qui devient très utile, dans le cas des matériaux anisotropes, pour la détermination du tenseur $\overline{\rho}$.

Utilisant un dispositif approprié, aux quatre contacts disposés en croix (fig. 3), nous avons élaboré une méthode sensible pour mettre en évidence les défauts macroscopiques situés près de la surface des pièces contrôlées, méthode d'autant plus exacte et sensible que le matériel a une résistivité plus grande.

Dans le cas du graphite nucléaire que nous avons étudié, cette méthode s'est révélée plus avantageuse au point de vue sensibilité, que les méthodes qui utilisent les ultra-sons, mais elle impose deux conditions, notamment: l'épaisseur des pièces contrôlées ne doit pas être trop grande et aussi, dans le cas d'un matériel anisotrope, les dimensions les plus grandes des pièces doivent être situées dans les plans perpendiculaires à la direction de pressage.

La présente étude contient des données expérimentales obtenues pour le graphite nucléaire. Des travaux sont en cours pour appliquer ces méthodes au contrôle d'autres matériaux conducteurs.

Bibliographie

1. van der Pauw. L. J. *Revue technique Philips,* 20,8, 234
2. Nuclear Graphite sur l'édition de R. E. Nightingale, Academic Press, New-York, London, 1962.
3. Andreescu, N. Une méthode de mesure de la conductibilité électrique des conducteurs massifs, isotropes et anisotropes; en cours de parution.
4. Andreescu, N. Calcul des perturbations dans le champ électrique, en régime électrocinétique produits par les fissures d'un conducteur massif; en cours de parution.
5. Făcăoaru, I., Negoitã, C. et Bernath, A. Măsurări si control cu ultrasunete. *Ed. Technicã,* Bucuresti, 1965.

The Mill Inspection of Steel Pipe at 2150°F

MERRILL M. GODSHALL, ROY A. NANCE and JOHN W. ALLEN, U.S.A.

ABSTRACT: A breakthrough has been made in the eddy-current inspection of materials at elevated temperatures. A new inspection technique is described which permits an eddy-current encircling coil inspection technique to be used on steel pipe at temperatures of up to 2150° F.* Data is included indicating that the test obtained is approximately the same as would be attained at room temperature using magnetic saturation eddy-current inspection techniques. The development of this technique is discussed along with the many advantages it offers.

Introduction

Eddy-current testing is one of the major nondestructive testing techniques used in industry today. Although first mentioned in technical papers in 1879 it was not used in industry until the early 1930s. Within the past decade it has become a primary inspection tool of the pipe and tubing industry. One of its major advantages is its ability to perform 100% inspection at high rates of speed.

This paper presents a new technique developed for the inspection of pipe at very high product temperatures. This permits product inspection during manufacture instead of waiting for room-temperature testing. Thus faulty material or manufacturing procedure can be detected in time to prevent a faulty product from being manufactured in quantity.

* Patent applied for.

The theory, operational requirements, and equipment design for the inspection of ferromagnetic materials at very high temperatures are discussed, and test results of prototype installation on a butt-weld pipe mill are presented. Although test results using these techniques have been to date limited to steel pipe, it is the opinion of the authors that they may be applied successfully to several other high-temperature inspection problems.

Eddy-Current Test Principles

Eddy currents are induced ac currents that flow in a metal part, and are produced by a changing magnetic field. The currents are not the same in all sections of the part, owing to the thickness and/or shape of the metal part, and the rate of change of the magnetic flux. The basic principle involves Ampere's law, $H = I/2\pi R$, i.e., there is a magnetic field strength associated with a current flow through a wire or coil. If a piece of metal is brought into the field of this flux, Faraday's law of electromagnetic induction states that there will be a voltage induced in the metal, $E = -Nd\theta/dt$. This induced voltage causes a current flow in the metal part, and the current is called an eddy current because it flows in a closed path. The eddy-current flow has a magnetic flux associated with it which opposes the flux that

produced it; this opposing flux reduces the initial current in the exciting coil.

From the above it is seen that there is electromagnetic energy transmitted into the metal. Part of this energy is dissipated into heat by the metal's resistance and some is reflected back to the coil. It is possible to monitor the coil's impedance and measure the effects of a piece of metal in the proximity of a coil. It is also possible to resolve the difference in impedance between a coil in air and the same coil near a piece of metal, or to distinguish the difference between a section of pipe with flaws and one without flaws.

The effectiveness of eddy currents in detecting flaws depends largely on the disruption of their flow by the flaw. The flow of eddy currents in a metal part is determined by the following factors:

(1) *Frequency of the exciting field.* This has an appreciable effect upon the depth of penetration of the eddy currents. As the test frequency increases the depth of penetration of the eddy currents decreases (commonly referred to as the skin effect).

(2) *Characteristics of the exciting field.* The shape and power level of the field affect both the orientation and magnitude of the eddy currents.

(3) *Electrical conductivity of the metal part.* The higher the conductivity, the more eddy-current flow that will be induced in the part.

(4) *Magnetic permeability of the metal part.* As this increases, the total eddy-current flow increases, and the depth of penetration of the eddy currents decreases.

(5) *Dimensions of the metal part.* Volume and shape of the metal part in the field of the test coil is a determining factor in the result of eddy-current flow.

(6) *Location of the part in the exciting field.* In general a high sensitivity is obtained as the test coil is brought closer to the test part.

(7) *Presence of discontinuities.* A crack, porosity, etc., within the metal part will disrupt the eddy-current flow pattern.

Figure 1 illustrates a piece of pipe passing through an eddy-current test coil. The change in eddy-current flow in a pipe which occurs when the defective area passes through the test coil will produce a change in the impedance of the test coil, which, when properly processed in the eddy-current instrumentation, will present an indication on a strip-chart recorder.

Figure 2 illustrates the inspection of a pipe in which the eddy-current flow patterns around a discontinuity such as a crack are shown.

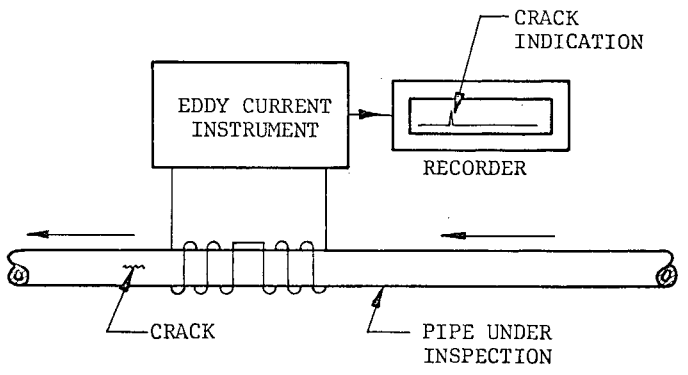

Figure 1. Eddy-current testing of pipe, using an encircling coil.

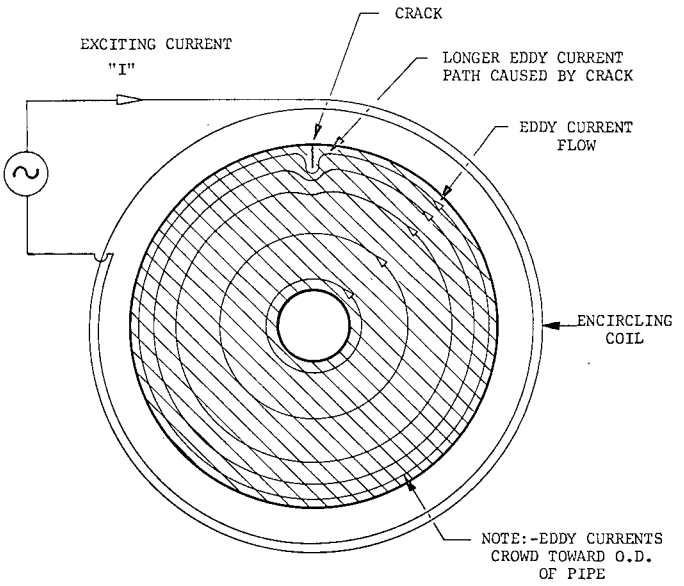

Figure 2. Heavy wall pipe section test using an encircling coil technique.

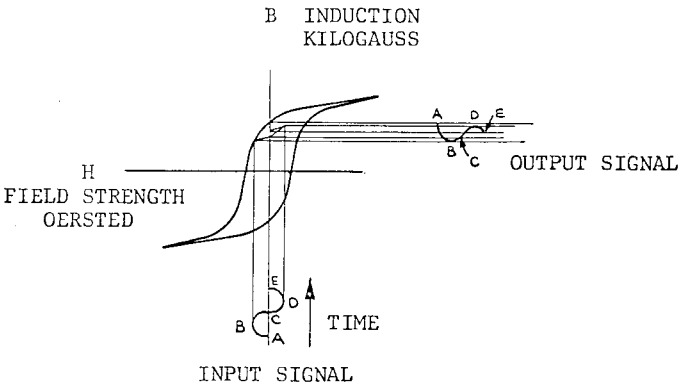

Figure 3. Unsaturated transfer characteristic.

Eddy-Current Inspection of Steel Pipe

The presence of relative permeabilities greater than unity in ferromagnetic materials presents two major problems in the inspection of such items:

(1) The presence of high permeability drastically reduces the depth of penetration of the eddy currents and prevents more than a superficial surface inspection.

(2) The internal stresses within the ferromagnetic part tend to be nonuniform producing great variations in the magnetic permeability of the part. Since the eddy current instrumentation is sensitive to changes which occur as the part being tested passes through the test coil, these permeability variations normally produce eddy-current signals which obscure any flaw information which is present. One method which has been used to eliminate this problem is the use of a strong dc field in the vicinity of the test coil. This provides magnetic saturation of the part and effectively reduces the permeability to unity.

Figures 3 and 4 show typical B-H curves for ferromagnetic materials and illustrate the transfer characteristics of the eddy-current signals as a function of permeability. There are many other types of transfer characteristics related to hysteresis loops but Figures 3 and 4 show one simple example.

It should be noted that distortion is present due to the nonlinearity of the hysteresis loop. The output signal is reduced considerably in Figure 4 as well as the distortion. This signal loss is compensated for by using increased instrument gain. The

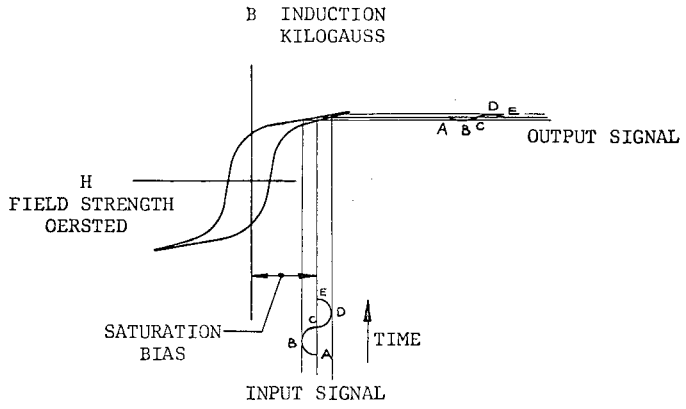

Figure 4. Saturated transfer characteristic.

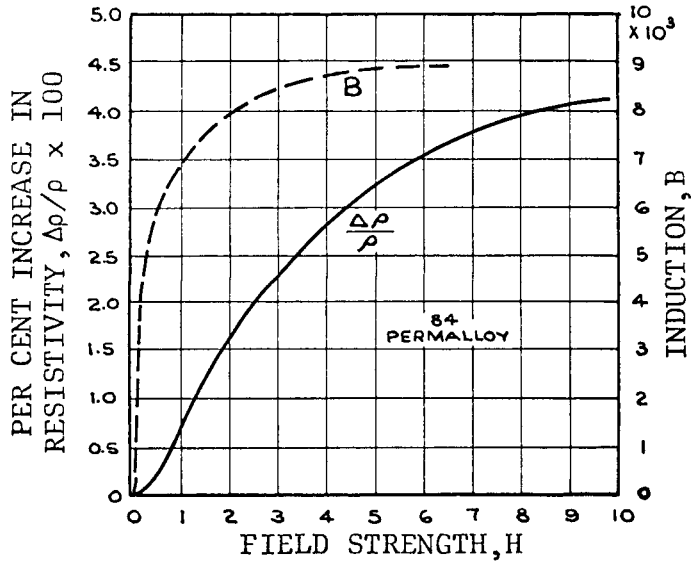

Figure 5. Resistivity vs. field strength.

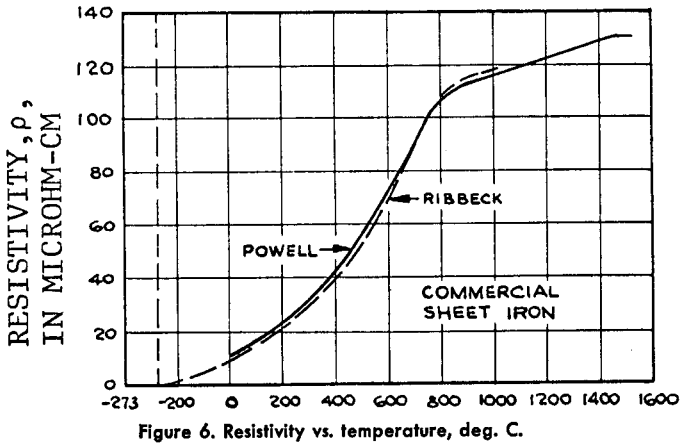

Figure 6. Resistivity vs. temperature, deg. C.

signal field strength and the saturation field strength are shown out of scale for purposes of illustration.

A secondary factor associated with high field strengths is an increase in resistivity* of the part as shown in Figure 5. This has the effect of increasing the depth of eddy currents in the metal by a factor of 2.

* R. M. Bozorth, Ferro-magnetism, D. Van Nostrand Company, New York, N.Y., 1951, pp. 55, 715, 726, 746.

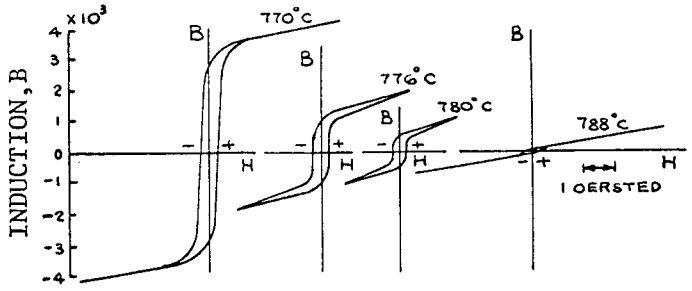

Figure 7. Hysteresis loops vs. temperature.

Inspection of Ferromagnetic Materials at Elevated Temperatures

By raising the temperature of the material being inspected above the Curie point, which is approximately 1400°F for low-carbon steel, it is possible to reduce the permeability to unity.

Figures 6 and 7 illustrate the effects of increasing temperature on both the resistivity and the hysteresis loop for ferromagnetic materials. Figure 8 shows a theoretical transfer characteristic above the Curie point, illustrating that the transfer

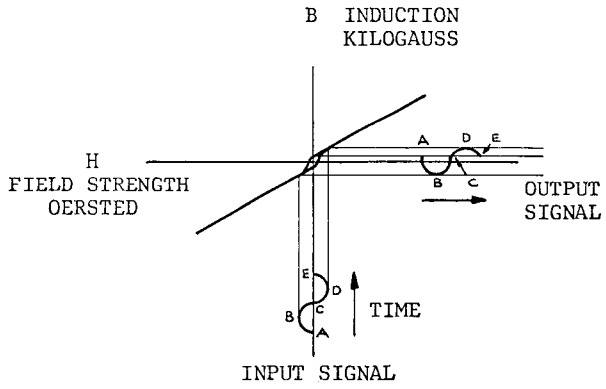

Figure 8. Transfer characteristic above the Curie point.

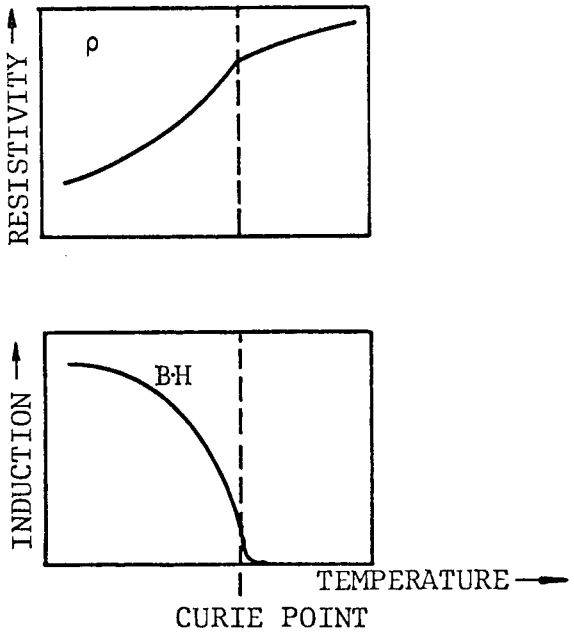

Figure 9. Resistivity, induction vs. temperature.

characteristic is essentially unity. The depth of penetration of the eddy currents is also increased due to the decrease in resistivity indicated in Figure 6. This is desirable in most instances since it provides better detection for defects on the interior of the pipe. Figure 9 illustrates the variations of both induction and resistivity with temperature.

By taking advantage of the physical characteristics of material being tested above the Curie point it is possible to inspect the product before handling marks have been introduced. It also eliminates the need for demagnetizing the product after a cold test using saturation techniques, and in addition permits an inspection early in the process, thereby eliminating manufacturing faults that would not normally be found until the part is tested after cooling.

The remainder of this paper describes a practical example of this inspection technique on a butt weld rolling mill where the temperature at the test station was 2150°F.

Designing Equipment to Work at High Temperatures

The basic eddy-current pipe inspection equipment involves a sensing coil, an eddy-current test instrument, an appropriate marking system, an alarm system, and recorder for permanent records. These are shown in Figure 1, except for the defect marking device.

In the design of a hot-pipe system (Figure 11), the instrumentation, which was a standard Budd Company Instruments Division RADAC* Model 440 with alarms, and the Budd Instruments Model 1023 Recorder, was remote from the hot pipe. This was done by using a specially designed high-temperature cable rated to 1000° F, sufficient to keep the cable at least 6 ft away from the hot pipe. It was connected to the test coil assembly in an externally water-cooled conduit.

Test Coil

The first problem was to design a test coil to work continuously at the elevated temperature. The windings must be maintained at their lower rated temperature. This was achieved by designing with the following considerations:

(1) A large annular spacing was used between the pipe and inside diameter of the coil to keep the heat transfer from pipe to coil at a minimum; (2) The coil was enclosed in a sealed weldment; (3) A cooling system was provided within the coil housing; (4) External water was applied for surface cooling.

Metal used for the test-coil housing had a hign electrical resistivity and was capable of operating at 2100° F. SS-310 has a resistivity of greater than 70 μΩ–cm, and can withstand 2100°F. Normally this temperature will be lower due to the

* Registered.

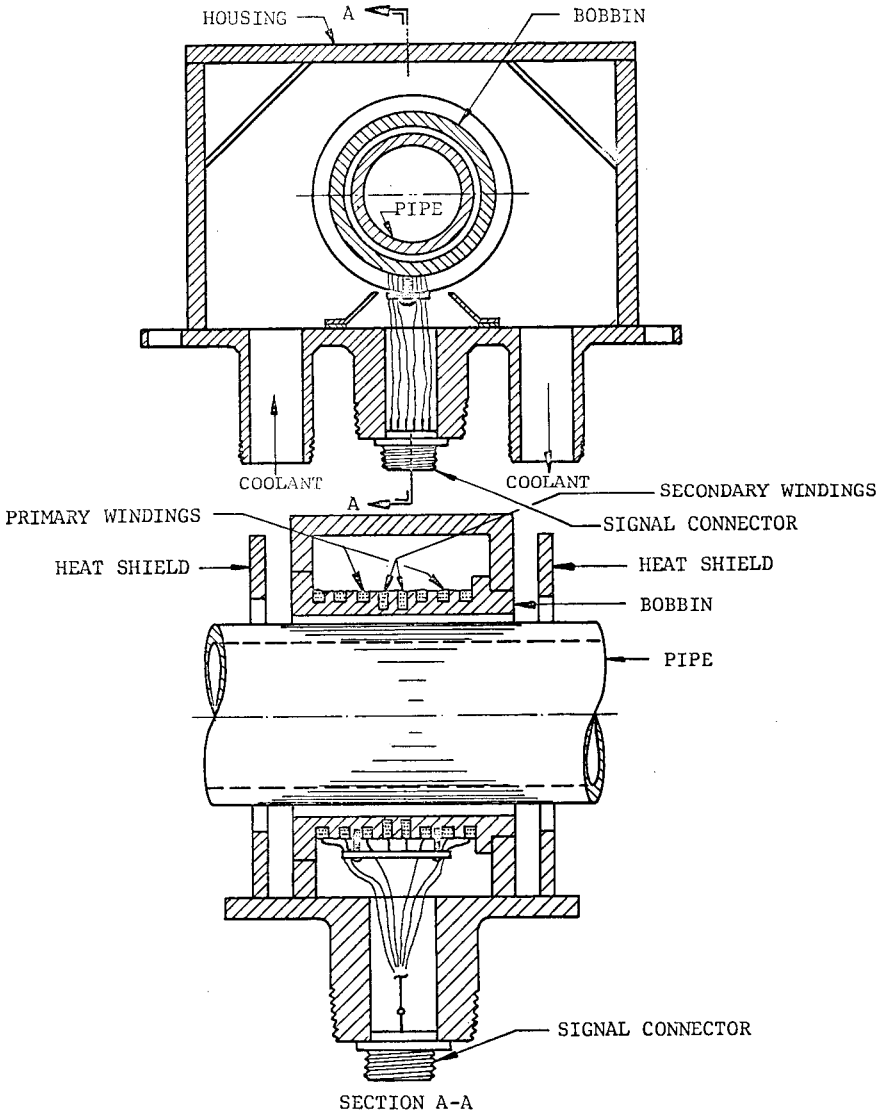

Figure 10
High-temperature test coil sections.

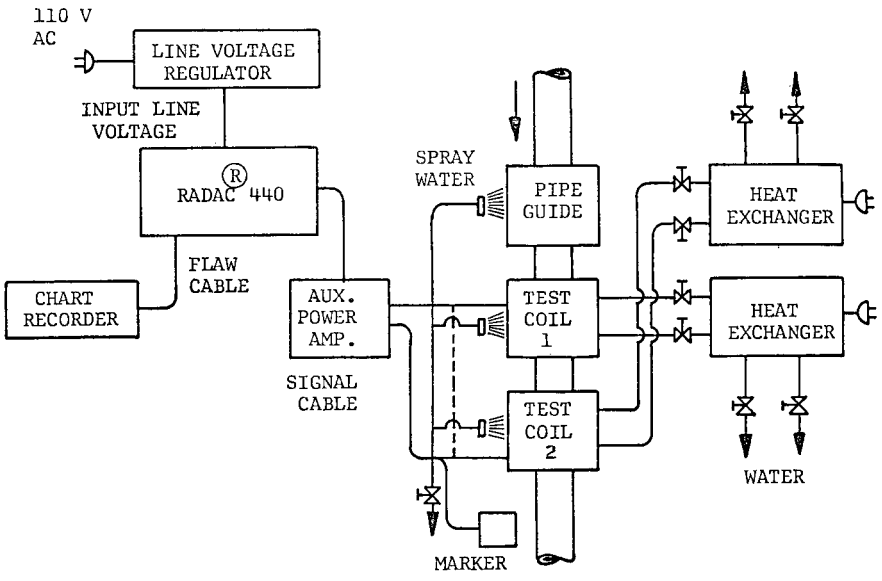

Figure 11
High-temperature block diagram.

water cooling. A bobbin was wound for the primary and secondary as shown in Figure 10. The flanges were to provide high thermal conductivity from the coil. The coil windings were coated with a high-temperature ceramic cement.

Test Coil Assembly

The test-coil assembly comprised two high-temperature test coils; one with $\frac{1}{8}$-in.-dia clearance, and the other with $\frac{1}{4}$-in.-dia clearance. These units were mounted on a common centreline on a baseplate. A conical guide was placed in front of the test coils with an opening slightly smaller in diameter than the test coil I.D. to protect the test coils during initial threading of the mill. The baseplate in turn was mounted to a bracket which had been mounted in the production line. This mounting permitted the quick removal of the test coil from the line when the mill was changed to produce different diameters of pipe.

The test-coil facility was installed in such a location as to satisfy the following mechanical considerations:

(1) The cutoff saw (downstream from the inspection station) caused no excessive pipe vibration that would produce extraneous eddy-current signals; (2) A means of initially threading pipe through the test coil was provided; (3) The sizing rollers held the pipe dimensions constant; (4) The droop between the rollers was negligible and constant; (5) The pipe centring was held constant by the sizing rollers; (6) Flaking (the breaking off of a fragment of the weld) on the weld was solved using a water spray. Stripping the skelp may be necessary in some cases; (7) Interchangeable coil sizes within a specific period of time (1 hour).

Test Coil Cooling

The stainless steel test coils each had pipes extending 1 ft through the main baseplate of the mill to allow oil line and coil cable connections at a protected point, Figure 13. The coils were cooled by separate oil cooler assemblies filled with special interpeen PPO oil coolant. Water was piped through the coolers in the usual manner. Additional cooling for each coil and the guide block was provided by a $\frac{3}{4}$-in.-dia water line flowing down on the top of each of them. The main baseplate had two vertical $\frac{1}{2}$-in. water lines (one on each side at the top), plus an array of 16 pin-holes in a water manifold falling across the entire top of the baseplate. The purpose of the water on the main baseplate was to maintain good dimensional stability at high temperature.

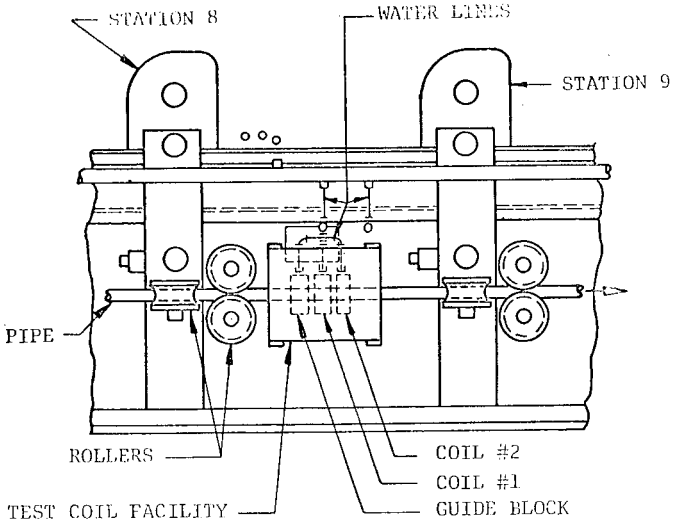

Figure 12. Test coil facility on pipe mill.

Other Equipment

The standard Budd Company Instruments Division Auxiliary Power Amplifier was used with the RADAC 440. Installed immediately following the test coil along the pipe line toward station 9, a solenoidal high-temperature marking facility was installed to mark the defects in the pipe, similar to the marking methods used at low temperatures.

Operations

Figure 14 shows the operation at 220 fpm at 2150°F. Neither the speed nor the temperature produced excessive noise signals.

Operation Results

The system was in the line continuously for 45 hours (a complete lot of that pipe size). It was operated for 16 hours and displayed alarm signals (caused by flaw signals that exceed a predetermined threshold level) for end welds at 9 position. These sensitivity positions are adjustable from 1 to 21 with 6 db (2:1) gain per step. This is the same sensitivity position required to find end welds as in the "cold" inspection system with $\frac{1}{4}$-in.-dia clearance coils. A "cold" system test refers to a room temperature test using the saturation coil technique. This proves beyond doubt the feasibility at this point, since the baseline of the

recorder was "clean" between end welds. It indicated defects such as laminations, "slag in the welds" at 14 position, and obvious differences in the weld from 9 to 15 position. The noise level of the recorder on good pieces of weld was "clean" (absence of any spurious signals) at 16 position. The instrument occasionally would indicate noise from a particular piece of questionable skelp at 9 position.

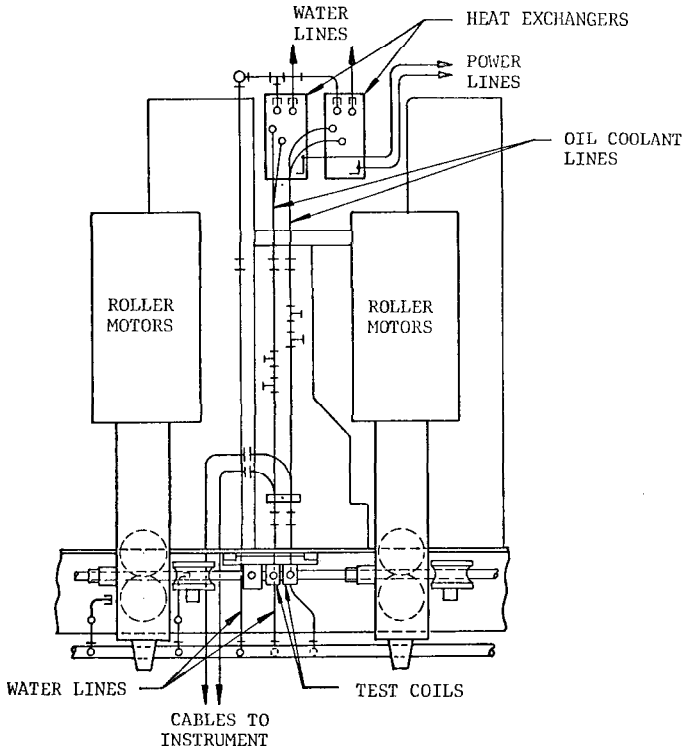

Figure 13. Test coil cooling, top view.

Defect Marking

One of the major problems in correlating the eddy-current information with an actual defect is the difficulty in making a durable mark on the pipe at high temperatures. Several techniques have been tried including the use of hot chalk or a gouge in the pipe in the area of the defect. The hot chalk burns off and the mechanical gouging destroys the pipe and prevents further eddy-current testing. Finally a flame spray metallizing technique using aluminum rod melted in an acetylene flame and sprayed onto the hot pipe was developed and provided a reasonably good mark detectable on the cooling racks. This technique appears satisfactory providing no further diameter reduction is encountered after the marking operation.

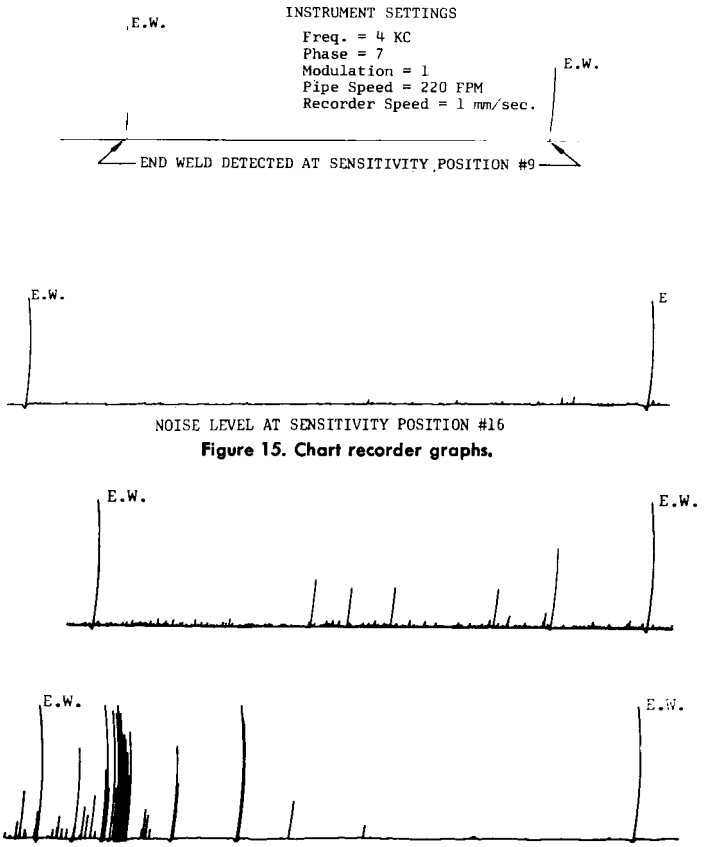

Figure 15. Chart recorder graphs.

Figure 16. Defects detected at sensitivity position No. 13.

Conclusions

1. The facility for prolonged testing of pipe at 2150° F has been demonstrated mechanically and electrically. The possibility of coil damage is no greater than in any other high-speed pipe mill operation.

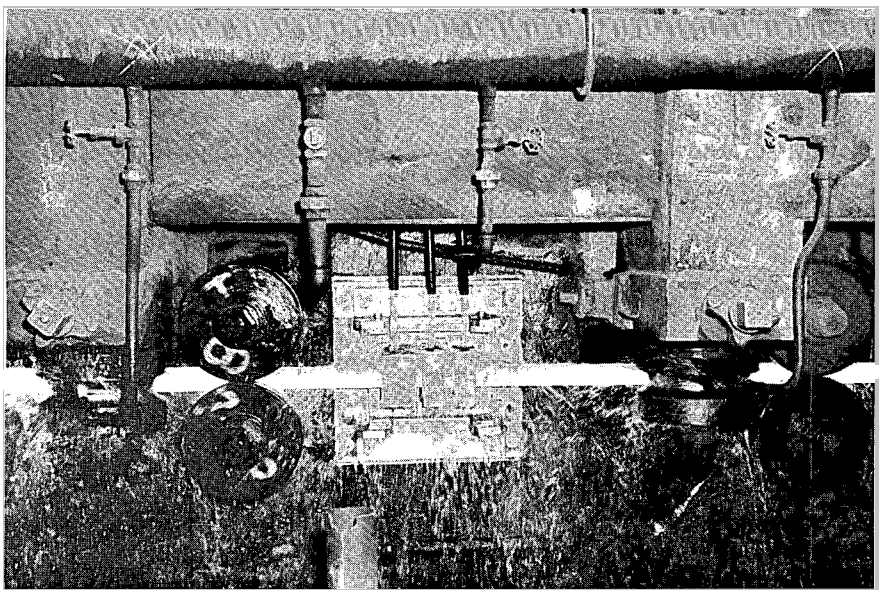

Figure 14
Hot pipe test on mill.

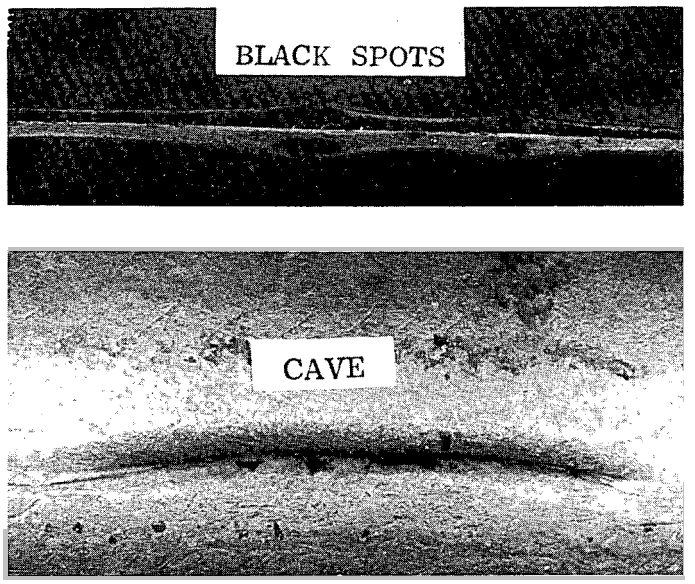

Figure 17. Black spots and caves detected by eddy currents at 2150°F.

2. The defect sensitivity appears satisfactory. (See chart recordings, Figures 15 and 16.) End welds are detected at sensitivity position 9 with the background noise at least 40 db below this level, except in cases of questionable skelp. These results are based on an initial test coil position adjustment. There is strong reason to believe that with better test coil positioning an even better defect-signal-to-noise-signal ratio is possible. It should be noted that there were no gross defect signals since the mill was running "good" pipe. Improved defect correlation requires, as with any other installation, time and experience.

3. Figure 17 shows photographs of the "black spots" and "caves" detected by the system at 2150° F.

4. Slight mechanical design improvement could be made to improve the unit as a production unit as a result of this installation.

5. The disassembly time was 1 hour for a size change. This is approximately the time that was allotted between normal size changes.

6. The general type and location of defects that this system under the foregoing conditions has detected, or could detect, are given in Table 2.

7. In spite of the marking difficulties this inspection technique can be extremely useful on a mill to prevent the manufacture of many tons of faulty pipe prior to its detection after cooling.

Acknowledgments

Thanks are expressed to the following for their support on this project:

R. Dahlberg, Ass't. Quality Control Superintendent, Youngstown Sheet & Tube Co., East Chicago, Ind., and J. Koneski, Applications Engineering, The Budd Company, Instruments Division, Phoenixville, Pa.

	"Cold" pipe test results	Hot pipe test results
Pipe speed	220 FPM	220 FPM
Pipe clearance	¼"	¼"
Frequency	4 KC	4 KC
Phase	6	6
Modulation	1	1
Defect—Endweld*	Sensitivity 9	9
Defect—Caves*	Sensitivity 18	?
Defect—Opens*	Sensitivity 18	?
Defect—Leakers*	Sensitivity 18	?
Defect—Slag*	Sensitivity —	14
*Gross type defects		

Table 2

Type and Location of Defects

Defect location	Defect type			
	Open weld	Lami-nations	Caves (inden-tation)	Slag in weld
O.D. 1"-4"	X	X	X	X
I.D.	⊗	?	?	⊗
Wall thickness .050"-.250"	—	—	—	—

Legend:
X Has
⊗ Could
? Maybe

Computer Design of Eddy-Current Tests

C. V. DODD and W. E. DEEDS,* U.S.A.

ABSTRACT: An analytical solution of eddy-current coil problems was sought in order to improve eddy-current tests. A method was developed of analyzing the physical properties of an eddy-current coil with the help of a large digital computer. These physical properties include eddy-current coil impedance, actual eddy-current distribution in the sample (and hence the sensitivity to small defects), and the induced voltages in various "pickup" coils. The technique has been applied to several specific cases, including a coil above a conducting plane, the same coil with a ferrite cup above a conducting plane, and a coil encircling a rod. This technique gives both further physical insight into and actual numerical results of eddy-current tests.

List of Symbols

Symbol	Name	MKS Units
A	Vector potential	*weber* metre
A_D	Vector potential at a defect	*weber* metre
A_R	Vector potential at the defect relative to the average value at the coil in air	
a	Distance between lattice points	metre
I	Applied current density	*ampere* metre^2
I_o	Applied current	ampere
i	Induced current density	*ampere* metre^2
j	Square root of -1	
l	Radius of a spherical defect	metre
L	Inductance	henry
N	Number of lattice points in the coil	
n	Number of turns on the coil	
R	Mean coil radius	metre
S	Spacing between coil and sphere in coil radii	
s	Distance	metre
t	Time	second
v	Voltage	volt
Vol	Volume	metre^3
z	Impedance	ohm
ϵ	Dielectric constant	*farad* metre
μ	Permeability	*henry* metre
σ	Conductivity	*mho* metre
ω	Angular frequency	*radian* second

Introduction

The starting point of any eddy-current test is the coil which generates the eddy currents. We have developed a method (sometimes called a relaxation or iteration process) of analyzing the physical properties of an eddy-current coil with the help of a large digital computer. In particular, these physical properties include eddy-current coil impedance, actual eddy-current distribution in the sample (and hence the sensitivity to small defects), and the induced voltages in various "pickup" coils. Within the present restrictions of axial symmetry and sinusoidal driving currents, the technique can be applied to a probe coil of any size and shape, with or without ferrite. The sample may also be any size and shape, with any conductivity and permeability. The technique has been applied to several specific cases, including a coil above a conducting plane, the same coil with a ferrite cup above a conducting plane, and a coil encircling a rod.

Research sponsored by the U.S. Atomic Energy Commission under contract with the Union Carbide Corporation.

* Consultant from the University of Tennessee.

Theory and Results

The calculations begin with the differential equation for the vector potential in a conductive, isotropic, inhomogeneous medium at low frequencies (below 10 MHz)(1):

$$\nabla^2 \vec{A} = -\mu \vec{I} + \mu\sigma \frac{\vec{A}}{t} + \mu \nabla \left(\frac{1}{\mu}\right) \times (\nabla \times \vec{A}) \qquad (1)$$

We next make the assumption of axial symmetry and sinusoidal driving currents. Both these assumptions are valid for most eddy-current test problems. This allows us to reduce our vector equation to one scalar equation for the components around the axis. Also the time dependence can be represented by complex numbers. After making these assumptions and expanding the various vector quantities the equation becomes:

$$\frac{\partial^2 A}{r^2} + \frac{1}{r}\frac{\partial A}{r} + \frac{\partial^2 A}{z^2} - \frac{A}{r^2} = -\mu I + j\omega\mu\sigma A - \mu \left[\frac{}{r}\left(\frac{1}{\mu}\right)\left(\frac{1}{r}\frac{rA}{r}\right) + \frac{}{z}\left(\frac{1}{\mu}\right)\frac{A}{z}\right]. \qquad (2)$$

This is the differential equation which we must solve. It is a very difficult differential equation to solve in a closed form, and, even if we obtained a closed-form solution, we would still need some computer approximations to evaluate our closed-form functions. Therefore, we chose to use an approximate method (2) to solve problems using this equation. We first lay out the problem on a two-dimensional lattice of points, in a plane extending outward from the axis of symmetry, as shown in Figure 1. We then use finite difference calculus to approximate the various terms in our differential equation. From this, the vector potential can be determined at a point in terms of the vector potential at the four nearest neighbours. The equation is:

$$A_{r,z} = \frac{(1 + a/r)\left(\frac{\mu_{r,z}}{\mu_{r+a,z}}\right) A_{r+a,z} + A_{r-a,z} + \frac{\mu_{r,z}}{\mu_{r,z+a}} A_{r,z+a} + A_{r,z-a} + a^2 \mu_{r,z} I_{r,z}}{2 + \frac{a}{r} + \frac{a^2}{r^2} + \frac{\mu_{r,z}}{\mu_{r+a,z}} + \frac{\mu_{r,z}}{\mu_{r,z+a}} + ja^2\omega\mu_{r,z}\sigma_{r,z}} \qquad (3)$$

The various values of $\mu_{r,z}$, $\sigma_{r,z}$, and $I_{r,z}$ for each point in the lattice are stored in the computer. The vector potential at the boundary of the mesh is set equal to zero. The computer then starts through the lattice, calculating (3) the vector potential at each point in terms of the neighbouring points. After a number of runs through the entire mesh, the value of the vector potential at each point will converge to the value predicted by the differential equation. Typically it takes a 70 × 70 mesh 400 iterations to converge within 1%, at a computation cost of $200. Once the vector potential is known, any physically observable electromagnetic phenomenon may be calculated from it.

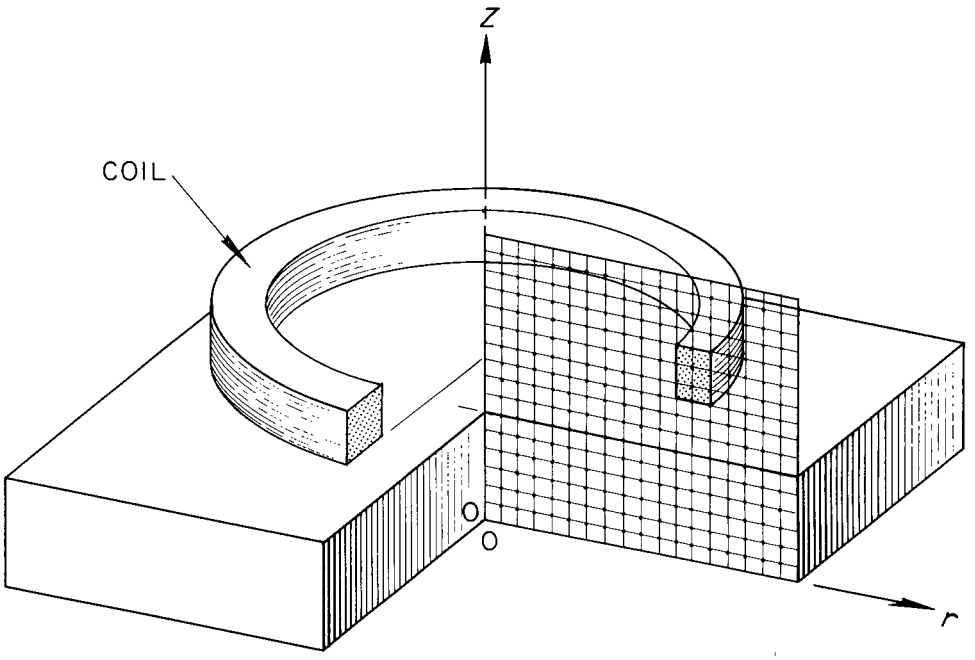

Figure 1
Layout of eddy-current coil analysis problem on a lattice of points.

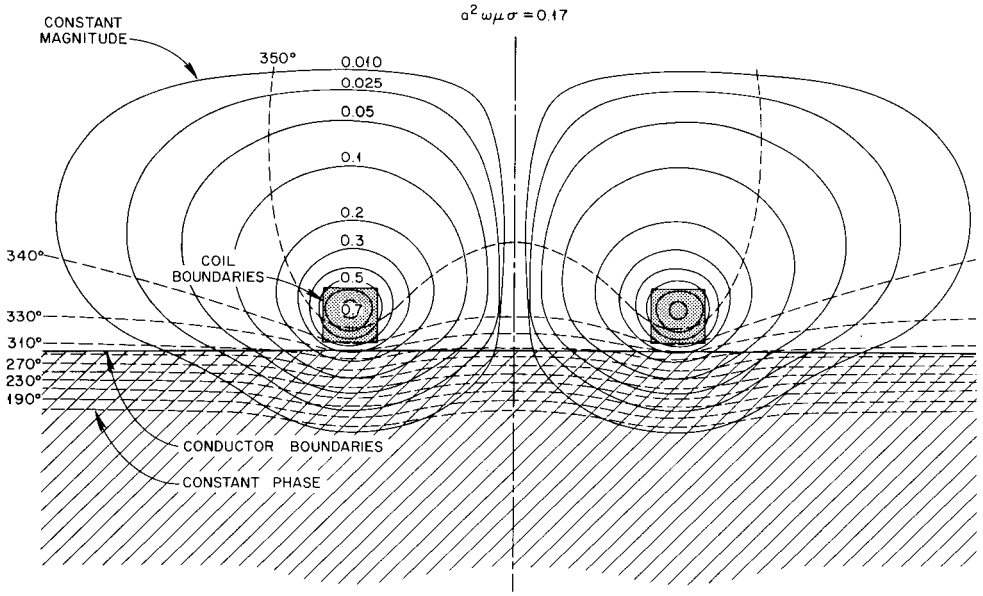

Figure 2
Coil above a conducting plane.

Figure 2 shows amplitude and phase contours of the vector potential for a square cross-section coil above a conducting plane. Note how the amplitude is attenuated and the phase is shifted by the presence of the metal. One of the properties that we can calculate from the vector potential is the induced voltage in the driving coil, given by:

$$dv = j\omega \vec{A} \cdot \vec{ds}, \tag{4}$$

or, in finite difference approximation:

$$v = j\omega a \sum_{\text{coil}} 2\pi\,(r/a)\,A_{r,z} \tag{5}$$

This same method may be applied to calculate the voltage induced in any pickup coil. It is a good approximation as long as the current density in the coil is much less than the eddy-current density in the metal. Once we know the voltage induced in the driving coil, we can calculate its impedance. The driving-coil impedance, normalized by dividing by the magnitude of driving coil impedance in air, is:

$$Z_n = \frac{j \sum_{\text{coil}} 2\pi\,(r/a)\,A_{r,z}\ \text{(with conductor present)}}{\sum_{\text{coil}} 2\pi\,(r/a)\,A_{r,z}\ \text{(with coil in air)}} . \tag{6}$$

The normalized impedance has been calculated for a number of different frequencies for a coil above a metal surface. The spacing between the coil and the surface, or the liftoff, has also been varied. For experimental confirmation the impedance was measured at different frequencies and spacings for a family of four coils of different sizes, but having the same relative dimensions. We can trade among the frequency, conductivity, and the square of the linear dimensions of the coil because they appear in our relaxation equation only as the product $a^2\omega\mu\sigma$. For example, doubling the frequency and halving the conductivity will still provide the same product. Figure 3 shows how the measured and calculated impedances agree. The accuracy of the measured values is rather poor in the low-frequency region and better in the higher frequency regions. The calculated values had some inaccuracy along the spacing

direction (along lines of constant $R^2\omega\mu\sigma$). This is due to the fact that impedance as affected so strongly by liftoff and this method of calculation does not define the precise location of the coil and the metal. The error is always less than one lattice space. The agreement in values of $R^2\omega\mu\sigma$ is quite good for the higher frequencies.

The coil inductance may be calculated by the relation:

$$L = \left(\frac{n}{N}\right)^2 a\mu \sum_{\text{coil}} 2\pi\,(r/a)\,A_{r,z}\,/\mu I_o \quad . \tag{7}$$

The values of the coil inductance calculated in this way were approximately 2% lower than the measured values. This is probably due to the fact that the boundaries should extend to infinity instead of only two coil diameters. The close boundaries (where the vector potential is assumed to be zero) have the effect of reducing the vector potential and, hence, the coil inductance.

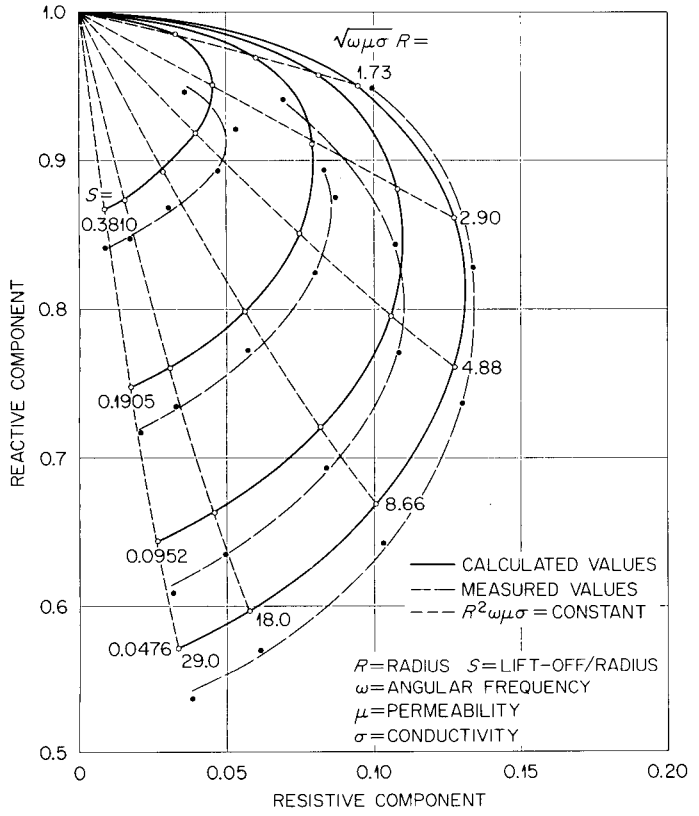

Figure 3. Normalized impedance of a coil above a conducting plane.

As an example of the use of this technique we shall show how it can be used to design an eddy-current coil for an impedance bridge instrument to measure the conductivity of aluminum. We shall stipulate that the coil diameter will be about 0.4 in. (1 cm) so that we can measure the conductivity of small parts. We assume that we want to operate at a point on the impedance plane with a ratio of lift-off-to-coil radius equal to 0.0476 and with $\sqrt{\omega\mu\sigma}\,R$ equal to 8.66. The impedance at this point on the plot in Figure 3 is a sensitive function of conductivity and the parasitic errors (interwinding capacitance, direct-current resistance) encountered in the measured values are small. The frequency may be calculated to be approximately 10 kilohertz.

If we specify that the coil should have an impedance of about 100 ohms to be compatible with the bridge, we can calculate the air inductance of the coil to be:

$$L_{air} = \frac{100}{(0.7)\,75 \times 10^3} \approx 2 \text{ millihenries} \quad . \tag{8}$$

The coil would need about 390 turns of No. 40 wire to have 2 millihenries inductance (4).

Figure 3 also shows some problems that arise in making the conductivity measurements. We note at the chosen point on the impedance plane that the impedance change is as great for only 10 mils (0.025 cm) of liftoff as it is for a factor of 4 change in the conductivity.

Another property that we can calculate is the actual eddy-current distribution. The eddy-current density which is given by,

$$\vec{i} = \sigma\vec{E} = -\sigma\frac{\vec{A}}{t} = -j\omega\sigma\vec{A} \quad , \tag{9}$$

is directly proportional to the vector potential and lags it by 90°. Thus in Figure 2 the phase and amplitude contours of the vector potential in the metal are also phase and amplitude contours of the eddy-current distribution. This, in turn, can be used to estimate the sensitivity of a coil to a defect. A defect can be represented as a current equal in magnitude and flowing in the opposite direction to the induced eddy currents. The vector potential of a coil with a defect present is the sum of vector potentials of the coil and conductor alone and the defect alone. The addition of the current of the defect to the eddy currents gives, of course, zero current flowing through the defect. Although the impedance change due to an actual defect is difficult to calculate, we may approximate the impedance change due to a small, spherical defect by: (5)

$$Z' = \frac{3}{2}\sigma\,\text{Vol}\,\omega^2\left(\frac{A_D}{I_o}\right)^2 \quad . \tag{10}$$

Or, in terms of parameters we have already calculated in our computer program, the normalized impedance is:

$$Z'_n = \frac{1}{2\pi}(a^2\omega\mu\sigma)\left(\frac{l}{a}\right)^3 \frac{A_R^2}{(R/a)^2 N^2 \text{coil}}\left(\sum 2\pi\,(r/a)\,A_{r,z}\right)^{e^2 j\phi/\mu I_0} \quad . \tag{11}$$

Thus, in Figure 2 the normalized impedance change for a small, spherical defect whose radius is 1/40 the coil diameter is:

$$Z'_n = 0.016\,A_R^2 e^{2j\phi} \quad . \tag{12}$$

Thus the impedance change is proportional to the square of the relative vector potential with a phase shift of twice that of the vector potential at the defect.

This technique may also be applied to fields with ferrite and ferromagnetic materials present. For instance, ferrites can be used to shape the eddy-current flow and increase the sensitivity to defects. Figure 4 shows how the phase and amplitude (and hence the eddy-current distribution) contours vary when we place a ferrite cup (relative permeability of 1000) around the coil shown in Figure 2. Notice how the ferrite concentrates the vector potential and, consequently, the eddy currents directly beneath the coil. This increases the sensitivity to defects and also gives a sharper pulse when the coil moves across a defect, which allows eddy-current instruments with time-differentiating defect-enhancement circuits to perform better. The normalized impedance change for a small, spherical defect is:

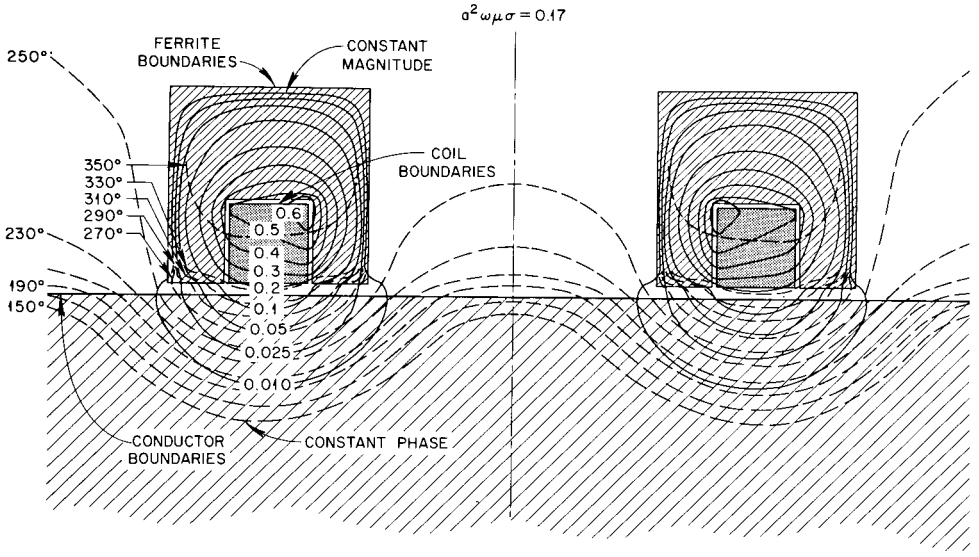

Figure 4
Coil with a ferrite cup above a conducting plane.

ORNL-DWG 66-12063

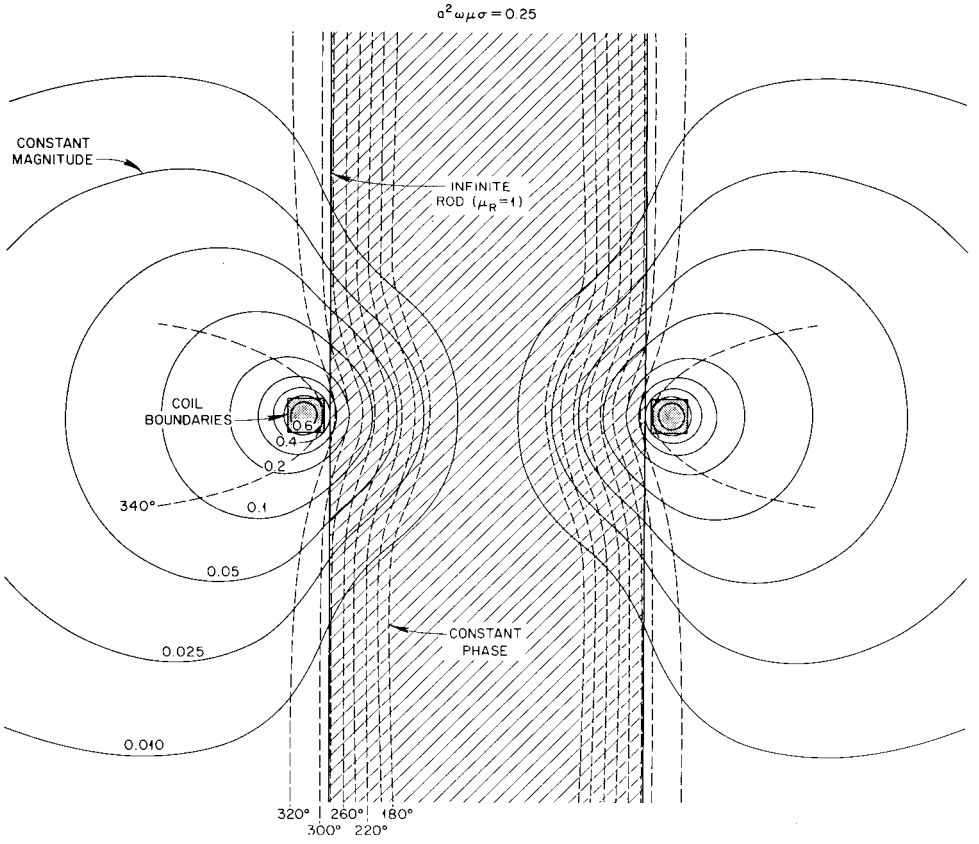

Figure 5
Coil encircling a conducting rod.

$$Z'_n = 0.054 \underset{R}{A^2} e^{2j\phi} \quad . \qquad (13)$$

Comparison of this with the preceding equation shows how ferrite has increased the sensitivity to defects.

We have also applied this technique to calculate the vector potential for rods. Figure 5 shows the vector potential of a coil encircling a nonferromagnetic rod. Figure 6 shows how the vector potential varies if we assume the rod to have a relative permeability of 200, making it ferromagnetic. Notice how the vector potential is attracted by the rod. Also the eddy-current density is relatively constant over a large outer portion of the rod and rapidly decreases toward the centre of the rod. As the frequency is increased, the relatively constant current over the outer portion of the rod remains constant, but the rate of decrease toward the centre of the rod becomes much steeper. This illustrates how this technique can sometimes uncover some unexpected results.

Conclusions and Discussion

A technique has been developed for application to a number of eddy-current problems and can be applied to many others. The restrictions of our present program, axial symmetry and sinusoidal driving currents, are not true limits. As computers grow larger and faster, we shall be able to program and solve problems with three-dimensional nonsymmetric lattices. Sinusoidal driving currents are only a convenience; they could be replaced by time-sequential currents and a time-sequential relaxation performed. A nonlinear medium can also be handled in a time-sequential relaxation if the nonlinearity of the medium is known.

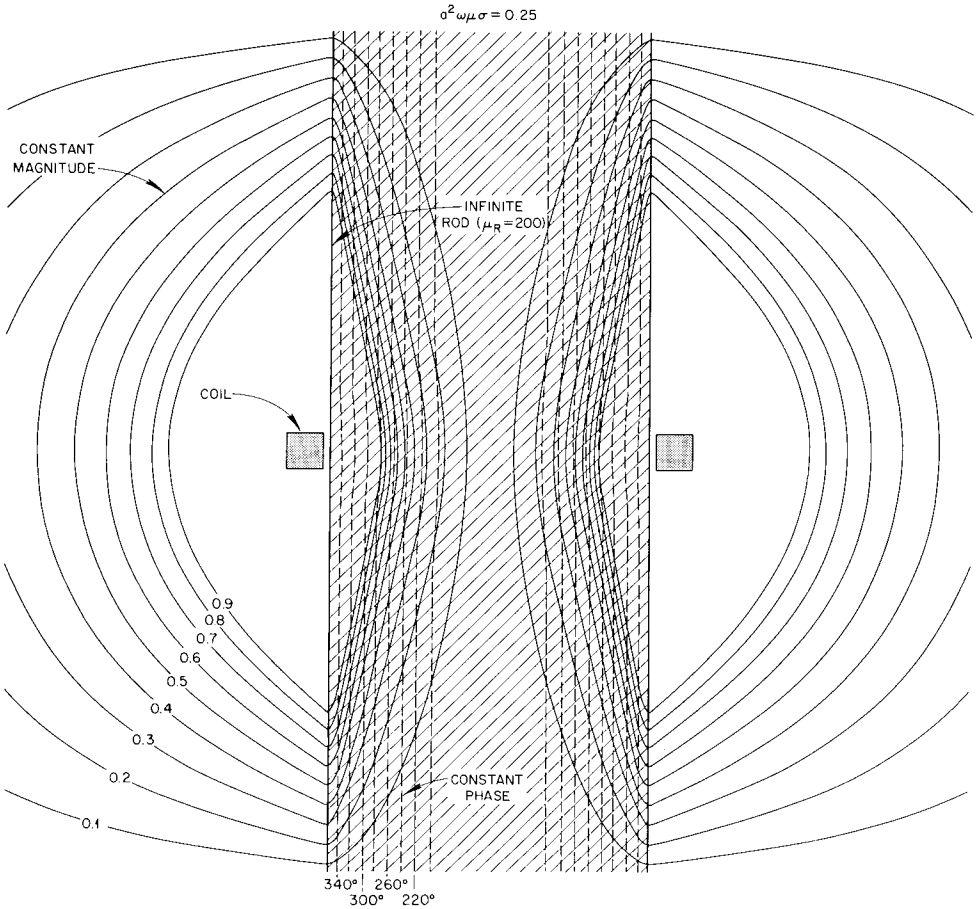

Figure 6
Coil encircling a ferromagnetic rod.

This technique gives further insight into eddy-current phenomena, allows the design of actual eddy-current systems, and takes the design of eddy-current coils from an empirical to a scientific basis.

References

1. Dodd, C. V. A solution to electromagnetic induction problems, ORNL-TM-1185, 1965.
2. Binns, Kenneth John, and Lawenson, P. J. Analysis and Computation of Electric and Magnetic Field Problems, Macmillan Company, New York, 1963.
3. Tunstall, G. N., and Dodd, C. V. A computer program to solve eddy-current problems (in preparation, 1967).
4. Dodd, C. V. *Microtecnic 5 and 6*, 18, 1964.
5. Burrows, Michael Leonard. A theory of eddy-current flaw detection, University Microfilms, Inc., Ann Arbor, Michigan (1964).

Eddy-Current Inspection of Rod During Hot Rolling

ANDERS ARNELO and AXEL VON HEIJNE, SWEDEN

Inspection on Final Product or in Process

Modern industry makes ever increasing demands on high and even quality in semi-fabricated products of steel and nonferrous metals. With a product such as wire rod, where length is many times greater than cross-section, testing by sampling can give only very restricted information on the quality of the product. Adequate knowledge can only be obtained by continuous control. When the speed of production in hot rolling is taken into account it is obvious that only the eddy-current method is applicable.

The automatic nondestructive testing of semi-fabricated products can be carried out either at separate inspection stations or in connection with the manufacturing process. When the inspection operation is of the discontinuous type, for example inspecting tubes, considerable handling equipment for transporting and sorting the product is necessary. The cost of such handling equipment can often represent a larger investment than the actual testing equipment. In a continuous inspection operation, applicable to products that are very long in comparison to their cross-section, the case is different. Here it is possible to adapt the testing equipment directly to the final manufacturing process, e.g. on the output side of a draw bench. In this type of application relatively little handling equipment is necessary.

It is general experience that when introducing quality-control techniques, the first step is always to inspect the final product. Eddy-current testing of cold-drawn wire has been used in many works for a relatively long time with good results. The next step is to attempt to inspect the product earlier in the process, partly in order to reduce the necessary testing capacity and partly to avoid further processing of defect material. It is therefore logical to apply eddy-current testing to the hot-rolling of rod.

Testing Hot-rolled Rod

Inspecting rod in the hot-rolling process, directly after the last rolling stand, gives maximum testing capacity and no extra handling equipment is necessary. Further, hot-rolled rod is usually very difficult to handle when cold and the unavoidable recoiling operation would give rise to irregular cold working of the rod, which in its turn would give electrical signals of the same type as caused by defects such as cracks. Between the last stand and the coiler, the hot rod, on the other hand, is straight and easy to guide so that transverse movement can largely be avoided. The speed is also high and relatively constant.

As is well known the eddy-current penetration into a tested material decreases in proportion to the increase of frequency. The following equation, which although only true for a semi-infinite plane, is sufficiently accurate for a short coil to permit qualitative discussion:

$$\delta = c\sqrt{\frac{\rho}{\mu \cdot f}}$$

where δ = depth of penetration, defined as the depth where the field strength will be reduced to 1/e or 37%,

ρ = resistivity

μ = permeability

f = frequency

c = constant

The resistivity of hot metal is higher than in the cold state and therefore for any given frequency the penetration is greater.

In the case of steel, the relative permeability is high for cold ferritic material. It is possible to increase the depth of penetration by magnetizing the cold material to near saturation. However, it is normally not possible to decrease the value of μ below 2 or 3. In the temperature range above the Curie point, 768°C (1414°F) iron is nonmagnetic with a relative permeability of practically 1. This, of course, means again that for any given frequency the penetration is greater for hot steel than for cold. Also the noise level is lower.

Conventional Inspection

The methods used up to now for inspecting rod have always been limited, for practical reasons, to testing relatively short lengths at each end. As far as is known, there are no national standards for this inspection, but a typical work standard can be cited as an example.

1. Cut off a number of turns; 2. Cut off one turn for testing; 3. Straighten this turn, cut to short length (roughly 1 ft), pickle and inspect under microscope; 4. Grade surface condition according to presence of cracks, pits, roughness etc. A scale of 0 – 5 is used. E.g. for valve rod the limit for depth of cracks is max 0.0012 in. (0.03 mm). 5. If test shows unsatisfactory condition, a further length of rod is removed and a new test made.

The main disadvantages of this method of inspection are:

a) Only the ends of the rod are tested, and purely statistically, the length tested in relation to the total length is very small, perhaps of the order of 0.05%; b) The sample is taken near the end of the rod and the information thus obtained is not representative of the main length. Experience shows that the fault frequency tends to be higher at the ends. However, eddy-current testing has shown that faults can occur in the main length of the rod even if the ends are free from faults. Eddy-current continuous testing gives information on all defects throughout the entire length of the rod. In evaluating the results it is always possible to disregard the defects in the neighbourhood of the two ends; c) Although end inspection gives so little information, it is expensive, partly because the tests themselves are time consuming, partly because the products must be stored in case they have to be retested.

Principles

The principles of eddy-current testing are well known and need only be mentioned briefly (1, 3). The material passes through a coil and current flowing through the coil sets up a magnetic field in the material. The changing magnetic field causes eddy currents to flow in the material. The changes in magnetic and resistive properties of the material due to faults influence the eddy currents and this effect is measured.

When applied to fault detection in rod the faults to be detected are so small compared with effect of changes in temperature that the rod must pass through two coils connected differentially in a bridge circuit.

To function satisfactorily an eddy-current tester for hot rod must be designed for temperatures between 200°C (aluminium) and 1100°C (steel) (390–2010°F) and a testing speed of between 10 and 30 m/s (1970 ft/min — 5900 ft/min). It must also be able to differentiate between genuine defects, such as cracks, inclusions, overlaps and spurious effects arising from changes in temperature, structure, shape, size, speed and vibration. Signals arising from these spurious effects are normally collectively termed noise. The equipment must be designed so that the signal-to-noise ratio is at an optimum.

Noise can arise slowly or rapidly. Changes in temperature are usually relatively slow while electrical interference is very rapid. The use of the differential coil method diminishes to a large extent the effect of slow variations but does nothing to the rapid variation.

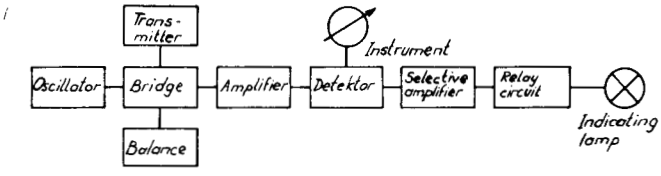

Figure 1. Block diagram of Metallverken's Metotest eddy-current tester.

Testing Equipment

In connection with the development of a new, completely automatic rolling mill for aluminium rod, equipment for drawing wire and manufacturing steel-reinforced aluminium conductors, Svenska Metallverken started development work on eddy-current testing equipment in 1949. The first version was used for testing cold-drawn wire. Later equipment was developed for hot rod. The principle of the method is shown in Figure 1. Patents were granted in several countries in 1955 and later (3).

In Metallverken's Metotest equipment the bridge including the differential coils is not completely balanced. A small unbalance voltage serves as a carrier wave on which defect impulses are modulated. The main advantage of this method is that the amplifiers and detector operate in their linear regions and that, as a result, any changes in the unbalance voltage, due, for example, to changes in temperature in the differential coils, will have no effect on sensitivity.

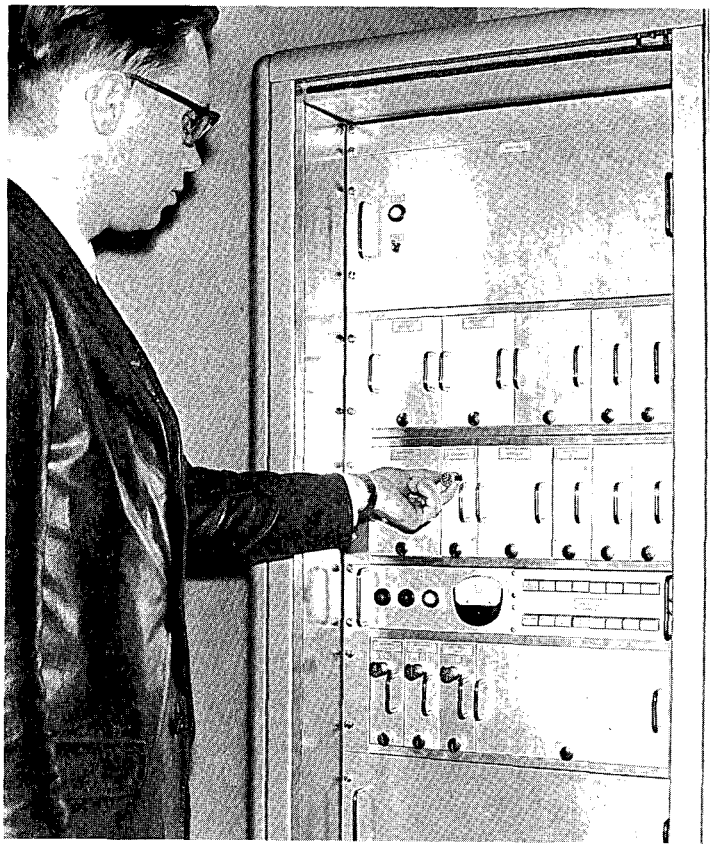

Figure 2. Instrument cabinet with main electronic equipment.

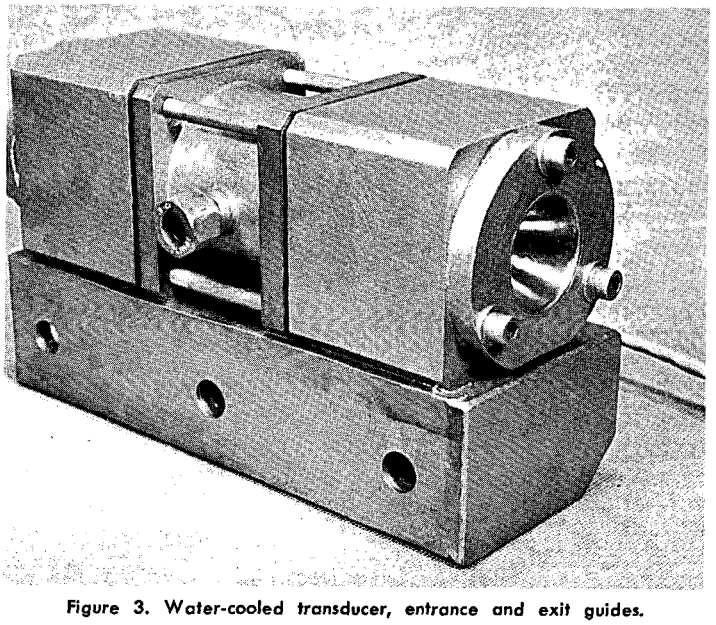

Figure 3. Water-cooled transducer, entrance and exit guides.

It is well known that the eddy-current changes, arising from different types of defects, their position in the cross-section of the material, and from other causes such as vibration and changes in dimension and speed, are at different phase angles compared to a reference voltage. The voltage, which is measured after the detector, is the vector sum of the unbalance voltage and any change in voltage arising from a defect passing through the coil. The phase of the unbalance voltage can be shifted so that it will combine with the fault vector to the maximum effect or be independent of the fault vector. Thus by changing the phase angle of the unbalance voltage one can discriminate between desired effects from cracks and undesired effects such as changes in speed.

The passage of a fault through the pair of coils gives rise to a pulse with a frequency which depends only on the speed of the material through the coils, the geometry of the coil and the properties of the defect. The detector is followed by a frequency-selective amplifier, tuned to the frequency of the fault pulses. In this way the signal-to-noise ratio is considerably improved.

The pick-up units with the differential coils are water-cooled and fitted with entrance and exit guides of wear resistant material to prevent damage from the hot rod, Figure 3. The coils are designed to produce a pulse frequency different from the dominating interference frequencies.

The equipment is completely transistorized and is built up of standardized plug-in units, Figure 2. There is an efficient system for the automatic supervision of the equipment and warning is given if a fault should arise in any circuit.

All equipment is very robust and experience has proved it capable of standing up to the arduous conditions in steel mills. The apparatus is set by means of decade thumb-wheel switches and once set no instruments have to be read. Running and first-aid maintenance are so simple that they can be done by semi-skilled personnel.

Aluminium

From 1950 to 1956 considerable experience was gained in the Västerås Works of Svenska Metallverken on the eddy-current testing of cold-drawn aluminium wire (2). Among other things it was found that the major proportion of faults were surface flaws and ferrous inclusions, originating in the hot rolling process or earlier. Detailed study showed that one of the most important reasons was that, during rolling, particles of a silicon-rich aluminum phase cladded to repeaters and guides through which the aluminium rod was passing. At irregular intervals these particles loosened from the guides and were rolled into the surface of the aluminium rod. Figure 4 shows schematically

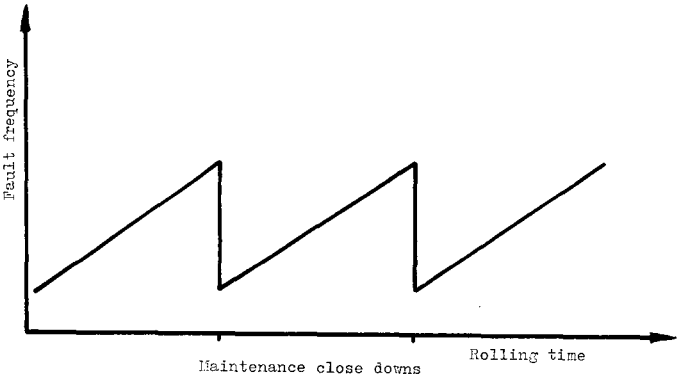

Figure 4. Fault frequency increases with rolling time, but drops when repeaters and guides are cleaned.

how this effect builds up cumulatively between maintenance close downs, when repeaters and guides were thoroughly cleaned. Maintenance could then be planned by using eddy-current inspection reports to indicate the condition of the mill.

A further example of the results of eddy-current testing is given by a study that was made at the same time on iron inclusions found in the drawn wire. Based on eddy-current inspection of the drawn wire, 4,000 samples which had shown defects were examined. In many cases the signals were due to iron inclusions and by treating the samples carefully, it was

possible to extract these inclusions and to analyze them metallographically and spectrographically. The carbon content and the presence of martensite or graphite indicated the origin of the iron particles. It was found, for example, that the iron strips holding together bundles of wire bars were removed by means of chisel and hammer. In this operation slivers of steel were pressed into the surface of the wire bar. In another case it was found that the aluminium wire bars were transported to the mill in ships carrying cast-iron scrap on their return journey.

Based on this experience and in view of the fact that testing during hot rolling would give higher production, it was decided to develop eddy-current testing equipment with transducers in the mill line. The first equipment was developed in 1957 and modifications have since been made, so that today equipment is available which is reliable and has a sensitivity accurately adapted to the particular problems in rolling aluminium rod.

Equipment of this type is now in successful operation not only in Metallverken, but also in aluminium rod mills in USA, Japan and Norway.

The rod is usually between $\frac{3}{8}$ in. and $\frac{3}{4}$ in. and rolling speed of the order of 10–25 m/sec (1970–5000 ft/min).

The water-cooled transducers are usually positioned immediately after the last pass, where the temperature is usually between 150 and 400°C.

In this position vibration in the rod is normally not great and the frequency-selective principle employed minimizes any vibration troubles that may occur.

In general eddy-current equipment can detect surface flaws, laps and inclusions. Since it is difficult to describe the size of a surface flaw quantitatively, it is usual to state the resolution in terms of equivalent area reduction compared with a standard fault, manufactured by reducing the area of the rod by turning. In our case we found that the average length of a surface flaw was about $\frac{1}{8}$ in. and the standard fault was made with this length. In hot-rolled rod a resolution of 0.5–2% area reduction can be achieved. An example is given in Figure 5.

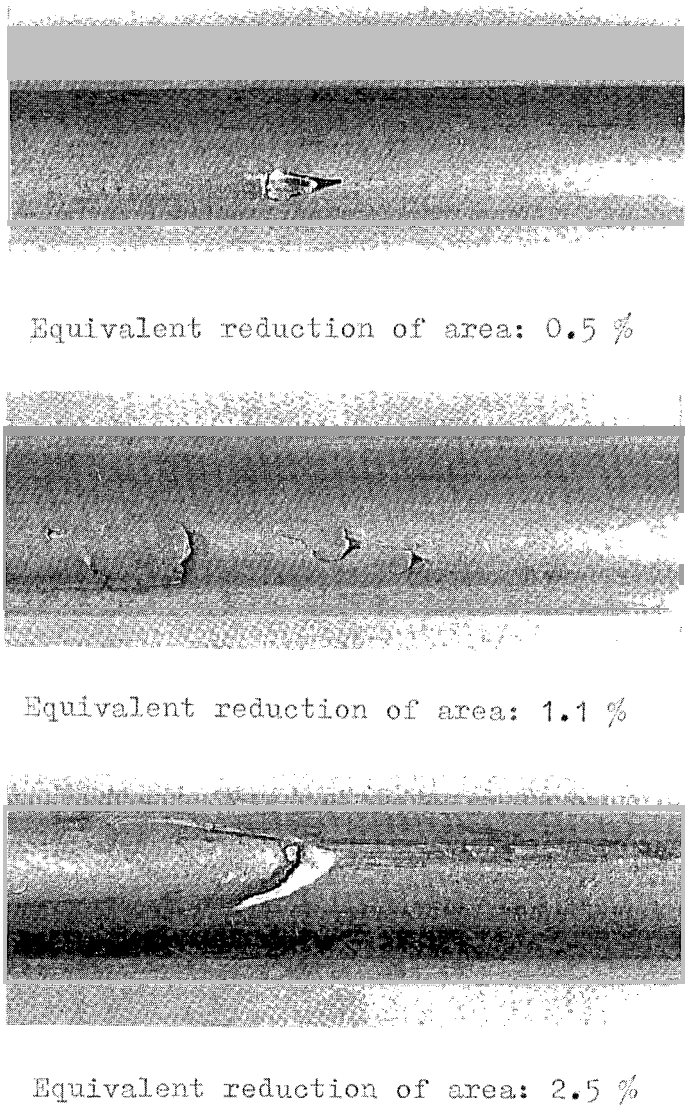

Figure 5. Surface flaws in hot-rolled aluminium rod. The fault signals obtained in the eddy-current tester correspond to the equivalent faults given.

Copper

When inspecting copper rod the temperature range is normally between 600 and 900°C (1110–1650°F) and the rolling speed roughly the same as for aluminium.

Copper is harder than aluminium and the consequent difference in rolling technique permits the use of higher sensitivity in eddy-current testing since the noise level is lower. The most important faults in copper rod are inclusions of foreign materials such as iron, copper oxide and nonmetallic particles. Practical tests using particles extracted from copper rod, detected by eddy-current inspecting, have shown that it is possible to detect iron particles of the order of 200 micrograms (0.02–0.1 mm^3) (1.2–6.1 $\times$ 10^{-6} cu. in.). Faults of this type are particularly embarrassing in rod which is to be drawn down to the finest gauges, since in drawing the dimensions of the inclusions are normally not changed and therefore their relative size compared to the diameter of the wire increases. At a certain stage an inclusion may therefore cause a rupture in the wire.

It has been found that the main causes of these inclusions are a) unsatisfactory cleanliness in the mill and b) slivers of iron loosening from the rolls. It has also been found that the frequency with which slivers loosen from the rolls increases with the rolling time between reconditioning. It is therefore possible to use eddy-current testing to follow continuously the condition of the mill.

Steel

It was soon found that there are similar problems in the hot rolling of steel, both high-alloyed steel, stainless steel and in many cases also carbon and low-alloyed steel—in particular for high-quality wire, such as is used for valve springs, ball-bearings and wire rope. The types of faults, however, are different to those encountered in aluminium and copper. One frequent cause is cracks and other defects remaining on the billet before rolling.

The first experiments with steel rod were made in 1959. The important difference between aluminium and steel is the high rolling temperature, 800–1000°C (1420–1800°F), and these original experiments were designed to develop a thermally stable and reliable transducer. When these experiments had proved successful, research projects were made in conjunction with two different steel works in Sweden in order to study the practical application of eddy-current testing. Testing equipment was set up in the mills and test runs were made on a large number of coils, during which the signals were recorded on tape. After preliminary analysis of the recordings, certain rings were chosen for further inspection. These were cut into short lengths, straightened and studied using a laboratory set-up.

Finally the electrical signals obtained were correlated with the results of ocular inspection of the rod and metallographic studies of the cross-section.

Based on these studies full-scale testing equipment was delivered to two mills in 1966.

As already mentioned the most important faults are cracks, and to some extent surface flaws. The resolution depends, as always, on the noise level. Experience has shown that this noise level, due largely to variations in the rod structure, in speed, vibration etc., varies from mill to mill, but as a general figure a minimum equivalent crack depth of about 0.002 in. (0.05 mm) can be detected.

In the same way as in aluminium, it is difficult to describe quantitatively the depth of a natural crack. Few cracks extend straight and radially; usually they are folded in an irregular manner. Sometimes a cross-section shows a broad notch, which an inspector may consider a shallow crack, but below which a deep crack can be hidden (see Figure 6). Further, it is common to find oxide inclusions or varying degrees of decarburization in connection with cracks. Both affect the amplitude and phase of the defect signal.

For these reasons it is necessary to express resolution in terms of equivalent crack depth or a standard fault. Since cracks dominate in steel, the standard fault normally used is a narrow notch, some half inch long, made preferably by some method giving a well defined, reproducible notch and which avoids all cold working. We have normally used air-abrasive cutting (4).

Since the eddy-current method employs two adjacent coils it is theoretically not possible to detect a continuous fault with exactly the same shape and size throughout its length. In practice, however, although long faults may be found they are always short compared to the total length of the rod. The beginning and the end of a fault can therefore be detected. Further, faults almost always vary in shape and size and major discontinuities and changes are detected.

In one case it was shown that an electrical signal corresponding to an equivalent crack depth of 0.012 in. (0.30 mm) corresponds to an actual crack depth of 0.0012 in. (0.03 mm) as judged ocularly by an inspector. The cross-section, however, (Figure 6) shows that below the crack there are oxide inclusions extending to a depth of 0.002-0.004 in. (0.05 to 0.1 mm). In another case, the eddy-current signal showed an equivalent crack depth of 0.006 in. (0.15 mm). This corresponded to an ocular judgment of 0.002 in. (0.05 mm). The cross-section showed, however, that the area around the crack was severely decarburized.

Normal speeds in steel rolling are between 5 and 30 m/sec (980-5900 ft/min), normal gauges are $\frac{1}{4}$ in.-$\frac{3}{4}$ in. (5.5-20 mm).

In steel mills the vibration problems are different from those in aluminium mills, mainly because steel rod is harder than aluminium. It is normally not necessary to position the transducer very close to the last mill stand. It can, in fact, be placed practically anywhere between the last stand and the next unit, either a chopper or a coiler. Since the guide pipes in the mill have a diameter several times the diameter of the rod, the transducer must be fitted with inlet and outlet guides, partly to guide the rod, partly to prevent mechanical damage to the transducer itself.

Detector Output

The signal obtained for each fault may be employed in various ways. The simplest is a signal lamp which lights up for every fault as it is detected. The signal can also operate a relay, which remains in the on-position until reset manually or by the end of the rod. Counters can be applied to count the number of faults in each coil or the number accumulated over any number of coils. The faults can be classified at different levels, each with its own counter. A digital high-speed counter and printer can be used to record the size level and position along the rod of every fault. This type of information is suitable for feeding into any kind of computerized system used in a modern rolling mill. A special computer unit can be used to operate large-size display units placed anywhere in the mill, for example for the operator's sorting of coils after they have cooled.

Conclusion

The foregoing examples have shown some of the applications of eddy-current testing to the inspection of hot-rolled rod. Although

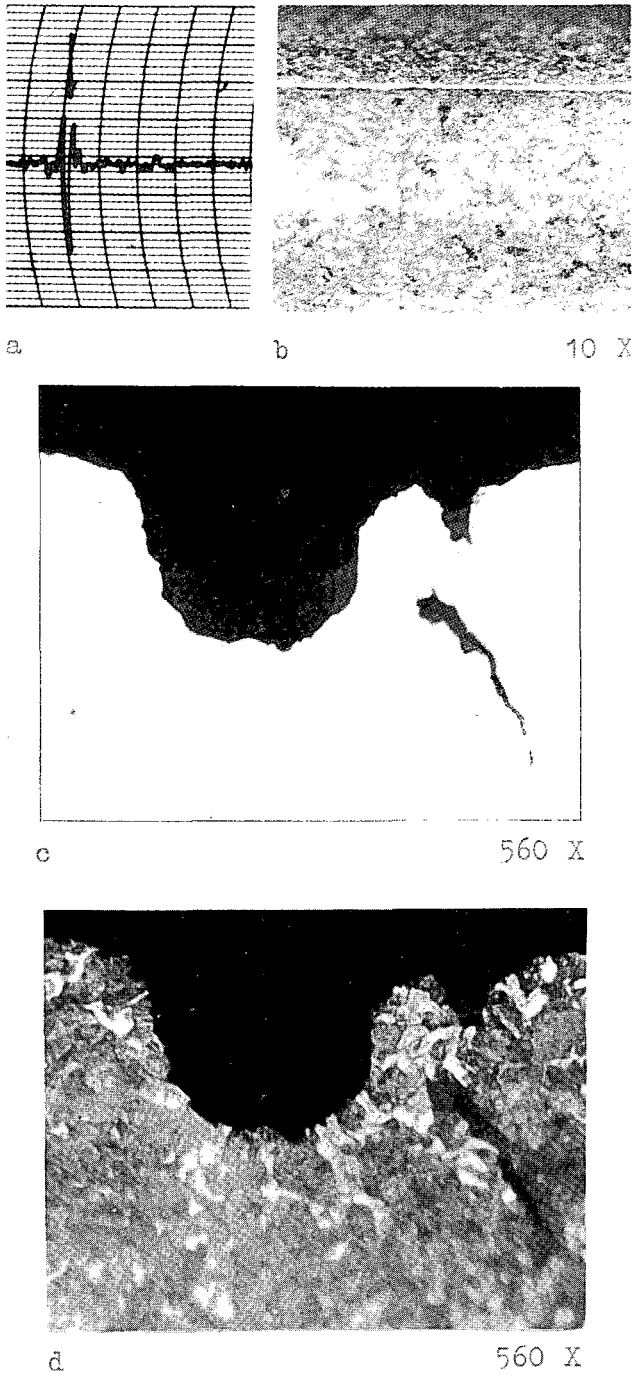

Figure 6. Flaw in hot-rolled carbon-steel rod.
a)Signal obtained with tester; b) Macro of surface; c) Cross-section, showing subsurface crack; d) Cross-section etched, showing decarburization.

eddy-current testing to the inspection of hot-rolled rod. Although apparent that we are only in the beginning of a development period. There is still a great deal to be done to develop better pick-up coils, in order to detect difficult faults, such as continuous unchanging cracks, narrow transverse cracks, and to be able to differentiate between different types of faults. One example is to separate surface-flaws from nonmetallic superficial inclusions.

The value of eddy-current testing lies in the fact that it permits practically 100 per cent inspection. Consequently it offers an effective means of ensuring constant high quality in the outgoing product. At the same time the personnel involved in inspection is kept to a minimum.

Another important aspect is that by analyzing the types of fault and the frequencies at which they occur, valuable information is obtained which can be fed back to improve the process. Since the method implies 100 per cent inspection a great amount of information is obtained, which can be presented in data processing language and is already suitable for treating in data systems—for example for regression analysis. Thus eddy-current testing supplies a basis for considerable improvement in product quality and mill output. It is in fact our opinion that eddy-current inspection of hot-rolled rod can be one of the most profitable of all applications of nondestructive testing.

References

1. Arnelo, A. The eddy-current testing method in non-ferrous metals. *Metallen* (Sweden) 20: 3, 1964.
2. Arnelo, A. and Leuchovius, K. Experience of eddy-current testing of wire and strip. *Metallen* (Sweden) 20: 3, 1964.
3. Patents: Sweden No. 179.407; USA No. 2.948.848; Canada No. 632.073 et al.
4. Arnelo, A. and Hedlund, B. Experience of standard faults in non-destructive testing of tubes (This conference).

Discussion

Q. DAVID STEIN, Picatinny Arsenal, Dover, USA:

It is considered a serious omission that you did not describe the transducer design or how you solved the various problems associated with high temperature. Was this planned?

A. The paper was directed towards people actually occupied in the testing of products and it was therefore felt that within the necessary time limit, a discussion of transducer design was outside the field of immediate interest. Moreover, many aspects of transducer design and the way in which temperature problems are solved are part of the know-how that is sold together with the equipment. Some features are the subject of patents but not all.

Q. R. N. CRESSMAN, Bethlehem Steel Corp., Bethlehem, USA:

My questions pertain to inspection steel rod:

1. Can you give the size range of rod that can be inspected? 2. What is the maximum test speed? 3. What is the spacing between the test coil and the rod? 4. Is the defect sensitivity dependent on rod size? If so, how? 5. Where are the test coils mounted on the mill line? 6. Are there any unusual problems in feeding the rod through the test coil? 7. Can you detect long seam-type defects that run the full length of the coil? 8. Is it necessary to use different test coils for different grades of magnetic steel? 9. How do you mark the location of the defects?

A. The size range of rod is normally from $\frac{3}{16}$"-1". However, studies are being made to increase this range. 2. Maximum test speed up to now has been about 6000 ft/min. However, this limit is based more on what present rolling mills accomplish than on the eddy-current testing equipment. 3. The spacing between the pick-up coil and the rod varies of course. The limits are shown on page 6 of the enclosed leaflet EM 317. 4. Defect sensitivity is dependent on rod size. The relation is extremely difficult to pin down, as it depends on a large number of factors. The limit is dependent on the signal to noise ratio and since in most applications in hot rolled rod that we have met the noise is, to about 90%, attributable to variations in the material being tested, it follows that interference and electrical noise within the equipment are unimportant factors. It is difficult to study this question using artificial faults on cold material since the noise level is different in hot material and is also dependent on many factors that pertain to the mill itself, e.g. temperature variations, vibration, changes in rolling speed, degree of decarburization etc. However, as a very general rule of thumb it can be said that resolution is roughly proportional to diameter, with a certain flattening off towards the lower end of the range. 5. The pick-up coil unit is mounted between the last mill stand and the coiler. The exact position depends of course, on the lay out of the mill. 6. If the pick-up unit and the rod guides are correctly designed there are normally no particular problems in feeding the rod through the pick-up unit. 7. Theoretically a seam type defect running the full length of the coil cannot be detected by differential coils. However, our experience is that such a defect extending throughout the entire length of the rod without appreciably changing its size, shape or position occurs extremely seldom. The experience that we have from steel mills using this type of equipment for over two years is that when long faults do occur they always vary in size so much that a series of small defect signals (of course in some cases also large signals) is obtained. By summing the number of faults or summing the total noise level along the rod (auxiliary units are available for this purpose) this type of fault can be kept under control where it occurs. 8. It is not necessary to use different pick-up units for different grades of magnetic steel since, when testing during hot rolling, the temperature is above the Curie point and therefore the relative permeability is 1. The resistivity also approaches roughly the same figure for many different qualities at the rolling temperature. This includes also the non-magnetic austenitic steels. 9. Up to now marking hot rolled rod has not been considered practical, partly because of the inherent difficulties of doing so, partly because the marking material tended to disturb following drawing operations and partly because the users did not want to cut out faulty parts from a coil. Instead a digital recording device is often used giving a recording such as is shown in the enclosed diagram. The number of each coil is printed, a figure is given for each defect within one of three classes and also the time from the beginning of the rod when each defect actually occurred. Since the rolling speed is practically constant the time that has elapsed from the moment that the front end of the rod passes the pick-up unit to the moment when a fault occurs is proportional to the distance from the front end of the rod. Other ways of treating the data are given in the enclosed leaflet.

It might be added that there is a tendency towards an increased interest in the problems of marking the location of defects and development work is going on to solve this problem.

In-Line Utilization of New Eddy-Current Test Systems for the Crack Inspection of Semi-Finished and Mass Produced Parts

E. F. FÖRSTER, GERMANY

Introduction

Among the various methods of nondestructive testing, eddy-current testing is specifically suitable for the automation of test procedures.

For this reason in the last years it has become more frequent that the design of complete new steel works included a fully mechanized installation for the nondestructive testing of the total output. Therefore, development work has been intensified to provide suitable test methods in the various stages of production, for instance, the production of tubes with wide ranges of diameter and wall thickness. It was a common feature of all these developments that they were built up on the basis of a careful investigation of the theoretical background. In addition, the problem of testing under extreme operating conditions caused by dirt, dust, vibrations and jerks had to be studied thoroughly. These influences complicate the utilization of automatic test installations in the production lines of steel works.

Experimental Results of New Encircling Eddy-Current Coils

Eddy currents are distorted if there is a defect in the wall of a tube. The distortion of the eddy currents produces a certain distortion of the magnetic alternating field in the vicinity of the defect. This distortion has been calculated theoretically* for the case of a cylindrical hole which was drilled through the wall of the tube. These theoretical results gave general rules for the optimum layout** of the encircling coils. It was the goal of the development to obtain coils with a very high defect resolution but which had a very small sensitivity to effects due to physical dimensions of the test material.

There is a general rule by which the quality of a well-designed test coil is defined: The narrower the signal due to a point-shaped defect and the stronger the suppression of signals due to dimension effects, the better is the test coil.

Figure 1 shows the record obtained from a borehole with a .040-in. diameter. In a copper tube of $\frac{5}{8}$ in. (16 mm) diameter, Figure 1 also shows the dimension effect which is due to a deformation by the traction device of a drawing bench. The record of Figures 1a and 1b was obtained by means of an XY-recorder. The horizontal coordinate shows the length of the tube in a reduced scale. This scale was obtained by means of a potentiometer having 20 turns which was driven by the tube under test.

The hole and the variation of the dimension were recorded with such phase settings that once, there was a maximum signal of the hole and the next time, there was a maximum signal of the dimension. This means the phase was set in two directions, one was the direction of the hole effect, the other, the direction of the dimension effect. In these tests the angle between the hole effect and the dimension effect was 45°.

Figure 1a was obtained with a standard eddy-current coil of conventional design. It had one primary coil and two secondary coils with opposite windings. Figure 1b shows the record of the same test piece with a new HR (high resolution) test coil. In this coil, the direction of the generating magnetic field was no longer parallel but vertical to the surface of the tube.

The substantial result shown in Figure 1b is the very high ratio of defect signal over dimension effect and the very narrow signal of the hole which is only half as wide as the signal in Figure 1a. Generally, the defect resolution of a point-shaped defect is best if the defect signal is as narrow as possible. This is seen in Figure 2 which shows records of the absolute defect depth in 4 test pieces.*

In an encircling differential coil, the defect signal is obtained by the local variation of the depth of the defect. The toothed curves in Figure 2 show such local variations. In general, these occur in very small zones. In a test piece, the larger the length which is affected by the coil, the more the effects due to the increase and decrease of the depth of defect can cancel each other out. Thus effectiveness of the test coil over a comparatively large length of test piece means a poor defect resolution. Conversely, an encircling coil which is effective over an extremely short length of test piece shows a good defect resolution. For this reason the recording of point-shaped defects at a scale of 1 : 1 has led to a quantitative analysis** of the conditions which must be met for the optimum defect resolution of the various coil designs.

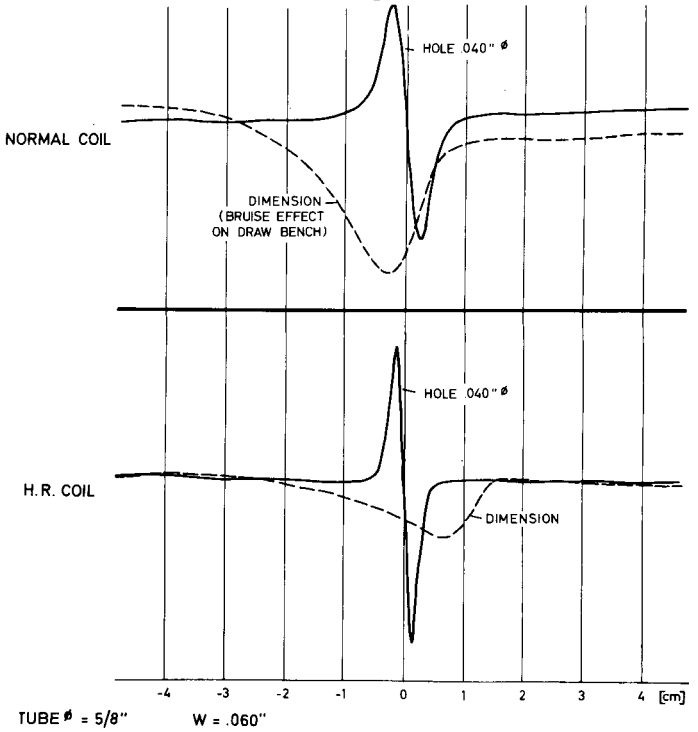

Figure 1. Indication of defects and distortion of dimension, by two different eddy-current test coil systems.

* Because of lack of space this calculation of the distribution of the magnetic field strength near a hole-shaped defect cannot be given in this paper.

** Because of lack of space no report about the exact design of the new test coils can be given. These theoretical and experimental results will be discussed more thoroughly in one of the next Förster Reports.

* This record of absolute defect depth was obtained with the Circograph (article IV) with rotating pick-up coils. The record of the test piece in a scale of 1:1 was obtained by attaching the chart to the test piece while the latter was fed through the Circograph.

** A report of this analysis of the encircling eddy-current coils will be given in another paper.

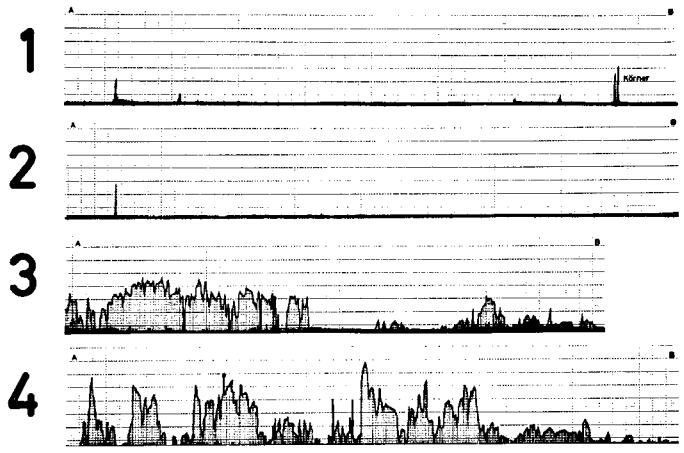

Figure 2. Distribution of crack depth along four steel rods.

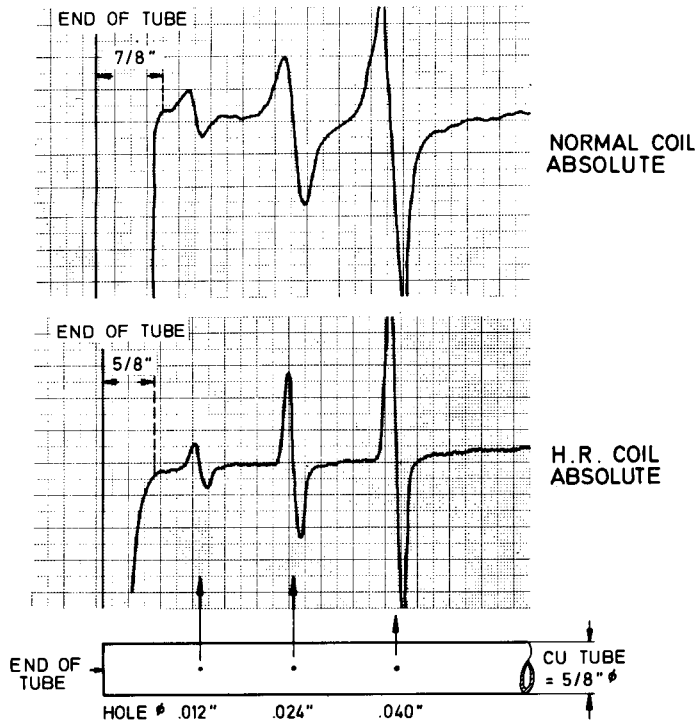

Figure 3. Record of three holes with diameters of .040 in., .024 in., and .012 in in a copper tube with a diameter of $\frac{5}{8}$ in. with the normal and the RH coil.

Figure 3 shows the record, in a scale of 1:1, of 3 holes with diameters of .040 in., .024 in. and .012 in. (1.0, .6, .3 mm). In a copper tube with a diameter of $\frac{5}{8}$ in. (16 mm), the 3 holes were drilled at a distance of $1\frac{3}{16}$ in. (30 mm) each. The smallest hole with the .012 in. diameter is $1\frac{3}{16}$ in. distant from the end of the tube. Thus Figure 3 shows the so-called end effect, too. This effect indicates the length of the uninspected end of the test piece or, in other words, the distance from the end of the test piece in which a given defect can be detected safely. The upper curve in Figure 3 shows that the defect indication of the 3 holes overlap each other. This curve was obtained with an eddy-current coil of the conventional type. In contrast to this, the lower curve of the new HR coil shows a considerably narrower defect signal over a much shorter zone. The upper curve in Figure 4 shows the result obtained with the test coils hitherto existing but the defect signal shown in Figure 3 was electronically differentiated. The end effect starts $\frac{7}{8}$ in. away from the end (21 mm). Between the 3 defects the record chart nowhere shows a horizontal line. That means that over the full length of the chart the effects of the defects superimpose each other. The middle curve of Figure 4 shows the results obtained with the new HR encircling coils. The much smaller width of effectiveness i.e. the narrower defect reading and consequently the higher defect resolution of the HR coil is clearly seen. Here the end effect begins $\frac{5}{8}$ in. (16 mm) in front of the end of the tube. In the bottom chart of Figure 4, the test piece does not travel through the HR coil with a free end but it goes "nose to tail" with the following test piece of the same type. There is no spacing between the two test pieces. Under these conditions the end effect is only $\frac{5}{16}$ in. (8 mm), which is half the end effect of the free end. Whenever the shortest possible uninspected end is desirable, "nose to tail" inspection is applied.

Defect Inspection of Very Thin Wires

The HR eddy-current coils described above refer to a diameter range of .040 in.–$5\frac{3}{16}$ in. (1–130 mm). For the diameter range of the very fine wire between .001 in. –.040 in. (.025–1 mm) a special coil technique has been developed.

With these coils for extremely small diameters, a very short test coil has been designed which does not indicate the variation of the depth of defect but its absolute value. The test coil is mounted in a small plug-in unit between two diamonds having a centre bore for centring the wire in the coil. The fine wire coils which are produced in batches and which cover diameter ranges between .001 in. and .008 in. (.025 and .2 mm) are

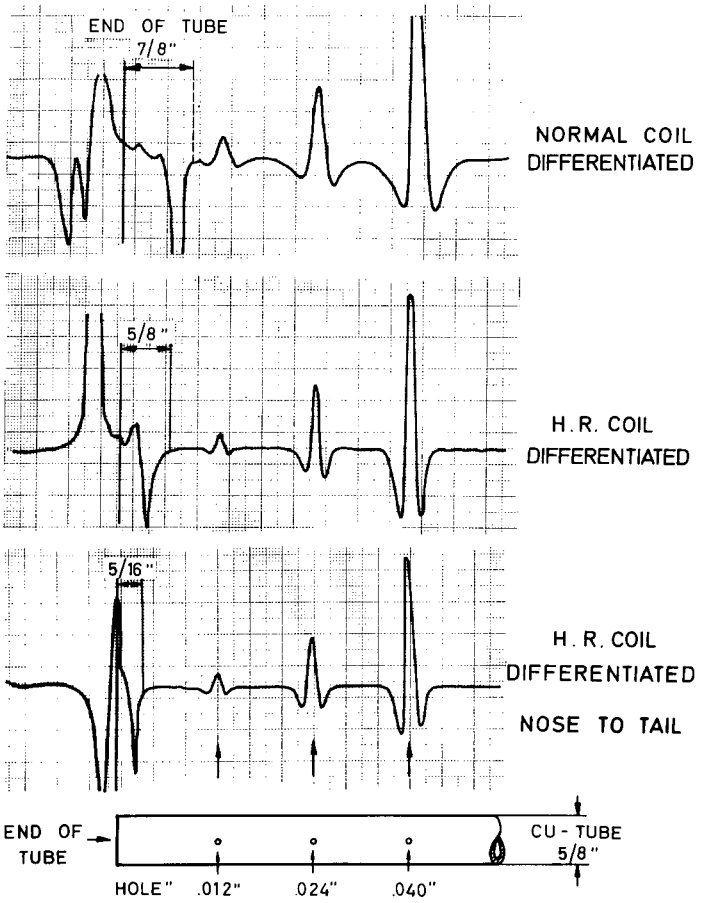

Figure 4. Defect signals of three holes (same as Figure 3) after electronic differentiation. Reduction of the end effect by HR coil and by nose-to-tail transportation of the test parts.

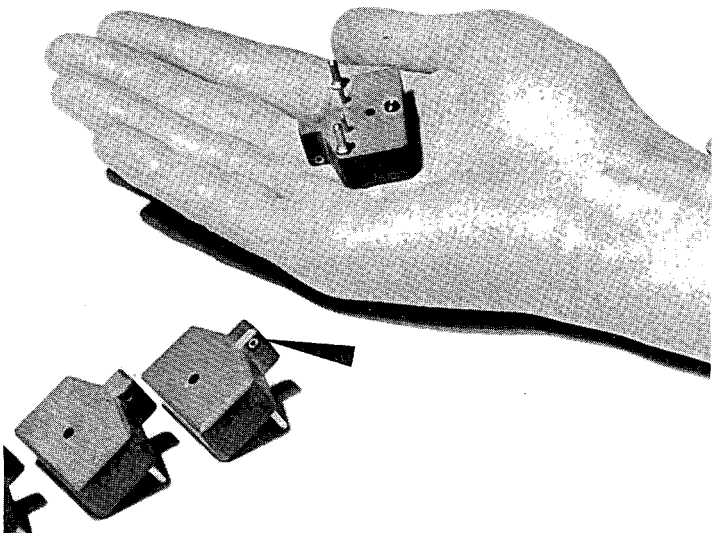

Figure 5. Test coils for fine wires, .001 in.–.008 in. dia (.025–.2 mm). The arrow shows the bore of the diamond die in the coil mounting.

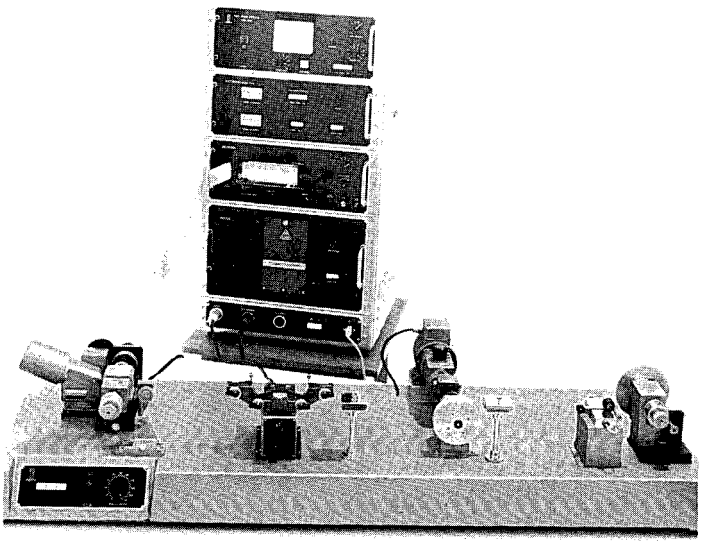

Figure 6. Fine-wire crack detector with electronic test system, recorder and counter printer for statistical defect evaluation and with mechanical rewind system and wire length meter.

operated in a frequency range between 50 and 800 Mc. The arrow, Figure 5, shows the bore in the diamond for threading in and centring the wire under test. The batch type production of such extremely small test coils is only possible by utilizing very accurate gauges and by the high precision of the single components.

Figure 6 shows a complete installation for the inspection of fine wires. In the background is a cabinet containing the electronics; in the foreground is a mechanical test device which recoils the wire under constant stress and avoids jerks. The instrument contains a recorder for recording the absolute depth of defect versus the length of the wire. Figure 7 shows such charts of a tungsten wire with a diameter of .002 in. (.05 mm). The relatively small background noise of the good sections and the high readings of the absolute depth of defects and their variation are conspicuous. The maximum of the defect reading in the defect signal which is marked by an arrow corresponds to the micrograph shown in Figure 8.

By means of the exact centring of the wires by diamond dies a very high reproductibility of the charts was obtained. Figure 9 shows the 6-fold repetition of the record of an identical piece of tungsten wire with a diameter of .002 in. (.05 mm).

The readings obtained for Figures 7 and 9 were obtained with a quantity of .0001 gram of tungsten. Such a quantity of tungsten is in the test coil at the same time.

The statistical evaluation of defects is of special interest for the inspection of wires. For this, the instrument shown in Figure 6 contains a digital counter-printer which can be set by push buttons to print any of the following information:

1. Number of defects per 10 m of the length of wires printed in steps of 10 m each.

2. Number of defects per 100 m of the length of wire printed in steps of 100 m each.

3. Total length of defects per 10 m of the length of wires printed in steps of 10 m each.

4. Total length of defects per 100 m of the length of wire printed in steps of 100 m each.

Figure 10 shows a part of such a printer chart for the evaluation of quality. As an example, in the left-hand chart a number, n_z, of defects are printed in steps of 10 m of wire length. The chart goes from 10-70 m. The right-hand chart shows the number, n_z, of defects in steps of 100 m for the first 600 m of a tungsten wire. Such printed charts as shown in Figure 10 are of specific importance for the engineer in the production line. The number, length and distribution of defects enables him to draw important conclusions as to the reasons defects occur.

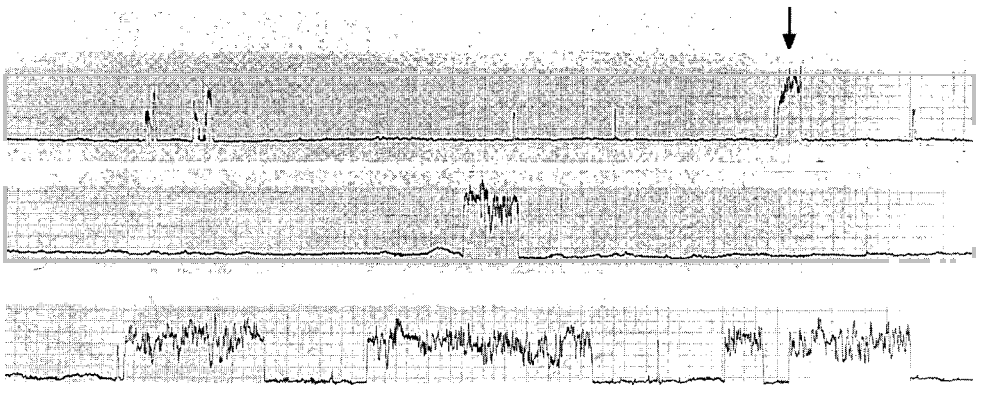

Figure 7
Recordings of the absolute depth of defects in tungsten wires with a diameter of .002 in. (.05 mm). The arrow shows the section from which the micrograph in Figure 8 was taken.

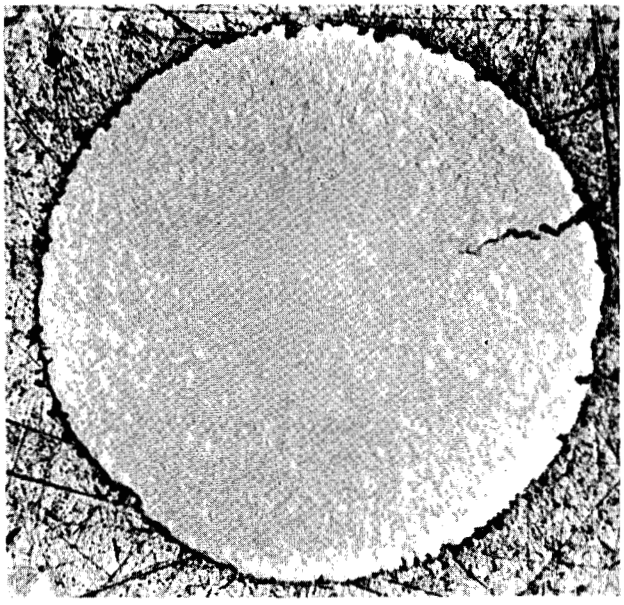

Figure 8. Micrograph of a tungsten wire .002 in. dia (.05 mm). Enlarged 1500X.

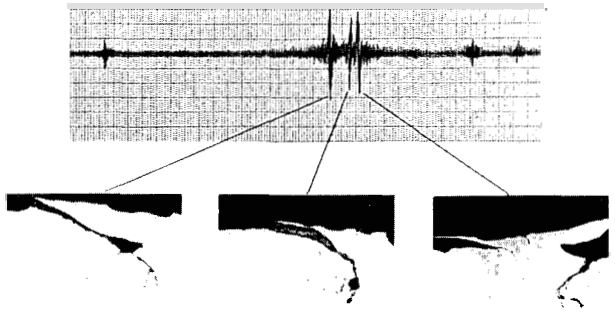

Figure 11. Record of defects in hot wires and their corresponding micrographs. Temperature 950°C (1700°F), test speed (4000 ft/min) (20 m/sec).

means of two adjustable acceptance limits. The quality mark of a wire coil determines its further use for high- or low-grade purposes or on its rejection.

Figure 11 shows part of a chart with defect readings and shows micrographs obtained from corresponding sections. The test speed was approx. 4000 ft/min (20m/sec) and the temperature of the wire was approx. 950°C (1700°F).

The defect inspection of very thin or hot wires is only mentioned as one example of the increasing range of application for eddy-current testing under extreme conditions. The prerequisite for meeting the requirements is the theoretical and experimental elucidation of the optimum layout of the coils as well as a highly advanced coil technology.

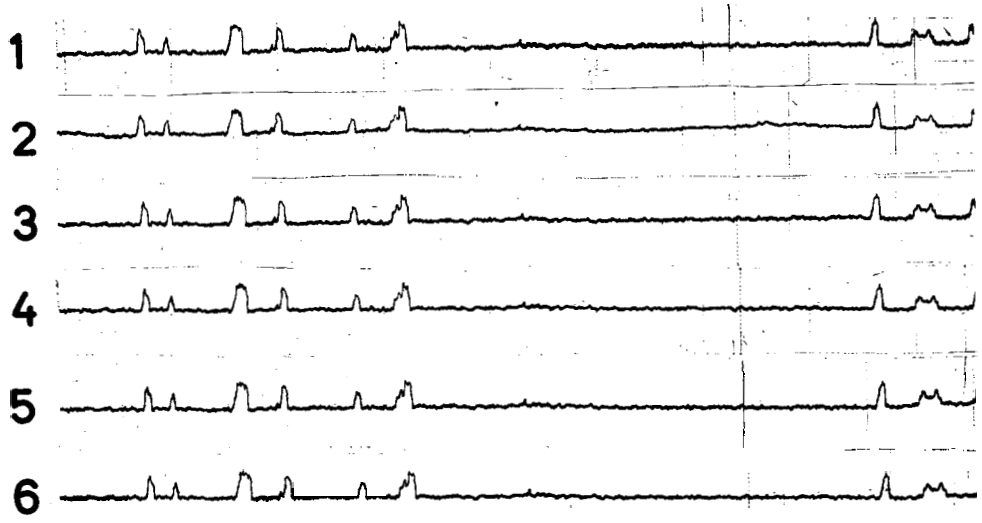

Figure 9
Six different records of the same piece of tungsten wire, 25 ft (8 m) long and .002 in. dia (.05 mm), for proving the high reducibility.

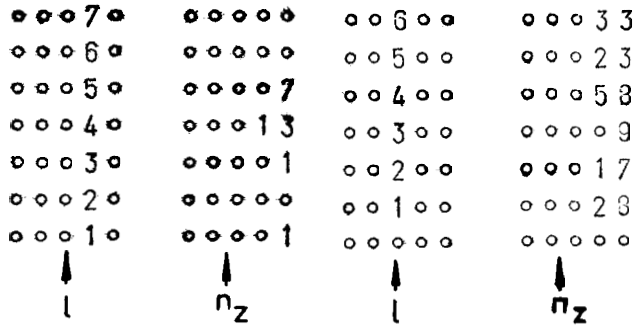

Figure 10. Printer chart for the statistical evaluation of quality. Number of defects n_z, printed for each 10 and 100 metres.

Defect Inspection of Hot wires at Approx. 1000°C (1800°F)

Recently, there has been a problem of defect inspection of red-hot wires at a high rolling speed. Immediately after rolling and coiling it should be known to which quality group this coil belongs. The quality group can be defined by the total number or the total length of defects in the coil. In addition it is possible to discriminate between defects of smaller and larger depth by

Eddy-Current Defect Detection by Pick-Up Coils

The defect resolution of the encircling coil could be substantially improved by theoretical investigation of the distribution of the magnetic alternating field near the defect. In a similar way the defect resolution of the pick-up coil could be improved by clearing up the theoretical background of the pick-up coil.

The task was to build pick-up coils that operate at a certain distance from the test piece and are still able to produce a sufficiently high field strength in the test piece. By developing a coil design with a field focussing effect, the defect inspection without contact between the pick-up coil and the material under test became possible.

As a function of the spacing between test coil and test piece, Figure 12 shows the height of the signal obtained from a given defect for a normal pick-up coil and a field focussing pick-up coil. For the distance O the readings of both coils were

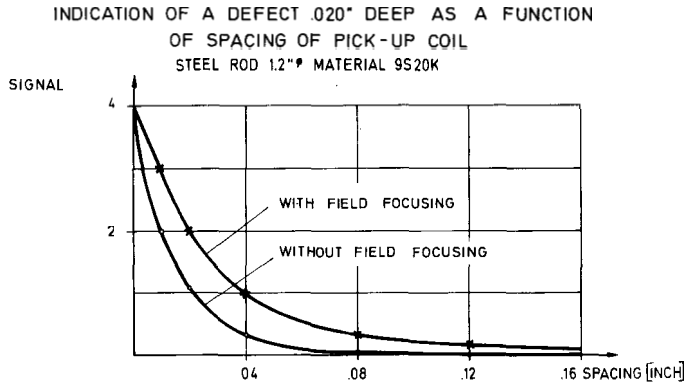

Figure 12. Height of defect signal as a function of the space between test coil and test-piece. Depth of defect: .002 in. (.5 mm).

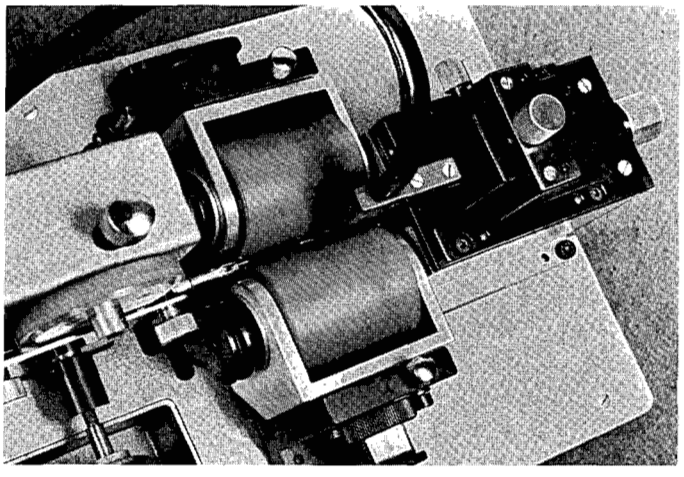

Figure 13. Mechanical device of the automatic test equipment for cylindrical products of small diameter. Inspection rate per hour: 10–15,000 pieces.

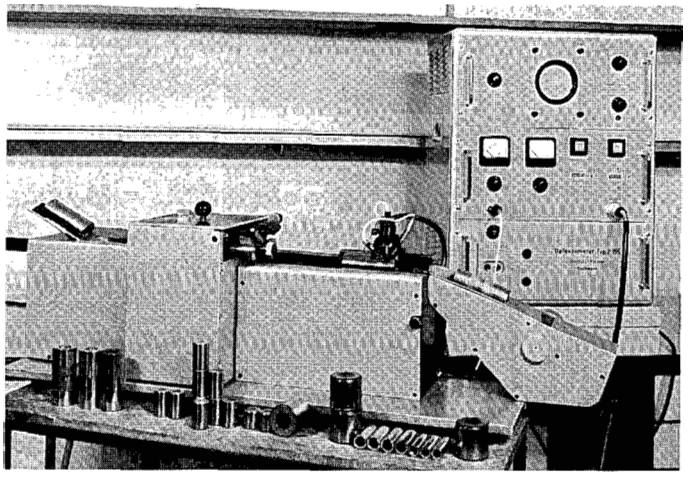

Figure 14. Automatic crack inspection unit for cylindrical mass-produced parts (axles, rollers, gudgeon pins, etc.).

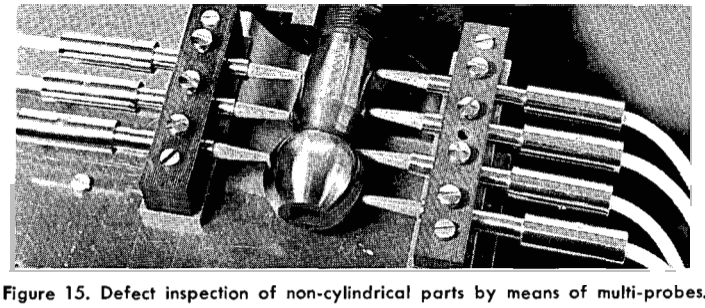

Figure 15. Defect inspection of non-cylindrical parts by means of multi-probes.

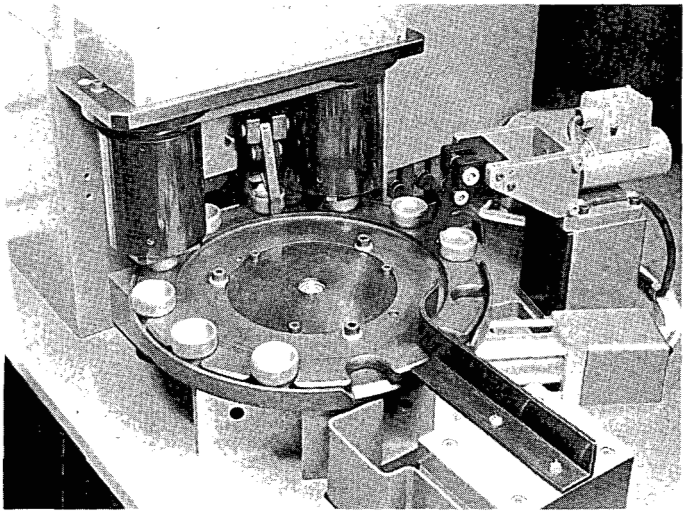

Figure 16. Automatic crack detection device for forgings.

adjusted to the same level. At a distance of .020 in. (.5 mm) the defect signal of the field focussing pick-up coil is twice as high. At the distance of .040 in. (1 mm) it is three times and at a distance of .120 in. (3 mm) it is five times as high as the defect signal of the normal pick-up coil.

In the following figures test devices utilizing focussing pick-up coils are shown. For these examples the pick-up coil is fixed and the test part moves. Figure 13 shows a mechanical device in which needles for needle bearings rotate with high speed and travel along the pick-up coil.

Approximately 10–15,000 needles per hour are inspected and automatically sorted with such a device. Figure 14 shows a very versatile instrument for fast, automatic crack inspection of cylindrical mass-produced parts such as axles, rollers, gudgeon pins etc. These parts are rotated by means of two rotating rollers. The axes of these rollers are slightly inclined to each other (principle of centreless grinding machine). Thus the test parts are transported along the pick-up coil. Auxiliary coils control the suppression of effects due to the leading and trailing ends. The test parts are fed pneumatically to the rotating rollers. The whole procedure of feeding the test part to the transportation device and of testing and sorting the good and the defective parts is controlled by a closed-loop system. This avoids choking of the test line.

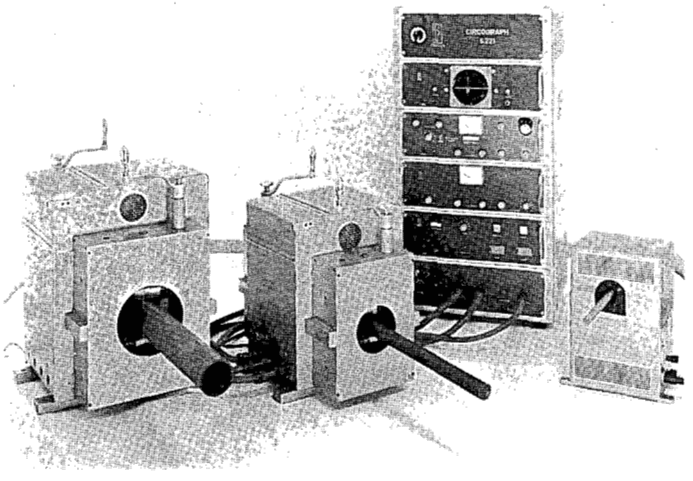

Figure 17. Circograph with three rotating heads.

By the simultaneous use of several pick-up coils, non-cylindrical test parts can also be tested for defects as shown in Figure 15. Here the ball pin under test is rotated mechanically and 7 pick-up coils simultaneously inspect the test part zones in which defects might occur. If only a certain area of a test part must be inspected, rotating pick-up coil devices can be moved over such a zone. In Figure 16 forgings are automatically inspected for defects in their upper area. On a turntable the test parts are moved in steps and those parts that are underneath the rotating pick-up coils are lifted and brought near the pick-up coils for inspection.

The circographs with rotating pick-up coils are applied for the inspection of a large diameter range of semi-finished products such as wires, bars and tubes.

At present four different rotating heads are in use and can be operated with the same electronics.

1. Ro 0 for a diameter range of .080 in.–.32 in. (2–8 mm).
2. Ro I from $\frac{3}{16}$ in.–1 in. (5–25 mm).
3. Ro II from $\frac{13}{16}$ in.–$1\frac{3}{8}$ in. (20–60 mm).
4. Ro III from 2 in.–5 in. (50–125 mm).

Ro 0, which is applied for the inspection of thin wires at a high test speed, has 100 rev/sec and four pick-ups, i.e. 400 test lines/sec. The largest rotating head Ro III has 40 rev/sec and two pick-up coils i.e. 80 test lines/sec.

Figure 17 shows the electronic cabinet of the circograph and the rotating heads Ro I, Ro II, Ro III. The rotating heads Ro 0, Ro II and Ro III have pick-up coils that are not in contact with the surface of the test material. According to the diameter of the test parts the pick-ups rotate around the semi-finished product in a distance between .010 in. and .12 in.

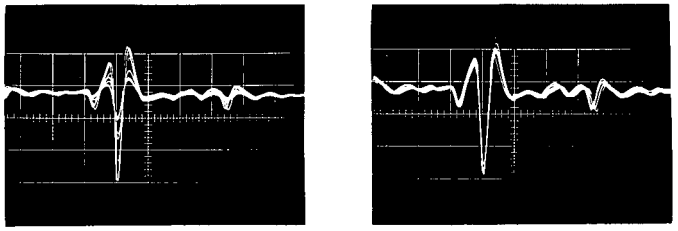

Figure 18. Defect signal of the circograph with and without automatic gain control.

The pick-up coils in the test coils have several functions:

1. defect inspection; 2. measurement of the spacing between pick-up and test piece; 3. switching off of the amplifier when the leading or trailing end of the semi-finished product passes the pick up coil; 4. generation of a control signal showing the degree of centring of the test part in the rotating head; 5. measurement of geometric properties of the material under test (out of roundness, diameter).

In addition to the defect signal, the complex pick-up coil generates a voltage which is only a function of its distance from the surface of the test piece. This "lift-off voltage" is used for the automatic gain control of the defect signals. According to Figure 12 the defect signal decreases when the spacing between the pick-up coil and the test piece increases. The lift-off voltage of the pick-up coil automatically controls the gain of the amplifier whenever the spacing between pick-up coil and test piece varies as in the case of a decentred or oval test piece.

In a certain range of spacing a specific defect will be signalled with the same amplitude no matter how large the spacing between the pick-up coil and the test piece. The lift-off voltage controls the gain of the amplifier automatically so that the gain increases with increasing spacing.

Figure 18 shows a defect signal obtained from a defect in a bar. The bar was placed in the rotating head and decentred in various steps. By this means the distance between the defect and the rotating coil was varied. The traces of the oscilloscope on the left-hand side in Figure 18 show the variations of the defect signal without automatic gain control. The variation of the amplitude of the defect signal is 5:1. The traces on the right-hand side were obtained after using the automatic gain control system. The defect signals remain practically constant.

For an eccentric position or an oval test piece this automatic gain control for the signal of a rotating pick-up coil is of general importance. If a round test piece is decentred the lift-off voltage is modulated with the first harmonic of the rotational frequency (if the pick-up coil makes one turn around a decentred round test piece there is one maximum and one minimum of the lift-off voltage). The display of this modulated lift-off voltage on the oscilloscope makes it possible to find out amplitude and direction of the eccentricity of the test piece in the rotating head. The lift-off voltage, which is modulated with the first harmonic, is used for mechanically balancing the rotating head in order to ensure an optimum centring of the test pieces while they travel through the test head. For an accurate geometric balancing of the test heads it is only necessary to adjust the position of the test head to a minimum modulation of the lift-off voltage. If the test piece is oval the lift-off voltage will be modulated with the second harmonic of the rotational frequency of the test head.

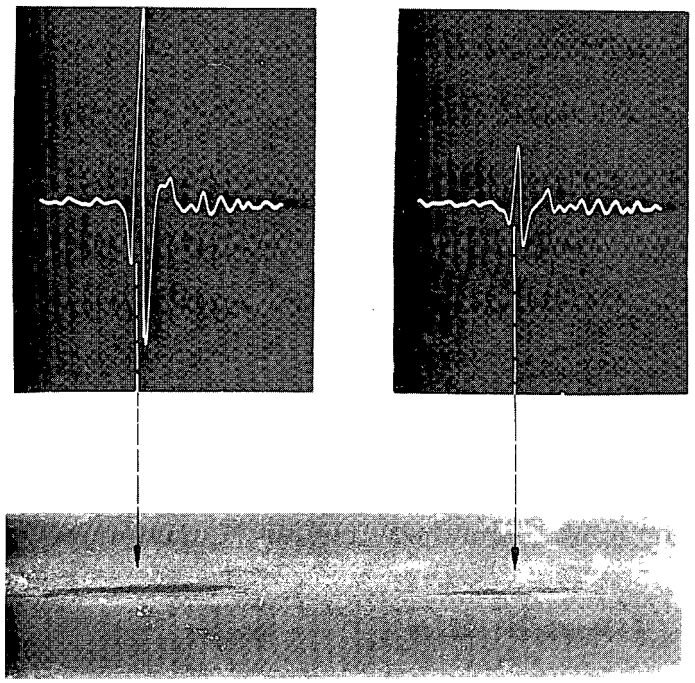

Figure 19. So-called folds in a seamless tube shown on the screen by representation of the "lift-off voltage".

Finally, the centre-line average of the lift-off voltage is a function of the diameter of the test piece. In addition to the crack detection the pick-up coil rotating in a distance around the test piece can be used for the determination of physical properties such as diameter, ovality, etc.

Another example in which the lift-off voltage gives important information is for the detection of folds in the tube. In

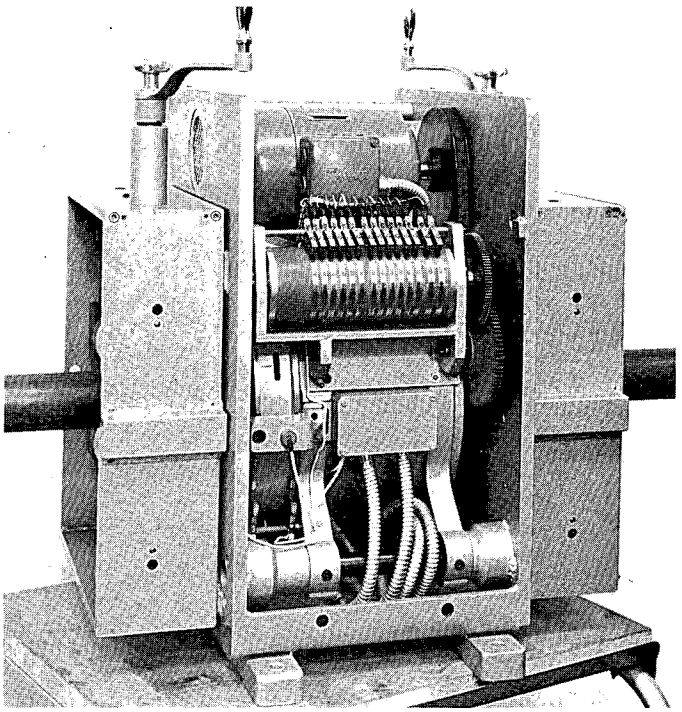

Figure 20. Rotating head of the circograph with the slip rings for every channel for paint-marking defects at their accurate location.

seamless tubes such folds occur from time to time as Figure 19 shows. As these folds represent only a geometric distortion but no separation of material, normally they cannot be found by means of eddy-current methods with encircling or rotating pick-up coils. Such coils are specifically designed for suppressions of such geometric effects. The lift-off voltage, though, indicates such folds as shown in Figure 19. The same is true for the display of so-called overfills and underfills in round billets.

In the inspection of heavier round material such as billets and tubes it is desirable to paint-mark the section in which there is a defect. Such a defect can be any place along the circumference of the test piece. For this reason the defect should be marked in its exact position on the circumference and, of course, its axial position. This is important if the defect must be conditioned. Paint-marks on the accurate location of the defect are obtained by panelling the circumference in 12, 16 or 24 "channels" according to 30°, 22.5° or 15° of the circumference

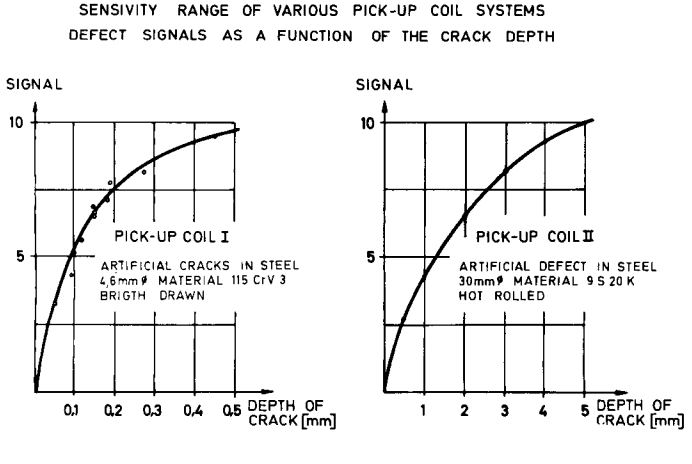

Figure 21. Sensitivity range of two pick-up coil systems for the lower and upper diameter range of the circograph.

of the test coil. There is a spray gun for every channel. Figure 20 shows the rotating head of the circograph with the slip rings for every channel. When a defect in the test material is detected the spray gun which belongs to the "channel" of this defect will be operated. Of course, there is a defined time delay for operating the spray guns according to the distance between the spray guns and the pick-up coils and according to the speed of the material under test.

In the lower size range of the circograph (e.g. wire inspection with Ro 0) much smaller defects must be found than in the upper size range (e.g. Ro III). For thin wires, defects as shallow as .001 in. (.025 mm) must be detected but quantitative measurements in the range of depth deeper than .020 in. (.5 mm) are not of interest.

For the large sizes, however, only defects deeper than .008 in. (.2 mm) are of interest but it should be possible to discriminate between a defect of .080 in., .120 in., .160 in. (2, 3 or even 4 mm). For this reason various pick-up coils for the various size ranges of the circograph were developed. Figure 21 shows the defect sensitivity of two pick-up coils for the lower and the upper size range.

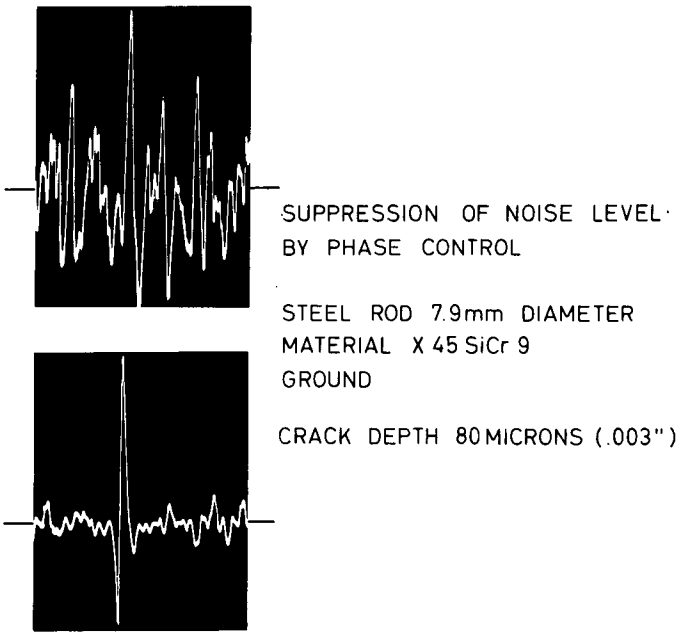

Figure 22. Suppression of the noise level by phase control.

The theoretical and experimental investigations of the pick-up coil showed that by principle it is not possible to cover the ranges of both the lower depth (.02 through .5 mm) and the higher depth of defect (.2 through 5 mm). For achieving a good defect resolution of pick-up coils it is necessary to design their shapes as well as the layout of the test instrument such that there is a maximum phase angle between effects of defects and effects due to the geometric properties such as diameter, out-of-roundness or roughness. Figure 22 shows an example of a defect signal of a defect with a depth of .003 in. (.08 mm). In the upper oscillograph curve the defect signal is nearly buried in the noise which is caused by geometric effects. In the lower oscillograph curve this noise due to roughness has been suppressed to a great extent by turning the instrument to an optimum phase selection. Figure 23 shows various defect signals and some of the corresponding micrographs with chromium steel parts having a diameter of .120 in. (3 mm.). The amplitude of the defect signal depends on the depth of the defect as well as on its direction with reference to the surface. Normally the depth of a defect is defined by its component vertical to the surface. If a defect

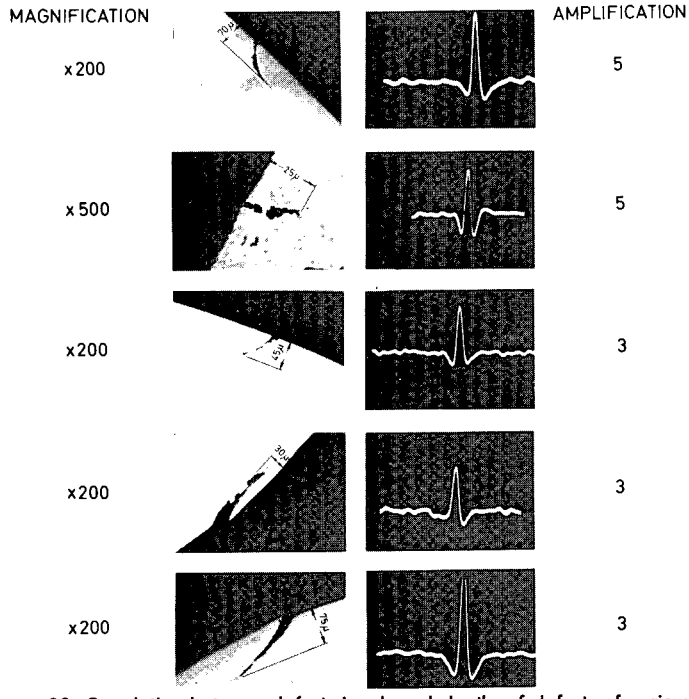

Figure 23. Correlation between defect signals and depths of defects of various shapes of defects.

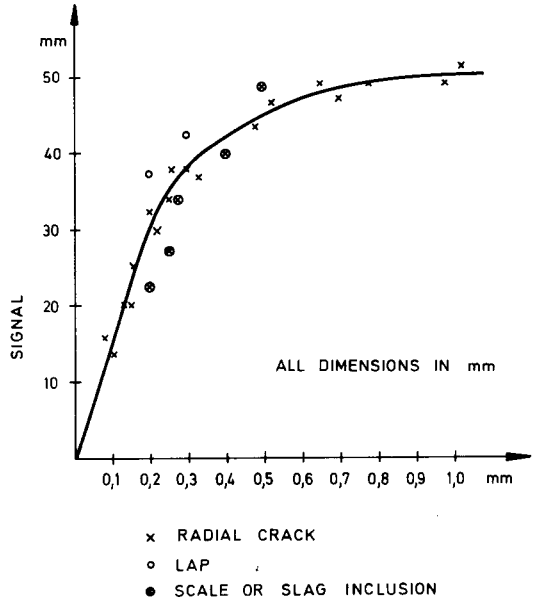

Figure 24. Correlation between depth of defect and defect signal found by circograph experiments.

is inclined to the surface (e.g. a lap) there is a higher signal compared with a signal of a vertical crack. This can be clearly seen in Figure 23. Frequently for specific grades of steel specific types of defects will prevail. An example of this is given in Figure 24.* There is a comparatively good correlation between the depth of defect and the defect signals. The data found by experiment show the relatively narrow band of error.

Comparison of Eddy-Current and Magnetographic Defect Signals

For a finished surface there is a good resolution by the eddy-current method. For hot-rolled material the defect resolution

* For the results of Figure 24 we are indebted to Klöckner Werke AG, Georgsmarienhütte, W. Germany.

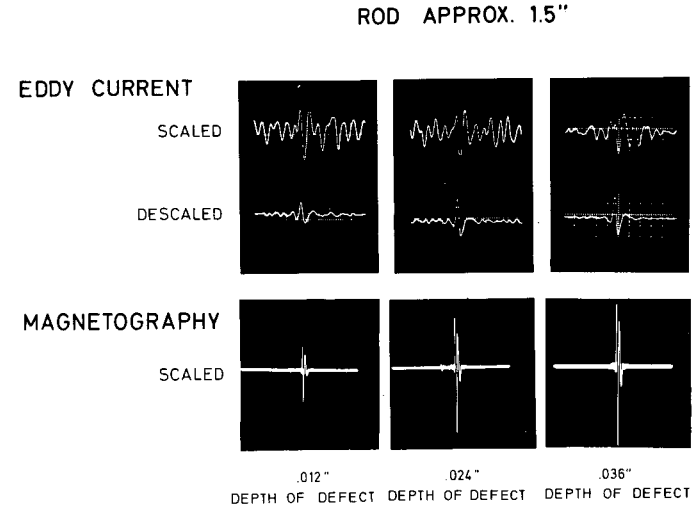

Figure 25. Comparison of the eddy-current and magnetographic methods on scaled and descaled steel rounds.

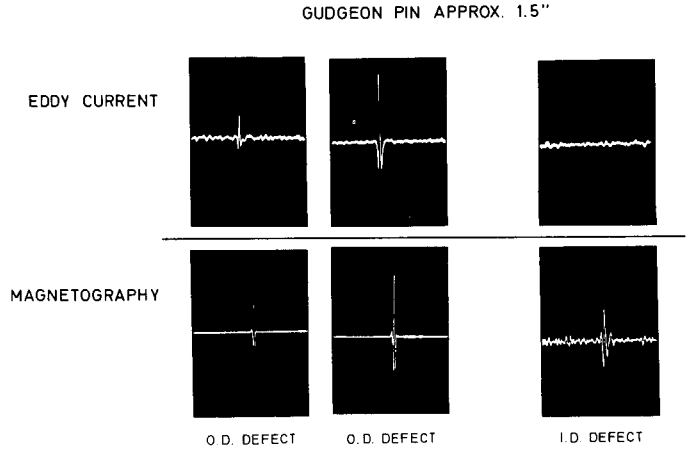

Figure 26. Comparison of eddy-current and magnetographic method on finished parts.

depends on scale conditions, its composition, its thickness and the presence of sharp edges.

For a long period numerous circographs have been successfully applied for the inspection of hot-rolled, semi-finished products. Nevertheless, the limitations of the circograph method which is given by thick scale must be mentioned. In Figure 25 the upper oscillograph curves show that the signals of three defects with depths of .012 in., .024 in., .036 in. (.3, .6 and .9 mm) are nearly buried in the background noise due to the scale. After the thick scale was removed the background noise was so far reduced that there was a good signal-to-noise ratio. (For the defect which is .9 mm deep the gain was reduced by 30% in order to see the full signal on the screen.)

In the bottom line in Figure 25 the signals obtained with the magnetographic method are shown. These measurements were made in the as-rolled condition before the scale was removed.

This example of heavily scaled material should be compared with another example of material with a finished surface. Figure 26 shows the indication of a very small seam in a gudgeon pin. The test parts were inspected with both eddy currents and magnetography. The top line shows defect signals obtained by the eddy currents and the bottom line those obtained by magnetography. In Figure 26 the resolution of both methods is almost equally good but it should be noted that—as shown in the two right hand traces—there can be no indication of a subsurface defect with eddy-current pick-up coils.

Figures 1-4 as well as 22-26 give important information for choosing the optimum test method.

1. For test parts having a surface that is not very rough, the eddy-current method utilizing a rotating pick-up coil is recommended. For defects open to the surface, the inspection is fast and has a good defect resolution.

2. Of all known nondestructive test methods the magnetographic method depends least on surface conditions. Both surface and subsurface defects are detected. For applying the magnetographic method, though, it is necessary that the test parts be magnetized by a yoke or a direct current during the full time of inspection. Only hardened test parts such as gudgeon pins, ball-bearing parts etc. can be magnetized before the test because in this case the residual field can be used.

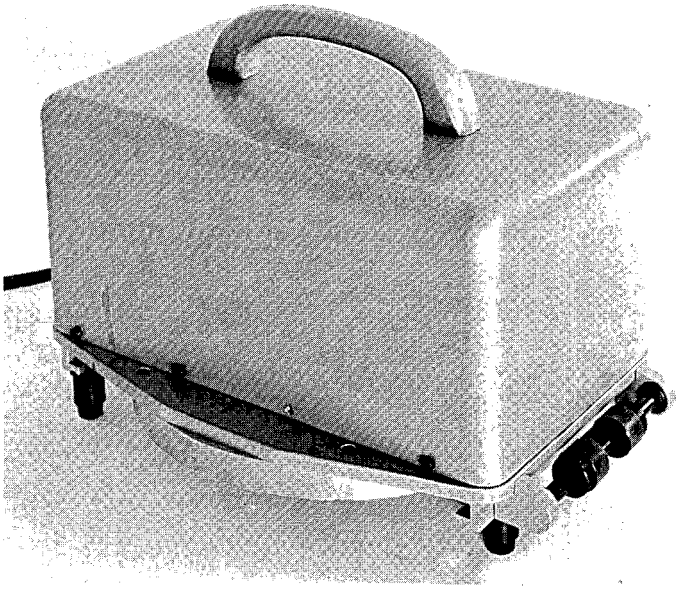

Figure 27. Rotating disc with eddy-current pick-up coil for the defect inspection of flat material.

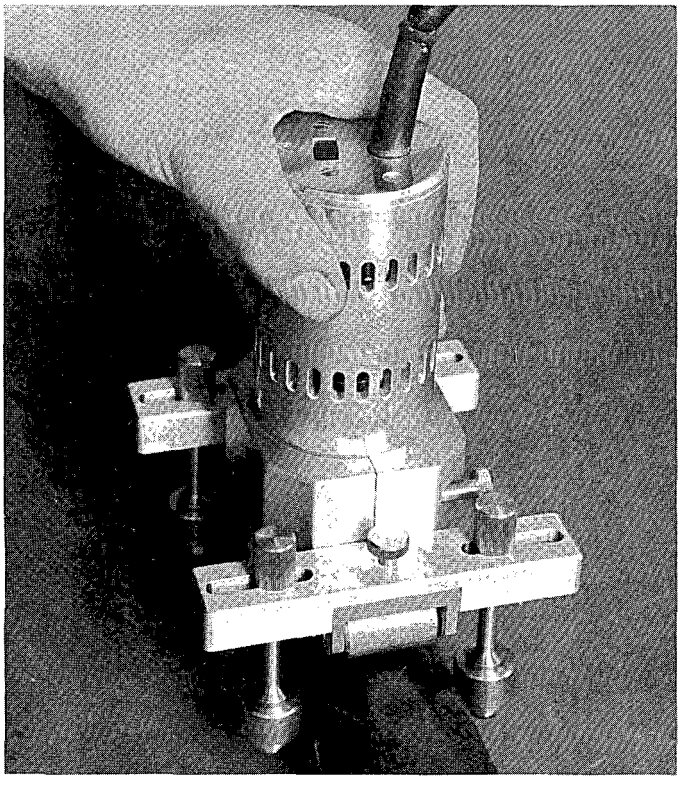

Figure 28. Rotating disc with eddy-current probe for the continuous inspection of welds for surface defects.

3. When there is heavily scaled material the magnetographic test method is superior, but when finished parts or, for example, hot-rolled straightened bars are to be inspected the eddy-current method is simpler because there is no need for magnetizing.

4. Eddy currents can be applied by utilizing encircling differential coils or rotating absolute pick-up coils. It is most advantageous to use a combination of encircling coils and rotating pick-up coils. The encircling coil detects even very short surface and subsurface defects but it does not have the same sensitivity for very small depth-variation. Such surface defects are indicated with full sensitivity by the rotating pick-up coil. In this case it is not necessary that the rotational speed of the pick-up coil be very high because the pitch of the scanning helix can be fairly large as the short defects are detected with the encircling coils.

Eddy-Current Pick-up Coils in Rotating Discs

There are various applications in which flat material has to be inspected for surface defects. Figure 27 shows such a rotating disc in which field focussing pick-up coils are mounted. The disc has a rotational speed of 50 to 60 rev/sec and there are four pick-ups on the circumference of the disc. Therefore there are 200 to 240 scanning lines/sec.

The disc is moved along, for example, the surface of a strip, similar to moving a vacuum cleaner. Thus, surface defects are detected. For larger sheets several rotating discs can be applied parallel to one another.

There are other applications in which a rotating disc has to inspect only a certain area e.g. each disc has to look at one side of a rectangular or hexagonal bar or the faces of stainless steel billets.

Figure 28 shows another example of a small rotating disc as it is applied for the testing of electrically welded tubes. Note that this application is for the detection of surface defects only. For surface defects the defect signals are fairly well proportionate to the depth of defects and they do not depend on their width. The rotating disc shown in Figure 28 maintains a relatively accurate acceptance limit. Although the resolution of the system is much higher it has proved to be of greatest interest to monitor all defects deeper than 12.5% of the wall thickness as claimed by the API standards.

Figure 29 shows a comparison of the eddy-current pick-up coil with the magnetographic method in the example of a welded tube with a diameter of 4 in. (100 mm). In the top line of Figure 29 the defect signals which were obtained with rotating eddy-current discs are shown. The bottom line shows the corresponding magnetography signals. The two lines in the middle show the peak-writer records of the eddy current and of the magnetographic method. The charts represent the full length of the tube. Figure 30 shows the micrographs which belong to the four defect signals in Figure 29.

If the question is to find, record or paint-mark surface defects only (e.g. in a welding line) the eddy-current method with rotating disc and 200 to 240 scanning lines/sec is very suitable.

A combination of the encircling coil method with the rotating disc in a welding line is also advantageous because under these conditions surface defects in the weld which have a very constant depth will be indicated with the full sensitivity by the rotating disc and encircling coils will detect short defects as well as I.D. defects.

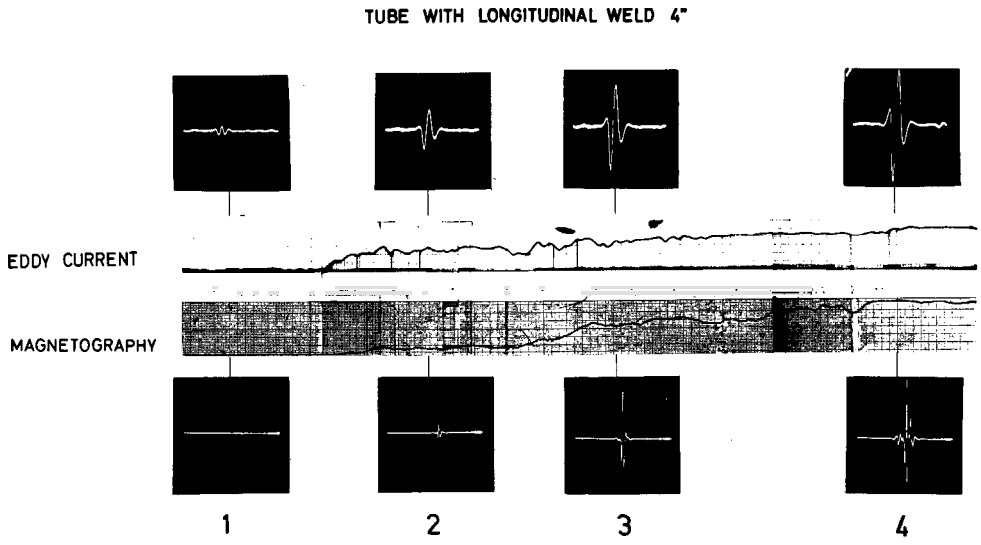

Figure 29
Comparison of the eddy-current method (rotating disc with pick-up coil) with the magnetographic method for testing welds in steel tubes.

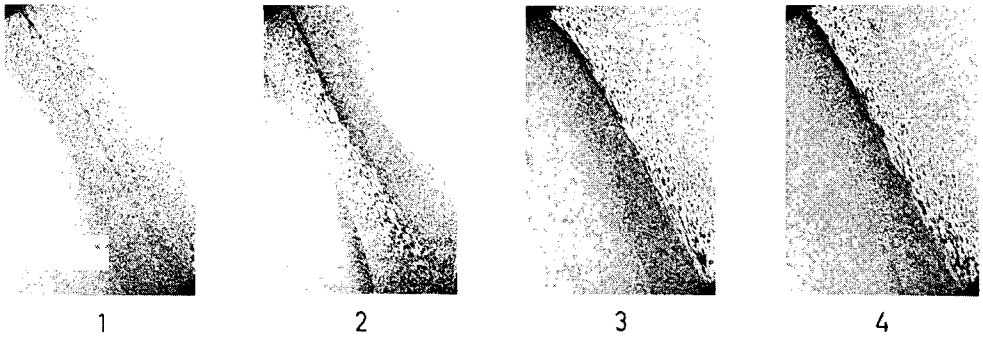

Figure 30
Four micrographs corresponding to the defect signals 1 through 4 of Figure 29.

New Components for Automation of Nondestructive Testing

More and more nondestructive testing methods operate as an integral part of fully automated installations. Therefore new auxiliary components have to be developed. In this paper the following new devices for automation are discussed. 1. proximity feelers; 2. slit monitors; 3. weld follower.

1. The proximity feeler should monitor: a) that the product to be tested is in a certain location; b) that the leading or trailing edge of the weld has arrived at the feeler; c) that the joint area has arrived in a certain location if the material under test is transported "nose to tail".

In a "nose to tail" operation photo-electric gates can no longer be used for monitoring. For proximity feelers in many phases barium-titanate crystals have been used in a magnetic bridge arrangement. But semi-finished products such as tubes and bars frequently have strong magnetic poles at their ends. For this reason disturbances are unavoidable when such magnetic direct field proximity feelers are used. Proximity feelers working on the induction principle are also in use but these have only a very short operating range.

The goal of this development was a proximity feeler which could monitor the leading or the trailing end or the joint area with an accuracy of a few millimetres. The distance of the feeler from the test material had to be as long as 1–1½ in. As the result of such a development Figure 32 shows the voltage of the proximity feeler while passing the leading or trailing end or a joint area. The distance between the feeler and the material under test was $1\frac{3}{16}$ in. (30 mm). The monitor is operated when the voltage goes through zero. This proximity feeler gives monitor pulses when the leading edge and the trailing edge or the joint area pass along. The pulses do not depend on speed and temperature of the material under test. If the ends or the joint area of the semi-finished product are far away from the proximity feeler, its voltage approaches zero. In another design of this feeler an additional voltage is obtained as long as the product is near the feeler. Thus, there is an additional discrimination between "product there" and "no product there".

2. The slit monitor is used for monitoring open welds. It is known that with differential coils only the beginning and the end of entirely open welds are detected. Figure 32 shows an eddy-current test system for welded tubes with a slit monitor coil. The electronic modules of this monitor are in the bottom rack of the cabinet.

The large diameter range in which such a slit monitor coil can operate is remarkable. For the whole range of tube diameters between $\frac{3}{8}$ in.–12 in. (10 and 300 mm) only two easily exchangeable coils are needed. In a coil with an inside diameter of 4 in. (100 mm) tubes in a diameter range of $\frac{5}{16}$ in.–3½ in. (15–90 mm) can be tested for open welds.

Figure 33 shows the voltage across the module terminals of the slit monitor as a function of the tube length. In the tubes with diameters of $\frac{13}{16}$ in., 2 in., 3½ in. (20, 48 and 90 mm) there were two slits with 8 in. and 24 in. (200 and 600 mm) each. The slit monitor signals three conditions:

a) tube with good weld: voltage = 0; b) tube with slit: voltage positive; c) no tube in coil: voltage negative.

For a tube with $\frac{13}{16}$ in. (20 mm) diameter which is in a coil having an inside diameter of 4 in. (100 mm) the fill factor is only 4%. Even under these conditions the voltage due to a slit in the tube is as much as 2 volts without any amplification.

3. The weld follower is used for accurately guiding test systems on the weld e.g. the rotating discs with eddy-current probes Figure 28. Such a device is needed because in a welding line there is very often a wandering of the weld. In the weld

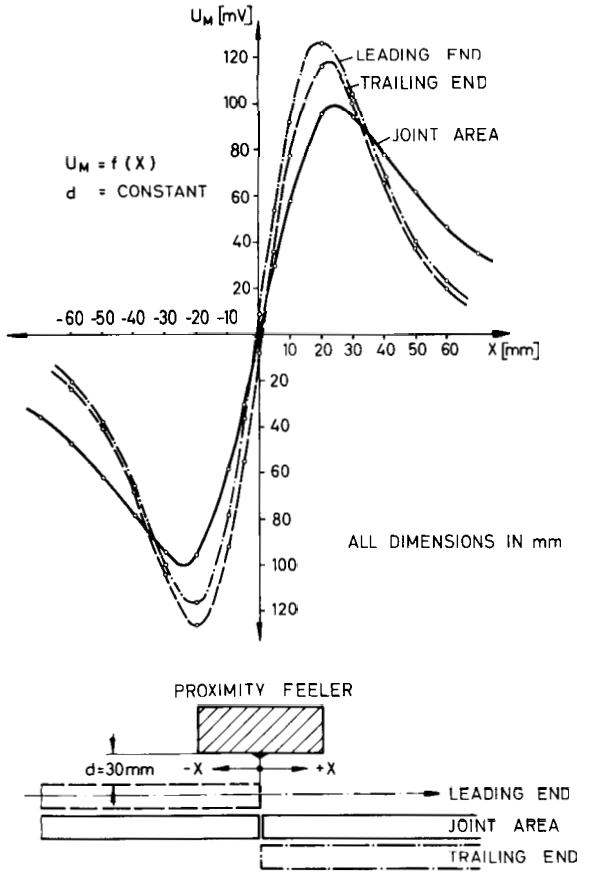

Figure 31. Voltage of proximity feeler when passing along the leading or trailing edge or the joint area of the tube. Distance between the proximity feeler and tube = $1\frac{1}{5}$ in. (30 mm).

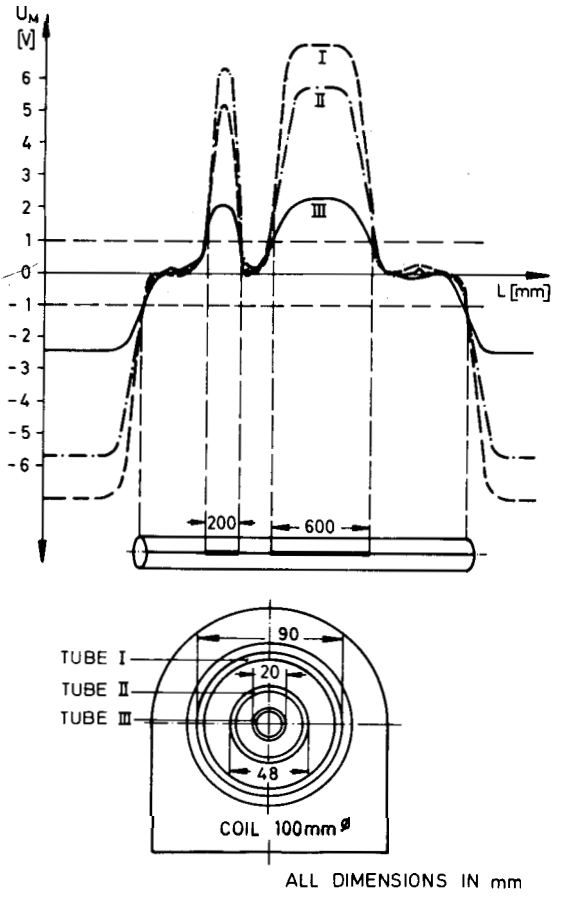

Figure 33. Voltage of slit monitor for good tube, open weld or for no tube. Tube diameters: approx. $\frac{13}{16}$ in., 2 in., $3\frac{1}{2}$ in. (20, 48 and 90 mm).

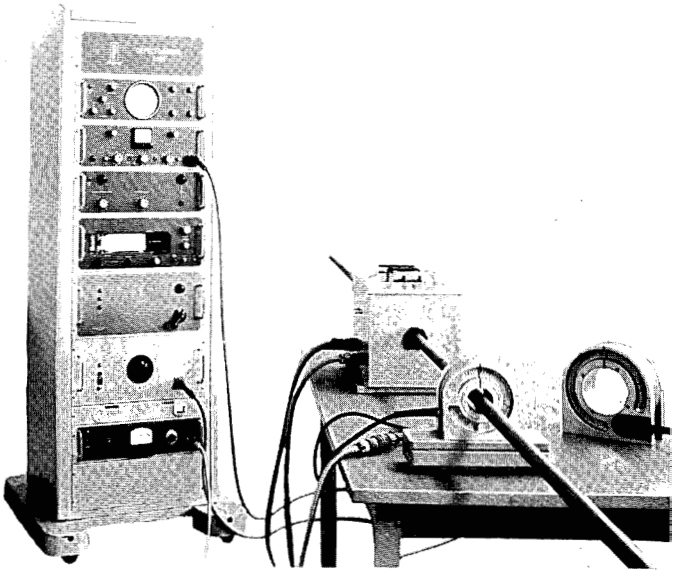

Figure 32. Eddy-current test installation for in-line weld testing with slit monitor and defect test coil.

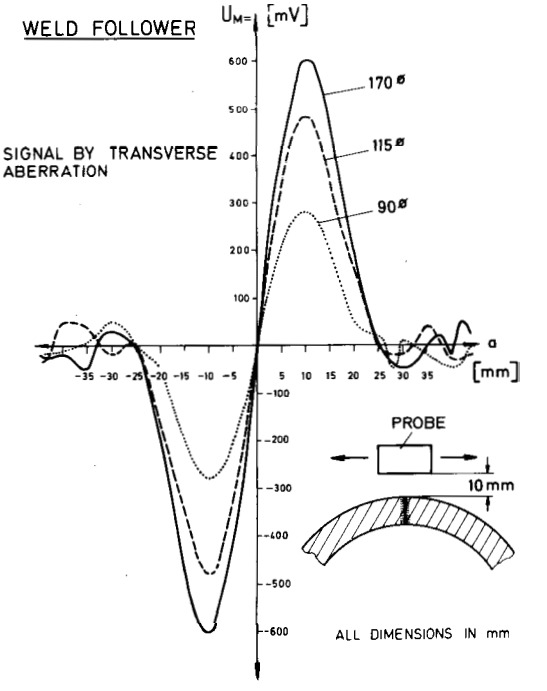

Figure 34. Voltage of weld-finder as a function of its transverse aberration from the weld.

follower a specific eddy-current probe is used. The probe feels the difference in permeability between the weld and the vicinity of the weld which was not heated during the welding process.

The standard distance of the weld probe to the surface is $\frac{3}{8}$ in. (10 mm). Figure 34 shows the voltage across the terminals

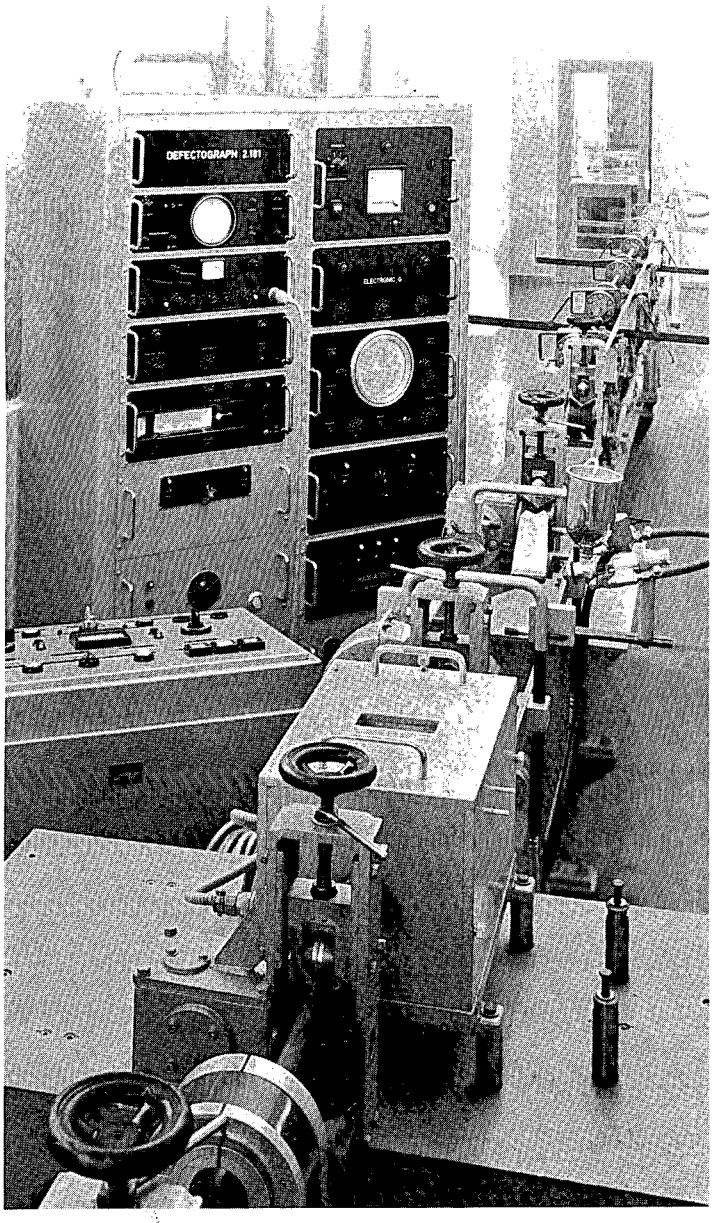

Figure 35. Automatic eddy-current test line for the simultaneous inspection of semi-finished products for defects and quality.

of the probe (without amplification) as a function of its transverse aberration from the weld. While the weld probe travels across the centre of the weld the voltage goes through zero with a very steep slope. With this voltage a servo-motor is controlled and resets the probe automatically to the weld if the latter has been wandering. The accuracy is approx. .040 in.–.080 in. (1–2 mm). The probe and the test system are fixed in one ring mount. Thus, the probe follows the weld in any direction it may wander.

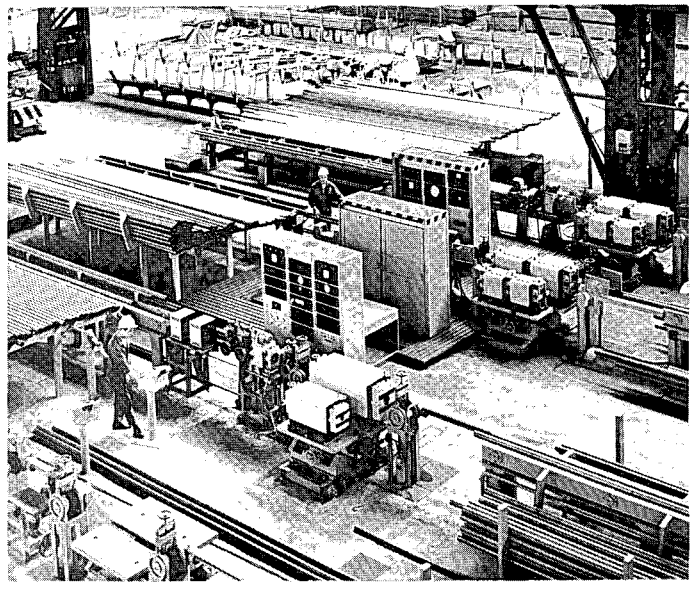

Figure 36. Four parallel installations for nondestructive eddy-current testing of tubes.

Fully Mechanized Installations for Nondestructive Testing

There is a strongly increasing tendency for setting up fully mechanized test lines with 100% inspection of production. The above mentioned progress in the field of nondestructive testing by means of electro-magnetic methods is important because:

1. the electro-magnetic test methods are specially suitable for automation; 2. the test speed is very high and can be as fast as 8000 ft/min (40 m/sec); 3. there is no need for touching the material during the test; 4. the tests are possible under extreme temperature conditions, up to 1000°C (1800°F); 5. the material under test remains dry so that several test procedures (e.g. for defects, mixtures, dimension, length, wall thickness and shape) can be adapted simultaneously. As an example of a combined inspection Figure 35 shows an automatic installation for simultaneous inspection for defects and quality (mixtures, hardness etc.).

In the foreground the test coil for quality is visible. Behind it there is the magnetizing yoke with the defect test coil. On the left hand side the control desk is seen on which the test operation is started by pushing a button and from there on the whole test procedure keeps going in a closed-loop system.

Such control desks are built for complicated test, sorting and conditioning procedures. In a welded line for instance it may be necessary to cut the tubes into sections of definite length but defective parts of the tube have to be cut out automatically. The proximity feelers will follow these defective tubings on their path while they are singled. At the end of the test line the tubes will be automatically sorted into groups—"good", "defective" or "scrap".

Numerous complicated test programs have been realized with such mechanized installations.

Figure 36 shows for parallel large installations for the nondestructive testing of tubes (of the fourth installation in the foreground only the support is visible). The tubes travel through the installation 24 hours a day with a speed of 400 ft/min (2 m/sec). They are inspected for O.D. and I.D. defects and for folds. In the installations, Figure 36, encircling coils and rotating pick-up coils are successfully combined.

Technical Session 8/ Surface Methods and Neutron Radiography

Removal Techniques in Penetrant Inspection Processes, Their Development and Effect on Sensitivity

R. E. BIRLEY, N. H. HYAM and J. TEBBENHAM, U.K.

Introduction

The history of penetrant inspection processes may be traced back to the simple oil and chalk methods in use a good many years ago. From this comparatively crude, but effective technique, modern penetrant inspection processes, based on visible and fluorescent dyes and utilizing a separate penetrant remover, were developed.

The incentive, especially in the aerospace industries, to develop these processes, is provided by the constant demand to improve the weight/strength ratios of engineering components, so that stresses have approximated ever more closely to the yield point of the materials of construction.

Consequently, the need has arisen to find surface discontinuities of ever decreasing dimensions, which can lead to premature failure during service. Because the materials of construction used in the aerospace industries are largely non-magnetic and thus preclude the use of magnetic-particle inspection, the need for sensitive penetrant inspection processes becomes apparent.

Principles

The principles underlying all penetrant inspection processes may be summarized thus:

Penetration

Penetrant is applied to the surface under examination and allowed to remain in contact sufficiently long to permit it to enter any discontinuities that may be present and which are open to the surface and free from contamination.

Removal of Excess Penetrant

The excess penetrant is removed from the surface of the component, leaving behind the entrapped penetrant in the discontinuities.

Development of the Penetrant Indications

The entrapped penetrant is drawn to the surface by means of a suitable developer to give a magnified indication of the discontinuity.

Performance

Several factors determine the performance and sensitivity of penetrant inspection processes:

1. The physical properties of the penetrant, which include: (a) The ability of the penetrant to enter a defect of minimal dimensions; (b) The weight of dye per unit volume of penetrant thus carried into the defect, i.e. the solubility of the dye in the penetrant; (c) The optical properties of the dye; its thin film characteristics, i.e. the minimum thickness of dye solution film which, when subjected to ultraviolet irradiation, is visible; and the intensity of the visible light emitted by it under standard conditions of ultraviolet irradiation; 2. The physical nature and condition of the surface to be examined and its preparation for penetrant inspection; 3. The nature of the discontinuity, its geometry and dimensions; 4. It is also necessary that the discontinuity be open to the surface and free from contaminants, including residues of cleaning compounds, which could preclude the entry of the penetrant or impair the fluorescence of the dyes; 5. Method of removing excess penetrant; 6. Nature of the developer.

Removal Methods

It is considered that, provided penetrant has entered a defect, the most critical and very often abused step in the penetrant inspection process is the removal of excess penetrant; and it is this particular aspect of penetrant inspection which is discussed in detail.

Four methods of penetrant removal are generally used:

1. Water rinsing; 2. A combination of water rinsing and solvent removers; 3. Solvent removers; 4. A combination of an emulsifier and water rinsing.

The object of all the above methods is to remove the excess penetrant from the surface and at the same time, allow the entrapped penetrant to remain behind in discontinuities open to the surface.

It is not easy to achieve this on a wide variety of materials and surface finishes with one penetrant; yet to a large extent, the success of the penetrant inspection process in locating surface discontinuities depends on this step. If the penetrant remover is too searching, then penetrant can be removed from surface discontinuities; on the other hand, if excess penetrant is incompletely removed, a high degree of background colour will remain which will reduce contrast and mask fine defect indications.

Of the four methods listed, numbers 1 to 3 are generally used in conjunction with red dye penetrants, while method 4 is generally preferred for use in conjunction with fluorescent penetrants. Most fluorescent penetrants are water insoluble and

hence are not directly water washable; to render them so, requires the use of an emulsifier. The emulsifier may be incorporated in the penetrant, or it may be applied as a separate operation.

Water-Washable Penetrants

Water-washable penetrants are formulated by incorporating surface-active agents in the solvent system. By varying the percentage of surface-active agent and its hydrophilic/lipophilic balance, the response of the penetrant to water washing can be controlled and adjusted. The term hydrophilic/lipophilic balance is explained more fully later.

The degree of susceptibility to water washing desirable in such a penetrant, is dictated by the surface texture of the components to be examined and the level of sensitivity required.

Rough surfaces, such as are presented by castings or shot-blasted sheet metal, require penetrants having exceptionally good response to water washing. However, high levels of water washability on difficult surfaces, can only be achieved at the expense of sensitivity, in the sense that there is an increased risk of washing penetrant out of fine, shallow defects.

Therefore, water-washable penetrants are generally reserved for less critical applications and are not normally used on highly stressed components. Ideally, a water-washable penetrant should be formulated for a specific surface condition. In practice, a range of two or three penetrants with varying susceptibility to water washing are sufficient to cover a wide range of applications.

Penetrant Removers

If a penetrant is not emulsifiable and therefore not directly water washable, then it must be exposed to a penetrant remover that will render it susceptible to water washing. For this type of process, the penetrant remover is applied as a separate operation. The sensitivity of the process can be controlled by varying the contact time between the penetrant and the remover. Experience has shown that these contact times are critical if maximum sensitivity is to be achieved. It has also been shown that if the surface film of penetrant is uniformly even and thin, only very brief contact times are required, thus contributing to the sensitivity of the process.

The action of a penetrant-compatible remover depends on the mutual solubility between it and the penetrant. Therefore, the contact period must be kept quite short, if appreciable dilution of entrapped penetrant is to be avoided.

It was therefore argued, that if a penetrant remover could be formulated in which the penetrant was insoluble, then the danger of dilution could be removed entirely. Also, if such a penetrant remover possessed high water tolerance, it would become possible to use a sprayed water rinse prior to immersion in the penetrant remover. This would ensure that a thin uniform film of penetrant covers the component.

It was considered that a penetrant remover, based on water and therefore insoluble in the penetrant, would satisfy two important requirements for achieving high sensitivity, namely: the presence of a uniform thin film of penetrant and the elimination of the risk of diluting entrapped penetrant or even removing it entirely by excessively long periods of contact.

Development work was therefore carried out, using dilute solutions of non-ionic surface-active agents, to test the validity of this argument. Large-scale trials were carried out on turbine blades that had been in service. These blades were electropolished and subjected to careful binocular inspection to identify all defects.

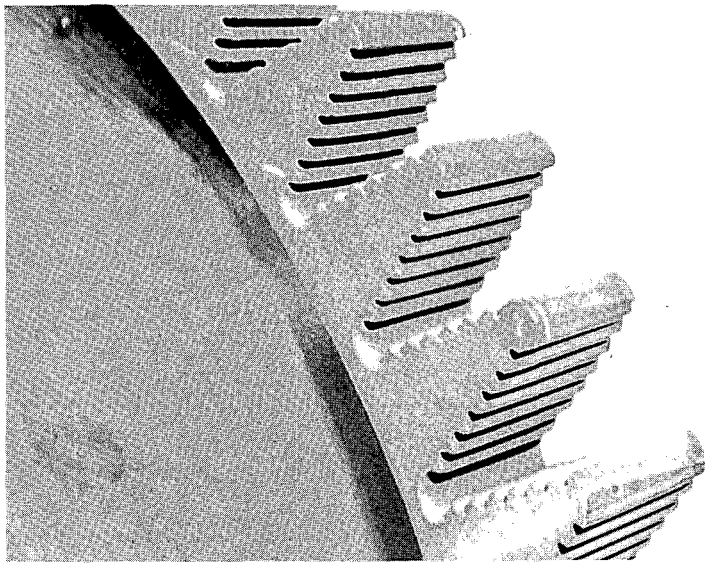

Figure 1. Typical fir-tree serrations on turbine disc.

Subsequently they were subjected to penetrant inspection, using high-sensitivity fluorescent penetrants, in one case with penetrant-compatible removers, and in the other with aqueous penetrant removers.

Further tests were carried out using a standard sensitivity fluorescent penetrant, again once in conjunction with a penetrant-compatible remover and once with an aqueous penetrant remover.

The results of these tests showed that a significantly higher level of sensitivity can be achieved with a given penetrant when used with an aqueous penetrant remover.

This novel approach to penetrant removal was the result of close collaboration between the user of the penetrant inspection process and the formulator. The idea was taken up by the aero-engine division of Rolls-Royce Ltd., and for several years the inspection of critical jet engine components has been carried out using a standard sensitivity penetrant in conjunction with a carefully formulated hydrophilic penetrant remover, such as ARDROX 9PR4 manufactured by Brent Chemical Products Ltd.

In view of the great importance of the penetrant removal operation, it is useful to consider penetrant removers in some detail. Because most penetrants are based on an oil-soluble dye system, the removal of excess penetrant, other than by liquid or vapour-phase solvent, depends on the formation of an emulsion with an aqueous cleaning phase.

An emulsion is a dispersion of one normally immiscible liquid in another. One liquid will be present as discrete droplets—the disperse phase—distributed through the other phase—the continuous phase. If the two phases are oil and water, it is possible to obtain two different emulsion systems, oil in water and water in oil. For the present purpose, only the oil-in-water system is considered. Oil may be dispersed in water by the application of mechanical energy, but the emulsion so produced is coarse and unstable. However, by the addition of a surface-active agent, the emulsion becomes fine grained, more stable and requires less mechanical energy to produce. If sufficient suitable surface-active agent is used, the emulsion can form on single contact of the phases. In this case, the chemical energy of the surfactant on its own produces an emulsion.

The chemical energy is manifested as a tendency of the surfactant molecules to reduce interfacial tension, to diffuse

rapidly to the phase interface, stabilize it and to occupy the maximum area. This latter function is accomplished by the formation of small droplets.

These properties of surface-active materials are derived from the presence in the molecule of two groups differing in their polar nature. Highly polar groups, such as the sulphate, sulphonate and quaternary nitrogen groups, together with the non-ionized less polar groups such as the ether, ester and amide groups, confer a tendency to water solubility and are termed hydrophilic groups. The hydrocarbon portion of the surfactant molecule will confer a tendency to oil solubility and is termed a lipophilic group. The relative power of the two types of groups within a surfactant molecule is often referred to as the hydrophilic/lipophilic balance, or H/L balance of the surfactant.

While ionizing polar groups are individually more highly hydrated than non-ionizing ones, an adequate total degree of hydration can be achieved if a sufficient number of non-ionizing polar groups are present. The extent to which the molecule is hydrophilic can thus be varied in smaller steps, since the effect of each non-ionic polar group is smaller. It has been suggested that one sulphate group is approximately equal to four polyether groups of the ethanoxy type.

Such non-ionic surfactants give the choice of a finely graded range of H/L values apart from other associated advantages such as the absence of ionizable matter and potentially corrosive inorganic residues.

The removal by emulsification of excess penetrant from the surface of a component is achieved by applying a separate solution of an emulsifier after the penetrant contact period has elapsed. The emulsifier, consisting of a blend of surface-active agents in a non-volatile solvent medium, diffuses into the penetrant layer; on subsequent water washing, the penetrant residues are converted into an emulsion in the water stream and carried away.

The surface-active agents have a fairly low H/L balance to confer on them solubility in the solvent. More efficient removal of excess penetrant can be achieved by increasing the H/L balance with the attendant risk of removing also very fine indications.

Penetrant removers, incorporating a surfactant, with excessively low H/L balance will leave a heavy background fluorescence. The margin between the two effects is often small and so the availability of penetrant removers with a finely graduated range of H/L balance is of great importance.

Another important consideration is the effect of the surface texture of the component on penetrant-removal efficiency. A relatively rough surface, as on a casting, requires an emulsifier with a higher H/L balance than one to be used on a smooth machined surface.

The Hydrophilic Removers

These consist of aqueous solutions of surface-active agents and corrosion inhibitors. They are generally prepared in the form of concentrates, capable of dilution with up to twenty times their own volume of water, before use. The surface-active agent system is highly hydrophilic and is insoluble in the penetrant as is the penetrant in it. It is this mutual insolubility which prevents any dilution of entrapped penetrant and consequent weakening of indications.

Its mode of action is probably a wetting process, whereby the reduced interfacial tension results in the oil phase of the penetrant being displaced by the aqueous remover.

Although hydrophilic penetrant removers form emulsions, these are not stable. This has the advantage that it makes easier the disposal of effluent arising from such a process. Additional advantages attaching to the use of hydrophilic removers are:—

1. They are not sensitive to contamination by water, and it is therefore possible and in some cases desirable, to rinse components with water only prior to immersion in the penetrant remover; this technique, which ensures the presence of an even thin film of penetrant over the entire area of the component, reduces the penetrant remover contact time required and therefore enhances sensitivity. It is not possible to use this method with the conventional penetrant-compatible remover, which is sensitive to water contamination. This technique also minimizes the amount of penetrant contamination carried into the remover and therefore extends its useful service life; 2. Although it is always desirable to minimize the penetrant remover contact time, this is in fact less critical in the case of hydrophilic removers, because of the mutual insolubility of the penetrant and the remover; 3. Hydrophilic penetrant removers are more economic by a factor varying between 5 and 20, according to the strength of the solution used.

Alternative methods of removing excess penetrant are provided by the use of what has been described as particulate removers. These methods have the merit that the danger of removing entrapped penetrant is practically absent, because the medium is in contact only with the surface of the metal and cannot enter into a defect.

In order to minimize the possibility of metal removal and peening over fine defects, plumstones, or similar materials of low abrasive properties, are used. The technique, known as 'plumstone blasting' has been used successfully and was found to be very sensitive. However, it is a rather tedious process and has found application only to a limited extent, such as for example, on turbine blades where very fine thermal shock cracks are sought.

Another abrasive technique described as 'vibratory barrelling' involves the use of an apparatus capable of being vibrated mechanically. It consists of a barrel filled with ceramic chips, preferably of triangular cross-section, and about $\frac{1}{4}$ in. size. The components to be treated in this manner are dispersed throughout the marble chips and the vibratory motion commenced. While the sensitivity achieved by this penetrant-removal technique is good, it has not found acceptance because mechanical damage can occur during this operation and not all surfaces of the components are cleaned satisfactorily.

Finally, a recent development in penetrant-removal techniques is represented by the use of a continuously moving column of foam. The initial impetus for investigating this method was provided by the necessity of inspecting the fir-tree slots on turbine discs for fatigue cracks.

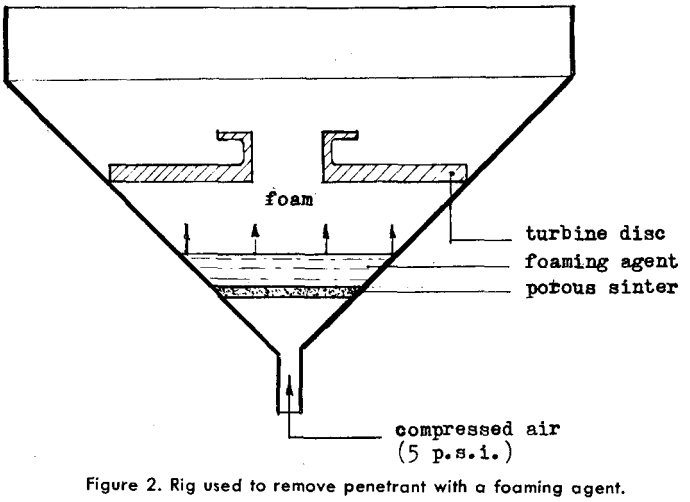

Figure 2. Rig used to remove penetrant with a foaming agent.

Using conventional penetrant-removal techniques, it was not found possible to achieve sufficiently low levels of background fluorescence to enable the very fine fatigue cracks to be clearly distinguished. Conversely, when background was completely removed by excessive washing, the indications were similarly removed.

It has been found that if a gentle stream of air is passed through a dilute solution of a hydrophilic remover, such as ARDROX 9PR4, a foam is generated which, if allowed to travel over the penetrant-contaminated surface, will clean it very efficiently. An interesting point about this is that although almost complete absence of background fluorescence is achieved, no penetrant is removed from even the finest cracks and indications are very clearly revealed.

For this method to be successful, it is necessary that the foam should be moving continuously over the surface. Trials have been carried out with this technique on turbine discs with known cracks. The defects had been previously located by first of all etching the discs anodically and subsequently inspecting them with a binocular microscope with X 15 magnification. Only 20 per cent of the defects were revealed by a standard penetrant inspection process using liquid penetrant removers, whether lipophilic or hydrophilic, and owing to high background fluorescence, they were difficult to identify.

When examination with the same penetrant was repeated, using the foam removal technique, 80 per cent of the known defects were readily identified. A third examination, using a high-sensitivity penetrant in conjunction with the foam removal technique, revealed all the defects with complete absence of background fluorescence. Subsequent metallurgical examination revealed that these cracks were very tight and varied in depth from .001 to .04 inch.

These results appear to show that the sensitivity of penetrant inspection can be increased considerably by the use of this technique.

The efficiency of foam removal is probably due to a number of factors, among them:—

(a) The increased surface energy associated with bubbles compared with the liquid phase. This view is supported by the rapid rate at which removal takes place; (b) The prevention of redeposition and the renewal of active foam provided by a continuously moving stream.

A possible view of the process is that of a rapid displacement or rolling-off action, in which the oily penetrant is carried away as small droplets at the junction between the foam lamellae.

The foam removal technique is considered to have a great potential not yet fully explored. The major limitation to the technique at present is the geometry of the component, which makes it difficult to fulfill the requirement that there be a free flow of foam over the surface to be cleaned.

In conclusion, it can be said that these developments in removal techniques amply illustrate the importance of this aspect of penetrant inspection in attaining maximum sensitivity. In fact, the levels of sensitivity that can now be readily attained, bring to the forefront the problem of interpretation and evaluation of small surface defects previously not revealed. The delineation of new standards in this field should lead to the establishment of even higher safety factors for critical applications of engineering components.

Discussion

Q. J. D. MARBLE, General Electric Co., Cincinnati, USA:

Would foam penetrant removal techniques work well on vapour blasted (water suspended grit) surfaces?

Is dry developer or wet developer preferred after foam penetrant removal technique?

A. Foam removal technique would be effective on vapour blasted surfaces. However vapour blasting is not recommended as a surface treatment prior to penetrant inspection, as it is an established fact that vapour blasting can peen over the mouths of cracks in a wide variety of materials and prevent penetrant from entering the crack.

Generally a dry developer is preferred; however, the use of wet dip developers is not precluded if the geometry of the component is suitable.

Q. DAVID STEIN, Picatinny Arsenal, Dover, USA:

In quoting increased detectability from 20% to 80% by use of the foam method, it was noted that in the sequence of the tests, the flaws were already known and located. Did your tests take this into account when you gave the increase in detectability?

A. Yes, the percentages were calculated on the number of known cracks. The presence of these cracks had been established by a critical metallurgical inspection. The point being that the best conventional penetrant inspection methods were only capable of locating 20% of these, whereas using foam removal, 80% were found with standard sensitivity penetrants and all known defects found using high-sensitivity penetrants.

Mechanisms Contributing to Fluorescence and Visibility of Penetrants

B. GRAHAM, USA

Introduction

Fluorescence is the name of the process wherein a molecule absorbs a photon of radiant energy at a particular wavelength, then almost instantaneously re-emits it at the same, or a slightly longer wavelength. It can be distinguished from phosphorescence, wherein the emission process continues over an appreciable span of time and at a much longer wavelength. Many natural organic materials exhibit some fluorescence, as do numerous synthetic ones. Fluorescent penetrants, however, commonly fluoresce whole orders of magnitude more brightly than most natural products.

Electronic Absorption

Fluorescent penetrants differ from other products because they contain one or more fluorescent dyes, compounds that have molecular structures especially suited for the production of fluorescence. A necessary, if not sufficient, condition that a fluorescing molecule must fulfill is that it absorb electromagnetic radiation within a rather specific wavelength range. This range lies between 150 mμ and perhaps 1000 mμ. It is called the electronic absorption range because absorption of photons

within the energy range leads to changes in the electronic configurations of molecules. Absorption of radiation in the infrared ranges leads not to electronic changes but rather to changes in the vibrational energy of specific atoms within the molecule. Infrared radiation therefore is absorbed by specific atoms and atom groupings within a molecule, rather than by electrons, hence its usefulness in chemical analysis. Absorption of the high-energy photons in the short wavelength part of the spectrum leads to complete removal of electrons, rupture of chemical bonds and breakdown of the molecule itself.

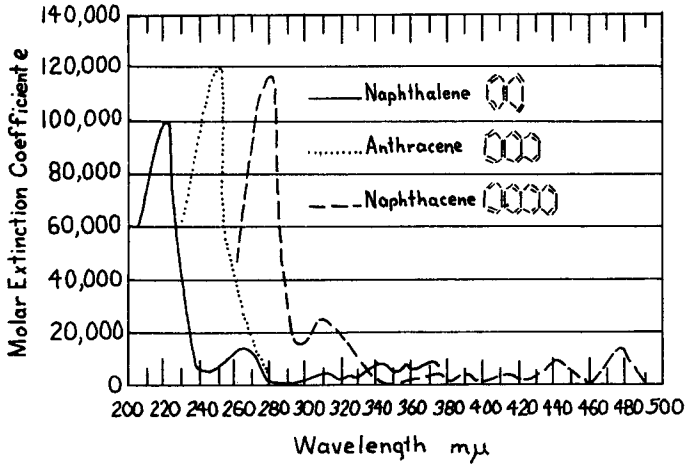

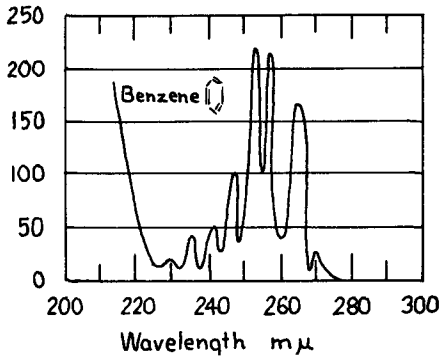

Figure 1. Absorption spectra of benzene and some homologs.

Ordinary dyestuffs show strong absorption in the electronic range, hence their vivid colours. While several types of chemical structures exhibit pronounced electronic absorption bands, the commonest dyes (both fluorescent and visible) are based on benzene rings or structures that closely resemble benzene rings. Benzene itself has several absorption bands in the far ultraviolet 240 to 270-mμ range. Since none occur within the visible part of the spectrum, it is colourless but many compounds containing one or more benzene rings, connected in certain ways, are highly coloured visibly, that is, they contain absorption bands in the visible part of the spectrum.

Figure 1 shows the absorption spectra of a homologous series of hydrocarbon compounds built up from benzene rings. Benzene, naphthalene and anthracene absorb only in the ultraviolet, while naphthacene and higher homologs have absorption bands within the visible region.

The units employed in Figure 1 are used throughout this paper. Since other units exist and have wide usage, those used here are explained: The abscissa is in wavelength units, millimicrons. One millimicron is equal to 10 Å units. Millimicrons are used to keep the numbers smaller. Other spectral units in common use are frequency and wavenumber (the reciprocal of wavelength). These units are used where energy relationships are important, as frequency of light radiation is directly proportional to its energy. We are concerned with light quantity rather than energy.

The ordinate is in units of "e", the molecular extinction coefficient. This is a molecular property, unique for each type of molecule and it has a continuous range of values throughout the absorption band of the molecule. The peak value of "e" is called "e_{max}", although many have multiple absorption peaks,

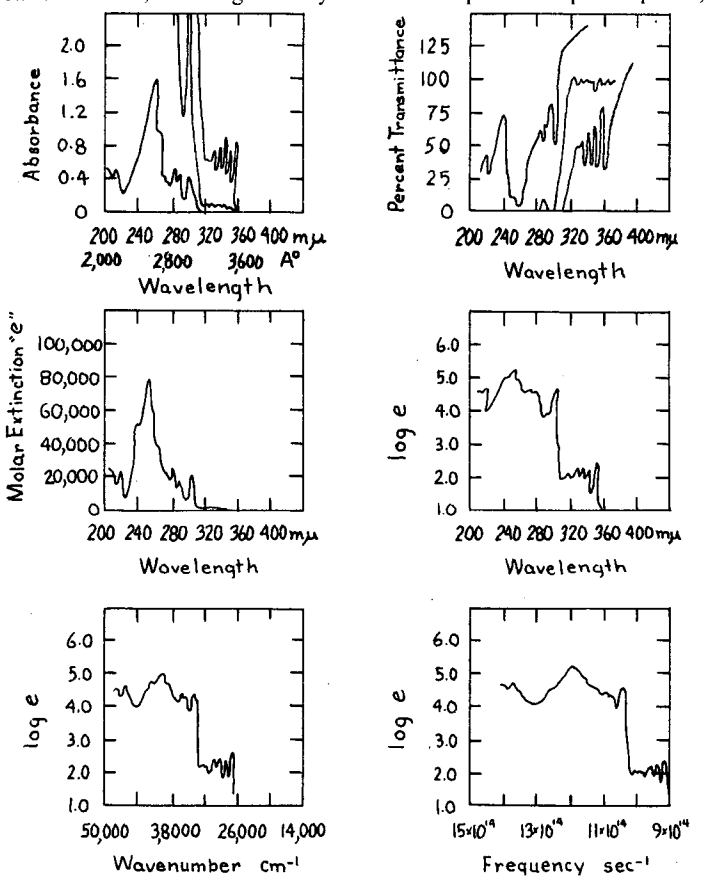

Figure 2. The absorption spectrum of phenanthrene, plotted with a variety of co-ordinate systems (Jaffe and Orchin, p. 12).

as can be seen in Figure 1. The value "e" itself is one of several definable absorption coefficients. Specifically, it is the one obtained from the Beer-Lambert law, when exponentials to the base 10 are used. The value "e" is also frequently plotted as log "e". When the material under study is unknown, its molecular concentration cannot be plotted and no value can be calculated for "e". In this case, ordinary transmission or optical density units must be used. Figure 2 shows the absorption spectrum of phenanthrene presented in several different ways. Note that most plots show a complicated fine structure in the 300 to 350-mμ range, while the "e" plot does not. For our purposes, these absorption peaks are too weak to be of any interest, and we lose nothing by choosing a coordinate system that suppresses them. For other purposes, such as elucidating molecular structures and electronic configurations and transitions, this weak, fine structure is important, and researchers would choose the log "e" type of presentation.

It has been mentioned that electronic absorption is accompanied by changes in the electronic configuration of the molecule in question, not just one or two electrons, but whole connected groups of them. In the benzenoid compounds these are referred to as π (pi) electrons, and most of the electronic

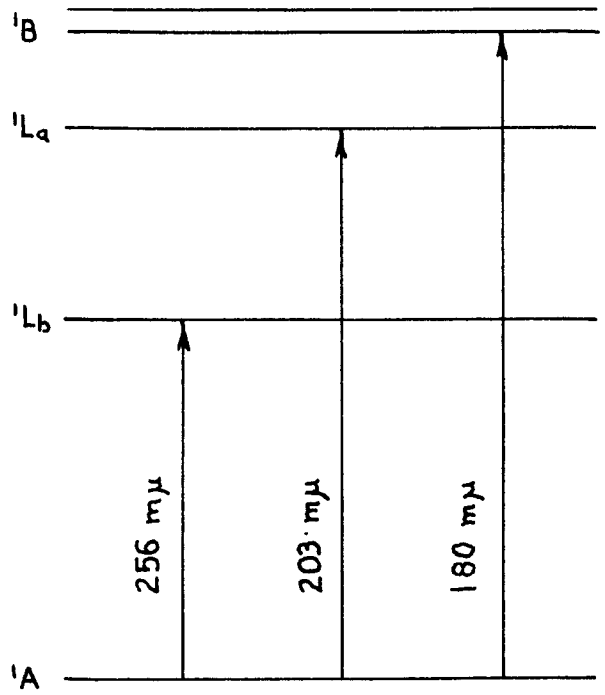

Figure 3. Term level diagram for benzene (Jaffe and Orchin, p. 244).

changes in compounds of interest to us, involve changes in their distribution within the dye molecules. The wavelength at which absorption occurs is of course related to the energy difference between the excited electronic state of the molecule and the original ground state.

In an approximate way, the energy levels associated with some of the absorption peaks in benzene are illustrated in Figure 3. The two highest levels correspond to absorption in the far ultraviolet, beyond the range shown in Figure 1. The ^1L_b band in reality is more complex than shown in this simple diagram, having at least eight observable peaks in Figure 1. The difference is due to the number of simplifying assumptions that are inherent in the energy-level diagram.

In the low-pressure gaseous phase, the absorption spectrum of a compound contains many lines, each characteristic of a specific electronic change, which occurs at an invariant energy. If the compound is again examined in a more condensed phase, it is seen that these sharp lines begin to spread out, and eventually fuse into broad bands. Figure 4 shows this phenomenon for benzene. Originally, the electronic processes are unperturbed, and only electrons are disturbed when radiation is absorbed. At a higher pressure, collisions between molecules begin to

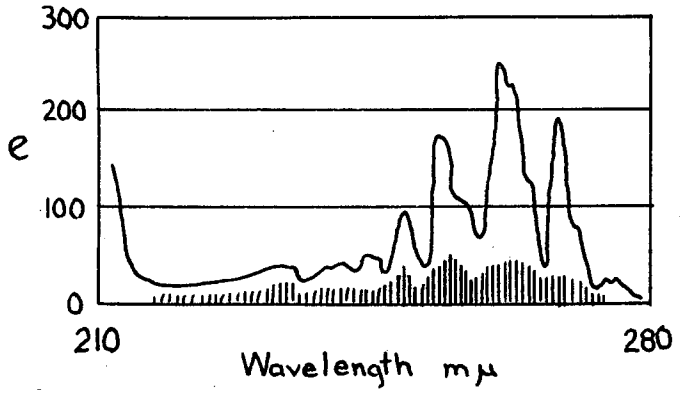

Figure 4. Benzene absorption spectra in liquid and vapour states (Gillam and Stern, p. 15).

interfere with the absorption process. Some change of molecular shape occurs on impact, which has a slight transitory effect on electron distribution. The narrow energy band for each transion becomes broadened because the molecules are no longer all exactly identical, and the spectral lines become blurred. In the liquid phase, these individual fine lines have by this process become smeared into a very few large bands, as molecular collisions became frequent.

Fluorescence

Under ideal conditions, a molecule that absorbs radiation can re-emit it at exactly the same wavelength. This has been observed for a number of simple compounds in the vapour state at very low pressures, and is called resonance radiation. More generally though, there is some energy loss and fluorescence occurs at slightly lower energy, that is, at a slightly longer wavelength. This happens because changes in the electronic

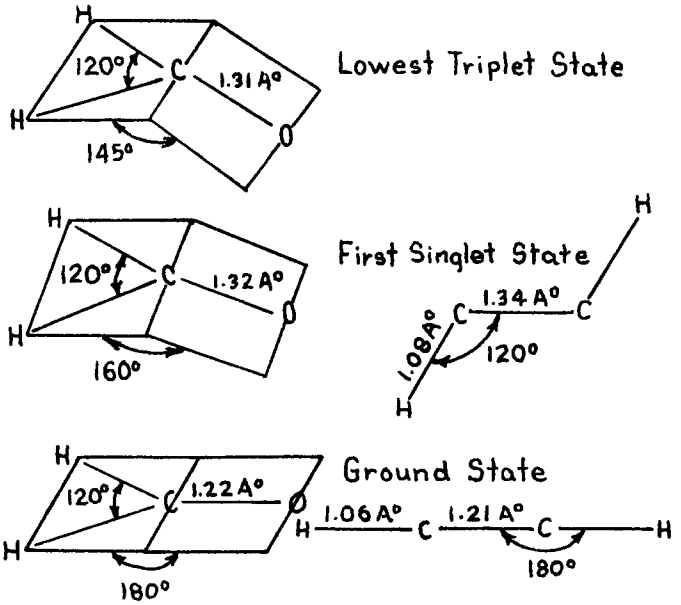

Figure 5. Configurations of lower excited states of formaldehyde and acetylene (Hercules, p. 14).

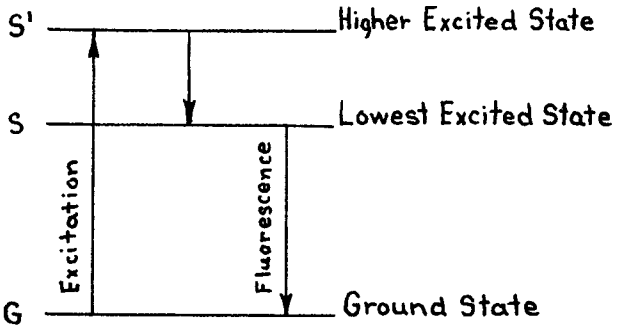

Figure 6. Generalized energy level diagram for a typical molecule.

distribution within the molecule can force changes in the shape of the molecule. Some of the exciting energy is used up in this process, and not quite so much energy is available for re-emission.

Figure 5 shows the configurational changes of a few molecules that have been elevated into some higher excited states. Rigid molecules, like phenol, undergo some dimensional change, but flexible molecules change their shape as well.

Some of the over-all energy relationships are summarized by the energy-level diagram for a typical molecule, shown in Figure 6. Excitation is normally to a higher energy level, say

S_2 due to the high energy of a 365-mμ photon. Various processes of internal conversion use up some of this energy, dropping the level to S_1. Once a molecule has absorbed this energy, and is elevated to an excited electronic state, it tends to lose it rapidly, normally within 10^{-6} to 10^{-7} seconds. The simplest mechanism of energy loss is by re-emission, that is, fluorescence. Obviously, fluorescence is not the only mechanism, as very many compounds, including nearly all dyes, do not fluoresce at all, and many that do, fluoresce with very low intensity. When the molecule returns to the ground state, S_1 to G, fluorescence can occur, if alternative paths are not available.

Several deactivation processes must compete with fluorescence. Some have been identified. One is called internal conversion. This process is quite rapid, and involves the conversion of electronic energy into vibrational energy of the atoms within the molecule, that is into heat. It is the favoured process when the molecule is flexible, as most linear molecules are. When the molecule is rigid, as many benzenoid compounds are, because of their interlocking ring structure, internal conversion is strongly hindered.

Another process is called external conversion, the transfer of energy, as heat, to surrounding molecules by collision. Anything that slows down the collision rate with the environment tends to diminish the extent of external conversion. For this reason fluorescent solutions are brighter at lower temperatures, or when the viscosity has greatly increased. A great many otherwise non-fluorescent dyes, such as auramine fluoresce only in solid solution, as in a hardened resin or plastic, as collision rate is low and molecular rigidity is forced.

Still another competing process is dissociation, wherein the absorption energy is large enough to destroy the molecule. This is the dominant mode of deactivation in molecules whose absorption bands lie in the highly energetic or ultraviolet portion of the spectrum. Dyes normally used in fluorescent penetrants, are chosen with absorption maxima around the 365-mμ output of the filtered black light. At this relatively lower energy level, dissociation is not a dominant process. However, some available fluorescent dyes are fairly unstable to 365-mμ radiation, fade rapidly and are seldom used. Nearly all known dyes show some sensitivity to ordinary black light, but not to a degree that interferes with normal penetrant inspection.

A much rarer deactivation process is a combination of internal conversion to a lower meta-stable excited state followed by slow re-emission at a much increased wavelength. This is known as phosphorescence. Figure 7 lists a number of organic compounds that exhibit phosphorescence. Figure 8 shows the energy-level diagram of Figure 5, with the inclusion of some alternative energy levels called triplet states, in opposition to the normal singlet states. Triplet states differ from singlets in that they represent different types of electronic configurations. To a first approximation, transitions between singlet and triplet states are forbidden. However, a few molecules, those in Figure 7 being examples, can undergo these transitions because of their peculiar configuration. When this happens, a molecule can drop to a lower T state and be trapped there long enough to emit phosphorescence, if a radiationless transition to the ground state does not occur. Occasionally collisions can lift a molecule from the T state back up to the S state, whence it can fluoresce. This is known as slow fluorescence.

Chemical compounds that show the most fluorescence are those whose structure reduces the probability of these several competing deactivation processes. These compounds are rigid, highly stable chemically, and selected to have useful absorption peaks in the near ultraviolet region. Other criteria must be met before they can be used in fluorescent penetrants. First they must be fairly soluble in ordinary solvents, and must not absorb

Compound	Wavelength of phosphoresonic band mμ	
α-Fluoronaphthalene	476.7	1.5
α-Chloronaphthalene	483	0.30
α-Bromonaphthalene	483	0.018
α-Iodonaphthalene	526	0.0025
β-Chloronaphthalene	476	0.47
β-Bromonaphthalene	473.8	0.021
β-Iodonaphthalene	475.2	0.0025
Benzene	340	7.0
Toluene	347	8.8
Phenol	350	2.9
Aniline	373	4.7
Benzoic acid	368	2.5
Acetophenone	384.5	0.008
Naphthalene	470	2.6
α-Aminonaphthalene	526	1.5
α-Nitronaphthalene	521	0.049
1,5-Dinitronaphthalene	502	0.11
Chrysene	505	2.5
Coronene	525	9.4
Triphenylene	420	15.9
Tetraphenylmethane	350	5.4
Tetraphenyllead	420	0.01

Figure 7. Lifetime of phosphorescence in several compounds (Jaffe, p. 549).

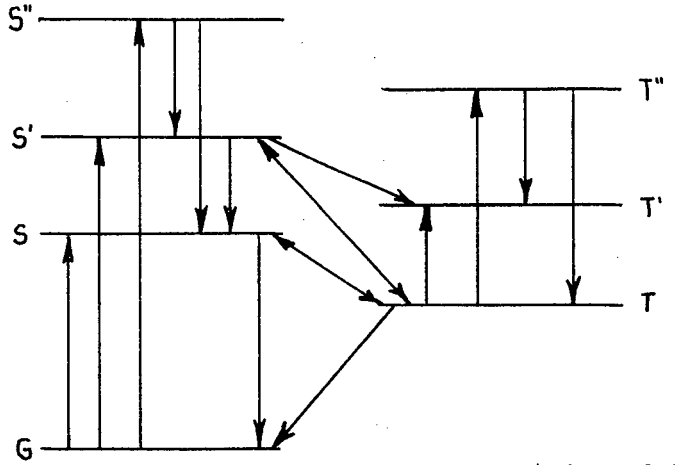

Figure 8. Energy level diagram showing phosphorescence (Jaffe and Orchin, p. 547).

light in spectral locations where it can interfere with fluorescence.

In addition, such compounds must have a high quantum yield of fluorescence. Quantum yield is of vital importance in a fluorescent dye. It can be defined as the fraction of excited molecules that fluoresce, or else as the ratio of photons of exciting light to photons of fluorescent light. Ideally it has a value of unity. Practically, because of competing deactivation processes, it is typically much less than one for even the best fluorescent dyes. Fluorescent efficiency, a related term, is the energy efficiency of the process. Even with a quantum yield of unity, fluorescence efficiency will be less than one, because the emitted photon has less energy (longer wavelength) than the exciting one. We are not concerned with energy as much as with quantity of light—number of photons—and prefer to deal with quantum yield. Fluorescent brightness of a penetrant is directly proportional to quantum yield.

The close correspondence of absorption and fluorescent spectra of a fluorescent substance shows up in combined plots, such as in Figure 9. In this figure, absorption is plotted in "e" units while fluorescence is plotted in arbitrary units (based on

current readings from a photomultiplier tube) chosen to give the same range of peak heights. It is quite common for the two spectra to be nearly mirror images, and to be close enough to overlap slightly. In fact if the two spectra do not show this close symmetry, it is a good indication that an S → T transition and phosphorescence are occurring. The fact that the typical dye's absorption and fluorescence peaks generally are quite close together causes problems that are discussed later.

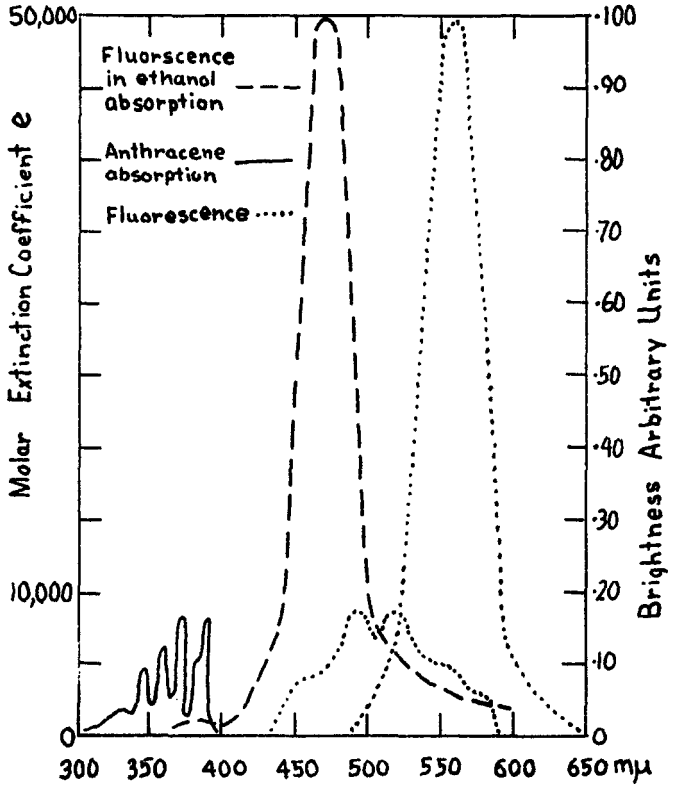

Figure 9. Symmetry of absorption and fluorescence spectra.

Fluorescence in Penetrants

In going from a general discussion of fluorescence to specific details of fluorescence in penetrants, it is important to consider the detailed physical properties of actually available fluorescent dyes. These are:

1. Fluorescent colour—the spectral location of the fluorescence band; 2. Fluorescent efficiency—brightness; 3. Absorption—both intensity and spectral location; 4. Solvent behaviour—solvent effect on location and intensity of both absorption and emission; 5. Stability—fastness toward heat and light.

Commercially available fluorescent dyestuffs span the visible spectrum. This allows penetrants to be made in nearly any desired fluorescent colour. Since the human eye is still the most commonly used sensing device, most penetrants are designed to fluoresce as close as possible to the eyes' peak response. Figure 10 shows the spectral response of the eye. It is sharply peaked, and colours that are distant from yellow are seen with much diminished sensitivity. For instance, a penetrant that fluoresces a pure blue, peaking at, say, 430mμ will seem only around 1 per cent as bright as one fluorescing a pure yellow of the same absolute intensity. Results like this place a severe penalty on penetrants of extreme colours, red ones as well as blue ones. Red fluorescent penetrants exist, but find their major use where a contrasting red colour is required and sensitivity demands are low.

There is a seeming exception to the rule that fluorescent penetrants should be as close to yellow as possible. Under very dim lighting conditions, the spectral sensitivity of the eye shifts its peak value from 555 mμ toward a limit of 510 mμ, in the blue-green part of the spectrum. This is known as the Purkinje effect, and is illustrated in Figure 11. Since fluorescent penetrant inspection takes place in darkened areas, it seems plausible that high-sensitivity penetrants should be made to fluoresce somewhere in this spectral region. This suggestion has been made quite often. Inspection of the existing data on the Purkinje effect shows that it does not begin to occur at all until brightness levels have sunk to 3×10^{-2} millilamberts or lower, then shifts downward continuously with decreasing illumination to the limit at levels just above pitch darkness, 10^{-5} millilamberts. Ambient visible light measurements made in a variety of inspection booths—at the point where inspection occurs—has invariably shown light levels of 10^{-2} millilamberts or more. At these levels the Purkinje effect has just barely begun to operate, and can be safely ignored. Most penetrants already show fluorescence peaks slightly below 555 mμ anyway. Even if inspection takes place in a light-tight room, visible light always is present, being emitted from (a) Fluorescent penetrant stain on the surroundings, including the inspector's hands and clothing; (b) Fluorescence from inspector's clothing, particularly white

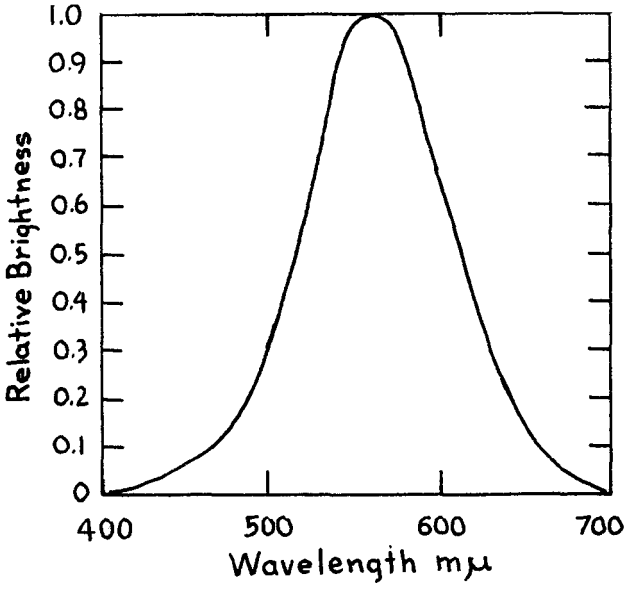

Figure 10. Visibility curve for normal eye.

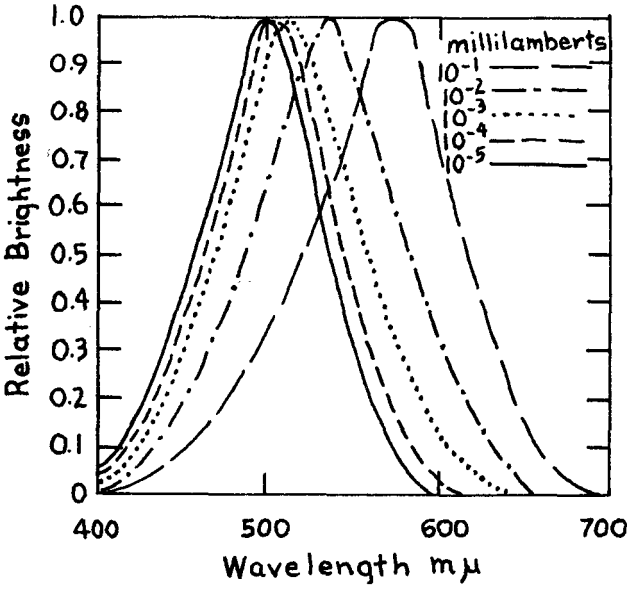

Figure 11. Visibility curve for normal eye under lower levels of illumination.

shirts, coveralls and lab coats; (c) Fluorescent background on surfaces being inspected; (d) Visible blue and red light emitted from the filtered black light itself; (e) The indications themselves.

The term fluorescent efficiency refers to the efficiency of the fluorescent dye in converting absorbed black light to visible light. This can be expressed in several ways—the previously defined quantum yield being the simplest. While some fluoragents at high dilution and low temperatures exhibit yields close to 1.0, most practical systems exhibit yields of no more than 0.1 at room temperature. Since quantum yield is directly related to brightness, it is important.

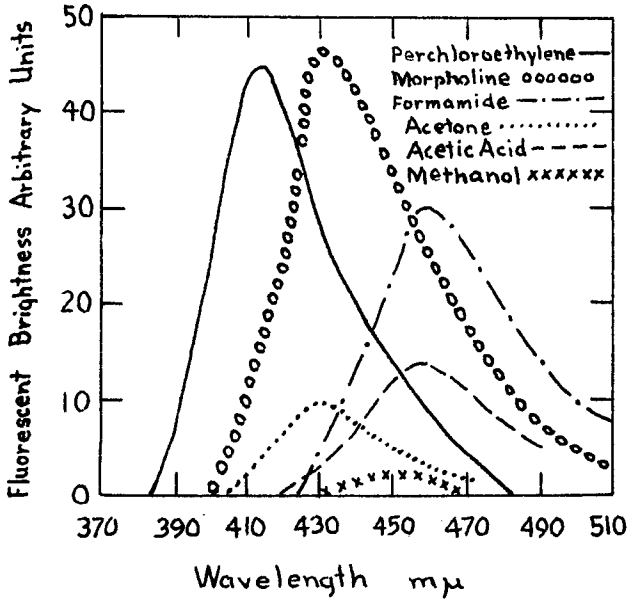

Figure 12. Spectra of cascading dye in various solvents.

Quantum yield has been shown to depend on the dye structure, but beyond this it is influenced by the medium in which the dye is dissolved. Figure 12 shows the fluorescent spectra for a blue fluorescent dye dissolved in five different solvents. The 20-to-1 range in fluorescent brightness shows that proper solvent selection is of extreme importance if fluoresence is to be maximized. Quantum yield is often effected by the

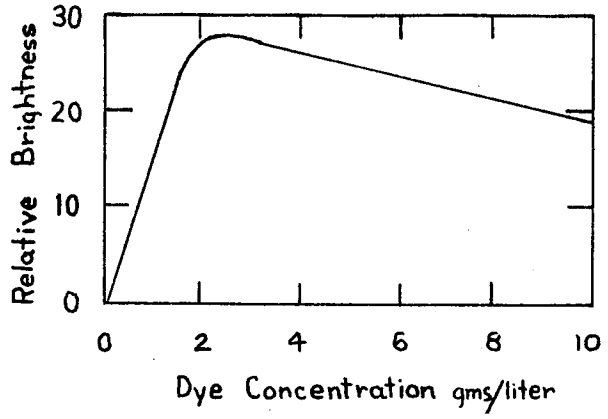

Figure 13. Concentration quenching of fluoral 5GA dye in naphtha.

concentration of a fluorescent dye. Typically it decreases with increasing dye concentration. Figure 13 shows some typical brightness losses that occur as dye concentration increases. This phenomenon is called concentration quenching. It limits the fluorescent performance that can be built into a penetrant by the brute force method of adding more and more dye.

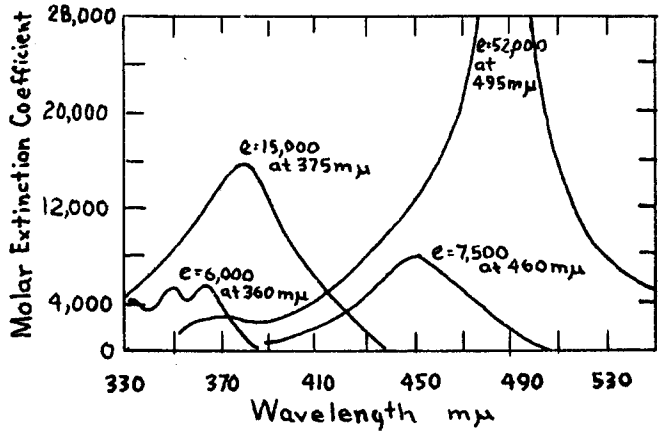

Figure 14. Absorption spectra of several penetrant dyes in dimethyl formamide.

Before a fluorescent penetrant can fluoresce, it must first absorb the exciting radiation. The fluoragents used in penetrants each have their unique absorption spectra, as illustrated in Figure 14. While the location and shape of these peaks are

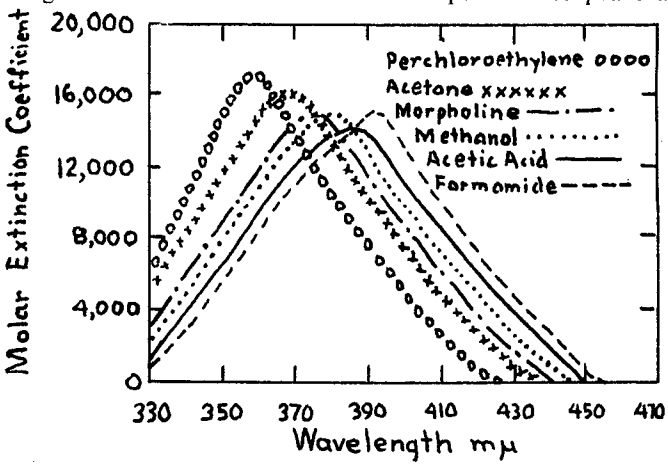

Figure 15. Absorption spectra of cascading dye in various solvents.

molecular properties of the dyes, there is some modifying effect due to the solvent. Figure 15 shows the absorption peaks of the same blue dye shown in Figure 12 dissolved in the same solvents. The effect is not as pronounced on absorption as on fluorescence, but it is still substantial.

The location and intensity of a fluorescent's absorption peak is extremely important, for the reasons developed below.

When monochromatic light is transmitted through a layer of light absorbing material, it is found that layers of the same thickness absorb the same fraction of incident light. Mathematically, this can be expressed as:

$$dI = -kI_o dl$$

where dI is the decrease in intensity of light originally of brightness I_o on passing through a layer of thickness dl. The constant k is a proportionality factor. Integrating, this gives us:

$$I_t = I_o\, e^{-kl},$$

where k is now called the absorption coefficient. Changing from natural logarithm to Briggsian logarithms gives:

$I_t = I_o \times 10^{-e'l}$, where e' is called the extinction coefficient. This is the mathematical expression of Lambert's Law.

Researchers working with light absorbing solutions are commonly more interested in concentrations of coloured solutions than in their thickness. It was also found that changes in light transmission fractions were also proportional to changes in the concentration of the absorbing species in solution, so that an equation very similar to Lambert's Law can be written

concerning concentration. This is known as Beer's law. Combining these two results in the Beer-Lambert law, the fundamental equation of spectrophotometry,

$I_t = I_o \times 10^{-ect}$ where c is concentration of the absorbing species, and e is the molar extinction coefficient.

While the amount of light transmitted through a solution is important for many purposes, we are more concerned with the amount of light that is absorbed. This is what leads to fluorescence.

The Beer-Lambert law of absorption states that

$$I_t = I_o \times 10^{-ect},$$

where I_t is the fraction of the total incident light, I_o, transmitted through a dye solution t cm thick, and having a molar concentration of c. The molecular extinction coefficient e is wavelength dependent.

In fluorescent penetrant applications we are more interested in the amount of light a dab of penetrant absorbs, since it absorbed light that leads to fluorescence.

Since $I_o = I_a + I_t$, $I_a = I_o - I_t$

and

$$I_a = I_o\ (1\text{-}10^{-ect}).$$

From this equation, we can compute the fluorescent brightness of a layer of penetrant t cm thick which has a concentration of c of a dye having a molar extinction coefficient (for the absorbed monochromatic light) of value e.

The apparent fluorescence F of a penetrant solution is proportional to the amount of absorbed light, I_a, and the quantum yield of the dye, Q, so that,

$F = kSQI_a$, where S is a factor covering the spectral sensitivity of the detector and k is a constant geometric factor that is determined by the fraction of the total emitted light actually entering the detector. Combining the two equations gives

$$F = kSQI_o\ (1\text{-}10^{-ect}),$$

a fundamental equation that describes apparent fluorescent brightness in terms of measurable quantities.

Let us examine this in some detail. Whenever the value of *ect* is three or greater, $F = kSQI_o$ within 0.1%. In this range, fluorescent brightness of a penetrant film is directly proportional to the intensity of the exciting light and the quantum yield of the dye. It also depends on the colour of the fluorescence, whether or not it matches the peak sensitivity of the detector. As *ect* decreases below three, the apparent brightness of the film can only decrease. Thus, for maximum fluorescent brightness, the *ect* value of a fluorescent penetrant solution should be kept close to three.

What factors tend to decrease the value of *ect*?

When the penetrant is viewed in a very thin layer, as in an extremely fine indication, t is small. Figure 16 shows photographs of four equally dilute fluorescent dye solutions, under

Figure 16. Uranine dye solutions at the same concentrations, diminishing thickness. Illuminated from above, viewed from side.

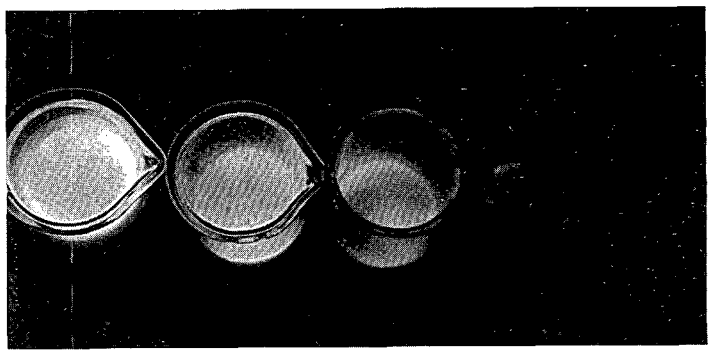

Figure 17. Same as Figure 16, but viewed from above.

black light. Observe that each is a different thickness, and that the band of fluorescence (where absorption also is taking place) is the same thickness. In the last two, the liquid layer is thinner than this, and not all the incident light is absorbed.

Figure 17 shows a top view of these four samples. It can be seen that the brightness is dependent on the thickness, once *ect*, (here determined by varying t alone) decreases below three. In normal penetrant solutions c is very much higher, and the range of phenomena, here magnified, occurs within a very small range. Unless e and/or c are large, then F is going to be low for fine indications, making them more difficult, if not impossible to see. When the dye concentration c is made large, it can offset the effect of small penetrant film thickness. Thus penetrants with large dye contents are capable of significant brightness even in very thin films, but c cannot be made indefinitely larger. Ultimately there is a limit to how much dye can be dissolved into a penetrant, but before this limit is reached, the quantum yield, Q, of the system is going to decrease, which itself will diminish fluorescent brightness.

The other alternative for maximizing *ect* is to maximize e. Since this is a molecular property, it can be maximized only by selecting an appropriate fluorescent dye, one having an *e max* in the desired spectral region, usually at 365 mμ. Small changes in solvent composition can change the location of the absorption peak, allowing it to approach more closely the ideal wavelength, but such effects are small, and do not allow just any dye to be matched.

For instance, a penetrant in use in the early 1950s, ZL-1A, contained a yellow fluorescent dye of good brightness and colour. Its *e max* occurred at a wavelength of 430 mμ in the blue. Excited with black light, 365 mμ, where e was only ¼ of its peak value, it was incapable of giving maximum sensitivity. Working only with this dye, there were only a limited number of ways available to improve such a dye solution: (a) We could use it only in relatively insensitive formulations, that were to be used on large cracks only (giving thick indications, large t); (b) We could increase c, by raising the dye concentration as far as possible until Q started dropping; (c) we could increase e by using blue exciting light that peaked around 430 mμ, the absorption peak of the dye. This method has been offered commercially, but suffers from two disadvantages. First, the blue light interferes with the visibility of the fine green-yellow indications. Yellow goggles are required to mask the blue light and restore the light-dark contrast of the indications. Second, the light source, a blue filtered incandescent bulb, contains only a small fraction of suitable blue light, and I_o is always rather low—hence F too; (d) We could use a dye that has a high e value for black light. Unfortunately, since most dyes have fluorescent emission peaks not too far from their absorption peaks, most, if not all, such dyes fluoresce somewhere in the blue, where eye sensitivity is low; (e) Even if *ect* is low F can be brought to a usable value for any penetrants by using intense illumination, by raising I_o an order

of magnitude or more about its normal values. This has been demonstrated effectively in our laboratory, where I_o can be increased 10× or more, although sheer mechanical, optical and electrical complications militate against its common use as a means of improving fluorescent penetrant brightness and sensitivity.

By the middle 1950s fluorescent penetrants had been developed as far towards maximum F as the limitations just outlined would permit. This was not far enough, as inspection needs at the time were beginning to demand larger values of *ect* while the smaller cracks being sought were shrinking the value of *t*. In the absence of a bright fluorescent yellow dye having a high value of *e* at 365 mμ, it seemed that little more could be done. At this point fluorescent dye cascading was discovered, and higher sensitivities instantly became available.

The cascading process employs two fluorescent dyes in a penetrant, one having peak absorbance at 365 mμ, and showing blue fluorescence, around 430 to 450 mμ, the second having peak absorbance around 430 to 450 mμ and a fluorescence peak around 530 to 540 mμ.

Essentially the original exciting energy is transferred to blue light which is absorbed on the spot by the other dye to be re-emitted as yellow. When properly done, none of the intermediate blue fluorescence shows, the fluorescence remains as yellow as if the blue dye is absent, but brighter.

Proper cascading demands a quite delicate operation of dye selection and blending. In fact it is easily possible to make fluorescent penetrants of diminished brightness. Such a result occurs because both dyes compete for the available black light. Since the blue fluoragent is much more absorptive of 365 mμ radiation, it gets the lion's share; I_o is low for the yellow fluoragent and its fluorescence is dim. If the blue fluorescence from the blue, or cascading fluoragent does not match that of the yellow, or cascaded fluoragent, it will not be absorbed, meaning a lot of blue fluorescence will be evident, with not much yellow. The result is a washed-out blue-green colour of low visual brightness. Only when the dyes are precisely matched in spectral characteristics does true cascading occur.

As seen in Figures 9 and 11, the choice of solvent has some influence on the fluorescent properties of the dyes. At the present level of technology, fluorescent penetrants are confined by the inflexible spectral limits that are imposed on them, the filtered mercury arc with its invariant 365 exciting radiation, and the human eye, with its invariant 555 mμ peak response. Operating between such fixed boundaries, the small adjustments that can be made on absorption and emission peaks of fluorescent dye combinations by solvent changes make solvent selection a critical part of the art of penetrant formulation.

A final property of fluorescent dyes is their fastness. Like ordinary dyes, fluoragents can be faded by black light exposure. This is primarily a chemical problem, and is not subject to the simple and rigorous physical controls that the other fluorescent properties respond to.

Developers and Fluorescence

The preceding portion of this paper has been concerned with fluorescence of fluoragent solutions, penetrants themselves, as seen in bulk or in thin layers. Penetrants however are not profitably observed in this manner. Almost always they are observed in indications, where they exist within a developer matrix. This, oddly enough, can change both the colour and brightness of a penetrant from its "pure" values. The combination of penetrant-plus-developer is commonly much brighter than penetrant alone, and is frequently a different colour as well. Work is proceeding in our laboratory that attempts to explain this behaviour and eventually place it under control.

Evidence is accumulating that verifies the development mechanism brought out by Thomas. Light scattering is at the heart of it, scattering that ensures complete utilization of the ultraviolet radiation incident upon an indication and complete emission of fluorescence. Brightness values several times higher than those of the original penetrant result.

Several types of developers exist. While their chief functions are to bring penetrant up out of voids and spread it out on the surface, they also boost maximum fluorescence, each type exerting its own influence on colour and brightness.

The simplest development step is to use no developer at all. Easily visible indications will occur in the absence of developer if these conditions are all fulfilled. First the defects must be large, so that penetrant seepage from voids occurs in fairly thick layers. Second, the dye concentration must be very high. Third, the penetrant must have a low surface tension, so that it seeps out easily. The first two conditions maximize *ect*, the third relates to surface properties. Such a development scheme looks good on large cracks, 0.001 in. or so across but fails utterly for fine cracks a few microns wide. Here *t* is small, and *ect* is so small that *F* of the indication is below the threshold of visibility. Therefore developers must be used for high sensitivity inspection of fine defects.

Dry developers are the simplest chemically, containing particles of simple chemical composition that are completely insoluble in and unreactive with fluorescent penetrants. While increasing indication brightness via the scattering process, they exert little influence on the colour of the penetrant in the indication. Made properly, of completely colourless powders, they absorb no radiant energy from the indication.

Wet developers, by contrast, have quite complicated compositions. Besides the necessary developing powders, they contain wetting agents, corrosion inhibitors and suspending agents. Some of these ingredients may be coloured, in which case they absorb light to the detriment of the indications' true colour and brilliance. Other constituents may dissolve into the penetrant that occupies the indication; as already noted, even small changes in penetrant solvent can alter fluorescence greatly. Since penetrants are normally made with optimum solvent constitution, the unwanted accidental inclusion of developer constituents can only hurt fluorescence, fluorescence may be reduced, or colour may be changed from the best eye-response values.

Solvent-based developers more often contain penetrant-soluble constituents (aside from the volatile-bulk solvent, which soon evaporates from the indications), and, much oftener than wet developers, they tend to cause penetrant indications to fluoresce a bluish colour. Some colour interference may be due to unmeasurable refraction and scattering processes that occur in the ultraviolet, between penetrant and particles. Even though solvent developers tend to blue indications, they function with high sensitivity, because their solvent action brings up more penetrant from the defects and spreads it wider than do capillary processes unaided by solvents.

Lacquer-based developers, though known for nearly three decades, have recently been receiving publicity. Their primary advantage, aside from providing a removable and fairly permanent record of an indication, is to offer a means of controlling the spread of an indication. Most developers create indications that are very much wider than the crack itself. A width magnification of 100X is not unusual. By careful application of a lacquer developer, this spreading can be limited to 5 or 10X, which allows a high resolving ability for tight networks of fine cracks. Of course, this does not give indications of high visibility (a

10μ-wide fluorescent line is much less visible than a 100μ-wide line), but it does fulfill an occasional need that other developers do not.

Based on materials, resins and plasticizers that dissolve in typical penetrants (and thus alter fluorescent brightness and colour), lacquer developers tend to form blue indications rather than yellow ones, even more than ordinary solvent developers. As blue indications are not remarkably visible, and since many lacquers have at least a faint bluish-white fluorescence anyway, lacquer developers still cannot be used to maximum advantage.

In fluorescent enhancement, lacquer developers suffer yet another disadvantage. Because the ultimate resin particles are very much finer than ordinary developer particles (and very much smaller than the wavelength of light) they scatter light inefficiently, and fail to show the fluorescent enhancement afforded by the other types of developers. Brightness can be increased by including scattering particles in the lacquer, but this tends to lower resolution and makes removal after inspection more difficult.

It cannot be said that any of these types of developer is superior, since each has its specialized use. The main idea to be emphasized is that each has some important effects on the appearance, size, brightness and color of indications, and must be considered a significant factor in the over-all fluorescent inspection process.

Discussion

Q. DANIEL POLANSKY, Silver Spring, Md., U.S.A.:
When cracks are said to be detected of a size 12 to 15 microns, how does one differentiate between cracks and surface finish?
A. The difference between an irregularity in surface finish and a crack is functional. A crack is relatively deep, compared to its width, and acts to concentrate stress at its tip. Normal surface irregularities are usually too broad to have this effect and are not normally considered to be cracks or defects. Occasionally, a particular deep and sharp machining mark will cause a failure by concentrating stresses at its tip. Such a mark could be considered a crack, certainly it would be considered a defect.

Conclusions

While the fundamental aspects of fluorescence are still incompletely understood, there is enough known about it to insure that penetrants will continue to be improved in the future as in the past. The large number of variables affecting fluorescence alone opens up many avenues to improvement. New dyes, with higher molar extinction coefficients and/or quantum yields may be discovered. New solvents may be found to improve brightness or eye-response matching. Different light sources may turn up, which will change the cascading balance or eliminate its need. Even variables having little to do with fluorescence can contribute a penetrant that fills the crack more fully, or washes out less completely, or spreads out of the crack more thoroughly, can yield bigger indications. The list is so long that it is hard to know where to start.

References

Jaffe and Orchin. "Theory and Applications of Ultraviolet Spectroscopy", 1962, Wiley & Sons, New York.
Gillam and Stern. "Electronic Absorption Spectroscopy", 1958, Arnold.
Forsythe. Smithsonian Physical Tables, 9th Edn., 1954, Smithsonian Institution.
Handbook of Colorimetry, 1936, The Technology Press, M.I.T.
Hercules. "Fluorescence and Phosphorescence Analysis", 1966, Wiley & Sons, New York.
Thomas. "An Analytic Approach to Penetrant Performance", Nondestructive Testing, Nov.-Dec., 1963.

Penetrants tend to fill any type of surface-open voids, cracks, pits, scratches, even screw threads. The selectivity of the penetrant for cracks and other sharp discontinuities arises during the removal step. It is very difficult to keep a residual trace of penetrant in a surface scratch say 0.005" wide by 0.005" deep during cleaning. If this discontinuity is 0.001" wide by 0.005" deep it is more difficult to remove it all, and the penetrant is much more apt to detect it as a defect.

As a result, penetrants tend to indicate those surface imperfections that are most apt to weaken the part and to overlook those that do not.

Nondestructive Replica Methods for Surface Examination

D. SCOTT and A. I. SMITH, U.K.

ABSTRACT: To examine microscopically and assess selected surface areas of large unwieldy test specimens, or to examine periodically the surfaces of large machine components in situ, replica techniques may be used to advantage. Plastic replicas may be made quickly and, to aid microscopic examination and allow investigation by interferometry, a highly reflecting surface can be produced by metal coating the replica in vacuo. For the examination of curved surfaces of small radius, pliable replicas made of softened cellulose acetate sheet are useful, as they can be flattened to facilitate focussing of the microscope. Stylus methods of surface assessment may be applied to replicas.

Electron microscopy is required to reveal the initiation of failure, and suitable replicas may be taken from large, in situ components. Surfaces that are too rough to be examined satisfactorily by optical microscopy can be examined by the electron microscope. Fracture surfaces and worn surfaces may be nondestructively replicated for electron microfractography.

The preparation, use, and advantages of different replica techniques are described, with illustrations of their use in various fields.

Introduction

For inspection purposes, quality control, and the examination of failed service components and test specimens, nondestructive methods of surface examination are preferred to methods that may cause damage and obliterate information which may be recorded by the use of other techniques of examination. Modern laboratories have to use all available investigational techniques, as specific information from each enables comprehensive data to be acquired.

Surface topography can greatly influence the frictional, wear and mechanical behaviour of engineering components, so the starting point in any inspection or investigation should be the examination and assessment of the original surfaces involved, to enable changes that are necessitated by service use or test conditions, to be determined from the used components. Many techniques are available to examine the topography of surfaces, but optical methods allow the specimen to be investigated without destroying it or subjecting it to strain or wear. However, in many instances, due to size or inaccessibility, it is not possible to carry out a direct microscopic examination of a surface, and replica methods may be used to advantage. Stylus methods provide an immediate numerical characterization

A

B

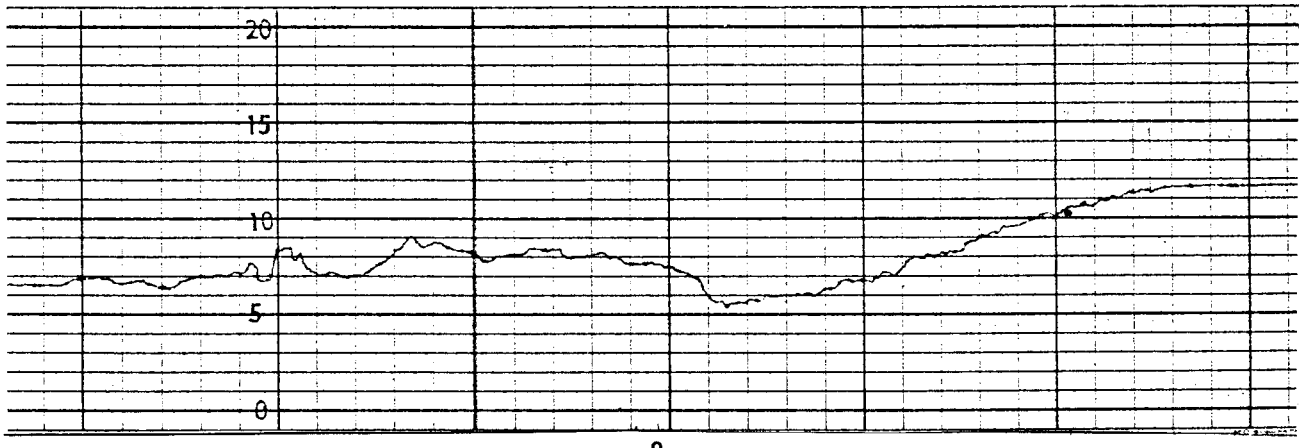

C

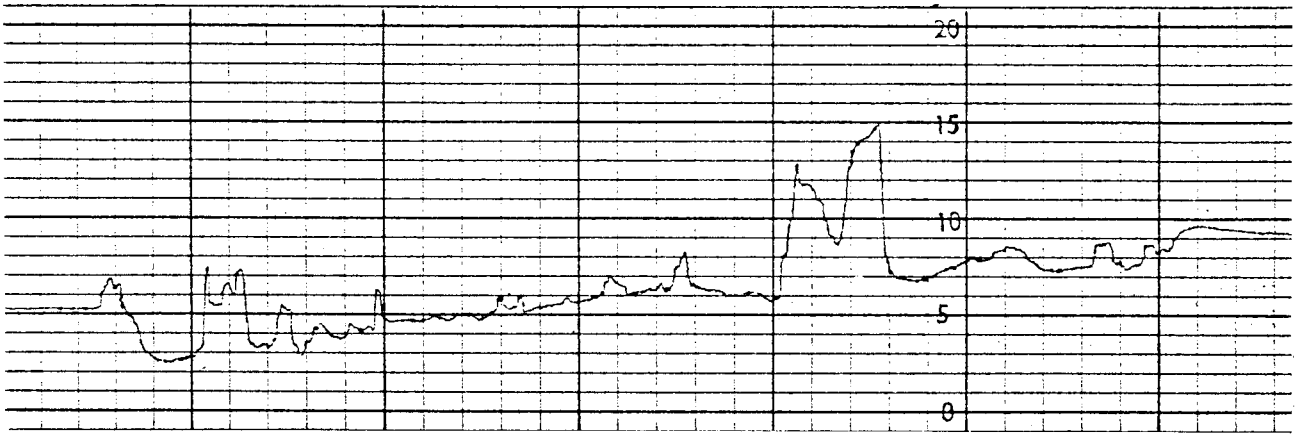

Figure 1. Replica and talysurf trace of the surface of a steel rail. A. (X6) Metal-coated plastic replica from the surface of a steel rail. B. (H=20X; V=1000X) Talysurf trace of smoother surface area of replica. C. (H=20X; V=1000K) Talysurf trace of rougher surface of replica.

of a surface such as 'centre line average' but they are subject to the uncertainty of the extent of surface damage done by the stylus itself. Thus for the assessment of the surfaces of soft materials damage can be avoided by carrying out the stylus measurement of surface replicas. Also, surfaces inaccessible to the stylus, such as the inner surfaces of small-diameter ball races or surfaces of components or specimens too unwieldy to be accommodated on the measuring instrument, may be assessed by stylus measurement of replicas.

Assessment by Optical and Stylus Methods

It is essential that replicas for assessment or examination of surfaces must be faithful reproductions of the surfaces from which they are taken. A large variety of materials and techniques can be applied to the replication of solid surfaces (1-5). What may be a satisfactory method for one solid surface may not give the best results on another, so that the method of replication must be selected from several possibilities. Plastic replicas such as those made from prepared kits (Scott-Bader, Crystal Field Kit) have been successfully employed for the examination and assessment of all types of surfaces. They may be made of the surface of large components in situ by isolating the area required with plasticine to form a reservoir for the plastic. On solidification, to aid microscopic examination and allow investigation by optical interferometry, a highly reflecting surface may be produced on the plastic replica by coating in vacuo with a film of aluminum. The periodic inspection of rails and locomotive driving wheels has been carried out by this method, to study surface changes due to different operating conditions and environment, and how they influence surface texture, frictional and wear behaviour. Figure 1 shows a photomicrograph of the metal-coated plastic replica from the surface of a rail at the exit of a station where some slipping of the locomotive wheels appeared to occur. Talysurf traces were easily obtained from the replicas.

Surface replicas have been successfully used to follow the running-in, the initiation and development of scuffing and the mechanism of rippling of heavily loaded hypoid gears without interrupting the testing procedure. Figure 2(A) shows a photomicrograph of the replica of the surface of a tooth of a hypoid gear, at a stage in the test when the noise level was beginning to rise. The use of interferometry, Figure 2(B), shows that the run-in, apparently smoothed surface was actually rippled.

For the assessment of curved surfaces of small radius, pliable replicas are useful as they may be easily flattened to facilitate focussing of the microscope and measurement by stylus or optical interferometry (6). Suitable replicas can be quickly made by firmly pressing softened, thin acetate sheet on to the surface. Acetate sheet 0.005 in. thick, moistened on one side with acetone, has been found to be successful for this purpose. These replicas can be examined by transmitted light or with reflected light, with or without a vacuum-deposited metallic coating to improve reflectivity. Coated, they are suitable for interferometry. Figure 2(C) shows a replica from a scored rippled tooth of a hypoid gear. Except by replica methods microscopic examination of the inaccessible, curved tooth surface would be difficult without destruction of the pinion by time-absorbing sectioning procedure. Figure 2(D), a talysurf trace across the replica, shows that small ripples are superimposed on the larger ripples of the surface.

Replicas for Electron Microscopic Examination

The finer topographical features of surfaces are beyond the resolving power of the optical microscope, and electron microscopy is a powerful laboratory technique required for surface examination. Also, the initial stages of many surface phenomena, such as wear, corrosion, and fatigue, which affect the useful life of machine elements occur on a very small scale and the electron microscope, with its enhanced magnification, can reveal fine-scale surface features of interest in the elucidation of such failure mechanisms.

The conventional electron microscope is a transmission instrument, and replicas suitable for transmission electron microscopy must meet exacting requirements. Besides being a faithful reproduction of the surface contour, the replica must possess sufficient contrast to permit ready interpretation of the surface features. It must be structureless so that any structure seen will be that of the specimen surface from which the replica was taken. It must be durable to withstand necessary handling and the strain and heating that accompany bombardment by the electron beam. The choice of replica material depends upon the nature of the specimen and the information required from it. Formvar replicas made from a 1 per cent solution of formvar (polyvinyl formvar) in chloroform have been found to satisfactorily replicate metal surfaces (7). When they are backed with a thick collodion film it is possible to remove thin formvar films of high contrast from metal surfaces without tearing and without any evidence of strain in the formvar. The specimen surface is flooded with formvar and then held vertically so that the excess solution drains off. When the chloroform has evaporated, a plastic film remains on the surface. The backing film is formed in a similar manner with a 2-per-cent solution of collodion in amyl acetate. A dry stripping method with adhesive tape, upon which supporting grids have been suitably placed, eliminates any wetting of the surface, contamination or corrosion involved in wet stripping procedure with water, from the specimen surface. Replicas may be shadowed with a heavy metal to improve contrast and to enhance the observation of fine detail. The adhesive tape and collodion backing are removed with amyl acetate. Single-stage formvar replicas may be somewhat difficult to interpret correctly as they are negative replicas, the valleys on the metal surfaces appearing as hills and vice versa. Photographic reverse printing of negatives of electron micrographs can facilitate interpretation (7).

Various two-stage replica techniques have been developed and the high-resolution carbon replica technique (8,9) has been found to be particularly effective in producing positive replicas. Carbon replicas are obtained by evaporating carbon on to the surface of a negative formvar replica by passing a heavy current through two pointed carbon rods lightly held together in a vacuum and then dissolving away the formvar. This leaves a carbon film which conforms exactly to the original surface and shows the irregularities in their true perspective. Not requiring to be stripped from a surface, the carbon replica can be made thin to allow better intensity of illumination and contrast. Also, carbon is much stronger than plastic materials, it is structureless and unaffected by the electron beam.

The true nature of various types of industrial surface finishes can be revealed by electron microscopic examination of carbon replicas. A typical finely ground workshop finish, about 7 micro-inches C.L.A., on a hardened steel gear is shown in Figure 3(A). The electron microscope shows the flowed uneven nature of the surface and thus dispels erroneous ideas about the smoothness of surfaces produced by this means. Running-in of such a gear produces a smoother, more highly reflecting surface, Figure 3(B). It is evident that the improved surface finish is due to plastic deformation of surface asperities. Initiation of surface damage, leading to scuffing and pitting failure of gears, can be followed by using carbon replicas taken from selected areas of gear teeth in situ without dismantling the test set-up, Figure 3(C) and (D).

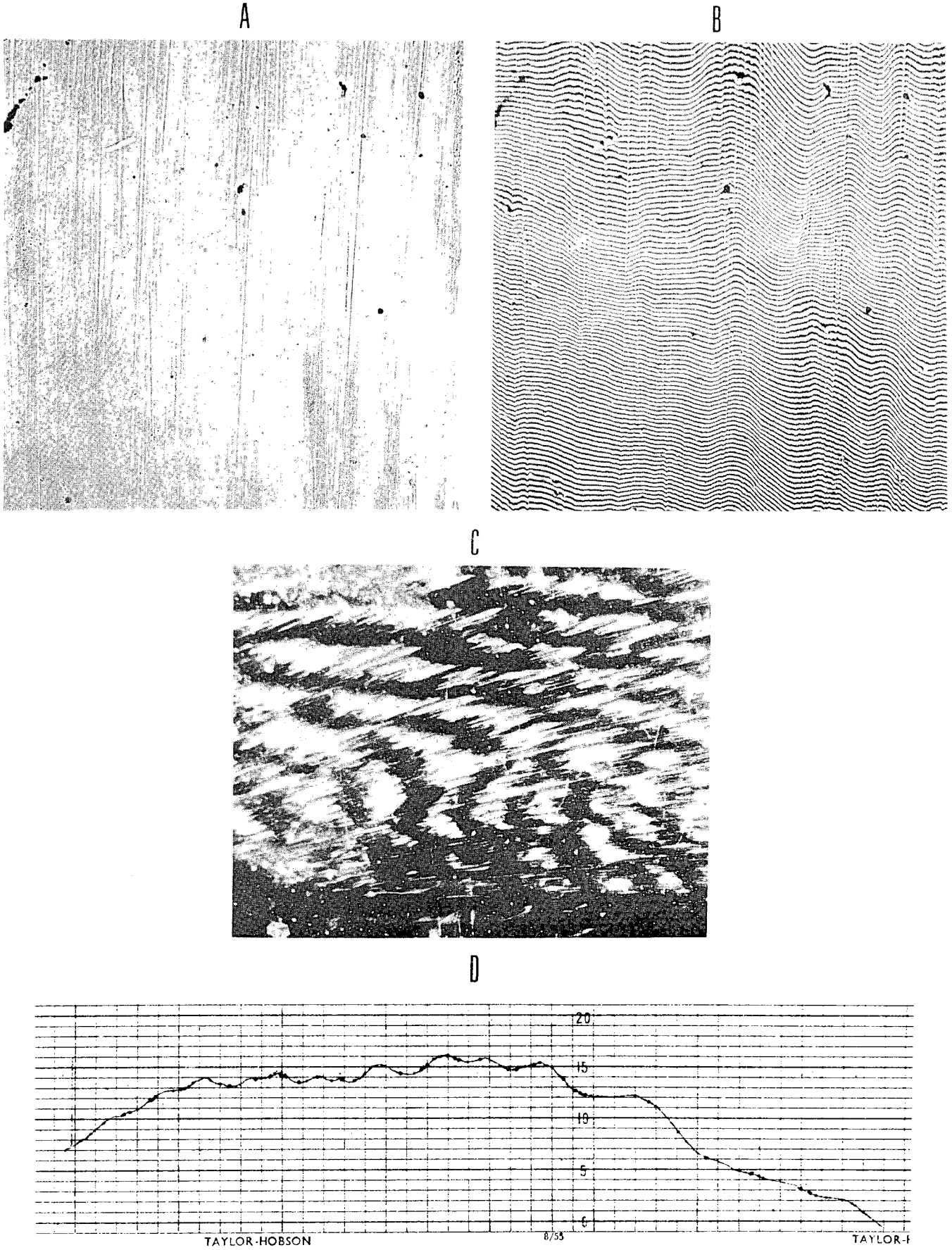

Figure 2. Metal-coated thick plastic and thin pliable replicas. A. (X60) Optical micrograph of a metal-coated plastic replica from a gear tooth, showing scoring. B. (X60) Interference micrograph of same area showing rippling. C. (X100) Metal-coated pliable replica from scored, rippled surface of a hypoid gear tooth. D. (V=2000X; H=200X) Talysurf trace showing profile of a large ripple and smaller associated ripples.

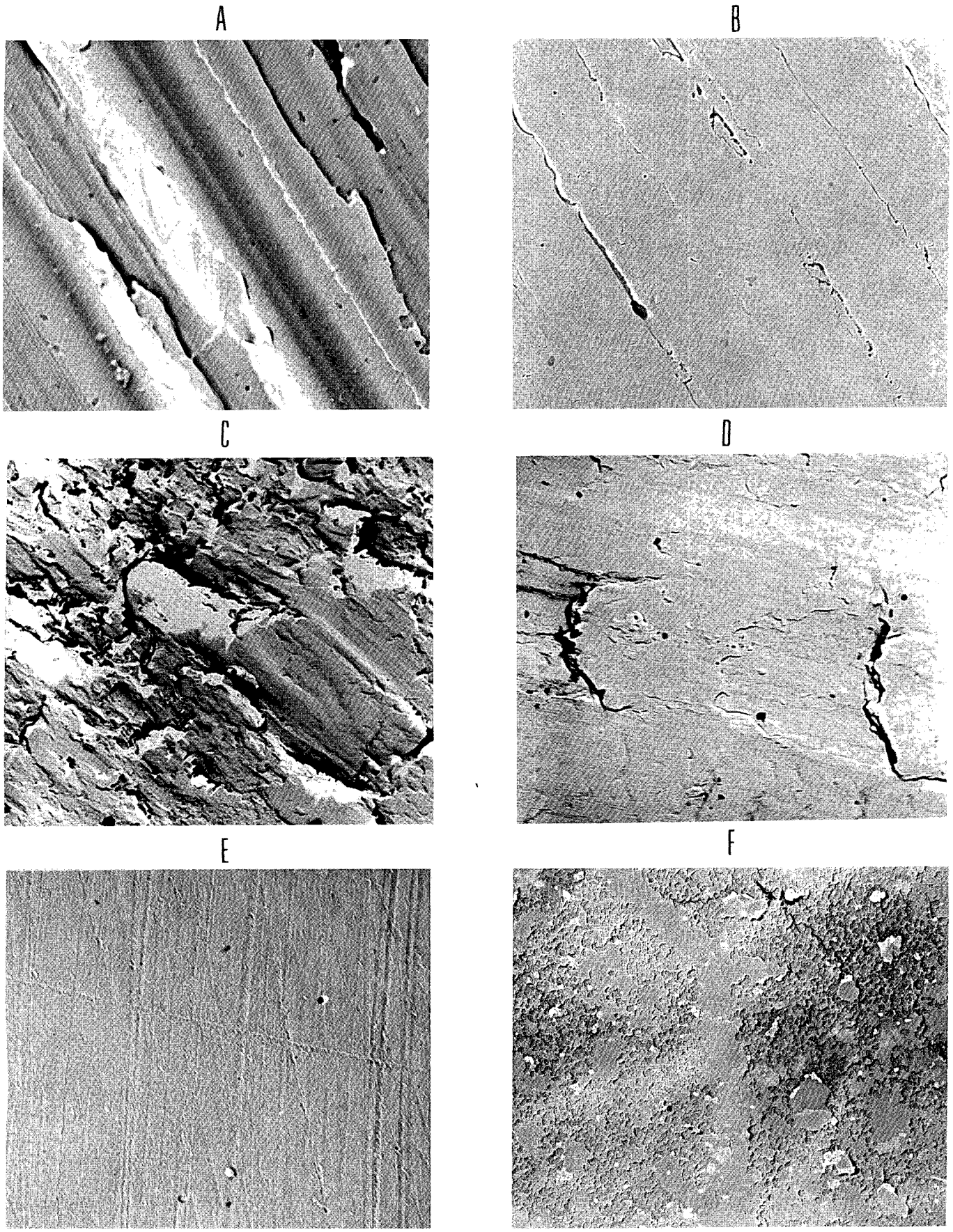

Figure 3. (X10,000) Electron micrographs from shadowed, two-stage positive carbon replicas. A. Finely ground surface of a gear tooth. B. Run-in surface of a gear tooth. C. Initiation of scuffing type failure of a gear. D. Initiation of pitting type failure of a gear. E. Diamond polished surface. F. Initiation of corrosion on the surface of a steel ball-bearing.

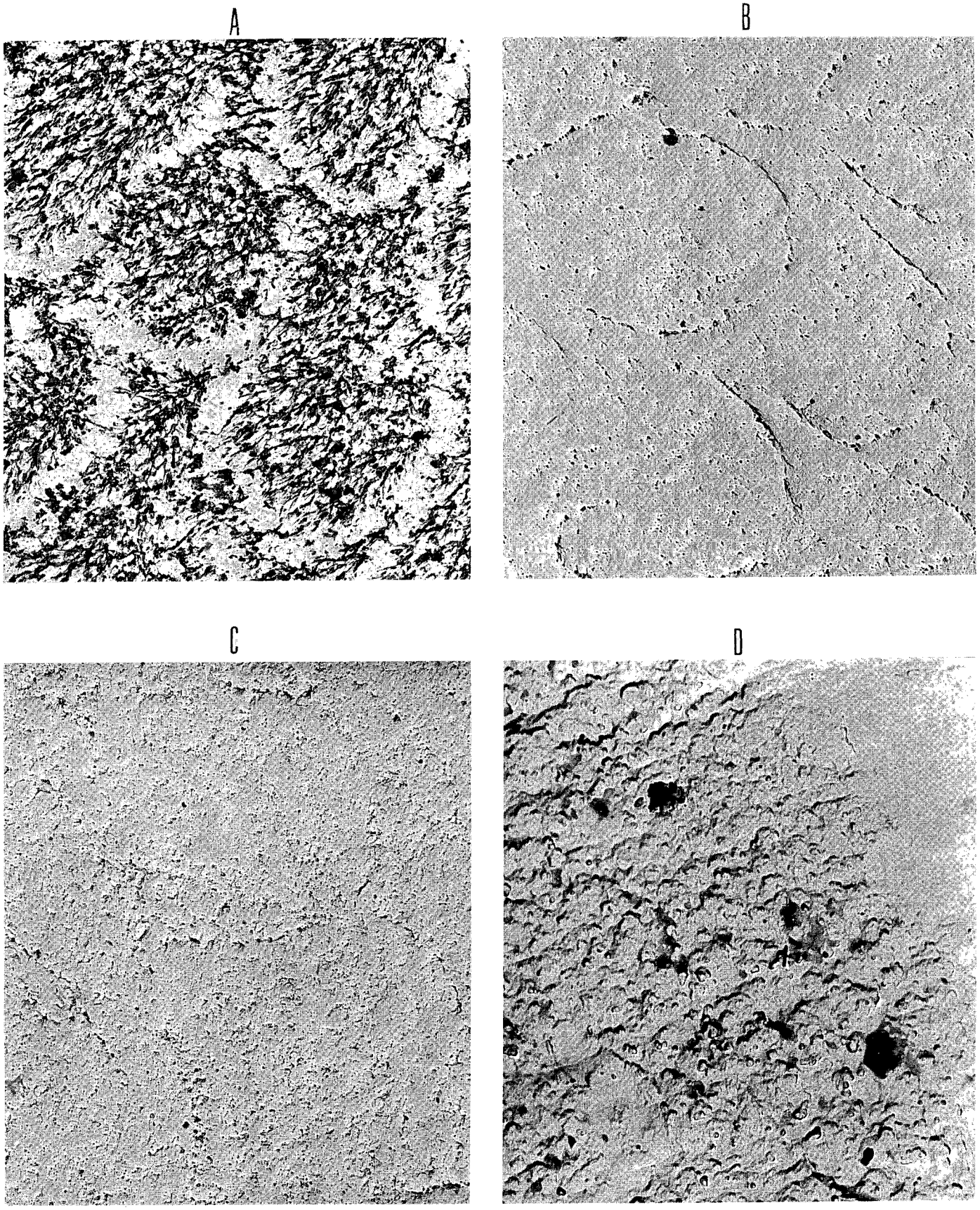

Figure 4. Electron micrographs of two-stage positive carbon replicas of surfaces. A. (X6000) Cell structure of a human tooth revealed by etching with lactic acid (milk). B. (X6000) Smoothed surface of a human tooth after brushing with a less abrasive type tooth paste; cell structure still visible. C. (X6000) Cell structure of a tooth almost removed by brushing with a more abrasive type of tooth paste. D. (X15,000) Initial stage of fretting damage on the surface of a titanium implant.

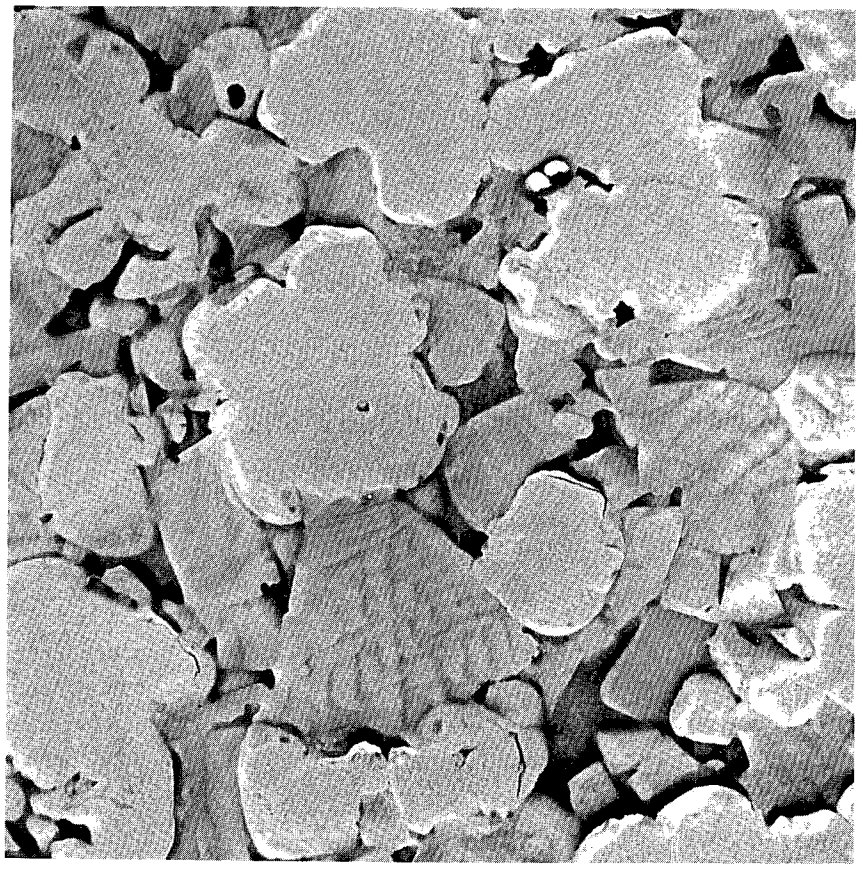

A

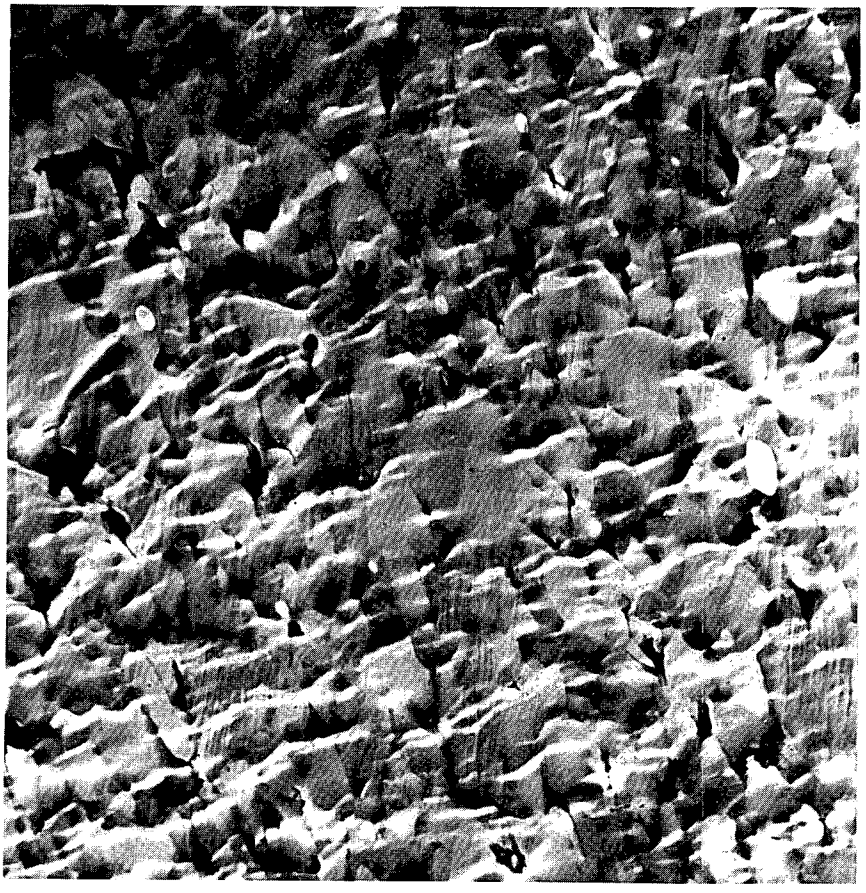

B

Figure 5
(×3200) Electron micrographs of shadowed, two-stage positive carbon replicas from the crater surfaces of carbide tools. A. Crater surface of cemented mixed carbide cutting tool. TIC particles have suffered less damage than WC particles. B. Crater surface of worn cemented WC cutting tool.

An improved, more uniform, mirror finish by optical standards and better than 1 micro-inch C.L.A. by stylus method can be obtained by diamond polishing. However, electron microscopic examination of a carbon replica still reveals the fine polishing marks of the $\frac{1}{4}$-micron diamond, Figure 3(A). By optical methods and stylus assessment, this surface is comparable with the run-in surface, Figure 3(B), but the examination of replicas at higher degrees of resolution shows important differences.

Use of electron microscopy in the examination of replicas from the bearing surfaces of races and rolling elements of advanced aero-engines, has revealed that what appeared to be staining by lubricant was the initiation of surface attack and corrosion traced to lubricant deterioration at elevated temperature, Figure 3(F). The abrasive action of different tooth pastes on the cleaning of human teeth has been revealed by electron microscopic examination of replicas from teeth, Figure 4. A cell structure is revealed by lactic acid (from milk) attack, Figure 4(A). Strongly abrasive tooth paste removes the etched surface but a less abrasive one smooths the surface with less removal of material, the cell outline still being visible, Figure 4(B) and (C). Electron microscopic examination of replicas from titanium implants which had given trouble in a human knee joint showed the presence of fretting action, Figure 4(D), fine debris being the cause of biological reaction and pain in the joint.

Besides showing surface details, replicas can embed and remove debris, contaminant particles, corrosion and lubricant reaction products from surfaces. Besides revealing the size and shape of such products, use of the electron microscope selected-area diffraction facilities can determine the structure of such particles and provide an indication of their source and the process of formation. Such information is useful in failure investigation.

Examination of Rough Surfaces

The application of optical microscopy to the examination of rough surfaces may offer some advantage over visual examination but is limited by the poor vertical resolution or depth of focus of optical instruments. The great depth of focus of electron microscopy, however, allows the examination of replicas of surfaces too rough for optical methods. Two-stage carbon replicas have proved useful for studying the rate at which cutting tools wear, one of the most important factors in machining from an economic point of view. Examination of craters or wear on the top surface of the tool in progressive stages of development, in different tool materials, under various cutting conditions has provided fine-scale information of use in confirming the mechanism of formation. The different appearance and wear rate of different constituents in a worn, mixed carbide, cobalt cemented tool tip, Figure 5(A), has indicated the advantage of such a tool over straight tungsten carbide, Figure 5(B). Titanium carbide particles appear to suffer less damage and wear than tungsten carbide particles.

Examination of Fracture Surfaces

The topography and characteristic markings of fracture surfaces are indicative of the mechanism of fracture which operated during the initiation of failure and crack propagation, thus the study of fracture surfaces, i.e. fractography (10), is useful in failure investigation. Owing to the low depth of focus of the optical microscope, interpretation of some fracture surfaces may be difficult. The microscopic topography and its relation to the causes and basic mechanism of fracture may be conveniently studied by electron microfractography (11, 12), using nondestructive replica methods. Replicas may be taken from selected areas of the fracture surfaces of large unwieldy engineering components.

Fine formvar replicas which form the first stage for positive carbon replicas of smooth surfaces may be difficult to remove without tearing from fracture surfaces, and nondestructive rough replica techniques such as the plastic/carbon replica technique have been developed (13). The first step is to obtain a thick, strong plastic replica of the surface. Acetate sheet, softened by acetone, can be pressed or clamped on to the fracture surface. When hard, it can easily be removed mechanically from the surface without damage. A thin film of carbon is evaporated on to the plastic replica, and the latter is then dissolved away in acetone leaving a thin positive carbon replica to be collected for examination, with or without metal shadowing to improve contrast. If the carbon is evaporated from a platinum/carbon rod at an acute angle to the surface of the plastic replica, replication and shadowing are effected simultaneously (14). An alternative method, sometimes more suitable for very large specimens, is to cast perspex on to the surface and cure it in situ to form the initial plastic replica.

Figure 6(A) shows a typical electron microfractograph of plastic or ductile fracture caused by the formation and coalescence of micro voids leaving concave depressions or 'dimples' on both fracture surfaces. Figure 6(B) shows 'river markings' typical of cleavage-type brittle fracture. Intergranular fracture may occur by the separation of crystals from each other along the grain boundaries; Figure 6(C) shows an example of intergranular fracture of a ball-bearing indicative of hydrogen embrittlement, due to environmental effects, being a contributory cause of failure. Electron microfractography can reveal striations or crack front arrest lines, characteristic of fatigue fracture, by progession of a crack under cyclic load, Figure 6(D).

Conclusions

Replica techniques are available for the nondestructive examination and assessment of surfaces. For large, unwieldy specimens and inaccessible or curved surfaces they offer, in some instances, the only convenient method of examination. They are most useful for periodic, in situ, surface examination. The replica technique used depends upon the nature of the specimen and the information required from it. Plastic replicas may be made quickly and metal coating improves reflectivity and aids microscopic examination and interferometry. Pliable replicas facilitate the examination of curved surfaces, and positive carbon replicas allow the surface irregularities to be observed in their true perspective. Rough surfaces may be conveniently replicated for examination by electron microscopy. Stylus methods of surface assessment may be applied to replicas.

Acknowledgments

The work described was carried out at the National Engineering Laboratory of the Ministry of Technology, and the paper is published by permission of the Director. This report is Crown copyright reserved and is produced by permission of the Controller of H.M. Stationery Office.

References

1. Drummond, D. G. The practice of electron microscopy. 1950. *Roy. Microscopical Soc.*, London.
2. Cosslett, V. E. Practical Electron Microscopy. 1951. Butterworths Scientific Publications, London.
3. Kay, D. H. Techniques for Electron Microscopy. 1965. Blackwell Scientific Publications, Oxford.
4. Kay, D. and Cosslett, V. E. Techniques for Electron Microscopy. 1961. Blackwell Scientific Publications, Oxford.
5. Thomas, G. Transmission Electron Microscopy of Metals. 1961. J. Wiley & Sons, London.
6. Scott, D. Optical microscopy in wear studies. 1957. *Proc. Inst. Mech. Engrs., Conference on Lubrication and Wear,* London, Paper 57, 670-673.

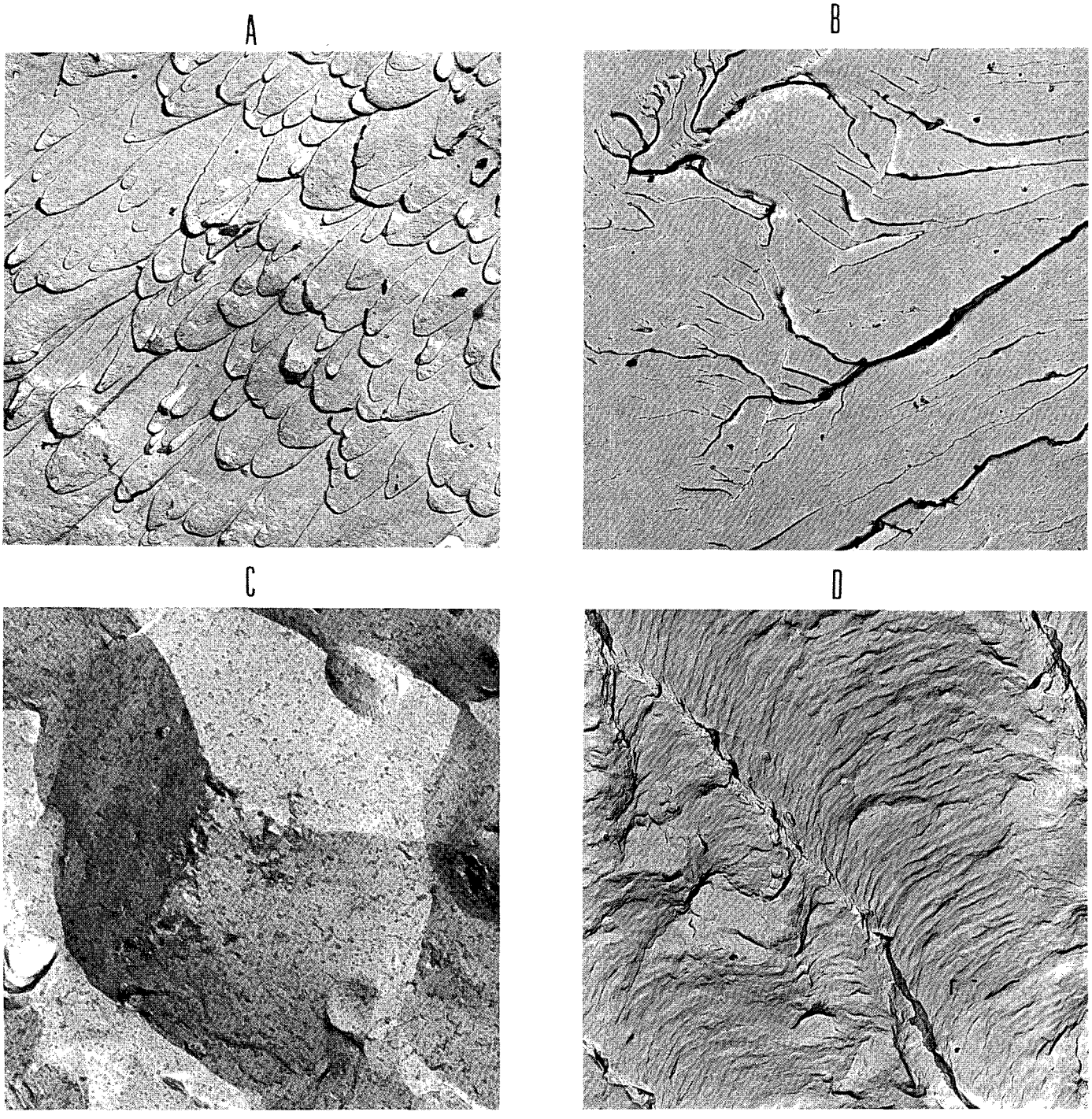

Figure 6. Electron micrographs of plastic/carbon replicas from fracture surfaces. A. (X2250) Ductile fracture of uranium, showing dimpled nature. B. (X4600) Brittle fracture of cast iron, showing typical river markings. C. (X15,000) Intergranular fracture of EN31 ball-bearing steel due to hydrogen embrittlement. D. (X10,000) Fatigue fracture of an aluminum alloy, showing characteristic striations.

7. Scott, D. and Scott, H. M. The electron microscope in the study of wear. 1957. *Proc. Inst. Mech. Engrs., Conference on Lubrication and Wear,* London, Paper 14, 609-612.
8. Bradley, D. E. A high resolution evaporated carbon replica technique for the electron microscope. 1954. *J. Inst. Metals,* **83**, 35.
9. Bradley, D. E. Uses of carbon replicas in electron microscopy. 1956. *J. Appl. Phys.* **27**, (12), 1399.
10. Zapffe, C. A. and Clogg, M. Fractography—A new tool for metallurgical research. 1945, *Trans. ASM,* **34**, 71.
11. Crussard, C., Borione, R., Plateau, J., Morillon, U. and Maratray, F. A study of impact tests and the mechanism of brittle fracture. 1956. *J. Iron and Steel Inst.,* **183**, 146-177.
12. Plateau, J., Henry, G. and Crussard, C. Influence of physicochemical conditions of grain boundaries on intergranular fracture. *ISI Special Report* 1964, 157-176. The Iron and Steel Institute, London, 1959.
13. Scott, D. and Scott, H. M. The electron microscope in the investigation of lubrication and wear problems. 1960, *Proc. Eur. Reg.,* Conference on Electron Microscopy, Delft, **1**, 535-538.
14. Bradley, D. E. A new approach to the problem of high resolution shadow casting—The simultaneous evaporation of platinum and carbon. *Proc. 4th Int., Conf. on Electron Microscopy,* Berlin, 1958, Vol. 1, 428. Springer-Verlag, Berlin.

Improved Resolution Neutron Radiography

B. L. BLANKS, D. A. GARRET and R. A. MORRIS, USA

ABSTRACT: Experiments in neutron radiography have demonstrated the feasibility of producing radiographs with image resolution comparable to that produced with x or γ radiation. Neutron collimation and imaging experiments by members of the Nondestructive Testing and Reactor Groups of the Los Alamos Scientific Laboratory are described in relation to the general problem of image unsharpness. Theoretical and experimental analyses of a neutron beam emergent from a simple collimating system are presented. Emphasis is placed on the angular divergence of the primary neutron beam and the resultant intensity pattern produced in the image plane. The theoretical analysis is shown to be basically correct for simple collimators and, in a qualitative manner, is applied to the more complex collimating systems employed in production neutron radiography. The results of production applications of neutron radiography at the Los Alamos Scientific Laboratory are described and include the detection of an O-ring in a nitrogen valve, the inspection of metallic-encapsulated high explosive components, and the detection of the boundary between different isotopic uranium compounds

Introduction

Recent experiments in neutron radiography confirm the feasibility of producing neutron radiographs with image resolution comparable to that of conventional x- and γ-ray radiographs. The results of neutron collimation experiments conducted by members of the Nondestructive Testing and Reactor Groups of the Los Alamos Scientific Laboratory are described in relation to the general problem of image unsharpness. Experimentally verified theoretical data for a single-slit neutron collimating system are presented. These data are applied to minimize source size as a partial cause of image unsharpness. Production applications of neutron radiography at the Los Alamos Scientific Laboratory are described.

The Neutron Source

The neutron source, because of its relatively large size, is the most significant factor contributing to image unsharpness. Image unsharpness is geometrical in character and is described by the equation

$$U_g = b(S/a) \tag{1}$$

where U_g is the image unsharpness, S is the maximum source dimension, b is the object-to-film distance, and a is the source-to-object distance.

Of the three factors used to define U_g, the term b is not influenced by the neutron source. If the quantity b is factored from both sides of equation (1), the term S/a can be used to characterize the source resolution capability for a given object-to-film geometry as follows:

$$\frac{U_g}{b} = \frac{S}{a} \tag{1a}$$

The term (S/a) is used in this paper as a measure of image unsharpness for a given object-to-image plane geometry.

The neutrons scattered by the object and the nondirectional scatter of the induced decay products in the imaging system contribute roughly similar amounts to image unsharpness, as do the corresponding components encountered in X-radiographic systems. However, the relative S/a value between neutron and X-ray systems differs markedly. Typical S/a values for industrial X-ray machines vary from 5.2×10^{-3} to 4.1×10^{-4}, whereas the ratio for the uncollimated neutron source employed in these experiments was approximately 5×10^{-2}.

Theory of Neutron Collimation

The requisite collimating system for neutron radiographic applications must produce a neutron beam possessing uniform flux and minimum angular divergence of the incident beam in the object plane. The magnitude of the S/a ratio of a neutron beam can be reduced by placing a Soller (1) slit in the beam. The original source area is divided into an approximately equal area of individual sources. Each source possesses a smaller S/a ratio than that of the original source by virtue of the reduction in the value of S.

The analysis of experimental data obtained from a two-dimensionally collimated beam would be difficult and laborious. For this reason, the experimental data obtained from a neutron beam transmitted through a simple, one-dimensional, single-slit collimator were first analyzed. The results of the analysis were applied in a qualitative manner to the more complex two-dimensional system.

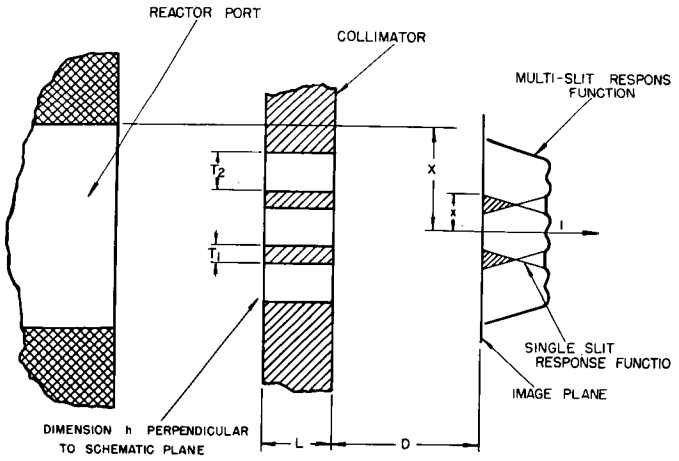

Figure 1. Multi-slit collimating system.

The Geometrical Beam

As a first approximation to a practical two-dimensional neutron collimator, the one-dimensional parallel plate system illustrated in Figure 1 can be employed. The collimator is assumed to possess totally absorbing and nonreflecting walls. This type of collimator produces an easily analyzed beam for which the neutron intensity at points in the imaging plane can be accurately predicted.

The parallel-plate collimating system is assumed to possess the following physical dimensions: collimator length, L; plate thickness; T_1; plate spacing T_2; collimator-to-image plane distance, D; and collimator height, h. The pretransmission neutron flux/unit solid angle (2) is I_0 n/cm^2/sec/sr. Assume that x is the coordinate in the image plane measured from the origin midway between the collimator plates in a direction normal to the neutron beam direction. The distance x is the coordinate for a single slit.

If $|x| \leq T_2/2$, the total neutron flux at the image plane due to transmission through a single slit is

$$I_1 = \left[\frac{h I_0 T_2}{(D+L)^2}\right] \tag{2}$$

Equation (2) represents a statement that the neutron flux at any point in the image plane is proportional to the total solid angle subtended by the source at point x. As the angles involved are small, the spherical surface of the solid angle is approximated by a plane surface.

If $|x|>T_2/2$, the point at x in the image plane "views" a smaller source from the single slit. The magnitude of the neutron intensity as point x is given by

$$I_2 = H I_0 \left[\frac{T_2(2D+L) - 2Lx}{2D(D+L)^2} \right] \tag{3}$$

Equations (2) and (3) represent the basic functions employed to calculate the neutron intensity pattern at an image plane produced by a perfectly absorbing and non-reflecting collimator having small angular divergence. Equation (3) indicates that the single-slit pattern width increases with the collimator-to-image plane distance, D. If the collimator consists of an array of more than one slit, individual single-slit patterns superimpose, producing a periodic intensity pattern as a function of

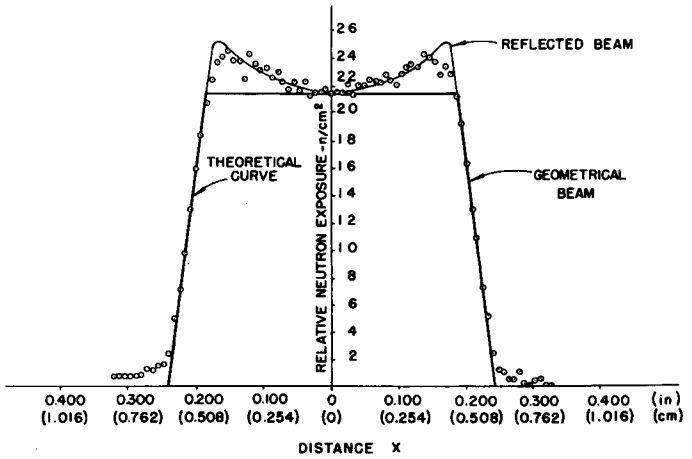

Figure 2. Theoretical and experimental response functions as a function of distance x.

distances x and D. The intensity pattern will possess a spatial period of $T_1 + T_2$. The theoretical intensity pattern for a single-slit system is illustrated in Figure 2. The pattern from a multi-slit collimator disappears completely for particular values of D. The maximum relative difference in neutron intensity in the imaging plane, R, is shown in Figure 3 as a function of the D/L ratio for various ratios, T_1/T_2. An expression for this function is given by

$$R = \left[\frac{\Delta I}{I} \right]_{max} \tag{4}$$

where ΔI is the maximum variation in intensity in the image plane, and I is the maximum image plane intensity.

The function R is periodic, decreasing from a value of one at D = 0 to zero for a particular value of D. As D is increased, the value of R alternately increases to some maximum value, less than one, and decreases to zero at a larger value of D. The ratio T_2/L is the largest value of the ratio S/a that can be attained for a particular collimating system. As the collimator-to-image plane distance is increased from zero, the S/a ratio decreases linearly from T_2/L to some minimum value. The minimum value depends upon the plate thickness, T_1. As the distance D is increased further, the S/a ratio again increases to T_2/L and decreases to a minimum value. The neutron flux remains relatively constant with increasing collimator-to-image plane distance. Results of experimentally verified calculations indicate that the system resolution can be increased by increasing the value of D. Small loss in flux results with increasing D, since $I=F(1/D)$ for such a system (1) (4).

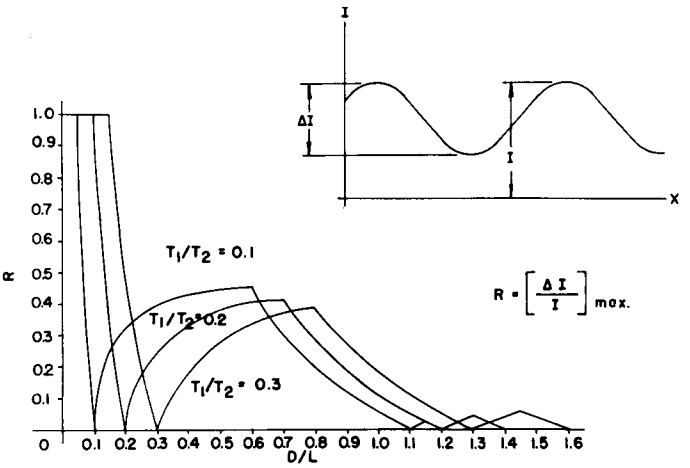

Figure 3. Theoretical R values as a function of $\frac{D}{L}$ ratios for various ratios $\frac{T_1}{T_2}$.

Perturbations Introduced by Wall Scattering

Neutron scattering from the collimator walls consists of (a) total reflection, and (b) regular isotropic or incoherent scattering. Both can increase the effective angular width of the beam, degrading the maximum resolution attainable.

Total reflection of a neutron beam incident upon a surface at near grazing incidence reflects the beam into the complementary solid angle with no loss in intensity. The magnitude of the solid angle for which total reflection takes place is a function of the maximum neutron energy. The critical angle is the largest angle for which a neutron beam of a given energy is reflected.

The same neutron beam is scattered in every direction with equal intensity by the process of isotropic scattering; i.e., the scattered neutron intensity is constant over 4 π steradians.

The critical angle for total reflection of a 2Å incident neutron on a phosphor bronze plate is 2.55×10^{-3} radians. The ratio of the totally reflected angles to the isotropically scattered angles is $2.55 \times 10^{-3}/4\pi$ or 2.03×10^{-4}. This indicates that the totally reflected intensity is larger than the isotropically scattered beam by a factor of 10^4. These calculations are based on the valid assumptions that:

(a) the incident neutron intensity is equal for both types of scattering, and (b) the collimator restricts the angular divergence of the incident intensity for both types of scattering to the same order of magnitude.

Isotropic scattering was ignored as a possible perturbation because of its relatively low magnitude, and only those perturbations contributed by total wall reflection were considered in the theoretical analysis.

The reflection from a single surface was analyzed and the results applied to the array of collimator surfaces. The surface employed was considered mathematically as a plane mirror which reflected all monoenergetic neutrons incident at an angle less than the critical angle, Θ_c, to the surface plane. The incident neutron spectrum was assumed to possess a Maxwellian distribution and was divided into small energy increments. Each increment was considered as a monoenergetic neutron beam, and the individual energy increments were then reflected from the plates.

The application of the scattering perturbation to the geometrical beam is illustrated by the light solid line of Figure 2 (2).

Perturbations Produced by Collimator Wall Penetration

Significant perturbations of the geometrical beam pattern are caused by neutron penetration of the collimator walls. This perturbation increases the apparent collimator aperture spacing.

Equations derived by Lillegraven (3) for γ-ray penetration of collimator walls were applied to a single-slit neutron collimating system having the following properties:

(a) plate material, phosphor bronze; (b) collimator length, 48 in. (121.9 cm); (c) plate spacing 0.375 in. (0.953 cm); (d) collimator-to-image plane distance, 6 in. (15.2 cm).

The results of the calculations indicated an apparent increase in collimator plate spacing of 0.03 in. (0.08 cm), or approximately 10%.

The Theoretical Collimator Response Curve

The theoretical response curve for a single-slit neutron collimating system is illustrated by the dark and light solid lines in Figure 2. The illustration presents the curves obtained from the geometrical beam and the perturbations introduced by critical angle scattering from the collimator walls. The theoretical curve does not take cognizance of the contribution by collimator-wall transmission since this effect was eliminated in the experimental analysis. It should be noted that this perturbation does exist in practical collimating system configurations.

Experimental Procedures—Neutron Collimating Systems

The neutron source utilized for the experimental portions of these investigations was the north thermal column of the Los Alamos Homogeneous Reactor (SUPO Model). This reactor is a water-moderated, graphite-reflected research reactor capable of producing a maximum neutron flux at the beam port of approximately 20 × 10^7 n/cm²/sec. The reactor components are illustrated in the sectional diagram of Figure 4.

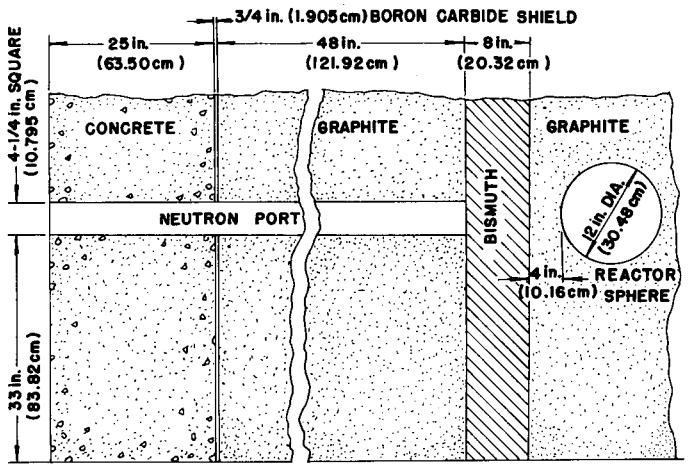

Figure 4. Sectional diagram, Los Alamos Homogeneous Reactor (SUPO model).

The collimated neutron beam pattern was recorded utilizing a 0.0003-in. (0.0008-cm) thick gadolinium imaging foil* in conjunction with Types AA and M Kodak Industrial X-Ray film. To obtain the highest resolution possible, the following measures were taken:

(a) The bakelite panels of rigid film cassettes were replaced by 0.125-in. (0.318-cm) thick reactor grade aluminum to reduce scattering, and (b) the radiographic films were positioned in a front film geometry; i.e., the film was placed in contact with, and on, the object side of the imaging foil.

Total Reflection Intensity—Single-Slit Collimation

The single-slit collimating system illustrated in Figure 5a was used to determine the totally reflected neutron intensity as a function of position in the imaging plane. The collimator walls were fabricated from phosphor bronze plates to the following dimensions: collimator length, 48 in. (121.9 cm); plate spacing, 0.375 in. (0.953 cm); and plate height, 3 in. (7.62 cm). Cadmium shields, opaque to thermal neutron transmission, were placed at the collimator ends and at intermediate points along the collimator walls. This measure eliminated neutron scatter from the reactor port walls. Placement of the shields allowed the perturbation introduced by neutron transmission through the collimator walls to be ignored and defined the geometrical beam in the absence of the removable phosphor bronze walls.

Experiments were conducted to determine the magnitude of film darkening produced at the image plane as a result of direct exposure to the neutron beam and by decay products resulting from neutron activation of the cadmium shields. No significant contribution from either factor was observed for collimator-to-image plane distances equal to or greater than 6 in. (15.2 cm).

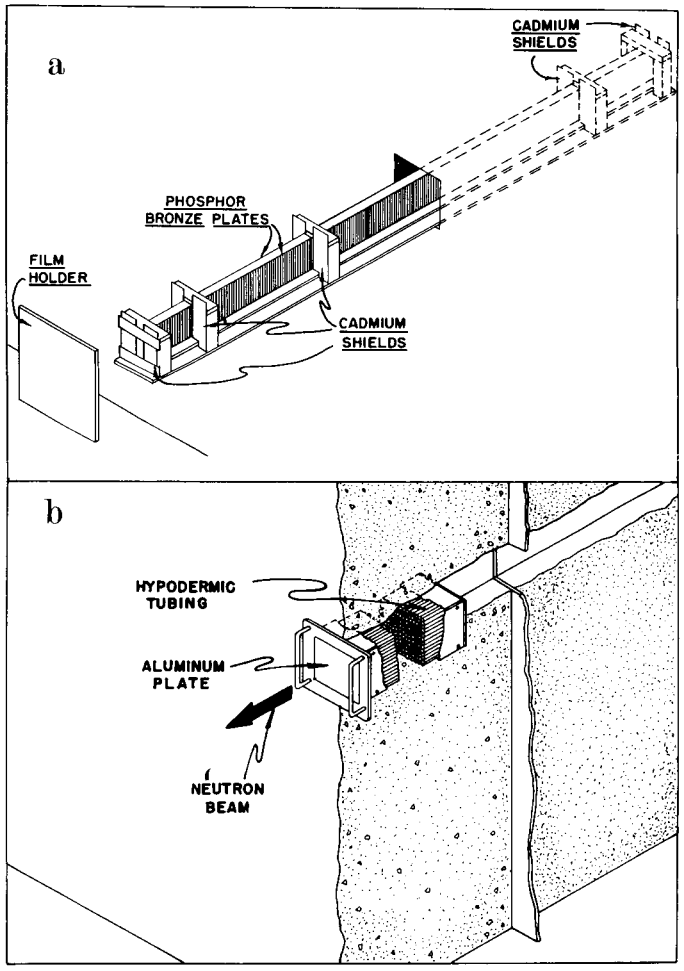

Figure 5. (a) Single-slit collimating system. (b) Tube collimating system.

To determine the geometrical beam pattern and the scattering contribution resulting from the collimator walls, exposures were made without and with the phosphor bronze walls in position, respectively. The exposures were made on Kodak Type AA Industrial X-Ray film at a pretransmission neutron intensity of 1.2 × 10^{10} n/cm². The X-ray films were cut from the same film sheet to ensure that the emulsions had similar characteristics. The reactor was operated under constant flux conditions. Imaging system placement and exposure were effected by an electrically-driven, electronically-controlled transport system. Films from the two exposures were hand-developed simultaneously.

The films were scanned with a Jarrell-Ash microdensitometer having a 0.0276 in. by 2.36 × 10^{-4} in. (0.7-mm × 6-micron) slit at a scan speed of 0.098 in./min. (2.5 mm/min).

* On loan from H. Berger, Argonne National Laboratory.

The densitometer data were converted to relative neutron intensity as a function of position x, in the image plane. The experimental data were normalized to the theoretical data and are illustrated by the circled points in Figure 2. The average film background was subtracted from the exposure density before the data were reduced to relative neutron intensity.

Pretransmission Collimation (Tube System)

The experimental verification of the single-slit collimation calculations indicated that these data could be applied in a qualitative way, to a two-dimensional tube or multi-slit system. A tube system is illustrated in Figure 5b.

These experiments were designed to yield collimator pattern data as a function of collimator-to-image plane distance for a tube collimating system. The system was fabricated from a stacked rectangular array of stainless steel hypodermic tubing. The collimator produced a maximum S/a ratio of 5.25×10^{-3}, which is comparable to that of an average X-ray system. This S/a ratio was effected with tubing of the following dimensions: outside diameter, 0.083 in. (0.211 cm); inside diameter, 0.063 in. (0.160 cm); and length 12.0 in. (30.5 cm).

The exposures illustrated in Figure 6a through 6f show the experimental patterns obtained on Kodak Type M Industrial X-Ray film, as a function of collimator-to-image plane distance for a pretransmission neutron intensity of 2.9×10^{11} n/cm^2. Beam pattern disappearance with increasing collimator-to-image plane distance is apparent from these radiographs.

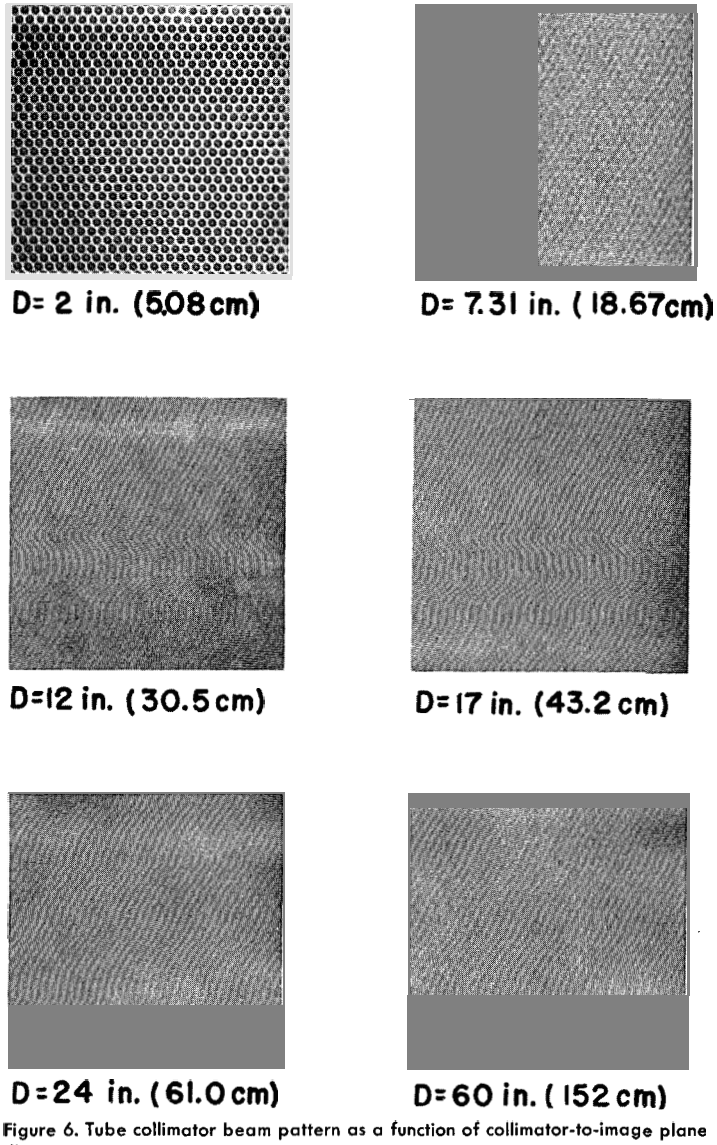

Figure 6. Tube collimator beam pattern as a function of collimator-to-image plane distance.

Application of Neutron Radiography

The application of neutron radiographic techniques to the solution of nondestructive testing laboratory problems has become a reality with the development of the tube collimation system at the Los Alamos Scientific Laboratory. Specifically, the technique has been applied to (a) the detection of hydrogenous seals in steel forgings, (b) the detection of voids in metallic encapsulated high-explosive components, and (c) the detection of isotopic separation in plasma thermocouple fuel pins.

The geometrical configurations employed for all applications described in this paper were identical; i.e. (a) collimator-to-image plane distance, 30 in. (76.2 cm); (b) collimator tube length, 12 in. (30.5 cm); (c) outside tube diameter, 0.083 in. (0.211 cm); (d) tube wall thickness, 0.010 in. (0.025 cm); and (e) object in contact with the cassette. A 0.0003 in.-(0.0008 cm) thick gadolinium imaging foil was employed in conjunction with Kodak Type M Industrial X-Ray film in a front-film geometry. (5) All films were exposed at an intensity of approximately 10^{10} n/cm^2 at the object plane.

Experiments were conducted to determine the feasibility of detecting a neoprene O-ring in an explosively-actuated nitrogen valve. The valve housing was a forging fabricated from corrosion resistant steel. The results of the application of γ and neutron radiography, respectively, to the problem are illustrated in the left- and right-hand reproductions of Figure 7a. Iridium γ-rays having an energy range from 137 to 651 keV and thermal neutrons at a moderator temperature of 330°K were employed in these investigations. The O-ring was present during the making of both radiographs; however, it was detected only in the neutron radiograph.

The bridgewire of a Type SE-1 detonator was exploded on the application of a voltage, resulting in partial burnup of the adjacent explosive. The system was composed of two high-explosive components, PETN and tetryl. The left-hand radiographic reproduction of Figure 7b shows the results of a 150-pkv X-radiographic examination of the detonator, and the right-hand reproduction, the result of a neutron radiographic exposure. The neutron radiograph clearly shows not only the void area adjacent to the bridgewire caused by partial PETN burnup, but also the boundary between the PETN and tetryl. A brass collar surrounding the high explosive masks any detail which might otherwise be observable in the high-explosive components in the X-ray radiograph.

Plasma thermocouple fuel pins were fabricated from different isotopic uranium compounds. The fuel pins were segregated into two regions, an upper region containing a ^{238}U and a lower region containing a ^{235}U compound. It was required to accurately define the boundary of separation between the two regions by a nondestructive technique. The left- and right-hand illustrations of Figure 7c are the results of a 150-pkv X-ray and neutron radiographic examination, respectively. It can be seen that the X-radiograph does detect some density change at the isotopic interface; the interface is, however, more apparent and better defined in the neutron radiograph.

Conclusions

The results derived from the single-slit collimator experiments verify the validity of theoretically derived collimator response functions assuming that the wall transmission perturbations are negligible. The periodicity of the image plane intensity pattern as a function of collimator-to-image plane distance was confirmed for the multi-slit collimating system.

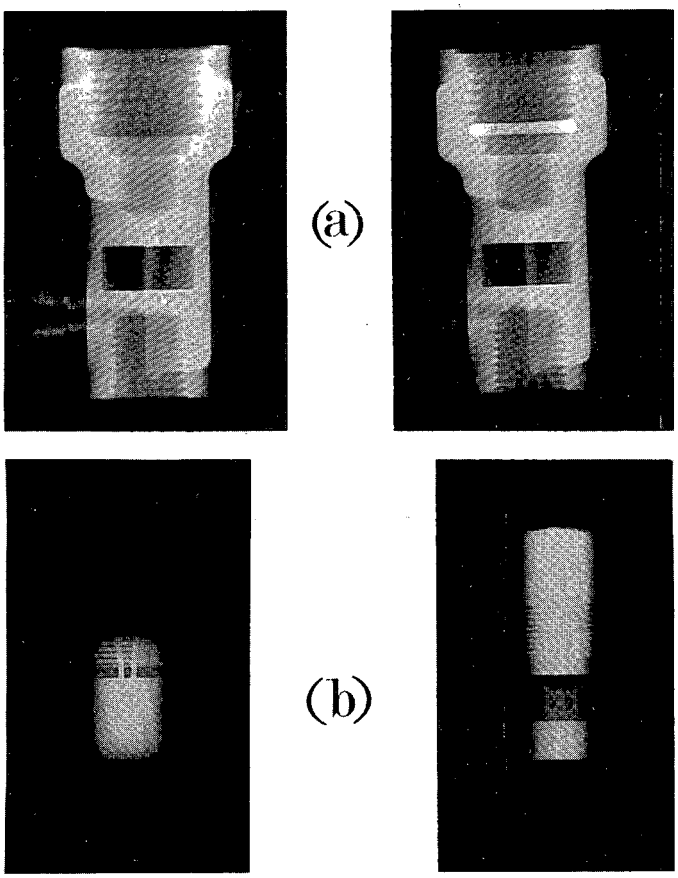

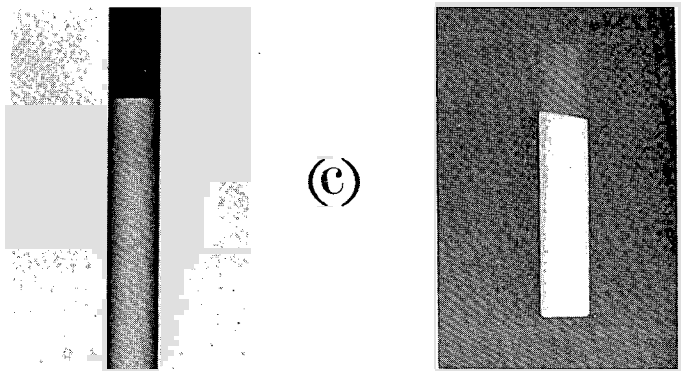

Figure 7. (a) O-ring detection (explosively actuated nitrogen valve). (b) Partial burnup of PETN (type SE-1 detonator). (c) Boundary of isotropic separation (plasma thermocouple fuel pin).

The single- and multi-slit collimation experiments led to the development of the tube collimator which has been applied to production neutron radiography at the Los Alamos Scientific Laboratory. The system, having an S/a ratio of 5×10^{-3}, confirmed the feasibility of producing neutron radiographs with image quality comparable to conventional X-ray radiographs.

Experiments will be conducted to investigate the feasibility of posttransmission static collimation and bidirectional dynamic collimation.

Acknowledgments

Appreciation is expressed by the authors to M. M. Thorpe of the Los Alamos Reactor Group for his assistance throughout the course of the experiment; to A. J. Demny and C. A. Baum for the graphic illustrations and to J. H. Smith, Radiation Section, Nondestructive Testing Group. The authors are also indebted to Dana E. Elliott, Group Leader, Nondestructive Testing Group, for his suggestions and encouragement regarding the preparation of this paper, and to H. H. Bybee, Jr.*, a Research Assistant in the Los Alamos Scientific Laboratory Summer Graduate Program, for his contributions to the successful completion of this phase of the investigations.

* Present Address—Electrical Engineering Department, University of Texas, Austin, Texas.

References

1. Soller, W., *Phys. Rev.* **24**, 158, 1924.
2. Morris, R. A., An investigation of neutron collimators and their application in neutron radiography. Thesis for the Degree of Master of Science in Physics, Univ. New Mexico, 1965.
3. Lillegraven, A. L., *J. Appl. Phys.*, **35**, 1974, 1964.
4. Egelstaff, P. A., Thermal Neutron Scattering, Academic Press, New York, 1965, p. 3.
5. Berger, H., *J. Appl. Phys.*, **34**, 914, 1963.

Discussion

Q. Dr. J. P. BARTON, S.A.R., Centre d'Études Nucléaires, Grenoble, France:

We have just heard a summary of ingenious methods to overcome the effect of masking lines cast by multi-channel Soller type collimators in neutron radiography. The problem of neutron beam collimation is certainly a very important aspect of neutron radiography. I think therefore the idea of the divergent collimator should be mentioned here. This is a principle which seems to me to overcome the difficulties of the multi-channel collimator mentioned in this summary, and can have some additional advantages.

Most neutron radiography has probably grown out of neutron beam physics, where it is necessary to extract a parallel beam from the broad source of the nuclear reactor core. Hence the Soller Slit Collimators. However, in the particular case of neutron radiography, it should be noted that a parallel beam is not a necessary requirement. Thus for a normal beam tube of diameter 'D' and length 'L' the neutron divergence is given by D/L where 'D' is measured at the outlet end of the tube; but the unsharpness of a point in the object cast on the detector screen is given by D/L where now 'D' is measured at the neutron source end of the tube. Hence a multi-tube parallel collimator can be replaced by a single divergent collimator of inlet diameter 'D' equal to the diameter of a single tube in the parallel collimator system. The outlet diameter 'O' of the divergent system may be large enough to radiograph sizable objects, as for the multi-channel system. If the lengths 'L' of the two alternatives are also the same it will be seen that they provide the same exposure rate

$$(\text{a function of } \frac{D^2}{L^2})$$

and the same unsharpness

$$(\text{a function of } \frac{D}{L}).$$

Overall distortion of the image for the divergent system can be exactly calculated, and will be negligible for normal values of

$$\frac{O}{L}.$$

The system appears to overcome very simply the problems of the multi-channel collimators discussed in the paper on Improved Resolution Neutron Radiography in that:

(1) There are no slats and therefore no mashing lines, and
(2) There is no problem of neutron critical reflection. In addition the collimator is comparatively cheap to manufacture, and the

displacement of moderator at the source end is minimized, which can have an important effect on the available neutron flux. This divergent collimator idea for neutron radiography has been widely tested and used in France over the past 18 months and I feel we can recommend the system. It would be useful to record the comments of Mr. Morris on these alternatives.

A. Dr. Barton's comparison between a Soller and pinhole collimator as they are used in neutron radiography is certainly pertinent but a good detailed comparison must be made between the two before a final verdict can be issued.

I disagree slightly with Dr. Barton that the exposure rate at the detector plane is the same for a pinhole and a Soller collimator. I contend that the exposure rate from a Soller collimator remains approximately constant as a function of distance between the object and collimator while for a pinhole collimator, the rate decreases as L^2, where L is the distance of the object from the pinhole. This can be seen if the flux, I_0, in the detector plane from *one* tube is given by:

$$I_0 = \frac{KD^2}{(T+L)^2} \tag{1}$$

where K is an arbitrary constant, D is the tube diameter, L the tube length, and T the distance from the detector plane to the exit side of the collimator. As the object is moved away from the collimator (T increases), the flux from the one tube decreases as expected. However, radiation from more tubes is added and imaged in the detector plane as T increases. The increase in flux due to the detector "seeing" more tubes is given approximately by calculating the increased area subtended at the collimator by the constant solid angle defined by:

$$\Omega = \frac{\pi D^2}{4L^2}$$

The number of tubes "seen" at any value of T is given by:

$$N = \Omega (T+L)^2 K' \tag{2}$$

where K′ is another arbitrary constant.

If the number of tubes "seen" by any point in the detector is multiplied by the neutron flux incident upon the point from one tube, the result will be equal to the total neutron flux at the detector plane.

$$I = NI_0 = \frac{\Omega (T+L)^2 K' K D^2}{(T+L)^2} = \Omega K'' D^2 \tag{3}$$

All of the terms on right side are constant. This shows in a qualitative fashion and with some approximations, that the flux from a Soller collimator is independent of the object-collimator distance.

This analysis ignores the fact that the variation of N as a function of T is in fact discontinuous. Between discrete steps in the N function, the total neutron flux on the detector will decrease according to the inverse square law. At each discontinuity in the N function, the total flux will increase to the original value. Without actually calculating the result, I would assume that the intensity function would exhibit a saw-tooth shape with an almost constant average level.

This constant level of flux at the detector plane would exist out to the value of T_0 where:

$$\Omega(T_0+L)^2 = \text{total beam area.}$$

For T larger than T_0, the flux would fall off inversely with the square of T. For the LASL collimator, $\Omega = 1.96 \times 10^{-5}$ steradians, L=12 inches, and the beam is approximately 16 square inches.

Solving the above equation for T_0 gives:

T_0=891 inches or 74.3 feet.

There can be no doubt that the presence of a masking pattern in the detector plane is a detriment that must be overcome. However, as I pointed out in the paper, these patterns are only significant when the detector is relatively close to the exit end of the collimator. As there is no significant loss in neutron flux as the detector is moved away from the collimator face, the pattern problem can be easily eliminated.

The existence of critical reflections from the walls of the tubes is only a problem when trying to calculate the exact effect they have on the image. In general, critical reflections can only increase the neutron flux in the detector plane without increasing the beam divergence. Critical angles are quite small depending on the tube material but are typically of the order of 0.1 degree. This is smaller than the divergence of the LASL collimator (0.3 degree) and so did not decrease the available resolution.

Dr. Barton's comments concerning the mechanical simplicity of the pinhole collimator are well taken and they certainly describe an advantage over the Soller collimator. However, I believe that there may be circumstances which require high resolution neutron radiography of relatively small objects, e.g., 4 to 6 inches when the neutron flux is relatively low (10^7 to 10^8 n/cm/sec for which the Soller collimator would be more useful than the pinhole. The price the experimenter pays for using a Soller collimator (and a relatively constant flux at the detector plane) is constant resolution. The inherent resolution in the radiation source as measured by the ratio of the source size to the source-to-object distance also remains constant for the same reasons that the flux remains constant. For the pinhole collimator, the larger the source-to-object distance, the better the resolution but the flux decreases by the inverse square law.

Q. ROY E. WYSNEWSKI, General Aniline & Film Corp., New York, USA:

Have you investigated X-ray film other than those mentioned in your paper to improve (a) system resolution, (b) enhance radiation response?

A. We have not investigated other films except to make trial radiographs with the extremely slow and fine-grained Type R film manufactured by Eastman Kodak. Again, the primary reason for restricting ourselves to one brand of film is the belief that basically, most industrial X-ray films are similar and the fact that Eastman Kodak films are readily available to us.

Q. RONALD HALMSHAW, Ministry of Defence (UK) RARDE, Sevenoaks, England:

I missed your statement of the material of the fine tube collimator—are they steel tubes?

A. The tubes in the collimator we use for production purposes are steel hypodermic tubing. This material was chosen primarily for its availability and not for any particular advantage it has in its reactions with neutrons.

Applications of Neutron Radiography Using a Pool Reactor

WAYNE A. CARBIENER, USA

ABSTRACT: The technique and apparatus used to obtain neutron radiographs of irradiated nuclear fuel specimens are described. The Battelle Research Reactor, a 2 Mw pool reactor, is used as a neutron source and all specimen handling and foil activation phases are carried out completely underwater, thereby using the reactor as a biological shield. Radiographs of clad and encapsulated fuel samples have been obtained. These radiographs have shown fuel pellet interfaces, cracking, fuel relocation, and swelling. Representative radiographs are included.

Introduction

The increasing role of nuclear energy in the nation's electrical power complex and a wide variety of other applications has brought about a continuing research and development effort to improve nuclear reactors. One of the primary areas of research has been the investigation of various reactor fuel mate-

rials. This continuing search for improved fuel has led to many extensive in-pile testing programs. Analyses of the tests have been limited owing to the destructive nature of the post-irradiation examination technique and the lack of knowledge about the timing of the observed effects. The desirability of nondestructive examination techniques has led to the application of neutron radiography to the reactor fuels research area. (1)

Neutron radiography is not confined to examination of radioactive materials but is valuable for other applications where X-ray and gamma radiography are limited (2, 3, 4, 5). However, the application of neutron radiography to the examination of irradiated materials has been the primary use of this tool at Battelle Memorial Institute, where a comprehensive nuclear fuels research program has been pursued for a number of years.

We have obtained neutron radiographs of more than a hundred clad fuel specimens, ranging in length from 4 in. to 10 ft, as well as several encapsulated samples. Many of these were obtained on a 1-2 day turnaround basis to meet test reactor startup requirements. Fission product activities up to 60,000 curies have been handled successfully since our work in this area was initiated in early 1965.

Method

Owing to the highly radioactive nature of the samples and the underwater operations employed, the transfer method of neutron radiography has been used exclusively in our efforts. Berger (6) has demonstrated the applicability of a variety of high-neutron cross-section materials for use in this and in the direct-exposure method of neutron radiography. We have used 5-mil indium foil as the screen material and Type AA film in our work.

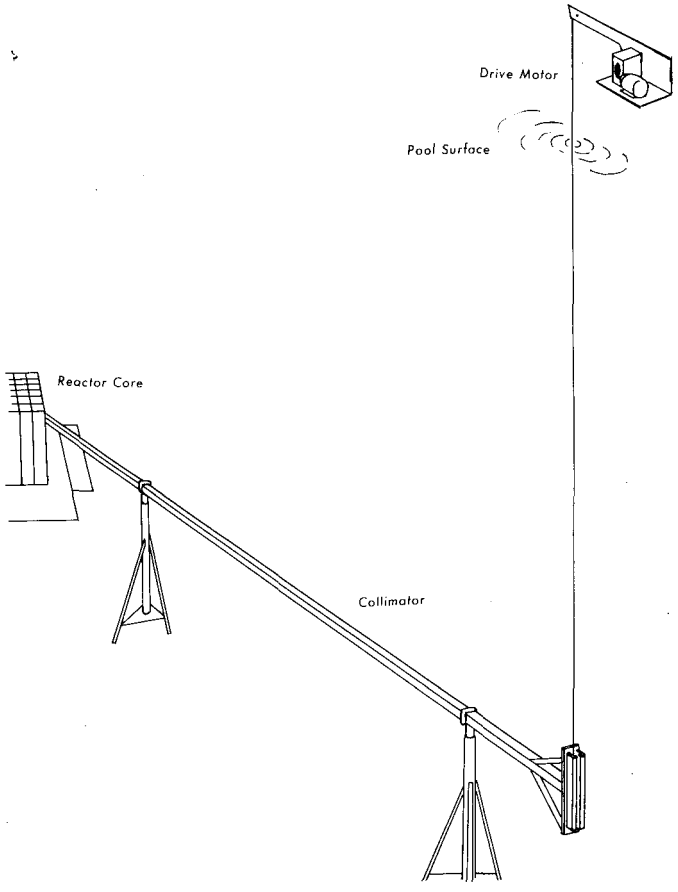

Figure 1. Neutron radiography apparatus.

The Battelle Research Reactor (BRR), a 2-Mw pool reactor, is used as the neutron source. A collimated beam of neutrons is obtained by immersing a $1\frac{1}{2}$-in. square, air filled, aluminum tube horizontally in the BRR pool about 6 ft above the floor. One end of the tube is positioned approximately $1\frac{1}{2}$ in. from the reactor core face at an oblique angle (Figure 1). A thermal neutron beam intensity of 1.2×10^8 n/cm^2/sec is available at the other end of the 12-ft-long collimator for radiographic applications with the reactor power at 2 Mw. The cadmium ratio for gold is about 6.5.

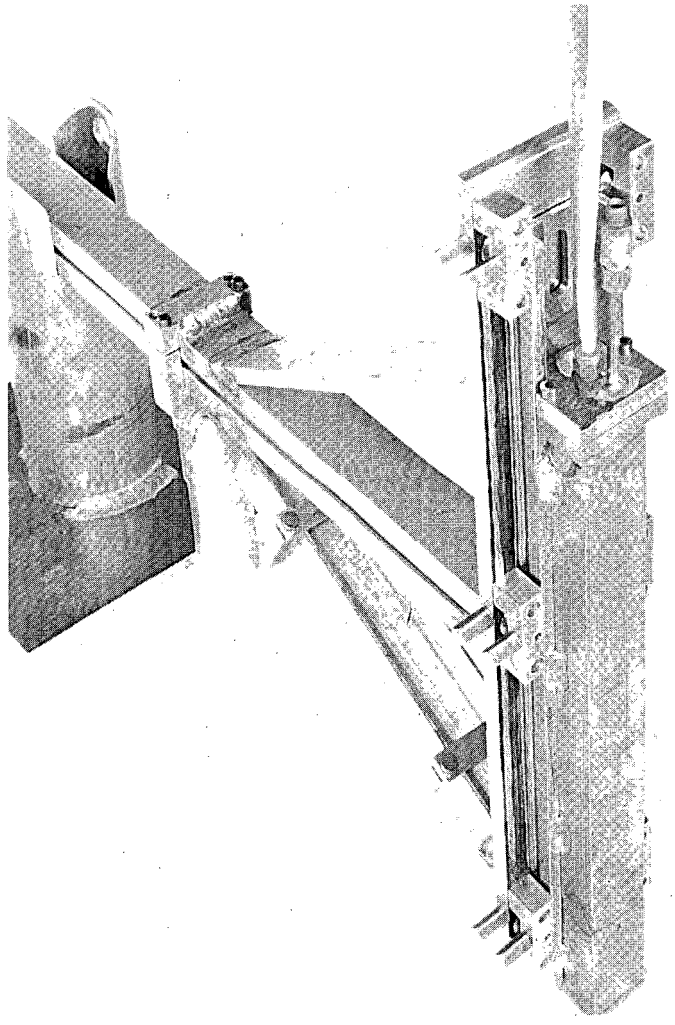

Figure 2. Sample fixture.

The exposure end of the collimator is equipped with three sets of V-shaped wheels to act as a guide for the sample fixture. The fixture (Figure 2) consists of a square can attached to a slotted plate. The V-shaped wheels run in the slots and position the fixture approximately 10 mils from the end of the collimating tube. The fixture is driven past the end of the collimator by a variable-speed gear motor mounted above the pool surface. In this manner the sample is scanned by the neutron beam, and a radiograph of specimens up to 12 in. long may be obtained. The fixture is fitted with purge lines so that after the samples are loaded underwater, the water remaining in the fixture is discharged by helium pressure. The samples and indium screens are both placed inside this fixture. The screen is backed by a cadmium sheet to reduce neutron backscatter. The internal arrangement of the fixture is shown in Figure 3 along with the arrangement used for capsule radiography.

In-pile test capsules are radiographed with lead-out hardware intact over reactor shutdown periods. The capsule is inserted in a close fitting tube (Figure 3) with the indium screen positioned behind the capsule in the water. The indium screen is removed in 12-in. lengths as the assembly is driven past the collimator. Scanning speeds used cover the range from 0.7 to 2.2 in./min. depending on the specimen geometry and film density desired. Fuel samples up to 10 ft long have been examined in a manner similar to that used for capsules.

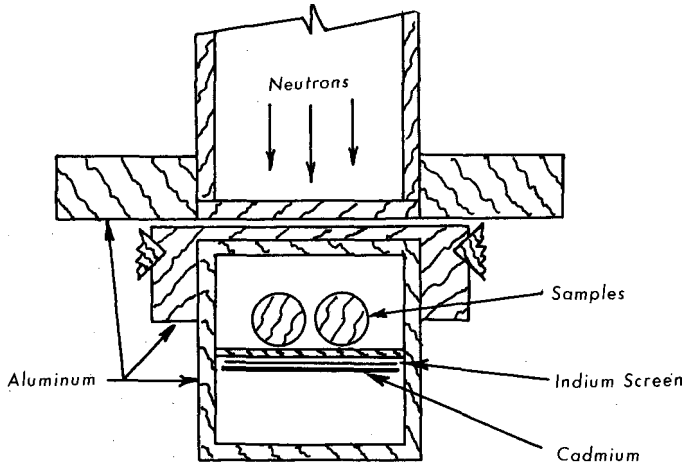

Clad Fuel Sample Fixture 1 ft long

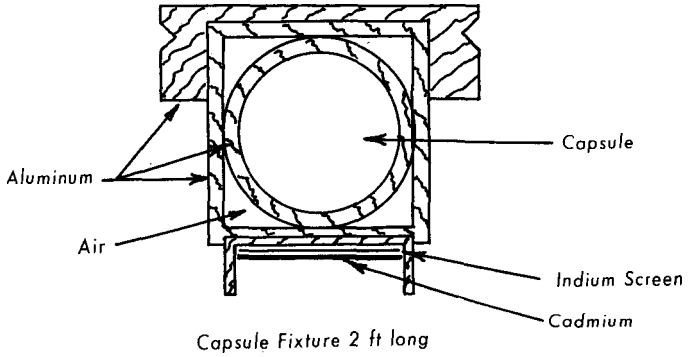

Capsule Fixture 2 ft long

Figure 3. Radiography fixtures.

Upon completion of the neutron activation of the indium screen, the screen is removed from the pool and allowed to decay in a cassette adjacent to standard X-ray film for approximately three half-lives. The decay time is varied, however, to compensate for the foil activity in achieving the desired resultant film density.

Results

The neutron radiographs of irradiated specimens obtained to date have been valuable in evaluating fuel and capsule performance. Figure 4 is an example of a capsule radiograph obtained prior to irradiation. Similar radiographs were obtained after each cycle of irradiation. The changes occurring during the test can be related to integrated neutron exposure by obtaining the specimen dimensional changes from the radiographs. Since the scanning technique used for radiography allows a 1:1 dimensional reproduction over the entire capsule or specimen area, these measurements can be reliably obtained. The capsule, in this case, was a double-walled, stainless-steel cylinder.

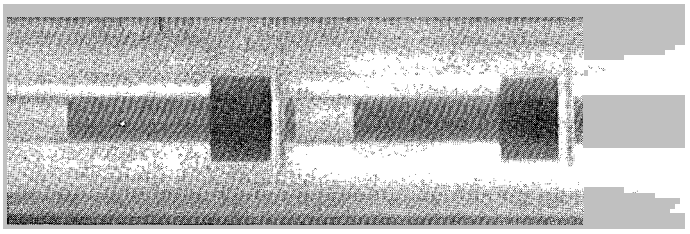

Figure 4. In-pile irradiation capsule.

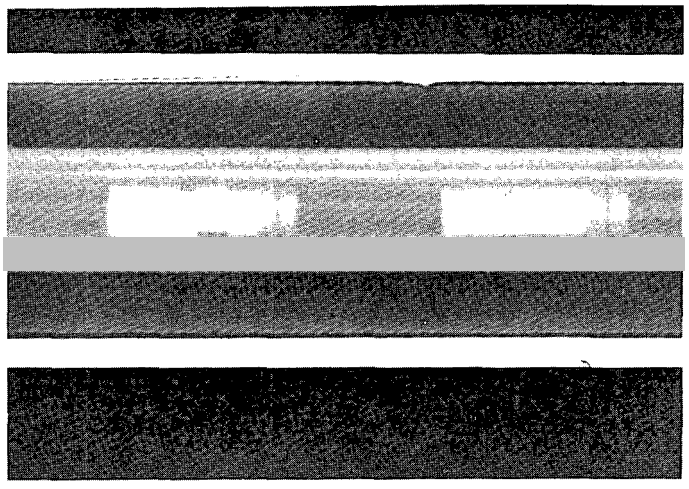

Figure 5. Double-walled irradiation capsule.

Figure 5 is another example of a fueled capsule which shows more internal fuel detail. This type of information relating to pellet interfaces, annular regions, cracks, and voids is indicative of that obtained from clad fuel samples which are not encapsulated.

Figure 6 shows a radiograph of two enriched uranium step blocks along with a perforated cadmium strip to present a measure of the resolution which has been attained. The longer uranium piece has steps of 8 mils over its length, the minimum thickness being 12 mils. The cadmium strip is drilled with 20- and 25-mil holes at varying separations. The strip is 20 mils thick. The remaining uranium piece was drilled to show the capability of detecting small holes in fuel material.

Conclusions

This neutron radiographic technique utilizing a pool reactor has proved valuable for the nondestructive examination of irradiated materials with extremely high activities. The use of the reactor pool water as a biological shield precludes the necessity of fabricating costly additional shielding and the water has not interfered with the radiographic process. Neutron radiographs obtained in this manner have shown fuel relocation, cracking, and swelling; and have also allowed the examination of capsule internals such as thermocouples, coolant levels, and sample positioning devices.

This nondestructive examination method has been a valuable tool for two applications. First, experimental capsules can be examined at intervals during a test to detect internal changes and develop radiation-effects information which can be related to integrated neutron exposure. This technique has also been of assistance in determining the advisability of continuing or terminating a test in view of safety and post-irradiation examination requirements.

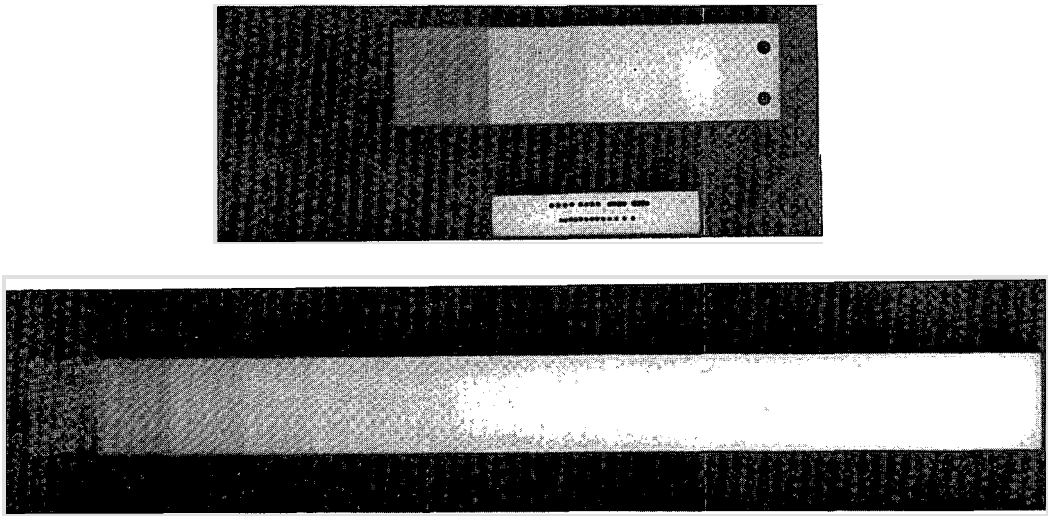

Figure 6
Radiographic test-pieces.

The second application of this technique has been the detailed examination of the clad fuel specimens upon completion of a test as an aid in determining the more advantageous locations for obtaining post-irradiation destructive test samples.

Currently underway are efforts to expand the application of neutron radiography to nondestructive examination of irradiated materials. As more experience is gained in the evaluation of radiographs, showing the internal changes taking place in the material, interim radiographs during a test will be more valuable in the analysis of the test results.

References

1. Berger, Harold and Beck, W. N. Neutron radiographic inspection of radioactive irradiated fuel specimens, *Nuclear Sci. and Eng.* **15**, 411-414, 1963.
2. Berger, Harold. "Neutron Radiography, Methods, Capabilities, and Applications," p. 113, Elsevier Publishing Company, Amsterdam, London, and New York, 1965.
3. Berger, Harold. A discussion of neutron radiography, Nondestructive Testing, **20**, 185, 1962.
4. Berger, Harold and Kraska, I. R. Neutron radiographic inspection of heavy metals and hydrogenous materials, *Materials Eval.* **22**, 305, 1964.
5. Berger, Harold, Talboy, James H. and Tylka, Joseph P. Determination of cadmium burnup in reactor control rods by neutron radiography, *Nuclear Sci. and Eng.*, **18**, 236-241, 1964.
6. Berger, Harold. Resolution study of photographic thermal neutron image detectors, *J. Appl. Phys.*, **34**, 914-918, 1963.

The Present Aspects of Neutron Radiography in Toshiba

TAMON INOUYE, SHINSUKE KAWASAKI, NOBUYOSHI WAKABAYASHI and KAZUYUKI OGAWA, JAPAN

ABSTRACT: Two beam ports of the 100-kW Toshiba Training Reactor are simply converted to two collimators for thermal neutron radiography having the neutron intensity of 2.5 $\times$ 10^5 n/cm^2-sec with a cadmium ratio of 3.5. Neutron radiographs are obtained by the image transfer method using an indium screen, and the direct method using a gadolinium screen which needs only 10 minutes to expose. One application of the image transfer method is to examine the nonirradiated and the highly irradiated nuclear fuels which cannot be done with X-ray radiography. This method is satisfactorily free from γ-ray fogging. The cadmium shadowing method, using cadmium compound solution by which it is possible to detect the hair cracks and a porous portion of the sample, suggests a number of application possibilities. Images obtained by thermal neutron radiography are analyzed by the technique of Fourier analysis. The optical transfer functions related to the unparallelism of thermal neutron beams in the process of image transfer from an activated indium screen to an X-ray film are derived, and compared with experimental procedures using a cadmium-made Siemens-star.

Introduction

Thermal neutron radiography(1) has been studied in connection with its possible application as a useful industrial testing tool, using two beam ports of the Toshiba Training Reactor. Good neutron radiographs are obtained by the image transfer and the direct method. One application of the image transfer method is to examine nuclear fuels, which cannot be done with conventional X-ray radiography. An interesting method is the cadmium shadowing technique using a cadmium compound solution by which it is possible to detect the hair cracks and a porous portion of the sample. Images obtained are analyzed by means of the spectrum analyses of line spread functions.

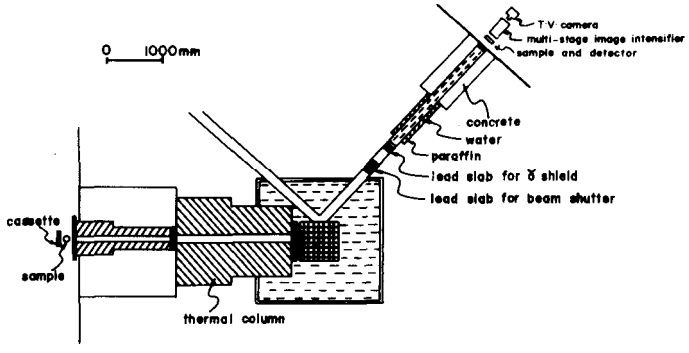

Figure 1. Experimental arrangement for neutron radiography in Toshiba Training Reactor.

Experimental Procedure

Collimated thermal neutron beams are obtained from two beam ports of the 100-kW Toshiba Training Reactor which were simply converted to two collimators as shown in Figure 1. One of them is constructed by pulling out the 100-mm^2 graphite rod in the centre of the thermal column and placing the collimator plug in front of it. The collimator is made by pouring paraffin into the stainless steel case. No cadmium is used, but a 50-mm-thick lead block is placed at the end of the thermal column as a γ-ray shield. The divergence of the thermal neutron beams is $\tan\theta = 50\text{ mm}/3535\text{ mm} = 0.014$ and the neutron intensity at the collimator exit measured with indium foils is 2.5×10^5 n/cm^2·sec. The neutron spectrum used for radiographs (cadmium ratio: 3.5) is very close to that of the reactor core (3.0), therefore graphite contributes greatly to the neutron collimation. Good neutron radiographs are obtained by the image-transfer method using a 0.5-mm-thick indium screen, and the direct method using a 0.3-mm-thick gadolinium screen. These methods require 50 min. and 10 min. respectively to secure radiographs. However, the quality of radiographs secured by the image transfer method, being free from γ-ray fogging, is better than that by the direct method. We have used the latter only for quick testing.

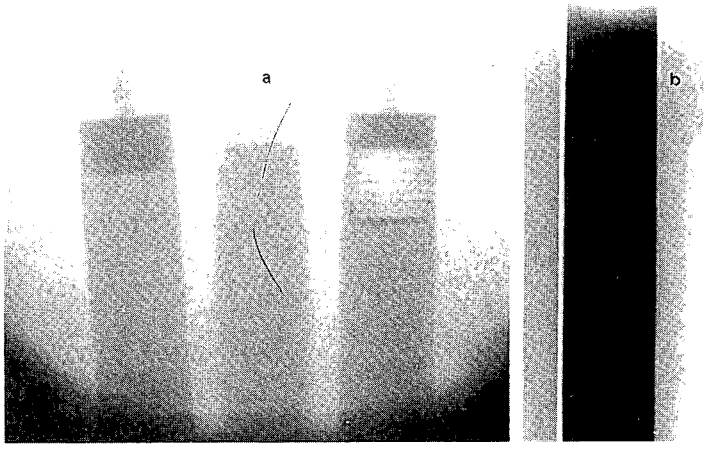

Figure 2. Radiographs of capsulated UO_2 fuels. (a) Taken with thermal neutrons. Irr. 50 min; Trans. 50 min with medium-speed Sakura-S X-ray film at 90 kW. (b) Taken with X-rays at 200kV.

Application to Nuclear Fuels

Inspection of Nonirradiated Fuels

Figure 2a shows the neutron radiograph of UO_2 fuels capsulated with stainless steel and zircalloy (centre). Figure 2b shows the X-ray radiograph (200 kV) of Figure 2a. The thermal neutrons seem to be superior to X-rays for the inspection of UO_2 fuels because of the high penetrating power for UO_2. Although it has the disadvantage of poor resolution, the neutron method can still detect about 5% of defects.

Inspection of Highly Irradiated Fuels

UO_2 pellets irradiated in GETR at 6×10^{13} n/cm^2-sec for two months were inspected (2). During the irradiation, the pellets were supposed to have been heated to about 3000°C in the centre and 2000°C near the circumference. These pellets were originally solid cylinders 12 mm in diameter and 12 mm long. Owing to the high temperature irradiation these pellets became coalesced, and the middle portion of the pellets was observed to have become hollow.

Inspection of Fuels by Shadowing Method

The sample pellet is a solid cylinder 24 mm in diameter, 24 mm long with a density of 10.3. Through the centre of the pellet along the axis, a 2.5-mm-dia hole was made by an ultrasonic tool and a tungsten wire of the same diameter was inserted. The pellet was then heated by applying electric current to the

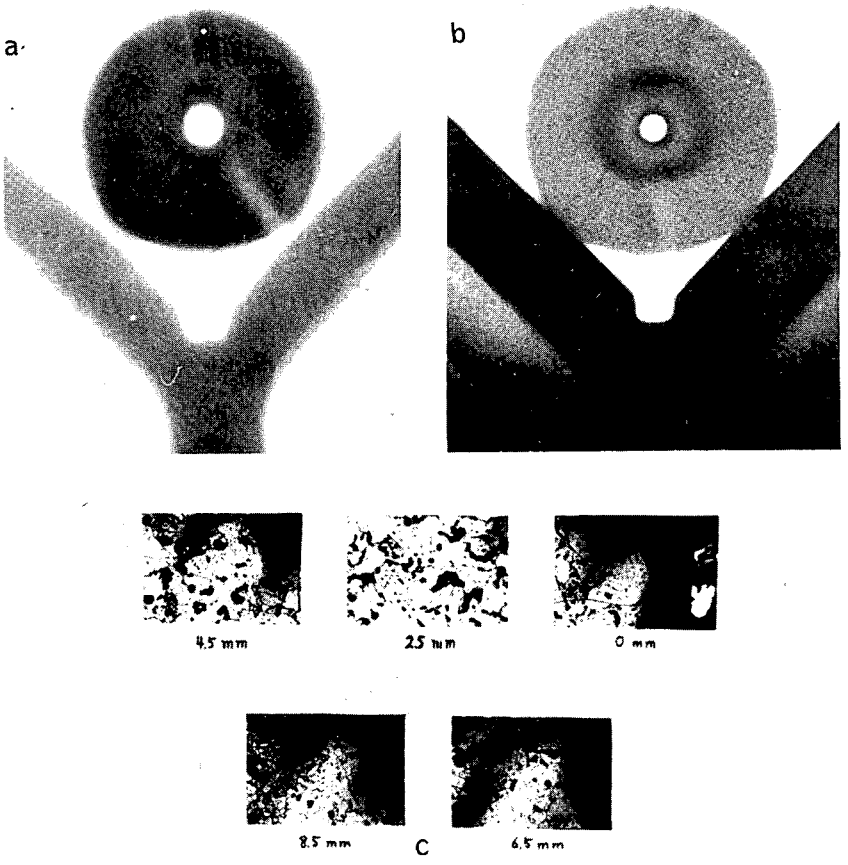

Figure 3
Radiographs of irradiated UO_2 pellets. (a) Taken with thermal neutrons. Irr. 40 min; Trans 1 hr with medium-speed Sakura-S X-ray film at 30 kW. (b) Taken with 15 Mev X-rays. (c) Radial variation of microscopic structure. Magnification, ×480; Etching: conc. H_2SO_4(1), conc. H_2O_2(3), and H_2O (6).

wire for two or three hours at 2800°C; it was then left to cool. The heat-treated pellet was dipped in saturated aqueous solution of cadmium chloride for several seconds, then the excess solution on the surface was wiped off, and the pellet was immediately radiographed. Figure 3a shows a concentric black ring which could not be observed with the X-ray radiograph as shown in Figure 3b. The cadmium salt is thought to have settled slightly in the part which has become porous. When the pellet was cut either axially or radially and observed with a microscope, structural differences were observed in the area corresponding to the black ring. Figure 3c shows the micrographs of the pellet cut perpendicular to the axis. Numbers on Figure 3c indicate the distances from the circumference to the centre hole. The part where the black ring appears can be seen in the insert marked 4.5 mm in Figure 3c.

Application to Hydrogen-containing Substances

The outstanding characteristics in the neutron radiographs of samples which contain some hydrogen can easily be seen when compared with X-ray radiographs. The defect in the structure of a lead-sheathed polyethylene cable cannot be observed in the X-ray (50-kV) radiograph, because the inner part of polyethylene sheathed with lead is perfectly black while the remaining part is transparent. In the neutron radiograph, on the other hand, the lead sheath is transparent and voids are seen dotted along the copper wire. The difference between the two methods can be also seen in the case of M-type high-frequency plug. X-ray and neutron radiography are complementary owing to the difference of absorption coefficient of the matter, and when the two methods are combined very useful radiographs are obtained; for example, Figures 4a and 4b show the images of a fuel-tank and gas lighter obtained by both X-ray and neutron radiography. Figure 4c shows the combination of the two radiographs. The over-all outline of the tank is clearly given by the X-ray image, while the positions and structures of the liquid pressurized gas, wick and packing are given by the neutron image as well as information on materials.

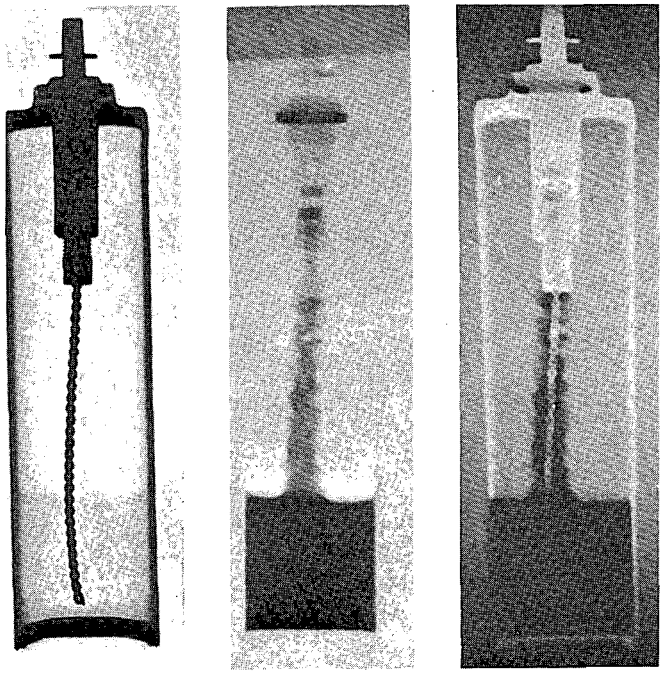

Figure 4. Combined radiograph of gas lighter.

Image Analysis of Thermal Neutron Radiography

Images obtained with thermal neutron radiography are analyzed by the technique of Fourier analysis. This technique is applied to the image transfer method using a 0.5-mm-thick indium screen. The resolving power of images is influenced by the unparallelism of thermal neutron beams, the image transfer from an activated indium screen to an X-ray film, and the existence of substances that contain hydrogen between a sample and an indium screen.

Optical Transfer Functions Related to the Unparallelism of Thermal Neutron Beams

The resolving power ν (3) related to the unparallelism of thermal neutron beams is obtained as $\nu = 0.59$ lines/mm from its optical transfer function using the value of $\tan\theta = 0.014$ which was calculated from the angle observed from the sample to the reactor core surface geometrically, and setting the length between the sample and the indium screen $l = 60$ mm. On the other hand, according to the experimental procedure using a cadmium-made Siemens-star which is often used in optics, the resolving power which is indicated as the turning frequency from the positive to the negative value of the function $H(\nu)$ is obtained as $\nu = 0.75$ lines/mm. Therefore, the divergence of the thermal neutron beams is estimated as $\tan\theta = 0.011$ which is about 30% lower than the value expected from the geometrical considerations. This fact indicates that the thermal neutron beam collimation is comparably well carried out at the surface of the reactor core.

Optical Transfer Functions in the Process of Image Transfer

We set $l = 60$ mm in the above case to observe the inverted image of a Siemens-star, but this value is larger than usual. Two line-spread functions using smaller values such as $l = 23$ mm and 9 mm show almost the same spread. Therefore, the optical transfer functions in the process of image transfer from a 0.5-mm-thick activated indium screen to a 0.25-mm-thick X-ray film. In this process, the resolving power of images is influenced by the screen thickness and the distance from the screen to the film. An activated latent image is got in the indium screen by means of exposing thermal neutron beams having the mean free path of about $\lambda = 1.3$ mm. The distribution of this image can be shown as $\exp(-z/\lambda)$, where the z-axis is perpendicular to the x-direction, which is taken along the surface of an X-ray film. Therefore, the line-spread function $h(x)$ of β and γ-rays at the surface of an X-ray film is given as follows.

$$h(x) = \int_{d}^{d+t} \frac{\exp\left(-\frac{z-d}{\lambda}\right) \cdot z}{x^2+z^2}\,dz + \int_{d}^{d+t} \frac{\exp\left(-\frac{z-d}{\lambda}\right) \cdot (z+f)}{x^2+(z+f)^2}\,dz$$

By Fourier transformation of $h(x)$, the optical transfer function in the process of image transfer can be obtained.

$$H(\nu) = \frac{\pi \cdot \exp\left(\frac{d}{\lambda}\right)}{2\pi|\nu| + \frac{1}{\lambda}} \left[\exp\left\{-\left(2\pi|\nu| + \frac{1}{\lambda}\right)d\right\} - \exp\left\{-\left(2\pi|\nu| + \frac{1}{\lambda}\right)(d+t)\right\}\right] \times \left[1 + \exp\left(-2\pi|\nu| \cdot f\right)\right]$$

This function always takes a plus value for every frequency ν, so the inverted image of a Siemens-star noticed by experimental procedure is not made in the process of image

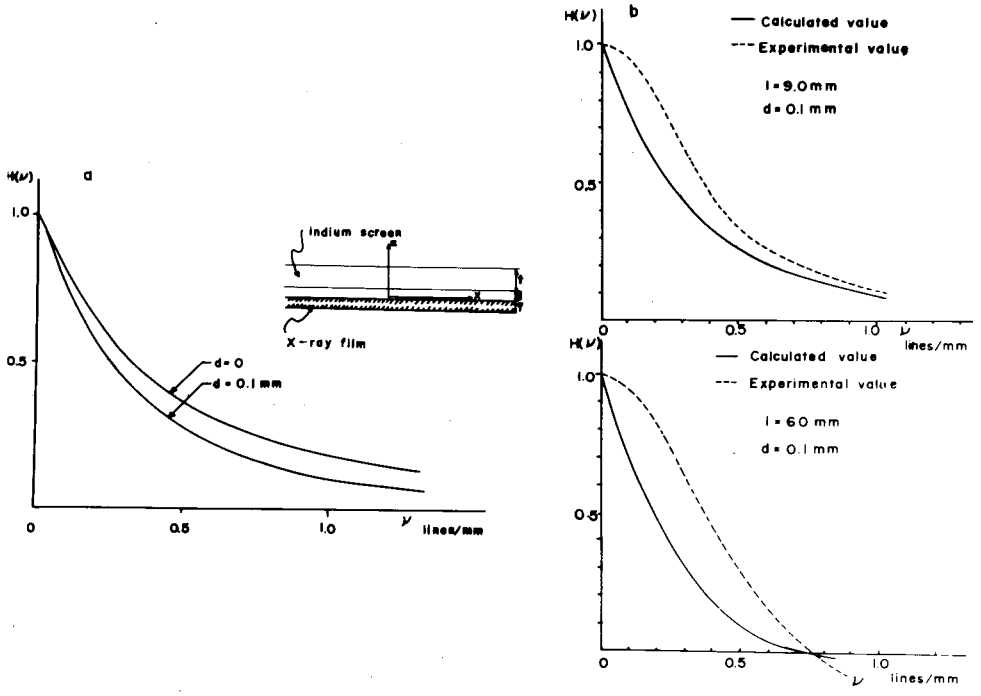

Figure 5
(a) Experimental arrangement of the process of image transfer between the indium screen and the X-ray film. Optical transfer functions of image transfer. (b) Optical transfer functions at l = 9.0 mm. (c) Optical transfer functions at l = 60 mm.

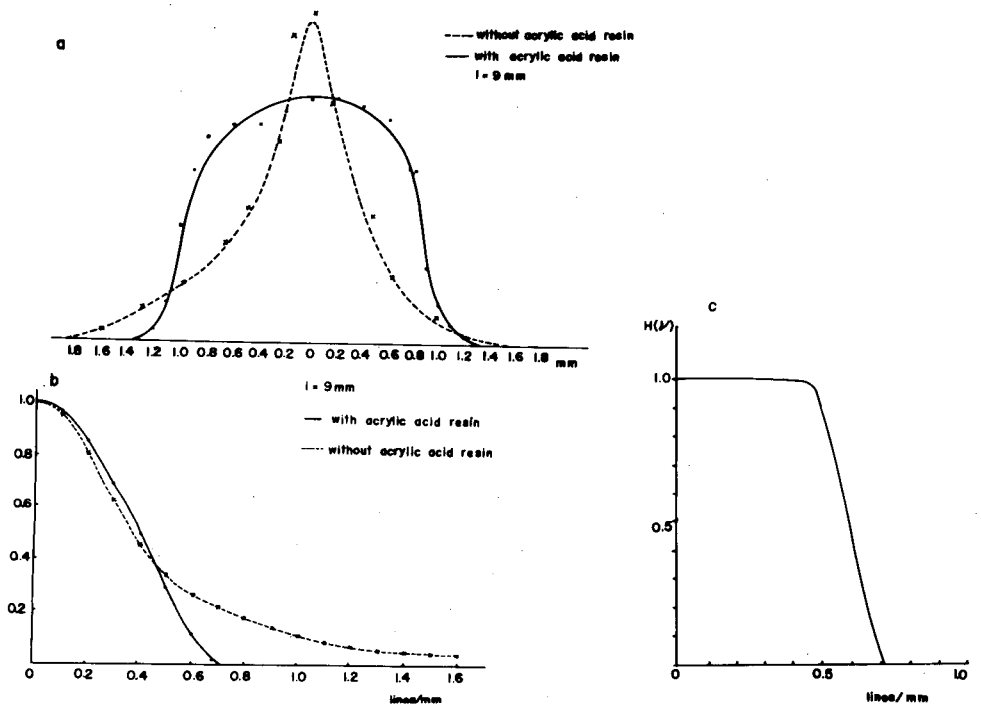

Figure 6
(a) Line-spread functions at l = 9 mm. (b) Optical transfer functions at l = 9 mm. (c) Optical transfer functions of acrylic acid resin of 9-mm thickness.

transfer, but comes from the unparallelism of beams. Figure 5a shows these functions in the case of $d = 0$ and 0.1 mm using the fixed value of $t = 0.5$ mm, $f = 0.25$ mm. Figure 5b shows the product of two H(ν) induced from the unparallelism and the process of image transfer in cases of $l = 9$ mm, 60 mm, and experimental values are also shown. They indicate that the experimental H(ν) includes higher frequencies than the calculated one. This tendency is caused by ignoring the limited range of β-ray beams which take the value of 4 mm. β-ray beams with a wide-aperture angle are scattered in the process of passing through the indium screen, therefore collimated β-ray beams are obtained.

Optical Transfer Functions Related to the Influence of Hydrogen-containing Substances.

Neutron images are influenced by substances containing hydrogen, such as acrylic acid resin. This influence is analyzed by using the same technique described before. Figure 6a shows the line-spread functions induced from the radiograph of step-wise acrylic acid resin, and the optical transfer functions in this case are shown in Figure 6b. Figure 6c shows the optical transfer function of a 9-mm-thick acrylic acid resin induced from the comparison of the two functions with and without the acrylic acid resin.

References

1. Berger, H. Comparison of several methods for the photographic detection of thermal neutron images: *J. Appl. Phys.* **33**, 48-55, 1962.
2. Ogawa, K. and Wakabayashi, N. "Irradiation Tests of UO_2 Fuel," Presented at the 3rd United Nations International Conference on the Peaceful Uses of Atomic Energy, 1964, Session 2.3/2.4.
3. Inoue, T. and Ogawa, K. A method of determination of thermal neutron beam collimation, *Nucl. Instr. & Methods,* **42**, 309-311, 1966.

Discussion

Q. Dr. J. P. BARTON, S.A.R., Centre d'Études Nucléaires, Grenoble, France:

In the summary on 'The Present Aspects of Neutron Radiography in Toshiba, Japan', a most interesting point was the relationship between observed and calculated collimation of a neutron beam. The divergence of the neutron beam was measured by a Seimens Star and Fourier Analyses method to be 30 per cent better than that calculated from the length and diameter of the beam tube. Two comments may be made on this.

Firstly we note that the beam tube was not lined with cadmium or other neutron absorber. Our own experience indicates that in this case many neutrons diverge from the sides of the tube, and the actual beam collimation is very much inferior to that calculated from the tube length. For example with a paraffin wax block of moderator surrounding a source of 14 MeV neutrons a 5 cm diameter tube of length 75 cm unlined, produces only the same beam collimator as a cadmium lined tube of length 25 cm. A difference of a factor of three. Thus we might expect the true neutron divergence in the Japanese case to be much larger than calculated.

Secondly we might note that photographic measurements often indicate much better beam collimation than would be expected. For example in our conical collimator of inlet diameter 1.4 cm and length 187 cm we would expect an image blur of 600 μ for a separation between object and image plane of 8 cm. In practice we can see in this case the separation of holes in cadmium down to 50 μ, and plastic wires can be distinguished down to 200 μ. Certainly this is not a true measurement of beam divergence, and the Seimens star method will be a more exact measurement. However, perhaps it is possible that both the calculated beam divergence (from the tube geometry) and the measured beam divergence (from the photographic method) are optimistic by about the same large factor, which would explain their agreement to within 30 per cent. This must, however, be very unlikely. Perhaps Mr. INOUE could comment on this question of possible errors in either the calculated or measured beam divergence.

A. In your first question, you have compared with the case of beam collimation of 14 MeV fast neutrons. When the source is the fast neutron emitter, then the contribution of thermalized neutrons from the sides of the tube will be important because a lot of thermalized neutrons diverge from the sides of collimator tube as you have mentioned in the comment. However, when the source is the emitter of thermalized neutrons, I do not think that the neutrons from the side surface are dominant. In our case, the source is the core of the nuclear reactor of swimming pool type, so the neutrons are well thermalized even at the end surface of the neutron collimator. According to this reason, I do not think that neutrons that diverge from the sides of the collimator tube significantly affect the neutron beam collimation.

For your second question, I cannot mention the most reasonable answer. One reason I can comment is the neutron intensity distribution at the end surface of the collimator tube. In our calculation, we have assumed that the neutron intensity distribution is constant on this surface. However, this is not confirmed. If the distribution is somewhat concentrated at the centre position, then the neutron collimation will be better than in the case of the constant distribution. In our case, the reactor core is very small, so it is not probable that the neutron intensity distribution is constant at the end surface of the collimator tube. This may be the reason of the discrepancy of thermal neutron beam collimations.

Technical Session 9/ Standardization—General

Development of Radiographic Standards for Castings

S. GOLDSPIEL, USA

ABSTRACT: Standards are urgently needed for radiographic (NDT) evaluation of common alloy castings to safeguard against failures due to hidden defects. These standards must be realistic to maintain balance between safety and costs. With these as an ultimate objective, the paper describes over five years of ASTM development work on Reference Radiographs, in which the U.S. Naval Applied Science Laboratory has been cooperating under the sponsorship of the Bureau of Ships. In addition, a summary is given of the Laboratory's work designed to develop objective bases whereby suitable reference radiographs can be designated as standards of acceptance for various types of castings. The discussion covers the following aspects: (a) development of steel, bronze and aluminum plate castings with defects of graded severity and most common radiographic indication types; (b) development of relationships between radiographic indications and mechanical properties using full section thickness specimens from 3-in. plate castings; and (c) considerations involved in making quantity reproductions of reference radiographs.

It is concluded that severity of radiographic indications can be used to assess performance of castings loaded in tension. However, radiography cannot be used alone to assess performance of castings loaded in bending (or flexure). In such cases, greater reliance must be placed on NDT methods which emphasize surface or near-surface discontinuities. It is also concluded that the new ASTM Reference Documents will adequately serve as radiographic standards for castings when various codifying activities prepare suitable implementing directives specifying acceptable severity levels for common types of discontinuity in various typical castings. In addition, the permanently stored plate castings developed for the ASTM Reference Radiograph documents can be used for production of new original radiographs for printing of future reissues; to make reference documents for new radiographic sources and techniques; and to prove capabilities of various other NDT methods for detection and assessment of internal flaws.

Background

The Navy Radiographic Standards for Steel Castings (1) promulgated in 1942 and still in use, include a compilation of actual industry production radiographs. They represent graded severity levels of most common discontinuity types, produced from steel casting sections not exceeding 2 in. thick. However, they lack the following two features, which technology has since recognized important in standards that can be used effectively:

a. Castings from which "standard" or "reference" radiographs are made should be available and stored for possible future reference, as for example in checking of improvements in sensitivity of detection which new radiographic sources, techniques and recording media may make possible at any particular time.

b. Radiographs used as standards of acceptance should be related to deterioration of engineering properties with increased severity of various discontinuity types.

ASTM Designation E71 (2), employing illustrations of the Navy Radiographic Standards for Steel Castings, was first adopted in 1947 as a tentative standard and until recently represented the only widely accepted document for specifying radiographic quality of steel castings for all of industry, as well as the Navy.

With the increased use of heavy-walled steel castings, involving section thicknesses up to 12 in., the Bureau of Ships has decided to modernize the existing standards, which were based on relatively thin-walled castings. Accordingly, it sponsored related project work at the Naval Applied Science Laboratory. Substantial funding on modernization of reference radiographs for common alloy castings including heavy-walled steel, high-strength Cu-base and related Ni-Cu alloys, tin bronzes and aluminum was started in 1962. For each alloy type, the intent was to include the largest section thicknesses in general use and simultaneous development of destructive test data to help in the establishment of more meaningful acceptance criteria. The work on the references was to be conducted, as much as possible, in cooperation with ASTM in order that completion be expedited and results receive industry acceptance. Cooperation was effected through a Laboratory representative on various task groups, who was to assure that:

a. The Navy's point of view is adequately reflected in the related work of ASTM; b. the development of required references be expedited at reduced cost to the Navy; and that c. special needs of the Navy, not reflected in references produced by ASTM, be supplemented by appropriate additional work at the Laboratory.

The important "special need of the Navy" results from the difference in the concepts of "Reference Radiographs" and "Standard Radiographs". "Reference Radiographs", as the term is used by ASTM, are sets of illustrations of graded severities of various discontinuity types, which cover a wide range of casting quality levels practically attainable in production with current know-how, without recommendations as to acceptability to particular applications. It is in pursuit of this policy, that the E71-52 document was revised recently (E71-64) to exclude a table of suggested classifications of castings by severity levels of common discontinuity indications. It is to be noted that, though the various gradations are established on basis of engineering judgment of competent engineers and metallurgists with many years of radiography experience, they are not backed by objective data relating discontinuity indications to effect on engineering property deterioration. Selected "references" become "standards" of radiographic quality acceptance, or "Radiographic Standards", when producer (vendor) and consumer (buyer) agree on using them as a basis of acceptance or rejection in a particular contract.

The Navy, as a large user of castings of radiographic quality, was first to develop and publish radiographic "standards" of acceptance to assure maximum uniformity in design, procurement, quality control, inspection and related activities with respect to castings in its far-flung establishment involving people of varied training, experience and points of view. The

Navy document, which was the basis of original ASTM E71 document, though based on judgment unbacked by actual data, listed 5 classes of castings established by arbitrary values of more or less loosely defined factors of (1) section thickness, (2) pressure (including temperature and superheat when steam is involved), (3) service stress, and (4) presence of impact and vibration. It has since been recognized that additional factors which must be considered in an over-all evaluation of radiographic quality in specific cases are: fatigue, exposure to penetrating radiation, accessibility for maintenance or replacement, and alloy type solidification characteristics. At best, however, (even with all factors of use currently considered in determination of radiographic classification requirements for a particular application) the acceptance criteria are largely qualitative and subjective.

Considerable improvement in the effective use of radiography as a nondestructive testing method for castings might result from an evaluation of the relationship between radiographic indications and change of mechanical properties. Availability of quantitative data, for example relating static tensile-test parameters and impact-bend to severity of radiographic indications, would be helpful in a more objective determination of standards of acceptance because such data could be used in conventional design calculations. While it is recognized that establishment of such relationships and their use is by no means easy, the trend in recent years has been to do so. Work of this type, but related to different materials or thickness ranges has been reported (3), (4), (5), but had to be extended to supply data for new alloys and especially for thicker sections of each.

Scope of Paper

This paper summarizes over five years of ASTM development work on Reference Radiographs, in which the Naval Applied Science Laboratory has been cooperating. In addition it discusses the Laboratory's related work on development of steel and bronze plate castings with defects of graded severity for most common radiographic indication types, development of relationships between radiographic indications and mechanical properties using full section thickness specimens from 3-in. plate castings; and considerations involved in making quantity reproductions of original selected reference radiographs. Finally, it outlines bases whereby suitable reference radiographs can be designated as standards of acceptance for various types of castings.

How ASTM Reference Radiographs Are Developed

Work on ASTM Reference Radiographs starts in Sub II of Committee E7, when a sufficient demand by producer and consumer interests demonstrates the need of new references. Considerations for establishing need for new references include (a) alloy type and solidification peculiarities; (b) thickness ranges and their influence on solidification or radiographic appearance of defects; and (c) radiation sources and their sensitivity of defect detection.

Upon approval of proposed work by the E7 Council, the chairman of Sub II appoints a Task Group chairman, who in turn establishes the Task Group personnel with equal representation of specialists in the field from producer and consumer interests. The Task Group, within general charge of the chairman of Sub II, decides on plans and conduct of its work autonomously. It agrees on the material to be produced for making the radiographs; thicknesses to represent ranges used by industry; representative discontinuity types and severity levels to be covered; dimensions of original radiographs; radiation sources to be employed for radiography; text material to accompany document; and method of original radiograph reproduction for ultimate quantity promulgation.

The detail work is accomplished by splinter groups whose decisions are subject to frequent reviews by the entire Task Group. When the selection of radiographs has been approved unanimously by the entire Task Group, the document is progressively subjected to ballot by Sub II and E7 membership. To provide bases for action on ballots, prototype albums of reference radiographs are made available for viewing at local and national meetings. Recommendations for changes and criticisms accompanying negative ballots, at each stage, are resolved by Sub II with the aid of additional studies, as necessary, by the Task Group. The process is generally painstaking and time consuming. This can be illustrated by work on document E186, "Reference Radiographs for Steel Castings for 2 to 4½ in. in Section Thickness." The selection involved many castings and frequent retaking of radiographs; 11 task group meetings and 5 Sub II meetings from March 1959 to June 1961, when the document was submitted for simultaneous balloting by Sub II and E7. The Administrative Committee on Standards of ASTM assigned the designation E186-62 to the recommended references on 16 April 1962. The references became an ASTM document on 28 May 1962. Difficulties in making reproductions by photography for the published document required its withdrawal. The problem of making improved reproductions was turned back to the Task Group and Sub II. As a result of special work, in which the Eastman Kodak Co. Research Laboratories assisted materially, a satisfactory method was evolved and a revised document E186-65 was issued almost 2½ years later. This aspect is described later in the paper.

Production of Plate Castings with Representative Radiographic Discontinuities

Plates, 3 in. thick and 12 in. × 14 in. in area, cast of approximately 0.30 carbon steel by 6 cooperating companies of the

Table 1

Chemical Composition and Tensile Properties of Plate Castings

(a) STEEL

	Chemical composition				Mechanical properties			
	%C	%Mn	%Si		T. S. 1000 psi	Yield Pt 1000 psi	% Elong in 2″	BHN
Number of specimens	49	49	49		47	47	46	47
Mean	0.26	0.58	0.41		68.5	36.3	31.4	128
Standard deviation	0.03	0.09	0.09		3.5	3.0	2.5	7
Minimum	0.19	0.42	0.25		60.9	31.1	28.0	112
Maximum	0.32	0.77	0.65		77.0	42.0	38.5	143
MIL-S-15083, Class B	−0.30	−0.60	−0.60		60.0*	30.0*	24.0*	—

(b) Mn-Ni-Al BRONZE

	Chemical composition				Mechanical properties			
	%Mn	%Ni	%Al	%Fe	T. S. 1000 psi	Yield Pt 1000 psi	% Elong in 2″	BHN
Number of specimens	58	58	58	58	58	58	58	58
Mean	12.4	2.4	7.5	3.2	97.0	44.2	33.2	167
Standard deviation	0.28	0.16	0.28	0.11	4.1	3.1	5.8	10.9
Minimum	11.7	2.1	7.0	3.1	90.8	32.8	12.5	149
Maximum	12.9	3.4	8.3	36	110.7	51.6	42.5	207
MIL-B-21230A, Alloy #2	11.0 to 14.0	1.5 to 3.0	7.0 to 8.5	2.0 to 4.0	90.0*	40.0*	200*	—

*Minimum

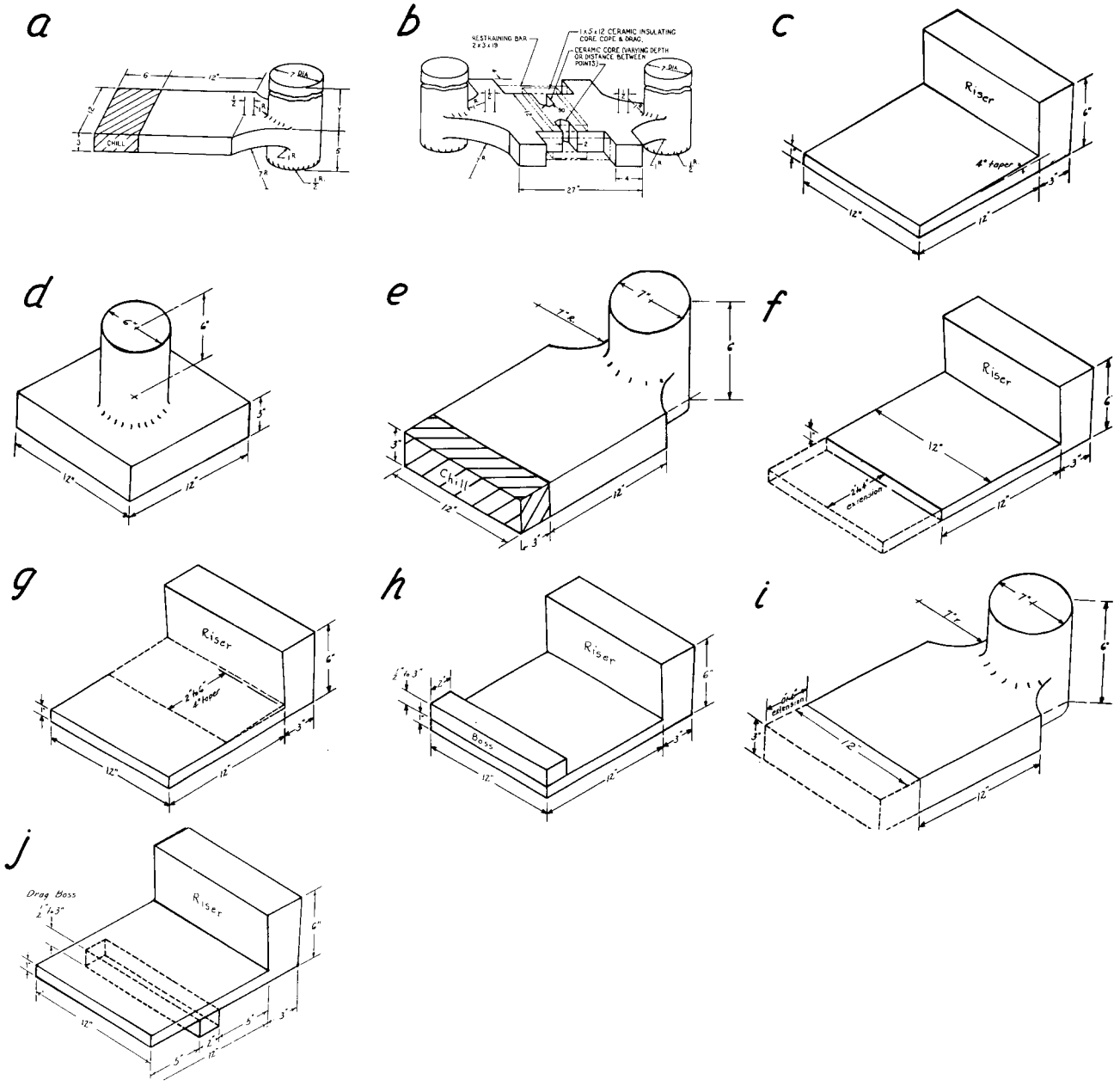

Figure 1. Foundry rigging used to produce plate castings with representative radiographic discontinuity types in graded severities.

Task Group (Blaw-Knox, Bonney-Floyd, Chapman Valve Mfg., Crane, General Electric and General Steel Industries Inc.) were used to develop the reference radiographs for the 2 to $4\frac{1}{2}$-in. steel castings (E186). All other plate castings for the selection of reference radiographs and destructive tests described in this paper were produced by or under the direction of the Naval Applied Science Laboratory. The following is a résumé of foundry procedures used to develop the various discontinuity types, which have been described in greater detail previously (6),(7).

A. Steel Plate Castings

Plate castings, other than those provided for E186 by cooperating companies mentioned above, were made of a composition complying with MIL-B-15083, Class B, Table 1(a). Typical rigging used in the foundry work is shown in Figures 1(a) and (b). It should be noted that even with the use of planned procedures (outlined below), the yield of usable castings was relatively low because random variables associated with casting technology and foundry metallurgy introduce extraneous discontinuity types and otherwise interfere with quality desired in "standard" plate castings. The following is a brief description of how the various defect types were introduced:

1. *Gas Porosity*—The total Si content of the heat was varied and deoxidation with Al eliminated.

2. *Inclusions*—Silica aggregate was introduced into approximately the mid-section of the mold and held with fine mesh steel wire screens which dissolved into the mass of metal during pouring.

3. *Shrinkage*—The three types of shrinkage included in the reference radiographs were produced by controlling the feeding and solidation gradients; e.g. using two risers, one at each plate end, while the plate length was varied; molds were poured with and without insulating pads placed, as deemed necessary, at bot-

tom and sides of the plate portion of the molds. The three shrinkage indication types (i.e., linear, dendritic and worm hole) were obtained more or less by accident.

4. *Linear*—The mold for castings with this discontinuity type made allowance for a longer plate than required for the finished length. It also had "ears" at corners at which tension was formed by resistance of restraining steel bars held between the ear portions of the mold. These plate castings were fed with two risers, one at each end.

5. *Inserts*—Two types of this discontinuity, i.e. chills and chaplets were used in this work, and both were produced in an identical manner. Various gradations were achieved by changing the area and thickness of zircon-bentonite wash applied to the metal inserts.

B. High-strength Copper-base Alloy Plate Castings

The alloy chosen for this work was a Mn-Ni-Al bronze, complying with composition requirements of MIL-B21230A, Alloy No. 2, Table 1(b) because this material has a narrow solidification range and dross forming characteristics of most of the alloys of high-strength Cu-base and related alloy castings (though somewhat to an exaggerated extent). Briefly the methods used to develop plates with varying severities of the most common discontinuity types for the alloy were as follows:

1. *Gas Holes*—For the 1-in. plate castings, the metal was melted and degassed by bubbling dry nitrogen through it for 30 to 40 minutes. Tapered plate castings, as shown in Figure 1(c), were poured in air using bonded, dry sand molds. The molds were placed immediately after pouring in a chamber where vacuum of 26 in. of mercury was applied during solidification. It was learned later that without the use of vacuum, gas bubbles did not form at all, but that with vacuum and without degassing an excess amount of bubbles formed. The procedure followed for the 3-in. plate castings was similar, except that degassing lasted from 45 to 120 minutes and the molds were as shown in Figure 1 (d).

2. *Inclusions*—For the 1-in. plate castings, silica particles of various sizes and amounts were fastened with sodium silicate to the ends of superston pins which were pushed into the drag of the green sand molds. The pins and inclusions were fused into the castings during pouring. The casting proper was a tapered 1-in. plate as shown in Figure 1(c). The procedure for the 3-in. plates was similar, except that the silica particles were fastened with sodium silicate to a copper screen which was suspended in the centre of the mold cavity as shown in Figure 1(e).

3. *Dross*—For 1-in. plate castings, the pattern used is shown in Figure 1(c). Castings with a small amount of dross were made by removing the screen normally used from the rigging and increasing the gate area. The latter was accomplished by increasing both the height and width of the gates. Medium amounts of dross were generated by introducing turbulence when clean metal was poured directly down the riser. The castings with large mounts of dross were made by pouring directly down the risers and allowing the floating dross in the ladle to stay with the metal stream. The procedure for the 3-in. plate castings was similar, except that the mold used was as shown in Figure 1(e).

4. *Shrinkage, Feathery*—For this discontinuity type, which applies only to the 1-in. castings, the plates were made with a mold, as shown in Figure 1(f), with extensions varying from 2 in. to 4 in. to obtain lower severity levels. The mold shown in Figure 1(g) with the plate having a 4° taper, varying in length from 2 in. to 6 in., was used to produce minor severity levels of shrinkage. The casting mold shown in Figure 1(h) with various appendages was used to produce intermediate levels of shrinkage. To produce the most severe grades of shrinkage, the mold was placed in a chamber and allowed to solidify under vacuum. The mold used for these castings is shown in Figure 1(c).

5. *Shrinkage, Linear and Spongy*—The "spongy" shrinkage type could only be developed for the 3-in.-thick plates and is considered to be a variation of the feathery type discussed for the 1-in.-plates. The difference in radiographic appearance between the sponge and feathery shrinkage types is mainly due to mass effect in cooling and reduction in detail resulting from superimposition of thicker layers of metal between the discontinuity and radiographic film. Both linear and spongy shrinkage were produced in castings poured with molds shown in Figure 1(i). Generally, the more severe levels were found in longer castings. However, the occurrence of either type seemed to be random and unrelated to the controlled variables.

C. Tin Bronze Plate Castings

The alloy chosen for this work was composition "G", MIL-M-16576(BUORD). Illustrations for sand inclusions, hot tear and inserts were retained from NAVSHIPS 250-537. The molds for the plates specially made for the new document were of green sand, rammed in tight flasks. Briefly, the methods used to produce the various discontinuity types were as follows:

1. *Gas Holes*—Gas holes were formed by mechanically entrapping gas in tapered plate castings of the type shown in Figure 1(c). Gas holes were also formed from dissolved gas added to the metal by bubbling ammonia or wet nitrogen.

2. *Shrinkage, Linear and Feathery*—Both types of shrinkage were found in castings with appendages shown in mold patterns, Figure 1(j). Either type of shrinkage occurred at random and the severity seemed unrelated to the size of the appendage.

New ASTM Reference Radiograph Documents for Steel and Bronze Castings

The results of the work on new reference radiographs for castings over the past five years of Committee E7 Sub II are summarized in Table 2 which lists by document: (a) designations; (b) applications as to material, thickness range and radiographic source types; (c) plate castings used, by material, size, total numbers cast and number finally selected for the references; and (d) reference document details, including discontinuity types, severity levels, film size and cognizant ASTM E7 Sub II Task Group. For each document the developed plate castings have been stored for possible future use on reissues, new radiographic techniques and even for proving other NDT techniques. To conserve expense and time for making original plate castings, references for alloys other than steel emphasized discontinuity types which are peculiar to the particular alloy types, and refer back to steel documents for discontinuity types which are substantially unaffected by alloy type.

Reproduction of Illustrations in Quantity from Prototype Album Originals

As briefly noted previously, the problems in the development of reference radiographs for the 3-in.-thick steel plates were not over when the prototype albums were completed and accepted by ballot at various committee levels. Thus the promulgation of proposed document E186 required that illustrations for each of 40 selected 3-in. plate castings, each radiographed with three radiation sources, be reproduced in quantity. For an initial issue of 100 sets this entailed production of 12,000 films each of which had to retain the essential detail of the originals including contrast, sensitivity, H&D density and colour. The first approach followed the traditionally used method of reproduction. This involved making of photographic intermediate trans-

Table 2

Tabular Summary for New ASTM Reference Radiographs for Castings

Document identification No.	Application			Plate castings used				Reference Document Details				Cognizant task group of ASTM COMM E-7
	Material	Thickness range (in.)	Radiation sources	Material	Size	Total No.	Selected No.	Discontinuity	Types	Severity levels per type	Film dimensions	
E186	Steel	2 TO 4½	1 MEV X-Ray Co–Co 10 TO 24 MEV X-Ray	MIL-S-15083 Class B	3″×12″×12″ to 18″×27″	165	40	Gas porosity	1	5	5″×7″	A
								Sand and Slag inclusions	1	5		
								Shrinkage	3	5		
								Linear	1	5		
								Inserts	2	5		
E280	Steel	4½ TO 12	10-24 MEV X-Ray Co-Co	MIL-S-15083 Class B	3″×12″×12″ TO 18″×27″	96	35	Gas porosity	1	5	8″×10″	A
								Sand and slag inclusions	1	5		
								Shrinkage	3	5		
								Linear	1	2		
								Inserts	2	5		
E272	High-strength Copper-base and nickel-copper *	TO 2	250 KVP X-Ray	MIL-B-21230A Alloy #2	1″×12″×12″	135	20	Gas porosity	1	5	5″×7″	D
								Inclusions, Sand and slag	1	5		
								Inclusions, dross	1	5		
								Shrinkage, feathery	1	5		
	,,	2 TO 6	2-MEV X-Ray	MIL-B-21230A Alloy #2	3″×12″×12″	170	25	Gas porosity	1	5		D
								Inclusions, slag and sand	1	5		
								Inclusions, dross	1	5		
								Shrinkage, linear	1	5		
								Shrinkage, spongy	1	5		
E310	Tin bronzes **	TO 4	250 KVP X-Ray	MIL-M16576 (Buord)	1″×12″×12″	44	15	Gas porosity	1	5		D
								Shrinkage	2	5		

*For discontinuities not shown appropriate steel reference radiographs can be used.
**For discontinuities not shown, either those retained from NAVSHIPS 250-537-1 or appropriate ones for steel castings can be used.

parencies on commercial film by photographing original radiographs from a light by use of a long range focal lens or by contact printing by use of a conventional printing box. Both these methods, when closely monitored under radiographic laboratory conditions, gave fair results in the past although the reproductions were considerably grainy and lacked the colour of original radiographs. Under shop production conditions, difficulties of control graininess gave nonuniform copies which, for the lower severity levels, became so bad at times that the relevant radiographic indications were illegible. Thus when the issues of document ASTM E186-62T first came out, complaints about their graininess was such as to cause their withdrawal until an improved method of reproduction was developed. The thickness of sections involved in the radiography of 3-in. steel plates for E186 and of the other documents, which by now were nearing completion (i.e. 6-in.-thick steel and 3-in-thick bronze plates, made the use of actual radiographs economically impractical. It may be noted that original radiographs were used for documents E192 and E155 which involves up to ¾-in.-thick sections of steel and aluminum, respectively. For heavy section thicknesses in the present instance, however, it was obvious that reproductions had to be made by a copying method. The Eastman Kodak Co. representative on Task Group A, which developed the E186 document, finally helped solve the problem with assistance of the company's research laboratory. Direct positive X-ray copying film, when properly exposed, yields reproductions which have almost identical contrast compared to the originals over a considerable density range. Figure 2 shows, for example, data for copying a radio-

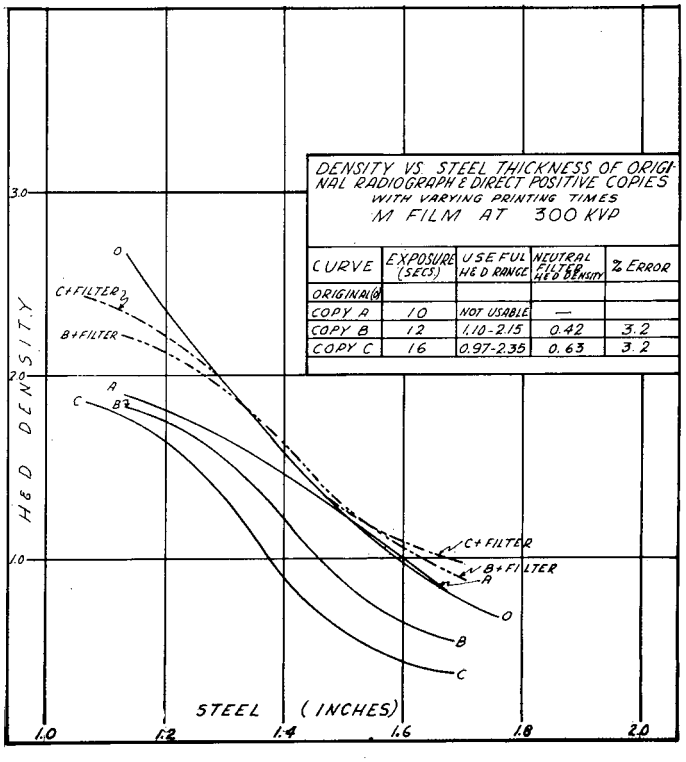

Figure 2. Direct X-ray film copies of steel step wedge radiograph.

graph of a step wedge on M film by using three different exposures. Curves B and C give copies which faithfully reproduce the contrast of the original over the range of 1.00 to 2.2 within 5%; whereas curve A shows such poor results as to be entirely unusable. In either case, however, the reproductions have a grain structure and colour which is comparable to those of original radiographs. However, they only reach a maximum density of about 1.9, because of the reversible nature of the emulsion. This density is considerably below the density of the original radiographs whose base and defects reach density values of 2 and 3 or more respectively. To achieve the densities of the original radiographs in copies it was finally decided that the reversible X-ray film copies be combined with sheets of commercial film which have been exposed to a uniform density. The density of the added film (or neutral filters) is such as to build up the combination to that of the original. In practice the neutral filters are prepared in advance to different uniform densities by varying exposures, and selected for use with suitable X-ray reversible film copies. For curves B and C of Figure 2 for example, use of neutral filters of 0.38 and 0.58, respectively will build up the density of reversible X-ray copies of the original wedge radiograph for a range of 1.0 to about 2.3 in terms of the original within about 5%.

Estimation of Heavy-Walled Casting Tensile Properties From Radiographs

Following is a brief summary of work to determine how static tensile strength properties correlate with severity level of representative radiographic discontinuities in full section specimens cut from 3-in. plate castings.

Materials—The materials studied were Class B steel (MIL-S-15083) (6)* and Mn-Ni-Al bronze (MIL-B-21230A, Alloy #2) representing a high-strength, narrow solidification, copper-base-type alloy.

Test Procedure—The tensile specimens were cut from plate castings accumulated during, and left over from, the selection of material for corresponding reference radiograph documents ASTM E186 and E272 for steel and high-strength bronze castings, respectively. The gauge section of all specimens were radiographed in plan and side elevation and evaluated for radiographic type of discontinuity and severity level by use of corresponding ASTM tentative reference radiographs. With few exceptions, which were noted for purposes of interpretation of results for

* Symbols in parentheses after discontinuity type are Code designations used for brevity on reference radiographs, and report tables, figures and discussions.

Table 3

Statistical Correlation Data between tensile Properties and Severity of Representative Types of Radiographic Indications in 3-in.-thick Steel and Mn-Ni-Al Bronze Plate Castings

(The slope is the deterioration per grade of severity and is given by the equation Y = a-bX, where Y is the property, X the severity of indication and a the average value for substantially sound plates.)

Discontinuity	Material	Tensile 1000 psi		Yield 1000 psi		% Elongation 4″ Gauge length	
		Slope	95% Tolerance limit	Slope	95% Tolerance limit	Slope	95% Tolerance limit
Gas porosity A	MIL-S-15083 CLASS "B" STEEL	−3.28	± 5.2	−0.43	*	−3.65	±5.0
Inclusions B		−0.03	*	−0.03	*	−1.36*	*
Linear shrinkage Ca		−8.11	± 6.2	−1.76	±2.3	−3.38	±4.8
Dendritic shrinkage Cb		−8.11	± 9.2	−0.69	±3.0	−1.22	±3.8
Worm-hole shrinkage Cc		−7.60	± 5.4	−1.43	±2.2	−3.46	±5.6
"Hot tears" D		−8.06	± 6.8	−1.23	±2.0	−4.40	±5.8
Chill inserts Ea		−2.58	± 5.2	−0.08	*	−2.59	±4.3
Chaplet inserts Eb		−4.93	± 5.4	−0.61	±1.9	−3.26	±3.8
Gas porosity A	Mn-Ni-Al BRONZE MIL-B-21250A; Alloy #2	−4.07	± 6.4	**	**	*	*
Sand inclusions Ba		−0.06	± 7.2	**	**	*	*
Dross inclusions Bb		−3.85	± 9.0	**	**	−1.20	±3.9
Linear shrinkage Ca		−3.62	± 8.4	**	**	−1.10	±2.6
Spongy shrinkage Cd		−3.58	±10.1	**	**	−0.93	±3.0

*No significant relationship indicate.
**Data not taken.

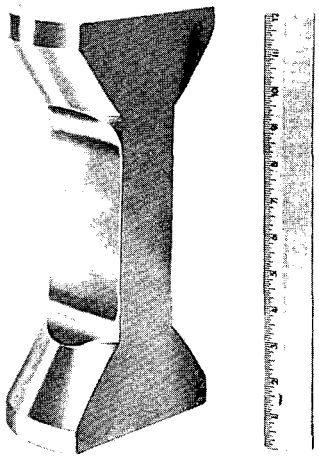

Figure 3. Full thickness tensile specimen produced from 3-in.-thick plate castings with representative radiographic discontinuities.

the effect, specimens chosen had no breakthroughs to the surface as determined by magnetic particle or penetrant inspection. The tensile specimen, shown in Figure 3 was designed to cope with limitations of original plate casting size and to assure that grips would not fail in tension, yield, or bearing prior to yielding of the gauge section. The cross-section of the specimens were 3 x 2 in. and the gauge length was 4 in. The specimens were pulled in the annealed and as-cast conditions for the steel and bronze castings respectively. The discontinuity types considered were as follows:

For steel	*For bronze*
Gas porosity	Gas porosity
Inclusions	Sand inclusions
Linear shrinkage	Dross inclusions
Dendritic shrinkage	Linear shrinkage
Wormhole shrinkage	Spongy shrinkage
"Hot tears"	
Chill inserts	
Chaplet inserts	

Test Data—For each specimen tested the following data were collected: radiographs of gauge section in plan and side elevation, photographs of fractures, percentage of principal alloying elements, the BHN and destructive tensile data. The yield point, determined by the divider method, is shown only for steels. The per cent elongation was determined from the change of the original 4-in. gauge length. Figures 4 and 5 are illustrative of data sheets for porosity and dendritic shrinkage for steel; while Figure 6 is for specimens with spongy shrinkage in Mn-Ni-Al bronze castings, respectively. Table 3 summarizes results of statistical regression analysis correlating tensile properties with severity level of various radiographic discontinuity types. Linear regressions were found to apply in all but the following:

For steel

Tensile, yield point and elongation for inclusions
Yield point for gas porosity
Yield point for chill inserts

For bronze

Elongation for gas porosity
Tensile and elongation for sand inclusions

Typical graphs of the relationships, with 95% confidence limits where applicable, are shown in Figures 7 and 8 for steel and Figure 9 for bronze.

Briefly, the results of this work can be summarized as follows:

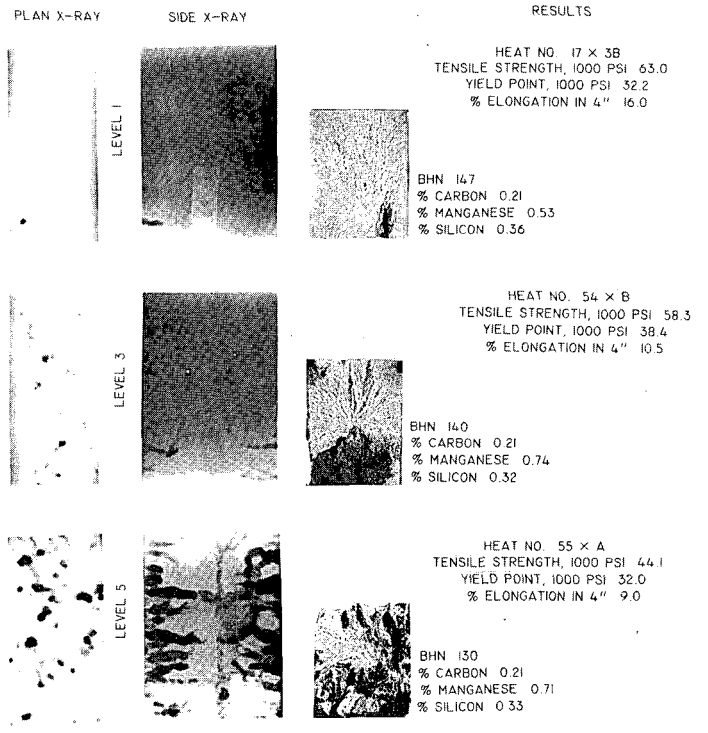

Figure 4. Representative steel casting tensile specimens with gas porosity, radiographic severity levels 1, 3 and 5.

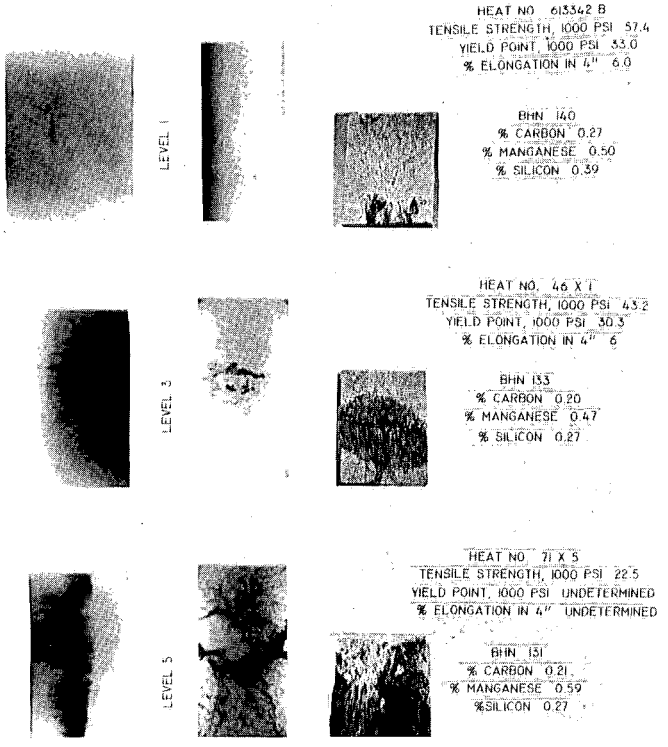

Figure 5. Representative steel casting tensile specimens with dendritic shrinkage, radiographic severity levels 1, 3 and 5.

Steel Castings

1. Visual graduation of radiographic indications obtained for steel castings yields severity levels which give linear regressions with respect to ultimate strength for all types of defects, except inclusions. 2. The deterioration in ultimate tensile strength of steel in the annealed condition may be estimated from the severity of radiographic indications. The deterioration is most

severe for linearly disposed discontinuities, such as shrinkage. 3. The yield point is practically unrelated to the severity of radiographic indications studied here, except for the most severe levels of the linear type. 4. Elongation of cast steel is drastically affected by soundness and cleanliness. Where elongation is important in design, the quality level of steel castings is indicated by the required elongation. 5. While radiographs of castings should by no means be used to replace tensile testing, the engineering strength of particular portions may be assessed with a high degree of confidence by use of relationships described here.

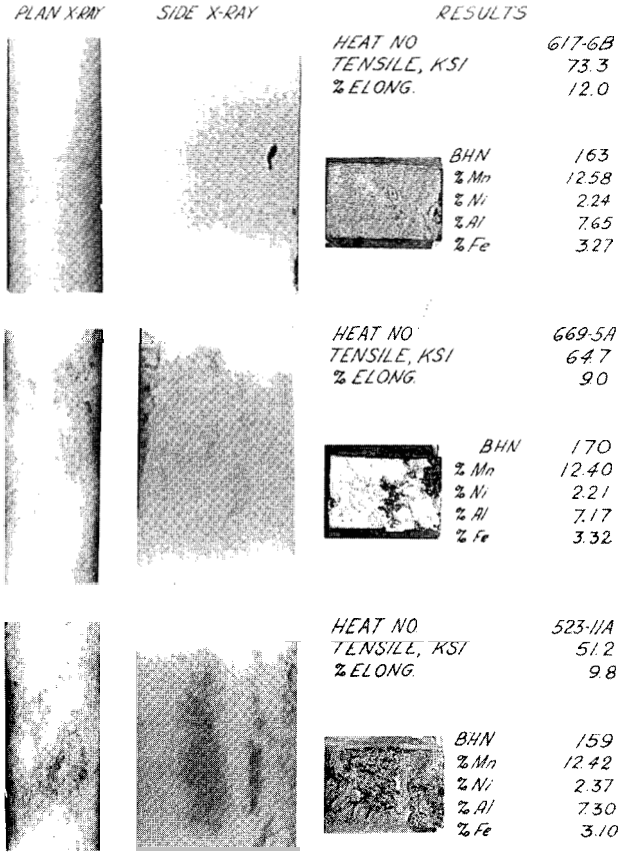

Figure 6. Representative Mn-Ni-Al bronze casting tensile specimens with spongy shrinkage, radiographic severity levels 1, 3 and 5.

Mn-Ni-Al Bronze Castings

1. While fewer data were available for some curves of this material, the trends shown for steel are verified for this material. 2. Slopes for most curves are somewhat smaller than for steel, possibly due to (a) non equivalence of severity levels for the reference radiographs of the two materials; and (b) relatively lower notch sensitivity of bronze. The general conclusion from this portion of the paper is that radiography can be used to assess degradation of castings subjected to tensile loading.

Estimate of Heavy-walled Casting Impact-bend Resistance from Radiographs

This is a summary of work to determine how impact-bend resistance of castings is affected by the severity level of representative radiographic discontinuities in full-section specimens cut from 3-in. plate castings.

Materials—The materials studied were the same as for the tensile work, i.e. class B steel (MIL-S-15083) (6) and Mn-Ni-Al bronze (MIL-B-21230A, Alloy No. 2) (5).

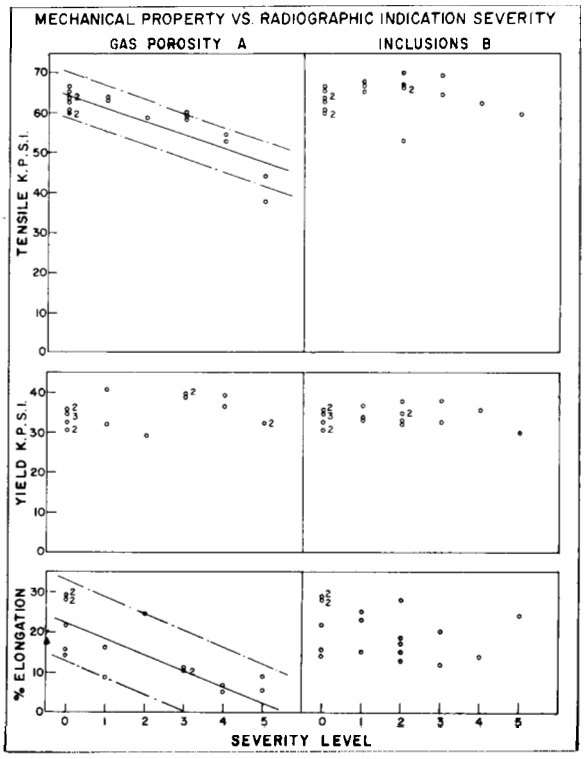

Figure 7. Graph of tensile properties vs. severity level of radiographic indications of gas porosity and inclusions in steel castings.

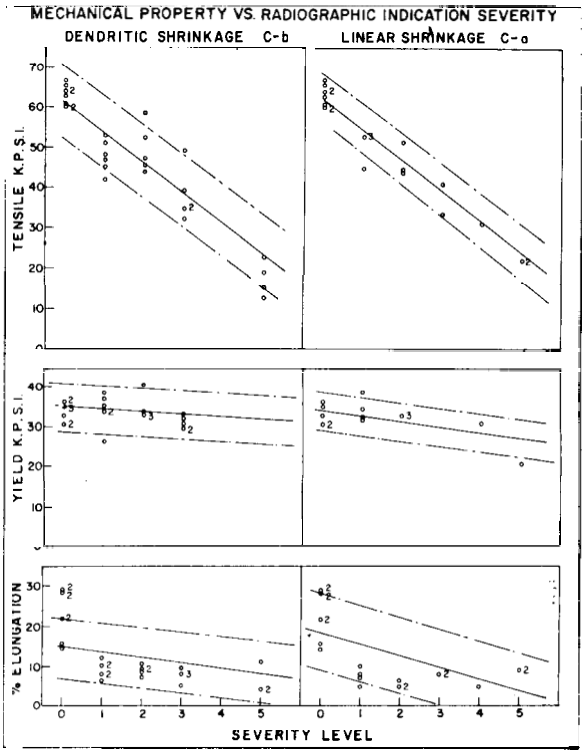

Figure 8. Graph of tensile properties vs. severity level of radiographic indication of dendritic and linear shrinkage in steel castings.

Test Specimens—Bars 3½ in. wide by 12 in. long were saw cut from 3-in. plate castings to include areas within their centres (in plan view) which resembled radiographic discontinuity types and severities shown in applicable ASTM reference radiographs. The rough edges produced by saw cutting were removed by light file dressing. The severity of the radiographic indications,

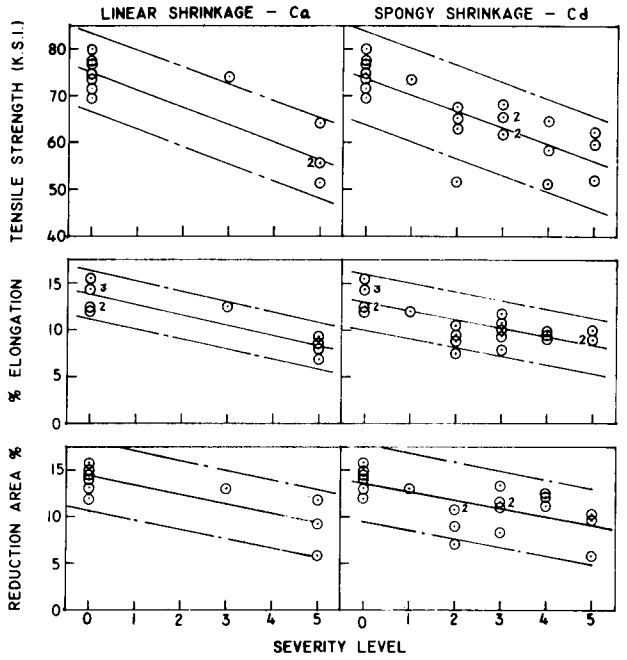

Figure 9. Graph of tensile properties vs. severity level of radiographic indications of spongy shrinkage in Mn-Ni-Al bronze castings.

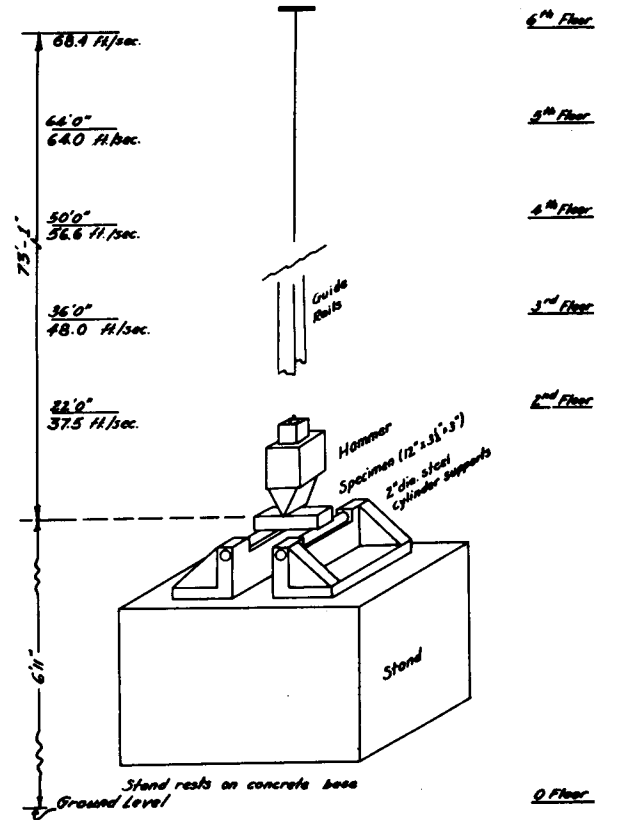

Figure 10. Experimental setup with specimen in position for "impact-bend" test.

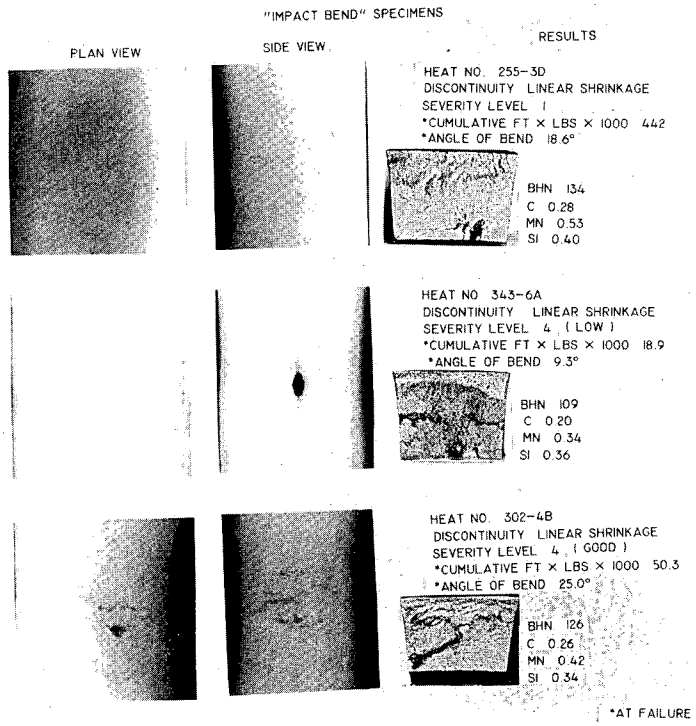

Figure 11. Representative steel casting "impact-bend" specimens with linear shrinkage, radiographic severity levels 1, 4 (low resistance) and 4 (good resistance).

for each specimen, was assigned by comparing Co-60 gammagraphs taken in plan and side elevation with illustrations of applicable reference documents.

Method of Test—The specimens were tested as simply supported beams at 10½-in. centres by dropping weights (in the form of hammers) from a height of 70½ ft. Three hammers were used, i.e. 100, 40 and 29 lb which gave, for the 75-ft drop-height used, applied energies per blow of 7050, 2820 and 2040 ft×lb, respectively. Figure 10 is a sketch of the experimental arrangement and shows a specimen in position for test on the Laboratory's guillotine impact machine. The maximum attainable velocity is about 68 ft/sec. The "cumulative angle of bend" at failure was the parameter ultimately used for correlation with severity level of radiographic indication in the specimen tested. This was based on preliminary experiments which showed that the slope of cumulative angle of bend vs. cumulative applied energy for material for the same heat treatment is independent of weight used, provided the impact results in plastic deformation of the specimen. In addition it was considered that the "total angle of bend" due to repetitive blows more closely reflects the capability of the material to undergo plastic deformation than the cumulative applied energy. Possible inaccuracies in the latter stem from variations in (1) departure from "free fall" conditions, due to contact of the hammer with guide rails; (2) shifts in point of impact between blows; and (3) losses due to elastic deformation.

The data for actual work to correlate "impact-bend" strength with radiographic indications were obtained for about 140 steel and 40 bronze specimens. Prior to start of tests a judgment was made on the probable energy which each specimen would take before failure. Generally, initial blows were applied with the largest hammer, while blows toward the end of tests were made with the small hammer. This procedure was used in an attempt to permit as close an estimate as possible of the cumulative applied energy at failure from the last blow. The tests for various specimens were stopped and considered failures on three bases, as follows: (a) fracture into two parts; (b) visible crack developed on surface; and (c) the angle of bend made further tests on the supports impossible. A data sheet was prepared for each specimen showing: copies of gauge section plan and side elevation radiographs and photographs of the fracture surfaces; and listing cumulative applied energy, angle of bend, chemical composition of major elements and BHN. The latter data were included for possible use in interpretation of results. The individual data were then integrated in tabular form by discontinuity and severity of radiographic

Table 4

Representative Data for Steel Casting Impact-bend Specimens with Various Radiographic Discontinuity Types

Heat No.	Discontinuity type*	Severity level	Cumulative applied energy ft/lb×1000	No. of blows hammer wt., lb			Angle of bend when test stopped, degrees	Sample fractured	Heat qualification Data				Remarks
				29	40	100			C	Mn	Si	BHN	
612972A	A	1	3.6	—	—	1	3.1	Yes	.32	.72	.23	126	Major indications less than $\frac{1}{16}$″ from tension surface.
18×4	A	3	7.3	4	—	—	3.6	Yes	.23	.66	.60	147	3 gas holes (2, $1\frac{3}{4}$″ long and 1, $1\frac{3}{8}$″ long) extending to tension surface.
324–4	Ba	3	3.6	—	—	1	6.0	Yes	.23	.53	.43	128	Fracture through major inclusion with porosity cluster near tension surface.
149–1	Ba	3	58.4	—	12	4	16.8	Yes	.25	.45	.49	138	Dispersed inclusions and gas porosity are are mostly internal.
255–3D	Ca	1	44.2	—	12	2	18.6	Yes	.28	.53	.40	134	Major indication terminates at tension surface.
343–6A	Ca	4	18.9	—	7	—	9.3	Yes	.20	.34	.36	109	Centre line with gas at tension surface.
302–4B	Ca	4	50.3	—	12	3	25.0	Yes	.26	.42	.34	126	Linear indications, are all internal in area subjected to low stress.
302–5B	Cb	2	44.2	—	12	2	22.6	Yes	.26	.42	.34	126	Dendritic shrinkage all internal in area subject to low stress.
57X–1B	Cb	4	1.1	1	—	—	0.9	Yes	.20	.57	.25	132	Major indication covers large surface area, terminating less than $\frac{1}{16}$″ from tension surface
302–3C	Cc	2	44.2	—	12	2	22.1	Yes	.26	.42	.34	126	Major discontinuity mostly internal, terminates at compression surface.
116–2	Cc	5	11.6	6	—	—	3.9	Yes	.24	.52	.32	—	Gross shrinkage cavity terminates at tension surface. Other stress raisers noted along tension fibre.
343–6B	Cc	5	32.2	—	12	—	14.4	Yes	.20	.34	.36	109	Flaw at centre line, $1\frac{9}{16}$″ above tension surface (closer to compression side).

*A—Porosity; Ba—Sand and slag inclusions; Ca—Linear shrinkage; Cb—Dendritic shrinkage; Cc—Worm-hole shrinkage

indications with notations as to depth and extent of indication in relation to surfaces and pertinent observation on site of failure. Illustrative data for steel with linear shrinkage are shown in Figure 11. Representative tabular data for steel "impact-bend" specimens are shown in Table 4. It lists, for steel castings, heat numbers, discontinuity types and severity levels of radiographs compared to ASTM document E186; cumulative applied energy in ft×lb when the test was stopped, number of blows applied with various hammers, angle of bend of specimen from the horizontal when the test was stopped, whether the sample actually failed at end of tests, principal chemical composition of heat, Brinell hardness, and remarks about size and location of defects determined from fracture. Similar data were obtained for Mn-Ni-Al bronze castings (7).

The salient point apparent from a study of data of Table 4, is that "impact-bend" resistance does not vary consistently with severity level of radiographic discontinuity. In addition resistance to "impact-bend" depends more on the sharpness of the discontinuity and its location with respect to the tension fibre than on amount present. Reference to a few samples will illustrate these points. For gas porosity (A), the angle of bend varies little with severity level and is of the order of magnitude from 3.0 to 3.6°. Specimen 612972-A1 (Table 4) had a major indication in the form of a narrow hole (inverted V) located at the tension surface and producing a high localized stress concentration. The fracture revealed that the failure occurred through this indication. Specimen 18×4 had three round gas holes, two about $1\frac{3}{4}$ in. long and one about $1\frac{3}{8}$ in. long, extending practically up to the tension surface. The difference in results of tension tests, based on radiograph appearance, would have been greater. However, the two specimens were practically the same as far as "impact-bend" behaviour is concerned. The effect of a stress concentration is the same regardless of number and size of defects in the inside of the section.

Specimens 255-3D, 343-6A and 302-4B, Figure 11, are illustrative of data for linear shrinkage (Ca). Specimen 255-3D is of a relatively good radiographic quality (i.e. severity level 1) but the major indication terminates close to the tension surface. It gave an angle at failure of 18.6°. Specimens 343-6A and 302-4B (Figure 11) were evaluated as having linear shrinkage, each of severity level 4. The first mentioned specimen failed at 9.3°, while the second one failed at 25°. The reason in the

difference of the behaviour of the two specimens (the latter showing better performance than even the sample with severity level 1 shrinkage) may be found in observations on the flaw locations. Specimen 343-6A had mainly centre-line shrinkage and some gas near the tension surface. It is the latter defect that probably caused early failure. On the other hand specimen

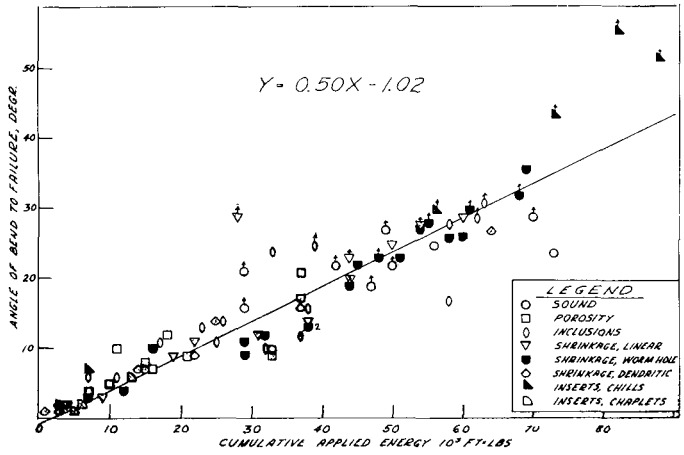

Figure 12. Graph of "angle of bend" at failure vs. cumulative applied energy for steel impact-bend specimens with representative radiographic discontinuities.

302-4B contains linear shrinkage severity level 4, all of which is internal and hence producing relatively low stress at the tension surface.

Figure 12 is a plot of "total angle of bend" (at failure as previously defined) vs. cumulative applied energy for all steel casting specimens considered in the study and including various discontinuity types. It proves that a linear relationship exists between the two variables at a correlation of 0.93. Hence, the total angle of bend can be used in attempts to establish correlations of "impact-bend" strength with severity level of radiographic indications for castings. Similar relationships were obtained for the bronze casting specimens (7).

Figure 13 shows plots of angle of bend (at failure) vs. severity level of radiographic indications in steel castings for porosity, sand and slag inclusions, linear shrinkage, dendritic shrinkage, worm-hole shrinkage, chill inserts and chaplet inserts. Similar plots for bronze have been published previously (7). Even a casual inspection of the plots shows that there is no correlation between the two variables. Of all discontinuity types considered, gas porosity in steel castings appears to be most detrimental to the ability of the material to resist "impact-bend"** energy. For all discontinuity types, location of the defect with respect to the tension surface is more important than the extent, as shown in plan radiographs evaluated with Reference Radiographs in a conventional manner. In short, this failure of radiography is mainly attributable to its failure to evaluate depth of defects, especially near the surface.

Though negative, the important conclusion from the "impact-bend" work is that performance of castings in bending cannot be reliably assessed with radiography alone as it is usually used and interpreted. For flexural loading greater reliance must be placed on NDT methods, which evaluate surface and near sub-surface discontinuities.

Need for Revised Radiograph Acceptance Criteria for Castings

With the development of reference radiographs for castings, described here (and similar ones nearing completion for large sand castings of aluminum alloys) improvement in interpretation of radiographs produced in nondestructive quality assurance tests for castings should be possible. The new references

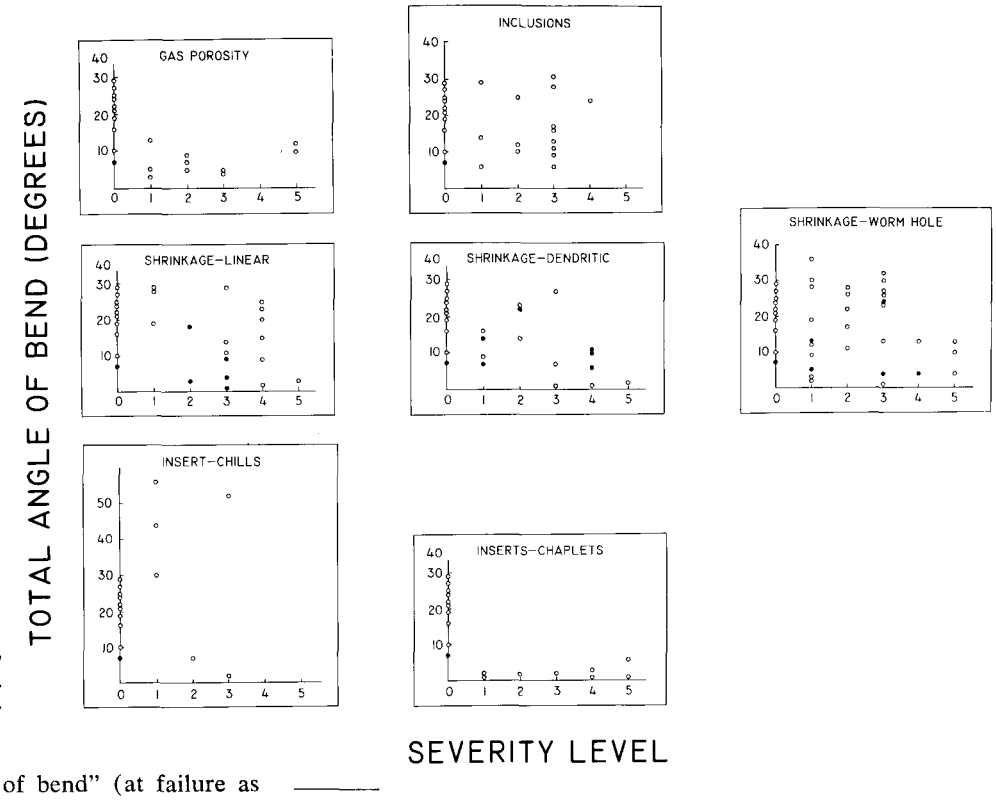

Figure 13. Plots of "angle of bend" at failure vs. severity level of radiographic discontinuities in steel-casting impact bend specimens.

** The term "impact-bend" has been deliberately placed in quotes throughout the paper. This is because the velocity attained by weights in tests described is probably too low to characterize the loading as true "impact". In the light of studies of materials considered here and of aluminum castings, it appears that the test merely reflects relationships between radiographic indications and ductility. In retrospect it is realized that similar results could have been obtained by the use of slow bending and that the failure is a function of the elongation the specimen is capable of undergoing during plastic deformation, as affected by stress raisers near the tension fibre of the specimen.

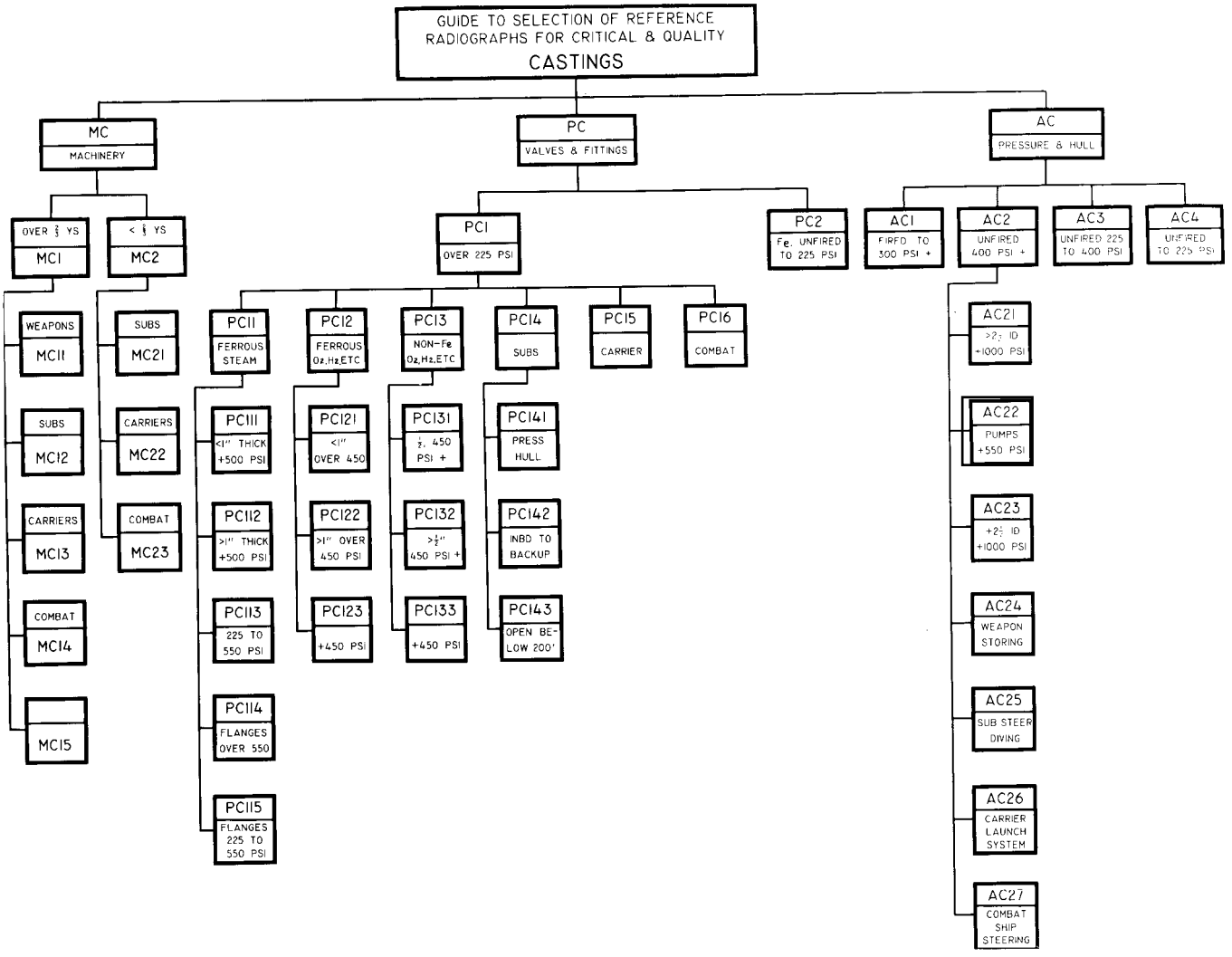

Figure 14. Suggested flow-chart presentation of casting classifications based on MIL-STD-278A.

consider the most common discontinuity types of alloys produced in considerable volume, and cover severity levels for a quality range from the most critical to the most ordinary applications. They also cover thickness ranges commonly in use. Most effective utilization of these references requires, however, a closer look on acceptance criteria. The high quality attainable in castings demonstrated by the lower severity level reference radiographs points to the direction which the foundry industry may work for and users can specify when critical applications are involved. For practical purposes, as long as very high-quality castings are difficult to make consistently, and costly at any rate, acceptance criteria must be developed to assure adequate safety commensurate with specific applications. Such criteria can best be established when stresses in castings and various portions of larger castings are known. Data for various typical geometry castings, which are at present rather sparse, must be developed as rapidly as possible. In the meantime a pragmatic solution for establishing realistic acceptance criteria is to develop classifications for castings by various factors. These should include: the end use loading and consequence of failure, pressure, temperature, involvement of lethal or explosive gases or liquids, alloy type, section thickness, etc. Figure 14 is a preliminary suggested flow chart presentation of possible classifications prepared by the writer on the basis of MIL-STD-278A. Such a classification (possibly revised for consistency, by deliberate collaborative work of designers, foundry technologists, metallurgists and NDT specialists) can provide a realistic basis for assignment of suitable severity levels for characteristic discontinuity types of applicable reference radiograph documents by alloy type and section thickness. For a specific application the designation could be "called out" as suggested in Figure 15. This sketch suggests an additional step, which has not been followed to date and which may encounter resistance even in the future. It considers discontinuities as shrinkage and non-shrinkage types and provides for possible use of different severity levels for each. This can be justified by the realization, supported by some test work, that deterioration of tensile strength with severity level is not the same for the two discontinuity types and that linearly disposed types are generally more degrading.

Admittedly, the task of developing clearcut classifications as suggested above is involved, especially since it must apply to old as well as new designs and to shelf items as well as castings produced for specific applications. To initiate the development of such a classification, several Sub II members and the chairman are trying to evolve a suitable Task Group to work up a suggested classification for industrial use.

Summary and Conclusions

The reference radiograph documents described should adequately serve as radiographic standards for castings when various

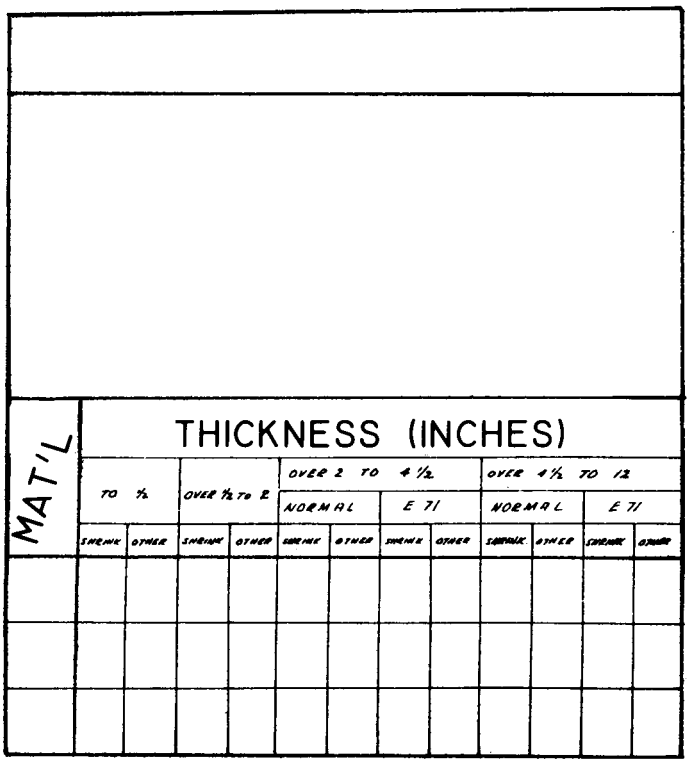

Figure 15. Suggested form for designation of radiographic acceptance criteria for castings.

codifying activities prepare suitable implementing directives specifying acceptable severity levels for common discontinuity types in various typical castings. In addition, the permanently stored plate castings developed for the new ASTM reference radiograph documents can be used for production of new original radiographs for printing future reissues; to make reference documents for new radiographic sources and techniques; and to prove capabilities of various other NDT methods for detection and assessment of internal flaws. The direct X-ray copy-plus-neutral-filter-combination reproduction of radiographs developed during this work offers a new method for quantity reproduction of radiographs, where section thickness makes originals impractical. Destructive tests demonstrate that severity of radiographic indications can be used to assess performance of castings loaded in tension. However, radiography cannot be used alone to assess performance of castings loaded in bending (or flexure). In such cases, greater reliance must be placed on NDT methods which emphasize detection and assessment of surface and near-surface discontinuities.

Acknowledgments

Grateful acknowledgment is made to the Navy (T. J. Griffin, Naval Ship Engineering Center, Code 6634B and G. Sorkin, Naval Ship Systems Command, Code 0342) for sponsoring the various projects summarized in this paper and to the management of the U. S. Naval Applied Science Laboratory (Capt. T. T. McGillicuddy, Commanding Officer and Director; E. J. Jehle, Technical Director; D. H. Kallas, Head of the Material Sciences Division; E. A. Imbembo, Head of the Metallurgy Branch) for guidance and supervision of the general work and for permission to present this paper.

References

1. Radiographic Standards for Steel Castings, NAVSHIPS 250-692-13 dated 1 July 1942.
2. Industrial Radiographic Standards for Steel Castings, ASTM Designation E71-52, adopted as tentative in 1947; as standard in 1952.
3. Goldspiel, S. Development of radiographic standards for castings, *Trans. Third Internat. Conf.* NDT, Tokyo and Osaka, Japan, March 1960.
4. Materk, L. J. Correlation of radiographically observed flaws with tensile properties of stainless steel castings, *Materials Research and Standards,* Vol. 2, No. 8, August 1962.
5. Briggs, C. W. Significance of discontinuities in steel castings on basis of destructive testing, *Materials Research and Standards,* Vol. 3, No. 6, June 1963.
6. Goldspiel, S. Development of reference radiographs for heavy-walled steel castings (2 to 4½" Sections), *Naval Applied Science Laboratory,* Project 5108-4, Progress Report No. 4 (SR 007-10-04, Task 0890) of 23 October 1964.
7. Goldspiel, S. and Lloyd, H. W. Radiographic indications and mechanical properties of bronze castings, *Modern Castings,* Vol. 49, No. 1, January 1966.

Discussion

Q. J. D. LAVENDER, BSCRA, Sheffield, England:
How were the castings heat-treated?

A. The steel specimens were tested in the annealed conditions (1700°F for two hours, followed by cooling in furnace); the bronze specimens were tested in the 'as cast' condition. These facts are noted in the text under "Test Procedure".

Q. Has any work been done on the effect of defects on fatigue strength?

A. Not for the work reported in the subject paper. Some work is now in progress to determine how bronze castings, which have been rejected on basis of current radiographic acceptance criteria, behave under simulated service performance (including fatigue loading).

Q. Where and when will the paper be published?

A. In the Proceedings of the 5th International Conference on NDT, subject to the conference's management.

Q. Is there, or has there been, any direct correlation between the use of these reference radiographs on castings, which subsequently failed in service?

A. Not to the knowledge of the author. At any rate, the references are out too short a time to expect feedback information, which is always difficult to obtain anyhow.

Q. Are there any ultrasonic standards in preparation?

A. No, not in the author's laboratory. However, when ultrasonic methods have been adequately demonstrated to have applicability to castings (at least to portions of critical large ones), there is no reason why some of the plate castings developed and stored for the reference radiographs cannot be used for the purpose. Obviously, only the better grades will be of any real relevance.

Q. Would there be any possibility of cooperation under BSCRA/SFSA agreement?

A. If this cooperation is being sought from SFSA, the question should more appropriately be put to its current Research & Technical Director, Dr. R. W. Zillman (c/o SFSA, 21010 Center Ridge Rd., Rocky River, Ohio 44116, USA). If the cooperation is being sought from the author, it would have to be cleared through official Navy channels.

The Development of Reference Radiographs for Steel Welds MIL-STD-779

R. M. GUSTAFSON AND E. L. CRISCUOLO, USA

ABSTRACT: A working group composed of representatives from each service of the U.S. Armed Forces has been engaged in developing a set of reference radiographs for steel weldments in the range of thickness from 0.030 in. to 5.0 in.

Before starting work on this development, an analysis of most United States references and standards was made. From this analysis the requirements for a new document that would satisfy most needs was obtained. In addition, a survey of many facilities yielded useful information. The thicknesses of greatest interest were 0.030 in., 0.080 in. $\frac{3}{16}$ in., $\frac{3}{8}$ in., $\frac{3}{4}$ in., 2 in. and 5 in. Original radiographs for the references were desired. Illustration size, defect type and grades were established. Assignments were made to several government organizations to develop the references for a specific thickness range. The first volume has been completed for thicknesses of 0.030 in., 0.080 in. and $\frac{3}{16}$ in. Other volumes are being developed. This work has been coordinated with Committee E-7 of the American Society for Testing and Materials.

Introduction

The demands of the military services for high integrity and improved quality in welded structures and parts has led to increased emphasis on nondestructive testing and inspection of welds. While a number of techniques are employed by industry, i.e., radiographic, ultrasonic, magnetic particle, penetrant and eddy-current, radiographic methods are probably the best established and are most generally specified for inspection of welds.

In 1960, the Materials Division of the Bureau of Naval Weapons and the Materials Laboratory of Wright-Patterson Air Force Base, faced with the need for more realistically assessing the quality of steel welds in weapon systems, organized a committee from all the services to review the problem.

The committee found that although there was a great deal of information available on inspection of steel welds there was: (1) a definite lack of coordinated standards that could be used for assessing defects in welds, (2) a lack of illustrative material that could be used by inspectors to aid in recognizing defects, and (3) a lack of information correlating weld quality with stress levels.

Accordingly it was recommended that a program be established to develop a set of graded reference radiographs for steel welds that would cover a wide range of material thicknesses, and could be employed to establish the quality of weldments for use at different stress levels. It was also recommended that the document include illustrative drawings that would supplement the reference radiographs and be useful to inspectors in the recognition of weld defects.

A project for accomplishing this work was established by the Department of Defense. As a first step a review was made of all known standards and specifications that related to the radiographic inspection of welds, with emphasis on steel welds. In addition, a questionnaire was sent to some 80 organizations seeking information on their specific needs in connection with radiographic inspection of welds. It was requested that they indicate the types of defects and the number of grades of each which they considered necessary for inclusion in a set of graded reference radiographs. Information was also requested on thicknesses of materials that should be covered, specific problems they had encountered, and any other information they deemed pertinent for the development of reference radiographs for steel welds.

The response was gratifying and showed strong interest of industry in the project, and the desirability for the development of a fully coordinated set of reference radiographs that could be used by government and industry on a national basis.

A number of documents used in connection with radiographic inspection of welds were reviewed. These included:

NAVSHIPS Document 250-692-2—X-ray Standards for Production and Repair Welds—Amendment 1, Jan. 1962

MIL-R-11468—Radiographic Inspection Soundness Requirements for Arc and Gas Welds in Steel—Department of the Army (Ordnance)

Document ABMA-PD-R-27A—Standards for Aluminum Welds—Army Ballistics Missile Agency, August 1959

Document API-1104—Standard for Field Welding of Pipe Lines—American Petroleum Institute No. 5L.

In addition, proprietary specifications and standards used by a number of aerospace companies were also reviewed.

On the basis of the above information, a program was formulated for a document that would include:

1. A set of graded reference radiographs for steel welds that would:

a. be applicable to all steel alloys ranging from 0.010 to 8 in. in thickness; b. show various types of defects in different degrees of severity; c. be composed of original radiographs.

2. A description of weld discontinuities and their radiographic appearance.

3. A set of illustrative drawings that would supplement the reference radiographs.

Based upon this survey, the thicknesses and the applicable range of thickness were selected, as shown in Table 1.

Table 1
Applicable Thickness Range

Master standard thickness (in.)	Metal thickness range (in.)
0.030	Over 0.010 to and incl. 0.050
0.080	Over 0.0500 to and incl. 0.125
0.187	Over 0.125 to and incl. 0.250
0.375	Over 0.250 to and incl. 0.500
0.750	Over 0.500 to and incl. 1.0
2.0	Over 1.0 to and incl. 3.0
5.0	Over 3.0

Table 2 lists the discontinuities to be illustrated in the reference radiographs. Included are eight types in five grades of progressively increasing severity, and single illustrations for seven types of ungraded discontinuities.

The following guide lines were provided for the preparation of the illustrative drawings that were to supplement the set of reference radiographs.

They would include a cross-sectional view of the weld, show the direction of radiation, position of film and location of the discontinuity. The drawings were to illustrate the appearance of the weld and the method most generally specified for the inspection of welds. Figure 1 shows one of the drawings included in the document.

After the broad outlines of the program had been formulated, it became apparent to the committee that the task was too large for any one laboratory or organization to accomplish.

The Bureau of Naval Weapons, which had been designated by the Department of Defense as the preparing activity for the

Table 2
Discontinuities Shown in Reference Radiographs

Graded types	No. of grades
Fine scattered porosity*	5
Coarse scattered porosity*	5
Clustered porosity	5
Linear porosity**	5
Slag inclusions	5
Tungsten inclusions†	5
Lack of fusion††	5
Incomplete penetration††	5
Ungraded Discontinuities—Single Illustration	
Transverse crack	
Longitudinal crack	
Crater crack	
Icicle	
Burn through	
Undercut	
Elongated porosity	

*For the 5-in. section no differentiation is made between fine and coarse porosity
**Single illustration for .030 in.
†Single illustration for 2.0 in.
††Single illustration for .030 in. and .080 in.

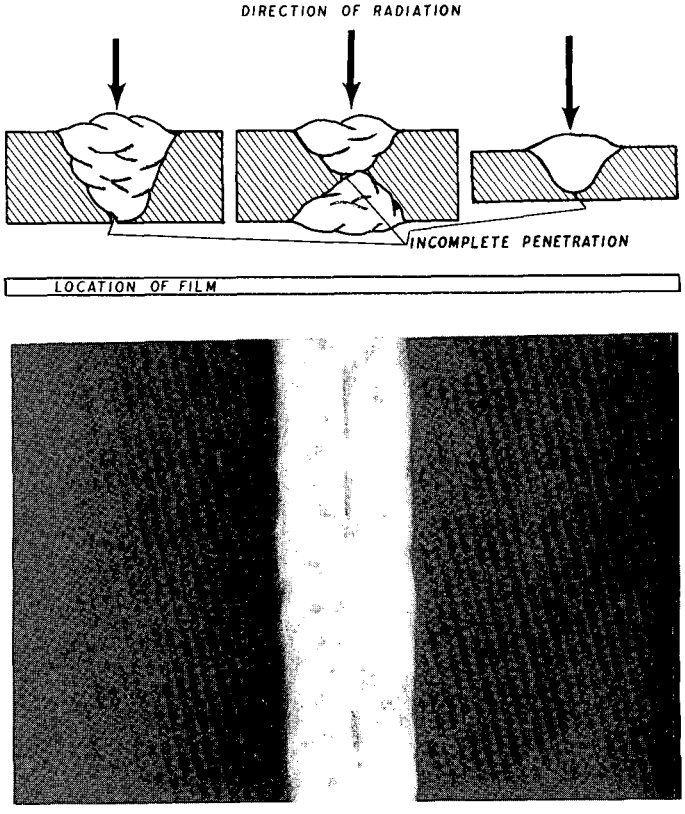

Figure 1. Sketch of weld cross-section and radiographic appearance.

reference radiographs (MIL-STD-779), had assigned to the Naval Ordnance Laboratory, White Oak, the primary task for preparation of this document.

The major obstacle was the preparation of welds that would have the necessary defects. To expedite this phase of the project each service agreed to accept a part of the workload. Table 3 lists the activities and their specific assignment.

Table 3
Assignments for Preparation of Master Plates

Activity	Thickness (in.)
U. S. Naval Ordnance Laboratory, White Oak, Silver Spring, Maryland	.030 and .080
Aeronautical Materials Laboratory, U. S. Naval Engineering Center, Philadelphia, Pennsylvania	.187 and .375
Warner-Robins Air Force Base, Macon, Georgia and Wright-Patterson Air Force Base, Dayton, Ohio	.750
U. S. Army Tank Automotive Center, Warren, Michigan	2.0
U. S. Naval Applied Science Laboratory, Naval Base, New York	5.0

To provide some degree of uniformity in the preparation of the master plates, the following guide lines were established:

Material to be Used

The base metal to be joined by fusion welding could be any type of steel. However, to permit the introduction of defects in varying degrees of severity, it was recommended that the steels be selected from those that had good weldability and in which the welding process could be readily controlled. The welding rods or electrodes were to be similar in composition to the parent metal with slight modification permissible to conform to commercial practice.

Weldments

The length of the weld desired for the radiographic standards could vary with the thickness of the plate being joined. The following lengths were recommended:

Table 4

Length of Welds—Master Test Plates

Plate thickness (in.)	Length for radiographic illustration (in.)	Minimum length of weld (in.)
0.030	2	4
0.080	2	4
0.187	4	6
0.375	4	6
0.750	6	10
2.0	6	10
5.0	6	12

The welds for plate thicknesses up to 0.375 in. were specified to be single V-groove butt welds, with back-up strips removed. Welds for plate thicknesses over 0.375 in. were specified to be double-V-groove or double-U-groove butt welds. The groove face was to be machined on all samples. Dimensions of the joint were to be in accordance with MIL-STD-22A*.

The method of welding was optional. However, it was to be accomplished in such a manner as to induce each of the imperfections to the degree of severity required. Defects incorporated into the weld were to be as natural as possible.

* MIL-STD-22A, Welded-Joint Designs, 24 October 1956.

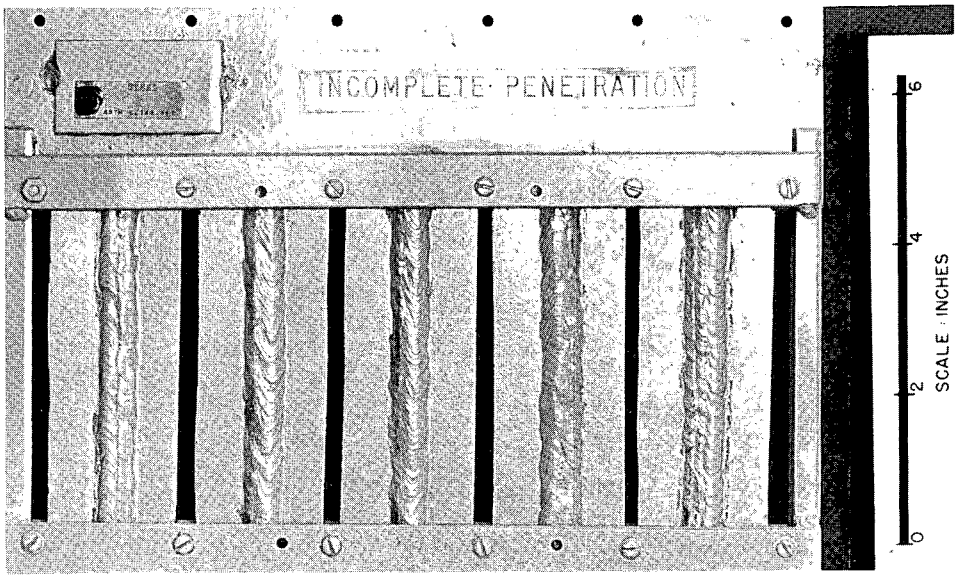

Figure 2
Fixture for holding weld plates for radiography.

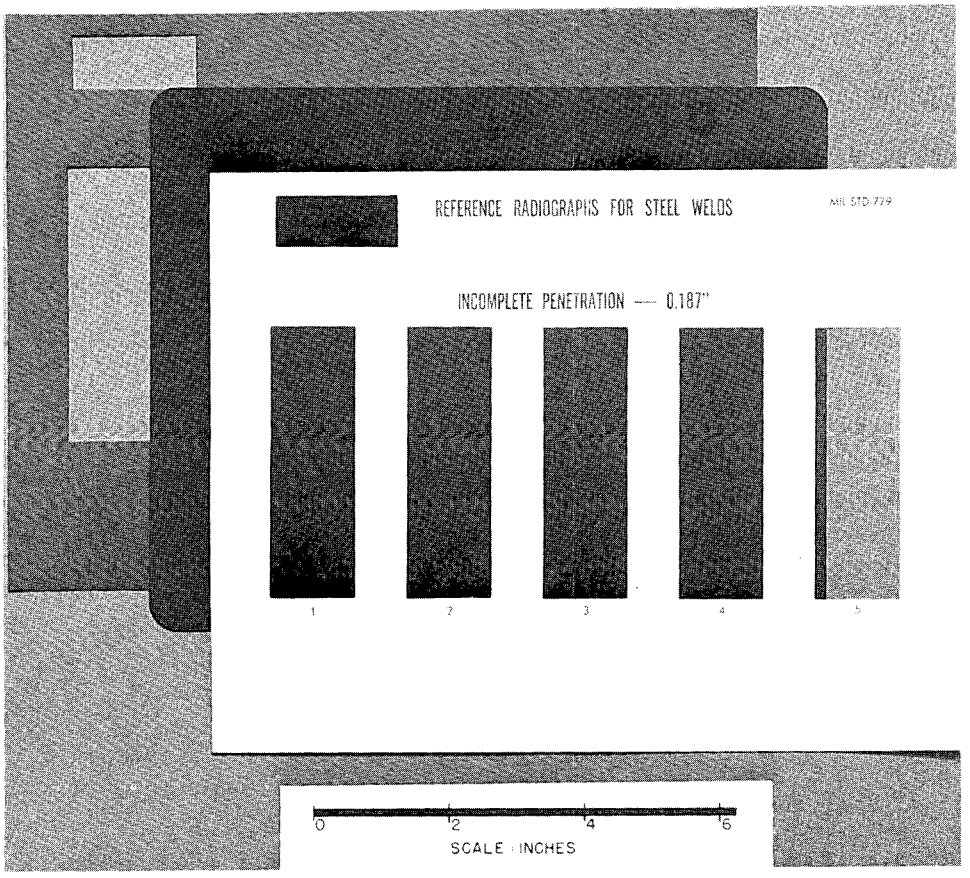

Figure 3
Radiograph with front and back masks.

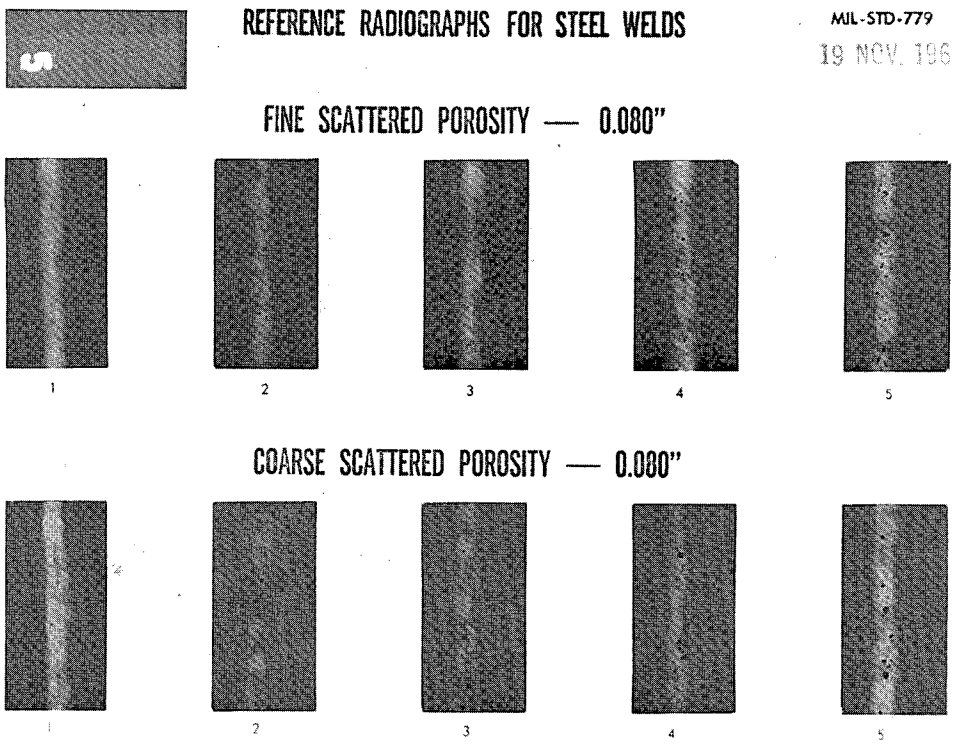

Figure 4.

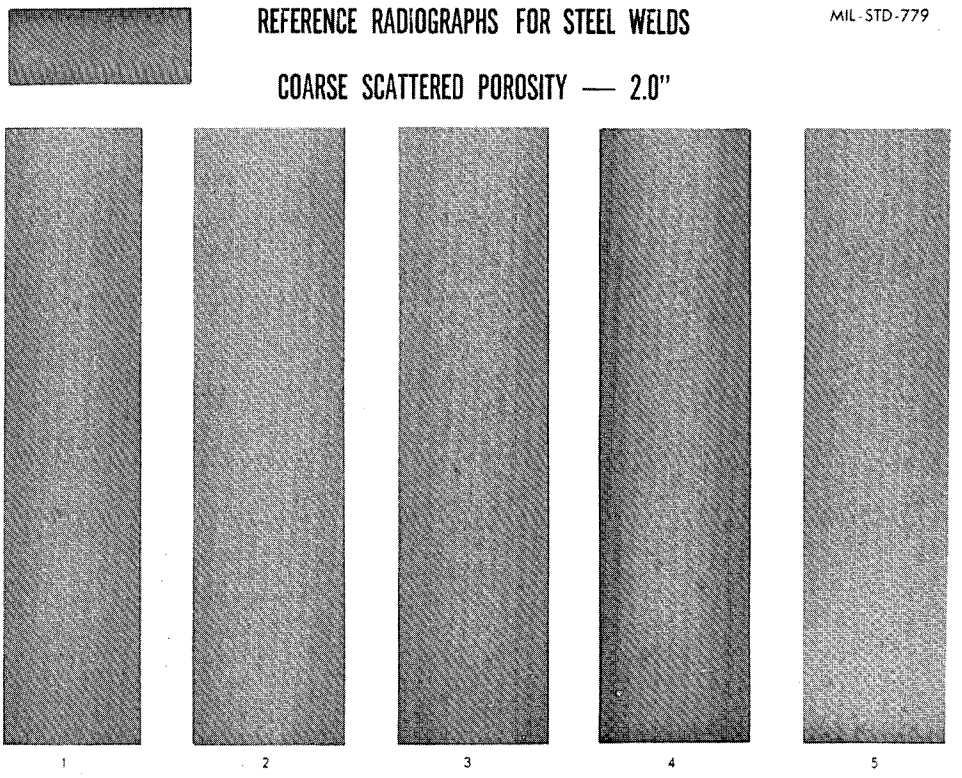

Figure 5.

If devices or special welding techniques were employed to achieve a certain type of defect, the practice employed was to be noted in the written history to be submitted with each approved master test plate.

Master Test Plates

The master test plates were to contain a section of weld that would illustrate each defect in the severity desired to be shown. To insure that the imperfections were present as desired, each activity was required to radiographically inspect the samples. Penetrameters were to be placed beside the weld and shimmed up to the height of the bead. It was recommended that the radiographs have an H & D density of 2 ± 0.2. Density strips for comparison purposes were provided by the Naval Ordnance Laboratory.

Shipment of Master Plates to NOL

The radiographs used by the activities to screen the samples were submitted to the committee for review. If they were considered acceptable the master plates were then shipped to NOL for use in the preparation of the final reference radiographs.

A complete history of the preparation of each master test plate was requested. This included data on welding technique, basic material, filler rods or electrodes, equipment and any other information that might be needed to duplicate the preparation of the specific master plate.

When the project is completed, the master plates and history of preparation are to remain in the custody of the Naval Ordnance Laboratory.

Reference Radiographs

The establishment of general requirements for weld flaws enabled us to proceed with the manufacture of weld plates. Since the need for the references for thin sections was most urgent, especially in the aerospace and missile industry, the 0.030-in. and 0.080-in. sections were the first to be developed. No special edge preparation was made for these but a removable backing and clamping plate was used. Weld lengths of 16-in. gave ample material from which to select a 2-in. segment for use in standard plates. The 0.187-in. and 0.375-in. plates were prepared with a single vee edge; a number of plates were made before a set could be selected. One thousand feet of weld for the 0.030-in. and 0.080-in. thicknesses was made using various techniques.

The range of severity for the graded type discontinuities was selected so as to extend from that just discernible, and what could be expected in the best quality weld, to that evident of poor workmanship and commonly rejectable in commercial practice. The ungraded illustrations are included for educational purposes. It was also necessary to make the grades for each defect type and thickness compatible.

After the final selection was made the welded plates were mounted together for ease in radiography. For example, all five grades of scattered porosity were mounted in a special holding fixture, as shown in Figure 2. This allowed the welds to be spaced so that they are centred in the paper masks. For the 2-in.-long illustrations it was possible to place 10 weldments on each page. In order to make the radiographic densities of each weld approximately the same, thin shims were added to balance each weld image. It was then possible to make a single radiograph for each page. This kept production costs down and allowed the use of original radiographs.

Table 5 shows the radiographic technique for each section thickness. The density tolerance was carefully controlled so that each radiograph for a given defect type is identical.

Figure 3 shows how each page is made up. The radiograph is sandwiched between a black paper mask on the back and a white front mask. The front mask contains information as to defect type, grade, thickness and identification. The surfaces of the masks (one side) and the radiograph (both sides) are coated with rubber cement and allowed to dry. They are then assembled with the image centred in the mask. The excess rubber cement is cleaned from the surfaces by means of a small paint roller. The finished pages are then assembled in a binder.

Table 5
Radiographic Techniques

Section thickness (in.)	Tube voltage
0.030	90 kv
0.080	120 kv
0.187*	150 kv
0.375*	175 kv
0.750*	250 kv
2.0*	2 mv
5.0*	2 mv

*Lead screens

Some of the defects covered by this document are illustrated in Figures 4, 5 and 6. As can be seen, Grade 1 has only a minor degree of scattered porosity while Grade 5 has a maximum amount—usually much more than can be tolerated in the loosest specification. Some attempt has been made to keep grades compatible from one thickness range to another. The upper left hand corner shows an ASTM penetrameter which indicates the image quality of the radiograph.

As mentioned previously, a second volume is almost complete and a third volume to cover the 5.0-in. thickness is being developed. As a result of this program the complete range of weld thicknesses will be covered.

Volume I has been reviewed by Task Group F of the American Society for Testing and Materials, Committee E-7, Subcommittee II. A number of recommendations made by the task group have been incorporated; for example, the clustered porosity illustrations were expanded from three to five. Only through close cooperation with ASTM and DOD committees were we able to achieve a realistic set of references. A comparison of the references with existing standards indicates that this document covers the range needed.

Summary

The development of a complete set of reference radiographs for weld inspection has been accomplished only through the efforts of the various participating DOD agencies. By dividing the workload we were able to develop the reference radiographs in a reasonable time.

Coordination with the ASTM task group was established early in the program and the inclusion of their comments allowed us to develop a document that is useful both to government and to industry. Such other key organizations as the Aircraft Industries Association, the American Welding Society and the International Institute of Welding have been kept informed of the progress of this work.

Volume I is complete and Volumes II and III are about 90% ready. The military version of Volume I, MIL-STD-779, has been issued to a limited number of government facilities. We will look to ASTM to fill the needs of industry. The weld plates and technical assistance necessary will be made available to them so that their version can be produced as quickly and as economically as possible. The primary intent of this document is for use as a reference to supplement weld specifications. No mention is made of acceptability levels; this must be determined by a primary specification.

REFERENCE RADIOGRAPHS FOR STEEL WELDS MIL-STD-779

COARSE SCATTERED POROSITY — 0.375"

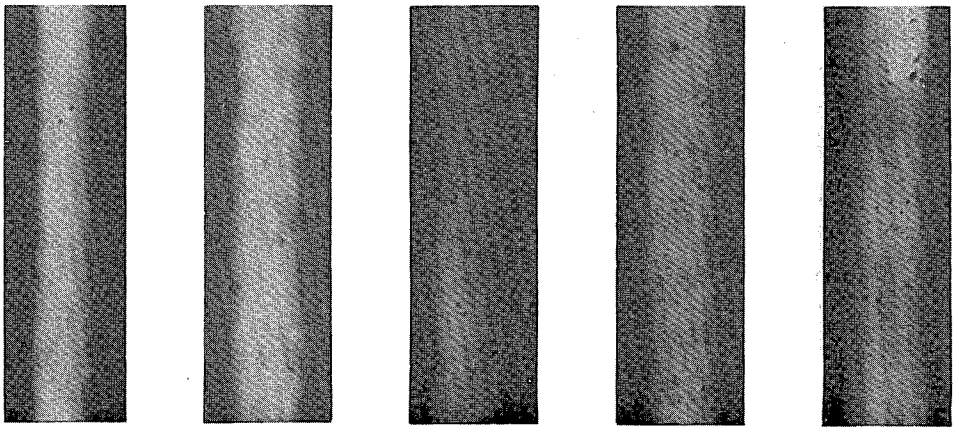

Figure 6.

Acknowledgment

The progress made in developing these reference radiographs is due to a coordinated effort by many participants. Special recognition is given to the contribution made by R. A. Youshaw (NOL) for his active participation. Other members of the present DOD Task Group are M. L. Stellabotte, W. J. Fedyna, W. F. Wulf, O. Gluck, B. W. Boisvert, W. P. Byrd, E. W. McKelvey, G. Farmer, Jr., and T. E. Dunn, Jr.

Contributing to the early formative work were B. R. Cantor, F. H. Martin, R. C. Rosenberger, I. L. Stern, H. Heffan, D. Polansky, F. S. Williams, S. Goldspiel, D. Barth, W. M. Sheppard, M. L. Foster and L. Fink.

The authors gratefully acknowledge the contributions made by all of the above mentioned individuals.

Nondestructive Testing Standardization in Great Britain

C. C. BATES and C. CAMPKIN, UK

ABSTRACT: The paper discusses the history and growth of standards and the establishment in the United Kingdom of the British Standards Institution as the national standards body.

The events leading to the formation of the British National Committee for Nondestructive Testing and of a British Standard Institution Technical Committee specifically for NDT i.e. M.E.E./169, are outlined.

Data on standards existing prior to 1957 and those produced in the decade to 31st December, 1966, and the procedure for initiating and producing standards, are discussed.

Reference is made to the 2nd International Conference on Nondestructive Testing, where a number of resolutions on international cooperation and standardization were discussed, and the authors suggest that the time is now appropriate for the establishment of a Technical Committee for Nondestructive Testing of the International Standards Organization, and recommend to the national standards bodies that they pursue this objective.

Introduction

The objective of the authors in presenting this paper is firstly to record the progress in standardization in nondestructive testing during the past decade in the United Kingdom, and to provide information on the NDT standards issued by the British Standards Institution; secondly to suggest the need for international coordination and standardization in NDT terminology, equipment and techniques, through the International Organization for Standardization (I.S.O.), by the establishment of a technical committee for nondestructive testing.

Any discussion on standardization should start with the standardization of the technical words that have agreed meanings and definitions. Language itself is changing more than ever today, when the progress of science and the growth of nations are making new demands on old words and definitions. Can we therefore commence with definitions of nondestructive testing and standards.

An accepted definition of nondestructive testing is:—

> A knowledge and experience in methods of inspecting, examining and testing materials and components without detriment to their physical properties or their service performance.

The Oxford Dictionary defines standards as:—

> A basis of measurement; a criterion; an established or accepted model; definite level of excellence or adequacy required, aimed at, or possible.

Standards are as old as recorded history with the Egyptian and Mesopotamian surveyors and architects mapping the fields and planning the temples, tombs and palaces. More than 5,000 years ago, the cubit, a unit of length, had reached a standard which did not vary much more than one part in two hundred from the mean. The Romans, with their great civil engineering achievements, roads, aqueducts and buildings, had reliable standards of length, area and volume. Thus, from early days, mankind has found it necessary to establish standards, so that diverse groups of people can work together to a chosen end.

Historical

British National Standardization

In Great Britain the establishment in the year 1754 of the Royal Society of Arts, in 1760 of Lloyds Register of Shipping and in

1762 of The Royal Society, may be regarded as the first concerted steps towards engineering classification and standardization in this country. However, although Sir J. Whitworth established the Whitworth Screw Thread Standard in 1841 and there was considerable activity in the middle and latter half of the 19th century in the field of standards for boilers and similar pressure vessels, progress was slow.

By the end of the 19th century the growth and expansion of engineering and the disadvantages arising from lack of national standards led to an Engineering Standards Committee being set up in 1901, by the Institution of Civil Engineers, which was soon supported by a number of other engineering institutions. This committee later became the Engineering Standards Association, was granted a Royal Charter in 1929, and adopted the present name of British Standards Institution in 1931.

Today the British Standards Institution is the national authority in the United Kingdom for the preparation and promulgation of standards, covering five main fields:—

Methods of test; Terms, definitions and symbols; Standards for quality and performance; Standards for dimensions; and Codes of practice.

Stated briefly, the principles observed in the preparation of British standards are:—

(a) that they shall be in accordance with the needs of industry and fulfil a generally recognized want; (b) that the interests of both producer and consumer shall be considered; (c) that standards are subject to periodic review.

Nondestructive Testing and British Standards Institution

The British Standards Institution has produced standards concerned with mechanical testing and inspection for years, including a small number concerned with nondestructive testing, chiefly radiography. However, normally proposals for the preparation of standards are not initiated by the Institution itself. They must, under normal circumstances, come from an outside body, and in Great Britain two major agencies in establishing the earlier nondestructive testing standards have been the British Welding Research Association and the Institute of Welding, both of which have sponsored a number of nondestructive testing standards.

Although the Institute of Physics had in being a nondestructive testing group and the Institution of Engineering Inspection had an active interest in NDT it was only in 1954 that nondestructive testing assumed a recognizable form as a body of knowledge and people, with the formation of the British Societies of Nondestructive Examination and Testing. With the establishment of recognized forums for nondestructive testing, and its increasing importance to industry in terms of safety and economics, so came a corporate and independent voice to call for standards and standardization in NDT.

At the first International Conference on Nondestructive Testing, held in Brussels in 1955, Great Britain was represented by individual societies, there being no single British representation. Prior to the second International Nondestructive Testing Conference, held in Chicago in 1957, a British National Committee was formed under the aegis of the British National Committee for Materials and Testing, through which a sister body was set up, the British National Committee for NDT. From this beginning, the British National Committee now comprises representatives of 24 engineering institutions or technical societies using or engaged in NDT, but does not itself directly undertake work on standards or other aspects of NDT. Its function is to guide and coordinate nondestructive testing in Great Britain and coordinate liaison in the international field.

In September, 1962, at the request of the British National Committee, The Institution of Production Engineers and the Nondestructive Testing Society of Great Britain held a joint symposium on standardization in nondestructive testing at Harrogate. This symposium was supported by the British Standards Institution, whose associate director opened the proceedings with a paper entitled 'The Value of Standards'.

The symposium consisted of three major sections:—

(a) The value of standards; (b) A survey of existing standards; (c) what additional standards are needed;

The industries concerned covered:—

(a) Aircraft; (b) Petrochemical; (c) Steel; (d) Shipbuilding; (e) Transport.

In an open forum at the conclusion, it was agreed by all that there was a need in sections of industry represented for further standardization in nondestructive testing in relation to the following:—

1. Standard methods of test, for those methods now coming into general use, viz: radiographic, ultrasonic and eddy current; 2. Standard specifications for such items of test equipment and ancillary apparatus that may be required in order to facilitate uniformity in testing; 3. Standards for quality levels, to be associated with the application of these methods of test to engineering materials and components (Ref. 1).

Concurrently with these activities, B.S.I. Technical Committee MEE/37 (Mechanical Testing of Metals) had reconstituted its Subcommittee MEE/37/11 (Nondestructive Testing) as a result of a request from the Institution of Production Engineers to prepare a glossary of terms for nondestructive testing so that the use of standard terms and definitions could be encouraged. About the same time the Institute of Welding, which was preparing an institutional recommendation covering the types and use of reference blocks for checking ultrasonic equipment proposed a revision of B.S. 2704:1956—Reference Blocks for routine checking of ultrasonic testing equipment.

The Engineering Divisional Council agreed that a glossary of terms should be compiled, covering penetrant, magnetic, ultrasonic, radiographic and eddy-current methods, and a small working party was set up to prepare a revised standard for ultrasonic reference blocks.

Meanwhile the Council of B.S.I., taking heed of the Harrogate proposals, which were subsequently endorsed by the British National Committee, called representatives of industry and all other appropriate authorities to a meeting on 10th July, 1963 of a new and over-all coordinating NDT Standards Committee—MEE/169.

Proposals for work and terms of reference were considered and tentatively agreed. Working panels were set up and the work started by MEE/37/11 was incorporated into MEE/169.

At a second meeting of MEE/169 held later that year the original terms of reference and scope of work were further discussed. The original terms were to prepare British standards for nondestructive testing, viz: standards for quality levels to be associated with the application of standard testing methods to engineering materials and components. This, however, has proved too ambitious a project and the terms of reference were modified to exclude quality levels and now stand as follows:—

To prepare British standards for the application of nondestructive testing tehniques to mechanical engineering materials and components, relating to the sizes and types of imperfections, but excluding quality levels, by means of:—

(a) Glossary of terms; (b) Methods of test, covering penetrant, magnetic particle, radiographic, ultrasonic and eddy current flaw detection etc.; (c) Specifications for testing equipment and ancillary apparatus to facilitate uniformity in testing, taking into account international work in this field.

Table 1

Standards Published to 31st December 1956

Reference	Title	Remarks
B.S. 2783 : 1956	Gamma-ray source capsules for radiography	Withdrawn, superseded by B.S. 3513
B.S. 2600 : 1955	General recommendations for the radiographic examination of fusion welded joints in thickness of steel up to 2 inches	Revised and reissued 1962
B.S. 1443 : 1952	Sizes of X-ray intensifying screens for medical and industrial use, excludes X-ray films for crystallography	Amendment P.D. 4558 May 1962
B.S. 1380 :	Method for determining the speed of sensitized photographic materials	Part I: 1962 Negative monochrome material for use in daylight
B.S. 1384 : 1947	Measurements of photographic transmission density	Confirmed 1962
B.S. 2704 : 1956	Reference blocks for routine checking of ultrasonic testing equipment	Revised and enlarged. Reissued 1966
B.S. 1881 : 1952	Methods of testing concrete	Under revision
Glossaries and Terminology		
B.S. 2737 : 1956	Terminology of internal defects in castings as revealed by radiography	
B.S. 2597 : 1955	Glossary of terms used in radiology	
B.S. 661 : 1955	Glossary of acoustical terms	
B.S. 499 : 1952	Glossary of terms (with symbols) relating to the welding and cutting of metals	Initially issued 1933, revised 1939. Part II issued 1948, revised 1952. Revised and reissued in 3 parts, 1965.
B.S. 233 : 1953	Glossary of terms used in illumination and photometry	
B.S. 661 : 1955	Glossary of acoustical terms	
B.S. 499 : 1952	Glossary of terms (with symbols) relating to the welding and cutting of metals	Revised and reissued in 3 parts, 1965
B.S. 233 : 1953	Glossary of terms used in illumination and photometry	

Table 2

Standards Published 1957–1966 Inclusive

Reference	Title	Remarks
B.S. 2600 : 1962	General recommendations for the radiographic examination of fusion welded butt joints in steel	Covers 8 individual techniques for X and Gamma-ray examination, does not establish radiographic standards of acceptance (See Table 1)
B.S. 2910 : 1965	General recommendations for the radiographic examination of fusion welded circumferential butt joints in steel pipes	18 X-ray and Gamma-ray techniques using three types of film
B.S. 3451 : 1962	Methods of testing fusion welds in aluminium and aluminium alloys, including radiography and dye and fluorescent penetrant methods	
*B.S. 3683	Glossary of terms used in N.D.T.	
Part I : 1963	Penetrant flaw detection	
Part II : 1963	Magnetic particle flaw detection	
Part III : 1964	Radiological flaw detection	
Part IV : 1965	Ultrasonic flaw detection	
Part V : 1965	Eddy-current flaw detection	

Table 2 (Cont'd)

Reference	Title	Remarks
*B.S. 3889 Part Ia : 1965 Part IIa : 1965 Part IIb : 1966 Part IIIa : 1965 Part IVa : 1965	Methods of N.D.T. of pipes and tubes Ultrasonic testing of ferrous pipes Eddy-current testing of ferrous pipes and tubes Eddy-current testing of non-ferrous tubes Penetrant testing of ferrous pipes and tubes Magnetic particle flaw detection, ferrous pipes and tubes	
*B.S. 3923 Part I : 1965 Part II : 1965 Part III : 1965	Ultrasonic examination of welds Manual examination of circumferential butt welds in pipes Automatic examination of welded seams Manual examination of nozzle welds	
*B.S. 2704 : 1966	Calibration blocks and recommendations for their use in ultrasonic flaw detection	(See also Table 1)
*B.S. 3971 : 1966	Image quality indicators for radiography and recommendations for their use	
*B.S. 4069 : 1966	Magnetic inks and powders	
*B.S. 4080 : 1966	Methods for NDT of steel castings	
B.S. 4094 : Part I : 1966	Data on shielding from ionizing radiation Shielding from gamma radiation	Metric units
B.S. 4097 : 1966	Gamma radiography exposure containers for industrial purposes and their source holders	Metric units
Glossaries B.S. 3455 : 1962	Glossary of terms used in nuclear science	
B.S. 2591 : 1958	Glossary of terms used in high-vacuum technology	
Terminology B.S. 499 : 1965 Part III	Welding terms and symbols Terminology of, and abbreviations for, fusion welding imperfections as revealed by radiography	(See Table 1)
Radiography B.S. 1443 : 1952	Sizes of X-ray film and intensifying screens for medical and industrial use, other than dental X-ray films and X-ray films for crystallography Amendment P.D. 4588: May 1962	(See Table 1)
B.S. 3490 : 1962	Size of industrial X-ray film (including film for crystallography)	
B.S. 3513 : 1962	Gamma-radiography sealed sources	(See Table 1)
B.S. 3385 : 1961	Specification for direct-reading personal dosemeters for X and gamma radiation	
B.S. 3664 : 1963	Specification for film badges for personnel monitoring	
B.S. 3890 : 1965	General recommendations for the testing, calibration and processing of radiation monitoring films	
B.S. 4031 : 1966	X-ray protective lead glasses	
B.S. 3783 : 1964	X-ray lead-rubber protective aprons for personal use	
B.S. 3510 : 1962	Symbols for denoting the actual or potential presence of ionizing radiation	

*Denotes standard prepared by Committee MEE/169

In addition, to maintain close liaison with other B.S.I. Committees dealing with the application of nondestructive testing techniques, and where necessary to make recommendations to these and other product-application committees regarding priorities of work.

It is the intention that MEE/169 Committee should be conversant with all work on British standards concerned with NDT so as to assist communications and provide a liaison section for this work.

Following the establishment of MEE/169 and the program of work, it was recognized by the Council of B.S.I. that one committee could not control and produce NDT standards for all spheres of industry and so further specialist industry committees were set up namely:—

Welding Industry WEE/-
WEE/34 N.D.T. of Welding

Aerospace Industry ACE/-
ACE/56 Aircraft Applications and Quality Levels

Nuclear Energy Industry NCE/-
NCE/4 Radioisotopes

Cement, Lime and Gypsum Products Industry CEB/-
CEB/4 Concrete Tests

Another group of committees is concerned with the application of NDT methods, and standards produced by these product committees can establish quality levels. A selected list of standards wherein NDT techniques or quality levels are specified is given in Table 4. It is realized by the authors that this list is in no way comprehensive but it does give an indication of the breadth and depth of the product fields covered.

Liaison between MEE/169 and other B.S.I. Committees is through the permanent B.S.I. Secretariat, by formal cross-representation and by personal contact between members of the various committees.

Table 1 lists the British standards for NDT that were in existence in 1956. In Table 2 is a list of standards that have been published in the past decade, including the glossary and standards prepared and issued under the aegis of the MEE/169 Committee.

A list of other work in hand which it is hoped will result in the issue of British standards is given in Table 3. In the remarks column is also given a code numbering relating to the rate of progress. From a study of this table it will readily be seen that a wide spectrum of NDT standards will be available for British industry in the course of time.

British Standards Institution

It will be readily appreciated that any national standard must not only appear to represent the views of the entire country concerned, it must in fact truly represent the cross-sectional views of that country. To instance the situation in Britain, the authors briefly list the structure and system of the British Standards Institution.

The B.S.I. is an independent body supported by both government and British industry, and although it receives a government grant, a large proportion of its funds is received from firms and trade associations and by individual subscribing members. It also obtains a reasonable proportion of its income from the sale of the standards it produces.

While its test house is not large, it does operate a control scheme for the constant checking of items that are covered by the Kite scheme of approval. Details of the Kite or certification marking system are given in the B.S.I. yearbook (2) as well as its close connections with the Standards Associates.

Control of B.S.I. is through its General Council (OC/-), upon which representatives of the various divisional councils, government departments and nationalized industries sit to lay down guidelines of policy, although the more day-to-day work is done through an Executive Committee (OC/5), consisting mainly of the chairmen of the various divisional councils.

The divisional councils, of which there are five, represent the major industrial divisions of the country, namely:—

Building divisional council (B/-)
Chemical divisional council (C/-)
Engineering divisional council (E/-)
Textile divisional council (T/-)
Codes of Practice (CP/-)

On each of these divisional councils are the elected representatives of the various industries standards committees, together with the nominated representatives of the major institutional bodies and government departments. The Engineering divisional council (E/-), which probably concerns the nondestructive testing section of industry most, has representatives from the following industries standards committees:—

Aerospace
Agricultural machining implements
Automobile
Chemical engineering
Cinematograph
Colliery requisites
Data processing
Electrical
Gas
Illumination
Instrument
Iron and steel
Mechanical engineering
Non-ferrous metals
Nuclear energy
Petroleum equipment
Refractory products
Refrigeration
Road engineering
Solid fuel
Surface coatings (other than paints)
Telecommunication
Welding

Additionally, representatives of such diverse organizations as the Trade Union Congress, the National Physical Laboratory, Crown Agents for overseas governments, etc., sit on the Engineering divisional council. Under the divisional council operates, as has been mentioned above, an industry committee. To instance only one, the "Mechanical Engineering Industry (MEE/-)" is composed of 48 representatives of the major institutions, trade organizations and governmental departments. Among these, to name a few, are, the Association of Consulting Engineers, Engineering Equipment Users Association, Machine Tool Trades Association, Radio Industry Council, etc. The particular industry council is the parent body for a number of individual technical committees under its direct control, e.g., MEE/169—Nondestructive Testing.

The individual technical committee may set up subcommittees, i.e., subcommittee MEE/169/1—Glossary of Terms, to produce standards direct, or it may set up panels, i.e. MEE/169/-/5—NDT of Steel Castings, to draft standards for approval of the main committee or the subcommittee.

Main or subcommittees may set up panels or working parties to deal with and consider a specific point.

Each representative speaks for the section of industry he represents, rather than a particular firm or organization, and each committee or panel elects its own chairman and is serviced by a permanent officer of the B.S.I. Like most organizations, the committees have power to co-opt specific experts to offer advice and comment whenever the need arises.

An engineering product involves, frequently, the producer of the basic material, the fabricator or constructor who does his work on it or with it, and the eventual user of the product. In some cases other interests exist. In many cases, NDT

Table 3

Standards in Preparation

Industry Committee concerned	Title of standard or description of work	Progress stage as at 31.3.66
AGE/–	Acceptance levels for the ultrasonic testing of light alloys	1
ELE/–	X-ray equipment—cable terminations	4
	X-ray equipment—film cassettes	6
	X-ray equipment—intensifying screens	2
INST/–	Measurement of flow in open channels—radioactive isotopes	4
MEE/– (MEE/169)	NDT—Magnetic inks and powders	4
	NDT of steel castings	3
	NDT—Spec. penetrants, magnetic inks and powders	4
	NDT—Steel forgings	
	Part 1—Ultrasonic flaw detection	
	Part 2—Magnetic particle flaw detection	
	Part 3—Penetrant flaw detection	
	Methods for NDT of plate material	
	Part 1(a)—Ultrasonic detection of laminations	
	Part 1(b)—Ultrasonic detection of inclusion clusters	
NCE/– (NCE/4)	Data on shielding from ionizing radiation	
	Part 2—Shielding from X-radiation	2
WEE/– (WEE/34)	Magnetic particle testing of welds	3
WEE/– (WEE/31)	Testing fusion welds in copper and copper alloys (metric units)	2
WEE/– (WEE/34)	Ultrasonic examination of welds	
	Part 1—Manual examination of fusion welded butt joints in ferritic steels (Revision B.S. 3923 Part 1)	3

Key to progress stages: 1. Work authorized
2. Drafting in hand
3. Draft circulated for comment
4. Comments under review
5. Approved for submission to industry committee
6. Approved for publication—with the printer

procedures and techniques are important to all these agencies and their collaboration in establishing acceptable and workable standards is clearly recognized.

Decisions in committee are not as of right taken on a majority vote, rather is it a principle to get common agreement, and here the chairman plays a vital and constructive part. However, when serious points of contention arise, this may mean a compromise, or even lowering of a standard. This, fortunately, does not arise very often, but if and when it does, it can be referred to an advisory committee for a ruling.

The system and structure of B.S.I. outlined above might seem complicated at first glance and even slow and cumbersome in operation. It is neither. Not only does the system work and work well, it can work fast. For instance, B.S.3971: 1966—Image Quality Indicators for Radiography and Recommendations for their Use—was initially discussed in committee in February 1965 and ten months later was ready for printing. This period included time for circulation of a draft, for receipt of comments, for the study of those comments, editing by B.S.I. of the final draft and preparation for printing.

British Standards are issued to and are available by most other national standards organizations, and are normally available for reading at most British Embassy and major libraries overseas and at home.

Producing a British Standard

The preparation of a standard for NDT is in no way unique, it follows common prescribed practices. The standard can be drafted either by committee or panel in committee assembled, or by members agreeing to prepare sections which are then discussed again by the assembled committee, or by the use of an existing industrial or governmental department standard acting as the draft for framework.

However, before any draft is prepared, it must be proved to the permanent directorate of B.S.I. that there is a need for such a standard and that the subject is not already covered by an existing British standard. Requests for a new standard are not normally received from individuals, rather must the request come from a trade association or engineering technical institution or society.

Having convinced the directorate that the need for such a national standard is required, and having obtained the approval of the particular industry committee which gives broad guide terms of reference in the case of a new committee, the B.S.I. then approach all the appropriate trade and industrial bodies to send and appoint their representatives.

At the first meeting this committee or panel examines its terms of reference, elects its chairman and decides how it might tackle the job of work. At the same time, a program or target date for the completion of the work or section of the work is invariably set.

Industry Comment

Although, as has already been mentioned, the committee is made up of representatives from organizations rather than individuals, it will be readily appreciated that any national stand-

Table 4

Application or Product Standards (wherein reference is made to N.D.T.)

Standard No.	Title	Remarks
B.S. 487 : 1963	Part II—Fusion welded steel air receivers Part II—Receivers to Class 1 requirements	
B.S. 806 : 1954	Ferrous pipe and piping installations for, and in connection with land boilers	(R)
B.S. 1113 : 1958	Section 5. Radiography is called for in this section dealing with inspection and testing	(R)
B.S. 1500 : 1958	Fusion welded pressure vessels for use in chemical, petroleum and allied industries Part I—Carbon and low-alloy steels. Sections 4 and 5 Part III—Aluminium. Refers to radiographic examination of welds	Manufacture, workmanship, inspection and testing refers to radiographic and ultrasonic methods
B.S. 1515 :	Fusion welded pressure vessels (advanced design and construction) for use in chemical, petroleum and allied industries Part I—1965—Carbon and ferritic alloy steels.	Nondestructive tests (none except for weld imperfections as revealed by radiographs and pressure tests).
B.S. 1894 : 1952	Electrode boilers of riveted, seamless welding and cast iron construction for water heating and steam generating	
B.S. 2070 : 1954	Steam receivers and separators	
B.S. 2633 : 1956	Class 1. Metal-arc welding of steel pipeline and pipe assemblies for carrying fluids. Refers to B.S.2910 and includes acceptance levels.	(R)
B.S. 2645	Test for use in improvement of welders, Part I	
B.S. 2654 : 1961	Part II—Site erection, inspection and testing	
B.S. 2790 : 1956	Cylindrical land steam boilers of welded construction (other than water tube boilers)	
B.S. 3351 : 1961	Piping systems for the petroleum industry. Refers to B.S. 2910 and gives acceptance levels	
B.S. 3451 : 1962	Testing fusion welds in aluminium and aluminium alloys	
B.S. 3915 : 1965	Carbon and low-alloy pressure vessels for primary circuits of nuclear reactors. Refers to radiographic and ultrasonic examination, crack detection and leak detection methods	
B.S. 3636 : 1963	Methods of proving the gas tightness of vacuum or pressurized plant. Describes 17 methods of proving gas tightness	

Key: (R) Under revision
(P) New standard or Part in course of preparation
The majority of the above standards relate to pressure vessels and welded items; somewhat unusual is:—B.S. 3197: 1960 Adze claw hammers, which specifies magnetic and hardness tests.

ard must not only be approved by industry at large, but also must be accepted and implemented by industry at large. Compulsory use of standards does not apply in Britain, except where particular legislation exists, although there are times when we individually feel there are cases when compulsion is desirable. As Britain is a trading nation, it is left for individual firms to decide whether, in order to maintain and expand their business, they should comply with Standards.

To get industry's comment and concurrence is therefore imperative. Thus, after the draft has been prepared by the committee and agreed, copies are circulated (free) to each trade association, institution or individual firm that might be interested and able to offer constructive comment. Sometimes such a document has hundreds of copies circulated. In the case of B.S. 3971 1966—Image Quality Indicators already mentioned, 611 copies were circulated for comment, and a reasonable issue will be 500-1,000 copies.

The recipients are normally given six weeks in which to prepare and return their comments, amendments, criticisms. This period may have to be extended when overseas comment is invited.

The permanent secretary, who in turn is an experienced and qualified individual in his own right, has then the formidable task of collating these comments for the committee to consider. As an example, in the case of nondestructive testing of pipes and tubes (eddy-current testing of non-ferrous pipes

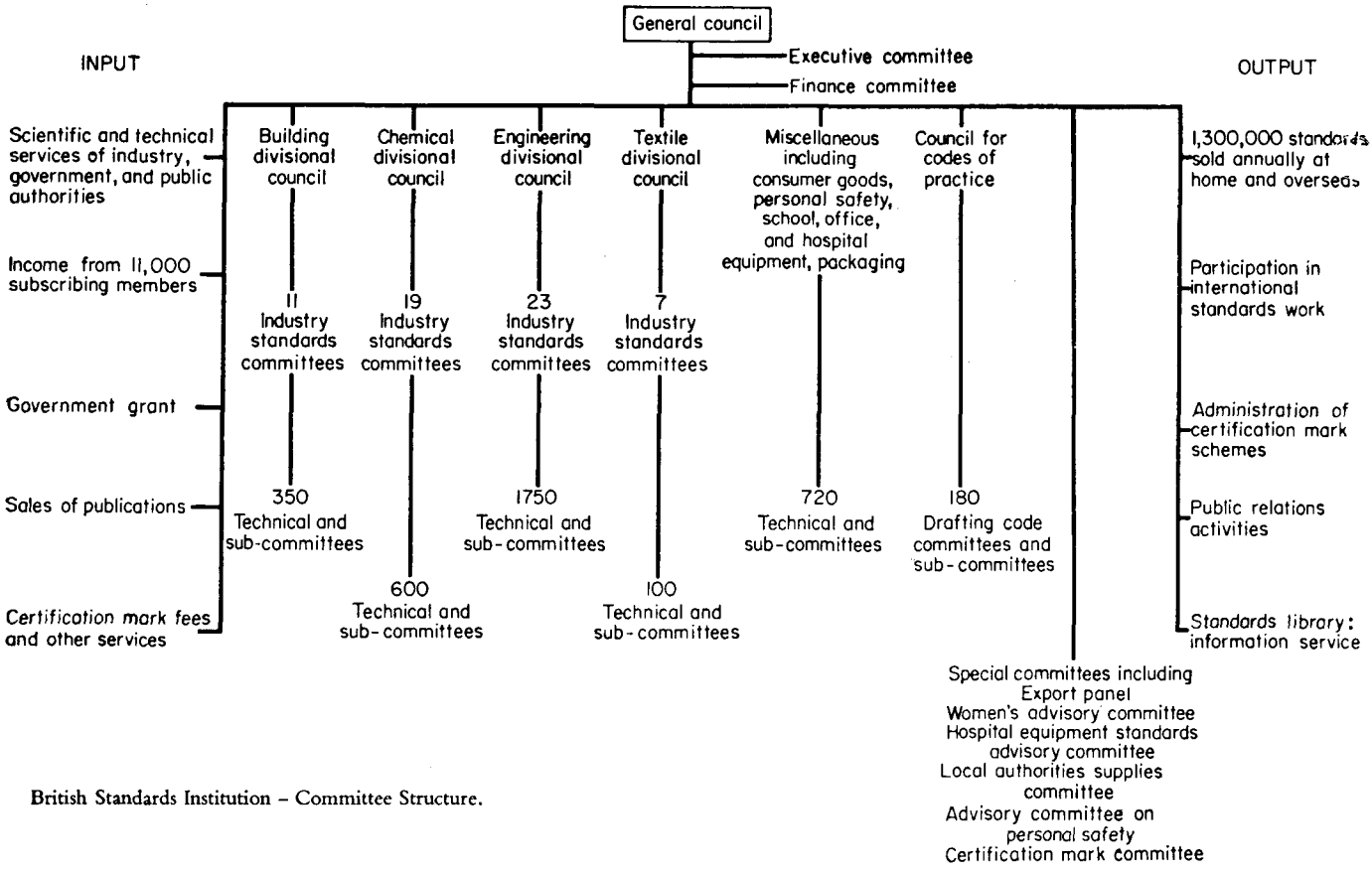

British Standards Institution – Committee Structure.

and tubes)—B.S. 3889, Part 2B, Document D65/9793,—thirty industrial comments were received, including one of two pages.

The committee has to decide which comments are worthy of serious consideration and the draft is amended. In some cases, a second draft may be circulated to industry, but in most cases the document is submitted to the appropriate industry standards committee and the divisional council for approval. In many cases this approval can be done on a postal basis, but where a particular section of industry disapproves, or a particularly strong objection is put forth, the final draft can be discussed in industry committee or divisional council.

Thus it will be seen that the system not only ensures that the views of British Industry are fully considered, but also that standards receive industry's blessing.

On occasions it is found there is insufficient experience or factual information available to produce a satisfactory standard, and investigations or research may be needed; for example, when dealing with "black light" for magnetic and penetrant flaw detection processes the requirement arises of specifying the "black light" intensity and a method of calibrating lamps. At the time of writing this paper there is no national centre for research in NDT to which such problems can be referred, and any work necessary has to be carried out by individual firms or research associations, etc., but there is a strong probability that such a centre will be established and operating by the time this paper is presented.

International Standards Organization

The B.S.I. is the formal and official link with international standardization organizations and provides the secretariat for many of their committees in addition to appointing British delegates to the various committees, working groups or sub-committees. It is indeed regrettable to record that of the seven international organizations—comprising no less than 200 committees—listed below there is not one committee whose primary function or term of reference is to coordinate or prepare international NDT standards or recommendations.

I.S.O. —International Standards Organisation (80 technical Committees). (Ref. 3).

I.E.C. —International Electrotechnical Commission (60 technical Committees).

C.E.E. —International Commission on Rules for the approval of Electrical Equipment (18 Committees).

C.I.S.P.R. —International Special Committees on Radio Interference (9 Working Groups).

C.E.N. —European Standards Co-ordinating Committee (27 Technical Committees).

C.E.N.E.L. —Committee for the Co-ordination of European Standards in the Electrical field. (Ref. 4).

A.B.C. —Conferences on the unification of standards (A.B.C.—America, Britain and Canada).

Table 5

A Selection of Some Other National Standards relating to N.D.T.

Country	Number	Title
U.S.A. (A.S.T.M.)	E 138–63	Wet magnetic particle inspection.
India	IS. 1182	General recommendations for radiographic examination of fusion welded joints.
Canada	48–GP–2	Spot radiography of butt welds in ferrous materials.
Czechoslovakia	CSN–05–1305	Classification of weld defects on radiographs.
Germany	DIN.54111	X-ray and Gamma-ray testing of welds on metallic materials.
Hungary	MSZ.4310 Parts 1–5	Nondestructive testing methods. General. Including dye penetrant and magnetic particle methods; radiographs; types and symbols of weld defects; classification and estimation of weld defects by X-rays and Gamma-rays.
Poland	M-69772	Radiographic determination of weld faults.
Spain	UNE.14011	Grading of welds by X-rays.
Russia	GOST.7512-55	Methods of inspection of welded seams by X-rays and Gamma-rays.
ISO Documents		
	44 N 244 / ISO(WEE)1473.X	Recommended practice for radiographic inspection of fusion welded butt joints for steel pipes up to 2-in. wall thickness.
	44 N 245 / ISO(WEE)1475.X	Recommended practice for radiographic inspection of fusion welded butt joints for steel plates up to 2 in.
	44 N 246 / ISO(WEE)1475.X	Radiographic image quality indicators.

We must pay tribute to the work of the International Institute of Welding which has produced standards that have formed the basis for I.S.O. recommendations.

Furthermore, there might be a glimmer of hope in a recent announcement from B.S.I., Memorandum 66/24817—19th October, 1966, following recommendations made by representatives of the Ministry of Technology in Bergen in May 1966.

(i) EFTA Ministers should give strong encouragement to industries, departments and to standards bodies to pursue the objective of getting early agreement on standards in the European and, where appropriate, in the international standards organizations; (ii) the national standards bodies should be pressed to make the strongest efforts to secure full acceptance of the results of these agreements in national standards without deviation, and public purchasing departments should be urged to take full account of such standards.

Not only were these recommendations submitted to and endorsed by the meeting in Bergen but they have been confirmed as part of B.S.I. policy and agreed by both the Ministry of Technology and the Confederation of British Industry.

Additionally, the U.K. has announced the decision to "go metric" over the next decade, using the rationalized M.K.S.A. system as adopted by I.S.O.—that is, the *Système Internationale* (S.I.), and British standards are now being produced using metric units.

Future Requirements

Nondestructive testing has a useful and important part to play in the economy of nations by assisting in the efficient use of materials and labour. This will only be achieved by a concerted effort and an understanding of the problems involved. Nondestructive testing engineers currently have four major tasks:—*First.* To establish national standards and international recommendations for NDT instruments and equipments, and to define test procedures, including the scope and limitations of particular methods and techniques, so that designers, inspectors, and other personnel can confidently and correctly specify nondestructive testing. *Second.* To improve the ability to locate, identify and describe imperfections so that materials can be classified or graded, enabling specifications for quality levels to be applied when necessary. *Third.* To expand the present range of methods and their speed of operation to enable them to be integrated into automated and flow-line processes, and on stream and other inspection procedures. *Fourth.* To expand the field of materials evaluation and the correlation of physical properties with those measurable by nondestructive methods.

Discussion

Most people can appreciate the value of standards, but having an appreciation is much easier than actually producing effective standards. In fact, the possession by a nation of an adequate number of reliable and realistic standards can be regarded as an index to the level of civilization and citizenship—for the production of standards of the right type and quality requires individuals and organizations who are prepared to devote considerable time and energy to a cooperative effort in producing documents that are useful nationally and ultimately internationally.

The production and maintenance of standards then involves a considerable amount of expertise, diverse skills and organization. In some spheres of life, e.g. weights and measures, standards have existed for many years: in other fields, such as NDT, which is still young in terms of the engineering industries, standardization is proceeding alongside the growth of knowledge and experience.

Inherent in this paper is the need for standards of quality or levels of acceptance. This is the field of standardization that is exceedingly difficult and in which most progress needs to be made. Unless some understanding is possible of the significance of imperfections or flaws, the establishment of levels of quality must remain a subjective judgment. NDT can assist in this difficult field in two ways. Firstly, by enabling sorting of materials and components into grades or classes, say, A.B.C.D.E., etc.; the appropriate grade then being selected for the required duty by the responsible people concerned. Secondly, by measuring the extent and rate of growth of defects in plant and

enabling an evaluation of their seriousness to be obtained. Those in the nondestructive testing field need to actively support all work being carried out in determining the significance of imperfections.

Conclusions and Recommendations

At the conclusion of the 2nd International Conference on NDT at Chicago in 1957, under the theme "Recommendations for Technical Development and Standardization", seventeen points were offered for discussion, including detailed suggestions for international cooperation (5). In the decade since then, individual countries have made progress in standardization, as it is hoped has been illustrated in this paper for Great Britain, and it is the authors' belief that the time is now appropriate for the establishment of international standardization. We therefore suggest that the International Standards Organization (I.S.O.) is the appropriate body and recommend to this conference that appropriate steps be taken to approach the I.S.O. for the establishment of a technical committee for NDT.

The authors would therefore like to propose to this meeting that:

(a) Now is the appropriate time for the establishment of an international committee to coordinate the preparation of international NDT recommendations; (b) It is agreed by all delegates that they will request (persuade, bring pressure to bear) their official national standards organization to recommend to the I.S.O. that I.S.O. does establish a separate Technical Committee to deal with NDT.

Acknowledgments

The authors, while acknowledging that the views expressed in this paper are individual rather than corporate, would like to express their appreciation to the Boards of the Central Electricity Generating Board and Corrosion & Welding Engineering Limited for their permission and encouragement to present this paper.

They would also record acknowledgments to the British National Committee for Nondestructive Testing and particularly to the British Standards Institution for their help and assistance in the preparation of this paper.

References

1. Standardization in Nondestructive Testing Symposium, Harrogate, 20th-22nd September, 1962. *The Production Engineer*, Vol. 41, No. 12, December 1962, pages 735-746, and January-February 1963, Vol. 42, No. 1 and 2, pages 17-47 and 84-94, the Institution of Production Engineers, London, England.
2. British Standard Institution Year Book (1966).
3. I.S.O. Memento (1966), I.S.O. General Secretariat, Geneva.
4. British Standards Institution Year Book Supplement. Publications by International Organisations, I.S.O., I.E.C., C.E.E., C.I.S.P.R. (1966).
5. Summary of Session on Recommendations for Technical Development and Standardization, Vol. XVI, No. 2, page 152, *Nondestructive Testing*, March-April, 1958. Society for Nondestructive Testing, Evanston, Ill., U.S.A.

British Standard Annual Report (1966). British Standards Institution, London, England.

"Standards for Industry," C. Douglas Woodward, Heinemann Educational Books Ltd., London (1965).

"An Introduction to Industrial Radiology," J. C. Rockley (1964), Butterworth & Co. (Publishers) Ltd., London, England.

Correlation of Conductivity to Mechanical Properties of Age-Hardenable Aluminum Alloys Using Eddy-Current Methods

DAVID D. SELTZER, USA

Introduction

Age-hardenable aluminum alloys 7075, 2014, 2024, and 2219 have been used in aircraft and aerospace applications based primarily on their strength-to-weight ratio. The strength and corrosion resistance characteristics of these alloys depend on close control of the time-temperature cycle during the solution heat treat and the subsequent aging of the material. The mechanical properties of these alloys specified in various materials specifications are obtained by appropriately heat treating the material in accordance with specification MIL-H-6088 (1).

In areas of service applications, degradation of mechanical properties occur because of either an accidental fire or the exposure of parts or vehicles to elevated temperatures long enough to decrease the strength of the material.

Degradation of mechanical properties may occur also by an unauthorized localized heating of machined parts prior to the straightening operation. Because control is lacking in this type of operation and also because there is the possibility of inducing residual stresses that may be detrimental in service, localized heating is prohibited in various specifications.

Improper processing during heat treat will lower the mechanical properties and will decrease the corrosion resistance of the alloys; for example, slack quenching occurs when the material is not cooled rapidly enough in a quench medium after the solution heat-treat cycle.

Degradation of mechanical properties can also result from improper aging. However, a controlled decrease in mechanical properties by precise overaging decreases the susceptibility of the alloys to stress-corrosion. To the designer a known and controlled loss in mechanical properties has value in certain applications and is better than risking catastrophic failure because of stress-corrosion.

In the past, degradation of mechanical-physical properties was not truly assessable except in a limited way by destructive tensile tests and the nondestructive hardness tests. The correlation of hardness values to ultimate tensile strength has never been too accurate, and reliability in its use for many years has been dependent more on either over-design of the structure or the result of actual service loads that occurred below the anticipated design load conditions.

Extensive studies have been conducted by the Martin-Marietta Corporation in the correlation of electrical conductivity to the mechanical properties of age-hardenable aluminum alloys using eddy-current methods (1 to 7 incl.). Studies on alloys 2014, 2024, and 7075 were directed primarily towards obtaining a correlation of conductivity, hardness, and ultimate tensile and yield strength. Results of these studies have been put into practical application, as in assessing accidental fire damage to aircraft structures, assessing slack-quenched conditions in aerospace hardware, and in assessing mechanical properties of aerospace hardware after controlled overaging.

The problem manifests itself in that, under conditions of severe overheating, identical values of conductivity can be obtained that have different values of mechanical properties. However, supplemental hardness-test information and occa-

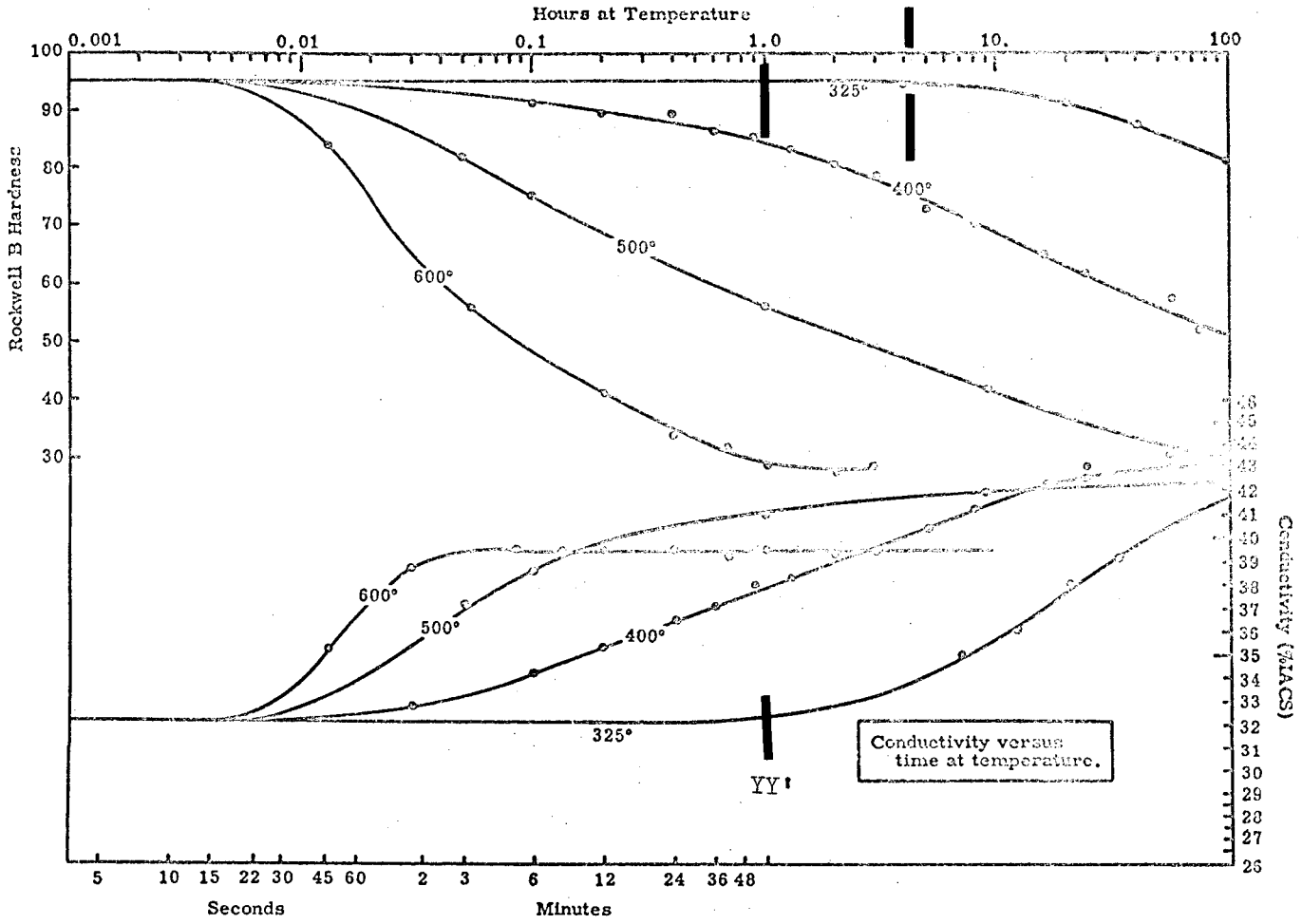

Figure 1. Conductivity and hardness vs. time at temperature on 7075-T6 aluminum alloy.

sional verification of the tensile strength will produce reliable results in establishing the mechanical properties without extensive destructive testing. In addition, the conductivity of different alloy systems overlap; therefore, it is essential to identify the alloy. Extrapolation of values from one alloy to another or the use of values derived for fire degradation, for those involved in degradation of properties because of slack quenching or controlled overaging, will result in errors.

Time and temperature are two of the critical parameters that produce the final physical characteristics. Knowing the metallurgical phenomena or transformation that occur in the alloys under various conditions, or understanding the methods used to arrive at the characteristics and recognizing the limitations of the eddy-current technique, are essential to the appropriate use of conductivity measurements in evaluating the mechanical properties of the age-hardenable aluminum alloys.

The correlative data, only parts of which are described in this paper, have permitted the continuously expanding use of the eddy-current instrument as a means of 1) verifying that proper process control in heat treat has been followed to obtain specified mechanical properties (ultimate and yield), 2) assessing the loss in mechanical properties owing to slack quenching or to overaging, 3) assessing the loss in mechanical properties owing to accidental fire or to exposure to temperatures detrimental to mechanical properties of the material, and 4) verifying mechanical properties obtained under closely controlled conditions of overaging to minimize material susceptibility to stress-corrosion, and still maintain minimum specified mechanical properties.

Equipment

Conductivity measurements in these studies were made with an FM-100 instrument that utilizes the principle of eddy currents to measure the electrical conductivity of nonmagnetic alloys (2). The instrument covers a range of conductivity from 8 to 103 per cent IACS (International Annealed Copper Standard). A probe acts as the leg of a Wheatstone bridge, and its impedance varies according to the conductivity of the material on which it is placed. When the probe is placed on a conductive material the bridge becomes unbalanced; the balance is restored by adjusting a capacitor that at the same time rotates a dial bearing conductivity figures. When the bridge has been balanced the conductivity reading on the dial is that of the material upon which the probe is placed.

Test Procedure

To obtain accurate measurements of conductivity, the instrument must be adjusted, calibrated, and used in accordance with instructions appearing in the instrument operation manual. Calibration is made using standards supplied with the instrument. The samples tested and the calibrating standards must be at the same temperature. The instrument probe should be applied to clean, fairly smooth, and flat areas. Anodic coatings and chemical films affect the accuracy. For materials ranging in conductivity from 28 to 40 per cent IACS, accurate readings are obtainable when the material thickness exceeds 0.040 in. The effects of specimen thickness, cladding, and lift-off adjustment in measurements of conductivity have been previously

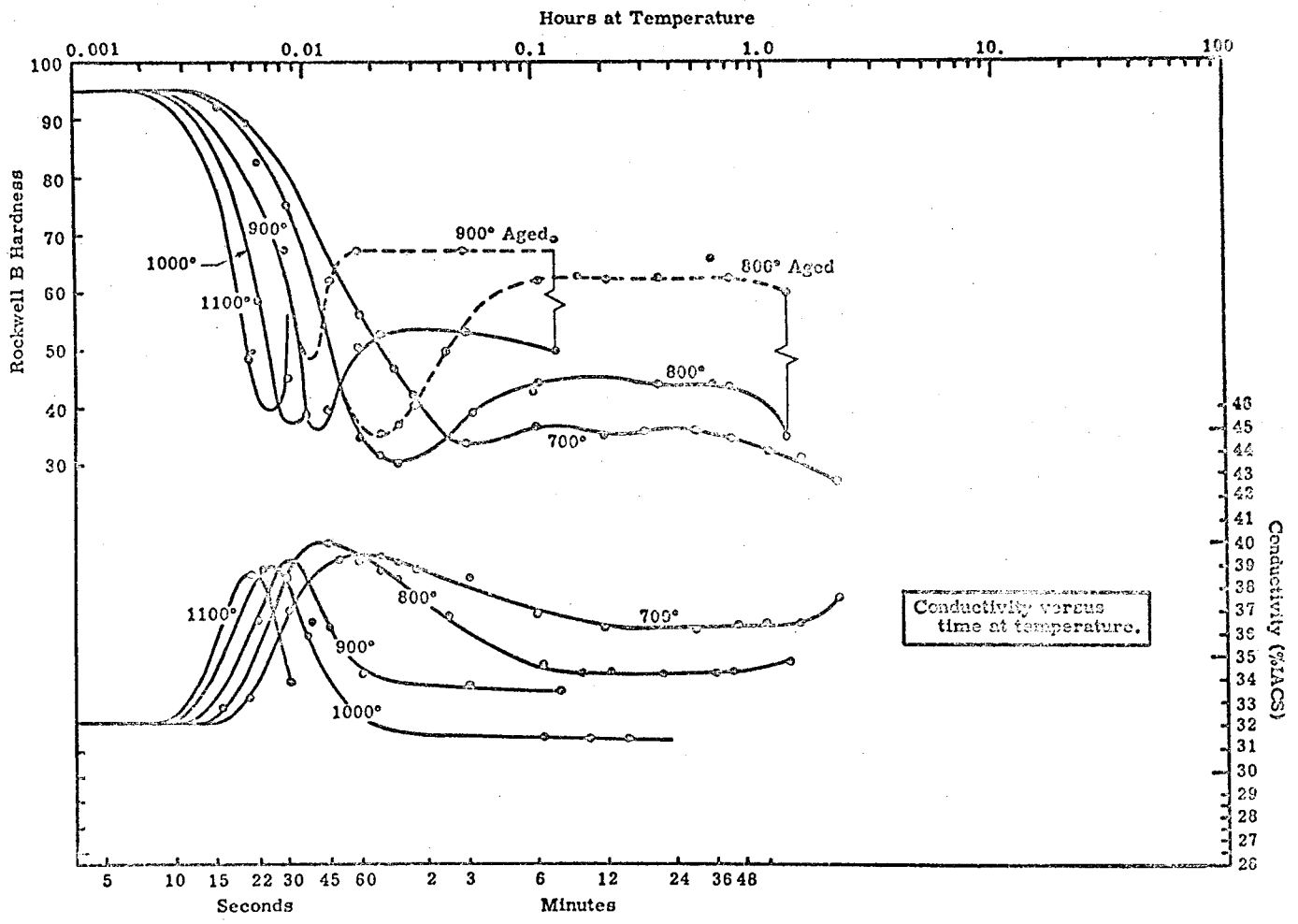

Figure 2. Conductivity and hardness vs. time at temperature on 7075-T6 aluminum alloy.

presented in a technical article (3). Parts curvature and edges also affect the accuracy of the conductivity reading.

Discussion

In this paper I describe several characteristic curves of mechanical-physical properties of age-hardenable aluminum alloys in which the alloy properties have been lowered or degraded by a number of heat treatments, e.g., controlled overaging, high temperature exposure, and slack quenching. It is my intent to describe briefly how these characteristic curves were obtained and to discuss primarily the value that may be derived from their use. For more detailed information on time-temperature effects, with respect to the characteristic curves derived, one may refer to the listed references.

Investigations have revealed that the exposure of aluminum alloy 7075-T6 to high temperatures results in a rise in conductivity accompanied by a drop in hardness and strength. A number of test specimens were exposed to various times and temperatures of overaging and high-temperature degradation. Conductivity and hardnesses were determined immediately after the exposure. The specimens were placed in a deep freeze to prevent natural aging and were tested subsequently at room temperature to establish their mechanical properties. The results, shown in Figures 1 and 2, illustrate that a decreasing hardness is mirrored by an increasing conductivity for the alloy when exposed to temperatures of 325° up to 1100°F for increasing times of exposure. A sharp reversal in slope at the higher temperature is ascribed to solutioning of the alloying elements with a subsequent increase in hardness and a decrease in conductivity, possibly owing to the setting of a strain in the metal lattice. Subsequent aging after exposure at the higher temperatures will result in a significant increase in hardness, without a rise in conductivity, owing to precipitation of the alloying elements. Figure 1 shows that the conductivity is more responsive initially to metallurgical change than to the hardness test. Note that line YY′ depicts a rise in conductivity at 325°F after 1 hour, while for the same temperature, a drop in hardness occurs after 4 hours of exposure. These characteristic curves are described in other parts of this paper in their application to controlled overaging to minimize the material susceptibility to stress-corrosion. The initial application of the graphical data in Figures 1 and 2 was in the evaluation of fire damaged aircraft structures and in cases of improper aging of the alloy. Above 600°F a curve reversal occurs (shown in Figure 3) that depicts the relationship of conductivity to hardness. Note that for curves obtained on material exposure above 600°F, each specimen can have a hardness reading that corresponds to two different conductivities and that depends on the time and/or temperature of exposure. Also, in a short-time high-temperature exposure, the conductivity readings may be identical, although the hardness readings would be dissimilar. This can be seen by drawing a vertical line along hardness R_B50 and noting that it intersects the 1000°F curve at 34 per cent and again at 39 per cent IACS. In a similar manner, a horizontal line along 35 per cent IACS conductivity would intersect the 1000°F curve at the approximate hardness of R_B86 and again at R_B45. Thus one would not know by either conductivity reading or

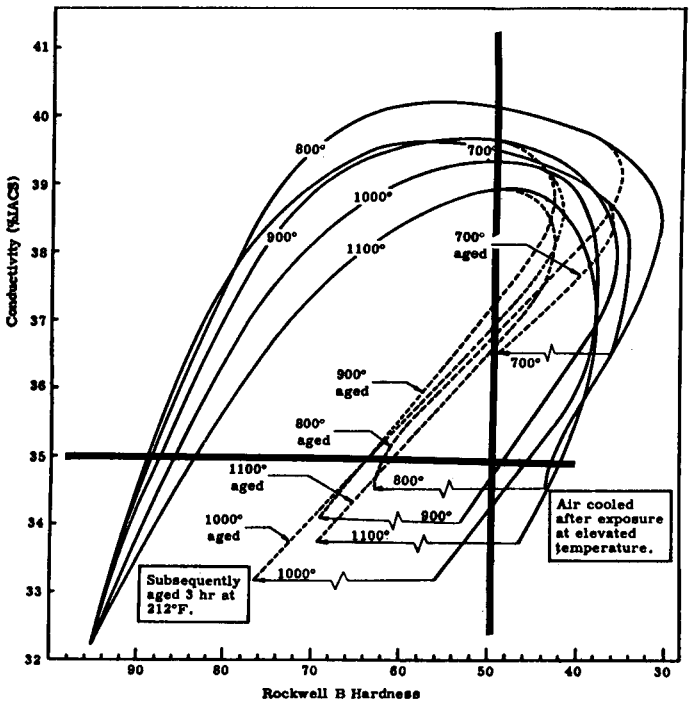

Figure 3. Conductivity vs. Rockwell B hardness on 7075-T6 aluminum alloy.

hardness reading alone that the material either was undamaged or was severely damaged by a high-temperature exposure. In this case a hardness reading to supplement the conductivity reading should be taken occasionally. Hardnesses falling to the right of a vertical line through the point of maximum conductivity would substantiate that the conductivity is on the downward or reverse slope and would indicate, therefore, that the material properties have been appreciably lowered. No reversal occurs from 325° to 600°F and a conductivity reading alone can be used to substantiate the mechanical properties (ultimate and yield strength).

In an extensive study by Chihoski, the resultant conductivity-hardness relationship based on various times and temperatures of exposure for 7075-T6 material were projected into isometric form as shown in Figure 4 (4). Isometric projections permit establishing the possible times and temperatures of exposure when they are unknown, provided that the conductivity and hardness can be measured. These data were applied practically when estimating time and temperatures of exposure in the case of jet-engine starts, with a noise suppressor attached, that retained excessive heat in the nacelles of the aircraft.

The correlation of conductivity to the ultimate and yield strength of 7075-T6 aluminum alloy are shown in Figure 5. Generally a conductivity of 32 to 35 per cent IACS depicted by the grey area of the graph is the T-6 material within the specification. Vertical lines have been drawn to indicate the minimum specified properties. The degradation or loss in mechanical properties resulted from various high-temperature exposures at various times. All tensile tests were conducted at ambient after the exposure. As cited earlier, specimens were stored in a deep freeze to prevent natural aging. Note that the loss in strength is more severe for high-temperature short-time exposures of T-6 material than for low-temperature long-time exposure even when the conductivities of the material are the same. This may be clearly seen in Figure 7.

The conductivity-ultimate tensile strength and the conductivity-yield strength of the various age-hardenable aluminum alloys are not identical. In contrast to 7075-T6 with a con-

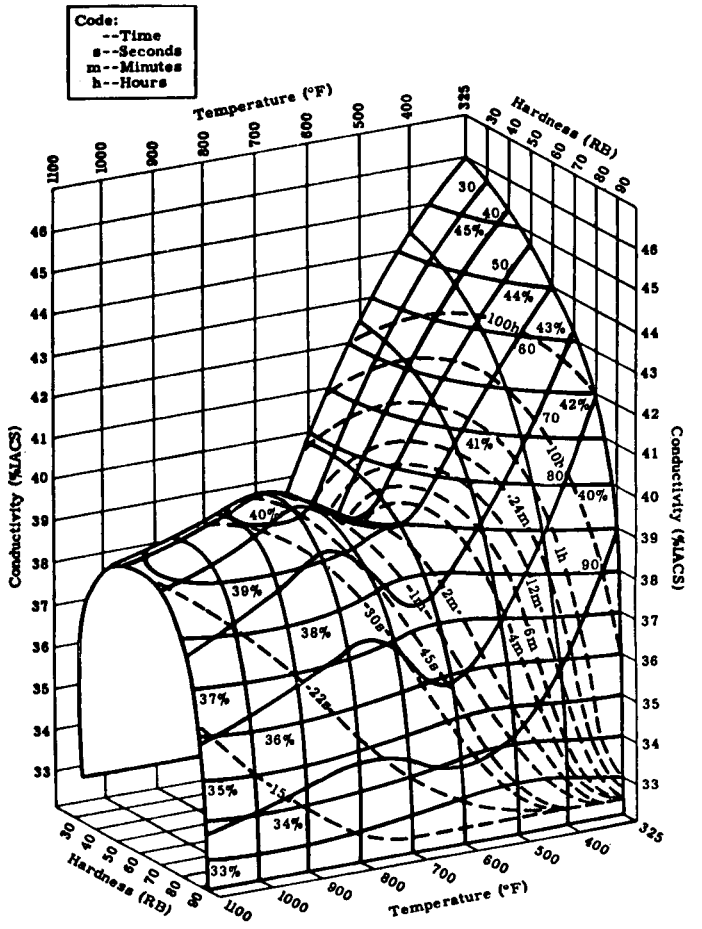

Figure 4. Conductivity vs. hardness vs. temperature of exposure with exposure times marked by isochronous lines on the surface of the curve for exposures of 7075-T6 aluminum alloy.

ductivity of 32 to 35 per cent, the alloy 2014-T6 generally indicates a conductivity of less than 39 per cent IACS for specified minimum properties. Minimum properties of ultimate and yield and their corresponding conductivity for alloys 7075-T6, 2014-T6, and 2024-T4 are shown in Table 1.

The conductivity-ultimate tensile strength relationship at ambient temperature for 2014-T6 subjected to overaging and/or degradation of mechanical properties by exposure to various

Table 1
Properties of Aluminum Alloys 7075–T6, 2014–T6, 2024–T4

Alloy	Specification	Tensile strength minimum	Yield strength minimum	Conductivity per cent IACS
7075–T6	QQ–A–287	72,000 psi (5062 Kg/cm²)	62,000 psi (4360 Kg/cm²)	32 to 35
2014–T6	QQ–A–255	64,000 psi	57,000 psi	less than 39
2024–T4	QQ–A–355	62,000 psi		less than 34.5

times and temperatures between 400° to 1100°F is shown in Figure 6. The area within A′B′B indicates material within specification; the area C′C′C (grey area) indicates material in the doubtful category of meeting the specification. The rise in

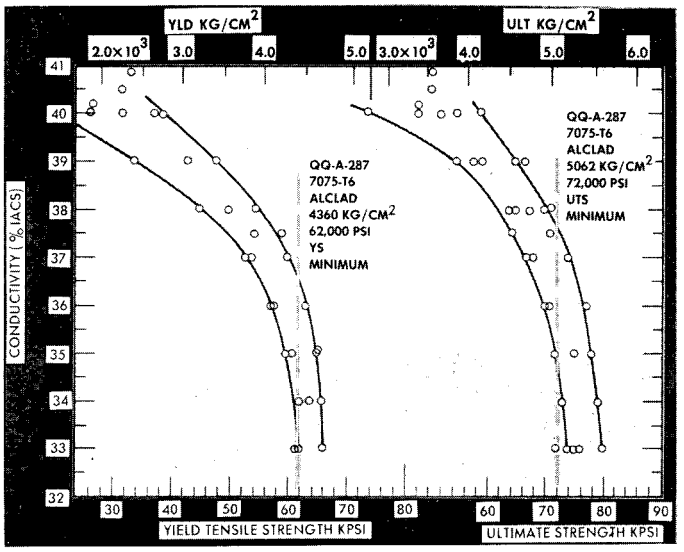

Figure 5. Conductivity vs. yield and ultimate tensile strengths.

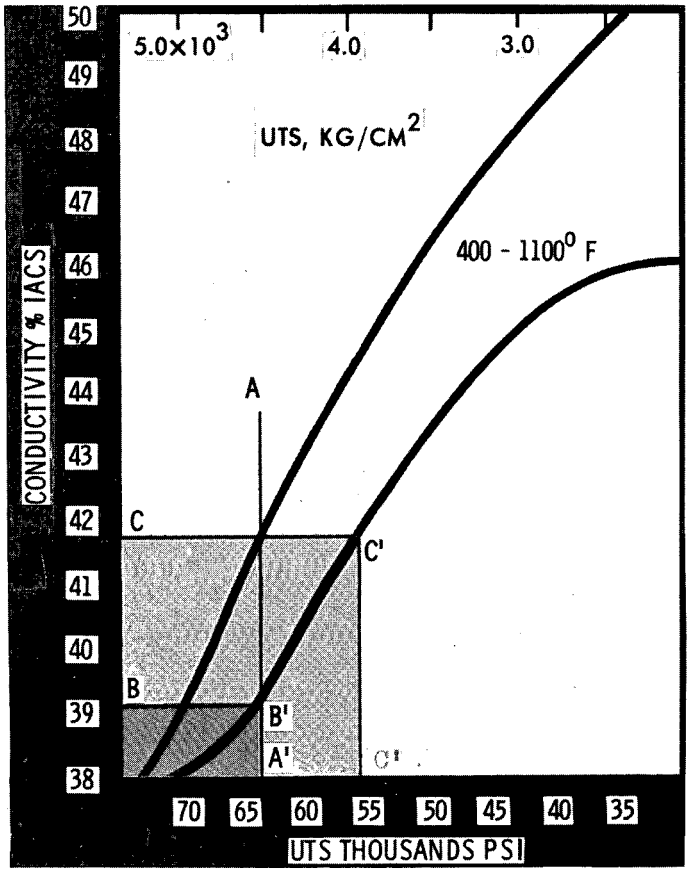

Figure 6. Conductivity vs. UTS for 2014-T6 for all temperatures.

conductivity of 2014-T6 material exposed to temperatures between 400° and 800°F is gradual with no reversal (5). In temperature exposures between 800° and 1100°F the conductivity curves of 2014-T6 material indicate a reversal similar to the characteristic curves described previously for alloy 7075-T6 (*see* Figures 3 and 15).

Earlier in this paper it was indicated that the loss in strength is more severe for high-temperature short-time exposures of 7075-T6 material than for similar material exposed

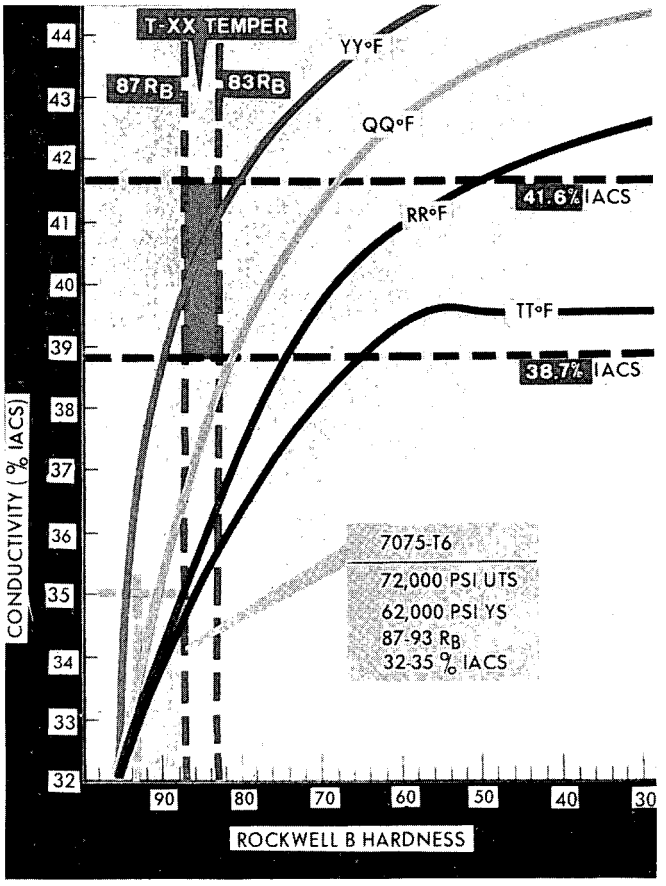

Figure 7. Conductivity vs. Rockwell B hardness on 7075-T6 aluminum alloy after exposure to various temperatures (°F) and times.

to low-temperature long-time exposure even though the conductivities are the same. The mechanical/physical parameters for 7075-T6 material within specification are depicted by the light grey area in Figure 7. The subsequent change in the hardness-conductivity parameters by controlled-overaging to the T-XX temper is depicted by the dark grey area. Note that temperatures higher than YY°F produce identical conductivities with a lowering of the hardness. A lowering of the hardness will also produce a decrease in the ultimate and yield strength. Material in the T-XX temper within the approximate parameters of hardness R_B83-87 and conductivity 38.7 to 41.6 per cent IACS, obtained by controlled overaging of 7075-T6 material at YY°F for a known period of time, will produce an approximate 15-per-cent loss in mechanical properties below specification. Material subjected to this controlled overaging lessens the possibility of failures due to stress corrosion.

Extensive testing needs to be done to establish the specification limit lines for conductivity and hardness related to a known probability of obtaining a specified ultimate and yield strength. Figure 8 shows a projection of possible limit lines for hardness and conductivity for the T-XX temper. To establish these limit lines more accurately a statistical number of tests on T-XX material aged at YY°F for a specified time are necessary to establish the Gaussian distributions of hardness, conductivity, ultimate and yield strength. The Gaussian distributions derived would subsequently be placed as an overlay on Figures 9 and 10. This would permit a more accurate definition of the specification limits of conductivity and hardness. In addition the determination of a known probability of meeting specified tensile and yield strength will permit extensive acceptance testing of T-XX material based primarily on conductivity and

hardness. This would result in a lesser dependance on destructive tensile testing which currently limits heat-treat lot acceptance on the basis of limited sampling.

Figures 11 and 12 show the characteristic curves of hardnesses and related conductivities of 7075-T6 based on various overaging temperatures for various time intervals. The characteristic curves may be used to project a development test program in establishing specific cycles of overaging or tempering with subsequent evaluation of material susceptibility to stress corrosion. For example, a series of vertical lines from the horizontal conductivity (38 per cent IACS) line intersecting each of the aging curves have been projected so that they also intersect with the corresponding hardness-aging curves. Note that for the identical conductivities (38 per cent IACS) the hardnesses are lowered and the scatter becomes greater as higher temperatures-shorter times are used in the overaging cycle. In Figure 11, approximately 30 hours of controlled overaging of 7075-T6 material at YY°F, depicted by the triangular symbol, produces an approximate hardness of R_B87 and a conductivity of 38 per cent IACS. This appears to be the near optimum compromise in which material susceptibility to stress corrosion and the loss in mechanical properties due to overaging are minimal. Figure 12 indicates that increasing the conductivity range from 38-40 per cent IACS, as indicated in Figure 11, to 40-42 per cent IACS will result in a lowering of the hardness. Therefore one would also expect an additional lowering of the ultimate and yield strength.

For years the general practice has been to use the hardness test to evaluate the mechanical properties of fire damaged and overheated structural aluminum alloys. The error of this practice can be seen in Figures 13 and 14 which illustrate the

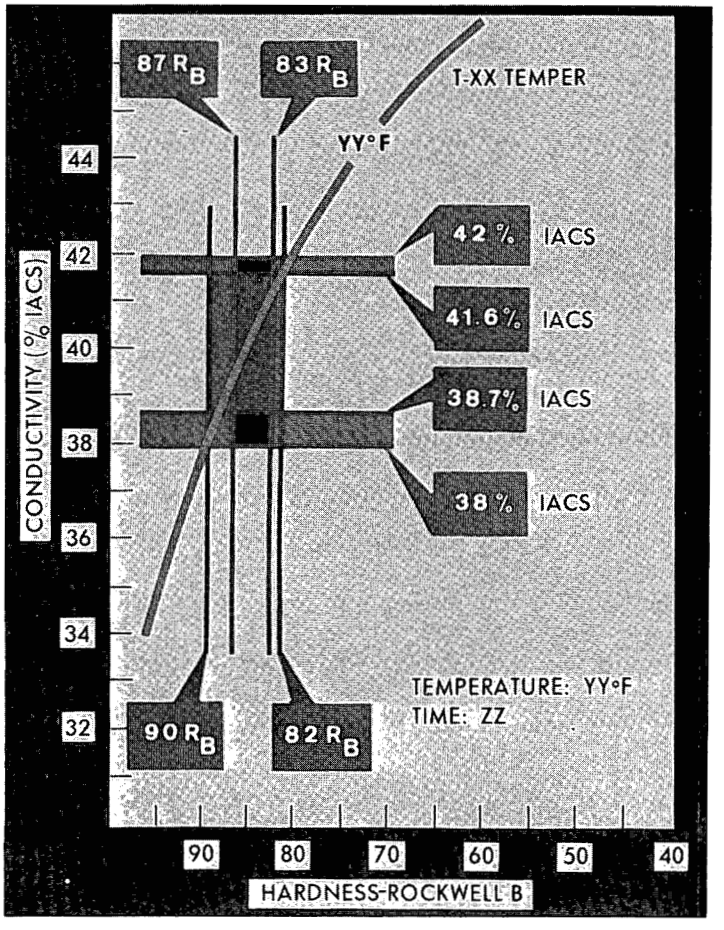

Figure 8. 7075-T6 aluminum alloy overaged at YY°F for various time intervals. Gauge: .250-in. nominal.

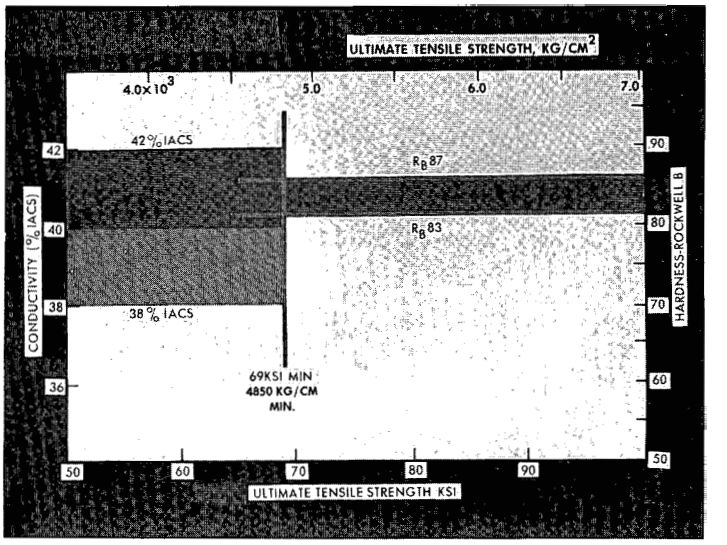

Figure 9. T-XX temper.

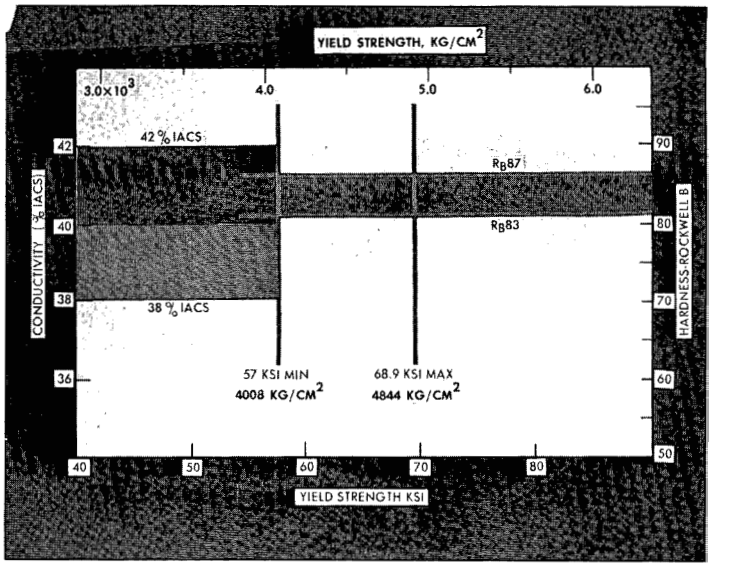

Figure 10. T-XX temper.

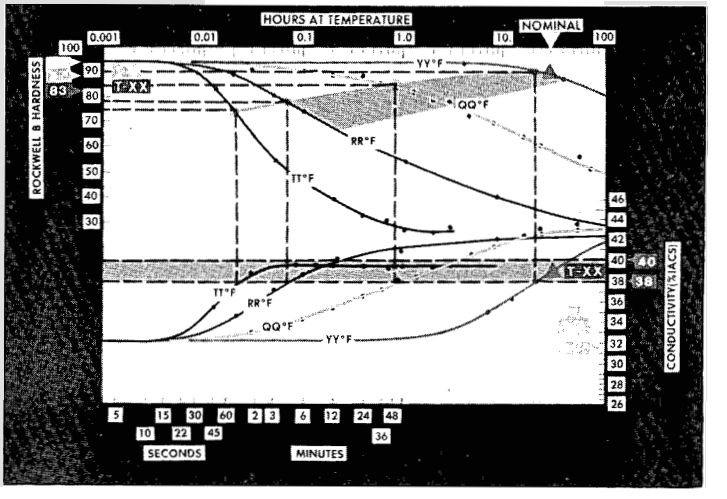

Figure 11. Conductivity and hardness vs. time at temperature on 7075-T6 aluminum alloy.

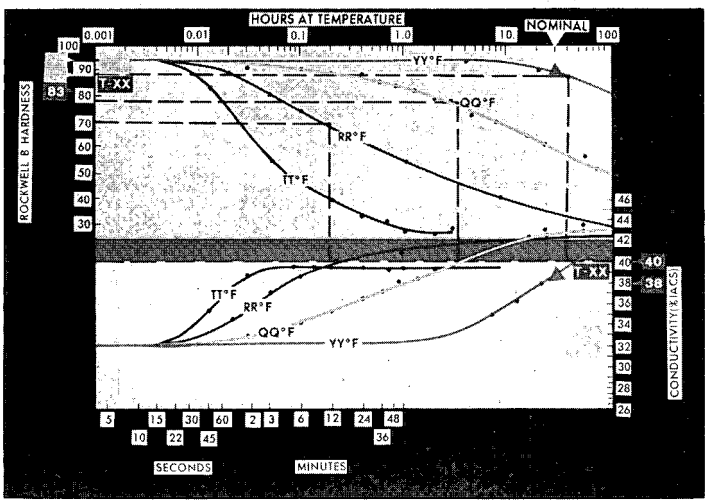

Figure 12. Conductivity and hardness vs. time at temperature on 7075-T6 aluminum alloy.

hardness relationship to ultimate and yield strength of 2014-T6 aluminum alloy. In these figures the grey area within the lines AA'BB' represent material within specification. Note however that the vertical lines AA' and BB' representing a hardness of R_B71, the lowest hardness acceptable by specification, will result in acceptance of material that is 4000 psi below the specification limit of 64,000 psi tensile and 12,000 psi below the specification limit of 57,000 psi yield. The possibility of error can be minimized by obtaining a conductivity reading with values falling within the parameters depicted by the shaded area of Figures 13 and 14 (5).

The correlation of conductivity to hardness of 2014-T6 alloy tested at ambient after exposure to various elevated temperatures are depicted in Figures 15 and 16 (5). The areas within the lines AA'BB' indicate material within the specification of 2014-T6 material. A conductivity above 39.5 per cent IACS is generally indicative of mechanical properties (ultimate and yield strength) below the minimum of the specification. As described earlier 2014-T6 alloy exposed to temperatures 800°F and above produce a reversal in the conductivity curve. Material suspected of reaching temperatures of 800°F and above require both a conductivity and hardness test to assist in the evaluation of the mechanical properties.

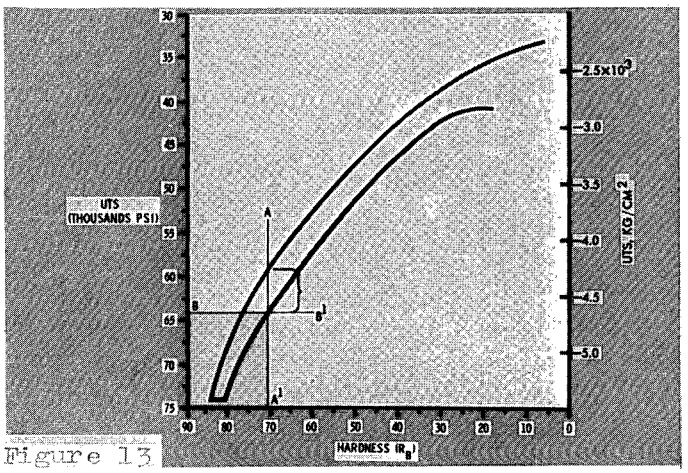

Figure 13

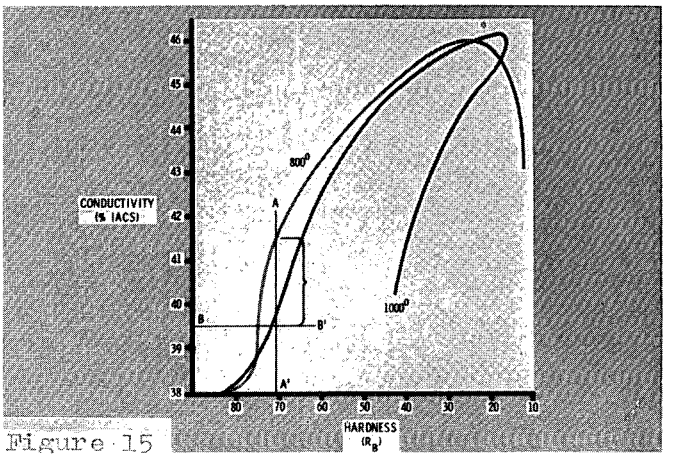

Figure 15

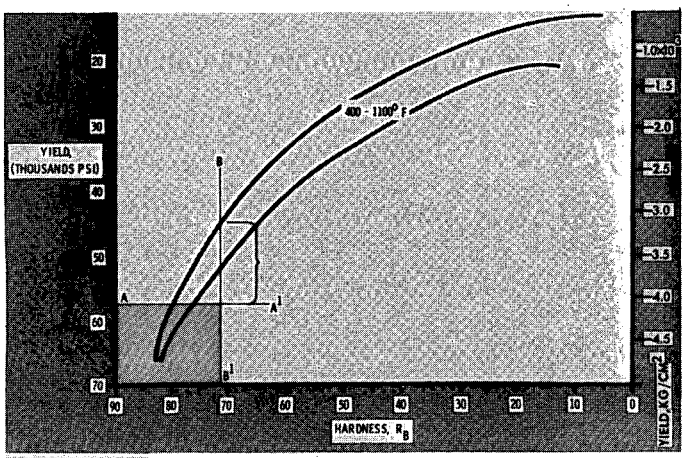

Figure 14

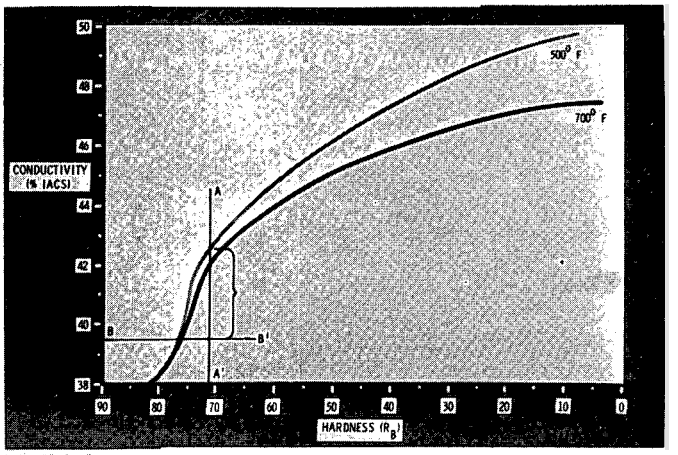

Figure 16

Figure 13. UTS vs. hardness for 2014-T6 at all temperatures. Figure 14. Yield vs. hardness for 2014-T6 at all temperature. Figure 15. Conductivity vs. hardness for 2014-T6 at 800° and 1000°F. Figure 16. Conductivity vs. hardness for 2014-T6 at 500° and 700°F.

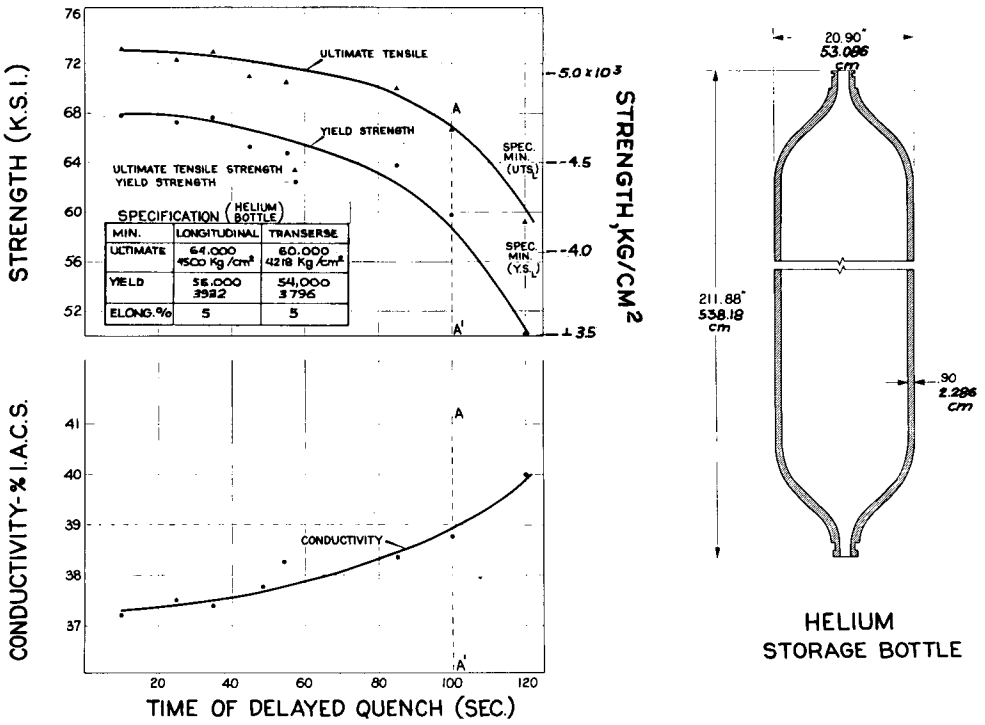

Figure 17
Properties of 2014 aluminum quench delayed and subsequently aged to T6 temper.

In selected cases the loss in the mechanical properties due to slack quenching may be evaluated by establishing the strength-conductivity relationship as shown in Figure 17. In this case the massive size, small entry and exit ports, and thick wall could produce a slack quenched condition on the inner wall of the helium storage bottle. To simulate slack-quenched conditions, a number of 1x1x8-in. 2014-T6 bars were solution-annealed and submitted to various time delays prior to quenching in water. The results are depicted by the characteristic curves for conductivity, ultimate and yield strength shown in Figure 17. Note that the vertical line AA′ through the three characteristic curves will permit material acceptance appreciably above the minimum specified mechanical properties.

Conclusions

It is concluded that: 1) A correlative relationship exists between the electrical conductivity, hardness, ultimate tensile and yield strength of aluminum alloys 7075-T6, 2014-T6, and 2024-T4; 2) Various characteristic curves for each of these alloys can be derived by using various times and temperatures to produce structural (metallurgical) changes; these changes directly affect the conductivity, hardness, ultimate tensile and yield strength; 3) By means of characteristic curves (appropriately derived to represent actual conditions) the conductivity and hardness can be used to:

(a) Verify that proper process control in heat treatment has been adhered to and that material meets specified mechanical properties.

(b) Assess the loss in mechanical properties resulting from slack quenching or overaging.

(c) Assess the loss in mechanical properties resulting from accidental fire or exposure to temperatures detrimental to the mechanical properties of the material.

(d) Verify specified mechanical properties obtained under closely controlled conditions of overaging to minimize material susceptibility to stress-corrosion.

Acknowledgments

The author expresses his gratitude to his former associates, R.A. Chihoski, D. Hunter, and R.R. Jones for the extensive testing and evaluation of data in the eddy-current studies. Appreciation is extended to K. Benjes and B. Kingsmore for metallurgical and mechanical test assistance. The author gratefully acknowledges the support of the Martin-Marietta Corporation in sponsoring these studies.

References

1. "Heat treatment of aluminum alloys, military specifications", *Military Spec.* MIL-H-6088C, Oct. 15, 1962.
2. FM-100, Magnatest conductivity meter, *Magnaflux Corpn.*, Chicago, Ill.
3. Chihoski, R. A., Jones, R. R., Hunter, D. and Seltzer, D. D. Effect of specimen thickness, cladding and lift-off adjustment on the conductivity of 7075-T6 aluminum alloy. *Proc.* 1st Nat. Symp. NDT Aircraft and Missile Components, San Antonio, Texas, Feb. 1960.
4. Chihoski, R. A., Jones, R. R., Hunter, D. and Seltzer, D. D. Effect of time and temperature exposures on the conductivity and mechanical properties of 7075 aluminum alloy sheet, using eddy-current methods. Martin Co. (Baltimore) May 1960 (*unpub.*)
5. Hunter, D. and Seltzer, D. D. Effect of time and temperature exposures on the conductivity and mechanical properties of 2014 aluminum alloy, using eddy-current methods. *Proc.*, 3rd Nat. Symp. on NDT Aircraft and Missile Components, San Antonio, Texas, Feb. 1962.

6. Martin Co. (Baltimore) Influence of chemical composition on the conductivity of wrought aluminum alloys in the T4 and T6 conditions. (*unpub.*)
7. Hunter, D., Jones, R. R., Seltzer, D. D. Effect of time and temperature exposures on the conductivity and mechanical properties of 2024-T4 aluminum alloy sheet, using eddy-current methods. *Proc.*, 2nd Ann. Symp. on NDT Aircraft and Missile Components, San Antonio, Texas, Feb. 1961.
8. King, W., Lifka, B. W. and Willey, L. A. Rapid control tests for 7075-T73 aluminum alloy products. *Materials Evaluation*, 1964.
9. Rummel, W. D. Characterization and evaluation of 2014 aluminum alloy by eddy-current conductivity techniques. *Materials Evaluation*, June 1966.
10. Hagemaier, D. and Basl, G. J. Evaluation of mechanical properties of 2014-T6 weldments by nondestructive (eddy-current) methods. *Materials Evaluation*, Jan. 1967.
11. Mueller, R. A. Relationships among the metallurgical condition, hardness and the electrical conductivity of aluminum alloys. *Thesis, Univ. Missouri*, Rolla, Miss. 1967.

Contrôles non destructifs de gaines d'éléments combustibles prototypes de réacteurs à neutrons rapides

J.-P. DUFAYET, A. SAMOEL ET B. SPRIET, FRANCE.

Introduction

Les études des réacteurs de la filière à neutrons rapides sont désormais orientées vers la réalisation de grandes centrales dont la puissance serait de l'ordre de 1000 MWe. Il a été décidé que l'étape intermédiaire entre le réacteur Rapsodie, réacteur de recherche, et les grands réacteurs industriels serait un réacteur d'une puissance de l'ordre de 250 MWe appelé Phénix. Les problèmes que soulève l'élément combustible de ce type de piles sont importants et nouveaux: ils trouvent leur origine dans les fortes puissances spécifiques et les forts taux de combustion de cette filière. Beaucoup d'incertitudes restent encore à lever avant de pouvoir fixer les limites des différents matériaux qui entrent dans la fabrication de l'élément combustible, et plus particulièrement de la gaine.

Pour le gainage, il est prévu d'utiliser l'acier inoxydable du type 316 dont la comptabilité avec l'oxyde et avec le sodium est satisfaisante (d'autres nuances de remplacement sont également envisagées: alliages à base de nickel, alliages de vanadium). Toutefois son emploi conduira vraisemblablement dans le cas de Phénix à fixer la température maximale de la gaine aux environs de 700° C. Si l'on est amené à adopter une valeur prudente du point chaud de la gaine, c'est d'ailleurs moins à cause des propriétés mécaniques de l'acier à cette température qu'en raison de notre mauvaise connaissance de l'évolution de ses propriétés sous irradiation.

On espère améliorer cette connaissance grâce à un important programme d'irradiations. Des éléments combustibles gainés d'acier inoxydable sont ou seront prochainement irradiés dans différents réacteurs à neutrons rapides aussi bien étrangers (E.F.F.B.R., D.F.R.) que français (Rapsodie). Ces expériences ont pour but de tester les solutions qui serviront de base à l'élément combustible de Phénix.

Les conditions de travail de la gaine sont particulièrement sévères. La gaine est soumise à des contraintes thermiques, et à des contraintes mécaniques dues au gonflement du combustible et au dégagement des produits de fission. La durée de vie de l'élément combustible dépend essentiellement de la tenue de la gaine; c'est pourquoi un gros effort s'est porté dans deux directions:

—choix du matériau de gainage en fonction de ses caractéristiques mécaniques à chaud et de sa résistance au fluage,

—amélioration de la qualité de la gaine.

Nous avons donc été amenés à développer des contrôles destructifs et non destructifs non seulement dans le but d'éliminer des gaines défectueuses, mais aussi de faire progresser les techniques de fabrication dans le sens de l'homogénéité des différents lots de tubes. Nous nous limiterons, dans cette communication, à décrire les méthodes d'essais non destructifs qui ont été utilisées pour contrôler des gaines destinées à être irradiées dans des réacteurs comme E.F.F.B.R., D.F.R., Rapsodie, EL III . . . Les contrôles ont été de plusieurs types: métrologie, courants de Foucault, ressuage fluorescent, essais sous pression interne. Les gaines sont constituées de tubes lisses, sans soudure, en acier inoxydable 316 (X 18 M Aubert et Duval); les diamètres intérieurs ont varié entre 5.20 mm et 6.25 mm, et les épaisseurs entre 0.35 mm et 0.45 mm (longueur maximale 1300 mm). Notre expérience actuelle se limite au contrôle d'environ un millier de tubes.

Métrologie

Appareillage

On dispose d'un banc EAM adapté aux nécessités de cet examen. Ce banc permet l'enregistrement continu des diamètres intérieurs et extérieurs de tubes d'une longueur maximale de 1.50 m; remarquons que, pour les diamètres intérieurs, il faut opérer «à la retourne», c'est-à-dire en mesurant sur 75 cm à partir de chaque embouchure.

Cet appareil se compose principalement (figure 1):

—d'une gouttière de guidage où le tube est poussé à la vitesse de 0.5 cm/s par une «locomotive» électrique;

—d'une tête de mesure transformant les variations de diamètre extérieur en signaux électriques par l'intermédiaire d'une capacité variable;

—d'une tête de mesure pour les diamètres intérieurs équipée d'un Diatest;

—d'un tiroir amplificateur qui permet d'injecter des données de chacune des têtes de mesure dans un enregistreur potentio-métrique à deux voies (un topeur repère les distances).

Il y a possibilité d'enregistrement simultané soit du diamètre intérieur et du diamètre extérieur, soit de l'une de ces données et de l'épaisseur (en faisant la différence). La gamme de mesure est comprise entre 4 et 8 mm; on dispose pour les étalonnages d'un jeu de piges et de bagues calibrées. La métrologie se fait en continu suivant deux génératrices à 90° l'une de l'autre; la figure 2 montre la métrologie d'un tube présentant des surépaisseurs de l'ordre de 10μ à une extrémité.

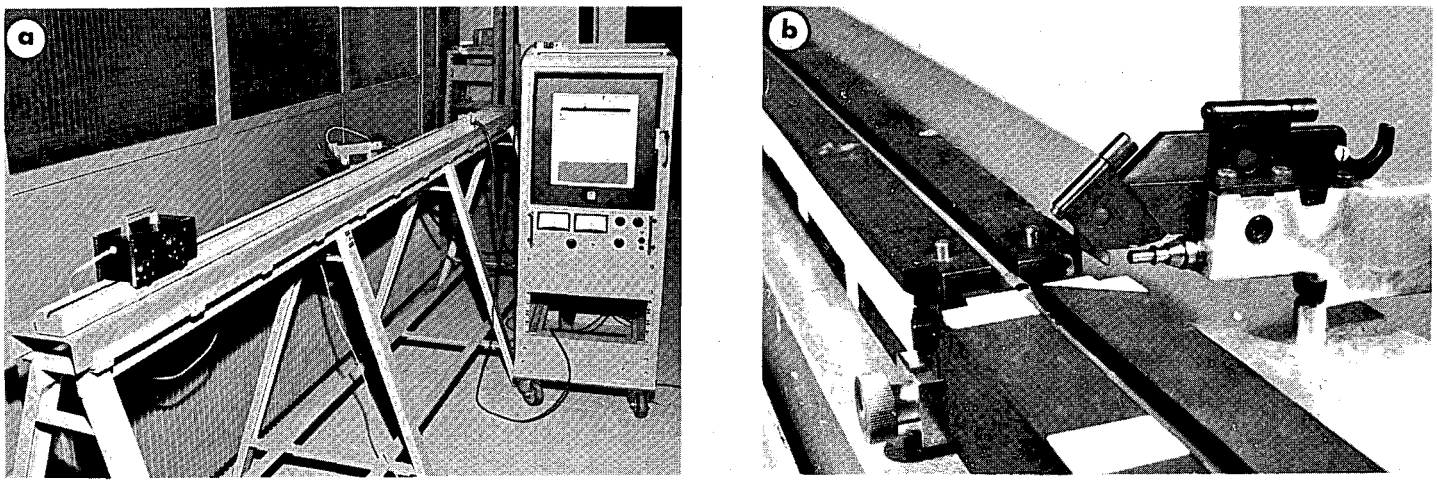

Figure 1. Banc de métrologie. a) vue d'ensemble; b) têtes de mesure.

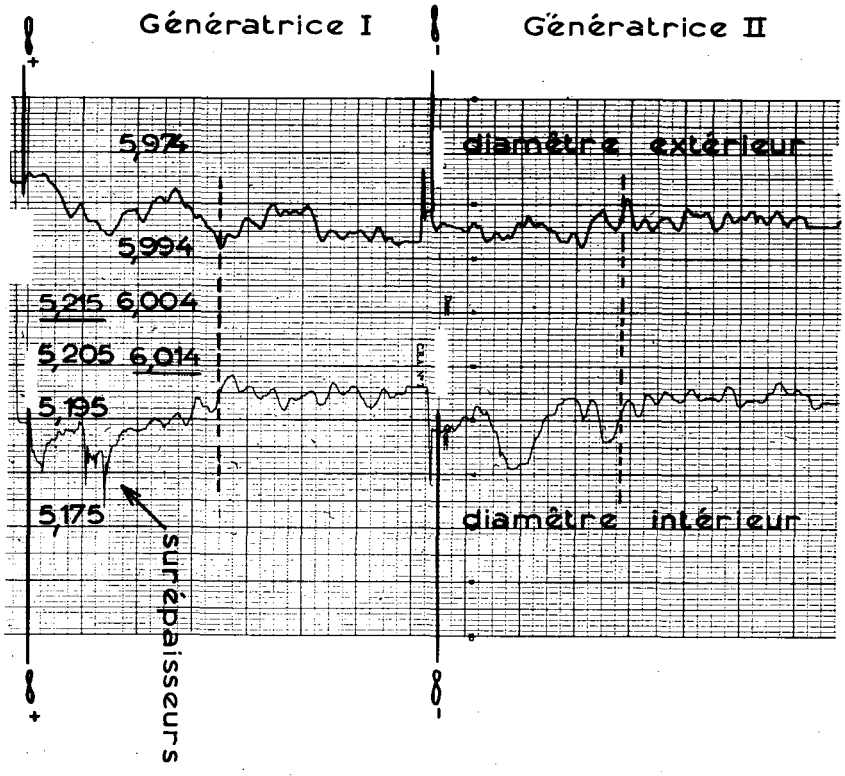

Figure 2
Courbes d'enregistrement métrologiques.

Discussion

La métrologie exige de sérieuses précautions pour obtenir une précision supérieure à 5μ sur le diamètre extérieur; sur le diamètre intérieur, la précision est voisine de .01 mm. Si les valeurs absolues ne sont connues qu'à 5μ près, par contre il est facile d'obtenir le micron en valeur relative. En ce qui concerne les dimensions des tubes, nous atteignons les limites de l'appareil précédent pour la mesure du diamètre intérieur sur une telle longueur.

Une autre faiblesse de l'appareil tient à sa faible vitesse de défilement qui entraîne des durées d'examen trop importantes quand le nombre de tubes dépasse la centaine. Comme nous pensons, dans l'avenir, avoir à contrôler plusieurs milliers de gaines à la fois, nous nous orientons vers une solution différente: mesure du diamètre extérieur par jauges mécaniques ou pneumatiques, mesure directe de l'épaisseur par ultra-sons (méthode de résonance). De cette façon, les problèmes posés à la fois par la longueur de la gaine et par le débit d'examen se trouveront résolus sans trop de difficultés.

Contrôle par courants de Foucault

Appareillage

Deux appareils différents ont été utilisés: le «Défectographe Förster» (figure 3a) et un montage de laboratoire (figure 3b). Nous ne reviendrons pas sur la description du premier appareil qui est bien connu. Rappelons seulement ses deux caractéristiques principales: une sélection de phase qui permet d'éliminer certaines variations d'impédance par un choix de l'axe de projection, un dispositif de différentiation qui favorise les impulsions rapides aux dépens des variations lentes.

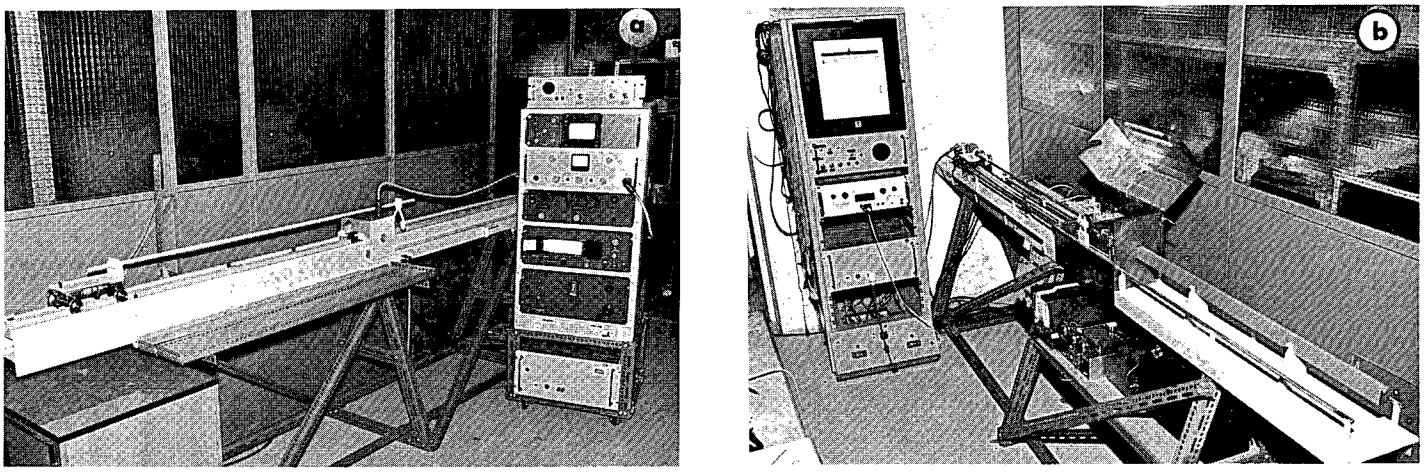

Figure 3. Appareils courants de Foucault. a) banc Förster; b) banc de laboratoire.

Le montage de laboratoire se compose essentiellement de deux bobines identiques encerclant le tube; elles sont placées côte à côte à une distance de 1 mm environ. Chaque bobine constitue à elle seule un circuit résonant parallèle (figure 4a), les oscillations étant entretenues par une triode (oscillateur Hartley: figure 4b). Les défauts, en modifiant le cours des courants induits dans le tube, provoquent des variations d'impédance de la bobine qui se répercutent sur la fréquence et l'amplitude des oscillations.

Ce système présente la particularité d'avoir un fort coefficient d'inductance mutuelle entre les deux bobines; le couplage est tel que les deux oscillateurs oscillent sinusoïdalement à la même fréquence. Lorsqu'un défaut apparaît au droit de la première bobine, il perturbe non seulement le premier circuit, mais aussi le second par suite de couplage.

En comparant les tensions V_{g1} et V_{g2} de chaque canal, on obtient une excellente sensibilité de détection. Cette tension V_g varie comme l'amplitude dans la mesure où les oscillations sont bien sinusoïdales. On constate que le passage d'un défaut dans la première bobine diminue V_{g1} et augmente simultanément V_{g2}; la différence V_{g1}-V_{g2} subit donc des variations importantes. Par contre des mesures de fréquence montrent que les variations de fréquence de l'ensemble des deux oscillateurs couplés sont du même ordre de grandeur que celles d'un seul oscillateur. Il y a donc intérêt à prendre un signal proportionnel aux variations d'amplitude des oscillations.

Le couplage se dose en ajustant la distance entre bobines. La sensibilité est maximale quand le coefficient de couplage est juste suffisant pour réaliser un accrochage des oscillateurs; quand le couplage dépasse cette valeur, la stabilité de l'ensemble augmente mais la sensibilité diminue. Les conditions de couplage peuvent être réalisées à volonté pour des valeurs très différentes de l'inductance mutuelle des deux bobines.

Le montage s'avère particulièrement adapté à la détection de défauts bien localisés (inclusions, fissures) puisque l'on compare deux portions très voisines du tube; au contraire les variations lentes dues à des changements dimensionnels (diamètre, épaisseur) sont absorbées. Cet effet peut encore être accentué

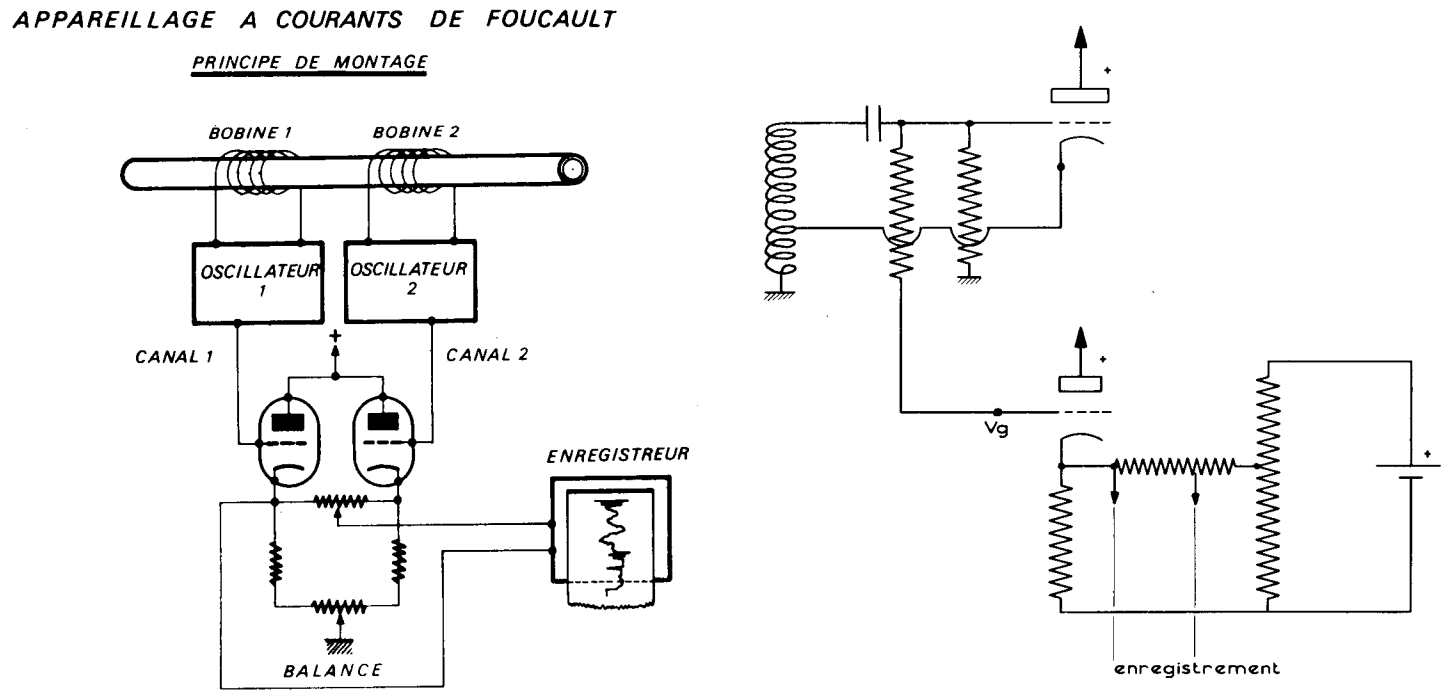

Figure 4. Courants de Foucault—Banc de laboratoire. a) principe de montage; b) schéma de l'oscillateur.

Figure 5a

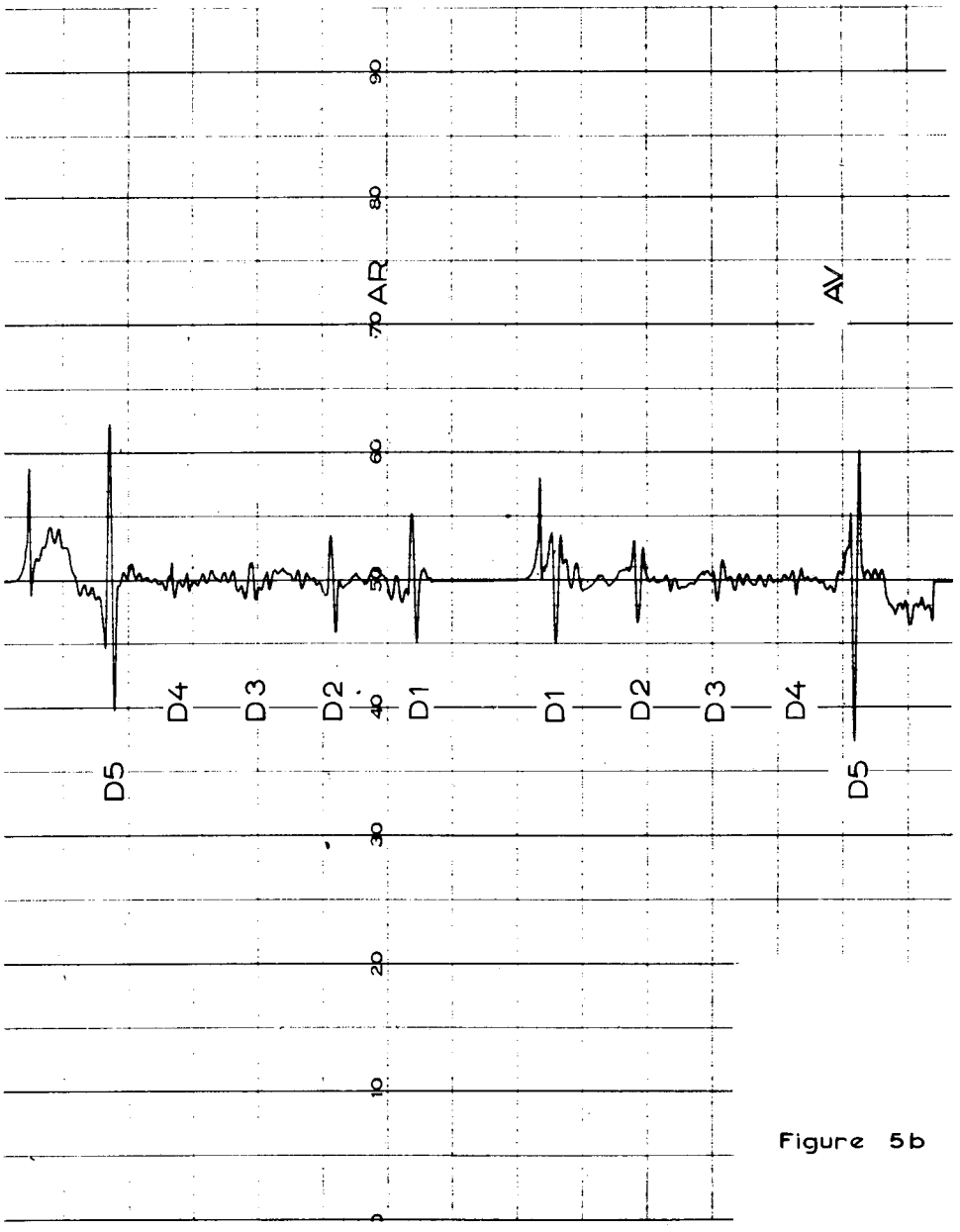

Figure 5b

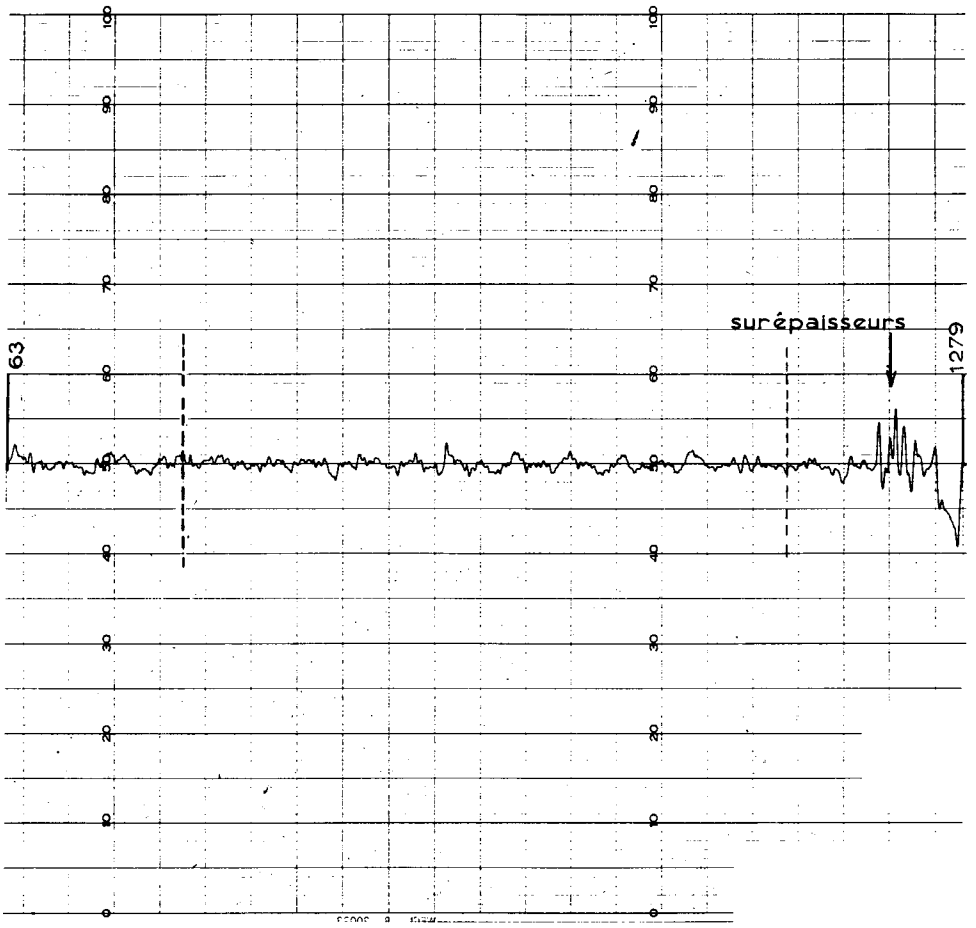

Figure 5 d

Figure 5
Courbes d'enregistrement aux courants de Foucault. a) signaux étalons au banc Förster; b) signaux étalons au banc de laboratoire; c) enregistrement d'un tube présentant des surépaisseurs internes (banc Förster); d) même tube au banc de laboratoire.

par l'emploi d'une différentiation. La sensibilité aux petits défauts sera augmentée en réduisant la longueur des bobines, et en limitant le champ extérieur.

Discussion

L'appareil «Förster» fonctionne avec une fréquence de 100 Kc tandis que le montage de laboratoire utilise une fréquence de l'ordre de 400 Kc. Il s'ensuit que le premier mettra mieux en évidence les défauts de la surface intérieure du tube, en particulier les surépaisseurs (figures 5c et 5d); il permet d'autre part d'augmenter le débit du contrôle grâce à sa grande vitesse de défilement (de l'ordre de 50 cm/s) et à ses possibilités d'enregistrement rapide. Par contre le banc de laboratoire a l'avantage de présenter une meilleure sensibilité pour plusieurs motifs: choix de la fréquence, faible vitesse de défilement (voisine du cm/s) limitant les perturbations apportées par des vibrations éventuelles, phénomène de couplage.

Le réglage des appareils se fait à l'aide de défauts étalons usinés sur un tube par électro-érosion. Suivant les cas et la sévérité du contrôle, on utilise des défauts de différentes dimensions et de différentes natures: trous, rayures transversales ou longitudinales, externes ou internes. La taille de ces défauts artificiels est mesurée directement sur des répliques. Les tubes sont alors classés en catégories, en prenant comme référence le

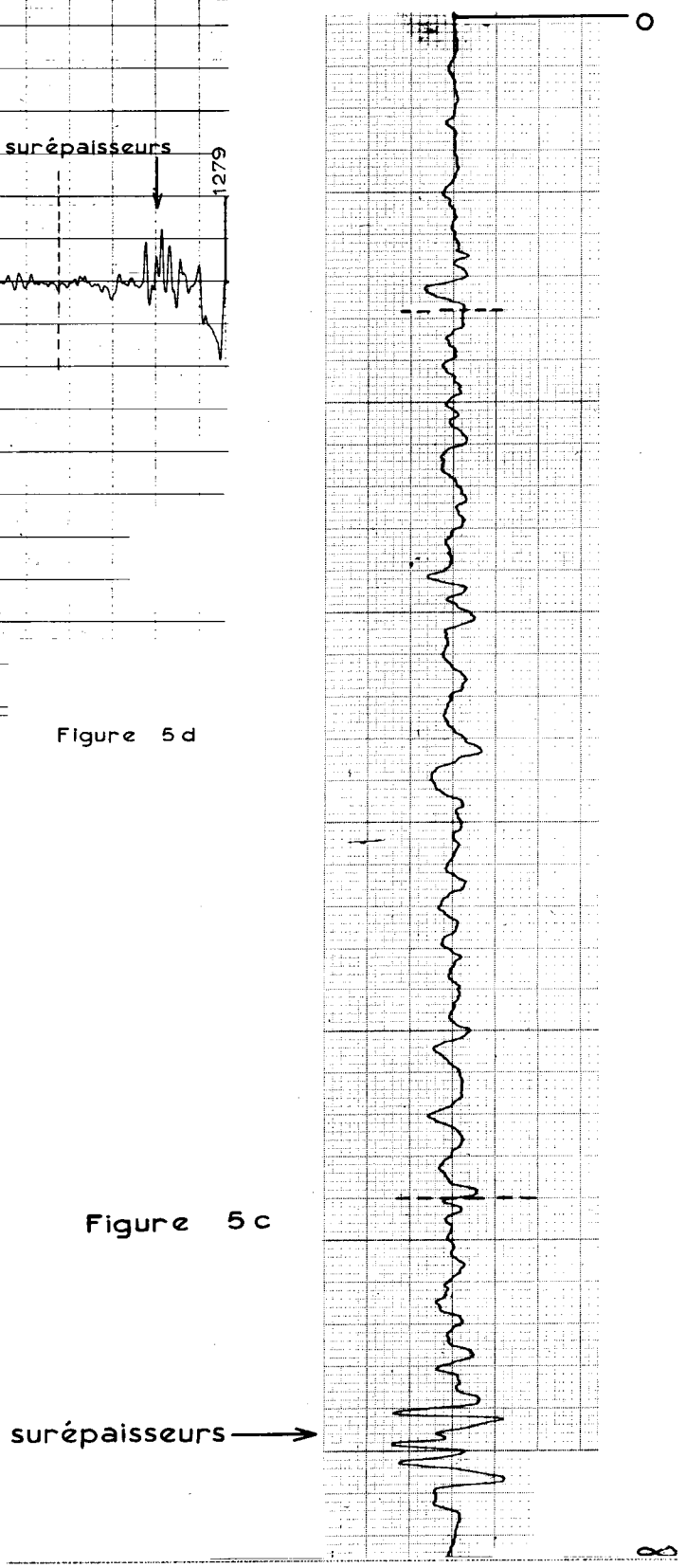

Figure 5 c

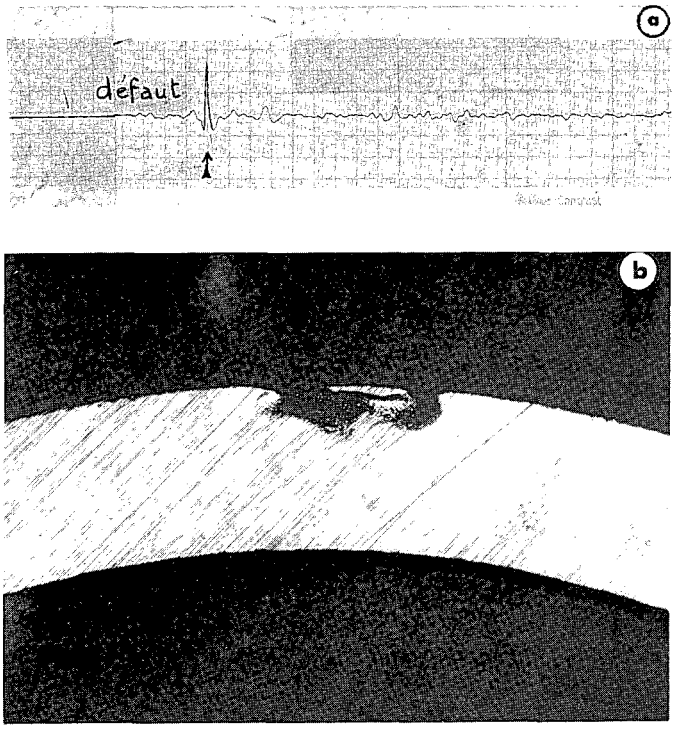

Figure 6. Défaut aux courants de Foucault. a) courbe d'enregistrement; b) défaut correspondant X 75.

signal donné par un défaut étalon. Les figures 5a et 5b montrent par exemple des signaux étalons correspondant à des défauts D_1 trou de diamètre 230μ, D_2 trou de diamètre 180μ, D_3 fente longitudinale (longueur 3 mm, largeur 90μ, profondeur 25μ), D_4 fente transversale (longueur 2 mm, largeur 80μ, profondeur comprise entre 25 et 40μ), D_5 trou de diamètre 320μ. Le signal donné par le défaut transversal ne se détache pas nettement du bruit de fond; viennent ensuite par ordre d'importance les signaux du défaut longitudinal, des trous de 180μ, 230μ, 320μ.

Les indications fournies par ces deux bancs (banc Förster et banc de laboratoire) sont assez complémentaires et nous les employons dans une optique différente. Tous les contrôles débutent par un examen à l'appareil «Förster» qui élimine rapidement les tubes ayant des défauts bien apparents, du type reproduit sur la figure 5 bis. Le banc de laboratoire permet alors une recherche plus approfondie des défauts, ainsi que leur localisation précise. Ce stade se révèle indispensable si l'on veut progresser dans l'identification des signaux, identification qui peut se faire par une étude micrographique (coupes successives dans la zone défectueuse), par une analyse de la forme du signal (les surépaisseurs donnent en particulier des signaux très caractéristiques), par des mesures de déphasage, d'amplitude, de fréquence...

Mais il faut bien avouer que, souvent, le problème reste entier, et c'est là la principale faiblesse de ce contrôle. Néanmoins nous continuons à développer le contrôle par courants de Foucault en raison de sa sensibilité, de son grand débit d'examen et de ses facilités d'automatisation. Notre objectif le plus immédiat consiste à monter un banc à très forte vitesse de défilement (voisine du m/s) utilisant le montage à bobines couplées. Nous pourrons aborder sans arrière-pensée un contrôle de série portant sur plusieurs milliers de tubes.

Contrôle par ressuage fluorescent

Généralités

Le ressuage fluorescent est basé sur le principe des liquides pénétrants. Pour augmenter le contraste et la sensibilité de la méthode, nous avons utilisé un pénétrant fluorescent, non lavable à l'eau (Zyglo Pentrex ZL 22). Le pénétrant ne peut être éliminé directement; il faut avoir recours à une étape intermédiaire qui est l'émulsification.

Les différentes phases du traitement se résument ainsi. La gaine, après un bain dans le pénétrant, est plongée dans l'émulsifiant (Zyglo Pentrex ZE 2) puis lavée. Le mélange pénétrant-émulsifiant est plus ou moins lavable suivant la concentration. En surface, le pourcentage de pénétrant est suffisamment faible pour que le lavage l'élimine totalement; par contre, dans les défauts, la concentration de pénétrant est trop importante pour que le mélange soit lavable. Les opérations suivantes consistent en un séchage puis un développement à l'aide d'une poudre très fine qui amène le pénétrant en surface.

L'observation de l'extérieur des gaines ne pose pas de problèmes particuliers; elle se fait en lumière ultra-violette. Pour l'examen intérieur, nous employons un endoscope à vision directe avec illuminateur séparé (figure 7a). Un dispositif d'entraînement automatique déplace la gaine par rapport à l'illumination et permet ainsi une vision continue sur toute la longueur (figure 7b); pour diminuer la fatigue de l'observateur, nous disposons d'un système de télévision en circuit fermé.

Discussion

Le ressuage fluorescent se révèle comme un outil complémentaire très utile. Grâce à l'endoscope, il est possible d'identifier certains défauts internes sans détruire la gaine; des défauts qui avaient une importance inquiétante aux courants de Foucault s'avèrent tout à fait inoffensifs: c'est le cas en particulier des surépaisseurs. Ces surépaisseurs sont très visibles, même en lumière ordinaire (figure 7c); elles se situent à 120° l'une de l'autre dans un plan diamétral. Pour cette raison, nous pensons qu'elles reproduisent des empreintes laissées sur le mandrin au cours de l'usinage.

En dehors du fait que le contrôle se limite à un aspect superficiel, le ressuage présente quelques inconvénients majeurs. En premier lieu, il fait appel uniquement au jugement personnel de l'observateur. L'importance de la tache fluorescente, et son intensité, lui donnent des indications sur le danger que peut présenter le défaut; la décision est prise en se basant sur l'expérience qu'il a de cette méthode. Ensuite le ressuage ne laisse aucune trace concrète du contrôle; pour pallier cette défaillance, nous avons monté un magnétoscope qui enregistre l'image télévisée. Ce début d'archivage est cependant loin d'être parfait car le dépouillement des renseignements consignés sur la bande magnétique ne peut se comparer à la lecture rapide et directe d'une courbe.

Nous considérons donc le ressuage comme une méthode d'appoint, limitée à des séries de gaines ne dépassant pas la centaine. Malgré sa lenteur et sa difficulté d'automatisation, ce contrôle est particulièrement efficace et sensible quand il s'agit de tubes aux formes complexes (gaines à ailette par exemple) qui se prêtent assez mal à d'autres essais non destructifs.

Essais sous pression interne

Conditions expérimentales

Après les contrôles par métrologie, courants de Foucault et ressuage fluorescent, les gaines ont été testées sous pression interne. La pression d'essai est définie par la norme ASTM 450

$$P = \frac{2\delta e}{D}$$

δ = contrainte exercée sur la paroi du tube

e = épaisseur du tube

D = diamètre extérieur

Nous avons utilisé systématiquement comme valeur de référence une contrainte de l'ordre de 17 kg/mm². Ce contrôle comporte trois étapes:

Figure 7
Endoscope. a) schéma; b) banc de défilement; c) aspect des surépaisseurs internes.

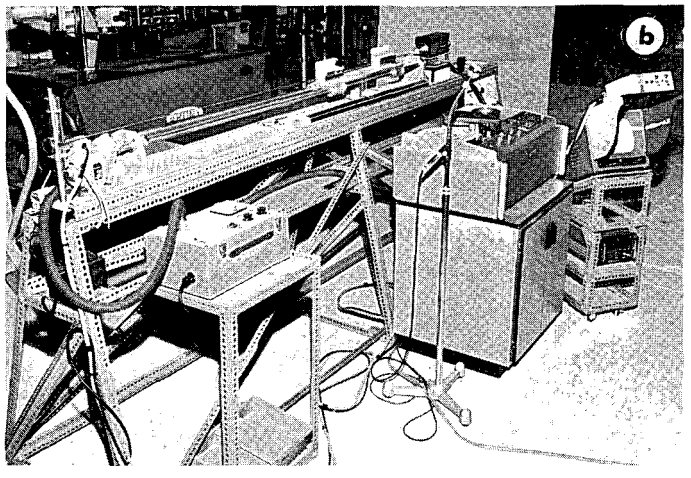

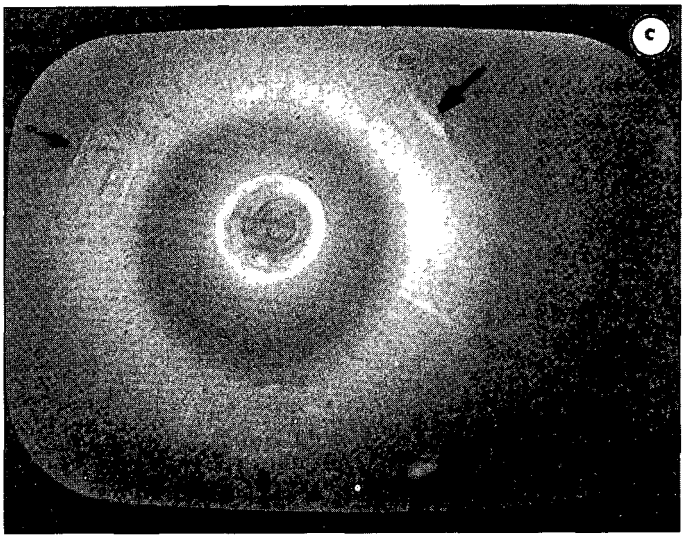

—une métrologie avant mise en pression
—essai en pression pendant 5 secondes
—une métrologie après mise en pression.

Les mesures se font suivant deux génératrices à 90° l'une de l'autre à l'aide du banc décrit au paragraphe II-1; nous nous sommes limités à une métrologie du diamètre intérieur et nous avons comparé les enregistrements obtenus avant et après pression.

L'essai est réalisé sous pression d'huile à température ambiante. La pression est obtenue au moyen soit d'un vérin hydraulique, soit d'un multiplicateur oléo-pneumatique. Des embouts avec joints toriques assurent l'étanchéité aux deux extrémités du tube. La figure 8 montre un banc permettant la mise en pression simultanée de huit tubes.

Discussion

Cet essai est non destructif, c'est-à-dire qu'il ne doit pas entraîner de déformations importantes empêchant l'utilisation ultérieure du tube. Dans les conditions choisies, l'augmentation de diamètre est en général très inférieure à 10μ, mais il y a la plupart du temps une déformation résiduelle permanente décelable par une métrologie soignée (bien que la contrainte maximale dans le tube soit bien inférieure à la limite élastique à 0.2% de l'acier).

Dans notre appréciation, nous tenons compte de l'allure de la déformation (progressive ou brutale), des déformations maximales et moyennes, de la longueur de la zone déformée, de la concordance de cette zone avec des défauts décelés aux autres contrôles. Cet essai sous pression interne peut révéler des défauts importants mais il n'a pas la sensibilité des méthodes précédentes. Il a l'avantage de faire travailler le tube dans des conditions relativement proches de la réalité et de tester son comportement d'ensemble; il est d'autant plus représentatif qu'il est effectué à une pression interne élevée mais la valeur de cette pression est limitée par les déformations qu'il est possible d'accepter.

Il n'y a pas de problèmes insurmontables dans l'extension de ce contrôle à de grandes séries; la cadence des essais dépend, pour la plus grande part, de la métrologie.

Conclusion

Dans cette série de contrôles, nous avons tout d'abord le souci de trier les tubes pour en retenir finalement les meilleurs. Le choix des critères de sélection se fait arbitrairement: tolérances en métrologie, amplitude du signal étalon aux courants de Foucault, opinion personnelle de l'observateur au ressuage, déformations maximales admissibles aux essais sous pression interne. Nous arrivons donc en fin de circuit à séparer les tubes

en lots parfaitement homogènes, répondant à des critères bien définis; plus les critères sont sévères, plus l'homogénéité du lot est grande.

Si nous pouvons classer les lots les uns par rapport aux autres en valeur relative, par contre une telle façon de procéder ne nous autorise pas à porter un jugement sur la qualité d'une fabrication. Cette étape sera franchie à partir du moment où il sera possible d'identifier sans hésitation tout défaut détecté. Dores et déjà, il nous a été possible de révéler la présence de défauts bien caractéristiques, se présentant sous la forme de surépaisseurs locales sur la paroi interne du tube. Après avoir décelé l'origine de cette imperfection (défauts d'usinage des mandrins utilisés lors de l'étirage), la méthode de fabrication a été modifiée en conséquence.

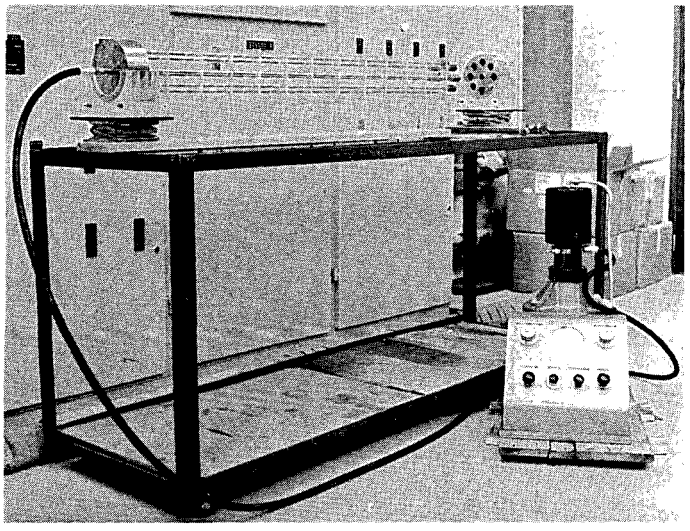

Figure 8. Banc d'essais sous pression interne.

L'accomplissement de cette étape «identification» doit faire l'objet d'une recherche longue et minutieuse; cette recherche est actuellement en cours chez nous. Elle ne peut aboutir qu'en élargissant le nombre de contrôles, aussi bien destructifs que non destructifs. Chaque type de contrôle a un domaine de sensibilité bien spécifique; les courants de Foucault sont sensibles aux variations locales de résistivité et de perméabilité (écrouissage, précipités magnétiques . . .), par contre les ultrasons réagiront mieux à des discontinuités de structure (fissures, trous . . .).

Pour augmenter notre source de renseignements, nous serons donc amenés dans l'avenir à développer le contrôle par ultra-sons, non pas comme une méthode concurrente des courants de Foucault mais comme une méthode complémentaire. D'autres indications nous sont apportées par des examens micrographiques en coupes successives; ils ont l'avantage de révéler la nature du défaut détecté et de relier directement le signal à un défaut visible.

Une dernière étape, et non la moindre, consiste à répondre à cette question: «dans quelle mesure les zones défectueuses ont-elles une importance sur la tenue mécanique de la gaine?». Il est bien évident qu'une surépaisseur, dans le genre de celles qui ont été mises en évidence au cours de ces contrôles, ne présente aucun danger; elle ne peut que gêner le remplissage du tube par les pastilles de combustible. Seuls des essais mécaniques nous permettent de voir à quel point les zones anormales correspondent à des zones de faiblesse réelle du tube. C'est dans cet esprit que nous effectuons des essais à caractère purement technologique: traction, fluage sous pression interne, fatigue sous contrainte cyclique.

En définitive, il faut sans cesse créer des méthodes plus perfectionnées de contrôles destructifs et non destructifs. À un stade préliminaire, elles servent à classer et à normaliser les lots de tubes. Ultérieurement les renseignements tirés de ces contrôles se révèlent indispensables pour corriger éventuellement les gammes de fabrication, de façon à assurer une production homogène et reproductible.

Technical Session 10/ Ultrasonics at Elevated Temperatures

Ultrasonic Testing of Solids at Elevated Temperatures

LAWRENCE C. LYNNWORTH AND EDMUND H. CARNEVALE, USA

ABSTRACT: High-temperature ultrasonic tests are required to measure and control materials early in processing. Illustrative examples at temperatures above 1000°K include thickness and temperature measurements in continuous casting of steel, and "pipe" detection to guide steel billet cropping. Laboratory studies up to 2800°K have demonstrated the feasibility of applying ultrasonics to these nondestructive testing problems. Longitudinal and shear waves are momentarily coupled at high pressure to bulk specimens. It is shown that shear waves offer some unique advantages over longitudinal waves, and that sometimes both waves are required to characterize a material ultrasonically. Techniques are described for measuring average temperature and temperature distribution within a solid along a chosen path by exploiting the temperature dependence of longitudinal wave velocity, shear wave velocity, and/or Poisson's ratio. In addition to the above nondestructive testing applications, high-temperature ultrasonic tests provide information on basic physical properties of solids. Using the Pana-Therm thin refractory wires have been ultrasonically tested beyond 3000°K. Results are presented for Mo and Re.

Introduction

At room temperature, ultrasonic testing of solids is now fairly common, both in nondestructive testing applications, and in the determination of elastic properties. At elevated temperatures, however, particularly above ~1000°K, ultrasonic testing of solids is rather uncommon. There are two obvious reasons for this. First, the need for high-temperature measurements has not been generally recognized or established. Second, transducer materials and coupling techniques suitable for routine, automatic ultrasonic testing at high temperature, have not been available.

The need for high-temperature NDT becomes more apparent if one accepts the argument that it is desirable to locate and evaluate defects or departures from specifications at their earliest occurrence, so that further work is not wasted on defective material. In a high-temperature process this implies high temperature NDT.

The need for high-temperature elastic properties data has become urgent this past decade, stimulated largely by the entry into and re-entry from space. Materials for rocket engines, heat shields, aerospace structures, and related experiments, must now perform reproducibly and maintain integrity at elevated temperature even up to their destruction temperatures. Tests have shown that ultrasonics can not only measure elastic properties up to the melting point, but also can provide information on other physical, metallurgical and chemical properties such as phase changes, recrystallization, carbiding, nitriding, etc.

Having thus pointed up the need for high-temperature measurements, particularly ultrasonic measurements, there remains the task of choosing or developing the required sound generating, detecting and coupling means for problems of interest. To simplify this presentation, we group the measurement problems into two areas, according to whether the specimen is of (1) bulk form (cross-sectional dimensions $> 5\ \lambda$), or (2) thin wire form (dia $< \lambda/10$).

For testing bulk solids, the commonly used NDT transducers are limited by Curie points substantially below 1000°K. Likewise the usual couplants would vaporize or ignite at elevated temperatures. By using high-pressure momentary dry contact, however, these limits have been avoided. Thus, MHz waves have been transmitted through bulk solids up to 2800°K, using no couplant at all. Dry high-pressure momentary contact is effective for both longitudinal and shear waves at elevated temperature. Such tests on bulk solids so far have been conducted on a laboratory scale. Extending these tests to production line NDT of bulk metals up to their melting point appears feasible. We consider three applications for which, in the laboratory, the momentary contact technique has been shown feasible: (1) thickness, (2) thermometry, and (3) defects such as "piping." Taking steel as an example, these three NDT problems are discussed in the temperature range ~1000 to 1800°K.

For specimens in wire form, where elastic and other properties are required up to the melting point, we have developed a new instrument, the Pana-Therm. This instrument automatically measures transit time of longitudinal (extensional) and torsional shear waves in a specimen, from which sound velocity and related quantities are derived. Attenuation can also be measured as a function of temperature.

Ultrasonic Testing of Bulk Solids

Momentary Contact, High-Pressure Coupling of Longitudinal and Shear Waves

In the past five years, the authors have found that many bulk solids—metals, ceramics, graphites, plastics, composites—can be tested with momentary contact techniques, at elevated temperatures which in some cases range up to 2800°K (1). The brief contact, ~0.1 second, is quite sufficient for ultrasonic pulses to interrogate the hot material, yet short enough that the specimen temperature is essentially unperturbed, and also short enough that the transducer is not overheated. Although ordinary couplants can survive very brief exposure to temperature above 1000°K, we found that couplants are not necessary at all, if sufficient pressure is applied between transducer probe and specimen. For machined surfaces, pressures of ~1000 psi suffice for longitudinal and shear waves. For rougher surfaces, high pressures are required: ~10,000 to 30,000 psi or higher. On the other extreme, if both probe and specimen are optically flat and are brought together into optical contact, no further coupling pressure need be applied. By avoiding the usual fluid

couplant, both longitudinal and shear waves can be momentarily pressure-coupled simultaneously across the same boundary.

Details of these techniques and their application to elastic moduli determinations have been presented elsewhere (1). Accordingly we describe three NDT applications: measurement of (1) thickness, (2) temperature, and (3) defects, in bulk steel between ~1000°K and the melting point, ~1800°K.

Measurement of Thickness

At room temperature, thickness is readily measured with ultrasonic resonance or pulse techniques, provided the material (i.e., its sound velocity), is known. At elevated temperature, however, owing to generally higher attenuation and rough surface conditions, pulse techniques are preferred. Unless sound velocity is known, steel thickness errors as large as 50% are possible, near the melting point. Through suitable measuring techniques, however, accuracies of 1% are attainable.

In steel processing above 1000°K, there are several situations where thickness measurements are desired. Examples include wall thickness of seamless extruded tubing (typical range, ~0.3 to 5 cm, on tubing of O.D. 25 cm), and solid-skin thickness of continuous cast steel (typical range, ~0.5 to 2.5 cm, on emerging from mold, to ~2.5 to 10 cm just before pinch (reducer) rolls or stirring coils). The continuous casting problem is discussed below, to illustrate the application of ultrasonics up to the melting point of steel, to show some of the advantages of shear waves over longitudinal waves, and to indicate the measurement possibilities using both waves simultaneously.

In continuous casting, molten metal passes from a ladle through a tundish, through a water-cooled copper mold, and then through various rolls. Details may be found in the literature.

The solidification front, or liquid/solid interface, is not smooth, due to dendritic growth. To simplify calculations, however, it is convenient initially to consider the interface smooth, corresponding to an abrupt acoustic impedance change. With this approximation, and using published data for density and sound velocity just above and just below the melting point, one can readily calculate that the amplitude reflection coefficient for longitudinal waves is about 10%. For shear waves, the reflection coefficient is 100%, because the molten metal cannot support a shear wave, and so exhibits a shear wave impedance value of zero. Theoretically, then, both longitudinal and shear waves can be reflected off the liquid/solid interface, but shear waves should provide ten times more sensitivity.

To determine whether ultrasonic pulses could be reflected from a liquid steel/solid steel interface under conditions simulating the continuous casting process to some degree, the following experiment was conducted. Cylindrical steel specimens, ~1 to 3 cm dia × 10 to 20 cm long were fitted with a water jacket (Figure 1) and a graphite sleeve (not shown) to contain the molten steel. A longitudinal or shear wave crystal, 0.5 to 3 MHz, was bonded to the cooled end. The opposite end, which was surrounded by a graphite sleeve, was subjected to an electric arc from a dc plasma torch operated at ~60 kw in the transfer mode. With the arc established, one end of the specimen was quickly heated to the melting point, and the curved molten interface advanced ~1 to 1.5 cm into the specimen. With the arc extinguished, the molten layer solidified. Oscillograms were photographed every few seconds during these runs, and were simultaneously observed continuously on another oscilloscope.

Results were that both longitudinal and shear waves were reflected at the liquid/solid interface. When the arc was first established, and the specimen heated up, but was not yet molten, the transit time increased. Then, after about 5 seconds, as melting proceeded, transit time decreased, corresponding to a shorter solid path. From the measured decrease in transit time, the liquid depth was estimated, and confirmed by momentarily dipping a fused silica rod into the molten pool immediately after turning off the arc. A second confirmation was obtained by noting, after complete solidification, the obvious change in appearance near the specimen's end. The characteristic oscillogram sequence showed the transit time increasing (on heating, before melting), then decreasing (during melting), increasing again (on solidification), and finally decreasing somewhat (on cooling in the solid state), approaching the initial value except for lost material. (This dynamic pulse transit time behavior is somewhat similar to that observed in ultrasonic ablation studies) (2).

From these observations, it was concluded that both longitudinal and shear waves offer a feasible, practical approach to measuring the thickness of continuous cast steel. (Kurz and

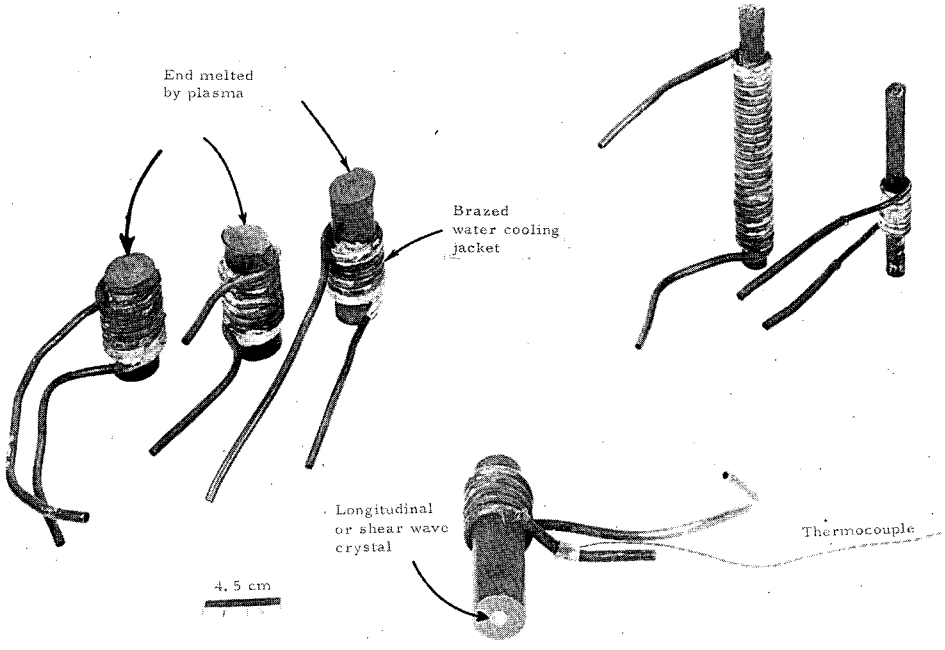

Figure 1
Some of the samples used in laboratory study which demonstrated the feasibility of ultrasonically measuring the thickness of continuous-cast steel.

Lux(3) independently found that *longitudinal* wave echoes can be received from solidification fronts in metals.) While the shear waves theoretically offer ten times more sensitivity than longitudinal waves, in our tests only a marginal advantage was apparent. However, if an additional requirement is considered, namely, that the probe or buffer rod shall have as small a diameter as possible, (in order to fit between existing closely-spaced rolls, and further, to achieve high pressure coupling, up to ~10,000 psi with minimum thrust) the shear waves offer a clear advantage. Because of this geometric restriction on allowable probe diameter, if a longitudinal wave were used, a series of unwanted echoes would follow the probe's end echo, due to mode conversions within the probe. Taziri et al.(4) point out the difficulty of suppressing such unwanted, spurious echoes. Using a shear-wave probe, however, echoes due to mode conversion are avoided. During the past two years, shear-wave probes have been in use at one steel company, to measure skin thickness of continuous-cast steel on a laboratory basis. It is hoped that the results of this program can be disclosed later this year.

[*Note added in proof:*

Other methods of avoiding the spurious echoes usually generated in the buffer between transducer and part being tested are also under investigation. Extensional waves in a bundle of wires, concentric tubes, roll of sheet metal, etc., for example, provide interesting alternatives to shear waves in a solid buffer rod, for NDT, especially at high temperature.]

To illustrate another application of shear waves, this time in conjunction with longitudinal waves, consider the problem of interpreting the measured ultrasonic transit time in terms of thickness. Assuming sound velocities have been measured as a function of temperature, to the melting point (Figure 2), one still needs to know the temperature. Depending on the thickness accuracy required, the temperature sometimes may be known accurately enough, based on theoretical considerations, or based on optical or thermocouple readings, or ultrasonic readings parallel to the surface, across a known path. If, however, temperature is not known accurately enough, so that there are really two unknowns, thickness and temperature, the following approach may be used.

This approach exploits the temperature dependence of Poisson's ratio. Since there are two unknowns, two independent measurements are required. Suppose these two measurements are longitudinal and shear-wave transit times, τ_L and τ_T, respectively, both measured over the same path. In a specimen of unknown thickness X and unknown temperature T (assumed uniform for the moment), the transit times are simply

$$\tau_L = X/V_L \text{ and } \tau_T = X/V_T$$

where V_L and V_T are longitudinal and shear-wave velocity, respectively. The ratio of these transit times is

$$\frac{\tau_L}{\tau_T} = \frac{V_T}{V_L} = \sqrt{\frac{1-2\sigma}{2(1-\sigma)}}$$

where σ = Poisson's ratio. The temperature dependence of σ is shown in Figure 3 for steel, aluminum, fused silica, hafnium and tungsten (1, 5, 6). The above equation for σ, and the σ vs T curves (Figure 3) show that measurement of τ_L and τ_T determines σ, which in turn yields T. Knowing T, the velocity vs T curves (Figure 2) can be used to interpret τ_L or τ_T in terms of thickness X.

When there is a temperature gradient in the thickness X, the above procedure yields a slightly erroneous T, because longitudinal and shear waves propagate at velocities which generally average the temperature gradient in slightly different manners (*see* Measurement of Temperature section below). The error depends on the material and temperature distribution. This method is limited to relatively large thicknesses.

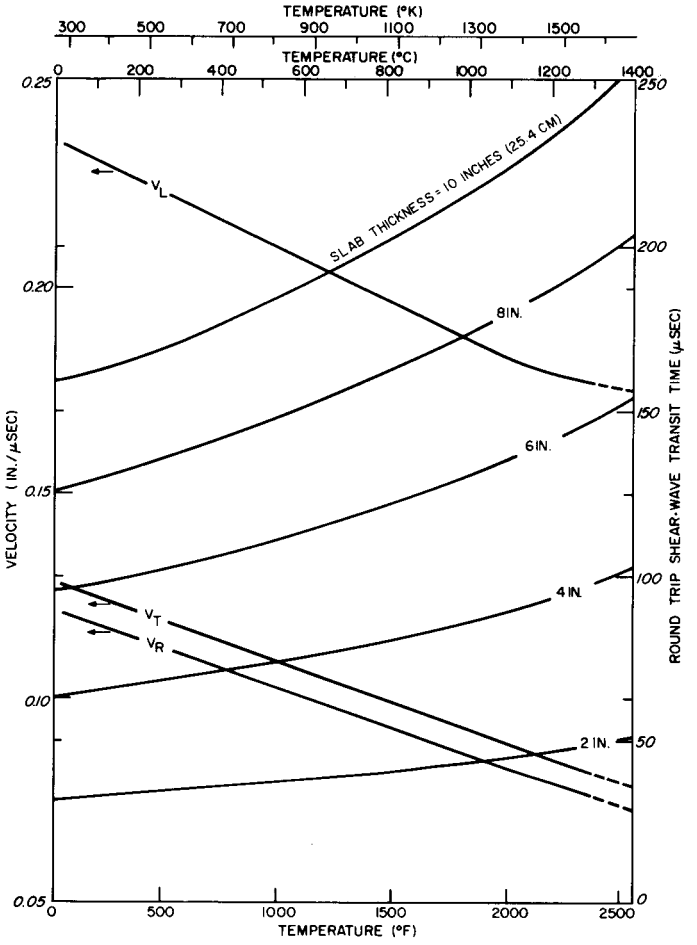

Figure 2. Velocity and transit-time vs temperature.

The above application illustrates how information may be obtained with shear and longitudinal waves that is not obtainable with longitudinal waves alone.

Measurement of Temperature

Determination of temperature from sound-velocity measurements was suggested nearly 100 years ago (7). The temperature dependence of the sound velocity may be measured in a gas, liquid or solid. Although the method is quite simple in principle, it has not been applied to high temperatures except in a few instances (8-10).

Uniform Temperature Within Material. We have measured longitudinal and shear-wave velocities in a number of bulk materials, typically 2.5 cm dia × 2.5 cm long, up to 2800°K in the case of tungsten, at frequencies of the order of 1 MHz (1). Results in a low carbon manganese steel are shown in Figure 2. For this material, the velocities are approximately linearly decreasing functions of temperature. The Rayleigh wave velocity V_R was calculated from V_L and V_T, and might be used to measure a surface temperature averaged over a depth of about one wavelength. In this section, however, we emphasize not surface temperature, but the generally inaccessible *interior* temperature within bulk material.

From the V_L and V_T vs temperature data (Figure 2), it is clear that τ_T is approximately twice as sensitive to temperature as is τ_L. Accordingly, we plot the round-trip shear-wave transit time vs temperature, with slab thickness as parameter, in Figure 2. From these curves, the thermometry accuracy can

be estimated, if one additionally knows specimen thickness, and transit time accuracy. The curves shift somewhat depending on composition, thermal cycling, and propagation direction within anisotropic material. Therefore the velocity-temperature curves should be established for particular applications, to determine the velocity band appropriate to the case at hand.

As an example, for a 5-cm slab, a 0.2-μsec change in round-trip time for a shear wave corresponds to a temperature change of about 10°K, or 1%, above ~1000°K. Sensitivity improves at higher temperatures, and for thicker slabs.

Nonuniform Temperature Distribution. When the material is not isothermal, the problem is the inverse of a case solved by Kalugin and Mikhailov (11), wherein a nonuniformly heated rod was cooled at the ends. They measured $T(x)$ with thermocouples and a pyrometer, and τ with ultrasonic pulses, and calculated $V(T)$. In the following, we suggest ultrasonically measuring $\tau(x)$ and, separately, $V(T)$, from which the unknown $T(x)$ can be calculated.

The "average" temperature calculated in this way from harmonic mean velocity measurements over a single path is the harmonic ultrasonic temperature, denoted $\overline{T}$. This $\overline{T}$ is higher than $< T >$, the arithmetic mean temperature, for materials in which velocity decreases as temperature increases. Furthermore, for materials in which σ increases as temperature increases, $\overline{T_T} > \overline{T_L}$, because the shear wave spends a greater proportion of time in the hot regions than does the longitudinal wave. Thus, for steel, $\overline{T_T}\,\overline{T_L}$, both of which are greater than $< T >$. Table 1 compares ultrasonic temperature with average temperature in a steel slab having a sinusoidal temperature distribution from the surface to the centre ($T_{max} = 1273$°K at the centre). It is clear that the ultrasonic "average" temperature $\overline{T}$ is in good agreement with the true average $< T >$, i.e., within 1% despite gradients of 500°K from centre to surface.

Table 1

Comparison of ultrasonic temperature with arithmetic mean temperature, in C1008 steel slab, assuming temperature distribution sinusoidal, $T_{max} = 1273$°K at centre, $V_L = 0.235 - 47.8 \times 10^{-6}$ (T–273° K) in./μ sec and $V_T = 0.128 - 35 \times 10^{-6}$ (T–273°K) in./μ sec for $273 \leq T \leq 1273$ (Figure 2).

Surface Temp., °K	Arith. Mean Temp. $<T>$, °K	Ultrasonic Temperature., °K			
		$\overline{T_L}$	% Error	$\overline{T_T}$	% Error
273	910	930	2.2	939	3.2
473	982	999	1.7	1002	2.0
673	1055	1062	<1	1067	1.1
873	1128	1131	<1	1132	<1
1073	1200	1201	<1	1201	<1
1273	1273	1273	<1	1273	<1

[Triangular and parabolic temperature distributions are analyzed in NASA CR-72339, Appx. I(20)]

Next we consider determining the temperature distribution T (x) from ultrasonic measurements over two or more paths. For square or rectangular bodies in which the *shape* of the isotherms is approximately known, measurements across the centre and across the edges may indicate whether the interior is hotter or colder than the surface. When there is a difference in the phase [e.g., austenite vs ferrite + pearlite in 4340 steel, (1) γ vs δ in iron (12)] of the interior material and the surface material, the transit-time difference becomes more pronounced over the centre and edge paths.

To approach the problem of ultrasonically measuring the point-by-point temperature distribution, consider first the analogous problem of optically determining temperature distribution in hot gases. For example, the relative intensity of a particular spectral line may be measured along a number of parallel chords. In a sense, an average temperature is measured along different paths. From these data temperature distribution may be calculated (13-18).

Analogous to the above optical determinations of temperature distribution obtained from integrated intensity measurements over different optical paths (generally parallel paths), an ultrasonic determination of temperature distribution may be obtained from measurements of integrated transit times over different acoustic paths (not necessarily parallel paths). In gases as hot as 17,000°K, our ultrasonic measurements of temperature distributions employ *differential-path* techniques (8). In solids, it appears feasible to determine temperature profiles, employing *different-path* measurements. Imagine the cross-section to be divided into n isothermal zones. Thus, we have n unknown temperatures to be determined, and need n different transit-time measurements. These measurements may be all longitudinal, all shear, or a combination of the two.

To interpret such measurements, one may solve the n equations, or follow Pearce's approach (15) and plot the transit-time distributions for assumed temperature distributions. One can then match an observed τ distribution (or velocity profile) to the corresponding T distribution. Results using this approach will be reported subsequently.

We have noted that when the material is not isothermal, $\overline{T}$ is usually somewhat higher than $< T >$. On the contrary, in gases, where sound velocity *increases* in proportion to the square root of temperature, the harmonic mean sound velocity indicates an average temperature *lower* than the arithmetic mean temperature.

In the thin-wire section below we also discuss thermometry using the Pana-Therm.

The present thermometry section may be concluded by noting that high-pressure momentary contact has been used to measure the temperature dependence of sound velocity $V(T)$ in many bulk solids. Using these results in reverse, sound velocity may be measured on bulk materials, and interpreted in terms of temperature, both in isothermal and nonisothermal conditions.

Measurement of Defects

The principal defect we are attempting to resolve is the well-known "pipe" in steel blooms and billets. The temperature of the piece is typically 1000 to 1400°K. Scale is present in varying degrees, depending on the grade and process. The steel is usually in motion but may be stationary in some installations.

Our earliest laboratory attempts used commercially available transducers protected with a sheet of Viton, and later, dual probes (angled buffer rods) following in principle the technique of Taziri et al. (4). The first approach suffers from probe overheating for specimen temperatures beyond ~1000°K; the second, from acoustic "short circuit" effects which limit the S/N ratio when testing scaled material.

To avoid these difficulties, two other techniques which appear to offer more promise are being developed. They are pulse-echo techniques, and employ either (1) a large-diameter longitudinal wave buffer rod, with small contact boss, or (2) a small-diameter shear wave buffer rod. These have been used successfully at room temperature but not yet at elevated temperature.

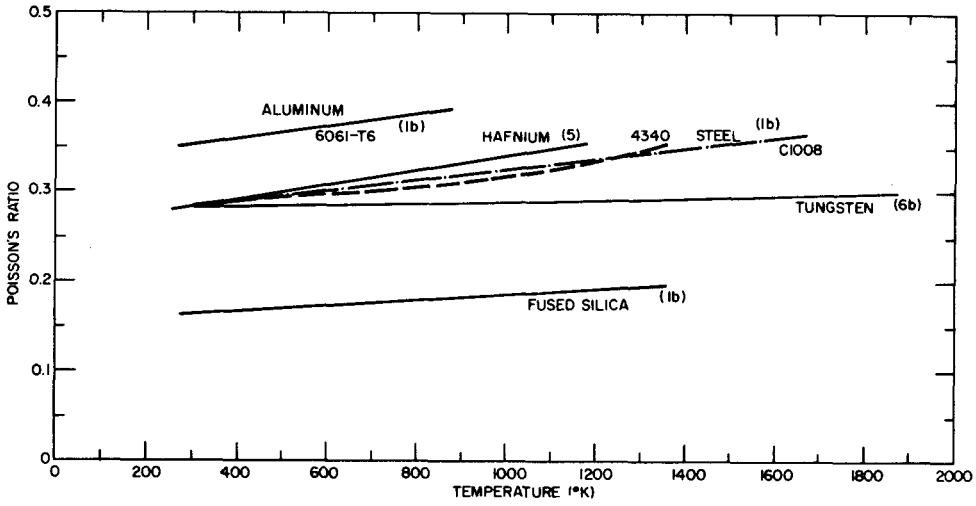

Figure 3
Poisson's ratio vs temperature, determined from longitudinal and shear-wave velocity measurements in bulk specimens.

In the following, design considerations such as length and diameter of buffer rod, crystal frequency and orientation, and coupling, are discussed for longitudinal and shear modes.

For pulse-echo probes the length of the buffer rod may be ~50% longer than the specimen thickness, to permit the defect and rear face echoes of interest to be resolved between multiple internal reflections within the buffer rod. For through-transmission measurements, shorter probes would suffice.

The diameter of the buffer rod depends on vibration mode, specimen thickness, "pipe" location, and again on whether pulse-echo or through-transmission testing is employed. For pulse-echo longitudinal wave testing, the diameter must be large enough so that mode conversions within the probe do not yield interfering echoes.

On the contrary, the diameter of a shear wave buffer rod may be comparable to that of the crystal, typically only 1 to 2 cm.

Shear-wave-test frequency would generally be about half that of the longitudinal-wave-test frequency, for a given specimen, and given probe diameter, to maintain comparable beam spreading and grain boundary scattering losses for the two wave types.

Another consideration regarding the choice between longitudinal and shear waves concerns the probabilities of detecting a given "pipe" defect. To compare these probabilities theoretically, incident shear and longitudinal wave beams of equal shape and wavelength are assumed. Intuitively, one might predict equal probabilities. For an ideal flat "pipe" normal to the beam, such intuition is correct, provided other variables are equal (coupling, attenuation, S/N ratio, etc.). Realistically, however, the "pipe" is neither flat nor normal to the beam. At oblique incidence, a longitudinal wave, on reflecting from the "pipe", is partly mode converted to shear. For a 10-cm-sq. billet, if the "pipe" is located with ± 1.2 cm from the axis and if the buffer rod is about 2.5 cm dia., echoes may be received from interfaces inclined up to 17° from the incident beam. At this angle, if $\sigma = 0.35$, nearly 20% of the incident longitudinal energy is "lost" due to mode conversion to shear. For these same conditions, shear waves having particle motion perpendicular to the "pipe" surface will be 50% mode converted. However, by orienting the shear wave probe so that particle motion is parallel to the "pipe" surface (i.e., generally parallel to billet axis), there is no mode conversion. Thus, compared to longitudinal waves, properly oriented shear waves should provide slightly higher reflection coefficients from a given obliquely oriented void defect.

To evaluate the above probe types experimentally, a pneumatic drive system is being used (Figure 4). While Figure 4 illustrates only an elementary reciprocating drive system useful in the laboratory, it is obvious that moving stock preferably would be inspected with a drive system that follows the motion.

On the production line, many system designs are possible, and may include belts, roller transducers, etc. At least one steel company has used a transducer in contact with a steel roll to obtain coupling to the 1300°K billet. When scale or surface roughness is so severe that pressure alone does not provide adequate coupling, the surface may be scalped prior to momentary acoustic contact.

From the above analysis, and laboratory experiments that we have performed, it is concluded that "pipe" detection is more difficult than thermometry or thickness measurement, because of the relatively small, irregular target. Shear waves offer two advantages over longitudinal waves: use of long, thin buffer rod, and an orientation-dependent reflection from oblique "pipe," which can be slightly larger than the longitudinal wave echo. Longitudinal waves, on the other hand, may offer advantages where couplants can be applied more easily than high pressure. There may also be cases where, under a given coupling pressure, and in the absence of any applied couplant, longitudinal waves may be easier to couple than shear waves.

Ultrasonic Testing of Wires

In the past decade, Bell (19) and his co-workers (10, 12) have tested numerous wire specimens, and obtained velocity and attenuation data by pulse-echo techniques up to the melting point. Bell et al. have shown that besides E, G and σ, information can be obtained on hysteresis effects at phase changes, nitriding, grain reorientations, crystal growth, etc. The authors' initial thin-wire experiments used Bell's unique double-pulse system.

To study wires ~0.05 to 1 mm dia × only ~2 to 5 cm long, however, the authors now use 3 to 5μ sec pulses and a new single pulse instrument, the Pana-Therm, to automatically measure transit times as a function of temperature. The principal reasons for testing such short specimens are to simplify attaining uniform temperature over the entire specimen, and to obtain localized temperature readings, when the wire is used as a thermometer element (20).

The Pana-Therm model 5000, Figure 5, measures the transit time (up to 999.9 μ sec) between the midpoints of the 3 db points of the echoes received from the front and rear

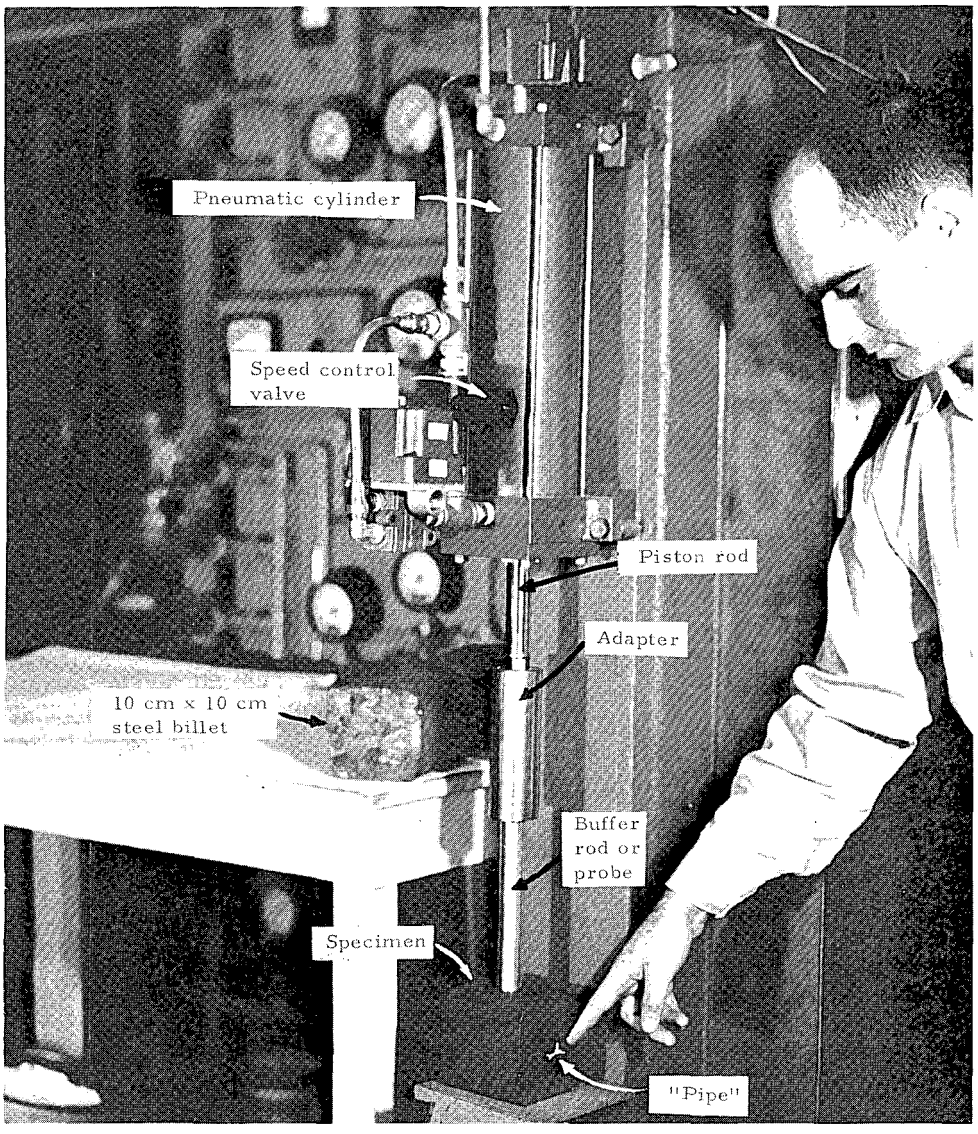

Figure 4
High-pressure momentary contact apparatus used in testing ultrasonic probes.

of the sensor or specimen. The average of ten such readings is displayed as shown, in digital and/or analog form. The analog voltage can also be recorded on a strip chart, and the echoes can be displayed on an oscilloscope for attenuation measurements. A new model, the Pana-Therm 5010, is available with improved blanking, echo polarity and time selection, for automatically monitoring pulse transit time and amplitude (20).

Figure 6 compares our preliminary thin-wire measurements of Young's modulus with independent data for polycrystalline Mo (6, 11) and Re (21). (Above ~1800°K, the discrepancy between our Mo data and that of Armstrong and Brown (6) is probably due to a temperature gradient.) Mo exhibits temperature hysteresis, which was substantially annealed out by soaking for two hours at ~2250°K. Hysteresis effects have been attributed to grain reorientations, and appear to depend in part on crystal anisotropy, prior work, and grain growth and recrystallization at elevated temperature. Re exhibits hardly any hysteresis. The excellent reproducibility of the Re data suggests its use as a thermometer, to measure temperature to 1% up to and beyond 3000°K. At its melting point, 3453°K., Young's modulus in Re falls to one-third of its value at room temperature. Mo, however, at *its* melting point (2883°K) exhibits a Young's modulus which has fallen to only half its room temperature value.

Thin wire thermometers were first studied in the Dragon Project (10, 12, 19). Such thermometers offer advantages in certain nuclear and prolonged heating applications, where geometry, materials reactions and other conditions preclude or limit the accuracy of pyrometers or thermoelectric devices. In general, the thin-wire sensor does not require electrical insulation. Uniquely, one single wire is able simultaneously to indicate temperature at one or more points. If required, torsional and extensional waves may be used simultaneously or sequentially, to take advantage of different reflection coefficients of the two waves at two sensor locations within one wire (20).

Another application of these techniques is NDT of thin wires, to determine uniformity. In selecting refractory wires for possible sensors, we found ~5% velocity variations at different points in a given wire. This inspection was accomplished by using a hand-held jig which pressed two pairs of steel dowel pins against the wire, at points 7.5 cm apart. Echoes were produced at these two contact points. As the jig was drawn along the wire, the time between echoes indicated uniformity of sound velocity.

Based on the above tests of elastic properties, thermometry applications, and wire uniformity testing, it appears that the Pana-Therm 5010 and related thin-wire techniques will be of increasing value in future materials studies.

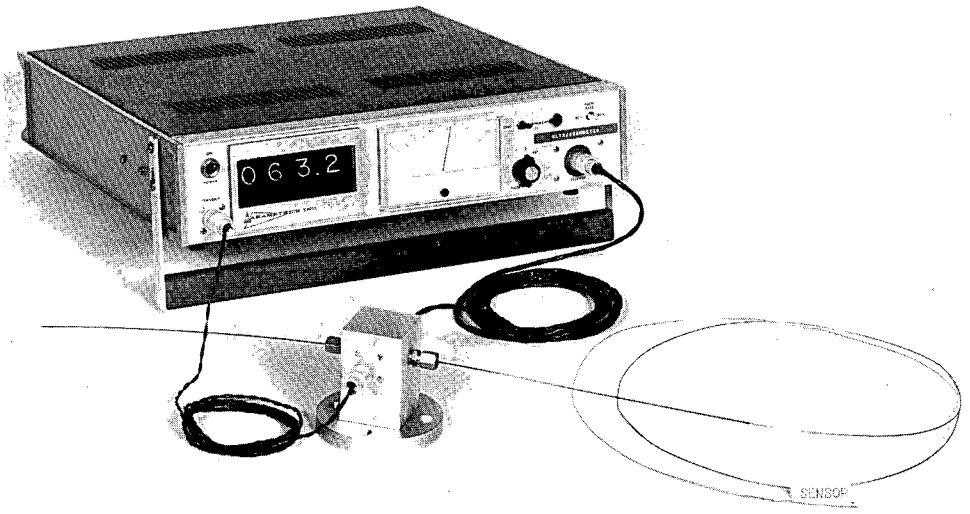

Figure 5
Pana-Therm Model 5000 automatically measures transit time in sensor, from which sound velocity, elastic moduli, Poisson's ratio, temperature, etc. can be determined. The system consists of the transmitter-receiver and readout instrument, transducer, lead-in wire and sensor. A newer instrument, Model 5010, provides more automatic features, greater versatility.

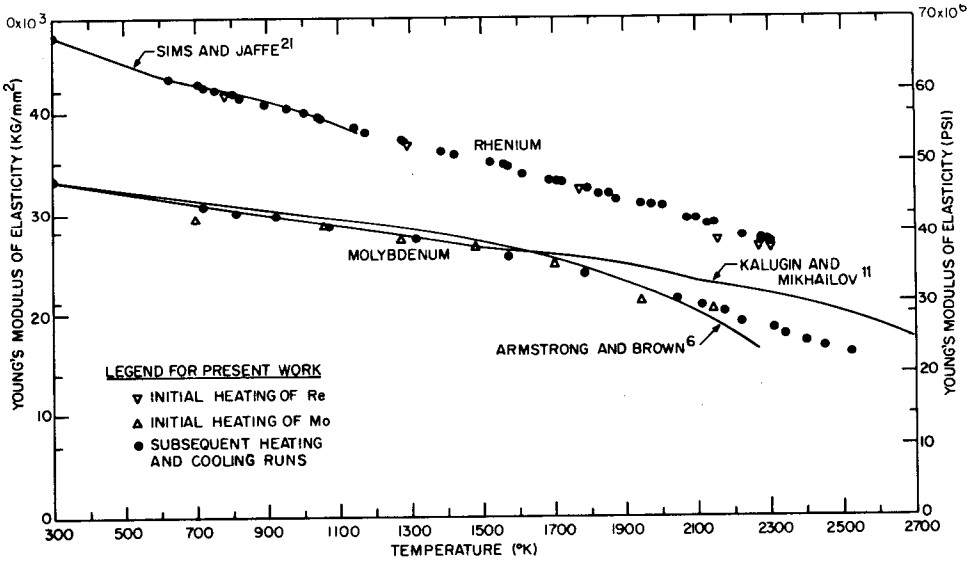

Figure 6
Young's modulus of elasticity vs temperature in Mo and Re. Experimental data points shown were obtained using the Pana-Therm of Figure 5. At the melting point of Re, 3453°K, the modulus falls to about 17000 kg/mm².

Conclusions

Ultrasonic testing of solids at elevated temperature is but a small part of the general field of high-temperature research and technology. Grosse (22) has aptly pointed out that this general field, while important as a frontier of science, is by no means a new frontier. Since prehistoric times, Grosse continues, attaining higher and higher temperatures characterizes successively more advanced civilizations. Accordingly, we anticipate NDT advances at increasingly elevated temperature (23). The present work illustrates this theme by showing how high-pressure momentary dry contact has permitted bulk solids to be ultrasonically tested in the laboratory up to 2800°K, in a manner potentially applicable to production-line NDT of materials up to their melting points. Additionally, Pana-Therm measurements of thin metal wires show that elastic properties can be easily determined at temperatures approaching the melting point. Ultrasonic thermometry using this thin wire system offers an alternative to thermocouples which may prove significant in high temperature and nuclear applications (20).

Acknowledgments

The authors gratefully acknowledge the encouragement and support of a number of patient individuals in the steel industry. The above work was also supported in part by the Office of Naval Research, and NASA. The authors are also indebted to Prof. J. F. W. Bell, of the Royal Naval College, Greenwich, and T. A. J. Jaques and E. A. Thorne, of the A.E.E., Winfrith, for personally communicating the detailed background and art of their thin-wire ultrasonic testing and thermometry. At Panametrics, Inc., B. R. Douglass, S. L. Klaidman and B. J. Spencer substantially contributed to the conduct of the experiments.

References

1. Carnevale, E. H., Lynnworth, L. C. and Larson, G. S., *J. Acoust. Soc. Am.*, **35**, 1883 (Abstract F6, Nov. 1963); **36**, 1678-1684 (Sept. 1964); **36**, 1999 (Abstract I2, Oct. 1964; *L.C.L. and E.H.C., Materials Eval.* **22** (9) 423 (Abstract, Sept. 1964); D21 in *Rpts. Fifth Int. Cong. Acoust.*, Liège, Belgium (7-14 Sept. 1965); 1965 IEEE Ultrasonics Symposium, Boston, Mass. (Dec. 1-3, 1965); *Materials Eval.* **23** (1) 29 (Abstract, Jan. 1965); *L.C.L. Materials Eval.* **25** (12) 265-277 (Dec. 1967); *Proc. 6th Symp. NDT*, San Antonio 323-361 (April 17-19, 1967).
2. Lynnworth, L. C., IN Morrow, C. T., Ely, L. P. and Smith, M. R. (ed.), *Proc. 6th Symp. on Ballistic Missile and Aerospace Tech.*, Vol. 4, 145-187, Academic Press, N.Y. (1961).
3. Kurz, W. and Lux, B. *Concast-News*, **4** (2) 3-6 (1965); Arch. Eisenhüttenwes, **39** (7) 521-530 (July 1968).
4. Taziri, I., Sekino, S. and Sasaki, Y. *Yawata Tech. Rpt.* 245 (Dec. 1963), this Proc., Sess. 10/2.

5. Dunegan, H. L., *Materials Eval.*, **22** (6) 266-272 (June, 1964). See especially App. A, for a derivation of the increment of delay $\Delta\tau$ caused by mode conversion across the buffer rod of dia D: $\Delta\tau = D(V_L^2 - V_T^2)^{1/2}/V_L V_T$. *See also* Reynolds, M. B., *Trans. ASM* **45,** 839-861, 1953.
6. Armstrong, P. E. and Brown, H. L., *Trans. Met. Soc.* AIME **230** 962-966 (Aug. 1964). *See also* Lowrie, R. and Gonas, A. Union Carbide Tech. Rpt. C-27 (Jan. 1965).
7. Mayer, A. M. *Phil. Mag.*, **45** 18 (1873).
8. Carnevale, E. H., et al. IN Temperature—Its Measurement and Control in Science and Industry, **3** Part 2, 959-967, Reinhold, New York (1962), and *J. Chem. Phys.*, **46** (8), 3040-47 Apr. 15, 1967, and IN Mannella, G. G., NASA SP-132, 73-103 (1967).
9. Apfel, J. H. *Rev. Sci. Instr.*, **33** (4), 428-430, 1962.
10. Thorne, E. H., P23 in *Proc. Fourth Int. Cong. Acoust.*, Copenhagen, 1962.
11. Kalugin, B. A. and Mikhailov, I. G. *Sov. Phys.-Acoust.*, **12** (1) 91-92, July-Sept. 1966.
12. Hub, D. R., J51 in *Proc. Fourth Int. Cong. Acoust.*, Copenhagen, 1962.
13. Hormann, H., *Z. Phys.*, **97,** 539-560, 1935.
14. Maecker, H., *Z. Phys.*, **136,** 119-136, 1953.
15. Pearce, W. J., *WADC Tech. Rpt.* 59-346, Feb. 1960; IN Dickerman, P. J., ed., *Symp. on Optical Spectrometric Measurements of High Temperatures,* Univ. of Chicago, 1960, 125-169, Univ. of Chicago Press, 1961.
16. Reed, T. B., *J. Appl. Phys.*, **32** (5), 821-824, May 1961.
17. Simon, L., *Optik,* **19** (12), 621-639, 1962.
18. Krakow, B., *Appl. Optics,* **5** (2) 201-209, Feb. 1966.
19. Bell, J. F. W., *Phil. Mag.*, **2,** 1113, 1957; J52 IN *Proc. Fourth Int. Cong. Acoust.,* Copenhagen, 1962; Bell, J. F. W., Doyle, B. P. and Smith, B. S., *J. Sci. Instrum.*, **43** (1) 28-31, 1966.
20. Lynnworth, L. C. et al., NASA CR-72339 (Aug. 1967), -72395 (Dec. 1967), AEC Rept. NYO-3906-4 (Sep. 1968); Space/Aeronautics **48** (4) 121-128 (Sep. 1967); "Ultrasonic Thermometry for Nuclear Reactors", IEEE *Trans. Nucl. Sci.* (Feb. 1969).
21. Sims, C. T. and Jaffe, R. I., *AIME Trans.*, **206** (8) 913-917, 1956; Sims, C. T., IN Gonser, B. W., ed. *Rhenium,* p. 26, Fig. 3, Elsevier, Amsterdam-New York, 1962.
22. Grosse, A. V., *Science,* **140** (3568) 781-789, May 17, 1963.
23. Beaujard, L., Mondot, L. and Kapluszak, M., *Rev. de Métallurgie* **62** 1187-1191, Dec. 1965; Brutcher Trans. No. 6832. Atkins, M. and Druce, M., *J. Iron and Steel,* 607-608, (June 1966).

Discussion

Q. Dr. A. NEMET, British National Committee for NDT, England: Since I understand that the probe is only in momentary, intermittent contact with the test piece, is it not necessary to make assumptions about the stationary temperature conditions of the transducer?

To what extent are these assumptions justified and what errors are introduced by variation of temperature of the test piece and of the contact time?

A. The high temperature probes described in this paper consist of a transducer bonded to the cooled end of a buffer rod similar to Fig. 1. The buffer rod protects the transducer from exposure to damaging temperatures. Thus, the transducer is easily kept cool. The contact end of the buffer rod, however, can indeed heat up, thereby changing the time delay and amplitude of the pulse apart from propagation effects within the specimen. These changes in the buffer rod are automatically measured and compensated for in our Pana-Therm instruments. In our laboratory, the ultrasonic probes and systems described in the paper have been used to test solids to ~3500°K, and gases and plasmas to ~20,000°K, without any observable errors due to overheating of the transducers or buffer rods (Ref. 1, 8).

Regarding errors in ultrasonic thermometry due to temperature variations in the specimen, when a bulk solid such as a steel billet is not isothermal, the ultrasonic wave propagates at a harmonic mean velocity which very nearly equals the velocity corresponding to the arithmetic mean temperature. The error or difference between the ultrasonic temperature deduced from the harmonic mean velocity, and the arithmetic mean temperature, is given in Table I for a sinusoidal temperature distribution, and in Ref. 20 (NASA CR-72339, Appendix I) for linear and parabolic distributions. Such errors are typically less than 1%, for variations up to 500°K in steel, and for variations up to 1000°K in certain refractory metals (e.g., Re).

Regarding ultrasonic thermometry errors due to variations in contact time, the following two cases may be considered. First, consider the case when the medium or test piece itself is the sensor. Here, contact usually should be as brief as possible, typically less than 1/10th of a second. The longer the probe contacts the specimen, the greater the error, due to the perturbing effect of the probe on specimen temperature. Second, consider the case when a foreign sensor such as a thin wire is brought into thermal contact with the region whose temperature is sought. Here, contact times are generally longer, depending on the thermal diffusivity and dimensions of the sensor. Measurements are accurate to the extent that contact time is long enough for the foreign sensor to achieve thermal equilibrium with the region in question.

The Ultrasonic Testing of Hot Steel Products

S. SEKINO AND Y. SASAKI, JAPAN

ABSTRACT: An apparatus for ultrasonic testing at high temperature was constructed in the blooming mill so as to detect mechanical "pipe" in a bloom or slab. The transducers were protected from heat by using stainless steel rods between the hot material and the transducers. The couplant used was mixed salt. Mechanical and shrinkage "pipe" can be detected above 1000°C, and the former can be cropped off exactly by the cropping shear.

Introduction

Today ultrasonic testing (UST) is widely used in the steel industry, but the method of testing hot steel products has not yet been established, although it has long been recognized as desirable. This method is important in certain processes, for example, in the case of the exact decision of the cropping position in the slabbing mill. At present, the only practical way to examine hot products nondestructively is the radiographic method using a betatron (1) which has many weak points, such as low sensitivity to flat defects, large initial and running costs, and the danger of radiation injury.

In hot UST, there are two main difficulties. One is the transducer, which generally stands up to 100°-300°C, whereas products should be capable of inspection at temperatures above 1000°C. The other difficulty is the couplant. Water or oil cannot be used at such high temperatures. In this paper it is explained how these two difficulties were solved by a practical test apparatus in a blooming mill.

Principle and Apparatus

To protect the transducers from heat, they were separated from the hot product by a water-cooled dual probe device. A single, reflection-type device (2) was difficult to apply because strong side echoes appeared, especially at low frequencies, such as 1 MHz. In the present study, a two-transducer, SE probe was adopted. Figure 1a shows the principle, and Figure 1b, the corresponding echo pattern, in which no side or surface

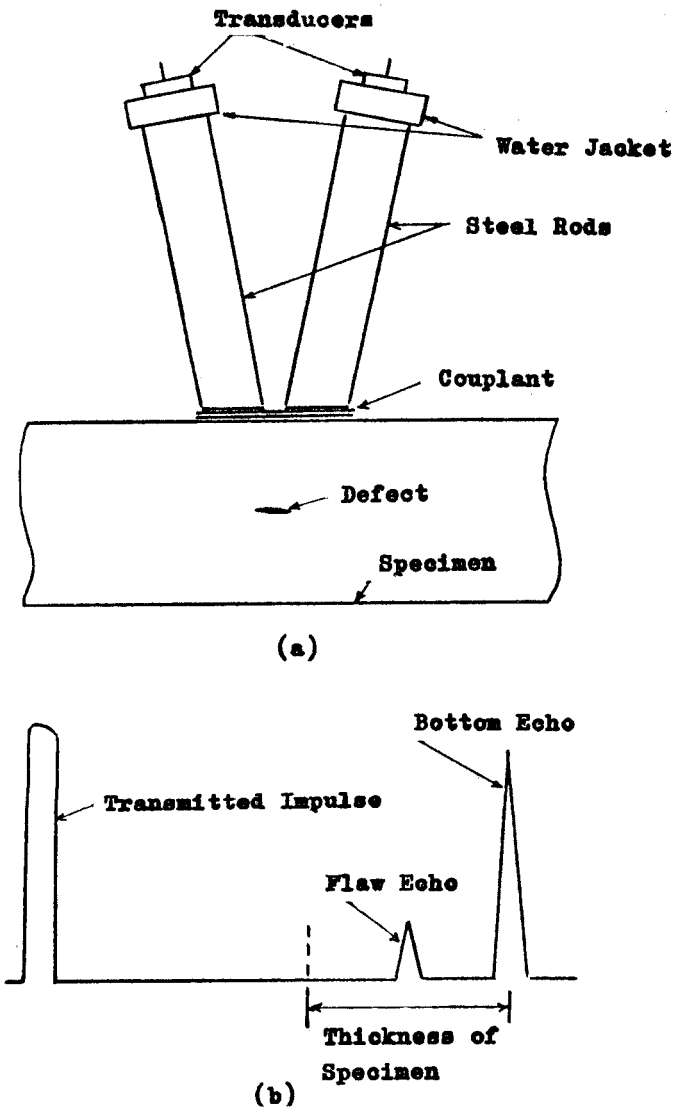

Figure 1. The principles of hot ultrasonic testing. (a) The two-probe, SE type with cooled steel rods. (b) The echo pattern of (a).

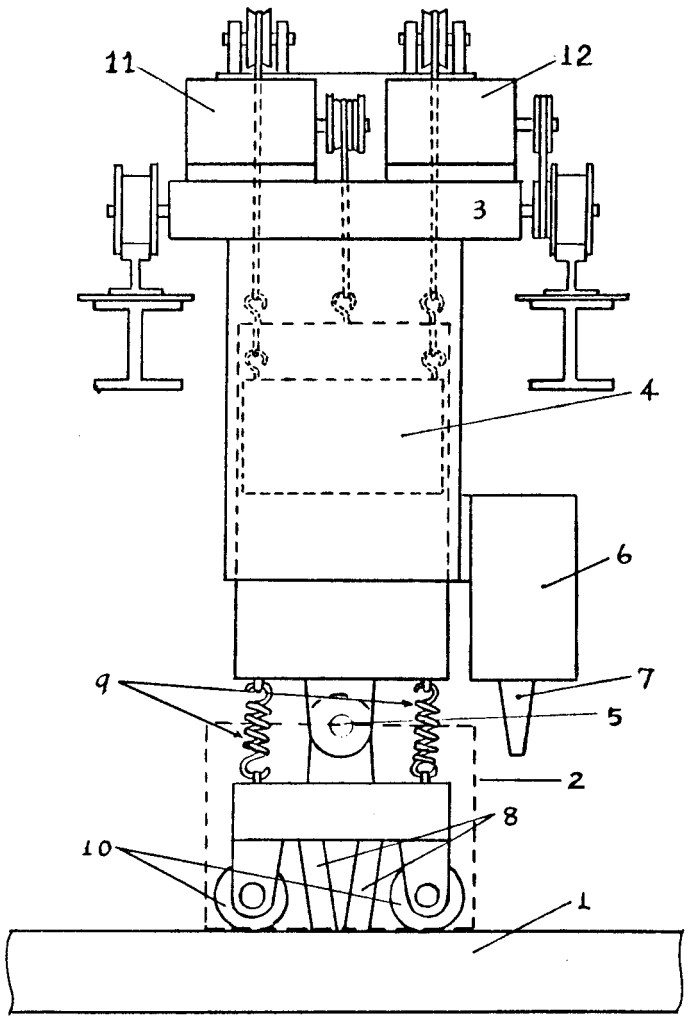

Figure 2. A schematic view of the on-line apparatus. 1. Slab; 2. measuring unit; 3. rack; 4. counterbalance; 5. free rotating axis; 6. salt powder mixer; 7. chute; 8. stainless steel rods; 9. spring; 10. wheel; 11. motor for vertical movement; 12. motor for horizontal movement.

echo is observed. If there are defects, their echoes would appear in the marked range.

Following are the couplant characteristics; it must be liquid at testing temperature; stable even above 1000°C; inexpensive, and easily available. A mixture composed of NaCl, $CaCl_2$, etc. was adopted, a liquid that is stable between 500°C to 1200°C. The only problem was the splashing of liquid salt when water is poured on.

Figure 2 is a schematic view of the apparatus. The total testing unit 2 which is suspended from the rack 3 is balanced with counterweight 4 and can be moved up and down easily. The rack can also be moved transversely to the rolling direction. The unit can turn around the axis 5, so as to follow the curved surface of the slab or bloom top. The separating device is made of stainless steel rods, 40 mm ϕ, inclined 8° from the vertical. The salt powder mixed with water is poured just behind the inspection point using the mixer 6 and the chute 7. It melts in several seconds and spreads to cover the region where the stainless steel rods contact the surface. The exact positioning of the "pipe" area is carried out by moving the hot material forward and backward, and moving the rack left and right. Figure 3 shows the apparatus being used in practice. It takes about one minute for one area measurement. The transmitting transducer is quartz, and the receiving one PZT-5, both 1 MHz.

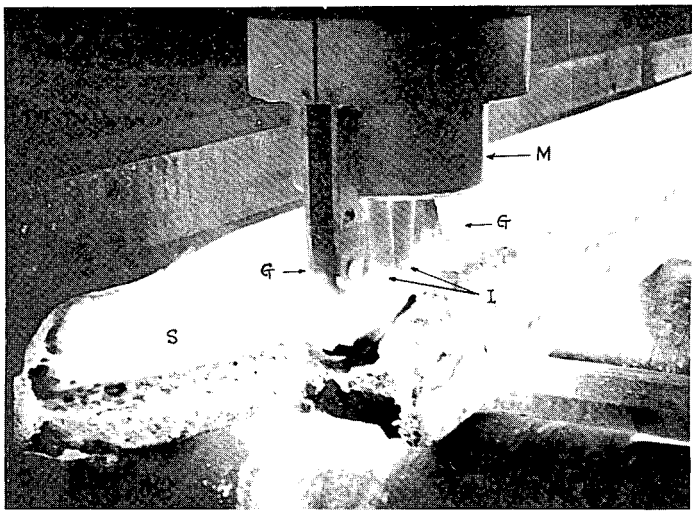

Figure 3. The apparatus testing a hot slab. M. measuring unit; G. guide roll; I. stainless steel rods; S. slab.

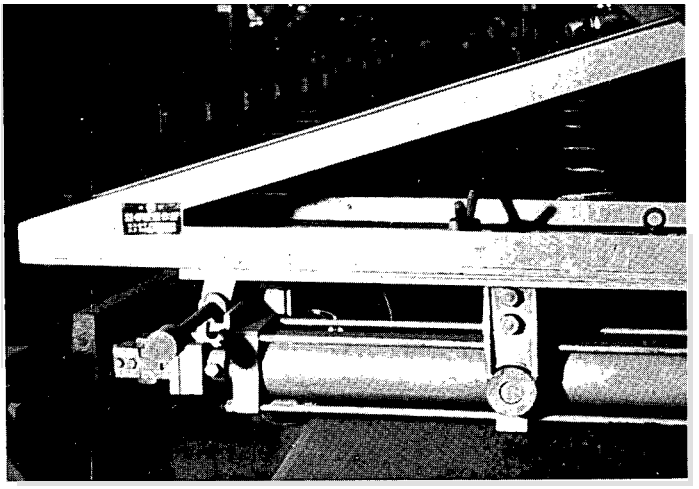

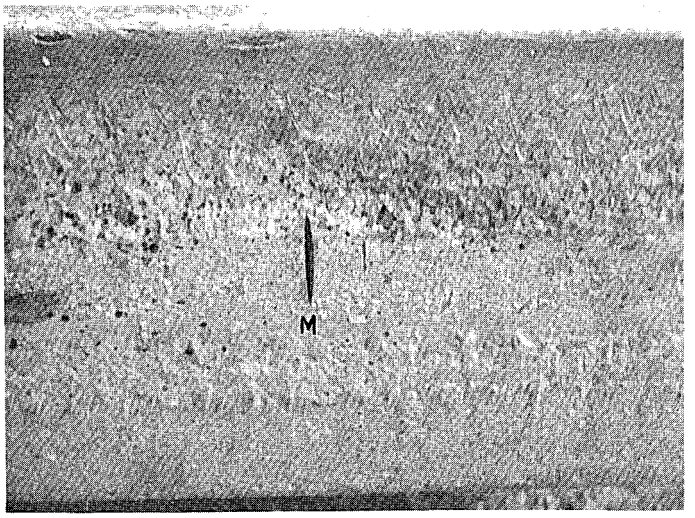

Figure 4. The marking device (upper) and (lower) a mark on the side of a slab.

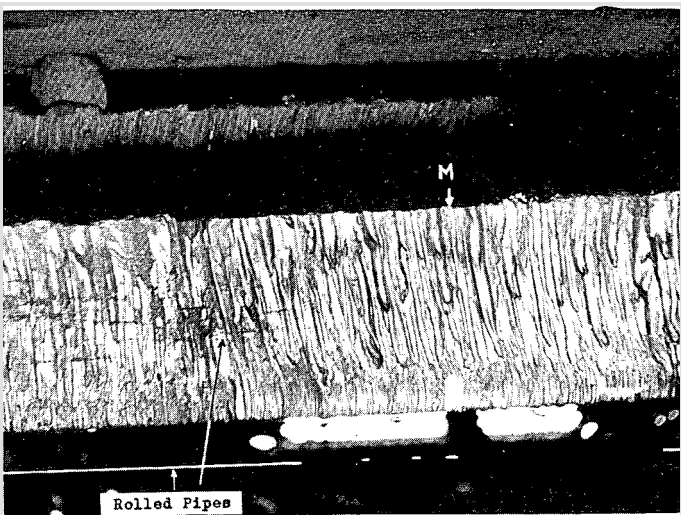

Figure 5. (Upper) M is the marked position; the hatched area is where F/B > 100% in cold ultrasonic testing, and the dotted line is the gas cut. (Lower). The gas cut section.

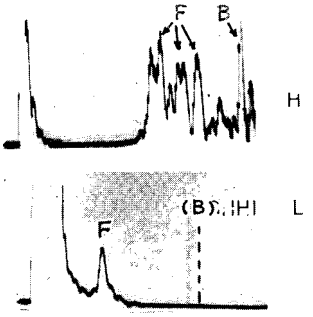

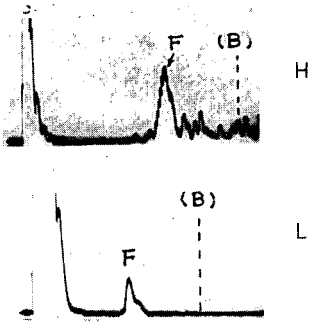

Figure 6
Echo patterns of a bloom in both hot and cold ultrasonic testing, and their corresponding cross-sections. H: hot state at 1000°C, with 1 MHz. L: cold state, by normal reflection method, with 2 MHz.

When the end point of the mechanical "pipe" is decided upon, it must be marked. The authors found no material suitable at such a high temperature, so adopted the mechanical marking of V-shape groove by air hammer. Figure 4 shows the marking device and the mark put on the side surface of the slab.

Results

After successful preliminary tests, the on-line test was carried out. Figure 5a shows, as an example, the marked position M, the area of F/B > 100% in cold UST, and also the gas cut line, and in Figure 5b, the gas cut section is shown, where it is clearly recognized as a rolled mechanical "pipe" extending to the point M in the middle of the section. The comparison of the results in the hot and cold states is excellent. The error is ±20 mm except in very extraordinary cases.

In plain carbon steel and in stainless steel, there is no difficulty in testing, but some silicon steel cannot be examined because of a large attenuation of sound.

A shrinkage "pipe" can be detected as well as mechanical "pipe". Figure 6 shows the hot and cold state test results of a bloom 200 mm square, and its corresponding section. The defect at the centre is a 1 to 2-mm ϕ rolled shrinkage "pipe".

Discussion

The above method is very inexpensive, highly sensitive, and rapid enough not to disturb the rolling process.

Future plans envisage automatic cropping of the slab or bloom at the marked position.

Scale has little harmful effect in practice, but it is certainly one of the reasons for bad coupling, and makes quantitative estimates difficult.

Cutting the shrinkage "pipe" in the hot state is not recommended, because it is extremely difficult to estimate the defects quantitatively, and to predict their harmfulness in the final products. So the aim of hot UST in the blooming mill should be the exact cropping-off of the mechanical "pipe".

Conclusions

1. Hot UST apparatus was constructed and set up in a blooming mill, and we were able to detect defects even above 1000°C.
2. It is difficult to evaluate the defect size quantitatively because of bad coupling conditions, curved surface, scale, and other unevenness. However, shrinkage "pipe", especially mechanical "pipe" can be detected with certainty.
3. Practical on-line application contributes to increased yield, quality improvement, and the control of steel making practices.

References

1. Luckerath, W., Fink, K. and Flossman, R. *Stahl u. Eisen*, **79**, p. 1638, 1959.
2. Farrow, F. and Falls, G. United States Patent, No. 2697936, Dec. 1954.

A Continuous Ultrasonic Test Installation for Steel Strip with Automatic Recording of Data

LUTZ BRAND, GERMANY

ABSTRACT: Ultrasonic test equipment with automatic recording for testing hot-rolled strips is described. Experiments showed that recording papers make screen observation superfluous. The abundance and length of the indications is of more importance than individual screens. Circumstances which influence the procedure are described and the possibility of achieving optimum test conditions is discussed. New developments may make further improvement of this testing method possible.

Introduction

The ultrasonic testing equipment described in this report was built for testing hot-rolled steel strip 200 to 700 mm wide. We have examined drawing and deep drawing qualities which are intended for cold forming and cold rolling.

The following figures present examples of the typical defects. We have compared the ultrasonic presentations with micro-sections and stretch tests.

Figure 1 shows the ultrasonic record obtained from very small inclusions. The flaw echo is very strong; the edge echo is not reduced; the amplification is relatively low.

A sketch shows the position of the inclusions and test-pieces in the strip. In this case, the drawing test has made no separations. The transverse micro-section shows the inclusions, which are aluminas and silicates.

These inclusions would probably not produce any defects unless the strip were cold rolled to very thin dimensions. In Figure 2 is a very thin but relatively broad inclusion band which was opened to a lamination by the stretch test. Of course coils with many defects of such a nature cannot be used for cold working or cold rolling.

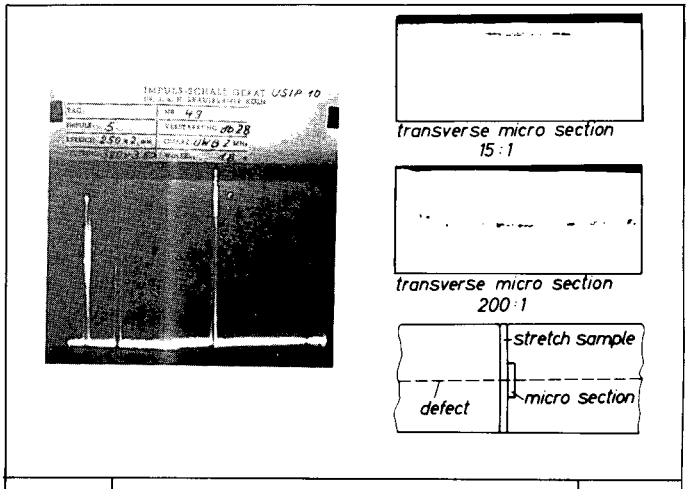

Brand 1967	Ultrasonic-scope of a small inclusion banding. Micro-sections and a sketch of sampling.	T.W. ↓ Fig. 1

If there are defects in the form of long bandings, test results are easily explained, and defects in the form of particular points have no significance for later processing.

Several writers have examined the question of how long and how big a defect should be in order to be certain of finding it with this method of testing. According to our experience the minimum size cannot be precisely determined.

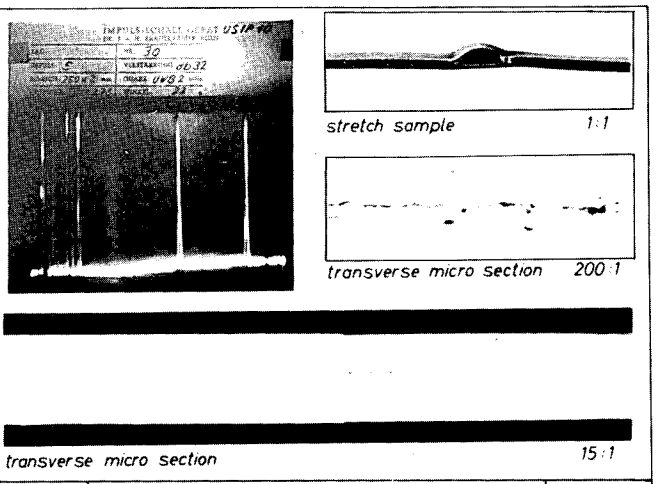

Brand 1967	Ultrasonic-scope of a slag banding. Micro sections and stretch sample.	T.W. Fig. 2

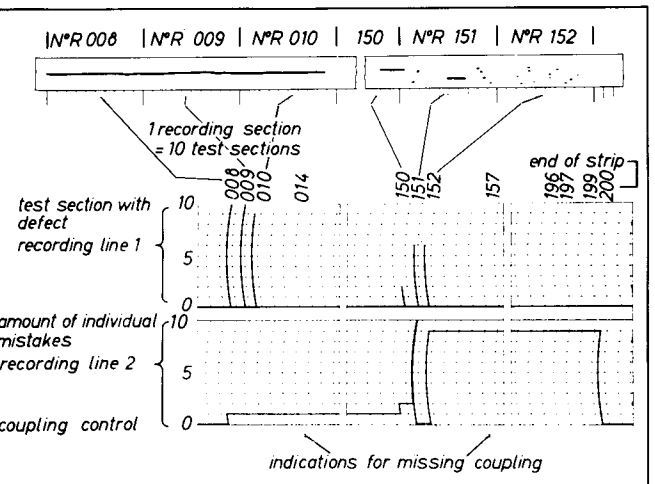

Brand 1967	Skelton sketch of a strip with defects and their recording.	T.W. Fig. 3

If there are accumulations of little defects, there are good indications. We believe that it is not only the size of the inclusions but more their form and their composition which have an influence on the testing results. With this technique it is not possible to determine the size of a defect. Also the comparison with artificial defects gives no reference to the size of the defect in the strip.

The test equipment with all mechanical and electronic apparatus was built by the firm Krautkrämer in Cologne, Germany. It was installed in the pickling line of the firm Wuppermann in Leverkusen, Germany, between the last neutralization tank and the hot air drying plant. In this location water coupling presents no difficulty because the drying plant follows. The strip passes the test equipment at a speed of 40 to 70 m/min. Rubber rolls are installed just in front of and behind the test equipment in order to guarantee the minimum noise from vertical movement of the strip. A detailed description of this test equipment was given in Stahl und Eisen, 1965, No. 9, 519-526. For those who have not had the opportunity to read this report, only the description of the automatic recording method is repeated.

Figure 3 is a schematic of a strip with defects and their recording. The recorder is writing in the transverse direction of the paper movement. The upper line gives the number of the test sections with defects for one recording section; the other line the number of defects altogether. If the defects are recorded, the stylus falls back to zero and begins again. The third line marks, with a little deflection, the missing coupling.

Our plotting shows a slag line with a length of three recording sections. Thrice the stylus gave the signal for 9 test sections with defects. Simultaneously only one particular defect was recorded. So the figure of this defect is defined. On the right are a lot of little defects. For three recording sections the stylus showed two test sections, and later for six respectively, with defects. Simultaneously the second line produced by the stylus recorded twenty defects.

The firm Krautkrämer has also developed another registration system. A printing apparatus is governed from the digital counters, and prints only one line for each recording section with defects, as described in the above mentioned number of Stahl und Eisen.

Both systems of recording are satisfactory, and the test engineer is able to note the defects, their species and their position in relation to the length of the strip, and in this way the quality of the coil.

Figure 4 illustrates some typical registration papers. The upper sheet is considered good. At three points a small number of short defects are seen. This coil is suitable for all uses to which ultrasonic testing may be put.

Lower on the sheet we see one zone with an accumulation of defects at one end of the coil. These are without doubt the rest of the head shrinkage. This part of the coil cannot be used for processing; if it is not possible to cut off the zone with defects on it, the whole coil must be rejected.

The test engineer's presence is not needed at all times during the test procedure. The automatic recording device allows him to determine the acceptance or otherwise of the coil at some later time.

Such tests not only prevent rejects from reaching the consumer, but also make possible close cooperation with the steel works. We can quickly examine many ingots or melts for freedom from slag and shrinkage and so determine the extent of testing needed. At first we test all deliveries of high-quality materials produced by the cold forming process, particularly those produced in multiple-stage presses. The evaluation of the records can be done later.

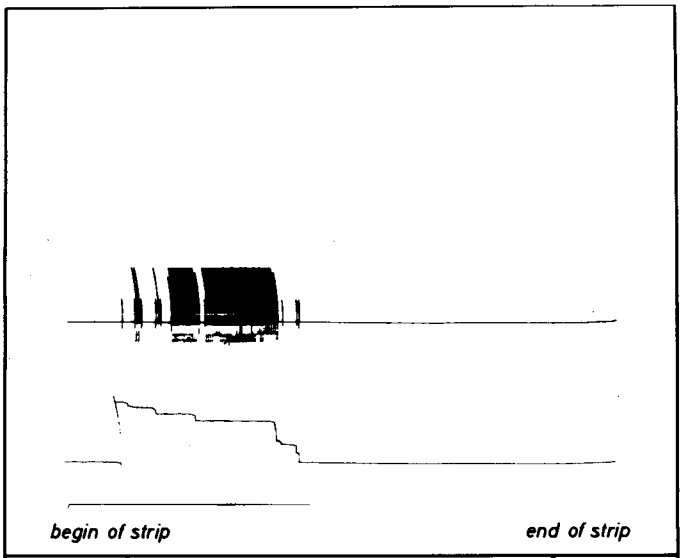

Brand 1967	Recording stripes of hot rolled strips (~200m long - ~219 yards long)	T.W. Fig. 4

The test engineer must be knowledgeable and experienced in this work.

We also accept commissions to carry out test surveys for quality or work in co-operation with the steelworks. Normally, one man can operate the test equipment, but if small lots with changing dimensions have to be checked, it is better to have a second man. Also if we test materials for extra high quality, two men are needed to attend to all installations, to keep an eye on the ultrasonic indications and to compare them with the record.

Optimum test conditions must prevail in order to be sure that the recording paper is correct. These conditions can be guaranteed only if all circumstances likely to influence the test results are known and respected. These circumstances and their influence are discussed later.

Lamb-wave Diagram of Group Velocity

This diagram has been widely discussed in the literature and general explanations are superfluous. For testing we use wave trains designated in the diagram with approximate horizontal lines. The testing frequency and thickness of the strip fix the zone in the diagram, and the angle of the probe fixes the wave train we use. It is best to use those wave trains that have no intersections with other wave trains in the questionable zone. In most cases we have to test strips between 2 and 4 mm thick. Usually we use probes with a frequency of 2 MHz; so the factor $f \times d$ gives values between 400 and 800 kc $\times$ cm. The test angles are between 9° and 12° by coupling with water. The wave trains belonging to these angles are A_0, S_0, A_2, S_2, S_3.

Some authors have reported the possibility of recording defects that are typical for the different wave trains. Our observations have confirmed this, but we have observed that nearly all wave trains can record defects if used with a high pulse intensity and amplification. It is necessary to test with a very overexcited edge echo.

Selection of the proper wave train depends on the accuracy of the frequency and the adjustment of probe angles. The exact frequency of a probe is not always known and the angle often has some deviations. These account for the differences between the theoretical adjustment and the best adjustment for detecting defects. We use calibration test plates with artificial defects or well known natural defects. This is especially useful if we change the probe, the ultrasonic apparatus or the dimensions of the strip.

With an adjustment that is in accordance with our experience, we observe the scope of the defect in the plate and correct the angle until we have the best presentation of the defect. An adjustment which gives the best edge echo can be wrong; the differences between the theoretical adjustment and the adjustment with a test plate often amount to 1°. During the testing of sheets, the adjustment will be corrected if the thickness of the sheet changes between its tolerances. Another influence is the abrasion of the plastic guide plate on the upper side of the probe tank.

Output of Ultrasonic Apparatus

To get good presentations of defects under unfavourable circumstances, for example, for a greater thickness of sheet and a longer scanning path, it is necessary to have a high output ultrasonic apparatus. Experience has shown that thick laminations give very small echoes, too small for the monitor's sensibility.

Figure 5 shows performance curves of some of the apparatus used. Types USIP 10 "amplified" and USM 1 "amplified" gave the best curves. Their amplifier was not linear, a particular advantage in this case.

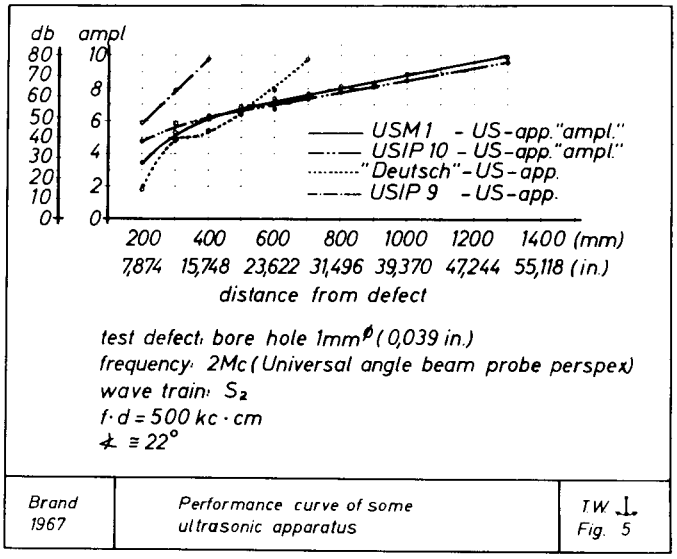

The curves were received on a test plate with an artificial defect, and the frequency was not varied. For this laboratory test we used an angle probe with an adjustable angle. The coupling was done with plexiglass and oil. For each apparatus the angle was adjusted to receive the best indication. The proper amplification relates to the defect echo, which is as high as the screen.

Influence of Cable Length

Plant conditions demand that ultrasonic and electronic apparatus be placed in a special control room, distant from the probe installation in the pickling line. It is useful to lay the cables in pipes, and as we used long cables it was interesting to find out how much pulse energy was lost in this way.

Actually for one metre of cable length nearly 1.5dB added amplification must be applied to balance the lost energy. We use a cable 10 m long and therefore need an additional amplification of 15dB.

Output of Probes

Because probe output has an important influence on the finding of defects in the strip, we compared the different probes

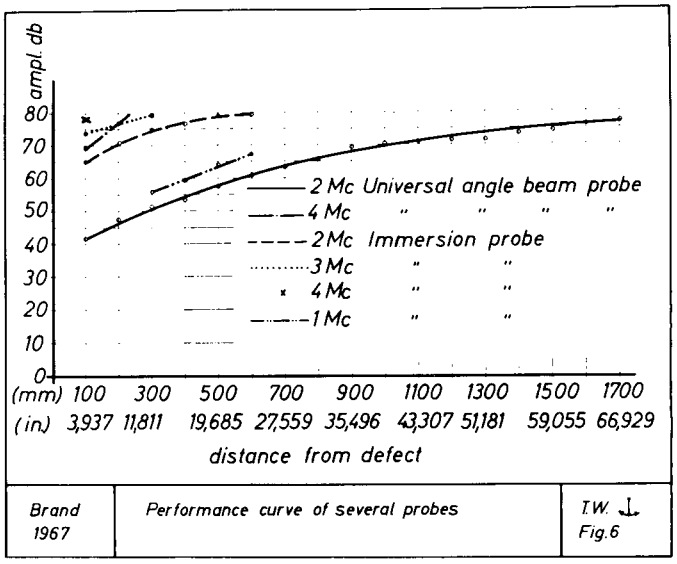

in a laboratory test. Figure 6 shows performance curves received with the same ultrasonic apparatus by the highest transmitter power. We have selected those angles that give an optimum presentation of the artificial defect.

The curves show that the universal-angle beam probe with a coupling over perspex and oil has the best output. Unfortunately, this kind of probe cannot be used with our test equipment at this high test speed because we would have coupling difficulties.

The 1-MHz immersion probe has good output, but only in a very small section does it give a clear presentation on the screen. Small strips cannot be tested with it, because the echo mountains of the transmitter pulse are so wide that the monitor gives wrong signals. By testing with higher amplification, which we need for strips with 500 to 700 mm width, we got too many disturbing echoes. Indications are received, but not from real defects.

The 2-MHz immersion probe shows a curve with a relatively favourable course, and its output is much better than that of the 3-MHz and 4-MHz probes. We used this probe almost exclusively. If we use a new probe we compare its output with this diagram, so we can be sure of getting comparable results.

Influence of Test Frequency

Figure 5 shows that it is possible to test with frequencies between 1 and 4 MHz, but the highest output is given by 2 MHz. Testing with 3 or 4 MHz can be profitable because the resolution of the higher frequencies is better. On the other hand, higher frequencies have greater attenuation. Therefore the use of this probe is limited to narrow strips. In most instances better range and higher output is preferable to resolution.

Adjustment of Angle, Precision and Consistency

It is possible to adjust the immersion probes between 0° and 15°. This corresponds to the angles between 0° and 27°36′ when coupling with perspex. Lamb waves can most often be excited by the immersion technique between 7° and 14°.

The precision of angular adjustment is controlled by calibration blocks. On the focussing scale the reading accuracy is about 10′ and the true angle deviates by less than 10′. This is not important for test results.

Lost motion of the worm gear can be eliminated if the adjusting screw is always turned from a less to a greater angle.

The Dead Zones

This procedure is designed to test the greatest possible part of the strip width and to record nearly all defects. It is not possible to test a streak along the edge of a strip. This streak has a width defined by the distance between the edge of the strip and the end of this zone and is disturbed by echoes arising from scattering rays in the water tank.

This zone would be broader if we tested with greater impulse energy and amplification. Then the monitor's range must be a greater distance from the transmitter's echo. Defects near the edge cannot be recorded. The same applies for the edge echo.

There are several ways to get small dead-zone echoes. One is to use the optimum wave train with a horizontal course as in the diagram. It is more important to test narrow strips this way because the percentage of dead zone echoes is higher in them. The other way is to lower the pulse energy and the amplification to get small echoes and a small dead zone. For wide strips we must use high pulse and amplification; therefore the latter method cannot be used for testing wide strips.

It is an interesting fact that, when testing a 500-mm-wide strip the dead zone on the probe side is about 130 to 150 mm, while on the opposite side it is about 50 to 100 mm. The actual tested zone is about 250 to 320 mm wide. We can accept these dead zones only because experience has shown that most defects are near the axis of the strip.

Test Velocity, Strip Guidance and Probe Guidance

Our test equipment works with a velocity of about 70 m/sec, whereas other comparable installations work at nearly 150 m/sec. The influence of the test velocity on the sensitivity of indications is not important when electronic recordings are used. Observation of the screen would be very difficult at this velocity and indications could easily be overlooked.

However, high strip velocity does make for coupling difficulties if the strip has "shape waves" caused by one side of the strip being thicker than the other, or if the strip is "flattering" (caused by both sides being thicker than the centre). To prevent jerky, vertical movement, two pairs of guide rolls are used in front of and behind the test equipment.

The probe container must follow the movements of the strip exactly. For to accomplish this, it is suspended in gimbels and a counterweight presses the container against the underside of the strip. It is possible to improve this arrangement if the container is spring supported, and this method must be used if the guide rolls cannot be assembled immediately in front of and behind the test equipment. These rolls are covered with rubber for squeezing off the water which is running with the strip out of the neutralization tank. Water in the scanning can produce indications and so simulate defects.

Steel Quality

In this equipment we test low-carbon steels in rimmed and killed qualities. In laboratory tests we have found that there is greater absorpition in the segregated zone of the rimmed steel than in zones free of segregations. However this has no influence on testing at right angles to the length of the strip, therefore the sensitivity of the process is nearly the same in testing killed or unkilled steels.

In testing high-carbon steels we could not find any disadvantageous effects, just as by steels with a higher percentage of manganese, copper and columbium. We have not tested and have had no experiences with steels with a high percentage of chromium, nickel and molybdenum. We found that a coarse grain intensifies attenuation. Charlet and Nouvet have given detailed descriptions of these effects. In testing hot-rolled strips we generally have grain sizes between ASTM 6 and 8 and therefore have no difficulty with this problem.

Strip Surface, Condition of Edges, Coilbreaks and Edge Waves

Usually strip surfaces are very smooth and free from scale. Rough shells, pinchings, overlappings and sharp-edged mechanical defects of the surface are usually defects in the material.

Damaged edges do not affect the test, because no indications of them are recorded. Coilbreaks could make for difficulties in coupling, if there is no straightening machine at the start of the pickling line. Indications such as those recorded for defects are not initiated by coilbreaks. If the probe container cannot follow the vertical movements of the strip as quickly as necessary difficulties arise with coupling. Methods to improve this situation have already been described.

Chances for Development

This testing process has been used with good results at the Wuppermann factory for more than five years. Rejects by customers have been considerably reduced, but not totally eliminated. We can find most of all defects, but not all.

To improve the sensitivity of the testing system the ultrasonic apparatus is capable of special amplification, and we cannot hope to do more in this direction. In any event, experiments are done with two probes, one for transmitting, one for receiving and installed in one container. This makes it possible to test with higher output without enlarging the dead zone. We can also use an additional amplifier direct on the transmitting probe to compensate for the transmitting energy lost in the cable.

Another interesting development by physicists of the firm Hoesch AG in Germany is a sound-optical system which is able to transmit ultrasonic waves at many angles simultaneously. These waves excite all the possible kinds of Lamb-wave trains. In testing with this system one uses all the possible wave trains at once. The chance that a defect may not be indicated because the optimum wave train for it is not used, is eliminated by this system. If it can achieve good output, we can look forward to a fundamental improvement in Lamb-wave testing.

Ultrasonic Evaluation of the Tensile Strength of Brittle Materials

ZDZISLAW PAWLOWSKI, POLAND

ABSTRACT: The paper deals with the determination of tensile strength of electroceramics and cast iron by ultrasonics. It is shown that the existing solutions to this problem have only limited range. This statement is based on the investigations of more than 400 specimens of lamellar and spheroidal cast iron of different grades, coming from four different foundries, as well as on the investigation of two different kinds of electroceramics.

A new approach to quantitative tensile strength measurements by ultrasonic is presented. It is shown that there exists a very simple relationship between the tensile strength of electroceramics and the reduced modulus of elasticity, the latter being approximately proportional to the quotient of longitudinal and transverse wave velocity. The same kind of relationship is valid for cast iron with lamellar and spheroidal graphite. The only difference in the relationship between electroceramics and cast iron are two material constants valid for the given type of material i.e. electroceramics and cast iron. These constants are independent of the different grades of cast iron and graphite configuration.

The relationship presented seems to have more general validity for all kinds of brittle materials. To evaluate the tensile strength of cast iron of an unknown origin, one has only to know the two material constants and to measure the velocity of longitudinal and transverse ultrasonic waves.

Introduction

In the last ten years several attempts have been made to evaluate the tensile strength of cast iron by ultrasonic methods. (2-4, 6, 8, 10). Two directions of approach are here discernible. The first approach is based on searching the dependence between the tensile strength and velocity of ultrasonic waves or the modulus of elasticity (Young's modulus) (2, 3, 4, 10). In the second, one tries to connect the tensile strength with the attenuation of ultrasonic waves (6, 7).

A modification of these two methods of approach is that proposed by Collaud and applied later by Felix (3, 4). They plot the tensile strength of cast iron against the quotient of longitudinal ultrasonic wave velocity and Brinell hardness number.

As far as we know, no successful method of evaluating the strength of porcelain with ultrasonics has been presented until now.

Critical Review

The existing methods of evaluating the tensile strength of cast iron are rather closely limited to a given grade of cast iron coming from a given foundry. The empirical relationships for lamellar cast iron cannot be extrapolated for cast iron with spheroidal graphite.

The reason appears to be that the relationships shown by various authors are not physically justified. There is no single criterion acceptable to all from which one can deduce the expected relationship. The formulae derived from the many investigations carried out serve only as confirmation of the lack of theoretical basis for the reported relations (1, 5, 9).

The limited range of the existing approach is illustrated in Figures 1a, 1b and 1c which are drawn on the basis of our own investigations carried out on more than 400 specimens of eight grades of cast iron from three different foundries. In addition we used the results obtained in the Laboratories of Technical Supervision Office in Warsaw for three grades of cast iron from one foundry. Thus the departure point for the critical proof of existing solutions and for the new approach consisted of 11 grades of cast iron from four different foundries. Some data for the tested material is presented in Table 1. It shows the number of specimens tested, the spread of strength, i.e. the lowest and the highest strength observed for a given sample size (population).

Table 1
Grades of Cast Iron Tested

No.	Foundry	Cast iron grade	The spread of strength $R_{r\,min} - R_{r\,max}$ in kg/mm²	The number of tested specimens
1	A	Zl 18	12.5—15.5	9
2		22	19.0—22.5	10
3		26	21.0—27.0	10
4	B	Zl 18	11.0—20.0	56
5		22	15.0—26.5	58
6		26	20.0—27.0	60
7		30	14.0—27.5	55
8	C	ZSF 10	47.0—57.5	64
9	D*	Zl 15	14.5—19.0	44
10		20	19.0—24.0	44
11		25	21.0—28.5	44
				454

*Courtesy Technical Supervision Office, Warsaw, Poland.

The relationship between the tensile strength and ultrasonic wave velocity (Figure 1a) shows very distinctly the differences for cast iron coming from different foundries, as well as the great dispersion of experimental values. The dotted areas in Figure 1a are those in which the points for particular samples

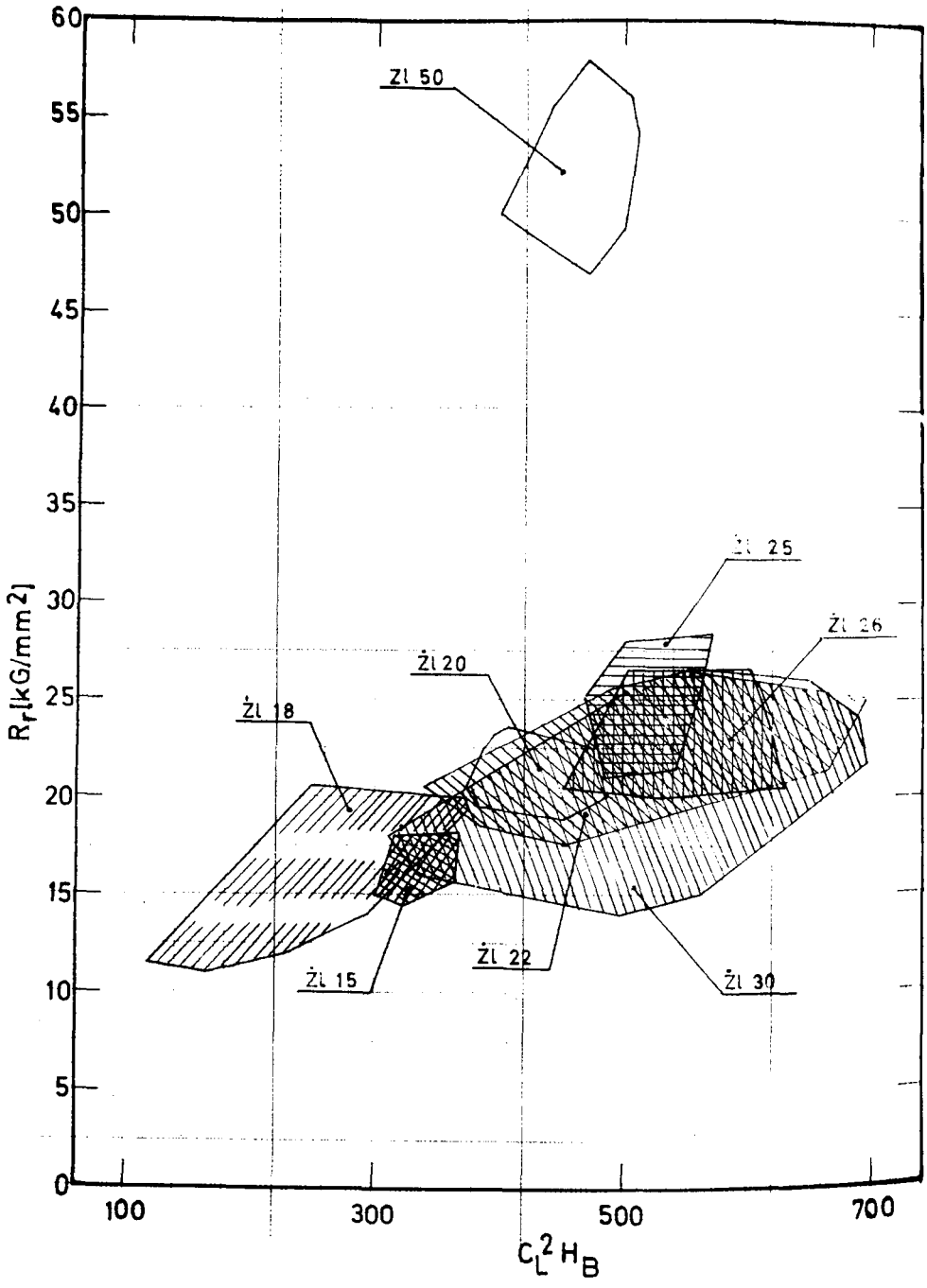

Figure 1(a)
The relationship of tensile strength against ultrasonic wave velocity for cast iron. The numbers in parentheses denote the number of specimens tested.

(populations) were found. In addition two areas for porcelain were also drawn. The numbers in parentheses give the number of specimens tested of a given grade of cast iron or porcelain. Although some authors hope to obtain better results when presenting the strength against the quotient $C_L^2 H_B$ of ultrasonic velocity and Brinell hardness number, in our investigations it appeared (Figure 1b) that the relationship for a wide range of tensile strength (including cast iron with spheroidal graphite), is a multivalued function of the independent variable $C_L^2 H_B$. In the case of porcelain (Figure 1c) one can easily see that there is no relationship at all between the strength and velocity of ultrasonic longitudinal or transverse waves.

Similar results were obtained for the relationship of tensile strength against the attenuation of ultrasonic longitudinal waves, and in the case of porcelain also for the attenuation of transverse waves.

The graphite structure of some of the tested specimens is presented in Figure 2. Although there is no correlation of tensile strength of porcelain against the longitudinal ultrasonic wave velocity, or attenuation, there is a definite correlation between the fracture surface appearance of the porcelain and the tensile strength. In Figure 3 some fracture surfaces are presented. Under each surface the number of the specimen, the load at fracture in tons, and the velocity of ultrasonic longitudinal waves is given. One can easily see that with increasing fracture strength the river-like pattern of the surface becomes more and more pronounced. The flat area near the starting point of the propagating crack is smaller and smaller as the strength increases. The "rivers" on the cleavage plane run in the direction of the propagating crack. A cleavage plane of similar appearance was observed for specimens of other kinds of porcelain. The river-like pattern and small area near the

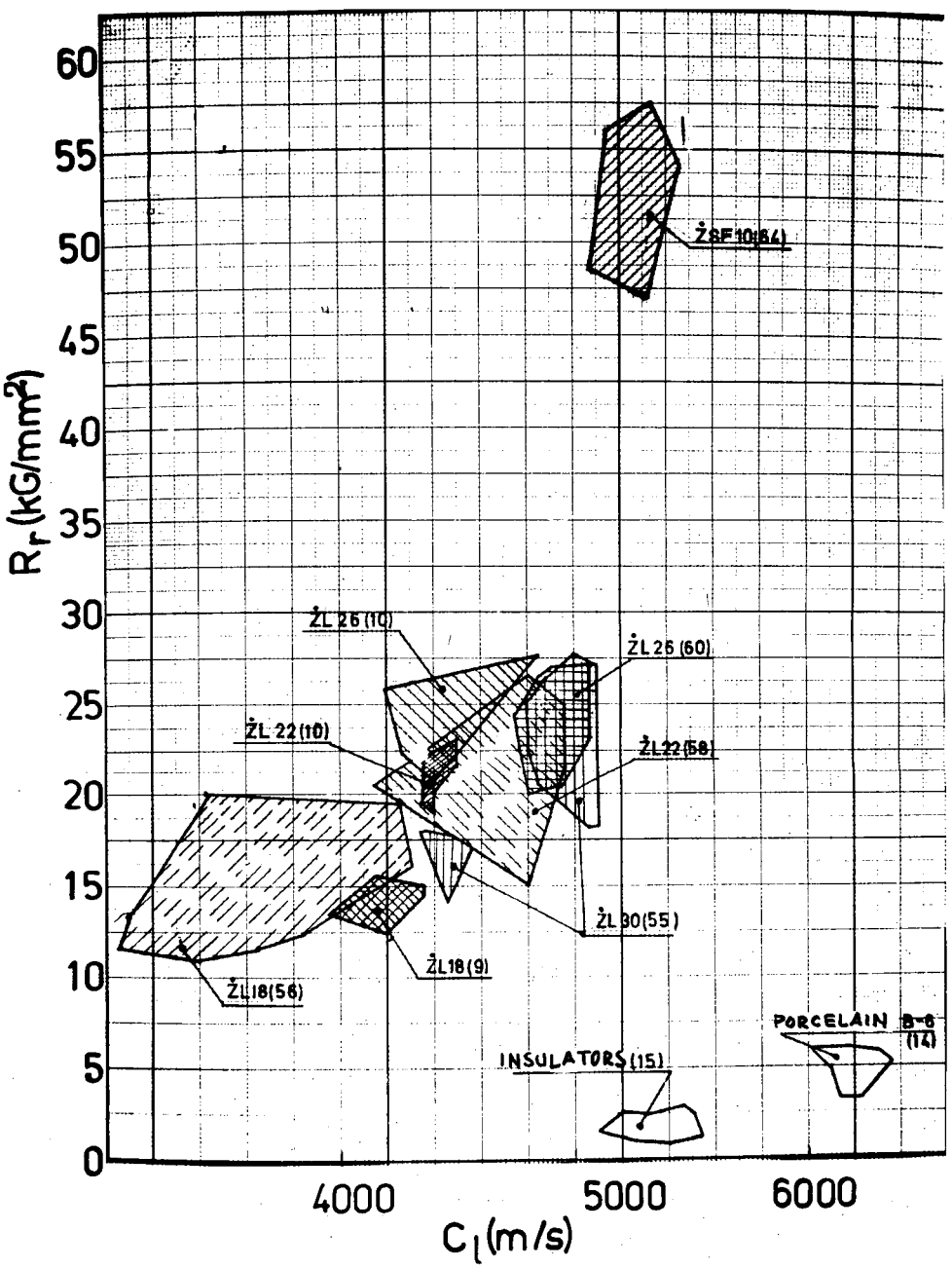

Figure 1(b)
The relationship of cast iron against $c^2_L H_B$.

starting point of the crack were invariably connected with high strength.

The Strength Criterion

The starting point for our approach to the evaluation of tensile strength of both cast iron and porcelain was the strength criterion. Both materials are nonhomogeneous. In cast iron there are graphite inclusions, which give rise to stress concentration. A similar source of stress concentration in porcelain is the porosity. The brittle fracture starts at the point of high stress concentration and propagates with great velocity through the whole cross-section.

In the areas of high stress concentration there is a three-dimensional state of stresses. Let us assume that the radial stress σr and the tangential stress σt are connected with the axial stress σi by the relation

$$\sigma_r = \sigma_t = k\,\sigma_i \tag{1}$$

where $k < 1$ is dependent on the severity of the crack, i.e. on the degree of stress concentration.

For a three-dimensional state of stresses, which is defined by the components of state of stresses or by the components of the stress tensor σ_r, σ_t, σ_i we may write

$$\epsilon = \frac{1}{E}[\sigma_i - \nu(\sigma_r + \sigma_t)] = \frac{\sigma_i}{E}[1 - 2\nu k] \tag{2}$$

For an uniaxial reference state of stress with the stress we have

$$\epsilon = \frac{\sigma_{red}}{E} \tag{3}$$

According to the strength criterion of Saint Venant, i.e., the strength criterion for maximum elongation, which predicts the behaviour of brittle materials, we obtain the relation

$$\frac{\sigma_{red}}{E} = \frac{\sigma_i}{E/(1 - 2\nu k)} \tag{4}$$

If now we put for the uniaxial state of stresses $\sigma_{red} = \sigma_i$, then to satisfy the equation (4) one must replace the modulus of elasticity by the reduced expression i.e. by

$$E_r = \frac{E}{1 - 2\nu k} \tag{5}$$

The introduction of the "reduced modulus" of elasticity according to equation (5) reflects the fact that the fracture is starting from a localized nucleus due to high stress concentration.

The Reduced Elasticity Modulus

In order to express the reduced elasticity modulus E_r by the velocity of ultrasonic longitudinal C_L and transverse C_T waves we put into formula (5) the expression (5)

$$G = \frac{E}{2(1+\nu)}, \quad \nu = \frac{E}{2G} - 1 = \frac{E - 2G}{2G} \tag{6}$$

Using these we obtain

$$E_r = \frac{E}{1 - 2\nu k} = \frac{E \cdot G}{G(1 + 2k) - kE} \tag{7}$$

One can easily see from equation (7) that in the case where no stress concentration occurs, i.e. in the case when $k=0$ the reduced modulus of elasticity is exactly equal to the Young's modulus, $E_r=E$.

The elasticity constants for isotropic materials, i.e. Young's modulus E, the shear modulus G and Poisson's ratio ν are connected with the velocity of ultrasonic waves by the relations

$$E = \delta C_L^2 \frac{(1+\nu)(1-2\nu)}{(1-\nu)}$$

$$G = \delta C_T^2$$

$$\nu = \frac{1 - 2(C_T/C_L)^2}{2 - 2(C_T/C_L)^2} = \frac{1 - 2a^2}{2 - 2a^2}; \quad a = \frac{C_T}{C_L} \tag{8}$$

Putting these expressions into equation (7) we obtain, after some transformations,

$$E_r = \delta \frac{C_L C_T}{C} \tag{9}$$

where

$$C = \frac{1 - 4k + 8ka^2}{6a - 8a^3}$$

The function $C(a)$ does not change very much for "a" values lying, for cast iron and porcelain, in the range 0.53 to 0.64 and 0.60 to 0.70 respectively. Thus if we further assume that the density changes are small or negligible, we may set

$$E_r \alpha = C_L C_T \tag{10}$$

This means that the reduced elasticity modulus defined by equation (5) is proportional to the quotient of ultrasonic longitudinal and transverse wave velocity, and can be conveniently replaced by $c_L.c_T$.

The Uncertainty Principle

Materials which behave in a brittle manner during tension or compression, have the deformation diagram, i.e. the diagram of tensile stress against the elongation, which can be seen in the first approximation as almost nearly linear. If we could accept that the critical value of strain is constant for the given kind of material, then one can see that the relation

$$R_r = E_r \cdot \epsilon_{cr} \tag{11}$$

is justified. Unfortunately we do get from experience the information that the critical value ε_{cr} at which the fracture starts is not constant, but has some statistical distribution. We must therefore rewrite equation (11) in a new form

$$R_r = E_r\, \epsilon_{cr}(R_r) \tag{12}$$

Assuming now that for the given tensile strength, the critical strain ε_{cr} is a linear function of R_r, we may write

$$\epsilon_{cr}(R_r) = \epsilon_{cr\ min} + m R_r = \frac{R_{r\ min}}{E_r} + m R_r \tag{13}$$

After putting expression (13) into (12) we obtain, after simple transformations,

$$R_r = \frac{R_{r\ min}}{1 - m E_r} \tag{14}$$

Adopting further that the proportionality constant $m=1/E_{r\ max}$, where $E_{r\ max}$ is the maximum value of the reduced elasticity modulus E_r we write equation (14) in the form

$$R_r = \frac{R_{r\ min} \cdot E_{r\ max}}{E_{r\ max} - E_r} \tag{15}$$

Let us now set

$$R_{r\ min} \cdot E_{r\ max} = A, \quad E_{r\ max} = B \tag{16}$$

we finally have

$$R_r = \frac{A}{B - E_r} \tag{17}$$

As one can see from the above, the constants A and B, appearing in equation (17) have strongly defined physical meaning. The constant A is the quotient the minimum strength

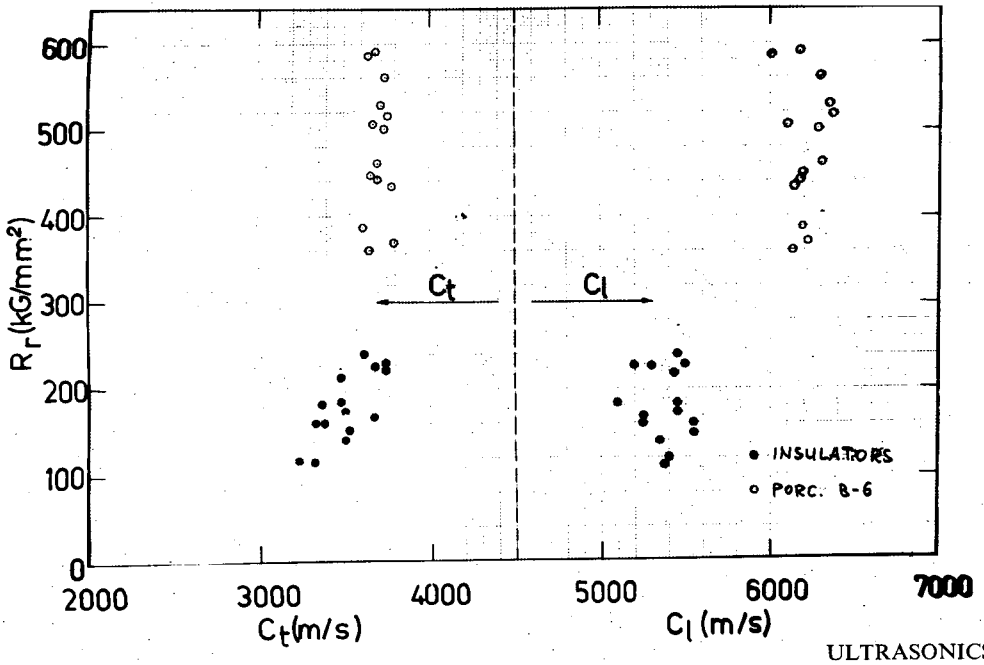

Figure 1(c)
The relationship of tensile strength of porcelain against the velocity of ultrasonic longitudinal C_L and transverse C_T waves.

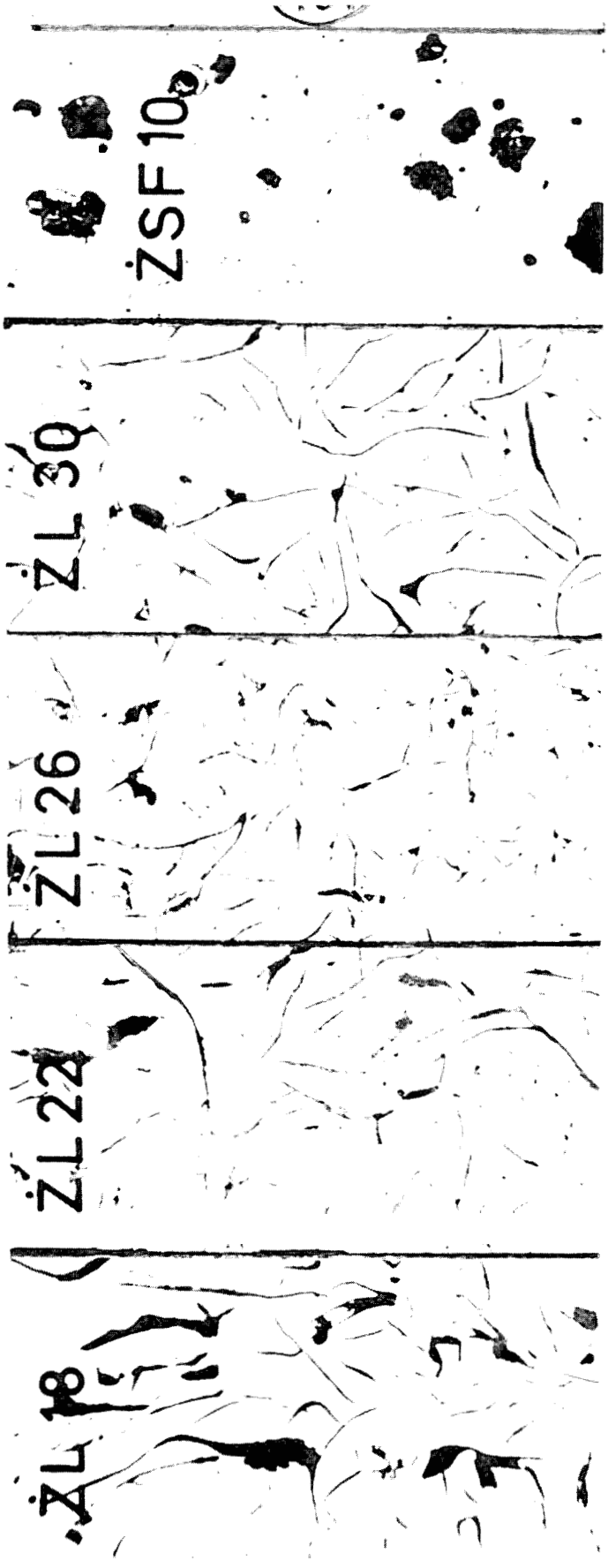

Figure 2. The graphite structure of some tested grades of cast iron × 100, repr. ~2.

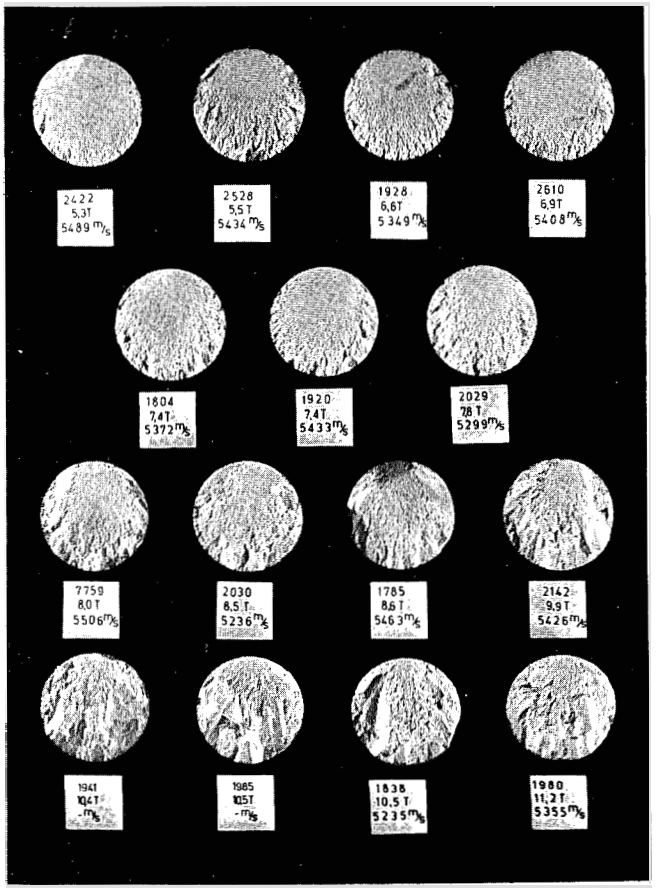

Figure 3. Fracture surfaces of porcelain insulators. Numbers indicate the specimen number, the fracture load in tons and the velocity of ultrasonic longitudinal waves in m/s. 1 T=1 metric ton=0.984 ton, 1 m/s=3.28 ft/sec.

multiplicated by maximum value of the reduced elasticity modulus. The constant B presents itself as the maximum value of the reduced modulus of elasticity for the given kind of material.

A very simple formal approach leads to the same relationship. If we assume that R_r is proportional to the strain

$$R_r = a + b'\epsilon \tag{18}$$

where a and b' are constants, we obtain after putting

$$\epsilon\,\alpha = R_r \tag{19}$$

the following expression

$$R_r = a + b\,R_r \tag{20}$$

which can be brought to the form

$$R_r = \frac{a}{1-b} \tag{21}$$

which is built similarly to equation (17). The constants a and b may be easily expressed by the constants A and B from equation (17).

Since R_r is dependent on the value of the critical strain ε_{cr} and the constants A and B have the meanings of material constants for the given material, equation (17) transformed into

$$R_r\,(B - E_r) = A \tag{22}$$

expresses the principle of uncertainty. This states that the difference of the reduced elasticity modulus multiplied by the tensile strength is constant.

Due to the general assumptions made in deducing equation (17) it seems that it will be valid for all kinds of brittle materials.

Experimental Verification of the Theory

To make an experimental verification of the theory it is convenient to rearrange equation (17) to the form

$$(R_r \cdot B - A) = R_r E_r \tag{23}$$

If we now put $\eta = R_r E_r$ and $(R_r B - A) = \xi$ then all the points obtained from the measurements should concentrate along the line passing through the origin and inclined 45° against the coordinates axis. If we do use another variable, namely $R_r E_r$ and $R_r.B$ then the regression line should be further inclined by an angle 45° and cut, on the coordinates axis, the segments A and $-A$ respectively. This form of presentation is very convenient to the statistical interpretation. It follows also from equation (17) that a linear dependence should exist in the coordinates $c_L.c_T$ and $1/R_r$.

In Figure 4, the results for 8 grades of cast iron—for Zl 18, Zl 22, Zl 26 (Foundry A), and Zl 18, Zl 22, Zl 26, Zl 30 (Foundry B), as well as for ZSF 10, are presented in the coordinates plane $R_r C_L C_T$ and $R_r B$. In general there were 313 specimens, and for 222 of them the mean values out of three specimens cut from the same bar. The specimens were cut from bars having a diameter of 30 to 40 mm. The diameter of specimens for tensile testing was 20 mm, the length 91 mm. The velocity of ultrasonic transverse waves was measured at 1 MHz frequency, that of longitudinal waves at 3 MHz.

In Figure 4 the regression line having the equation

$$R_r = \frac{150}{18.75 - C_L C_T} \; [kg/mm^2] \tag{24}$$

is shifted by a segment $A = 150$ to the right from the origin. The value cut on the horizontal axis exactly equals the quotient of minimum tensile strength and maximum reduced elastic modulus, replaced in our case by the $c_L.c_T$. The regression line was obtained with the help of the least-squares method. In Figure 4 we set, instead of the reduced elastic modulus, the corresponding values $C_L C_T$ in accordance with equation (10).

Table 2
Some Values of Mechanical and Acoustical Properties of the Cast Iron Tested

	R_r kg/mm²	$C_L.C_T$ (m^2s^{-2}), 10^{-6}	R_r $(B-C_LC_T)$ (kgmm^{-2} $m^2s^{-2})10^{-6}$	R_r *estimated* kg/mm²	$\Delta R = R_{r\,estim} - R_r$
Foundry A					
Zl 18	14.5	9.30	137.03	15.9	1.4
	15.0	10.10	129.75	14.9	−0.1
	13.5	9.12	130.00	16.4	2.9
Zl 22	19.5	10.75	175.50	18.8	−0.7
	20.0	10.75	160.00	18.8	−1.2
	22.0	10.60	179.30	18.4	−1.6
Zl 26	27.0	12.00	182.25	22.2	−4.8
	21.5	10.60	175.23	18.4	−3.1
	21.0	10.50	173.25	18.2	2.9
Foundry B					
Zl 18	15.5	9.10	149.38	15.6	−0.1
	15.0	8.49	153.90	14.6	−0.4
	15.0	9.92	147.45	15.3	0.3
Zl 22	19.1	11.25	143.25	20.0	0.9
	24.1	12.22	157.37	23.0	−1.1
	19.6	11.51	141.90	20.7	1.1
Zl 26	20.7	12.51	129.17	24.0	3.3
	24.4	12.75	146.40	25.0	0.6
	25.4	12.69	153.92	24.8	−0.6
Zl 30	22.5	12.24	146.48	23.0	0.5
	27.0	12.97	156.06	26.0	−1.0
	26.5	12.95	153.70	25.9	−0.6
Foundry C					
ZSF 10	54.0	15.88	154.98	52.2	−1.8
	54.5	16.05	147.15	55.6	1.1
	50.0	15.87	144.00	52.0	2.0

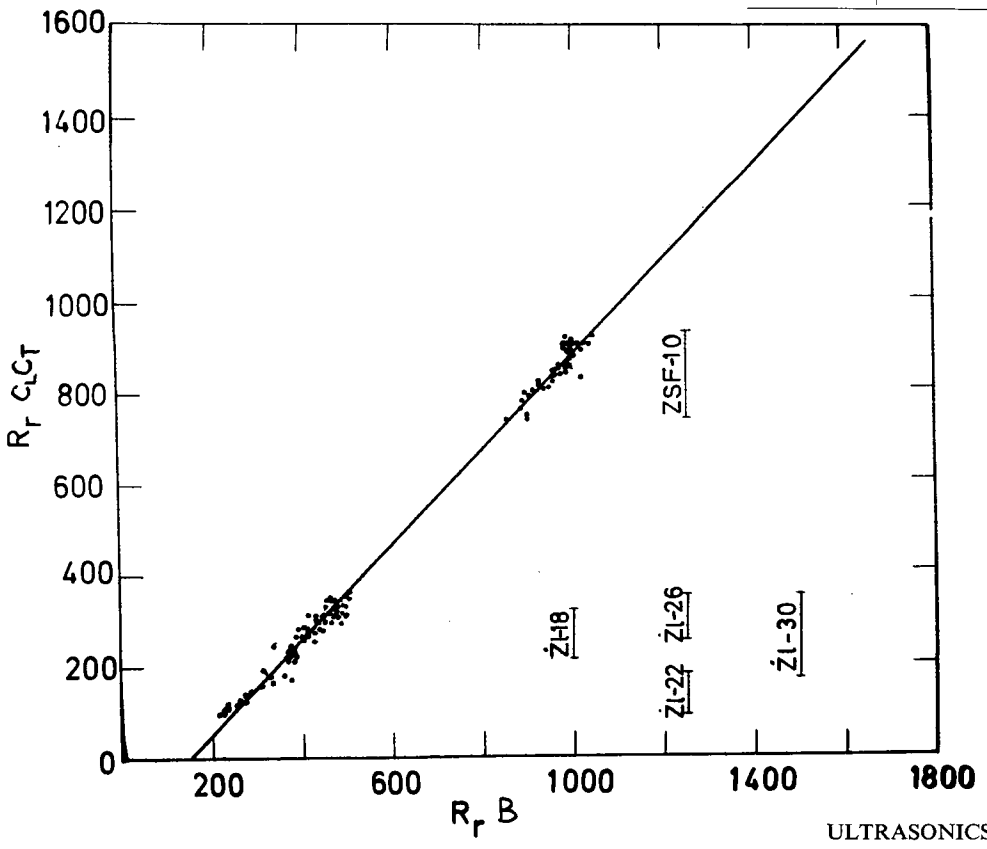

Figure 4
The relationship $R_r c_L c_T$ against $R_r B$ for cast iron. Eight grades of cast iron (cf Table 1), 313 specimens.

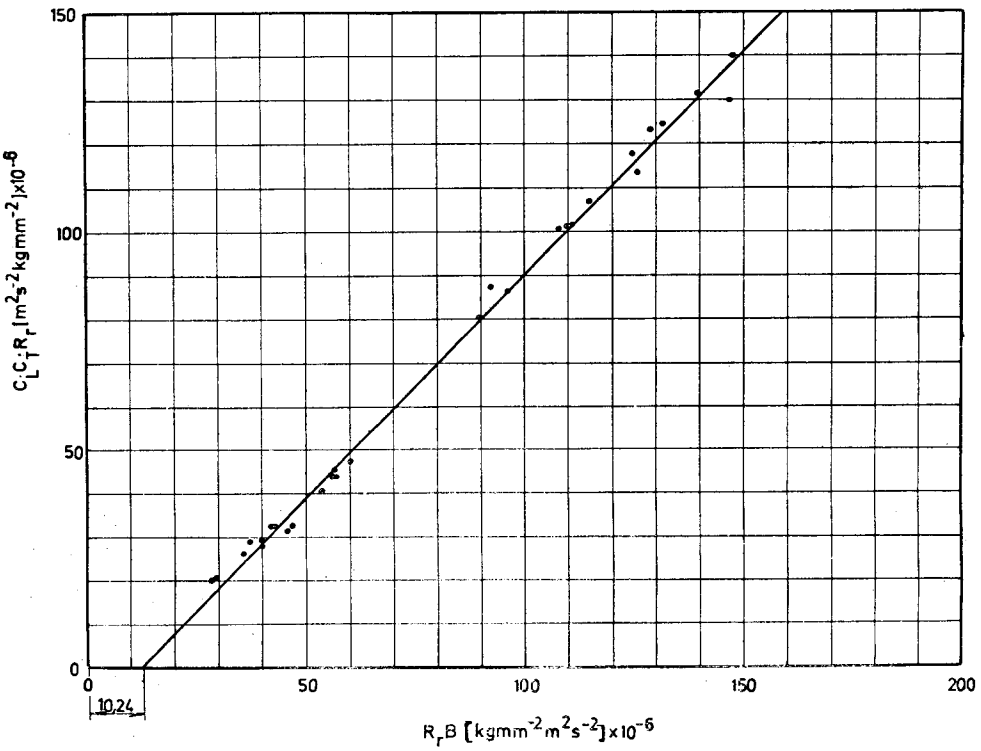

Figure 5
The relationship $R_r C_L C_T$ against $R_r B$ for porcelain (two grades of porcelain).

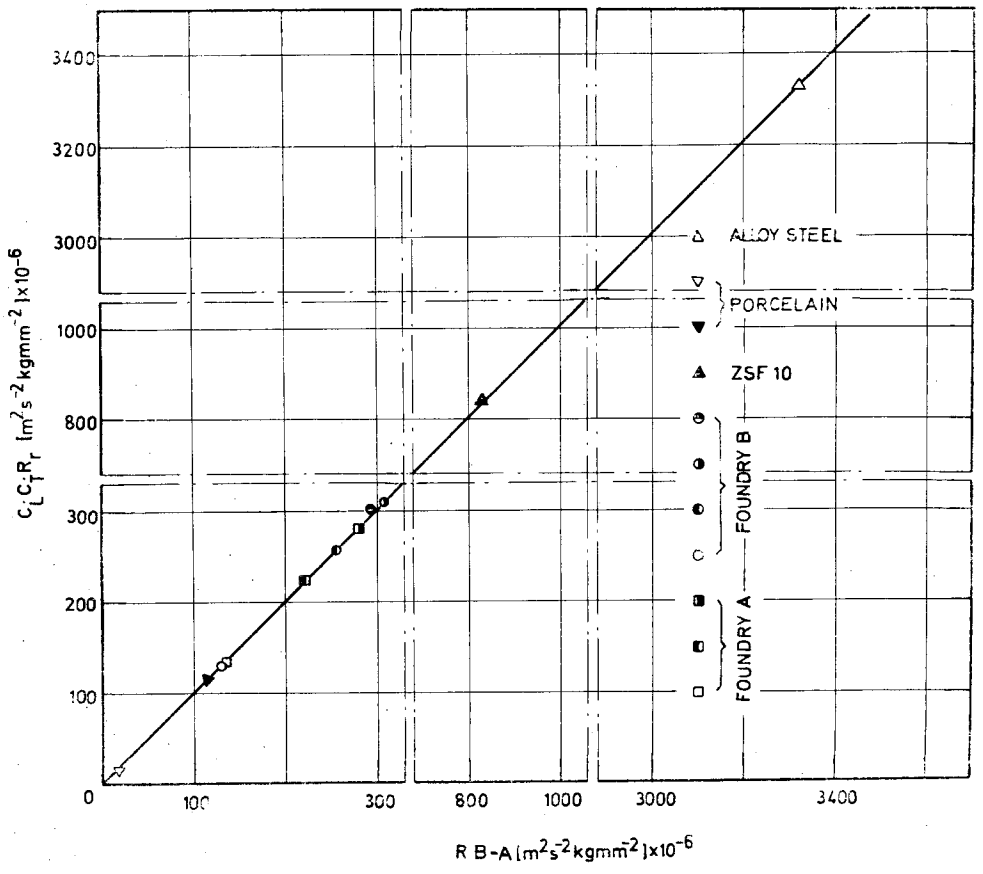

Figure 6
Mean values for different grades of cast iron and porcelain brought to a common line.

For electrotechnical porcelain we derived, by the least-squares method, the following regression line

$$R_r = \frac{10.24}{25 - C_L C_T} [kg/mm^2] \tag{25}$$

The results for porcelain are presented in Figure 5. As in the case of cast iron the regression line and the results distributed randomly along this line are presented in coordinates $R_r C_L C_T$ and $R_r B$. Owing to this the line intersects the horizontal axis at 10.24 i.e. the value of A for porcelain.

In Figure 5 the results for two kinds of electroceramics are given. The specimens tested had the form of 76-mm-dia insulators and specially prepared 20-mm-dia probes. The velocity of ultrasonic waves was measured at the frequency 6 MHz.

In Figure 6 the results for cast iron and porcelain are brought to the common line crossing the origin of the coordinates axis and inclined by an angle 45°. This was obtained by plotting $R_r C_L C_T$ against $R_r B - A$. In order to have a clear picture of the relation only mean values for the given kind of cast iron and porcelain were introduced into the figure. As it was expected by theory, all the points lie around the theoretical line. In the figure an additional point was introduced, for alloy steel, which behaves in a brittle manner in simple tension. In this case the constants A and B are somewhat higher than for cast iron.

Discussion

Some values for randomly chosen specimens of cast iron are presented in Table 2, where a comparison is given between the predicted values and values obtained from tensile tests. Similar results are presented for porcelain in Table 3. The mean values of mechanical and acoustical properties of the tested cast iron grades are shown in Table 4.

One easily can see from the tables that the difference between the estimated tensile test values amounts to only several per cent for cast iron. The accuracy of the estimate can be more accurate when the evaluation is based on the mean values of velocity taken from several tests. For porcelain the mean deviation from the "true" values is about 14%. As one can see from Table 3, for specimens of porcelain B-6 the deviations were 97% and 80.5% in two cases. The probability of such values occurring is quite high when short specimens are tested. This is due to the slight deviation of the axial load even then when the test is very carefully carried out. The unavoidable departure from the axial loading in tensile tests diminishes the "true" value of the tensile strength as can be seen from Table 3. For the insulators whose length is much greater than that of the probes such great deviations were not observed. It is still worth pointing out that the errors in measuring ultrasonic wave velocity have a greater influence on the evaluated strength for high strength than for lower strength. For example let us as-

Table 3
Mechanical and Acoustical Properties Two Kinds of Porcelain

No.	P kg	R_r kgcm^{-2}	C_L ms^{-1}	C_T ms^{-1}	$C_L C_T$ (m^{2}s^{-2}) $\times$ 10^{-6}	$R_r C_L C_T$ (kgmm^{-2} · m^{2}s^{-2})10^{-6}	$R_r(B\text{-}C_L C_T)$	$R_{r\,estimated}$ kg cm^{-2}	$\Delta R = R_{est} - R_r$	$\lvert\Delta R\rvert$ %
				Insulators						
1941	10400	224	5300	3750	19.9	44.6	11.4	201	−23	10.2
1838	10500	226	5210	3750	19.5	44.1	12.4	186	−40	17.7
1985	10500	226	5500	3690	20.3	45.9	10.6	218	− 8	3.5
1980	11200	241	5450	3620	19.7	47.5	12.8	193	−48	19.9
2142	9900	214	5430	3480	18.9	40.5	13.0	168	−46	21.5
2030	8500	183	5100	3370	17.2	31.5	14.3	131	−52	28.4
7759	8000	172	5450	3510	19.1	32.9	10.1	173	1	0.6
1785	8600	185	5450	3480	19.0	35.2	11.1	171	−14	7.6
2029	7800	168	5250	3690	19.4	32.6	9.4	183	15	8.9
2528	5500	118	5400	3230	17.5	20.7	8.9	137	17	14.3
1920	7400	160	5550	3340	18.5	29.6	10.4	157	− 3	1.9
1804	7400	160	5250	3380	17.8	28.5	11.5	142	−18	11.2
1928	6600	142	5350	3500	18.7	26.6	8.9	162	20	14.0
2610	6900	149	5550	3530	19.6	29.2	8.1	190	41	27.5
2422	5300	114	5380	3320	17.9	20.4	8.1	144	30	26.4
				Specimens of porcelain B–6						
12	1620	590	6180	3680	22.7	133.9	13.5	445	−145	24.6
6	1610	586	6020	3640	22.0	128.9	17.6	332	−254	43.3
20	1520	559	6300	3740	23.5	131.4	8.4	682	123	22.0
1	1465	528	6350	3720	23.6	124.6	7.4	732	204	38.6
13	1340	515	6370	3760	23.9	123.1	5.7	930	415	80.5
8	1390	506	6100	3670	22.4	113.4	13.2	394	−112	22.1
11	1420	501	6280	3740	23.5	117.7	7.5	682	181	36.0
4	1226	461	6300	3690	23.2	107.0	8.3	569	108	23.4
10	1265	446	6190	3670	22.7	101.2	10.3	445	−1	0.2
16	1200	442	6180	3700	22.9	101.2	9.3	487	45	10.2
5	1310	434	6150	3780	23.2	100.7	7.8	569	135	31.1
7	1060	386	6190	3620	22.4	86.5	10.0	394	8	2.1
14	1020	371	6220	3800	23.6	87.6	5.2	731	360	97.0
18	980	361	6130	3650	22.4	80.9	9.4	394	33	9.1

Table 4
Mean Values of Mechanical and Acoustical Properties of Grades of Cast Iron Tested

	Foundry A			Foundry B				Foundry C	Foundry D		
	Z1 18	Z1 22	Z1 26	Z1 18	Z1 22	Z1 26	Z1 30	ZSF 10	Z1 15	Z1 20	Z125
C_L [m/s]	4161	4405	4500	3715	4736	4962	4884	5322	4080	4350	4685
C_T [m/s]	2306	2457	2498	2375	2503	2548	2614	2991			
$C_L \cdot C_T$ $[m^2/s^2] \times 10^{-6}$	9.60	10.70	11.25	8.80	11.80	12.60	12.70	15.90			
R^r [kg/mm^2]	14.22	20.95	24.65	14.97	21.48	24.42	23.15	53.19	17.36	21.25	25.68

sume a 5% error in the measuring of $c_L.c_T$ for the value $c_L.c_T = 24 \times 10^{-6}$ m^{2}s^{-2}; then we have an error in strength amounting to 54.5%. The same error in ultrasonic wave velocity measurement, i.e. 5%, for $c_L.c_T = 22 \times 10^{-6}$ m^{2}s^{-2} gives a 24.2% error in estimated strength.

The mean values for mechanical and acoustical properties presented in Table 4 show some differences in longitudinal wave velocity for cast iron having approximately the same tensile strength. This, together with the statistical analysis of the values $R_r(B-C_LC_T)$, shown in Table 3 is discussed elsewhere (7).

Conclusions

The results presented confirm the supposition that there exists a general relationship between the strength of brittle material and the velocity of ultrasonic longitudinal and transverse waves. To estimate the strength only two material constants have to be known and they have sharply defined physical meaning. The material constants seem to be the same for materials having the same crystallographic structure. To prove this statement, further experiments are needed on materials other than those that are the subject of this paper.

References

1. Brunarski L. Gleichzeitige Anwendung verschiedener zerstörungsfreien Prüfmethoden Zur Gütekontrolle des Betons, Wiss. Zeit. Hochsch. Bauwesen Leipzig, Sonderdruck, (1963), 191-197.
2. Bierwirth, G. Zerstörungsfreie Prüfung von Gusstucken durch Ultraschall, Giesserei **44,** (1957), 477-485.
3. Felix, W. Der Elastizitätsmodul als Hilfsmittel bei Qualitätsbeurteilung von Gusseisen. Giesserei **10,** (1963), 6-11.
4. Felix, W. Nondestructive tensile testing of cast iron. *Metal Progress,* **83,** (1963), 91-95.
5. Filipczynski, L., Pawlowski, Z. and Wehr, J., Ultrasonic Methods of Testing Materials, Butterworths, London, 1966.
6. Jarvis, J. A. F. Determination of tensile strength of cast iron by ultrasonics. Proc. Fourth Intern. Conf. NDT, Butterworths, London, 1964, 173-175.
7. Pawlowski, Z. Statistical Interpretation of Ultrasonic Testing Results, to be published.
8. Reti, P. Gütekontrolle von kugelgraphitischem Gusseisen mit Ultraschall. Wiss. Z. Hochsch. Schwermaschinenbau, Magdeburg, **3,** (1959), 195-202.
9. Sawczuk, A. and Brunarski, L., Ultradzwiekowe badanie jakosci i jednorodnosci betonu w konstrukcjach. Zesz. Probl. Nauki Polskiej, XXVI, 1965, 396-409.
10. Ziegler, R. and Gerstner, P., Die Schallgeschwindigkeit als kennzeichnende Grösse für die Beurteilung von Grauguss. 24 Intern. Giessereikongress, Stockholm 19-24. VIII, 1957, Vortrag Nr. 6.

Project Apollo–Automated Ultrasonic Bond-Quality Inspection

C. C. KAMMERER, USA

ABSTRACT: This paper describes the conception, design, development, construction, and operation of two large ultrasonic inspection systems. These systems are used to determine and record bond quality on all adhesive bonded assemblies of the Saturn S-II booster and the Apollo Command and Service Modules. Both systems use turntables to rotate the test parts—most of which are revolute sections—and use tape-programmed drives to position ultrasonic water-squirter assemblies on opposite sides of the parts for the ultrasonic inspection. The ultrasonic information is recorded on scale models of the test parts. These systems are the largest ultrasonic inspection machines ever built, and several advances in "state of the art" were made during their development.

Introduction

Five hundred pounds of fuel are needed to place each pound of the manned Apollo capsule in orbit for a lunar voyage. The NASA Project Apollo will stand 360 feet tall above the launching pad, will weigh roughly six million pounds and will be placed in orbit by three Saturn booster rockets, together generating 8.7 million pounds of thrust. These staggering figures clearly show why honeycomb sandwich structures have gained increasing demand by the aerospace industry where strength at the lowest weight is basic for extending payload delivery capabilities to the maximum.

The Space and Information Systems Division (S&ID) of North American Aviation, Inc., Downey, California, was awarded the contracts to build the Apollo Command and Service Modules, the Lunar Excursion Module adapter panels and the Saturn S-II booster which all use bonded honeycomb panel

structures. Similar assemblies are also used on the Saturn SIC and S-IVB currently undergoing development by other companies for the same project.

During the conceptual stages of the manned lunar space program, the Quality Assurance Department of S&ID organized an evaluation team to investigate all methods of the non-destructive testing of honeycomb assemblies to establish the most suitable means for determining the quality of the adhesive bonds. Known inspection methods and techniques were repeatedly compared and analyzed by the team. Their findings indicated ultrasonic testing to have the most promise for determining the integrity of all bonded honeycomb assemblies. The study further showed that this method of testing would indicate a good bond only when the adhesive had surface molecular attachment. Automatic testing and recording systems complemented with rigid process control were deemed mandatory to assure reliability of the test results.

Development of Inspection Techniques

The primary purpose of performing an inspection on these components and assemblies is to determine the quality of the attachment of a panel facing sheet, or several laminated sheets (doublers), to the honeycomb cell structure (core), and attachment of the core to the facing sheet and doublers on the opposite panel side. Initial tests indicated that an inspection could be performed by either the pulse-echo technique, in which propagated ultrasonic waves are reflected by a lack of bond back to the generating transducer, or by the through-transmission technique in which the propagated ultrasonic wave travels through a well-bonded panel on to a receiving transducer.

The through-transmission technique was considered most satisfactory if sufficient wave energy could be generated to propagate through the thick and highly attenuative honeycomb structures owing to the fail-safe nature of such an inspection. Any obstruction in the path of an incident ultrasonic wave, whether it be a facing sheet detachment, fractured core, or other refracting interface, would prevent a wave from reaching its intended goal.

To prove the practicability of a through-transmission inspection vs. pulse-echo inspection for specific cases in question, test panels were fabricated, duplicating the more complex cross-sectional geometry of the Apollo and Saturn S-II assemblies. These test panels, with controlled void patterns at all sandwich interfaces, were subsequently inspected with different types of ultrasonic equipment using several types of wave propagation and detection principles.

Results of preliminary investigations showed ultrasonic through-transmission techniques to be the most suitable for reliably detecting voids at all interfaces of adhesive-bonded structures. The low signal-to-noise ratio obtained from commercially available ultrasonic equipment used during the development tests indicated that the limitations of the equipment were attributed primarily to transducers and not instrumentation. Several problems, such as establishing the type of wave propagation which exists when coupling waves through complex adhesive-bonded honeycomb structures, also affected the transducer design parameters.

The tests and data gathered showed that propagation through the panel skins was longitudinal, with wave fronts parallel to the skin, while propagation through the cell walls was a complex combination of shear and surface waves. Mode conversion would, consequently, take place at least twice through a simple sandwich structure during a through-transmission test. Losses resulting from the conversions and acoustical impedance mismatch at the many interfaces indicated the need for high-power transducers.

High conversion efficiency transducers from 0.5 to 5 MHz were required to adequately inspect all panel configurations including sandwich structures with 0.010-in.-thick chem-milled facing sheets. Special low damped, high "Q" ceramic transducers were developed specifically for this purpose. The frequency, power, and sensitivity requirements were such that standard immersion-type ultrasonic instrumentation could be selected.

System Concept

In addition to developing ultrasonic techniques, a general concept of mechanical scanning and recording systems was evolved. The NDT systems group of the Budd Company, consulting with the S&ID Quality Reliability Assurance Department of NAA designed and constructed both the Apollo and Saturn S-II inspection systems after repeated evaluation of the inspection parameters. The design criteria for both systems changed many times during the conceptual stage as the design details of the panel assemblies were refined.

The system performance required for inspecting Apollo and Saturn S-II panel assemblies evoked many new component and system-design concepts, heretofore not used with ultrasonic inspection equipment, and the considerable improvement to several previously adequate support equipments. The large size and complex geometry of the space vehicle panels posed numerous tooling problems in both the panel and transducer assemblies. An absolute static and dynamic position tolerance of the assemblies had to be maintained to assure the necessary location and attitude relationship of all assemblies during an automatic inspection mode.

All the panel assemblies requiring inspection were either flat or bodies of revolution which indicated that individual rotating-type fixtures, XY scanners, and turntables would be appropriate to permit a greater inspection rate than would be realized with one universal inspection tool. This original concept was discarded as the panel geometry developed, and it was realized that greater versatility was required, including the capability of through-transmission inspection of the entire part. Turntable assemblies, unaffected by protrusions, were therefore selected to support and position the parts so that transducer programming of only two axes would be required. The through-transmission inspection technique further necessitated the design of a centreless-type turntable to provide adequate space for a rigid inner transducer positioning assembly.

Proper synchronization of the inner and outer transducers for the through-transmission inspection of space vehicle panels was the foremost design consideration. During the conceptual stages, tracks, for guiding and supporting both the inner and outer transducer assemblies, were thought the most reliable and simple method for maintaining synchronization. Since the panels did not have plain geometric shapes or uniform cross-sections and, because the system versatility was greatly limited as to the size and geometry of the panels, an independent three-axes position program of the transmit and receive transducers became a part of the fundamental design.

The test results of the ultrasonic inspection would be subjected to analysis by the S&ID Quality Reliability Assurance Department, as well as other responsible departments, for acceptance or rejection. Therefore, the data accumulated had to be presented so as to preclude any chance for ambiguity regarding the orientation of specific test information. The task of displaying such a permanent inspection record created the need for a new recorder design that would indicate clear, interpretable, and precisely situated test results capable of displaying the unbond conditions as to size and extent of the unbond, preferably as a halftone shading. It was reasoned that a reduced size model with an electrosensitive surface, exactly duplicating the panel shape

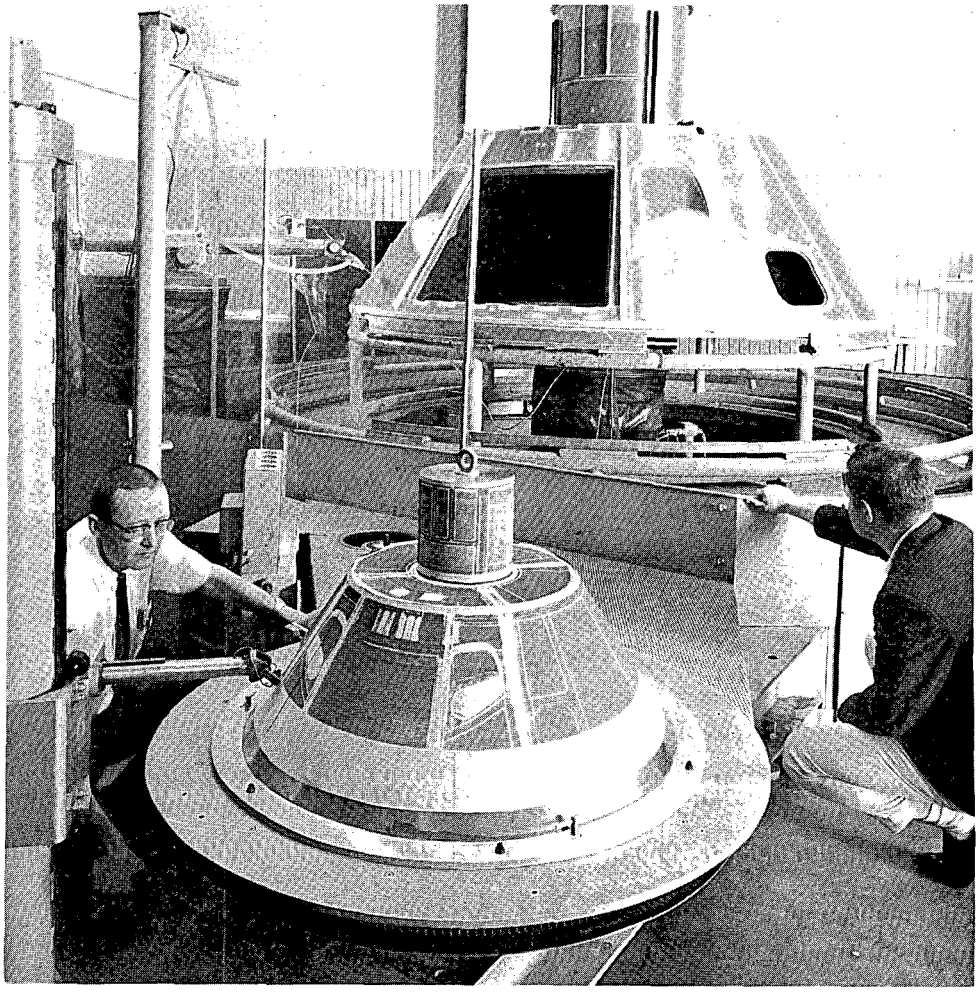

Figure 1. Ultrasonic "C" scan recorded results of an Apollo Command Module crew compartment forward section. The scaled down recording depicts bond integrity with single honeycomb cell resolution.

to be inspected, would provide the recording surface geometry ideal for interpretation (Figure 1). The model would be supported and rotated by a synchronized turntable and a recording stylus assembly would translate the transducer-to-panel-surface relationship. A three-dimensional recording would be produced when test voltages, matched to the coating sensitivity, were applied to the stylus thus causing "writing" during a specific bond condition.

Engineering Design

The above system concept briefly describes the basis for the individual component design. Since all of the primary functions were interrelated and because of the size, complexity, and integrated nature of the systems, design consideration was given to facilitate assembly at the S&ID Downey and Seal Beach inspection sites.

Transducer Positioning Assemblies

The Apollo and Saturn S-II System performance requirements were closely related as to function, accuracy, and inspection speed. The relative size and complexity of the panel assemblies characteristic to each system greatly affected the appearance, detail design and program of the two systems. The relatively small Apollo (Figure 2) with a maximum panel diameter of approximately 12 ft, consisted of cylindrical, truncated, hemispherical and flat sections with varying lengths, and non-symmetric internal and external protrusions.

However, the Saturn S-II (Figures 3 and 4) consisted of bulkhead and LH-2 tank panels approximately 33 ft in diameter without extensive protrusion.

The Apollo inner transducer positioning assembly had to retract to an out-of-the-way position for inspecting the service module bulkhead and aft section of the inner crew compartment panels. Conventional (horizontal and vertical) "XY" transducer positioning assemblies were employed to position the inner and outer transducers vertically and horizontally. The vertical support tubes were anchored in 15-ft-deep casements in the concrete floor to permit full retraction of the vertical booms. The inner transducer cross-feed tube was required to extend rigidly to cantilever the transducer 7 ft from the centre and also telescope during positioning and to have a total length of 4 ft so as to clear obstructions in the truncated command module (Figure 2) section. Double-geared rack-drive tubes, approximately 3½ ft long, were designed to achieve this.

The Saturn S-II outer transducer positioning assembly (Figures 3 and 4) was designed to support a transducer approximately 20 ft horizontally, inward from its anchored position, while maintaining a rigid support structure. Inner and outer two-axes support booms were constructed, in lieu of curved tracks, to position the transducer carriages tangent to two points on both the inner and outer bulkhead surfaces to provide the necessary transducer support structure profile. Search tubes, extending perpendicular from the carriage axes, were used to position the transducers with respect to the boom axes. Inner and outer transfer tables pivoted the associated transducer carriage from the lower booms to the upper booms to facilitate the transfer of the carriages. The outer double-boom assembly was constructed to pivot to an out-of-the-way position to permit the inspection

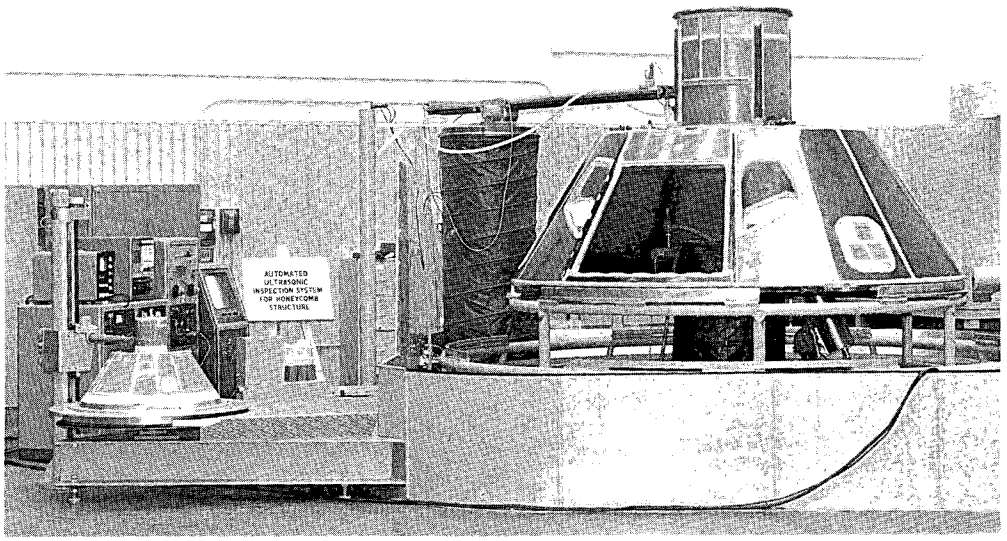

Figure 2.
Forward inner crew compartment with instrumentation in background consisting of two ultrasonic detectors with frequency range of 0.5 to 25 MHz, gate adapters, punched tape reader with positioning translator, and closed-circuit TV for monitoring clearance of inner transducer.

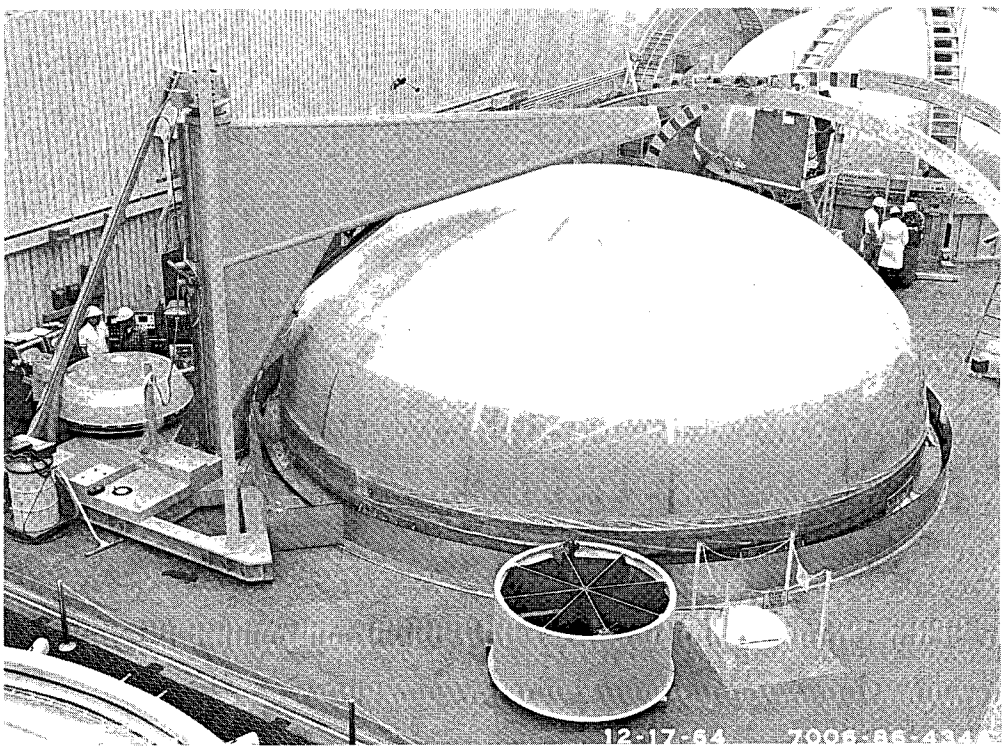

Figure 3.
Saturn S-II common bulkhead during an ultrasonic inspection. The massiveness of the structure is evident by comparing the bulkhead to the personnel standing behind the $\frac{1}{5}$ scale recorder model.

of an LH-2 tank section. An inner vertical boom was provided to extend into position for the inspection of these tanks.

Both systems were also equipped with transducer gimbal motions to control the transducer attitude with respect to the search-tube axes. All of these motions were accomplished with stepping motors that impart an exact and repetitive motion (each command signal causes 1.8° of armature rotation) when properly controlled. Both systems thus required six channels of stepping-motor control to provide the necessary independent control of three inner and three outer transducer motions.

Centreless Turntable Assembly

The turntable assemblies consisted basically of two main components: (1) a thrust race supported by the concrete floor, and (2) a rotary table with radial and axial thrust-bearing stations equally spaced around the table. The radial thrust bearings were included to maintain concentricity of the table with the race, while the axial thrust bearings supported the space vehicle and table assembly with tooling load. A chain drive was selected to provide positive positioning of the assembly to assure synchronization of the part table with the reduced scale recorder model table. Variable-speed drive motors permitted the high inertial turntable loads to be started, rotated, and stopped without losing synchronization. The Saturn S-II turntable was also equipped with a two-speed motor starter fluid coupling to further reduce the initial chain load.

Three-Dimensional Recorder

Recorder models were fabricated and electrosensitive coatings were sprayed on the conductive forms to provide a recording surface that would not deteriorate with age, that could be handled without extreme care, that would provide several shades of halftone information with good resolution ability, and that did not require a special environment. The last criterion ruled out coatings such as photographic emulsions, facsimile recorder surfaces and other duplicating coatings. The parameters required

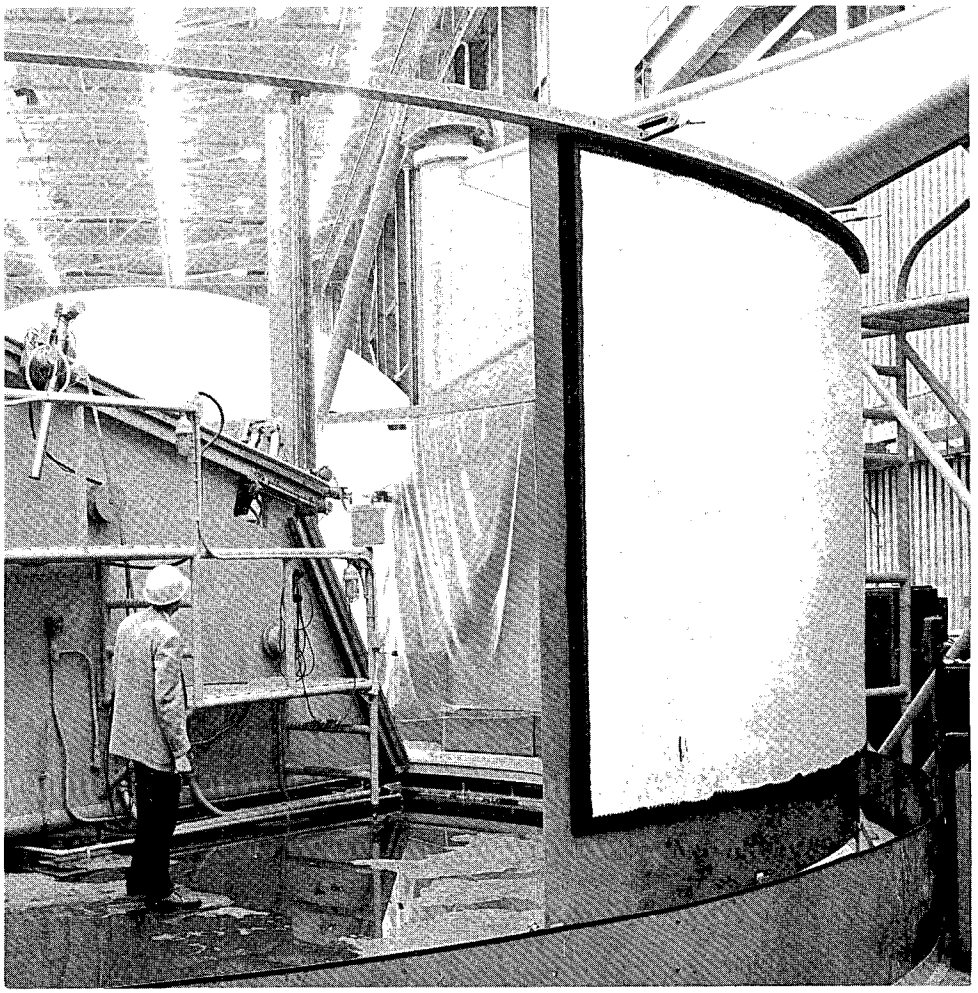

Figure 4.
Saturn S-II LH-2 tank quarter panel inspection for insulation bond integrity. The outer and inner transducer carriage assemblies used for bulkhead inspection are parked out of position during tank wall inspection.

for applying coatings developed specifically for the Apollo and Saturn S-II panel assemblies were too rigid to maintain except under laboratory-controlled conditions. Models were subsequently developed to approximate the panel configurations yet permit a dry-type "weather map" halftone recording paper to be wrapped around the form and held in contact with the form surface. Some difficulty was encountered when the slight arc generated by the stylus, during the recording process, produced electrical signals detrimental to the sonic unit operation. The harmful effects were successfully eliminated by a bypassing network. Reduced scale three-dimensional halftone recordings of the various Apollo and Saturn S-II panels were thus sucessfully obtained.

Tape Programming

Eight-channel tape readers were employed by both systems as the program control. Since the position and gimbal motions of both the inside and outside transducer assemblies required an independent program, six channels were designated for their control. One channel was used to control the transducer positioning logic during an automatic inspection cycle, and the eighth remaining channel was used to control the turntable angular velocity necessary to maintain a uniform surface inspection speed and recorder-writing density.

The program information was generated with the aid of a high-speed computer coded with the necessary mold-line equations for both the inner and outer surfaces of a specific panel assembly. A complete series of calculations was performed and the data thus obtained were stored on magnetic tape and transferred, by a punched tape computer, to mylar tape in a usable coded form.

The programmed tape is indexed past the tape reader photocell head to initiate the operation of each controlled function. The hole arrangement for each stepping-motor channel satisfies the previously computed transducer position change as required to conform to the panel geometry being inspected. Since the tape reader is only required to initiate automatic, programmed transducer indexing each turntable revolution, the function is provided with a control to permit the transducer index increment to be adjusted by the operator.

Acceptance and Production Testing

Initial ultrasonic inspection of the Apollo and Saturn S-II assemblies was performed on the regular production assemblies as they were available during the acceptance testing period. Acceptable performance capabilities of both systems required the satisfactory inspection of one of each of the representative honeycomb sandwich configurations illustrated in Figures 1, 3 and 4.

Each assembly required careful preparation prior to its inspection to assure that water from the squirter assemblies could not enter through joined areas such as laps, closeouts, or joggles and become entrapped within the sandwich structure. Possible leak-path areas were sealed with a strippable maskant consisting of a masking tape base later coated with a solvent-evaporate, low-adhesion elastomer. The sealing technique provided a seam impervious to water penetration that could

readily be removed and cleaned off without leaving a residue.

The prepared assembly was then set in place on the turntable with the applicable tooling. The position and relative clearance of the assembly surface and protrusions with respect to the transducer water squirters was checked and adjusted. The pressure to the water squirters was adjusted and the instrumentation, recording model, and all program controls were readied for an automatic inspection as required by the specific test (Figures 2, 3 and 4).

A production "C" scan inspection of the entire assembly and its associated test standard was subsequently performed to verify the systems' production inspection capabilities. All suspected void areas recorded were further evaluated by complementary ultrasonic techniques such as contact, resonant, frequency-shift, sonic, and dimensional checks to locate voids to their respective sides and interfaces, to facilitate their repair.

Redesign of the water squirter assemblies was then accomplished to lengthen the effective sustained water column. The design geometry was altered ultimately to permit a distance of up to 12 in., in several instances, to be maintained from the squirter orifice to the inspection surface. Distances of up to 6 in. were reliably maintained at all times. (Figure 1)

Discussion

The development of the Apollo and Saturn S-II ultrasonic systems has led to the rapid advancement of new automatic inspection equipments. Principally, the use of stepping motors, because of their reliability and ability to provide an exact and positive motion when activated, permitted the development of remote-controlled synchronizing assemblies which made design of the systems possible. The adaptation of punched tape-reader programming to ultrasonic inspection systems further contributed to the feasibility of systems capable of automatically inspecting geometric shapes previously considered impractical. This programmed method of positioning readily adapts to many other complex positioning and synchronizing needs frequently encountered by inspection departments.

More than 2,000 Apollo and Saturn S-II adhesive bonded assemblies have been successfully inspected by the S&ID Quality Control Departments since the installation of both ultrasonic inspection systems. The photographs illustrate the results that can be achieved with such a programmed "C" scan inspection system (Figures 1 and 2). Results of the many tests performed attest the wisdom of selecting ultrasonics and the over-all systems concept described as the method for reliably nondestructively testing the many bonded structures.

Figure 5. Inner and outer squirters directing a water column couplant to both sides of a standard test panel. Calibration standards are located adjacent to production parts for sensitivity evaluation to ensure inspection reliability.

The design, fabrication, erection and operation of the complex and unproven systems have experienced only minor problems which, in most instances, were resolved during the installation period. Result: the "state of the art" of testing techniques and testing equipments has been advanced and refined to meet the challenge set forth by the NASA Apollo Space Program.

Technical Session 11 / Applications

Nondestructive Detection of Contents, Radiation Leakage and Sources in Containers Packed for Transportation

JÓZEF DOMANUS, POLAND

ABSTRACT: Nondestructive testing has been applied to the leakage of contents from packages by a radiometric method, and the leakage of radiation either by an autoradiographic or radiometric method to determine whether such packages have, during transportation, kept their containment and shielding properties.

The containment vessel is assessed for leakage in a pressure tank by the air-bubble test, and if none are observed, the radioactivity of the water is measured.

Admissible quantities of radioactivity in water have been determined by which it can be established whether the vessel is leaking.

Testing for radiation leakage of lead containers involves the detection of defects in the radiation shielding. A radiation source placed in the packaging is used for this purpose.

As radiation detectors either X-ray films (autoradiography) or a scintillation counter is used to scan the package (radiometry).

To determine the sensitivity of both methods, test containers were used with artificial defects.

A combination of characteristic film curves with lead attenuation curves, gave new curves from which defect depths could be read vs. film-density increase.

With the radiometric method a recording count-rate meter was used, calibrated against artificial defect depths.

In both methods theoretical values gave higher readings, due to the influence of scattered radiation.

Analysis of results permitted the establishment of new criteria of failure.

Packaging of Radioactive Materials for Transportation

Like other dangerous goods, radioactive materials must submit to special regulations to assure safe transportation. The potential hazards presented by such materials consist of external radiation emitted by the radionuclides, and the possibility of contamination of persons and materials in case of the release of the radioactive contents of a package.

External radiation may endanger both the health of persons in contact with the radioisotopes, and the photographic materials transported with them.

To avoid such risks radioisotopes must be transported in special packages that provide adequate control of both external radiation and contamination.

The general rules for safe transportation of radioisotopes are laid down by the International Atomic Energy Agency in its *Regulations for the Safe Transport of Radioactive Materials, (1964), (Revised Edition)* (1).

Packages in which radiation sources can be safely transported must be so constructed as to prevent release of the radioactive contents (i.e. containment), and must limit external radiation to the prescribed level (i.e. shielding).

The adequacy of the packages in preventing loss or dispersal of radioactive contents and retain the efficiency of its shielding properties may be proven by a series of tests.

These tests have been elaborated on by the International Organization for Standardization (ISO) (2), which provides technical specifications and procedures to facilitate application of the requirements of IAEA for the safe transportation of radioactive materials.

The specifications for contents leakage and radiation leakage tests have been elaborated on in Poland by the Polish Secretariat of the ISO/TC 85, Subcommittee SC 4 *Radioisotopes* (of which the author is a chairman) and are based on investigations performed in the Nuclear Research Institute and the Electrotechnical Institute in Warsaw.

As the tests for containment and shielding integrity are used as criteria of failure for the packages under test, they are of primary importance to the designer as well as the user of the packages.

Detection of Contents Leakage

Subcommittee SC4 *Radioisotopes* has proposed in document N 32 (3) a specific method for testing contents leakage, based on the investigations of the Nuclear Research Institute in Warsaw.

These investigations consisted of determining the sensitivities of the so-called "bubble" and "activity" tests for leakage detection.

A complete draft ISO proposal on the contents leakage test is proposed by ISO in document N 63 (2).

The Bubble Test

One of the simplest methods of leak detection is immersing the containment vessel in liquid and observing gas escape from it in the form of a stream of gas bubbles.

To assure good streaming of gas bubbles it is necessary to pressurize the containment vessel before testing and then to create a difference in pressure between the gas in the vessel and the gas space above the liquid.

The possible existence of threshold pressures for very small leaks was investigated, below which no streaming of gas bubbles occurs. This was done with very small openings ranging down to the diameter of 30 microns.

Initially it was proven that even for the smallest openings (8.8×10^{-4} mm^2) after about 15 min of pressurization the test vessel could be filled with air of the desired pressure. The vessel was then immersed in water and streaming air bubbles were observed.

As it was difficult to produce openings smaller than 30 microns and because comparatively high threshold pressures were observed by other investigators (4), the region below 30 microns was not investigated.

In this area another method of leak detection was proposed. When pressure in the test vessel was lowered, and a certain

pressure was reached (called threshold pressure) the bubbling of air stopped. In Figure 1 threshold pressures are shown for different diameters of test openings. As can be seen, for the smallest openings (8.4×10^{-4} mm^2) the threshold pressure was 250 mm Hg and was rapidly falling down to c.a. 20 mm Hg for larger openings.

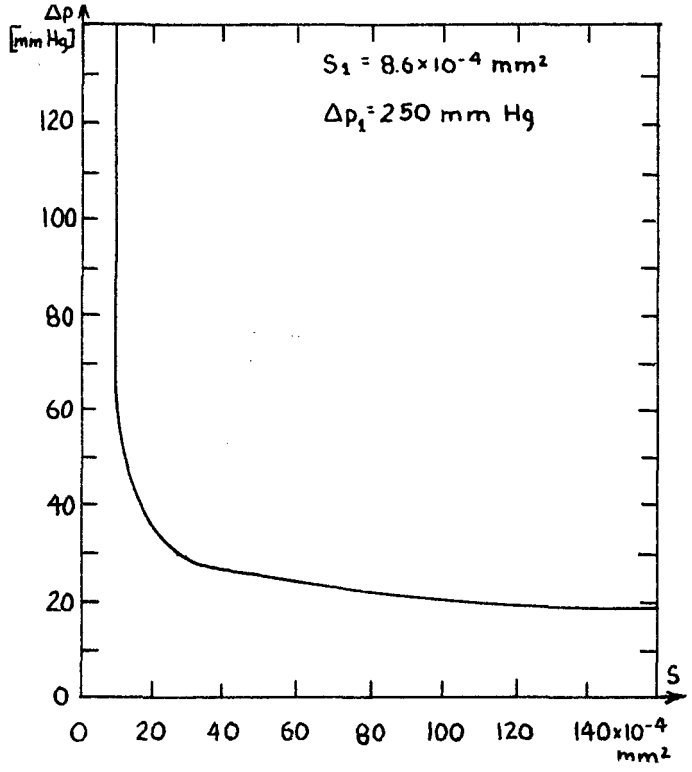

Figure 1. Threshold pressure for different cross-sections of test openings.

The Activity Test

With the same equipment another method of leak detection was investigated. The test vessel was filled with radioactive solution (1% solution of NaCl, containing radioactive Na 24) and the active leaking from the test vessel into distilled water in the measuring tank was measured. The results of those measurements are shown on Figure 2.

As can be seen, no threshold is observed and one can expect that even for smaller openings leakage will occur, even without any difference of pressure.

This method of leak detection is much more sensitive than the bubble test, but needs special measuring instruments for the measurement of the radioactivity of the water in the measuring tank.

Standard Contents Leakage Test

Apart from the investigations described above, a standard contents leakage test has been proposed by ISO, as follows:

A sample container, filled during the assembly of the package with an active solution, is placed in a measuring tank. The tank is submitted to air pressure of 2 ata for a period of 15 min.

The tank is next filled with distilled water, which should reach at least 40 mm above the upper wall of the container under test. After complete immersion of the container in water, air pressure in the tank is reduced to atmospheric pressure and streaming of air from the container is observed through walls or observation windows of the tank. If no stream of air bubbles appears within 5 minutes, the measuring tank with the

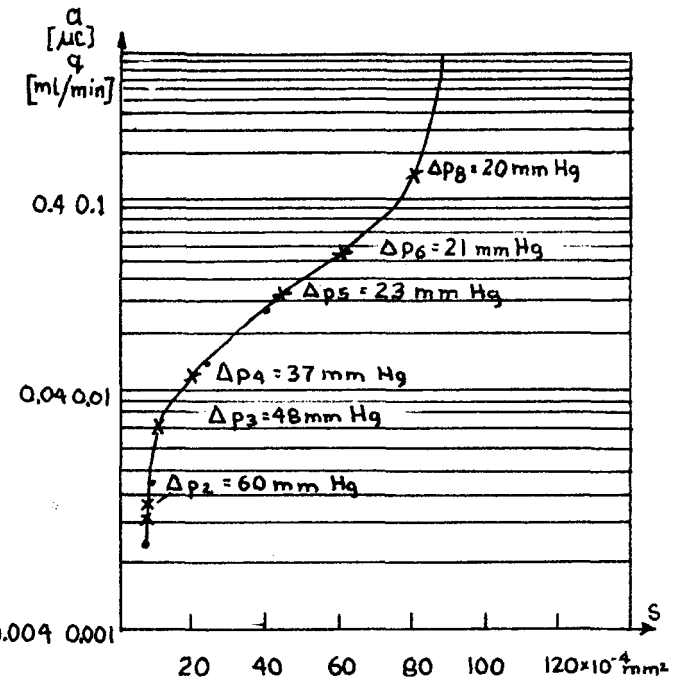

Figure 2. Active leakage (a) and leakage rate (q) for different cross-sections of test openings.

container is turned to positions in which all the walls of the container are consecutively placed parallel to the surface of the water, still at a depth of at least 40 mm, so that each part of the inner surface of the containment vessel be brought into contact with the active solution for at least 5 min.

If, after the test is repeated twice, no stream of air bubbles is observed, a sample of water of at least 10^{-1} l volume is taken from the measuring tank and its activity measured in a beta- or gamma-ray measuring set-up.

As a result of a discussion on a recent ISO meeting held in Warsaw in June, 1966, a new criterion for contents leakage was accepted.

The containment vessel may be regarded as leakproof (within the limit of 1.5×10^{-5} l in 10 min) if the activity of the sample water taken from the measuring tank is not greater than the sensitivity of the measuring instrument used for the measurement of beta or gamma activity, providing that the specific activity of the active solution, introduced into the containment vessel prior to testing was calculated from the following formula:

$$a = S \frac{V_T}{V_S} \cdot \frac{1}{L} \text{ (Ci/l)}$$

where: S=sensitivity of the measuring instrument—in Ci,
V_T=volume of distilled water in the measuring tank,
V_S=volume of water sample,
L=1.5×10^{-5} l in 10 min—minimum detectable leakage.

e.g. using a measuring instrument capable of detecting 2×10^{-9} Ci of gamma activity, a measuring tank of 7.5 l water capacity and taking a water sample of 10^{-1} l volume the specific activity of the active solution to be introduced into the containment vessel prior to the test shall be:

$$a = 2 \times 10^{-9} \frac{7.5}{10^{-1}} \cdot \frac{1}{1.5 \times 10^{-5}} = 10^{-2} \text{ (Ci/l)}$$

The containment vessel may be considered as leak-proof if the activity of the water sample taken from the measuring tank is not greater than 2×10^{-9} Ci.

Detection of Radiation Leakage

Preliminary investigations performed in 1963 in the Electrotechnical Institute (5) showed that transport packages used for transportation can be tested for radiation leakage by two comparatively simple methods.

It was felt both by the ISO as well as IAEA, that the final formulation of the radiation leakage test must be preceded by research that would have a valid scientific background. Therefore on the suggestion of the Polish Standards Committee a research contract was granted by the IAEA to the Industrial Radiology Department of the Electrotechnical Institute in Warsaw under which a standard method for testing packaging of radioactive materials for radiation leakage was to be developed.

The results are described in a special report (6) and have served as a basis for the formulation of the ISO radiation leakage test (2), the background of which was given in a separate ISO document (7).

It was proposed to test transport packaging for radiation leakage by two methods: autoradiography and radiometry. During the final elaboration of those methods it was decided to use three gamma-ray radiation sources.

Ir 192 is mentioned as a reference source by the IAEA regulations so it was used here, too. Unfortunately, due to its comparatively low energy it is unsuitable for great thicknesses of lead. Therefore Co 60 was used for the greater lead thicknesses; Cs 137 was also used, as it presents great advantages of having a monochromatic gamma-radiation and long half-life.

The activities of these three radiation sources were chosen so as to guarantee reasonable exposure times in autoradiography and high sensitivity of the radiometric method.

The radiation sources used throughout the investigations were standard radiography (point-like) sources.

To confirm the results obtained during the autoradiographic and radiometric testing ordinary radiography was made for the lead containers tested for radiation leakage. For that purpose a 15 × 15 mm Co^{60} source was used, having an activity of 300 Ci.

Throughout the investigation Polish standard transportation packages were used with a lead shielding of lead-in-steel containers (type K) of 25, 50 and 90 mm.

Autoradiographic Method

In this method a sealed radiation source is placed within the containment vessel and the packaging is wrapped outside with X-ray films. An image of the internal defects in the shielding is produced on the X-ray films, and acts as an evaluation of the shielding adequacy.

X-ray films. To reduce both the source activity and the exposure times to a minimum, X-ray films of the highest sensitivity were chosen (Kodak-Kodirex). On those films densities between 1 and 2 had to be reached.

Taking into account the filtration of gamma radiation through 25, 50 and 90 mm of lead, the different X-ray sensitivities for those filtrations and the focus-film distance for different dimensions of the containers wrapped with X-ray films (used with lead intensifying screens) exposure times for Kodak-Kodirex films could be calculated. It was necessary to obtain film densities from 1 to 2, when exposed to Ir 192, Cs 137 and Co 60 sources of 1 Ci activity (Table 1). As can be seen, K-25 containers can be easily autoradiographed with all the three types of sources, whereas K-50 containers can be examined only with Cs 137 and Co 60, and K-90 with Co 60 only.

Table 1

Exposure Data for Ir 192, Cs 137 and Co 60 gamma-ray Sources of 1 Ci activity for Kodak-Kodirex X-ray Films with D = 1 and D = 2 Densities

Container	Type / Lead shield—mm / FFD—m / Distance factor		K 25 25 0.11 83	K 50 50 0.13 59.3	K 90 90 0.17 34.5
Attenuation factor	Ir 192		60	1590	—
	Cs 137		20	263	20000
	Co 60		3.29	14.25	149
Required dose on film in Ir	Ir 192	D = 1	0.15	0.15	—
		D = 2	0.4	0.4	—
	Cs 137	D = 1	0.07	0.07	0.07
		D = 2	0.175	0.175	0.175
	Co 60	D = 1	0.4	0.35	0.3
		D = 2	1.0	0.9	0.75
Required dose at 1 m from source in r	Ir 192	D = 1	0.114	4.4	—
		D = 2	0.307	11.8	—
	Cs 137	D = 1	0.0146	0.353	39
		D = 2	0.041	0.885	97
	Co 60	D = 1	0.0169	0.09	1.52
		D = 2	0.0422	0.231	3.83
Required exposure for 1 Ci source	Ir 192	D = 1	14'	8.85 h	—
		D = 2	37'	23.7 h	—
	Cs 137	D = 1	2.5'	1 h	110 h
		D = 2	6.9'	2.5 h	272 h
	Co 60	D = 1	47″	4.1 '	1.15 h
		D = 2	1.9'	10.5'	2.9 h

Characteristic curves of X-ray films. To be able to evaluate the findings of the autoradiographs and to translate the difference of X-ray film densities into radiation-dose variations, it was necessary to dispose of characteristic curves of the X-ray films and screens used for autoradiography.

As X-ray film sensitivity varies with the energy of radiation reaching the film, the influence of lead filtration on the composition of the gamma-ray spectrum was taken into account. This was done for Ir 192 up to 25 mm of lead, for Cs 137 up to 50 mm, and for Co 60 up to 90 mm, and adequate characteristic curves were used in the final computations.

Lead attenuation curves. For the evaluation of lead shield decrease on the basis of the readings taken from the autoradiograph it was necessary to take into account lead attenuation curves. These are published in various documents (e.g. in a Polish Standard 8), and in the described investigations broad beam attenuation curves were used. From those curves attenuation factors were read for 25, 50 and 90 mm of lead.

Evaluation of the autoradiographic findings. By combining the data available from the attenuation curves of lead with those of the characteristic curves of X-ray films, obtained for different filtrations of lead, one can evaluate the density readings

of the autoradiographs and compute therefrom both relative radiation doses as well as lead thicknesses of the defective spots of the examined containers.

This can be done in the following way. If one takes as basic film density the density measured on the autoradiograph in the parts where the density is uniform, then any increase of density on the autoradiograph in the area of the uniform density will mean that in this spot the dose increase that has caused this density increase, is due to the lead shield decrease. In the spot where the decrease of the shield occurs, the attenuation of gamma radiation decreases too. Therefore if one takes different attenuation factors for different lead thickness from the attenuation curves and divides the attenuation factor for the basic density by the attenuation factor corresponding to the decreased lead thickness, one obtains the relative dose increase factor. Knowing this dose increase factor one can further calculate the film density corresponding to this increased dose. This can be done by using adequate characteristic curves of X-ray films.

If D_0 is the basic film density for which the calculations are done, then for this D_0 one takes the reading of the dose necessary to produce D_0 for the basic lead thickness d_0. For the defective spit, with lead thickness of $d < d_0$ the corresponding film density will be $D > D_0$. Knowing the dose increase factor one must multiply it by the dose D_0 read from the characteristic curve. For the resulting dose one must read the new film density D from the characteristic curve, corresponding to the new filtration d. Repeating this operation consecutively for different values of lead shielding d one can compute new curves giving lead shield decrease and radiation dose increase vs film density on the autoradiograph. Repeating this operation for different basic film densities one can compute a whole set of curves.

Instead of presenting on the graphs absolute densities under the defective spots, one can calculate density differences between the defective spots and the surrounding "sound" parts and thus obtain density-increase values for the defects shown on X-ray films.

This was done and a series of curves was produced on which defect depths were calculated vs density increase on the autoradiograph. Examples of such curves are shown on Figure 3.

Sensitivity calibration. The above method of evaluating of autoradiographic findings was based on computations done for ideal autoradiographic conditions, in which such factor as, for example, scattered gamma radiation was not taken into account. To take into account all those factors the autoradiographic method has been calibrated for sensitivity. This was done as follows: two types of test containers (spheres and cylinders) were used, which were especially manufactured for that purpose as model containers. They had uniformly thick lead shields, of the same thickness as the regular containers 25, 50 and 90 mm.

On the outside of the test containers artificial defects were drilled in the form of calibrated cylindrical openings (diameter equals depth) of the following diameters: 1; 2; 3; 4; 5; 7.5; 10 and 15 mm.

Using those spherical and cylindrical test containers autoradiographs were made on which the artificial defects could be seen.

Analysis of results obtained during calibration. From the analysis of the results the following conclusions can be drawn.

The practical limit of defect detectability with the autoradiographic method proved to be a defect of 2 mm. On some autoradiographs a 1-mm defect could sometimes be seen, but

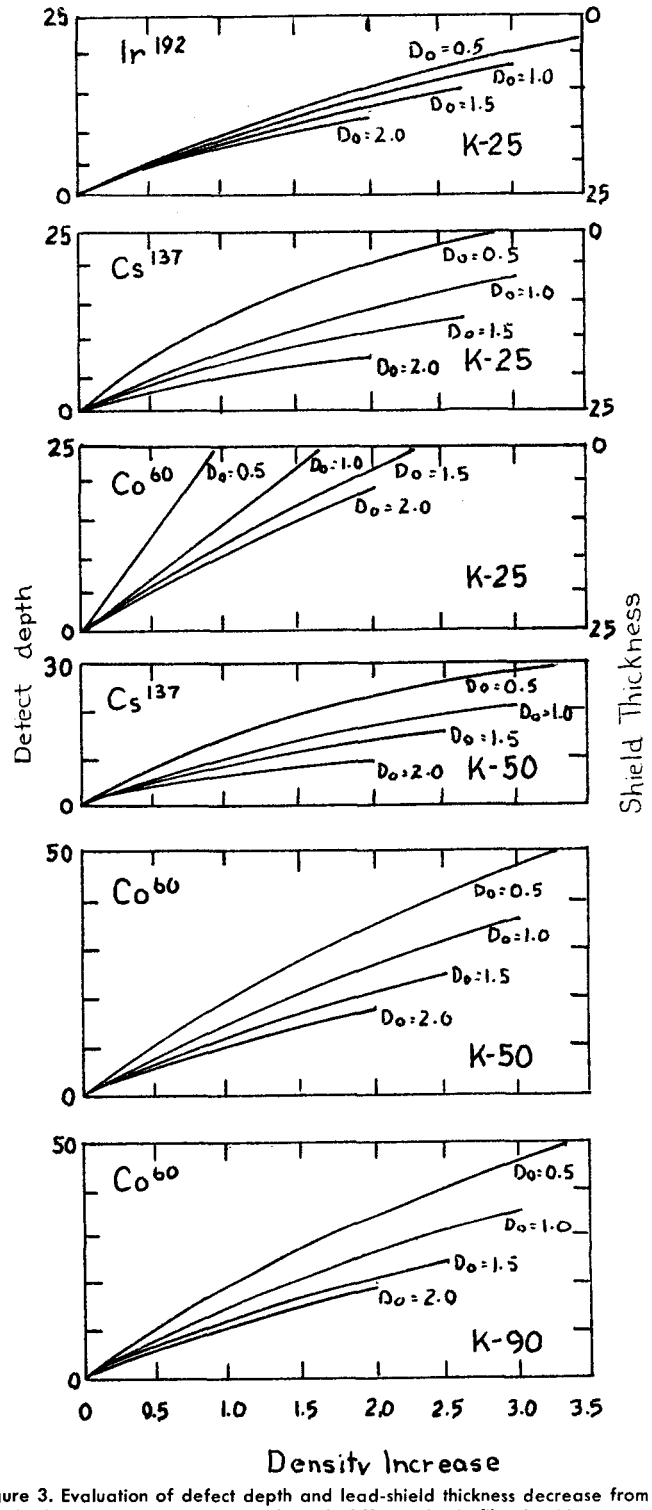

Figure 3. Evaluation of defect depth and lead-shield thickness decrease from the density increase on autoradiographs with different basic film densities.

due to the very small surface of such a defect it was practically impossible to measure film density differences caused by it on an ordinary densitometer.

In general, the autoradiographic readings show lower thickness decrease under the defective spot than those calculated for the calibrated defect depths.

This is due to the effect of scattered radiation, which causes the basic film density in the immediate vicinity of the defective spot to be greater than expected and therefore the measured density difference is lower than the calculated one. This is more

visible for defects of larger diameter, as the scattered radiation covers a larger field in such instances.

Actual autoradiographic examination. During the investigation about 40 K-series containers were examined by the autoradiographic method.

The container was placed on a rigid X-ray film cassette, loaded with X-ray film, sandwiched between two lead intensifying screens.

At the same time a flexible X-ray cassette was placed around a 1-mm aluminum drum, which was necessary as a film support, because the containers had some protruding parts such as handles and steel rings.

On the top of the drum a second rigid cassette was placed on which the autoradiograph of the plug could be taken.

Ordinary radiography. To be able to identify defects revealed by autoradiography, an ordinary, normal radiography test was made of the containers using a Co 60 source of 300 Ci activity.

The ordinary radiographs have confirmed the findings of the autoradiography.

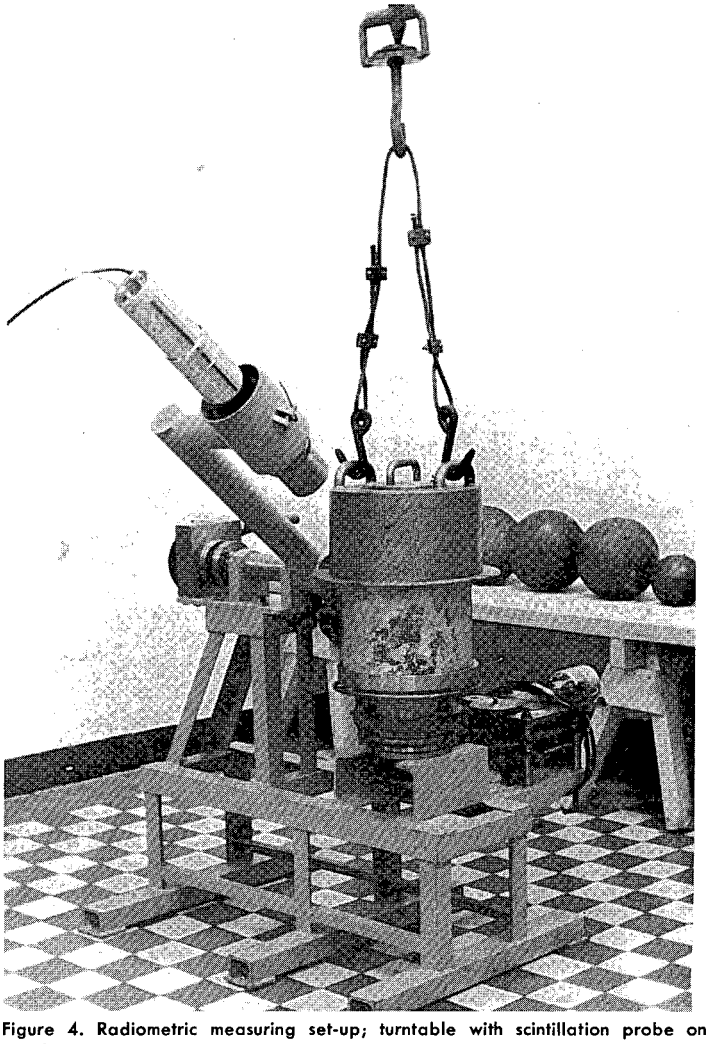

Figure 4. Radiometric measuring set-up; turntable with scintillation probe on rotating arm.

Radiometric Method

Testing procedure. The container to be tested, with the radiation source inside its containment vessel, is put on a turntable so that the source is located on the rotation axis. The radiation detector, consisting of a scintillation probe, is placed in a suitable lead collimator. The probe is held by a rotating arm, fixed to the turntable. The axis of rotation of the probe intersects the axis of rotation of the turntable—and the axis of the tested container—at the point where the radiation source is located.

Thus by moving the rotating arm, with the probe, around the turning container a complete scanning can be obtained. After each 360° rotation of the turntable the probe is turned 10° around the source. So the scanning is done by 10° steps.

All the elements of this measuring set-up can be seen on Figure 4.

A scintillation counter is used with a 1-in NaJ/Tl/ crystal, placed in a conical lead collimator with a 5-mm front opening. A count-rate meter and recorder are used with different measuring ranges from 5×10^2 to 10^6 cpm. The measurements are made using a 0.5-s time constant, 0.285-rpm speed of the turntable and 1.905-cm/min chart paper speed.

Sensitivity calibration. For calibration purposes the same two types of test containers were used as in autoradiography.

For each defect the count rate was measured twice on the 6-decade preset scaler with preset time of 30 s measured by the decade-preset electronic timer.

The readings were made when the collimator was facing the centre of the calibrated opening as well as a spot located in the middle of two consecutive openings. The results of each

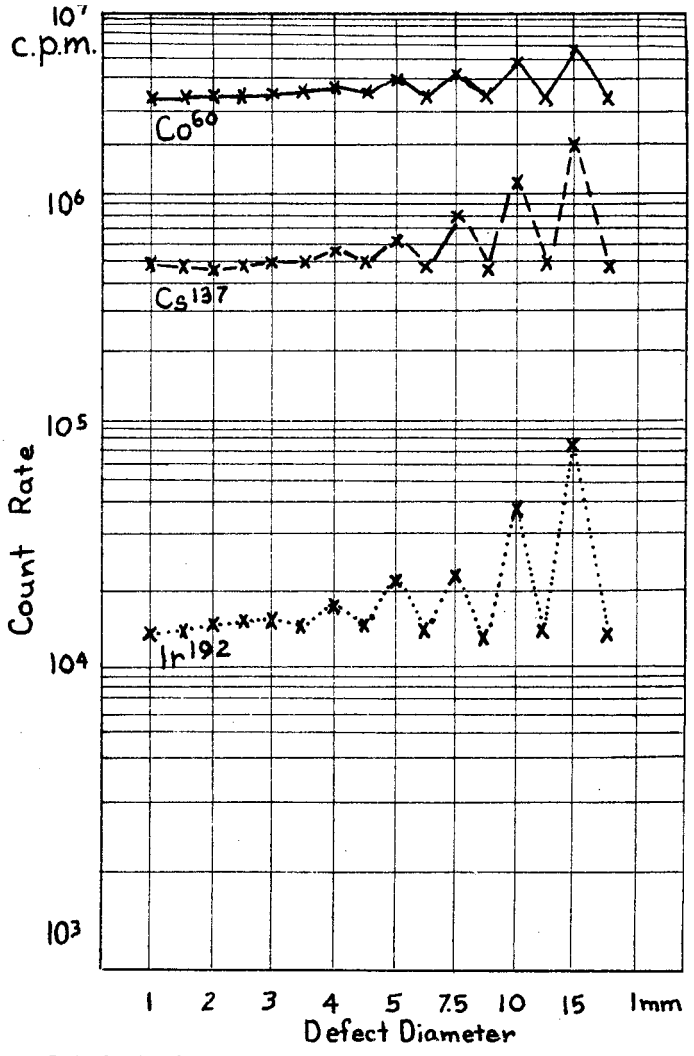

Figure 5. Artificial defects in cylindrical lead containers detected by the radiometric timer and scaler technique.

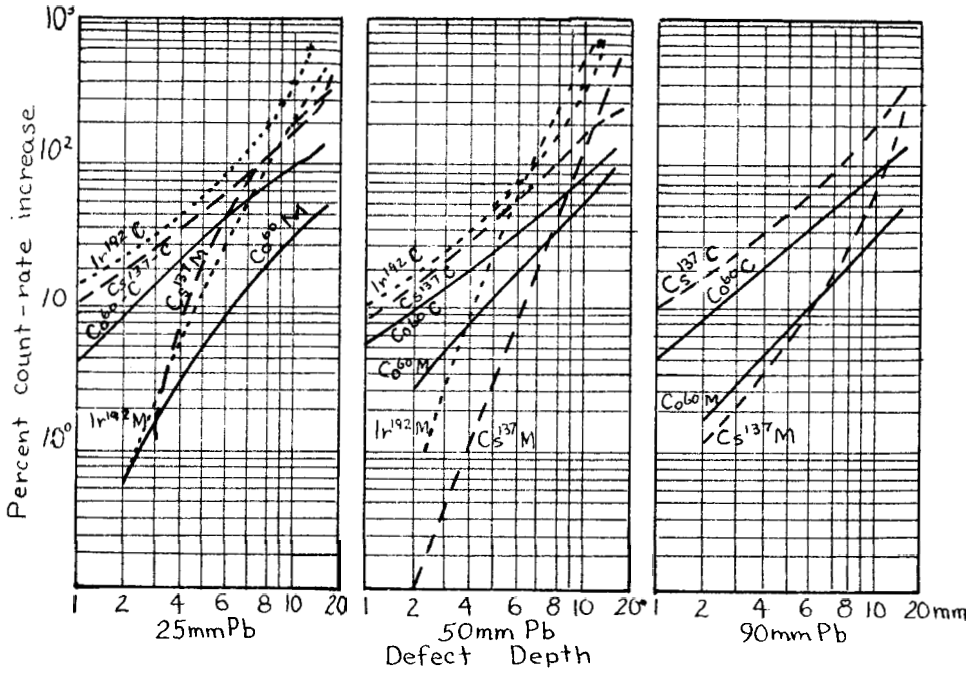

Figure 6
Per cent count-rate increase for different defect depths in lead containers. M—Measured by radiometric method: C—Calculated from attenuation curves.

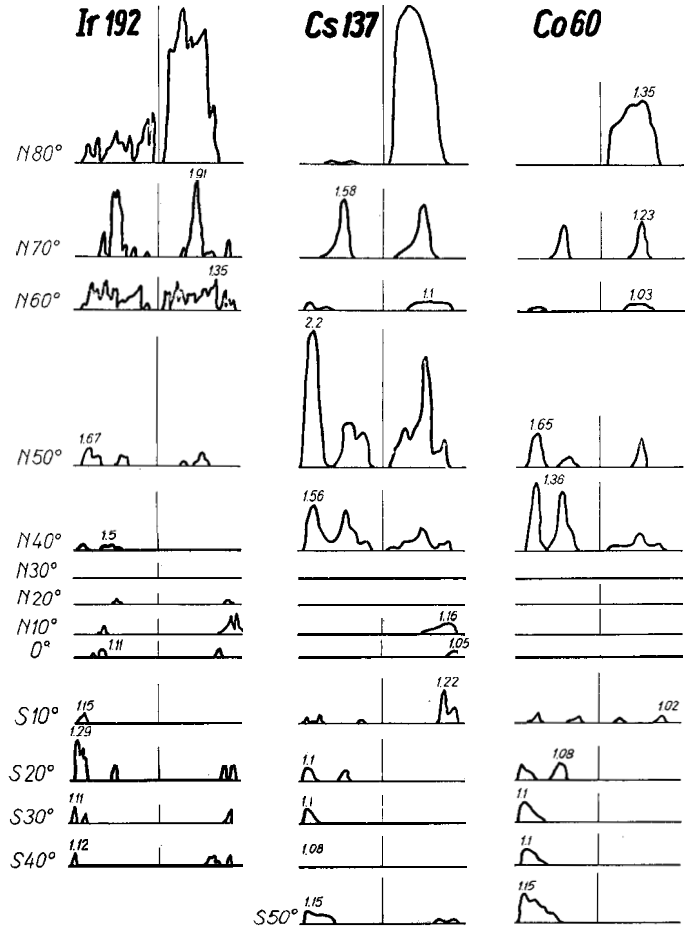

Figure 7. Defect detection in lead transport containers by the radiometric method.

two countings were added together and were recorded on graphs as count rates in c.p.m. (*see* Figure 5).

The best way to compare the results of measurements obtained with the same test containers but with different radiation sources, is to calculate the per cent count-rate increase for different artificial defects. This is shown on Figure 6.

Besides the measured values (M) on these graphs calculated values are given for (C). As can be seen there are great differences between measured and calculated values due to the effect of scattered radiation.

Those results were obtained with the most sensitive measuring technique i.e. a scintillation counter used with a preset timer and scaler. However this technique is very time-consuming and therefore cannot be recommended for routine measurements and can be used only as a reference method.

Routine measurements can be performed by using the testing procedure described above, in which the tested container is rotated at constant speed and the count-rate readings of the scintillation counter are recorded on chart paper.

Detection of defects in the K-series containers. Three K-series containers were examined by the radiometric method. These were the containers in which most visible defects were detected by the autoradiographic method. They were examined with Ir 192, Cs 137 and Co 60 radiography sources.

As it is impossible to reproduce all the graphs taken during the scanning of the three containers with different radiation sources, only those parts of the graphs are reproduced for each container that showed count-rate increases above the basic value, and which can be considered as representing defects discovered in the containers under examination. Therefore while evaluating the readings of the measuring probe it is enough to take into account only the highest readings on the graphs taken for particular inclination of the probe. This was done, and on Figure 7 for the highest peaks figures are inscribed giving the relative count-rate increase, corresponding to those peaks.

Comparison of Sensitivities of Both Methods

The measurements performed on test containers with calibrated artificial defects permit direct comparison of the sensitivities of both methods.

This comparison shows that with autoradiography, higher detection sensitivity can be obtained and the results of such findings are closer to those calculated from the attenuation curves of lead.

The results of the comparison are shown in Table 2, where the calculated values are also listed.

Table 2
Comparison of Autoradiographic and Radiometric Sensitivities

Calibrated defect depth mm	Calculated or measured values	Per cent dose increase for different lead-shield thickness in mm and radiation sources used							
		25			50			90	
		Ir 192	Cs 137	Co 60	Ir 192	Cs 137	Co 60	Cs 137	Co 60
2	C	30	20	15	25	20	10	20	10
	A	25	—	21	—	16	6	—	15
	R	—	—	—	4.2	—	—	—	—
3	C	50	32	21	42	30	18	30	19
	A	40	25	30	—	20	15	—	15
	R	—	0.5	—	7.7	0.19	—	—	—
4	C	70	49	30	62	47	25	50	26
	A	45	32	20	—	15	20	—	19
	R	—	14.5	2.5	21	9.3	3.5	—	—
5	C	95	62	37	85	62	32	68	34
	A	75	60	28	—	47	31	—	10
	R	41	41.5	7.1	49	25	5.65	—	—
7.5	C	170	115	58	160	110	52	115	55
	A	100	70	40	—	90	35	—	34
	R	73.5	71	26	103	56	23.2	—	14
10	C	300	170	80	260	170	76	180	78
	A	180	95	58	—	165	78	—	78
	R	124	117	52	>100	>55	>25	71	37
15	C	770	400	125	580	260	135	380	140
	A	450	120	90	—	240	120	—	150
	R	>235	>120	150	>100	>55	>25	240	84

NOTE: C—Calculated values. A—Autoradiographic findings. R—Radiometric findings.

Standard Radiation Leakage Test

Radiation source used for testing. A sealed radiation source, the dimensions of which should be as small as possible, should be placed within the radiation shielding to be tested. For lead shields of small and medium thicknesses (up to 70 mm) Ir 192 should be used as the gamma-radiation source. For higher shield thicknesses Cs 137 should be used. If the packaging under test is to be used for one particular radionuclide only, that radionuclide may be used as the radiation source.

If the radiation leakage test is to be performed by the autoradiographic method then the activity of the source should be such as to produce on X-ray film a density (D) not less than 1 in a reasonable period of time (say 5 hours).

For the radiometric method the activity of the source should be such as to produce sufficient count-rates in the scintillation counter to guarantee reliable and reproducible measuring indications, when the scintillation counter detector is equipped with a suitable collimating system and is located at minimum practicable distance from the radiation source (e.g. 50 cm).

Test procedure for the autoradiographic method. The characteristic curves of the X-ray film should be derived experimentally, taking into account the thickness of the lead shielding of the package under test, since the thickness of the lead will affect the spectral composition of the gamma radiation reaching the film. By a combination of this curve with that for the attenuation in lead of the gamma radiation to be used, a calibration curve can be derived to give the relationship between the X-ray film density and the lead shielding thickness.

The entire surface of the package should be covered with the X-ray film. If protruding parts of the packaging make this impossible then that part of the package affected by the protruding parts should be enveloped with a metal sheet (e.g. 1-mm thick aluminium) parallel to the surface of the affected part.

The exposure time should be chosen so as to reach a film density (D) not less than 1. After processing the X-ray film, its densities should be assessed on the densitometer and any density differences should be calculated. Using the X-ray film calibration curve referred to above, any decrease in lead shielding thickness can be determined.

Test procedure for the radiometric method. The package should be put on the turntable, with the measuring probe aimed at the centre of the radiation source within the package during the whole process of testing. By turning the turntable and rotating the probe around their axes of rotation, a complete scanning of the package should be made. A scanning is considered complete if, after each turn of the turntable, the rotating arm is moved not more than 10 degrees. The readings of the count-rates of the scintillation counter should be recorded. The maximum count-rate differences should be computed.

Sensitivity of the method. The minimum loss of radiation shielding detectable using these methods is that equivalent to half-value-layer of lead for Ir 192 used as a reference gamma radiation source.

Since the above value represents the threshold of detection, test results which give a shielding loss equivalent to not more than half-value-layer of lead for the reference source on a surface not greater than 1 cm^2 may be interpreted as an indication of no significant loss of radiation shielding.

In evaluating the results of the radiation leakage test, attention must be drawn to the fact that while the sensitivity of the autoradiographic and radiometric methods assures the detec-

tion of minimum losses of radiation shielding that are greater than one half-value-layer of lead for the reference radiation source, this does not mean that a container may be considered as leak-proof if it has lost one HVL of lead on its entire surface or a great part thereof.

Both the autoradiographic and radiometric methods permit the detection of defects of as small a cross-section as 2 mm, and the evaluation of these local losses of shielding is done with the accuracy of one HVL for Ir 192 taken as the reference radiation source.

References

1. Regulations for the safe transport of radioactive materials. 1964 revised edition. Safety series No. 6. International Atomic Energy Agency, Vienna, 1965.
2. International Organization for Standardization. Draft ISO Proposal on the contents leakage test and radiation leakage test. ISO (TC 85)(SC 4) Secretariat-36/63. August, 1966.
3. International Organization for Standardization. Remarks on the necessity of introducing a specific contents leakage test into ISO recommendations and IAEA regulations. ISO (TC 85) (SC 4) Secretariat-19/32, March, 1965.
4. King, R. C. Vacuum leak testing of radiation source capsules. RNL—3664. January, 1965.
5. Domanus, J. and Wolski, M. Testing of transport packagings of radioactive sources for radiation leakage. Electrotechnical Institute, Industrial Radiology Department, Warsaw, 1963.
6. Domanus, J. The development of a standard method for testing packagings of radioactive materials for radiation leakage. Final report on the research project made under International Atomic Energy Agency Research Contract No. 251/RB, Warsaw, 1966.
7. International Organization for Standardization. Remarks about the new formulation of the radiation leakage test. ISO (TC 85) (SC 4) (WG 3) Secretariat-23/36, May, 1966.
8. Polish Standard PN-62/J-80001. Protective materials and devices against X- and gamma-rays. Fixed screens.

Progress in Nondestructive Testing in Aero Engine Manufacture

I. L. F. GLOVER, USA

ABSTRACT: A large number of different types of nondestructive testing techniques are used during the manufacture of an aero engine. The methods described include the application of ultrasonics to the inspection of rotor discs, welds and plastics and other systems for material sorting and the determination of coating thickness. Many of the techniques described are used on a production basis, but other methods still under development are also discussed.

Introduction

To achieve the necessarily high standard of airworthiness required of a modern aero engine a very precise quality control must be exercised at all stages of its manufacture. An important part of this quality control is the application of nondestructive testing techniques. However, due to the complex physical shapes of the components, the exotic materials used and the high level of cleanliness required, a very large range of nondestructive testing systems are employed. These range from dye penetrant, magnetic ink and radiography to eddy currents and ultrasonics.

In the following discussion it is intended to consider principally the applications of the latter two methods specifically to the field of aero engine inspection. Although the methods outlined are specific in themselves, nevertheless it is felt that they may be of direct interest to those concerned in the more general field of nondestructive testing. It should be pointed out, however, that these methods constitute only a very small part of the range of nondestructive techniques developed for use in this field.

Ultrasonics

Disc Inspection

One of the oldest and most well established methods of ultrasonic testing in the aero engine industry is that of the inspection of forged turbine and compressor discs. Being critical components it is essential to maintain a high degree of cleanliness and also for economic reasons it is preferable to detect harmful internal defects as early as possible in the manufacturing process, to eliminate further unnecessary machining. The defects in these components are usually lamellar in nature as a result of the forging and therefore are very thin with respect to the disc section thickness, which may be as large as 6 in. Radiographic methods are unsuitable as they have a maximum sensitivity of about 1.5%, whereas a 5 MHz ultrasonic pulse echo system is capable of detecting defects in this plane of less than 0.020 in. dia.

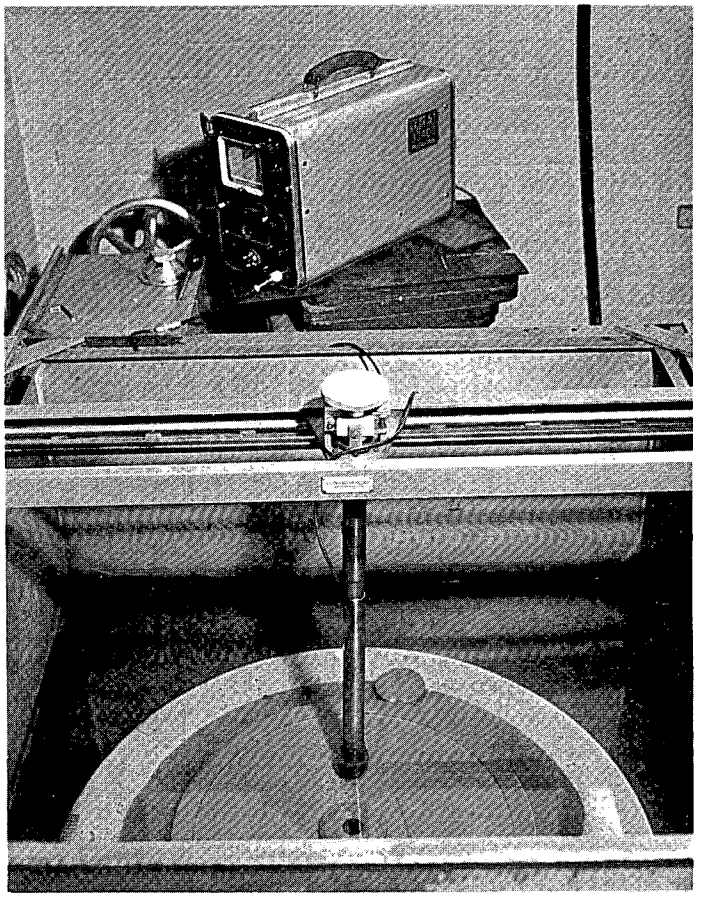

Figure 1. Ultrasonic examination of a turbine disc.

With the system employed the disc is immersed in water and scanned using a compressional wave probe normal to the surface and at a frequency of about 5 MHz (Figure 1). By automatically linking the rotation of the disc with the radial movement of the probe, a complete gramophone scan is

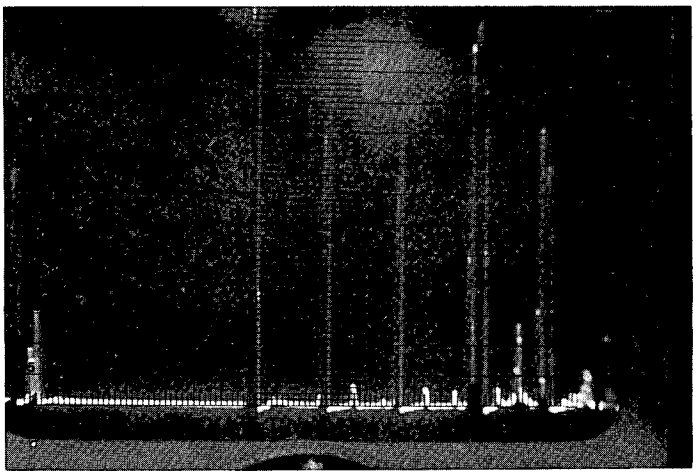

Figure 2. C.R.T. presentation of a satisfactory disc.

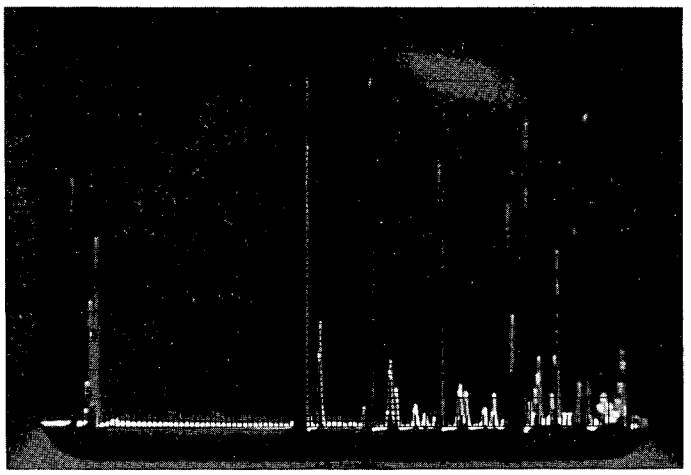

Figure 3. C.R.T. presentation of a defective disc.

achieved. In order to reduce probe manipulation to a minimum the disc is machined, prior to inspection, to a rectilinear profile so that the probe has only to be normalised at the commencement of the inspection cycle. A conventional type of A-scan presentation is used (Figures 2 and 3) as the system is capable of providing both more direct information, and higher sensitivity than either B or C-scan. The standards of quality applied vary from a defect diameter of 0.020 to 0.080 in., depending on its position.

Although this method of inspection has proved its worth, it is still often unfavourably compared with radiography because of the lack of a permanent record, which is an essential feature of the latter system. Considerable effort is being employed to overcome this problem by the application of automatic recording and some of the steps taken are briefly outlined. Improvements in design and monitor construction make it possible now to monitor very small defect indications and the use of A.G.C. (automatic gain control) units or Gaussian probes enable a constant sensitivity with depth to be maintained. Accurate control of the monitor gate position and width is necessary to keep it between the front and back surface echoes. By using an interface trigger unit the gate may be made to start after the front echo and at present work is under way to produce a similar device which will trigger from the back echo. Recent developments in recording techniques have resulted in the facsimile recorder which employs a current-sensitive paper capable of reproducing all shades from black to white. With this system it is possible to display defects pictorially in three dimensions with the depth co-ordinate being provided by the 'tone' of the defect indication. Hence a system may soon be available for complete pictorial recording of defect location and magnitude on an entirely automatic basis.

Shaft Inspection

A field of inspection closely allied to that just described is that of hollow shafts. These components can vary in diameter from a few inches upwards and with lengths up to 6 ft. In some cases these shafts have large bell ends with diameters up to 2 ft.

Wall sections can range from $\frac{1}{8}$ in to $\frac{1}{2}$ in and the standards of inspection are similar to those outlined previously. Clearly a system using a single transmitter/receiver longitudinal probe is of little use due to the problems of dead zone, which occur as a result of the large front surface pulse. Commercial probes of 5 MHz frequency rarely have a front surface pulse less than 0.25 in. and usually the pulse is somewhat larger. The system chosen uses a double probe with the transmitter and receiver mounted side by side. This configuration, if used in contact, gives good near-surface resolution due to the lack of a front-surface pulse. However, as the system was required to be automated, a gap scanning system was chosen where a small gap of the order of a few thousandths of an inch exists between probe and component. The coupling is achieved by a water bubbler and this results in both good coupling and no probe wear. At present the system is still being developed, but the method involves the rotation of the shaft about its axis and the scanning of the probe along its surface, resulting in a helical scan. The probe-to-surface distance is accurately controlled by means of servo motors and micro switches.

Reinforced Glass Fibre Components

An entirely different field that has recently been explored using ultrasonics is that of 'fibre-glass' components. The basic materials inspected consist of a glass-fibre mat or cloth which is bonded together in a series of layers using a resin system, which may vary from an epoxide to a polyester. The sections to be inspected vary from a few thousandths of an inch up to a few inches. It is proposed to discuss just two examples of the use of ultrasonics in the inspection of these materials and the limiting cases are considered.

At the large end of the scale is the problem of entry ducts which may be 4 ft dia and 4 ft long with a wall thickness varying from about $\frac{1}{4}$ in. to $\frac{1}{2}$ in. The method of manufacture is such that voids or delaminations may occur, or gas bubbles may be produced during the curing cycle. Although small defects of this type may be tolerable, large defects of the order of $\frac{1}{4}$ in. to $\frac{1}{2}$ in. dia are deemed undesirable. The use of low-frequency probes is essential because of the high attenuation and scattering of the ultrasonic energy due to the inhomogeneous structure. The frequency used is usually in the range 0.2 MHz to 1.5 MHz and clearly a large probe diameter is preferable to increase the energy available. Due to the large surface area of the component, its somewhat irregular nature and the need to detect defects in the order $\frac{1}{4}$ in. to $\frac{1}{2}$ in. dia a contact method employing hand scanning would be impracticable and therefore an immersion method is employed. A reflection technique is not normally possible for two reasons. Firstly the relatively thin sections could not be inspected using a single probe because of the very large width of the front-surface pulse obtained with low-frequency probes. Secondly as a consequence of the 'layered' type of construction, numerous spurious echoes would be received from the glass/resin interfaces due to the different

acoustic velocities in the two materials. This type of inspection can be conveniently carried out by using a through-transmission system. A double-probe system using a transmitter on one side and a receiver on the other poses mechanical scanning problems, so a reflector was used in place of one probe and the other used as a combined transmitter and receiver. The probe is placed inside the component which rests on rollers and the reflector is placed on the base of the immersion tank (Figure 4). In this method the echo received from the reflector is monitored to detect the presence of the defects. By employing this method an improved relative sensitivity to defects is achieved due to the double passage of the beam through the component. A further advantage is that the system does not require the component surface to be exactly normal to the ultrasonic beam as long as the reflector is correctly aligned. Any slight irregularities in the surface or eccentricity of the component do not, therefore, affect the amplitude of the received signal. It has been found that defects in the form of air bubbles, voids or delaminations greater than $\frac{1}{4}$ in. dia in a section approximately $\frac{1}{2}$ in. will attenuate the signal appreciably (often greater than 6 dB). Thus the indication obtained is easily monitored and areas of interest can easily be chart recorded to see the actual shape of the defect detected.

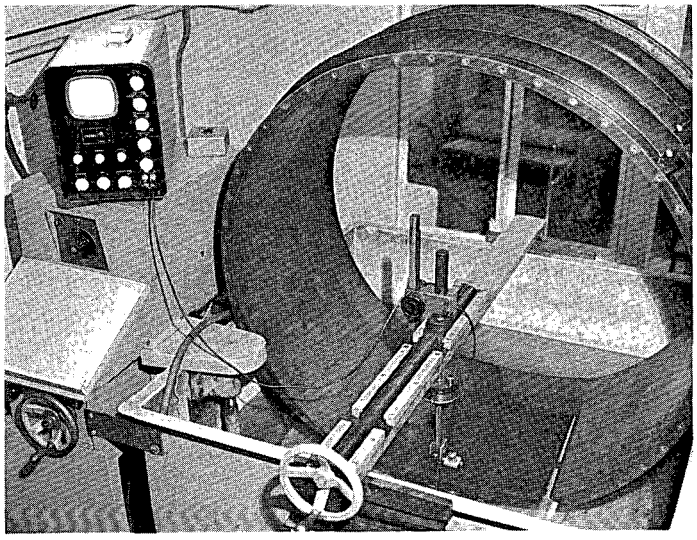

Figure 4. Ultrasonic examination of an entry duct.

This type of through-transmission system has also been used to good effect at the other end of the scale on micro-electronic circuit boards. Here the requirements are somewhat similar to that above, as the base material of the boards is again a glass-fibre reinforced resin system. The boards are approximately 2 in. by 1 in. by 0.006 in. thick with a copper face on one side 0.001 in. thick. During construction a number of boards are bonded together in stacks using an epoxy adhesive. It is essential that no voids or gas bubbles should be present in this glue line and it is for this reason that ultrasonic inspection is required. The voids to be detected are of the order of 0.030 in. diameter. The technique evolved is similar to the previous method, but due to the thinner sections involved, it is possible to use frequencies of up to 5 MHz or even 10 MHz. By using focussed probes an increase in sensitivity can be achieved as the area inspected is smaller. A single or double probe through-transmission method may be used, but it has been found that a single focussed probe with a reflector at the focus and the board near to the reflector is the most sensitive configuration. By using a line-by-line type of scanning system and linking the movement to a facsimile recorder a direct photographic readout is possible.

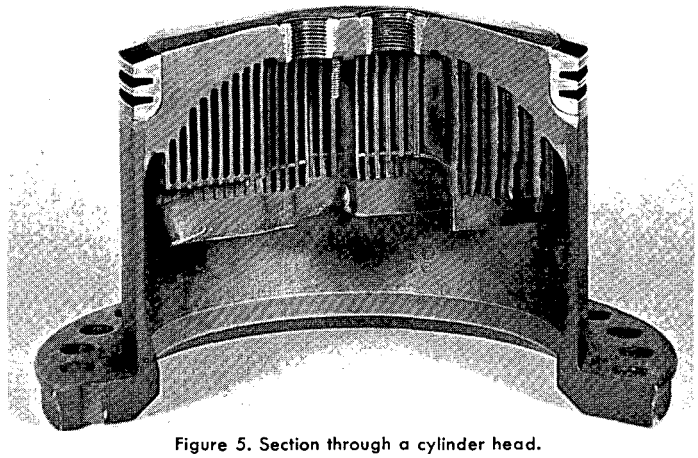

Figure 5. Section through a cylinder head.

This type of system is now being extended to see if potted circuitry can be inspected. However, the entrapment of air in components such as condensers and transistors is likely to make this rather complicated. By using a facsimile recorder it is hoped that with a knowledge of the component layout, any voids or air bubbles detected could be associated with the internal components and then any other voids would represent defects in the circuitry. These types of defects are harmful, as often the circuits have to undergo very large 'g' forces and extremes of temperature.

Cylinder Head Inspection

The discussion so far has only been concerned with the inspection of new components, the purpose of the inspection being to detect the presence of harmful internal defects in finished components or to detect defects in partly machined components as supplied by sub-contractors, in order to eliminate further unnecessary machining of defective components. However, the use of ultrasonics is also an important one in the field of overhaul inspection.

A particularly interesting aspect has been the use of ultrasonics for detecting fatigue cracking in piston engine cylinder heads. These heads are fabricated from a copper base alloy and a typical component, which has been sectioned, is shown in Figure 5. Fatigue cracks can occur from the ring carrier radius and propagate into the cylinder head. Previously a dye-penetrant surface-inspection method was applied, but clearly before this was applicable the ring carrier had to be removed. As this is shrunk on it necessitated an induction heating method for its removal. However, having removed the ring a further grinding or machining operation was necessary to remove the carbon deposit on the radius before penetrant inspection was practicable.

To facilitate this inspection without ring removal, an ultrasonic shear-wave system was developed. It was found that by producing a shear wave in the head, from the angled face at the top, it was possible to detect the cracks in question. The most suitable angle of shear is about 35 to 40 degrees in the material, and with this configuration the beam strikes the cracks approximately normally. Initial experiments were carried out using a standard shear-wave contact system. However, in view of the problems of coupling on the curved face and the large number of components involved, an automatic immersion scanning system was developed. A typical arrangement is shown in Figure 6. A 5-MHz longitudinal wave-immersion probe is employed with a diameter of 10 mm. By using a 1-in. water

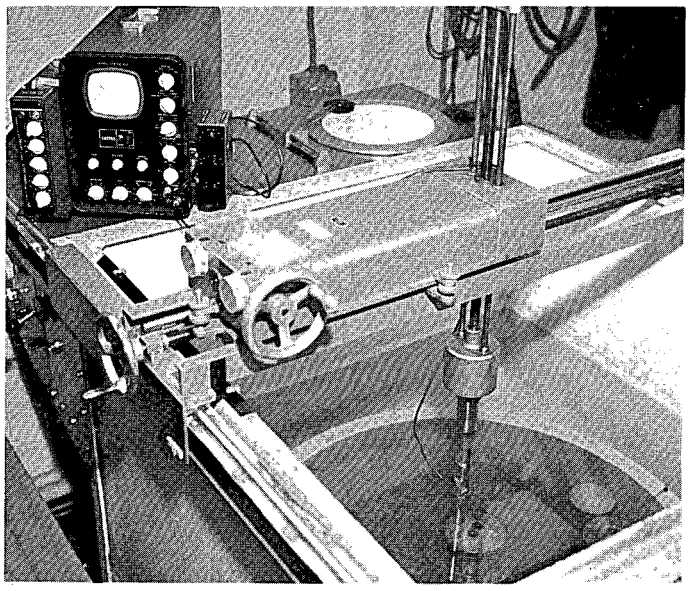

Figure 6. Automatic cylinder head inspection unit.

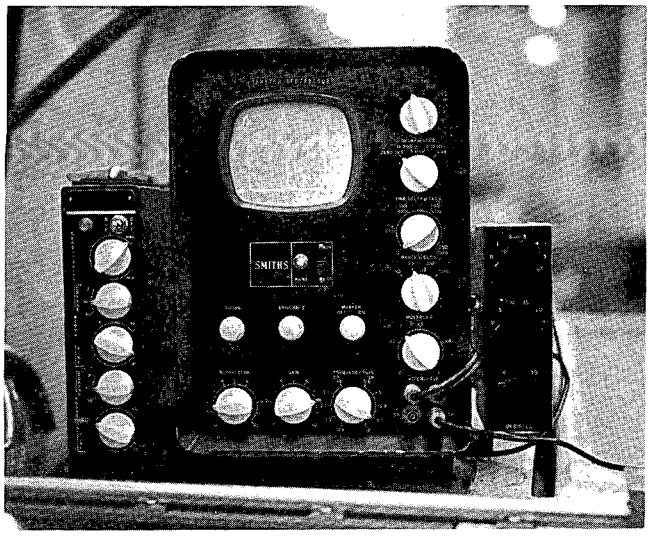

Figure 7. Flaw-detector presentation of a satisfactory head. (Light opposite switch, top left, is off.)

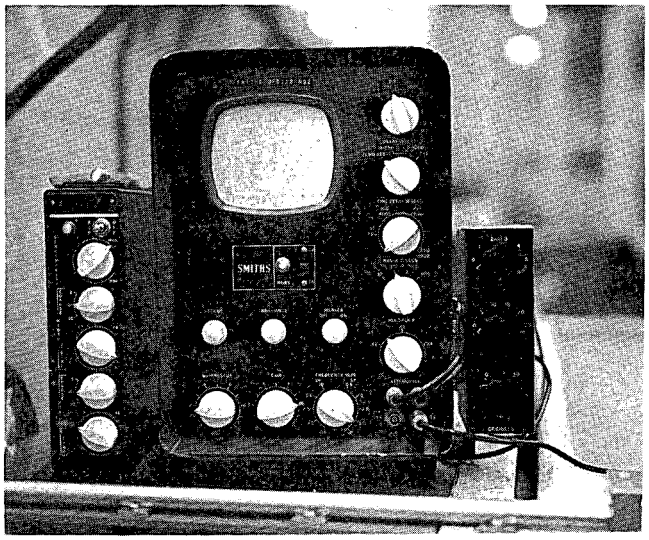

Figure 8. Flaw-detector presentation of a defective head. (Light opposite switch top left, is on.)

column, and angling the probe, the necessary shear wave is induced in the head, by mode conversion at the water-to-metal interface. A gating system is used in conjunction with the flaw detector to enable the defects to be monitored (Figures 7 and 8). By rotating the component about its axis with the probe at the requisite radius the defects will occur at one depth on the flaw detector. By setting the gate to correspond to this position, the defects may be satisfactorily monitored. The output from the flaw alarm can be fed to a circular chart recorder, which then displays the defects graphically (Figure 9). The threshold of the monitor is set to trigger on cracks above the acceptance level applied. A typical fatigue crack detected by this system is shown in Figure 10.

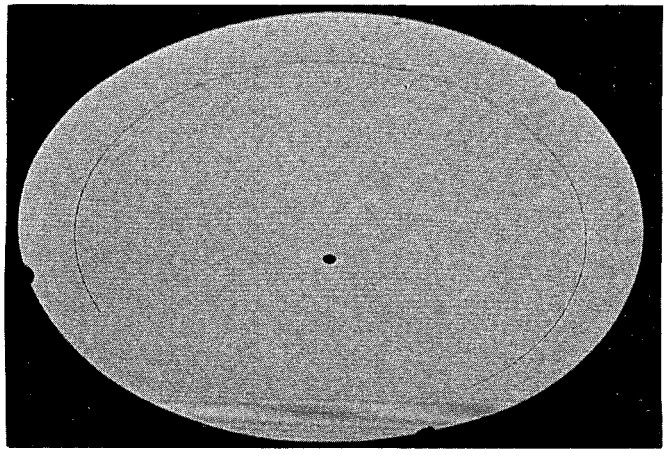

Figure 9. Chart record of a defective head.

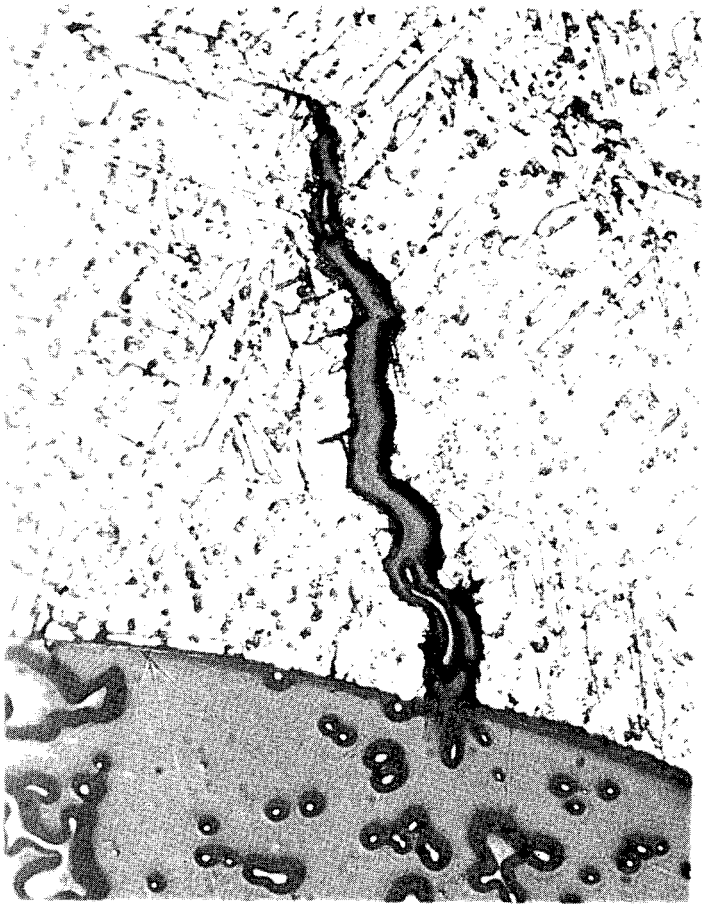

Figure 10. Microsection showing a fatigue crack—X50.

So far many hundreds of cylinder heads have been inspected and a very good correlation has been obtained when the ultrasonic indications have been compared with the penetrant tests applied after ring removal. It has been found in certain cases, which have been investigated by metallurgical sectioning, that this method is more sensitive than the penetrant system that it replaced.

Weld Inspection

Nondestructive testing techniques for weld inspection are generally well established and in common use. The most usual system employed is radiography, but where the section thickness is large, such as in ship building, or remote such as in pipe welding, then ultrasonics is applied. Gas or electric arc welds are also found in aero engine construction, but one of the most commonly used welds in this industry is a resistance spot or seam weld. X-ray systems are capable of detecting voids and cracks in resistance welds, but they give no information about the nature of the weld itself. To date no satisfactory nondestructive testing technique has been devised for this type of inspection so we investigated the possibility of using an ultrasonic resonance system.

It has been found that on adhesive bonded metal joints considerable information could be obtained from the study of the resonant frequency of the bonded joint. Since a spot weld is similar in construction, except that fused metal is used as the adhesive, it was thought that a similar method could be applied. The system used a freely vibrating crystal which could be placed on the weld surface. When placed in contact with a piece of sheet metal the probe resonant frequency was altered and the probe oscillations damped, both these effects being observed on a cathode ray tube. On welding a second piece of sheet to the first and then rechecking, the probe damping was increased and the resonance point changed. In the case of a very poor weld with a small nugget, the damping effect was reduced and the frequency shift was small. Tests were carried out on seam welds in nickel-base alloys and for this purpose the existing crystal was carefully shaped to fit the weld width, which was slightly smaller than the original crystal diameter. It was found that a correlation could be obtained between the resonance pattern observed and the weld nugget size as determined by subsequent metallurgical sectioning. By using suitable gating circuits it was also possible to detect the illusive stuck weld where no fusion had taken place. However, although very promising, two major problems revealed themselves. Due to the contact system employed acoustical coupling varied appreciably with the surface roughness of the weld. A further problem was created by the multiplicity of weld sections involved as these welds were used to join sheets of very widely differing section thickness. When using a resonance method a different set of operating conditions was required for each weld section inspected.

Although this system is at present not suitable for a production application, it is hoped that the development of improved crystal types will enable some further work to be carried on in the future.

The recent use of electron beam welds in aero engine construction has introduced a further nondestructive testing problem. Some success has been achieved in the use of shear-wave techniques for the detection of certain types of defect, which elude the X-ray eye of the radiographer. Lack of penetration is a common problem where a box type of construction is employed and the reverse side of the weld is invisible. This type of defect is particularly harmful as it can act as a nucleus for fatigue failure. In welds of this type with wall sections of the order of 0.1 in., 5% lack of penetration can easily be detected by using an 80° shear-wave technique. Development of this method is likely to enable even small amounts of lack of penetration to be detected accurately.

Material Sorting

Apart from defect detection in new and used components using the ultrasonic systems mentioned above and the more generally discussed dye penetrant, magnetic and radiographic methods, nondestructive testing is extensively applied in the field of material identification and metal sorting.

The aero engine consists of a vast range of components of different shapes and materials. However, in some cases, two different components may have the same physical shape but be manufactured from different materials. Although very strict precautions are taken to ensure that material mixing does not occur, a problem still exists.

Naturally components are marked if possible; however, due to the complex machining and heat treatment process necessary to produce some components, such as turbine blades, it is clear that often it is impossible to ensure the component is marked at all phases of its life. Strict quality control is applied to guard against mixed materials, but as an aid to this control and to enable mixed materials to be sorted if this did occur, various nondestructive sorting methods have been developed.

The main physical characteristics that can be measured are conductivity, permeability, thermoelectric properties or chemical composition. It is to be assumed that a difference in chemical composition occurs, but there may also be different heat treatment and variations in surface condition to consider. A principle sorting problem is that of separating nimonic alloys which are a series of nickel-based materials used for the manufacture of turbine blades. The difference in chemical composition between the alloys in this series is small, so the sorting method has to be very sensitive. Two methods are applied in conjunction to enable the whole series to be sorted. A measurement of conductivity may be made using an eddy-current system, where the phase is carefully chosen to be sensitive to this parameter only. The hand probe is placed on the component in question and instead of reading conductivity directly, the null position meter of the bridge is used as a sensitive indicator, to improve the separation of alloys with very similar conductivities. As overlapping of conductivities can occur within the nimonic series a second sorting method is required to separate these alloys. By placing a heated metal probe onto the component, which acts as a cold junction, and by connecting the probe and component to a sensitive amplifier and galvanometer, the thermoelectric E.M.F. generated may be measured. This method is highly sensitive to small changes in chemical composition and may be used with the previous system to enable a complete check to be carried out on the material identification of these alloys. A system of measuring permeability directly is now available and this has proved useful in sorting certain austenitic alloys and similar materials. If neither of the previous methods is applicable then a chemical spot check may be employed, which although satisfactory in certain cases, is rather outside the scope of this discussion. However, this chemical check may be applied indirectly in some cases due to the different etching properties of various alloys. In this way rogue components may be spotted during routine etch inspection due to the different type of attack which may have taken place.

Coating Thickness Determination

A further example of nondestructive testing techniques, again outside the limits of defect detection, is that of coating-thickness measurement. Present trends in aero construction have lead to

the use of a very wide range of both base materials and protective coatings. Coupled with the problem of complex shape and very tight tolerances on the coating thickness, this sphere has proved to be one of the most absorbing and interesting.

The types of coating and substrate may be classified:—

(a) *Coatings*

(i) *Non metallic*
Paint, anodic films, oxides, etc.

(ii) *Metallic Coatings*
Electroplating, sprayed metals and fused metallic carbides.

(b) *Substrates*

(i) *Light alloys*
Magnesium, aluminium.

(ii) *Ferromagnetic materials*
Steels and nickel.

(iii) *Non magnetic materials*
Austenitic steels, titanium and nimonics.

To cater for the range of possible combinations of the above, it has been necessary to employ a number of techniques which are now briefly described.

Eddy-Current Methods

These are suitable generally for light alloys with insulating coatings such as paint or anodic films. The technique relies on the well known 'lift off' effect, where the eddy-current field induced in the substrate is reduced by the presence of the coating. This method is also applicable to certain plated coatings as long as a reasonable difference in conductivity exists between coating and base material. The equipment employed has operating frequencies from 100 Kc/s to above 10 MHz. The use of careful jigging of the handheld probe is usually necessary to minimize edge effects.

Magnetic Methods

Here various forms of the old magnetic lift-off gauge are employed, but the modern equipment often uses a low-frequency type of eddy-current system. The materials inspected vary from plated coatings to paint films on a ferromagnetic base. By suitable probe jigging it has been found that it is now possible to measure down to coatings of the order of 0.0003 in. to an accuracy of 0.00005 in. Edge effects still prove a problem, but the use once more of jigging and representative test-pieces can be used to minimize this effect.

Thermoelectric Method

This system has already been mentioned in conjunction with sorting and it is the same type of equipment that is employed. This method is often overlooked, but is particularly useful where a ferromagnetic coating such as nickel is applied to a ferromagnetic base. Clearly, neither of the previous methods are applicable so this fills quite an important gap.

Point Magnetic Field Method

A recent problem has been that of measuring tungsten-carbide flame plating on a titanium alloy base. The previous methods are not applicable, so the system devised relies on the fact that the coating is magnetic and the titanium non-magnetic. The coating is magnetized in local areas by means of a hemispherical tipped magnet. The point field retained in the coating is subsequently measured by scanning with a sensitive point-field probe. A good correlation is obtained between the value obtained and the thickness of the coating. This system has an added advantage in that edge effects associated with other methods are considerably reduced, so relatively small surface areas can be inspected.

Beta-Particle Backscatter Method

Diffusion coatings are often applied to cast-nickel or cobalt-alloy turbine blades to improve their high-temperature properties. This type of coating is applied by heating the blade in a box of aluminium powder and alumina until fusion occurs. Unlike plating, a direct intermetallic bond is created by the presence of a diffusion zone. Eddy-current techniques cannot be applied due to the insufficient difference in the conductivities of coating and base and the coarse dendritic structure of the substrate.

At present a Beta-particle backscatter system is being developed so that the present rather laborious method of hardness checking and metallurgical sectioning on test-pieces can be replaced by a speedy accurate system capable of operation on finished components in a truly nondestructive manner.

Beta particles emitted by a radioactive isotope such as Promethium are allowed to fall onto the surface of the specimen, which then backscatters the received particles. The level of this backscatter depends on the atomic number of the element involved and, therefore, if the atomic weights of the coating and base are sufficiently separated, the coating may be measured. The measuring head employs a sensitive scintillation counter connected to a scalar or ratemeter which gives a direct readout in thickness. Using this system it is hoped that an accurate measure of the coating thickness may be obtained rapidly and easily.

Present and Future Development

So far I have discussed systems that have been developed or are in the late stages of development for use in the specific sphere of aero engine inspection.

However, I should like to conclude by mentioning some other development projects at present under way.

Measurement of hardness by using an ultrasonic method. It is hoped that this system could be used to enable more elaborate hardness explorations to be carried out on critical components without producing large harmful indentations which result from Vickers or Rockwell testing.

The nondestructive determination of creep life on turbine blades has been an unattained goal in the field of aero engine manufacture for many years.

Following some recent success in this field it is hoped that a system may be developed eventually to make this form of testing a practical possibility.

Infrared scanning systems are being evaluated to see if a simple system can be devised for the inspection of fibre-glass components, with a view to detecting defects at present not detectible by ultrasonic systems.

A simple mechanical follower system is being developed to see of contour following could be practised on ultrasonic testing of discs. This system would eliminate the costly and wasteful practice of rectilinear machining employed at present. Development work is still very much in the early stages, but a simple mechanical follower has been manufactured and its evaluation has been commenced.

The author expresses thanks tc the Directors of Bristol Siddeley Engines Limited for permission to publish this paper which contains only his own opinions.

Application of the Ultrasonic Testing Technique to the Quality Evaluation of Cast Iron Rolls

SOJI SASAKI AND KUNIO ONO, JAPAN

ABSTRACT: Ultrasonic testing techniques described here involve two procedures for evaluating the quality of cast iron rolls; the estimation of the thickness of the hardened layer and the detection of inner flaws.

The estimation of the thickness of the hardened layer is performed by the pulse-echo method and for this purpose special types of local immersion probes were developed. Experiments made on chilled and grain rolls proved that the ultrasonic frequency suitable for measuring the thickness of the hardened layer depends on the material structure of the object; especially in the grain rolls, the frequencies lie in the range lower than 3 MHz.

In detecting inner flaws, comparatively low frequency is preferable such as 0.75 or 0.4 MHz and combined type probes with resonant coupling were developed.

The equipment has a display system by which the thickness of the hardened layer or the existence of inner flaws can be interpreted by B-scan representation.

Introduction

Cast iron rolls, such as chilled rolls or grain rolls which are widely used in rolling mills, present some problems in the field of ultrasonic testing techniques.

In order that a cast iron roll performs its function, it is important that the thickness of the hardened layer, which forms the outer shell of the roll, be held within a suitable range and that inner flaws be substantially avoided.

When the thickness of the hardened layer is less than adequate the roll cannot be guaranteed for its designated life usage. On the other hand, when it is too thick the roll may tend to break down. Moreover, when the hardened layer is not uniformly thick along the roll, the rolling characteristics may be inadequate in operation.

If there is a flaw of considerable scale in a roll, it may accidentally cause the roll to break down. Thus the problem arises of how to apply ultrasonic testing techniques for estimating the thickness of the hardened layers on cast iron rolls and for detecting inner flaws.

The ultrasonic pulse-echo method for measuring chill depth on castings or chilled rolls has been examined by Smith and Fuller (1). However, to measure the thickness of hardened layers on grain rolls, it is necessary to take into account their structural difference, i.e. dispersion of graphite flakes in the hardened layer which cause ultrasonic scattering and attenuation.

When detecting inner flaws, an effort is also required to overcome the impediment of ultrasonic scattering and attenuation.

This paper describes some experimental results and the techniques developed to meet the above requirements.

Estimating the Depth of the Hardened Layer

The thickness of the hardened layer is estimated by the pulse-echo method, which measures the time interval between the echo signal from the roll surface and the return signal initiated by scattering at the boundary between the hardened layer and the inner core region.

Figure 1 shows an example of echo signals representing chill depths of specimens cut from a chilled roll. The experiments were made by the single-probe immersion method, where the ultrasonic energy is normally inserted from the chilled face and the ultrasonic frequency is 5 MHz. The time interval t, between the peak of the surface echo S and that of the boundary echo B, is in proportion to the chill depth d.

Since in the chilled roll an acoustical discontinuity is well defined at the structural boundary, the scattered echo signals

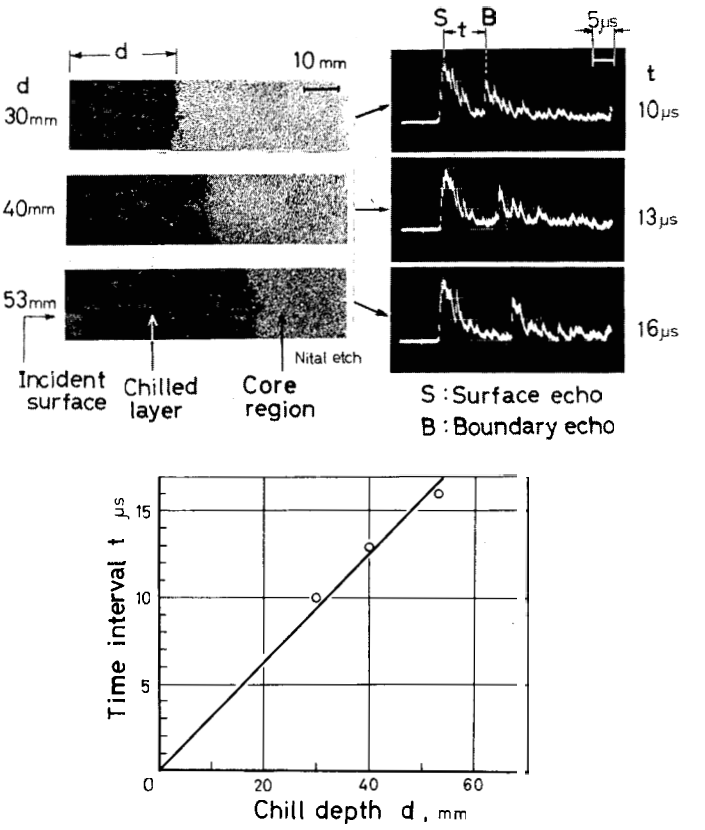

Figure 1. An example of experimental chill-depth measurements from chilled specimens.

from the boundary can be easily distinguished. This discontinuity is mainly due to graphite flakes in the inner core in contrast to their absence in the outer chilled shell.

In a grain roll, however, since graphite flakes are dispersed in the hardened layer as well as in the inner core, the acoustical discontinuity is so indistinctly formed that the scattered echo signals from the boundary are not so clearly observable as in the case of a chilled roll. In order to distinguish the signals of the scattered echoes at the boundary from those of the other structural echoes, the following procedures are employed:

(1) selection of the suitable ultrasonic frequency in accordance with the acoustical property of the structure of the test roll.

(2) identification of the echo signals as a pattern by means of the B-scan method.

It is experimentally observed that the ultrasonic frequencies suitable for measuring the depth of the hardened layer lie in the 3 MHz or less range. When the frequency is too high, too much scatter occurs in the hardened layer to observe the boundary echo when it is too low, the resolution of the echoes is so reduced that the boundary echo can hardly be observed.

For measuring the thickness of the hardened layer, a type of local immersion transducer assembly has been devised to control the intensity of the surface echo that would mask the boundary echo, especially if the hardened layer were thin. The assembly is constructed as shown in Figure 2. In the probe a pair

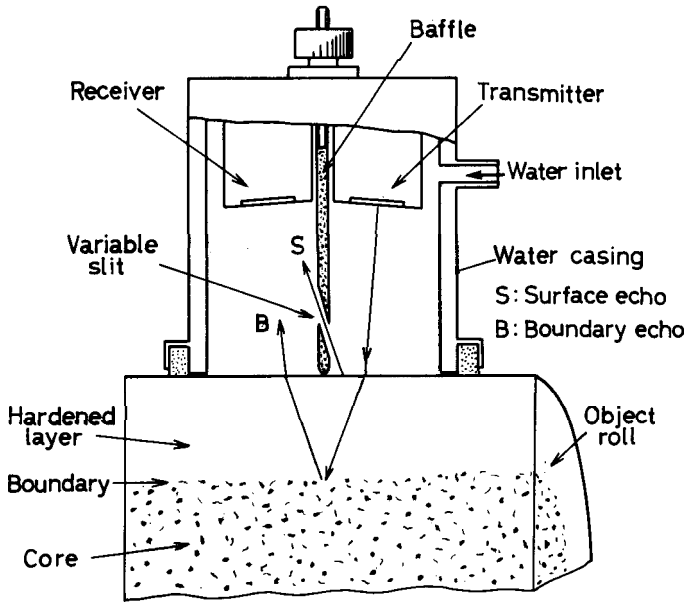

Figure 2. Illustration showing the probe system for measuring the thickness of the hardened layer.

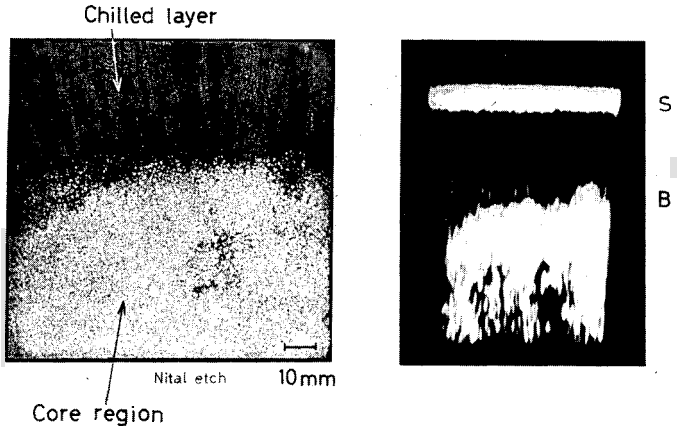

Figure 3. A chilled specimen and its echo pattern.

of barium-titanate transducers are separately mounted; one is a 20 × 20 mm transmitter and the other a 20 × 15 mm receiver. Situated between the transducers is a baffle with a variable slit to pass the surface echo reflected at the roll surface to the receiver. The complete assembly is approximately 80 × 60 × 100 mm.

In operation, the probe is moved along the roll surface, keeping acoustical contact between the transducers and the test material, with a water medium filling the casing. Ultrasonic energy once projected into the roll travels through the hardened layer, partly scatters at the boundary zone and is detected by the receiver. The time interval between the surface echo and the boundary echo gives the thickness of the hardened layer.

Figure 3 shows a chill-depth echo pattern of a specimen cut from a chilled roll. The experiment was performed at the ultrasonic frequency of 5 MHz.

Figure 4 (b) shows the pattern of an accidental case in which differing thicknesses of the hardened layer along the periphery of a grain roll are displayed; the destructive test revealed the nonuniform thickness of the hardened layer as shown in Figure 4 (a). Figure 4 (c) shows the echo pattern of the normal section where a uniform depth of about 47 mm was confirmed for the hardened layer.

The echo patterns in Figure 4 were obtained in the following way. The horizontal sweep line, whose brightness is controlled by the echo signals, is scanned vertically from the top to the bottom and is synchronized with the probe scan along the periphery of the rotating roll. Consequently, when the test roll accomplishes one revolution, a frame of the echo pattern is completed. This represents the depth distribution of the hardened layer.

Detection of Inner Flaws

The metallic structure of the cast iron roll is usually so coarse that high-frequency ultrasonic energy is considerably dispersed and attenuated. This dispersion and attenuation obstruct the detection of flaws in the roll.

To attain sufficient penetration through the test roll and to pick up the internal echoes, a comparatively low ultrasonic frequency, less than 1 MHz, is preferable. Therefore, the fre-

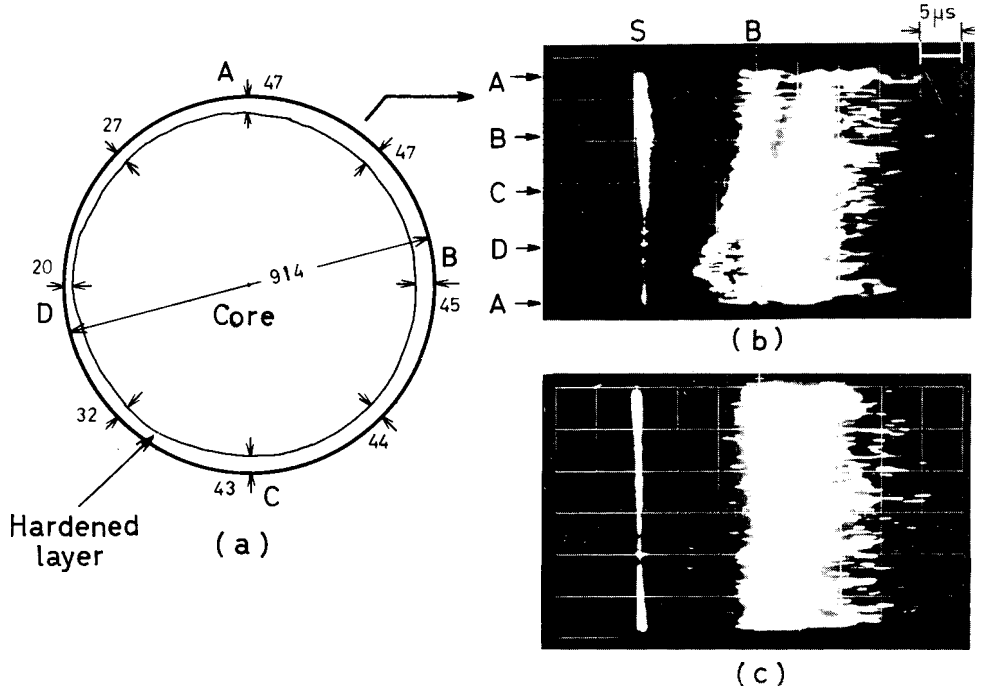

Figure 4
Thickness distributions of the hardened layer observed in grain roll specimens: (a) sketch of a section showing nonuniformity in the hardened layer; (b) echo pattern corresponding to (a); (c) echo pattern corresponding to a normal section showing uniform thickness, about 47 mm, of the hardened layer.

quencies of 0.75 and 0.4 MHz are provided for flaw detection. A combination probe where a transmitting transducer and a receiving transducer are mounted separately in a single head, has been developed to minimize the dead zone near the surface of the test-piece. Both transducers are 30 × 20 mm lead-zirconitanate. To protect the transducers from damage the resonant coupling method is employed, by inserting a half-wavelength plate between the transducers and the test-piece. Several plexiglass coupling plates are shaped to fit the cylindrical surfaces of rolls ranging 500-1000 mm in diameter. The effective thicknesses of the plates corresponding to the frequencies 0.75 and 0.4 MHz are designated as 1.7 mm and 3.2 mm. Machine oil both lubricates and forms the acoustical contact between the plate and the object.

The B-scan representation method is also used so that flaw echo patterns are displayed clearly on the cathode ray tube and distinguished from other echoes scattered in the roll.

Figure 5 shows echo patterns of defects in a grain roll specimen. The test specimen was cut from a plate work roll originally 904 mm in diameter and 3405 mm in length, and two artificial defects 7 mm and 3 mm in diameter, were drilled in one section normal to the face. The echo signals from the artificial defects are easily distinguished from those of the other echoes and represent the locations of the defects.

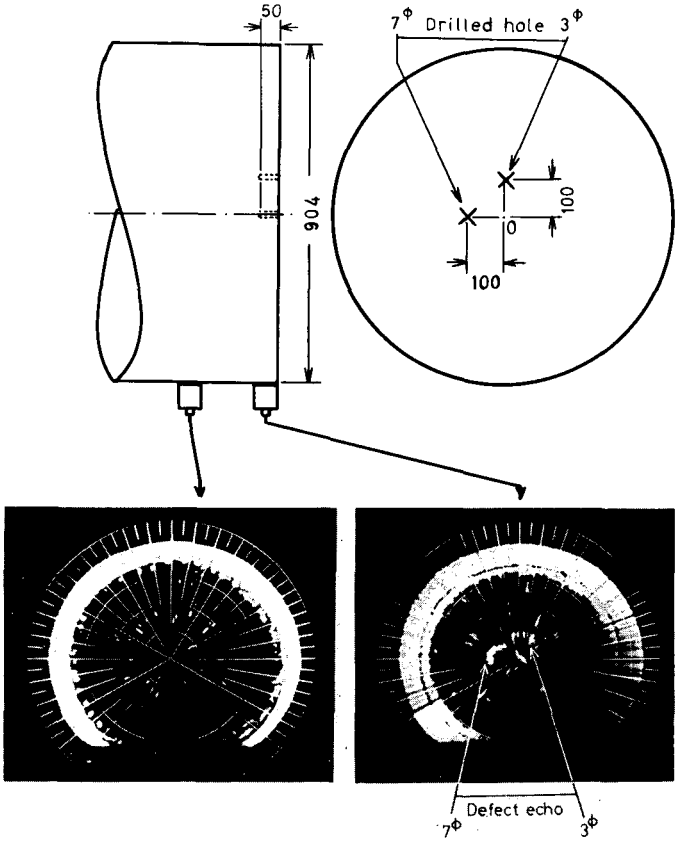

Figure 5. Acoustic sectional views of a grain roll specimen: left, free from defect; right, including artificial inner defects.

The circular patterns were obtained in the following way. The sweep line on the cathode-ray tube, whose brightness is controlled by echo signals, rotates synchronously with the roll specimen so that the rotation centre of the sweep line corresponds to the roll axis. Thus the echo pattern represents the acoustic sectional view of the roll being tested.

Apparatus for Practical Use

The apparatus for practical use, Figure 6, was developed from the results of experiments similar to those previously described.

The electronic equipment consists of the following devices: transmitter and receiver circuits; two sets of cathode-ray oscilloscopes—i.e. A-scope and B-scope and a signal synchronizing unit. The system of transmitter and receiver circuits is similar to that of ordinary ultrasonic pulse-echo flaw detectors. The ultrasonic frequencies provided are 5, 3, 2.25, 1.5, 1, 0.75 and 0.40 MHz.

The transmitter circuit supplies impulses to the transmitting transducer at the repetition rate about 1 kc/s. The receiver circuit, amplifying echo signals detected by the receiving transducer with the gain about 100 dB, produces video signal output and introduces it to both the A- and B-scope.

The A-scope monitors the waveforms of echo signals or measures the time intervals between the peaks of those signals. The B-scope, provided with a storage type cathode-ray tube, shows the inner flaws or the hardened layer thickness without photographic processes.

The B-scan representation when measuring the hardened layer thickness is such that the voltage signal proportional to the rotating angle of the test roll is applied to the vertical input of the B-scope. Consequently, the vertical scanning of the sweep line is accomplished as shown in Figure 4. To display the sectional view on the B-scope, rotational scanning is employed where two series of saw-tooth sweep signals, one subjected to amplitude modulation in sine form, the other in cosine form, are applied to the vertical and the horizontal input, respectively, of the B-scope.

In addition to the electronic equipment, a lathe mechanism is used to turn the test roll and the motion of its centre axis is electrically transmitted to the signal synchronizing unit by means of synchro-transmitter and receiver. The angle of rotation of the test roll is shown by the dial indicator on the panel of the signal synchronizing unit.

Conclusion

The techniques described are now employed in the production line for estimating the thickness of the hardened layer and for detecting inner flaws in cast iron rolls; they prove effective in ensuring the quality of the products.

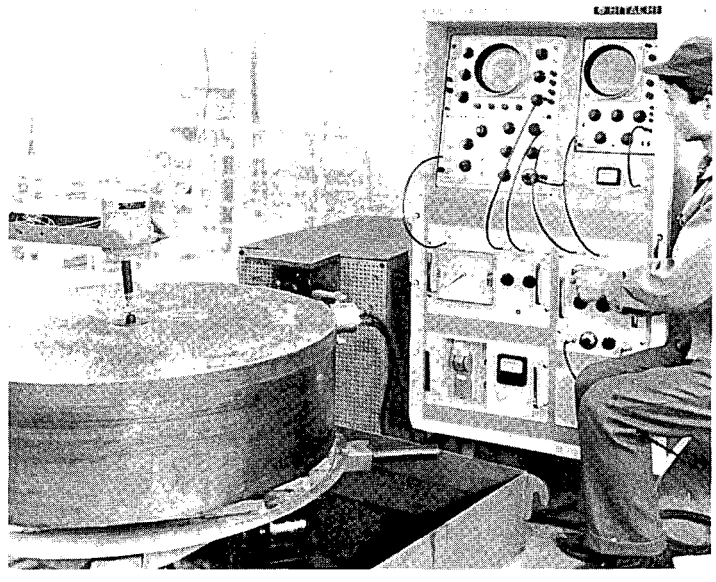

Figure 6. Experimental layout of the ultrasonic test equipment.

The next step is to accumulate test results with a number of products and to establish the standard procedures for inspection.

Acknowledgments

This work was supported by Hitachi Metals Ltd. The authors wish to express their gratitude to Dr. K. Miyashita, vice-president of the company, for his encouragement and to T. Asakura, Engineering Associate of the company, for helpful discussions.

The authors also appreciate the co-operation of the Wakamatsu Factory staff, especially Dr. M. Suenaga, T. Yamasaki and Y. Takezaki.

Grateful acknowledgment for helpful discussions is tendered to Dr. K. Katagi, Chief of the research section in the Hatachi Research Laboratory.

Reference

1. Smith, J. I. and Fuller, A. G. Measurement of chill depth on cast iron test pieces and rolls. *B.C.I.R.A.* **12**, 1964, 319-326.

Discussion

Q. NEIL A. SINCLAIR, General Dynamics Electric Corp., Boat Division, Groton, USA:

I am interested in various approaches to the propagation of ultrasonic waves in cast iron and equivalent materials. Did you investigate approaches other than lowering the frequency, such as focussed beams or special transducers or pulsers?

A. The illustration of the probe system in Figure 2 shows only the principle for measuring chill depth. I may say that contour transducers were employed on occasion, which generate ultrasonic beams focussed at the surface of an object and produce divergent ultrasonic fields in the subsurface region, so that acoustic discontinuities even in the near-surface could be detected.

Composite Nondestructive Testing of Steel Castings: The Radiographic-Ultrasonic Method

ROMAN RACKWAL, POLAND

Introduction

Radiographic testing of steel castings is expensive and time consuming, while the preliminary application of ultrasonic testing can reduce the cost and time of the examination.

The radiographic image of the defect forms the basic material for the composite application of testing. The results of ultrasonic testing are referred to the radiographic results.

It is proposed to introduce an industrial composite application of testing, based on:

1. Radiographic standards of defects;
2. Measurement of the attenuation of the ultrasonic beam;
3. Evaluation of the oscillographic image.

The premise is accepted that such details as cross-section, surface roughness and microstructure of pieces tested ultrasonically must be similar.

Laboratory Examinations

The radiographic testing of carbon steel castings with wall thicknesses from 50 to 90 mm (2 in. to 3½ in.) was performed with a GRM-750 type gamma radiographic machine with a Co^{60} source, having activity of ca 250 Ci.

Polish Foton-Defectofilm X-ray films with 0.2 + 0.2 mm lead screens were used. The ultrasonic testing was done with a DI-10 ultrasonic apparatus.

Double-purpose (transducer + receiver) probeheads with barium titanate crystals were used. The frequency generally used during the testing, was 2 MHz and the surface of the casting was roughly ground by hand.

For the attenuation measurement, a type TP-2 capacitance attenuator was used, calibrated directly in decibels.

The composite testing of castings was performed in the following manner:

—a network of coordinates was put on the radiograms, forming fields of 20 × 20 mm;

—in each field the attenuation of the ultrasonic beam was measured;

—simultaneously the oscillographic picture was evaluated (eventually photographed).

Typical results of testing are illustrated in Figures 1 to 7; the attenuation being based on the following principles:

attenuation up to 18 db — white fields
" 19 ÷ 24 db — light-grey fields
" 25 ÷ 30 db — dark-grey fields
" 31 ÷ 36 db — black fields
" not measured — X

As can be seen, the oscillographic picture for high amplification contains echoes from reflections in the Perspex layer of the double-probe head. These echoes are called "disturbing echoes," but one can isolate these echoes from those of large defects. The echoes from small defects, however, cannot be isolated.

The results of the attenuation measurements show that there exists a correlation between the attenuation of ultrasonics, and concentration of defects, evaluated on the basis of radiographic pictures.

Principles of Industrial Testing

In Table 1, the principles of evaluation of the kind, magnitude and concentration of defects on the basis of ultrasonic testing are given.

For this evaluation the following data are necessary:

—appearance or not of a defect echo that can be isolated from the disturbing echoes: attenuation in the measured field related to the field in which radiography has not showed any defects.

In practice, industrial testing will be performed along the following lines:

—performing radiographic testing of a small series of castings or selected parts of castings with similar cross-section;

—testing ultrasonically to verify the principles, given in Table 1;

—serial ultrasonic testing of many details with radiographic control of a few details.

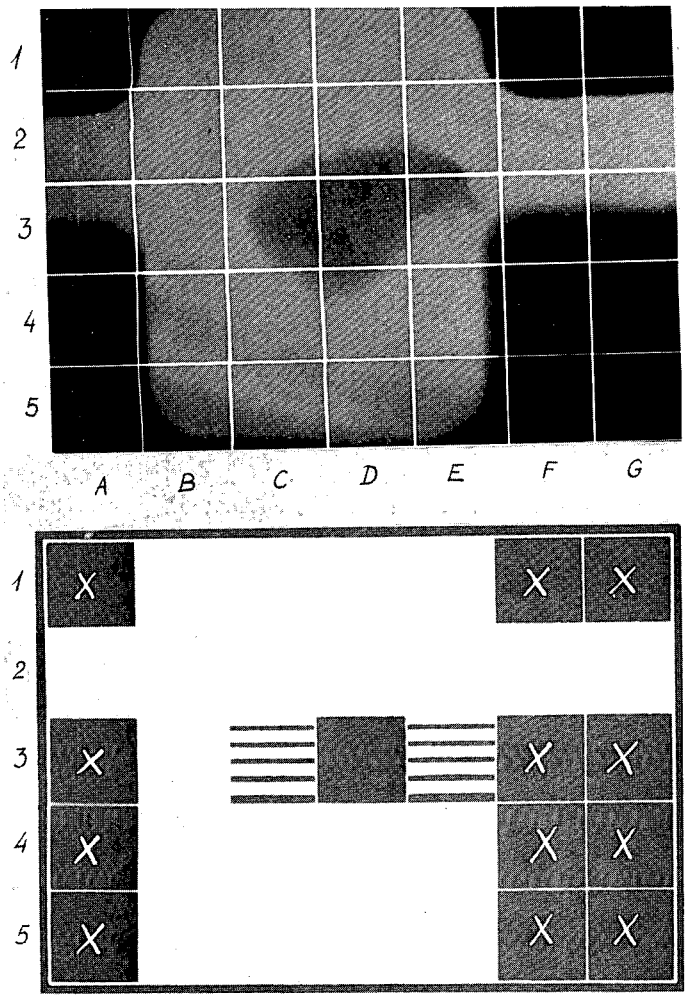

Figure 1. Castings with shrinkage cavities. Top, radiogram with network; below, attenuation diagram.

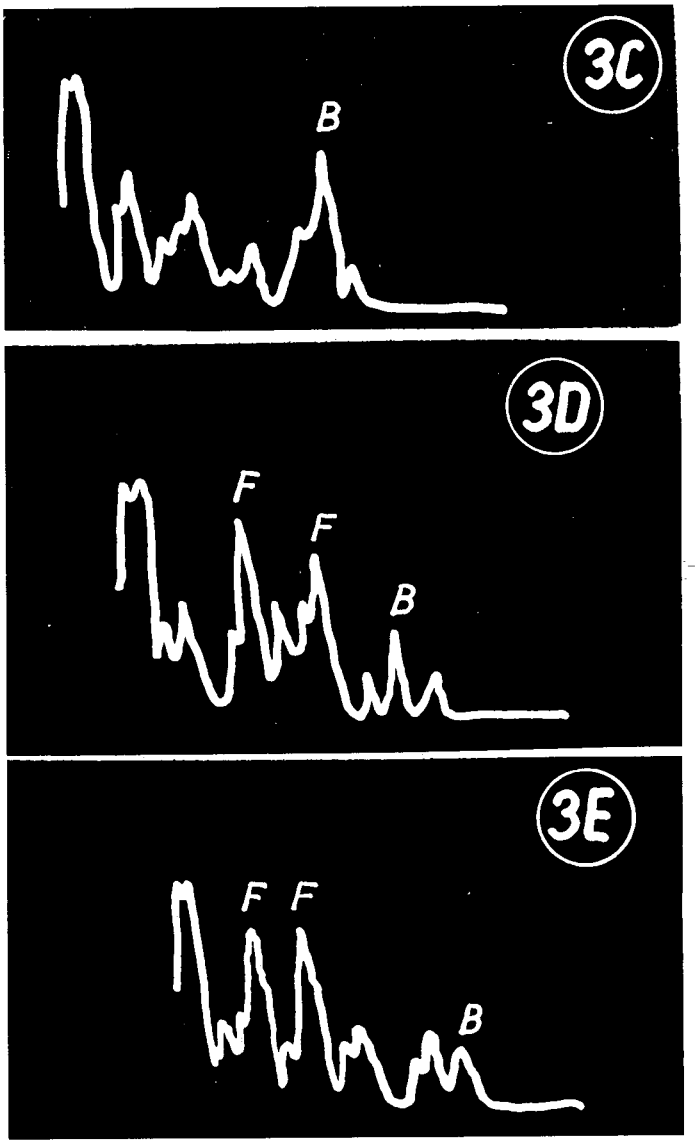

Figure 2. Oscillographic pictures of spots examined by ultrasonics of a casting with shrinkage (coordinates referring to Figure 1, top, are circled). B = bottom echo; F = flaw echo.

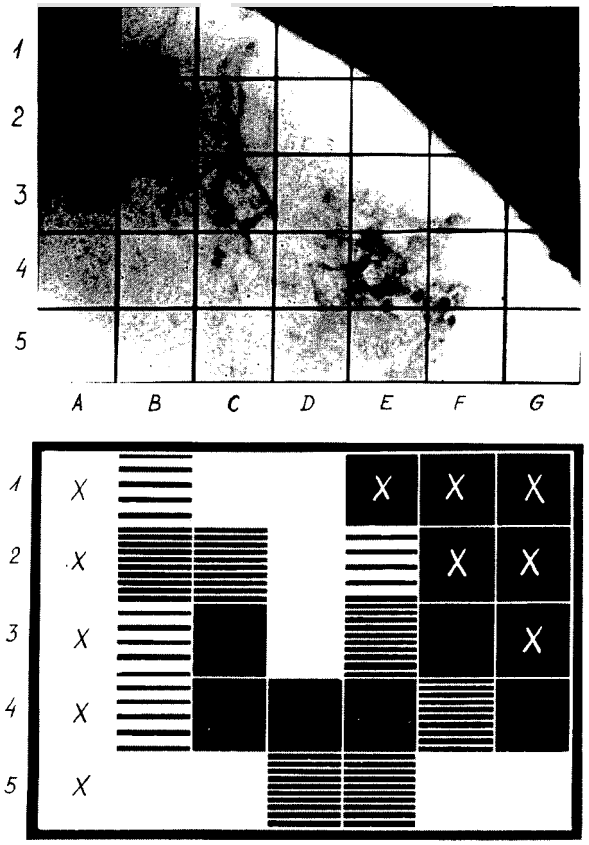

Figure 3. Castings with shrinkage. Top, radiogram with network; below, attenuation diagram.

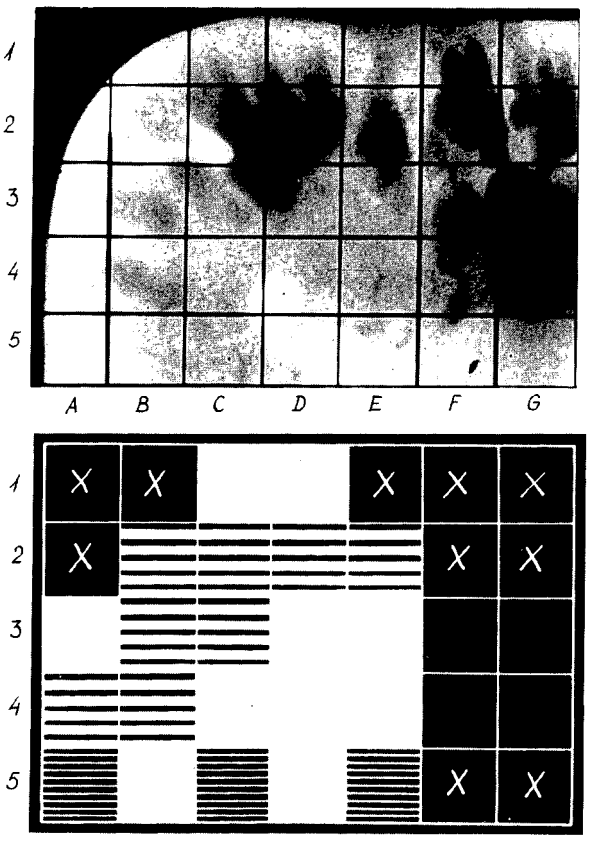

Figure 5. Casting with blowholes. Top, radiogram with network; below, attenuation diagram.

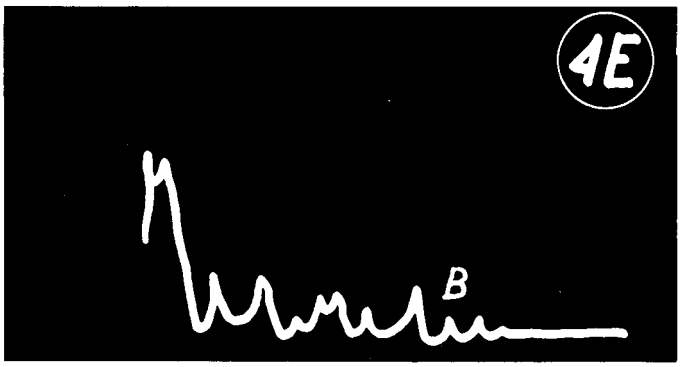

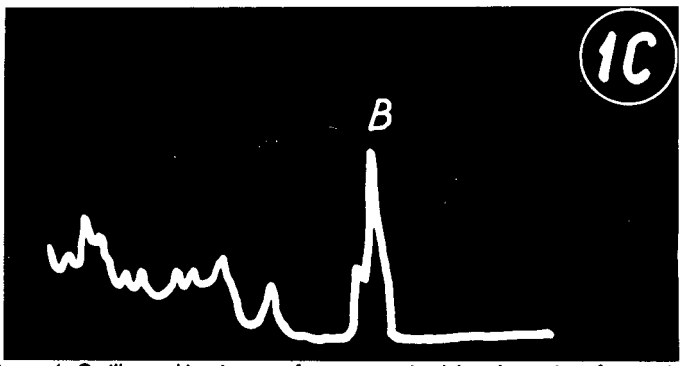

Figure 4. Oscillographic pictures of spots examined by ultrasonics of a casting with shrinkage (coordinates referring to Figure 3, top, are circled). B = bottom echo; F = flaw echo.

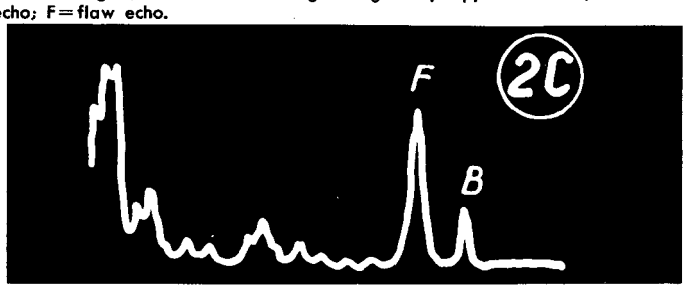

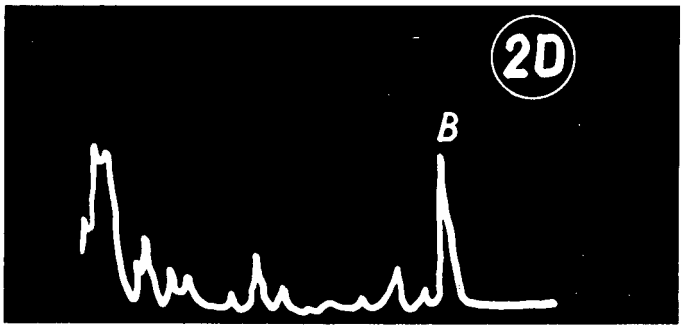

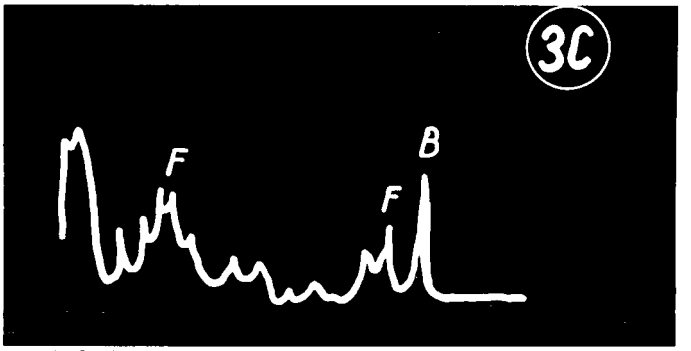

Figure 6. Oscillographic pictures of spots examined by ultrasonics of a casting with blowholes (coordinates referring to Figure 5, top, are circled). B = bottom echo; F = flaw echo.

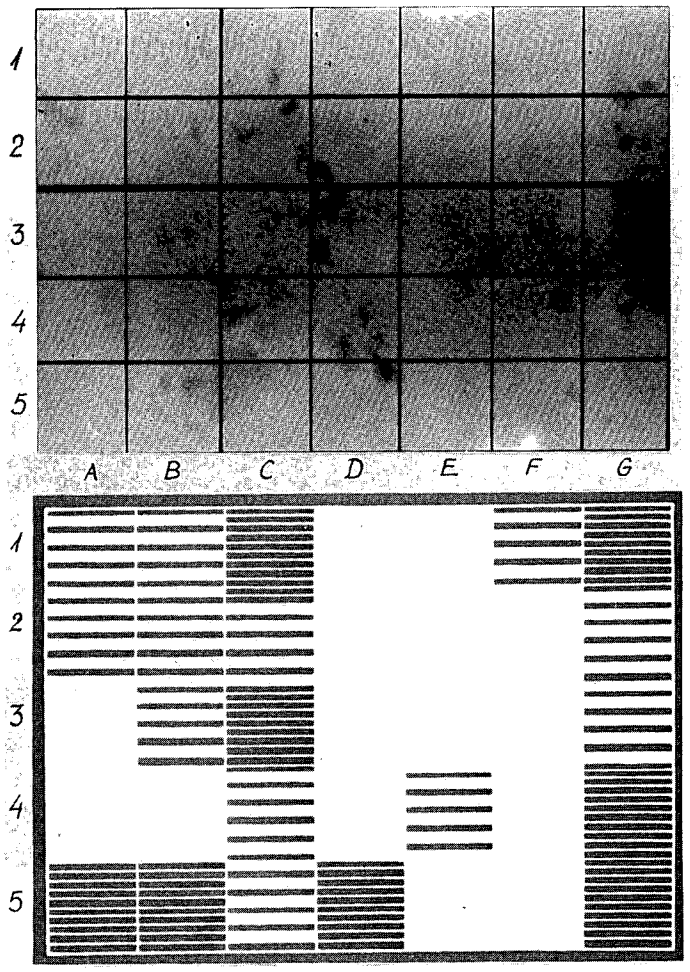

Figure 7. Casting with sand inclusions. Top, radiogram with network; below, attenuation diagram.

Table 1

Principles of evaluation of the kind, magnitude and concentration of defects in steel castings, on the basis of ultrasonic testing

Appearance of defect echo	Attenuation of ultrasonic beam in decibels		
	0 ÷ 18	19 ÷ 30	above 30
Lack of defect echo	Tiny blowholes and inclusions	Concentration of blowholes and inclusions. Shrinkage and small shrinkage cavities.	Large concentrations of blowholes and inclusions. Large shrinkage.
Defect echo exists	Lack of defect giving echoes	Large blowholes, cavities. Cracks and lack of fusion.	Largest blowholes, cavities. Wide cracks and lack of fusion.

Conclusions

Results have shown the possibility of applying ultrasonics in testing steel castings. The radiographic method will be the criterion for the composite method.

Ultrasonic testing does not reveal very small defects that will be of importance in critical castings.

The composite method may have the widest application for castings in the middle quality class. In many cases radiographic testing for such castings is not economical. In such instances ultrasonic testing, controlled by radiography, may give good results.

Castings of middle quality constitute a large percentage of the general production of castings. Hence the application of a cheap testing method may give good economical results.

Ultrasonic Nondestructive Inspection of Round Tubes and Bars by the Rotating Probe Method

CARY E. HOHL, USA

ABSTRACT: Ultrasonic testing of tubing and round bars has generally been accomplished by the rotation of the material being tested.

This paper describes ultrasonic inspection equipment, for round tubes and bars, in which several ultrasonic test probes are mounted in a fixture which rotates around the material at speeds of up to 3,000 rpm, and in which the probes are so fixed as to scan the material simultaneously in a clockwise, counter-clockwise, and longitudinal direction. All probes are pre-aimed for optimum test results which provides practically equal sensitivity on I.D. and O.D. of tubes.

Defective material can be audibly signalled, marked, sorted, recorded, data-processed and evaluated.

Advantages of the rotating probe method over material rotation methods for inspection of round bars, pipes and tubing are:

1. Higher testing speeds, 10:1 or more.
2. Excellent flaw-recognition properties.
3. Flexibility, due to the possibility of selecting from various evaluation devices or combinations thereof.

Introduction

Ultrasonic testing of rods and pipes of high-quality material has been common practice for many years. This is because it was realized early, that in contrast to other nondestructive testing methods, ultrasonic testing guarantees good fault recognition, even in the interior of the test samples, independent of material thickness.

At present ultrasonic testing techniques offer the only possibility for complete and automatic testing of round rods and pipes of all dimensions at high scanning speeds, for surface faults as well as inclusions.

Since the demand for 100% tested semi-finished material is steadily increasing, and more and more material must be tested, automatic ultrasonic testing units are employed on an increasing basis in all branches of industry which manufacture or process semi-finished material.

Underlying Principles

Before introducing the fastest ultrasonic test unit now available for the testing of rods and pipes, let me explain briefly the various ultrasonic test procedures used in practical applications.

Manual Test

To locate longitudinal flaws in pipes or rods, an angle probe is coupled to the sample so as to direct sound beams transverse to the longitudinal axis. In the case of a rod (Figure 1, left), the obliquely adjusted beam circulates within the rod in the shape of a polygon, resulting in a fault indication on the screen of the attached pulse-echo ultrasonic flaw detector as soon as a longitudinal fault is located. In a pipe (Figure 1, right), the sound follows a zig-zag path, detecting inside and outside longi-

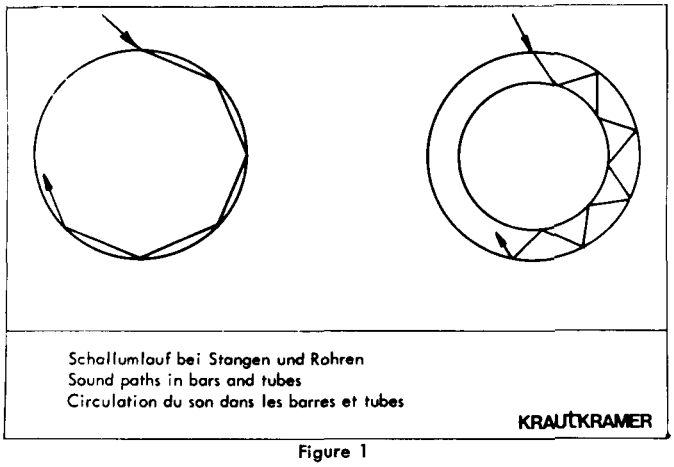

Figure 1

tudinal faults. The probe is manually rotated around the test sample so that, independent of the position of the fault, an indication relative to the depth of the fault is achieved. The screen indication is visually evaluated by the operator. Testing with only one angle probe (Figure 2), in a clockwise direction only, permits overlooking flaws which lie at unfavourable angles. To avoid this, a second test (Figure 3) in a counter-clockwise direction (test probe rotated 180°) must be performed.

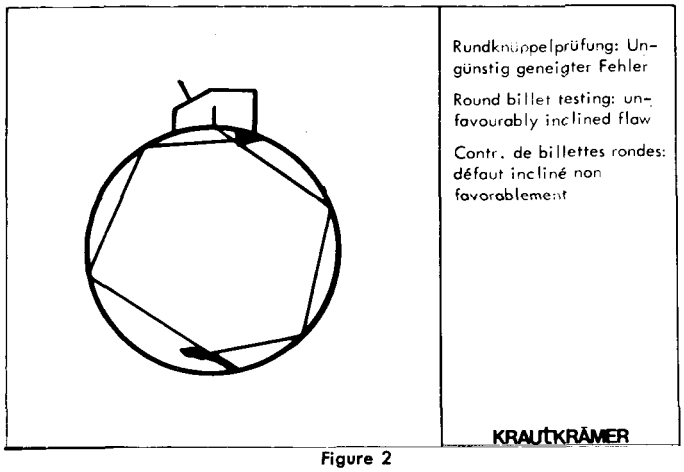

Figure 2

First Stage of Automation

An angle probe is mounted in a test saddle which is equipped with a connection for running water so that with a constant supply of water, good coupling of the test probe to the sample is guaranteed. If the sample is rotated, only longitudinal advance of the test saddle is required. Depending on the speed of rotation of the sample and the minimum flaw length to be detected, the test speed is increased considerably, compared to the simple manual test. If visual evaluation of the screen indications proves to be too strenuous for the operator, or too unreliable, the screen can be observed by an electronic monitor. The latter emits a go-no go signal as soon as the flaw echoes exceed a certain preselected level, thus indicating a flaw that exceeds the permissible limits. The go-no go signal may trigger an optical or an acoustic

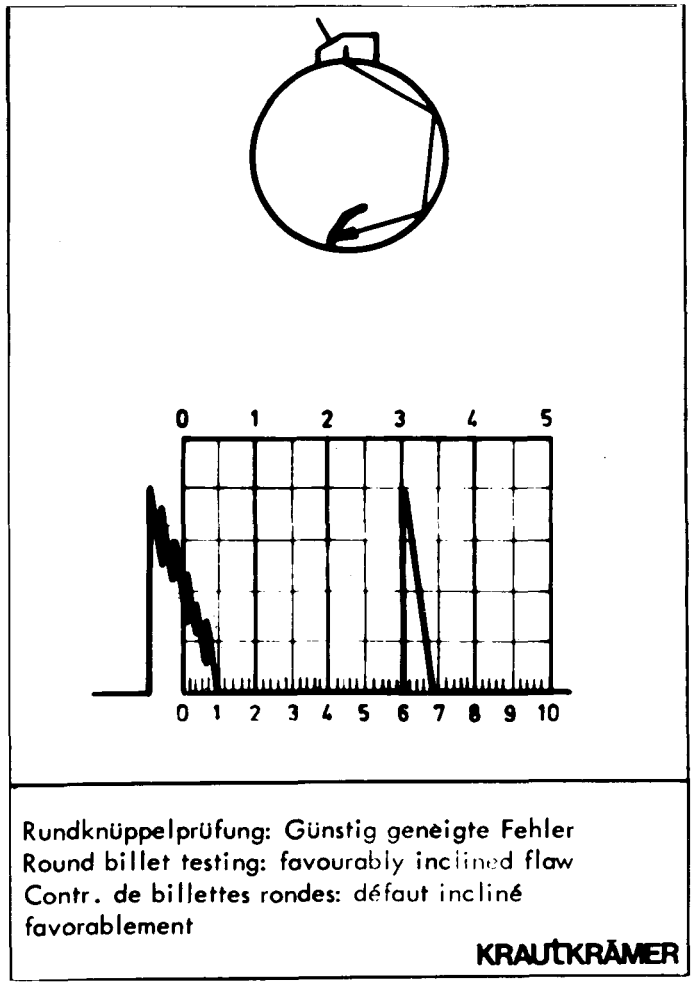

Figure 3

signal device which must be acknowledged by the operator. To locate all unfavourably angled flaws, two systems are required, one with a probe testing clockwise, the other with a probe testing counter-clockwise. The alternative is two separate tests of the material, with the sound circulating in the oposite direction during the second test.

Second Stage of Automation

Instead of the test saddle with one angle probe, a dual probe with running water connection is used. With the same arrangement as described before, two tests are now conducted simultaneously with two sound beams circulating in opposite directions. Advantages lie in the positive detection of all longitudinal flaws independent of their angle of inclination, and positive monitoring of probe "coupling". If a double probe is used, the time required for a second scan is eliminated. Therefore, all other conditions remaining equal, the test speed is increased by a factor of 2.

Third Stage of Automation, North America

Many companies favour immersion testing, where tubes are spiralled under water past an immersion probe aimed at the material at the optimum angle to detect undesirable flaws. An advantage is constant coupling, but care must be taken to maintain proper entry angle of the sound beam into the material. Because of the difference in sound velocities in water, as compared to steel or aluminum, every single degree of change in probe angle results in a 4-degree change of the sound angle in the material. Most test installations of this type limit the rotational speed of the material to 300 rpm, although some claim

to get satisfactory results, free from effects of vibration, up to 600 rpm. Tubes must be plugged to keep water from the interior, since water drops can give flaw signals. If tubes are tested unplugged, air bubbles in the tubes can give flaw signals. All surfaces of the material under test, as well as the probe face, must be free of air bubbles.

Third Stage of Automation, Europe

Because, in immersion testing, there is a buffer zone of water between the test probe and the material surface, the S-E (German, Sender-Empfanger) method, testing with separate transmitting and receiving probes, is employed so that interference echoes from more or less rough surfaces do not cause distracting indications on the screen. Following a spiral path, the test-pieces move through a water-filled tank in which (Figure 4) a pair of probes are directed in a certain way toward the sample. The transmitter probe S(T) beams obliquely into the wall of the sample and produces a wave which circulates the material.

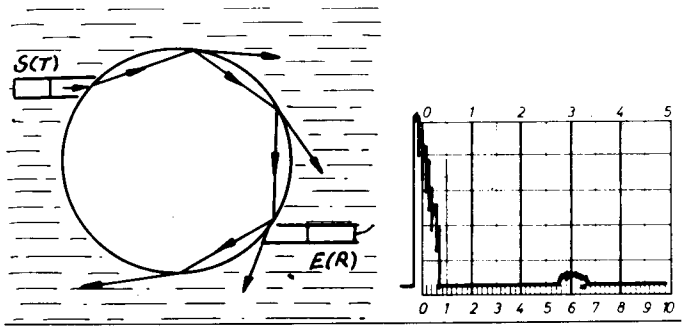

RMBHV - Anordnung
RMBHV - Position of probes
RMBHV - Position des palpeurs

KRAUTKRAMER

Figure 4

In the case of flawless material, the portions of the wave reflected into the water cannot reach the oppositely located receiving probe E(R). If there are longitudinal flaws, the sound waves reflected by the flaws into the water strike the receiving test probe. Maximum indication, for instance, will result in an external flaw located at the marked location.

The advantages of this method are the constant coupling of the test probe to the sample, since the test is carried out without direct contact (water between test probe and sample), and in the totally mechanical advance of the material under test, with probes in a fixture straddling and guided by the test sample. This system contains two pairs of test probes for maximum detectability of all longitudinal flaws. Each pair (transmitter and receiver) forms one testing plane. For positive detection of all inclined flaws, the ultrasonic beams of the two planes circulate in opposite directions.

Fourth Stage of Automation

This stage is accomplished by the use of the rotating probe round tube and round bar tester, described in detail. The rotating probe method incorporates all advantages of the immersion S-E method mentioned above, and in addition, offers a considerably higher test speed. The material is moved only in the longitudinal direction (without rotation) while the ultrasonic probes rotate at approximately 3,000 rpm around the material. With the same scanning density (distance between the individual loops of the scanning spiral), the test rate is increased by a factor of approximately 10:1.

The Rotating Probe, Tube and Bar Tester

This comprises assemblies, as shown in Figure 5: a) The Testing Unit; b) The Guiding Device; c) The Evaluation Unit.

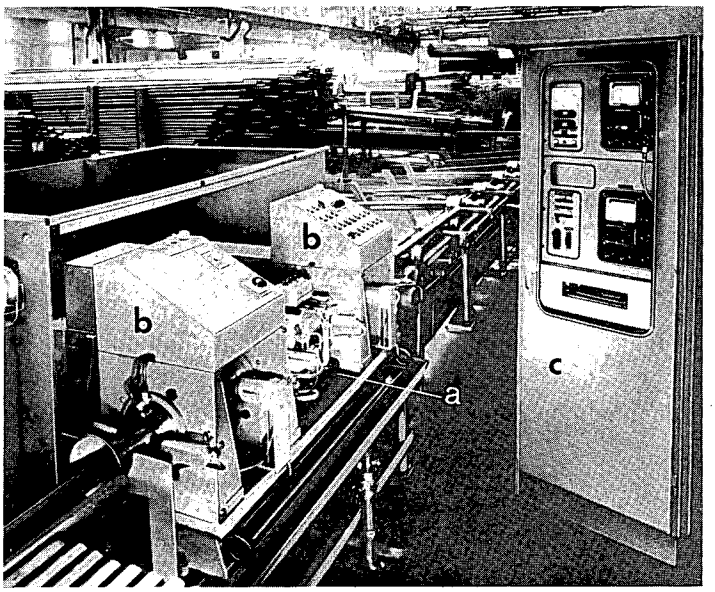

Figure 5

Testing Unit

The essential component of the test machine is the rotary test block which contains the test probes with either 1, 2 or 3 test planes, depending on the requirement. Generally pipe is simultaneously tested for longitudinal and transverse flaws.

For longitudinal flaw scanning, two planes in the test block are necessary. Each plane has two test probes (Figure 6)

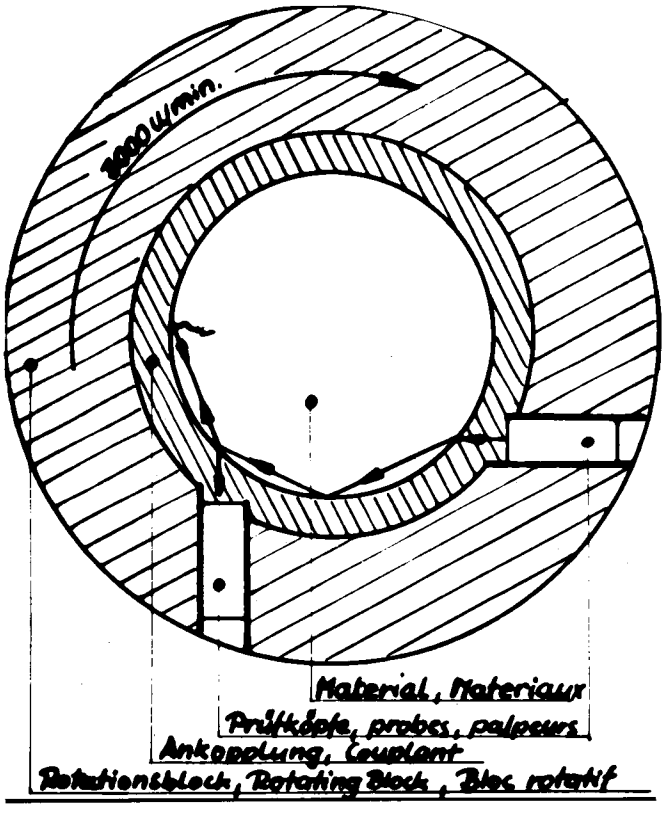

Rotationsprüfblock
Rotating block
Bloc rotatif de contrôle

KRAUTKRAMER

Figure 6

which, by means of the S-E method, cause two sound waves to circulate simultaneously in opposite directions in the wall of the pipe.

The third plane contains another probe, the sound beam of which is aimed at the material axially at an angle and directed along the centre line of the pipe. It receives an echo when a transverse fault is encountered.

Since the path of the sound beam depends very much on the sample dimensions, the test probes in the rotary test block must be exactly aligned for these dimensions.

The rotary probe block is used to test tubing for longitudinal and transverse internal and external flaws, and to test bar stock for longitudinal defects at or near the surface.

In the rotary probe block test blocks, the probes are aimed with the help of sample tubes, pipes or bars. The test specimens contain artificial external and internal defects of a defined depth and length. The choice of the angle of incidence is very critical. Very small changes in the aim have an effect on the "quality" of the rotary probe block.

The "quality" of a test block is defined in general as the difference between the maximum defect echo amplitude and the noise echo amplitude (in the range of the defect echo). A test block is "good" if this defect to noise ratio is 8 dB or more; that is, if the defect echo height is higher, by about $2\frac{1}{2}$ times, than the noise level. When a rotary test block is manufactured for the testing of tubes and pipes, a second value for "quality" is important; that is, the difference between the echo amplitudes of internal and external longitudinal defects of the same depth. If this difference is 4 dB or less, the test block is "good", providing the previous condition is met at the same time. The adjustment of the optimum probe positions in a rotary test block for one size specimen (outside diameter of bar stock, outside diameter and wall thickness of tubes) should only be made by Krautkramer to maintain our guarantee of performance.

A rotary probe block made for bar stock testing, optimally adjusted for a given diameter, can be used for the testing of other bars with nearly the same outside diameter if the guidance of the material is controlled precisely through the test block. In general, bar stock with a diameter of ± 2-mm difference from the nominal diameter, can be tested with the same test block and with enough accuracy for general practice. Here there are no longer the optimal ratios as with the optimum diameter, and the difference between defect echo amplitude and noise level is going to decrease, perhaps to even less than 8 dB.

For probe blocks designed for a given tube dimension, (meaning tube O.D. and wall thickness) the ratio of the flaw indications to the noise level decreases when tubes with a slightly different dimension are tested. Also, the ratio of the echo amplitudes of internal and external defects becomes worse, differing perhaps by more than 4 dB.

Our answer to the question, "What tubes with nearly similar dimensions can be tested with a probe block manufactured for another tube size?" must be combined with the question, "What deviation from optimum test conditions can be tolerated?" In general, when testing tubes with different dimensions, the difference between internal-external defect echo amplitudes becomes more with 4 dB. With wide testing tolerances and with proper guidance, tubes which differ in their external diameter by ± 1 mm (with ROT 50, $\frac{3}{8}$"-2") and ± 2 mm (with ROT 120 1.2"-4.8") are "testable". Also, some tubes are "testable" whose wall thicknesses differ to a specified degree from the dimension for which the probe block was manufactured. A numerical value statement is only possible if the permitted difference between the internal and external echo amplitude is stated in advance. A probe block only delivers optimum test results when it is used on tubes with the dimensions for which it was designed.

Experience has shown that satisfactory test results can be obtained with a stock of from 2 to 4 probe blocks, depending on the wall-thickness range, for tubes with the same outside diameter. Here the wall thickness should not be more than 20% of the external diameter.

The rotary probe blocks for test systems ROT 50 and ROT 120 are designed for certain *diameter ranges*. A probe block can be adjusted by Krautkramer for tubes of other diameters, (and for tubes with other wall thickness) if the new diameter is in the same diameter range.

Water is used as a coupling medium. It is pumped under pressure into the interior of the rotary test block, filling it completely. By giving the block the proper shape, perfect coupling is achieved at the high rotational speeds.

Electrical connection between test probes and the pulse-echo ultrasonic flaw detector is accomplished by means of inductive coupling between the test block and the stator of the test machine. Thus slip rings, which cause contact difficulties and are subject to severe wear, are avoided. The ultrasonic flaw detectors operate at as high a pulse frequency as possible (about 3,000 cps), so that maximum ultrasonic pulses per block rotation result in a good scanning density. In the case of the ROT 50, there are nearly 60 impulses per spiral rotation. On a normal boiler tube of 37-mm dia, the impulses on the tube surface are about 2 mm apart. Thus it is guaranteed that flaws are optimally located by an ultrasonic pulse, independent of their location relative to the tube circumference, and that the resulting echo is proportional to the depth of the flaw. In order to obtain maximum reproducibility, the ultrasonic flaw detector is not self-synchronized. Instead, it is designed for external synchronization, obtaining synchronization impulses from the rotary test unit which, by means of an impulse transmitter, supplies the required number of impulses per test-block rotation.

Reproducible indications also demand that the position of the test probes, relative to the axis of the samples, remains unchanged. Since the test probes in the rotary test block are cast in place, care must be taken that pipe being tested moves through the test block perfectly centred. Actually, the guidance accuracy must be ± 0.2 mm, so that a flaw recognition accuracy of 0.1-mm flaw depth can be guaranteed. With simple handling methods, this accuracy can only be achieved when the test samples are not out of true, or bent. Since in most cases this cannot be guaranteed, early customers who purchased only a test machine had additional expense for accurate handling devices in order to obtain the desired flaw detection accuracy. This caused us, based on these experiences of our customers, to develop a suitable guiding device, which, together with the test machine, forms a complete structural unit. In the case of the ROT 50 (Figure 5) this guiding device consists essentially of 4 tripping rollers which are pneumatically activated and automatically adjust to all test sample diameters between 10 and 50 mm. Since the contact pressure is adjustable up to 500 Kg. even slightly warped test samples move perfectly centred through the machine. Warping up to 2 mm per metre is generally permissible.

Combined with the guiding device there are two pairs of driving rollers, located ahead of and after the test unit. The rollers contact the pipe by means of pneumatically driven cams. Six photo cells note the passing of the test samples and actuate the engagement or disengagement of the tripping and drive rollers.

In the case of the ROT 120, which tests samples up to 120 mm O.D. it is not possible as with the ROT 50, to guide

the test samples on a solidly mounted test machine. Here, because of the inflexibility of thick pipes or bars, the test machine must be mobile and follow the movements of the test sample. The guidance is provided by two tripping rollers which are mounted on the test machine and which, pneumatically operated, adjust to all product diameters between 35 mm and 120 mm. If the test sample deviates horizontally or vertically, the floating table makes it possible for the machine to follow this movement, thus maintaining the required concentric position with respect to the test sample as determined by the tripping rollers. The drive of the test samples is not accomplished by means of a separate driving device but by the roller beds ahead of and after the test result.

Evaluation

If a test sample contains flaws, echoes appear on the screen of the ultrasonic flaw detector the height of which is proportional to the depth of the flaw. Thus the screen could be visually observed and evaluated if, as is usually the case, due to the high scanning speeds, the echoes did not appear so very briefly. In addition to the possibility of overlooking flaws, there is the danger of operator fatigue. Therefore one has to depend upon an automatic evaluation device which does not possess these two human limitations. Additionally, the evaluation device should also mark the location of the flaw and perhaps, sort the samples according to the depth, length, and possibly even the number and distribution of flaws.

Since the demands vary considerably, there are various evaluation devices for the ROT units, that offer, depending upon the combination, various evaluation possibilities.

The following evaluation devices are available.

Sorting and simultaneous signalling: The go-no go monitors which are series-connected to the ultrasonic flaw detectors cause, at the occurrence of the flaw echo, an instantaneous optical or acoustical signal. In addition, the signal "reject" is flashed to the storage relay which is checked prior to the sorting.

Marking at the end of the test sample: The flaw signals are transmitted from the go-no go monitors to a storage relay which is activated by the first signal, and transmits the latter to a marking device as soon as the test sample has passed through the test device, triggering an end contact. Generally, the marking device is located so that the marking is accomplished at the end of the test sample. If the marking must be in accordance with the type of flaw (longitudinal flaw, transverse flaw), then each monitor must be equipped with a storage relay and a marking device.

Marking of the flaw location: A delaying device stores the flaw indication signal from the go-no go monitors until the respective pipe section moves past the marking device. The delay is "transport synchronized", that is, it depends on the advancing speed of the test sample.

Sorting and marking by means of the automatic evaluator: The automatic system includes a counter storage unit with preselection which receives one impulse per test block rotation, when simultaneously, a flaw signal is received by one of the monitors. There is a choice of two different evaluation systems:

A.—In the simpler case, marking and sorting into the "reject bin" takes place at the occurrence of a single flaw indication, independent of the length of the flaw.

B.—If the counter is activated only after receiving two impulses, marking and sorting takes place only when a flaw is longer than the distance travelled by the test sample during two test-block rotations.

Thus, the flaw recognition accuracy of the unit relative to the smallest detectable flaw length can be selected by the proper advancing speed adjustment. The flaw recognition accuracy relative to the depth of the flaw is adjusted by the sensitivity adjustment of the monitors.

During the first two simple evaluations the test samples are individually moved through the unit. In the case of the third and fourth evaluation a choice of individual and end-to-end transport of tubes is possible. For most installations, the fourth evaluation has become the standard although different requirements are possible.

It could be required for example, to sort the test samples into several categories not only according to flaw depth and length, but also according to the number and distribution of the flaws. This demand can be realized although it requires a more complex evaluation system. Additionally, an impulse transmitter is needed which, coupled with the roller bed, emits a certain number of impulses per advance distance of the test sample. These impulses subdivide the test sample into test sections. The respective test sections are judged faulty, if simultaneously with these impulses, flaw signals are received by the evaluation system while the test sample moves through the test machine. The automatic evaluation system counts the faulty test sections and causes sorting into two, three, or four bins, depending upon how many long flaws there are, and how long the flawless sections are. Simultaneous marking makes it possible to differentiate later between flawless, slightly objectionable, and unusable sections of each piece tested.

Summary

The efficiency of these units is the combination of:

1. *High testing speed* due to the high rotational speed of the test probes.

2. *Good flaw recognition properties,* to some degree achieved through perfect guidance of the test samples (ROT 50) or the test unit (ROT 120), respectively.

3. *Flexibility*, due to the possibility of selecting from various evaluation devices or combinations thereof.

The fact that to this date some 40 units have been sold, all of which are in constant use, is proof that the units are a success.

Automated Quality Control of Electrical Steel in a Production Line

J. A. VDOVIN AND A. I. KADOCHNIKOV, U.S.S.R.

Introduction

Technical progress in electrical machine-building engineering is based on the scientific achievements and the developments of other branches of engineering, primarily that of metallurgy. The production of magnetic wires for electrical machines and transformers, different components of electrotechnical equipment, etc., involves millions of tons of electrical sheet steel every year. The degree of perfection achieved in the production of these articles and, hence, to a certain extent the general technical and economical level, are very much characterized by the magnetic properties of the steel used.

Consequently, the reduction of electrotechnical loss in steel and the increase of its magnetic permeability presents an important economic task. It is obvious that the most complete use of the magnetic properties of electrical steels already achieved is by no means less important. The best use of these properties is provided only by strict control of the basic magnetic properties of steel used in production. Gradation lists of magnetic properties of electrical steel designated by corresponding marks are established by national standards. The real grade of the given batch of metal can be determined only by measurements. Thus, the control of magnetic electrical steel is systematically carried out by steel plants. This control is aimed at obtaining sufficiently complete and reliable data on the magnetic properties of any batch of steel produced.

Accordingly, it is important to use proper methods and apparatus to carry out mass control and sorting of large batches of electrical steel. This control should be a) continuous, b) non-destructive, c) automated, d) quick. As the control should not damage any of the metal tested it must be conducted according to the sizes and shapes designed by standards, i.e. on sheets and coils.

Labour and time costs expended in testing and sorting are more, rather than less, significant to the economy of the method than are metal costs. Obviously, the techniques of continuous control and sorting would become simpler if the number of characteristics measured and accounted for were fewer.

The choice of main parameters required for mass control is of paramount importance. At present it seems reasonable to control the quality of soft magnetic materials intended for use in variable magnetic fields according to their dynamic characteristics, providing the test conditions are as close as possible to real working conditions. The choice of such characteristics and the elaboration of proper methods of control require further exploration; in particular, it is necessary to study the laws which the dynamic characteristics obey under given conditions.

Theory

In view of the above, the problem of conditions in which the testing is carried out is the first to be considered. It is necessary, when measuring the dynamic characteristics, to fix not only the external field amplitude H_e and the flux amplitude ϕ but also the form of their dependence on time. The preferable way is to test the material under the sinusoidal flux variation ($\phi=\phi_m \sin \omega t$). The practical ways to attain these magnetization conditions are available in many works (1).

Besides the certainty of the dynamic characteristics the condition $\phi=\phi_m \sin \omega t$ results in a fact to which we are liable to attach great importance. Thus it appears that a set of dynamic hysteresis loops obtained at different ϕ_m as well as a set of static loops, have a kind of limiting loop. Let us explain the conclusion. The electromagnetic process in a sheet material found in a longitudinal uniform field is described by the following expressions:

$$\frac{\delta H}{\delta Z} = j \tag{1}$$

$$\frac{\delta j}{\delta Z} = \sigma \frac{\delta B}{\delta t} \tag{2}$$

where H,B,j are magnetic field strength, magnetic flux density and eddy-current density of a given sheet, σ is specific conductivity, t is time. The Z-axis of the coordinate system is perpendicular to the biggest lateral sides of the sheet.

To obtain a particular solution corresponding to the established periodical process (variation) one must also set an edge function, i.e. the dependence of the field on the surface of the sheet on time, or the dependence of the current density on the surface of the sheet on time. Thus the solution of the equations (1) and (2) under the given static dependence $B=f(H)$ and without any phenomena conditioning the so-called "magnetic viscosity" would be unambiguous. By integrating (2) along the thickness of the sheet we find that the current density in the surface layer of the sheet is proportional to $d\phi/dt$. It means that for the given sheet the condition $\phi=\phi_m \sin \omega t$ should unambiguously define the functions describing the skin-effect. If we now imagine that the external field amplitude increases so that ϕ_m actually reaches the saturation flux, the further increase of the field amplitude would have no practical influence on the magnetization process. Consequently, a limiting dynamic loop is obtained. For detailed illustration of the above, let us consider two particular cases.

1. The case of a weak skin-effect when the flux density amplitude may be thought non-dependent on the Z coordinates. In this case the ascending branch of a dynamic loop (i.e. the relationship between

$$H_e \text{ and } B = \frac{\phi}{S}$$

is shifted to the right, and the descending branch to the left, the degree of the shift being defined as

$$\Delta H(\overline{B}) = \frac{1}{3} \sigma \delta^2 w \sqrt{\overline{B^2}_m - \overline{B}^2} \tag{3}$$

where $B_m=\phi_m/S$, S being the cross-sectional area of the sheet. With increase of the external field amplitude H_m (the sinusoidal flux is retained) the amplitude B_m rises to reach the value approaching B_s and with the further increase of H_m the expansion of the loop practically stops.

From Eq. (3) the dynamic coercive strength is

$$H_{cd} = H_c + \frac{1}{3} \sigma \delta^2 w B_m \tag{4}$$

and the maximum dynamic coercive strength is

$$H_{cd}^{max} = H_c + \frac{1}{3}\sigma\delta^2 w B_S \tag{5}$$

The eddy-current loss related to the unit of volume in the case considered is known to be expressed by

$$P_e = \frac{1}{6}\sigma\delta^2 w^2 B^2_m \tag{6}$$

Thus the maximum loss would be

$$P_e^{max} = \frac{1}{6}\sigma\delta^2 w^2 B^2_S \tag{7}$$

It follows from (5) and (7) that

$$P_e^{max} = \frac{1}{2} w B_s (H_{cd}^{max} - H_c) \tag{8}$$

The proportionality factor in this case appears non-dependent on the thickness and the specific conductivity of the explored sheet.

2. The case of a limiting non-linear dependence of B on H when the ascending branch of a static hysteresis loop can be expressed in the following way:

$$B = \begin{cases} -B_S \text{ at } H < H_c \\ -B_S < B < +B_S \text{ at } H = H_c \\ +B_S \text{ at } H > H_c \end{cases}$$

Now the following expressions are obtained:

a) for a dynamic hysteresis loop

$$H_e = H_c + \frac{\sigma\delta^2 w B^2_m}{2 B_S}\left(1 + \frac{\bar{B}}{B_m}\right)\sqrt{1 - \left(\frac{\bar{B}}{B_m}\right)^2} \tag{9}$$

b) for a dynamic coercive strength

$$H_{cd} = H_c + \frac{\sigma\delta^2 w}{2 B_S} B^2_m \tag{10}$$

c) for eddy-current loss

$$P_e = \frac{\sigma\delta^2 w^2}{4B_S} B^3_m \tag{11}$$

At B_m-B_S Eq. (9) becomes an expression for a limiting dynamic loop and from (10) and (11) the maximum values of

$$H_{cd}^{max} \text{ and } P_e^{max}$$

are obtained, the expression for P_e^{max} coinciding with (8). The last circumstance is of great importance, presenting the possibility of replacing the loss of control by the coercive strength control.

Not to confine ourselves to these two somewhat extreme cases, we have considered in a special paper a kind of an intermediate case (2). The static magnetic characteristic was taken in the following form:

$$B = \begin{cases} -B_r + \dfrac{B_S - B_r}{(1 + \zeta|H|)^2} \text{ at } H \gtrless 0 \\ -B_r < B < +B_r \text{ at } H = 0 \end{cases}$$

The existence of a limiting loop in this case was also confirmed, the expression (8) remaining true. Furthermore the correlation appearing between the limiting loop and the loops approaching it, which are most widely used in practice, is confirmed. This correlation promises a high practical value of the control according to characteristics of the limiting dynamic loop.

Methods and Apparatus

The knowledge of peculiarities of the magnetization process with sinusoidal flux variation, and in particular, the presence of a limiting loop, may be useful in elaborating methods of the quality control of electrical steel. It is known that the possibility to evaluate the quality of a material by its coercive strength on a limiting static loop has proved rather useful. These measurements do not require a precise setting of the magnetizing current and a preliminary determination of the cross-sectional area of the sample. It is a temptation to find a similar possibility for control by means of dynamic characteristics as well. The dependence existing between the maximum eddy-current losses and the limiting dynamic coercive strength gives reason to replace the direct measurement of maximum losses by the more convenient automated measurement of the limiting dynamic coercive strength. The simple relation existing between the characteristics of the limiting loop and those of the loops adjoining it which are most widely used in practice, allows an easy establishment of the necessary relationships.

In accomplishing such a control one is apt to meet with difficulties connected with the determination of the flux-density value in a test-piece. In principle, only the magnetic flux may be directly measured. The magnetic-flux density value is obtained by calculation with a preliminary determination of the cross-sectional area of the test-piece. This is done by weighing or by means of different kinds of thickness gauges. The separation of these operations in space and time and the unavoidable setting of the measuring apparatus in accordance with the thickness data obtained complicate the control process. To get rid of the shortcomings of the above method a new method of magnetic-flux density determination in sheets and coils with magnetization along the limiting dynamic loop was developed (3).

This method consists of practically simultaneous measurement of the magnetic flux in the sample ϕ_m with a given magnetic field strength H_e and saturation flux ϕ_S in the same cross-section of the sample. Considering that the fluxes ϕ_H and ϕ_S are proportional to the cross-sectional area of the sample, by the value of this ratio and the known value of the saturation flux density B_S for the given grade of steel the actual flux density in the sample is obtained, which is B_H. The block diagram of such an apparatus for the flux density measurement is shown in Figure 1. The measured portion of the sheet or coil is periodically magnetized in a solenoid along the limiting symmetrical loop at the top of which the flux density is sufficiently close to the saturation flux density of the given material. The measurement process consists in determining the relation

$$\frac{\phi_H}{\phi_S} = \frac{B_H \cdot S}{B_S \cdot S} = \frac{B_H}{B_S} \sim B_H$$

with the aid of logometer I.

Logometer I is connected across two measuring coils 4 and 5 wound on a solenoid: one of them is connected through rectifier 3 with a linear characteristic crossing the zero-point of the coordinate system, and the other through the phase-regulated commutator 6. This commutator operates in phase with commutator 8, which controls coil 7 serving to measure the instantaneous value of the mean field strength in the measured portion of the field. The phase angle corresponding to the appearance of a square-wave pulse may be adjusted with the help of phase-regulator 10. Permanent-magnet instrument 11 serves as

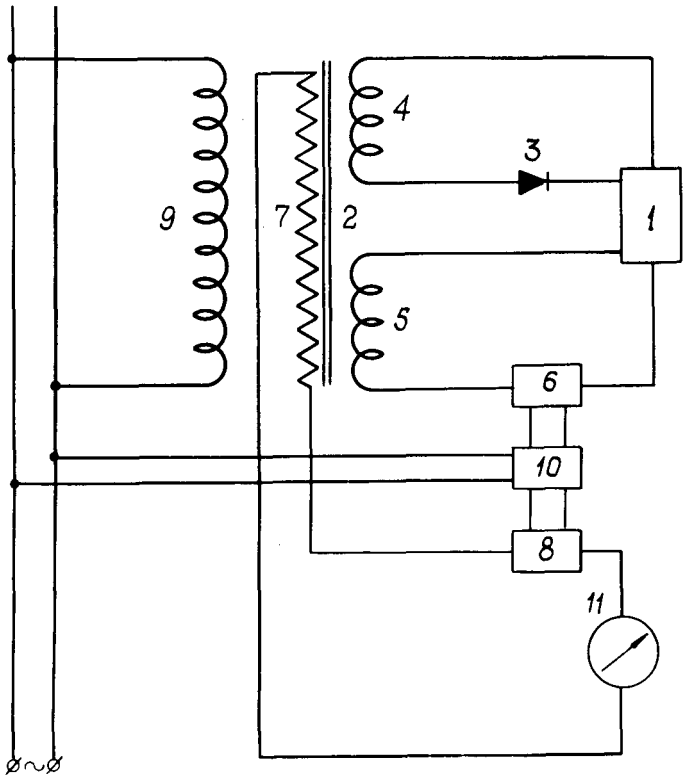

Figure 1. Block diagram of the flux density measuring device.

a field strength indicator. The phase-regulator permits the establishment of the phase necessary for the flux density measurement at a given field strength value. The commutations in the circuit of the coils occur in phase, so the average value of the current in the circuit of coil 5 is proportional to the instantaneous values of the flux. Under these conditions the logometer readings are proportional to the ratio of the flux density in the sample with a given field strength to the saturation flux in the same sample. On the basis of the above method a modified apparatus for nondestructive control was developed (4).

The apparatus consists of three principal parts: a supply unit ensuring a sinusoidal flux, a solenoid and a measuring unit with a computing device (logometer). The magnetization of the measured portion of the sample takes place in a solenoid on the frame of which there is a magnetizing winding uniformly diswinding uniformly distributed along the middle part of the tributed along the whole length of the solenoid, and a measuring frame $\frac{1}{3}$ of its length). The solenoid has two through longitudinal slots. One of them contains the test-piece, the other has, on a special frame in the middle part of the solenoid (along $\frac{1}{3}$ of its length), a measuring coil and a compensating winding.

The measurement of a magnetic flux in test sheets presents certain difficulties because, on the one hand, the measuring coil cannot in every case be wound directly on the test-piece and, on the other hand, the cross-sectional area of the solenoid slot should be sufficient to allow free movement of the sample. A big "air" gap existing between the measuring winding and the sample which may be a hundred times as big as the cross-section of the sample, and a high magnetization field strength lead to that the magnetic flux in the "air" gap constitutes a considerable portion of the total flux.

It is evident that the emf part existing in the measuring winding due to the flux in the "air" gap should be compensated before the measured data of magnetic fluxes ϕ_H and ϕ_M are applied to the logometer windings. This is achieved with a special compensating winding placed on a general frame together with a field coil and connected in series and in opposition to the measuring winding. The number of turns of the compensating winding was found from:

$$W(\bar{\bar{S}} - \underline{\underline{S}}) = W_K \cdot \bar{\bar{S}}_K$$

where W and W_K are the number of turns of the measuring and the compensating windings, respectively; $\bar{\bar{S}}$ and S_K are the area of one turn of the measuring and the compensating windings, respectively.

The variations of $\underline{\underline{S}}$ should be neglected to their $\bar{\bar{S}}$ small magnitude. In view of the variable character of the field the compensation should be accomplished in a sufficiently wide field strength range. The results of compensation of the magnetic flux in the "air" gap for sheets of different thickness are presented in Figure 2. The instantaneous field strengths are plotted on the x-axis, and the relative compensation error on the y-axis. As is seen from the curves, the error does not exceed 0.2%.

To obtain the voltages and currents necessary for operation of a computing device without any increase in the number of turns of the measuring and the compensating windings of the solenoid, a push-pull power amplifier, working in an "ultralinear" duty, was included in the circuit. As the output transformer in the amplifier has two identical secondary windings the solenoid may have only one winding. The variation in the cross-sectional area of the sample as well as in the amplitude and phase of the voltage feeding the solenoid magnetizing winding brings about a change in amplitude, phase and wave form of the magnetizing current. Consequently, before every new measurement of the magnetic flux, if any of the above stated changes have occurred, the original field strength at which the flux density is measured, should be reset by adjusting the commutation phase of the phase-regulated circuit with a phase-regulator.

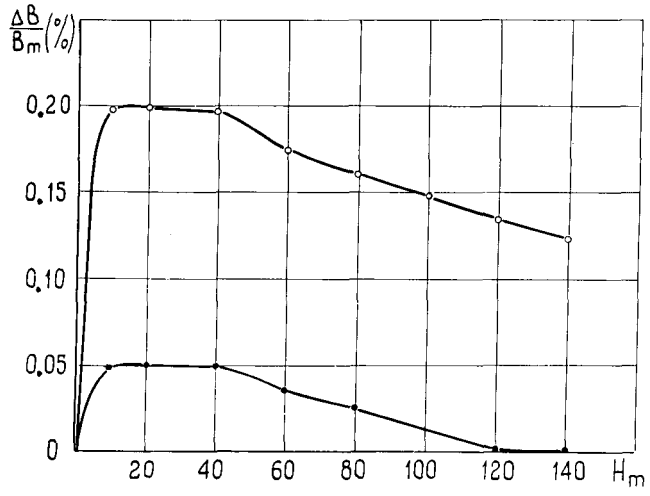

Figure 2. Relative error of the magnetic flux compensation in the solenoid air gap for a sheet 0.37 mm thick; and for a sheet 0.29 mm thick.

At high-speed flux-density measurements, such an adjustment is difficult to accomplish by hand. To eliminate this shortcoming a new circuit with self-regulated commutators was developed allowing a continuous flux-density measurement with a given field strength, independent of the above-mentioned variations (5). The operating principle of such a circuit lies in that the commutation moment of phase-regulated commutators 6 and 8 corresponds to a definite value of the magnetizing current and, hence, of the magnetizing field strength. This is accomplished by excluding phase-regulator 10 and connecting a

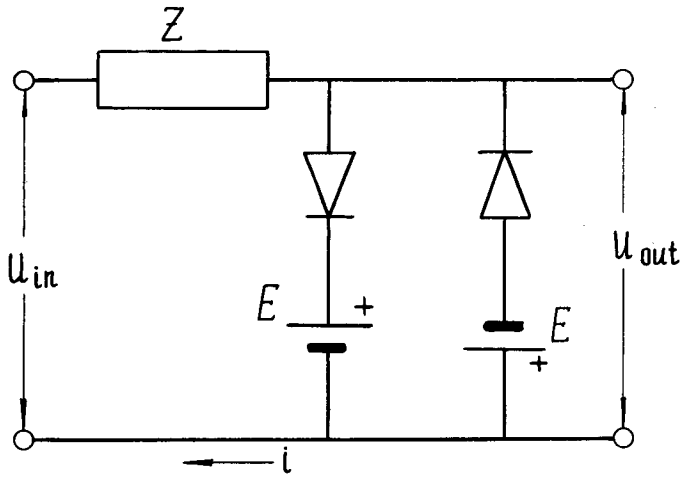

Figure 3. Diode limiter with diodes connected in parallel.

primary winding of a special square-wave generator for control of these commutators in series with the solenoid magnetizing winding. Let us consider the operating principle of the generator (6). The change in polarity of the output voltage amplitude limiters for sinusoidal voltage (Figure 3) depends principally on the type of limiting resistance Z used. With an active limiting resistance the transition from one polarity to another is accomplished proportionally to the input voltage sine curve while with an inductive resistance the case is somewhat different. This is due to a phase shift between the current and the input voltage, which is the principal peculiarity of the circuit. Let us consider the accompanying processes. (Figures 3 and 4.)

Assuming that U_{in}–$V_m \sin wt$ and neglecting the forward resistance of the rectifier and the battery resistance we obtain for the input circuit

$$V_{in} \sin wt \mp E - L\frac{di}{dt} = 0 \qquad (12)$$

The upper sign before E corresponds to $i > 0$ (the conventional positive direction of the current i is shown in Figure 3 by an arrow), and the lower sign corresponds to $i < 0$. By integrating (12) we obtain

$$i = -\frac{V_m}{wL}\cos wt + \frac{\pi}{2}\cdot\frac{E}{wL}f(wt) \qquad (13)$$

where $f(wt)$ is a saw-tooth function with a unit amplitude. Thus i consists of two components, each of them being shown separately in Figure 4. The phase shift between the curves i_a and i_b is defined by the position of the peaks of the saw-tooth curve i_b which must correspond to the moment when current i passes through zero. In the interval $\Delta\alpha$, if i is equal to zero (diodes are biased off), the voltage U_{out}, which before this was equal to $\pm E$ tends to attain the values that U_{in} takes in this interval (Figure 4). As a consequence of the current phase lag caused by inductance U_{in} value in the interval $\Delta\alpha$ has a sign opposite to what it had before this interval. Hence, U_{out} would reverse its sign by leap. As soon as its absolute value exceeds E the i current is not equal to zero and U_{out} retains its value up to the next moment when U_{out} becomes equal to zero. So U_{out} has a square form. It is evident that in the $\Delta\alpha$ interval it is required that $|U_{in}) > E$.

The square-wave generator used by us is presented in Figure 5. The square-wave voltage here is derived from the transformer windings. Use is made of the phase shift between the emf and the current in the secondary winding II. This current is equal to:

$$i_2 = -\frac{n_1}{n_2}i_1 + \frac{\pi}{2}\cdot\frac{E}{wL_2}f(wt) \qquad (14)$$

Eq. (14) shows that with a given i_2 it is possible to choose the necessary commutation moment by selecting a proper E value, i.e. to select the field at which the flux density should be measured.

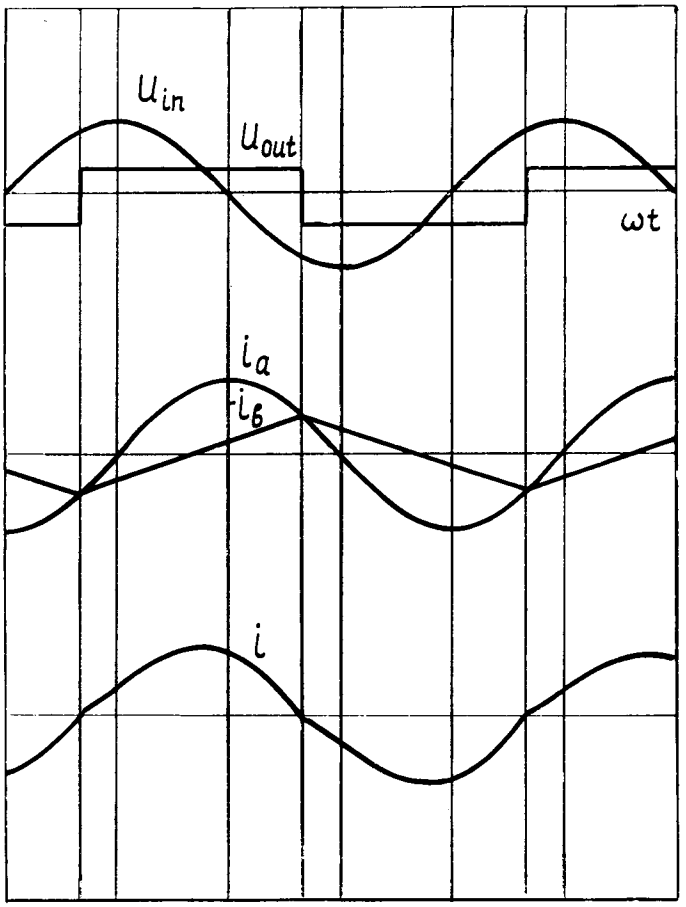

Figure 4. Processes occurring in the circuit for obtaining square-wave pulses.

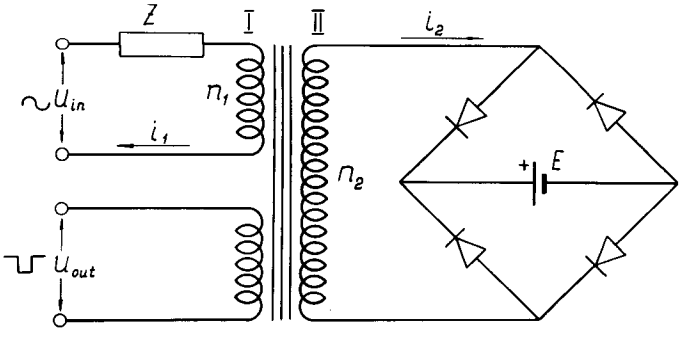

Figure 5. One version of a square-wave generator.

A circuit including such a generator was tested and showed that if the magnetizing current change does not exceed 50%, the field variation at which the flux density is measured, is equal to 1-2% and the error in the measured flux density value does not exceed 0.1-0.2% as long as the measurements are made on a gently sloping portion of the curve. The voltage division in the integrator output was made by a standard electronic self-compensating potentiometer, its measuring device following the ratio change of the quantities being measured and producing a continuous record of its values on a paper tape.

The output voltage of the integrator included into the measuring circuit ϕ_S serves for evaluating the cross-sectional area of the tested portion of the sheet.

$$\underline{\underline{S}} = \frac{E_0}{4 f w B_s}$$

where f is the current frequencyl; W_2 is the number of turns of the measuring winding; E_0 is the mean emf value of the measuring winding.

In view of close tolerances in sheet width (1%) the thickness of the tested section is determined by the known value of $\underline{\underline{S}}$ with an error not exceeding 0.01 mm.

Simultaneously with the magnetic flux and thickness measurements the dynamic coercive strength is also measured on the limiting loop in a similar manner(7). The latter can be used for evaluation of the specific losses in sheets or in moving steel tape.

References

1. Kryg, W. Avfrechterhalfung der sinusförmigen Induction bei hohen Feldstärken in Prüfjochen für Electrobleche. *Archiv für technisches Messen,* 1962, 1 322, 323, 1963. 1 324.
2. Vdovin, Yu. A., Kadochnikov, A. I., Polovnikova, L. A. and Khan, Ye. B. K probleme kontrol'a kachestva m'agkikh magnitnykh materialov po dinamicheskim kharakteristikam. *Defektoskopia* No. 3, 1966, pp. 55-69.
3. Yanus, R. I. and Vdovin, Yu. A. Sposob opredeleniya magnitnykh svoystv elektrotekhnicheskoy stali. Avt. svid. No. 124547 kl. $21_e 37_{10}$.
4. Vdovin, Yu. A. and Polovnikova, L. A. Skhema s avtoupravl'ayemymi kommutatorami dla nepreryvnogo kholodnokatanogo elektrotekhnicheskogo zheleza. AVTOMATICHESKY KONTROL'I METODY ELEKTRICHESKIKH IZMERENIY. *Trudy IV Konferentsii,* t. II, 1962.
5. Vdovin, Yu. A. Ustroystvo dla opredeleniya svoystv elektrotekhnicheskoy stali. Avt. svid. No. 155232 kl. 6 01_e, 37_{10}.
6. Vdovin, Yu. A. and Kadochnikov, A. I. Generator napr'azheniy pr'amougolnoy formy. *Elektromekhanika* No. 5, 1962, pp. 557-559.
7. Koppelman, F. Der Vekformesser Messung Verlustziffer ganzer Dinamo-ader Transformator blechtafeln. E u M. 1951, N 9, s 225-229.

Technical Session 12/ X-Ray Techniques

Radiography of Parts with Wide Variations in Thickness

JOSEPH H. D'ADLER-RACZ, USA AND MICHEL SEVRIN, BELGIUM

ABSTRACT: In case of uniform thickness, the best image quality will usually be obtained with the highest radiographic contrast. On the radiograph of an irregularly shaped part, many details may be lost in the areas that are penetrated too much or not enough. Also, some undercut near the edges may reduce the image quality.

The purpose of this paper is to establish the radiographic technique, assuring the highest image quality for a given range of material thickness.

The latitude in thickness may be increased by using higher "kV" and by filtering the X-ray beam. Experimental results are reported and discussed.

The image quality is measured by means of American and European indicators, and compared for the suggested, the conventional and the gamma-ray techniques.

A practical diagram is proposed, which may be used to radiograph irregularly shaped pieces, or parts having wide variations in thickness.

Finally, some newly designed X-ray units, which are particularly suitable for the proposed radiographic technique, up to 400 kV, are described.

Introduction

In case of nearly uniform thickness, the best image quality will usually be obtained with the highest radiographic contrast. For this purpose, kilovoltages as low as possible should be used, in conjunction with the maximum mA available. The practical limit depends upon the size of the focal spot, which in turn depends on the resulting power (kV × mA.). It was experimentally demonstrated, that for equal film density and exposure time, mA have to be doubled if kv are decreased by about 10%.

On a radiograph of a piece with wide variations in thickness, there may be unpenetrated and overexposed areas on the film. If these areas are large enough, it is possible to use a high-intensity viewer, and cover the light areas which may blind the observer. Another well known technique consists of a sandwich of different type films in the same pack, but the inspection of a single film will always be preferred.

As already discussed in a previous paper (1), there is an additional problem when the pieces are smaller than the film, or have some holes. The long wavelengths of the X-ray spectrum produce an undercut on the image, thereby spoiling the edges.

The purpose of this paper is to define the optimum limits of film density, and to find out the corresponding radiographic technique, assuring the highest image quality for a given range of material thickness.

Film Density

The gamma of the usual X-ray films decreases rapidly under density 1.0, so we consider this density a minimum for good image quality.

The film contrast will of course be excellent up to density 4-6, depending on the type of film. However, if the intensity of the viewer was adjusted to a maximum tolerable brightness in the density 1 areas, we found the upper limit of good evaluation by a normal human eye, at about density 3.0.

Latitude in Thickness

By means of a step wedge, we plotted in Figure 1 the exposure time needed to obtain densities 1 and 3 on film Gevaert D 7, for different thicknesses, and we used 200, 300 and 400 kV constant potential, with 10 mA.

The difference of thickness, comprised between the lines corresponding to densities 1 and 3, defines the latitude in thickness, covered by a good evaluation of the film. We found it to be:

8 mm=$\frac{5}{16}$″ steel at 200 kV
12 mm=$\frac{1}{2}$″ steel at 300 kV
16 mm=$\frac{5}{8}$″ steel at 400 kV

Image Quality

It is obvious that higher kV reduce the radiographic contrast. Therefore we have to demonstrate that this loss is largely offset by the improvement of film evaluation.

As a typical example, we radiographed 3 thicknesses and placed on each some American and European image-quality indicators. We obtained the densities and penetrameter sensitivities (in % of the thickness) shown on Figure 2.

At 370 kV the 25-10=15 mm thickness range is within the desired 1 to 3 film density, but it is not so at 200 kV. Although the radiographic contrast is certainly higher at 200 kV, it appears clearly that the penetrameter sensitivity did not increase at all, but even decreased in some cases.

We extended this comparison to Cs 137, but in this case the contrast is decreased to such an extent that there is a definite loss in penetrameter sensitivity.

It would have been quite proper to use 200 kV for a 25-mm uniform thickness, but as there is a 10-mm minimum thickness, a film exposed at 370 kV will be more pleasant to evaluate, with a slight gain in penetrameter sensitivity, and a much shorter time:

200 kV: 5′45″ with 3 mA
370 kV: 11″ with 3 mA
Cs 137: 24′ with 5 Ci

Practical Diagram

The 1 to 3 density range being proved to be a good basis for the definition of latitude in thickness, we established in Figure 3 a practical diagram for the radiographic technique.

For instance, considering a part varying from 27 to 41 mm thickness, the 14-mm latitude will call for 350-kV constant potential. The exposure time will be 15 sec with 10 mA.

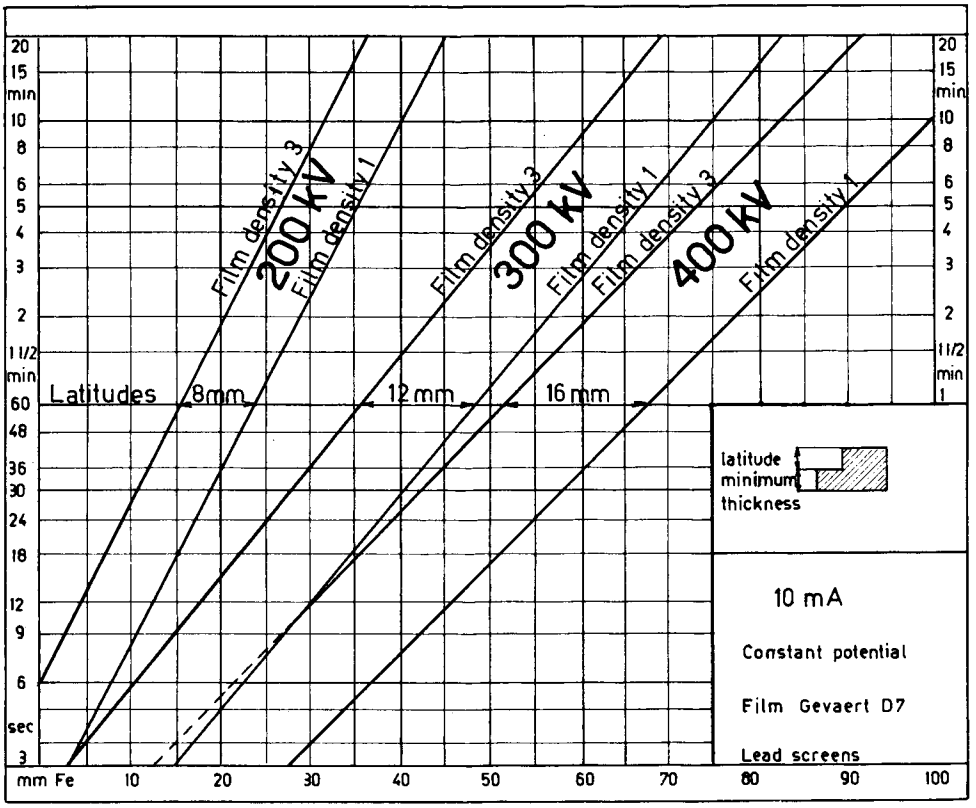

Figure 1
Exposure data for film density 1 and 3.

FF = 4' 1225 mm	200 kV 17 ma . min			370 kV 33 ma . sec			Cs 137 2 Ci . h		
Fe:	10 mm (3/8")	18 mm (3/4")	25 mm (1")	10 mm (3/8")	18 mm (3/4")	25 mm (1")	10 mm (3/8")	18 mm (3/4")	25 mm (1")
N=	>5	1.46	0.58	3.08	1.65	0.96	1.55	1.28	1.03
DIN	>4 %	1.4 %	1.6 %	2.2 %	2.1 %	1.6 %	2.5 %	2.8 %	>4 %
AFNOR	5.7 %	4.5 %	3.2 %	4 %	4.5 %	2.8 %	10 %	5.5 %	3.2 %
ASME	>2.5 %	2.1 %	2 %	2.5 %	2.1 %	2 %	>2.5 %	2.1 %	2 %

Figure 2
Densities and penetrameter sensitivities obtained.

Additional Filtration

When the minimum thickness is zero, the use of a copper filter on the tube port is recommended, and in some cases a lead filter covering the cassette.

Its optimum thickness is a matter of experience, but the diagram given in Figure 3 will again be very useful. The absorption of copper being about 1.4 times more than steel, this should be added to the minimum thickness of the part X-rayed.

Let us take the example of a small part, in which 3 to 14 mm of steel must be inspected. A 6-mm copper filter is equivalent to 8.4 mm of steel. Thus the total minimum thickness is 11.4 mm. The latitude being 11 mm, according to Figure 3 the right technique will be: 260 kV and 10 sec with 10 mA. In Figure 4, this radiograph is compared to another one exposed at 160 kV, 1 min, 10 mA. There is no doubt that the 260 kV are preferable for general inspection of the whole part.

Equipment Used

Today there is no problem in producing such high kV as unusually compact and even mobile X-ray units are available. Although for this evaluation we used a large 400-kV constant potential, 10-mA double-focus unit, of self contained design,

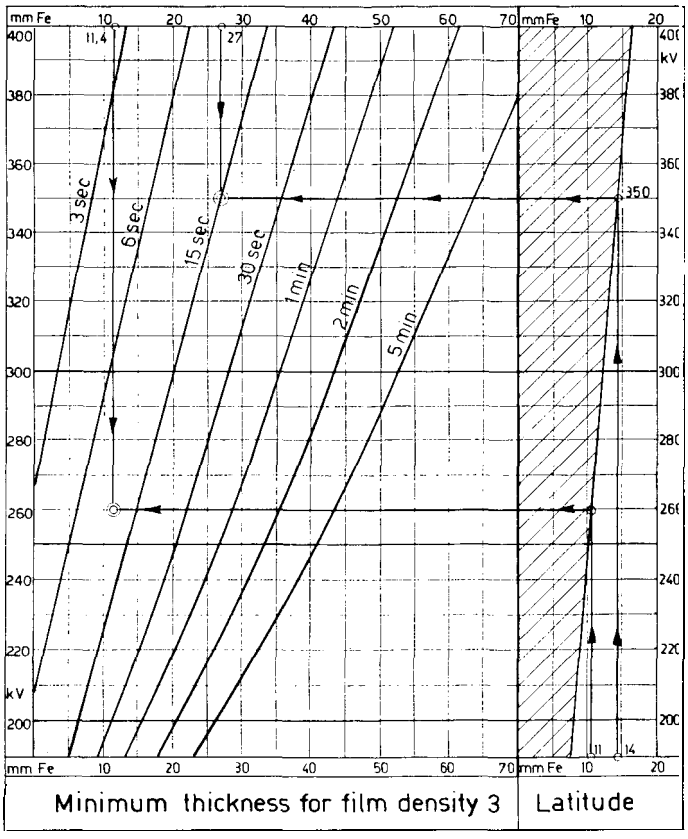

Figure 3. Latitude and exposure time for 10 mA constant potential.

a portable 400-kV machine has recently been developed (Figure 5). Its weight being only 95 kg (215 lb) it is possible to apply, on site, the radiographic technique developed in this paper.

Conclusions

For the radiography of parts with wide variations in thickness, not only the radiographic contrast, but also the resulting film density should be considered.

It is demonstrated that the best image quality is obtained when the film density ranges from 1 to 3.

When the minimum thickness is small, or in the case of irregular shaped pieces, additional filtration should be used.

A practical diagram is given for quick determination of the best radiographic technique, depending upon the range of thickness involved.

Bibliography

1. d'Adler-Racz, J. Influence of high voltage wave form and inherent filtration of X-ray generators on image quality; *Materials Evaluation,* V. 24, Sept. 1966, No. 9, 503-506.

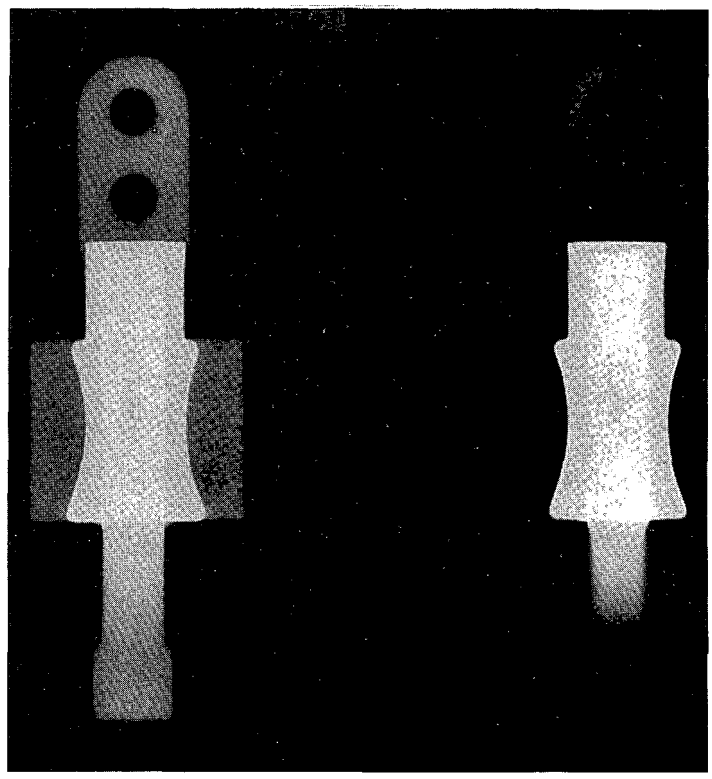

Figure 4. Radiographs of a small part; left, 260 kV; right, 160 kV.

Figure 5. 400-kV portable unit.

Discussion

Q. RONALD HALMSHAW, Ministry of Defence (UK) RARDE, Sevenoaks, England:

What thickness of copper filter (on the X-ray tube) do you recommend for use with 400 kV X-rays?

I have found advantage in using this type of filter in most cases of radiography of varying-thickness specimens—do you agree?

A. We certainly agree that in case of variable thickness it is generally recommended to use additional filtration, depending on the minimum and the latitude of thickness being covered.

A very common error is to use a beryllium window tube for radiography of transistors and similar small pieces. The radiographs are much better with 1-3-mm aluminum inherent filtration.

As an example of heavy material, let us consider a 2-in.-thick steel block with different borings, and covering not the whole film. We found the best result at 400 kV with a 20-mm copper filter on the tube port, and 2-mm of lead on the film.

Q. PIERRE RUAULT, Gaz de France, France:

1. Quand l'auteur précise que le contraste est amélioré quand l'énergie des photons décroît, peut-il préciser si cette hypothèse s'applique pour des émulsions de qualité identique ou différente, et de quel contraste il parle. 2). Pense-t-il qu'il y a une relation entre le contraste dont il parle et la qualité d'image jugée d'après ou IQI. 3). La qualité d'image est-elle appréciée objectivement ou subjectivement. Dans ce dernier cas, l'auteur est-il satisfait de juger sub-

jectivement un résultant qui dépend de très nombreaux paramètres. **A.** 1. Nous avons utilisé pour nos comparaisons des émulsions de qualité identique, exposées et traitées de la même manière. Nous entendons par contraste le rapport de la variation de noircissement à celle de la variation de l'exposition au rayonnement, toutes autres conditions restant identiques. 2. Nous pensons que le contraste est un des éléments qui agit sur la qualité d'image jugée d'après un IQI. 3. Les indicateurs de qualité d'image ont été lus par plusieurs observateurs, dans des conditions identiques, et nous avons constaté très peu d'écarts de la valeur moyenne communiquée. Le but de cette évaluation étant comparatif, nous considérons cette méthode comme suffisamment objective.

Errors due to the X-ray Technique in Stress Measurement

MITUGI IWAMOTO AND HATUTARO KIKUCHI, JAPAN

ABSTRACT: Roughly classified, there are two methods of X-ray stress measurement, one using photography and the other using a Geiger counter.

Taking up the possibility of errors in the former, the authors studied theoretically and experimentally the following three types of errors:

1. Caused geometrically in photography.
2. Depending on the variation of photographic time.
3. Occurring in the distance measurement of the diffraction pattern after photography.

Results have confirmed that both the Glocker method and the $\sin^2\psi$ method may cause a serious error in extreme cases; it was found that some of the factors inducing these large errors can be experimentally identified, while others cannot. From this standpoint, the Geiger counter method was found the best for eliminating as many factors inducing these errors as possible. On the other hand, it is also pointed out that this method has its own drawbacks in other respects.

Introduction

The principle of the conventional stress measurement by X-ray consists in measuring the lattice distortion from the diffraction pattern due to characteristic X-rays and therefrom determining the stress. This is a very effective form of nondestructive inspection for stress, particularly residual stress. But for the purpose of industrial application, the reliability of measurement is vital and accordingly it becomes necessary to clarify the possible sources of errors inherent in the measurement.

The possibility of errors occurring in the measurement of lattice distance by photography is discussed in theory and experiment, and only such factors as directly affect the errors are described.

Industrial applicability of a Geiger counter for eliminating as many of these factors as possible is confirmed. The following discussion is based on the assumption that the surface stresses are always plane ones.

The Photographic Method

The diffraction condition for the lattice distance d and the wave length of the characteristic X-ray λ is expressed by Bragg's law:

$$\lambda = 2d \sin\theta$$

For the purpose of finding d from the above equation, θ is directly obtained or calculated from the measured diffraction pattern.

In the photographic method, the distance between the surface to be measured and the film must be known, in order to find θ. The standard practice is to put calibrating powder (usually, nondistorted metallic powder) on the surface to be measured and take simultaneous pictures of the diffraction patterns of both. And in case the stress in only one direction is to be measured, more than two pictures must be taken with the tangential angle ψ of the incident ray changed to various angles.

Suppose errors occur in the true value of θ in the process of the diffraction pattern being photographed and θ being found. Then such errors may be classified as follows:

1) Errors due to deviation from the right angle of the angle formed between the incident ray and the film surface in photography.

2) Errors due to difference in the blackness of the diffraction pattern as fixed on the film.

In the group of pictures taken with varied angles, under constant photographic conditions, the blackness of the diffraction pattern and its background differs from picture to picture.

This is due to the fact that the intensity of scattered X-rays is minimal in the tangential direction to the measured plane and maximal in the normal direction to it; and that the size and number of crystal grains exposed to diffraction differ from picture to picture.

3) In addition to 1) and 2) above, errors may be due to the film being double coated. Here the errors due to the difference in blackness between the diffraction pattern distance of the measured object and the calibrating powder and the errors due to the effect of calibrating powder on the camera length when the latter is found from the former, ought to be taken into account.

4) Errors liable to occur in the microphotometer measurement of the diameter of the diffraction pattern from the diffraction picture.

The above errors are discussed one by one, both theoretically and experimentally.

Theoretical Discussion

Errors Due to Deviation, etc.

At the top in Figure 1 is shown the geometrical shape of the diffraction pattern in photography. If in spite of $\delta \neq 90°$ in this figure, the distance between the diffraction pattern of the calibrating powder and that of the measured object is measured assuming $\delta = 90°$, the error caused thereby ($\Delta\rho$) will be expressed as below; but this is the case of $\delta = 90°$ and the diameter of diffraction pattern being 50 mm.

$$\Delta\rho_2\zeta' = (X_1 - X') \times \frac{50}{2X_1} - (R' - Y') \times \frac{50}{R' + R''}$$
$$= 25 \times \frac{\sin(\delta - \pi/2)}{\tan 2\zeta_1} \times \times \frac{\{\tan^2 2\zeta' - \tan^2 2\zeta_1\}}{\{\cos(\delta - \pi/2) - \sin(\delta - \pi/2) \cdot \tan 2\zeta'\}} \quad (1)$$

$$\Delta\rho_2\zeta'' = (X_1 - X'') \times \frac{50}{2X_1} - (R'' - Y'') \times \frac{50}{R' + R''}$$
$$= 25 \times \frac{\sin(\delta - \pi/2)}{\tan 2\zeta_1} \times \times \frac{\{\tan^2 2\zeta_1 - \tan^2 2\zeta''\}}{\{\cos(\delta - \pi/2) + \sin(\delta - \pi/2) \cdot \tan 2\zeta''\}} \quad (2)$$

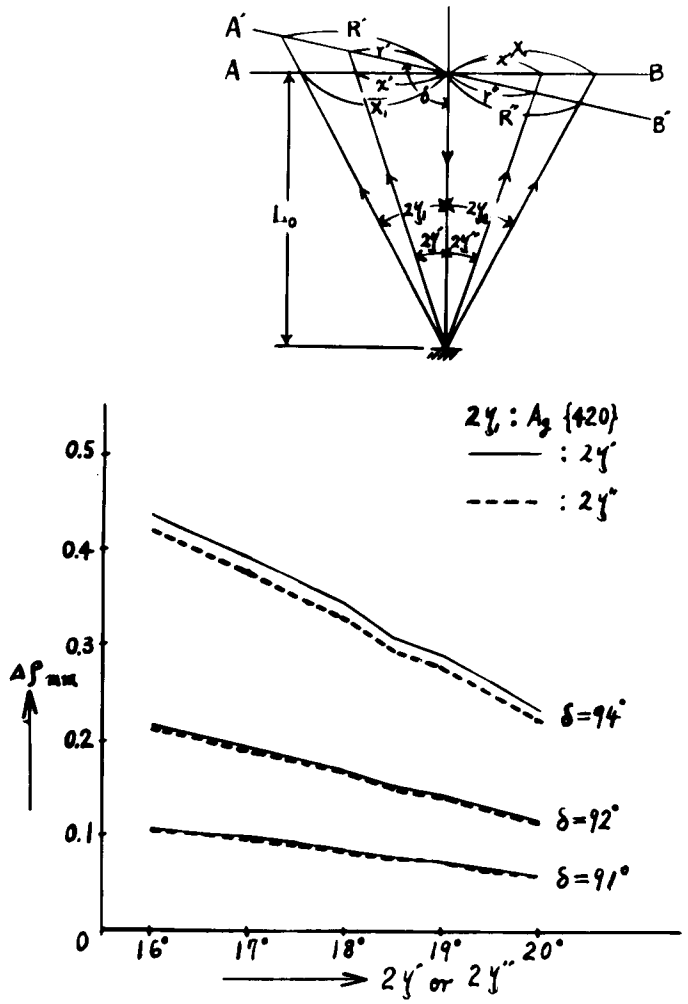

Figure. 1. Relation between $\Delta\rho$ and diffraction angle $2\zeta'$ or $2\zeta''$.

If in equations (1) and (2), 2ζ is supposed to be due to 420 of Ag by C_o-K_α ray of characteristic X-rays, the relation between $\Delta\rho$ and $2\zeta'$ or $2\zeta''$ may be represented by Figure 1.

According to this figure, the value of $\Delta\rho$ causing a direct error in the value of θ will be so large as not to be ignored in relation to the value of $2\zeta'$ or $2\zeta''$ at $\delta=91°$. A countermeasure for this is to adopt the diffraction line of one of the diffraction pictures, because the stress is measured not from the absolute value of θ but from the gradient of θ to $\sin^2\psi$. Another measure will be to find an exact value of δ by a different procedure and make a similar correction to Figure 1. Theoretically speaking, the following may be said about the latter measure, but the experimental results usually do not agree with the theoretical values. Namely, when Au powder is radiated by C_oK_α ray, the same picture exhibits two diffraction patterns of 420 and 331 of Au. In the measurement of camera length from these two diffraction patterns, if there is no distortion, theoretically both ought to be equal at $\delta=90°$. When $\delta=90°$, the camera length L will change in relation to $2\zeta_1$ as follows:

$$\frac{L_o' - L_o}{L_o} = \frac{\cos(\delta-\pi/2) - \cos^2(\delta-\pi/2) + \sin^2(\delta-\pi/2)\cdot\tan^2 2\zeta_1}{\cos^2(\delta-\pi/2) - \sin^2(\delta-\pi/2)\cdot\tan^2 2\zeta_1} = K \quad (3)$$

From equation (3), the relation between K and $2\zeta_1$, may be represented by Figure 2. In this figure, when $\delta = 90°$, K will be the larger, the larger the value of 2ζ. Namely, the camera

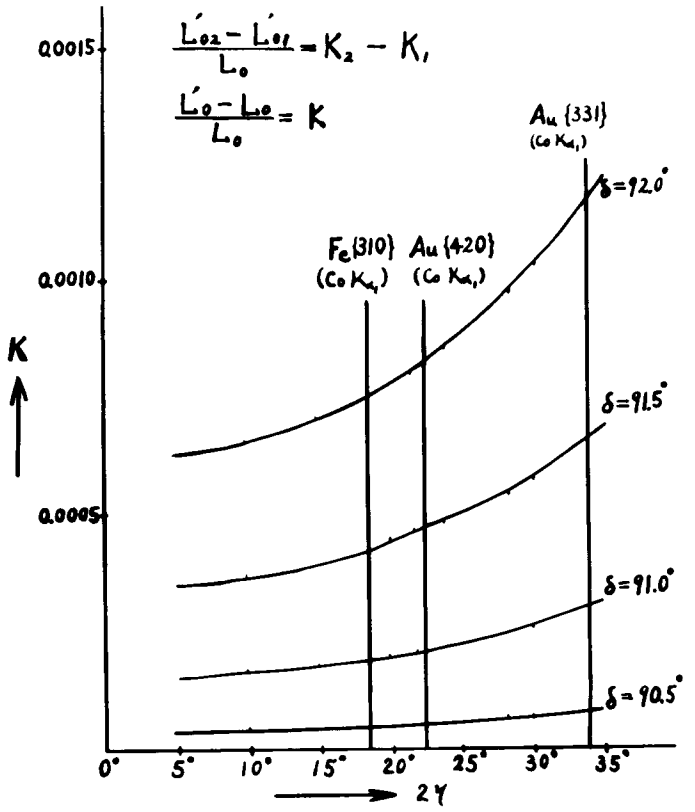

Figure 2. Relation between k and 2ζ.

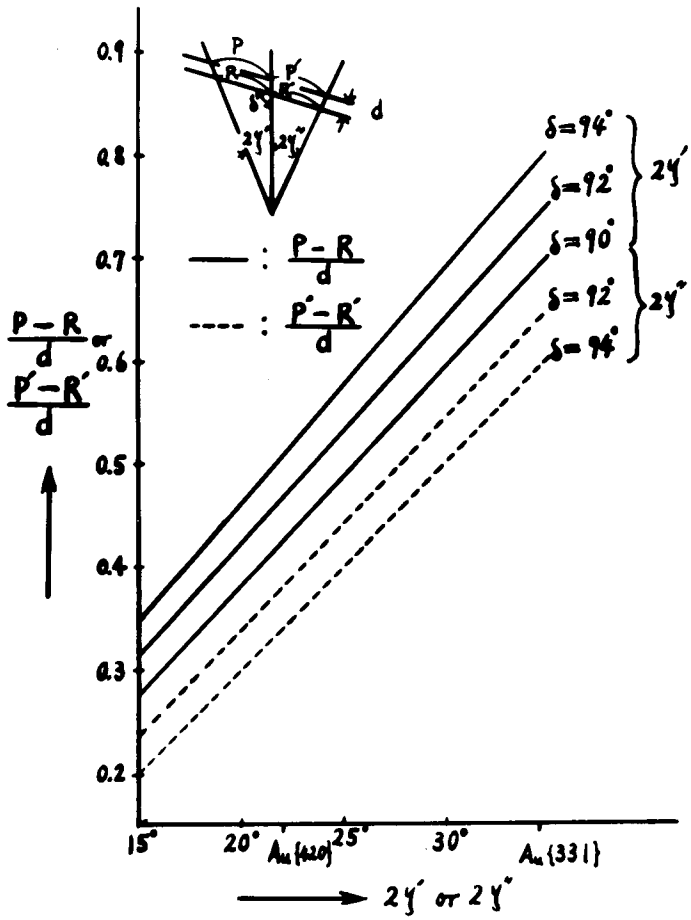

Figure 3. Relation between (P-R)/d, (P'-R')/d and $2\zeta'$ or $2\zeta''$.

length obtained for 420 will be equal to or smaller than the one obtained for 331. However, the experiment shows in most cases that L_{331} is smaller than L_{420} (1). This is treated later under experimental discussion.

As seen from Figure 2, the influence of camera length on possible errors is negligibly small.

Errors Due to Double Coated Film

When a double-coated X-ray film is used, the X-ray will fall on the film surface with greater inclination, the greater the value of 2ζ is, and accordingly, the diameter of the diffraction pattern will tend to be larger; geometrically this tendency may be indicated in Figure 3.

Usually in the double-coated film, d is equal to about 0.24 mm; and when $\delta = 92°$ the radius of 331 of Au will in the extreme cases be about 0.15 mm longer than in the single-coated film. As a matter of fact, this characteristic depends on the blackness of the diffraction line. But under the principle of measuring the stress under constant conditions, it would suffice to find the changing value of θ; therefore the above-mentioned dependence may not be a very important factor. Nevertheless, it is worth considering indirectly in the observation of diffraction phenomena.

Errors Liable to Occur in the Microphotometer Measurement of the Diffraction Pattern Distance

When the difference in blackness of the diffraction pattern is measured by the microphotometer, errors may slip in unless constant measuring conditions are maintained with full consideration of the characteristic of the meter. Care should be taken at this point, because the amount of error has a direct bearing on the measured values.

Experimental Discussions

In X-ray stress measurement by photography it is most important to take clear-cut diffraction patterns of both the calibrating powder and the measured object on a single film. Therefore it is necessary to know the characteristics of the diffraction pattern that directly influence possible errors in stress measurement.

There follows a typical example of testing to investigate errors attributable to the difference in blackness of the diffraction patterns.

Experimental Procedure

A steel rail containing about 0.7% C was annealed and the area to be measured was electrolytically polished. Cr powder for calibration was strewn on the polished surface for diffraction pattern photography under Cr-Kα ray, with the voltage 35 kV, the current 20 mA, the collimator $1\phi_{mm}$, the films, double coated no-screen, high-(D), medium-(C) and low-sensitive (B), screen-type (E); single-coated, no-screen (A), the filter being V-foil.

Exposure time was set: 7, 15, 30, 60, and 120 minutes for the film (D); 60 minutes for (A), (D) (E); 300 minutes for (C) and 360 minutes for (B). Photos were taken with the distance between sample and film maintained constant; they were developed under constant conditions.

Photometry of the diffraction pattern on each film was made, using a photo-multi type microphotometer, and the diffraction pattern distance was measured by the peak method.

The diffraction picture taken on film (D) under 60 minutes exposure was circumferentially microphotographed at every 15° and the diffraction pattern diameter (2R) of Cr 211 and the distance ($\triangle$ Y) between the pattern for Cr 211 and the pattern for Fe 211 were measured.

As for the other films, the value of 2θ for the pattern of Fe 211 was measured with reference to that of Cr 211.

Experimental Results

Figure 4 shows a typical diffraction picture taken under typical experimental conditions. In this photo, the blackness of the pattern for Cr 211 looks greater than that of the pattern for Fe 211. The change of diameter (2R) relative to the circumferential angular change (α) of the pattern for Cr 211 and those of the radial distance between the pattern for Cr 211 and the pattern for Fe 211 relative to the change (α) were estimated from the microphotometer data obtained under the same conditions; the results are given in Figure 5, which also indicates the difference in blackness of the pattern for Cr 211 or for Fe 211 relative to the change (α). It is seen that the diameter of the

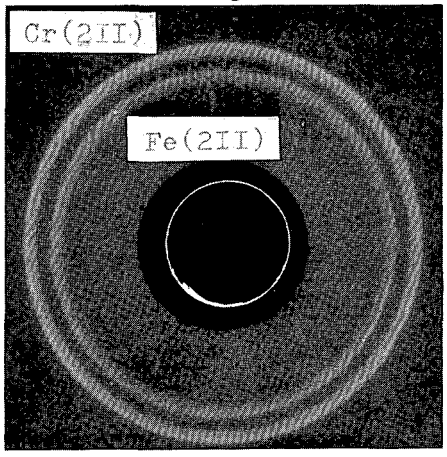

Figure 4.
A typical diffraction picture.

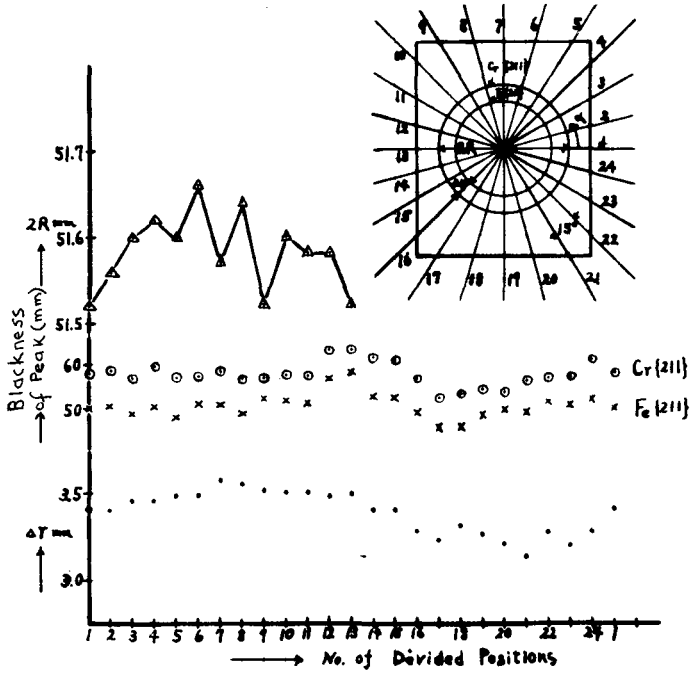

Figure 5. Relation between Δr, 2R and number of divided positions in Figure 4.

pattern for Cr 211 makes a complicated change with the change (α), maximum difference in diameter being 0.15 mm. Also $\Delta\gamma$ makes a complicated change, with the difference between maximum and minimum being as large as 0.45 mm; if expressed in terms of the diffraction angle (θ), $\Delta 2\theta$ will amount to about 0.45°. The residual stress of this sample was about −5 kg/mm^2 by the Geiger-counter method. The experimental results suggest that any change in 2R and $\Delta\gamma$ originates from the statistical distribution changes in the size and number of

crystals involved with diffraction which influence the intensity distribution of scattered rays and that of radial diffraction lines at each measured point of the pattern. It is easily conceivable that such $\Delta\gamma$ change will also appear on a definite diameter of the diffraction pattern which has been measured with the tangential angle varied several times.

Accordingly, the $\Delta\gamma$ change with only the exposure time varied—all the other conditions being fixed—was measured to investigate the effect only of the relation between the intensity distribution of scattered rays and the characteristics of photographic emulsion. The results turned out as Figure 6-a, which shows the relation between exposure time and the diffraction angle 2 θ of Fe 211 as found with reference to the diameter of pattern for Cr 211 as base in each film; even in this case, the value of 2R differs from one to another of the five photos. Similarly, the change of 2 θ for Fe 211 depending on the kind of film turned out as Figure 6-b, which shows that 2 θ changes considerably with exposure time and no specific tendency is observed in this change. The 2 θ change depending on the kind of film is equal to 0.1° at maximum and there is no great difference in the value between right and left; and this value is always larger than the value at zero lattice distortion. Together with Figure 6-a, this fact suggests that the cause is the relative weakness of the Fe diffraction line as compared with the Cr one. From this it may be surmised that it is a secondary influence which does not directly affect the errors in stress measurement.

The above mentioned 2 θ change with the change only of exposure time seems to be caused by the change in the blackness distribution on the film through the change in the time integral values of the diffraction line intensity and scattered ray intensity owing to the characteristics of photographic emulsion and exposure-time variation.

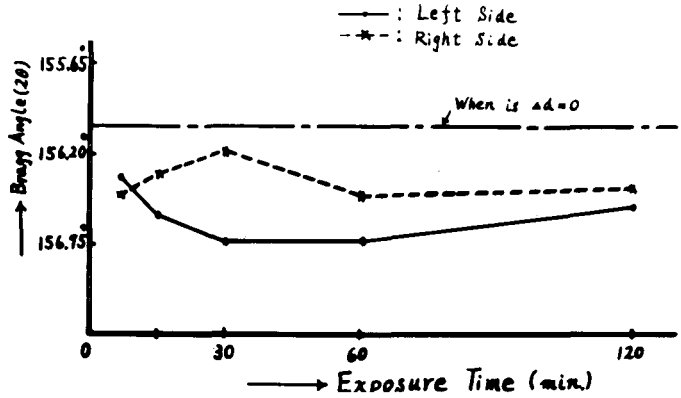

Figure 6a. Relationship of 2θ– exposure time.

Experimental results suggest that the errors are induced through the following causes: the measured object is an alloy containing more than two elements; the calibrating powder is laid on the surface of the measured object; the diffraction line intensity distribution is photographed on a film; the blackness distribution of the diffraction pattern is measured by the microphotometer; and the irradiated area is reduced. The only method free from these sources of error is direct use of a Geiger counter for measurement of the diffraction line intensity distribution; in this case, however, the X-ray-irradiated area will not be as small as that by the photographic method, but not so large as to hamper its practical industrial application.

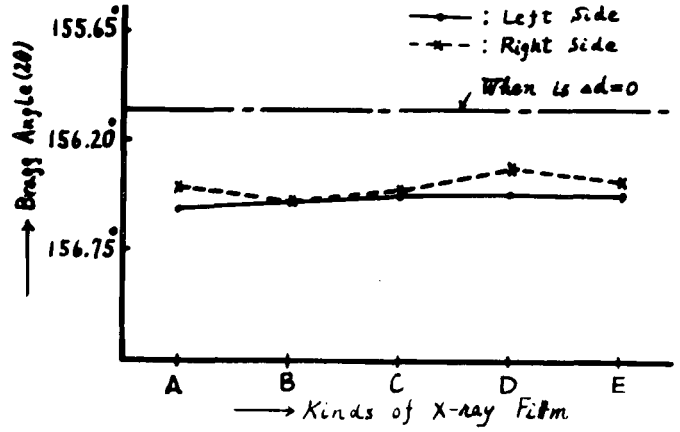

Figure 6b. Relationship of 2θ– kinds of X-ray film.

Summary

In the $\sin^2\psi$ method which is the most reliable measuring technique for photography, it is common practice to take more than four pictures with varied tangential angles; thereby the diffraction pattern for which the value of 2 θ is to be found for each value of ψ is not identical, and usually the background and the diffraction line intensity distribution differ also. In the industrial application of this measuring technique it would be very difficult to keep these conditions absolutely identical. Under usual conditions, the error of 2 θ may occasionally exceed 0.5° even when the ideal diffraction pattern as indicated in Figures 5 and 6a and b appears. Meanwhile, in order that the precision for Fe may be less than 1 kg/mm^2 in the 2 θ–$\sin^2\psi$ diagram at $\psi = 0°$, 15°, 30° and 45°, it will be necessary to measure the value of 2 θ to an accuracy of less than about 0.01°. The allowable limit of error permitted in drawing a straight line by the least-squares method, even if the error of 2 θ changes relative to ψ or $\sin^2\psi$, ought to be less than 0.1°. However, the above experimental discussion shows that said error can amount to over 0.5°; thus the values measured by the photography method will entail large indeterminate deviations from the true value of stress or residual stress. Moreover, secondary errors due to theoretical discussion may be induced and accordingly there is a likelihood of large errors slipping into the measurement of residual stress, which defy any comparison of measured values with other methods.

Conclusion

It has been confirmed that the photographic method, one of the X-ray stress measurement techniques, is not free from technical errors depending on the materials in the measurement of lattice distortion. These errors will induce considerably large errors in the stress values, particularly residual stress values obtained even by the supposedly most reliable $\sin^2\psi$ method. The source of such errors has been traced, but the cause involves some physical phenomena which defy satisfactory interpretation and wait for future elucidation. If this trouble is to be circumvented, the Geiger counter method is recommended.

Reference

1. Iwamoto, H. and Kikuchi, H. On the exposure time in X-ray stress measurement by the photographic method. *J. Soc. Materials Science Japan,* Vol. 13, No. 135, 923-929, 1964.

L'influence de la sensibilité spectrale des émulsions et de la composition spectrale des rayonnements ionisants dans la qualité des images radiograhiques

P. A. RUAULT, FRANCE

Introduction

Pour mieux préciser l'objet de notre étude, nous croyons nécessaire d'expliquer très brièvement les raisons qui l'ont motivée. Pour cela, nous allons préciser ce que nos conceptions sur le contrôle radiographique par rayons X et γ ont peut-être d'original.

Un contrôle est destiné à mettre en évidence les défauts, et principalement, ceux qui présentent la plus grande nuisance pour la pièce dans laquelle ils se trouvent, compte tenu de ses conditions de service. Quand l'ouvrage est soumis à des efforts de traction, ce sont les défauts de forme aiguë qui sont, de beaucoup, les plus dangereux, principalement quand ils affectent un métal de caractéristiques mécaniques élevées, pour lequel l'adaptation du métal est moins bonne. La recherche des défauts fins et aigus peut nécessiter la mise en œuvre de techniques particulières d'examen, parce que leur très faible dimension transversale peut les faire échapper à l'investigation si leur direction n'est pas identique ou très voisine de celle du rayonnement incident. Pour illustrer ce dernier point, nous avons procédé à la radiographie d'un bloc en acier dans lequel étaient usinées trois fentes parallèles de largeur égale à 30 μ environ. L'irradiation s'est faite suivant deux techniques différentes, d'une part en utilisant un tube à rayons X à foyer émissif ponctuel disposé face à l'une des fentes, d'autre part, une source linéaire de rayons γ, de longueur suffisante pour qu'une portion soit face à chacune des fentes. La première technique, si elle permet une bonne détection de la fente disposée face au foyer, ainsi que l'obtention d'une bonne note de qualité l'image jugée d'après un IQI à trous et gradins du type AFNOR-IIS, se révèle incapable de mettre en évidence les deux fentes mal orientées. La seconde technique permet de voir les trois fentes, mais elle introduit un flou géométrique tel que les trous de l'IQI disparaissent.

La figure 1 montre les résultats obtenus, et met en évidence la différence de comportement fondamentale des défauts de forme ronde et de forme aiguë, du point de vue de leur possibilité de détection par radiographie. Cet exemple montre que la recherche d'un faible flou géométrique n'importe vraiment que pour la détection des défauts ronds, semblables par leur forme aux trous d'un IQI, mais qu'il peut être souhaitable de disposer de gros foyers pour la recherche des défauts très fins, ou mieux encore, de mettre en œuvre simultanément plusieurs foyers fins collimatés. Indépendamment du rayonnement qui peut être orienté dans les directions parallèles à celle des défauts les plus probables, cette technique des gros foyers, ou des foyers multiples, permet de disposer d'un débit de dose important, favorable à l'emploi d'un film à grains fins, donc nécessairement lent, mais indispensable pour permettre la détection des défauts fins. Les figures 2 et 3 montrent bien les différences dans la détection des défauts, suivant qu'ils sont de forme aiguë ou ronde, quand on fait varier conjointement l'énergie du rayonnement, sa direction par rapport à celle des défauts recherchés et la nature des émulsions employées. Il est bien évident que l'emploi des foyers multiples ou de grandes dimensions provoque, nécessairement, une perte de contraste de l'image radiographique, quand la densité de base du cliché reste constante. Pour élever ce contraste, une solution simple s'offre, qui est de profiter de l'accroissement du contraste du film quand sa densité de base augmente, ainsi que le montre la figure 4 qui exprime, pour diverses émulsions, l'évolution de la densité optique en fonction de la dose de rayonnement reçue par le film, et plus encore la figure 5, qui montre l'élévation du contraste de l'image d'un objet quand la densité de base des clichés s'accroît. Nous parvenons, actuellement, à lire des clichés dont la densité de base est de l'ordre de 6 et à mesurer cette dernière jusqu'à une valeur de l'ordre de 7.5. Pour permettre cela, nous avons dû réaliser un négatoscope à éclairement constant asservi automatiquement à la densité du cliché par un système électronique commandé par une cellule photoélectrique. De cette façon, le lecteur est protégé contre une fausse manœuvre, très gênante et même dangereuse avec des éclairements très intenses, et la lecture se fait dans des conditions constantes d'éclairement et même de qualité spectrale de la lumière. Un densitomètre à amplification logarithmique et échelle dilatée a également dû être réalisé.

La mise en pratique des techniques décrites nous a contraint à remplacer l'IQI par un dispositif non tributaire du flou géométrique auquel nous avons demandé en outre:

—de juger *objectivement* et *seulement* la qualité de la technique opératoire de prise de cliché, contrairement à l'IQI, où la lecture est faite de façon subjective et ne permet pas de savoir si un mauvais résultat provient du cliché, des conditions de lecture ou du lecteur.

—de permettre une surveillance rapide et systématique de la qualité des clichés, et pour cela, nous avons réalisé un dispositif qui fait automatiquement cette lecture et permet, sans aucune difficulté, de vérifier ainsi la qualité de plusieurs centaines de clichés en une heure.

Les conditions de lecture sont maintenant imposées et précisent, entre autres, l'éclairement minimal émergent du cliché en cours d'examen, la distance et la durée maximale de lecture.

L'acuité visuelle et la perception des contrastes seront désormais périodiquement contrôlées sur la vue des lecteurs des clichés. Ces examens seront pratiqués par les médecins de travail, dans le cadre du contrôle médical périodique des travailleurs, au même titre que les contrôles médicaux particuliers exigés par les réglementations en vigueur pour les agents professionnellement exposés aux rayonnements ionisants.

C'est la recherche du contraste maximal de l'image radiographique qui nous a conduits, en plus des études brièvement énumérées ci-dessus, à préciser le domaine optimal d'emploi des appareils d'émissions, compte tenu de la réponse spectrale du film employé: c'est l'objet essentiel de notre étude et dont nous allons maintenant décrire brièvement les techniques mises en œuvre et les résultats obtenus.

L'absorption d'un rayonnement monochromatique par une paroi se fait par divers mécanismes, qui dépendent, entre autre, de l'énergie du rayonnement primaire incident. On sait, en particulier, que, pour des énergies croissantes $h\nu_0$ des photons incidents, les mécanismes d'absorption existants ou prédominants seront successivement:

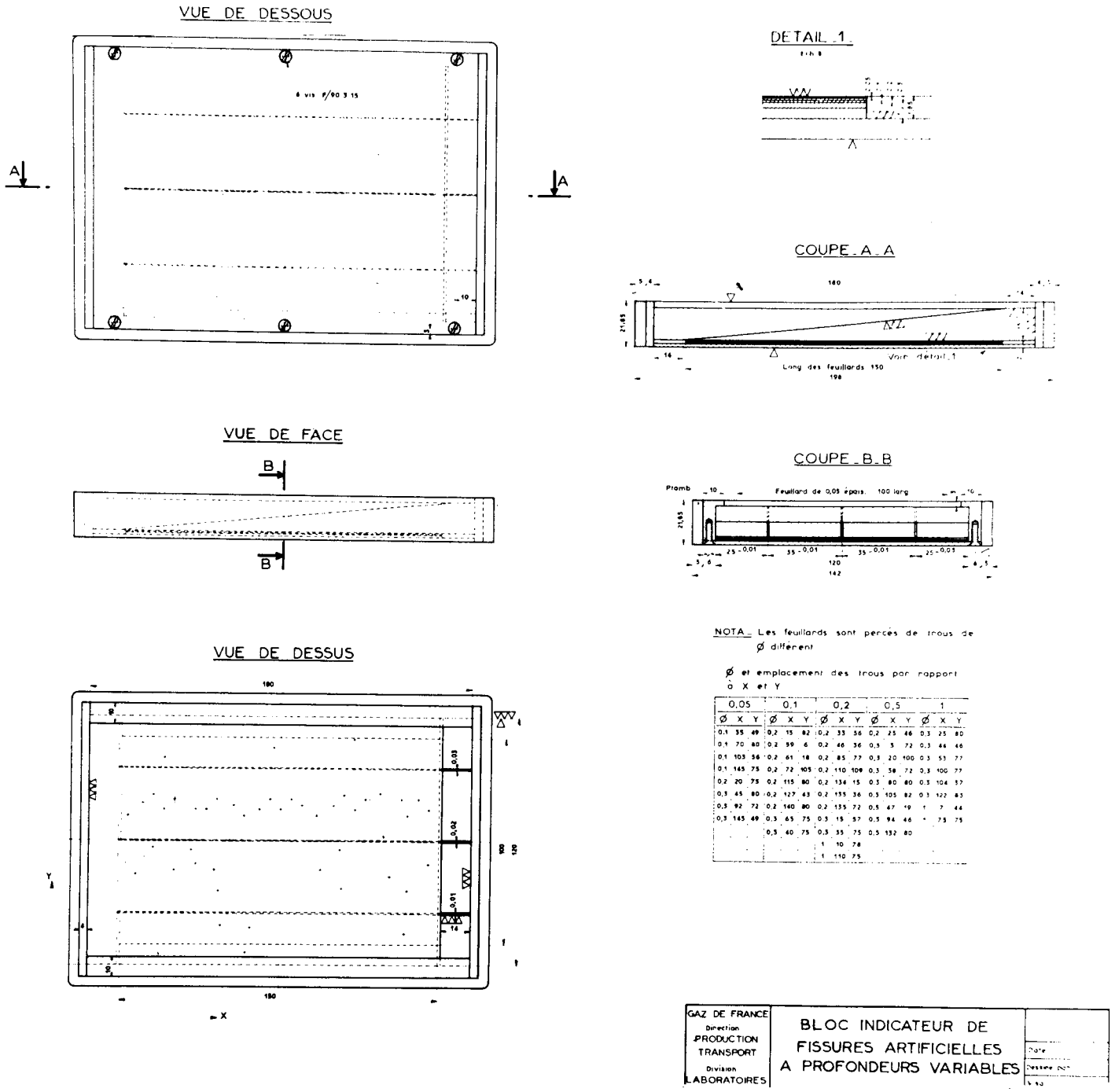

NOTA Les feuillards sont percés de trous de Ø différent

Ø et emplacement des trous par rapport à X et Y

0,05			0,1			0,2			0,5			1		
Ø	X	Y	Ø	X	Y	Ø	X	Y	Ø	X	Y	Ø	X	Y
0,1	35	49	0,2	15	82	0,2	33	56	0,2	25	46	0,3	25	80
0,1	70	80	0,2	59	6	0,2	46	36	0,3	5	72	0,3	46	46
0,1	103	36	0,2	61	18	0,2	85	77	0,3	20	100	0,3	53	77
0,1	145	75	0,2	72	105	0,2	110	109	0,3	58	72	0,3	100	77
0,2	20	75	0,2	115	80	0,2	134	15	0,3	80	80	0,3	104	57
0,3	45	80	0,2	127	43	0,2	155	36	0,3	105	82	0,3	122	83
0,3	92	72	0,2	140	80	0,2	135	72	0,5	47	19	1	7	44
0,3	145	49	0,3	65	75	0,3	15	57	0,5	94	46	1	75	75
			0,3	40	75	0,3	35	75	0,5	132	80			
						1	10	78						
						1	110	75						

GAZ DE FRANCE Direction PRODUCTION TRANSPORT Division LABORATOIRES	BLOC INDICATEUR DE FISSURES ARTIFICIELLES A PROFONDEURS VARIABLES	Date Dessiné par N°

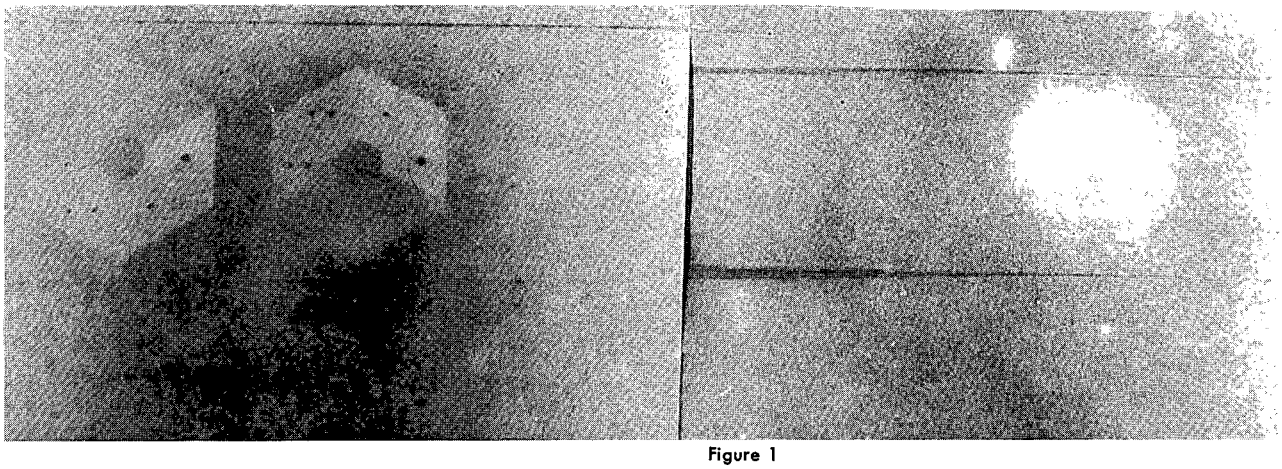

Figure 1

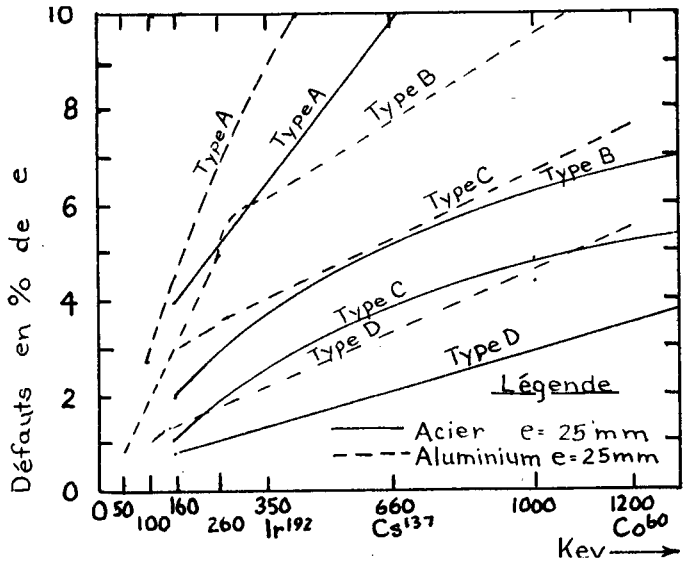

Figure 2. Détection des défauts fins en fonction du film et du rayonnement flou géométrique <0.2 mm.

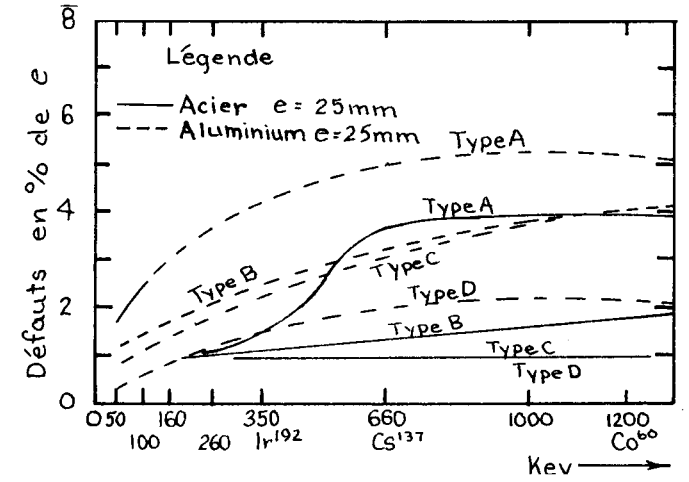

Figure 3. Détection des gros défauts (φ 8 mm) en fonction du film et du rayonnement flou géométrique <0.2 mm.

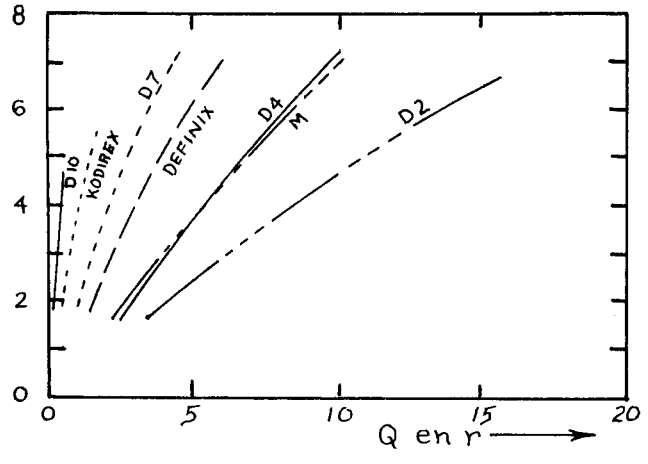

Figure 4

1°) La diffusion électromagnétique sans changement de longueur d'onde: elle se produira principalement dans un domaine où les énergies $h\nu_o$ des photons X ou γ incidents seront inférieures à celles qui sont nécessaires pour extraire un électron de sa couche électronique. Pour ce dernier cas, on a l'absorption par effet photoélectrique. Ces deux phénomènes sont prépondérants en radiographie médicale, ou encore dans la radiographie à faible énergie des parois en alliage léger ou en plastique. On aura alors $h\nu_o < Wnl$ formule bien connue dans laquelle h est la constante de Plank

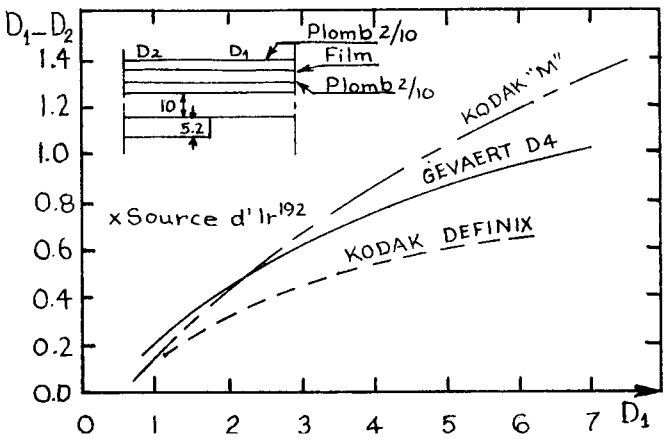

Figure 5. Détermination expérimentale de la course du contraste différentiel en fonction de la densité de base des clichés.

ν_o la fréquence du rayonnement incident

Wnl l'énergie de liaison de l'électron

avec le noyau de l'atome auquel il appartient.

Cette énergie dépendra des nombres quantiques total et azimutal qui définissent le rayon et la forme de l'orbite à laquelle appartient l'électron considéré.

2°) La diffusion Compton avec changement de longueur d'onde. Elle se produit quand l'énergie des photons est très supérieure aux énergies de liaison Wnl des électrons avec les noyaux des atomes. Dans ce cas, l'équation donnant la répartition des énergies après l'expulsion de l'électron d'énergie de liaison Wnl par le photon incident d'énergie $h\nu_o$ est:

$$h\nu_o = Wnl + \tfrac{1}{2}mv^2 + h\nu'$$

Les deuxième et troisième termes du second membre de cette équation expriment respectivement l'énergie cinétique transmise à l'électron et l'énergie restante du photon secondaire. L'amplitude de ce phénomène est très grande pour des énergies allant d'une centaine de keV à quelques MeV, elle est prépondérante sur les autres mécanismes d'absorption entre environ 400 à 500 keV et 4 à 5 MeV. C'est donc elle qui l'emporte de beaucoup dans l'absorption des rayonnements X et γ utilisés dans la plupart des industries faisant appel à la radiographie pour vérifier leur produit.

3°) À partir d'environ 1 MeV, le photon peut disparaître pour donner naissance à une paire d'électrons, l'énergie du rayonnement se retrouvant sous forme de masse des électrons créés. Ce phénomène devient prépondérant au-delà de 4 à 5 MeV. Ces divers mécanismes se composent pour donner une absorption totale qui est la résultante des diverses courbes d'absorption correspondantes à chacun des processus décrits. La courbe exprimant le coefficient d'absorption total passe par un minimum qui dépend de la nature de l'élément absorbeur; il est respectivement de 3.5 MeV, 10 MeV et 22 MeV pour le plomb, le cuivre et l'aluminium.

Ces divers effets peuvent s'accompagner de phénomènes qui en découlent, telles que l'émission des raies de fluorescence et l'émission d'électrons Auger (effet photoélectrique interne).

L'image radiographique qui est obtenue après traitement chimique approprié du film, va résulter de l'action des divers rayonnements et particules sur lui.

Le but de notre étude est d'étudier l'importance relative de ces rayonnements secondaires émis par la paroi émergente en cours d'examen par rapport au rayonnement primaire transmis par cette paroi et leur action sur la formation de l'image radiographique.

Conditions nécessaires pour obtenir une image radiographique correcte

Les variations d'intensité de rayonnement émergent résultant de variations d'absorption sont traduites sur le film par des noircissements différents. L'image radiographique est donc caractérisée par un noircissement de base sensiblement constant, sur lequel sont perceptibles des détails de formes diverses, pouvant présenter un écart de noircissement en plus ou en moins, dont l'amplitude dépend en partie des caractéristiques physiques et géométriques de l'anomalie qui l'a provoquée.

En assimilant au bruit de fond d'un appareil électronique la densité de base du cliché, et à un signal le détail perceptible provoqué par un défaut ou une anomalie et dans l'hypothèse où les conditions d'examen et l'acuité visuelle du lecteur sont correctes, pour que le signal provoqué par le défaut soit perceptible, il faut réunir les conditions suivantes:

—une amplitude du signal suffisante, c'est-à-dire un rapport $\frac{\text{amplitude du signal}}{\text{amplitude du bruit de fond}}$ suffisant

—une forme favorable du signal, c'est-à-dire un rapport $\frac{\text{amplitude du signal}}{\text{largeur du signal}}$ le plus grand possible

Diverses études sur ces conditions ont été effectuées par divers auteurs (1-2-3-4-5-6-7) pour préciser l'influence de certains paramètres. Pour notre part, notre contribution consiste à rechercher comment varie l'amplitude du signal quand le spectre transmis par la paroi se modifie: soit parce que l'épaisseur ou parce que la qualité du rayonnement émis, varie. Ces modifications du spectre transmis vont modifier, parfois de façon importante, l'amplitude du signal produit sur le cliché par le défaut par suite des rapidités différentes du film pour les diverses longueurs d'onde qui lui parviennent.

Tracé de la courbe de sensibilité spectrale d'une émulsion

Il est bien connu qu'une émulsion radiographique possède une réponse spectrale non linéaire vers les basses énergies. Toutefois, les études traitant de cette question sont peu nombreuses et ne font généralement l'objet d'aucune publication. Nous avons donc voulu déterminer l'ampleur du phénomène, et pour cela, nous avons procédé au tracé expérimental d'une courbe de réponse spectrale d'un film d'utilisation courante.

Deux difficultés se présentent pour mener à bien une telle étude:

—disposer:

—de rayonnements monochromatiques ou assimilables, de diverses énergies correctement connues,

—d'un appareillage de mesure de dose dont la lecture soit indépendante de l'énergie du rayonnement utilisé.

Obtention de rayonnement homogène

Certains radio-isotopes émettent un rayonnement monochromatique d'énergie bien connue, cependant ils proviennent souvent d'éléments chimiques rares ou précieux et pour lesquels les activités disponibles sont très faibles. Nous avons utilisé ces radio-éléments seulement pour étalonner le spectromètre multicanaux avec lequel a été réalisé cette étude, et nous avons recherché les épaisseurs de filtration nécessaires pour que le rayonnement hétérogène correspondant au spectre continu émis par un tube à rayons X soumis à une tension secondaire déterminée, devienne homogène. Nous pouvions ainsi disposer d'une intensité suffisante de rayonnement pour exposer un film dans un temps raisonnable. Pour cela, nous avons diaphragmé le faisceau de rayons X par un premier collimateur présentant une ouverture de 0.2 mm de diamètre, le faisceau émergent traverse alors un filtre placé devant un second collimateur ayant une ouverture de 10 mm de diamètre, puis le faisceau ainsi transmis est capté par le cristal du compteur à scintillation dont les signaux sont analysés par l'ensemble spectrométrique. On détermine alors, pour une tension secondaire de fonctionnement du poste à rayons X déterminée, et une distance compatible avec une émission de photons ne provoquant pas la saturation de la sonde, l'épaisseur de filtre nécessaire pour que l'énergie du rayonnement filtré ainsi obtenu devienne indépendante de l'épaisseur de filtration. À ce moment, le coefficient d'absorption est devenu constant et le rayonnement homogène. Cette détermination se fait sur un graphique qui représente la fonction

$$\mu x = \log \frac{I}{I_0}$$

La valeur recherchée correspond au point à partir duquel cette fonction devient linéaire.

L'appareillage utilisé pour ces mesures a été le suivant:

a) *Radio-éléments de référence pour l'étalonnage du spectromètre*

Radio-éléments	Énergie en keV de la raie utilisée pour l'étalonnage
Césium 137	32
Gadolinium 153	41
Mercure 203	72
Baryum 133	79
Gadolinium 153	97
Gadolinium 153	103

b) *Appareils à rayons X*

5-50 kV BALTEAU—foyer 1 × 1 mm—débit maximal 20 mA filtration propre: 2 mm Beryllium

utilisé avec un débit électronique de 5 mA pour les tensions secondaires inférieures à 50 keV

200 kV BALTOSPOT—foyer 1.5 × 1.5 mm—débit maximal 3 mA filtration propre, 3.6 mm Aluminium

utilisé au débit maximal pour les tensions supérieures à 50 kV

c) *Filtres utilisés*—

Aluminium pour les tensions de 20-30 et 40 kV.

Cuivre pour les tensions de 40-80-100-120-140-170 et 200 kV

d) *Spectromètre S A M 60* à 60 canaux, à mémoire, avec enregistreur et bloc d'impression et utilisé avec une sonde à scintillation dont l'élément actif est un cristal de 25 mm de diamètre de INa activé au Thallium.

Les résultats obtenus sont représentés sur les figures 6 et 7 concernant respectivement les tensions secondaires comprises entre 20 et 40 kV et celles comprises entre 80 et 200 kV.

Ces courbes permettent de fixer les valeurs des épaisseurs de filtration à partir desquelles le rayonnement X obtenu est

homogène, et d'en préciser l'énergie. Le tableau suivant résume les résultats obtenus.

Tension secondaire V appliquée au tube à rayons X en kV	Nature du filtre	Épaisseur minimale de filtration en mm	Énergie du rayonnement E homogène obtenu en keV	E / V
20	Aluminium	3	18	0.9
30	»	12	25.7	0.84
40	Cuivre	1	35	0.88
80	»	3	61	0.76
100	»	6	74	0.74
120	»	10.6	97	0.80
140	»	15.8	115	0.82
170	»	19.8	128	0.75
200	»	23	145	0.72

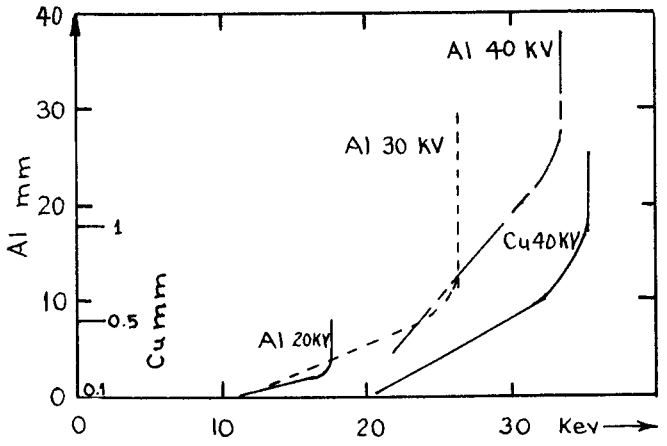

Figure 6. Filtration avec aluminium et avec cuivre 5mA.

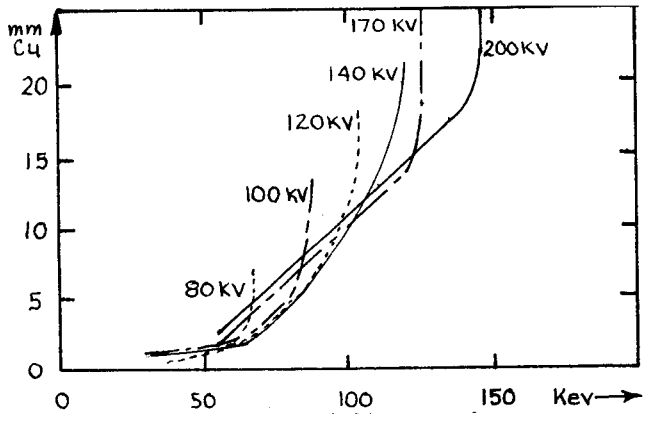

Figure 7. Filtration avec cuivre 3mA.

Mesure de la dose choisie pour irradier le film étudié aux diverses énergies retenues

Pour étudier la réponse spectrale de l'émulsion étudiée, nous avons irradié des films appartenant au même lot, avec une dose constante que nous avons choisie égale à 500 mR et avec des rayonnements homogènes d'énergies connues et croissantes, telles qu'elles résultent du tableau précédent. Pour mesurer la dose que recevait le film, nous utilisions des dosimètres à thermoluminescence au fluorure de lithium avec un appareil lecteur réalisé par la Société CONRAD. La réponse des dosimètres au fluorure de lithium, munis de films correcteurs pour la mesure en basse énergie, est linéaire à partir de 25 keV environ.

Les doses sont déterminées à partir des lectures faites sur trois dosimètres irradiés simultanément. Elles sont retenues si la dispersion entre les trois lecteurs reste inférieure à 5% et, dans ce cas, la valeur adoptée est la moyenne arithmétique des trois valeurs mesurées.

On procède à diverses irradiations pour des doses croissantes; les films irradiés à une certaine énergie sont alors développés dans des conditions rigoureusement semblables, et on trace la courbe exprimant la variation de densité en fonction de la dose. De telles courbes sont données à titre d'exemple sur la figure 8 pour diverses énergies de rayonnement. À partir de ces graphiques, on détermine alors aisément la densité correspondant à la dose de 500 mR pour chacune des énergies. On ob-

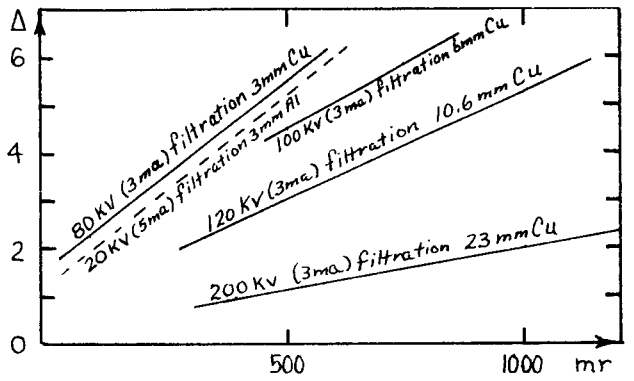

Figure 8. Courbes de noircissement.

tient alors une courbe représentée à la figure 9a. Si elle met bien en évidence la non-linéarité de réponse de l'émulsion pour les énergies inférieures à 140 keV, elle ne constitue pas, à proprement parler, la courbe de sensibilité spectrale, laquelle exprime la variation de dose en fonction de l'énergie pour obtenir une densité constante. Toutefois, lors de la prise de cliché, c'est la densité qui exprimera les variations de dose et d'énergie. Pour des films de caractéristiques voisines mais provenant de fournisseurs différents, les courbes obtenues sont pratiquement les mêmes.

Influence conjointe de la sensibilité spectrale de l'émulsion et de la composition spectrale du rayonnement transmis par la paroi examinée

L'émulsion ayant une réponse spectrale non linéaire avec l'énergie des photons qu'elle absorbe et les photons transmis par une paroi pouvant avoir des énergies et des orientations diverses par suite des phénomènes de diffusion, il est important de rechercher comment l'émulsion traduit les différences d'absorption du rayonnement primaire dont les écarts d'intensité qui en résultent se superposent à un spectre de rayonnement d'énergie plus faible.

Nous avons procédé à cette recherche avec trois spectres différents:

—le spectre continu de rayonnement X émis pour des tensions secondaires, respectivement de 140 et 200 kV,

—le spectre de raies γ émis par une source de radio-iridium 192.

Nous interposons entre le foyer émissif et l'élément détecteur de l'ensemble spectrométrique, des épaisseurs croissantes de cuivre avec les rayons X et d'acier avec les rayons γ considérés.

Pour chacune des épaisseurs de filtration adoptée, nous comptons le nombre de photons enregistrés par le spectromètre, d'une part en considérant la totalité des photons présents dans le spectre transmis quelle que soit leur énergie, d'autre part seulement ceux dont l'énergie est comprise entre 25 et 100 keV, bande dans laquelle la réponse spectrale du film n'est pas linéaire.

Nature du rayonnement	Absorption (filtre)		Spectre complet		Bande spectrale 25 — 100 keV	
	Nature	Épaisseur	Nbre de photons	Log Nbre photons	Nbre de photons	Log Nbre photons
R × 140 kV	cuivre	1.5	162 667	5,2113	92 512	4,9662
		2.5	157 377	5,1969	97 618	4,9895
		4	155 185	5,1908	107 519	5,0314
		5.2	164 702	5,2167	100 893	5,0038
		6.2	158 697	5,2005	97 704	4,9899
		7.2	147 906	5,1699	84 632	4,9275
		8.2	138 174	5,1404	71 911	4,8568
		9	128 423	5,1086	61 778	4,7908
		10.6	117 905	5,0715	49 712	4,6964
		12	108 130	5,0339	44 055	4,6440
		13	103 257	5,0139	43 566	4,6391
		14	99 009	4,9956	45 858	4,6614
		17	86 604	4,9375	45 716	4,6600
		17.8	81 593	4,9116	46 183	4,6644
		19.8	76 066	4,8811	49 398	4,6937
		21.8	68 210	4,8338	51 365	4,7106
R × 200 kV	cuivre	3	171 124	5,2334	101 871	5,0081
		4	163 275	5,2129	104 897	5,0208
		5.2	153 128	5,1851	98 669	4,9942
		6.2	154 673	5,1894	98 735	4,9945
		7.2	163 625	5,2138	106 769	5,0284
		9	165 774	5,2195	107 583	5,0317
		10.7	157 877	5,1983	90 360	4,9560
		12	152 477	5,1832	78 329	4,8939
		16	154 282	5,1883	63 590	4,8034
		17.8	152 289	5,1826	57 370	4,7587
		19.8	150 989	5,1789	57 100	4,7572
		22.6	148 816	5,1726	59 829	4,7769
		24.1	147 153	5,1678	71 716	4,8556
		27	144 681	5,1604	84 524	4,9270
		29	142 596	5,1541	88 238	4,9457
		31	140 697	5,1483	98 738	4,9945
		36.2	137 433	5,1381	109 642	5,0779
Iridium 192	acier	0	100 000	5,000	23 435	4,3698
		1	91 278	4,9603	20 143	4,3041
		4.05	86 283	4,9359	18 550	4,2683
		6.2	80 299	4,9047	16 872	4,2271
		7.8	76 715	4,8848	16 215	4,2099
		11.85	66 769	4,8245	14 213	4,1526
		15.16	57 071	4,7564	11 983	4,0785
		19.65	49 908	4,6981	10 538	4,0227
		25.85	40 111	4,6032	8 284	3,9182
		30.70	33 885	4,5300	6 996	3,8448

Les résultats obtenus figurent dans le tableau de la page suivante. Ce tableau permet de tracer alors les courbes représentées sur la figure 10, qui amènent les remarques ci-après:

1°) les courbes obtenues avec l'iridium 192 décroissent régulièrement, aussi bien pour le spectre total que partiel.

2°) les courbes obtenues avec les rayons X émis à 140 kV et 200 kV sont assez différentes. Celles qui concernent le spectre total décroissent constamment et assez régulièrement. Au contraire, celles qui concernent la bande spectrale 25-100 keV sont très dissemblables. On peut y distinguer trois domaines:

—un premier domaine, situé au-dessous de 4 mm de paroi pour 140 kV, et 9 mm pour 200 kV, où la courbe est sensiblement horizontale, avec une légère concavité vers le haut;

—un second domaine, situé entre 4 et 13 mm pour 140 kV et 9 à 20 mm pour 200 kV, voit la courbe du spectre partiel décroître rapidement. C'est cette partie de courbe qui définit les limites d'utilisation optimale de l'énergie d'émission considérée;

—un troisième domaine voit la courbe représentative du spectre partiel remonter plus ou moins rapidement. Dans ce cas, l'émission secondaire devient très importante, son intensité augmente alors que celle du rayonnement primaire décroît. Le rapport

$$\frac{\text{rayonnement secondaire}}{\text{rayonnement primaire}}$$ croît très vite.

Pour mieux comprendre l'importance très grande de ce fait, nous avons enregistré le spectre transmis par une paroi de 19.8 mm de cuivre traversée par le rayonnement X provenant d'un appareil fonctionnant sous une tension secondaire de 140 kV. Le résultat est représenté à la figure 4b. Chaque cran correspond à un canal du spectromètre. On observe deux pics nets, l'un à 120 keV environ qui correspond au rayonnement primaire tranmis, l'autre à 65 keV qui correspond à une émission secondaire de forte intensité. On distingue également un troisième pic vers 30 keV.

Comme cette figure le montre, l'intensité des rayonnements secondaires diffusés ou émis par la paroi radiographiée est sen-

siblement supérieure à l'intensité du rayonnement primaire transmis, ce qui a pour effet de diminuer le rapport

$$\frac{\text{signal}}{\text{bruit de fond}}$$

par élévation de ce dernier. L'affaiblissement de ce rapport est considérablement accentué par le fait que l'émulsion est beaucoup plus sensible aux photons secondaires de basse énergie qu'aux photons primaires d'énergie plus élevée, qui *seuls* contribuent à l'obtention de l'information recherchée.

Le rapprochement des figures 9a et 9b tel que nous l'avons représenté met bien en évidence ce phénomène.

Dans le cas considéré, les quantités (doses) des divers rayonnements transmis ou émis par la paroi sont proportionnelles aux surfaces des deux pics de la figure 9b, soit 40% pour celui qui concerne les énergies de photons supérieures à 100 keV et 60% pour celui qui concerne les photons d'énergie inférieure à cette valeur.

En ne considérant, pour simplifier notre raisonnement, que l'énergie maximale de chacun des pics principaux soit respectivement 120 et 65 keV, le rapport de la rapidité de réponse du film pour ces deux valeurs est d'environ 4. Ce coefficient représente l'amplification de la densité due aux photons de 65 keV par rapport à celle qui résulte de l'action des photons de 120 keV. Dans ces conditions, la densité de base résulte, pour 10% de la valeur du rayonnement primaire, et pour 90% de celle du rayonnement diffusé. C'est donc seulement sur ces 10% que se manifesteront les variations dues aux différences d'absorption provoquées par la présence de défauts de compacité.

Les expériences décrites montrent la grande importance qu'il faut accorder à la composition spectrale du rayonnement X ou γ transmis par une paroi. Les résultats trouvés avec les rayonnements émis sous des tensions secondaires de 140 et 200 kV semblent conduire à une limitation des épaisseurs maximales pour lesquelles la qualité de la détection des défauts est bonne. Au-delà des épaisseurs de 13 et 20 mm pour les deux tensions considérées, la proportion relative de rayonnements secondaires dans le spectre qui parvient au film croît très vite. Toutefois, des expériences en cours montrent qu'il convient de distinguer les défauts proches de la paroi contre laquelle est disposé le film, de ceux qui en sont éloignés. Il peut arriver que le rayonnement secondaire participe à la détection d'un défaut et même améliore le contraste avec lequel il est perçu. Pour cela, il suffit que les photons secondaires aient une direction voisine de celle des photons primaires et que l'épaisseur comprise entre le défaut et le film soit telle qu'une portion appréciable de ces photons diffusés puissent parvenir au film sans provoquer une nouvelle diffusion. Tout se passe alors comme si la radiographie était effectuée sur la seule épaisseur Δ_e par deux rayonnements d'énergie $h\nu_0$ pour le primaire, et $h\nu'$ pour le secondaire. Nos essais ont montré que, pour un matériau déterminé, suivant l'énergie des photons primaires et l'épaisseur de la filtration, on observait l'émission de photons secondaires pouvant avoir une énergie assez bien définie (voir figure 9b). On peut donc faire, pour cette émission secondaire, le même raisonnement que pour les photons primaires et considérer qu'il existe un domaine d'épaisseur pour lequel ils auront un rôle bénéfique sur la détection des défauts qu'ils rencontreront.

On conçoit que ce résultat ne peut être observé que pour les défauts proches de la paroi contre laquelle se trouve le cliché et avec un rayonnement diffusé de direction aussi proche que possible de celle du rayonnement primaire. Dans le cas contraire où le défaut n'est pas proche de la paroi d'émergence des rayonnements, les photons secondaires de faible énergie seront absorbés avant de parvenir au cliché en donnant naissance à

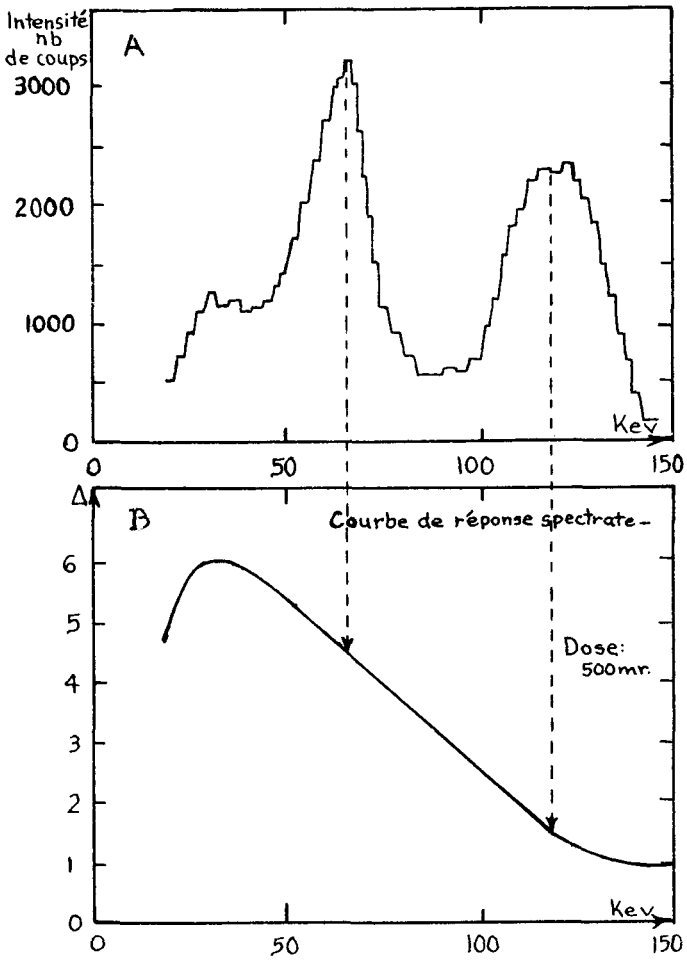

Figure 9. Composition spectrale du rayonnement émis sous 140 kV avec filtration 19.8 mm cuivre.

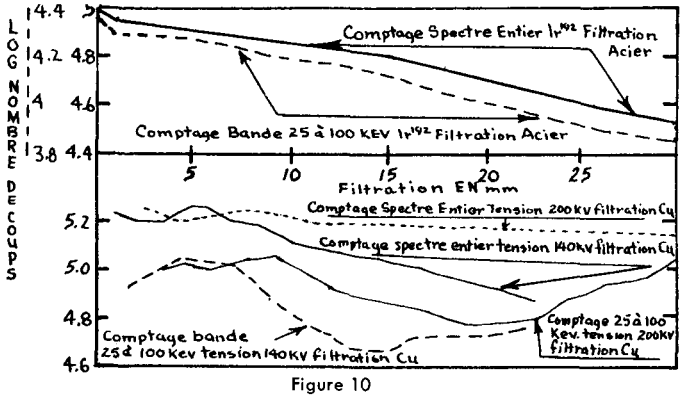

Figure 10

d'autres photons moins bien orientés ou à des photoélectrons. Si le défaut débouche, les rayonnements diffusés de toute nature, quelles que soient leur direction et leur énergie, participeront à la formation de l'image et pourront accroître, parfois de façon importante, le contraste de cette dernière. La figure 6 résume cette analyse des phénomènes étudiés, qui demandent une expérimentation soignée sur des modèles présentant des défauts à diverses profondeurs afin de vérifier comment se modifie le contraste de leurs images.

Conclusions

Nos expériences semblent montrer que pour chaque matériau il existe une tranche d'épaisseur bien définie pour laquelle la qualité spectrale du rayonnement permettra la meilleure détection possible d'un défaut en mettant en œuvre un rayonnement

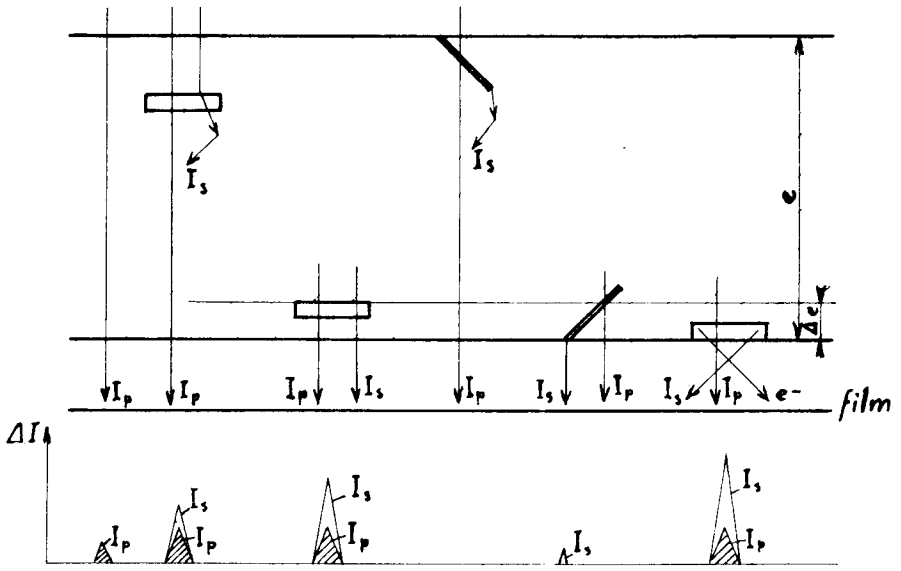

Figure 11
Représentation schématique de l'amplitude des divers signaux provoqués par les différents défauts représentés.

primaire de qualité donnée. Ce domaine d'épaisseur optimale diffère sensiblement de celui qui est indiqué par les fabricants d'appareillage à rayons X et se situe très en dessous des valeurs portées sur les notices d'emploi.

Il semble préférable de radiographier une pièce avec un rayonnement d'énergie relativement élevée, si l'on évite ainsi une émission secondaire dont l'énergie moyenne se situe dans le domaine spectral où l'émulsion présente sa plus grande rapidité. L'écart des intensités du rayonnement primaire transmises respectivement à travers le défaut et à côté de celui-ci diminuera, mais le contraste de l'image radiographique au moment de la lecture du cliché augmentera, et la détection du défaut sera finalement améliorée.

Bien entendu, les autres précautions usuelles concernant
—le rayonnement: incidence, filtration, etc.....
—le film: qualité, traitement, densité élevée, etc.....
—l'examen du cliché: qualité du négatoscope, de la linéarité émergente et ambiante, etc.....
contribueront également à la bonne qualité des images radiographiques.

Bibliographie

1. Halmshaw, R. The image on a radiograph and its interpretation; 4th International Symposium in Industrial Radiography, Gevaert Anvers, 31/3—1/4/66.
2. Charlet, E. et Nouvet, A. Étude de l'influence des conditions géométriques de pose sur la qualité d'image en gammagraphie; 4ème Symposium Gevaert Anvers.
3. Ruault, P. A. Aspects particuliers de la qualité d'image radiographique et gammagraphique dans l'industrie du gaz; 4ème Symposium Gevaert Anvers.
4. Weber, H. Die Abbildung von natürlichen Fehlern und von Testfehlern in Durchstrahlungsaufnahmen; 4ème Symposium Gevaert Anvers.
5. Von Bentz, W. Aufnahmetechnik und Bildgüte von durchstrahlungsaufnahmen an Stahl bis 400 mm Dicke; 4ème Symposium Gevaert Anvers.
6. Criscvolo. Radiography and visual perception; Non-destruction Testing—Nov.-Dec. 1962.
7. Becker, E. Der Einfluss der Unschärfen auf Filmaufnahmen mit gamma; Strahlenquellen Material Prüfung—Vol. 6 n° 2 (1964).

Relations Between Radiographic Image Quality and Film Density

W. BOCK, E. MUNDRY AND D. SCHNITGER, GERMANY

Introduction

In the history of industrial radiography there have been many different views as to the density of X-ray and gamma exposures. From the literature of the thirties we learn that at that time densities around S=1 were preferred (1-7).

Though Schiebold (8) stated as early as 1936 that a favourable range for sensitivity was $0.5 \leq S \leq 2.5$, only in later years have higher sensitivities been used. In 1951, Vaupel and von Wetterneck demanded exposure densities of at least S=1.5 for Ir-192(9) and O'Connor and Hirschfield obtained the best image quality for Co-60 radiographs in the range of $3.0 \leq S \leq 3.5$ (10).

Similar results from other papers point to the most favourable densities of fine-grain films with heavy metal screens for X-ray and gamma radiation at about S=2.5 (11-13), sometimes even between 3 and 4 (14). Systematic studies showed the most favourable densities at ca. 1.5-3.0 (15-22). Some standards contain data on useful densities between S=1.3 and S=3.0 depending on the exposure technique (23,24).

Since there are very strongly diverging opinions on the choice of densities in practice it is the scope of this paper to find, by completing the Möller-Weeber theory of image quality, the relation between radiographic image quality and density by theory and experiment. Possible contradictions should be cleared up. Last but not least, the influence of view-box brightness is discussed and recommendations for the most favourable film densities and lowest brightness are stated.

Theory of Image Quality at Any Given Density

To express the image quality of an industrial radiograph as a numerical value, penetrameters with artificial flaws of various shapes and sizes are generally used. The detectability of the arti-

ficial flaws gives units of measurement to assess the image quality. In this paper wires with circular cross-sections are used as test flaws. The wire images have the advantage of being much longer than they are wide; that means that we can limit the theoretical calculation of the wire sensitivity to a two-dimensional method and can use, for the consideration of the film unsharpnesses, the simpler line-spread function instead of the point-spread function.

Radiation Characteristics

The essential content of the theory of Möller and Weeber as the basis of this paper should be briefly outlined here because relevant reports have as yet been published only in German, so we cannot assume this theory to be generally known.

According to this theory the best attainable wire sensitivity can be computed for a given exposure set-up and radiation quality. A set-up according to Figure 1a is given: A wire with the diameter d lying on the opposite side of the film on a piece of material of

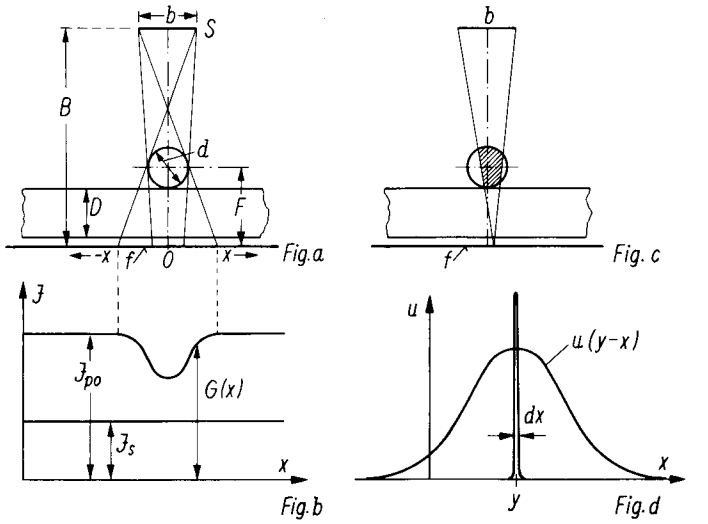

Figure 1. Geometry (a and c); curve of intensity in the film plane (b), and blurring by film unsharpness (d).

the thickness D is reflected on the film f by the radiation source S. The film to focus distance is B, the film to wire centre distance is F and the diameter of the focal spot is b. It is assumed $b<B$ and $d << D$; these conditions are satisfied generally in practice. As to the shape of the intensity behind the piece of material in the film plane (Figure 1b) the following statements can be made (x being the coordinate of film length): $G(x)$ describes the total intensity; it is lower behind the wire than at both sides of the wire. $G(x)$ comprises two components i.e. the intensities of scattered radiation I_s and of primary radiation I_p. Because $d << D$ $I_s(x) =$ const, while $I_p(x)$ depends on the associated total irradiated material thickness according to the absorption law. Beside the wire $I_p(x) = I_{po} =$ const. For the continuous energy distribution of the Bremsstrahlung a mean absorption coefficient $\bar{\mu}$ and for the finite size of focal spot a mean irradiated wire thickness $\bar{d}$ are introduced. With the intensity I_o in front of the material we have

$$I_p(x) = I_o \cdot exp\,\{-\bar{\mu}[D + \bar{d}(x)]\} \tag{1}$$

As for the imaging of the wire, the absolute intensities are not of interest but only the difference, $\Delta I(x)$, between the intensities at the place of wire image and of places outside the wire image; this means the shape of the intensity absorbed by the wire in the film plane. Regarding $d << D$ and $\bar{\mu}\,\bar{d}(x) << 1$, we get

$$\begin{aligned} \Delta I(x) &= I_p(x) - I_{po} \\ &= I_{po}\{1 - \bar{\mu}\,\bar{d}(x)\} - I_{po} \\ \Delta I(x) &= -I_{po}\,\bar{\mu}\,\bar{d}(x) \end{aligned} \tag{2}$$

The irradiated mean wire thickness d, which is assigned to the point x on the film, must be calculated from the covered wire cross-section divided by the distance of the two marginal rays in the plane parallel to the film through the wire centre.

Film Unsharpness

Next we must take into account, in the formula of $\Delta I(x)$, the inherent unsharpness of the film-screen combination, which is produced on every exposure by lateral transportation of energy. If every part of energy associated with an infinitesimal width dx is scattered sidewise in the film-screen combination according to the function $u(x)$ (Figure 1d), the superposition of all incident scattered intensity parts produces the broadened shape of intensity:

$$F(y) = \cdot \int_{-\infty}^{+\infty} G(x) \cdot u(y - x) \cdot dx \tag{3}$$

y and x are coordinates of film length in this convolution integral. According to (26) the spread function can be described by functions of the form

$$u(x) = a \cdot e^{\pm \gamma x}$$

But the assumption of a simple triangle function as

$$u(x) = c \cdot x + g \tag{4}$$

alone gives an adequate approximation (25). Such a triangle function, the half-width of it being the film unsharpness u_i, permits the solution of the integral $F(y)$ completely in an analytical form, a solution which has as yet been approximated only graphically (25). The shape of the absorbed intensity by the wire integration produces

$$\Delta I(y) = -I_{po} \cdot \bar{\mu} \cdot h(y) \tag{5}$$

$h(y)$ contains the relation between the wire image and all geometrical values—the geometrical unsharpness included—and the film unsharpness u_i. We have calculated the function $h(y)$ given in the Appendix. It consists mainly of root and arc cos expressions, which cause no difficulty in electronic computer programming.

Introduction of the Density Parameter

Only the shape of the intensity absorbed by the wire has so far been calculated. In order to get the corresponding shape of density on the film the gradation qualities of the film material must be considered and the film density has to be introduced. To maintain the analytical method of calculation, the density $S = f(\log E)$ necessitates its introduction as an additional parameter into the Möller-Weeber theory. For that purpose we have recorded in the BAM the characteristic density curves of 24 types of films: the densities have been measured within the range of $0 < S \leq 6.8$ with a Macbeth densitometer with sufficient accuracy. Corresponding to the recommendations of the IIW-document (32) the density curves of nearly all film types within the range of $0.5 < S < 5.0$. fitted the exponential functions of the form $S = c \cdot E^m$, c and m being characteristic constants of each film type. The differentiation of the exponential function gives

$$\Delta S = m \cdot S \cdot \frac{\Delta E}{E} \tag{6}$$

Since the radiation intensity I is proportional to the exposure value E within the limits of radiographic interest, we get with the equ. (5) and $I = I_s + I_{po}$

$$\Delta S(y) = -m \cdot S \cdot \frac{\bar{\mu}}{1 + k} \cdot h(y) \tag{7}$$

$k = \frac{I_s}{I_{po}}$ is the ratio of scattered radiation intensity to primary radiation intensity outside the wire. $\Delta S(y)$ describes the shape of the wire-image density compared to the evenly darkened background. The expression is clearly constructed. The negative sign indicates that the density in the wire image is less than that of the adjacent area. The first two values m and s give the influence of the film characteristics, $\frac{\mu}{1+k}$ accounts for the influence of absorption and scattering properties of the irradiated material with regard to radiation quality. $h(y)$ describes the dependence of the wire image on the geometrical and film unsharpness. Measured values are available (25, 26) for μ and k in relation to the energy and the thickness of the irradiated material, for u_i in relation to the energy. They were used for the calculations in this paper. Values for m are taken from our own measurements of the density curves mentioned above.

Limits of Perception and Determination of Wire Sensitivity

The final determination of the wire sensitivity proper from the calculated wire images requires in addition the knowledge of the limits of perception of the human eye and its dependence on the shape of image detail to be observed. Möller and Weeber confirmed with special penetrameter plates (25) that the smallest density differences ΔS_{min} perceptible by the human eye depend to a large degree on the shape of the image detail observed. The test-plates consisted of pairs of aluminium plates of which one longitudinal edge was chamfered in such a way that rectangular, trapezoidal and triangular density profiles of differing widths and slopes could be produced by irradiation. The crest values of the density profiles were measured with a photometer. A number of observers determined the values of ΔS_{min} as a function of slope and width. This catalogue of density profiles was used for the final determination of wire perceptibility. Trapezes are drawn as similar as possible to every calculated wire image. These trapezes must have the same height and slope as any trapeze of equal width of the catalogue, if the respective wire is to be just perceptible. A certain wire sensitivity corresponds to this wire.

Theoretical Determination of Wire Sensitivity as a Function of Density

If we accept the density S as the only variable parameter, the other exposure parameters remaining constant, we can find with the method discussed here in addition to (25) the relation between wire sensitivity and film density. Equ. (7) shows that the crest value of a wire profile, or more generally speaking the image contrast, increases when the product $m.S$ increases. Since the density is combined with the gradation γ by

$$\gamma = ln\ e \cdot m \cdot S \qquad (8)$$

within the validity range of $S=c \cdot E^m$ it means that the wire sensitivity increases as long as the gradation increases. The maximum of the wire sensitivity should therefore be attained at the inflection point of the density curve. As the inflection point of the usual middle and fine-grain films lies at densities above $S=5$, we can expect that the wire sensitivity for these films increases with the density at least up to $S=5$. Furthermore when evaluating the perceptibility of wires, Ricco's law known in physiological optics, has to be taken into account. It states that for sharp imaging of an object within the range of the fovea the threshold value of the human eye is given by the product of the brightness of the object and the area of its image on the retina, as soon as this area falls below a certain value, which depends on the brightness of the field of vision (27). Applied to the problem of wire perception it means that the density profile of wires below a certain diameter, which are still to be seen, requires a higher crest value ΔS_{min} the smaller the wire diameter. It can therefore be expected that the increment of the image quality due to film gradation plotted against density becomes smaller after reaching a certain image quality index, the narrower the wire profiles reaching the limits of perception of the human eye.

Determination of ΔS_{min}

Since within the range of boundary energy between 50 keV and 400 keV with higher densities and rather thin material thicknesses, wire diameters reach the perception threshold, where Ricco's law has a non-negligible influence on the perceptibility, the relation between the density difference ΔS_{min} and the geometry of the density profile must be correctly known for the computation of the image quality. We therefore made investigations for wire diameters $d < 1$ mm (0.04in.) in addition to (25). To save time, wires were used instead of test slits. The image profiles of small wires can be taken in good approximation as triangles, which are determined in addition to the crest value of the profile by only one geometrical value, namely the slope or the base length. In regard to a special case discussed later we chose as geometrical value the width of the profile at the point where S has fallen to 40% of the crest value; for this width was in all experiments equal to the wire diameter itself with a tolerance of $\pm$ 1%.

The experiments were carried out with finest grain films between 0.02/0.02 mm ($\sim$ 1 mil) Pb-screens and a tube tension of 180 kV. The distance from the wire sets to the film was small enough to produce no recognizable geometrical unsharpness. For a constant exposure time t_g and the resulting background density crest values of the wire profiles in the range of $\Delta S=0.05$ to $\Delta S=0.2$ were obtained. The much smaller crest values of the density profiles near the perceptibility threshold could not be measured any more with a microphotometer. They were produced at a known height in an additional series of exposures by placing the wires only during a certain part (partial exposure time t_T) of the total exposure time t_g on the film. So they reached only a fraction ΔS_T of the full density difference ΔS_g, which was measured by the Schmidt-Haensch microphotometer (25). The just perceptible wire was determined from the partial exposures by several observers, and the associated value Δ_T which is equal to the wanted value ΔS_{min} was computed from

$$\frac{\Delta S_T}{\Delta S_g} = \frac{t_T}{t_g}.$$

In Figure 2 the ΔS_{min} values obtained this way are plotted against the wire diameter. We recognize below about 0.4 to 0.5 mm clearly the influence of Ricco's law. For decreasing diameters the minimum density difference ΔS_{min} required for the detectability increases. The curve is given by a broken line for the bigger diameters, because this range leads to density profiles, which are to be approximated more expediently no longer by triangles, but by trapezes being determined by two geometrical values.

Example

In a concrete example the image quality was determined as a function of the density by theory and experiments and the results were compared. The data of exposure were:

B=1000 mm (39.4")
b= 4 mm (0.16")
D= 20 mm (0.79")
u_i= 0.17 mm (0.07")
300 kV, Adox M2 (0.02/0.02 mm Pb)

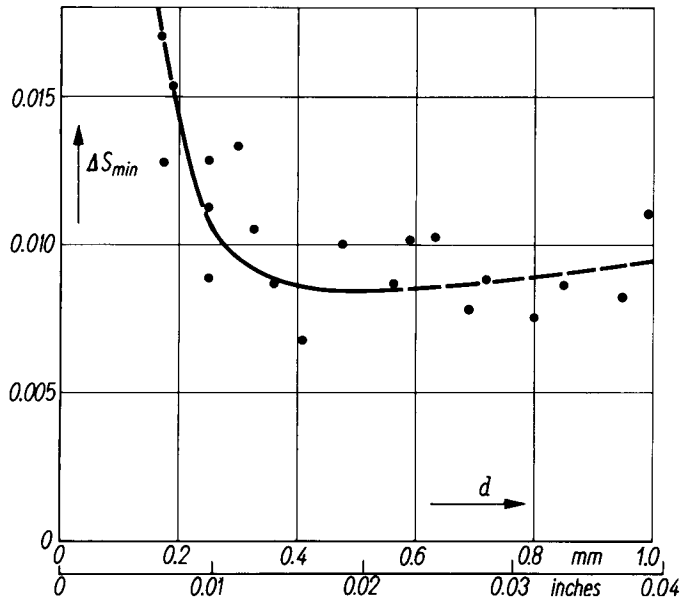

Figure 2. Density difference $\triangle S_{min}$ of lowest perceptible profile vs. wire diameter d.

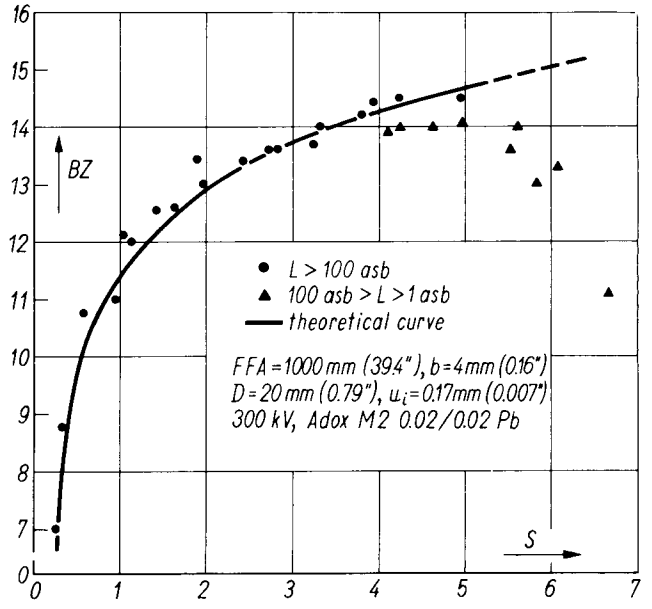

Figure 3. Image-quality index BZ vs. density S (BZ = 6 — 10 l°g d, d[mm] = diameter of the thinnest perceptible wire.

The equation (7) describing the curve of wire image density in regard to the even background density was programmed for a Zuse 23 ZV computer to allow the computation of ΔS as a function of the place y for any wanted density and any wire diameter in satisfying little steps of y. The just perceptible wire was determined out of the number of profiles calculated for a given density by comparing it to the ΔS_{min} values. With the definition of the image-quality index BZ=6-10 log d according to the German standard DIN 54 109/2 (28) the corresponding BZ values were obtained, which are plotted against the density in Figure 3 (full line). Firstly the image-quality index increases fast in the range of little densities. With increasing densities the increment becomes smaller, but there is no maximum in the investigated density range. For the example chosen here the maximum has to be expected around or above the density $S=6$. Its place is determined by the influence of Ricco's law by the shape of the characteristic film curve and for certain circumstances also by other influences as e.g. the acuity of the human eye. In no case can it be at densities behind the point of inflection of the characteristic film density curve.

The experimental determination of the image quality indexes was carried out with a Seifert & Co. 400 kV set-up. The films were evaluated by the 4 observers who had counted the wires for the determination of ΔS_{min}. So the influence of different evaluation rules and sensitivities of the eyes was kept down. The general evaluation rule used was the same as defined in an earlier paper on the experimental determination of the relation between image quality and film density (29). For reasons discussed further on the brightness on the observed film side was carefully watched during the evaluation. The brightness was measured in apostilbs (asb) or millilamberts (ml; 10 asb=1ml); it was checked on every evaluation by a Schmidt & Haensch brightness meter. The data characterized in Figure 3 by circles had always a brightness greater than 100 asb (10 ml). Agreement with the computed curve is good.

Influence of Brightness

The data symbolized in Figure 3 as triangles, were determined at brightnesses L between 100 and 1 asb (10 and 0.1 ml). Caused by the limited luminosity of our view box the brightness was, for these data, getting smaller with increasing film densities. For the last point, for example, it was only 1 asb (0.1 ml). We can see from these data that the image quality decreases rapidly with decreasing brightness below 100 asb (10 ml).

This behaviour was already found in an earlier investigation (29). A typical example is given in Figure 4. Again the image-quality indexes of a series of Gevaert D2 films exposed to 200 kV is plotted against density. The series was evaluated at different view-box brightnesses given in arbitrary units. We learn that the maximum of the curve shifts with decreasing brightness to smaller densities; the maximum itself getting smaller.

The shape of the experimentally found image-quality index curve of Figure 3 at higher densities represents a general behaviour, which becomes understandable when we take into consideration that the contrast sensitivity of the human eye depends

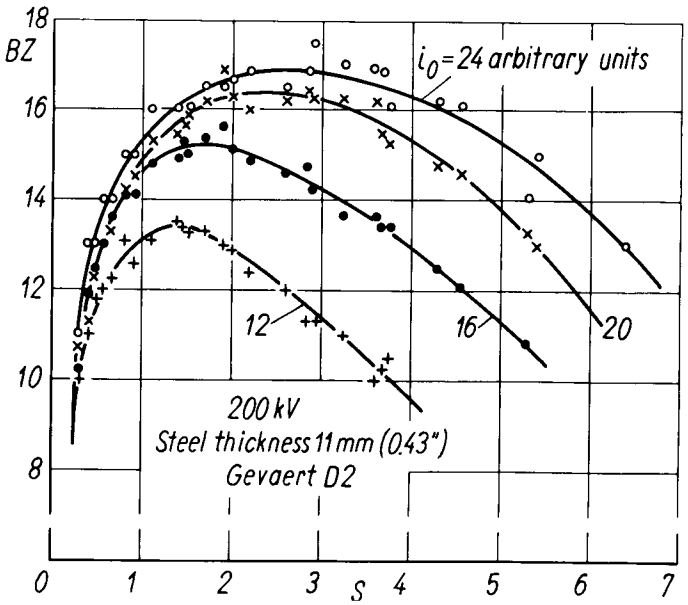

Figure 4. Image-quality index BZ vs. density S for different brightnesses i_0 of the view box.

strongly on the brightness. If two directly adjacent areas have the brightness L and $L \pm \Delta L$, the difference ΔL being just perceptible, then the contrast sensitivity means the ratio $L/\Delta L$. A survey of the whole relevant brightness range is shown in Figure 5, where the contrast sensitivity according to data from physiological optics (27,30) is plotted against brightness; the ordinate on the right gives the corresponding density differences ΔS_{min}. If we want to operate at maximum contrast sensitivity, which is necessary for a full utilization of the film information, we must ask for brightnesses on the observers film side of at least 10^2 asb (10 ml). Below 100 asb the contrast sensitivity decreases rapidly. At 1 asb (0.1 ml) the density difference ΔS has to be three times as much as within the maximum range of the curve in order to be still recognized. To get maximum contrast sensitivity a film with the density $S=5.0$ requires a view box with a brightness of at least $L=10^{5}+^{2}=10^{7}$ asb (10^6 ml), a film with the density $S=6.0$ $L=10^8$ asb. One of the two devices by which the data of Figure 5 were determined had, however, only a maximum brightness of $10^{6.2}$ asb respectively $10^{6.6}$ asb without ground glass, the other one reached $10^{7.1}$ (asb*). This means that films with densities of S≈4 and above could not be evaluated any more by instrument no. 1 with maximum contrast sensitivity and therefore the wires related to the expected image quality indices BZ=14 to BZ=15.5 could not be found.

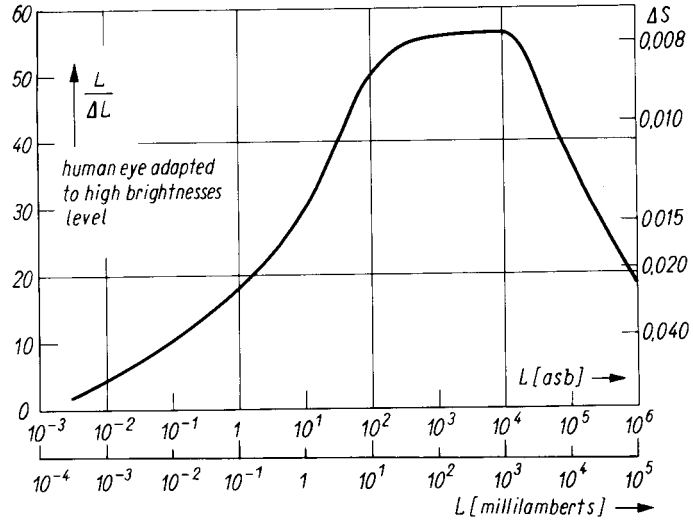

Figure 5. Threshold contrast sensitivity L/△L vs. brightness L.

There is also another effect which increases with decreasing brightness reducing the wire sensitivity when brightnesses are too small. If the eye has to adapt from light to darkness the visual angle α_{min} under which an object is just detectable increases. But this means that the decreasing contrast sensitivity is superposed at lower brightnesses by the decreasing of acuity, where the three values brightness, contrast sensitivity and visual angle are interdependent (31,32,27).

Therefore in the evaluation of X-ray films attention should be paid to a satisfying brightness on the observers side of the films, if the detectability of small details is important. For these cases we recommend brightnesses at 100 asb (10 ml), if possible at 200 or 500 asb.

Conclusions

From the theoretical considerations and their experimental confirmation we learn that the image quality improves rapidly with increasing density and then moves towards a maximum. From the results of the example investigated here one could deduce the claim that X-ray films should have densities from $S=4.0$ to $S=6.0$, view boxes of relevant brightnesses provided. The following arguments speak against the derivation of binding regulations and their inclusion in standards:

1. The way by which such high densities are produced cannot be neglected (29).
2. The light energy absorbed in films at high densities leads to such a heating of the film that damage to it during the evaluation cannot be prevented by normal technical aids.
3. The gain in image quality with increasing density becomes smaller and smaller, the technical expenditure for the production and evaluation of such exposures, however, gets bigger and bigger, so that economical considerations should not be neglected.

The choice of densities $S > 4$ should in our opinion be reserved for special test problems, where economic aspects are of secondary importance to the highest image qualities.

Summary

The present paper deals with the problem of how to introduce density as a parameter into the Möller and Weeber theory of image quality expressed by wire sensitivity when irradiating material with X- and gamma-radiation; how the wire images are to be computed analytically and how the image quality finally depends on the density. For that purpose we first examined how the film gradation depends on the density. It was shown that within the range of $0.5 < S \leq 5.0$ the characteristic curves of almost all investigated fine-grain films can be described as exponential functions and that a linear relation exists between gradation and density; therefore the gradation could be replaced by the density itself. Thus it was possible to compute for different densities the shape of contrast, which describes the wire image, and to determine theoretically the wire sensitivity as a function of density by comparison with the contrast threshold values of the human eye, which were also determined as a function of density. These values are compared with the experiments, the influence of brightness on image quality is discussed, and optimum film densities are stated.

References

1. Berthold, R., and Hellmich, H. Kesselprüfung mit Röntgen- und Gammastrahlen. Mitt. Vereinig. Grozkesselbes. (1932) No. 40, p. 251/79
2. Berthold, R. Leistung und Wirtschaftlichkeit der Röntgenprüfung von Schweizungen. Elektroschweizung (1932) No. 11, p. 201/05
3. Berthold, R., and Riehl, N. Grundlagen der Werkstoffprüfung mit Gammastrahlen. Z.VDI 76 (1932) No. 17, p. 401
4. Berthold, R. Möglichkeiten und Grenzen der Grozbildaufnahmen mit Röntgenstrahlen. Arch. Eisenhüttenwes. 8 (1934/35) No. 9, p. 425/26
5. Berthold, R., and Zacharow, M. Untersuchungen an Röntgen-Verstärkerschirmen.Z.Metallkde. 28 (1936) No. 2, p. 40-42
6. Fischer, O., and Vaupel, O. Die Durchstrahlbarkeit von Beton mit Röntgen- und Gammastrahlen. Beton u. Eisen 37 (1938) No. 5, p. 87/91
7. Berthold, R., Ebert, Fr. and Vaupel, O. Röntgen-Durchstrahlbarkeit von Stahl bei Röhrenspannungen bis 1 Million Volt. Stahl u. Eisen 60 (1940) No. 16, p. 339/41
8. Schiebold, E. Die Bedeutung der Röntgen-Grob- und Feinstrukturforschung für die Giezereifachwelt. Vortrag auf dem Giezerei-Kongrez 1936, Düsseldorf. Düsseldorf: Giezerei-Verlag 1936, 40 p.

*We were able to use this instrument through the courtesy of M. Ruault, Gaz de France, Paris.

9. Vaupel, O, and v.Wetterneck, N. Ueber die Anwendbarkeit radioaktiver Isotope in der Werkstoffprüfung, Versuche mit Iridium 192. Metall 5 (1951) No. 13/14, p. 293/94
10. O'Connor, D. T., and Hirschfield, J. J. Some Aspects of Cobalt Radiography. Nondestr. Testing 10 (1951) No. 1, p. 33/39
11. —— Reduction of Exposure of Time in Gamma Radiography. Nondestr. Testing 11 (1953) No. 4, p. 28/33
12. Polansky, D., Case, D. P. and Criscuolo, E. L. The Investigation of Radioisotopes for the Inspection of Ship Welds. Nondestr. Testing 17 (1959) No. 1, p. 21/25
13. Holloway, J. A., Polansky, D. and Criscuolo, E. L. Analysis of Radiographic Techniques. Nondestr. Testing 18 (1960) No. 5, p. 337/40
14. Youshaw, R. A., and Maddy, W. R. Radiography of Cast High Explosives. Nondestr. Testing 20 (1962) No. 5, p. 325/31
15. van Ouwerkerk, L. The Relative Advantage and Limitation of Nondestructive Testing Methods. Nondestr. Testing 16 (1958) No. 2, p. 113/27
16. Schiebold, E. and Becker, E. Bildgüte und Fehlererkennbarkeit bei Filmaufnahmen mittels Röntgen- und Gammastrahlen. Wiss.Z.d.Hochschule f. Schwermaschinenbau Magdeburg 3 (1959) No. 2, p. 117/32, insbes. p. 125
17. Becker, E. and Vorsprach, F. Prüfung von Aluminium mit Ir-192. Freiberger Forschungsh. 38 (1960), p. 231/40, insbes. p. 236
18. Schiebold, E., Becker, E. and Vorsprach, F. Zur Anwendung des Agfa-Texo-F-Filmes in der zerstörungsfreien Werkstoffprüfung mit Gammastrahlen. Isotopentechn. 1 (1960 No. 1, p. 2/9
19. Fink, K. Neue Ergebnisse bei der Anwendung des Betatrons in der Werkstoffprüfung. Techn. Mitt., Essen (1960), p. 162
20. Becker, E. and Slaba, I. Untersuchungen mit dem tschechischen Betatron. Wiss.Z.d.Hochschule f.Schwermaschinenbau Magdeburg 5 (1961) No. 1, p. 61/68
21. Becker, E., Schöning, H. G. and Tschorn, G. Untersuchung der Bildgüte mit einer Co-60-Strahlenquelle von 20 Ci. Isotopentechn. 2 (1962) No. 4, p. 97/101
22. Fink, K. and Woitschach, J. Aufnahmetechnik bei der Schweiznahtprüfung mit Betatron-Röntgenstrahlen. Schweizen und Schneiden 14 (1962) No. 4, S. 137/49
23. British Standard 2910 (1957): General Recommendations for the Radiographic Examination of Fusion welded Circumferential Butt Joints in Steel Pipes
24. ISO TC 44: übernommen aus IIS/IIW-36-59, Doc. V-113-59 (1959): Recommended Practice for the Radiographic Inspection Pipes up to 2 Inches (50 mm) Wall Thickness
25. Möller, H., and Weeber, H. Die Bildgüte bei der Durchstrahlung von Werkstoffen mit Röntgenoder Gammastrahlen von 0,1—31 MeV. Forschungsber.d. Landes Nordrhein-Westfalen No. 1305. Köln/Opladen: Westdeutscher Verlag 1963.
26. Möller, H. and Weeber, H. Die innere Unschärfe von Durchstrahlungsaufnahmen im Energiebereich von 0,1 bis 31 MeV. Archiv f. Eisenhüttenwesen 35 (1964) p. 891-901
27. Schober, H. Das Sehen, Bd. II. VEB Fachbuchverlag Leipzig 1964
28. DIN 54 109: Bestimmung der Bildgüte von Röntgen- und Gamma-Film-Aufnahmen an metallischen Werkstoffen
29. Mundry, E., and Bock, W. Ueber den Zusammenhang zwischen Bildgüte und Filmschwärzung bei der Durchstrahlungsprüfung mit Röntgen- und Gammastrahlen. Materialprüf. 6 (1964) No. 8, p. 265/71
30. Wahl, K. Lichttechnik. Fachbuch GmbH Leipzig 1954
31. Ruault, P. A. Aspects particuliers de la qualité d'image radiographique et gammagraphique dans l'industrie du gaz en France. Vorgetr. anläzl. des 4. Symposiums über Industrielle Radiographie 1966 in Antwerpen
32. Criscuolo, E. L. Radiography and Visual Perception. NDT 1962, No. 6, p. 373/379
33. Doc IIS/IIW—184-65: Recommendation Concerning Sensitometric Tests on Radiographic Films without Screens or with Lead Screens

Appendix

The function $h(y)$ from Equ. (7) is calculated as $h(y) = \beta \cdot f(y)$

with $\beta = \dfrac{d^4 \cdot B^3}{64 \cdot b \cdot F(B-F)^2} \cdot \dfrac{1}{\overline{u_i}^2}$ and

$$
f(y) = \begin{cases}
+ (ay + c)\sqrt{1 - (ay + c)^2}\ 2\{\tfrac{1}{3}[1 - (ay + c)^2] - 2{,}5\} \\
- (ax + c)\sqrt{1 - (ax + c)^2}\ \{\tfrac{1}{3}[1 - (ax + c)^2] - 2{,}5\} \\
- (az + c)\sqrt{1 - (az + c)^2}\ \{\tfrac{1}{3}[1 - (az + c)^2] - 2{,}5\} \\
- (ay - c)\sqrt{1 - (ay - c)^2}\ 2\{\tfrac{1}{3}[1 - (ay - c)^2] - 2{,}5\} \\
+ (ax - c)\sqrt{1 - (ax - c)^2}\ \{\tfrac{1}{3}[1 - (ax - c)^2] - 2{,}5\} \\
+ (az - c)\sqrt{1 - (az - c)^2}\ \{\tfrac{1}{3}[1 - (az - c)^2] - 2{,}5\} \\
\\
+ 2\{2(ay + c)^2 + \tfrac{1}{2}\} \arccos(ay + c) \\
- \{2(ax + c)^2 + \tfrac{1}{2}\} \arccos(ax + c) \\
- \{2(az + c)^2 + \tfrac{1}{2}\} \arccos(az + c) \\
- 2\{2(ay - c)^2 + \tfrac{1}{2}\} \arccos(ay - c) \\
+ \{2(ax - c)^2 + \tfrac{1}{2}\} \arccos(ax - c) \\
+ \{2(az - c)^2 + \tfrac{1}{2}\} \arccos(az - c)
\end{cases}
$$

$$x = y - u_i \qquad a = 2\frac{(B - F)}{B \cdot d}$$

$$z = y + u_i \qquad c = \frac{b \cdot F}{B \cdot d}$$

Discussion

Q. Jos. H. d'ADLER-RACZ, Balteau S.A., Belgium:

In case of the different curves of read-out sensitivity shown, was the intensity of the viewer constant for each curve, or adjusted in view of an optimum?

A. In Figure 4, four different but constant intensities of the viewer were used. In the case of Figure 3, the intensity was adjusted to produce an optimum for the evaluating person showing these values as dots. Triangles are shown when the viewer intensity was too low to fulfil this condition.

Q. PIERRE RUAULT, Gaz de France, France:

L'auteur a-t-il essayé d'améliorer la perception de fins détails sur des films à haute densité, en supposant qu'il ne dispose pas d'un éclairement suffisant, en utilisant une loupe à faible grossissement, entre 2 et 5. Il semble qu'une telle pratique permettrait de bénéficier plus longtemps de l'amélioration de la qualité d'image avec la densité et s'accommoderait d'éclairement plus faible.

A. On ne s'est pas servi d'une loupe à faible grossissement, parce que ce mémoire couvrait seulement l'étude de la perception de fins détails sur le film en autant qu'une telle perception est liée à la densité et à l'éclairement du film. On n'a pas eu recours non plus à quelque autre aide technique.

Layer-Radiography with a Betatron

YŪGORO ISHII AND AKIRA KANNŌ, JAPAN

ABSTRACT: Layer-radiography with a betatron was applied to thick steel weldments to determine locations and shapes of defects. The fixed radiation source method was applied to movable samples, and the tomographic method was applied to samples welded directly to the 3000-ton fatigue testing machine.

The extent of fading in both methods was the same, and the sectioned layer width, with a 2-per cent detectability of the wire type defect, was determined to be 6 mm in the layer-radiography of a 100-mm thick steel plate.

Simultaneous four layer-radiography was applied with a 6-mm sectioning interval and four pairs of lead screens of 0.3 mm thickness. This method could detect almost all defects that could be detected by ordinary radiography.

Slag inclusion, a crack model and a nozzle weld part model were investigated and the defect locations were determined with a precision of 1 mm. The cracks, which were inclined to the radiation direction within an angle of the rotation, were detected more easily by layer-radiography than by ordinary radiography.

Introduction

The determination of locations and shapes of defects in thick steel plate weldments is frequently required because this information is considered indispensable in the analysis of mechanical test results.

Although there was no previous example of the application of layer-radiography with a betatron for nondestructive inspection, it was considered to be a very effective method for measuring locations and shapes in thick steel weldments.

Two methods were applied; the tomographic method and the fixed-radiation source method.

The tomographic method was applied to samples that were welded directly to the 3000-ton fatigue testing machine, setting the apparatus on one of the columns.

The fixed-radiation source method was applied to movable samples in a betatron radiography room. The apparatus used in the tomographic method was also used in this method, changing the driving mechanism.

The two methods showed quite similar results in the extent of fading of images which deviated from the sectioned plane. The preliminary experiments for the 3000-ton samples were then done in the betatron radiography room by the fixed-radiation source method.

This paper deals mainly with the experimental results on artificial defects. Slits were substituted for cracks, and rotated in the steel blocks. Slag was made artificially in welds. Drill holes with various diameters and at different locations in a steel block were used as the reference standard for the measurement of the extent of fading of defects deviating from the sectioned plane.

A nozzle joint model with artificial defects was layer-radiographically investigated and the results were compared with those of ordinary radiography.

Experimental results show that layer-radiography is superior to stereo-radiography in measuring the defect locations and shapes in nondestructive inspection.

Mechanism of Layer-radiography

A 15-MeV betatron is used as the radiation source; it has a 0.2-mm focus size and a 20-r/min.m of radiation intensity. The X-ray generator head is only about 780 kg in weight and is set on a carriage. This carriage is set on the layer-radiographic apparatus.

Fixed Radiation Source Method

Although light in weight, it is necessary to prepare a rigid set for the rotation of the head around the sample and prepare enough area when using the tomographic method. If the sample and the X-ray film are rotated around each axis at the same speed, at the point where the two axes are parallel to each other and on the same plane, including the fixed radiation source point, a layer-radiograph can be obtained. In the fixed-radiation source method, the apparatus has no need of such requirements. However, for this report the same apparatus was used in both methods by changing the driving mechanism. It was applied to movable samples in the betatron radiography room. Since simultaneous multilayer-radiography was considered an indispensable factor in the practical use of layer-radiography, this method was tried as well as the tomographic method. Figure 1 shows the mechanism for simultaneous multilayer-radiography in the fixed-radiation source method. The X-ray film is placed at y_2 distance from the film rotation axis. A plane which is at y_1 distance from the sample rotation axis is radiographed without obscurity, if y_1 and y_2 have the following relation;

$$y_1 = y_2 . R/R+r$$

where R is the distance from the rotation axis to the radiation source, and r is the distance between the two rotation axes. In the experiments reported R and r are 100 cm and 60 cm respectively. Any layer of the sample may be layer-radiographed by varying the film position. The enlargement ratio of the images of each film is R+r/R. The fixed-radiation source method is easily put to practical use.

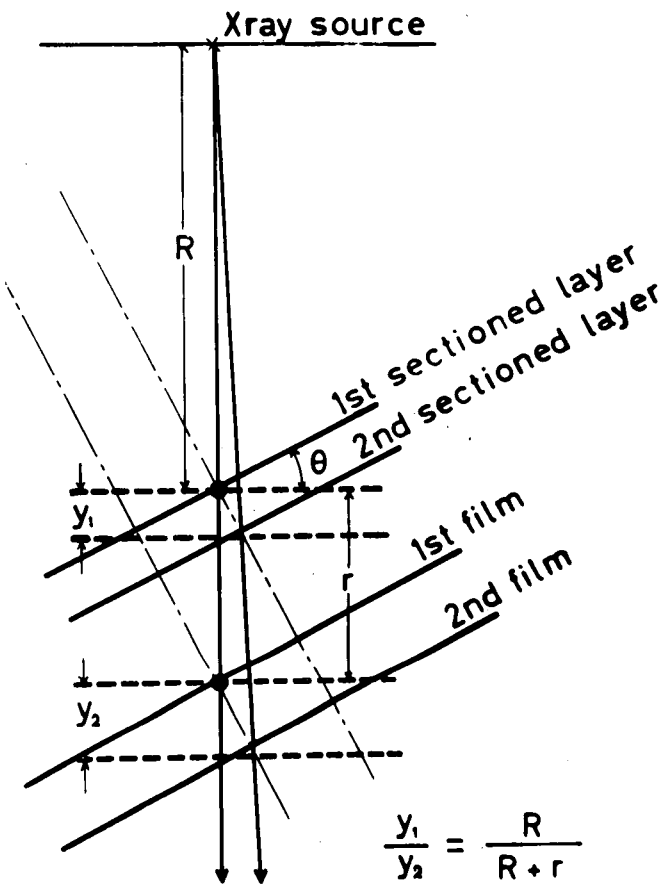

Figure 1. Mechanism of multilayer-radiography of the fixed-radiation source method.

Tomographic Method

The apparatus is set on one of the columns of the 3000-ton fatigue testing machine. Changing the driving mechanism to the tomographic method from the fixed-radiation source method, the apparatus is rotated around the sample with the betatron and the X-ray film facing each other. The tomographic method is shown in Figure 2.

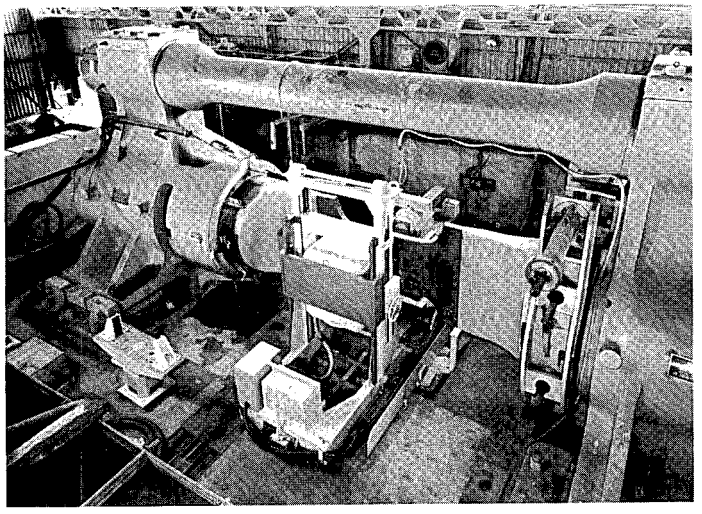

Figure 2. Application of tomographic layer-radiography to a sample of a 3000-ton fatigue testing machine.

The X-ray was well shielded so that the betatron could be operated four hours in a week.

Rotation Angle

The image gap between the image of zero rotation and the image of θ rotation was calculated in both methods, and varying the rotation angle the extent of fading of the images were examined (1).

From these results a rotation angle of $\pm$ 30 degrees was chosen, because the images deviating from the sectioned plane faded almost equally in a 60-degree or over rotation angle for a 100-cm-thick steel plate, due to the increase of the X-ray absorption in larger angles than 60 degrees.

Exposure Time and Film Density

For the layer-radiography an exposure time of 20% more than that for ordinary radiography of a 100-mm-thick steel plate with a 60 degree rotation angle was required (1).

In layer-radiography the images that deviate from the sectioned plane give a scattering effect on the X-ray film. If the ratio of the quantity of the direct ray to that of the scattering ray is constant, a high film density is favourable for photographic contrast. Film density of over 2.0 was chosen.

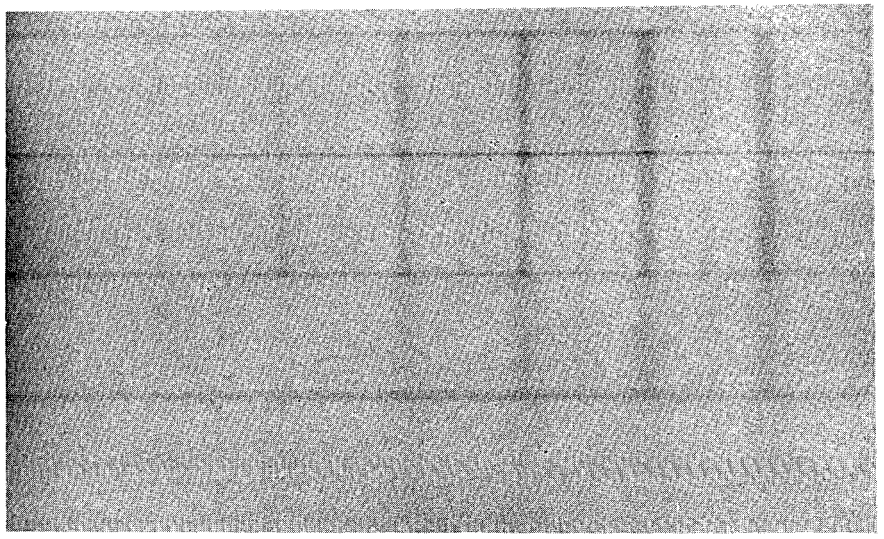

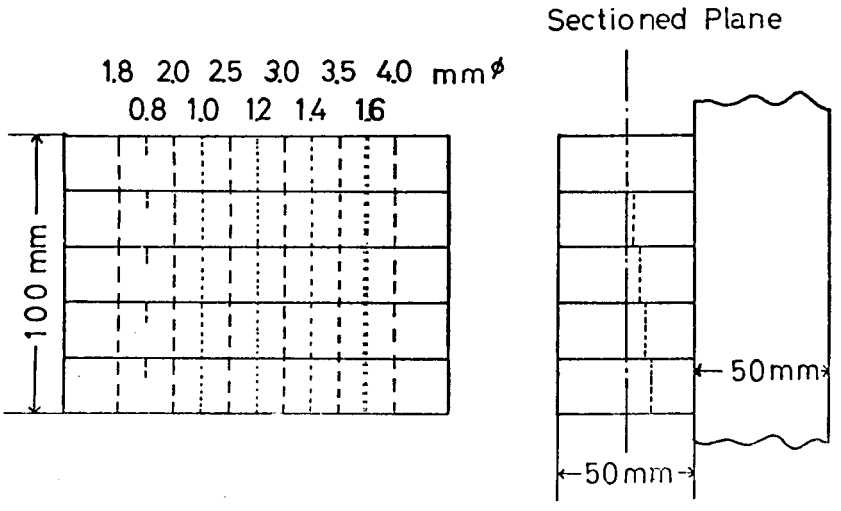

Figure 3
Layer-radiograph of the reference standard which has a series of wire type defects.

The rotation time for one shot can be varied from 2 min to 12 min with this apparatus.

Film densities in multilayer-radiography vary corresponding to their positions. Density differences occur mainly from the decrease of X-ray intensity by the absorption of lead screens in simultaneous four-layer radiography. The density differences estimated from the characteristic curve of the fine-grain type film (SAKURA RR) is about 0.15 at a 2.0 film density and 0.25 at a 3.0 film density, due to the X-ray absorption differences by a 1.8-mm plate which corresponds to three pairs of lead screens. In practice these values varied because the lead screen surfaces were not quite in the same condition. Despite the difference in densities it had no effect on the image qualities. It was not necessary to change the combination of the intensifying screens and X-ray film types as in the low-energy X-ray method.

Sectioning Width

For observing the fading of images that were on the other planes from the sectioned plane of the sample, artificial defects were used as reference standards.

One of them had drill-holes parallel to the rotation axis in a line of various hole diameters in a 2-cm-thick steel plate 5 cm wide. Five plates of this type were piled up so that the drill-hole lines made a step-like alignment deviating 2.5 mm horizontally. The drill-hole diameters are 4, 1.6, 3.5, 1.4, 3.0, 1.2, 2.5, 1.0, 2.0, 0.8 and 1.8 mm from right to left (Figure 3).

The other reference standard was made by piling 2.6-mm-thick steel plates, each with one line of drill-holes of various diameters; 9.0, 6.0, 4.0, 3.5, 3.0, 2.5, 2.0, 1.5, 1.0, 0.5 mm. These lines were not superposed vertically. This standard was set so that the thickness direction made a right angle to the sample rotation axis.

These standard samples were layer-radiographed with a single film. The visible diameters were plotted to the deviated distances from the sectioned plane. The images which showed their originals to some extent were plotted as visible. Figure 4 shows the experimental results. The ASTM equivalent percentage was calculated according to Criscuolo's equation (2).

The results show that the wire-type defects have a greater tendency to fading than the hole-type defects.

If a 2-per cent defect sensitivity for the wire-type defect is required, the sectioned layer width is determined to be 6 mm. With this sectioning interval, the samples were layer-radiographed with one or several shots by the simultaneous multilayer method. Any defect detected by ordinary radiography was almost always detected on at least one film.

After estimating the defect locations roughly, the second fine sectioning around the estimated locations was made. Comparing the obscurities of the images on each film, the defect location was determined precisely. The fine sectioning interval was about 2 mm.

Slag Inclusion

Artificial slag inclusion was made in the weldment of a 100-mm-thick steel plate. After the inclusion was layer-radiographed and stereo-radiographed, the sample was brittle-fractured across the defect. Figure 5 shows the cross-section of the slag inclusion, the ordinary radiograph, and a series of layer-radiographs.

The layer-radiograph was somewhat obscure because of the other part of the image which deviated from the sectioned layer. The extent of the obscurity increased remarkably when the sectioned layer itself deviated from the defect. Figure 5 shows that, when the sectioned layer deviates about 1 mm from the defect, the obscurity of the image increases markedly.

In practice, the interval of sectioning planes is about 2 mm in the fine sectioning. Then it is not difficult to choose the image which has less obscurity. By this method the spread of a defect in the direction of the radiation can be estimated with a precision of 1 mm.

By stereo-radiography, only the location of the centre of the slag is estimated, because the width of the defect obstructs the correspondence of the images of the two X-ray radiographs.

Crack

Although the detection of a crack is rather difficult by radiography if the crack depth is not favourable to the direction of the radiation, the measurement of its depth is sometimes required. Stereo-radiography of the crack is almost impossible, because of the inability of radiographical detection in at least one direction.

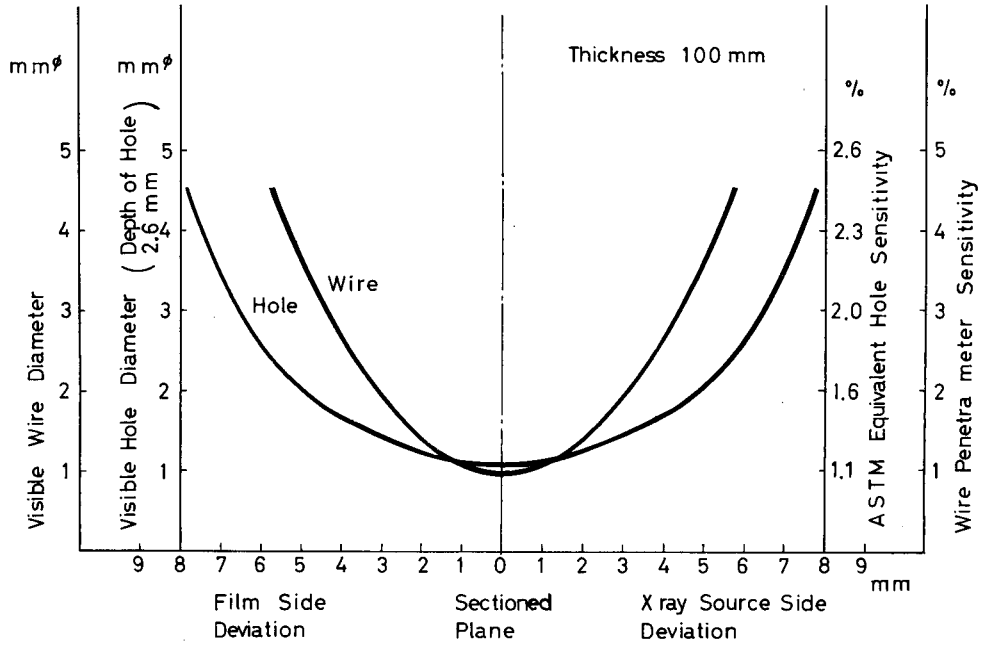

Figure 4
Relationship between the visible diameters of artificial defects, which are wire and hole types, and the distances from the sectioned plane in layer-radiography.

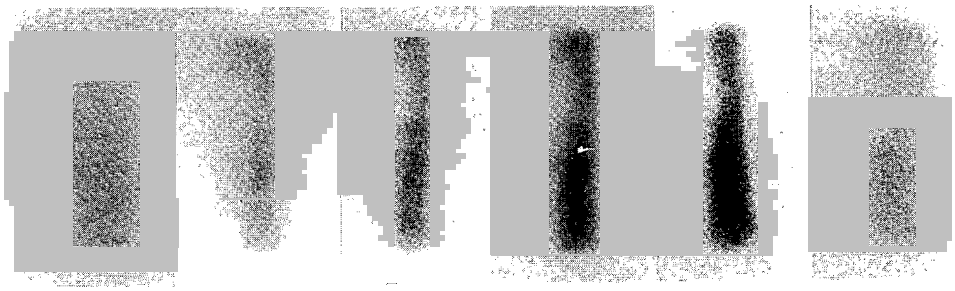

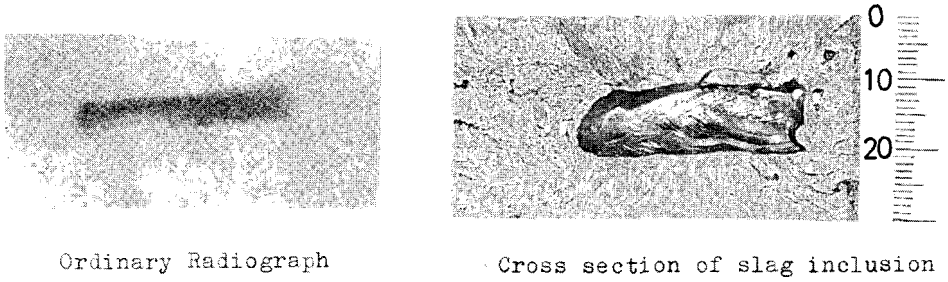

Figure 5
A series of layer-radiographs of a slag inclusion, and the ordinary radiograph and cross-section of the slag obtained by a brittle fracture across the slag.

In this report, the artificial crack was examined by layer-radiography. These artificial crack models are 5 cm in length, and 15, 10 and 5 mm in depth. The width of the crack is changed by the thickness of the spacer. The direction of the depth is varied by rotating the slit inside the steel block. The sample was made 100 mm thick by adding steel plates.

Fading of Crack Image

The three crack models were piled up so that the cracks made one plane. The sample was layer-radiographed from the source side to the centre of the cracks. The cracks were recognized when they were sectioned at 1.5 mm or less off from their edges. This means that the cracks fade to an equal extent, despite their different depths, and that the images deviating from the sectioned layer work mainly as the scattering ray, and the crack is not radiographed only when the depth direction becomes parallel to the direction of the radiation.

Angle of Crack and Detectability

Ordinary radiography could not detect the crack which had a 0.2-mm width and an inclination over 20 degrees to the direction of the radiation. The crack of 15-mm depth had a wide, vague image and could not be recognized as a crack when it inclined 20 degrees to the direction of the radiation.

With layer-radiography the crack with a 30-degree rotation angle could be recognized. The crack with a 35-degree angle could be recognized vaguely. Image fade-out occurred at 1.5 mm from the edge.

These experiments show that cracks are more easily detected than by ordinary radiography if the crack depth directions are inclined within the rotation angle of the layer-radiography.

Nozzle Model

One of the advantages of layer-radiography is that this method can investigate a part that is hidden by other parts. As one of the complex shapes examined, a nozzle weld part model was investigated by layer-radiography. This model consists of three main parts; a 100-mm-thick base-plate with a hole, a multi-ring-layer which has drill-holes as artificial defects, a pipe with a 200-mm outside diameter and a 100-mm inner diameter. Some of the rings are inserted in the base plate hole; the others are piled up at the foot of the nozzle pipe. This model also has a weld fillet model ring around the foot of the nozzle.

Simultaneous four-layer radiography with about a 6-mm sectioning interval was applied as the first stage of layer-radiography. After a rough estimate of the defect locations from the obscurities of the images, the second-stage layer-radiography with about a 2-mm sectioning interval was conducted around the roughly estimated locations. Comparing the obscurities of these films, the clearest image was chosen as indicating the nearest point to the defect location. Then the estimate was re-made with a precision of 1 mm. Figure 6 shows the layer-radiograph and the ordinary radiograph of the sample.

Conclusion

Betatron layer-radiography was tried on thick steel plate weldments and artificial defect models to obtain the precise locations and shapes of defects. The conclusions obtained are as follows.

1. Fixed-radiation source layer-radiography is a very effective method for a heavy X-ray generator such as a betatron, and can be applied to movable samples readily. The results obtained from this method are the same as those of the tomographic method, experimentally as well as theoretically.
2. The film density differences in simultaneous four layer-radiography with four pairs of 0.3-mm lead screens do not markedly affect the radiographic sensitivity in each X-ray film.
3. The sectioned layer width with a 2-per cent sensitivity of the wire-type penetrameter is about 6 mm in the layer-radiography of a 100-mm steel plate. Layer-radiography with a 6-mm sectioning interval detected almost all defects that are detectable by ordinary radiography, where R and r are 100 cm and 60 cm respectively.

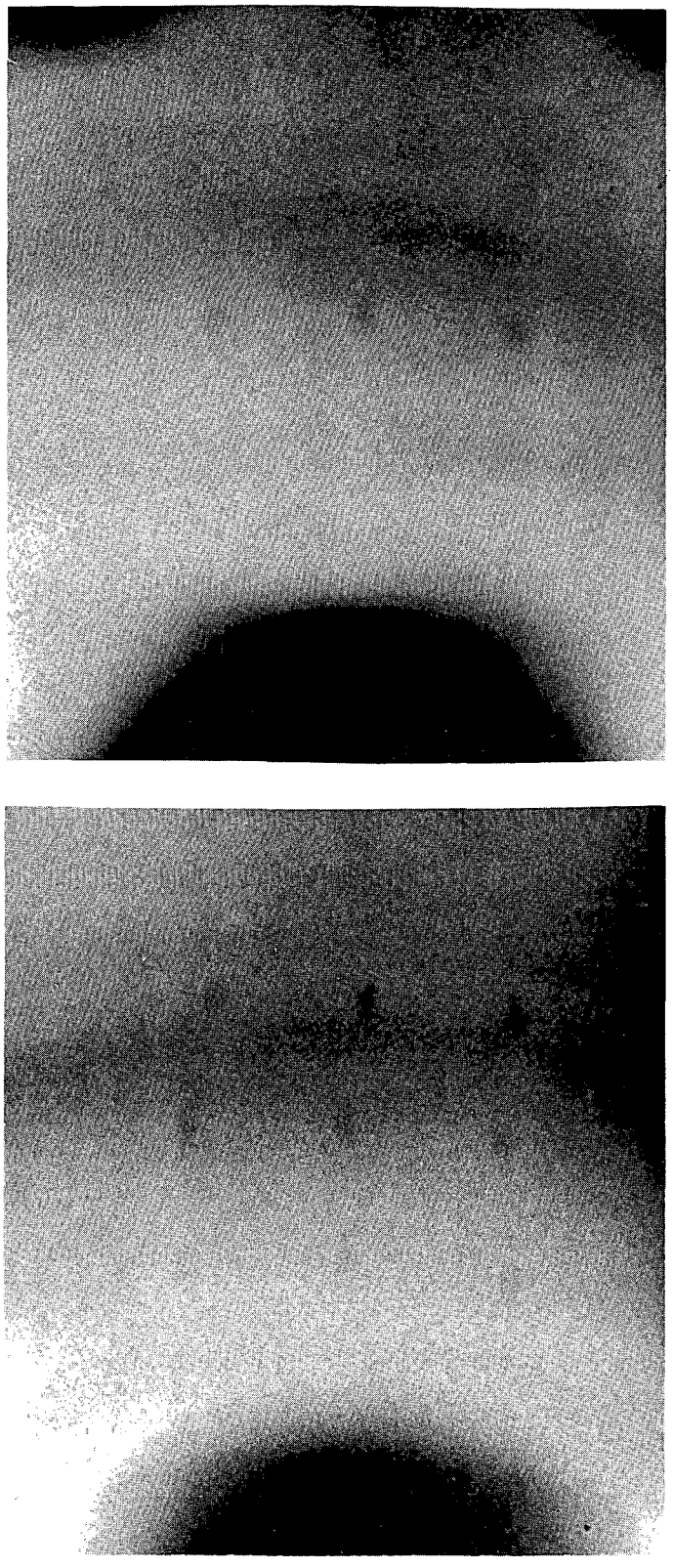

Figure 6. Layer-radiograph (upper) of a nozzle weld part model and an ordinary radiograph (lower).

4. Radiographic sensitivity on the sectioned plane is same as that of ordinary radiography.
5. Extent of a crack is determined by layer-radiography, while it is difficult to do so with stereo-radiography. If the crack depth direction makes an angle smaller than the rotation angle, layer-radiography shows superior detection of the crack than ordinary radiography according to crack model experiments.
6. The extent of the defect in the radiation direction only can be determined by layer-radiography, because of the width of the defect.
7. The location of many defects of a comparable size are determined only by the layer-radiography, because of the difficulty of the correspondences of the defect images.

References

(1) Ishii, Y. Ogura, Kannõ, A. and Sakaki. Layer-radiography with a 15-MeV betatron, *J. Nondestructive Inspection*, Vol. 14, No. 12.

(2) Criscuolo, E. L. and Polansky, D. The application of radiographic specifications, *Nondestructive Testing*, March-April, 1962.

Radiography within the Energy Range 100 kV to 15 MeV with ORWOCOLOR Films

H. U. RICHTER AND D. LINKE, GERMANY

ABSTRACT: Radiography with color films produces more information in the two additional parameters, hue and saturation, than does conventional black-and-white radiography.

Among the many techniques possible to produce color radiographs the direct technique was more closely investigated with the use of conventional color films. The transformation of the radiant energy into visible colored light was accomplished by the aid of fluorescence screens. The color contrast was increased by second-stage colored light exposure during the development process. Detailed densitometric investigations have been made and are disclosed. From the changes in hue and saturation it is possible to determine changes in the thickness of radiographed material. Also determinable from the hue is the tendency (decrease or increase) of such a change. An optimum exposure is possible by using the screen combination Zn Cd S / Pb 0.15. Exposure diagrams for radiant energies ranging from 100 kV to 15 MeV are presented. Exposure time and wire sensitivity are more unfavourable with conventional color films than with black-and-white radiography. The advantages associated with the color radiography are summarized.

Symbols Used

Exposure	B	(mA x min)
Thickness of material	d	(mm)
Color density	D	(–)
Color density behind blue filter	D_B	(–)
Color density behind green filter	D_G	(–)
Color density behind red filter	D_R	(–)
Focus-to-film distance	FFA	(cm)
Time of first-stage development	T	(min)
Time of second-stage exposure with green light	t_g	(sec)
Time of second-stage exposure with red light	t_r	(sec)
Intensifier screen combination	front screen/back screen	

Introduction

Owing to the two additional parameters, hue and saturation been published by Beyer (2, 3, 4, 5), Parish and Pullen (6), as can be obtained from conventional black-and-white radiography, which is characterized by brightness only. The many tested and suggested techniques for producing color radiographs have been described in detail by Richter and Linke (1). Of particular advantage to nondestructive testing of materials are the direct methods (not simulated), where a special or conventional color film is directly exposed to X-rays. Results of such tests have been published by Beyer (2, 3, 4, 5), Parish and Pullen (6), as well as by Richter and Linke (7).

In these tests, two different possibilities for transforming radiant energies and/or radiant intensities into visible colored light were employed:

a) The individual three color-sensitive layers of the color film are different in their sensitiveness to X-rays (Table 1, Figure 1). Color films especially sensitized for X-ray exposure permit, of course, of considerably shorter exposure times than conventional color films sensitized to visible light (1, 8).

b) Fluorescent intensifier screens transform the energy of X-rays into the visible range of the electromagnetic spectrum. The emission of fluorescence light lies, with the conventional types of screens (ZnS, Zn Cd S, Ca WO_4), in different wavelength ranges and results, therefore, in differences of hue on the exposed color film.

The following tests were carried out according to method "b" with the use of conventional ORWOCOLOR positive film PC 7. The development was done according to ORWOCOLOR instructions K 4 (9).

Table 1

Sensitive layer	Relative exposure (X-rays)	
	ORWOCOLOR Positive PC 7	KODAK Ektacolor-Print (6)
Blue	1	1
Red	2	16—20
Green	12	3—7

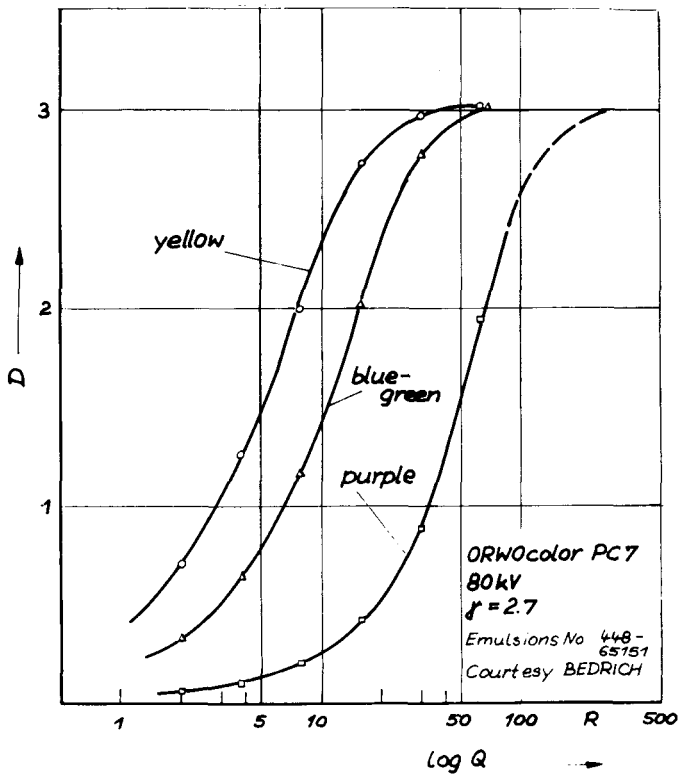

Figure 1. Partial color densities of the individual color layers of ORWOCOLOR film PC 7.

Densitometric Fundamentals

Detailed densitometric investigations were made in order to discover the optimum exposure parameters.

Energy Transformation

Tests on aluminium step-wedge penetrameters with a constant exposure were carried out, using the screen combinations M 100 / Pb 0.15 (M = Ca WO_4), ZnS / Pb 0.15 and Zn Cd S / Pb 0.15, in order to ascertain the influence exercised by different fluorescence light on the color densities. Informative tests with ORWOCOLOR negative film NT 17 disclosed

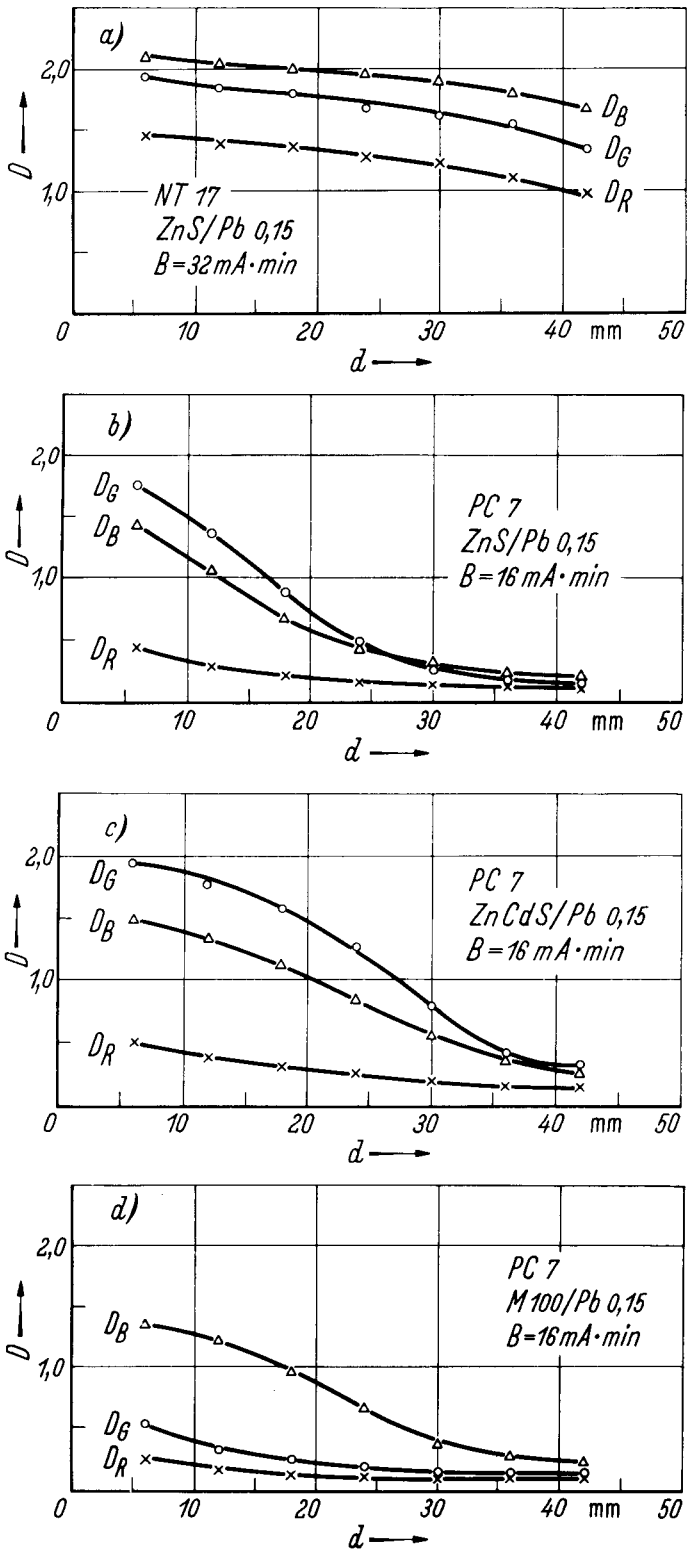

Figure 2. Partial color densities on ORWOCOLOR films NT 17 (negative film) and PC 7 (positive film) with different screen combinations and exposure of aluminum step-wedge penetrameter.

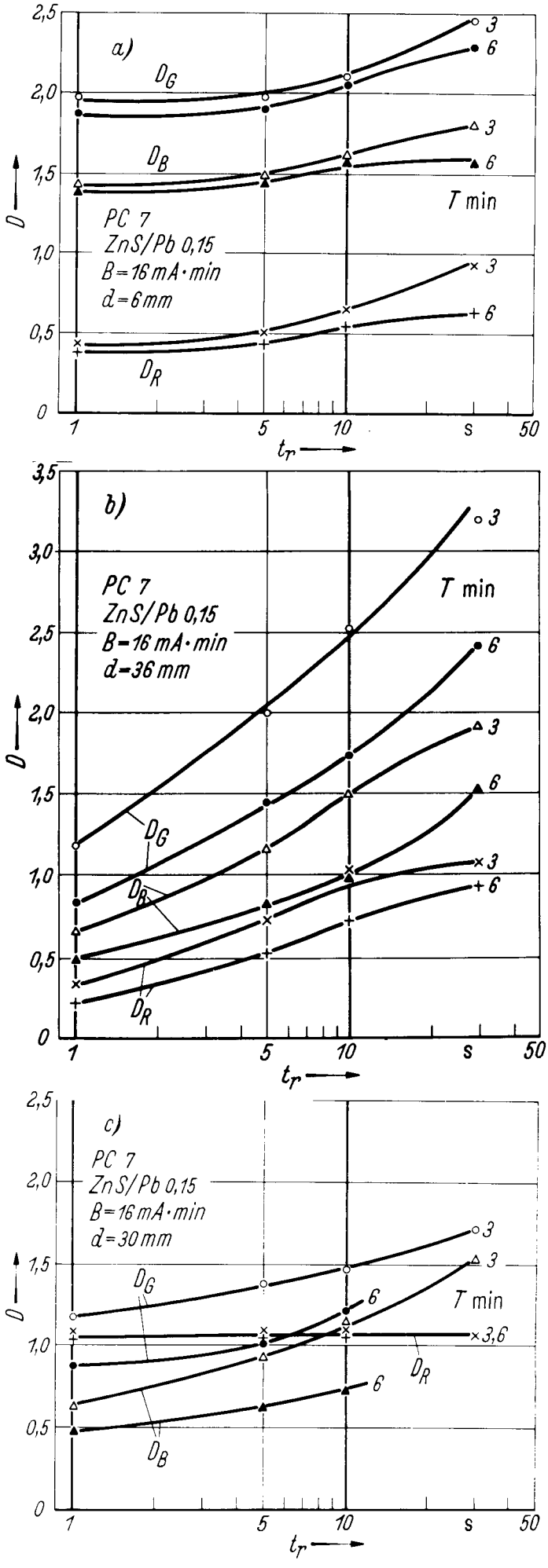

Figure 3. Partial color densities on ORWOCOLOR film PC 7 with varied times of first-stage development and second-stage exposure as well as second-exposure colors, with exposure of aluminum step-wedge penetrameter.

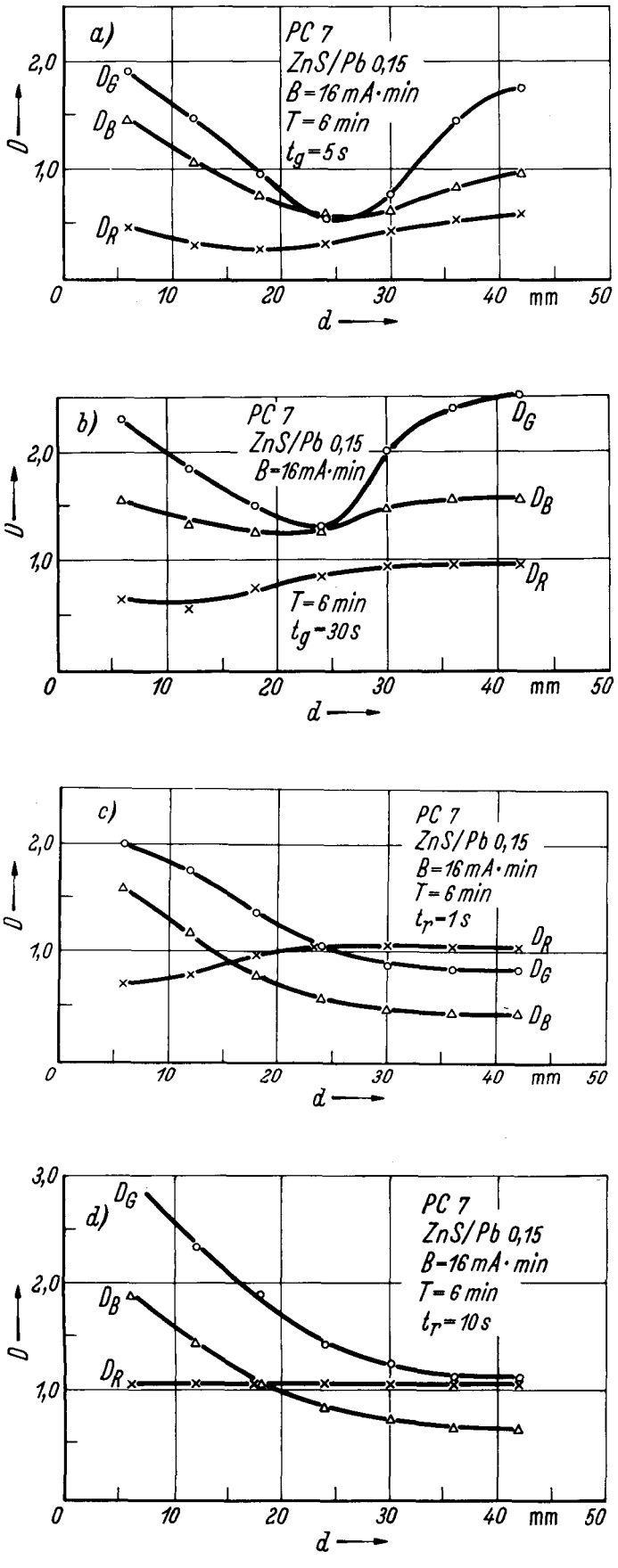

Figure 4. Partial color densities on ORWOCOLOR film PC 7 with second-stage exposure to green and red light respectively, depending on the material thickness of the exposed aluminium.

that with this film the partial color densities D_R, D_G, and D_B diminish only a little with increasing material thickness (Figure 2). The curves of the color densities are almost parallel so that, with different material thicknesses (or material densities), no hue changes but only changes in color density appear.

Using ORWOCOLOR positive film PC 7, a great influence of the material thickness is perceptible. The screen combination Zn Cd S / Pb 0.15 exhibited the most extreme differences of color density.

Increase of Color Contrasts

For increasing color contrasts Bryce (10, 11) has been recommended interrupting the processing of the color film after a certain time of first-stage development (12, 13). Subsequently the color film has to be subjected to a second-stage exposure to colored light. By this procedure, a colored exposure of the relatively thick or dense ranges takes place, which up to that stage had been unexposed or underexposed by the X-radiation. The ranges already exposed remain uninfluenced, since the silver image produced in the top layer through the first-stage of development acts like a black filter. Thereafter the procedure of developing is continued and finished in the usual way.

In these cases, the second exposures were carried out by the aid of green and red light of different duration and constant intensity (24 volt, 40 watt, 40 cm distance). The degrees of hue density rise as the duration of the second-stage exposure increases. The values with short times of first-stage development (T = 3 min) are higher than with long times (T = 6 min). On larger material thicknesses (d = 36 mm) too, the influence of the first-stage development time increases. (Figure 3).

As compared with shots without a second-stage exposure (Figure 2) it will be noted that, with a second exposure to green light and an equal second exposure time, the partial color density D_G shows a marked minimum (Figure 4). This minimum, however, implies an ambiguity of the color density, since there is an equal color density value for two different material thicknesses. Thus, different material thicknesses and material densities are featured by different colors, the time of second exposure (Figure 4) being without influence.

Generally it was ascertained that the color of the second-stage exposure increased the selective color density on the color film on those areas of the radiograph which, on account of too thick or too dense a material, were largely unexposed before. With this, an essential increase in color contrast is obtained. That means that different thicknesses of material also show different colors, so that the radiographed thickness of material can be determined by the change in color (Figure 5).

For practical material testing it is noteworthy that greater thicknesses or densities of material display a color different from those of lesser thicknesses or densities.

The diagrams shown here were made with a white "color" as a ground color (Figure 7). Normal material defects, such as cracks, pores, etc., appear in a blue hue, because the radiographed thickness or density of material was diminished in consequence of these defects. Heavy metal slag, such as may appear for instance in tungsten-inert-gas-welding (WIG), are displayed in a red hue.

Fundamentals of Test Techniques

Exposure

The exposure diagrams show that with the different radiant energies that were investigated for the screen combinations with different exposures and material thicknesses respectively, the differences in color as stated appear (Figure 6). Universal tests on aluminium with different screen combinations disclose that the

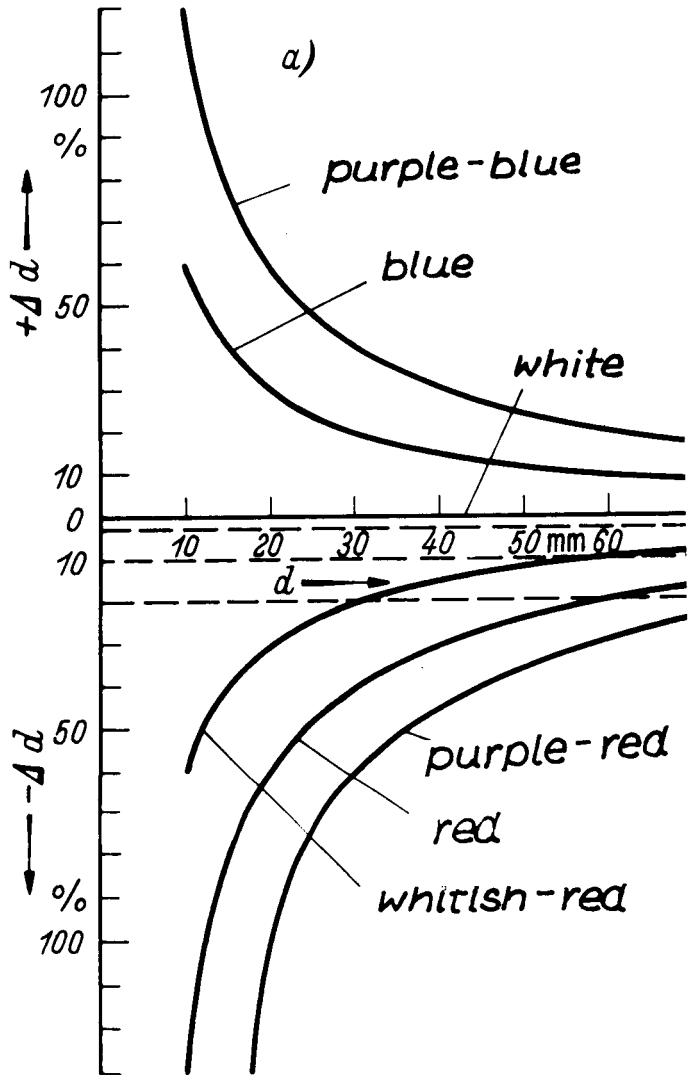

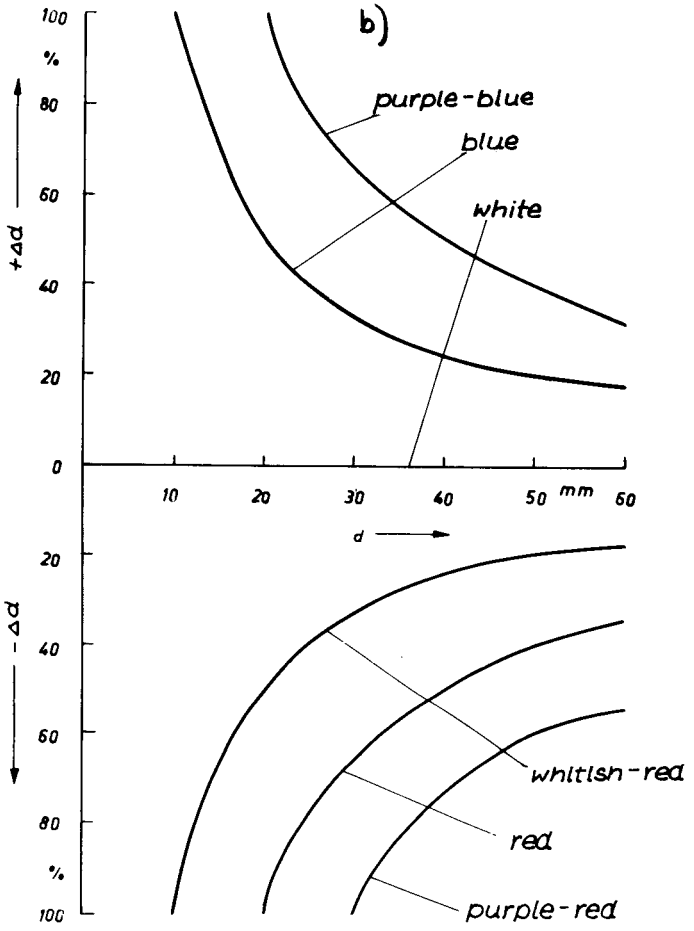

screen combination Zn Cd S / Pb 0.15 calls for a minimum exposure, whereas the screen combinations M 100/Pb 0.15 and Zn S / Pb 0.15 require an exposure approximately three times as long. Therefore, the necessary exposures with conventional color films and optimum screen combinations being used are in general still about 5 to 15 times as great as in black-and-white radiography.

Wire sensitivity

The relative wire sensitivity was likewise ascertained by the aid of step-wedge penetrameters. The tests with conventional color films showed somewhat poorer results (Figure 7) in relation to those obtained with special black-and-white X-ray films. Particularly interesting is the influence of secondary exposure to colored light during the process of developing. Those areas of the radiograph that were exposed to colored light only during the developing process, display an improvement of their informatory content. These areas of the radiograph contain a great color density of the second exposure color. But it is most remarkable that, with an equal gradation ($\gamma=2.7$), the color film allows a greater thickness range to be evaluated with but slightly less wire sensitivity than is possible in black-and-white radiography.

Conclusions

The tests described permit the following statements to be made:

a) Color radiographs comprehend a large range of material thickness and/or material density, displaying high contrasts at the same time.

b) Differences in thickness and density of material, and consequently material defects too, are shown not only by brightness differences, but also by different hue and saturation respectively.

c) In accordance with the tendency—i.e. with the increase or decrease in material thickness and/or material density—different hues and degrees of saturation respectively are shown.

d) The differences in hue and saturation respectively make it possible to determine quantitatively the depth extent (in the direction of radiation) of defects of the material.

e) Wire sensitivity is somewhat smaller than in black-and-white radiography.

f) The thickness range capable of being evaluated is, with the same gradation, greater than in black-and-white radiography.

Further investigations will still be necessary in order to search out the possibilities and the bounds of color radiography more comprehensively. Color radiography is apt to open up new fields of application in nondestructive material testing.

References

(1) Richter, H.-U. and Linke, D. Grundlagen und Verfahren der Color-Radiografie Die Technik 21 (1966) 424.

Figure 5. Diagrams for quantitative determination of the percentage of changes in radiographed thicknesses of material by evaluating the different hues.

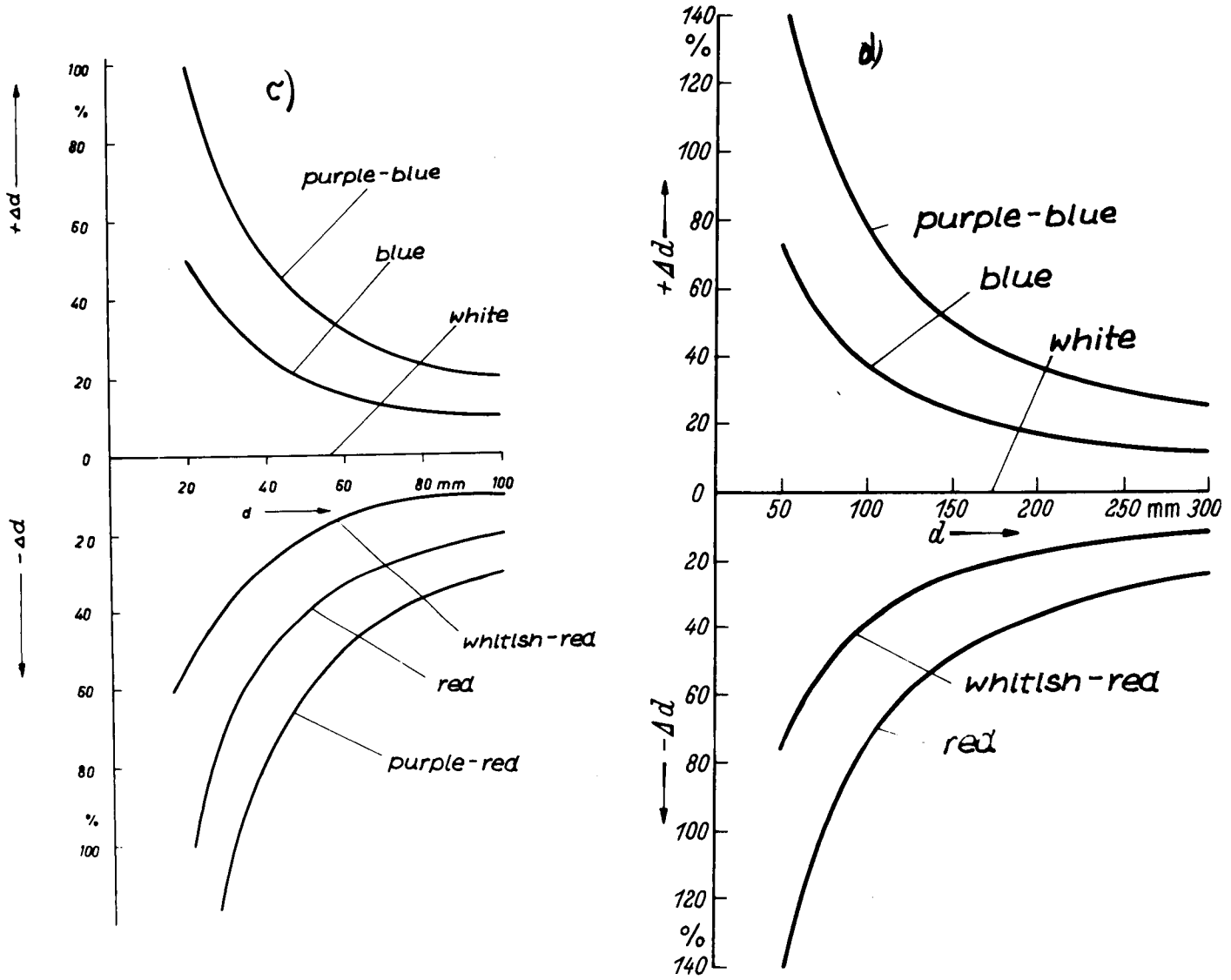

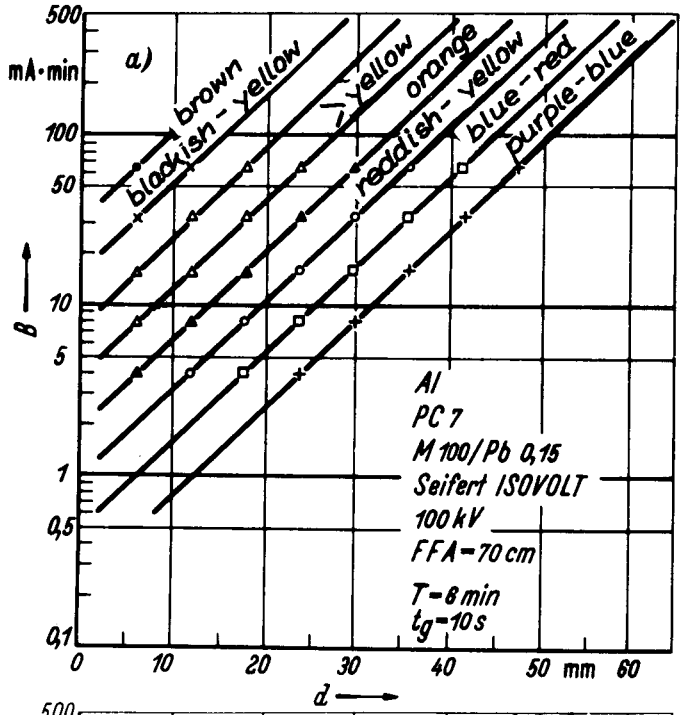

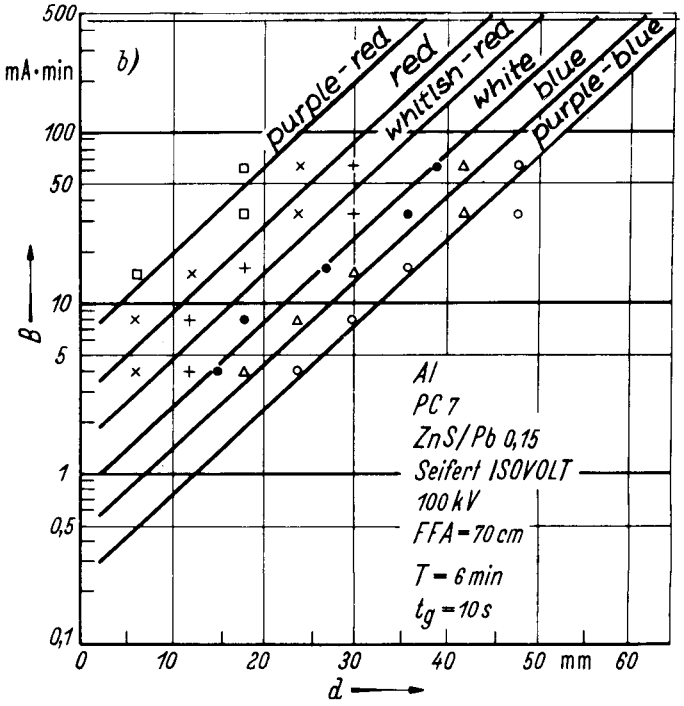

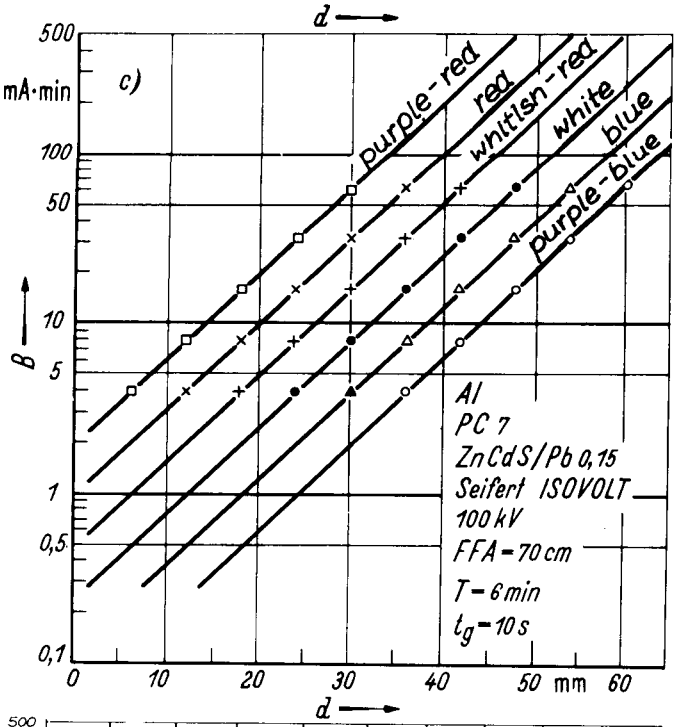

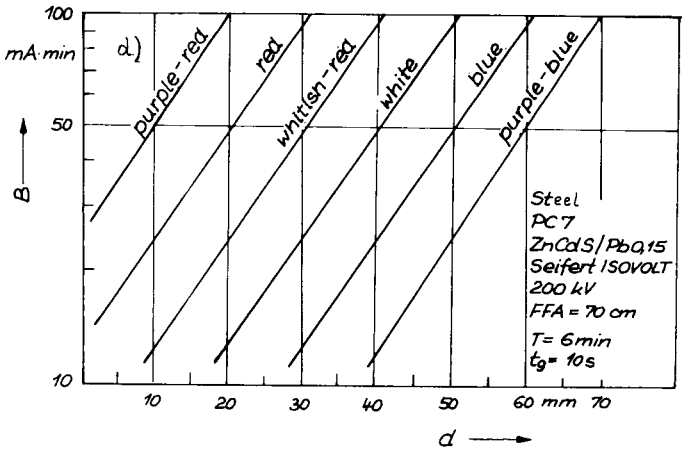

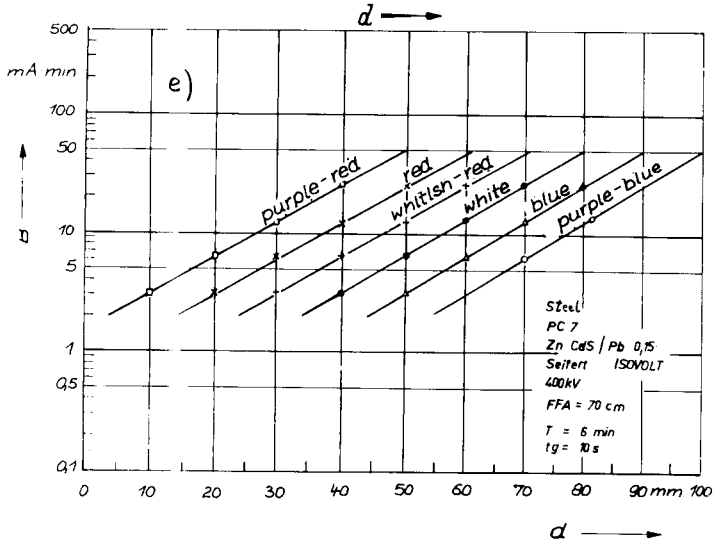

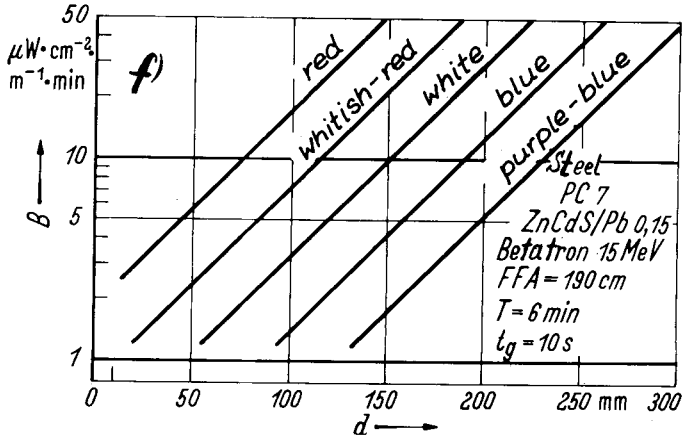

Figure 6. Exposure diagrams for color radiography on aluminum and iron within energy ranges from 100 kV to 15 MeV for ORWOCOLOR film PC 7.

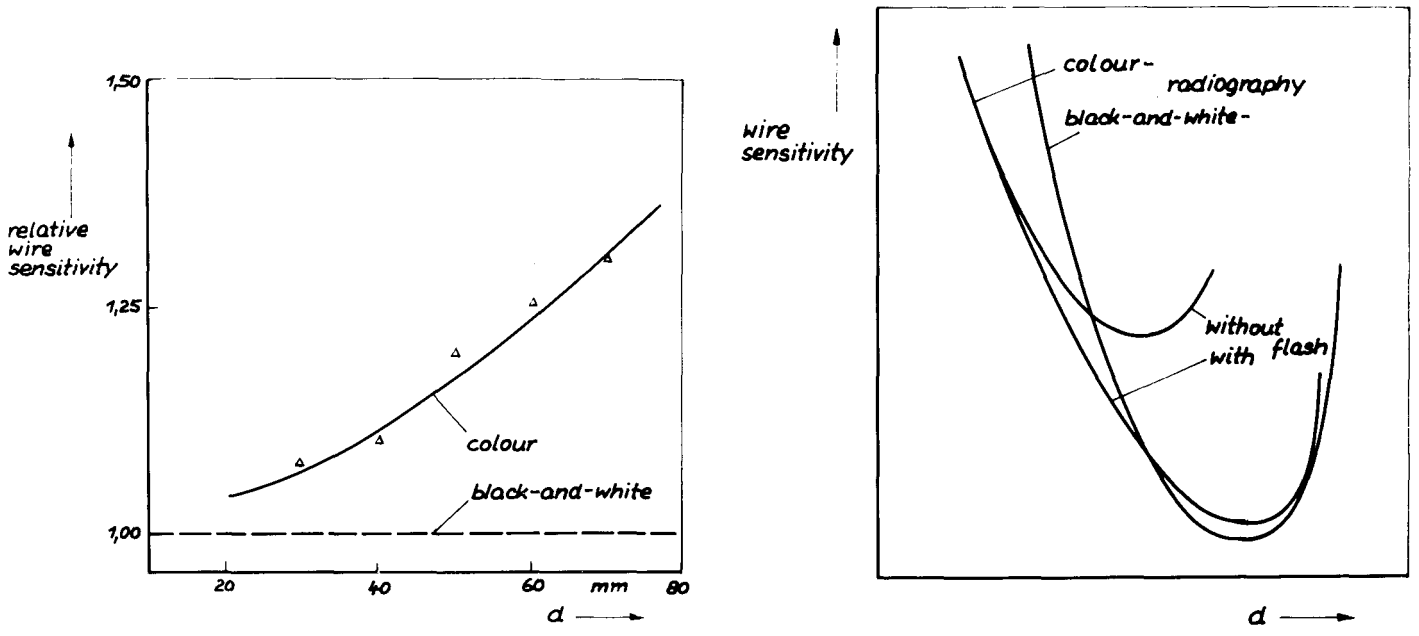

Figure 7. Relative wire sensitivity on parts of the film, without and with second-age exposure (black-and-white radiography = 1).

(2) Beyer, N. S. New Techniques in radiography. *Proc.* Third Annual Symposium on Nondestructive Testing of Aircraft and Missile Components, San Antonio, Texas/USA 1962.

(3) Beyer, N. S. Color-radiography. *Proc.* Second Annual Symposium on Physics and Nondestructive Testing. Argonne National Laboratory, Argonne, Ill./USA 1961.

(4) Beyer, N. S. and Staroba, J. F. Recent development in the production of color-radiographs. 26th National Conference of the Society for Nondestructive Testing, Chicago, Ill./USA 1966.

(5) Color-radiography-neutron. *Welding Eng.,* (1962) 68.

(6) Parish, R. W. and Pullen, D. A. W. The development of colour radiography into a routine service at A.E.R.E. Harwell. *Brit. J. Nondestructive Testing,* 6 (1964) 103.

(7) Richter, H.-U. and Linke, D. Color-Radiografie, ein neues Verfahren der industriellen Werkstoffprüfung, *Die Technik,* 21 (1966) 561.

(8) Industrielle Farbenradiografie, Gevaert-Agfa N.V., Mortsel/Belgien 1965.

(9) Orwo-Rezepte, VEB Filmfabrik Wolfen, Wolfen/GDR 1964.

(10) Bryce, A. Experimental color radiography, *Brit. J. Radiol.* 28 (1955) 552.

(11) Bryce, A. Color-radiography *in*: Clark, G. L. 'Enzyklopedia of X-rays and Gamma-rays' New York: Reinhold Publishing Corporation 1963.

(12) Wise, L. K. Colour-radiography, the photographic considerations, *Brit. J. Nondestructive Testing,* 8 (1966) 2.

(13) Richter, H.-U. and Linke, D. Farbmetrische Grundlagen der industriellen Color-Radiografie, *Die Technik,* 21 (1966) 497.

A Method for the Classification of Industrial X-Ray Film

D. POLANSKY AND E. L. CRISCUOLO, USA

ABSTRACT: The introduction of new X-ray films over the past ten years has resulted in the loss of identification of a given film type as being in a specified ASTM class. At the present time four classes are established based on a brief general description. The recent introduction of automatic processors and new developers has further outdated the present classification system.

A study has been conducted to evaluate the various parameters that might be used to characterize a particular film. Factors such as graininess and resolution are not as yet measured in a satisfactory manner. Recently developed methods of measuring resolution, such as the line spread function and modulation transfer will be reviewed. These methods should be of value in future classification of film. Specifically, the characteristics such as speed and average gradient should form the basis of a film classification system. It is proposed that a speed-film contrast index, $\eta = \bar{G}\sqrt{r}$, be used to classify film.

Introduction

Existing methods of classifying X-ray film are proving inadequate to the requirements of modern inspection needs. There are several reasons for this situation. The development of automatic processors with their relatively short cycle of dry exposed film to dry radiograph has modified the characteristics of film. The processing cycle with its higher temperatures required changes in the developing solution; this affected the granular appearance of some films. In addition, the continuing demand for increased resolution and finer grained film resulted in the introduction of several new X-ray films. The result has been that there is no method for purchasers to classify the newly developed film. One can purchase as many as half a dozen different films that are characterized as having high contrast and fine grain.

One of the early systems for rating industrial film was given in a paper by Kahn, Imbembo and Bland presented to the Annual Meeting of the American Society for Testing and Materials in 1949(1). They rated film as type I or type II, with type II being the film used with fluorescent screens. Within type I they differentiated between films by the speed rating for a net density of 1.0 and 1.25. The slowest film was designated as having very fine grain and high contrast while the fastest film (about 15 times faster) was described as extremely fast, moderately high contrast.

In 1957 the Navy published an interim Federal Specification for Film, Radiographic, Industrial and Medical (W-F-00350 Navy-Ships, 28 August 1957). This specification followed the ASTM published system as to class and type of film. In addition it had a table that listed the speed at several energies. The following table is from that specification.

Here the energy dependence of a film can be noted and at a given energy the finer grain film has the slowest speed. The final table in that specification lists the classes and identifies several films in each class. Unfortunately the wide latitude of speed within a given class gave rise to the question of differentiating between the films in a given class. Finally, the introduction of several new films and the inevitable question "What class is it"?, indicated that the film classification system should be updated.

Table 1

Film Speed and Contrast Range

Type	Class	100 kV range*	200 kV range*	Gamma Ray*	Average Gradient
I	1	2.0–3.8	1.0–2.2	0.1–0.4	3.0–3.5
	2	5.2–9.5	2.5–5.2	0.5–1.0	2.5–3.0
II	4	17.0–29.4	6.5–12.0	1.0–2.1	2.2–2.8
		6.0–11.5	3.0–6.5	0.5–1.5	1.7–2.2

*Film speed as given is proportional to the numerical rating—the larger number indicates less roentgens are required to achieve a given film density.

Requirements of an X-ray Film Classification System

If we are to update the present system or to introduce another one we should meet some rather broad requirements. The system should be flexible enough to include future film changes and developments. It must be definitive; at different energies or densities the film characteristics should be listed. In addition, standard test procedures must be agreed upon by manufacturer and consumer through the exchange of ideas at meetings such as SNT and eventually formalized in ASTM or ASA standards.

After reviewing the literature and having discussions with film manufacturers and film users it became apparent that there was general agreement that some changes were necessary. The specific properties of film to be measured were widely discussed and some accord was reached on several parameters.

The characteristic of speed could be measured within ±20 per cent. The average gradient could be measured within ±10 per cent (2). It was felt that the aging property of film was adequately covered by the manufacturer's expiration date. What is implied by this date is that the speed and average gradient are within the tolerance of the specification. The graininess of film is a difficult thing to express and it was felt that this characteristic is implicit in the definition of speed. The uniformity of the emulsion on a given sheet is probably best indicated by a comparison to a visual reference standard. The establishment of a visual reference standard is in the future. One of the more informative features of film, its

resolution, is one of the most difficult to measure in radiography. At the present time there is no agreement on a means of measuring resolution; however some recent experimental work indicates a beginning in this direction.

Film Resolution

The resolving power of a film (resolution) is described as the ability of photographic emulsions to record fine detail. While this definition is quite general, it is important to bear it in mind while discussing various methods of measurement in order to see that the method fills this requirement. Graininess is a good film indicator but it is difficult to measure. It also does not take into account the effect of screens on image resolution. Because of these difficulties no attempt has been made to evaluate the film by this parameter at the present time. Other methods of resolution measurement are visibility of holes, unsharpness and spatial frequency.

The threshold visibility of holes in a test object has been used to indicate film resolution. An absorber with several shims of different thickness each containing a series of holes with decreasing diameter is radiographed. Then the relative contrasts

$$\frac{\Delta X}{X}$$

is plotted on log-log paper against the smallest hole diameter perceptible. The data from each film results in a straight-line plot that is parallel to that for other types of film; the position of the lines is an indication of film resolution. An example of a curve is shown in Figure 1. The position of the lines is related to the signal to noise ratio and at the centre of the curve follows the relationship (3).

$$c = \frac{k}{d}, \text{ where } c = \text{contrast}$$

d = hole diameter

k = constant related to the threshold signal to noise ratio

It should be noted that as the hole diameter is increased the contrast level reaches a lower threshold limit. This threshold contrast limit is the same for detection of large areas. As the contrast is increased the smallest hole size detectable is also limited. These limits are shown by dotted lines. The method of measurement is of limited value to evaluate film resolution since the limits of detection appear to vary considerably among several readers.

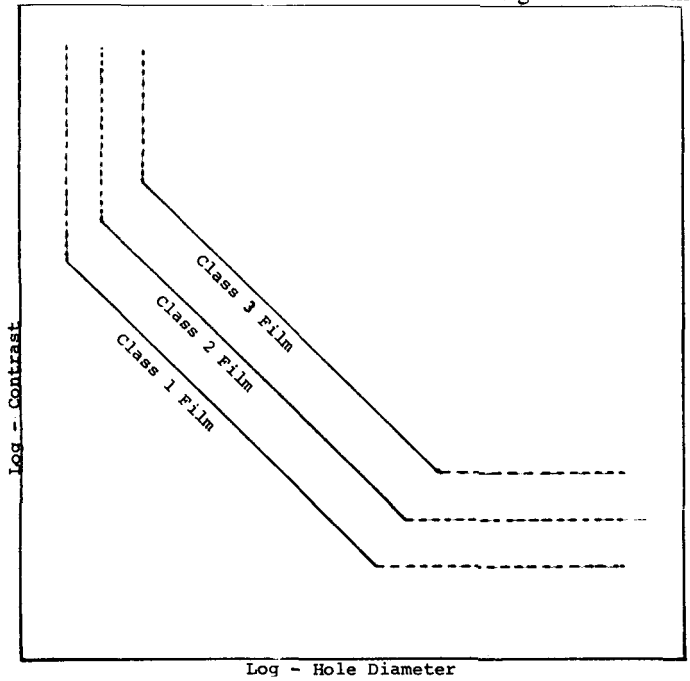

Figure 1. Minimum hole size vs. contrast for several films.

Film unsharpness is also used to evaluate resolution. In the measurement of unsharpness, a radiograph of a step wedge is made. By means of a scanning microdensitometer a density profile is measured and a numercial value of unsharpness is obtained by Klassens method (4). This method does not take into account the shape of the curve. It attempts to fit a straight line for the "S"-shaped unsharpness curve. Obtaining and measuring the unsharpness curve is difficult because the object edge must be carefully aligned with the X-ray beam.

In addition, all other unsharpnesses in the system must be reduced so that they are negligible. While this method is valuable it does not give a number that indicates an absolute value of resolution.

More recently, the line-spread function and modulation-transfer function have been used to evaluate films. The line-spread function can be described as the resulting intensity distribution on a film due to a line of radiation of microscopic width. This intensity distribution produces on the film a density variation that has a bell shape. By convoluting this function with a sine function the spatial frequency concept can be introduced. This convolution is called the modulation-transfer function. The results obtained give information similar to the line-test chart used in specifying TV resolution.

Recent experiments (5) have enabled direct measurement of the spatial frequency of films at 10 MeV. This work is still in progress and does offer a possible method for the measurement of radiographic resolution of film. In this film classification work no attempt has been made to evaluate this parameter.

Measurement of Speed and Average Gradient

There has been considerable interest in the past few years in the use of betatron radiation for the inspection of propellent. The use of this energy range for film classification meets our immediate needs. The experimental technique used to gather the film classification data was as follows:

Energy	10 MeV
Absorber—	3 HVL of propellant placed adjacent to the film
Intensifying Screens—	.060″ lead front .010″ lead back
Processing Equipment—	Kodak Model B Processor with liquid chemicals

The radiation field was such that density variation across the film was no greater than 0.04. Strips of film 1 in. wide by 3 in. long were placed in a 14″ × 17″ cassette. Films of the three major U.S. manufacturers were checked. A series of exposures were made, the entire series of film developed and the densities read on a Macbeth Ansco densitometer. The data were plotted on semi-logarithmic paper (density—log exposure) and from these plots the values of average gradient and relative speed were obtained, as shown in Table 2.

In this data it is noted that the average gradient between densities of 2.0 and 4.0 gives values that distinguish between films in a given class. The gradients at the lower density range are equivalent for at least six films. It appears therefore that this added measurement can be of value in a classification system.

Table 2
Speed and Gradient of Films with 10 MeV

Film no.[1]	ASTM Class	Relative Speed at D=1.5	Relative Speed at D=3.0	Average Gradient .5–2.5	Average Gradient 2.0–4.0
1		1.5	.7	3.0	4.7
2		1.7	.8	2.9	5.3
3	1	2.7	.9	2.2	4.2
4	1	2.7	.9	2.7	4.1
5	1	3.2	1.5	2.9	6.1
6	2	19.6	9.0	2.7	5.5
7	2	11.9	3.3	2.5	3.3
8	2	13.9	6.4	3.1	4.9
9[2]		1.0	.4		

[1] X-ray film are from Ansco, Dupont and Kodak. Films are numbered from one through 9.
[2] Film number 9 was arbitrarily selected as having unit speed to reach a density of 1.5.

Speed-Film Contrast Index

Of the parameters discussed it appears that the measurement of speed and average gradient gives reproducible numbers. The question one asks is, "Can these numbers be combined to produce an index that differentiates between film"?

Film speed is inversely associated with resolution; in general the faster the film the poorer the resolution. Film speed is also an inverse measure of the number of photons and photoelectrons that interact with the film. With these interactions there is associated the statistical deviation of a random process that is proportional to the square root of the number of events. One can assume that the recording ability of film is proportional to $\sqrt{r}$ where r = roentgens incident on the film. Thus $\sqrt{r}$ is one parameter used in the establishment of a film index.

Film gradient, the other parameter, is the slope of the density-log exposure curve at a given point. The average film gradient is the slope between two arbitrary density points. Increased film resolution is reported to be a direct result of higher film gradients. One can assume therefore that the film contrast index is proportional to the average gradient. Combining the two parameters into a single speed-film contrast index η, where $\eta = \bar{G}\sqrt{r}$ should give us a number that differentiates between the film types.

Since the measurements at 10 MeV gave good results, it was decided to make additional preliminary measurements at 200 kvp to investigate the energy dependence. The 200 kvp data were taken in an experimental manner similar to the technique used at 10 MeV. The energy of 200 kVp was achieved as specified in ASA PH 2.8—1964, Sensitometry of Industrial X-ray Films[(2)].

Table 3 shows the speed contrast index at two different energies. η_1 is calculated with the average gradient between densities of 0.5 and 2.5 and $\sqrt{r}$ is measured at a density of 1.5. η_2 is calculated with the average gradient between densities of 2.0 and 4.0 and the $\sqrt{r}$ is at a density of 3.0. The film strips in this comparison were developed by hand at 68°F in Kodak rapid X-ray developer.

Let us look at the speed-film contrast values in relation to our objective. A differentiation is maintained between the classes. Within a given class there is a significant difference between several films. The system does not become obsolescent with the introduction of finer grained film (slower speed) or film with increased gradients.

Let us refer to the table again and briefly consider the effect of X-ray energy. At these two energies the values are generally consistent with each other with the exception of the new films recently introduced. Even in this case the only gross deviation is with film number 2. If this difference is consistent when checked again it may be necessary to have tables of η versus selected X-ray energies.

Table 3
Speed—Film Contrast Index

Film No.	ASTM Class	η_1 10 MeV	η_1 200 kVp	η_2 10 MeV	η_2 200 kVp
1		5.6	5.1	19.2	14.3
2		7.5	5.4	32.6	15.6
3	1	2.6	2.0	7.9	7.3
4	1	2.4	2.9	13.3	11.1
5	1	3.8	3.2	13.8	11.7
6	2	1.1	1.1	3.1	3.4
7	2	1.4	1.4	4.9	4.2
8	2	1.6	1.4	5.3	4.2

As previously stated we had an immediate interest in the response of films used in the X-ray range of 10-25 MeV. The two sets of films that were exposed simultaneously at 10 MeV with those listed in Table 3 were developed in different developer systems. The second set was developed in a Model B X-OMAT with Hunt liquid chemicals and the third set was hand developed in Kodak Rapid chemicals. Following the established procedure of plotting the characteristic curves, measuring the average gradients at the selected points and determining the exposure to give the required densities, we calculated the speed contrast index η. Table 4 lists the results obtained.

In this table it is noted that the two liquid developers in general give similar results; that is, the previously designated classes of film give separated values of η. Within a given class it is noted that one developer gives superior results, that is, film number 7 if used at η_1 level appears better suited to the Hunt chemistry. At the η_2 level an advantage in chemistry is not evident for this film. At the η_1 level all three chemistries give compatible results with a slight difference in films 1 and 2.

At the higher density level, the development of film by hand at 68°F gave consistently higher index values. This is in agreement with the observed fact, that developing film at increased

Table 4
Speed—Film Contrast Index

Film No.	Class	$\eta_1 = \bar{G}_1\sqrt{r}_{1.5}$ X-OMAT MX589 Chemical	X-OMAT Hunt Chemical	Hand Dev. Kodak Rapid Chemical	$\eta_2 = \bar{G}_2\sqrt{r}_{3.0}$ X-OMAT MX589 Chemical	X-OMAT Hunt Chemical	Hand Dev. Kodak Rapid Chemical
1		4.7	3.8	5.6	13.2	11.0	19.2
2		3.9	5.8	7.5	13.9	20.0	32.6
3	1	2.0	1.6	2.6	6.4	5.0	7.9
4	1	2.4	1.9	2.4	7.0	6.8	13.3
5	1	3.1	3.8	3.8	10.5	8.8	13.8
6	2	1.1	1.0	1.1	2.6	3.0	3.1
7	2	1.1	1.8	1.4	3.7	3.0	4.9
8	2	1.2	.9	1.6	3.6	3.5	5.3
9		2.2	2.0	2.2	6.4	6.0	9.2

temperatures (both X-Omats operated at 81°F) increases the apparent graininess of a film. Since increased graininess degrades resolution at the minimum observable threshold limits, the effect of decreasing value of η is in the right direction.

For the facilities that use megavolt radiation and automatic processors it is concluded that the calculation and tabulation of η_1 and η_2 values will be of value in determining film response in the complete radiographic system.

Summary

Many of the parameters that can be used to classify film are very difficult to measure. As a result of this study it was found that the film speed and average gradient can be used for this purpose. While resolution is an important consideration, it is not advisable at this time to use it to gauge film.

A simple method of combining film gradient and speed is to take the product of film gradient and the square root of exposure $\overline{G}\sqrt{r}$ (where exposure is defined as the roentgens incident on a film to achieve a given film density). This product is defined as the speed-film contrast index η. Experimental results at 200 kVp and 10 MeV indicate that the η can distinguish between film types. The development of three sets of film in three different chemistries also showed that this method of classifying film gives consistent and distinctly different values of η for the different classes of film.

In conclusion, this method of classifying film has the following advantages:

1. It gives a separate number for each film type and does show small differences between different film.
2. It is simple to use and to calculate.
3. It provides for future introduction of new films.

It is proposed that the speed-film contrast index be used as the means of classifying film in their response relative to a specified energy, screen and chemical processing combination.

Acknowledgments

The authors wish to acknowledge the contribution of D. P. Case of the NOL Staff for his assistance in gathering the film data. Our thanks also to representatives of the various film manufacturers for their cooperative efforts on this task. Members of ASME and ASTM contributed through discussion of the many problems involved.

References

(1) Kahn, N. A. Imbembo, E. A. and Bland, J. Film rating factors for industrial radiographic film for use with Universal Exposure Calculator. Presented at 1949 Annual Meeting of the American Society for Testing and Materials.

(2) American Standard Method for the Sensitometry of Industrial X-ray Films for Energies up to 3 Million Electron Volts—American Standards Association, PH 2.8, 1964.

(3) O'Connor, D. T. and Criscuolo, E. L. The quality of radiographic inspection, *ASTM Bull.* No. 213, April 1963.

(4) Klassens, H. A. Measurement and calculation of unsharpness combinations in X-ray photography. *Philips Res. Reports,* Vol. I, No. 4, pp. 241-249, Aug. 1946.

(5) Criscuolo, E. L. and Dyer, C. H. Measurement of spatial frequency response of radiographs. Presented to Society for Nondestructive Testing, fall, 1965.

Discussion

Q. RONALD HALMSHAW, Ministry of Defence (UK) RARDE, Sevenoaks, England:

Your method of classifying films is a most interesting one and will be valuable if the measuring techniques can be standardized between different laboratories and countries. The most difficult measurement is the dosage received by the film; are you proposing standard techniques of measurement for different kilovoltages which other laboratories can reproduce? Should you not consider film-screen combination rather than just a film?

A. Rather than measure the dosage received by the film, we propose to measure the dosage incident on the film. This dosage was measured using integrating ionization chambers. When properly calibrated, these chambers are accurate within plus or minus 5 per cent. The measurement of dosages at X-ray energies above 2 MeV should definitely be standardized; we used a one-eighth-in. (3-mm) lead cap around the thimble chamber, while some laboratories prefer the 11.5-cm cube of lucite.

We originally began to develop a system to classify film only and found that what we have is the response of film to a given X-ray energy-screen and processing combination.

Evaluation of the Strength of Castings Based on Radiography

ZBIGNIEW GODLEWSKI, POLAND

ABSTRACT: In this report one method classifying castings with flaws is presented which is supported by comparison with specific deformation (contraction) work and the ratio of plastic deformation resistance to cleavage strength.

This method was verified during strength investigations and radiographic examinations.

Introduction

Radiographic testing makes possible the detection of flaws hidden in material, although this does not necessarily constitute the measure of its quality.

Today methods sensitive enough to detect any defective parts are available, but only in a few cases is it possible to predict the behaviour of the material under working conditions. The well known ASTM method classifies castings by grade on the basis of reference standard radiographs which are yardsticks that vendor or purchaser may use as they see fit(1). These standards are based on the experience and needs of purchasers and users and as yet are not subject to a broader approach by accurate investigations as well as strength calculation. Attempts to organize the problem of quality evaluation for castings have been made in other countries as, for example, in the report issued recently by the Zentral-institut für Giessereitechnik in Leipzig or the Csepel-Works in Budapest(2). All these interpretations of the results of testing are subjective and their influence should be minimized; it is felt that a verdict on the quality of a casting (good or bad) should be objective. There are two ways to investigate the influence of flaws upon the properties of castings:

—statistical—which requires many experiments, and

—analytical consisting of analytical evaluation of the influence of well defined flaws upon the properties required for a given casting.

Gillemot (3) is following the analytical method in research on flaws in weldings and J. Nemec (4) on flaws in castings.

Object of the Investigation

It is well known that flaws in castings take the form of holes acting as notches and causing the effect of concentration of stress. In any kind of stress that depends upon the shape and the number of defects, the strength of material is characterized by specific deformation. L. Gillemot in (5) has shown that the amount of specific deformation, or contraction, depends mainly on the factor of stress concentration but is independent of the size and shape of the tested sample. Its value can be calculated from the equation:

$$A = \frac{\delta_k \lambda_k}{\lambda_k + 1} \tag{1}$$

where: δ_k —true stress on the boundary of uniform distortion;

$\lambda_k = \ln(1+e)$ —elongation on the boundary of uniform distortion;

ε —true elongation on the boundary of uniform distortion.

Since the material with the flaw is usually destroyed during mechanical examination within the boundaries of uniform distortion therefore δ_k can be considered as the cleavage strength and ε as the total true elongation. On the other hand the state of stress caused in the sample under test, can be best characterized (based on the theory of N. N. Dawidenkow—J. B. Friedman (6)) by the ratio of plastic resistance δ_a to the cleavage strength of a given material R_0

$$r = \frac{\delta_a}{R_0} \tag{2}$$

The magnitude of the numerator depends upon the type of flaw that effects the concentration of stress. The denominator is dependent on the material only. The lowest value δ_a corresponds to yield point Qr of a flawless material.

The increase of this value δ_a may be observed in the brittle cracking of the sample, which results from the type of stress of the material and the shape and type of defect. The material is susceptible to brittle cracking the more the above ratio increases.

The object of investigation is the relationship between the change in specific deformation contraction and the change in stress intensity due to the shape, size and orientation of flaws detected by radiographic methods: $A = f(r)$.

Figure 1 represents this change, calculated with the following assumptions:

—cylindrically shaped castings are subject to tensile stress produced by tensile forces applied along their axis;

—the casting has a flaw in the form of an ellipsoid hole, whose short axis is situated in the axis of the cylinder;

—main stresses so formed are of the circumferential, radial and axial type and can be determined by factors of concentration of stress α' and α'', which have been assumed for the ratios of half-diameters of ellipsoids to the radii of curvatures at given load conditions after H. Neuber (7);

—the tensile crack rupture takes place within the limits of uniform distortion, while the true tensile stress (in cross-section, not impurities of the flaw) is assumed to be cleavage strength;

—the change of work is represented by the ratio

$$\frac{A_{no}}{A_i} = \frac{\alpha'_{no}(\alpha'_{no} - \mu\alpha''_{no})}{\alpha'_i(\alpha'_i - \mu\alpha''_i)} \tag{3}$$

where: α'_{no} and α''_{no}—factors of stress concentrations for the most disadvantageous case $t/\zeta = 40$

α'_i and α''_i—factors of stress concentration for less dangerous cases $t/\zeta < 40$/lower value t and ζ —constant

μ— Poisson's ratio.

The magnitude r (equation 2) was calculated assuming that resistance to plastic deformation attains the value of reduced stress after the hypothesis of M. T. Huber (the so-called hypothesis of energy of distortion in pure shape) since:

$$r_i = \frac{\delta_{Qi}}{R_0} = \frac{\delta_{Hi}}{R_0} = \sqrt{(\alpha'_i)^2 + (\alpha''_i)^2 - \alpha'_i \alpha''_i} \tag{4}$$

The Experiments

Investigations were carried out on 120 ordinary cast-steel samples (up to 0.3-0.4% C). The samples were prism-shaped with over-all dimensions 60 × 60 × 300 mm ($2\frac{3}{8}$ in. × $2\frac{3}{8}$ in. × 12 in.) having a special feeding system to facilitate

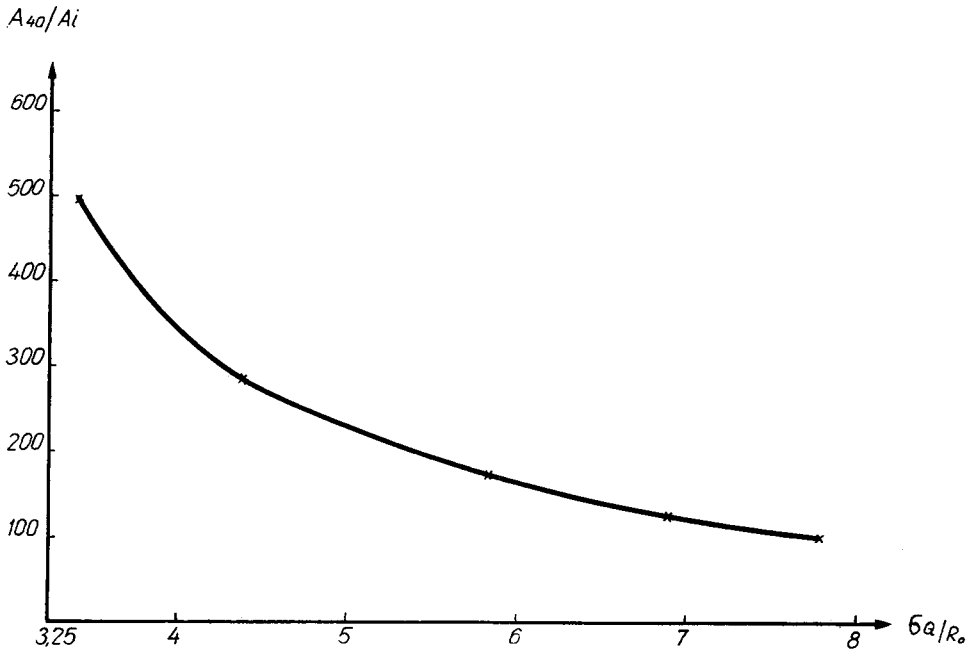

Figure 1.

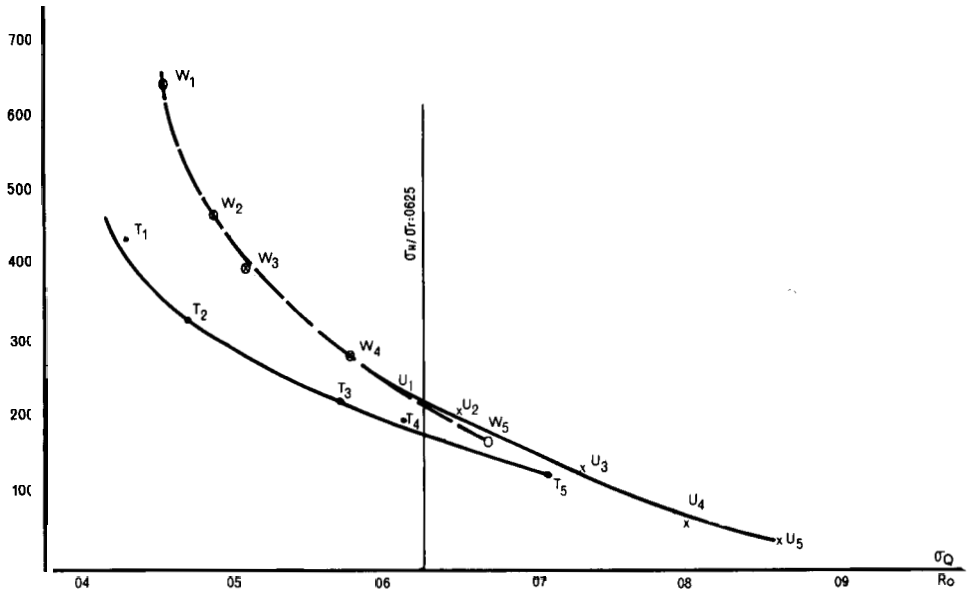

Figure 2.

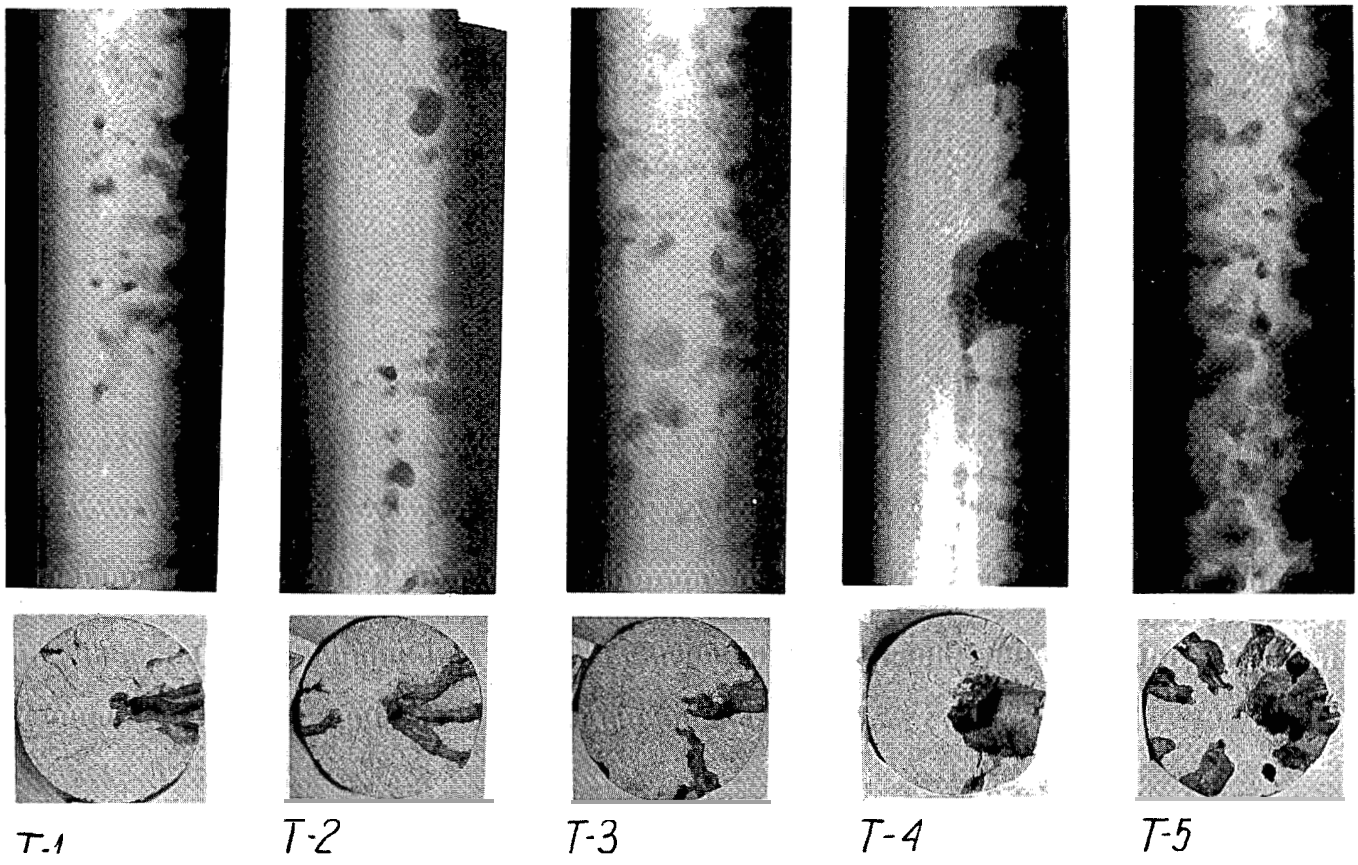

Figure 3.

the formation of defects such as shrinkage holes and blowholes inside the specimen. In order to detect flaws and define their orientation in the castings the samples underwent a preliminary examination by radiography using Co-60 gamma-radiation, and were annealed at 850° C (1562° F) for two hours. A cylindrical shape was given to them by machining and then they were tested for tensile strength by fastening in ring chucks. Dimensions of the tested section were 35 × 140 mm (1⅜ in. × 10¾ in.). These machine-shaped samples were radiographically examined again using Ir-192 and tested for tensile strength by applying the load 100 t (220,000 lb) and minimal speed of extention 20 mm/min. (¾ in./min).

As a result of those investigations the following values were defined

1. Maximum tensile force and strength limit
2. Load at the yield point
3. Elongation and construction of the sample
4. Extentiongraph whose coordinate of elongation was magnified 8 times
5. Photographs of ruptures

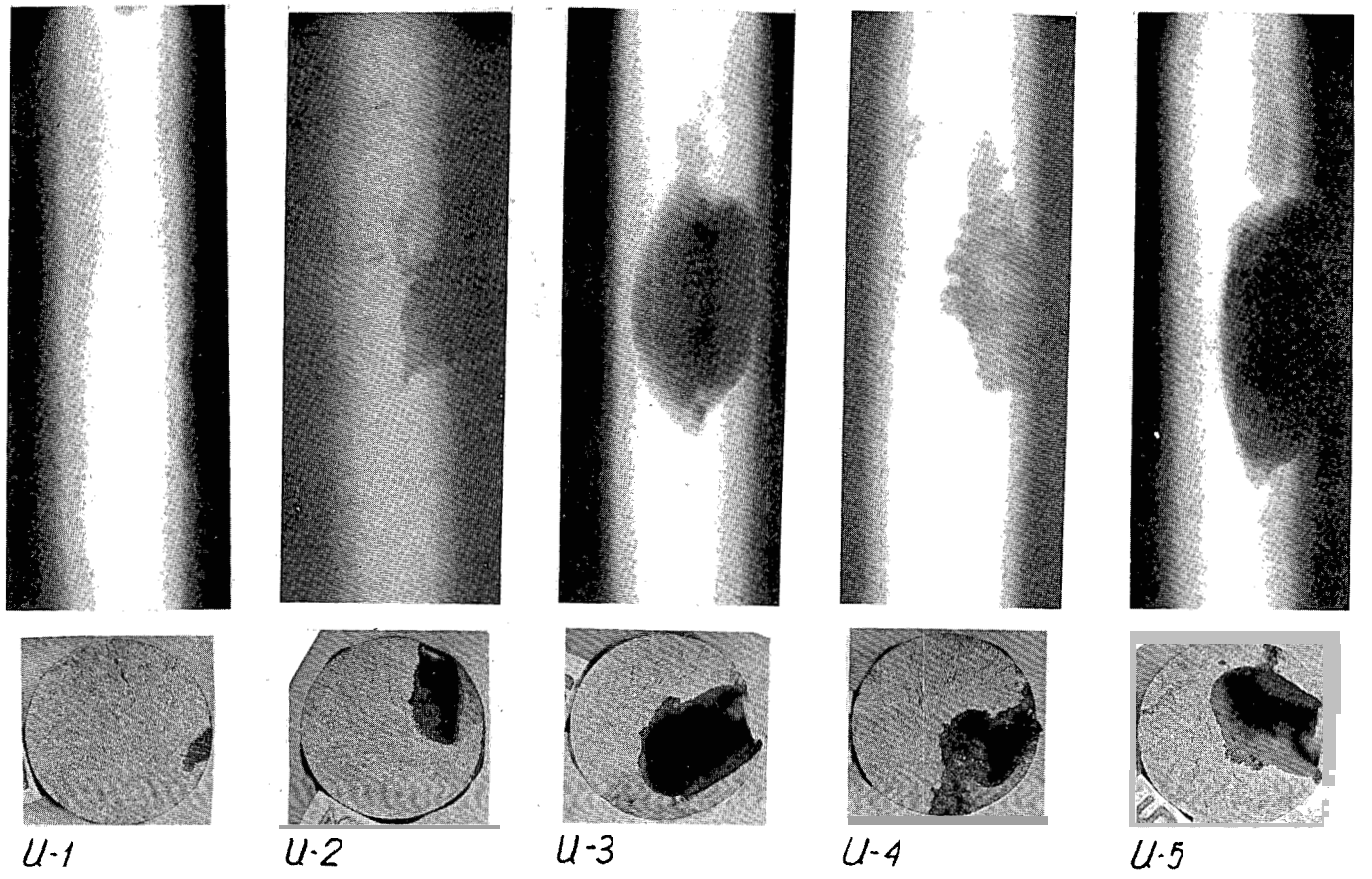

Figure 4.

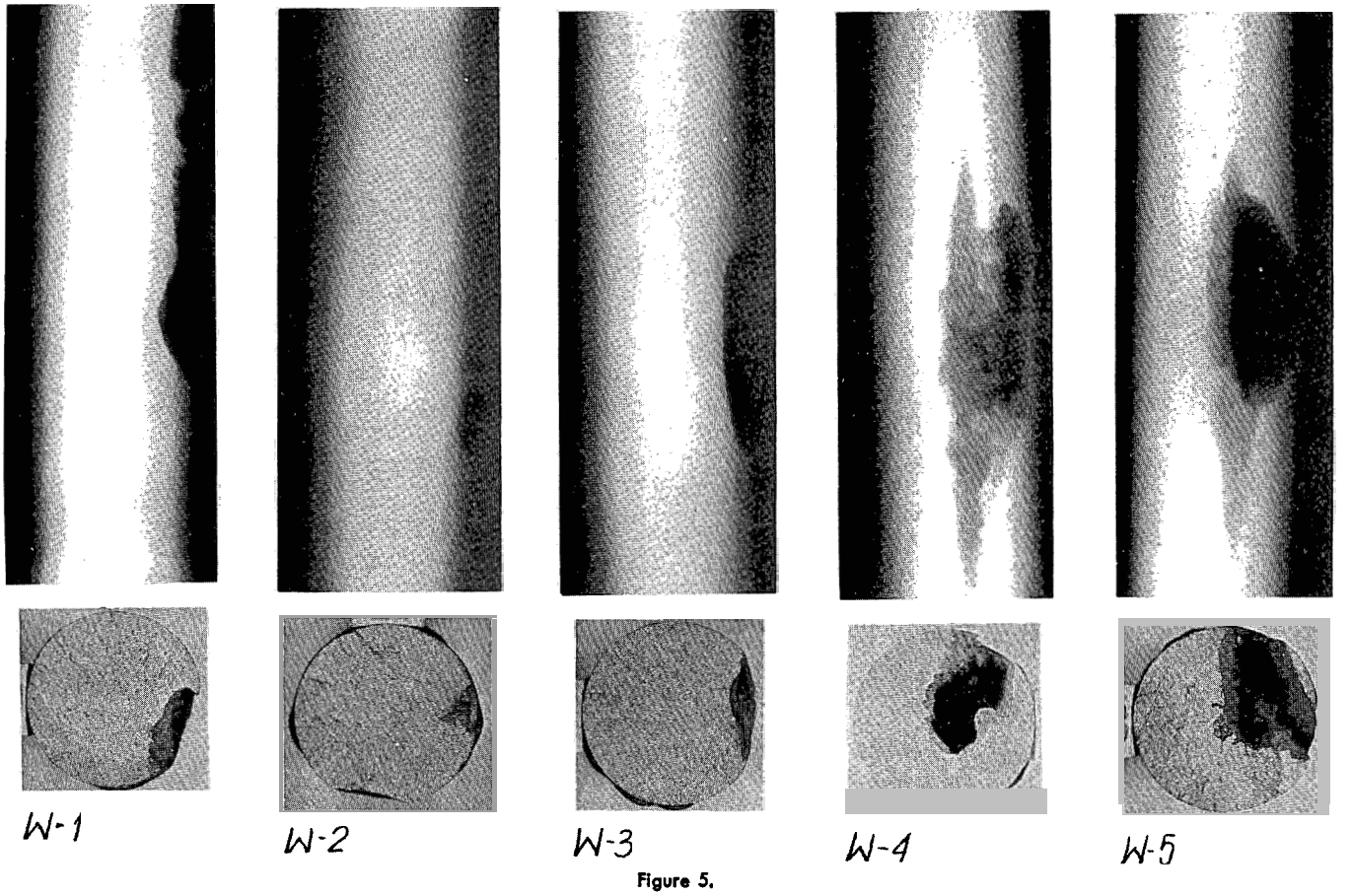

Figure 5.

Those results were evaluated in respect to the calculations of specific deformations, i.e. contraction (equation 1). True tensile stresses were calculated and the true cross-section of the ruptured sample determined by subtracting the areas measured by planimeter on the photograph showing the rupture and the flaw. From the diagram of extension the relative elongation was determined as well as for $\triangle 1 = 0.02\%$ of the measured length of the samples—the resistance to plastic deformation. It was assumed that the cleavage strength is equal to the true tensile strength.

Results of Research

The change of specific deformation (contraction) and the ratio of plastic resistance to cleavage strength is shown in Figure 2. Results of the research are shown by the broken-line curve. This curve and the calculated curve (Figure 1) are identical in shape.

The comparison between the results obtained during the investigations of strength and radiographic investigations can serve as a basis for the following conclusions:

Figures 3, 4 and 5 show radiographic pictures of some samples tested for tensile strength, and depict rupture. Those in Figure 3 show that the samples had many very small blowholes, the radii of which are very small and for which $t/\varphi \approx 1$. Figure 4 shows radiographs of samples having equal tensile strength of the order 52 kg/mm² (≈ 73,000 lb/sq in.) with single shrinkage holes that are larger but for which the ratio $t/\varphi > 1$.

Figure 5 shows similar defects inside samples of greater tensile strength—68 kg/mm² (≈ 95,200 lb/sq in.).

Figure 6* illustrates the change in suitable amount of specific deformation (contraction) and the resistance to plastic deformation.

The curve on the left is related to the samples shown in Figure 3, having numerous blowholes, and the curves on the right are related to those in Figures 4 and 5, which have single shrinkage holes.

Therefore, with the appearance of numerous blowholes the specific deformation (contraction) decreases at a rate greater than the ratio increase of resistance to plastic deformation compared with the case in which single flaws, such as shrinkage holes, are present.

Classification of Castings Undergoing Radiographic Examination

According to the theory of Dawidenkow-Friedman (7), developed by T. Pelczynski (1), there is a stipulated plastic deformation of the material under a given load during a state of stress, which is defined by the formula:

$$\frac{\delta_H}{\delta_r} > \frac{Q_r}{R_0} \qquad (5)$$

where δ_H = reduced stress after the hypothesis of M.T. Huber
δ_r = reduced stress after the hypothesis of the highest (greatest) true elongation.

In the case studied we assume that:

$$\frac{\delta_H}{\delta_r} > \frac{\delta_Q}{R_0} \geqslant \frac{Q_r}{R_0} \qquad (6)$$

If the curves on Figure 7a correspond to curves of Figure 6, which show the results of a series of investigations and observations, and a coordinate is plotted corresponding to the ratio δ_H/δ_r, then all defects effecting a drop in specific deformation (contraction) down to the values represented by the dotted lines to the right of the above mentioned line will effect the brittleness of the material. Material with such flaws is not subject to plastic distortion. In turn a material, the flaws of which are likely to bring about a change of specific deformation to the values lying inside of the dotted area and to the left of coordinate δ_H/δ_r will be subject to plastic distortions in the state of stress, is defined by this ratio.

This results from the following consideration (10):

Figure 7b represents a few straight lines in coordinates δ_Q–δ_r and at various angles corresponding to:

$\operatorname{tg}\alpha_0 = \frac{Q_r}{R_0} = r_0$ —material without flaws

$\operatorname{tg}\alpha_1 = \frac{\delta_{Q1}}{R_0} = r_1$ —material with flaws of the "y" type

$\operatorname{tg}\alpha_2 = \frac{\delta_{Q2}}{R_0} = r_2$ —material with flaws of the "x" type

$\operatorname{tg}\alpha = \frac{\delta_H}{\delta_r} = z$ —material subject to stress under working condition.

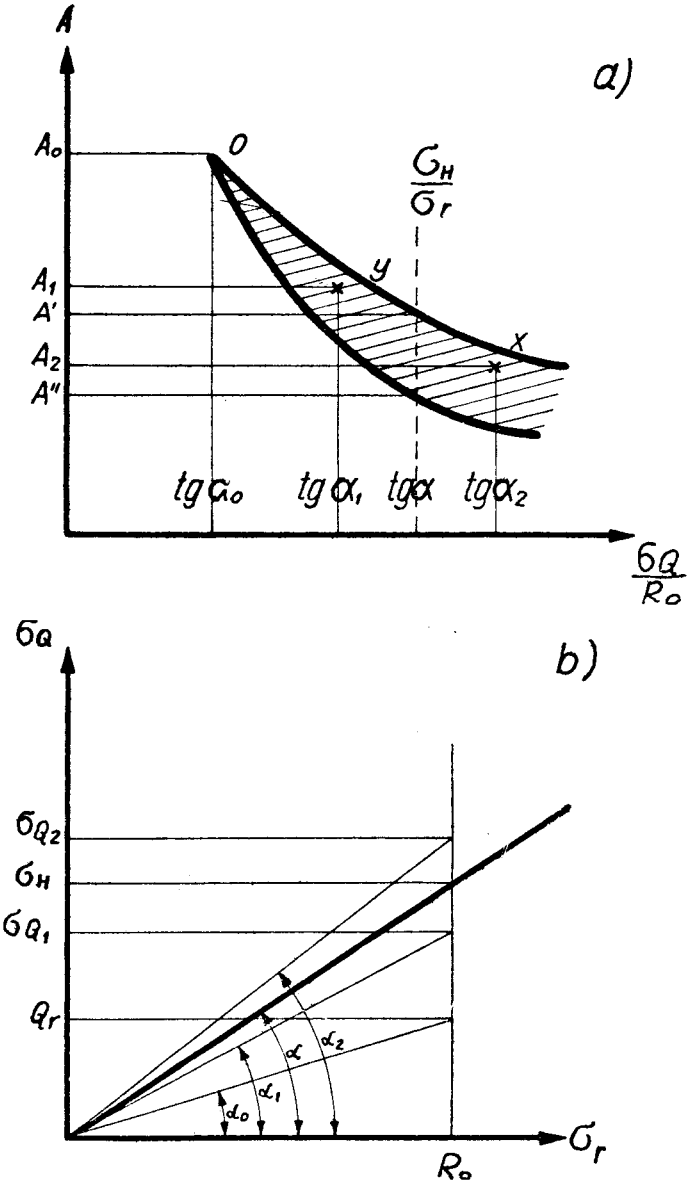

Figure 7.

*EDITOR'S NOTE: Figure 6 was not available at press time.

Moreover coordinates were plotted corresponding to the values Q_r, δ_{Q1}, δ_{Q2}, δ_H and R_0. The line inclined under the angle α_0 corresponding to $\delta_H = Z\delta_r$ will first cross the ordinate Q_r and then the δ_{Q1} and finally R_0.

It does imply that the reduced stress δ_H will first attain a value equal to the yield point of the material without flaws, or a value of the resistance to the plastic distortion of the material with flaws of type "y". The sample will follow cracking as soon as the reduced stress attains the value R_0.

The general requirement in respect of non-brittle castings such as cast iron, is that they be not susceptible to brittle cracking and plastic distortions. Coming back to Figure 7a the defect of type "y" and the other giving the value A and δ_Q/R_0, and those lying inside the dotted area at the left from abscissa δ_H/δ_r, may be defined as permissible and those at the right not permissible. This can be expressed as:

$$\alpha_1 < \alpha < \alpha_0$$

Figure 6 shows that for $\delta_H/\delta_r = 0.625$ flaws T_1—T_4 may be permitted, radiographic pictures of which are represented in Figure 3 at the left in respect to the vertical line as well as the flaw U_1 (Figure 4) and flaws W_1—W_4 (Figure 5), provided the material has better strength properties.

Conclusions

The outlined method of comparison of the strength properties, with the results of radiographic examinations, may establish the foundation for the quality classification of castings. The relationship between the size of flaws such as shrink holes and blowholes and change of specific deformation (contraction) and the ratio of plastic resistance to the cleavage strength has been determined and experimentally proven.

This permits recognition of such flaws in the casting, which may be, by virtue of working conditions, defined as permissible or not permissible.

Determination of this relationship for flaws of another type requires other experiments on artificially produced reference flaws, the pattern of which must have various and well defined values for t and radii of curvature ϕ, as well as the distance to the outer surface of the casting.

References

1. ASTM—Reference radiographs for steel castings up to 2 in. in thickness. E 71-64 (in English).
2. Zerstörungsfreie Werkstoffprüfung von Gusserzeugnissen. Bewertung und Klassifikation von Gussfehlern an Hand von Radiogramen. Manuscript Zentrall-Institut für Giessereitechnik-Leipzig 1963. p. 1-8, (in German).
3. Gillemot, L. Materialprüfung Bd 3 1961 Nr 9 p. 330-336, (in German).
4. Nemec, J. Publication of Conference—o nedestruktivnej kontrole odliatkov—Dom Techniky Bratislava, 1966 p. 70-78, (in Slav).
5. Gillemot, L. Zeszyty Problemowe Nauki Polskiej XXVI—1965, p. 514-525, (in German).
6. Friedman, J. Mechaniczeskije svoistvo mettalov Moskwa, 1948, (in Russian).
7. Neuber, H. Kerbspannungslehre Springer Verl. Berlin 1958, (in German).
8. Godlewski, Z. Defektoskopowe Metody Badan i Oceny Odlewów, Prac. Inst. Podst. Probl. Techniki. PAN, Warszawa 1961, (MS in Polish).
9. Pelczynski, T. Przeglad Spawalnictwa XI, 1959 p. 85-90, (in Polish).
10. Godlewski, Z. Slevarenstvi XIV 1966, No. 6, p. 227-230, (in Slav).

Automation in Radiology

R. HALMSHAW, U.K.

ABSTRACT: Where a radiograph is taken to check specific points—e.g. an assembly detail—some form of automatic viewing and assessment is feasible. The type, usefulness, and extent of such systems is discussed.

Extensive automation of the technique of radiography-on-film does not however seem a very practical proposition, partly because of the number of operations required to produce a processed radiograph and because the number of variables involved makes a standard quality of radiography difficult to maintain if the skill of the individual radiographer is eliminated.

Scanning and television-fluoroscopic techniques, in which at some stage the radiographic information is in the form of an electrical signal, seem much more promising as automatic inspection methods. Possible methods of converting these techniques into automatic systems are discussed.

The capital cost of an automatic system is likely to be considerable and its value must be assessed in terms of the comparative cost of a skilled radiographer.

Introduction

Most present-day techniques of industrial radiology make use of radiography-on-film; scanning techniques using a detector, and fluoroscopy, are not extensively used, but new forms of image intensifier systems now being developed for medical radiological work seem likely to find use in industrial applications and these might greatly extend the uses of fluoroscopic techniques.

At the present time "automation" is a fashionable subject and it is natural to see how usefully it may be applied to various inspection processes including industrial radiology. With television-fluoroscopic techniques, in which at one stage the information is in the form of an electrical signal, there is clearly suitable opportunity for applying electronic monitoring, sorting and processing systems.

Strictly, the term "automation" as used in engineering circles implies a system with a feed-back, such that corrections for variations in operating conditions are automatically applied to the equipment. This type of system has not yet been developed for any radiological process, but some stages of the process can be made more automatic than they are at present and it is worthwhile considering what can usefully be accomplished. The justification for the development of automatic systems seems to be:—

1. The high cost of skilled labour presently required for nondestructive testing; considerable training and experience are required to produce a satisfactory operator and this cannot be done cheaply; 2. The requirement for the inspection technique to match the production, in terms of inspection speed; 3. The need for greater inherent reliability of inspection—the elimination of human errors; 4. The more rapid production and feedback of information from the inspection process.

Radiography-on-film

Essentially the process of radiography can be considered as four sub-processes:—

1. setting up and exposing the radiograph; 2. processing the film; 3. viewing and interpreting the image; 4. decision and action on the findings.

Some use of automatic methods can theoretically be applied to at least three of these stages.

Clearly, automatic systems would have to be far more complex if they were designed to handle stores of different shapes and sizes, and it is probably not worth considering any but the simplest example of radiographic inspection of large numbers of the same item. One large application of routine radiography is to the inspection of ordnance fuses and it is of interest to consider how useful automatic methods have been or would be in this field. The fuses are loaded into racks and sometimes require orienting in a particular direction relative to some external feature of the fuse; the rack is then moved in front of the X-ray machine together with a loaded film cassette; the X-ray set is switched on to make a pre-determined exposure. Much of this could be automated: the racks of fuses and the cassettes could be handled on a moving belt system with automatic switching on of the X-ray set when the fuses are in position, and the equipment to do this would be far from complex. In practice, however, automatic handling has been tried but not found to be worthwhile; it leads to a greater complexity of switching, in particular of interlocking safety circuits, and complicates the changeover from inspection of one pattern of fuse to another.

Stage 2, the film processing, can be made automatic and rapid progress has been made in the development of automatic processing units. A typical modern unit will process all film sizes up to 14 in. × 17 in. with a "dry-to-dry" time of less than 2 minutes. For ordnance fuse inspection however, the radiographs are inspected while still wet to reduce the time during which racks of fuses must be held prior to acceptance or rejection.

In practice, standardization of processing, through the use of automatic units, has outstripped the standardization of X-ray equipment and the inherent variations in X-ray film due to age and storage conditions.

For viewing and interpreting radiographs there have been several attempts to develop automatic electronic systems. It can be argued that human film reading will always result in some errors, even when such factors as lack of experience, inadequate viewing conditions, and tiredness are eliminated. Recent experiments organized by the author on behalf of the International Institute of Welding have highlighted this problem. Radiographs containing a series of standard images (image-quality indicators) were circulated to experienced radiographers in a number of countries for "reading". No instructions were placed on the film viewing conditions or on the reading-time, and the readings obtained by about 60 observers were studied. Consistency of reading was found to vary with the quality of the radiographs; it was found that there was a greater spread in reading values on the gamma-radiographs and on the exposures made with salt intensifying screens, i.e. the comparatively unsharp radiographs.

The extremes of consistent (Film A) and inconsistent (Film B) readings, out of a series of 40 radiographs are shown in Table 1.

Table 1

Number of observers seeing N elements on the image

		No. of elements, N (holes or wires) seen*							
		6	7	8	9	10	11	12	13
No. of observers reading N	Film A	—	—	—	4	51	9	—	—
	Film B	—	1	8	19	34	1	—	—

* A change in N of ± 1 represents, on these films, a change in sensitivity of about 25% of the actual sensitivity. Thus on film B, the sensitivity was read as from 2.5% to 1.0% compared with a "true" value of 1.2%.

More importantly, from the point of view of automatic film reading, these experiments clearly showed that workers in different countries use different standards for the limit of discernability of the image, and that unless very experienced, an observer seeing the same film several times was not entirely consistent. It seems reasonable to assume that the same or greater inconsistencies will occur in the interpretation of radiographs of complex objects when the human reader is required to look for a series of features. Experiments by Tuddenham (1) with medical diagnostic radiographs have shown, in an even more startling manner, the fallibility of human judgment. Out of a series of 200 chest radiograph readings, "significant abnormalities" were overlooked in 20-30% of the readings; the experiments were conducted using experienced radiologists. If an instrument can be made for automatic film reading, it would be possible to greatly reduce the errors in judgment which can at present occur.

Several points need to be considered, however,

1. An image on a radiograph is basically a density discontinuity; under suitable viewing conditions the eye can discern contrasts of 1.4% (a density difference of 0.006). Can an instrument be made to be as sensitive as the human eye? 2. The human eye, because it scans an image and mentally integrates the information, can cope with blurred and grainy images with little or no loss in contrast discrimination; 3. A human film reader will see abnormalities on a radiograph outside the specified items which he is looking for; thus, in a fuse, a cracked spring would be seen and reported even if the inspection was nominally only for the presence or absence of the spring. There is, therefore, a bonus of information which is unlikely to be produced by any electronic reader; 4. A human observer will quite easily recognize the image of a helical spring, whatever the orientation of the spring: although electronic character recognition machines are being developed, this is a very difficult task for any instrument to perform; 5. In general in radiography of such items as fuses, orientation of the fuses, and positioning on the radiographs is not accurate enough for the images to be exactly alike. Again, the helical spring is a typical example; the human observer easily takes account of slight differences in the image while the electronic system would not do so as easily.

In summary, for the relatively complex images of assemblies, it would appear that there are many advantages in retaining human film readers, even when large numbers of the same store are involved.

In some applications of radiographic inspection, however, interpretation is a simpler business. For high-quality welding of thin structures, virtually any weld flaw shown by radiography is cause for either rejection or investigation, and for vessels such as rocket propellant tanks, thousands of feet of weld-radiography are involved. The problem of automatic film reading is inherently simpler than in fuse inspection, for three basic reasons:—

(1) Because the specimen is very thin, better definition of detail on the radiographs is possible; (2) For similar reasons, a high contrast image can be obtained; (3) The area of film to be examined is a long narrow strip, rather than a large area, and scanning is simplified.

This problem has been examined by Sheldon (2) and it is worthwhile examining the techniques which he proposes, together with other possibilities, to see whether they could be applied to radiographs of more complex specimens.

Design of an automatic film reader

Three ways in which the image on a film radiograph could be converted into an electrical signal are:

(1) By projecting the film image onto a television camera tube, with suitable optical reduction, so that the light variations are converted into video signals; (2) By using a bank of small

photocells to examine discrete areas; (3) By using a line-scan photometer.

The simplest system would be a photometric system in which a photo-electric detecting head is moved to cover small areas on the radiograph and the output is compared with that from a similar cell covering the same area on a master radiograph. By appropriate choice of area, allowance could be made for slight variations from the standard image (Figure 1), such as the rotated helical spring or slight displacements of a component, without impairing the alarm signal when a genuine abnormality appears. A more serious problem would be image location on the radiograph and slight variations in radiographic quality due to processing, etc. so that it would be necessary to have some form of automatic compensation for variations in background density and contrast.

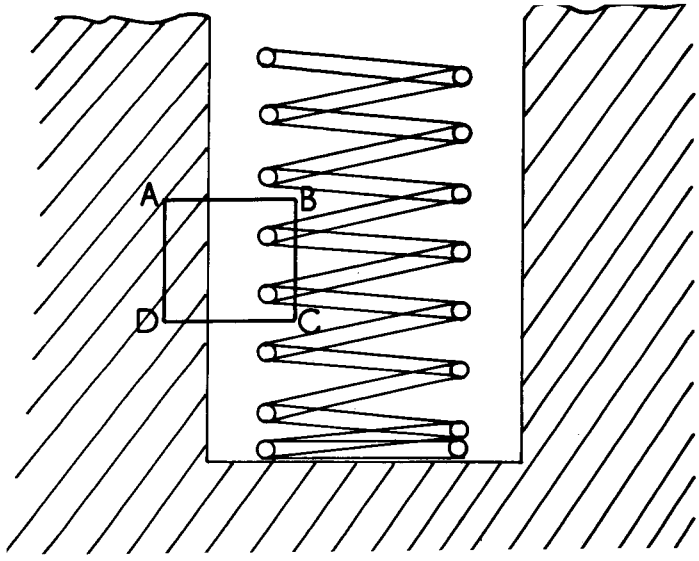

Figure 1. Helical spring in a well. If area ABCD is monitored, the presence or absence of the spring will be shown and the spring may be rotated without significant change in the light intensity received. The area ABCD must be located accurately in relation to the edge of the cavity.

A similar scheme can be envisaged using a line-scan system. The two images are scanned simultaneously and the two signals cancel one another out in a differential amplifier, so that any differences appear as positive or negative pulses (Figure 2).

The comparison could be made in terms of pulse heights, pulse time or both. A helical spring image would not cancel out if the spring has been rotated, but it would be possible to check the presence or absence of a spring by comparison with a sample image with no spring present. To succeed, such a system requires a much higher degree of standardization of the radiographic parameters and positioning than is now used in routine radiography.

Using a television camera tube the definition required can be adjusted in terms of the line scan used, in relation to the optical reduction of the image employed. Thus a 405-line image, looking at a film area of 4 in. $\times$ 4 in. would be equivalent to detecting detail down to 1/100 in. The video signal would be converted into digital form by means of a differential amplifier (Figure 3) so that the edge of an image on the film is recognized as an abrupt change in video voltage and a flaw is registered as a sequence of two pulses of opposite polarity. Information concerning tonal value is lost. To produce a satisfactory pulse, the periphery of the image must be sharply defined and it has been found that on many radiographs the sharpness of definition is not adequate. This lack of definition may be due to radiographic factors, inherent unsharpness, etc., or may be intrinsic to the component, e.g. cylindrical items radiographed along a diameter.

Even assuming that satisfactory pulses could be obtained, a machine to compare these in height and time with the pulses from a standard image would be very complex. Essentially, it would be a computer of the type used for character recognition, having a memory system.

For weld flaws, Sheldon (2) has suggested that the information required can be reduced to nine parameters and that this includes the density difference between the flaw image and background. The parameters describing each image are stored on nine delay-lines and the information obtained in digital form on each parameter is compared with predetermined limits. If the image is unacceptable all the parameters are printed out and in practice this printing-out time limits the speed of operation.

Automatic Radiological Inspection—Direct Systems

It might be argued that if scanning of the radiograph can be used as an inspection method, then as the film is merely a

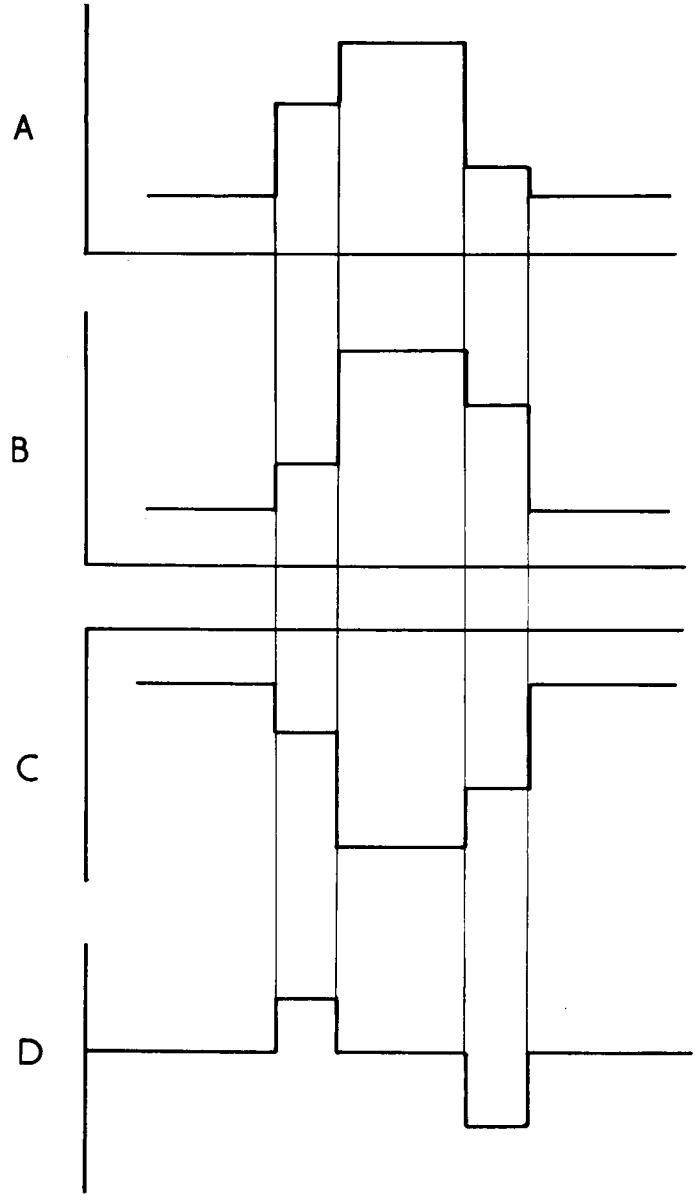

Figure 2. Illustrating the method of optical line scan across the image: A—light intensity-distance curve across image to be examined; B—scan across reference image; C—reference image inverted; D—difference between A and C. Positive or negative pulses on D show image abnormalities.

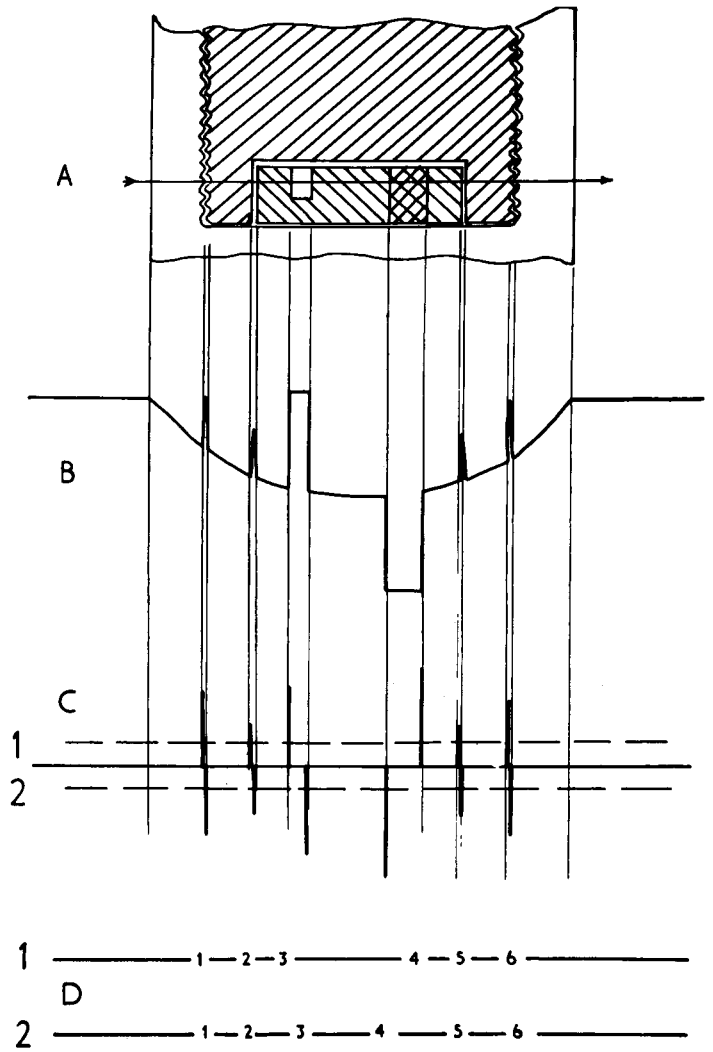

Figure 3. Illustrating conversion of a video signal into digital form: A—scan is taken along line shown through image of an assembly; B—video signal; C—differentiated signal; D—digital pulse counts along levels 1 and 2 on C.

permanent record of the spatial variations in intensity across the X-ray image, the whole of the photographic process could be eliminated and the sampling done directly on the X-ray beam after transmission through the specimen.

This is possible and has been successfully applied, but use of the photographic process has two advantages:—

(1) It is an integration process in which the total number of X-ray quanta incident within the film exposure time is recorded, so that statistical fluctuations in the number of these quanta are minimized; (2) Scanning, masking and detection of light quanta is generally simpler than for X-ray quanta.

There is the incidental advantage that the film provides a permanent record which is available for visual inspection or re-check.

Three systems of automatic radiological inspection which have been used successfully are as follows:—

(a) Using a gamma-ray source and a G.M. or scintillation counter to monitor the thickness of a uniform tube by means of a spiral scan. The method can be extended to non-uniform thickness "tubes" where the variation in absorption is regular and can be predicted. The source is generally placed inside and the detector outside, with collimation on both. Essentially, any local change in absorption is recorded, and this may be due to internal cavities or to a change in wall thickness. The collimated area, size of source, rate of scan and sensitivity are related mathematically and have been discussed by a number of authors, notably McGonnagle (3). To be detected, the cross-sectional area of a flaw must be a significant percentage (typically 5–10%) of the collimated area, so that unless the latter is made very small, which implies a very slow inspection rate, the method is not efficient for the detection of linear flaws such as cracks. An alarm system can be made to register or record any variations in count-rate above or below predetermined limits, and these limits can be programmed to cover expected thickness variations such as webs inside a hollow cylinder. The method is chiefly applicable to large uniform tubes which have to be inspected in quantity and successful applications have been described by Hinsley (4) and McClung (5). Gamma-ray sources are usually used, because of the constancy of their output over short periods, which eliminates one variable.

(b) Successful systems have been built in which a gamma-ray source and a detector "look at" a limited cross-section of an assembly and compare the transmitted intensity with that through a known correctly assembled specimen. The system can be made automatic with mechanical handling arrangements. The method has been applied to a number of ordnance components, such as the detection of the presence or absence of the sealing ball in cartridge primers, but in practice a number of limitations were found:

(i) In a complex specimen the machining tolerances on individual components along the path of the X-ray beam can collectively represent a considerable change in absorption, comparable to the presence or absence of the item being checked;

(ii) It is a slow process: in the case of the primers, these can be radiographed on film or X-ray paper forty or more at a time, and film reading for the presence of a sealing ball is not difficult or slow. There is a loss of incidental but useful information compared with film, e.g. the presence or absence of filling;

(iii) Automatic sorting systems using X-ray transmitted intensity as a criterion of acceptance. In the machines which have so far come to the notice of the writer, a single discrimination level is used as a 'go-no go' criterion, but multi-level systems are also possible.

The response signal is coupled directly to a mechanical sorting gate so that the components are automatically separated in accept and reject lots.

The method has been used for such varied applications as filled containers, pharmaceutical packages, sorting potatoes from stones during harvesting.

Television—Fluoroscopy Systems

By using image intensifier systems, particularly those involving a television system, one can obtain image sensitivities comparable to those on film; these may be viewed comfortably in ordinary room lighting, without any dark-adaptation of the

inspector or any radiation hazard. Since the information in the X-ray image is available in this equipment as an electrical signal, it is natural to consider the application of automatic reading techniques using this signal.

Again, the complexity of the system depends on the information required. One possible application, which the author collaborated in assessing, is the fluoroscopic inspection of hot steel billets using a television X-ray image-intensifier and a high energy X-ray source (linac or betatron). The aim was to locate the ends of centre-line cavities in the rolled billet as an aid to accurate cropping: experiments showed that images of cavities, of the size which metallurgical considerations suggested it was necessary to locate, could be clearly shown on the fluoroscopic screen. By their nature, these cavities tend to occur on the centre line of the billet and it was proposed to monitor the television display signal over a limited number of lines on the raster for any sudden change which would represent the image of a cavity moving across the image area. The signal would be processed, so that it had to be repeated on several successive scans and on several adjacent lines at the same location, before being accepted as genuine. Two probable obstacles were envisaged:—

(1) The image of a cavity, with these fluoroscopic techniques, is not sharp, so that the edge of the image does not cause a sharp, well-defined signal; (2) The human eye is very adept at viewing a noisy unevenly bright image and picking out relevant detail from the background. Using a monitoring system it was thought probable that a much greater signal-to-noise ratio would have to be accepted; this is equivalent to a poorer sensitivity.

For reasons entirely unconnected with the feasibility of this proposal for automatic-monitoring, this application has not yet been tried in practical industrial conditions, but the technique proposed is clearly applicable to other inspection problems. With television circuits, automatic brightness control and contrast adjustment have already been shown to be possible.

This application is a relatively simple one so far as image interpretation is concerned; it is limited to the detection of an "edge" greater than a predetermined size and contrast. The interpretation of more complex images will require more sophisticated techniques, as already discussed, probably involving the use of a computer.

Conclusions

While techniques for automatic image interpretation, either from film or fluoroscopy, are feasible, they are exceedingly complex, for all except the simplest problems. While they are potentially capable of greater reliability and speed of operation than human film reading, the factors of

(i) cost; (ii) inherent unreliability of any very complex equipment; (iii) staff required for setting-up and maintaining the equipment, must be compared with the problems and cost of training radiographic interpreters to be more expert and reliable. The human film reader is always capable of providing some useful extra information from the image, which would not be available from a programmed machine.

It is fashionable to suggest that computer systems should be used to replace humans whenever possible and this is a reasonable argument when the computer performs a task that is impossible or excessively tedious by the more conventional method, but radiographic film reading does not yet come into this category. It seems doubtful, therefore, whether there is any real practical advantage in using complex and very expensive equipment to gain what would only be a slight improvement in reliability.

References

1. Tuddenham, W. *Radiology*, **78**, (5), 694, 1962.
2. Sheldon, L. and Eppler, W. G. Proc. of 4th Int. Conf. on NDT London 1963. (Butterworth.)
3. McGonnagle, W. J., Beyer, N. S. Progr. in N.D.T. Vol. 5 (Heywoods, London) 1964.
4. Hinsley, J. F. Nondestructive Testing. (McDonald & Evans, London) 1959.
5. Foster, B. E. and McClung, R. *Materials Evaluation*, **23**, (4), 1965.

Discussion

Q. DR. A. NEMET, British National Committee for NDT, Richmond, England:

Since the main advantage of radiography is in making use of the human brain in obtaining the maximum amount of complex information contained in the radiograph, I agree with Mr. Halmshaw's conclusions. That is to say, automation would lose the correlating capacity of the trained brain of the experienced radiographer. We have no such reservations in automating ultrasonics simply because the information is limited. However, I missed in his paper and, in fact, in the whole of the Conference, reference to Xeroradiography, which figured at previous conferences. This technique lends itself to automation and its disappearance is certainly not due to its technical limitations but probably only to commercial policy of the manufacturers.

A. Xeroradiography is an interesting and valuable process which has been neglected, probably because no manufacturer has produced large-size selenium-coated plates of high quality at a reasonable price. In my opinion it is a process which is not very suitable for automation. It would be possible to scan the "electric charge image" on the selenium plate and present the result on a television monitor screen, or to gate the signal through an alarm system, but if the selenium plate has to be part of the system it would seem simpler and more satisfactory to produce the normal powder image for viewing; this final stage is simple and brings in the usual advantages of using the human eye for interpretation. Again, an automatic "reading" system could be devised for xeroradiographic image, but this brings in the same limitations as a film reading system.

The Radiographic Evaluation of a Welded Structure Designed with Fatigue Strength

H. KIHARA AND Y. ISHII, JAPAN

ABSTRACT: Discussed is a method of evaluating the quality of a manually-welded structure designed with fatigue strength taken into consideration. In this method, the evaluation is done as follows. Rejections are determined by the relationship between the severity of the defect and the pulsating tensile fatigue strength. The probability of rejections occurring in defective areas, such as porosity; and in defect length, such as slag inclusion and lack of fusion, are assumed from the average number of defects in a certain area, based on the law of defect distribution. Consequently a welded structure is evaluated by the average number of defects, the severity of defects, and the rate of defective area or the defect length.

Introduction

Radiography of long weld-line structures is carried out by the spot inspection method for reasons of economy. As on extension of reference (1), this paper describes the scientific evaluation of structure quality. In the case of a structure designed for a static load, but which is not likely to cause a brittle fracture, whatever defects may be included will not substantially affect the tensile strength, except by reducing slightly the elongation, as long as the structure is of the quality expected from normal welding (2)~(6). For such welded structures, radiography by random sampling is important as a form of quality control performed in parallel with the welding. Welding defects have great bearing on brittle fracture and fatigue strength, but this discussion is confined to the quality evaluation of welded structures designed with consideration of fatigue strength. Moreover, as it is common to remove the reinforcement from such structures, only the unreinforced, manually-welded structures are considered.

Distribution Law of Manually-Welded Defects

For the successful quality evaluation of a welded structure on the basis of defects revealed by spot inspection, the law of defect distribution must be established. As yet, the laws of distribution are available only for porosity and slag inclusion (lack of fusion included) of a manually-welded structure. Crack, and incomplete penetration, which are also serious defects, occur very rarely and no laws of distribution for them have yet been found. Little attention has been paid to undercutting, because it is an external defect, although it does sharply lower fatigue strength; accordingly, no law of distribution available has been established for it. For this reason, the present paper deals with porosity, slag inclusion, etc.

Periodicity of Defect Distribution

If there were any periodicity in defect occurrence under varied conditions, the data obtained would differ depending on the manner of spot inspection. However, it has been reported (7)(8) that there is no such periodicity.

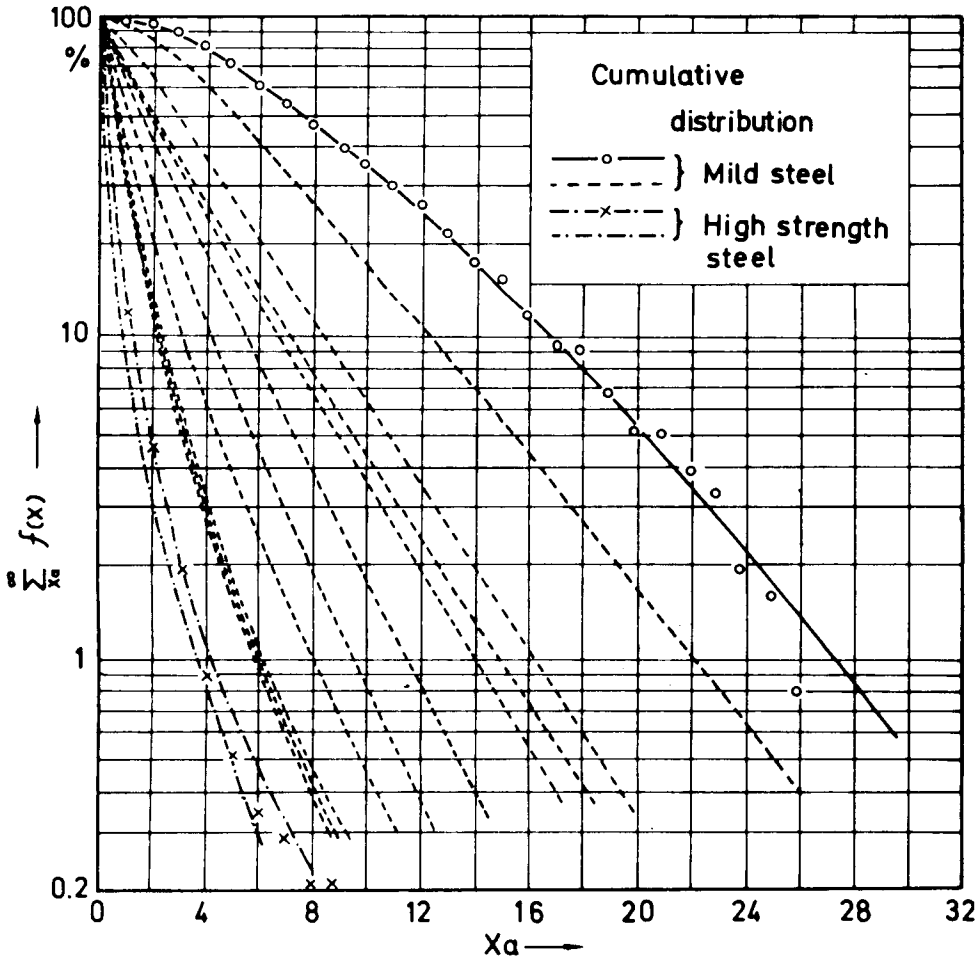

Figure 1
Cumulative relative frequency of defects in a 5-cm division.

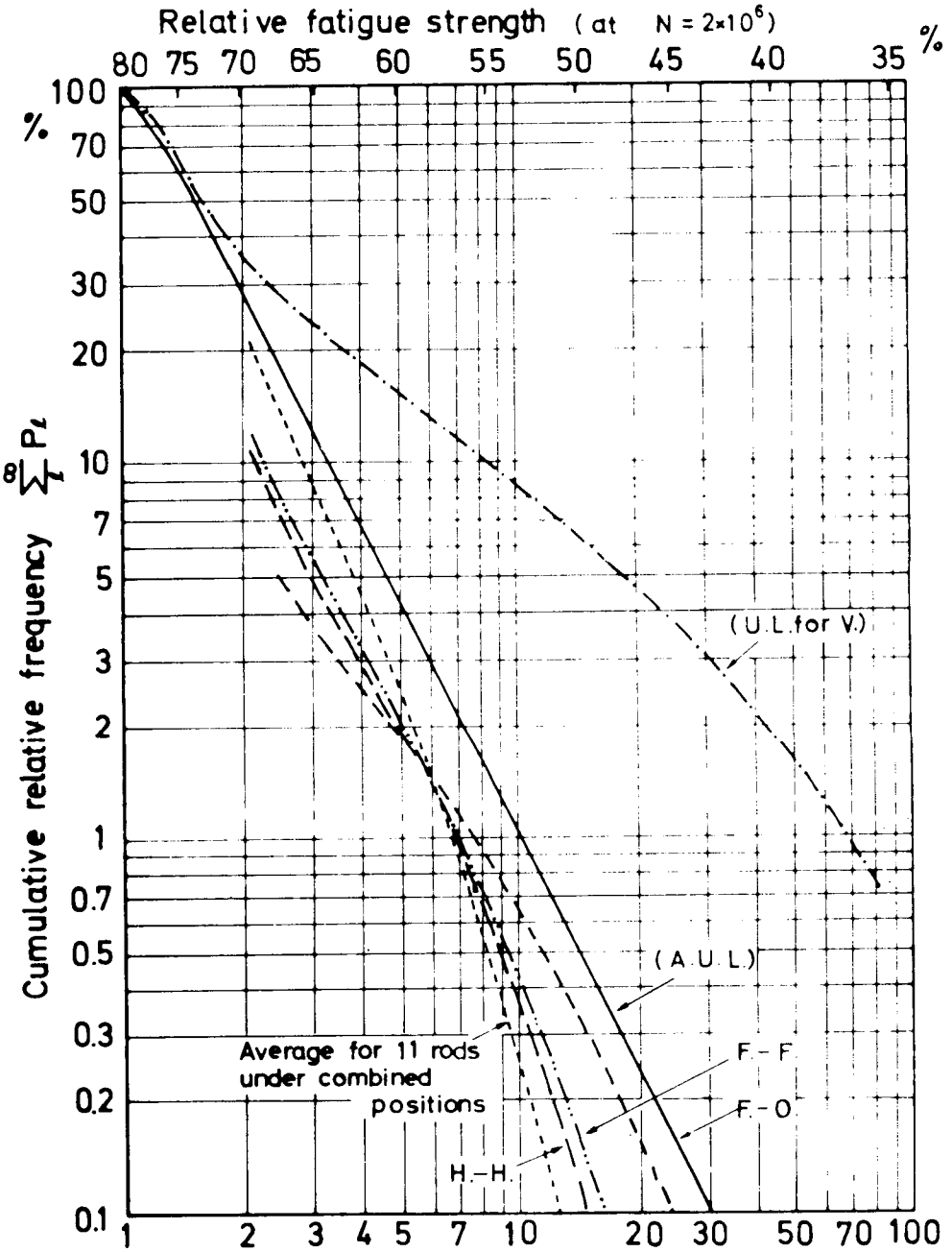

Figure 2
Defect length and its cumulative relative frequency. U.L. for V.—upper limit for vertical position: A.U.L.—average upper limit: F.-F.—flat-flat: F.-O.—flat-overhead: H.-H.—horizontal-horizontal.

Law of Distribution

The distribution law of defects actually occurring in manual welds has been found as follows. Radiographs, taken continuously for 5cm divisions were checked for the number of defects, χ, contained in each division. Then the relationship between the number of defects and the cumulative relative frequence,

$$\sum_{\chi\alpha}^{\infty} f(\chi)$$

was found as shown in Figure 1. (7)

The curves in this Figure correspond to the respective structures continuously radiographed and have been derived from weld lines of 10~100m; for example, the measuring points are indicated for only two of the curves. From the results of measurements, the relation between the average number of defects, χ, and their variance for a 5-cm division (width of about 10mm of weld line) was found as follows:

$$\sigma^2 = \frac{1}{N} \Sigma (\bar{\chi} - \chi_i)^2 = 2.5\bar{\chi}^{1.1} \qquad (1)$$

This distribution concerns structural steels of 20~25mm plate thickness. According to equation (1) the variance and the average number of defects are not independent, and accordingly one or the other will suffice for the evaluation of welded structures.

Relative Frequency of Defect Size in Manual Welds

The relation between the size of defects in welds and their relative frequency has been investigated for a large number of

welds on plates of about 20mm thickness. Figure 2 shows the relation between the defect length and the cumulative relative frequency for the eleven rods in Figure 1, as executed from the combined position, and other welds as executed from flat-overhead, flat-flat and horizontal-horizontal positions.

According to these figures, the vertical position is likely to cause long defects such as slag inclusions. Complicated curves in these figures suggest the difference in the law of distribution applicable between porosity and slag inclusion. Meanwhile, the intersection of weld lines is often chosen as the spot inspection point, but it should be emphasized that there is no evidence that these are particularly vulnerable.

Quality Evaluation of Welded Structures by Spot Radiography

How to evaluate the quality of a welded structure, with the strength of it as a whole taken into account, from the images of defects on X-ray radiographs taken at random with consideration of the above conditions is discussed. For this purpose, the relation between defect, and strength, and the law of defect distribution must be used. The discussion is confined to structure evaluation considering the effects of porosity and slag inclusion on fatigue strength, and brittle fracture evaluation is reserved for another time.

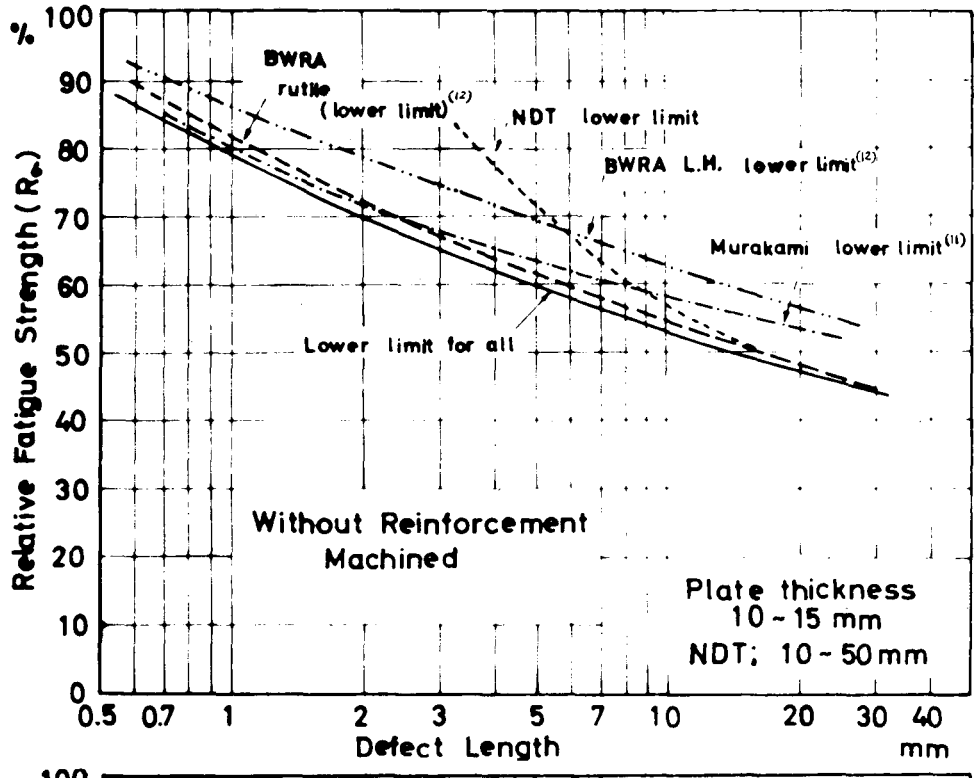

Figure 3
Relation between lengths of slag inclusion and lack of fusion in welds and pulsating tensile fatigue strength. (Extrapolated value of strength for 0.3-mm defect as 100.)

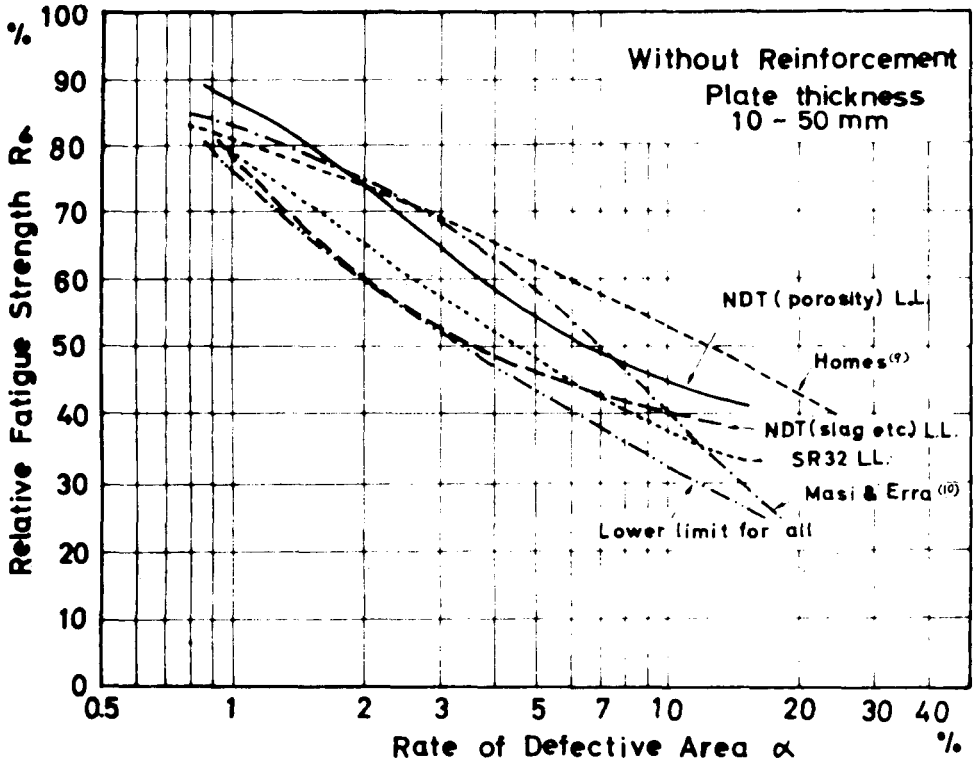

Figure 4
Relation between rate of defective area in welds and pulsating tensile fatigue strength at $N = 2 \times 10^6$.

Reduction of Fatigue Strength Due to Weld Defects

For investigation of the effect of weld defects on the fatigue strength, the rate of defective area, mainly porosity and the length of defects when slag inclusions are involved, was investigated. The percentages of the lower-limit data from the above investigations, compared to strength extrapolation for absence of defect, or for 0.3mm defect, are shown in Figures 3 and 4. The region below the lower limit curves will be regarded as safe.

Method of Investigation

The quality of welds, i.e. the defect distribution, is evaluated in terms of the average number of defects contained in a certain area and the distribution of defect sizes. By this method, the structure is accepted or rejected depending on the probability of having an area with a dangerous rate of defective area and length of defect that are calculated from the average number of defects in a certain length of weld, and the distribution of defect length on random-sample radiographs, for the whole weld line. If no single area likely to be rejected is included, there is no alternative but to make a 100% inspection and correct all major defects.

Suppose the whole weld line is split into N divisions, n divisions out of them are chosen and the average number of defects, $\bar{x}$, in these divisions (for convenience sake, 5-cm divisions) is considered. Then, the value of $\bar{x}$ will differ depending on the mode of sampling. But if the average number of defects in a 100% inspection is indicated as $\overline{X}$, $\bar{x}$ and $\overline{X}$ will be expressed respectively as follows:

$$\overline{X} = \frac{1}{N} \sum_{i=1}^{N} x_i \quad , \quad \overline{\bar{x}} = \frac{1}{n} \sum_{i=1}^{n} x_i \quad . \tag{2}$$

Thus, on the average, $\bar{x}$ agrees with $\overline{X}$. If the variance of $\bar{x}$ is put as σx,

$$\sigma_{\bar{x}}^2 = \frac{N-n}{N-1} \frac{\sigma^2}{n} \quad . \tag{3}$$

If N is larger than n, $\sigma_{\bar{x}}^2 \fallingdotseq \sigma^2/n$.

And if n grows very large, the x distribution will be Gaussian with average $\overline{X}$ and variance $\sigma_{\bar{x}}^2$. As the over-all variance σ will be unobtainable, the sampling value will be adopted, namely, the following $S_{\bar{x}}$ will be substituted for $\sigma_{\bar{x}}$:

$$S_{\bar{x}} = \sqrt{\frac{S^2}{n}} = \frac{1}{n} \sqrt{\sum_{i=1}^{n} (\bar{x} - x_i)^2} \quad , \tag{4}$$

and $\overline{X}$ will be estimated from $\bar{x}$ and $S_{\bar{x}}$. Accordingly, the probability of $\bar{x}$ fitting into the limits of $\bar{x} \pm 2S_{\bar{x}}$, is about 95% and of fitting into $\bar{x} \pm 3S_{\bar{x}}$ about 99%. For practical purposes, estimation may be made with $\overline{X} = \bar{x} \pm 2S_{\bar{x}}$.

Estimate of Strength from Slag Length

Plotting the relation between the length, l, and its relative frequence, P_l, for the upper limit of combined and vertical positions, we get the solid lines in Figure 5. Figure 1 shows cumulative relative frequency of 5-cm divisions that contain more defects than x_a for various weld structures. The relation between the average number of defects, $\overline{X}$, as found from the weld line represented by each curve, and the values of x_a has been plotted in Figure 6 with the cumulative relative frequency, $\sum_{x_a}^{\infty} f(x)$, as parameter.

Suppose a spot inspection is made of a weld line with L metres as unit length, and $\overline{X}$ is found by the above statistical method. Let us discuss how to evaluate the quality of a welded structure when L metres is set at 5 cm and it is required that there be included no more than one area where the specified fatique strength cannot be satisfied (there is no guarantee that such an area will be included, so long as it is a spot inspection). In this case, the total number of defects contained in L metres is $\overline{X}L/0.05 = 20\,L\overline{X}$ and the number of defects longer than l will be $20L\overline{X}\sum_{l}^{\infty} P_l$. Therefore, the above requirement will be expressed by:

$$20L\overline{X} \sum_{l}^{\infty} P_l \leqq 1 \tag{5}$$

and accordingly,

$$\overline{X} \leqq 1/(20L \sum_{l}^{\infty} P_l) \tag{6}$$

The $\overline{X}$-Rσ relation has only to be established about a specific L, utilizing the relation between the defect length, l, and the relative fatigue strength, Rσ, in Figure 3, the relation between the probability of presence of defects longer than l, i, e; $\sum_{l}^{\infty} Pl$, and l in Figure 2, and the relation between $\overline{X}$ and $\sum_{l}^{\infty} Pl$ in equation (6). The two chain-line curves in Figure 7 represent the $\overline{X}$ − Rσ relations as obtained about L = 10 m from the average upper limit curve for combined positions, and the upper limit curves for vertical position. Namely, $\bar{x}$ is determined by sampling; $\overline{X} = \bar{x} \pm 2S_{\bar{x}}$ is found from equation (4) and is compared with $\overline{X}$ obtained from Figure 7 for decision to accept or reject.

Estimate of Strength from Rate of Defective Area

The percentage of the total sectional areas of defect existing in a definite area (here 10×50 mm^2), to the nominal sectional area of the specimen is called the rate of defective area. To find this rate, the probable sectional area of a single defect must be determined. For this purpose, the relation between the defect length, l, and its depth, h, must be established. If the experimentally obtained points are plotted and indicated as $h = \sqrt{l^2}$, this will be slightly larger than the average value; therefore, it will be safe to put the area of a defect with length l, i.e. Sl as equal to $l_{\frac{3}{2}}^{3}$. However, considering the condition of manual welding, it might be put as $h_{max} \fallingdotseq 5$ mm (l = over 25 mm). Distributions of defects by sectional areas with $Sl = l_{\frac{3}{2}}^{3}$ are shown for the average upper limit of combined positions and for the upper limit of the vertical position by the broken-line curves in Figure 5. Since the product of this area x, its relative frequency, is the probable contribution of a defect to that sectional area, the total sum, i.e.

$$k = \sum_{l=1}^{\infty} P_l S_l \tag{7}$$

will be the probable sectional area (average sectional area) of a defect, if there is only one defect. Substituting $k = \sum_{l=1}^{l} P_l S_l$, the relations between l and k for the average upper limit for combined positions and that for the vertical position are shown in Figure 5, in which the complexity of the $P_l S_l$ curve seems to be due to the blended distributions of porosity and slag inclusion. The relative frequence declines with an increase in defect size, but k ought to converge to a certain value, because the defect cannot grow infinitely. In the diagram, however, k of the upper limit for the vertical position will not easily converge. But the rate of defective area being counted for 5-cm divisions, then in the above method of estimation, the maximum value of l may be put as 5 cm, and any length larger than 5 cm may be split into two. Thus, we may set

$$k = \sum_{l=1}^{50} P_l S_l = 7 \text{ mm}^2.$$

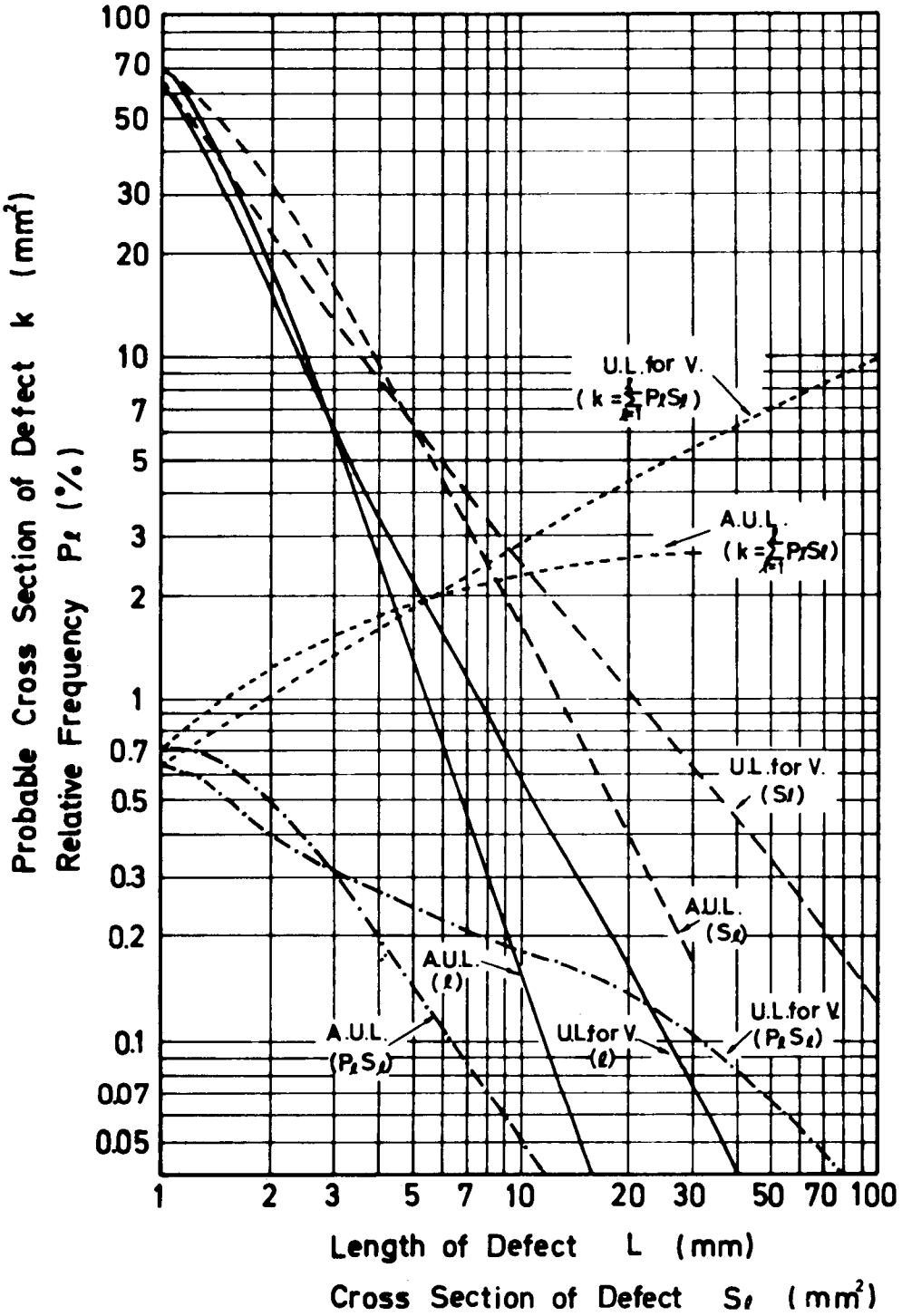

Figure 5

Applying this method to the case of L = 10 m, if 10 m is split into 5-cm divisions and in one of these divisions the relative fatigue strength is permitted to be lower than the specified value $R\sigma$, the probability will be $(0.05/10) \times 100 = 0.5$. This means that rejected areas will be included at a probability of 0.5%. When the average upper limits for combined and vertical positions are plotted under the above consideration, one defect, if it exists, will probably have sectional areas of $k = 3$ mm² and $k = 7$ mm² as calculated on the safe side from Figure 5. Meanwhile, if a 5-cm division contains x_a defects, the rate of defective area, α, in said division will, with plate thickness tmm, be as follows:

$$\alpha = \frac{k\,x_a}{50t} \tag{8}$$

Substituting $t = 20$ mm, and $k = 3$ mm² and 7 mm² for the average upper limits for combined and vertical positions in (8), the relation between α and x_a is found. On the other hand, from the α–$R\sigma$ relation in Figure 4, the relation between x_a and $R\sigma$ is derived. Further, the relation between x_a and $\bar{X}$ is obtained from the 0.5% curve of Figure 6. Thus, from all these relationships the relation between $\bar{X}$ and $R\sigma$ can be established; the solid-line curves in Figure 7 have been obtained in this manner.

According to these results, the decrease in fatigue strength depends predominantly on the length of defect while the average number of defects is small; but when this average exceeds a certain limit, the strength depends predominantly on the rate of defective area. The rate of defective area, α, is vastly influenced by the plate

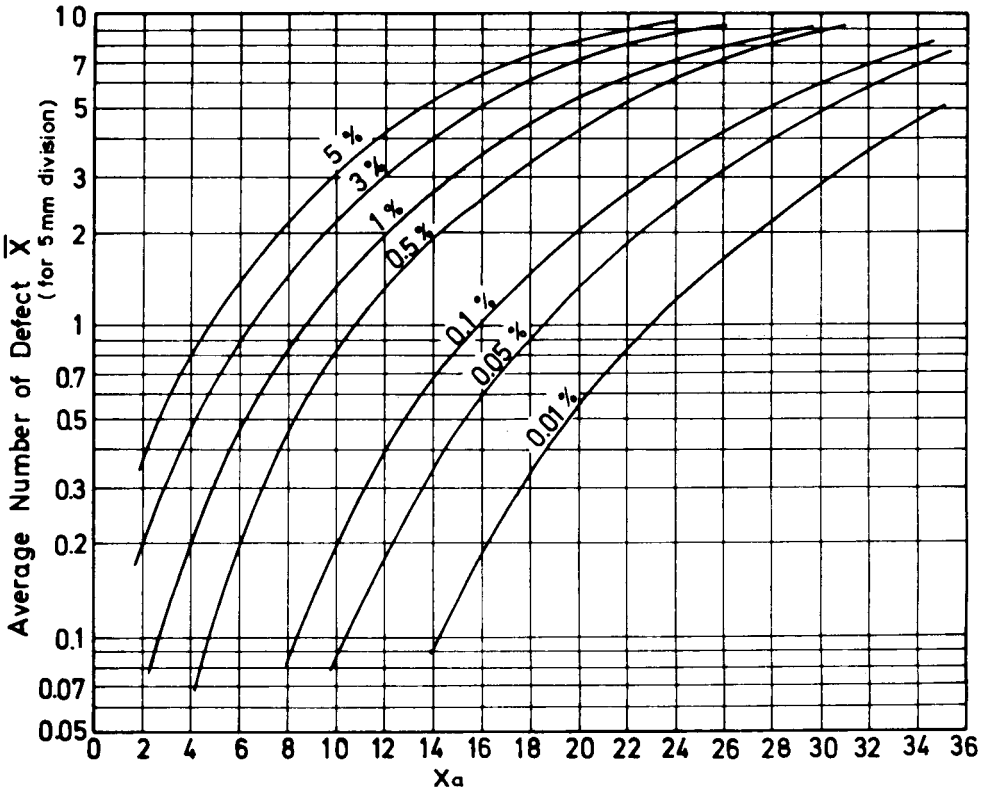

Figure 6
Relation between $\overline{X}$ and χ_a with cumulative relative frequency as the parameter.

thickness, but the length of defect has little bearing on the plate thickness. Thus, when porosities and wide slag inclusions are very numerous, the strength will be governed by the rate of defective area.

A structure will be accepted in evaluation, if $\overline{X} < \overline{\chi} - 2S\overline{\chi}$ for a given $R\sigma$, and will be rejected if $\overline{X} > \overline{\chi} + 2S\overline{\chi}$. But when $\overline{\chi} - 2S\overline{\chi} < \overline{X} < \overline{\chi} + 2S\overline{\chi}$ the inspection must be repeated before a decision on acceptance or rejection can be made. In this context negotiations must be made between maker and customer.

The above results were obtained chiefly from plates of about 20 mm thickness and the data cannot be called ample. Therefore, it is desirable that the accuracy of estimation be improved through investigations of both the defect distributions in the sampled X-ray radiographs and the relation between defect and strength.

Generally the values are taken on the safe side except for values like χ_a.

Conclusions

The above discussion concerns manual butt-welds of about 20-mm thick plates. The experiments on fatigue strength show that with increasing plate thickness, the effect of a central defect on the strength will be weaker than one located near the surface. As the actual tests on strength indicate, a large central defect does not cause a fracture, but a small defect, like a surface fissure which does not show on an X-ray film, initiates cracking. Accordingly, the method of quality evaluation described here should be considered applicable only to welds with no fissures, incomplete penetrations, undercuts or reinforcements. Lastly, a brief study was made of welds containing cracks and undercuts or having non-machined reinforcements.

The authors' study (2), indicates that the length of the crack is not significant. When the crack occurs near the surface, the pulsating tensile fatigue strength of a weld drops to about 50% of that of a non-defective part; presence of undercuts results in a similar decline of strength. The effect of incomplete penetration is greater than that of slag inclusion. Further, if there is reinforcement at the number of cycles in pulsating tensile fatigue test $N=2\times10^6$, the strength will be reduced to about 50% even if no defect is contained; and if reinforced at $N=5\times10^4$, the presence of reinforcement ceases to be influential.

In conclusion, only about half the high-cycle fatigue strength of a non-defective part can be guaranteed unless the reinforcement is machined away and it is confirmed by magnetic inspection that no surface near-surface cracks exist in the welds.

The authors are determined to push this program of research vigorously and they hope to be able to publish a follow-up paper.

References

(1) Kihara, H. Radiographic sampling in the inspection of ship structure. Pre-prints of 4th Int. Conf. on NDT (1963), 7.
(2) Relation between defectiveness of welds of 302B steel and their strength: Japan Welding Engineering Society, (1966).
(3) Green, W. L., Hamod, M. F. and McCauley, R. B.: Welding Research Supplement May (1958), p. 2065.
(4) Bradley, J. W. and McCauley, R. B.: Welding Research Supplement Sep. (1964), p. 408.

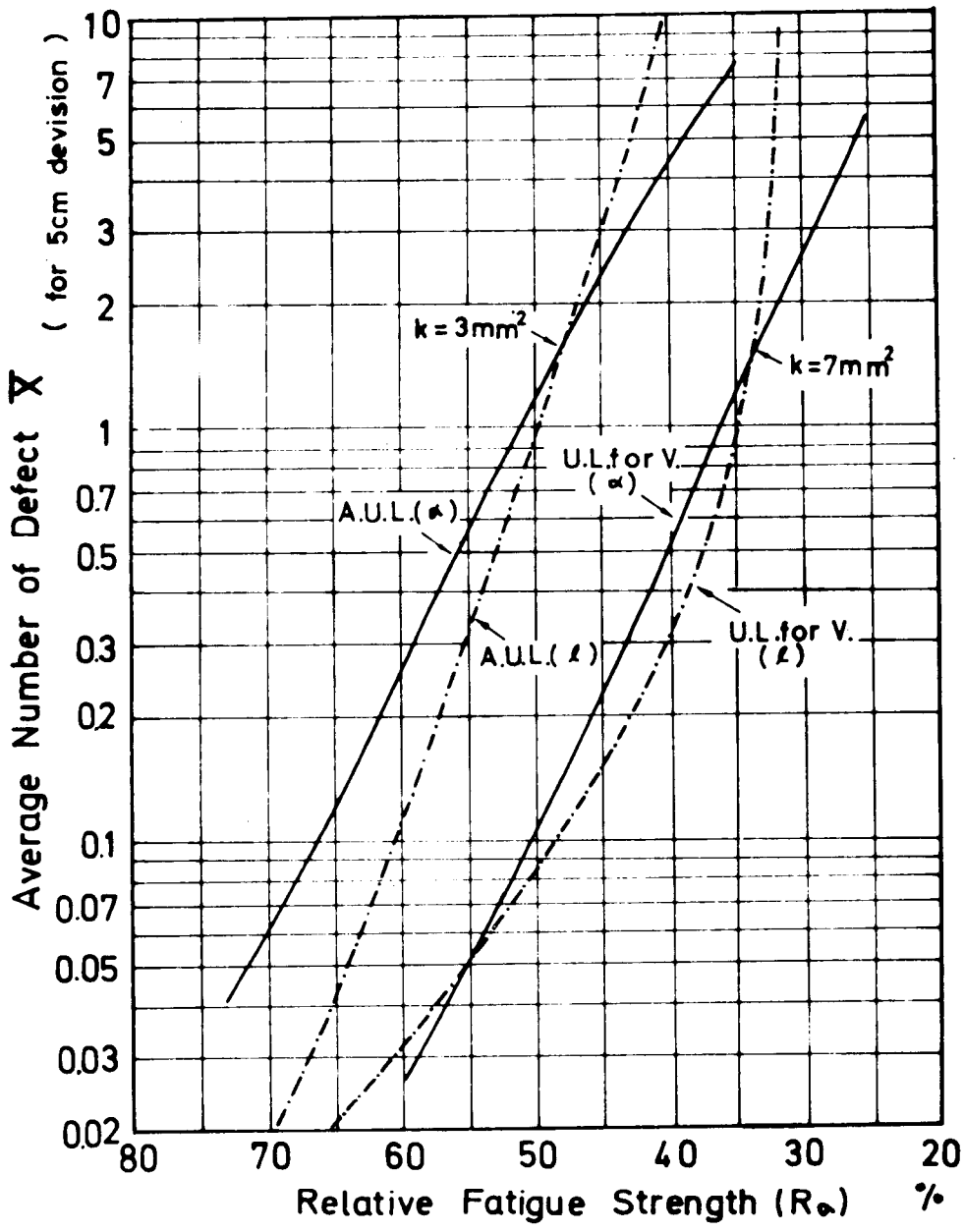

Figure 7
Relationship between the pulsating tensile fatigue strength Rσ and the average number of defects for 5-cm division when, on 10 m of weld line, only one area (5 cm) is permitted to be short of relative fatigue strength.

(5) Nondestructive testing of welds and their strength (1960). The Society of Naval Architects of Japan.

(6) Kihara, H. and Ishii Y.: Proceedings of Third Internat. Conference on NDT (1960), p. 91.

(7) Ishii, Y. and Nakada, M.: Journal of Nondestructive Inspection, Vol. 10, No. 5 (1961), p. 214.

(8) Ishii, Y. Report of Transportation Technical Research Institute, No. 49 (1962), 1.

(9) Homès, G. A.: Arcos, Vol. 15, No. 89 (1938), p. 1951.

(10) Mase, O. and Erra, A. Metalluria Italiana, 45, (1953), 8, p. 273.

(11) Murakami, N.: Unpublished.

(12) Newman, R. P.: BWRA Research Report April, (1963), No. D2/4/62.

Flaw Detection in Finned, Thin-Walled Tubes

V. V. GORSKY, V. T. PRONYAKIN, E. M. LOVYAKIN AND V. M. ZAKHAROV, USSR

ABSTRACT: Finned thin-walled tubes are used for canning reactor fuel rods. Helical fins on the outside surface of the tubes are made for spacing fuel rods in a subassembly (1). The canning tubes must be of very high quality to maintain the integrity of the fuel elements during reactor service.

For ultrasonic testing of the finned tubes we made two types of apparatus, and an eddy-current apparatus for measuring the wall thickness. For ultrasonic testing of the finned tubes we used Lamb waves. When the Lamb waves are propagated in the finned part of the wall it transforms and interacts with longitudinal and transverse sound waves which are reflected from the side surfaces of the fin. Thus, the total amplitude depends on the profile of the fin. The presence of the fins reduces the sensitivity of the ultrasonic inspection of the tubes and complicates the testing apparatus (2).

The purpose of our work was to study the sensitivity of the two-probe ultrasonic method (through-transmission immersion technique) and the one-probe ultrasonic method (reflection immersion technique) for the detection of longitudinal defects in finned thin-walled tubes.

The Two-Probe Apparatus

A schematic view of the two-probe ultrasonic testing of the three-finned tube and a block diagram of the apparatus are shown in Figure 1. The transmitter and receiver probes are placed on the outside surface of the tube symmetrically about the fin. The angle of incidence of the ultrasonic wave on the tube surface between the fins is taken to generate in a thin wall a definite mode of Lamb waves. To test a whole cross-section of the tube there are three pairs of ultrasonic probes spaced 120° apart. The probes are mounted in a plexiglass holder.

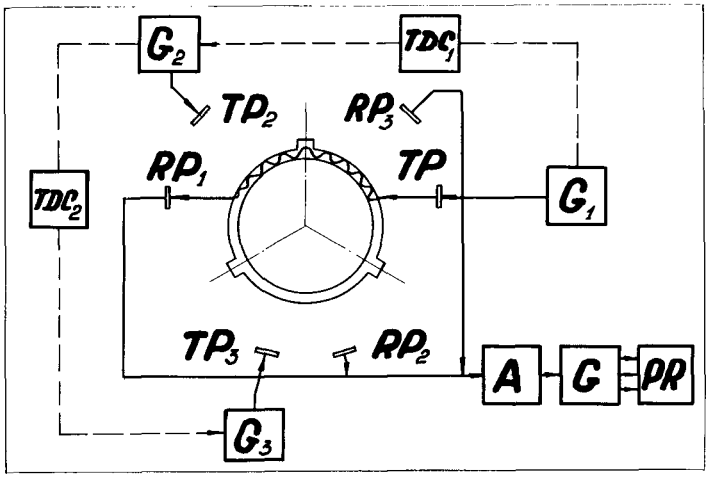

Figure 1. Block diagram of the apparatus and schematic view of the two-probe ultrasonic testing of a 3-finned tube: G_1, G_2, G_3—pulse generators; TDC_1, TDC_2—time delay circuits; TP—transmitting probe; RP—receiving probe; A—amplifier; G—Gate; PR—pen recorder.

The transmitter probe of the first pair of probes TR_1 is excited by the free-running pulse generator PG_1. The transmitting probes of the two other pairs are excited one after another by the pulse generators PG_2 and PG_3. The time delay between three pulses is achieved by means of the two time-delay circuits DC_1 and DC_2. Time-delayed ultrasonic pulses pass through the coupling medium and propagate in the part of the wall being tested. Then the pulses received are fed to the common amplifier A. The time selection of the ultrasonic pulses into the three channels is accomplished by means of the gate circuits G. The pulses in each channel are amplified and fed into the three-channel recorder R. If, for example, there is a crack on the inner surface of the tube some part of the sound waves is reflected by it and the ultrasonic field strength on the surface of the receiver probe is reduced. The pen recorder shows reduction of the signal level.

The complete installation for two-probe ultrasonic testing three-finned tubes (Figure 2) consists of the axial transport device (1), small immersion tank (2) with probe assembly (3), instrument support (4) and three-channel pen recorder (5). Two sets of profiled guiding wheels (6) pull the tube through the test tank (2). The proper position of the probe holder in relation to the tube is achieved by using the tube as a support member for the probe holder. The probe holder is pressed to the tube (through a teflon prism) with four springs. Water escaping through the bushes of the test tank is fed into the degassing tank (9) by a small centrifugal pump. Both the tanks are connected by a pipe.

Electronic instrument (10) is transistorized.

Technical Performance

1. Axial speed of the tube, m/min	3-4
2. Frequency of the pulsed ultrasound, MHz	9-10
3. Pulse repetition rate, pulse/sec	3000-4000
4. Sensitivity to defects	
a depth, μm	60-70
a length, mm	5
5. Recording, three-channel H320-3 pen recorder	

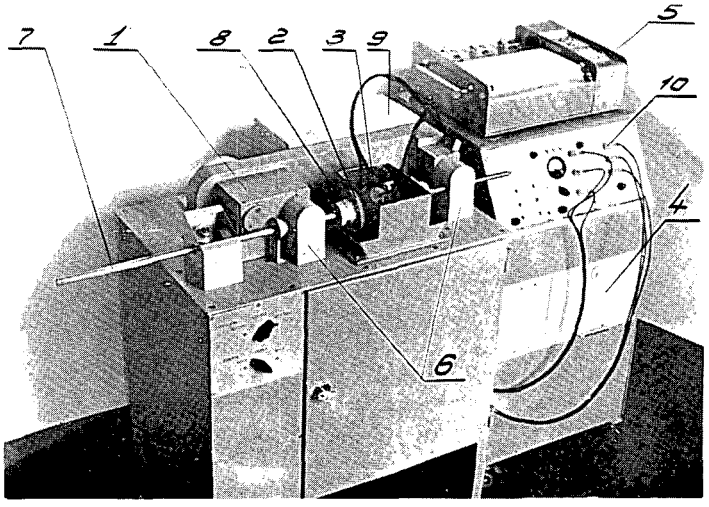

Figure 2. General view of the installation for the two-probe ultrasonic testing of a 3-finned tube: 1. axial transport device; 2. immersion water tank; 3. probe assembly; 4. instruments support; 5. 3-channel pen recorder; 6. profiled guiding wheels; 7. tube; 8. seal; 9. degassing tank; 10. electronic instrument.

Sensitivity to defects on the outer and inner surfaces of the tube is the same. The through-transmission technique ensures the detection of defects, the direction of which do not coincide with the axis of the tube. Figure 3a shows a record. The right trace refers to two longitudinal cracks on the bore (under the fin) of a different depth (105 and 57μ m) and a length (2 and 5 mm). Figure 3b shows the metallographic cross-section of the first crack. The defects 50-60 μm deep reduce the level of the trace by 20%, irregularity fluctuations by 10%.

The One-Probe Apparatus

A schematic view of one-probe ultrasonic testing finned tubes and a block diagram of the apparatus is shown in Figure 4. Probe (1) is inserted into the bore of the tube (2). The commercially available pulse-echo instrument type UDM-1M was used. This flaw detector can provide ultrasonic pulses up to 6 MHz.

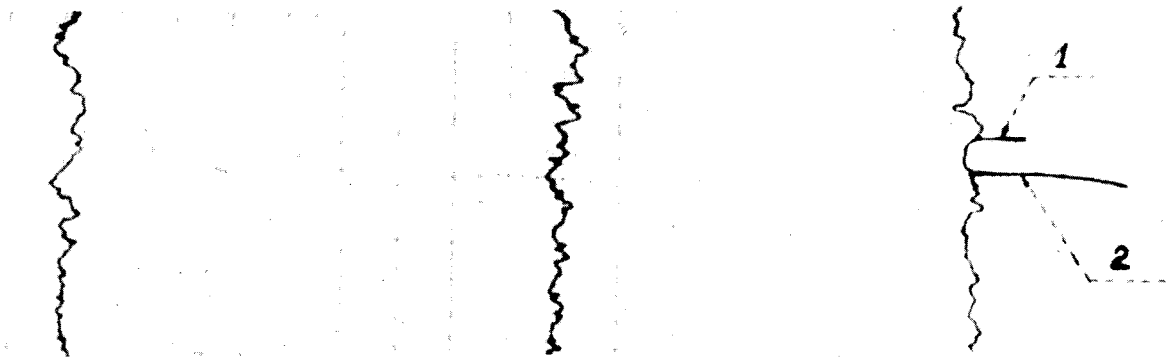

Figure 3a) Part of the inspection record. 1. longitudinal cracks, 57 μm deep; 2. longitudinal cracks, 105 μm deep.

Figure 3b) Section through defect 1. (X400).

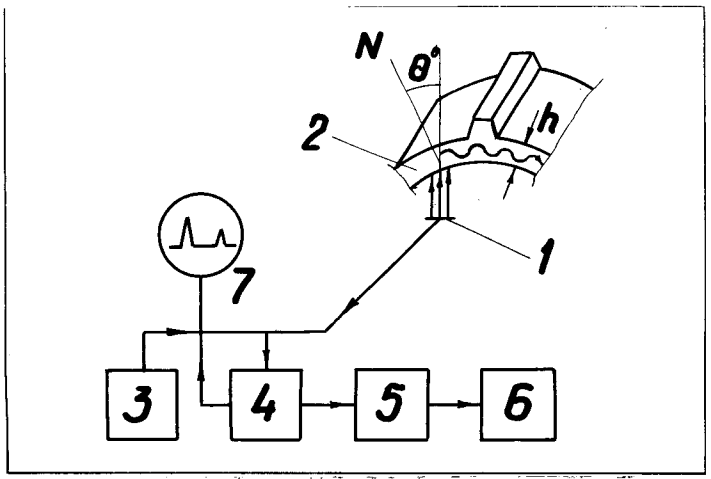

Figure 4. Block diagram of the apparatus and schematic view of the one-probe ultrasonic testing of finned tubes: 1. probe (transmitter-receiver); 2. part of the finned tube; 3. pulse generator; 4. amplifier; 5. gate; 6. light signal; 7. oscilloscope.

The pulse repetition rate was increased to 3800 pulses/sec. The angle of incidence and the frequency of the ultrasonic waves were chosen so as to generate in the wall modes S_0 (1 symmetrical) and a_0 (1 asymmetrical) of Lamb waves. The best results were obtained for f.h.$\geqslant$2.2-2.4 MHz.mm. In this case the amplitude of the reflected signal from the fin is less than the amplitude of the reflected signal from the defect 20 μm deep on the inner surface of the tube. However, the same amplitude of the signal reflected from the defect on the outer surface was received only for the defects more than 70 μm deep. The greater sensitivity to the defects on the inner surface is due to the direct reflection from the defect and the presence of the surface waves that propagate in the thin layer of the inner surface of the tube.

Figure 5 shows a combined transmitter-receiver probe assembly. The probe consists of a rectangular lead zirconate-ti-

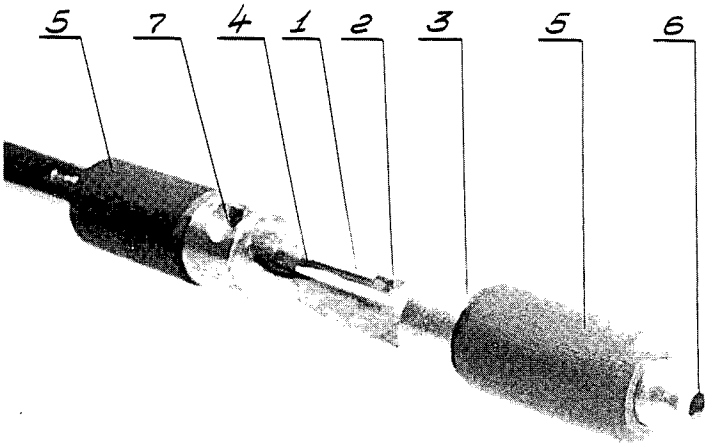

Figure 5. Transmitter-receiver probe assembly: 1. transmitter-receiver piezocrystal; 2. pin; 3. body; 4. electrode; 5. tight spigots; 6, 7. channel holes.

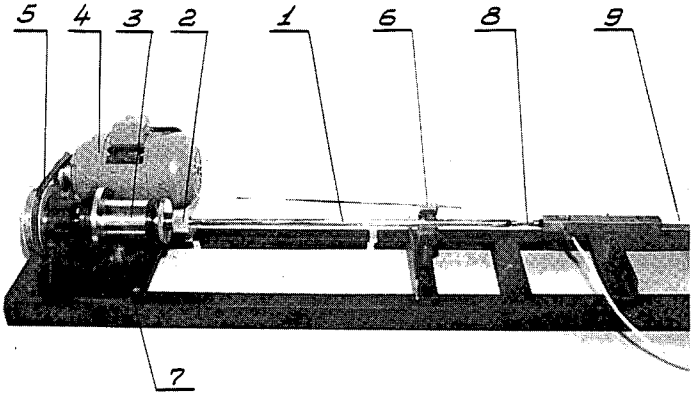

Figure 6. Installation for one-probe ultrasonic testing of finned thin-walled tubes: 1. tube; 2. holder; 3. spindle; 4. motor; 5. belt drive; 6. split bearing; 7. connection; 8. probe.

tanate crystal 2.5 mm × 10 mm in size. It is cemented by electroconductive epoxy resin filled with silver powder to a flat surface of a pivoted pin (2). The other electrode of the coaxial cable is soldered at the radiation face of the crystal. The crystal is covered with a waterproof compound.

To eliminate spurious signals from air bubbles passed through the tube water, we made a bypass channel in the holder with the inlet entry positioned in the centre of the head of the holder. When the speed of rotation of the tube is more than 400 rev/min the air bubbles are forced by water to the axis of rotation of the tube. Thus, the water with air bubbles passes through the bypass channel without entering the region where the crystal is placed.

A photograph of the installation for one-probe ultrasonic testing of finned thin-walled tubes is shown in Figure 6. Tube (1) is rotated by an electric drive. Water is pumped through the bore of the tube. Probe (8) is inserted into the bore by another electric drive. Water escaping the bore is collected in a small tank not shown in Figure 6.

Technical Performance

1. Rotation speed of the tube, rev/min	650–950
2. Speed of the axial movement of the probe, m/min	1.7–2.5
3. Frequency of the pulsed ultrasound, MHz	4.5–6
4. Pulse repetition rate, pulses/s	3800
5. Sensitivity to defects	
a) on the outer surface	
a depth, μm	70–80
a length, mm	0.5
b) on the inner surface	
a depth, μm	15–25
a length, mm	0.5
6. Recording	light and sound signals

Comparisons of both ultrasonic methods, the complexity of the mechanical parts of the installations and of the electronic instruments and some other parameters show the advantage of the one-probe ultrasonic installation excluding the sensitivity to the defects on the outer surface of the tube.

The Eddy-Current Apparatus

The thickness of the wall between the fins is measured by eddy-current. A block diagram of the apparatus is shown in Figure 7. The apparatus measures the relative impedance variations of two pick-up coils L_u and L_k which are incorporated in a

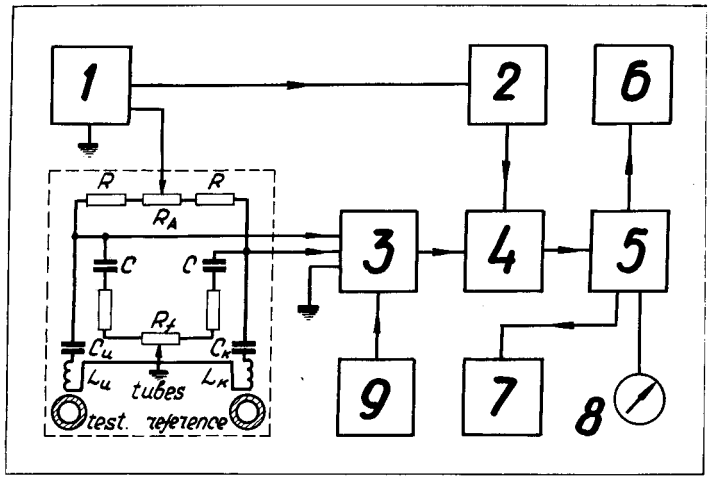

Figure 7. Block diagram of the apparatus: 1. oscillator; 2. phase shift; 3. differential amplifier; 4. phase detector; 5. amplifier; 6. alarm signal; 7. pen recorder; 8. microampermeter; 9. rectifier.

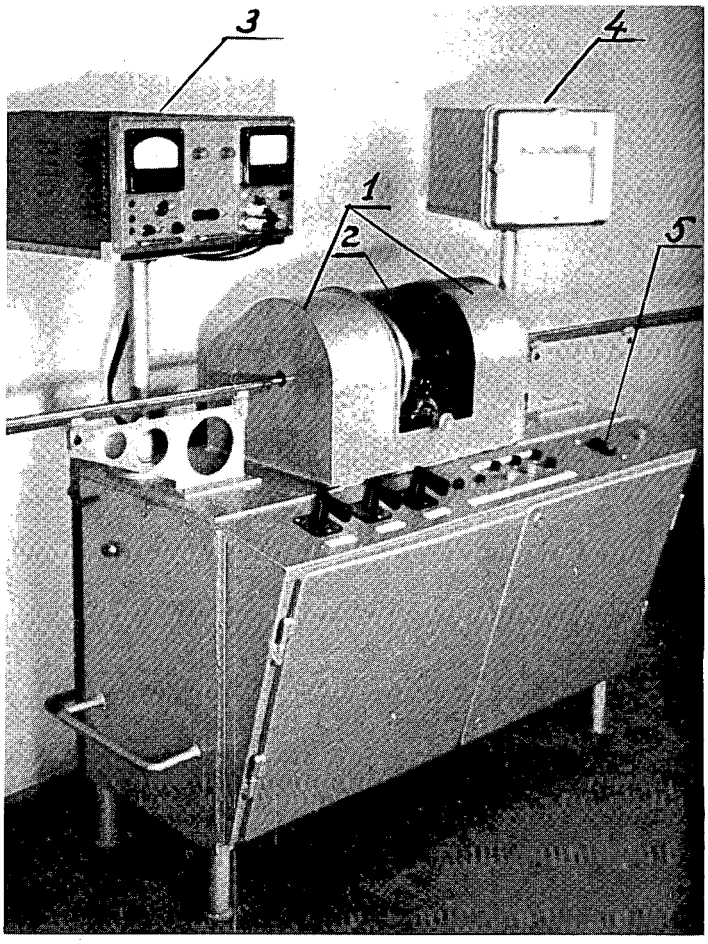

Figure 8. Installation for measurement of the wall thickness of finned tubes: 1. axial transport devices; 2. pick-up coil; 3. instrument; 4. pen recorder; 5. automatic control arrangement.

resonant bridge circuit. One of the coils is placed on the reference tube, while the tube to be tested is traversed beneath the second coil L_u. The passage beneath the pick-up coil of the tube, the wall thickness of which deviates from the reference tube, temporarily unbalances the bridge. The unbalance voltage is amplified by the differential amplifier DA and then is detected by the phase detector PD. Bucking voltage is fed from the phase adjusting circuit PS (to avoid the influence of changing the air gap between the pick-up coil and the tube). The output from this phase detector after a further stage of amplification drives a conventional pen recorder PR and an alarm signal and is measured by the direct-reading instrument PI.

The photograph of the complete installation is shown in Figure 8. It consists of two axial transport devices (1), pick-up coil (2), pen recorder (4) and automatic control arrangement (5).

Technical Performance

1.	Inner diameter of finned tubes, mm	4–20
2.	Wall thickness, mm	0.2–0.8
3.	Number of fins	2,3,4,6
4.	Speed of axial movement of the tube, m/min	1–6
5.	Diameter of the tested area, mm	5
6.	Accuracy, % of the wall thickness	2

References

1. Zaimovski, A. S., Kalashnikov, V. V., Golovnin, I. S. Heat-producing elements of nuclear reactors. Atomizat, Moscow 1966.
2. Gorski, V. V., et al. Flaw detection in thinwalled tubes. Non-destructive testing in nuclear technology. Proc. Symp. on NDT in Nuc. Technol. 17-21 May 1965, Bucharest, 1965.

Technical Session 14/Ultrasonic Standardization

A Proven Method of Selection and Standardization of Ultrasonic Probes

L. NIKLAS AND H. STOLL, GERMANY

ABSTRACT: A method based on technical data is presented giving figures for the application limits of the following points: Nominal frequency, including the spurious resonances of probes. Figures to describe the performance of the sound fields. These are: the near-zone length N, the angle of divergence in the far zone, and the effective diameter of the probe D_{eff}. Separate figures for the instrument sensitivity S_e and the probe losses L_p are given. From the difference in these two figures, using the AVG diagram, we find the minimum detectable defect size at any given distance.

To establish the resolution the damping factor d is given. In the appendix, the equations to calculate the resolution from this damping factor d is given.

A method of measurement is discussed covering the near-surface resolution for any given defect diameter.

List of Symbols

N	= near-zone length of a probe
D_{eff}	= effective probe dia
λ	= wave length
γ	= angle of divergence in the far-zone cone
S_e	= sensitivity of unit in db
L_p	= probe loss in db
d	= damping factor
r_m	= theoretical resolution for two echoes if the second one is m dB lower than the first one
c	= sound velocity
f_0	= nominal frequency of probes
ρ	= density of material

Introduction

For nondestructive testing by the ultrasonic pulse-echo method there is no ideal electro-acoustic transducer. Each probe must be a compromise between sensitivity, resolution and ruggedness. Therefore, it is necessary to have a method, based on technical data, to select the most suitable probe for any test problem.

In this paper the technical characteristics of ultrasonic instruments are only used when they are directly related to the probe characteristics.

To be useful, the method of selection should answer the following questions:

1) What is the minimum defect size detectable at any given distance? In practice the question is often worded this way: What gain-control setting should be used to detect a given size defect at a given distance?

2) What is the minimum distance between two defects that will give separate indications? (Depth resolution and sound beam divergence).

The working temperature range, ruggedness, waterproofing, etc. are also important, but owing to space limitations these items are not discussed.

In presenting the answers to these questions by means of a method based on technical data, we are quite aware that, in ultrasonic testing, we do not normally have laboratory conditions. The influence of surface roughness, irregular defect surfaces and insufficient coupling will bring tolerances into the measurements. We have to accept these tolerances in the answers to the problem. Nevertheless, the method presented is not artificially simplified. It takes into account the complex form of the sound field of the probe and the electrical matching of the probe to the instruments.

To illustrate the hazards of a simplified evaluating method, let us make a test in accordance with a popular method, which specifies measurement of the echo height obtained from the flat-bottom hole in the Series A Alcoa No. 1 test block (0.4 mm or 1/64-in. hole at 76 mm or 3 in. distance). Comparing two 4 MHz probes of 20- and 24-mm diameter (Krautkramer Q4S and Q4T), we find by this method that the 20-mm probe is six times more sensitive than the 24-mm probe. If we repeat this test with the same flat-bottom hole at 500-mm distance, we find the opposite: the 24-mm probe has twice the sensitivity of the 20-mm probe. If we accept the echo height from the Alcoa No. 1 test block as a sensitivity standard for the probes in question, we are in error by a factor of 12. The reason for this discrepancy is due to the following: for the 20-mm probe, the hole in the Alcoa block is just in the near-zone maximum (see Figure 2). The 24-mm probe has a near-zone minimum at the same distance.

Probe Characteristics

Nearly all probe characteristics are dependent on frequency. Therefore, we should first define the nominal frequency. We know that for damped oscillating systems such as probes, the resonant frequency and the natural frequency have different values. An ultrasonic pulse is generated mostly by the free ringing of the crystal; only a negligible part is due to forced vibrations. Therefore, the nominal frequency should be the natural frequency of the probe.

Pulse-echo instruments do not generate at a single frequency, but rather over a wide bandwidth of several MHz. Therefore, the manufacturer has to insure that there are no spurious resonances in the neighbourhood of the natural frequency.

Measurement of the probe frequency can be done by wave analysis of the echo signal from a thin plate. The previously recommended procedure of counting the high-frequency oscillations of the echo with an oscilloscope is not very accurate, and fails to detect cases where the probe has more than one resonant point. Figure 1a shows the wave analysis of a 4-MHz probe with only one resonant point. Figure 1b is the oscillogram of

the same echo. Figure 1c shows the frequency analysis of a probe with distinct spurious resonance at 3.8 and 4.2 MHz. In the corresponding oscillogram (Figure 1d) the influence of this spurious resonance is not visible. Under test this last probe produces distinct deviations in defect-size measurements. Such a probe must be rejected in practice.

Accurate wave analysis can be made with instruments designed for the measurement of broadcast interference. They are superheterodyne receivers covering a wide frequency range, having a bandwidth of at least 9 KHz, and incorporating a calibrated gain control. The measurements (Figure 1) were made with a Siemens type B83600.

To select a probe of suitable frequency we must first determine from the AVG diagram (Figure 3) what is the minimum detectable defect size. Secondly, we should not forget that sound attenuation increases with frequency. The selection of a suitable frequency is often a compromise between the defect detectability and the attenuation.

AVG Diagram, Near-Zone Length, Divergence

In the practice of ultrasonic testing the technician should be constantly aware of the sound-field shape. A Schlieren picture (Figure 2) shows its typical shape. Close to the probe we have the near zone, characterized by the fact that the total sound intensity is nearly independent of distance, but sections of the beam show periodic variations in intensity. The last maxima lie in the centre of the sound beam at the distance:

$$N: \frac{D_{eff}^2}{4\lambda_o},$$

the near-zone length. This near-zone maximum has a long-drawn shape of nearly two wavelengths diameter and half N length. At this distance the normal probe behaves much the same as a focussed probe. At greater distances, in the far zone, the sound beams open conically with the angle of divergence: $\sin\gamma: 1.2\ \lambda / D_{eff}: 0.3\ D_{eff}/N$

These are the most important characteristics of the sound field. In the AVG diagram, Figure 3, they find their quantitative application. This diagram gives the decrease of sound energy (measured in db) resulting from distance and defect size. The sound energy decreases because part of it bypasses the defect and also part of the reflected energy bypasses the probe.

We assume that the theoretical foundation of the AVG diagram and its practical application is known (1, 2).

From the shape of the sound field we establish the following rules for the selection of probes:

1) For most sensitive detection of small defects at a given distance we select a probe with a near-zone length equal to the distance.

2) For the same application at very short distances we use specially focussed probes.

3) To find large defects at long distances and to make quantitative defect size measurements, we select probes with shorter near-zone lengths than the defect distance.

Because of the variations of sound pressure in the near zone, the detection of defects is difficult and quantitative measurements in this range are subject to large errors. More suitable probes for this range are special quasi-Gaussian probes, which have an equalized near zone.

Sensitivity

The AVG diagram shows that the back echo from a thin plate (thinner than the near-zone length) is an excellent sensitivity standard. In this range the sound-energy loss is nearly independent from plate thickness. Of course, we must use a plate

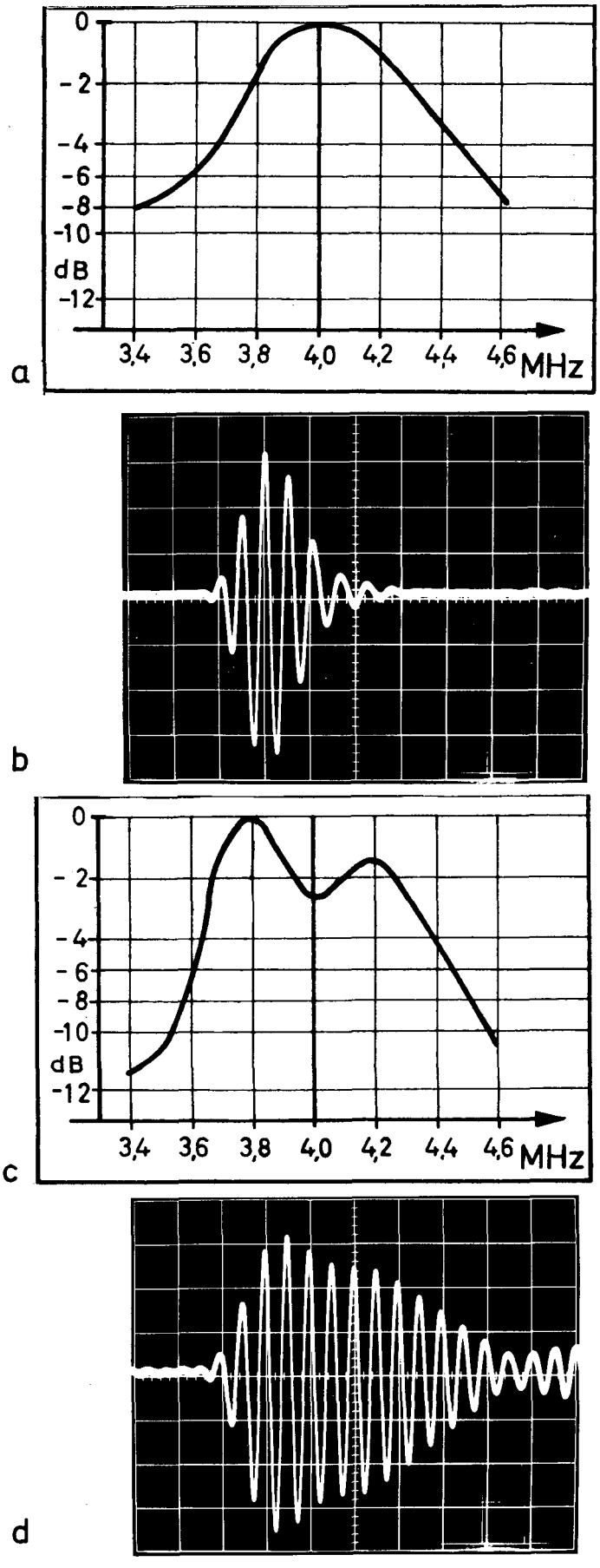

Figure 1

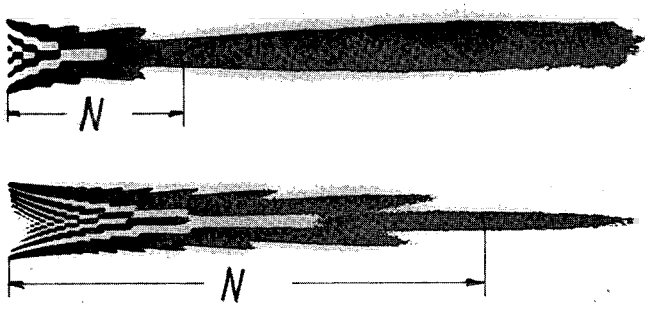

Figure 2

of low-attenuation material. In practice the over-all test sensitivity of the instrument is limited by the thermal noise of the amplifier. To establish a sensitivity figure, we first measure the height of the noise on the screen with the gain set at maximum. Second, we bring the back echo from the thin plate to the same screen height and define the gain control setting as zero db. All modern pulse-echo instruments have a gain control calibrated in db. To obtain the sensitivity figure, we only need to read reserve S (difference between the gain setting for the back echo of a thin plate and maximum gain). With this sensitivity figure we find from the AVG diagram directly, the minimum detectable defect size for any distance.

Generally a probe will be used with several different ultrasonic instruments and vice-versa. It is therefore an advantage to have the sensitivity figures for probes and instruments separately. These values are obtained by simple measurement of a-high frequency voltages with an oscilloscope and of b-impedances with a bridge.

Taking v_e as the peak voltage of a pulse equivalent in height to the thermal noise of the instrument, and R_e as the input impedance of the instrument, then

$$\frac{v^2_e}{2R_e}$$

will give us the minimum peak pulse power detectable by the instrument.

Taking v_p as the peak voltage of the transmitter pulse and R_p as the electrical impedance of the probe,

$$\frac{v^2_p}{2R_p}$$

will give the peak transmitter pulse power. The sensitivity of the instrument S_e in db is defined as the ratio of both powers:

$$S_e: 10 \log \frac{v^2_p R_e}{v^2_e R_p} \text{ (db)}$$

Manufacturers who have not standardized their probe impedances R_p must give the sensitivity figure S_e for every probe impedance R_p. S_e is the figure representing the power reserve of the instrument. In practice this reserve must compensate the following energy losses:

1) Conversion losses from electrical to sound energy in the probe and sound losses in the damping device of the probe.

2) Losses in sound propagation and reflection by the defect. These can be established quantitatively from the AVG diagram.

3) Re-entry losses: only part of the reflected energy enters the probe.

4) Conversion losses from sound to electrical energy in the probe and matching losses in the unit.

For a thin plate of negligible attenuation the sound energy losses in 2 above are 0. The other losses (1, 3 and 4 above) can be grouped together as total probe losses L_p. To measure L_p, we put the probe on the thin plate and measure the transmitter peak pulse voltage v_p, the echo peak voltage v_e, the electrical impedance of the probe R_p and the electrical input impedance R_e. From this we calculate the ratio of transmitter pulse energy to echo pulse energy:

$$L_p: 10 \log \frac{v^2_p R_e}{v^2_e R_p} \text{ (db)}$$

Taking the difference S: S_e—L_p to the AVG diagram we obtain the minimum detectable defect size.

Example: Taking an ultrasonic instrument (Krautkramer· USIP 10) we measure S_e: 157 db, for the probe (Krautkramer· Q4S) L_p: 55 db. The difference is S: 102 db. From the AVG diagram, Figure 3, we see that 0.2 mm dia flat-bottom defects are detectable at 1-m distance, and 2-mm dia defects can be detected at 10-m distance. In practice we have to subtract from the energy reserve S, the energy losses for attenuation and for imperfect coupling between probe and the test specimen.

Technicians who have to make frequent measurements of S_e and L_p can save time by making the measurements on one standard probe for each frequency. All other values can be measured by comparison with this standard. A quartz crystal cemented to an aluminum plate was found to be a good arrangement for this purpose. In practice we have to remember that the probe figure L_p is dependent on the material under test, especially if the probes have an acoustic matching device. Therefore, it would be recommendable for manufacturers to specify the probe figure L_p for typical materials such as water, aluminum and steel.

Damping Factor

To have good depth resolution the oscillation of a probe must be damped. A quantitative figure for this is the damping factor. It is defined as the amplitude ratio of any oscillation to the next one in the same pulse. The damping factor is dependent on the acoustic impedance of the material, therefore it should be given for steel, aluminum and water. Also of great interest is the damping factor d for a standard rough surface in steel (i.e. a surface with 60° teeth spaced 1 mm) coupled to the probe with water or oil. In practice we find that this value is close to the value for water.

In most probe types the matching device between the unit and the crystal is built in the probe. The technician should remember that the total value of the damping factor is made up of electrical and mechanical damping.

For several instruments on the market the damping factor is also dependent on the sensitivity setting of the instrument itself. In these cases, the value for the damping factor should be given for low, medium and high gain settings.

To measure the damping factor, we pick up any echo from the probe with a highly damped crystal. This pick-up crystal should have a resonant frequency at least three times higher than the probe under test. The pick-up echo is displayed on a wide-band oscilloscope and the damping factor is measured from the amplitude ratio within the pulse. Because of spurious resonances in the probe, the flank of the echo may not have a uniform drop. In these cases, we measure the damping factor from the mean envelope of the pulse. To obtain an accurate value, it has been proven in practice that the flank of the pulse should be measured from the maximum down to 1% of the maximum. If the damping factor in this range is not uniform, we should take the minimum value found.

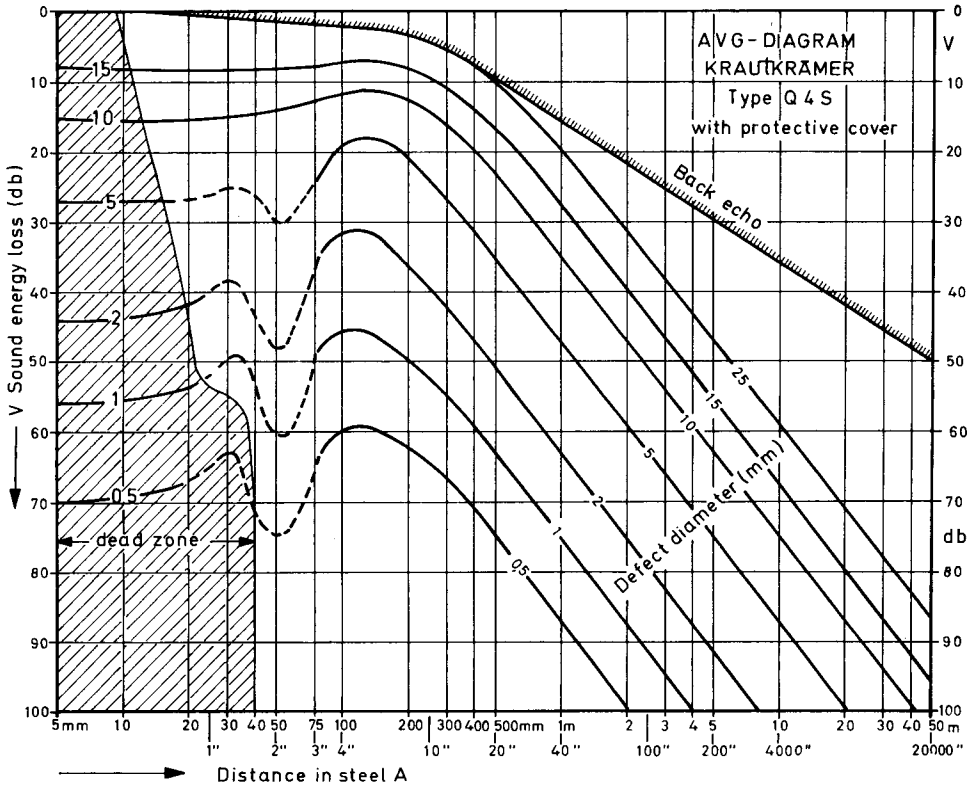

Figure 3

The amplifier of the instrument has tuned circuits with a certain amount of damping. The damping factor for the instrument is defined the same way as for the probes and is measured with a short electrical pulse. Normally the damping factor for the unit is much higher than for the probes. If this is not the case, the lower value found for the instrument must be used to qualify the system of instruments and probe.

Theoretically, it is possible to measure the damping factor with the pulse-echo instrument itself. But only a few of the instruments on the market are suitable for the purpose, because some amplifiers have a dead zone directly following any echo pulse. This effect presents a higher damping value than that which really exists. Damping factors measured from instruments having such "cosmetics" are irrelevant. Such "cosmetics" do not increase the resolution, but only replace the normal pulse with a shorter one followed by a dead zone.

In the literature we sometimes find the value for the mechanical Q instead of the damping factor d. The relation between the two is:

$$Q: \pi/\log_e d$$

We prefer the value for the damping factor, because it can be measured directly. Also for pulse-echo purposes probes with increasing Q have less resolution.

For a probe with a given damping factor we find the resolution from the calculation in the appendix (See Figure 4).

From the calculations in the appendix we learn the following:

The higher the damping factor d, the higher the resolution. But this rule is not always valid for the near-surface resolution. This resolution is also dependent on the probe loss L_v, the damping of the matching device and other influences. It is possible for probes with higher damping to have lower near-surface resolution. From this, we learn that the near-surface resolution cannot be stated for the probe alone or for the instrument alone; it is a figure for the system: instrument and probe.

Quite often specifications require that the back-echo of a plate of given thickness be fully separated from the initial pulse. This type of specification does not meet practical requirements, because normally we want to detect small defects close to the surface, rather than the back-echo of plates. Using the AVG diagram, we can extend the plate method to a method that has been proven in practice for the near-surface resolution.

We start with the normal plate test and bring the back-echo of the plate to 50% screen height. The figure for near-surface resolution, or dead-zone length, is the plate thickness where the initial pulse and back-echo merge together. The exact point of "merging" is defined as follows: the back flank of the initial merges with the back-echo at 6 db below the maximum echo height (not half the echo height). This limit of 6 db drop is dependent on distance, due to the sensitivity drop following the initial pulse. It must be measured for each plate thickness separately. This first plate resolution value is marked on the back-echo curve of the AVG diagram Figure 3. The probe is put on a thick plate in an area free of defects and the gain is increased x db. The distance at which the back flank of the initial pulse falls below the 6 db limit is plotted on the AVG diagram x db below the back-echo value. Repeating this measurement for different values of x, we establish the curve which gives the dead-zone length for different defect sizes (hatched area, Figure 3).

This measurement is incorrect if the sensitivity drop following the initial pulse is not taken into account. This sensitivity drop can be measured with a pulse generator, coupled at high impedance. A measuring pulse from the generator is set at half screen height at a point equivalent to a large distance. If this measuring pulse shows a drop of a db at the previously measured dead-zone length, then we use the (a-x) db value instead of the x value to plot out dead-zone length on the AVG diagram.

Probes that are to be used on rough surfaces, should be measured on a test plate with a standardized rough surface. Such a surface has 60° teeth and 1-mm tooth width.

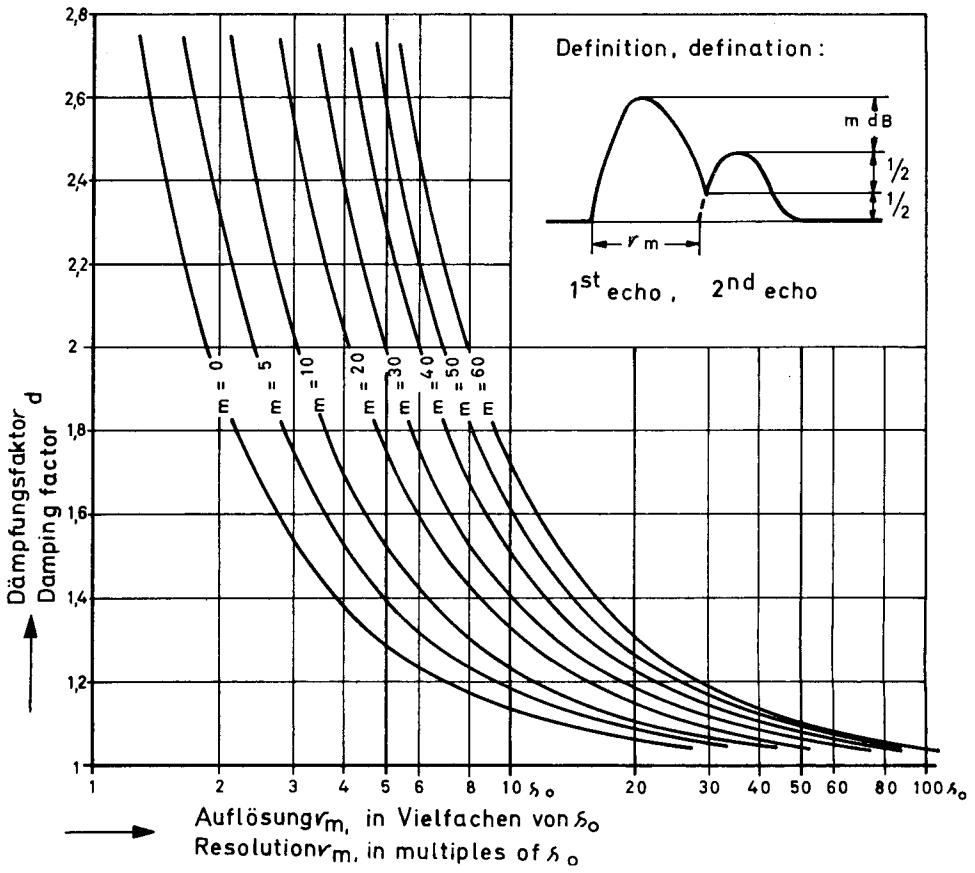

Figure 4

In practice there is another important zone: the pulse-influence zone. This is the distance in which the defined measuring pulse drops by a factor of 3 db in large distances. Within this pulse-influence zone it is not possible to make a quantitative defect-size measurement, without making special corrections for the sensitivity drop. (This zone is not shown on the AVG diagram Figure 3, because, for the unit under test, the pulse-influence zone is shorter than the near-surface resolution).

Final Remarks

The method described is mainly designed to select the most suitable probe for a given problem.

Mistakes can happen if the method is used to qualify probes and instruments from different manufacturers. For instance, if the instrument sensitivity S_e and probe losses L_p from manufacturer A are both high and the same values from manufacturer B are both low, it is a mistake to assume that the high-sensitivity unit from manufacturer A together with the low-loss probes from manufacturer B would be an ideal combination. In such case, it is possible that the only difference is that manufacturer A has the matching transformers on the instrument and manufacturer B puts them in the probes. Mixing probes and instruments is not possible because it usually results in serious electrical mis-match.

Other characteristics of probe-instruments systems, such as reliability, stability, brilliance and freedom of jitter of the screen, cannot be evaluated in a few simple figures.

Literature

1. Krautkramer, J.U.H. Werkstoffprüfung mit Ultraschall, Springer-Verlag, Berlin 1966, pp. 75-80.

2. Krautkramer, J. Determination of the size of defects by the ultrasonic pulse-echo method, *Brit. J. Appl. Phys.* 10 (1959) p. 240-245.

Appendix

A probe of frequency f_0, with a damping factor d, when excited with a short pulse gives a damped sine oscillation with the envelope:

$$f_s(t) = A_0 e^{-tf_0 \log_e d}$$

If this pulse is received by the same probe the envelope has the form:

$$f_e(t) = A_1 t e^{-tf_0 \log_e d}$$

In the time

$$t_m = \frac{1}{f_0 \log_e d}$$

the oscillation rises from 0 to maximum amplitude

$$\frac{A_1}{e f_0 \log_e d}.$$

Afterwards the oscillation decreases with the amplitude ratio between oscillation n and $n+1$:

$$\frac{n}{n+1} d.$$

To calculate the resolution we take the first pulse:

$$f_1(t) = A_1 t e^{-tf_0 \log_e d}$$

and the second pulse, which starts at some later time and has an amplitude m db lower than the first one:

$$f_2(t-a) = A_1 10^{-\frac{m}{20}} (t-a) e^{-(t-a) f_0 \log_e d}$$

We define: the second pulse is separately indicated if at t: a_m the first pulse is decreased to half the maximum height of the second pulse. This height is:

$$\frac{f_2^{max}}{2} = \frac{a_1 10^{-\frac{m}{20}}}{2ef_0 \log_e d}$$

For the time resolution a_m we have the equation:

$$a_m e^{-a_m \log_e d} = \frac{10^{-\frac{m}{20}}}{2ef_0 \log_e d}$$

In this time the pulse travels the distance $r_m = \frac{1}{2}ca_m$ (forward and back) and in the medium with sound velocity c. For the resolution r_m we have the equation:

$$r_m e^{\frac{2r_m}{c} f_0 \log_e d} = \frac{c\, 10^{-\frac{m}{20}}}{4ef_0 \log_e d}$$

Figure 4 shows the solution of this equation.

This solution is not valid for the near-surface resolution. In this case a lot of other oscillations are superimposed, and a separate study is necessary to clear up the case.

Example: For a low damped probe (Krautkramer Q4S) the damping factor in steel is measured: d: 1.55. At 4 MHz we have a wavelength 1.5 mm. From Figure 4 we read the resolution for two echoes of equal height: $m = 0$, $r_0 = 3$ mm. If we have to resolve a defect of 1-mm dia from the back echo: $m = 55$db (AVG diagram). For this condition we find $r_{55} = 18$ mm. For the same probe on the standardized rough surface, we find d 1.3. In this case we find $r_0 = 7.5$ mm and $r_{55} = 28$ mm.

In practical application we should pay attention to the calculation, especially if m has large values. One should make use of the r_m value only in cases where we have to compare the resolution of probe types which are to be used with the same instrument.

Ultrasonic Evaluation of Mechanical Inhomogeneities of Materials

I. MALECKI, POLAND

The Definition of the Inhomogeneity of Materials

Inhomogeneity of materials is a notion depending on the methods applied and the accuracy of investigation. Even apparently continuous media show structural inhomogeneities when passing through microscopic or submicroscopic investigations.

Research carried out during the last 20 years proves that electric, mechanical and optical properties of solids depend not only on the structure of their crystal lattice but mainly on the defects of this lattice.

Actually, crystals having perfectly ranged atoms in all directions do not exist. The structure of real crystals is far from the perfect spatial lattice structure.

In the case of solids it is often convenient to adopt an elementary lattice cell as a unit of the structure of matter. Such an approach concerns, in principle, crystals; however, amorphous bodies, especially glasses and liquids, also have certain arrangements of atoms called short-range order though they do not possess a defined lattice cell.

The dimensions of lattice cells of crystals vary considerably in the range of several Å.

Besides crystal lattice imperfections, the inclusions of foreign bodies, porosity and phase discontinuity also create inhomogeneities. Until recently in nondestructive ultrasonic testing inhomogeneities comparable with the wave length were considered as material inhomogeneities. At present, the measurements of inhomogeneities of several orders of magnitude smaller than the wave length are allowed, e.g. absolute measurements of the micoporosity and of the density of dislocations. In the case of relatively small inhomogeneities in comparison with the wave length, the classical definition of different specific acoustic impedances ρc is no longer valid. It seems that the definition of different free energies, characteristic for a volume unit of the regions considered, should be adopted as definition in the case of small inhomogeneities. The influence of the free energy on the wave propagation parameters consists in an increased absorption of the wave energy in regions of higher free energy. Hence, certain atom arrangements of a crystal having an excess of free energy in relation to the remaining atoms may be considered as inhomogeneities (dislocations, grain boundaries).

Such a definition permits the investigation by acoustic methods of all kinds of inhomogeneities that are significant for the technical properties of materials, including crystal lattice imperfections. In future, the possibility of evaluating the electronic structure of crystals by nondestructive tests is to be expected.

The development of acoustic nondestructive tests tends in the direction of measurement of phase velocity and attenuation of ultrasonic waves, which are both closely connected with the micro- and macrostructure of materials. Generally, structural changes affect the attenuation more than the propagation velocity, and therefore the former is of particular interest from the point of view of nondestructive tests.

In certain cases the application of velocity measurements for the detection of inhomogeneities in materials is desirable. The investigations on absolute porosity carried out in Poland during 1956-64 may serve as an example (1).

The attenuation mechanism is considerably more complicated than the effect of structure on the ultrasonic wave velocity. Its simplification, found in technical literature, seems unjustified. This simplification consists in the treatment as a whole of components of the resultant measured attenuation. These components result from different physical effects and are not additive, as their contribution to the attenuation may vary depending on the measuring method.

The aim of this paper is to attempt to classify and partly determine quantitatively the components of the attenuation of ultrasonic waves resulting from the macro- and microstructure of the material.

Kinds of Inhomogeneities and their Effect on the Attenuation of Elastic Waves

It seems correct to distinguish the following mechanisms of ultrasonic wave attenuation:

Attenuation by Diffraction

This kind of attenuation is caused by the scattering of the acoustic wave without change of its frequency and type of vibration. The inhomogeneity is then treated as the source of a disturbance wave superposed on the progressive acoustic wave.

If the medium is assumed lossless, the power balance for waves of a given frequency is of course satisfied, i.e. the disturbance wave has a power equal to the power extracted by the obstacle from the progressive wave.

If the dimensions of the obstacle are small in relation to the wavelength, the velocity potential of the disturbance wave may be expressed by the formula

$$\Phi' = \Phi_1 \sum_{m=o}^{\infty} \frac{(-j)^m (2m+1)\, kaP_m(\cos\Theta)}{j'_m(ka) + \mathrm{j}n'_m(\mathrm{ka})} [j_m(ka)n'_m(ka) - n_m(kr)j_m'(ka)] \quad (1)$$

where r = distance from the observation point to the obstacle centre

a = radius of spherical obstacle

Φ_1 = velocity potential of progressive wave

P_m = Legendre polynomial

θ = angle between the direction of progressive wave and vector r

k = wave number

j_m, n_m = spherical Bessel's and Neumann's functions of the m[th] order

This formula is deduced by the resolution of the progressive plane wave into a series of spherical waves, which are connected with components of the disturbance wave by means of boundary conditions on the surface of the obstacle. In first approximation the obstacle is treated as perfectly rigid. The influence of the obstacle elasticity can be introduced without special difficulties as a corrective term.

The power taken by the disturbance wave from the progressive wave is:

$$N = \Phi^2 2\pi \sum_{m=0}^{\infty} (2m+1) \sin^2 \gamma_m \quad (2)$$

where γ_m = angle determined by the equation

$$j'_m(ka) - jn'_m(ka) = jL_m e^{-j\gamma_m} \quad (3)$$

If ka << 1 the scattered wave is approximately a spherical wave of the zero order.

The picture obtained in the case of a single obstacle is distorted in an inhomogeneous medium by the effect of neighbouring obstacles and thereby by the occurrence of secondary reflections.

From the point of view of nondestructive testing the scattering mechanism has two characteristic features:

a) a part of the scattered wave is added to the progressive wave and thanks to multiple reflections the path of the scattered wave is greater than that covered by the progressive wave. This results in rendering the front of a pulse signal less steep. b) the reflection of scattered waves from the side boundaries of the sample may give origin to parasitic pulses or to a certain change of the amplitude of the main signal.

Attenuation by Change of Wave Mode

This kind of attenuation differs from the former in that scattering is accompanied by the change of the wave mode. This phenomenon takes place at reflections from inhomogeneities in a solid medium. For a spherical, perfectly compliant obstacle in a solid the formula expressing the power of a transverse disturbance wave caused by the passage of the longitudinal wave is:

$$N = \frac{1}{Q} 384\gamma^3 (1 + 2\gamma^2)^3 / 2\, kaI_1 \quad (4)$$

where $\gamma = \sqrt{\frac{\mu}{\lambda}}$ (μ and λ — Lamé constants)

Q = the complex function of γ and ka

$k = \frac{2\pi}{\lambda}$

a = radius of spherical inhomogeneity

I_1 = intensity of incident wave

A simpler relation is obtained for a reflection from an inhomogeneity having the shape of a perfectly compliant thin circular disc. The vector potential of the transversal wave is then:

$$\Psi = \frac{2}{3\pi} \Phi \frac{(k_t a)^4}{1 + \frac{3}{4}\left(\frac{k_t}{k_1}\right)^2} \left(\frac{k_1}{k_t}\right) \frac{1}{\zeta} e^{-ik_t a\zeta} \sin\theta \quad (5)$$

where k_t and k_1 = wave numbers of the transversal and longitudinal waves

ζ = distance from the disc expressed in coordinates

a = radius of disc

θ = angle between the axis of the disc and the direction of propagation of the incident wave.

This type of attenuation occurs at reflections of longitudinal waves from a flaw placed under a certain angle in reference to the direction of propagation of the wave.

If the dimensions of the obstacle are large in relation to the wavelength the wave potential is determined by the formula:

$$\Psi = \Phi_1 \frac{D'_t}{D_1} \quad (6)$$

where D'_t and D_1 are matrices of coefficients depending on cos θ and sin θ.

The scattered wave of the type considered has a different velocity than the progressive wave. The scattered wave, being reflected from neighbouring obstacles or side boundaries of the sample, reaches the receiver at a different time than the progressive wave. In the case of the application of a pulse method this fact causes the appearance of parasitic pulses, and in the case of using a continuous signal it may cause apparent changes of the attenuation constant depending on the shape of the sample.

Attenuation by Friction on the Boundary of Inhomogeneity

The attenuation consists in the conversion of the elastic waves into heat (nonlinear process of frequency conversion).

This kind of attenuation occurs if elements of the medium move tangentially in reference to one another. The losses in hydrosole may serve as an example in which suspended particles move freely in the medium, and thereby their presence does not give origin to scattered waves. The attenuation is then due to the viscosity of the medium. The formula deduced by H. Lamb may be applied here:

$$\alpha = \frac{kV_2}{2} \left[\frac{1}{6}(ka)^2 + \left(\frac{\rho_2}{\rho_1} - 1\right)^2 \frac{q}{q^2 + \left(\frac{q_2}{q_1} + s\right)^2} \right] \quad (7)$$

where $q = \frac{9}{4\beta a}\left(1+\frac{1}{\beta a}\right)$; $S = \frac{1}{2}+\frac{9}{4\beta a}$;

$\beta = \sqrt{\frac{\omega}{2\mu'}}$ (μ'—dynamic coefficient of viscosity)

V_2 = volume part of suspension

a = radius of suspension

In this category of losses those caused by dislocation motions should be classified.

Attenuation by Inhomogeneities of Anisotropy. If areas having different spatial orientation of mechanical and thermal properties exist in the material, and the dimensions of these areas are small in relation to the wave length, the following mechanism is valid. The stresses caused by acoustic waves inside a region (e.g. a crystallite) may be considered uniform, but on the other hand, due to anisotropy, the differences in the distribution of deformations and temperatures occur, resulting in higher thermal losses than in a homogeneous material.

Attenuation by Processes in the Boundary Layer. The boundary layer between homogeneous regions (e.g. crystallites) affects in a considerable degree, though as yet not well known, the manner of attenuation of elastic waves. One of the causes may be the low thermal conductivity of the boundary layer, causing the occurrence of a high-temperature gradient and thereby the appearance of a strongly attenuated temperature wave. The attenuation factor of this wave is approximately:

$$\alpha_T = \sqrt{\omega\rho\, C/2\,\kappa} \tag{9}$$

where C=specific heat, κ= average heat conductivity of the material. The calculation of the thermal balance gives the energy loss per volume unit:

$$E = \frac{\gamma}{T_0}(\text{grad } T)^2 \tag{10}$$

what for the adopted assumptions corresponds to an attenuation constant of the longitudinal elastic wave:

$$\alpha_1 = \frac{C_1\,\alpha_c^2\,T_0}{2a}\sqrt{\frac{\omega\,\kappa}{\rho\,C^3}} \tag{11}$$

where α_c = coefficient of thermal expansion
2_a = grain diameter
κ = heat conductivity
c_1 = sound velocity
C = specific heat
ρ = medium density

The losses in the boundary layer have, however, usually a much more complex character and their theoretical analysis is difficult.

Attenuation Caused by Dislocation

An elastic wave, progressing in a medium which contains linear lattice imperfections under the form of dislocations, causes a motion of these dislocations which may be described approximately (for infinitesimal wave amplitudes) by the equation of a vibrating string. These oscillations are accompanied by a partial conversion of the elastic wave's energy into heat, which is taken into account by the numerical factor B in the string equation. The calculation of this factor for a given medium is presented in the papers of Leibfried (2) and Mason (3). For dislocations considerably shorter than the wave length, the attenuation constant due to dislocation damping is expressed for the stream amplitude independent component, by the formula (4):

$$\alpha_t\,[db/\mu s] = 8{,}68.10^{-6}\,\Omega\,\frac{(1-\nu)^2}{\pi^4\,Gb^2}\,\Lambda\,L_e^4\,B\omega^2 \tag{12}$$

where Ω= orientation factor concerned with the stress effective in moving dislocations
ν = Poisson's ratio
G = shear modulus
b = Burger's vector
Λ = dislocations density
L_e = effective length of dislocation loop
B = damping constant
ω = angular frequency

Attenuation by the Phonon-Phonon and Phonon-Electron Interactions

Such interactions result in the thermal effect caused by crystal lattice vibrations. However, only for hypersonic waves of frequencies above 1000 MHz such an attenuation may be treated as closely dependent on the atomic crystal structure.

In this case the value of losses is determined by the nonlinearity of vibrating systems and thereby by the terms of the third order in the expression for the energy of an anharmonic oscillator. The Hamiltonian of the system contains then a supplementary term of the type:

$$H = \frac{1}{3!}\sum U_i U_j U_k \vdots A_{ijk} \tag{13}$$

where $U \vdots A$ is the product of displacement vectors and of the tensor A of potential forces of the system.

Depending on whether at phonon interaction the resulting wave vector is preserved (normal process) or undergoes a change (umklapp process) the value of dissipated energy changes.

General Method of Phonon Representation of the Mechanism of Elastic Wave Attenuation

The attenuation mechanism by phonon-phonon interaction mentioned as the last item of the classification may be applied, by analogy, for representing other types of attenuation. Every acoustic wave may be represented as a flux of so-called macro-phonons or, in other words, one may attribute to it a formal quantum character. For this purpose it suffices to adopt (in the formulae describing the mutual phonon-phonon interaction, and in the definition of the phonon itself) an arbitrarily chosen constant H instead of the reduced Planck's constant h. Such a quantization of the acoustic wave has no direct physical sense but only expresses the approximation by which a continuous process is substituted by a discrete process generally easier to calculate, especially when using computers.

Lack of space does not permit development of this method here, therefore only main principles are presented:

a) The conversion of the acoustic energy into other kinds of energy is determined by operators b of creation and b* of annihilation expressed by the formula

$$\begin{matrix} b \\ b^* \end{matrix} = \frac{1}{\sqrt{2H}}\left(\sqrt{m\omega}\;U \pm \frac{i}{\sqrt{m\omega}}P\right) \tag{14}$$

where U and P = shift and momentum of the macrophonon.

b) the wave scattering corresponds to the three-phonon process in which the wave vector of the progressive wave

(of the primary phonon) $\vec{k_1}$ and the vectors of the waves appearing as a result of scattering satisfy the relation:

$$\vec{k_1} + \vec{k'_1} + \vec{k_2} = \vec{g} \tag{15}$$

where $\vec{g}$ corresponds to the inverse of the lattice vector. In the adopted system of analogies, "lattice" should be considered the set of the centres of inhomogeneities.

c) The change of the wave mode may be represented by attributing to the macro-phonon spin properties and by determining the behaviour of the complex polarization unit vector e_1^{-i}. The spin is then determined by the expression:

$$\overline{S} = \frac{H}{i} \sum_{jkl} b^*_j \, b_k \, e_1^{-j*} \, e_1^{-k} \tag{16}$$

d) friction processes and the processes occurring in the boundary layer are expressed similarly to the phonon description of thermal vibrations of the crystal lattice.

e) the dispersion of phase velocities which may occur in an inhomogeneous medium is analogous to a quantum dispersion of a wave.

The macro-phonon method sketched above may prove to be useful in the consideration of phenomena in which several of the above mentioned attenuation mechanisms appear simultaneously.

Conclusion

The effects of various types of inhomogeneities on the attenuation of ultrasonic waves show the usefulness of attenuation measurements for systematic investigating macro- and micro-inhomogeneity of materials.

The advantages of sonic and ultrasonic methods are: a) The possibility of adjustment of the wave length in a very wide range depending on the kind and magnitude of inhomogeneities. b) The easy choice of a modulation system of acoustic waves (pulses, continuous waves, frequency modulation) which permits adjustment of the measuring method to the given shapes and dimensions of the tested samples as well as to their acoustic parameters.

References

1. Ranachowski J., Doctoral thesis, Warsaw, Inst. of Electrot., 1963
2. Leibfried, *Zs. Phys.*, 127, 344, 1950
3. Mason, *J. Appl. Phys.*, 35, 2779, 1964
4. Truell, Elbaum, *Encyc. of Phys.*, XI/2—Acoustics II, Springer, 1962

Focused Ultrasonic Beams

J. T. McELROY, USA

ABSTRACT: The successful application of ultrasonic flaw-detection techniques is highly dependent upon the search unit. The ability to direct the propagated ultrasonic beam to the area of interest in a controlled manner is most desirable in immersion testing. The use of focused-beam search units provides us with a method of enhancing the sensitivity, resolution, and directivity of any immersion ultrasonic system. The requirements of today's ultrasonic testing demand that we understand and exploit any method that will greatly contribute to our ability to test more thoroughly.

This paper is a guide for selecting focused ultrasonic search units. It is based on a development program designed to analyze, measure, and categorize the focal characteristics of commonly used immersion search units. The data were compiled, and reduced to charts and graphs which describe the "lens radius to crystal diameter ratio" as a means of categorizing the focal length and beam diameter characteristics of focused search units.

Introduction

The propagation pattern of energy from an ultrasonic search unit is fundamental. Understanding this energy pattern is mandatory if one is to utilize fully the search unit in nondestructive testing problems. Although energy emitted from a search unit can be controlled and directed through use of acoustic lenses, the design of the search unit must be carefully engineered for maximum inspection efficiency consistent with size, frequency and focal parameters. Inspection requirements dictate the choice of search unit. Some applications require low-frequency, large-diameter beams for deep penetration; others require high frequencies with extremely small beams to define minute defects.

The focusing of the sound energy propagated from the search unit can be accomplished with different lens materials. In this text, I discuss the plastic lens in combination with a water medium. Sound velocity is slower in water than it is in plastic; therefore, concave lenses are used to focus the sound energy. The diameter of the crystal radiator and the radius of curvature of the lens dictate the focal characteristics. A large number of combinations of crystal diameters and lens radii is possible. This paper considers only the most common search unit sizes used in today's ultrasonic testing.

The Flat Search Unit

Before attempting to analyze and categorize the characteristics of the focused search unit, a brief review of the flat or nonfocused search unit is in order. The most important characteristics of the nonfocused search unit are the ratio between crystal diameter and ultrasonic wavelength and the analysis of the near and far field beam patterns. These are basic factors from which we measure the influence of the acoustic lens. The directivity of the propagated energy is a function of wavelength which in turn is determined by $\lambda = c/f$ where:

λ = wavelength,
c = velocity within the medium,
f = frequency.

For good beam directivity (less than 5° dispersion angle), we must consider both frequency and crystal diameter. The minimum recommended D/λ ratio (crystal diameter:wavelength) is 20. The inherent divergence from crystals with a smaler D/λ ratio is difficult, if not impractical to overcome with the use of an acoustic lens.

Table 1
Recommended Minimum Search-unit Diameter

Frequency MHz	1λ Dimension in Water		Recommended 20λ Crystal Diameter	
	inches	(mm)	inches	(mm)
0.5	0.117	(2.97)	2.35	(59.69)
1.0	0.0587	(1.49)	1.17	(29.72)
2.25	0.026	(0.66)	0.521	(13.23)
5.0	0.012	(0.31)	0.234	(5.94)
10.0	0.0059	(0.15)	0.117	(2.97)
15.0	0.0039	(0.099)	0.078	(1.98)
20.0	0.0029	(0.074)	0.059	(0.15)

$$\lambda = \frac{\text{Velocity (Water 1.49 mm/}\mu\text{sec)}}{\text{Frequency}}$$

Table 1 lists the dimensions for 20λ (in water) crystal diameters at frequencies from 0.5 MHz to 20 MHz.

In applications requiring the use of low frequencies, it is not possible to obtain small beam diameters. While the addition of an acoustic lens to a crystal does not eliminate consideration of this D/λ restriction, it does provide a means of producing a small, well-defined beam from large diameter piezoelectric radiators.

The radiation pattern from any driven element is composed of two zones of energy known respectively as: (1) the Fraunhofer zone, or far field, and (2) the Fresnel zone, or near field. In immersion testing, the energy used is primarily that of the far field. Contact ultrasonic testing involves both the near and far fields. The Fresnel zone extends from the last peak in the energy pattern (last maximum pressure point) towards the search unit. The Fraunhofer zone extends outward from the last peak of the energy pattern. The last peak is located at the axial point Y_o^+. The axial positions of the maxima (Y^+) and minima (Y^-) for plane circular piston radiators can be described by the following equations:

$$Y^+ = \frac{4a^2 - \lambda^2 (2m+1)^2}{4\lambda (2m+1)}, \quad \text{where } m = 0, 1, 2 \qquad (1)$$

$$Y^- = \frac{a^2 - \lambda^2 m^2}{2m\lambda}, \quad \text{where } m = 1, 2, 3 \qquad (2)$$

In these equations:

Y^+=position of maxima along central axis,
Y^-=position of minima along central axis,
a=radius of crystal,
λ=wavelength of sound in medium.

In water, λ^2 is insignificant as compared to the radius, a, thus, at the last peak where $m=0$, Eq. (1) reduces to

$$Y_o^+ = a^2/\lambda \qquad (3)$$

For most ultrasonic immersion applications, Eq. (3) is adequate.

Figure 1. Schlieren image of focused search unit.

The beam in the far field is homogeneous and well-defined. However, in the near field, where the beam is still in the process of forming its wave front, there are many areas of high and low energy.

Where it is possible, it is desirable to perform the ultrasonic inspection with the area of interest positioned in the far field. In this region, the beam is uniform, and interpretation of a defect is not influenced by the undulations of the near field, however, it is not always possible or convenient to operate in the far field. Table 2 lists the theoretical position of the Y_o^+ points in water for various crystal diameters at frequencies of 1.0, 2.25, 5.0, 10.0, 15.0, and 25.0 MHz.

Table 2
Theoretical Position of Y_o^+ in Water

Crystal Frequency (MHz)—Inches

Crystal Diameter	1.0	2.25	5.0	10.0	15.0	25.0
3/16″	—	—	0.75	1.5	2.25	3.75
3/8″	—	1.35	3.0	6.0	9.0	15.0
3/4″	2.4	5.4	12.0	24.0	36.0	60.0
1″	4.26	9.6	21.3	42.6	63.9	—

Crystal Frequency (MHz)—(Millimetres)

Crystal Diameter	1.0	2.25	5.0	10.0	15.0	25.0
7.92	—	—	19.05	38.1	57.2	95.3
9.53	—	34.3	76.2	152.4	228.6	381.0
19.05	61.0	137.0	305.0	610.0	914.0	1524.0
25.40	108.0	244.0	541.0	1082.0	1623.0	—

The theoretical Y_o^+ points, in water for the higher frequency search units are at distances too great to be convenient for most applications where thin metal sections are to be tested. The metal-path does, however, offer velocities which are in the order of four times faster than water; thus, λ becomes longer. As λ increases, the water-path distances to the Y_o^+ region will be less (Eq. 1, 2). Yet it can be readily seen that when using a ¾-in. (19.05 mm) diameter, 10 HMz nonfocused search unit for the inspection of ¼-in. (6.35 mm)-thick aluminum sections, the water-path should be 23 in. (584 mm) to allow the use of the Y_o^+ region of the beam. Consequently, we find that much testing of thin metal sections at the higher frequencies is conducted at shorter, more convenient water-paths, and thus use the undesirable near-field region of the beam. Focused search units offer a solution to this problem.

The Focused Search Unit

The propagated energy pattern is extremely important in understanding the action of a focused search unit. Point Y_o^+ is the best defined energy zone in the radiated beam. As previously indicated, it is desirable in immersion testing with flat search units to utilize the region from approximately Y_1^- through the Y_o^+ point and extending into the far field. In focused ultrasonic inspection, only the zone in the region of Y_o^+ is used.

Through the use of acoustic lenses, the beam pattern can be manipulated to provide distinct advantages. The schlieren image illustrated in Figure 1 ably illustrates how the beam can be made to converge at a specific point in the propagation medium. With these lenses, it is possible to shift the position Y_o^+ toward the search unit. The Y_o^+ point will now become the focus of the

acoustic lens. Figure 2A and 2B shows that the Y_o^+ region for a ¾-in. (19mm) diameter 5 MHz search unit with an acoustic lens is now at 2.5 in. (63.5 mm). The addition of the lens to this search unit has moved the Y_o^+ point from 12 in. (305 mm) to 2.5 in. (63.5 mm).

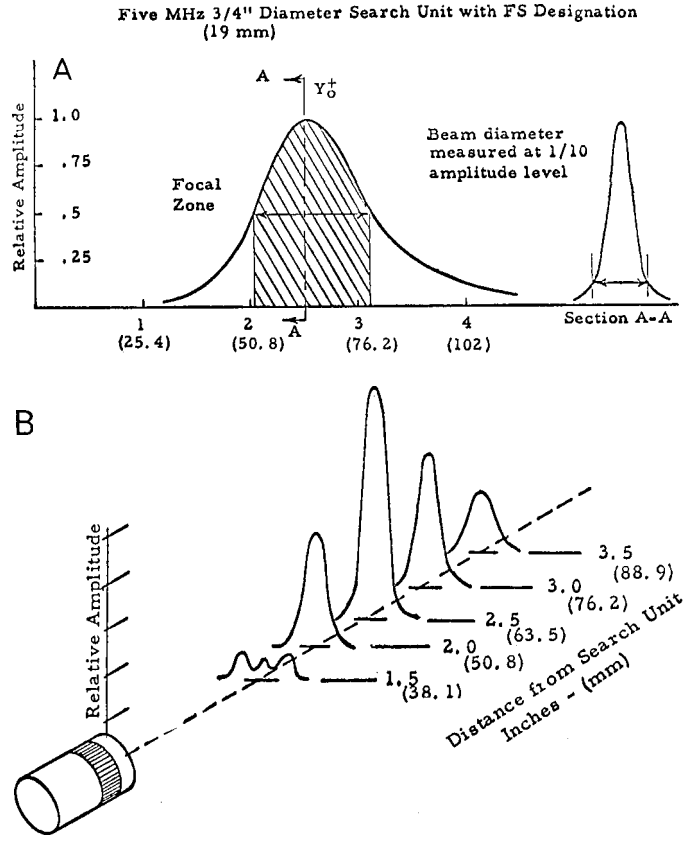

Figure 2. Energy propagation from a focused search unit. A. Axial plot of beam intensity. B. Focused sound-beam profile.

Figure 3 is a recording of the beam profile at 25 positions along its focal pattern. Such recordings are produced by the technique described in Automation Industries, Inc., Report TR 66-5, "Identification and Measurement of Ultrasonic Search Unit Characteristics". These recordings show how the addition of an acoustic lens draws both near and far field toward the search unit. The energy reflected from a small steel ball target is used for the sound-beam profile. The dynamic cycle-to-cycle radio-frequency response of the search unit is displayed on an oscilloscope and recorded with an open-shutter camera. A critical analysis of the beam characteristics is made by this technique. Figure 4 relates these sound-beam profiles to a Schlieren image of the same search unit. It is of interest to note that none of the characteristic Fresnel zone energy distribution patterns (Y_o^+, Y_1^-, and Y_1^+) are distorted by the effects of the lens. They are simply moved in closer to the search unit. This method of sound-beam profile recording describes these effects with near-perfect correlation to the theoretical.

Referring again to Table 2, the Y_o^+ for a ¾-in. (19 mm) diameter 10 MHz search unit is theoretically a distance of 24.0 in. (610 mm). The data presented later in this report shows that with the addition of the proper lens to this search unit, the Y_o^+ (focal point) can be pulled into a water-path distance of only 2.5 in. (63.5 mm). The beam diameter at this point will be small, highly concentrated, and well-defined. This high concentration of the beam energy enhances both the sensitivity and resolution capabilities of the search unit. Later sections of this text record the beam diameters that can be achieved by focused search units.

Focal distance can be defined as the water-path distance from the lens to the focal point. The focal zone is the distance between the half-amplitude points of the focused pattern, and is the usable portion of the focused beam. The focal distance for a simple spherical lens of small aperture (lens radius to crystal diameter ratio less than 3:1) can be described as:

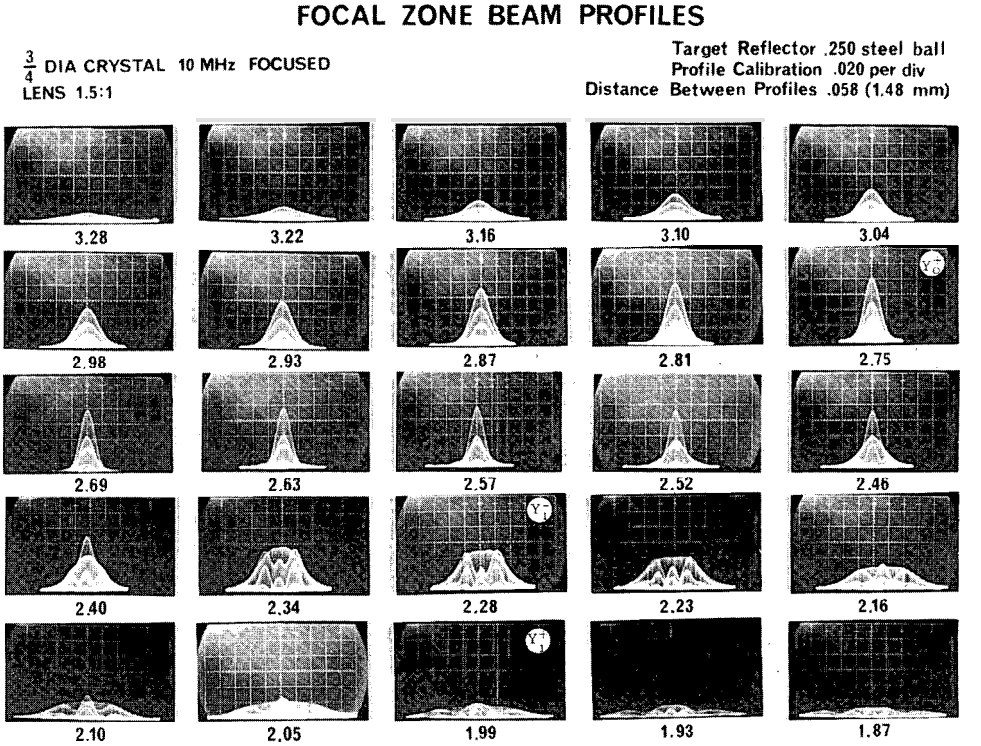

Figure 3
Incremental profiles along the sound-beam length.

$$R = F\left(\frac{n-1}{n}\right), \qquad (4)$$

where

R=lens radius of curvature,

F=focal distance of lens,

n=index of refraction of lens material.

For cast epoxy resin lenses:

n=1.86 in a water medium

$$\frac{n-1}{n} = .464$$

This equation is adequate only when defining lenses of short focal distance and it does not consider the effects of attenuation and aberrations.

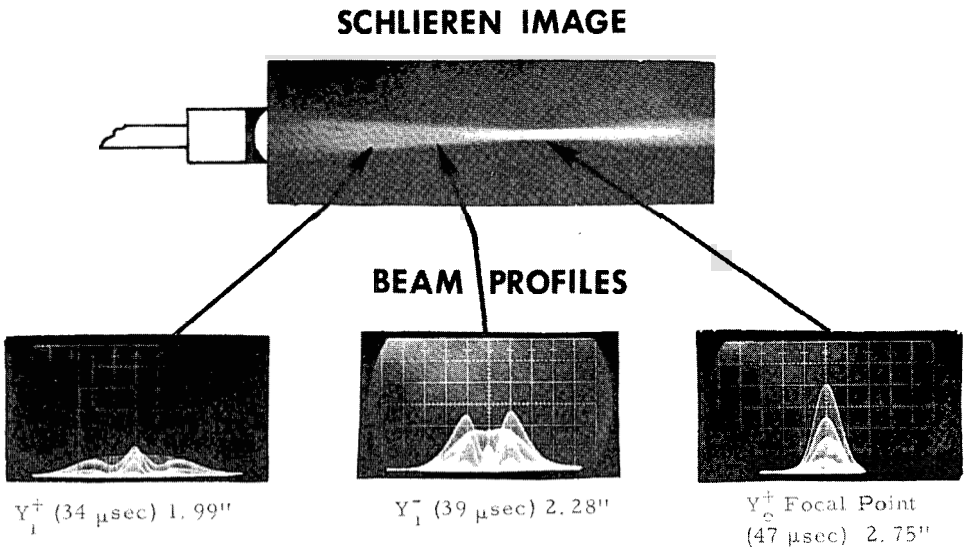

Figure 4
Correlation between the Schlieren and sound-beam profiles of a focused search unit.

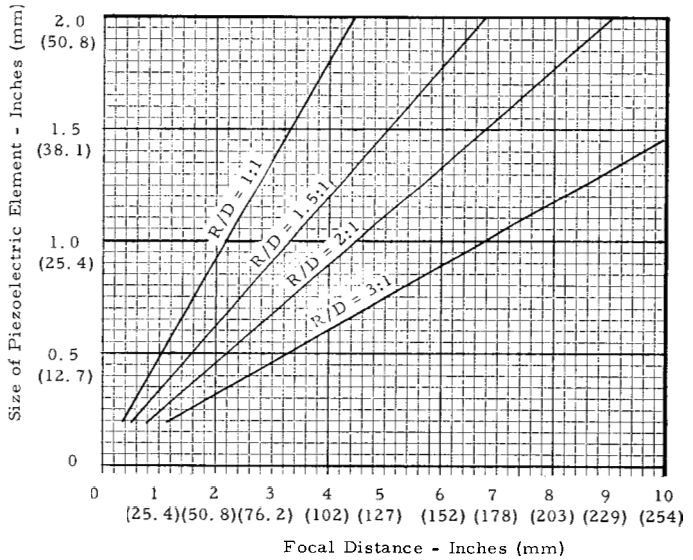

Figure 5. Calculated curves for plastic lenses.

To determine the focal properties of a search unit, it is convenient to relate the focal point to the ratio of the radius of curvature of the lens and the crystal diameter (R/D ratio). Figure 5 shows a calculated family of curves of various R/D ratios. At frequencies above 5.0 MHz, the plotted curves may deviate somewhat from the calculated points. This can be attributed to such factors as attenuation, lens loss, and mode conversion in the lens and transmission medium. Distance amplitude curves of the sound beams will provide a plot of the focal properties of a search unit. To use Figure 5, first choose the size of the crystal element that is appropriate for the search unit. Next, determine the point at which the energy should focus. Project to the R/D ratio that corresponds to the size of the element. The sharper the radius of curvature, the lower the lens ratio, the shorter the focal zone.

Figure 6 describes the influence of a metal section on the focused beam. Since sound velocity is higher in metals, the beam will reach its focal distance much sooner. Therefore, when selecting a focused search unit, thickness of the material to be inspected must be considered. The over-all focal distance will be foreshortened by the effect of the metal. In Figure 6 the sound beam has maximum concentration at $\frac{1}{4}$ in. (6.35 mm) in the aluminum block when the water-path is 2.4 in. (61.0 mm). Table 3 gives other examples of the influence of metal sections for other testing conditions.

Table 3

Comparison Focal Distance for Water-path only and Focal Distance for Combined Water and Metal-path

Crystal Diameter	Lens R/D	A	B	C
$\frac{3}{16}$ in. (7.92)	1.5:1	.63 in. (1.6)	.35 in. (0.89)	.06 in. (0.15)
$\frac{3}{8}$ in. (9.53)	1.5:1	1.34 in. (34.0)	.81 in. (2.05)	.12 in. (0.30)
$\frac{3}{4}$ in. (19.0)	1.5:1	2.57 in. (65.3)	1.52 in. (38.6)	.25 in. (0.64)

A = Focal distance in water only; B = Nominal water-path distance to aluminum; C = Nominal focal distance in aluminum.

Cylindrically focused rectangular search units are valuable in specialized testing applications such as thin-walled tube, round bar, etc. Such a search unit is especially sensitive to fine line cracks that exist either at the surface or subsurface within the wall of the tubing.

Characteristics of Focused Ultrasonic Beams

The objective of this study is to measure critically and to analyze the focal lengths and beam dimensions of commonly used focused search units. From the data, charts and graphs were compiled showing characteristics of lens radius, focal

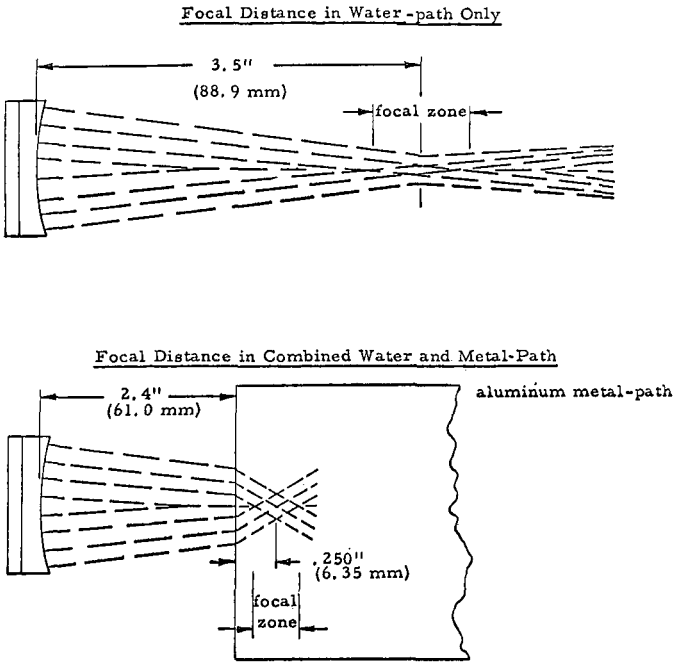

Example shown:
Sound velocity in aluminum is 4.25 times faster than it is in water:

$$\frac{\text{velocity in Al}}{\text{velocity in water}} = \frac{6.25 \text{ mm}/\mu\text{sec}}{1.49 \text{ mm}/\mu\text{sec}} = 4.25$$

Thus, if the desired focal point in aluminum is at a depth of .250", the operational water-path will be:
(6.35 mm)

$$3.5" - (.250" \times 4.25) = 2.4"$$
$$88.9 - (6.25 \times 4.25) = 61.9 \text{ mm}$$

Figure 6. Examples of focal distance in water and metal-path.

distance crystal diameter, beam diameter, and the ratio of lens radius:crystal diameter, (R/D) ratio. These charts and graphs can be used to predict the following:

a) Focal distance for a given combination of lens radius and crystal diameter; b) Beam diameter at the focal point for a given combination of lens radius and crystal diameter; c) Optimum radio of lens radius; crystal diameter (R/D).

Each search unit used in this study was investigated by profile recording for beam homogeneity. These profiles were made before focusing to insure beam symmetry.

Beam-diameter and beam-width measurements were made using a micrometer screw to generate the transverse movement. In all cases, the target used was a steel ball of the smallest diameter which would still yield an adequate signal. The beam diameters and widths were measured from the 1/10th amplitude, through the peak, to the 1/10th amplitude point on the opposite side. Care was taken to make this measurement on the exact centre line of the crystal. The search units chosen for this study were 20 or more wavelengths in diameter at their respective frequencies.

The lenses on all search units were cast epoxy resin, free of porosity, and cast directly on the face of the search unit. Sound velocity of the epoxy was 2.79 mm/μsec. Special care was taken to insure that the apex of the lens occurred at the exact centre of the crystal. Thirty-six combinations of lens radius:crystal diameter configurations were used to compile the data.

Figure 7 illustrates the relationship between the empirically measured focal distance and the lens radius:crystal diameter

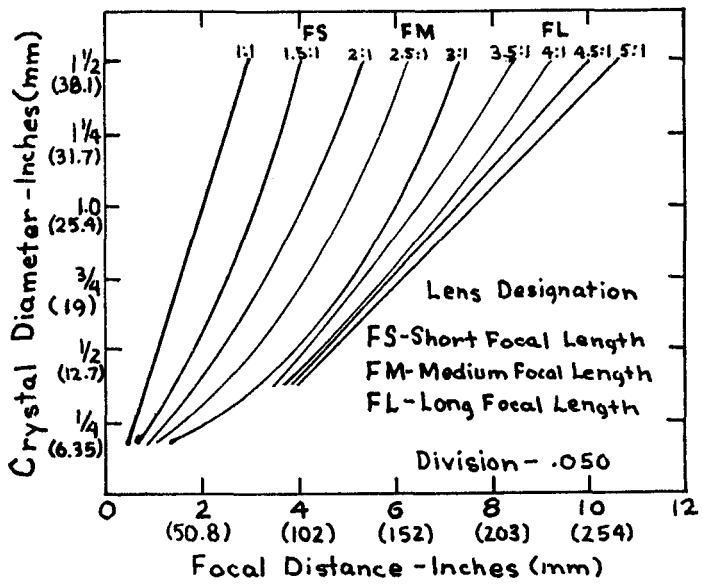

Figure 7. Relationship between crystal diameter, lens radius and focal distance.

(R/D) ratio for the various crystal sizes. As the R/D ratio becomes larger than 3:1, and the focal zone of the lens approaches the natural Y_o^+ point of the crystal in an unfocused condition, these curves will become sensitive to frequency.

The curves shown in Figure 7 with R/D ratios greater than 3:1 are based on a crystal frequency of 5 MHz. The focal distances of lower frequency crystals will be found at a slightly shorter water-path distance and at a slightly longer water-path distance at higher frequencies.

The designations FS, FM and FL have been assigned to lens configurations that produce nominal short, medium and long focal length distances for specific crystal sizes.

Designation		*Lens Radius: Crystal Diameter (R/D Ratio)*
FS	=	1.5:1
FM	=	2.5:1
FL	=	4.0:1

These designations appear on all charts and graphs in this paper. Table 4 lists the focal distance and beam diameters for the various designations.

The focal distance for most practical applications is independent of frequency for a given crystal diameter, lens radius combination. This is only true, however, when the crystal diameter:wavelength D/λ ratio is 20 or more and R/D is not greater than 3:1. For example, if a 1/4-in. dia crystal with a resonant frequency of 2.25 MHz were plotted, its focal distance and beam-diameter characteristics would deviate drastically from those recorded for a 1/4-in. 10 MHz search unit with an identical lens configuration. This is due to the beam divergence that results when a crystal radiator has a D/λ ratio considerably smaller than 20.

Rectangular crystal sizes are cylindrically focused with the focal plane across the width dimension. The length of the crystal can vary and have no effect on the focal characteristics if the length is maintained at two or more times greater than the width.

Table 4

Focal Characteristics of Designated Lens Configurations

Crystal Size		Lens Designation	Focal Distance in Water		Beam Diameter or Width at Focal Distance in Water	
inches	(mm)		inches	(mm)	inches	(mm)
$\frac{3}{16}$ dia	(7.92)	FS	.630	(16.0)	.023	(0.58)
$\frac{3}{16}$ dia	(7.92)	FM	1.00	(58.4)	.044	(1.12)
$\frac{3}{8}$ dia	(9.53)	FS	1.34	(34.0)	.030	(0.76)
$\frac{3}{8}$ dia	(9.53)	FM	2.20	(55.9)	.055	(1.40)
$\frac{3}{8}$ dia	(9.53)	FL	3.00	(76.2)	.087	(2.21)
$\frac{3}{4}$ dia	(19)	FS	2.57	(65.2)	.054	(1.37)
$\frac{3}{4}$ dia	(19)	FM	4.00	(102)	.095	(2.41)
$\frac{3}{4}$ dia	(19)	FL	5.25	(133)	.155	(3.94)
$1\frac{1}{2}$ dia	(38)	FS	4.25	(107)	.135	(3.43)
$1\frac{1}{2}$ dia	(38)	FM	6.5	(165)	.235	(5.97)
$1\frac{1}{2}$ dia	(38)	FL	9.25	(234)	.375	(9.53)
$\frac{3}{16} \times \frac{3}{4}$ (7.92 × 19)		FM	.580	(14.7)	.038	(0.965)
$\frac{1}{4} \times 3$ (6.35 × 76.2)		FM	1.60	(40.6)	.054	(1.37)
$\frac{3}{8} \times 2$ (9.53 × 50.8)		FM	1.96	(49.7)	.160	(4.06)

Conclusions

I have found the tables and graphs produced by this study can be used very effectively as a general guide in selecting focused search units for a given test application.

Due to the bulk of the data recorded during the course of this study it was not possible to present it entirely within the limits of this printing. However, the curves shown in Figure 7 and the data in Table 4 provide a very useful condensation of the total data. A complete series of charts and curves are available in Automation Industries, Inc., Research Division, Technical Report TR 66-40, available on request.

References

1. Heuter, T. F., Bolt, R. H. *Sonics,* John Wiley and Sons, New York (1955).
2. McElroy, J. T. A method of identification, measurement, and recording ultrasonic transducer characteristics. Automation Industries, Inc., Technical Report, TR 64-22 (1964).
3. McElroy, J. T. Focused ultrasonic beams. Automation Industries, Inc., Technical Report, TR 6508, (1965).
4. McMasters, R. C. Nondestructive Testing Handbook, Vol. 2, 1st Edition, The Ronald Press Co., New York (1959).
5. O'Neil, H. T. Theory of focusing radiators, *J. Acoust. Soc. Am.,* Vol. 21, pp. 516-526 (1949).
6. Posakony, G. J. and McMasters, R. C. The analysis of focused ultrasonic test techniques. Automation Industries, Inc., Technical Report No. 601 (1960).
7. Van Valkenburg, H. E., Wilson, R. A. and Okha, W. R. Ultrasonic inspection equipment program. Sperry Products Technical Report, TR-065, (December 1965).
8. Zeutschel, M. F. The measurement of ultrasonic transducer characteristics, HW81955 (1964).

Discussion

Q. MATTHEW J. GOLIS, Ohio State University, Columbus, USA:

1. Did you investigate the effects of introducing a flat interface into a spherical wave front system?

2. Did the "far field" remain coherent beyond the focal zone, even for short focal length lens system?

A. 1. Through the course of this work we used a steel ball reflector to make all focal distance and beam diameter measurements. However, in my experience I have not found a deviation between the focal distance as measured on a flat plate.

2. Our interest during this study was primarily the measurement of the focal distance, the length of the focal zone and the beam diameter in the focal zone, thus we did not make any quantitative measurements in the far field beyond the focal zone. The energy, beyond the focal distance, is defusing very rapidly and for most practical applications is not usable.

The beam profiles shown in Figure 3 were carried out to 0.5 in. beyond the focal point. At this distance it is evident that the beam, though defusing, is still coherent.

I know Mr. Golis has experience in viewing focused beams with Schlieren techniques and we have also noticed that in a Schlieren image there does appear to be a null in the centre of a focused beam at greater distances, beyond the focal zone.

Q. N. O. CROSS, Esso Research & Engineering, Florham Park, USA:

Have you tried using two focused transducers in a send-receive set-up?

A. I assume your question refers to the use of focused transducers in a testing application where a send-receive technique would be used.

Yes, we have. As a transmitter, a focused transducer is valuable in applications where a small, intense beam is required to improve defect definition. As a receiver, the focused transducer has the advantage of a larger "capture angle". That is, energy arriving at the transducer in an angular approach is refracted by the lens and presented to the crystal at a lesser angle that is more effective in exciting piezoelectric response.

Some Examples of Ultrasonic Testing in Swedish Industry

J. TILJANDER, G. FOLKESTAD AND S. INGEVALD, SWEDEN

ABSTRACT: Some examples of the application of ultrasonic testing in the electrical, mechanical engineering as well as the sulphate and sulphite paper pulp industries are given.

Examples from the electrical industry deal with the problem of inspecting the quality of brazed connections in electrical contacts, the ultrasonic inspection of cracks in bolts in big electrical generators without the expensive demounting of a big part of the generator, and an investigation on ultrasonic inspection and strength in the thickness direction of heavy plate.

After a short description of the design of the STAL turbine, the quality requirements for some particular forgings are given. These include blade, ring, disc and rotor forgings.

The requirements for nondestructive testing of a forged ring with a diameter of 3 to 4 m are indicated in detail. This ring is part of the second-stage gear wheel for a marine propulsion turbine. Some further examples from the turbine industry deal with nondestructive testing in receiving inspection and in production.

For about 15 years the Swedish Steam Users Association has used ultrasonic methods for inspection in the pressure vessel and steam boiler field. Some instances are discussed where ultrasonic inspection has proved to be of great value.

The measurement of wall thickness in sulphate digesters and in tubes in recovery boilers is also dealt with, as well as experiences in the examination of cracks in riveted joints in a great number of sulphite digesters after prolonged service. These inspection measures are taken at fixed intervals and are intended to enable the longest possible service life without impairing reliability.

Brazed Connections in Contacts

This paper describes an investigation that has been made at ASEA to compare two different testing techniques, namely ultrasonic examination and radiographic examination.

The contacts are built up on a body of copper on which a layer of silver or silver cadmium has been brazed. With these contacts it is essential that a very good brazed joint be obtained between the copper and silver layer. A poor bond will cause the layer to loosen after a number of contact operations and the contact will eventually be destroyed.

The thickness of the layer varies between $\frac{1}{64}$ in. (0.5 mm) and $\frac{5}{64}$ in. (2 mm) and that of the copper usually between $\frac{1}{64}$ in. (0.5 mm) and $\frac{3}{4}$ in. (20 mm). This difference in the thicknesses, the shape of the layer (plane or curved) as well as the geometrical shape of the contact have necessitated the adoption of different techniques for the examination of the bond. Some contacts can be tested more easily by ultrasonic than by radiographic examination, while the reverse applies to others. A preliminary investigation was therefore performed for the purpose of trying to coordinate the two testing techniques.

Fifteen different types of contacts of varying shapes and sizes were selected. About ten or more of each type were tested so that the investigation involved in all more than 200 layers. Some of the contacts were cut in two after examination.

From the test results the following can be concluded. When the bond was good, both the radiographic and the ultrasonic examinations gave similar results. If the bond was of a poorer quality, it was sometimes difficult with both techniques to estimate exactly the percentage of good bonding surface. Occasionally larger deviations were obtained, which proved to be caused by hydrogen embrittlement. This influenced the ultrasonic image, but could not be detected on the X-ray film.

The presence of a few very small flaws could be established by radiographic examination but not by ultrasonic examination. Larger flaws or a larger number of small flaws could be indicated equally well by ultrasonic as by radiographic examination.

The thickness of the material of the contacts proved to be the factor that determines in the first place the choice of the testing technique. Ultrasonic examination is unsuitable for contacts with a thickness of less than $\frac{5}{64}$ in. (2 mm), whereas it can be used practically always for greater thicknesses. Radiographic examination gave a good picture of the nature of the bonding surface for thicknesses up to $\frac{1}{4}$ to $\frac{5}{16}$ in. (6 to 8 mm). Over $\frac{5}{16}$ in. (8 mm), on the other hand, satisfactory results could not be obtained with increasing material thickness. The geometrical shape of the contact could also hinder the use of both techniques.

As a consequence of these results a proposal for a testing procedure was put forward, where, however, economic considerations were also taken into account in the choice of technique. In those cases where both techniques were technically equivalent, the costs of the testing decided the issue.

Relationship between Ultrasonic Wavelength and Grain Size

It is sometimes observed during the ultrasonic examination of steel castings and forgings that the material displays a rather poor sound transmission. The reason for this may be, if there are no flaws present, the coarse structure of the material.

In a coarse structure the short waves of the high frequencies are greatly spread out, the transmission of the sound waves through the material is hindered, and disturbing echoes from the grain boundaries occur. These disturbing echoes can be observed on the screen in the form of "grass". In the case of large grain sizes and higher frequencies the echo image breaks down. This effect is said to be extremely severe when the grain size lies in the vicinity of the wavelength of the sound waves and begins to become noticeable already at one tenth of the wavelength of the sound wave.

This can give rise to the idea that it would be possible to determine the grain size in a material by means of ultrasonic waves so as to be able to draw certain conclusions regarding the heat treatment of the material.

An investigation involving four grades of steel, including one stainless steel, was carried out to check the relationship between grain size and wavelength. The dimensions of the test specimens were selected so that the sound path was 2 in. (50 mm). Grains of varying size were obtained by means of annealing at different temperatures. The test specimens were tested from low to the maximum possible frequency. The results could finally be compressed into a diagram, where the wavelength was plotted as ordinate and the grain size (number of grains per mm) as abscissa, see Figure 1. The fully drawn curve shows the boundary frequency where the ultrasonic image breaks down. The broken curve joins those points where the grain size is just equal to one tenth of the wavelength. As expected, these two curves lie rather close together.

Crack Detection on Bolted Joints in Stator

This case can be said to be a typical example of field work in ultrasonic examination. The actual examination itself is not particularly remarkable from the technical point of view. What complicates the work, and also makes it interesting, is the circumstances around the case, the prehistory leading to the job, the practical preparations for the dismantling, etc., preliminary technical and economic consequences resulting from the investigation. All this applies irrespective of whether the technical results are positive or negative.

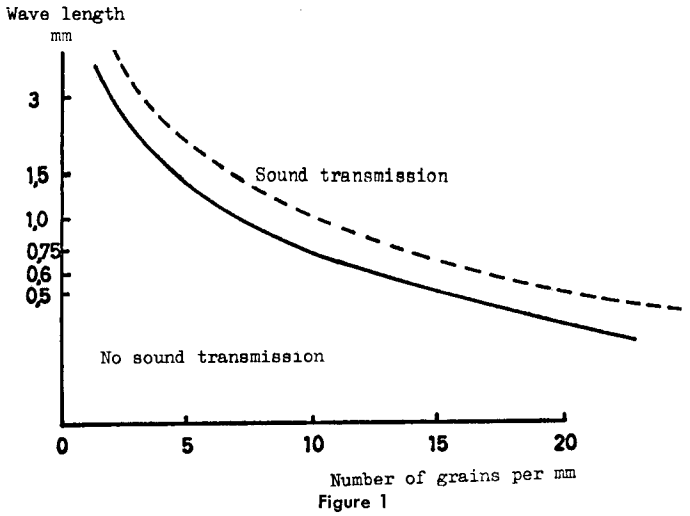

Figure 1

Some of the bolts retaining the dovetail keys in a generator in a power station had burst, which had resulted in contact in the air gap between rotor and stator. The repairs were supplemented by reinforcing of the bolted joint in the dovetail keys. It was felt that the same operation should also be carried out on the other generator in the power station. First, however, it was desired to find out whether there were any fatigue cracks present in the bolts; such cracks had in fact been found on generator I.

The conditions for the crack detection were as follows. The bolts were threaded into a fixing plate for the dovetail keys and therefore inaccessible from the outside of the stator. To be able to reach the bolts from their head end (inside the stator), it was necessary to dismantle the stator which, for several reasons, it was desirable to avoid. It was therefore necessary to make the bolts accessible for ultrasonic examination from the outside by some means, and the only solution proved to be the drill holes in the fixing plates exactly opposite the bolts and to introduce a probe through the hole. A special probe with elongated shaft was acquired for the examination and this could be introduced into the 4-in. (100-mm) deep holes, which were plane drilled in the bottom to permit good contact between the probe and the bolt.

Before the investigation on the generator could be started, preliminary tests had naturally to be made to discover whether any results could be obtained and to determine the limits for the flaw detection.

If a probe is placed against a bolt, an image is obtained on the screen displaying two echoes: one from the plane surface of the head, the bottom echo, and the other from the slot in the head, which is $\frac{1}{4}$ in. (6 mm) nearer, the trace echo. If an incision is made in the bolt by the head, a third echo is obtained, the flaw echo. In this case it was not a matter of detecting any incision made in the bolt but a natural crack, which had arisen owing to bending stresses. Such a crack does not run in a plane perpendicular to the longitudinal axis of the bolt, but always appears to try to deflect towards the bottom of the groove in the middle of the head. Such a crack will not give any echo at all. Nevertheless, an indication is obtained of the presence of a crack in that the sound beam is partly shielded, and as a result a certain reduction of back reflection takes place. If the trace echo and bottom echo are equally high there is no indication of a crack. If the bolt is in good condition the same screen image is obtained in all positions. On the other hand, the reduction of the bottom echo gives a faint indication of a crack.

With these experimental results as a basis, the investigation could be carried out according to plan on the stator, quickly and reliably. As has already been mentioned, the actual ultrasonic examination was not particularly demanding from the technical point of view apart from the preparations. On the other hand, the pleasant economic consequences were a source of satisfaction. If it had not been possible to carry out this investigation by means of ultrasonic examination, it would have been necessary to dismantle the entire stator and transport the parts to the workshop, and then back again to the power station and so on. The costs for this, together with the drop in income experienced by the power supplier, would probably have amounted to several hundred thousand Sw. Cr. All this was avoided in this case.

Strength in the Thickness Direction of Heavy Plate

When heavy plate is ultrasonically examined, indications are often obtained from larger or smaller flaws in the plate, which are found mainly to consist of slag inclusions. These defects reduce the strength of the plate in the thickness direction and may lead to the formation of cracks and fracture in the plate.

When welds in heavy plate are ultrasonically examined, indications are obtained from flaws located not in the weld but in the plate within the weld. This is a matter of actual cracks, ruptures in the plate material.

When this happens, it is a very serious situation, since it concerns structures subjected to relatively high stresses. Carrying out the necessary repairs is not only frequently troublesome, but also time-consuming and expensive.

This problem with cracks in conjunction with welding is nothing new, but it has been established that the crack frequency has increased, and more and more cases have occurred during recent years.

It is well known that rolled plate has a lower strength in the thickness direction than in the rolling direction; as a result of various investigations $\sigma_{Bth} \backsimeq 0.7\ \sigma_B$ is given as a general value. If the plate is, practically speaking, free from flaws and the stresses are moderate, this strength is often adequate. However, if macroscopic flaws such as, for example, slag are present, these constitute stress raisers, which can result in ruptures in the material.

Several questions concerning the mechanical properties in the thickness direction have not yet been solved. Certain of them are of a matter of some urgency. The following questions, for example, may be asked:

1. How much of the strength is utilized in different types of structure? 2. How are the toughness properties of plate related to different degrees of stress? To what exent is the material capable of withstanding tensile stresses? 3. To what extent is the strength reduced by so-and-so many and so-and-so large flaws?

The last question is one of the most important and if it could be satisfactorily answered, many difficult problems met in the ultrasonic examination of materials could be solved.

One can, and should, continue to ask such questions, even if one cannot expect to have them answered immediately.

4. What measures should be taken to prevent the occurrence of fracture in material, which may result in a breakdown in our structures? 5. What can be done to improve the toughness properties and strength of plate in the thickness direction?

The difficulties involved in welding plate subjected to stress in the thickness direction, however, have become so pronounced during recent years that it was found necessary at ASEA to make a start on tackling the problem. It soon became apparent that it would be impossible to begin an investigation that would be as complete and comprehensive as desired. A start was therefore made on a smaller scale to enable a program to be

drawn up for future investigations on the basis of the experience gained. The primary objective of this preliminary investigation was to find out:

a. to what extent the strength is reduced by the presence of slag in varying degrees; b. to what extent ultrasonic examination is capable of indicating the reduced strength properties of plate.

This preliminary investigation was limited to ultrasonic examination, magnaflux testing and strength testing as well as to a structure investigation.

Test Material

The investigation was made on plate of grades SIS 1312 and SIS 1411. The test material was taken from plates that had been ultrasonically examined as a matter of routine (see Table 1). The plates had been supplied from different steelworks.

Table 1

Test material

Plate marked	Steel grade	Thickness mm	Thickness in	Result of routine ultrasonic test
A	SIS 1312	20	$\frac{3}{4}$	Rejected
C	SIS 1312	20	$\frac{3}{4}$	Approved
E	SIS 1312	40	$1\frac{1}{2}$	Rejected
G	SIS 1312	60	$2\frac{1}{2}$	Rejected
K	SIS 1411	40	$1\frac{1}{2}$	Approved
T	SIS 1411	40	$1\frac{1}{2}$	Approved

A chemical analysis of the plate material showed that all the values complied with the specifications. Standard tensile tests were performed to determine the strength.

Results of the Investigation

Ultrasonic Testing. The plates of grade SIS 1312, marked A, C and E, $\frac{3}{4}$ in., $\frac{3}{4}$ in. and $1\frac{1}{2}$ in. (20 mm, 20 mm and 40 mm) were found to contain a large number of small flaws, which were fairly uniformly distributed in the plate. The $1\frac{1}{2}$-in. (40-mm) plate yielded slightly larger flaw indications than the $\frac{3}{4}$-in. (20-mm) plates.

The $2\frac{1}{2}$-in. (60-mm) plate, marked G, had unevenly distributed flaws with very small areas free from flaws among larger parts with flaws of varying size. A few test specimens displayed a reduction of 50 to 80 per cent of the bottom echo.

The plate of grade SIS 1411, marked T, had a limited area of a few dm^2 (about 50 sq in.) in size with flaws and was otherwise free from defect. A reduction in the bottom echo of 50 to 100 per cent occurred within the area of the flaws. The other plate of grade SIS 1411, marked K, proved to be particularly free from flaws. From the testing point of view the part of Plate T free from flaws could also be considered to be a perfect plate.

During the ultrasonic examination it was observed that the attenuation of the sound varied greatly between different plates. The transmission of the sound was attenuated greatly in the material displaying low strength values, irrespective of whether there were any flaw echoes or not. The number of bottom echoes as a measure of the attenuation is given in Table 2.

All the test material was also ultrasonically examined after normalizing. An extremely interesting discovery was made in this connection. A remarkable change in the ultrasonic image was obtained in plates of grade SIS 1312. The passage of the sound waves through the material was considerably improved and the amplitude of the flaw indication decreased considerably and even disappeared in some cases. Representative screen images of the plate material A in the rolled state and normalized state are reproduced in Figure 1.

Table 2

Number of bottom echoes as a measure of the attenuation

Plate marked	Tensile strength σB kp/mm²	σB kpsi	σBth kp/mm²	σBth kpsi	Number of bottom echoes
A	41.8	59.6	22.6	32.2	1
C	40.5	57.9	26.1	37.3	2
E	40.5	57.9	26.7	38.2	1
T	40.9	58.5	39.3	56.1	8
K	44.7	63.8	46.6	66.5	8

Magnaflux Testing. The magnaflux testing of test specimens from plates marked A, C, and E resulted in a large number of indications from rolled out slag inclusions, which appeared to be rather uniformly distributed in the plate. The plate marked G as well as the part with flaws of plate T displayed slag lines and slag layers. No indications of slag lines or slag accumulations were obtained from the magnaflux testing of plate K and the part of plate T free from flaws.

Strength testing. The results of the tensile tests in the thickness direction are shown in Table 3.

Table 3

Tensile test in the thickness direction, rolled state

Material	σBth thickness direction min kp/mm²	min kpsi	max kp/mm²	max kpsi	mean kp/mm²	mean kpsi	σB rolling direction mean kp/mm²	mean kpsi	σBth/σB %
A	21.9	31.3	22.9	32.7	22.6	32.3	41.8	59.7	54
C	25.7	36.7	26.3	37.6	26.1	37.3	40.5	57.9	65
E	24.4	34.8	27.8	39.8	26.7	38.2	40.5	57.9	66
G	16.0	22.9	31.8	45.5	23.5	33.6	41.4	59.2	57
K	46.3	66.2	47.0	67.2	46.6	66.6	44.7	63.7	104
T (free from flaws)	37.8	54.0	41.2	58.8	39.3	56.2	40.9	58.5	96
T (with flaws)	7.5	10.7	32.9	47.0	19.4	27.7	—	—	—

The above values were obtained from tests on specimens in the rolled state. The values for the tensile tests after normalizing are given in Table 4.

As can be seen from Table 3, the plates of grade SIS 1312 have a considerably lower strength in the thickness direction compared with the rolling direction. In addition, plate G displayed a considerable dispersion. The strength values for plates K and T (part free from flaws) of grade SIS 1411 lie on the same level as those for the strength in the rolling direction. The test-pieces from these plates were also the only ones to show any evident signs of contraction, K 30 per cent, T about 15 per cent.

The tensile tests on material that had been normalized prior to welding gave, with one exception, approximately the same or slightly higher values than those obtained before normalizing. Normalizing after welding, on the other hand, appears to result in a reduction of the strength. This tendency was still more pronounced with the normalizing of finished test pieces.

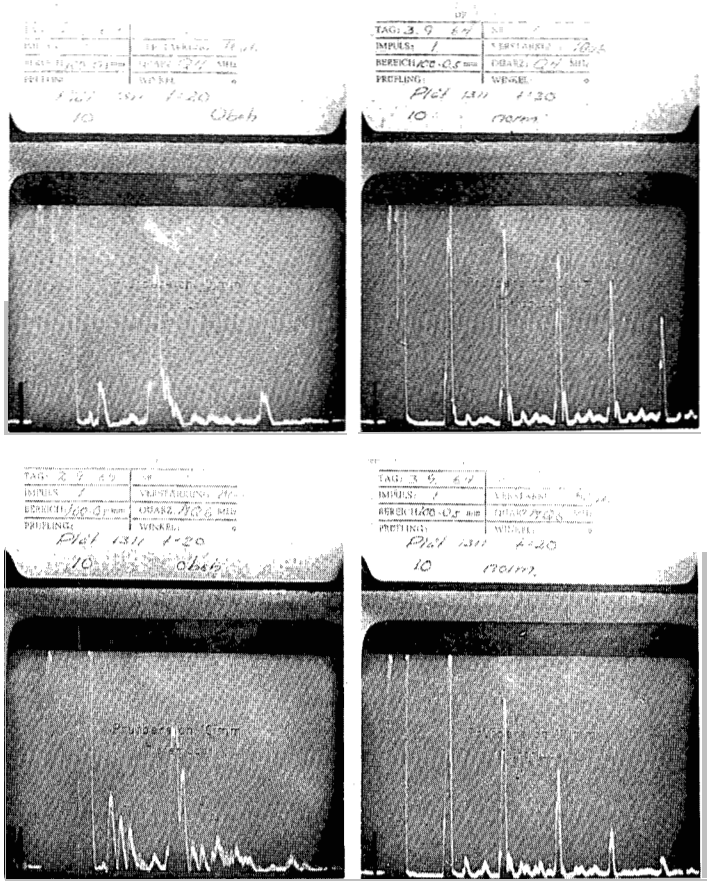

Figure 2. Screen images of plate material A. Left—material in rolled state; upper, frequency 4MHz; lower, frequency 6 MHz. Right—material in normalized state: upper, frequency 4 MHz; lower, frequency 6 MHz.

Table 4

Tensile test in the thickness direction after normalizing

Material	σBth min kp/mm²	min kpsi	max kp/mm²	max kpsi	mean kp/mm²	mean kpsi
a) Normalizing before welding						
A	21.0	30.0	24.0	34.3	22.4	32.0
E	26.9	38.4	29.1	41.6	28.0	40.0
G	17.6	25.1	31.2	44.6	27.1	38.7
K	46.3	66.2	48.5	69.3	47.8	68.3
b) Normalizing after welding						
A	20.3	29.0	21.0	30	20.8	29.7
E	23.9	34.2	25.3	36.2	24.5	35.0
T (free from flaws)	35.5	50.7	36.7	52.4	36.1	51.6
c) Normalizing of finished test-pieces						
A	17.4	24.8	18.1	25.8	17.8	25.6
C	20.2	28.8	22.1	31.6	20.9	29.8
T (free from flaws)	32.7	46.7	34.4	49.1	33.4	47.7
T (with flaws)	7.2	10.3	27.4	39.1	17.1	24.4

Examination of Structure

An examination of the relationship between the microstructure and the strength in the thickness direction was carried out. In the assessment of the structure the appearance of the perlite, the grain size of the material and the slag content were taken into account. The dimension point measuring technique was used for determining the amount of slag.

The following conclusions could be drawn from the investigation. It was established that the presence of slag has a pronounced influence on the strength. This is often lower in the thickness direction than in the rolling direction, and a high strength in the thickness direction was only obtained in material relatively free from slag. The relationship between tensile strength and hardness, σ_B: H_B, is considered to be constant for steel. In this investigation it was established that the relationship between tensile strength in the thickness direction and hardness is not constant, but decreases with increasing slag content. Furthermore, it has been found that neither the grain size nor the structure of the perlite appear to have influenced the tensile strength of the material.

Summary

As a result of the investigation the following conclusions can be drawn concerning the material tested:

1. The strength in the thickness direction of the plate can be very low, depending on the presence of slag. High values can be obtained on plate of good quality. 2. A certain relationship prevails between the results from the strength and ultrasonic tests for plate in the rolled state. Plate having a low strength, resulting from slag inclusions, generally gives an ultrasonic image with flaw indications and reduction of the bottom echo. Even if major flaw indications are absent, it appears that plate causing a pronounced attenuation of the sound in the ultrasonic examination has a low strength in the thickness direction. 3. Plate with small flaw indications and a pronounced attenuation of the bottom echo yielded, after normalizing, a considerably changed ultrasonic image with reduced flaw echoes and improved sound transmission. The normalizing does not lead, however, to any real improvement in the strength. 4. The magnaflux test gives an extremely informative picture of the presence of slag. The magnaflux images show very good agreement with the result from the ultrasonic and strength tests.

Investigations Planned for the Future

The investigation reported here has had only limited scope. A continued, more comprehensive investigation has been commenced, where, for example, the scope of the mechanical strength tests will be increased. The purpose of this investigation is to:

1. try to determine the relationship between the strength and the ultrasonic image; 2. try to clarify the problems associated with normalizing and its influence on the ultrasonic image and the strength properties; 3. try to clarify the problems associated with the formation of cracks occurring in conjunction with welding; 4. to obtain design data for permissible stresses in the thickness direction.

Some Examples of Ultrasonic Testing Methods Used by STAL-LAVAL

The technical development within the power and heat production field has created steam and gas turbines with higher pressure and temperature operating conditions. The demand to be profitable has also forced the designers to make more compact and reliable plants with higher outputs. A consequence of this is the development of the materials towards high-strength, heat-resistant steel and alloys with requirements of homogeneity and purity. This has in its turn resulted in nondestructive testing methods having an important role in production to eliminate defective materials used and for the control of certain operations of manufacturing, such as welding, soldering etc.

The STAL-LAVAL group manufactures steam and gas turbines for power and/or heat consumption, marine propulsion turbines and auxiliary alternator turbines, heat exchangers for different purposes, refrigeration plants for ships, etc.

This paper describes the nondestructive testing needs in our technical specifications of delivery of some important parts, and also gives some examples of the application of nondestructive testing in our receiving and manufacturing inspection departments.

In the STAL turbine, which is a reaction turbine with radial steam flow, the blades are placed between two or more parallel rings, which together form a blade ring. An inner turbine system consists of a number of such blade rings with increasing diameters, placed concentrically in relation to each other, as shown in Figure 3. The steam flows from the centre radially outwards, and through different blade-angles two consecutive rings receive an opposite rotating direction. All the blade rings with the same rotating direction are fixed to the same turbine disc, which in turn is connected to a generator. Consequently the STAL turbine consists of two oppositely rotating turbine systems, each connected to its own generator. For higher ranges there is an axial system to each of the radial systems. This axial system has a conventional design with forged rotors, with up to six different stages.

The radial blades are made by a 13% Cr steel, delivered as bars. The bars are ultrasonically tested by the supplier, primarily as regards slag inclusion of macro-size. The axial blades are made by the same steel from bars or delivered as normal forged pieces. The largest axial blades have an over-all length of 3 ft (0.9 m). For the forged blade blanks we prescribe ultrasonic testing with at least a frequency of 2 MHz and also a magnetic particle examination or dye check test depending on the material.

The blanks for blade rings are made by modified 13% Cr Mo steel. All the ring blanks are checked ultrasonically with a frequency of 4 MHz.

The radial turbine disc consists of a disc with a shaft and is ultrasonically tested on all surfaces with a frequency of at least 2 MHz, normally 4 MHz, and specially at the change between disc and shaft, where there is a risk of rupture during the forging.

The axial turbine rotors are made of forged blanks with a weight of 5-6 tons. These are ultrasonically tested in both radial and axial direction with a frequency of at least 2 MHz, normally 4 MHz. As we do not have any centre bore we are specially interested in having the centre-line of the rotor free from defects of any kind.

In our main propulsion machinery there is a gear for reducing the number of revolutions from the turbine to a lower number for the propeller. This is made in two steps and for the second reducing gear wheel we have a diameter of 10 to 13 ft (3 to 4 m). The rim for this wheel is made of forged non-alloyed steel and has a breadth of about 3 ft (1000 mm) and a thickness of 4 to 8 in. (100 to 200 mm). In order to have a perfect toothed surface in this wheel a material with a very high grade of freedom from slag inclusions is required. To fulfil this requirement our technical specifications for delivery demand the following specifications for nondestructive testing:

> Ultrasonic testing with regard to inner defects (segregations, cracks, flakes, slag inclusions etc.) to be made after heat treatment and rough-machining. The forging to have a good surface finish of about 40 μm in order to ensure close contact between the probe and the forging. The test preferably made at a frequency of 4 MHz with the min. frequency 2 MHz. The forging to be tested in both axial and radial direction. Axial examination of the forging to be made from both ends.
>
> If only a few small indications appear during the axial test, their approximate number is stated in a report and the maximum flaw echo amplitude as well as the amplitude of the pertinent bottom echo are given as a percentage of full screen height.
>
> If there are remarkable defects in the forging, each flaw echo and pertinent bottom echo is stated in a report as mentioned above, and the defects are marked on a sketch of the forging. The defects must also be marked on the forging with an indelible colour.
>
> In the radial examination the whole surface of the forging is scanned, preferably from the inside, to get distinct reflections from that part of the forging which is to be cut to teeth. The quality of the forging is judged with respect to the location, spread and concentration of the defects in two radial zones defined below.
>
> *Zone 1*
>
> The first zone consists of the outer portion twice the thickness of the external machining allowance + tooth height + 0.4 in. (10 mm), altogether approximately 1.6 in. (40 mm) for bigger wheels.
>
> In zone 1 only small, widely spread defects are allowed. Each flaw echo and corresponding bottom echo is to be noted in the report and plotted on a sketch of the forging.
>
> *Zone 2*
>
> The second zone encloses the remainder of the thickness of the rim. The bigger flaw echoes and pertinent bottom echoes

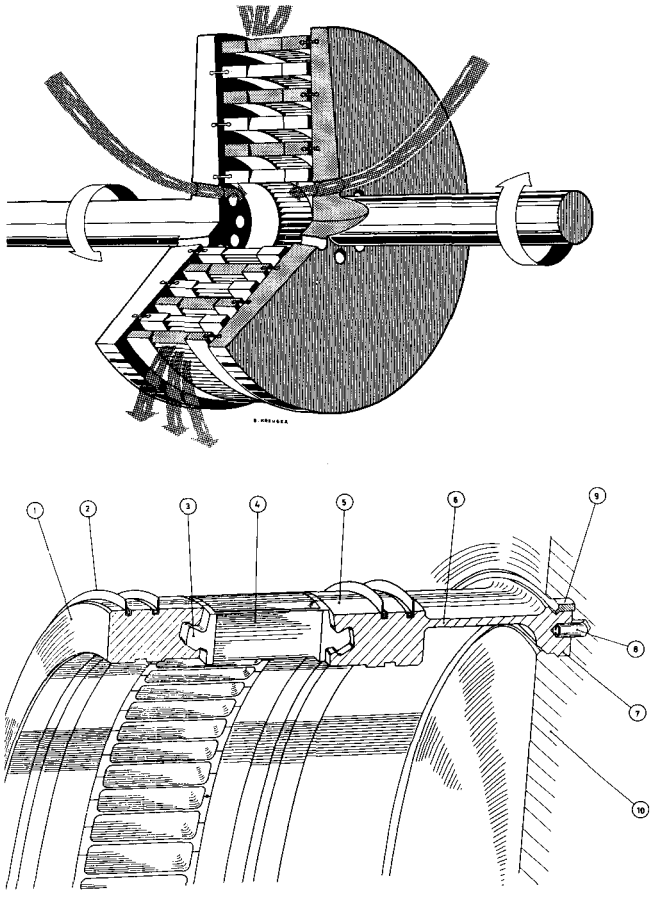

Figure 3. STAL turbine, upper; a section of a blade ring, lower.

are to be written in the report and plotted on a sketch of the forging. The concentration of the defects is defined as the number of echoes per sq.dm.

The supplier gives STAL-LAVAL a report and sketches of the ultrasonic test results for consideration, after which STAL-LAVAL advises whether the forging may be delivered.

For steel castings we send a drawing of the nondestructive testing examination to the foundry. In this we state the type of nondestructive testing which is applied on the different parts of the casting. This depends on the grade of strain of the finished detail, the quality of the material and the geometrical formation of the casting. Mostly we state ultrasonic testing and X-ray examination, where possible. A report of the examination and the radiograms are sent to us together with the casting.

On basis of the reports from the supplier's nondestructive testing we carry out, in our receiving control department, a verifying nondestructive test. This is also influenced by experiences with earlier deliveries from the supplier. For ultrasonic testing we use manual scanning, depending on the variation of parts in size, geometrical form and material.

In our radial turbines the blade rings are an important part. The ring blanks undergo a very extensive material inspection in our work which, apart from special tensile and impact tests, examination of the structure and checking slag-inclusions, also includes an ultrasonic examination of each blank. We use a 45° miniature angle probe for 4 MHz and as couplant a normal grease-oil or a paper-paste named Modocoll.

The material defects that can occur are slag-inclusions, cracks, flakes and so on. Since the finished blade ring in some sections has a thickness of only 0.04 to 0.12 in. (1 to 3 mm) and is rolled fixed on the turbine disc, a very small defect can cause a rejection of the material. An example of such a material defect is shown in Figure 4.

Many of our governor valves, turbine casings and heat exchangers are made of fabricated parts and are so shaped that it is impossible to do an adequate radiograph examination. In these cases we use ultrasonic examination by means of both normal and angle-beam probes. We have for a long time made a routine examination of all turbine bearings by checking the binding between the layer of bearing metal and the ground metal. Here we use normal probes with a frequency of 6 MHz.

Some Examples of Ultrasonic Testing by the Swedish Steam User's Association

Ångpanneföreningen (Swedish Steam User's Association) has for about 15 years used the ultrasonic method in connection with its control and inspection activity, which concerns pressure vessels, steam boilers, lifts and hoisting installations. Some examples are given of the application of ultrasonic testing that have shown great value in evaluating the functional stability of actual units.

In the pulp industry a special type of steam boiler is used, so-called recovery boiler units. These are fired with evaporated liquor from the cooking process. The furnace in a modern recovery boiler is composed of four vertical tube walls consisting each of about one hundred tangent tubes. The dimensions of the tubes are for example 2 in. × 7/32 in. dia (50 × 5.5 mm). The furnace in such a steam boiler can have a base of 20 × 25 ft (6 × 7 m) and a height of 70–100 ft (20–30m). In older units these tubes were protected by cast-iron blocks. In most of the modern recovery boilers these blocks have not been used, thereby exposing the tubes, in some cases, to corrosion. A tube failure in the furnace can cause a complete blow-out of the unit through secondary effects in the smelt on the bottom of the

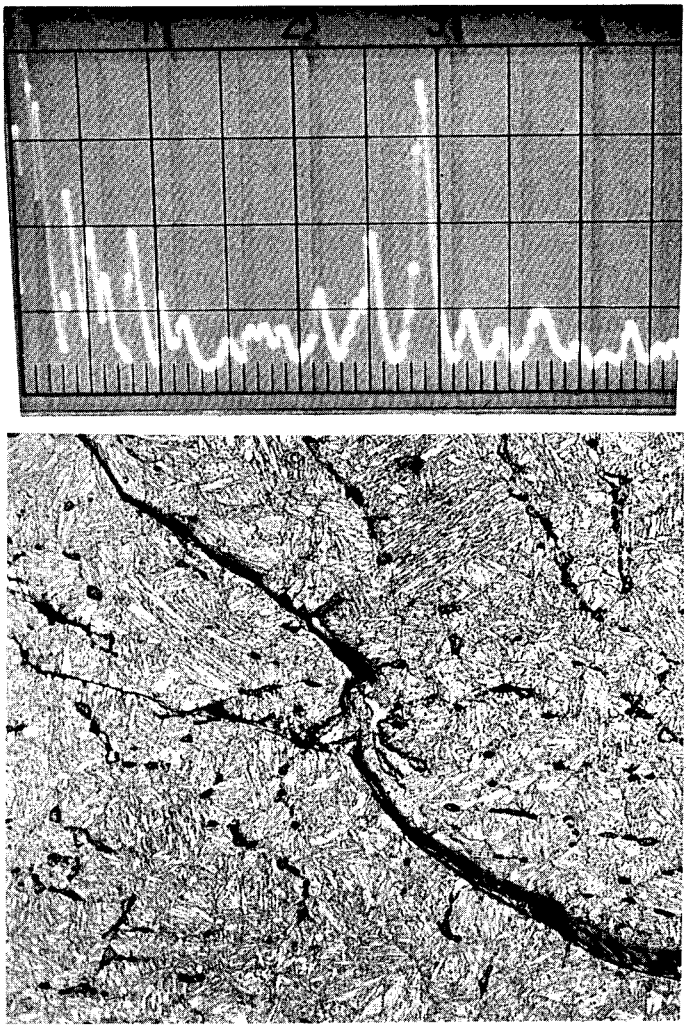

Figure 4. Defect in a blade ring. Upper, A-scan indication; lower, section through defect, X150 etched in 10% oxalic acid.

furnace. One single tube burst can thus lead to considerable economical loss besides the risk of personal injury. Since this corrosion on the furnace side of the tubes was observed, comprehensive measurement of the tube thickness by ultrasonic instruments was started in the spring of 1964. Measurements were made on the impulse-echo Krautkrämer instrument, type USIP 10 W. The transducer used is a so called "finger-tip-probe" with separate transmitter and receiver crystal and a frequency of 6MHz. The instrument permits an accuracy of reading of 0.004 in. (0.1 mm). The maximum measuring error under normal working conditions is 0.008 in. (0.2 mm). A two-man team can in an hour check about 500 measuring points. The result of measuring is stated in corrosion diagrams which give a direct picture of the scope of corrosion on a wall or wall section. Figure 5 shows the result from two measurements made at a 12-month interval on the lower part of the same tube wall.

The results from these measurements are the basis for:

1. Judging of possible exchange of tubes; 2. Means of decreasing corrosion, such as changed firing conditions; 3 research made to clarify the reason for the corrosion attack.

Another example where ultrasonic testing has shown its value is on pipes in circulation systems for sulphite digesters. An actual case refers to a pipe system made of acid-resistant material of austenitic quality with a carbon content of 0.06%. In the pipe system there are several large bends manufactured through the warm forming of ⅛-in. (3 mm) plate. After some

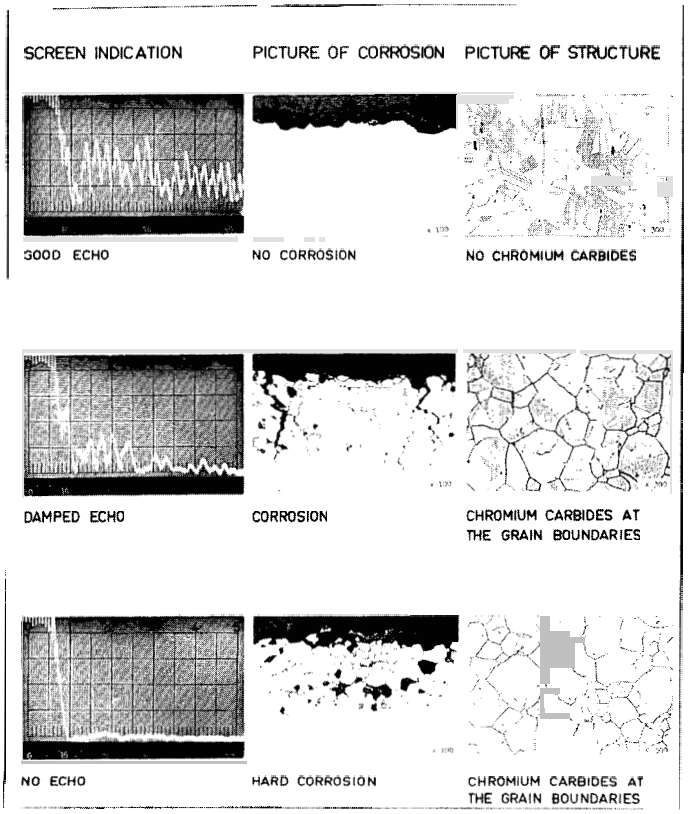

Figure 5. Pipes for circulating of sulphite solution. Material, UHB stainless, 4 mm.

time of operation two bends broke down in series. The reason was so-called grain-boundary corrosion due to chromium carbide formation in the grain boundaries. It was reliably established that only a few bends, through unsuitable heat treatment during manufacture, had been exposed to the risk of carbide formation. By ultrasonic testing one could easily distinguish faulty and (through corrosion) more or less affected bends from faultless ones. In this way the tube system could, with a short shut-down, be repaired through exchange of faulty tube details. When testing, a single-crystal straight-beam probe with 7/32-in. dia (5 mm) was used. When testing faultless plate, a series of multiple echoes were obtained in the usual way. For a light corrosion attack a striking moderation of the oscillogram was obtained; for heavy attacks no echo was obtained due to spreading of the sound at the corroded grain boundaries. The oscillogram at different degrees of corrosion appears in Figure 6.

Today, in the Swedish cellulose industry there are still about one hundred old sulphite digesters of riveted design. These digesters are lined with acid-resistant brickwork with single external butt straps in the rivet joints. From the point of view of strength this is not a good design. In addition, the environment is corrosive and cracks often arise on the inside of the external butt straps. Previously these rivet joints were examined by removing small specimens from the straps. Since 1954 such rivet joints have been examined by ultrasonic instruments. The examination normally comprises about 25% of the total rivet-joint length, with emphasis on the joints that are the most stressed or, for some other reason, can be expected to be in bad condition. In spite of this examination being considerably broader than the previous method, it can be carried out at a considerably lower cost, and a much shorter shut-down. Krautkrämer equipment is used for the examination. The butt straps are tested systematically with 45° angle probe. Due to varying surface conditions on different butt straps, calibration is made on each strap against a fixed rivet hole. To get more equivalent surface conditions, sandblasting of the surface is nowadays recommended. Through laboratory tests and through practical experience it has been possible to establish a certain connection between echo amplitude and depth of crack. Other methods for determining the depth of the cracks have been found to be too time-consuming. The cracks established are drawn schematically on a sketch showing the respective rivet joint part, and the estimated crack depth. When testing in this way, with an interval decided upon according to the crack frequency and crack depth, a good picture of the condition of a digester is achieved.

A further example of Ångpanneförenigen's application of the ultrasonic is the measurement of the thickness of pressure vessels, tanks and pipings exposed to corrosion or erosion. Such measurements are also made during operation at temperatures up to about 400°C (750°F). Weld examination with ultrasonic instruments has become of greater and greater importance. In several cases severe crack formations in welds have been detected with this method, information not possible with other nondestructive testing methods. Ångpanneföreningen has found more and more applications for the ultrasonic method and has found it a valuable aid for safely evaluating the effective use of various types of equipment.

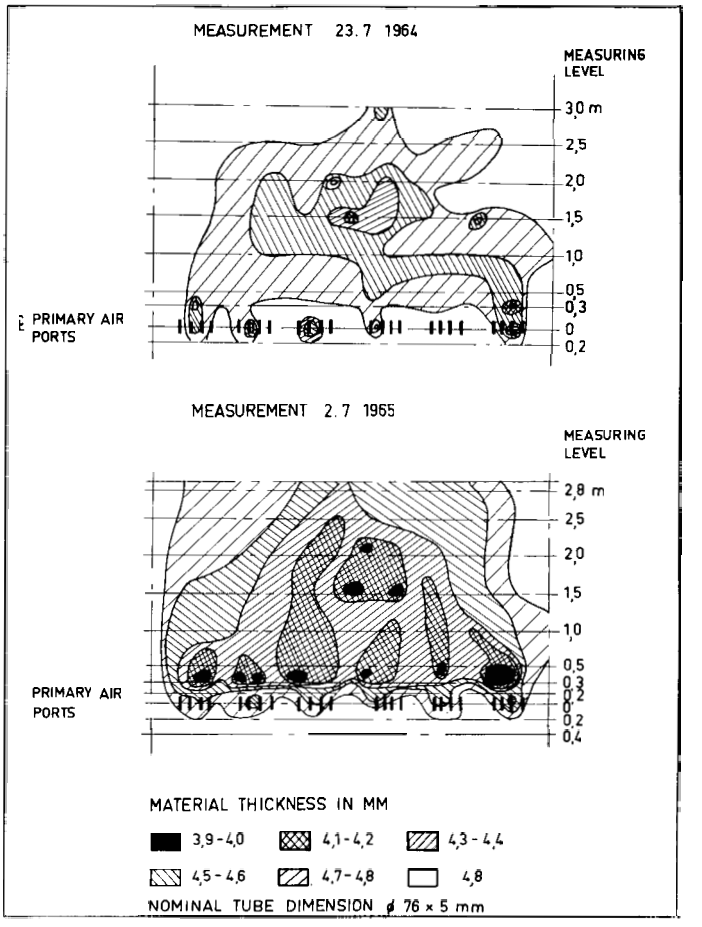

Figure 6. Recovery boiler. Material thickness of tubes in furnace according to ultrasonic measurements. Backside wall.

Theory and Application of Ultrasonic Multiple Echoes in Specimens with Semipermeable Interfaces

E. MUNDRY, GERMANY

ABSTRACT: If plane parallel specimens are tested with ultrasonic pulses of normal incidence, sometimes abnormal reflectograms with flaw echoes of initially increasing amplitude with increasing number of multiple back reflections can be observed. After reaching a maximum the echo amplitude decreases, similarly to a normal sequence of multiple echoes. This phenomenon can be explained as characteristic of the existence of a semipermeable interface inside the specimen. A complete theory of multiple echoes in such cases is developed, including special phenomena of interference. The main criteria of the calculated reflectograms are maxima and zero points in the envelopes of all intermediate and bottom echo sequences. The theoretical results are not only valid for simple interfaces, but for more complicated semipermeable layers, too.

To prove the theory, some experiments of different kinds were carried out on a model specimen consisting of a glass-mercury combination. All experimental results are in good quantitative agreement with the theory.

Some applications to practical problems of nondestructive testing are discussed: Testing of metallic bearings, shrink fits, brazed joints etc.; testing of plates, billets and other semiproducts; judgment of echoes from single defects; measurement of phase shift with direct probe-to-specimen contact; testing of spot welds in thick plates.

1. Introduction

If plane parallel specimens are tested with longitudinal ultrasonic pulses of normal incidence, reflectograms are sometimes observable, which seems to disagree with the normal conception of the formation of multiple echoes. Figure 1a shows a normal reflectogram with one sequence of bottom echoes and one sequence of flaw echoes, decreasing both monotonously with

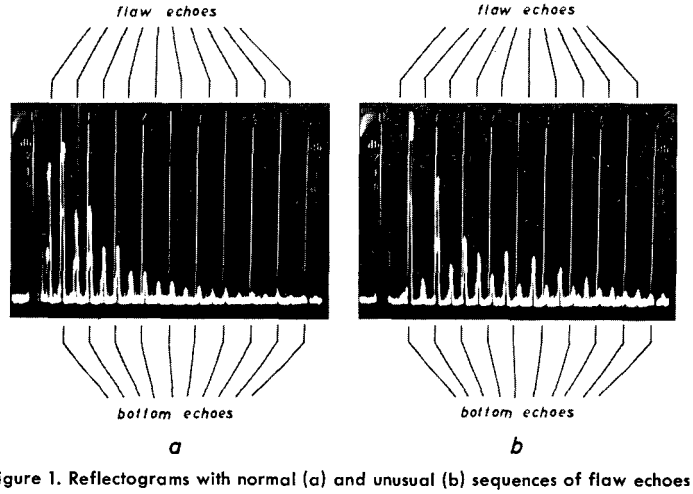

Figure 1. Reflectograms with normal (a) and unusual (b) sequences of flaw echoes

increasing path length. Since the pulse energy along the pulse path from echo to echo due to ultrasonic extinction, geometric and reflection losses becomes smaller and smaller, it is clear that the echo amplitude must decrease with increasing distance from the initial pulse. In apparent contradiction to this, the echo amplitude in the sequence of flaw echoes in Figure 1b at first increases and then decreases after having reached a maximum.

This phenomenon was mentioned by Grabendörfer and Krautkrämer (1), and was interpreted as a characteristic of the existence of semipermeable interfaces in the specimen. This paper deals with an exact theoretical explanation of such reflectograms, the verification of the theory by model tests, and discusses the applicability to practical problems of nondestructive testing. Some examples are described.

2. Theory of Multiple Echoes

If there is a semipermeable interface O_1 in a specimen parallel to its scanning surface O_0 and its opposite surface O_2, an ultrasonic pulse of normal incidence will always be divided into one transmitted and one reflected part, whenever it passes the interface (Figure 2, top left). In the course of its multiple reflections the initial pulse therefore splits into an increasing number of "single pulses". The pulse paths of the single pulses are shown in schematic representation at the bottom of Figure 2, whose scale of transition time τ is adapted to the reflectogram above. Each single pulse can be characterized by 3 integral numbers (m, n, q), specifying how often the pulse has passed the different sections

$$\overline{O_0O_2},\ \overline{O_0O_1} \text{ and } \overline{O_1O_2}$$

of its total path—each to and fro—(Figure 2 top right).

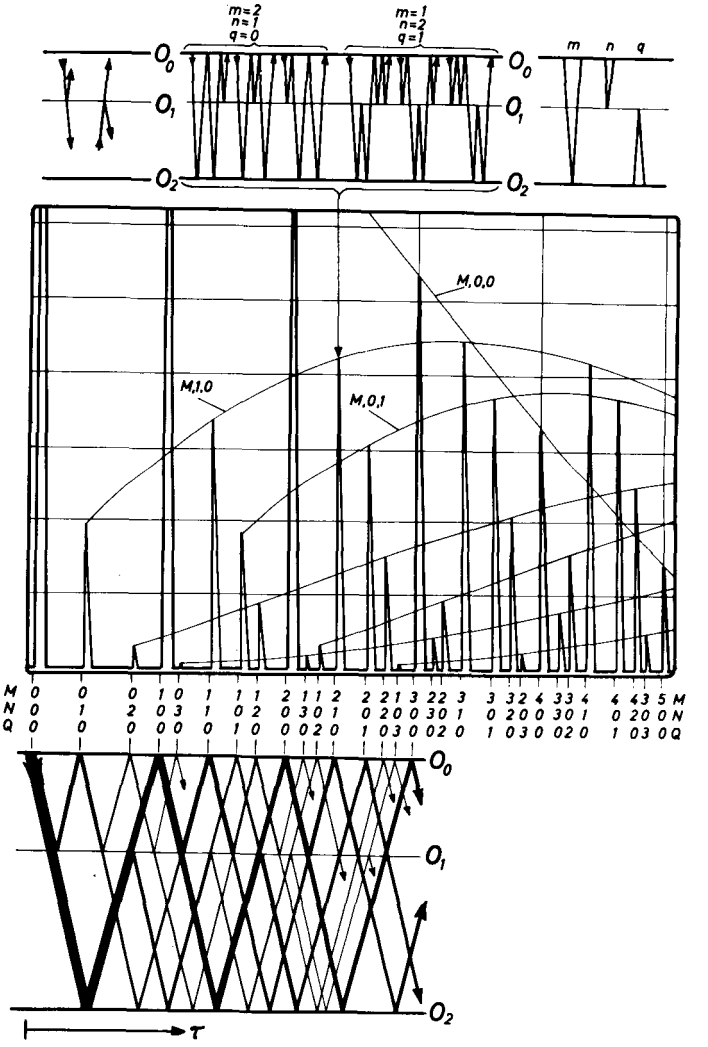

Figure 2. Formation of a reflectogram in a specimen with a semipermeable interface.

Primarily a group of several single pulses belongs to one given triplet of values (m, n, q). They differ from one another only in the kind of succession, in which the three sections mentioned above are passed. All single pulses of one group combine to a common pulse which shall be called "group pulse". Examples for such two groups with $(m = 2, n = 1, q = 0)$ and $(m = 1, n = 2, q = 1)$, each containing 3 single pulses, are shown in Figure 2 above.

Nearly all echoes of a reflectogram are formed by superposition of several group pulses. To bring the relatively complicated reflectograms into order, all these echoes are combined in one sequence, each of which is an equal distance from the preceding bottom echo. Furthermore it is possible to assign 3 integral numbers (M,N,Q) to each echo; the numbers are a measure for the total transition time whose meaning is very similar to that of the triplet (m,n,q) of the single pulses. Below each echo of the constructed reflectogram in Figure 2 the values of M,N, and Q are added, and moreover, the peaks of all echoes in one sequence are connected by a smooth curve, which shall be called "envelope of a sequence" or for short "envelope", which must not be confused with the envelope of a single pulse. The most important characteristics of the reflectograms can be taken from the envelopes as defined above. In order to determine their shape it is necessary to calculate the amplitudes of the single pulses and group pulses and lastly the echo amplitude.

Amplitude of Single Pulses

A single pulse, characterized by the triplet (m,n,q) has been reflected $(m + n - 1)$ times at the surface O_0, $(m + q)$ times at the surface O_2, and $(n + q)$ times at the interface O_1, and it passes through the interface in each of both directions m times. Neglecting all ultrasonic losses and assuming some other simplifying conditions, the sound pressure amplitude of such a single pulse is therefore

$$p(m,n,q) = P_0 R_0^{m+n-1} R_1^{n+q} R_2^{m+q} (1-R_1^2)^m \qquad (1)$$

P_0 is the sound-pressure amplitude of the initial pulse; R_0, R_1, R_2 are the reflection factors of the faces O_0, O_1, O_2.

Amplitude of Group Pulses

After having covered their pulse paths, which are different in detail, but of equal total length, all single pulses of one group arrive simultaneously and cophasally at the surface O_0, i.e. at the ultrasonic probe. The sound-pressure amplitude $P(m,n,q)$ of the group pulse built by them is therefore

$$P(m,n,q) = A(m,n,q)\, p(m,n,q) \qquad (2)$$

$p(m,n,q)$ is the amplitude, $A(m,n,q)$ the quantity of the single pulses in the group. Due to the possible different combinations of the m,n, and q pulse-path sections of the types

$$\overline{O_0O_2},\ \overline{O_0O_1} \text{ and } \overline{O_1O_2},$$

the combinatorial analysis gives

$$A(m,n,q) = \frac{(m+n)!}{m!\,n!}\,\frac{(m-1+q)!}{(m-1)!q!} = \binom{m+n}{n}\binom{m-1+q}{q} \qquad (3)$$

and as an additional condition

$$m = 0 \rightarrow q = 0 \qquad (4)$$

Echo Amplitude

All echoes in a reflectogram like Figure 2 with value of $M \geq 2$ are built by several group pulses with different triplets (m,n,q), each of them to be calculated according to Eq. (2). An example is the echo with $(M=2, N=1, Q=0)$, which is a superposition of the two group pulses $P(2,1,0)$ and $P(1,2,1)$, containing 3 single pulses each. Such superpositions are unavoidable, because there is always

$$\overline{O_0O_1} + \overline{O_1O_2} = \overline{O_0O_2}$$

For that reason all group pulses $P(m,z,z)$ with arbitrary values of $z=n=q$ compose the bottom echoes (M,O,O), being $M=m+z$. All group pulses with $n > q$ build up the echoes (M,N,O), being $M=m+q$ and $N=n-q$. The last possible case $q > n$ is analogous. Hence all echoes of a reflectogram belong either to the bottom echoes (M,O,O) or to a sequence of intermediate echoes of the kind (M,N,O) or (M,O,Q). According to this, for each echo in Figure 2 at least one value N or Q is equal to zero.

Generally the reflection and transmission factors, which appear in the specimen, are not real but complex magnitudes, e.g. if the specimen does not contain a simple interface, but a semi-permeable layer of one or several other materials of different characteristic impedances. This means that all group pulses composing one echo are not inphase. In order to obtain the echo amplitude, the complex sound pressures $P(m,n,q)$ of the group pulses must be summed up instead of their sound pressure amplitudes $P(m,n,q)$. The echo amplitudes, i.e. the observable heights of the echo peaks in the reflectogram, are then proportional to the absolute value of this sum:

$$H(M,N,Q) = C \left| \sum_{\mu=0}^{M-1} P(M-\mu, N+\mu, Q+\mu) \right| \qquad (6)$$

The constant of proportionality C depends on the sensitivity of probe and apparatus, the probe-to-specimen contact etc. The result of the calculation is

$$H(M,N,Q) = C\, P_0\, R_0^{M+N-1}\, R_1^{N+Q}\, R_2^{M+Q}\, (1-R_1^2)^M \cdot \sum_{\mu=0}^{M-1} \left[\binom{M+N}{N+\mu} \binom{M-1+Q}{Q+\mu} \left(\frac{R_1^2}{1-R_1^2}\right)^{\mu} (-1)^{\mu} \right] \qquad (7)$$

for $M \geq 1$ and with the additional condition, that at least one of the values N or Q must be equal to zero, R_0, R_1, and R_2 are the absolute values of the complex reflection factors. Each term of the sum in Eq. (7) represents one group pulse, and all group pulses can be classified in one type with even numbers μ and in another with odd numbers μ. The group pulses of one type are in phase with one another, and between the two types there is a phase difference π.

A more detailed description of the theory is given in (2). Moreover, Eq. (7) is valid for any semipermeable "zones", e.g. for simple interfaces, more complicated layers of given thickness etc. It must be assumed that no ultrasonic extinction takes place in this zone, and that one ultrasonic pulse contains so many single oscillations, that it can be approximated by a harmonic wave train. A generalization of the theory on several semipermeable zones in the specimen is outlined in (2) also.

Discussion of Reflectograms

Eq. (7) was evaluated numerically within the wide range $0.01 \leq R_1 \leq 0.9$. Due to the probe-to-specimen contact R_0 was varied as a parameter within the range $0.7 \leq R_0 \leq 1.0$. The opposite surface was assumed to be a free surface, i.e. $R_2 = 1.0$. Four examples of calculated reflectograms for two values of R_0 and R_1 each are plotted in Figure 3. The scale of transition time τ is divided by the values M of the bottom echoes, the echo amplitudes $H(M,N,Q)$ are plotted in arbitrary units. The bottom echoes are represented by full lines, the intermediate echoes by dashed lines. In order to get clear reflectograms, all echo sequences with $N \geq 4$ and $Q \geq 4$ are omitted.

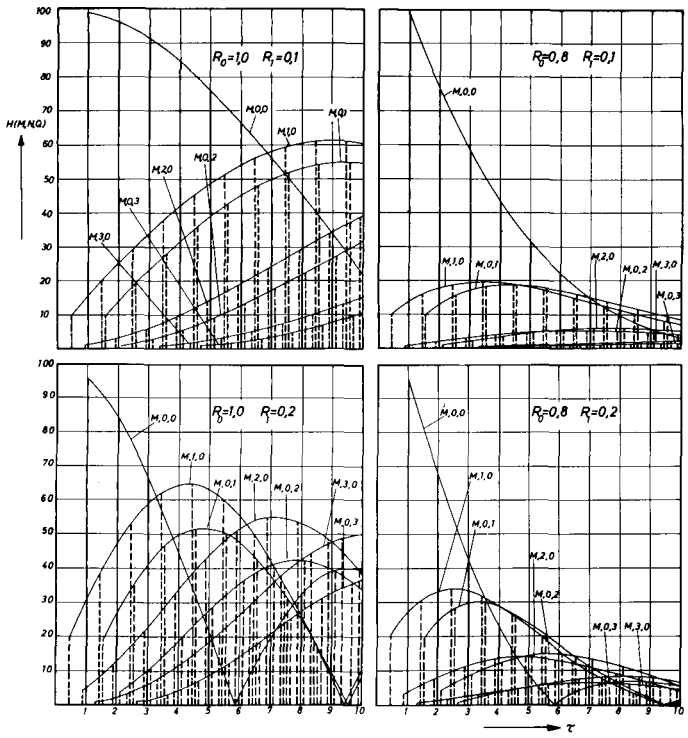

Figure 3. Calculated reflectograms for two values of R_0 and R_1 each.

The main characteristics of all calculated reflectograms are zero points and maxima in the envelope of the sequence of bottom echoes and in each sequence of intermediate echoes at different distances to the initial pulse. The distances between zero points and initial pulse—measured in units of M—depend only on R_1, those between maxima and initial pulse depend on R_0 and R_1. With the help of a more detailed analysis of the calculated reflectograms special diagrams can be constructed, in which the positions of the zero points or maxima at the time base of the reflectograms, i.e. their distances from the initial pulse, are plotted against R_1 in the case of the maxima with R_0 as a parameter. Using such diagrams the reflection factor R_1 of a semipermeable zone in a specimen can be read directly from the reflectogram. Due to the limited number of figures in this paper no such diagram is shown, but in (2) several examples are given. Qualitatively one can say that the value of R_1 is the smaller, the larger the distance between zero points or maxima and initial pulse. It is a considerable advantage of the theory, that due to the clearness of a reflectogram the evaluation of R_1 by reading the maximum or zero points from the reflectogram is the easier, the smaller R_1; and this is possible even when the first intermediate echo is too small to be observed or measured clearly.

Special Cases According to Echo Interferences

If the specimen is divided by the interface or zone into two parts in such a manner, that the pulse transition times in the sections $\overline{O_0O_1}$ and $\overline{O_1O_2}$ (see Figure 2) are nearly equal to each other, the echoes interfere with each other and, apart from the bottom echoes in the reflectogram, only one sequence of intermediate echoes remains observable, and the position of each intermediate echo is in the middle between two bottom echoes. All echoes with

$$2M+N+Q=1 \quad (1=1,2,3,\ldots) \tag{8}$$

have nearly equal total transition time and compose one interference echo with the echo amplitude E_1. Even values of 1 lead to bottom echoes, add values to intermediate echoes. When only extreme values, i.e. maxima and minima of interference echo amplitudes are investigated, this echo amplitude can be calculated very easily by a simple recurrence formula:

$$\begin{cases} E_0 = C P_0 \\ E_1 = E_0 R_1 \\ E_2 = E_1 R_0 R_1 \mp (1-R_1^2) E_0 \\ E_2 = E_2 R_0 R_1 \mp (1-R_1^2) \underbrace{[E_1 R_0 \mp E_0 R_1]}_{e_2} \\ \cdot \\ \cdot \\ \cdot \\ E_1 = E_{1-1} R_0 R_1 \mp (1-R_1^2) \underbrace{[E_{1-2} R_0 \pm e_{1-2} R_1]}_{e_{1-1}} \\ \cdot \\ \cdot \\ \cdot \end{cases} \tag{9}$$

The upper signs are valid for the one extreme case, those below for the other one. Both cases differ very considerably from one another. For small values of R_1 near the initial pulse the first case gives intermediate echoes of maximum and bottom echoes of minimum amplitudes, in the second case it is vice versa. Only in the first case the reflectograms are similar to those discussed in section 2. An example for both cases with equal values of R_0 and R_1 is shown in Figure 4 together with some experimental results.

Of course similar phenomena of interference take place too, if the pulse transition times in the two sections

$$\overline{O_0O_1} \text{ and } \overline{O_1O_2}$$

are not nearly equal, but nearly in an integral ratio to each other. In (2) the theory of interference echoes is discussed in detail.

3. Verification of the Theory by Experiments on a Model

Since real specimens like metallic bearings, shrink fits, brazed joints, etc. are unsuitable for testing the theory quantitatively, a special model of a specimen with one semipermeable interface was constructed. The main part of the model is a mercury-filled vessel with an exchangeable bottom plate of optical glass. The bottom surface of the glass plate and the free mercury surface are the two surfaces of the specimen, and the interface glass/mercury is semipermeable with a rather small reflection factor R_1, according to the small difference between the specific impedances $\rho\ c$ of glass and mercury ρ being the density and c the longitudinal wave velocity. Using several kinds of optical glasses as bottom plates, it was possible to obtain several values for R_1 within the range $0.06 \leqq R_1 \leqq 0.16$. Using an immersion technique by dipping the relatively small mercury vessel into a large water vessel with the ultrasonic probe in its botttom, it was possible to measure the reflection factor R_0 at the "scanning surface" of the specimen very carefully and easily according to Roderick and Truell (3), or to calculate this value from the characteristic impedance of glass and water. In the same arrangement the ultrasonic extinction in glass could be measured, that in mercury is negligibly small (4). The geometric losses caused by diffraction effects in the ultrasonic field of the probe, could be corrected according to Seki Granato and Truell (5). Thus experimental and theoretical results could be compared quantitatively. In (6) the whole experimental arrangement is described in detail.

As a first series of experiments all echo amplitudes of one reflectogram within the range between initial pulse and fourth bottom echo were measured in decibels. After having corrected all geometric and other ultrasonic losses, the unknown reflection factor R_1 of the interface was calculated about 15 times by application of Eq. (7) to 15 different ratios of different intermediate and bottom echo amplitudes. As theoretically expected, all values agreed with one another very well and do not depend on the special echo combination chosen. If the mercury is carefully cleaned of its oxide film, the average of the measured values of R_1 moreover agree with the theoretical value, which is calculated from the characteristic impedances. In most cases with several optical glasses the agreement was better than 0.7% although mercury cannot wet the glass.

By choosing suitable quantities of mercury it is possible to produce the two extreme cases of interference echoes. Since the true value of R_1 was known from these experimental results, these reflectograms could be compared directly with theoretical calculations described in section 2. An example is given in Figure 4. The left reflectogram shows maximum intermediate and minimum bottom echoes, the right reflectogram minimum bottom echoes in the neighbourhood of the initial pulse.

In another sort of experiment the phase shift from echo to echo, which is theoretically expected to be zero or π—so that all echoes can be classified into one type in phase with echoes and another one of phase opposition—was controlled by observing the non-rectified echo signals on an oscilloscope with a widely spread time base.

Finally an attempt was made to imitate a special case of interference echoes of theoretical interest with $R_0 = 1.0$ and $R_1 = 1\sqrt{2}$, using a $CaCl_2$ solution of suitable concentration instead of mercury. In this case all intermediate echoes must be of equal amplitude, and the bottom echoes alternate from echo to echo of minimal and maximal amplitude (2,6).

Since all theoretical considerations are verified quantitatively by the experimental results, it can be assumed, that the reflectograms and their formation are described exactly by the theory of section 2.

4. Applications to Problems of Nondestructive Testing

Testing of Metallic Bearings, Brazed Joints, Shrink Fits etc.

Metallic bearings, brazed joints, shrink fits etc. are specimens with semipermeable interfaces and zones respectivey. The reflection factor of such an interface can be used to obtain information about the quality of the specimen. Usually the amplitude of the first echo and seldom that of another echo from the interface or the ratio of this amplitude to that of a bottom echo is used as a direct characteristic of quality (7-14). Since the echo amplitude or the ratio of two amplitudes depends not only on the reflection factor, but on ultrasonic extinction and geometric losses too, the results of such tests are not generally valid, but only usable for the special conditions of the type of specimen. This disadvantage can be avoided when the amplitudes $H(0,1,0)$ of the first echo from the front of the interface, $H(1,0,0)$ of the first bottom echo, and $H(1,0,1)$ of the first echo from the back of the interface are taken into account. If this is possible, the reflection factor R_1 can be calculated by a simple approximative formula, which is independent of R_0 and of all ultrasonic losses:

$$R = \sqrt{\frac{1}{1 + H^2(1,0,0)/H(0,1,0)\,H(1,0,1)}}$$

Until now it was not known what corrections to this formula are necessary, when specimens with curved surfaces are tested.

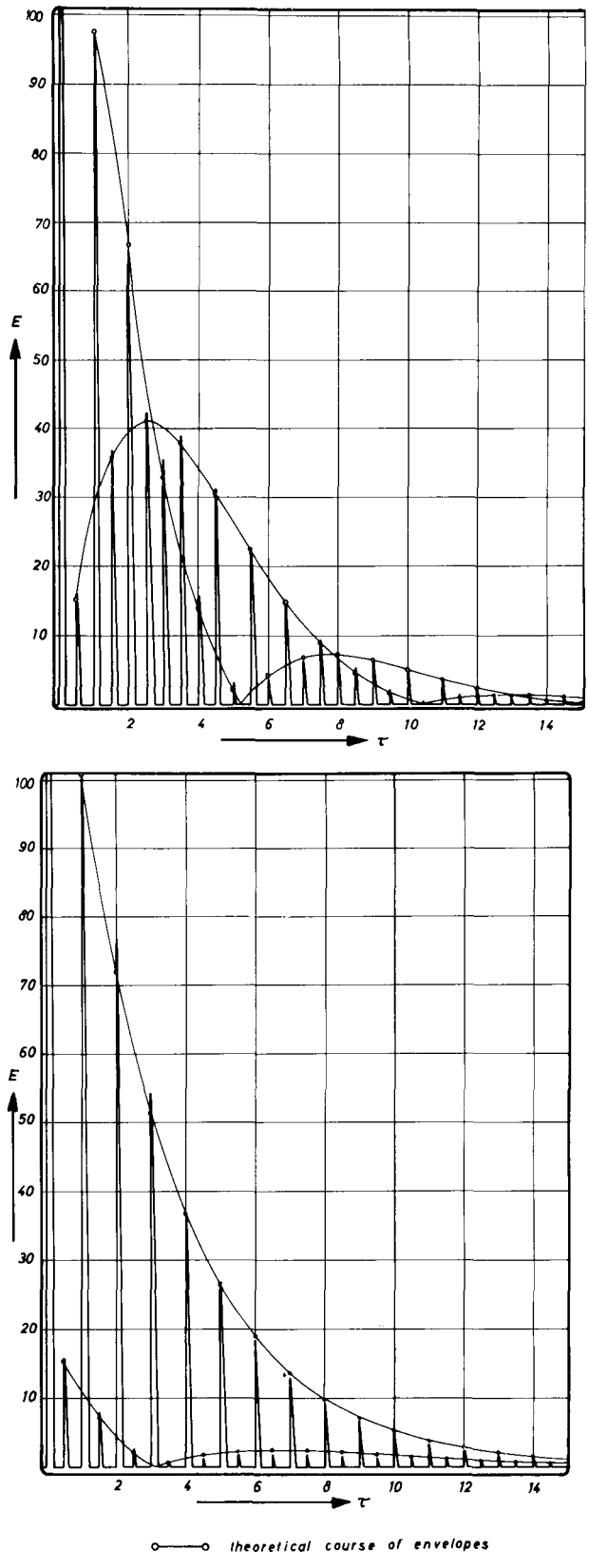

Figure 4. Measurements and calculations of reflectograms for the two extreme cases of interference echoes.

Testing of Plates, Billets and other Semiproducts

Sometimes semiproducts, e.g. steel plates, contain many very small inclusions in a netlike distribution. The sum of these in-

clusions behaves like a semipermeable interface or layer with a relatively small reflection factor, producing a sequence of flaw echoes with a maximum in its envelope at a rather long distance from the initial pulse. Such groupings of inclusions can be very harmful to the subsequent treatment or to the purpose for which the semi-products are needed. In order to trace such layers ultrasonically it is necessary to look at a long sequence of multiple echoes, because the first flaw echo often is too small to be noticed clearly. It is assumed that there exists an interrelation between the reflection factor of such zones and the quality of the semiproducts. Therefore the quality can be rated by application of the theory. Two examples of steel plates 10 mm thick are given in Figure 5. Since the distance between initial pulse and maximum in the envelope of flaw echo sequence in Figure 5a is larger than that in Figure 5b, the quality of the steel plate in the case of Figure 5a is better than that of Figure 5b. A rough evaluation leads to reflection factors of $R_1 \approx 0.06$ for Figure 5a and $R_1 \approx 0.1$ for 5b.

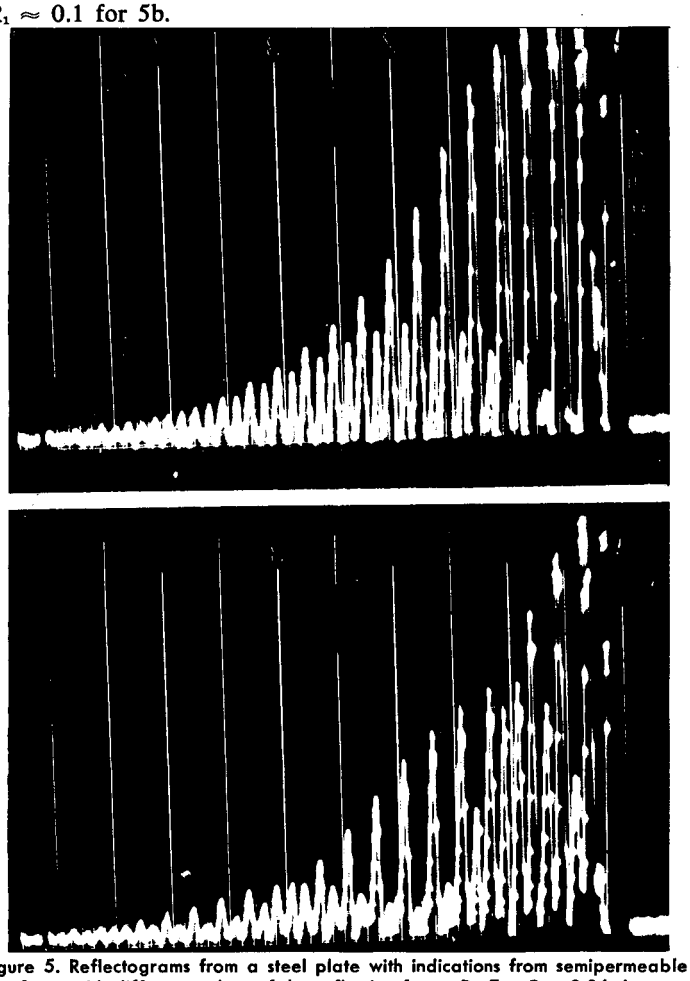

Figure 5. Reflectograms from a steel plate with indications from semipermeable interfaces with different values of the reflection factor R_1. Top $R_1 \approx 0.06$; bottom, $R_1 \approx 0.1$.

Since such areas of small inclusions rather often are an accompanying phenomenon of segregations, it seems possible to find segregation zones and to judge their influence on the quality of a semiproduct.

Judgment of Echoes from Single Defects

When the size of a defect is determined from the amplitude of its flaw echo, usually total reflection at the defect is assumed (15–22). Therefore the result must be wrong, when the defect is only partially reflecting. But perhaps additional information is available by observing the multiple echoes. When a defect lies in the far field of the ultrasonic probe, it can be decided with certainty whether the cause of a little flaw echo is either a small, totally reflecting defect or a large semipermeable interface. A semipermeable zone can probably be identified when it is smaller than the cross-section of the sound field. In order to clarify within what limitations this is a practical possibility, additional experimental and theoretical work must be done.

Measurement of Phase Shift with Direct Probe-to-Specimen Contact

If a normal probe is coupled directly to the specimen, each reflection of multiple echoes at the coupling area is connected with a phase shift $\varphi \neq \pi$ (23-25). This is important e.g. for accurate measurements of ultrasonic velocity using an interferometric method, since an unknown phase shift $\varphi \neq \pi$ causes an unknown systematic error. The phase shift φ and its dependence on surface conditions, probe type, pressure of coupling etc. can be measured, if a model of a specimen is used similar to that described in section 3. One case of extreme amplitudes of interference echoes (see section 2) must be produced two times, at first using an immersion technique and then direct probe-to-specimen contact, all other conditions remaining constant. The difference of pulse transition time in the variable section of the specimen between these two cases is a direct measure of the phase shift φ (6).

Testing of Spot Welds in Thick Plates

If the thickness of spot-welded plates is large enough or if the ultrasonic pulses are short enough, so that multiple intermediate and bottom echoes can be separated completely from one another, the spot welds can be tested with the usual pulse echo technique and with a simple normal probe. Experiments with spot welds of 24 mm dia in steel plates of 10 mm thickness have shown that not only defects inside the nugget are easily detectable, but that areas of incomplete welding can be identified too, if the multiple echoes are observed within a range of about 10 bottom echoes. These areas of incomplete welding, which surround the nugget, if this is too small, and which shall be called "ringzones", behave like semipermeable interfaces (26). The reflectogram in Figure 1b is an example for a ring zone indication. By application of the theory the reflection factor R_1 of the ringzones was rated. In many cases it was found that it lies within the range of $R_1 \leq 0.2$, and even $R_1 \leq 0.1$ was not infrequent. With these rather small values of R_1 the well known difficulties in testing spot welds ultrasonically can be explained easily.

With the assumption that there is an interrelation between largeness and reflection factor of a ringzone on the one hand, and their influence on the shear strength of the spot weld on the other hand, an attempt is made to define an "ultrasonic quality number"

$$K = c\, R_1^2 \frac{Z_{max}}{E} \qquad (11)$$

R_1 is the reflection factor; $R_1 = 1.0$ is valid for defects inside the nugget; Z_{max} the amplitude of the highest intermediate echo and E that of the following bottom echo. c is a constant, which was chosen as $c = 1$ for ringzone indications and as $c = 0.1$ for indications of defects inside the nugget. Thus it was considered that the influence of those defects on the shear strength is rather small. According to this definition one expects that the shear strength of a spot weld is the better, the smaller K is.

In Figure 6 the maximum shear force S, measured in shear tests, is plotted against the quality number K. The expected tendency can be seen clearly.

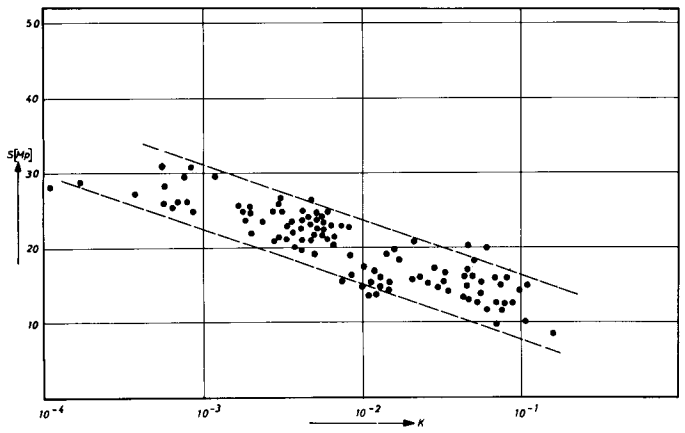

Figure 6. Interrelation between shear force S and ultrasonic quality number K of spot welds.

Conclusion

All applications of the theory are based upon the fact that a sequence of multiple intermediate or bottom echoes often contains additional information, which cannot be obtained from the first intermediate and bottom echo only. In order to get a clear idea of the real advantages of the applications of this theory to practical problems of nondestructive testing, further theoretical and mainly experimental investigations must be carried out.

References

1. Grabendörfer, W. and Krautkramer, J. Über Impuls-Echo-Prüfung an plattenförmigen Körpern; *Z. Metallkunde* 49 (1958); 1; p. 22/26.
2. Mundry, E. Über das Verhalten teildurchlässiger Zwischenflächen bei der zerstörungsfreien Materialprüfung mit Ultraschall, Teil I: Theorie; *Materialprüfung* 8 (1966); No. 12.
3. Roderick, R. L. and Truell, R. The measurement of ultrasonic attenuation in solids by the pulse techniques and some results in steel; *J. Appl. Phys.* 23 (1952); 2; p. 267/79.
4. Schaafs, W. Molekularakustik; Springer-Verlag (1963); p. 404.
5. Seki, H., Granato, A. and Truell, R. Diffraction effects in the ultrasonic field of a piston source and their importance in the accurate measurement of attenuation; *J. Acoust. Soc. Am.* 28 (1956); 2; p. 230/38.
6. Mundry, E. Über das Verhalten teildurchlässiger Zwischenflächen bei der zerstörungsfreien Materialprüfung mit Ultraschall, Teil II: Modellversuche und Anwendungsmöglichkeiten; *Materialprüfung* 9 (1967); to be expected in No. 4.
7. Hetzler, M. and Michalski, A. Ultraschallprüfung von Preßpassungen; *Werkstattstechnik u. Maschinenbau* 43 (1953); 7; p. 321/25.
8. ————Ultraschall-Schrumpfsitzprüfung von Blockaufnehmern für Strangpressen; *Z. Metallkunde* 46 (1955); 1; p. 6/11.
9. Krächter, H. Versuche zur zerstörungsfreien Prüfung von hartgelöteten Stumpfstößen an Kupfer; *Materialprüfung* 3(1961); 8; p. 297/99.
10. Deutsch, H. Erweiterte Anwendungsmöglichkeiten des Ultraschall-Verfahrens durch die Tauchtechnik; Mitteilungsblatt d. Niedersächs; *Materialprüfungsamtes* (1961); 1; p. 21/24.
11. Peters, B. F. An ultrasonic method for evaluating bonds in large metallic bearings; *Materials Evaluation* 22 (1964); 6; p. 257/59.
12. Jahn, P. Ultraschallprüfung von Lötverbindungen an hartmetallbestückten Werkzeugen; *Schweißtechnik* 15 (1965); 3; p. 115/17.
13. Richter, H. V., Linke, D. and Jahn, P. Zur ultraakustischen Prüfung von Verbundmetallen; *Maschinenbautechnik* 14 (1965); 4; p. 169/76.
14. Matting, A. and Heidemann, A. Entwicklung eines Gerätes zur zerstörungsfreien Prüfung von Lagerschalen mit Ultraschall; *Materialprüfung* 8 (1966); 5; p. 175/80.
15. Krautkramer, J. Fehlergrößenermittlung mit Ultraschall; *Arch. Eisenhüttenwes.* 30 (1959); 11; p. 693/703.
16. Byrne, B. R. Détection ultrasonore des défauts. Étude générale des facteurs affectant la signification des résultats obtenus par sondage avec echo; *Rev. Mét. Mém. Scient.* 56 (1959); 2; p. 231/56.
17. Claydon, D. G. W. Defect assessment using ultrasonic waves; *Progr. in Non-Destructive Testing,* 2 (1960); p. 165/87.
18. Rumsey, J. C. V. Interpretation of ultrasonic echo amplitude; *Brit. J. Appl. Phys.* 12 (1961); 1; p. 25/29.
19. Opel, P. and Ivens, G. Fehlergrößenermittlung mit Ultraschall an Schmiedestücken; *Arch. Eisenhüttenwes.* 33 (1962); 5; p. 311/16.
20. Knorr, W. and Ricken, H. G. Untersuchungen zur Messung der Schallschwächung und Ermittlung der Fehlergröße mit Ultraschall; *Arch. Eisenhüttenwes.* 33 (1962); 5; p. 317/26.
21. Kimura, K. Y. Approximate calculation of flaw echo height in ultrasonic pulse echo method; *Trans. Nat. Res. Inst. Metals, Japan* 4 (1962); 2; p. 104/10.
22. Zottmann, W. Beitrag zur Fehlergrößenermittlung beim Ultraschall-Impuls-Echo-Verfahren; *Arch. Eisenhüttenwes.* 35 (1964); 4; p. 353/58.
23. Krautkramer, J. Die Messung der Ultraschall-Schwächung nach dem Echolot-Verfahren; *Gießerei, Techn.-Wiss.,* Beih. 45 (1958); 20; p. 1067/75.
24. Schmauch, H. and Bentz, W. Ein kombiniertes Zeit-und Phasendemodulationsverfahren zur Messung von Schallgeschwindigkeiten mit handelsüblichen Ultraschallimpulsgeräten; *Z. f. angew. Phys.* 6 (1954); 4; p. 168/71.
25. Krautkramer, J. and Krautkramer, H. Werkstoffprüfung mit Ultraschall; Springer-Verlag (1961); p. 264.
26. Mundry, E. Untersuchungen über die zerstörungsfreie Prüfung von Punktschweißungen in dicken Blechen mit Ultraschall; *Schweißen und Schneiden* 19(1967); to be expected in No. 4.

Discussion

Q. MATTHEW J. GOLIS, Ohio State University, Columbus, USA:

In the simplified case of no reflection within a plate, do you feel that the distribution viewed on a U.T. screen can be used as a rough estimate of the extent of the field? Assume the plate has an air backing.

A. Taking into account the presumptions made for simplifying the theoretical treatment of the problem—first of all plane longitudinal waves of normal incidence [2]*—the theory cannot give any information about sound pressure distribution, near field length, beam spread, or other characteristics of the sound field of a normal probe, because all influences of this sound field are eliminated intentionally.

No reflection within the plate ($R_1=0$) means that no semipermeable interface exists; air backing of the plate means total reflection at the back face, $R_2=1$. In this case we have no intermediate echoes and only a normal, monotonously decreasing sequence of bottom echoes. Their amplitudes are

$$H(M,O,O) = C.P_0.R_0^{M-1}$$

That follows from a simple consideration about plane-wave echoes from a plane parallel specimen or from an application of lim $R_1 \to 0$ to equ. (7), which should be written for this purpose in the form of

$$H(M,N,Q) = C \cdot P_0 \cdot R_0^{M+N-1} \cdot R_2^{M+Q} .$$

$$\cdot \sum_{\mu=0}^{M-1} \left[\left(\frac{M+N}{N+\mu} \right) \left(\frac{M-1+Q}{Q+\mu} \right) R_1^{N+Q+2\mu} (1 - R_1^2)^{M-\mu} (-1)^{\mu} \right]$$

With $R_2 = 1$, $N = Q = 0$ we get for the bottom echoes

$$H(M,O,O) = C \cdot P_0 \cdot R_0^{M-1} \left\{ \left(\frac{M}{0} \right) \left(\frac{M-1}{0} \right) R_1^0 (1 - R_1^2)^M + \right.$$

$$\left. + \sum_{\mu=1}^{M-1} \left[\left(\frac{M}{\mu} \right) \left(\frac{M-1}{\mu} \right) R_1^{2\mu} (1 - R^2_1)^{M-\mu} (-1)^{\mu} \right] \right\}$$

and

$$\lim R_1 \to 0 \; H(M,O,O) = C \cdot P_0 \cdot R_0^{M-1} \{1 + O\} = C \cdot P_0 \cdot R_0^{M-1}.$$

If theoretical and experimental results are to be compared, geometric losses and other facts must be considered. This has been done in [6]* by using results from Seki, Granato and Truell [5]* and other authors, see also paper No. 2/6.

In the real case of a plane parallel plate without reflecting interfaces, small transverse wave echoes are sometimes observable between the bottom echoes [1]*. Most of them are built by several "single-pulses", similarly to the composition of an echo from a semipermeable interface. It is still unknown whether these transverse wave echoes can give information about the sound field, because their amplitudes have not yet been calculated theoretically.

Q. W. A. DUKES, Explosives Research & Development, Essex, England:

Would Dr. Mundry please comment on the possible ultimate applicability of his analysis to the examination of organic-adhesive joints between metallic adherends, and particularly multi-laminar joints?

A. An application of the theory in its present form to such test problems seems to be not very useful. The following circumstances must be considered:

1) As mentioned in the paper, the interpretation of the reflectograms is the easier, the smaller the reflection factor R_1 of the interface, see the two examples in Figure 5, with $R_1 \approx 0{,}1$ and $R_1 \approx 0{,}06$. Though we did not yet measure the reflection factor of adhesive joints precisely, according to some rough experiments with one adhesive joint between two thick metallic adherents (see 3) we can assume that the value of R_1 is rather high, e.g. within the range $R_1 > 0.8$. In this case, and with the preliminary assumption of only one adhesive layer inside the specimen, it seems much more useful to observe the simple sequence of multiple echoes

$$H(O,N,O) = C \cdot P_0 \cdot R_0^{N-1} \cdot R_1^N \quad (N = 1,2,3, \ldots .)$$

from the front side of the organic layer than to take bottom echoes H (M,O,O) from the specimen or intermediate echoes H (M,O,Q) from the back side of the layer into account, because the decrease of the sequence H (O,N,O) depends clearly on R_1 and therefore gives an easily readable quality indication.

2) The metallic adherends must be at least so thick or the pulse duration so small, that the echo indications on the screen do not overlap each other, and the pulse deformation due to frequency depending interference phenomena by passing through the thin organic layer must be negligible. Otherwise the theory must be extended from monochromatic processes to the whole Fourier spectro of the pulses.
3) The ultrasonic absorption inside the organic layer must be negligibly small.
4) A generalization of the theory to multi-laminar joints is possible indeed and outlined in [2]*, but will become rather complicated.
5) Before the analysis can be applied to such complex problems as the examination of multi-laminar adhesive joints, first of all it should be proven by simple experiments on simple test specimens, whether the reflection factor of an organic adhesive layer can be correlated clearly enough to the mechanical strength of the joint.

To give a complete answer to the question, additional investigations considering reflection and adsorption behaviour of the organic layer, influences of thicknesses of organic layers and metallic adherends etc. would be necessary. But at present such investigations would be of more academic and perhaps of little or no practical value.

* References on p. 440.

* Reference on p. 440.

Evaluation of Small Discontinuities in Non-Metals with Microwaves

DAVID W. PRINE, USA

ABSTRACT: Microwaves provide an excellent tool for nondestructive testing of non-metals. We are capable of detecting very small discontinuities by any of several microwave techniques. However, when it becomes necessary to evaluate these discontinuities as to size, shape or depth within the sample, many problems are encountered.

By using a microwave impedance plotter which automatically displays a polar plot of the phase and amplitude of the reflected microwave signal, we have found answers to some of the questions that arise when one attempts defect evaluation.

The Impedance Plotter

The detection of small discontinuities by microwaves in non-metals has been accomplished by a variety of means at wavelengths as long as 5 cm. The greatest sensitivity has been achieved with instruments of the interferometer type. The interferometer, or bridge, is a very sensitive device and under the right conditions very small discontinuities may be detected. If detection is all that is necessary, the interferometer is quite sufficient for most applications. However, if evaluation of various discontinuities is required, this task can become very difficult, if not impossible.

The output signal from a bridge is a complex function of the amplitude and phase changes in the reflected signal. Amplitude and phase are in turn complex functions of the many variables present in a particular application. In an attempt to gain a better understanding of the effects of these many variables and to clarify some of the seemingly contradictory results obtained in interferometry, we constructed a device known to microwave engineers as an impedance plotter. This device, or similar ones, is described in a number of microwave measurement texts (i.e., Measurement at Centimeter Wavelengths by D. D. King, Boston Technical Publications, Inc., 1965).

The impedance plotter used was chosen mainly for its simplicity of construction. Referring to Figure 1 it consists of four capacitive probes and associated detectors, placed along the axis of a transmission line, with $\frac{1}{8}$-wavelength spacing between probes. The probe samples the standing wave pattern

on the line and, if alternate probes are connected to the input of two differential amplifiers, the amplifier outputs have the form—

$$V_1 - V_2 = \rho \cos 2\psi \tag{1}$$

$$V_3 - V_4 = \rho \sin 2\psi \tag{2}$$

where V_1, V_2, V_3, V_4 = outputs from detectors

ρ = magnitude of voltage reflection coefficient

2ψ = phase angle of voltage reflection coefficient

The voltage reflection coefficient is defined as the ratio of the reflected wave voltage (travelling towards the generator) to the incident wave voltage (wave travelling towards load) at a particular reference point on a transmission line. This ratio is a complex number and, hence, has both amplitude and phase. For a loss-less transmission line—

$$\rho = \frac{\frac{Z_r}{Z_o} - 1}{\frac{Z_r}{Z_o} + 1} \tag{3}$$

where Z_r = terminating impedance, and

Z_o = characteristic impedance of line.

Thus we see that ρ contains all the available information about the termination of a transmission line. Furthermore, since we may make the incident wave constant, ρ is a measure of the amplitude and phase of the reflected wave. If the signals represented by Eqs. (1) and (2) are connected to the x and y deflection plates of a cathode ray oscilloscope, we will have a polar plot of the phase and amplitude of the reflected wave displayed on the scope.

We are presently using this device to study, in detail, the complex process by which one detects small discontinuities in non-metals with microwaves. We are using the impedance plotter to perform a series of carefully controlled idealized experiments in the hope that we can gain from this a better understanding of the interactions between the many complex processes involved in defect detection. We also hope to increase the value and usefulness of microwaves as an NDT tool by giving us some ability to evaluate and sort defects with microwaves.

Spherical Defect in Infinite Sample

The first case is that of the perfectly reflecting spherical defect in an infinite loss-less sample. This is the simplest case and as such will serve by defining a set of absolute theoretical limits on more practical cases. We first consider the amplitude and phase of a reflected signal for a constant defect size as functions of antenna aperture and position of defect. The defect is a 5/16-in.-dia metallic sphere, supported by a non-reflecting jig mounted on an x-y-z mechanical manipulator in front of the antenna being used.

A slide screw tuner is used to cancel out the residual reflection from the antenna. Microwave absorber panels are positioned to cancel out any stray reflections. In Figure 2 we see a plot of the amplitude and phase of ρ for a defect as it is positioned on the axis of the antenna and moved from the face of the horn to some arbitrary distance. The phase and amplitude change continually with position, which produces a spiral. Zero distance corresponds to the maximum amplitude point on the spiral. Figure 2 was taken for a small rectangular horn antenna. We may readily observe the effect of varying the size of the antenna aperture by making a series of such plots for

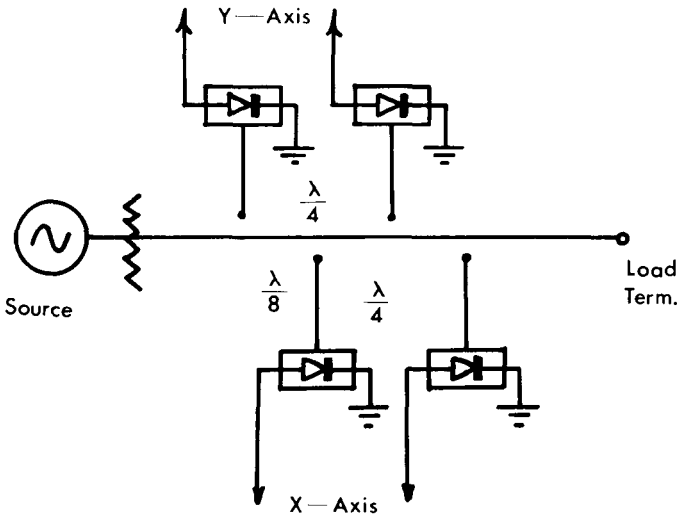

Figure 1. Showing schematic diagram of microwave impedance plotter.

various apertures. The variation of amplitude with distance for three cases is summarized by the curves shown in Figure 3. Here we see that, although the initial signal is largest for the smallest aperture, its high decay rate soon makes the signal smaller than that of the next largest aperture. The largest aperture displays a peak in amplitude at some distance from the horn due to Fresnel diffraction effects. Hence, for a particular distance range, an optimum aperture exists.

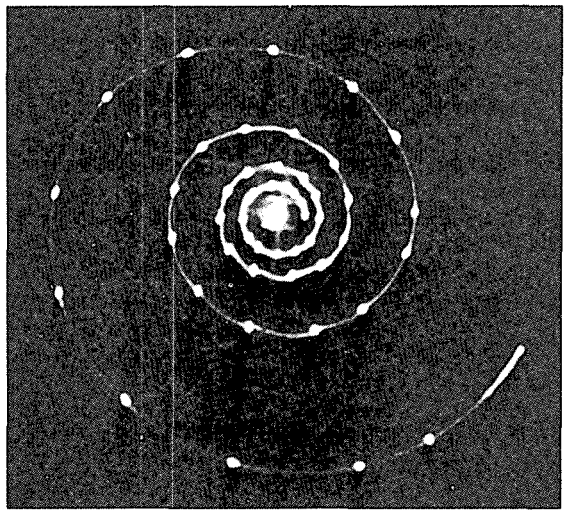

Figure 2. Showing ρ locus for $\frac{5}{16}$-in. steel sphere moved along the axis of the antenna from the antenna face to some arbitrary distance.

We should also point out here the significance of the phase data. Phase angle changes constantly with position and goes through 360° for each half wavelength distance from the antenna. Hence, we can easily determine the position of our defect by measuring its phase difference from our zero reference and multiplying this by the appropriate propagation constant for our medium. Some errors will result for distance very close to the aperture (i.e., a small fraction of a wavelength) due to diffraction effects. However, these errors are quite small. The repetitive nature of the phase angle introduces no ambiguity for the case discussed above because, along with phase, amplitude also changes, and hence we have successive turns of a spiral for each half wavelength distance. Hence, for

a particular defect and an infinite sample there is a single combination of phase and amplitude of reflected signal for any position, assuming that we also keep the antenna constant for our tests.

Fresnel Zone Plate

The antennas discussed in the previous section are all fairly small aperture horn-type antennas. We have seen how the aperture size determines an optimum range of inspection. The largest aperture used was about 32 sq. cm. in area. Its useful range extended out to approximately 15 cm. We decided to explore the possibility of other antennas, with the hope of extending the range of inspection.

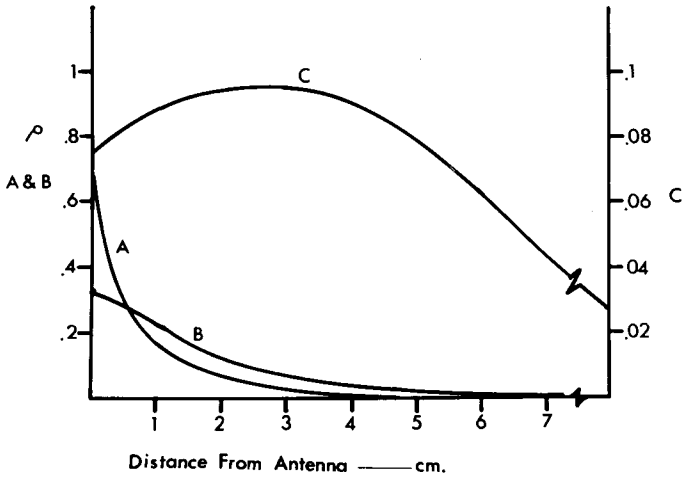

Figure 3. Showing graph of amplitude of ρ vs. distance for several small horn antennas.

To confine or focus the microwave beam at a distance of the order of a meter or so from the antenna it was felt that some form of microwave lens would be quite useful. Because of the rather large wavelength of microwave energy as compared to visible light a lens to be of any use at microwave frequencies is quite large. The cost of the materials and the machining problems involved on a dielectric lens prohibited the use of such a device for this experiment. We decided instead to construct a Fresnel zone plate. The Fresnel zone plate consists of a series of circular concentric rings of equal area. If we allow only alternate rings to transmit energy at some particular wavelength we find that at some point on the opposite side and on the axis of the zone plate the energies from all of the alternate transmitting zones add up in phase. This produces the effect of a focussed spot and, hence, the zone plate has many of the same properties as an ordinary lens.

A Fresnel zone plate with a focal length of 50 cm at a frequency of approximately 10.5 gigahertz was designed. This lens is approximately one metre in diameter which, for this focal length and at this frequency, allowed us to have 16 zones. The lens was constructed in the following manner. The zones were drawn on a good quality of drafting paper, then alternate zones were painted with a silver conductive paint. The lens was mounted on a rigid frame and is shown in Figure 4. With the lens placed at approximately twice the focal length from a small horn which approximated reasonably well a point source of microwave energy, the energy was concentrated in a focal zone at twice the focal length of the lens on the opposite side of the lens. Field plots of this focussed spot showed the focal zone to be in the shape of a right circular cylinder with tapered ends; this axis of the cylinder being the axis of the lens and the surface of the cylinder containing those points where the electric field

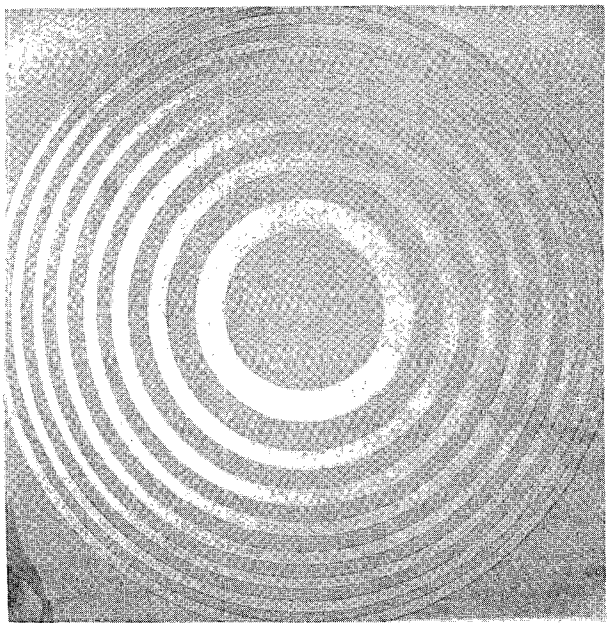

Figure 4. Showing experimental 10.5 gHz Fresnel zone plate.

intensity is half its value on the axis. The midpoint of the cylinder's axis was at the 2f point for our lens. The signals obtained on our impedance plotter by scanning our spherical defect through this focal zone with the Fresnel zone plate was comparable to the signal received from the same defect approximately 10 cm from the largest horn used in the previous measurements.

Size of Defect

All the previous experiments were for constant defect size; we now explore the effects of varying the size of the defect. Backscattering of electromagnetic energy by conductive spheres is discussed in a number of texts. This is one of the few geometries that submits readily to rigorous theoretical analysis. We find that the backscattered power is proportional to a fictitious cross-sectional area known as the scattering cross-section. If the wavelength is very small with respect to the radius of the sphere, the scattering cross-section is equal to the geometric cross-section. Hence, the backscattered power is proportional to the square of the sphere's radius. If we now allow the radius of the sphere to decrease we find that the above relationship holds true until we reach a region where the sphere's radius is comparable to the wavelength. Now the effects of certain natural resonant modes for the surface currents induced in this sphere become evident and our scattering cross-section oscillates in ever-increasing amounts about the geometric cross-section. If we allow our radius to decrease further, eventually we reach a point where the radius of our sphere is small compared to a wavelength and now the oscillations cease and the scattering cross-section decreases rapidly, as the square of the geometric cross-section or the fourth power of the radius. These regions are clearly shown in Figure 5. Here we see the scattering cross-section normalized to the geometric cross-section, plotted as a function of radius normalized to wavelength for metallic spheres. The three regions previously discussed are known as the optical ($a>\gamma$), resonance ($a\approx\gamma$) and Rayleigh ($a<\gamma$) regions where a is the sphere's radius and γ is the wavelength of the electromagnetic radiation. In the microwave portion of the electromagnetic spectrum and for most NDT applications our wavelength and defect dimension are such that we are either in the lower portion of the resonance region or in the Rayleigh region.

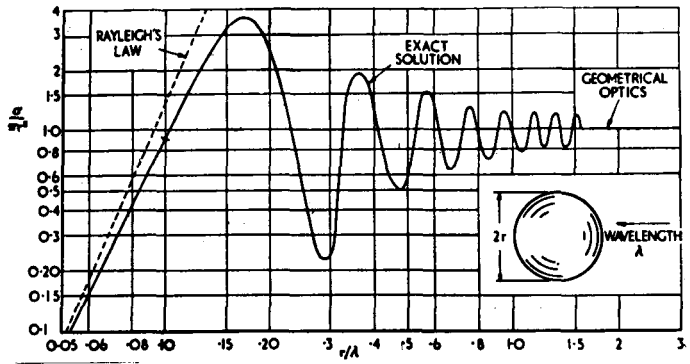

Figure 5. Showing electromagnetic backscattering for metallic sphere (normalized).

To make the above data more representative of what can physically be observed, we need to replot our curve in the unnormalized form. We shall choose a specific wavelength, our particular wavelength of operation 2.86 cm, and plot scattering cross-section vs radius of sphere. The results of this are shown in Figure 6. If we illuminate our sphere at a fixed distance from our horn at a wavelength of 2.86 cm and measure the amplitude of the reflected power, the values should lie on this curve. Since the amplitude from our impedance plotter is proportional to ρ which is proportional to reflected voltage, it will be necessary to square our readings from the plotter if they are to fall on this

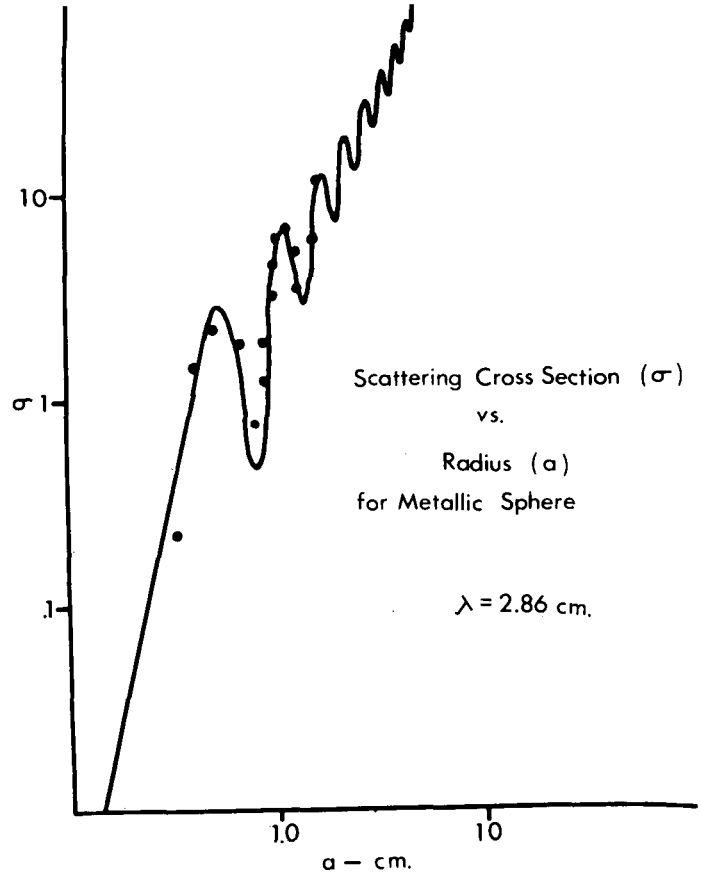

Figure 6. Showing electromagnetic backscattering at 10.5 gHz for metallic sphere.

curve. The points shown in Figure 6 are taken from our impedance plotter for a series of spheres of varying radii. There are certain approximations in the scattering cross-section calculations that produce negligible error as long as certain criteria are satisfied. These criteria are that the sphere be illuminated by plane waves and that the distance to the sphere be great enough to allow us to consider it a point source. For very small spheres these criteria are satisfied for very short distances from the horn, and hence the data in the Rayleigh region is accurate even for the small distances encountered in NDT applications.

However, at small distances a departure for large spheres becomes evident. Backscattering cross-section is a function of size, shape and material. However, the regions discussed above exist for all possible cases. The resonance region's upper limit depends greatly on shape and material, its lower limit is not so strongly affected. Therefore, it is possible to use a lower limit approximation for a wide variety of cases with a fair amount of success. This lower limit approximation depends mainly on radius or diameter of the defect at right angles to the direction of propagation of the wave. We may thus say that practically the lower limit of the resonance region is where

$$\frac{4\pi a}{\lambda} = 1 \tag{4}$$

where a = radius of defect
λ = wavelength of radiation

It is important to define this limit, because only below it can we correlate directly amplitude of signal and size of defect under any conditions, assuming that it is impractical to operate in the optical region. Within the resonance region at best we can only define a range of sizes for a given amplitude which may vary over 2:1 or greater.

Effect of Finite Sample Size

We have repeatedly pointed out that we are conducting our experiments on essentially infinite samples. When a sample has finite size, further complications due to internal reflections and refraction may enter into the problem, further complicating the picture. The subject of the effect of finite size of sample and geometry of sample on our ability to detect defects with microwaves is indeed a very complex subject and as such is beyond the scope of this paper. However, we would like to discuss one particular case which will show some of the problems that one may run into. In any flat planar sample of finite thickness microwave energy impinging on the front surface is partially reflected. That energy which is not reflected propagates through the sample and is partially reflected at the back surface of the sample. If we place a conductive plate at the back surface of our sample, this back surface reflection becomes total. As a result of this total back reflection we have two waves propagating in opposite directions within one sample. If scattering and dielectric losses are negligible, the resultant of this is a standing wave with well defined nulls occurring at intervals of half wavelength from our back-plate. The result of this standing-wave pattern is that our sensitivity to defects located at various positions from the metallic backing displays a space periodicity. In fact, if the defects are laminar in nature and oriented such that their plane is parallel to the surfaces of the sample, these defects will be undetected at points every half wavelength from the metallic back-plate. This particular effect has been observed in a number of actual applications wherein gross defects located at various distances within a sample were in some cases quite easily detected and in others not detectable at all. We simulated this condition also in a controlled experiment by placing small pieces of metallic foil on polyfoam supports on a metallic plate. The polyfoam supports did not affect the microwave beam. We located the metallic discs at quarter wavelength intervals from the back-plate. We then scanned the sample and found that those defects which were located at the half-wave points were not detectable at all, whereas those located at quarter-wave points stood out quite strongly. This effect, of course, will

not be quite as pronounced when the sample material is a fairly glossy material. Also, if the metallic back-plate is not present, the back-surface reflection is not as large and, hence, the nulls in the standing-wave pattern are not complete nulls.

Conclusions

The microwave impedance plotter has proven to be a very useful tool in our efforts to gain a better understanding of the complex process of defect detection and evaluation with microwaves. We have seen that the range of distance from the antenna over which we wish to inspect governs the size of the antenna aperture. The larger the aperture, the farther away the optimum inspection range.

If we wish to inspect over greater distances than a few centimetres, some form of microwave optics becomes necessary. The Fresnel zone plate provides a simple, economical solution to this problem.

We have shown that the phase of a microwave signal from a defect is directly related to its distance from the antenna.

Frequently in actual applications of microwaves to defect detection, a lack of correlation between defect size and amplitude of microwave signal has been observed. Two independent phenomena responsible for this lack of correlation have been observed with the aid of our impedance plotter. The first of these phenomena is inherent in electromagnetic scattering phenomena. This effect may be eliminated by choosing our frequency of operation such that the ratio of defect radius to wavelength is less than $\frac{1}{4}\pi$.

The second phenomenon that leads to a lack of correlation between signal amplitude and size of defect is due to finite sample size. We find that our defect sensitivity is space-periodic within a sample due to interference between internal reflections within the sample. In a sample this effect is greatly accented by the presence of a metallic back reflector.

Principal Session A/ Training and Qualification

Personnel Qualification for NDT in the U.S.A.

H. HOVLAND, USA

The human element in our manufacturing and fabrication processes constitutes a variable that is responsible in large measure for the need for quality control and, in turn, nondestructive testing. This variable is usually minimized as processes are automated but still exists since man must control the machine.

In nondestructive testing, the confidence level of the test is greatly affected by the human factor. For instance, the confidence level depends on:

1. Technical competence in selection of test methods; 2. technical competence of people performing the tests; 3. technical competence of people evaluating the tests; 4. technical capability of equipment and accessories used in the tests.

The recognition of the need for minimum competence levels of people performing nondestructive tests was shown by the U.S. Air Force Procurement Division in 1939 when they required laboratories performing radiographic and magnetic-particle testing to be approved by them before permitting them to test parts and assemblies used in aircraft. A group of test parts with known defects were supplied prospective laboratories to be tested. An Air Force representative witnessed the test and examined the equipment. Personnel and laboratories that passed the test were assigned stamps, and performance to their standards was periodically checked.

Likewise, the U.S. Navy Bureau of Ships used test blocks of various materials and thicknesses to qualify laboratories for performing tests on various materials.

The Nuclear Submarine Group of the Navy issued a document known as 250-1500 which prescribed a much more elaborate system of qualification for nondestructive testing personnel and laboratories permitted to work on Navy nuclear material.

Many organizations and laboratories have for years had their own training programs and have maintained careful surveillance on the qualification of personnel and equipment of subcontractors performing nondestructive test services for them.

The need for some recognized performance standards was becoming more and more apparent because of the increased use in industry of NDT brought about by the demand for assurance of product reliability, particularly in the areas of Aerospace and Atomic Energy requirements. A need also existed in the field of international business for a common ground for defining the level of nondestructive test performance. In addition, it was being suggested that the Military Quality Control Operations, in support of military procurement, which had established and supervised performance standards for some NDT operations such as magnetic-particle, penetrant, and to a degree, X-ray, was not planning to enlarge their program to include certification of other nondestructive testing operations, but rather was planning to place the responsibility for all operations on the contractor. This has, in fact, been done through several DOD and Military Specifications. They contain the wording which requires the contractor to assure that adequate process quality-control measures are established, including those for nondestructive tests and qualification of personnel. Hence, the Society had several requirements to fulfill in developing a Personnel Qualification Document. They are:

a. To meet government qualification of personnel requirements; b. to assure that personnel are sufficiently trained and experienced to perform critical inspection such as the requirements of the nuclear vessel section of the ASME Code; c. to provide management with subjective evidence relative to effectiveness of training and technical status of NDT employees; d. to provide a goal for continual study and upgrading of personnel in NDT.

The SNT program on personnel qualification received its formal start at the November, 1962 National Meeting of the Society for Nondestructive Testing, in New York City. At this meeting a panel discussion was organized by the Society's Technical Council for the purpose of reviewing the subject of qualification of NDT operations and to examine the various aspects of such a program. Canada had just embarked on a Certification Program for Industrial Radiographers. This had required some 5 years of intensive effort on their part and they had experienced many diverse ideas of educational and experience levels needed for levels of certification. We were fortunate in having as a panel discussor at the 1962 meeting, Mr. William Havercroft of the Canadian Department of Mines and Technical Surveys from Ottawa, Canada. The initial panel discussion at the 1962 SNT National Meeting reached four conclusions regarding operator qualification. These were:

a. That an immediate need existed for a document relating to qualification of NDT personnel; b. that the need was recognized by industry and government activities; c. that they were willing to cooperate in generating such a document; d. that the Society for Nondestructive Testing, acting through its Technical Council, was the agency to proceed with this program.

At this time the SNT Technical Council established a task force consisting of a chairman and six other members selected to represent a general cross-section of industrial users of NDT. The task force was expanded to include about 18 people of diverse backgrounds in industry, military and technical groups. All were well qualified in nondestructive testing. Two had an important part in the development and implementation of the NAVSHIPS 250-1500 program. Represented were materials producers and fabricators, aerospace and nuclear groups and general nondestructive testing laboratories. Naturally, there

were diverse opinions expressed as to the proper approach to the many facets of personnel qualification and certification. This task force has become a permanent division of the SNT Technical Council. Presently the division consists of approximately 30 members.

The task force proposed a four-phase program which included:

a. A document defining in simple terms the recommended levels or qualification requirements for NDT personnel; b. preparation of a training course outline for each method; c. preparation of an examination or test system whereby applicants could demonstrate their qualifications; d. recommending arrangements for the administration of NDT personnel certification.

A document covering the first step was prepared and discussed at an open membership meeting during the SNT Spring Convention in Los Angeles in March of 1963, and again in Atlantic City in June, 1963, where a published version, in the May-June, 1963 SNT Journal, was reviewed. Further revisions have been made since that time.

Essentially, the Personnel Qualification Document establishes three levels of qualification described as Levels I, II, and III. The scope of operation for each level as well as education and experience requirements are defined in the document. In general, an NDT Level I performs specific tests within an NDT method and under the direction of a Level II or Level III. A Level II, in addition to directing the activities of an NDT Level I, must be able to set up and calibrate equipment and be familiar with equipment capabilities and limitations. A Level II must be able to apply suitable inspection techniques, interpret indications, and evaluate them in terms of applicable codes and specifications. An NDT Level III must be capable of establishing techniques, interpreting specifications and codes, designating the particular test method and techniques to be used, and interpreting test results. He must be capable of evaluating results in terms of existing codes or specifications or assist in establishing test criteria when none exists. Each of these three main levels may be divided into more specific sub-levels.

Recommended training courses have been developed for each method. They list subject matter to be covered and recommend instruction periods in hours according to subject matter for Levels I and II. A list of recommended training references are provided for each method.

The third part of the program, the preparation of an examination or test system whereby applicants could demonstrate their qualification, has also been developed. The document describes three areas of knowledge on which applicants should be examined:

1. General knowledge of the NDT method; 2. specific knowledge relative to the specific type of work being done; 3. practical knowledge through actual performance on test specimens.

A grading system based on the three general test areas, giving weighted values for each area is described; also, the recommended minimum numbers of test questions in the different areas is given. Sets of the test questions have been gathered for the five major NDT methods: penetrant, magnetic-particle, X-ray, ultrasonic and eddy-current and described as Levels I, II or III.

Part four of the program, recommending arrangements for the administration of NDT personnel certification, is covered in the document by making it the responsibility of the employer of the NDT inspector to establish written procedures concerning all phases of certification and to maintain examination records for NDT Levels I and II. Level III may qualify by examination or by written verification of qualification by his employer.

The initial publication of the Personnel Qualification Documents consisting of Supplement "A", Radiography; "B", Magnetic-Particle Testing; "C", Ultrasonic Testing; "D", Penetrant Testing and "E", Eddy-Current Testing, were published in October, 1966. Appendices 1 and 2 for Supplements D and E, which are the general examination questions are not yet published. They should be available in late 1967.

It may be of interest to know that to date, approximately 1000 sets have gone out to industry, technical societies and private organizations. Many have been ordered by organizations and people in countries other than the United States.

The Personnel Qualification Division of the Technical Council—SNT—will continue to review the documents and make such additions, deletions or changes that enhance their use and the effectiveness of the documents.

Discussion

Q. JOHN A. DUTRA, San Francisco Bay Naval Shipyard, Vallejo, USA.

You indicated that the employer would assume responsibility for qualifying personnel at the various levels. This implies that each company has a qualified examiner to conduct the various examinations. What certainty do we have that the qualifier is qualified to examine within the guidelines set by the SNT?

A. An employer or organization that represents their facility as qualifying their NDT personnel under SNT-TC-1A must maintain a file with documentary evidence that reveals: SNT-TC-1A, Paragraph 7, Certification; sub-paragraph 7.6 states: "When requested the employer shall furnish a written statement verifying the qualification of any NDT Level III individual." It further states under subparagraph 7.7, "At the option of the employer an outside agency may be engaged to provide Level III services. In such instances the responsibility of certification must be retained by the employer utilizing outside services.

Q. R. D. BARER, Pacific Naval Laboratory, Victoria, Canada.

The American Level III is an intriguing one, particularly insofar as the qualifications are concerned. I think certifying of this level could present many problems. It seems to me that most people at this level have grown into the responsibility over years of detailed and then broader experience. Would Mr. Hovland care to amplify what the thinking is on establishing a qualifying procedure at this level?

A. The purpose of Personnel Qualification of NDT personnel is to provide a guide for training and examination of personnel performing nondestructive tests so that we might have a fairly uniform system by which to evaluate their capability to perform tests. Under SNT-TC-1A the functions of a Level III person therefore, are basically administrative. The documentation by the employer of the Level III person's experience and education should reveal to third parties his capability for the job. For instance, I know many welding engineers who are capable of directing welding operations, who perhaps could not qualify to make the weld they specify. If the buyers' examination of the Level III documentation by his employer fails to meet the standards of the buyer, the buyer still has the prerogative of making such examinations as he deems necessary and of accepting or rejecting the ability of the organization to perform the nondestructive test he requires.

Q. R. BEALE, DeHavilland Aircraft Co., Downsview, Canada.
Does the panel feel that the integrity of NDT operators is affected by their status within a company. For example, would unionized personnel have the same allegiance to their company and work as staff personnel?

A. Mr. Walter Offner of San Francisco raises substantially the same question so I would direct this reply to both.

Integrity cannot be written into a code or standard. However, the documentation of all facets of education, training examination and certification required by SNT-TC-1A will in my opinion reveal to a buyer or third party the degree of compliance with SNT-TC-1A. Where an organization's inspection group is under the production manager's direction, smart buyers look twice! Usually a Level III person in an organization is a staff person and as such has the responsibility for the technical quality and confidence level of the nondestructive testing operation whether or not they are performed by union personnel. I see no connection between union affiliation and integrity.

Q. WILLARD C. MINTON
In our work with industry, we repeatedly find people in management and elsewhere, who expect and even demand that there be a "Level 0" grade for personnel. In other words, a "probe pusher", "dial reader", or "powder duster", and that this man be certified in some way as "qualified". Comments, please.

A. The question you raise is perhaps one of the very reasons for development of the Personnel Qualification Document. Under this document the "probe pusher" or "powder duster" as you call them need not be qualified under any level but this person is not permitted to evaluate test results or to accept or reject material. This function is that of a level II or a level III person who must be qualified. The people you describe as Level "0" should remain at that level until such time by training, education and examination they can qualify for a grade in which industry can have confidence in their test operations.

Q. W. C. BORCHELT, Procter and Gamble Co., Ivorydale, USA.
What progress is being made towards acceptance of ultrasonic devices by the ASME Boiler Code Committee?

A. I understand that the ASME Code Committee on Section III, Nuclear Vessels have incorporated the requirement that personnel performing nondestructive tests shall be qualified in accordance with SNT-TC-1A. This will be in the new edition.

I know of no instances where the ASME code gives specific approval to ultrasonic devices. They do, however, specify reference plates for ultrasonic tests and reference the procedure to ASTM E-164-60T or E-114-55T.

Training and Certification of NDT Personnel in UK

B. R. BYRNE AND L. MULLINS, UK

Historical

With most new industrial techniques, consideration of training usually arises only when such techniques have proven successful. Meanwhile, newcomers pick up whatever knowledge they can from those already practicing the techniques. Training in nondestructive testing in Great Britain has mainly followed this pattern.

Fortunately for engineers, their earliest nondestructive test —oil and whitewash—was relatively simple, and easily learned. However, with the industrial use of radiography, dating from 1917 and the introduction of the magnetic-particle test about 1922, the question of specialized training soon became more pressing and more complex; the total number of people involved was, however, small. Even in 1939 there were fewer than twelve industrial radiographic installations in Great Britain and, with few exceptions newcomers learned the techniques only by working in established laboratories.

In 1939 an urgent need arose for systematic training because of the rapidly expanding application of nondestructive tests essential for the reliability of military equipment. Within a short period there was a heavy demand for radiographers to examine castings for aircraft, and welded joints in ships and other structures. As no training facilities existed at technical colleges, a commercial organization (Kodak Limited) set up a two-week course of about 75 teaching hours on the theory and practice of industrial radiography. At that time, in fact, there was no other attempt anywhere to provide training in any branch of nondestructive examination.

Even with the adoption of ultrasonic flaw detection by industry in the early 1940s and the appearance of eddy-current methods and new types of liquid penetrant a year or so later, there was still no comprehensive training course available on either basic principles or applications.

Towards the end of the decade a few technical colleges had planned evening courses on radiography (in 1947 the Northampton Polytechnic in London offered a two-year course), and for a few years the British Welding Research Association gave ultrasonics a prominent place in its Summer Schools. Sources such as these provided background knowledge but there was little chance for any student to undertake serious practical work. Even with the formation two years ago at the Institute of Welding in London of a school which specializes in applied nondestructive testing, the program of practical work undertaken is still only sufficient to give knowledgeable technicians some appreciation of the science (and the art), and to establish guidelines for its correct application. The same is true of two other training centres set up more recently. It is in the nature of the case very difficult in the time and with the funds commercially available to bring operators (still less technicians) in even one branch of NDT to a standard of competence, reliably certifiable by examination, which will enable prospective employers to regard them as fully trained. The Kodak School of Industrial and Engineering Radiography set up as a wartime measure is, however, still producing trainees whose theoretical and practical ability is reported on in detail, and is one of the very few places in which thorough practical grounding is to be had. Smaller schools set up by engineering concerns and by the Boards of some of the nationalized industries (1) for the benefit of their own employees (and those of their sub-contractors) also aim to produce dependable operators, though not in the field of radiography. The emphasis in these courses is on the practical aspects.

B. R. Byrne, Consultant in Nondestructive Testing, 99 Portsmouth Road, Guildford, Surrey, England.
L. Mullins, Kodak Limited, Harrow, Middlesex, England.

The Need

The type of training required depends on the responsibility and functions of the person concerned. The main classifications are as follows:—

1. The surveyor or inspector acting for the purchaser: 2. The person in the producing firm who is responsible for the quality of the work: 3. The person in charge of the nondestructive testing department: 4. In some instances, the senior assistants in the NDT laboratory. (These, where they exist, will be carrying authority delegated by the head of the department.) 5. The less skilled personnel who are engaged full-time on some specific application of NDT working largely under supervision. A few of these may succeed in qualifying for higher posts but most of them will be limited to their particular job, for which they need careful training.

These groupings merit further discussion.

1. The Purchaser's Surveyor

The surveyor or inspector will be independent of the producing firm. He will, in general, be extremely busy and will have to cover far more than the NDT aspects of the contract. Consequently, his knowledge of NDT will, of necessity, be restricted to those aspects which are relevant to his job. It is therefore important to give him instruction only in those parts of the subject which are essential to enable him to do his job properly. It is unfair, and unnecessary, to complicate his training beyond this. Such a statement, as might be expected, needs qualification. For instance, it is not enough to teach an inspector what the radiographic images of defects look like. He must know how the images are formed and he must know the importance of variations in the technique. As a guide he should be taught the background of the appropriate British or other national standards. He should certainly know enough about the subject to enable him to judge an operator's ability. Much of this background can be provided in the form of lectures, preferably illustrated; and such people are likely to gain most from the courses in applied NDT described below. Some supplementary coaching in the practical aspects will not only be of educational benefit but will also help to make the whole idea of further study more palatable.

2. The Producer's Chief Inspector

The duties of the man responsible for the quality of workmanship within the producing firm will be somewhat more specialized but he will need essentially the same kind of instruction. This should be supplemented by knowledge of the economics of NDT and of those aspects of the production cycle most favourable to its application. For instance, he may be able to arrange for inspection to be introduced at a more appropriate stage; or it may be possible for him to influence design during the early discussions on the contract so that NDT is simplified or even rendered unnecessary. He should be sufficiently well acquainted with NDT to be able to say when a method proposed by the purchaser is inappropriate or misleading and therefore useless. The acquisition of this kind of knowledge is to some extent a matter of experience but is also a feature of specialized coaching (some of which will come from his NDT assistant).

3. The Producer's Chief NDT Technologist

This man requires all the training he can be given, and it should be extended to associated subjects. However skilled in the art of NDT he will have very limited scope unless he is knowledgeable concerning the whole range of products covered by the producer's activities. This may be very extensive, covering both metallic and nonmetallic materials in a wide range of cross-sections. Again, without a solid foundation in physics and metallurgical engineering, he will be unable to talk on common ground with the foundryman, the welding engineer and forgemaster. In fact this man should be so well trained that he will inevitably be marked for promotion. In this way a most important aspect of NDT can be resolved, namely, the restricted scope and relatively low ceiling of the NDT technologist. Until such prospects of promotion, with better access to the "power structure" of the organization, become the recognized way up for NDT personnel, as it is for others, there is bound to be difficulty in recruiting, training and retaining the best men who, let it be said, do have to be technical and intellectual "all-rounders" if the firms employing them are to get the very best out of NDT.

4. The Senior Assistants

Naturally, the senior assistants of each division of the NDT department will need access to the same training facilities as their leader, since they occasionally have to assume major responsibilities for which they must be properly equipped, and are also in direct line of succession.

5. Rank and File Personnel

For the less skilled personnel some form of simple, specialized training should be the personal care of the head of the department, who should do all possible to ensure that junior laboratory assistants and operatives are properly schooled. They should not be left to "pick it up" from fellow workers who, even when themselves technically competent in the full sense, are not necessarily good teachers.

For the "older workers" (who, according to government surveys, comprise 50% of the labour force (1)) special teaching methods, such as programmed learning, deserve to be explored. Many such men find useful employment as assistant inspectors practicing some form of NDT in large firms where their technical attainments are of less importance than their steadiness and continuity of effort.

It must of course be remembered that among junior staff there will be some who, with encouragement and active assistance, will in due course benefit from the more advanced training planned primarily for the seniors.

The Training Facilities Available

Some comments have already been made on this subject in the opening paragraphs. The purpose of the present section is to supplement the earlier remarks.

Many technical colleges throughout the country are now providing short courses of, say, 10 to 12 lectures on all aspects of NDT, but very few have the equipment available to provide the necessary practical experience. Where they have, the time is too restricted to provide adequate practical training. Sometimes the courses have been started because of the demand from local industry. Otherwise they have arisen because of the enthusiasm of certain members of the college staffs, not all of whom had experience of NDT in industry. Fortunately some colleges have recruited local specialists in NDT to help in planning, and sometimes in running, the courses. Despite such limitations, these courses have made a worthwhile contribution to training and have in this way assisted in meeting the needs, but they are not the real answer to the problem.

A praiseworthy attempt to meet the needs of one branch of nondestructive testing was made about 9 years ago, when the City and Guilds of London Institute established a syllabus for a course in industrial radiography, occupying a total of 700 hours of instruction. Successful students are awarded a certificate

by the Institute. Unfortunately this course has not attracted many candidates, perhaps for reasons such as the following:—

1) the training demands a good basic knowledge of the sciences; 2) the course extends over a period of at least 3 years; 3) managements, in general, do not appear to have given the course much support; 4) local demands for training radiographers are very quickly satisfied and economic class sizes become impossible.

There have been attempts to change the syllabus to reduce the amount of associated knowledge necessary, but with no better success. Courses to the City and Guilds' industrial radiography syllabus were run by only a very few technical colleges. It is doubtful whether such courses are now available. The Institute is currently considering a comprehensive 4-year course to cover radiographic, electrical, ultrasonic and liquid penetrant methods. There seems, however, to be little assurance that its reception will necessarily be any warmer than that accorded to the industrial radiography course. The same uncertainty will attach to any courses planned by the British National Committee for Nondestructive Testing, which is also actively interested.

There is, therefore, still a need for well-run courses covering all methods of NDT and lasting, say, at least 12 months, with ample facilities for practical work; and to ensure maximum effect the instructors should have industrial experience in the methods they are teaching. This need for practical know-how constitutes the main reason why such courses are not available. The provision of equipment of sufficient variety and scope to justify running a course is very costly. A collection of suitable work-pieces is also required. These are not easy to obtain. The cost of preparing them (sketches, radiographs, macro-etched sections) is high. This would of itself not prevent some colleges making the necessary outlay but the number of students would. It is impossible to say how many students would come forward for training each year, but it is questionable whether this would at first exceed 100 throughout the whole country. Consequently, only about 5 training centres, at the most, would be justifiable and, to bring in the maximum student intake, these would obviously have to be centred on industrialized areas. This would almost inevitably lead to the necessity for some students to stay at colleges too far from their homes for daily commuting. One can only hope that the recently introduced Industrial Training Act will lead to a satisfactory solution to the problem.

Apart from the courses run by technical colleges, there are only three other training units in Great Britain open to all. These are named in chronological order of inception:—

(a) A four-week course (140 hours) in industrial radiography, run by Kodak Limited, (2) including extensive practical work, incorporating formal examination and assessment of the student. A two-week course for surveyors is also available; the main difference from the four-week course is that much less practical work is undertaken, and the emphasis in the lectures is upon those aspects of greatest importance to surveyors.

(b) Courses, predominantly of lectures, run for surveyors and others by the School of Applied Nondestructive Testing, which is organized jointly by the Institute of Welding and the Nondestructive Testing Society of Great Britain. Appreciation courses last 5 days and study courses 8 to 10 days.

(c) A four-week course in all NDT methods offered by Ilford Limited. This includes practical work but, here again, the brevity of the course means that it can provide only a basic knowledge of each method.

The situation outlined above is likely to be perpetuated until industry realizes that NDT worth doing is worth doing well, and that it can only be done well by using properly trained staff. Industry, in fact, owes it to itself to encourage the experienced teachers already in the field by giving support to the approved courses soon to be launched, and by taking a more constructive interest than hitherto in its intake of trainee personnel.

Details of the three courses named are given in the Appendices.

Qualifications in NDT

The City and Guilds of London Institute certificate in industrial radiography mentioned earlier is the only academic qualification currently available in Great Britain in any aspect of nondestructive testing.

The Nondestructive Testing Society of Great Britain offers its Associateship to those accepted by its Council as having the necessary experience and ability. So far, this qualification has been granted by the Society on the basis of evidence submitted by the candidate and his sponsors in relation to education, experience, ability and responsibility. For some time the Society has been trying to establish a qualifying examination, but this has met with many difficulties and no workable scheme has yet been found.

In the absence of any nationally accepted qualification, two important inspection authorities, namely the Aeronautical Inspection Directorate of the Ministry of Aviation, and Lloyd's Register of Shipping, have, for many years, had a system of approving inspectors for specific types of work coming under their survey. Although the principles of the two systems are very similar, minor differences of detail exist. Lloyd's Register of Shipping, for instance, expect firms applying for approval of their radiographers to send them to the 4-week course described under (a) above and to ensure that they take the examination at the end. The Register then takes into account the examination result, the practical ability and experience of the candidate, and the conditions under which he will be working, which must also be approved. Subject to the satisfaction of the Register, the radiographer becomes known as an "approved radiographer". This qualification is held by the radiographer only for so long as he remains with the firm for which he is approved and for so long as his work there continues to satisfy the Register. If the radiographer moves to another firm coming under Lloyd's Register survey, the firm must apply for his re-approval. Generally this is straightforward, but if the Register considers it necessary, they can ask for the radiographer to take a refresher course and to sit the examination again.

The A.I.D. system differs mainly in that the candidates need not take a prescribed course of training, and the theoretical and practical examination is organized by the A.I.D. on its own premises. Both organizations approve the operator for specified work only, e.g. pressure vessels in ferrous materials, welds in ships' structures, or light alloy castings for aircraft.

Selection of Personnel for Training

Since there are no courses leading to a professional qualification, a firm wishing to appoint a technician or an operator must either attract an industrially qualified man already in employment or select someone for training. As the training is likely to be costly both in time and money it is, on the whole, best to choose someone already in their own employ who has the basic educational qualifications. Preferably he should already be familiar with the technical background to the firm's activities, and be in turn sufficiently well-known to the management for practical assessment of his drive, his capacity and that elusive quality indispensable in NDT personnel—integrity.

For a technician a thoroughly sound background education is required, covering two or more of the disciplines involved in nondestructive testing, e.g. mathematics, physics, metallurgy

or electronics, plus a good knowledge of the use of the English language. (The art of writing a good report begins with this.)

For an operator the chief need is for competence and manipulative skill in the practice of one particular branch of NDT. Gaps in the formal education of the trainee (he may have had none to speak of since leaving school) must be filled with appropriate coaching in elementary mathematics, including simple equations, simple graphs, an introduction to the decimal system, and to logarithms together with practice in the preparation of simple reports.

Both types of trainee will require access to a selection of the technical books and journals which give space to the various aspects of NDT encountered in their industry. If they are sufficiently capable and enthusiastic, membership of one of the technical societies devoted to NDT will be open to them. The value of such cross-fertilization among others engaged on similar work is self-evident.

Conclusions

To those who are aware of the full scope and value of NDT as an aid to engineering reliability and who have its interests at heart, the present state and status of training facilities are discouraging. The courses presently offered are no more than leak-stopping operations. No improvement can be expected until industry as a whole is more enlightened, more conscious of the value of NDT as a science as well as a craft, and more readily disposed to pay the right kind of salary to the right kind of man.

Though the courses described in this paper have indeed been welcomed, their very success is actually regarded in some quarters as sufficient proof of the assertion that NDT technique is something that almost anybody can "pick up" and apply successfully with little prior training or formal education; an attitude which is reflected in the choice of school dropouts as new entrants to NDT inspectorates and in the manner of selecting personnel for attendance at courses which are in fact sometimes beyond their scope.

There is also a general failure to realize that the future development of NDT, like its progress to date, can only be the product of cultivated minds and skills, the supply of which calls for organization and should no longer be left to the workings of chance.

Appendix

The Kodak School of Industrial and Engineering Radiography, Kodak Limited, Harrow, Middlesex.

The school was established in 1942 to help meet the ever-increasing wartime demand for industrial radiographers. As the requirement was to train personnel as quickly as possible, a lengthy and comprehensive course covering all aspects in detail was out of the question. It was equally clear that in a short course, lasting a few weeks at the most, it would be impossible to give adequate training in the specialized aspects of the subject. The prime problem was therefore to decide what could be omitted. A survey of the knowledge actually *used* by the average industrial radiographer revealed that a sound grasp of certain basic aspects of the subject would suffice to enable an intelligent technician to undertake straightforward radiography.

For example, some knowledge of the electrical circuits used was considered desirable to enable students to fully appreciate the differences in output and in operation between various types of X-ray equipment. It was not thought necessary that they should master such technicalities as latent-image theory, but it was clear that they should understand what happens during the processing of a film, so that they could appreciate the importance of following good practice and recognize the consequences of faulty technique.

Accordingly the syllabus and practical exercises were planned with these basic aspects in mind. The successful results of such intensive training proved that these concepts were right. Accordingly these same principles have been followed in devising all subsequent courses, which have been reviewed year by year to ensure that the training is in line with modern practice.

Regarding the current courses, the comments apply both to the four-week course and the two-week course mentioned earlier, but it should be noted that the time for practical work is much less in the latter course, which is primarily intended for surveyors and inspectors. (The need for a surveyor to be able to contribute to the rational interpretation of radiographs and to assess the efficacy of the techniques by which they are produced, is obviously of first importance.)

The syllabus is arranged around the basic requirements mentioned earlier, with sufficient supplementary theoretical work to enable the trainee to develop his knowledge and skills further by studying text-books, and technical papers and British standards on industrial radiography. Training in the practical aspects of the subject is given in the form of exercises arranged to supplement the information given in the lectures. To ensure that the maximum value can be derived from the practical work, the work-pieces chosen as specimens are selected from welds and castings containing defects. The identification of these defects provides exercise in the interpretation of radiographs, thus effectively relating the work to the problems to be encountered after training. The four-week course occupies a total of 140 training hours.

A major problem in running intensive courses of this kind is the very varied technical background training of those attending the course, but small classes of twelve and a high staff-student ratio (1 to 4) enables additional help in the way of private tuition to be given where necessary. Accordingly the school has never found it necessary to impose any qualifying entrance examination, as employers generally select personnel well able to benefit from the courses.

Students with a good knowledge of the basic sciences, with intermediate degree passes, and with National Certificates in metallurgy, engineering and allied subjects, have all done well. Experience has shown that those students who have studied mathematics, physics and chemistry for about two years or more at school have little or no difficulty in understanding the basic theory. The better the basic knowledge is in these subjects, the better the student gets on.

Although students with no such basic background have achieved a high standard, they were exceptional.

Experience in the routine practice of industrial radiography is also helpful, provided that the student is willing to reconsider and, if necessary, revise some of the methods he uses.

The School of Applied Nondestructive Testing

This is a joint venture prompted by the Institute of Welding and the Nondestructive Testing Society of Great Britain. Its courses are held at the Institute of Welding in South Kensington, London, and its organization is similar to that of the School of Welding Technology (now in its tenth year), in that the courses are aimed primarily at lower- and middle-management personnel, e.g. from newly appointed inspectors or "surveyors" and technicians to chief inspectors, plant- or production-controllers and works managers. A certain proportion of NDT specialists and other senior personnel in industry and in the universities also avail themselves of the facilities. The use of

the word "applied" in the title of the school derives from the fact that most of the instruction given concerns the application of technique rather than the theory or practice of method, and that the lecturers (most of whom are able to give their services free) are all experienced men who earn their living in various branches of nondestructive examination and are moreover in the forefront of their profession. Included among them are specialists from Germany and Holland.

The number of courses offered during each session (September to April) varies with the demand and with the estimated market. The full range covered to date is as follows:—

5-day Appreciation Courses

(a) NDT methods and techniques for engineers and inspectors (the basic course for which no previous knowledge of NDT is required);

(b) NDT applied to tubes and pipes (ferrous and nonferrous, welded and otherwise);

(c) NDT applied to plant maintenance;

(d) NDT of welded joints (special applications). This is an advanced course for NDT technicians, inspectors and designers. The coverage includes resistance welds, spot welds and nozzle welds in power generating plant.

Study Courses

(e) Interpretation of Radiographs (castings), (Engineers and Inspectors) ..... 8 days

(f) Interpretation of Radiographs (welds), (Engineers and Inspectors) ..... 8 days

(g) Practical Ultrasonic Weld Inspection, Basic theory and practice for Inspectors (Course approved by Lloyd's Register) ..... 10 days

In these study courses approximately two-thirds of the total teaching time is devoted to practical work.

With one exception, the aim throughout is not to teach the skills required for using equipment but to impart the kind of information that an engineer can *use* when assessing the quality of inspection or when taking decisions. For instance, the courses on radiographic interpretation include a simple account of the merits and demerits of various types of X- and gamma-ray equipment and a talk on film processing designed to help an inspector to recognize the difference between good practice and bad. Tutorial exercises in appreciation (using classified radiographs) are accompanied by talks on the pattern and scope of the inspection procedure which the inspector must follow in order to understand the radiographic image in the first place, before detailed interpretation can commence.

An exception in regard to operative skill is seen in course (g), "Practical Ultrasonic Weld Inspection". Of all the methods currently employed, ultrasonics is the one least understood by industry as a whole. This course lays down the correct guidelines to newcomers by presenting echo-sounding as a precise discipline. One lecture period is allotted to the metallurgy of the plate material in which welded joints will be made, and a review of specifications for the ultrasonic inspection of heavy steel plate.

A new lecture room has recently been designed around the intensive use of closed-circuit television, three television cameras with 23-inch monitors being used for every course to provide close-up views of the lecturers' sketches, illustrations and practical demonstrations. The room accommodates 24 students at a time on study courses (working in pairs with the necessary equipment) or twice that number on appreciation courses where equipment is demonstrated but not (generally) used.

Each course is planned afresh on the basis of past experience supplemented by workable suggestions put forward by students in their critique of the previous course.

Ilford Limited, Nondestructive Testing Centre, London

Assessment of the needs of industry for training facilities and advice in the use of the different methods led this Company to set up the Nondestructive Testing Centre in January 1964 at the London headquarters of the X-ray Division, Tavistock House North, Tavistock Square, London, W.C.1.

The aim of the Centre is to equip those engaged in NDT with the knowledge to implement a specific technique to satisfy an investigation or inspection requirement, whether it be applied to a circumferential weld on a pipe line, fatigue crack in an aircraft spar, or whatever material evaluation is necessary. Concentration is on the fundamentals of the NDT methods.

An intensive four-week course covering the theory and practice of radiography and ultrasonics with an appreciation of dye and fluorescent penetrants, magnetic particle and electrical (eddy-current) methods, is provided.

The program is in two sections: a) radiography; two and a half weeks; b) ultrasonic testing and appreciation of other methods; one and a half weeks.

General Training

The course follows a logical progression, specialist lecturers of national repute putting across the strict sequence of essential information so that all levels of students are accommodated.

The syllabus constitutes a framework within which there is a tutorial relationship between lecturers and students. This ensures that individual problems may be catered for. At no time during the four days' practical radiography and the ultrasonics practical are students permitted to become merely observers since adequate equipment is available for their use.

Acceptance of training in terms of the academic level of applicants was considered to be a problem but experience has shown this need not be so; a general engineering background provides a suitable foundation. The participants in the training benefit considerably from the cross-section of skills represented; metallurgists, inspectors at all levels, insurance engineer surveyors, technical assistants training as radiographers or ultrasonic operators, physicists—representation is international from a wide industrial front.

It is during the discussion and practical sessions that the inspection problems are presented for group analysis. This is feasible since apart from the tutorial staff many of the course members are experienced in NDT but are attending the course to revise prior to attempting approval examinations, or are radiographers training in ultrasonics, and vice versa.

The practical exercises are designed to highlight the parameters of control for each method. A technique sheet is compiled by the students for each task to be assessed as to layout, reference to line diagrams or photographs, standard terminology, the correct use of penetrameters or references and the economical use of resources.

If the technique is for X or gamma radiography, particularly for 'on site' inspection, compliance with the code of practice regarding protection of personnel is discussed.

Constant observation and implementation of worthwhile suggestions arising from the students' course critique ensure that the training does not become routine and is always abreast of modern practice.

References

(1) Byrne, B. R. Finding, training and organizing personnel for nondestructive testing. *Br. J. NDT*, v. 8, no. 4, Dec. 1966.

(2) Mullins, L. and Grimwade, E. J. The training of industrial radiographers. *The Quality Engr.*, v. 26, no. 1, Jan.-Feb. 1962.

Discussion

Q. C. CAMPKIN, Central Electricity Generating Board, S-W Region, Bristol, England:

In Great Britain changes are taking place in the field of technical education and training. The qualification by part-time means, in a person's own time, will not be adequate. The Nondestructive Testing Societies are working towards technical colleges and institutes providing the education and training to syllabi established by societies and educationalists.

The Society is also hoping to establish corporate membership of the Society as a recognized qualification. We recognize that examinations in technical competence are only one part. The degree of responsibility and personal character must also be assessed, which cannot always be done completely objectively.

A. Mr. Campkin's remarks are supplementary to the paper, but it remains to be seen how many technical colleges set up courses to the syllabus. The likely student intake will only rarely justify the very considerable expense of providing the essential; moreover there is the problem of getting staff with practical experience for day courses. It would be interesting to know how he proposes assessing the degree of responsibility and personal character.

Q. FRED BYWATER, Ontario Hydro, Toronto, Canada:

What measures are taken to ensure that NDT practices are kept up to date? Sources of research? (nationally, internationally, etc). Is there any pre-planning with quality control groups so that NDT can be placed in the production line to the best advantage in order to reduce or eliminate work etc. and for follow up? In other words, is NDT used as a preventative measure rather than a remedial one? Are the results fed back to design for future reference?

A. (Byrne and Mullins) Mr. Bywater's contribution raises many interesting questions but these are outside the scope of this paper, except to say that any training course should be continually brought up to date in line with current practice. For instance, every new British Standard on nondestructive testing should be brought to the attention of the student.

Q. COLIN C. BATES, Corrosion & Welding Engineering Ltd., Redhill, England:

Perhaps Mr. Heselwood might like to make further comment on the industrial training board set up in Britain, and the NDT training section of the same. He might make some reference on such courses as organized by the British Steel Castings Research Association.

A. (Byrne and Mullins) Regarding Mr. Bates' inquiry, the Industrial Training Boards are still very largely in their early stages. Two have already accepted an established course in industrial radiography run by a commercial organization, as qualifying for a supplementary grant to employers sending employees for the training. The Foundry Trade Training Board has set up a panel to work out a suitable training syllabus for nondestructive testing training in the industry but training to this syllabus is in its early stages and it would be premature to comment on how it is working out.

Education and Qualification of Personnel in Japan

Y. TADA, JAPAN

Education and Training

It is well recognized that the capabilities of nondestructive testing personnel are important in evaluating the results of such testings. Of nondestructive testing methods used in Japan, the radiographic and magnetic-particle methods have been in use for 30 years with the later introduction of ultrasonic and penetrant methods for nearly 17 years.

About 16 years ago all these testing techniques were given the collective name of nondestructive testing and adopted in the process of production in Japan.

As these techniques were new to those who are in the relevant field as well as in industry, it was found necessary to provide the opportunity for both education and training to personnel engaged in such jobs. The situation of Japan in those days was such that there had been no agency to provide any education in this area, and the engineers who were responsible for nondestructive testing had to teach and train themselves with the aid of a poor collection of literature on the subject, most of which was obtained from abroad.

In 1952 The Japanese Society for Nondestructive Inspection (NDI) was founded for the purpose of promoting the art of nondestructive testing as well as cultivating and increasing nondestructive testing personnel.

In response to the expectations the NDI held a lecture course covering the entire range of nondestructive testing techniques in 1953. Nondestructive testing covers the techniques of radiographic, ultrasonic, magnetic-particle, penetrant and so on, according to the specific method. Therefore, nondestructive testing personnel should be classified as respective specialists depending on the specific method.

As early as 1953 the NDI offered specific lecture and laboratory training courses on nondestructive testing, depending on the methods to be applied.

The practice has been continued to date and these NDI courses have given the best opportunity of education and training to the nondestructive testing personnel in Japan.

These NDI courses are held on the four different subjects of radiographic, ultrasonic, magnetic-particle, and penetrant methods, and strain measurement. The four different sections correspond to four different committees formed within the NDI. It is a matter of discussion whether the subject of strain measurement should be included as one of the nondestructive testing techniques, but in Japan, strain measurement has been accepted as one, in view of the fact that it is often used for testing of products.

Each section holds lectures and laboratory training meetings for three to five days each year. Lectures are given for half the period and training for the rest. Lectures comprise fundamentals of each nondestructive testing technique and ordinarily make reference to the latest development in the particular technique, accompanied by demonstrations. This has proved useful in stimulating the interest of trainees, thus encouraging them to acquire the techniques discussed.

It is now recognized, that nondestructive testing should not be limited to a single specific method but should include a combination of several different methods as may be needed for better testing. For example, conventionally, radiography was used exclusively for testing welded joints in a structure, but nowadays the ultrasonic or magnetic-particle method has been applied as

the need has arisen. Thus NDT personnel are required to test welded joints not only by the radiographic method, but also to evaluate them by any of the other methods that are considered more advisable to use. The basic need is apparently for personnel to find out any possible defect in the welds, and use what is the most suitable of the different methods, ultrasonic or magnetic-particle, etc. Consequently, nondestructive testing personnel are required to be familiar with the entire range of methods available plus the capability for evaluating products.

To meet the demand the NDI has offered a lecture and laboratory training course covering the whole scope of nondestructive testing techniques, attendance at which includes personnel of comparatively high qualifications.

I have discussed the fact that the most effective education and training ever offered in Japan on nondestructive testing are these courses by the NDI, but some of the technical schools have also provided education on nondestructive testing.

Short nondestructive testing lectures are included in the subjects taught in most of the technical high schools in Japan. The ministry of education has recommended that these schools be equipped with nondestructive testing facilities, out of special funds.

In the summer of each year technical high school teachers have been given the opportunity of attending nondestructive testing lectures for one week or so.

A considerable number of university engineering departments offer lectures on nondestructive testing as one of the subjects of engineering. The engineering department of Osaka University has classes on the engineering of nondestructive testing.

Some industries provide nondestructive testing education and training, which is helpful to those who cannot afford to attend the NDI courses or receive school education. Some of the nondestructive testing companies have developed training materials of their own and use them to educate and train their employees.

In these days the regularly organized NDI lecture and laboratory training courses have been made good use of, and the number of training-within-industry programs has been decreased, although some industries provide fundamental education on nondestructive testing techniques.

Certification

Qualification by Law

Nondestructive testing personnel dealing with radiation as involved in radiographic testing are required by law to successfully pass national examinations provided in accordance with the laws for safety and security.

(1) The law concerning prevention from radiation hazards due to radioisotopes, etc., by Science and Technology Agency.

(2) Ordinance on safeguarding against radiation hazard, by Ministry of Labour.

The qualifying requirements provided for by (1) are applicable for nondestructive testing personnel engaged in radiographic jobs using gamma rays with radioisotopes, X-rays over one million volts, and neutrons.

The qualifying requirements stipulated by (2) apply to radiographers for radiation whatever its energy may be. Accordingly, ordinary radiographic testing cannot be carried out by those not qualified for the requirements of (2).

This ordinance was put into effect in 1965, and 7,000 personnel have qualified.

It should be noted, however that these legal qualifying requirements are intended primarily for the safety of human beings and do not qualify for, nor certify to technical levels of radiographers.

Certification of Nondestructive Testing Companies by Japanese Welding Engineering Society

In Japan, inspection of welding jobs is carried out most extensively by radiographic testing. Radiographs were taken at the inspection sections of manufacturing companies such as shipbuilding dockyards, and fabricators of chemical plants. More recently, however, most of these jobs are undertaken by companies specializing in radiographic testing. This ensures application of more reliable and experienced techniques in radiography and provides economic advantages to the fabricators, who do not have supply test facilities or train personnel.

It is important to note that as nondestructive testing specialist companies increase in number, their technical levels are not all equal. Some companies may operate on a well qualified level and some on a low one. It is expected that a few of the low-level companies may be seriously impairing the standard of nondestructive testing. This results in the need for checking nondestructive testing companies for their technical capabilities. It is rather difficult for manufacturing companies to do the job, so it was felt that the checking should be undertaken by a neutral organization.

The Japanese Welding Engineering Society attempted to meet the need by forming a Radiographic Testing Committee (RAC) and having the committee check and qualify nondestructive testing companies on their technical capabilities and levels of radiographic testing. Nondestructive testing companies thus qualified are then certified by the Society.

The requirements for qualification are that they have a certain standard of testing facilities and the testing personnel consists of more than two supervisors and more than five technicians. Such supervisors and technicians have to be qualified by examination by RAC.

This system of certification has been in effect for two years and has contributed in increasing the reliability of the certified nondestructive testing companies. It has proved successful, but the certification is available only to companies, not to individuals.

Qualification of Nondestructive Testing Personnel by NDI

It is evident that the reliability of nondestructive testing is dependent on the technical capabilities of nondestructive testing personnel. It is therefore very important to qualify these personnel on a technical level and to certify their qualifications.

In Japan there are many specifications for various manufactured products that require nondestructive testing by qualified personnel, and the matter of personnel qualification is becoming an urgent need.

Several years ago the NDI organized a subcommittee within the radiography committee, and it has been discussing the question of qualification of radiographic testing personnel. It has recently become clear that qualification should not be limited to radiographers, but that all nondestructive testing personnel should be subject to qualification. Two years ago the Committee for Certification of Nondestructive Testing Personnel was formed and has been planning a possible system for qualifying nondestructive testing personnel.

The code of qualification under consideration is still at the drafting stage and the outline is as follows:—

Three levels of qualification are proposed as shown in Table 1.

The strain measurement technique is taken as one of the nondestructive testing methods for reasons already mentioned, although no country other than Japan has done so.

The examining and certifying agency is the NDI.

Comparison of the Japanese system of certification with those by other countries indicates that the NDI system is similar to the SNT specifications of the U.S.A., since both classify nondestructive testing personnel into three grades and give similar classifications of nondestructive testing methods. The main difference is that in the U.S.A. the certifying agency is the industry employed, and in Japan it is the NDI.

In Canada, radiographic testing personnel are classified in two grades which correspond to the lower two grades of qualification in Japan, and the Canadian system of examination is similar to the Japanese one since it is administered by the government.

Table 1

Grade	Requirements
Special Grade	Personnel of this grade shall have sufficient knowledge and training on all of the nondestructive testing techniques. They shall be capable of planning and performing NDT tests and also of establishing evaluation criteria and making evaluations. They may be allowed to call themselves certified NDT inspectors.
1st Grade	Personnel of this grade shall have sufficient knowledge and training about the nondestructive testing method certified (hereinafter referred to as certified NDT method). They shall be capable of planning and performing NDT tests and also of calibrating equipment setup when necessary, and reading and evaluating results and interpreting related specifications. They shall also be able to establish acceptance criteria involved and to develop reports on NDT test results.
2nd Grade	Personnel of this grade shall have general knowledge and training on equipment and operating procedures involved in the nondestructive testing method certified. They shall be qualified to operate equipment and perform tests under the direction and guidance of 1st grade personnel, but not authorized to designate the particular testing method to be used and evaluate the results for acceptance.

The seven different nondestructive testing methods in Table 2 are under consideration for qualifying purposes.

Table 2

Ordinary X-ray radiographic testing
High-energy radiographic testing
Ultrasonic testing
Magnetic-particle testing
Eddy-current testing
Liquid penetrant testing
Strain measurement

In my personal opinion, it is fair and just if a neutral agency can provide coordinated qualifying examinations for nondestructive testing personnel, and thus help to level out the technical skills of all qualified personnel.

To conduct such an examination, all the subjects of study necessary for the applicant to be familiar with would have to be presented to him. It would also be necessary to present typical examination problems. For this purpose we are preparing textbooks, the contents of which will include those of Supplements of Recommended Practice No. SNT-TC-1A accompanied by further technical details or explanations. We propose that the textbook will contain a full range of well-rounded information for the nondestructive testing candidate to master.

We are of the opinion that any nondestructive testing operator should not only know how to operate devices and equipment, but also should have full background knowledge of the tests. Our NDI certification system will be made effective this year or next.

Suggestion for Establishing an International Certification of Nondestructive Testing Personnel

The U.S.A. and Japan have adopted the same system of classification for nondestructive testing personnel level, namely 3 classes. Although the Canadian system is applicable only to radiographic testing personnel, the two classes correspond to the two lower classes of the U.S.A. and Japan. There appears to be no radical difference in the qualifying requirements specified by the three countries.

Therefore I think there is a strong possibility of establishing an international system by which all nondestructive testing personnel can be qualified and certified on the same basis. To do this, it would be necessary for each country's specifications for qualification and certification to be similar. Further it would be necessary for each country to make exchange information available on personnel certification systems quickly, and to establish its own standards from an international point of view. Such efforts would result in minimizing the differences in qualifying requirements or standards established by each country, and eliminate any obstacles to the future establishment of an international agency for nondestructive testing qualification and certification.

The exchange of industrial products in the world increases each day, and nothing but inconvenience will result if methods, standards and requirements for qualification continue to be different from country to country.

I believe that the time has come for the International Conference on Nondestructive Testing to move ahead for international cooperation and make a decision to do something in support of such an idea.

Discussion

Q. A. C. WALKER, National Research Council of Canada, Ottawa, Canada:

I would like to know what kind of specimens are used for training personnel? Are they actual, defective parts and, if so, do you have some system for collecting such parts from industry?

A. We use weld and casting specimens for training personnel. It is difficult, however, to get a number of specimens with all patterns of defects, and a limited number of typical defective part specimens are employed. These defective parts are produced specially for the specimen purposes. We do not collect actual defective parts from industry since this practice has proved to be unsuitable in our past experience, which showed that though a large number of actual defective parts were collected from industry, they unfortunately did not include those with required patterns of defects. Furthermore, we are of the opinion that a great variety of defective part specimens are not always necessary for the purpose of training personnel on testing techniques, and such personnel will be able to obtain enough knowledge of defect images with the aid of radiographs or indicative photos of many different defect patterns.

Such references available include reference radiographs of IIW and ASTM as well as the collection of standard radiographs for radiographic tests and reference atlas for ultrasonic testing issued by the Japanese Society for Non-Destructive Inspection(NDI).

The standard NDI radiographs consist of a number of radiographs on defects as classified according to the Japanese Industrial Standard. The standard is under revision and re-edition of the NDI radiographs is expected to be made to the JIS as revised.

Certification of Radiographic Personnel in Canada

W. E. HAVERCROFT, CANADA

Introduction

Potential hazards both in the use of penetrating radiations and in the interpretation of their results when applied to the inspection of critical safety items, make some form of control over their use mandatory. There have been many illustrations of injury and loss of life due to exposure to harmful radiation and to improper quality control of critical components. The rapidly expanding science of nondestructive testing demands that skilled personnel be available to avoid these hazards and to prevent the great waste of manpower and materials which are a result of improper practice.

One of the first problems of this nature in Canada was concerned with obtaining skilled personnel to carry out aircraft radiography. The Royal Canadian Air Force established its own procedures for approval of personnel with the help of the Mines Branch in Ottawa and this eventually became the basis of the present C.G.S.B. Standard for the Certification of Industrial Radiographic Personnel.

It is the purpose of this report to discuss the preparation of the Canadian Government Specifications Board Standard 48-GP-4, the standard itself, the present status of the certification program and some problems which should be considered in regard to the training and qualification of all NDT personnel.

History

The Canadian Government Specifications Board (CGSB) is a federal government body charged with the responsibility of preparing specifications and standards at the request of government agencies. The Board proper is made up of the deputy heads of government departments and agencies and operates through technical committees in the various commodity fields for which specification work is undertaken. Membership on these committees is held by representation of the interested government agencies and of the main elements of the industry concerned.

The need for standardization resulted in the formation of a committee on nondestructive testing with a sub-committee on industrial radiography. The sub-committee recognized the fact that qualified personnel were needed if full benefit was to be derived from any specification it might issue. It was decided that the group should look into the desirability of certifying industrial radiographers and, if necessary, prepare a document outlining the certification procedure.

This group was established in 1956 and in 1960 agreement was reached on the many problems involved. A standard designated 48-GP-4 "The Certification of Industrial Radiographic Personnel" was then issued.

CGSB Standard 48-GP-4

This standard establishes two levels of certification. A Junior Industrial Radiographer is defined as one who carries out industrial radiography under supervision and is not responsible for establishing techniques or for the assessment of radiographs. A Senior Industrial Radiographer, on the other hand, is a fully qualified man who can assume full responsibility for a radiographic laboratory and staff.

It was necessary to set up standards of eligibility for applicants without penalizing those with years of experience, but who lacked a basic education. The education and experience requirements set forth in the standard for Junior Grade certification can be briefly stated as follows:

1. Grade 12 education or equivalent—one year of experience in industrial radiography.
2. Elementary School—two years experience.
3. A minimum of five years experience in radiography and related fields for those who did not complete their elementary education.

Eligibility requirements for Senior Grade candidates follow a similar pattern.

1. Three years experience as a certified Junior Grade industrial radiographer.
2. Six years experience of which three years must involve duties comparable to those expected of a Senior Grade radiographer.
3. Grade 12 education or equivalent—two years experience as a certified Junior Grade industrial radiographer.
4. University graduation or equivalent in science or engineering plus one year of experience as a certified Junior Grade industrial radiographer.

A candidate must be able to satisfy at least one of the conditions stated above in the level of certification he requests.

The standard 48-GP-4 also outlines the type of written and practical tests to be carried out by the examining authority, the percentage of marks to be obtained and states that a radiographer must be recertified if he is not employed for a continuous period of one year in the work for which he is certified.

Application of the Standard

The Mines Branch of the Dept. of Energy, Mines and Resources agreed to act as the Examining Authority for the CGSB. It agreed to prepare the written and practical tests, conduct the tests, assess the results, and issue a certificate to successful candidates.

The Radiation Protection Division of the Dept. of National Health and Welfare are also represented on the Certification Committee. The Division's interest in the program made the committee members aware of the radiation hazard involved and of their responsibility to include radiation safety in the qualifying tests. The dangers involved in the handling of radioactive materials by inexperienced personnel stress the need for the standard.

It was decided that questions on radiation safety would be a part of the examination and that a passing grade on this subject would be required before certification was granted. Subsequently, the Radiation Protection Division agreed to prepare the test papers dealing with radiation safety and to assess the results.

Applicants for Junior Grade certification are required to write three papers. The first deals with questions on the general knowledge of industrial radiography, the second with darkroom processing procedures, a prime responsibility of the Junior Grade radiographer, and the third with the problems of radiation safety. The time required for the three papers is usually one day.

The Senior Grade applicant, as noted earlier, must pass both a written and a practical test. He is required to write a paper on general radiography to assess his knowledge of the theoretical aspects of the subject, a paper concerned with radiation safety and another concerned with each category in which he seeks certification.

He may be certified in the following categories:

(a) Light Alloy Castings and Forgings; (b) Welds and Weldments; (c) Heavy Metal Castings and Forgings; (d) Aircraft Structures.

To date certification has not been granted in the Aircraft Structures category. This will begin as soon as the method of conducting the practical tests has been completed. These tests will be conducted at the National Defence (Air Force) nondestructive testing laboratories at Trenton, Ontario. Complete aircraft and aircraft components from both military and civil aircraft will be available on which applicants may carry out designated radiographic tests.

The Mines Branch will continue to act as the Examining Authority and conduct the remainder of the examinations.

It is hoped this cooperative effort will provide a sound method of assessing a radiographer's ability to do a proper job in the rapidly expanding field of aircraft radiography.

Present Status of the Program

The written portion of both the Junior and Senior tests are carried out in many centres across Canada. They may be given in any area where an invigilator can be found to conduct them. Most of the practical tests have been given in Ottawa, although the Pacific Naval Laboratories at Esquimalt, B.C., and the Northern Alberta Institute of Technology in Edmonton, Alta. are conducting both written and practical tests for applicants in western Canada.

Since Canada is a bilingual country certification tests are arranged to be given in English or French at the option of the applicant.

To date there are approximately 400 certified Junior Grade industrial radiographers in Canada and approximately 165 certified Senior Grade radiographers.

Although the program is relatively new it has been readily accepted by both industry and government in Canada. The RCAF abandoned its certification procedure in favour of this new national standard. The Atomic Energy Control Board saw in it a means of safeguarding industrial workers and announced that as of January 1st, 1966, all industrial radiographers using radioisotopes are required to be certified as Senior Grade Industrial Radiographers.

The certification program has been in effect for only a few years; however, the sub-committee has become aware of certain basic facts.

(a) A good elementary education is essential if a candidate is to successfully complete the written examinations; (b) Before certification is granted in any of the nondestructive testing methods a candidate must have some experience in the particular test method. (c) A system of control must be established whereby the certifying body is kept informed of personnel who may be removed for extended periods from the work for which they are certified. The certifying body must decide when recertification is necessary. (d) There is a great need for courses of instruction, lectures and practical training in industrial radiography or any of the nondestructive test methods.

In order to encourage instruction in industrial radiography the sub-committee is preparing an instruction manual which may be used by schools or other organizations wishing to establish lecture courses on this subject. It will also serve as a reference book for use by personnel preparing for the certification examinations.

Considerations

A number of countries have similar training and qualification programs in one or more of the nondestructive testing methods. Although there is much to be done at the national level it is possible that some thought and effort at the international level may appreciably reduce the problems to be encountered.

Let us consider some possible advantages of a qualification and certification system acceptable in whole or in part by two or more countries.

(a) Duplication of training of personnel could be reduced; (b) A country would be more willing to accept materials or products from another knowing that nondestructive tests had been made with qualified personnel; (c) Delays in the fulfillment of contracts due to the "checking out" of personnel may be avoided. In times of emergency this could be important.

Many problems would have to be resolved before such an agreement could be reached; however, there are some fundamental problems which could be considered at this time.

(a) Agreement upon terminology and definitions commonly used in nondestructive testing; (b) The adoption of an international classification system of NDT personnel based upon duties. This would allow an exchange of information on personnel qualifications to have meaning; (c) Agreement upon the levels of knowledge and experience necessary to carry out the duties within each classification; (d) The preparation of "a course of instruction outline" for each classification. This could be used as a foundation upon which national instruction courses could be based.

One object of the Standing Committee for International Cooperation within the field of Non-Destructive Testing is to promote collaboration, in association with national organizations on nondestructive testing, in the formulation of international standards. Perhaps these national organizations who are represented by members of the Standing Committee should be encouraged to work together on the above problems.

An organized exchange of information dealing exclusively with the training, qualification and certification of nondestructive testing personnel is worthy of consideration.

Discussion

Q. F. H. GOTTFELD, F. H. Gottfeld GmbH, Koeln-Lindenthal, Germany.

What can be done to change the attitude of the clients? They ought to ask for the quality of the tests and their limitations first, and for the costs afterwards?

A. We must show them that savings and quality go hand in hand, and are not in opposition as many believe. We must impress them with potential financial losses due to this attitude even though it is difficult to attach actual cost figures to such losses.

Q. JACQUES MENETRIER, Appareils Gamma Siar, Paris, France:

Regarding international coordination for the problems of formation and qualification of NDT personnel, which organization could become the centre for this international coordination?

An international centre is absolutely necessary to coordinate and sometimes encourage the initiatives dealing with projects and

specifications of national organizations or interested firms if a country does not have a national organization.

A. If countries attempted to follow a procedure prepared by an international group such as the International Committee on Nondestructive Testing, no doubt less conflict would occur in the acceptance of codes, specifications, test procedures etc. between nations. I believe the International Committee on Nondestructive Testing could prepare such a procedure. Naturally each country would conduct its own programs in training and qualification of personnel, very likely within the main NDT group in that country. In a country where no such group exists then one should be formed, even though it may be very small.

Q. WALTER A. PYCHYL, The Steel Co. of Canada Ltd., Welland, Canada:

Do I understand that only the use of isotope now require certifications at this time? When will the use of X-ray equipment require certification (mandatory) and at what level of certification? Would you expect that operator certification would be mandatory on an operation using X-rays where there would be little change, if any, in techniques, operating practices or product, from year to year?

A. Your question appears to be in three parts. For the first, certification to the CGSB standard is not mandatory in itself. The Atomic Energy Control Board, however, requires that personnel using radio-isotopes for industrial radiography be certified or supervised by certified personnel. There is no such requirement for radiography using X-rays.

X-ray safety committees advocate similar requirements, however, it is not possible to say when this may come about or the level of certification that may be required.

For the last part of your query, may I say that mandatory requirements in radiography have been based solely on radiation hazards. Therefore changes in technique, operating hazards, etc. may have no bearing on where operator certification is mandatory or not.

Q. G. F. HOGERVORST, Toronto Iron Works Ltd., Toronto, Canada:

Will there be a certification process for purchaser's inspectors in the pressure vessel field? Quite a few of this category have come through the ranks, having perhaps worked as layout men or welding supervisors or fit-up foremen etc., thereby acquiring a lot of knowledge on the general process and procedure of fabrication, but hardly any in the nondestructive testing aspect of it. These people do sometimes become acceptance inspectors for the purchasers, and at times it does create a problem, though in most cases a minor one.

A. This problem has been discussed by the NDT committees of the CGSB; however, no action has been taken. I believe the Canadian Welding Bureau is concerned with the qualifications of inspectors and supervisory personnel, and this may include the pressure vessel field.

Q. JACK MCKINNON, Warnock-Hersey Co. Ltd., Halifax, Canada:

What steps are being taken on the certification of ultrasonic technology?

A. The CGSB has a group working on the certification of ultrasonic testing of personnel. The main difficulties are in the establishment of suitable test procedures and in finding an organization capable and willing to conduct the certification program.

Q. PIERRE RUAULT, Gaz de France, France:

The quality of the result of a radiographic inspection depends on three broad areas:

1. The technique used; 2. the competence of the operator, but also his physiological abilities, particularly for certain types of inspection (sharpness of vision, appreciation of contrasts....) 3. the quality of the reading (sharp and clear, etc. . .). What do the authors think of the relationship between these various factors?

A. (Mullins and Byrne) Mr. Ruault's summary of the important factors is unquestionable. However capable the operator, he must be given the proper facilities to do his job efficiently. This is an aspect which is too often ignored by employers.

A. (Tada) It is true that the results of radiographic examination are dependent on the parameters that Mr. Ruault points out. Therefore we are trying to limit radiographic techniques to standardized specifications.

However, it is apparent that specifications can be no more than what they are, and each person who makes tests is required to have full knowledge about these parameters to enable him to adjust his environment or conditions to the best advantage. Our lectures and training programs reflect these points, especially for the radiographic inspector.

A. (Havercroft) Candidates applying for certification tests differ widely in the degree of tension or nervousness experienced prior to the tests. Some appear extremely tense. We allow them to do some of the practical tests first. In becoming acquainted with the surroundings and equipment the tension gradually disappears. It is essential that the supervisors maintain a friendly attitude and the ability to put the candidate at ease. Of course, pleasant surroundings and working conditions help in this regard.

Principal Session B/ Correlation of Weld Defects

How Dangerous Are Weld Defects?

R. WECK, U.K.

What Has Experience to Teach Us?

The pressure vessel shown in Figure 1 is a liquefier of 650-gallon capacity built in 1937, which formed part of a refrigeration plant. It was constructed in accordance with the B.E.S.A. standard then in use for a working pressure of 220 lb sq in. at a service temperature of −35°C. It had not been stress relieved after fabrication but had been hydraulically tested to 375 lb sq in. before commissioning. It was in use for a period of 17 years, from 1937 until 1954, and was then put into storage until 1961

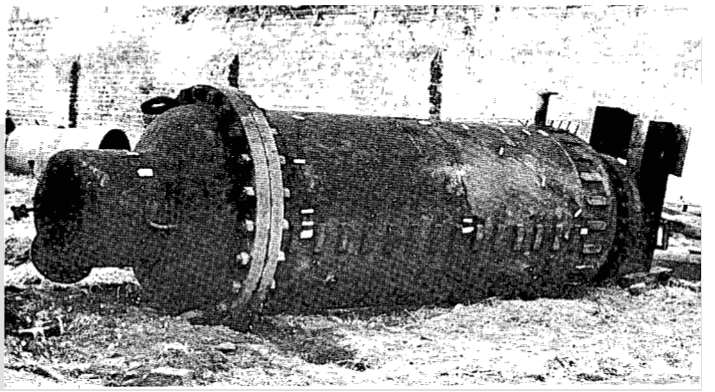

Figure 1. General view of CO_2 liquifier and header, showing longitudinal weld and lacing straps.

when it was intended to be recommissioned as a storage vessel for CO_2. At that time it was inspected by an insurance company when it was discovered that there was practically continuous lack of fusion throughout the length of the longitudinal butt weld, and recommissioning was abandoned. The longitudinal as well as the circumferential welds were "reinforced" by butt straps, symptomatic of the lack of faith in welding and in particular the lack of confidence in the reliability of butt welds 30 years ago. On the face of it, the continuous lack of fusion seems a very good reason for anxiety and the butt straps. The idea of "reinforcing" a suspect butt weld by butt straps looks terribly naive to us today when we know that butt straps if anything make matters worse by producing stress concentrations rather than reductions in stress, and when we know how easily a brittle fracture, if it ever started in the butt weld, would pass through the straps.

However, despite severe defects and despite the butt straps, the vessel gave satisfactory service over many years and would have continued to do so. It would have been almost worthwhile preserving it as a museum piece if it had not been put to even better use by testing it to destruction to find out how serious the weakening effect of the defects was.

A decision, of course, had to be made on the testing temperature since no information was available on the low temperature notch toughness of the material—in 1937 the significance of this property in relation to brittle fracture was not appreciated—it was assumed that for the mild steel from which the vessel was constructed and which was nowhere less than 0.48 in. thick, it would be about −5°C for 15 ft/lb Charpy V-notch. It was expected that failure would take place through the longitudinal butt welds.

It was calculated that at 900 lb sq in. pressure the circumferential membrane stress would reach the yield point of the material. The vessel was cooled to −8°C and it failed at a pressure of 500 lb sq in., i.e. at more than twice the working pressure. The failure, of course, was, as expected, by brittle fracture, which originated from a severe defect at the intersection of two welds shown in Figures 2 and 3. However, the crack only ran for a distance of about 8 in. when it was arrested, and the surface of the flaw was heat tinted indicating that it had been present ever since the vessel had been made and had been there throughout its service life. The flaw was situated in an area of stress concentration and the average stress in this area due to the change in shape was raised to at least yield level at working pressure.

The opportunity of testing a structure to destruction after it had been in service over a long period does not occur very often, but there can be no doubt that there are many structures still in service today which were constructed at a time when neither welding nor methods of nondestructible examination had been developed and which are continuing to give perfectly satisfactory service despite the fact that, like the present example, they are afflicted with quite serious defects.

Of course, when brittle service failures are experienced, the origin in practically every case reported and documented in the literature is associated with some kind of flaw and yet the number of structures that have failed is very small indeed in comparison with the number of defective structures which must be assumed to be in service today.

The explanation for this, of course, is quite simple—it takes more than the presence of a defect to cause brittle fracture. Residual stresses and in particular the changes in mechanical properties at the tip of a sharp planar defect due to the heating and deformation caused by welding are now known to be as important as is the third factor: the notch ductility of the material at the lowest service temperature to be experienced. The ancient liquefier tested has obviously been saved from failure in service by the hydrostatic test at a pressure of 375 lb sq in. carried out at a temperature above the transition temperature

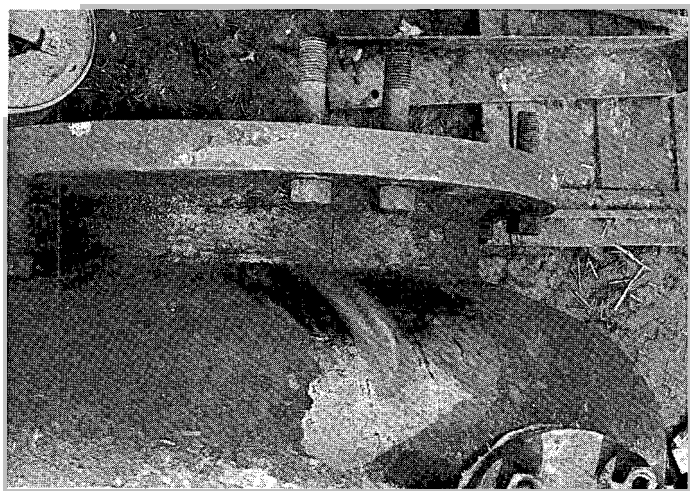

Figure 2. Close-up of short crack in vessel.

of the material, since had it been carried out below the transition temperature the vessel would undoubtedly not have been commissioned because it would have failed during the hydraulic test. The effect of prior overstrain above the transition temperature, provided it does not extend an existing flaw, is now known to render defects innocuous in relation to brittle fracture at temperatures below the transition temperature.

The only rational conclusion one may come to from this particular experiment is that even very severe weld defects of a character that would rarely occur—and if they did occur would not be tolerated today in any type of construction whose failure would present a risk to life or property—are not nearly as dangerous as the excessively severe inspection criteria almost universally in force today might lead one to expect. If it is remembered that for a very long time structures perforated with vast numbers of rivet holes have given perfectly satisfactory service, it seems absurd that today the fabricator is compelled to eliminate from welds in Class I pressure vessels and other important structures almost every trace of scattered porosity.

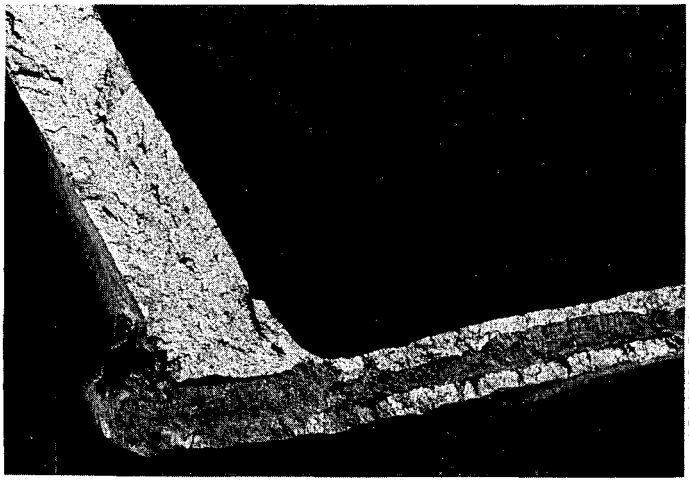

Figure 3. Close-up of flaw at point of initiation of fracture.

Codes for Weld Quality

In most countries the construction of welded structures of any importance is supervised and controlled by an inspection authority and in the last resort approval depends on the judgment of this authority. There are few other fields in industrial technology that offer so much scope for conflict and controversy and everybody in touch with industrial practice knows a good many cases where the fabricator considers the judgment of the inspection authority to be arbitrary and too severe. This is, of course, almost inevitable in a field where it is impossible to lay down standards in numerical terms. Practically every other requirement in construction—the properties of the material, the dimensions of the structure and its form—can be defined in numerical terms and while it has become increasingly obvious that some of these requirements are not very logical, there can at least be no argument about them. In relation to defects in welds the situation is different. Although attempts have been made—the A.S.M.E. Code being one example—to lay down acceptance criteria for defects, these attempts have not been very successful. To eliminate the element of arbitrary judgment, there is a persistent clamour on the part of the fabricator to have the standards of performance to which he is expected to work, codified.

Considering the scarcity of empirical and experimental data at this time any attempt to create and enforce rigid mandatory standards of acceptance will only make matters worse in the long run. The problem is complex and with the information so far available it is quite impossible to draw up a code that would take account of all the circumstances that must be considered in any judicious assessment of a defect in relation to the risk it may present for the satisfactory performance of a structure. Our factual knowledge in this field is continuously increasing—and could increase faster if a concerted international program was undertaken. A code introduced now would in large part have to be based on pure guesswork. Once a code becomes established, however, it takes many years to change it. It seems preferable to maintain the present flexible situation, however irritating it may be from time to time, rather than to freeze, as it were, requirements with a rigid code which it would take many years to change.

Defects and Failure

Defects are only relevant in relation to the possibility of initiating or facilitating structural failure. This can take place only in one of six ways:

1. Ductile failure as a result of overload which will produce excessive deformation prior to rupture; 2. Elastic or plastic instability; 3. Creep; 4. Corrosion and stress corrosion; 5. Brittle fracture; 6. Fatigue.

In relation to failure, defects have three effects: (a) They reduce a cross-section of area and augment the average stress; (b) As discontinuities they produce stress concentrations; (c) Defects, where they are in contact with the corrosive medium, may not offer the same resistance to corrosion as the metal.

The diminution of cross-sectional area in most cases is relatively small and the modest increase in average stress as a consequence of this reduction is irrelevant in relation to any possible modes of failure because even with design stress at a higher level in relation to yield point or proof stress than is customary today, there would always be an ample margin to cover the relatively modest stress increase involved. In cases, however, such as in certain aluminium alloys where the strength of the weld metal may not match the strength of the parent metal, and where the static tensile strength of the joint is further diminished by the presence of defects in the weld, design stress should in any case be based on joint strength and not on parent metal strength so that even a defective weld would not be unduly overstressed.

As far as the risk of failure by corrosion is concerned, defects, entirely surrounded by solid metal which do not penetrate to the surface in contact with the corrosive medium are without significance. Lack of fusion or the presence of slag inclusions

in the root pass in contact with the corrosive medium may lead to corrosive attack but so, of course, may the presence of ferrite in stainless steel welds which would not normally be classed as defects. Where protection from corrosive action depends on the maintenance of a continuous oxide film, corrosion may take place in crevices or cracks in a material normally resistant simply because at the bottom of a crack or a crevice, lack of oxygen may prevent the renewal of the protective film.

Effect of Stress Concentrations Caused by Defects

The most important aspect of the problem, however, arises solely from the fact that stress concentrations are discontinuities and discontinuities of any kind always produce stress concentrations. Stress concentrations, however, are known to be relevant only in relation to the possibility of failure from brittle fracture and failure by fatigue.

There is very little information at present on the effect of defects, or for that matter stress concentrations, on the possibility of creep rupture failure. No experimental work at all has been carried out in this field. To do so would clearly be a very costly and lengthy undertaking which could only be accomplished by effective international cooperation. However, there is also little evidence that creep failures in service have been found to be associated with weld defects. This perhaps is the reason why the problem—if it is a problem—has not received attention.

Before considering fatigue and brittle fracture, brief reference must also be made to impact loading. The rates of loading normally occurring in engineering even if they may be fairly fast, such as water hammer in a pen-stock, do not introduce aspects essentially different from the problem of failure under purely static loading. Ductile failure, failure from instability or brittle fracture can, of course, be caused by impact loading as readily as by static loading. At very high rates of loading, produced by explosives which would not normally have to be considered by the engineer except in as far as he may be concerned with military constructions such as submarines, the behaviour of the material itself changes, and it is known that even very ductile materials will shatter into fragments without prior plastic deformation when subjected to shock from explosives of the highest velocity. Normally, however, if the engineer is concerned with impact loading conditions at all he will have to consider quite modest loading speeds compared with those resulting from explosives. There is undoubtedly an influence of straining speed on the transition temperature from ductile to brittle fracture in steel, but if this is taken into account the criteria for accepting defects in structures exposed to impact need not differ from those where only static loading has to be taken into account. Provided that under the rates of loading in question the material can still be relied upon to behave in a ductile manner, even severe defects will have little effect on the over-all strength and performance of the structure.

Brittle Fracture

It is in relation to the risk from brittle fracture that defects really become important. No case of brittle fracture in a welded structure has ever occurred that did not initiate from a weld defect.

Having said this it is important to emphasize that we need concern ourselves only with low-stress brittle fracture, that is, the risk of failure by brittle fracture at stresses lower than the design stress, since yield-point fracture will never occur in practice. Stresses producing a state of general yield over a very large area of the structure will not normally occur unless a very serious mistake in design calculations has been made.

The distinction between yield-point fracture and low-stress fracture is important in relation to the role of defects. Yield-point brittle fracture could initiate from a defect of sufficient size provided the material was at a temperature well below its Charpy V-notch transition temperature, whereas low-stress brittle fracture requires in addition the presence of very high residual tensile stresses in the region of the defect. It follows that even fairly large crack-like defects perhaps equal in length to the plate thickness could be tolerated in a structure that has been stress relieved and that was not subjected to fatigue even if service temperature of the structure was below its transition temperature. To put it in another way; since for low-stress brittle fracture to occur there must be: (a) A crack-like defect (ordinary porosity not extended by cracking would not constitute a risk); (b) High residual tensile stresses in the region of the crack; (c) A service temperature well below the Charpy V-notch transition temperature.

The elimination of any one of these three factors would eliminate the risk of brittle fracture. That is to say, at a service (or test) temperature above the transition temperature even large crack-like defects (provided fatigue is absent) can be tolerated and stress relieving is unnecessary. In a stress-relieved structure, defects can be tolerated even if the material is brittle, and if serious crack-like defects are eliminated, stress relieving is unnecessary even if the material is brittle. One may go further still and say that stress relieving can be omitted even in the presence of fairly large crack-like defects (not exceeding plate thickness in length), even in material that is brittle at the lowest temperature reached by the structure, provided that (a) the structure has been subjected to an overload test at a temperature well above the Charpy V-notch transition temperature before being put into service, and (b) that, at temperatures below the transition temperatures, applied stresses are lower than those experienced in the overload test.

Experience has shown that only elongated crack-like defects present any real danger in relation to the initiation of brittle fracture. This is because only such defects produce strain concentrations of sufficient magnitude at their pointed ends under normal service loading to make brittle fracture initiation possible.

Fatigue

Fatigue failure is probably the most common type of failure in welded construction, but only a relatively small number of all such failures experienced are the direct result of the type of weld defect—porosity, blow holes, slag inclusion, lack of fusion, etc.—that occurs accidentally and gives rise to the usual arguments between inspectors and contractors. Deliberate defects, such as one that occurs when either no weld preparation for a butt weld is shown on a drawing, or a preparation

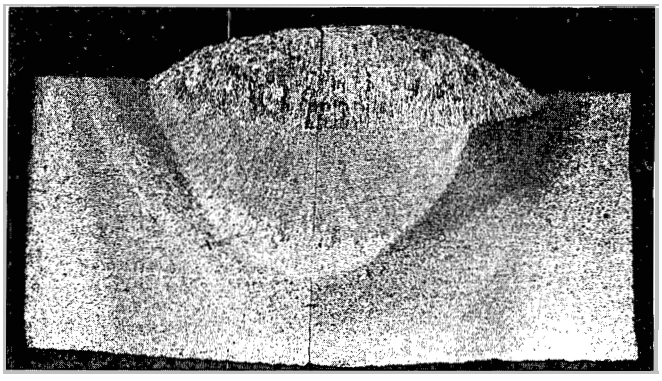

Figure 4. Incomplete penetration butt weld. Many fatigue failures and brittle fractures have been initiated by this deliberate defect designed into the structure. Such welds should never be permitted.

which will permit welding only about halfway through the plate thickness, (Figure 4) are known to have caused fatigue failures in service.

The reason, of course, is obvious. In such a weld, which hardly deserves the name, the abutting surfaces of the unwelded part of the plate constitute an exceedingly sharp and deep fissure which under cyclic stressing of even quite low magnitude will propagate almost from the start and penetrate very rapidly through the weld. The incomplete penetration butt weld should be prohibited for all but non-load carrying structures. It is as dangerous in respect of brittle fracture as it is in respect of fatigue.

Newman (1) showed that if this type of defect is present in circumferential butt welds of B.S. 806: Class B mild steel pipe of $6\frac{5}{8}$ in. o.d. and $\frac{3}{8}$ in. wall thickness it would reduce the fatigue strength in reversed bending for 2 x 10^6 cycles to $\pm$ $1\frac{1}{4}$ tons/in.^{2} which is only between 15% of the fatigue strength for unwelded pipe ($\pm$ $7\frac{1}{2}$ tons/in.^{2} to $\pm$ 11 tons/in.^{2}; mean $8\frac{1}{4}$ tons/in.^{2}) and 35% of the fatigue strength of sound butt welds ($\pm$ $3\frac{3}{4}$ tons/in.^{2}).

Most fatigue failures experienced in practice, with the exception of those due to this particular defect, stem from bad design of detail and this is one of the consequences of our using completely outdated methods of design. The fatigue resistance of a structure is determined by the magnitude of the stress at points of stress concentrations. Generally, in ordinary conventional design methods, we calculate only average stresses but ignore the stress concentrations due to such things as abrupt changes in section, sharp corners, attachments and other discontinuities. In a riveted girder, for instance, we calculate the maximum bending stress—making allowance for the loss of cross-sectional area due to rivet holes—but we ignore the fact that the actual maximum stress in the cross-section where the maximum bending movement occurs will be nearly trebled at the edge of each rivet hole. From experience we know, however, that using conventional methods of design and permissible stresses it is quite safe to ignore this local stress increase and that riveted girders with certain notable exceptions (such as the stiffening truss of the Manhattan suspension bridge in New York which failed from fatigue after 40 years) are reasonably immune from fatigue failure for many years.

Welded design, however, may introduce much more severe stress concentrations—and not by virtue of defects in the welds—than riveting, and it is a result of this fact that fatigue failures in welded structures are so common. For instance, the fatigue strength for two million cycles of a welded plate girder with a continuous web-to-flange weld will depend on whether the flanges are welded to the web by continuous automatic welding or by manual welding with its inevitable stop-start points when the electrode is changed. As a result of the stop-start points the fatigue strength of the manually welded plate girder will be about 9 tons/in.^{2} in terms of maximum bending stress in the flange and that of the automatically welded girder without stop-start points in the web-to-flange welds will be 11 tons/in.^{2} to 12 tons/in.^{2}. A butt weld in the flange may reduce the fatigue strength to 7 tons/in.^{2} and a transverse fillet weld attaching a stiffener to the flange will reduce the fatigue strength of the girder flange still further to about 5 tons/in.^{2}. It is obviously quite immaterial to argue about even a serious defect in the butt weld of the flange if right next to this butt weld there is a transverse fillet weld across the flange. Continuous lack of root fusion, the most serious defect by far, will reduce the fatigue strength of the butt weld to only 6 tons/in.^{2}, which is not as large a reduction as that produced by the transverse fillet weld.

Defects, in as far as they produce stress concentrations,

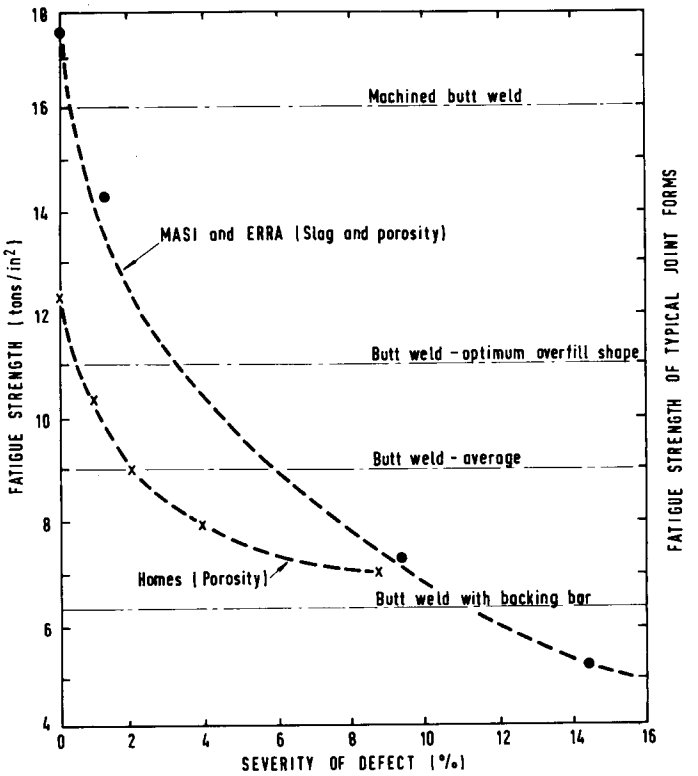

Figure 5. Effect of porosity on fatigue strength of butt welds. Porosity of 2% can be tolerated without detrimental effect on fatigue strength of unmachined butt welds, whereas porosity of only 1% would lower fatigue strength of machined butt welds. (Mild steel.)

lower the fatigue strength of welded joints. However, it does not follow that, in structures subjected to fatigue, defects in welds cannot be tolerated. The diagram in Figure 5 illustrates the results of fatigue tests carried out on butt welds with differing degrees of porosity. Although the fatigue strength falls with increasing porosity the diagram shows that porosity less than 2% could be tolerated in an unmachined butt weld with the overfill left on, whereas, of course, porosity of only 1% would reduce the fatigue strength of a machined butt weld by 6 tons/in.^{2} from 16 tons/in.^{2} to 10 tons/in.^{2}.

What decides whether a defect can be tolerated is the actual stress existing at the point where the defect occurs. If the fatigue strength of the weld for the appropriate number of cycles that the structure is expected to survive, even with this defect, does not fall below the stress known to exist at the particular point, there is no reason to remove the defect.

It must be remembered in this context that in design for fatigue one cannot use a safety factor by choosing a permissible stress which is only a fraction of the fatigue strength. If it is known that the fatigue strength of a butt weld free from defects and with the overfill machined off is 16 tons/in.^{2} for two million cycles, there is no reason why this figure should not be used in design. Safety lies in the fact that failure will not take place in less than two million cycles. If on the other hand a stress lower than 16 tons/in.^{2} is used in design for some other reason than fatigue, a weld completely free from defects need not be insisted on. If one chooses such high design stresses, one must, of course, be certain that the number of cycles of maximum load has been correctly estimated for the life of the structure. Lower design stresses may have to be used, perhaps because the structure may very occasionally have to withstand an overload equal to twice the normal design load. This would not be expected to produce fatigue if it were only experienced a few times during the life

of the structure; nevertheless in this case the design stress for normal loading might have to be reduced to 8 tons/in.^{2}. However, if it is, fairly severe defects may be tolerated in the butt weld as is evident in Figure 6 (Newman and Gurney (2)). On the right are shown the fracture surfaces of butt welds containing various types of defects typified by numbers DIB3 to DIB10 and on the left are given the S-N diagrams—that is, stress versus number of cycles to failure—obtained experimentally for these joints. Included in the diagram are two further lines giving the fatigue strength for defect-free welds both with the overfill left stress levels in the British Standard for Steel Girder Bridges (B.S. 153) for three classes of butt welds (see the accompanying on and machined off. The three dotted lines give the permissible Table).

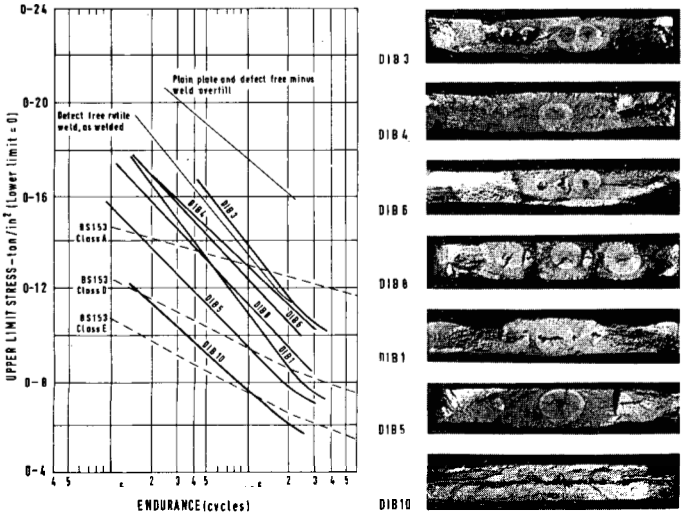

Figure 6. Fatigue S-N diagrams for butt welds tested in tension between zero and maximum stress. The photos on the right show the fatigue failures for different types of defect of increasing severity (downwards) corresponding to S-N diagram.

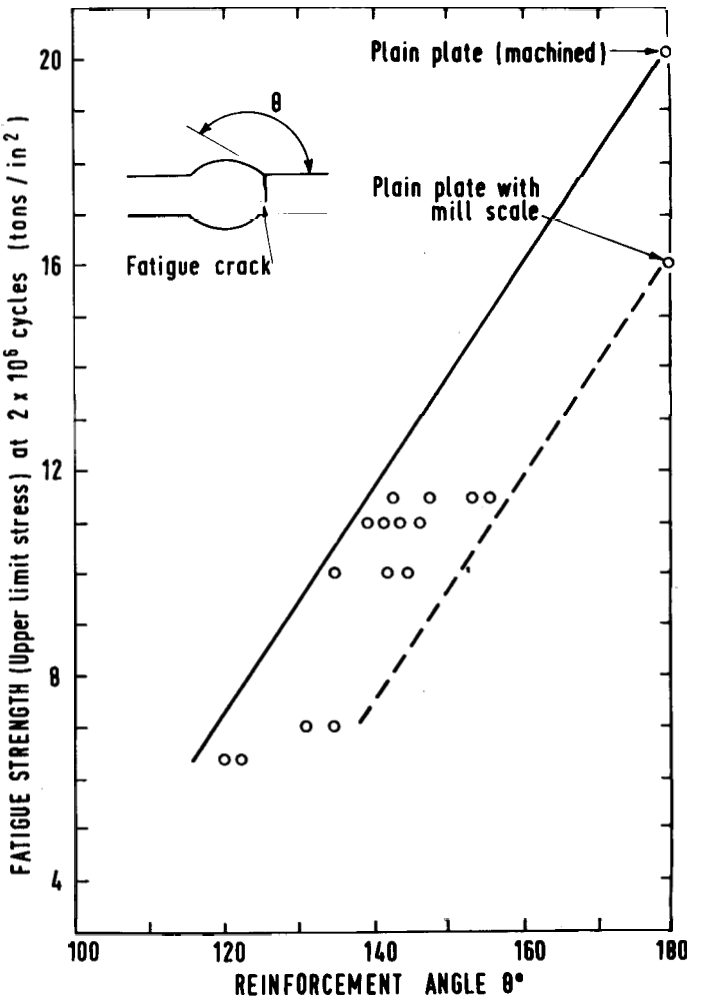

Figure 7. Fatigue strength of butt welds diminishes with decreasing angle included between tangent to overfill and plate surface.

It will be seen that for Class A design stresses, perfect butt welds with the reinforcement machined off are essential but that all manner of defects—except continuous lack of fusion—are acceptable for Class E for two million cycles. For less than two million cycles even that defect is acceptable at a much higher design stress.

Definition for Classes A, D and E butt welds (B.S. 153)

A	D	E
(i) Plain steel in the as-rolled condition with no ga cut edges.	Members fabricated with full penetration transverse butt welds having the weld reinforcement dressed flush and with no undercutting.	Members fabricated with transverse butt welds, other than previously mentioned, or with transverse butt welds made on a backing strip.
(ii) Members fabricated with continuous full penetra tion longitudinal or transverse butt welds with th reinforcement dressed flush with the plate surfac and the weld proved free from defects by non destructive examination, provided also that th members do not have exposed gas cut edges Welds shall be dressed flush by machining o grinding, or both, which shall be finished in th direction parallel to the direction of the applie stress.	Members with continuous longitudinal fillet welds with start-stop positions within the length of the weld.	Members fabricated with full penetration cruciform butt welds.
(iii)	Members of mild steel to B.S. 15 (mild steel for general structural purposes) or B.S. 2762 (notch ductile steel for general structural purposes) fabricated or connected with rivets or bolts.	

It is particularly irritating in relation to the whole argument about defects that it focusses attention on defects revealed by nondestructive testing—porosity, slag inclusions, etc.—but completely ignores those that one can see just by looking at the joint, but which, for no earthly reason, are assumed not to matter.

In another investigation carried out by Newman and Gurney (3) on the effect of the angle formed between the plate surface and the overfill they have shown (Figure 7) that the fatigue strength of perfect, defect-free butt welds may vary between 6 tons/in.^{2} for an angle of 120° to 11 tons/in.^{2} for an angle of between 140° to 160°. Comparing these figures with the S-N curves in Figure 7 it is obvious that if such an acute angle as 120° is tolerated for any butt weld one can tolerate also at the same time the continuous lack of root fusion defect without reducing the fatigue strength to below 6 tons/in.^{2}, and even for an angle of 160° one can still tolerate some fairly hefty slag inclusions.

Newman, in the investigation on the fatigue strength of butt welds in pipes, found that fatigue failure invariably started from the root of the weld (Figures 8 and 9) irrespective of whether or not a backing ring was used and whether the root of the weld was machined or not. Any additional defects, even such gross defects as those shown in Figure 10, had no effect in lowering the fatigue strength any further. In one particular case where fatigue failure started from the root of the weld the lack of sidewall fusion defect shown in Figure 11 was found after the broken specimen was examined and even this very serious defect could not compete with the overriding effect of the stress concentration in the perfectly sound and normal root of the butt weld.

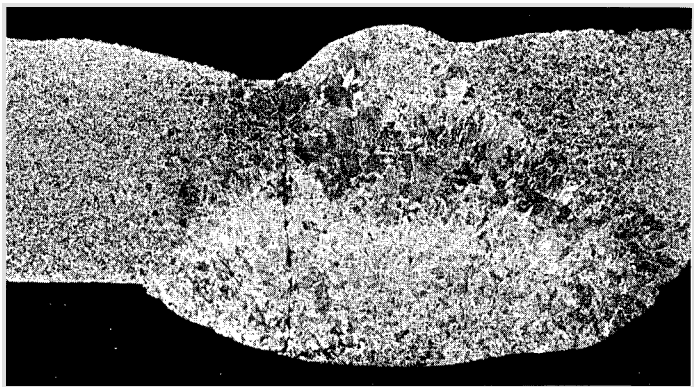

Figure 8. Fatigue crack in circumferential pipe weld starting from root overfill.

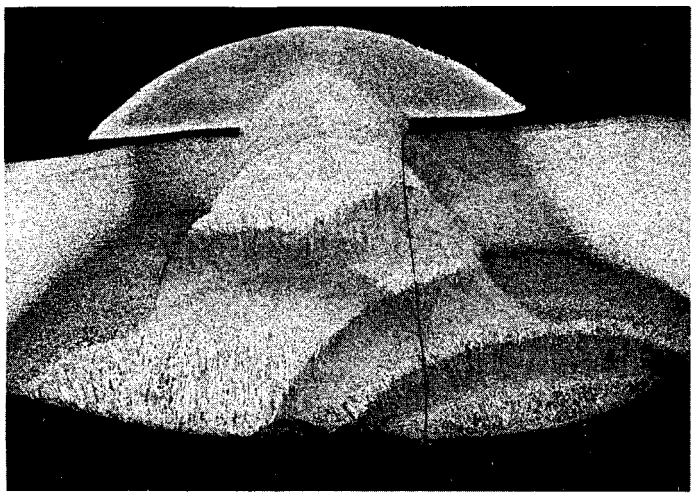

Figure 9. Fatigue crack in circumferential butt weld of pipe starting from notch between backing ring and pipe wall.

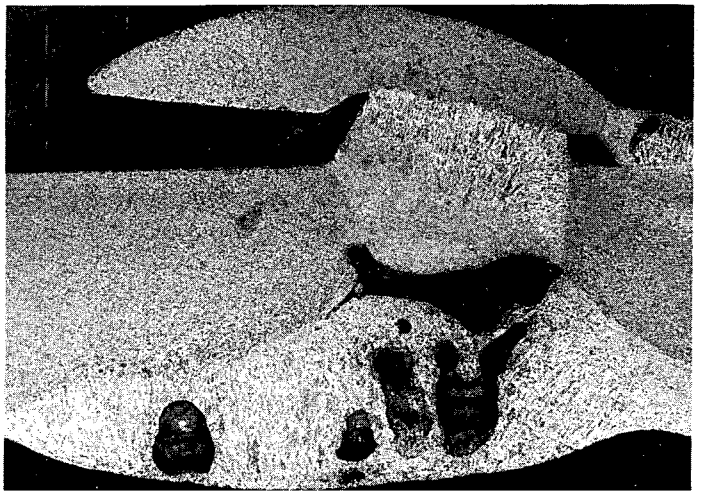

Figure 10. Gross defects in circumferential butt weld in pipe had no effect on bending fatigue strength. (Pressure strength may, of course, be reduced.)

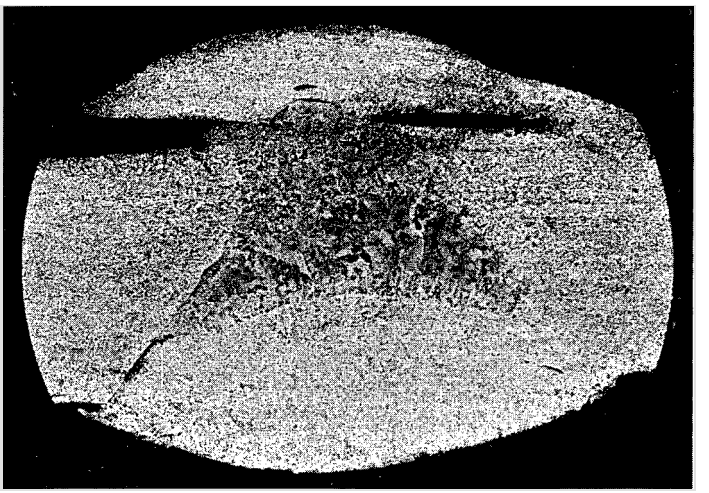

Figure 11. Lack of sidewall fusion in circumferential butt weld in pipe had no effect on bending fatigue strength of pipe. Fatigue failure started from perfectly normal and acceptable weld root.

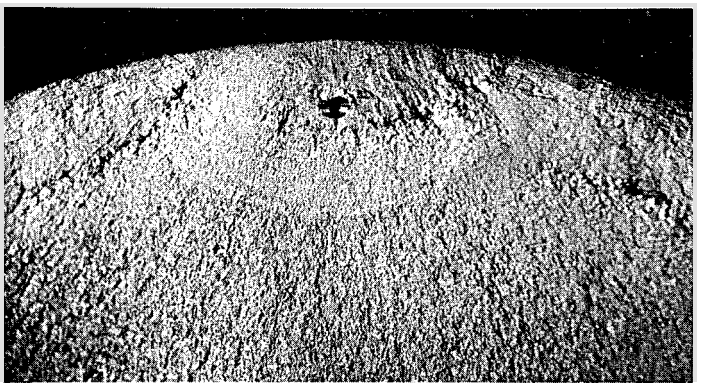

Figure 12. Fatigue failure starting from small subsurface pore in experimental shaft reclaimed by welding. The shaft prior to 'reclamation' was, of course, virgin material and had not suffered any previous fatigue.

In assessing the fatigue reducing effect of defects in welds one must consider first and foremost the over-all fatigue strength of the structure or component. Fatigue failure will start from the most sensitive point and this may not be—and very rarely is—a weld defect. The rolled surface of the plate itself produces a reduction in fatigue strength from 20 tons/in.^{2} to 16 tons/in.^{2} (Figure 7), the overfill of the butt weld produces a further reduction and so will any trace of undercut. What

stress concentration effects may be produced by defects may be simply swamped by the effect of other stress concentrations.

If, however, there are no other stress concentrations than those due to the weld defect even a single small sub-surface pore may produce fatigue failure and reduce fatigue strength. In a very extensive investigation of the problem where machinery shafts reclaimed by welding frequently fail from fatigue very soon after they have been put into service, Dawes (4) found that fatigue failure in 0.32% C steel shafts reclaimed by welding, and machined, would take place (at ten million cycles) at between ± 9.5 tons/in.^{2} to ± 11.5 tons/in.^{2} rotating bending fatigue stress, which he estimated to be only about 65% of the fatigue strength of the original machined but unwelded shaft, and that fatigue failure would originate even from a single small pore as that shown in Figure 12. This is not really surprising when it is remembered that a small pore will locally produce a stress concentration of nearly three, and that if this is the only stress concentration present in the whole of the shaft, fatigue failure will start from this pore and the fatigue strength of the shaft will be reduced, though as will be observed not to a third of the strength, i.e. not proportionately to the stress concentration factor.

A few examples presented in this survey illustrate the complexity of the general problem of tolerance levels for defects in welded structures. The subject is more complex even than has been indicated because the position of the defect in relation to the surface of the joint is important in joints made in thicker material. The location of a defect in a field of residual stresses, whether tensile or compressive, may influence the effect of the defect both on fatigue strength and brittle fracture strength. However, to make decisions on accepting or rejecting welds by ignoring all the experimental information now available is most unscientific and puts the engineer in the same class as the medicine man of a primitive tribe. Admittedly a great deal more experimental information is needed but enough is available already to show that the importance attached to certain types of defect is frequently grossly exaggerated and may, in fact, divert attention from other undesirable features in design and execution.

References

1. Newman, R. P. The influence of weld faults on fatigue strength with reference to butt joints in pipelines. *Trans. Inst. Marine Engrs.*, 1956, 68, 153-172.
2. Newman, R. P. and Gurney, T. R. Fatigue tests on ½-in. thick transverse butt welds containing slag inclusions. *Brit. Weld. J.*, 1964, 11, 7, 341-352.
3. ———— Fatigue tests on plain plate specimens and transverse butt welds, *Brit. Weld. J.*, 1959, 6, 12, 569-594.
4. Dawes, M. G. Ferritic steel shafts reclaimed by welding and metal spraying. *Brit. Weld. J.*, 1963, 10, 8, 418-427.

Discussion

Q. RONALD HALMSHAW, Ministry of Defence (UK) RARDE, Sevenoaks, England:

Were the curves showing defect length against strength for various defects, based on a series of experimental results on actual welds? If so, were these welds stress-relieved or "as welded"?

How do these results compare with calculations based on fracture toughness theories?

A. The curves showing defect length against strength for various defects have all been obtained on the basis of fatigue tests with actual welds in the as-welded condition. Stress relieving may reduce fatigue strength still further, as has also been demonstrated experimentally.

I am not sure that I understand the second question because fracture toughness theories do not permit at present any prediction of reduction in fatigue strength.

Q. HERMAN GREENBERG, Westinghouse R&D Centre, Pittsburgh, USA:

I agree wholeheartedly with Dr. Weck's comments that we place undue importance on some types of weld flaws, namely porosity and slag inclusions; however, I cannot agree as to lack of fusion and crack-like flaws. I am somewhat surprised that Dr. Weck did not utilize fracture mechanics concepts and data in his presentation nor did he utilize K_T concepts when considering the effects of flaws on fatigue strength. I am very much opposed to the concept of hydrostatic tests at 1½ or 2 times the service pressure for fear that these high stresses will rupture the metal between nonmetallic inclusion concentrations and subsequently cause failures which otherwise would never have occurred.

I would appreciate receiving a copy of Dr. Weck's paper in order to prepare a formal discussion for the proceedings.

What is being done to change the British acceptance standards for weldments?

A. Recent experimental work carried out in the laboratories of the British Welding Research Association has shown that lack of fusion and certain crack-like flaws are not as serious as one might have expected, although of course they produce a decidedly greater reduction in fatigue strength than porosity and certain types of slag inclusions. There is no evidence to show that the K_T concept has been adequately developed in relation to fatigue, particularly in relation to ductile materials, to permit reliable application of fatigue strength reduction from flaw size.

I am not sure what Mr. Greenberg means by "acceptance standards for weldments" but in Britain no such standards exist in the sense of the porosity charts in the ASME Code.

Q. J. E. BENSON, Canadian General Electric Co. Ltd., Peterborough, Canada:

The last illustration of Dr. Weck's paper was apparently intended to illustrate the serious effect of a small defect compared with the small effect of previously shown large defects. It seems likely that the real cause of failure of the welded shaft was the residual stress resulting from the weld and that failure would have occurred even if the defect had not been present. Do any of the discussors wish to comment?

A. Mr. Benson's presumption that failure would not have occurred if the shaft had been stress relieved, is quite erroneous. Stress relieving, as has been shown by experiment, makes no difference to fatigue strength; in fact it could reduce the fatigue strength still further as compared with a shaft in the as-welded condition if the heat treatment produced surface decarburization.

The reason why such a small defect has such a pronounced influence on fatigue strength must be seen in the fact that the fatigue strength of the shaft is very high compared with the fatigue strength of unmachined components.

Q. JOHN KEITH PARKINSON, Montreal Locomotive Works Ltd., Montreal, Canada:

Would you comment on the present practice of welders stamping an identification stamp adjacent to the weld, often in H.A.Z. This is with reference to your comments on the effect of a small undercut or of over fill on the strength of the weld.

A. The practice of stamping cannot be condemned too severely whether the stamp is in the heat affected zone or not. In certain types of steel, severe work hardening and strain ageing can occur and there are quite a number of failures reported in the literature which have been initiated from the sharp notches made by inspectors' stamps.

The Detection and Identification of Weld Defects

A. de STERKE, NETHERLANDS

General Aspects and Definitions

Since the particular branch of nondestructive testing sometimes referred to as "defectoscopy" is unfortunately still suffering from vagueness in many respects (contrary to nondestructive measurements), there are a number of questionable subjects on which to focus attention. There is, to start with, the expression "weld defect".

It is questionable whether the use of this term is justified, as long as the significance of the imperfection is not established. As such there is a certain contradiction in the title of this paper. Once an imperfection has been identified as a discontinuity which, based on the present knowledge of its significance in relation to service performance, is detrimental, the term "defect" is justified.

Meanwhile it is worth mentioning that most of the studies to evaluate weld defects refer to their influence on mechanical strength. In many cases, however, it is not so much strength, but surface condition, which determines their significance. In this respect, gas inclusions, rather harmless as far as their influence on strength is concerned, may be unacceptable if they tend to increase the risk of leakage. If they are open at the surface they may impair, with surface smoothness and consequently with corrosion, resistance and cleanliness. Thus, discontinuities may be unacceptable in one case and called defects while in another situation be regarded merely as an imperfection.

From this consideration it becomes obvious that identification of discontinuities is very important. However, identification is always the second step in defectoscopy; first comes the *detection* of inhomogeneities.

It is essential to differentiate between these two aspects of nondestructive examination as the requirements for each of them, with respect to the appropriate nondestructive testing techniques, differ.

For instance, in radiography, the detection is mainly determined by the exposure technique, but the identification by the conditions of viewing.

Another example can be found in ultrasonic testing where the detection of imperfections calls for a reasonably wide spread of the ultrasonic beam while on the other hand the identification can better be accomplished by the use of a more or less pencil-like beam. With a narrow beam the determination of shape, location, orientation and size can be better accomplished.

No doubt for detection and identification there are different requirements.

It seems worthwhile to define more closely first of all what has to be understood as detection and what is meant by identification in this connection.

Detection

This can be defined as the possibility of readily and clearly indicating the presence of a discontinuity in material by a nondestructive testing method, in an economically justifiable way. Obviously in this definition vagueness is still present; for instance what is meant by "readily indicate"?

This seems a rather flexible expression and the same comment also applies to the provision "economically justifiable". These two requirements are, after all, very closely connected because the examination must be of such a nature that it can be matched with production or, at least, it should not cause a prohibitive delay in the delivery of the finished product.

The speed of examination, however, is very much determined by the testing sensitivity required. It is therefore very important that the tests are based on well considered standards of acceptance, stating at least the nature and minimum size of the defects to be revealed.

The time required to repair any unacceptable defects found cannot of course be considered a part of the nondestructive test, but it is an extension of the production time needed to obtain the required quality level. It should, however, be realized that the speed of examination can be considerably influenced by the amount of discontinuities present in the piece under test.

This is particularly true for manual ultrasonic weld testing, where every imperfection demands special attention and the question of what is or what is not economically justifiable is difficult to answer. It cannot simply be settled by stating a given percentage of production costs. For example in less critical structures 1% or 2% of the processing costs may be thought high, but in other cases it may be economically justified to spend as much money on testing as on the production of a certain part when it has a key position in a critical structure. It is not only important to consider the production costs of the particular component, but also to appreciate the consequences and the cost of failure.

What should be understood by "clearly indicate" in the definition given? An experienced operator will observe a flaw indication, for instance, during ultrasonic testing, which may be unnoticed by the unskilled observer until his attention is drawn to the particular indication on the screen. The same may apply in radiography, where fine details like cracks should be discerned; they also may remain unnoticed to the untrained observer until an experienced person indicates their existence.

It seems therefore to be reasonable to accept that the statement "clearly indicate" refers to the situation where a nonexpert, once informed about a particular flaw indication, is able to see it and to differentiate it from irrelevant indications. To express the definition still more clearly, one can consider the opposite situation.

It is not true to claim viable defect detection when a multitude of operations are required involving an unreasonably long testing time and putting the testing costs on an economically unacceptable level.

With regard to the second step in testing, that is the identification, a similar definition can be given.

Identification

Identification can be defined as the possibility of readily characterizing discontinuities in a material by nondestructive testing in an economically justifiable way, stating their nature, shape, precise location, orientation and size. From what is known today about the influence of weld defects on service performance, it is obvious that identification in this sense is of paramount importance.

On the other hand one is inclined to question the use of sophisticated nondestructive testing methods to reveal small internal imperfections in conventional welded structures. Would it not be better to spend the money devoted to testing on achieving smooth merging contours in the welded joint? Care-surrounded structures like nuclear reactors, air- and spacecrafts obviously call for still further perfection of nondestructive testing methods, but do normal structures require this attention?

Nondestructive testing engineers would certainly appreciate somewhat more guidance as to the future developments and requirements in the different branches of industry.

Detection of Weld Defects by Radiography

The most widely accepted nondestructive testing technique for welds is still radiography, as long as the thickness does not exceed 2 to 3 in. It therefore seems reasonable to consider first the aspects of radiography in connection with flaw detectability. Starting with the most simple case, the butt weld, there are no severe problems in the detection of the so-called three-dimensional flaws, at least when their dimensions exceed 2.5% of the material thickness. Lower percentages mentioned as a criterion for image quality, for instance 1.5%, refer to discontinuities which are relatively long, for example like the wires found in the wiretype image quality indicator.

However, this low figure is not valid for local discontinuities of a restricted length, for instance a spherical inclusion. Nevertheless the sensitivity of radiography to detect such three-dimensional flaws is generally considered to be adequate.

In view of the data which predict their influence on strength, it seems that improvements in radiography in this direction are redundant.

In the case of the so-called two-dimensional defects, the picture is quite different and in fact far less acceptable. Although the same percentage may be valid for crack-detectability, it is assumed that the crack has sufficient width, and runs nearly parallel to the direction of the passing rays. The detection of two-dimensional defects is therefore the weakest point of radiography.

Although for some ten years the general opinion was not too pessimistic about this characteristic, one was inclined to suppose that, at least some parts of a crack would run reasonably parallel to the direction of radiation; comparative radiographic and ultrasonic studies show more and more that the situation is not that favourable. This, in the first place, should lead to some caution, as soon as radiography reveals the presence of a crack and be a reason for further investigation.

After all, cracks found either in the weld or in the heat-affected zone are the most serious defects; they indicate some severe condition with regard either to weldability or to residual stresses.

This observation leads to discussions on acceptance criteria of defects and is, as such, outside the scope of the present paper but a further elaboration would certainly be worthwhile.

It does lie within the scope of this paper, however, to consider what measures could be taken to improve the situation and achieve the best possible results in radiographic crack detection. Should the use of more appropriate fine-grain film emulsions be advised? Here the fine grains improve definition and the steeper film characteristic may improve contrast. However, a slower film requires a relatively longer exposure time. If a normal grain film for the detection of three-dimensional defects were chosen, the selection of a fine-grain film for the detection of two-dimensional cracks introduces a factor of five to seven in the exposure time. Would it not be better to accept the coarser grain film but make better use of time by increasing the number of radiographs instead?

It would be possible to extend the radiographic examination by angular shots at the same weld location. For instance five exposures; the normal shot, plus two extra exposures on either side of it, taken at angles of 10° and 20° from the normal. Clearly the angular shots require a longer exposure time because of the greater material thickness to be penetrated and therefore this technique does not seem very practicable.

Investigations show that for cracks longer than 10 to 15 mm there is only a minor improvement in crack visibility when normal and fine-grain films, differing not less in speed than a factor 7, are used. The visibility of short cracks and small inclusions is improved by the use of fine-grain film.

As the exposure time may be set for economic reasons (and this is often the case) the use of fine-grain films calls automatically for the application of harder rays. The result is that the desired gain in definition and contrast is almost eliminated by loss of contrast due to decreasing half value layer.

If, for the moment the favourable possibilities of ultrasonic testing in connection with the detection of two-dimensional flaws are not considered the best use of the testing budget can be made by taking a maximum number of low kV exposures on normal grain film. For the detection of lack of side fusion, angular shots are not so much a game of chance and may give better results, particularly when the unfused areas are of appreciable width. Besides, their presence can often be deduced from the appearance of accompanying inclusions.

The examination of fillet welds is, in general, much more complicated. Nevertheless three-dimensional defects can be found reasonably well.

The detectability of two-dimensional defects is still more difficult than in a normal butt weld. Generally, relatively high energies are used to obtain low-contrast over-all pictures in spite of the thickness variation inherent to the type of weld.

Notwithstanding the restrictions which have been highlighted there are no serious handicaps in the application of radiography. It is practically insensitive for the weld structure, which makes it the only practical method for the detection of internal weld defects in austenitic structures and, with increasing thickness, the detectable thickness variation improves.

For detection of three-dimensional discontinuities, radiography is almost ideal. The chief requirement is the correct selection of radiation energy for the given thickness to obtain optimum results.

In normal radiography focal-spot size plays a far smaller part than is often believed on the basis of conventional considerations of geometry. For the three-dimensional defects it is of no practical influence on defect detectability and for two-dimensional defects it may even effect a small improvement.

The situation is different when direct enlargements are made, a technique which is worth more attention; the influence of focal-spot size may then become a dominant factor in film unsharpness. Meanwhile improvements can still be made.

In particular, radiologists are still worried when they observe that at least 80% of the total film density in cobalt gamma radiography on four inches of steel is due to radiation scattered in the object and only the remaining 20% is caused by the primary beam. Also the use of lead back-screens is questionable; they seem useful to obtain a specified density, but add little or nothing to the formation of the image of the weld since their intensifying effect comes mainly from radiation scattered in the back-screen. It is a much better practice to use copper screens for cobalt radiography; however, an exposure 3 times as long is then required.

Some remarks inviting criticism, may conclude this paragraph. Suppose the existence of fine cracks in a particular welded structure is likely and creates risks. In this case use of fine-grain, high-contrast films is recommended, unless the radiographic examination can be supplemented by ultrasonic testing. A peculiar situation may sometimes arise when structures are made to general specifications not requiring fine-grain films but indicating at the same time that all cracks are unacceptable.

What should be done when crack-like indications are found, hardly visible on the coarse-grain film?

It would seem sensible from the technical point of view, to select a better film. This viewpoint, however, is often questioned as it does not comply with the letter of the specification. "What one does not know causes no woe" sometimes seems, under these circumstances, more appealing than the collection of optimum information for subsequent critical analysis, a situation comparable to driving with welder's glasses in dense traffic to see less and feel safer.

A similar undesirable situation is found when ultrasonic testing is used as a supplement to radiography but where acceptance criteria are based on the information given by the film. A clear ultrasonic flaw echo signal is disregarded if not confirmed on the radiograph and yet it is likely that this very indication is obtained from a crack-like defect.

Detection of Weld Defects by Ultrasonics

Again confining our subject to detection in the first place, we observe that ultrasonic testing is much more influenced by characteristics of the weld to be examined than is the case in radiography.

The most important factors are: 1. surface condition (influence on coupling and beam distortion); 2. geometry (influence of weld contours, backing strips, etc. on occurring irrelevant indications); 3. condition of the parent metal (influence on attenuation, scattering and occurrence of shadow effects due to laminar discontinuities); 4. structure of the weld (influence on sound propagation of austenitic structures).

Another important factor, much more important than in radiography, is the quality of the operative, particularly if manual weld scanning is involved. Not only his skill but also the means and abilities at his disposal to perform correct equipment calibration are most essential and determine the success or failure of the test.

In general, ultrasonic testing is regarded as the best method with which to detect internal two-dimensional discontinuities. In the absence of a better method, some restrictions must be recognized, for example, with decreasing width slits become transparent to ultrasonic waves and the critical condition is approached when the slit opening falls below 10^{-7} mm. Although this seems extremely small, even more severe conditions may exist when cracks (or other two-dimensional discontinuities) are present in the central region of a weld; due to stresses developed by contraction of the weld metal the surfaces of such a discontinuity may be pressed so firmly together, that the reflection factor approaches zero. Their detection before stress relieving (if at all possible) would require much higher frequencies than are normally used and may appear impracticable. Another risk in ultrasonic crack detection, often overlooked, is the increase in directionality of the reflected beam with increasing flaw size. Cracks large enough to be found radiographically may be missed during the ultrasonic test, very much to the surprise of ultrasonic advocates; however, the use of two ultrasonic probes in tandem soon brings the excitement down to an acceptable level. Whenever such a situation arises, for instance when lack of side wall fusion is expected, a single-probe scan should always be complemented by double-probe scanning to reveal gross defects, having smooth surfaces.

The possibility of finding small imperfections by ultrasonics has been shown for many years, but it will be appreciated that the results of laboratory tests yield no direct measure of test sensitivities which may be achieved in practice. As a guide, an experienced operator can detect, during a normal routine weld inspection, discontinuities having minimum dimensions of length 5 mm and depth 2 mm; even a defect 1 mm in depth may be found if it is located near to, or at, the weld surface, irrespective of the weld thickness.

The limiting factor is not so much a matter of equipment or technique but to a far greater extent the human factor, which is involved in the combined action of physical scanning, observation and the mental correlation of the observations with the internal weld condition. This takes time and as the signal-to-noise ratio decreases, more and more time is needed; this implies that the ultimate limitation lies in the presence of irrelevant indications.

It is outside the scope of this paper to describe techniques but a number of publications cover this subject already.

Detection of Weld Defects Magnetically

Detection of imperfections at the surface of magnetic materials is most commonly accomplished by the magnetic-particle method. The use of the so called magnetographic method, whereby the strayfield pattern is transferred to magnetic tape, has certain advantages in that it is more sensitive for the detection of subsurface defects.

However, the method is still in the development stage and, for surface inspection, it is not yet of sufficient interest, unless inspection on a mass production system is envisaged. The conventional magnetic-particle testing is a very reliable and sensitive method for the detection of surface defects.

While surface condition certainly has some influence—the smoother the better—shape and dimensions of the object have no appreciable effect when the prod method is applied. In addition, the influence of structure and plate condition are insignificant in the case of normal carbon steels. The heat affected zone in high-strength steels might show sufficient difference in permeability to cause a magnetic leakage field, and consequently a magnetic indication can be obtained. In comparison with radiography and ultrasonic testing the method offers more reliable and clearer information on surface defects at less expense.

For the detection of internal or even sub-surface defects in welds it is, in general, not a good method. Polished surfaces are then required and relatively high current densities should be applied to obtain reasonable results. Selection of the magnetizing current strength is much more critical than in the case of surface inspection and should be related to the optimum value of the relative permeability during magnetization.

Very little data on the minimum defect size which may be found in a particular material thickness are available. The detection of a 20-mm-deep crack in a 25-mm-thick weld is certainly possible, but most people think defects must be revealed in terms of a few per cent of the thickness. Under ideal conditions (polished surface, etc.) for a plate having a thickness of 25 mm, a 15-mm-deep crack located 10 mm below the surface gives only a very faint indication. A 3-mm-deep crack should be as close as 6 mm below the surface to be revealed under ideal conditions.

Detection of Weld Defects by Penetrant Testing

There is little or no doubt that penetrant testing is a most practical method for the detection of surface defects in non-magnetic materials. However, this does not imply that it is also the most simple method and that, for this reason alone, it could replace magnetic-particle surface inspection when normal steels must be examined. The difficulty in making a satisfactory penetrant test is often underestimated and this may be partly due to the name, which suggests that penetration

is the most important factor in the effectiveness of the test. This in fact is not true. It is correct to say that unless liquid has penetrated into the defect the method cannot work but unless it comes out again, and interacts with the developer, no defect is shown.

There are many unsatisfactory ways of removing the penetrant from the component and unfortunately, due to lack of appreciation of the method, they are often applied. First of all, excessive washing spoils the indication. Washing must take place in such a way that background indications due to normal surface irregularities are only just removed. Another fault in manipulation lies in the application of the developer. If a wet developer is used it should be applied with a minimum of liquid carrier as this also may wash out the remaining penetrant liquid from the defect. It is often overlooked that the finer the imperfection the smaller the quantity of penetrant liquid taken up in this minute reservoir and the more reason to treat it with the utmost care.

Misleading effects may also be due to insufficient drying time after pre-cleaning and the excessive use of developer, as a layer of developer which is too thick may conceal the indication.

Identification of Imperfections in Welds

Since not all defects have the same influence on service performance, their identification (once detected) is important. There is still another object in their identification, namely the initiation of remedial or, even better, preventive action. Identification of imperfections from the indications produced requires basic knowledge of the material in which they occur. For weld examination it means that weld shape, welding process etc., must be known, otherwise a good interpretation of the indications is very difficult to achieve, if not impossible. This is true for all methods of examination and important as this is such basic information is also required to establish an optimum technique of examination.

To set significant standards for the acceptance of weld defects one assumes that all defects present in the weld can be detected, identified and measured by some nondestructive testing method. The last aspect seems the most problematical, as flaw-size determination is still a source of much trouble. In the following, the four main methods of testing are considered again, but from the point of identification alone.

Identification by Radiography

Until now the radiographic image offers the best possibility for the identification of internal weld imperfections, although there are some restrictions. In the full sense of identification one would like not only to characterize the nature of the discontinuities present, but also define their shape, position, orientation and size. Flaw depth, orientation and size cannot be fully established from the radiograph alone but may be guessed when weld shape and welding process are known.

The only way to measure flaw size depends on density measurements, a rather tiresome and not very accurate method. Microdensitometry, providing correct steps have been taken for calibration, may offer some possibilities but it is increasingly inaccurate with decreasing flaw width—yet then the flaws become most interesting. On the other hand radiography provides an extremely good impression about the nature, length and distribution of the discontinuities in a weld, and a reasonable impression of their shape.

With regard to the determination of their nature, a good deal of experience is required for good interpretation, in particular when the imperfections are located in an area common for different types, e.g. incomplete penetration and incomplete root fusion.

The radiologist often bases his interpretation on previously made sample radiographs, the particulars of which have been checked by subsequent destructive tests. Moreover general collections of reference radiographs are useful to put the characterization and grading of the discontinuities on a common footing. The situation is still open for much improvement; not only should existing collections of radiographs be brought more up to date and be subdivided for different types of welds but also the essential element in the interpretation of radiographs, namely viewing, deserves more attention. The major efforts put into better radiographic practices designed to gain only a small part of one per cent in sensitivity are in real contrast to the rather simple conceptions one meets with regard to film viewing.

Of course barbaric film viewing against the sunlight window is out of date but nevertheless the results of sophisticated radiographic techniques are often diminished by the application of old fashioned viewing practices. The tendency to increase film density in an endeavour to obtain better contrast is not matched by the instalment of suitable film viewers.

Good viewing of radiographs having a density of 2.5 requires a brightness of at least 10.000 Lux. A good film viewer should furthermore have adequate brightness-control over a range from 100 to 30.000 Lux, sufficient cooling to prevent film damage, facilities for film masking and possibly automatic dimming or closing when the film is removed. For optimum viewing a little more attention should also be paid to the optics behind it. After all, we deal with two emulsions, the pattern of which should be accurately superimposed.

Ultrasonic Identification

To identify defects in ultrasonic testing is a much more complicated, a much more difficult and mostly a very lonely task. In critical circumstances the ultrasonic operative, lacking the encouraging remarks normally surrounding his colleagues in the radiologists group, and far from the stimulating atmosphere of the viewing room, has to find out the facts for himself on site, warm or cold, dry or wet, high or low.

Walking along the boundaries of unbelief he is engaged in a continuous struggle between responsibility and looking for trouble until he reaches a conclusion, in spite of the optimist who created the specification in the firm belief that conclusions are only drawn at a later stage.

The operative knows, and if he is wise admits, that porosity and similar small three-dimensional flaws, nicely presented on a radiograph, are difficult to detect in a routine scan, let alone identify individually. But identification of large discontinuities is not always simple either. It requires a great deal of skill and, besides good equipment, a set of well selected probes. Flaw identification from the appearance of its echo signal indication alone is like identifying a person from his silhouette. A characteristic nose would help, providing he faces in the right direction.

Secondary circumstances—for instance, movement—may disclose further characteristics, also in a metaphorical sense. Fundamental particulars for identification are derived from flaw location. Great accuracy is therefore exercised in calibration and in locating techniques; preferably location is made in a direct scan. Subsequent scanning is necessary to discover the orientation and reflecting properties of the discontinuities. Compared with radiography there are certainly some advantages with respect to identification, e.g. the possibility of determining quite easily the depth and orientation of the discontinuity.

However, determination of nature and shape is much more difficult and with the present ultrasonic equipment it is nearly impossible to differentiate between gas cavities, slag inclusions, and little cracks. It is mostly the location of the defect which brings the experienced operative to a cautious statement. He is faced with a similar problem when two-dimensional discontinuities must be distinguished.

Is it a crack, lack of fusion, or is it a lack of fusion ending in a crack? Is it incomplete penetration, lack of fusion in the root or a crack in the rootlayer?—many questions, to which it is very difficult to give a definite answer.

It may be that it is not necessary to look for such a degree of accuracy in identification, providing three-dimensional discontinuities can be well separated from two-dimensional flaws of appreciable size. But what is appreciable size and how can it be assessed? This latter question leads to a more detailed consideration of ultrasonic flaw-size determination.

In considering this problem the first thing to agree upon is the accuracy required. In view of the many factors playing a part in the ultimate influence of weld defects on service performance, it is a little difficult to believe that an "absolute accuracy" (whatever this may be) is necessary. Should, for the time being an accuracy of plus or minus 2 mm be acceptable it would be a good deal closer to practice.

Two basic techniques for flaw-size determination have been developed. In the first place there is the technique whereby the probe is placed in an optimum position to receive a flaw echo and the echo signal height produced is compared with the indication from a known discontinuity (flat bottomed hole, saw cut, etc.). Since all of these artificial defects are ideal reflectors (air-filled, smooth and flat) they produce greater echo indications than real weld imperfections, which are irregular and often filled with matter having an acoustic impedance much closer to that of the metal under test.

A similar principle is applied when calibration curves are used, such as AVG diagrams of Krautkramer.

In the other size estimation technique, the probe is moved to obtain the full envelope of the flaw-echo indication and from the dynamic screen image thus obtained a certain estimate of flaw size is made.

Both methods have their advantages. The first method is rather simple in its application and particularly suitable when the orientation of the flaw is known. However, deviations from normal incidence of some five degrees reduce the accuracy by more than 25%. Another disadvantage is that the total reflecting area is responsible for the echo obtained and it is impossible to differentiate between the length and depth of the flaw.

In this respect the second method offers better possibilities but here the probe characteristic should be determined precisely before any measurement of flaw size can be made. Theoretically the method works alright; however, in practice it is rather complicated and requires great skill and well selected probes to establish the contours of the imperfections. This is due to both equipment and scanning conditions. As far as the equipment is concerned, it is mainly the probe which gives rise to difficulties. Polar diagrams, according to the textbooks, have a rather simple shape but in practice can show considerable irregularities. The boundary of the beam is often not so well defined as expected and sound distribution in the beam may have an irregular pattern. Some probes show a very peculiar polar diagram and in some cases one is even apt to think that the beam has no single axis, but more. It is obvious that this circumstance makes flaw-size determination complex. After all, a rumpled ruler is not a very useful aid to measurement.

Investigations to determine beam characteristics more accurately are going on in many laboratories. They are hampered by the fact that no suitable beam calibration blocks have yet been developed. But it is to be expected that they are soon to come and that, from then on, better specifications for the requirements of probes for flaw-size determination can be given. Although the use of well selected and calibrated probes is essential, other features of the equipment, for instance paralax-free C.R. tubes (having the scale marking at the inside of the tube) are also important.

With regard to the conditions of examination it should be borne in mind that variations of coupling during manual scanning and inaccuracies in probe manipulation may already introduce amplitude differences of 10 dB and this consequently may result in inaccuracies in the measured flaw size.

Identification of Surface Defects

Whether found magnetically or by the penetrant method, identification of surface defects can best be accomplished by normal optical methods.

Sometimes grinding or polishing may be required to determine the true nature of an imperfection under the microscope. Attention should be given to magnetic indications caused by local differences of permeability due to structural changes, for instance at the boundaries of the H.A.Z. The length is easily established and today fairly reliable equipment is on the market to determine the depth.

In the case of sub-surface flaws, their identification is very difficult. Also in this respect magnetic-particle testing is not of much use for hidden flaws.

Observations

Some general supplementary observations can be made:

a) the several nondestructive tests mentioned are complementary: in some cases, application of two or more methods is advisable to obtain the best picture of the internal weld condition.

b) the extent of nondestructive testing should be related to the materials and joint details involved and, also, the service conditions should be taken into consideration, so that the most sensible test may be chosen.

c) the examination of welds with complicated shape, for instance connections of muzzles, is in general very difficult and yet such welds may represent the most important areas with a view to occurring stresses.

d) in many cases the nondestructive test should be regarded as a means for quality control, a guidance for welding technologists and for the welding operation rather than a search for defective welds which need repair.

e) the examination of welds in austenitic steels in thicknesses over 2 to 3 in. is an unsolved problem as far as crack detection is concerned.

Discussion

Q. PIERRE RUAULT, Gaz de France, France:

The author thinks that the size of the focus has no great influence on detection of defects of three dimensions. How does he explain the decrease of the IQI values when the size of focus increases?

Why does the author say that contrast is improved by a decrease of photon energy, without influence of film-grain size?

The quality of a radiographic result relies on three factors: namely, film quality; quality of the man looking at the negatoscope; examination conditions. How does the author appreciate the

part of failure coming from every one of them? Has the author an analytical method of judging separately every one of these three influences?

A. With regard to the first question raised by Mr. Ruault, it is the author's belief that for those three dimensional defects which seem detrimental according to the present knowledge, there is no appreciable influence on its detectability when one considers the normal range of focal spot sizes used in radiographic equipment. It is true that higher IQI values can be obtained with decreasing focal spot size. However, in practice the unsharpness of the contours of significant three dimensional defects do not interfere with their detectability.

If radiography is applied to search for cracks, which in fact is a questionable subject anyway, it is from the scientific point of view necessary to strive for the best possible image quality, which can be derived from an IQI. However, I do not believe that an IQI figure gives an indication for crack detectability.

Regarding your second question, I do believe that the radiographic contrast is improved with decreasing photon energy and unless insufficient measures are taken to prevent scattered radiation from reaching the film, also increased film contrast may be expected. Influence of radiation energy on film grain size is well known and is proved by practical investigations.

On the third question, I feel that this was outside the scope of my presentation, however, I must admit that I have no analytical method to judge separately the influence of film quality, quality of the observer and influence of viewing conditions on the ultimate detectability and identification of weld defects on radiography.

Recommendations of viewing conditions are the subject of study in IIW Commission V sub-commission A, in which also the eyesight of the observer will be taken into consideration. It is obvious that here also other factors play a part, for instance fatigue of the observer, and available reading time per film, depending on the number of films he has to read per day.

Q. N. O. CROSS, Esso Research and Engineering, Florham Park, USA:

In the use of angle beam U.T. examination we have verified the difficulty in correlating signal amplitude with discontinuity size for certain slow shapes and geometrics. Does not the use of some system which can quantitatively record the change in CRT echo profile or envelope shape as the search unit is traversed across the flaw appear as a reasonable approach to evaluating not only the area and predominant type (planar, spherical or cylindrical) of the discontinuity?

A. The remark of Mr. Cross points to one of the difficulties still encountered in ultrasonic testing.

I believe that the suggested record of flaw echo envelop contains indeed information about both area and nature of the flaw. The accuracy with which the area can be estimated depends largely on the orientation and reflecting properties of the flaw. Generally one would apply this method of flaw size determination when discontinuities are expected being large compared to the wave length applied.

Q. RONALD HALMSHAW, Ministry of Defence (UK) RARDE, Sevenoaks, England

It seems to me that the author has greatly oversimplified the problems of radiographic techniques and so reached some false conclusions. For instance, in the radiography of 1-in.-thick steel welds, if one changes from a medium speed film technique to a fine-grain film technique, one does not usually increase the exposure time by a factor of 5 or 7: other parameters would usually also be changed, and it can be shown that by a slight increase in KV a better radiograph can be obtained with the same exposure time.

Also the author's comments on the influence of X-ray tube focus size, were based on experiments with high-energy X-rays. They are not applicable to lower X-ray energies.

A. With regard to Mr. Halmshaw's comments I must confess that some of my remarks can be regarded as simplifications. As I remarked in the introduction of my paper I was invited to submit a provocative rather than didactic contribution and it is difficult to achieve such a situation if no playground is left for discussion.

Nevertheless I think that from the practical point of view my statements are not *per se* leading to false conclusions. Suppose the filmtypes under consideration are Kodak Industrex D and Kodak Microtex. Here a factor of nearly 7 is involved. For the thickness Mr. Halmshaw suggests of 1 in. of steel, an exposure of 15 mA. min. would require 205 kV to obtain (on Kodak D) a density of 1.75 with 0.125 front and back lead screens.

To obtain the same density on Microtex requires, for the same exposure of 15 mA.min., a kilovoltage of at least 280 kV. This means an increase of 75 kV, which in my appreciation is not a slight increase.

It would require the use of heavier radiographic equipment, which is no real drawback for tests in the factory but has no doubt its influence on working pace in the field. Since the basis of the observation in my paper was the best use which can be made of a given testing budget I still think there is room left for further discussions.

With regard to the second part of Mr. Halmshaw's remark I would like to repeat the comment given above to Mr. Ruault, knowing that this is again an invitation for discussion. I fully agree that for lower X-ray energies the geometrical unsharpness is the dominating factor in the total unsharpness. Nevertheless it does not have great effect on detectability of three dimensional discontinuities of a size regarded nowadays as significant in classical medium stressed structures. As such my provocative remark was intended as a warning against an overestimation of the influence of focal spot size on detectability of three dimensional flaws.

Standards for the Acceptance of Weld Defects

ROY B. McCAULEY, USA

Past participation in the activities of the International Institute of Welding has taught me caution in the use of a term the translation of which may have a variety of meanings. One of these terms has been present in the title of every paper in this session. The term is *defect,* which is related to the term *defective,* and calculated to be classified with such crimes as murder, treason, etc. However, it is also possible to look at the positive side of this dilemma and say that the choice of such a word simplifies greatly the treatment of this paper. Obviously then, there can never be standards for the acceptance of defects and we must reject every part, welded or not, which has been proven to be defective through the containment of defects. Our choice at this point then is to reject the part or repair it. As we study the possibility of repair, we must determine whether repair is economical or whether reliability has been reduced as you modify these unnamed items to restore the product from the state of being defective to being acceptable. By this time it is necessary to turn our attention to the naming of the nameless items. After hours of attempting to determine the difference between the terms *flaw* and *defect* with my British colleagues, neither term seemed to be adequate. Perhaps the term *discontinuity* may fit. Certainly it is long enough to be adequately professional.

If the term discontinuity would serve, it has the fortunate capability of having its existence defined as a *physical inhomogeneity* without the prejudice of the term *defect.* The inhomogeneity can be identified and described with the effect upon product service, life or use, and hence a quantitative

acceptance may be determined. Standards then have as their purpose the defining of the limits of acceptability in the identification of the discontinuity by the nature of the intended service. These types of standards may then serve both in design and production as well as product development.

Probably one of the earliest and most powerful of the specifications to produce a reliable manufactured product is the Power Boiler Code of the American Society of Mechanical Engineers. In 1909 this group took the task of unification and modernization of the various boiler codes authorized by numerous states in the United States. In 1914 this society issued its first "Power Boiler Code". Since that time it has issued seventeen major revisions of the code, with numerous interim addenda. Probably much of the continued success of this code was a logical beginning. The logic was continued with the combined use of Design—Manufacturing—Inspection —Material—Safety—and Research. In 1914, the concept of design related to manufacturing and inspection through the code stamp, and the impartial boiler inspector was most effective. An addendum in 1930 recommended the use of welding. The use of radiography and penetrameters as reliability tools were recommended to gain the grade of Class 1 welding. Then the 1931 edition of the code incorporated these concerns and added fusion welding to the boiler manufacturing capability.

Since the beginning of the American Society of Mechanical Engineers pressure-vessel research and specification analysis have continued. Today some fourteen countries of the world have developed their own pressure-vessel specifications. Additional countries use these specifications but conduct independent research in their own country. However, the concern of each group for local problems or the tall tales carried from one country to another, (and suffering in the retelling) has caused a new crisis. For example, if a contract were let in Germany, Sweden, Holland, Finland or Czechoslovakia for a particular pressure vessel of mild steel for room-temperature service at a working presure of 600 psi, and sent to New Zealand for installation, the walls of the vessel would be just $\frac{1}{2}$ the thickness required by the code at the point of installation. The conditions for the pressure vessel are rather ordinary and the results show a great inconsistency between these groups. Perhaps the pressure-vessel specification groups have been more diligent about inter-country exchange of research and study than others. By this means they have been able to focus more attention on their problems. More often we find those who have no problems are either naive or dishonest. In addition the pressure-vessel groups have been the leaders in the direction of logical control of manufacturing for much of our industry. In fact, the lack of similar more appropriate manufacturing control by other industries, is a real concern at the present time.

It is recognized that standards are useful and a very important engineering tool. They tell a manufacturer what is required of him to permit a fair price or bid to be submitted and a clear contract and execution to be accomplished. These standards permit the buyer a measure of the performance of the industry and a measure of the product. Without these necessary assurances many miscarriages of contractual manipulation may be accomplished.

On the other hand, certain negative problems also arise from standards. Tests for materials and assemblies may remain primitive and naive because of the fear that more complex tests with less accurately defined interpretation may cause confusion. Design may become over-simplified and discourage the desire or initiative of study groups to investigate newer and more venturesome product configurations. Standardization may lead to fixed prices where, because of the risk of capital equipment, new methods may be discouraged. Often the performance asked of new processes and materials cannot be answered by current methods. The question may then be raised whether or not present techniques are being reviewed with the purpose of examining current acceptance criterion.

Probably one of the earliest specifications concerning the evaluation of weld discontinuities in the U.S. was an Ordnance Department specification of the U.S. Army AXS-476 dated July 15, 1939. Here a series of reference radiographs were collected and classified as to the type of weld, fillet or butt (groove) and the type of discontinuity. These radiographs were further qualified as to whether the indications were acceptable, border-line acceptable or not acceptable. Rejectable defects were listed as:

1. Porosity (uniformly distributed, linear or cluster distribution); 2. Slag inclusions; 3. Improper fusion (incomplete fusion); 4. Incomplete penetration (inadequate joint penetration); 5. Undercuts; 6. Cracks (longitudinal, transverse, crater and plate cracks); 7. Lack of prescribed fit.

The scope of the standard is noted as applicable to all ordnance material for which radiography is required. Additional methods of inspection and the use of penetrameters was also described. The type of radiographic exposure by example suggested a single radiograph in the direction perpendicular to the surface with film, if possible, parallel and close to the surface, except in the case of a fillet weld where it was nearly 45° to the surface.

In general the standard in 1939 drew from the experience of a supply of radiographs of the type of manufacturing typical of a fabrication at the time. The authors were attempting to up-grade the current welding quality by revealing to the manufacturer the nature of the weld soundness. Cracks were not permitted, however, it is quite unlikely that many cracks would be revealed by the inspection procedure. Inspection seemed directed to revealing longitudinal cracks in the fillet weld and other discontinuities such as crater cracks and cracks perpendicular to the surface, in butt welds. The likelihood of finding other configurations is a gamble. Porosity is considered and tolerated. Comments about pores—10% of plate thickness in $\frac{1}{2}$-in. plate material and 7% of plate thickness in $2\frac{1}{2}$-in.-thick material with single cavities whose maximum length equal plate thickness are noted. However, the illustrated examples almost rule out linear and cluster porosity. Slag was permitted in single lengths up to $\frac{1}{3}$ T, with the seam of lengths no greater than T in a 12T total. T is equal to plate thickness. Distance between inclusions must exceed 6 times the length of the longest inclusion. When imperfect fusion, incomplete penetration and undercut were revealed, these discontinuities were then called to the attention of the inspector, and his decision was then based upon the conditions of service. Warnings of a process out of control indicate that these conditions would be called to the attention of the manufacturers.

It might be assumed that the design agencies were aware of the current quality of manufacturing and considered the "typical soundness" in their calculations. Surface analysis was the problem of the visual inspector and it is assumed that he used his own criterion of good surface appearance and symptomatic indications. The earlier pressure-vessel codes solved the surface problem by grinding or blending. The ordnance group did this in part; however, many welds were left in the "as welded" condition and became a problem of inspection. Surface inspection aids to visual inspection such as magnetic-particle and liquid-penetrant techniques greatly assisted the visual methods.

In rapid succession various additional supplements concerning the nondestructive testing procedure followed to

improve the X-ray or X-ray image. Still, however, the geometry of the fillet weld and the single exposure by radiography persisted. This also was coupled with the rather variable concept of where inspection was to be used. Should the radiography be of 100% of the welds, of the structure, or how should the burden be carried? On occasion when radiography began to be a sample lot program, repair caused a manifold increase in the amount of inspection. With this acceleration in manufacturing cost, both the buyer and seller became concerned that inspection became an open end in the purchase agreement. To the bidder it seemed that with some small inconsistency in manufacturing he could suffer a substantial change in cost. For the buyer, he was concerned for his product with the numerous repairs required. For many years these two groups sat down together to develop specifications which each could understand and use in process and manufacture. The bidder was usually concerned about less inspection to reduce price, and the buyer concerned that he had adequate inspection to assist in a guarantee of serviceability.

The term *serviceability* then became the concern of many groups. A review of inspection criteria which are not related to design were of the first order of business. However, while it was possibly not true in all areas, the costs relegated to serviceability testing seemed to discourage study in this realm. Some designers began to consider the concern of the state of stress in service with the design analysis. However frequently between the time of the final blueprint and the finished manufactured part numerous expedient modifications frequently took place. Even the designer could not be sure that the design stress analysis was still valid. Although the need for final product analysis from the viewpoint of both a design verification and a basis of in-service study was obvious, the cost of testing time delay caused hasty decisions to terminate manufacturing, and to ship.

Such problems as plate laminations caused concern. However when the extent of laminations became considerable, it caused an analysis of the expediency of the project. All too often the weld which allowed the inspector to find the lamination was repaired by closing the seam at the weld. In short, it would be too difficult or expensive to replace the plate, so the weld was merely replaced.

When plate rupture took place frequently, notch ductility of the material was studied. Then for some unfortunate reason the notch ductility as a measure of plate performance became part of the general code of the plate material, and never part of the acceptability of the assembly concern. Actually the needs for notch ductility vary in the fabricated product and also vary in the plate production. It could well be that each may vary in opposition. For example, specification concerns for notch toughness values in an easy-to-test region may dictate that the fabricator place in remote regions, (those regions most likely to have high near balanced triaxial loading), the least ductile material because testing complications free this region from control. Frequently the notch ductility is lower in heavier plate. More than likely the heavier plate is due to increased stress requirements. Is it clear that when fabrication is complete that the worst combination of problems have not culminated at the most critical point in the part? One further point concerning notch ductility and thickness. Some codes relieve the fabricator in the area of joint efficiency if stress relief is employed. With thick plate the fabricator may well choose to use slightly heavier plate to avoid the stress-relief problem. It also could be that his plate-notch ductility capability continues to suffer with increased plate thickness. There may be some concern to consider the plate properties in stress relief where local residual stress may reduce final assembly capability.

A review of current specifications reveals a certain piecemeal historical development caused by progressive chronological modification. With time, weld fit-up has been generally improved, welding materials have become more reliable, and welding processes have become more efficient. Inspection equipment can now reveal more minute discontinuities and techniques, now employ more varied tests and locations. With these new capabilities, new demands for inspection criteria have been met. Is this the proper trend? Possibly only the price of the manufactured article is raised rather than serviceability as well. The increase in price may also reflect a reduced market.

The principal question to be faced is, will the part do the job for which it is intended? Once again the prime concern is product serviceability and reliability. In many industries this concern was passed by as a needless expense. Today with new test methods available an additional review of product analysis may have merit. Numerous recently publicized failures have stressed the unit concept. The concern was not in the area of parts inspection or specifications, but with a final analysis of the assembled unit. Final service analysis has proven to be quite a surprise to some machinery. Often they find that their rugged model built to take punishment is so constrained by strengthening members, that a less complex and more economical model outlasts the "ruggedized" unit.

If at all possible the reporting of test indications should include information that can be employed beyond the manufacturing area. If development research is to plan serviceability, testing and design is to review the case of the prototype and the product, and manufacturing should be capable of a production review in terms of prior inspection criteria. Inspection should not make its findings in radiographic or ultrasonic jargon, but in terms that can be used in design and stress analysis.

A review of tests and testing will readily prove that many tests which specifications cherish are not contributing to our serviceability analysis. For example, weld metal tension testing may contribute to a raw materials evaluation but will not be

Table 1

USA	A.S.M.E. Boiler & Pressure Vessel Code—1965 Section I—Power Boilers Section II—Nuclear Boilers Section III—Unfired Pressure Vessels American Petroleum Institute 1104 Standard for Welding Pipe Lines and Related Facilities 5LX High Test Line Pipe American Welding Society D2.0-66 Welded Highway and Railway Bridges Military (Partial list of general and draft documents) NAVSHIPS 250 Series (e.g. 1500 and 637 types) MIL-STD 779, CE 260
UK	British Standard 1515 Fusion Welded Pressure Vessels—Part 1, Carbon and Ferritic Steels British Standard 1500 Fusion Welded Pressure Vessels—Part 3, Aluminum (Drafts of Parts for: Austenitic Steel Fusion Welded Pressure Vessels; Copper and Copper Alloy Pressure Vessels.) British Standard 2633—Class 1, Arc Welding of Ferritic Steel Pipework for Carrying Fluids
Poland	Polish Standard PN-60/M-69773 Classification of Welded Joints on the Basis of Evidence Supplied by Radiographs
Holland	Dienst Voor Het Stoomwezen VKR-7-5DFT, Evaluation of Acceptance Limits for Inhomogeneities Revealed by Radiography
Japan	Standards for the Visual Examination of Welds in Hull Construction

Table 2

Maximum Permissible Porosity Indications in Radiographs per 6 inch Length of Weld

Weld Thickness (in.)	Total Area of Permitted Porosity (sq. in.)	LARGE—Pore Size (in.)			MEDIUM—Pore Size (in.)			FINE—Pore Size (in.)		
		Approx. Fraction	Decimal Value[1]	No.	Approx. Fraction	Decimal Value[1]	No.	Approx. Fraction	Decimal Value[1]	No.
1/8	.0075	—	—	—	—	—	—	1/64	.014	49
1/4	.015	—	—	—	3/128	.025	31	1/64	.0138	100
1/2	.030	3/32	.10	4	1/32	.031	40	3/128	.0195	101
3/4	.045	1/8	.125	4	1/32	.034	50	3/128	.024	99
1	.060	1/8	.125	5	5/128	.039	50	1/32	.0275	101
1½	.090	1/8	.125	7	3/64	.048	50	1/32	.034	99
2	.120	1/8	.125	10	7/128	.055	51	5/128	.039	100
2½	.150	1/8	.125	12	1/16	.061	51	3/64	.044	99
3	.180	1/8	.125	15	1/16	.068	50	3/64	.048	99
3½	.210	1/8	.125	17	5/64	.073	50	7/128	.052	99
4	.240	1/8	.125	20	5/64	.078	50	7/128	.055	101

[1]These values used for calculating total area of permissible porosity given in second column.

effective as an assembly property analysis. In fact any uniaxial test may prove to give only relative analysis. Plate properties may show that an inordinate amount of concern has been given to connections. Tests directed to finding cracks rather than conforming to test configurations will certainly reveal internal cracks in structures accepted as having "no cracklike flaws". Would some realism here be in order?

A recent review of international specifications concerned with criteria for weld inspection was made by Commission V of the IIW. Their document V-332-66 notes that five countries of the world have specifications of this type. Table 1 has expanded the International Institute of Welding document to some degree. While some countries have acceptance criteria in their pressure vessel codes, these reflect the criteria of the U.S.A. or the U.K. for the most part.

It would be impossible to review the development of all world discontinuities in this paper. Because porosity studies seem to be under current consideration, this particular criterion may serve to illustrate a specification trend. Again in reference to the American Society of Mechanical Engineers we note first use of internal soundness as an acceptance basis in 1931. At this time sample X-ray film was used to set the limit of acceptability. In 1951 the film gave way to charts on porosity. This method permitted the standard committee a more flexible tool to describe acceptable radiographs. However, acceptance was still within the confines of the language of the inspection group. In 1962 a revised set of charts was produced which permitted the size of pore to be increased but permitted fewer pores to be accepted. In 1965 the tables were supplemented with a tabular indication of "maximum permissible porosity indications". Table 2 is a copy of the porosity chart from the ASME Power Boilers Section I. Other portions of the code are similar. If one can assume that the code speaks of spherical porosity it is quite clear that the ASME porosity specification employs roughly a 1% loss in cross-section by porosity as its criterion. For the intended service and the structural configuration of necks and nozzles employed to do the power transducing of heat to electrical energy, it is quite likely that one part of the unit may be asked for three times the service of another. In a review of the total job the strict case of 1% loss in section may prove a severe inequity.

A recent U.S. military specification has been developed to expand acceptance for a variety of service requirements. Five levels of porosity are recommended which fall approximately in the range of 1, 2, 4, 7 and 10% loss in cross-section. The motivation for this study was an examination of the real requirements of service.

Many stress analysts have used a classical Timoshenko analysis of a spherical cavity in a tension field as an adequate study of spherical type gas porosity in static load service. If a gas pore of 0.015 in. in radius is internal in a section, the average stress is increased to a value slightly more than two times, actually 2.04 at the edge of the hole. A stress concentration factor, K of 2.04. This K-value then decreases with distance from the hole as: $K=1.27$ at 0.005 in. from the cavity, 1.11 at 0.010 in. and 1.009 at 0.030 in.

These values are meaningless however unless we consider the material performance. Again consider the material a 200,000 psi yield strength high tensile strength steel with a 4% strain at rupture was examined for its capability of absorbing or redistributing local stress concentration. A K of 6.0 for the material indicates that in the tension field stress concentrations of this magnitude are absorbed, far more than the 0.015-in. porosity would indicate. Hence the problem may simply be loss in cross-section in this case. A porosity study in the static case indicates that original plate properties may be produced where a loss of cross-section of mild steel of 40,000 psi yield strength up to 7% may be occasional. With 100,000 psi yield strength material a loss of cross-section up to 5 or 6% may be present with original plate properties obtained. These figures may suggest further need for criteria re-evaluation.

Many specifications note the concern for cluster or linear porosity. This problem too, may be considered by this analysis. The interaction of two adjacent cavities may well increase the magnitude of the stress concentration at the pore edges. An analysis of two 0.015-in. pores first in contact and then removed specific distances was calculated. A K of 3.08 is revealed for the pores in contact. Thus even in contact the most severe case of linear porosity the K-value is well below the plate capability of 6.0. Table 3 indicates that the stress concentration drops off rapidly as the pores separate. Previous studies of porosity tests in mild steel and quenched and tempered steel failed to reveal the need for extra concern in the linear and clustered cases, other than being related to a loss in cross-section. The stress analysis gives additional weight to this conclusion.

As the standards groups review practical service the possibility of fatigue-type loading is cause for evaluation. R. E. Peterson has put this phenomenon on a quantitative basis with extensive test correlation. He defines his "notch-sensitivity factor" $= q$ as:

$$q = \left(\frac{K_f - 1}{K_t - 1}\right)$$

where

K_f = fatigue-notch factor

$$= \frac{\text{Endurance Limit of unnotched specimens}}{\text{Endurance Limit of notched specimens}}$$

and

K_t = the theoretical stress concentration factor where results are obtained by photoelastic materials.

Table 3

Interaction of Two Pores as the Distance of Separation is Increased

K	Pore Spacing in Per cent of Pore Diameter
3.08	0.0 (Contact)
2.12	0.1
1.60	0.2
1.20	0.3
1.12	0.4
1.08	0.5
1.05	0.6
1.03	0.7
1.02	1.0

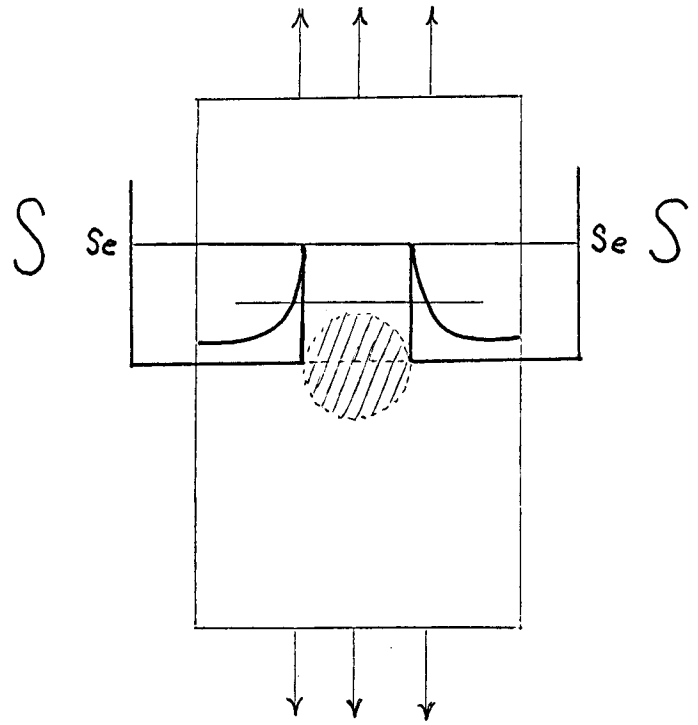

Figure 1. Stress distribution. $S = Se_1$.

The notch sensitivity factor is a property of the material and also a function of the notch radius, r. As the notch radius becomes small, K_t increases, however, q decreases and clarifies the problem of the infinite radius crack. Thus the relationship considers the material as non-homogeneous and recognizes actual grain structure.

When we consider the stress distribution across a section which contains a hole it is noted that the stress gradient at the edge of the hole is maximum. However if the load is just sufficient to bring the peak stress up to the fatigue limit, S_e, as in Figure 1, it would not be expected to produce fatigue failure because the volume of material at this stress value is zero. Due to grain structure some finite volume of material must be at the fatigue limit before a crack will form. One way of expressing this is to say that the fatigue limit stress must exist at some

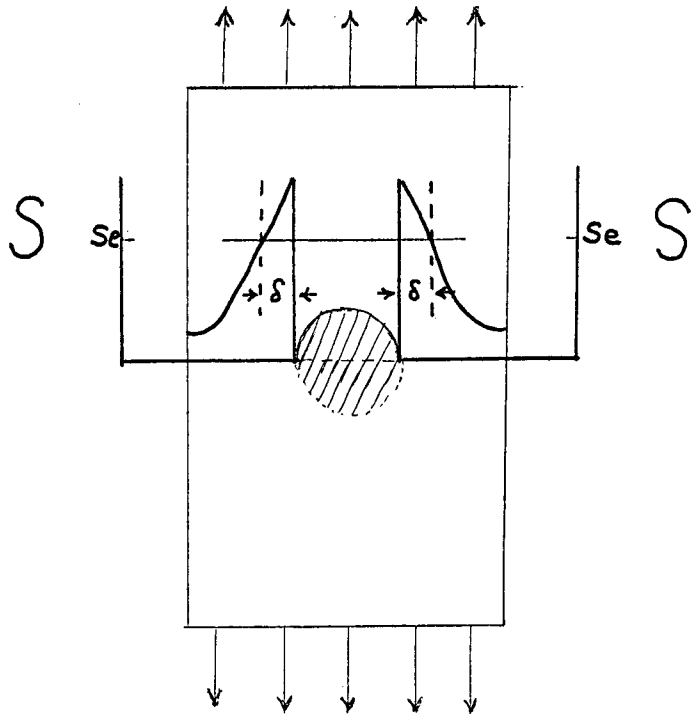

Figure 2. Stress distribution. $S > Se_2$.

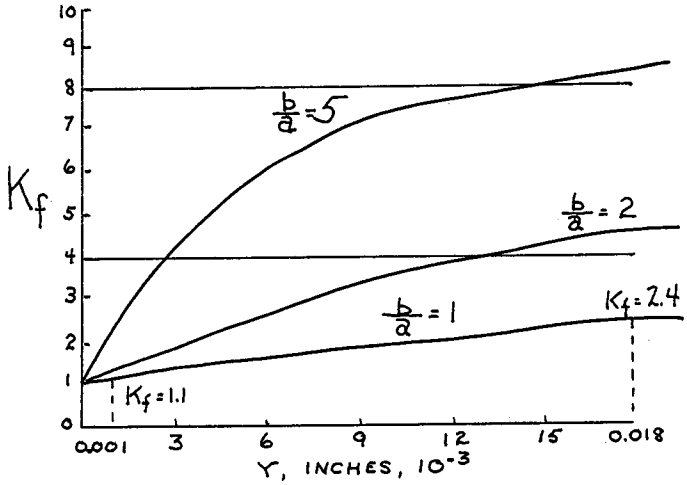

Figure 3. Strength reduction factors; elliptical holes and elongated cavities.

finite depth, δ below the surface (see Figure 2). The steeper the stress gradient the higher the load required to produce fatigue failure. The dimension, δ, is a material property. In general, hard fine-grained materials have small δ values while the values for soft-grained materials are large.

Peterson has estimated the relationship between K_f and notch radius, r, for three cases, (1) an elliptical hole or external notch, (2) an elongated cavity, (3) an ellipsoidal cavity. Figure 3 shows K_f plotted against r for the first two cases. For each ellipse b/a is equal to 1, 2, or 5. K_t starts at 1.0 for "r" = 0 and would approach K_t as r becomes larger.

For a round hole through a plate or a worm-hole cavity where $b/a = 1$, if $r = 0.001$ then $K_f = 1.1$. The plate is not weakened more than 10%.

With a cavity radius of 0.036 in. or a radius of 0.018; $K_f = 2.4$. With the theoretical K_t at 3.0 the notch sensitivity factor becomes 0.7. These particular tests were conducted in a 100,000 psi U.T.S. steel with a δ of 0.002. The low value of q gives support to the fact that porosity need not be a concern.

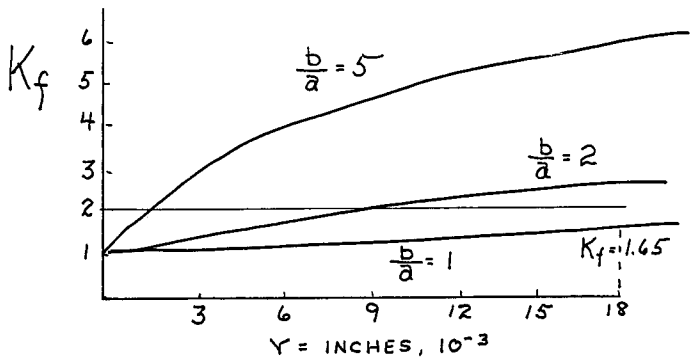

Figure 4. Strength reduction factors; ellipsoidal cavities.

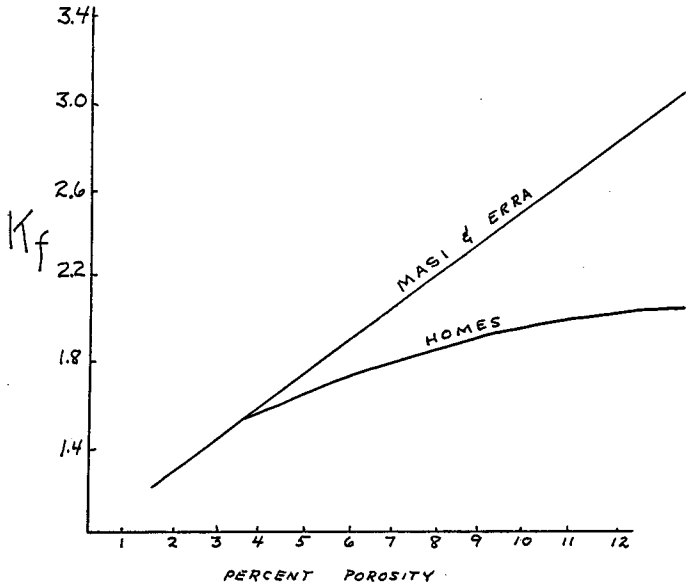

Figure 5. Effect of porosity on strength reduction factor.

Nominal Joint Thickness Inches	Maximum Allowable Pore Size	Allowable Total Pore Index	
		Class I	Class II
0.091 Thru 0.120	0.036	180	240
	% Porosity	4.25–5.6	5.66–7.42
0.121 Thru 0.160	0.042	210	280
	% Porosity	4.34–5.75	5.81–7.67
0.161 Thru 0.200	0.048	240	320
	% Porosity	4.55–5.6	6.05–7.52

Figure 6. Porosity requirements—weldments—rocket systems.

This should not be considered a case to replace the service test but only further justification for the study.

Figure 4 is the case of the ellipsoidal cavity. The curve for $b/a = 1$ shows the weakening effects to be expected from spherical cavities such as those produced by porosity. A pore of 0.018 in. radius produces a K_f of 1.65. The fatigue strength has been reduced about 60% of its basic value. Now the theoretical K_t for this case is 2.04, and the "q" becomes 0.625. Peterson also shows that K_t is markedly lower when the cavity is filled with another material, even if that material has a modulus of elasticity only $\frac{1}{4}$ that of the base metal. Tungsten inclusions may fit this case while slag inclusions may have less than an 8 million psi modulus. Even so the potential capability of the system may place both slag and porosity problems in the province of deserving reviewed study as acceptance criterion.

Two studies by Homés and Masi-Erra showed that with mild steel tested in alternating tension that at the 5% porosity level the strength reduction factor of approximately 1.7 or a 60% reduction of the fatigue strength. Homés' results indicates that at 5% K_f is 1.68 and at 7% K_f is 1.78 (Figure 5).

Encouraged by low fatigue cycle tests typical of rocket systems, Young made a study of porosity requirement for this field. Figure 6 shows the results of this work with an addition, insertion 6, considering percentage loss of section due to porosity. Two classes of work are considered and levels of porosity of approximately 6% and 7% are indicated. This work indicates that low-cycle fatigue service and prior work in static tension and impact are justified in predicting that review in porosity standards are in order. Most certainly serviceability studies may well permit new designs and cost reduction of useful products.

Standards for the acceptance of weld defects and all material are a logical and sound business practice. It is as sound as a contract to buy or sell. Many misfortunes arise when two parties have not effectively communicated, and standards are most capable of narrowing the gap of misunderstanding. However the method of hastily constructing standards based upon some simple technique of evaluating current production often becomes a deterrent to progress. With evaluation on the opposite side of the situation, carefully constructed standards have the advantage of becoming a major boon to the industry. Here standards are the result of long-range growth and development, based upon studied experience. Often the keeping of significant records of material, inspection, manufacturing procedure, design analysis and serviceability analysis are the principal ingredients.

Reference has been made to the significance of serviceability analysis, which is logically the ultimate answer. This test, however, comes at the end of manufacture where costs and time are critical. Therefore if any test is missing, serviceability analysis is usually absent. This is truly amazing, for with this fact it is admitted that only high-production industries use this valuable test. However, it is no secret that often startling information is revealed by service testing competitive products. The same attention paid to in-house products would be more effective by many orders of magnitude.

When standards are documented and products are tested it is startling how manufacturing emphasis changes. Also inspection can alert manufacturing of an increased discontinuity trend which may be corrected before any production is rejected as being defective. Designs become classic in line and manufacturing attention to critical regions is routine, and less critical regions receive statistically occasional analysis. The review of the discontinuities and their effect on service also becomes an important function of design, manufacture, and reliability. As well, repair becomes a clear-cut manufacturing procedure with no sacrifice in properties, only improvement. The logic in every case is clear, calculated proof of each step in manufacture, and decision making in inspection—the result a better product.

Report Session

Training and Qualication of NDT Personnel

PROFESSOR R. C. McMASTER, USA, *Session Chairman*

The authors of the papers on Training and Qualification of Nondestructive Testing Personnel are to be congratulated on the basic and important work they have undertaken, on which they have reported so clearly at this session. I should like to congratulate each author on his contribution. The development of parallel concepts in several great nations of the world is illustrated in these papers and is in itself a confirmation of the need and of the methods being developed for certification and control of personnel involved in interpretation and use of nondestructive tests in industry and other applications.

Canada has been a pioneer in certification of radiographic personnel and has provided a guide to many other countries in their development of similar certification techniques. Mr. Havercroft's report on Certification of Radiographic Personnel in Canada provides a historical review and identification of junior and senior grade certification standards. The existence of the examining authority provided by the Mines Branch of the Department of Energy, Mines and Resources is a national asset not presently duplicated in the United States, for example. The availability of a national standard with approximately 400 certified junior grade and 165 senior grade radiographers is a tribute to the pioneering effort of the members of the committees who have contributed to this development. Their interest in international collaboration in the field of nondestructive testing is to be commended.

The parallel development of certification systems in Great Britain as reported by W. C. Heselwood in Training and Certification of NDT Personnel in Great Britain represents a highly significant achievement. Mr. Heselwood's report on the historical development and recognition of the needs for such certification was most illuminating. The degree of humour, practical insight, and intelligent compromise between conflicting needs and demands frankly described in this report represents the challenge which each nation faces in developing such certification standards.

Professor Tada's report Education and Qualification of Nondestructive Testing Personnel in Japan presents a clear historical record of the development of the Japanese society for nondestructive inspection and its achievements during the past 15 years. Dr. Tada's emphasis upon the need for more than one basic nondestructive testing method to assure the reliability of weldments and other test objects is to be commended. In addition, Japan has developed programs for teachers of technical high schools and for university department faculty. To an educator it is particularly pleasing to know that the engineering department of Osaka University has classes on the engineering of nondestructive testing.

The attainment of laws dealing with radiation protection and of national examinations to assure safety and security under the laws represents a useful result of the efforts of individuals who have contributed their services to advance the field of nondestructive testing. The certification of nondestructive testing companies by the Japanese Welding Engineering Society and of nondestructive testing personnel by the Japanese nondestructive inspection society represent major contributions toward safety and proper application of nondestructive tests. Dr. Tada has compared the Japanese systems with those of Canada and the United States and suggests a strong possibility that an international system could be established wherein all nondestructive testing personnel can be qualified and certified on the same basis.

Mr. Harold Hovland's report on the personnel qualifications document SNT TC-1A of the American Society for Nondestructive Testing records the achievement over the past several years of hard-working committees on certification of nondestructive tests personnel. These committees have prepared training documents, examination questions, and procedures for the presentation of courses and certification of personnel who have received such training. Mr. Havland's delineation of the factors which contribute to the confidence level which can be applied to nondestructive test procedures is significant of all those who undertake this type of task. The fact that documents for several basic test methods have been published and approximately 1000 sets made available to industry, technical societies and private organizations, has been a major contribution to the standardization of nondestructive test certification in the United States.

Collectively the efforts reported in this session represent a basic trend in the field of nondestructive testing and contribute to the professional status of this field of engineering service. Critical to effectiveness in assuring reliability in industry and other applications is the integrity of the individuals and of the philosophy and programs used to implement certification procedures. There can be no question of the need for and value of these types of efforts which have led to useful national procedures for assurance that nondestructive testing and inspection are carried out to adequate standards.

As an individual involved in nondestructive testing leading to new methods and new concepts for their implementation, the session chairman recognizes the validity and need for certification and standardization efforts. However, the one question which remains always to be carefully considered is the possibility that by implementation of fixed standards for certification and specific types of knowledge, a limitation may be placed upon further introduction of novel methods and advanced methods of interpretation of test results. Methods for up-dating and for revision of the basic information, and of standards for its application, must exist. The next generation of nondestructive test systems may be much more complex than the present methods in

use. In particular, it is possible that further use of electronic computers and other methods of evaluation, and of quantitative efforts to relate nondestructive test indications to the precise dimensions and nature of discontinuities, and to the probable service life remaining in structures, will become vitally important. Thus, flexibility and provision for change, as new methods are developed and proven to be valid, should always be provided in the establishment of standards and methods for certification and training of personnel for our rapidly growing field of nondestructive testing.

REPORT OF MEETINGS OF THE INTERNATIONAL COMMITTEE

W. E. Havercroft

Two meetings of the International Committee for Nondestructive Testing were held in the Mount Royal Hotel, Montreal, during the Conference. The first meeting on Sunday, May 21st and the second on Thursday, May 25th.

Sixteen delegates representing 11 countries were present at the first meeting at which time the following action was taken.

(a) The terms of reference of the International Committee which had been revised by the delegates from Canada, Germany, Great Britain, Poland and the United States were adopted by the delegates.

The revision included a change in name of the committee from "The Standing Committee for International Co-operation within the Field of Nondestructive Testing" to "The International Committee on Nondestructive Testing".

(b) The invitation submitted by the delegate from Germany Dr. R. Seifert to host the Sixth International Conference on Nondestructive Testing in Germany in 1970 was unanimously accepted by the committee.

A total of 21 persons representing 14 countries attended the second meeting of the committee. Czechoslovakia's request for membership on the committee was welcomed and unanimously accepted by the delegates. The Czechoslovak Scientific and Technical Society named Ing. L. Cizek and Dr. M. Baimler as their representatives to the committee, these gentlemen were welcomed to the meeting.

Discussions were held on the future activity of the Committee and on matters relating to the Fifth International Conference on Nondestructive Testing which could be of benefit to future Conferences.

It was recommended that the International Standards Organization (ISO) be approached to establish and support a Technical Committee on Nondestructive Testing.

CLOSING SESSION—SUMMARY

Dr. G. H. Tenney

The final session of this impressive Fifth International Conference on Nondestructive Testing is now completed. As Session Chairman it is my desire to express sincere thanks to our Canadian friends for making this Fifth International Conference a reality. Having played an active part in all five conferences and having been on the international scene in the field of nondestructive testing since 1951, I believe that I am in a position to say that this conference, which now enters the history of nondestructive testing, has been at least as successful and informative as its four predecessors. By now it is firmly established that the nondestructive testing profession encompasses the entire world. Through international conferences great progress has been made in the dissemination of technical knowledge across the borders and over the oceans. These are indeed great contributions. In addition I wish to emphasize a much more important impact of these conferences and that is the opportunity to meet each other, to know each other, and to establish a common denominator based on personal knowledge and friendship. These human factors are, in the final analysis, the heartbeat of human endeavour toward peace on earth. Let us include in our philosophy the motto of our host city Montreal—"Concordia Salus"-—Salvation through Harmony.

It has been my privilege to introduce three gentlemen who have ably summarized some of the achievements of the Conference.

My good friend Dr. R. C. McMaster, Professor at Ohio State University and my predecessor as President of the American Society for Nondestructive Testing, has reported on the recommendations of the session dealing with the training and qualification of personnel.

It was an honour to present Professor Dr. G. Homès of the University of Brussels, Belgium, an elder statesman in the field of nondestructive testing and General Chairman of the First International Conference on Nondestructive Testing held in Brussels in 1955, who reported on the recommendations made at the session dealing with the correlation of weld defects.

Last, but not least, it was a special privilege to introduce a man whose efforts helped to make this informative gathering possible, the General Chairman of this Conference, Mr. William E. Havercroft, who reported on the meetings held by the International Committee for Nondestructive Testing.

I wish to thank these gentlemen for their reports of activities that have taken place during the five days of the conference in the beautiful "Expo 67" City of Montreal. Another major milestone to be remembered and appreciated has been placed on the road of progress in nondestructive testing. Let us be mindful that the road continues and that the next milestone will be established when we meet again in Germany in 1970.

PRESENTATION OF STANDARDS

A set of standards prepared by the British Standards Institution relating to nondestructive testing and welding was presented to the Canadian Council for Nondestructive Technology by Messrs. C. C. Bates and C. Campkin of the United Kingdom.

The gift was acknowledged by Mr. W. E. Havercroft, President of the Canadian Council for Nondestructive Technology, who expressed thanks to the donors, to the British Standards Institution and to the British National Committee for Nondestructive Testing for this gesture of international cooperation and friendship.